BIOLOGICAL AND MEDICAL PHYSICS, BIOMEDICAL ENGINEERING

For further volumes:
http://www.springer.com/series/3740

BIOLOGICAL AND MEDICAL PHYSICS, BIOMEDICAL ENGINEERING

The fields of biological and medical physics and biomedical engineering are broad, multidisciplinary and dynamic. They lie at the crossroads of frontier research in physics, biology, chemistry, and medicine. The Biological and Medical Physics, Biomedical Engineering Series is intended to be comprehensive, covering a broad range of topics important to the study of the physical, chemical and biological sciences. Its goal is to provide scientists and engineers with textbooks, monographs, and reference works to address the growing need for information.

Books in the series emphasize established and emergent areas of science including molecular, membrane, and mathematical biophysics; photosynthetic energy harvesting and conversion; information processing; physical principles of genetics; sensory communications; automata networks, neural networks, and cellular automata. Equally important will be coverage of applied aspects of biological and medical physics and biomedical engineering such as molecular electronic components and devices, biosensors, medicine, imaging, physical principles of renewable energy production, advanced prostheses, and environmental control and engineering.

Ute Linz
Editor

Ion Beam Therapy

Fundamentals, Technology, Clinical Applications

With 235 Figures

Springer

Editor
Dr. Ute Linz
Forschungszentrum Jülich
52425 Jülich, Germany
u.linz@fz-juelich.de

Biological and Medical Physics, Biomedical Engineering ISSN 1618-7210
ISBN 978-3-642-21413-4 e-ISBN 978-3-642-21414-1
DOI 10.1007/978-3-642-21414-1
Springer Heidelberg Dordrecht London New York

Library of Congress Control Number: 2011940320

Cover design: eStudio Calamar Steinen

Printed on acid-free paper

Springer is part of Springer Science+Business Media (www.springer.com)

Preface

In 1995, when I had the privilege to edit the first comprehensive volume on ion beam therapy (IBT), the world celebrated the 100th anniversary of Röntgen's discovery of a new kind of ionizing radiation, a finding which has significantly impacted medicine, biochemistry, and material science. X-rays became the foundation of several new disciplines for and within medicine such as radiology, radiography, radiobiology, radiation therapy, radiosurgery, but also radiation protection or X-ray technology and engineering for diagnostic and therapeutic equipment.

This new compendium will appear 110 years after Röntgen received the Nobel prize in physics, the first ever awarded. It is also the 65th anniversary of Robert R. Wilson's visionary publication in *Radiology* where he postulated the advantages of accelerated ions as a radiation source for therapeutic application. James M. Slater, the doyen of clinical proton therapy, commemorates these and other important milestones of radiation therapy that have enabled the development of IBT up to its current state in the introductory chapter of this book. The first section continues to view IBT and its place in the treatment of cancer from various angles including socioeconomic aspects.

In the second section, the physical and radiobiological fundamentals of IBT are described. Preclinical assays are presented and computer models to calculate the effects of various ions.

Clinical results cover a large part of this book because, in recent years, IBT experience has been gained for tumors of most organs. From ocular and skull base tumors to thoraco-abdominal and pelvic tumors or tumors of the extremities, promising data are reported, and it will become clear that IBT is applicable not only to fixed targets but also to highly mobile tumors that change their shape and location during a single treatment fraction.

Two sections are devoted to the technology required for IBT, from individual components to turn-key commercial concepts. Pros and cons of various accelerator types or the challenges of superconducting magnets are key topics. Beam spreading techniques, dosimetry, safety and control systems, and quality assurance

are explained, and how a gantry should be designed that offers precision, ease of handling, and maximum flexibility to the therapist.

The section *Patient Positioning and Treatment Planning* covers IBT-relevant issues of imaging, planning, positioning, and online irradiation control. Colleagues from Loma Linda, Boston, Chiba, and Jacksonville share their valuable experiences concerning the start-up of a new facility or an upgrade of an already operating center.

Radiation therapy still experiences new developments all intended for safer and more successful treatment of the patient. IBT is part of this progress and experiences significant changes itself. Despite some rather surprising recent decisions by industrial players, new facilities, will soon be able to study carefully and systematically ions of the first ten elements of the periodic table to find out which ions are best suited for which indications. However, IBT will not only be judged on its clinical excellence. In a world of health economics, any new diagnostic or treatment modality will have to compete economically with existing devices or techniques. New technical concepts which promise to lower the cost of IBT by promoting smaller units or single-room facilities will, therefore, complete the last section on *Future Developments*.

This book is the common achievement of many experts from around the world. Their background as clinicians, physicists, biologists, computer scientists, engineers, or health economists reflects the highly interdisciplinary character of the field of IBT. All participants want to share their expertise with those who need to know more about this still novel radiation therapy option, with those who consider to do research in IBT, with the interested public, and with patients and their relatives who might want to learn about the background of this treatment modality and the clinical experience gained.

I am very much indebted to all the contributors of this book. It has been a great pleasure to be part of this international community of motivated and dedicated scientists.

I am also grateful to the Forschungszentrum Jülich, in particular to Sebastian Schmidt and Georg Büldt, for constant support and the permission to edit this book and to Claus Ascheron of Springer Publishing for endorsing this publication.

My sincere apologies go to all those whom I was pushing too hard to meet one or the other deadline.

Jülich
October 2011 *Ute Linz*

Contents

Contributors

Dr. Hiroshi Akiyama Particle Therapy Systems Design Department, Hitachi Ltd. Power Systems Company, Saiwai-cho 3-1-1, Hitachi-shi, Ibaraki 317-8511, Japan, hiroshi.akiyama.qj@hitachi.com

Dr. Jose Alonso Lawrence Berkeley National Laboratory, 1 Cyclotron Road, Berkeley, CA 94720, USA, jralonso@lbl.gov

Dr. Masayuki Baba National Institute of Radiological Sciences, Research Center of Charged Particle Therapy, Anagawa 4-9-1, Inage-ku, Chiba, 263-8555, Japan, baba@nirs.go.jp

Dr. Christoph Bert GSI Helmholtzzentrum für Schwerionenforschung, Planckstraße 1, 64291 Darmstadt, Germany, c.bert@gsi.de

Dr. Eleanor A. Blakely Life Sciences Division, Mail Stop 977R180, Lawrence Berkeley National Laboratory, 1 Cyclotron Road, Berkeley, CA 94720, USA, eablakely@lbl.gov

Dr. Stéphanie Bolle Clinical Division, Centre de Protonthérapie Institut Curie, Campus Universitaire, 91898 Orsay, France, stephanie.bolle@curie.net

Dr. John Cameron ProCure Treatment Centers, 420 N Walnut Street, Bloomington, IN 47404, USA, john.cameron@procure.com

Dr. Polly Y. Chang Molecular and Genetic Toxicology, Biosciences Division, SRI International, 333 Ravenswood Ave, Mail stop: PN175, Menlo Park, CA, 94025, USA, polly.chang@sri.com

Dr. Stephanie E. Combs Abt. für Radioonkologie und Strahlentherapie, Universitätsklinikum Heidelberg, Im Neuenheimer Feld 400, 69120 Heidelberg, Germany, stephanie.combs@med.uni-heidelberg.de

Prof. Dr. James D. Cox Department of Radiation Oncology, M.D. Anderson Cancer Center, University of Texas, Houston, TX, USA, jcox@mdanderson.org

Dr. Giacomo Cuttone Laboratori Nazionali del Sud – INFN, Via S. Sofia 64, 95123 Catania, Italy, cuttone@lns.infn.it

Dr. Jean Datchary Department Radiation Oncology, Institut Gustave Roussy, 114 rue Edouard Vaillant, 94805 Villejuif, France, jean.datchary@igr.fr

Prof. Dr. Dr. Jürgen Debus Klinik für Radioonkologie und Strahlentherapie, Universitätsklinikum Heidelberg, Im Neuenheimer Feld 400, 69121 Heidelberg, Germany, juergen_debus@med.uni-heidelberg.de

Prof. Dr. Thomas F. DeLaney Radiation Oncology, Francis H. Burr Proton Therapy Center, Massachusetts General Hospital, Harvard Medical School, 30 Fruit St., Boston, MA 02114, USA, tdelaney@partners.org

Dr. Rémi Dendale Clinical Division, Centre de Protonthérapie Institut Curie, Campus Universitaire, 91898 Orsay, France, remi.dendale@curie.net

Dr. Hartmut Eickhoff GSI Helmholtzzentrum für Schwerionenforschung, Planckstraße 1, 64291 Darmstadt, Germany, h.eickhoff@gsi.de

Dr. Thilo Elsässer Siemens Healthcare AG, Imaging & Therapy, Particle Therapy, Hofmannstr. 26, 91052 Erlangen, Germany, thilo.elsaesser@siemens.com
and
GSI Helmholtzzentrum für Schwerionenforschung, Planckstraße 1, 64291 Darmstadt, Germany, t.elsaesser@gsi.de

Prof. Dr. Wolfgang Enghardt Technische Universität Dresden, OncoRay – National Center for Radiation Research in Oncology, Fetscherstr. 74, 01307 Dresden, Germany, wolfgang.enghardt@oncoray.de

Dr. Loïc Feuvret Department Radiation Oncology, Groupe Hospitalier Pitié-Salpétrière, 47-83, Blvd de l'Hôpital, 75013 Paris, France, loic.feuvret@psl.aphp.fr

Dr. Fine Fiedler Helmholtz-Zentrum Dresden-Rossendorf, Institute of Radiation Physics, PO Box 510119, 01314 Dresden, Germany, f.fiedler@hzdr.de

Dr. Jay Flanz Francis H. Burr Proton Therapy Center, Massachusetts General Hospital, Harvard Medical School, 30 Fruit St., Boston, MA 02114, USA, flanz@hadron.mgh.harvard.edu

Prof. Em. Dr. Reinhard Gahbauer Department of Radiation Medicine, A.G. James Cancer Hospital & R. Solove Research Institute, Ohio State University Medical Center, Columbus, OH 43210, USA, rgahbauer@aol.com

Dr. Kenneth P. Gall Still River Systems, 300 Foster Street, Littleton, MA 01460, USA, kgall@stillriversystems.com

Dr. Ismael Ghorbel Department Radiation Oncology, Institut Gustave Roussy, 114 rue Edouard Vaillant, 94805 Villejuif, France, ismael.ghorbel@igr.fr

Dr. Michael Gillin Department of Radiation Physics, University of Texas, M.D. Anderson Cancer Center, Houston, TX, USA, mgillin@mdanderson.org

Dr. John Gueulette Université Catholique de Louvain, UCL – IMRE 5469, Av Hippocrate 55, 1200 Brussels, Belgium, john.gueulette@uclouvain.be

Dr. Daniel Habermehl Klinik für Radioonkologie und Strahlentherapie, Universitätsklinikum Heidelberg, Im Neuenheimer Feld 400, 69121 Heidelberg, Germany, daniel.habermehl@med.uni-heidelberg.de

Prof. Dr. Jean-Louis Habrand Department Radiation Oncology, Institut Gustave Roussy, 114 rue Edouard Vaillant, 94805 Villejuif, France, habrand@igr.fr
and
ARCHADE - Centre François Baclesse, 3 av. Général Harris, BP 5026, 14076 Caen cedex 5, France, jl.habrand@baclesse.fr

Prof. Dr. Oliver Jäkel Klinik für Radioonkologie und Strahlentherapie, Universitätsklinikum Heidelberg and Heidelberger Ionenstrahl-Therapiezentrum, Im Neuenheimer Feld 450, 69120 Heidelberg, Germany, oliver.jaekel@med.uni-heidelberg.de

Dr. Dan T.L. Jones iThemba LABS, P.O. Box 722, Somerset West, 7129 South Africa, jones@tlabs.ac.za

Yves Jongen Ion Beam Applications SA, Chemin du Cyclotron 3, 1348 Louvain-la-Neuve, Belgium, yves.jongen@iba-group.com

Dr. Andrzej Kacperek Douglas Cyclotron, Clatterbridge Centre for Oncology, Wirral, CH63 4JY, UK, andrzej.kacperek@ccotrust.nhs.uk

Dr. Tadashi Kamada National Institute of Radiological Sciences, Research Center of Charged Particle Therapy, Anagawa 4-9-1, Inage-ku, Chiba, 263-8555, Japan, t_kamada@nirs.go.jp

Dr. Shingo Kato National Institute of Radiological Sciences, Research Center of Charged Particle Therapy, Anagawa 4-9-1, Inage-ku, Chiba, 263-8555, Japan, s_kato@nirs.go.jp

Dr. Paul J. Kim Massachusetts General Hospital, Department of Radiation Oncology, 100 Blossom St., Cox 3, Boston, MA 02114, USA, kimpx1@gmail.com

Prof. Dr. Andre Konski Department of Radiation Oncology, Wayne State University School of Medicine, Barbara Ann Karmanos Cancer Center, Detroit, MI 48201, USA, akonski@med.wayne.edu

Prof. Dr. Hanne Kooy Francis H. Burr Proton Therapy Center, Massachusetts General Hospital, Harvard Medical School, 30 Fruit St., Boston, MA 02114, USA, hkooy@partners.org

Dr. Detlef Krischel Bruker Advanced Supercon GmbH, Friedrich-Ebert-Str. 1, 51429 Bergisch Gladbach, detlef.krischel@bruker-asc.com

Dr. Daniela Kunath Helmholtz-Zentrum Dresden-Rossendorf, Institute of Radiation Physics, PO Box 510119, 01314 Dresden, Germany, d.kunath@hzdr.de

Prof. Dr. Zuofeng Li University of Florida Proton Therapy Institute, Department of Radiation Oncology, 2015 North Jefferson Street, Jacksonville, FL 32206, USA, zli@floridaproton.org

Dr. Ted Ling Department of Radiation Medicine, Loma Linda University Medical Center, 11234 Anderson Street, B 121, Loma Linda, CA 92354, USA, teling@llu.edu

Dr. Dr. Ute Linz Forschungszentrum Jülich, Leo-Brandt-Str. 1, 52425 Jülich, Germany, u.linz@fz-juelich.de

Prof. Dr. Ramona Mayer EBG MedAustron GmbH, Viktor Kaplan-Straße 2, 2700 Wiener Neustadt, Austria, ramona.mayer@ebgmedaustron.at

Prof. Dr. Nancy P. Mendenhall University of Florida Proton Therapy Institute, Department of Radiation Oncology, 2015 North Jefferson Street, Jacksonville, FL 32206, USA, menden@shands.ufl.edu

Dr. Hidetsugu Nakayama Department of Radiology, Tokyo Medical University, Shinjuku 6-1-1, Shinjuku-ku, Tokyo 160-0022, Japan, hnakayam@tokyo-med.ac.jp

Prof. Dr. Koji Noda Department of Accelerator and Medical Physics, National Institute of Radiological Sciences, Research Center of Charged Particle Therapy, Anagawa 4-9-1, Inage-ku, Chiba, 263-8555, Japan, noda_k@nirs.go.jp

Dr. Tatsuya Ohno Gunma University Heavy Ion Medical Center, Showa-machi 3-39-22, Maebashi, Gunma, 371-8511, Japan, tohno@gunma-u.ac.jp

Dr. Toshiyuki Okumura Proton Medical Research Center, Department of Radiation Oncology, University of Tsukuba, Tennodai 1-1-1, Tsukuba, Ibaraki 305-8575, Japan, okumura@pmrc.tsukuba.ac.jp

Dr. Katia Parodi Heidelberger Ionenstrahl-Therapiezentrum, Im Neuenheimer Feld 450, 69120 Heidelberg, Germany, katia.parodi@med-uni-heidelberg.de

Dr. Eros Pedroni Center for Proton Therapy (CPT), Paul Scherrer Institut, 5232 Villigen, Switzerland, eros.pedroni@psi.ch

Dr. Pascal Pommier Department Radiation Oncology, Centre Léon Berard, 28, rue Laennec, 69373 Lyon, France, pommier@lyon.fnclcc.fr

Marlen Priegnitz Helmholtz-Zentrum Dresden-Rossendorf, Institute of Radiation Physics, PO Box 510119, 01314 Dresden, Germany, m.priegnitz@hzdr.de

Dr. Eike Rietzel Siemens Healthcare AG, Imaging&Therapy, Particle Therapy, Hofmannstraße 26, 91052 Erlangen, eike.rietzel@siemens.com

Steven Rightnar Department of Radiation Medicine, Loma Linda University Medical Center, 11234 Anderson Street, CSP A-1010, Loma Linda, CA 92354, USA, rightnar@dominion.llumc.edu

Dr. Carl J. Rossi, Jr. Department of Radiation Medicine, Loma Linda University Medical Center, 11234 Anderson Street, CSP A-1010, Loma Linda, CA 92354, USA, crossi@llurm.org

Dr. Narayan Sahoo Department of Radiation Physics, University of Texas, M.D. Anderson Cancer Center, Houston, TX, USA, nsahoo@mdanderson.org

Prof. Dr. Hideyuki Sakurai Proton Medical Research Center, Department of Radiation Oncology, University of Tsukuba, Tennodai 1-1-1, Tsukuba, Ibaraki 305-8575, Japan, hsakurai@pmrc.tsukuba.ac.jp

Niek Schreuder ProCure Treatment Centers, 420 N Walnut Street, Bloomington, IN 47404, USA, niek.schreuder@procure.com

Dr. Reinhard Schulte Department of Radiation Medicine, Loma Linda University Medical Center, 11234 Anderson Street, B 121, Loma Linda, CA 92354, USA, rschulte@dominion.llumc.edu

Prof. Dr. Daniela Schulz-Ertner Radiologisches Institut am Markus-Krankenhaus, Wilhelm-Epstein-Str. 4, 60431 Frankfurt, Germany, daniela.ertner@fdk.info

Dr. Helen A. Shih Massachusetts General Hospital, Department of Radiation Oncology, 100 Blossom St., Cox 3, Boston, MA 02114, USA, hshih@partners.org

Prof. Jacobus Slabbert iThemba LABS, P.O. Box 722, Somerset West, 7129 South Africa, jps@tlabs.ac.za

Prof. Dr. James M. Slater Department of Radiation Medicine, Loma Linda University Medical Center, 11234 Anderson Street, CSP A-1010, Loma Linda, CA 92354, USA, jmslater@dominion.llumc.edu

Prof. Dr. Jerry D. Slater Department of Radiation Medicine, Loma Linda University Medical Center, 11234 Anderson Street, CSP A-1010, Loma Linda, CA 92354, USA, jdslater@dominion.llumc.edu

Dr. Andres Sommer Siemens Healthcare AG, Imaging&Therapy, Particle Therapy, Hofmannstraße 26, 91052 Erlangen, andres.sommer@siemens.com

Dr. Shinji Sugahara Department of Radiology, Tokyo Medical University, Ibaraki Medical Center, Amimachi-chuo 3-20-1, Inashiki, Ibaraki 300-0395, Japan, ssuga@tokyo-med.ac.jp

Prof. Dr. Koichi Tokuuye Department of Radiology, Tokyo Medical University, Shinjuku 6-1-1, Shinjuku-ku, Tokyo 160-0022, Japan, ktokuue@tokyo-med.ac.jp

Kazuo Tomida Particle Therapy Systems Design Department, Hitachi Ltd. Power Systems Company, Saiwai-cho 3-1-1, Hitachi-shi, Ibaraki 317-8511, Japan, kazuo.tomida.zf@hitachi.com

Prof. Dr. Hirohiko Tsujii National Institute of Radiological Sciences, Research Center of Charged Particle Therapy, Anagawa 4-9-1, Inage-ku, Chiba, 263-8555, Japan, tsujii@nirs.go.jp

Dr. Stanislav Vatnitsky EBG MedAustron GmbH, Viktor Kaplan-Straße 2, 2700 Wiener Neustadt, Austria, stanislav.vatnitsky@ebgmedaustron.at

Prof. Dr. André Wambersie Université Catholique de Louvain, UCL – IMRE 5469, Av Hippocrate 55, 1200 Brussels, Belgium, andre.wambersie@uclouvain.be

Dr. Udo Weinrich GSI Helmholtzzentrum für Schwerionenforschung, Planckstraße 1, 64291 Darmstadt, Germany, u.weinrich@gsi.de

Prof. Dr. Shiao Y. Woo Department of Radiation Oncology, James Graham Brown Cancer Center, University of Louisville, 529 S. Jackson Street, Louisville, KY 40202, USA, sywoo001@louisville.edu

Dr. Andrew Wroe Department of Radiation Medicine, Loma Linda University Medical Center, 11234 Anderson Street, CSP A-1010, Loma Linda, CA 92354, USA, awroe@dominion.llumc.edu

Dr. Naoyoshi Yamamoto National Institute of Radiological Sciences, Research Center of Charged Particle Therapy, Anagawa 4-9-1, Inage-ku, Chiba, 263-8555, Japan, nao_y@nirs.go.jp

Dr. X. Ronald Zhu Department of Radiation Physics, University of Texas, M.D. Anderson Cancer Center, Houston, TX, USA, xrzhu@mdanderson.org

Abbreviations

AAPM	American Association of Physicists in Medicine
ACC	Adenoid cystic carcinoma
ACR	American College of Radiology
ADT	Androgen deprivation therapy
ASTRO	American Society for Therapeutic Radiology and Oncology
AVM	Arteriovenous malformation
BED	Biologically effective dose (not to be confused with biologically equivalent dose EQD = BED/(RBE+dfraction/α/β))
BESSY	Berliner Elektronenspeicherring-Gesellschaft für Synchrotron-strahlung (now part of HZB), Berlin, Germany
BEV	Beam's eye view
bNED	Biochemically no evidence of disease
CAL	Centre Antoine-Lacassagne, Nice, France
CBCT	Cone beam computed tomography
CCD	Charge-coupled device, light-sensitive integrated circuit
CCO	Clatterbridge Centre for Oncology, Wirral, UK
CERN	Conseil Européen pour la Recherche Nucléaire (European Council for Nuclear Research), Geneva, Switzerland
CF	Conventional fractionation, ca. 2 Gy per fraction, 5 times per week
CI	Confidence interval
CIRT	Carbon ion radiotherapy
CMOS	Complementary metal oxide semiconductor
CNAO	Centro Nazionale di Adroterapia Oncologica (National Center for Oncological Hadrontherapy), Pavia, Italy
CNRS	Centre National de la Recherche Scientifique (National Center for Scientific Research of France)
CNS	Central nervous system
COMS	Collaborative Ocular Melanoma Study
CPO	Centre de Protonthérapie de l'Institut Curie, Orsay, France
CPU	Central processing unit

CR-39	Columbia Resin-39, trade mark for a thermoset polymer used as nuclear track detector
CRT	Conformal radiotherapy
CSS	Control and safety system
CT	Computed tomography
CTC	Common toxicity criteria
CTV	Clinical target volume
CW	Continuous wave
DICOM	Digital Imaging and Communications in Medicine, a standard for the exchange of information in medicine
DKFZ	Deutsches Krebsforschungszentrum (German Cancer Research Center), Heidelberg, Germany
DRR	Digitally reconstructed radiograph
DTL	Drift tube linac
DVH	Dose-volume histogram
DWA	Dielectric wall accelerator
ECHED	European Clinical Heavy-Particle Dosimetry Association
ECR	Electron cyclotron resonance
EORTC	European Organization for Research and Treatment of Cancer
ESS	Energy selection system
EULIMA	European Light-Ion Medical Accelerator
FFAG	Fixed-field alternating gradient (accelerator)
FHBPTC	Francis H. Burr Proton Therapy Center, Boston, USA
FPTI	Florida Proton Therapy Institute, Jacksonville, USA
FWHM	Full width at half maximum
GHMC	Gunma University Heavy Ion Medical Center
GSI	Helmholtzzentrum für Schwerionenforschung (formerly Gesellschaft für Schwerionenforschung, Society for Heavy Ion Research) Darmstadt, Germany
GTV	Gross tumor volume
GyE	Gray Equivalent or RBE-weighted dose (still widely used unit even though according to ICRU-IAEA Joint Report 79 the unit should be replaced by Gy (RBE))
Gy (RBE)	RBE-weighted or effective dose, see also GyE
HCL	Harvard Cyclotron Laboratory, Cambridge, USA
HIMAC	Heavy Ion Medical Accelerator Chiba, Japan
HIT	Heidelberger Ionenstrahl-Therapiezentrum (Heidelberg Ion-Beam Therapy Center)
HMI	Hahn-Meitner-Institut, (now part of HZB) Berlin, Germany
HU	Hounsfield unit
HZB	Helmholtz-Zentrum Berlin, a merger of HMI and BESSY, Berlin
IAEA	International Atomic Energy Agency
IBT	Ion beam therapy
ICER	Incremental cost-effectiveness ratio
ICUR	Incremental cost-utility ratio

IFJ	Instytut Fizyki Jadrowej (Institute of Nuclear Physics), Krakow, Poland
ICRU	International Commission on Radiation Units and Measurements
IGPT	Image-guided proton therapy
IGRT	Image-guided radiation therapy
IMPT	Intensity-modulated (particle or proton) therapy
IMRT	Intensity-modulated (X-ray or photon) radiotherapy, see also IMXT
IMXT	Intensity-modulated X-ray therapy, see also IMRT
INFN-LNS	Istituto Nazionale di Fisica Nucleare - Laboratori Nazionali del Sud (National Institute of Nuclear Physics - National Laboratory of the South), Catania, Italy
INSERM	Institut national de la santé et de la recherche médicale (National Institute of Health and Medical Research of France)
Kerma	Kinetic energy released in matter, defines the kinetic energy transferred by indirectly ionizing radiation to the first generation of secondary particles divided by the irradiated mass
keV	Kiloelectronvolt
LBL	Lawrence Berkeley National Laboratory, Berkeley, USA
LCR	Local control rate
LD_{50}	Lethal dose 50%, kills 50% of a sample population in a specified period of time
LEBT	Low-energy beam transport
LED	Light-emitting diode
LEM	Local Effect Mode
Linac	Linear accelerator
LLUMC	Loma Linda University Medical Center, Loma Linda, USA, (recently named James M. Slater, M.D., Proton Treatment and Research Center)
MCS	Multiple Coulomb scattering
MDACC	MD Anderson Cancer Center, Houston, USA
MEEI	Massachusetts Eye and Ear Infirmary, Boston, USA
MGH	Massachusetts General Hospital, Boston, USA
MKM	Microdosimetric Kinetic Model
MMP	Matrix metalloproteinase
MOSFET	Metal-oxide semiconductor field-effect transistor
MPRI	Midwest Proton Radiotherapy Institute, (recently named Indiana University Health Proton Therapy Center), Bloomington, USA
MRI	Magnetic resonance imaging
NCCHE	National Cancer Center Hospital East, Kashiwa, Japan
NCI	National Cancer Institute, Bethesda, USA
NIRS	National Institute of Radiological Sciences, Chiba, Japan
NPTC	Northeast Proton Therapy Center (now FHBPTC), Boston, USA
NSCLC	Non-small cell lung cancer
NTCP	Normal tissue complication probability
OAR	Organ at risk

OER	Oxygen enhancement ratio
OSL	Optically stimulated luminescence
PET	Positron emission tomography
PMMA	Polymethylmethacrylate
PMRC	Proton Medical Research Center, Tsukuba, Japan
PPIC	Parallel-plate ion chamber
PROG	Proton Radiation Oncology Group (USA)
PSA	Prostate-specific antigen
PSI	Paul Scherrer Institute, Villigen, Switzerland
PT	Proton therapy
PTC-H	Proton Therapy Center (at MDACC), Houston, USA
PTCOG	Particle (formerly Proton) Therapy Co-Operative Group
PTV	Planning target volume
QA	Quality assurance
QALY	Quality-adjusted life year
QUANTEC	Quantitative analyses of normal tissue effects in the clinic
RBE	Relative biological effectiveness
REM	Roentgen equivalent man (replaced by SI unit Sievert: 1 Sv=100 rem), still used in the expression "REM counter" for a neutron equivalent-dose meter
RF	Radiofrequency
RFQ	Radiofrequency quadrupole
RT	Radiotherapy or radiation therapy
rms	Root mean square, $x_{\mathrm{rms}} = ((\Sigma_{i=1}^{n} \quad x^2)/n)^{0.5}$
RPC	Radiological Physics Center, Houston, USA
RTOG	Radiation Therapy Oncology Group (USA)
SAD	Source-to-axis distance
SBRT	Stereotactic body radiation therapy
SEER	Surveillance Epidemiology and End Results, a source for cancer statistics in the USA
SEM	Secondary (electron) emission monitor
SMN	Secondary malignant neoplasm
SOBP	Spread-out Bragg peak
SSD	Source-to-skin distance
Sv	Sievert, unit for dose equivalent
TACE	Transarterial chemoembolization
TCP	Tumor control probability
TERA	Terapia con Radiazioni Adroniche (an Italian Foundation for Therapy with Hadronic Radiations)
TLD	Thermoluminescent (or thermoluminescence) dosimeter, detector measuring light emitted from a crystal upon heating as function of radiation exposure
TPS	Treatment planning system or software

TRIUMF	Tri-University Meson Facility (Canada's National Laboratory for Particle and Nuclear Physics), Vancouver, Canada
TSL	The Svedberg Lab, Uppsala, Sweden
UCL	Université catholique de Louvain, Louvain-la-Neuve (Belgium)
UCSF	University of California, San Francisco, USA
UICC-TNM	Union for International Cancer Control-Tumor-Nodes-Metastases, a widely used system to classify the extent of cancer spread
VEGF	Vascular endothelial growth factor
VOI	Volume of interest
WPE	Westdeutsches Protonentherapiezentrum (West German Proton Therapy Centre) Essen, Germany

Part I
Ion Beam Therapy in Perspective

Chapter 1
From X-Rays to Ion Beams: A Short History of Radiation Therapy

James M. Slater

Abstract Radiation therapy (RT) developed in several eras. Patients' needs for more effective treatment guided the efforts. The development of ion beam therapy (IBT) can be seen as a corollary in this continuous endeavor to optimize disease control while minimizing normal-tissue damage. It could not have materialized, however, without the curiosity, ingenuity, and perseverance of researchers, engineers, and clinicians who developed important enabling technologies.

1.1 Introduction

Prior to the advent of ionizing particle beams, medicine had few options for treating some malignant and benign diseases. Physicians' needs for new techniques to address these problems formed a vacuum, clearly demonstrated immediately following the discovery of X-rays in November 1895. By the first few months of 1896, X-rays were being used to treat skin lesions prior to any understanding of the beams' physical or biological characteristics. The driving force was, of course, patients' overwhelming need of treatment for uncontrollable and debilitating diseases.

Radiation medicine developed over four major eras: the era of discovery, from Röntgen's discovery to about the late 1920s; the orthovoltage era, from the late 1920s through World War II; the megavoltage era, which began with higher-energy linacs for therapy in the 1950s, and, with refinements such as intensity-modulated X-ray therapy (IMXT), is still ongoing. Within this scheme, the roots of IBT fall into the third or megavoltage phase, with the first treatment of humans in 1954.

J.M. Slater (✉)
Department of Radiation Medicine, Loma Linda University Medical Center, 11234 Anderson Street, CSP A-1010, Loma Linda, CA 92354, USA
e-mail: jmslater@dominion.llumc.edu

U. Linz (ed.), *Ion Beam Therapy*, Biological and Medical Physics, Biomedical Engineering, DOI 10.1007/978-3-642-21414-1_1,

Only in the mid 1980s did a first hospital-based proton facility become feasible. These eras represent a continuum rather than a succession of distinct periods, but are a convenient way to assess the evolution of RT and IBT as a sophisticated part of it.

In each era, the fundamental impetus for improvements came from patients' needs for effective disease control while retaining or improving quality of life. These needs aroused the curiosity of physicians, physicists, and biologists, who, in their own ways in each of the eras, performed studies aimed at better understanding the tools they were working with and learning how to use them optimally for patients' benefit. A kind of teamwork occurred in all of the eras, although often no formal teams existed; an overarching goal – better patient treatment – guided the efforts. The development of ion beams is part of this process.

1.1.1 The Discovery Era

During this period of 30–35 years, the roots of RT were established. This era saw the discovery of the atom and various subatomic and electromagnetic particles; investigators strove to learn how to use them therapeutically.

The salient discovery was Röntgen's in 1895 [1], although X-rays were produced earlier – if unwittingly – by others [2]. His report was followed soon by Becquerel's on the phenomenon of radioactivity [3] and, in 1898, by that of the Curies on the discovery of radium [4]. Becquerel and Curie reported on the physiologic effects of radium rays in 1901 [5]. Such discoveries stimulated speculation that radioactivity could be used to treat disease [6]; indeed, X-rays were used to treat a patient with breast cancer in January 1896 [7]. By 1904, RT texts were available [8, 9]; reports of the use of X-rays and radium (curietherapy) occurred throughout the first decade of the twentieth century.

In retrospect, it is clear that lack of knowledge of the biological effects and mechanisms of actions of the new rays led to much morbidity and poor cancer control [10]. However, such outcomes led physicians to ponder better modes of delivery; radiobiologists to study the effects of the rays on cells; and physicists to investigate the properties of these newly discovered radiations. Physics research led to the discovery of radioactive isotopes, which later were used for intracavitary and interstitial therapy; the same research led ultimately to an understanding of the structure of the atom.

As the era progressed, biologists began to understand the relationship between time and dose on cell survival. A crucial discovery occurred when Regaud [11] and Coutard [12] studied alternative ways of delivering the total radiation dose. Until that time, treatment was generally administered in one or a few large doses. Regaud demonstrated that fractionated therapy would eradicate spermatogenesis permanently; Coutard later showed that applying external beam therapy similarly could control head and neck cancer without the severe reactions and late effects that single large doses caused. These findings established that normal cells are better

able to recover from radiation injury than cancer cells and led radiation therapists to employ dose fractionation.

During this era also, Coolidge developed a practical X-ray tube, allowing physicians to deliver higher-energy X-rays (180–200 kV) to deeper tumors [13]. Until then, X-rays were used mainly to treat superficial tumors. High-voltage transformers were also developed. Subsequently, physicists and engineers developed techniques to better measure the dose of radiation with X-rays.

The path to charged-particle therapy begins with Ernest Rutherford, whose work spurred understanding of atomic structure. Rutherford explained radioactivity as the spontaneous disintegration of atoms; he helped determine the structure of the atom; and he was the first to note that one element could be converted to another. A complete bibliography of Rutherford's works is available online, as part of a comprehensive site devoted to him [14]. The reader is referred to that source for publications relating to discoveries noted herein.

In 1896, Rutherford began to use X-rays to initiate electrical conduction in gases; he repeated the study with rays from radioactive atoms after Becquerel's discovery. In 1898, he discovered that two separate types of emissions came from radioactive atoms; he named them alpha and beta rays, the latter of which were shown to be electrons. He showed that some heavy atoms decay into lighter atoms, and in 1907 demonstrated that the alpha particle is a helium atom stripped of its electrons. He and Geiger developed a method to detect single particles emitted by radioactive atoms. He investigated whether alpha particles were reflected from metals, discovering that some alpha rays were scattered directly backward from a thin film of gold; a massive yet minute entity, the atomic nucleus, turned back some alpha particles. In 1911, Rutherford proposed the nuclear model of the atom. One of his students, Niels Bohr, placed the electrons in stable formation around the atomic nucleus; the Rutherford–Bohr model of the atom, with later modifications, became standard, and Rutherford scattering is still used today in basic and applied research.

Wilhelm Wien, in 1898, had identified a positively charged particle equal in mass to the hydrogen atom. In 1919, Rutherford demonstrated that nitrogen under alpha-particle bombardment ejected what appeared to be nuclei of hydrogen; a year later, he equated the hydrogen nucleus with the charged entity that Wien had discovered. He named it the proton.

The discovery of X-rays, then gamma rays, then the structure of the atom with electrons, protons, and neutrons marked the first era. It was one of physical and biological experimentation to determine and understand the characteristics of the newly discovered beam and the effects of such rays on cells and tissues. Especially following the work of Rutherford, radioactive elements were also identified and diligently studied, as well.

As treatment began with these new types of radiation prior to adequate knowledge of their characteristics and effects, errors were made and patients were injured. However, as knowledge and understanding increased during this era, two major divisions of radiation medicine – diagnosis and therapy – were developing; physicians were diagnosing many diseases and malignant tumors were being treated, some of them successfully.

1.1.2 The Orthovoltage Era

The period from roughly the late 1920s to 1950 encompasses this era. Patients' needs for treatment of deep tumors were addressed largely by radium-based intracavitary and interstitial irradiation, in the absence of deeply penetrating external beam sources. It was also a transitional period: physical developments that led to supervoltage (approx. 500 kV–2 MV) RT were being made [15]. During the 1920s, advances in physics and engineering led to increased understanding of subatomic particles and techniques for energizing and focusing them.

The first supervoltage X-ray tubes, built by Coolidge [16], were the basis of the linear accelerator, developed by Widerøe in 1927 and described in a German journal in 1928. E.O. Lawrence, despite knowing little German, used Widerøe's equations and drawings to conceptualize the cyclotron [17]. By the late 1920s, particle accelerators began to be constructed. Following the invention of the linear accelerator, devices operating on the principle of applying a potential difference were developed by Van de Graaff in 1929 [18] and by Cockcroft and Walton in 1932 [19, 20]. The cyclotron, also based on the principle of applying a difference in potential, was invented in 1930 by Lawrence and Livingston [21]. At Lawrence's laboratories at the University of California, Berkeley, accelerated particles were used to bombard atoms of various elements, forming, in some cases, new elements. Lawrence's brother, John, a physician, along with Robert Stone, pioneered neutron radiation for medical treatments [22].

Electron beam therapy became a practical and useful therapeutic option in 1940, when Kerst developed the betatron [23, 24]. The first machine produced 2 MeV electrons; later devices yielded up to 300 MeV. Medical research in particle therapy was largely sidelined during World War II, but high-energy physics investigations were spurred, notably in the effort to develop an atomic bomb. Some who worked on it, notably Robert R. Wilson, became instrumental in the development of IBT.

One major advance during this period was the synchrotron, conceived independently and at about the same time (1944–1945) by Veksler in the Soviet Union and McMillan in the United States. McMillan gave priority to Veksler [25]. The central concept was phase stability, by which high energies could be achieved without the need to build ever larger cyclotrons. Phase stability became the basis for all high-energy proton and electron accelerators thereafter. More importantly for medical use, the synchrotron made it easier to vary the energy of acceleration and thus the depth of penetration in tissue – needed for optimal radiation treatments. The first, the Cosmotron at Brookhaven National Laboratory, began operation in 1952 [17].

1.1.3 Megavoltage Era

The megavoltage era encompasses the years from about 1950 to 1985, although, as noted, in some respects it is still in progress. A major advance, in response to

the continuing need to treat tumors located in deep tissues, was the development of cobalt teletherapy machines and megavoltage linear electron accelerators. Cobalt teletherapy was capable of producing beams equivalent to approximately 1.3 MV X-rays. Electron linacs began to become clinically available as early as the mid 1950s [26], but widespread application occurred in the 1960s and 1970s. Their higher energies (4–6 MeV in earlier machines; 10–20 MeV in later units) made possible increased depth of penetration, greater skin sparing, and improved disease-control rates, which often doubled or tripled, through delivery of higher doses [27, 28]. There was still a major limitation, however, because the radiation sources, X-rays or gamma rays (cobalt), were difficult to control as they passed through tissue: they scattered laterally and passed beyond their targets, exiting patients opposite the point of entry and causing excessive radiation in normal tissues surrounding the tumors. To overcome this, radiation oncologists and medical physicists developed multifield treatment plans to spread unwanted radiation to larger volumes of normal tissue, thereby reducing the high dose to any one region. This tactic helped to reduce visible effects, but also increased the total dose delivered to normal tissues (volume integral dose). Doses sufficient to control many tumors were still unattainable because of continued acute complications and late effects caused by injury to normal tissues.

During this era, radiation medicine advanced as a discipline. Well-designed clinical studies demonstrated the efficacy of modern methods of delivering RT. One of the earliest was done by Gilbert Fletcher at the University of Texas M.D. Anderson Hospital; it demonstrated clearly that megavoltage treatment resulted in improved survival in cancer of the uterine cervix [29]. The founding of the American Society for Therapeutic Radiologists (ASTR) in 1966 (originally the American Club of Therapeutic Radiologists, founded in 1958) occurred partly as a means of encouraging careful studies such as those done by Fletcher. As time progressed, radiation therapists began to emphasize themselves primarily as radiation oncologists; in 1983, the organization became the American Society for Therapeutic Radiology and Oncology (ASTRO) [30].

In many respects, the megavoltage era is still in progress, although the development of higher-energy electron accelerators is quite mature. In recent years the emphasis in photon RT has been on conformal techniques, featuring computerized control and approaches such as IMXT. The intent, as has been true throughout the megavoltage era, is to deliver a more effective dose to the target volume while reducing the dose to tissues that do not need to be irradiated. One might think of it as the multiportal approach brought to its logical conclusion; indeed, the approach was anticipated by rotational arc therapy, popular for a time in the 1970s and 1980s. IMXT can conform the high dose to the target volume, but the modality employs a greater number of portals and thus traverses a greater volume of normal cells. IMXT beams are still composed of photons; their absorption characteristics in tissue remain unchanged.

1.1.4 The Era of Ion Beams

The groundwork for IBT was laid in 1946 when Robert R. Wilson wrote the landmark paper in which he proposed that protons accelerated by machines such as Lawrence's could be used for medical purposes as well as scientific investigations [31]. In a conversation with the author, Wilson said that his insight was inspired by the medical work that Lawrence and Stone had done at Berkeley. In the immediate postwar years, higher-energy accelerators were just becoming available. Wilson reasoned that protons, among the charged particles, offered the longest range for a given energy and were then the simplest and most practical for medical use.

Wilson's interest in the medical use of protons never ceased. When he was selected as first director of the National Accelerator Laboratory (later Fermilab), he encouraged the idea of a proton treatment facility. In 1972, Fermilab investigators proposed such a facility. However, physicians in the Chicago area advocated a neutron facility at the laboratory instead. After Wilson resigned the directorship in 1978, others at Fermilab, among them Miguel Awschalom, Donald Young, and Philip Livdahl, continued to believe in a patient-dedicated proton facility.

The first clinical use of a proton beam occurred at Berkeley in 1954 [32]; limited investigational proton treatment lasted for a few years afterward, until Berkeley scientists, notably Cornelius A. Tobias, began investigating biologically similar helium ions. Tobias was a nuclear physicist who, early in his career, became interested in applying physics to biology and medicine. His fundamental research interest was on the effects of ionizing radiation on living cells, and he, like Wilson, foresaw the advantages of therapeutic ion beams long before most radiation oncologists did [33, 34].

Proton therapy (PT) began to spread to other physics laboratories around the world. The second use of a physics research accelerator for PT occurred in Uppsala, Sweden in 1957. Physicians at MGH, led by a neurosurgeon, Raymond Kjellberg, began employing protons in 1961 for neurological radiosurgery; pituitary adenomas were first so treated at Harvard in 1963 [35], followed by fractionated PT for other malignant tumors in 1973 [36, 37], under the leadership of Herman D. Suit. Proton beam therapy began at Dubna, Russia (then USSR), in 1967; subsequently, other Russian facilities began operating at Moscow in 1969 and at St. Petersburg in 1975. The Japanese experience began in 1979, at Chiba; another facility opened at Tsukuba in 1983. At the Swiss Institute for Nuclear Research (now the Paul Scherrer Institute), PT commenced in 1985 [38].

The development of the world's first hospital-based proton facility began in 1970 at LLUMC with a feasibility study that revealed three major missing supportive developments that prevented optimal use of protons for patient treatments: computer competence, digital imaging (computerized tomography scanning), and computer-assisted treatment planning that could allow the physician to visualize the ionization pattern superimposed on the patient's anatomy and thereby plan treatments with the precision necessary to realize the benefits from these well-controllable charged

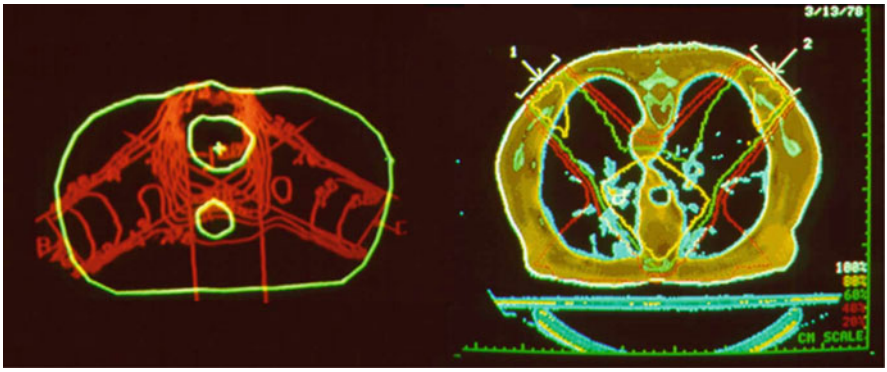

Fig. 1.1 Examples of data output from the computer-assisted treatment planning systems developed at LLUMC in the 1970s. The image from the first (ultrasound) planning system, for a patient treated in 1973, is shown at *left*; a planning image from the second LLUMC system, which employed CT scans, is shown at *right* for a patient treated in 1978. In addition to reproduction of the patient's anatomy, the CT-based system allowed assessment of density variations as the X-ray beams passed through tissue

particle beams (cf. Chap. 34 for details). Industry provided sufficient computer competence and the needed imaging technology by the early 1980s. LLUMC investigators began developing the concepts needed for computer-assisted radiation treatment planning in the late 1960s and completed the first unit, utilizing ultrasonography, in the early 1970s [39]. In the mid-1970s, this was converted to a CT-based unit, using one of the first GE scanners developed (Fig. 1.1). This system provided electron density data, which made possible placement of the Bragg peak precisely within the designated treatment volume [40]. Michael Goitein at MGH expanded the planning system to three-dimensional capabilities, thus providing excellent treatment-planning capabilities for heavy charged particles [41, 42]. The establishment of such planning systems provided one of the essential prerequisites for proton (and other heavy charged-particle) RT [43]. By 1984, all prerequisites for establishing optimal ion beam facilities for clinical use were in place. This was clearly recognized by some of the staff at Fermilab and at the MGH and LLUMC departments of radiation medicine.

The author approached the leadership of Fermilab, Deputy Director Philip V. Livdahl and Director Leon M. Lederman, who agreed to provide Fermilab support for developing a conceptual design for such a clinical facility; to continue with development of an engineering design; and to produce the accelerator, beam transport, and beam delivery systems for LLUMC to begin PT clinical trials (Figs. 1.2 and 1.3). A major turning point in PT, therefore, occurred in 1990, with the opening of the world's first hospital-based proton treatment center at LLUMC. This event occurred more than 20 years after the author and colleagues began to investigate and work toward developing such a facility [44, 45].

Protons were selected as the particle of choice at LLUMC because the relatively low LET of protons as compared to that of heavier ions would allow selective

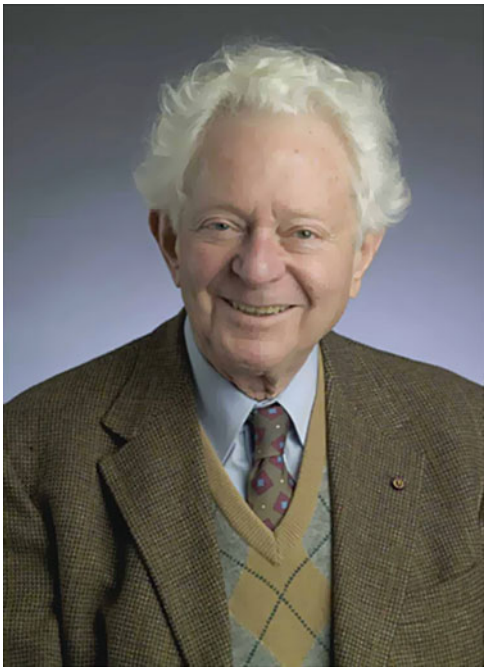

Fig. 1.2 Leon Lederman, Ph.D., Director of Fermilab from 1979 to 1989; recipient of the Nobel Prize for Physics in 1988. In 1986, Dr. Lederman approved Fermilab's collaboration with LLUMC in developing the world's first hospital-based proton treatment center

destruction of the invasive cancer cells growing among normal cells, as had been demonstrated for many years and documented by the worldwide data from using photons (X-rays). By this period, the RBE was known to be very similar for the two kinds of radiation. Loma Linda investigators realized that optimal applications and accumulation of meaningful clinical data could be made only in a facility designed to support patient needs and to operate within a medical environment, with access to a large patient volume and the supporting services available in a medical center. To date, over 15,000 patients have been treated at LLUMC.

Protons were not the only particles investigated for therapy. In the 1960s and 1970s, some physicists and radiation biologists were enthusiastic about the therapeutic possibilities of negative pi-mesons and ions heavier than the hydrogen nucleus. It was then not a given in the minds of many that the particle employed most commonly would be the proton.

Basing their suggestions on the pion capture phenomenon, Fowler and Perkins proposed pi-mesons for clinical use [46]. Pions were expected to become clinically desirable [47], and trials were conducted at three centers: Los Alamos National Laboratory, the Paul Scherrer Institute in Switzerland, and TRIUMF, in British Columbia, Canada. Although some successful outcomes were reported [48–50], in general, the anticipated clinical outcomes did not materialize.

Fig. 1.3 Two Fermilab personnel who helped make the hospital-based proton center at LLUMC a reality. Philip Livdahl (*left*) was Deputy Director of the laboratory in 1986, when the decision was made to proceed with the center. Livdahl had been a colleague of Robert Wilson; he shared Wilson's commitment to proton therapy. Lee Teng, Ph.D. (*right*), shown with the Loma Linda proton synchrotron under construction in the late 1980s, was the chief designer of the accelerator

Helium ion therapy was begun at Berkeley by Tobias and colleagues in 1957 [51]; some notable outcomes supervened [52–54]. Clinical studies with heavier ions were begun by Joseph R. Castro and associates in 1974 [55, 56]; Tobias elucidated the molecular and cellular radiobiology of the particles [57]. Advantages of heavy ions, though appealing theoretically, were not well-understood clinically; the Berkeley studies were undertaken partly to help develop this understanding. Several trials were conducted by Castro and colleagues; some clinical applications were studied, notably specialized indications such as bone sarcomas and bile duct carcinomas [58–60]. However, the cost of developing and delivering heavy ions eventually could not be justified by the relatively limited patient experience, as had been true in the pion trials [61]. Studies of heavy ions shifted to Japan and Germany, under the leadership of such individuals as Hirohiko Tsujii at Chiba and Gerhard Kraft at Darmstadt.

Today, several ion beam facilities operate around the world, including facilities in the United States, Japan, Germany, Russia, France, Canada, China, England, Italy, South Africa, South Korea, Sweden, and Switzerland. Most centers offer protons, but carbon ion therapy is available at HIMAC (Chiba) and HIBMC (Tatsuno) in Japan, and at HIT (Heidelberg), in Germany. The two latter centers offer both protons and carbon ions [62]. Thousands have been treated to date with carbon ion therapy [63, 64], but Eickhoff and Linz note that "systematic experimental studies to find the optimum ion have not yet been pursued" [65]. They speculate that ions with atomic numbers greater than 6 are "unlikely to undergo a clinical revival," but those with atomic numbers between 1 and 6 may be alternatives to carbon.

1.2 Perspective

The development of IBT was a response to the need to preserve normal tissue as much as possible, so as to lessen the side effects and complications that often barred delivery of sufficient dose levels to control tumors, even in the mature megavoltage era. Investigations by physicists and radiation biologists from the 1940s to the 1970s pointed to the superiority of charged particles in comparison to photon and neutron beams. Both Wilson and Tobias told the author that they found it easier to explain and demonstrate the advantages of protons and other ions to fellow scientists than to physicians. As evidence mounted, however, some physicians recognized the physical attributes of ions and were able to understand how these attributes would translate into clinical advantages beneficial to patients.

From the clinician's point of view, the advantages ultimately rested on the fact that ion beams are precisely controllable in three dimensions, while photon and neutron beams are less controllable in two dimensions and are uncontrollable in the third. The controllability of ion beams, in the hands of skillful physicians, provides a superior tool for cancer therapy and for dealing with difficult-to-treat benign diseases.

Curing patients who have solid tumors requires controlling those tumors at their site or region of origin. Normal-tissue damage, whether occasioned by surgical trauma or effects of radiation or chemotherapy, restricts the ability to ablate malignant cells.

Keeping the volume integral dose to normal tissues as low as possible is a fundamental issue in radiation medicine. Rubin and Casarett demonstrated that there is no "safe" radiation dose, in terms of avoiding sequelae in irradiated normal tissues [66]. Later, Rubin and colleagues noted a "cascade of cytokines" in mouse lung tissue exposed to doses that might be considered trivial, leading to pulmonary fibrosis [67]. Biological studies are now commonly finding other injury mechanisms.

Research, therefore, is always ongoing to develop new techniques to overcome these imposed limitations of normal-cell damage. Proton and other charged-particle beams are one outcome of such research.

Any radiation beam, regardless of the basic particle employed, can destroy any cancer cell – or any living entity – if the dose is high enough. Historically, therefore, the limiting factor in radiation medicine has been the normal cell and the need to avoid irradiating normal tissues, so as to permit normal-tissue repair and avoid treatment-compromising side effects. This was the fundamental reason behind dose fractionation and multiportal techniques. During the early years of radiation medicine, the major problem of practitioners was their inability to focus the invisible radiation beam precisely on the invisible tumor target.

Improvements in imaging technologies, along with computer-assisted, CT-based radiation treatment planning, enabled radiation oncologists to deliver precision external-beam radiation treatments to any anatomic site. This advance was limited, however, because conformity with photon beams, which has reached a high degree

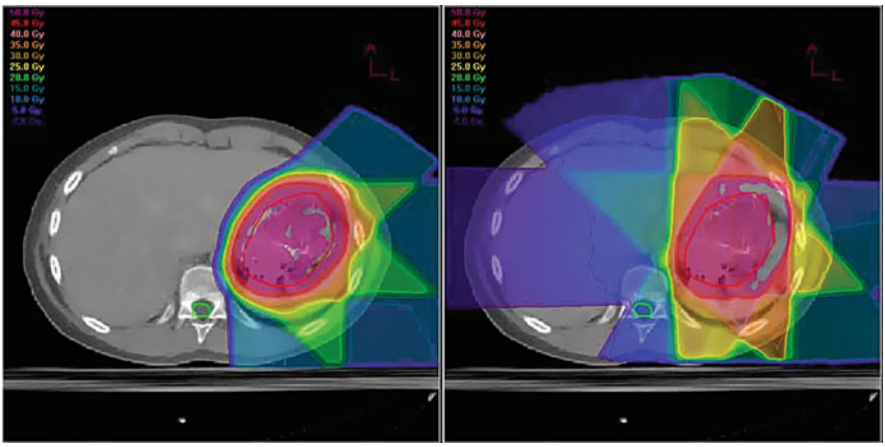

Fig. 1.4 An example of improved controllability needed to spare normal tissues from unnecessary radiation. A 3-field proton plan (*left*) is compared with a 6-field IMXT plan for treating a large liver cancer. Both modalities effect similar high-dose coverage of the clinical target volume (*red outline*), but the superior controllability of the proton beam enables the physician to avoid most of the normal liver tissue receiving low-dose irradiation in the IMXT plan

of precision with IMXT, requires a trade-off: an increased normal-tissue volume integral dose. Ion beams forming a Bragg peak offer a means to achieve the needed increased conformity – i.e., sparing a greater volume of normal tissue – (Fig. 1.4) because of their charge and increased mass.

Physicians using ion beams can now plan treatments to place the Bragg peak in targeted tissues and avoid unacceptable normal-tissue effects. Such capability is facilitated not only by precision therapy planning but also by precision positioning and alignment (cf. Chaps. 33 and 34). This creates a new focus for research and development in the upcoming era. Included in this era, one can expect studies on cell organelle effects with each particle and delivery technique used, and ultimately, biological dosimetry to be developed and merged with physical dosimetry for further improvements in treatment planning. We can also expect to use much more optical imaging fused with our more conventional imaging techniques to better understand the physiological attributes and biological effects of targeted cells and nearby normal cells following treatment. In future years, this increased understanding of cell physiology should help provide a more reasonable rationale for selecting the particle of choice, the fractionation schedule, and the total dose to use for each patient. Technological advances are also occurring in the development of radiosensitizers and radioprotectors, which will further enhance the physician's ability to optimize treatment.

This cyclical process, ongoing since Röntgen's discovery, should take us ever closer to an ideal treatment, wherein only "bad" cells are destroyed and "good" survive. Research will continue; the prime motivator, as always, will be the ongoing effort to meet patients' needs as optimally as possible.

References

1. W.C. Röntgen, Über eine neue Art von Strahlen. Vorläufige Mitteilung. In: Sitzungsberichte der physikalisch-medicinischen Gesellschaft zu Würzburg, Sitzung **30**, 132–141 (1895)
2. M. Lederman, The early history of radiotherapy: 1895–1939. Int. J. Radiat. Oncol. Biol. Phys. **7**, 639–648 (1981)
3. A.H. Becquerel, Sur les radiations émises par phosphorescence. Compt. Rend. Acad. Sci. **122**, 420–421 (1896)
4. P. Curie, M. Curie, Sur une substance nouvelle radioactive, contenue dans la pechblende. Compt. Rend. Acad. Sci. **127**, 175 (1898)
5. A.H. Becquerel, P. Curie, Action physiologique des rayons de radium. Compt. Rend. Acad. Sci. **132**, 1289–1291 (1901)
6. T.G. Lyon, The Roentgen rays as a cure for disease. Lancet **1**, 326 (1896)
7. E.H. Grubbé, Priority in the therapeutic use of X-rays. Radiology **21**, 156–162 (1933)
8. C. Beck, *Roentgen Ray Diagnosis and Therapy* (Appleton, London, 1904)
9. L. Freund, *Elements of General Radiotherapy for Practitioners* (Rehman, New York, 1904)
10. H.S. Kaplan, Basic principles in radiation oncology. Cancer **39**(Suppl 2), 689–693 (1977)
11. C. Regaud, R. Ferroux, Discordance des effets de rayons X, d'une part dans la peau, d'autre part dans le testicule, par le fractionnement de la dose. Compt. Rend. Soc. Biol. **97**, 431–434 (1927)
12. H. Coutard, Principles of X-ray therapy of malignant disease. Lancet **2**, 1–12 (1934)
13. W.D. Coolidge, A powerful Röntgen ray tube with a pure electron discharge. Phys. Rev. **2**, 409–413 (1913)
14. J. Campbell, Web site on Lord Ernest Rutherford, including a comprehensive bibliography at http://www.rutherford.org.nz/bibliography.htm (accessed 4 March 2010). Campbell is the author of a comprehensive biography: Rutherford Scientist Supreme, (AAS, Christchurch, New Zealand, 1999)
15. R.F. Robison, The race for megavoltage. Acta Oncol. **34**, 1055–1074 (1995)
16. W.D. Coolidge, Cathode-ray and Roentgen-ray work in progress. Am. J. Roentgenol. **19**, 313–321 (1928)
17. E.D. Courant, Early Milestones in the Evolution of Accelerators, in *Reviews of Accelerator Science and Technology*, vol. 1, ed. by A.W. Chao (World Scientific, Singapore, 2008), pp. 1–5
18. R.J. Van de Graaff, A 1 500 000 volt electrostatic generator. Phys. Rev. **38**, 1919–1920 (1931)
19. J.D. Cockcroft, E.T.S. Walton, Experiments with high velocity positive ions. Proc. R. Soc. Lond. A **129**, 477–489 (1930)
20. J.D. Cockcroft, E.T.S. Walton, Experiments with high velocity positive ions. (I) Further developments in the method of obtaining high velocity positive ions. Proc. R. Soc. Lond. A **136**, 619–630 (1932)
21. E.O. Lawrence, M.S. Livingston, The production of high speed light ions without the use of high voltages. Phys. Rev. **40**, 19–35 (1932)
22. R.S. Stone, J.H. Lawrence, P.D. Aebersold, A preliminary report on the use of fast neutrons in the treatment of malignant disease. Radiology **37**, 322–327 (1940)
23. D.W. Kerst, Acceleration of electrons by magnetic induction. Phys. Rev. **58**, 841 (1940)
24. D.W. Kerst, The acceleration of electrons by magnetic induction. Phys. Rev. **60**, 47–53 (1941)
25. E.M. McMillan, The origin of the synchrotron. Phys. Rev. **69**, 534 (1946)
26. C.J. Karzmark, N.C. Pering, Electron linear accelerators for radiation therapy: history, principles, and contemporary developments. Phys. Med. Biol. **18**, 321–354 (1973)
27. R.J. Berry, Therapeutic uses of X-rays. Int. J. Radiat. Biol. **15**, 873–895 (1985)
28. H.S. Kaplan, Historic milestones in radiobiology and radiation therapy. Semin. Oncol. **6**, 479–489 (1979)

29. G.H. Fletcher, Supervoltage radiotherapy for cancer of the uterine cervix. Br. J. Radiol. **35**, 5–17 (1962)
30. ASTRO Web site, http://www.astro.org/AboutUs/SocietyHistory/index.aspx (accessed 4 Mar 2010)
31. R.R. Wilson, Radiological use of fast protons. Radiology **47**, 487–491 (1946)
32. M.L.M. Boone, J.H. Lawrence, W.G. Connor, et al., Introduction to the use of protons and heavy ions in radiation therapy: historical perspective. Int. J. Radiat. Oncol. Biol. Phys. **3**, 65–69 (1977)
33. C.A. Tobias, J.E. Roberts, J.H. Lawrence, et al., Irradiation hypophysectomy and related studies using 340 MeV protons and 190 MeV deuterons. Peaceful Uses Atom. Energy **10**, 95–96 (1956)
34. C.A. Tobias, Failla Memorial lecture. The future of heavy-ion science in biology and medicine. Radiat. Res. **103**, 1–33 (1985)
35. R.N. Kjellberg, A. Shintani, A.G. Frantz, B. Kliman, Proton beam therapy in acromegaly. N. Engl. J. Med. **278**, 689–695 (1968)
36. H. Suit, M. Goitein, J. Munzenrider, et al., Evaluation of the clinical applicability of proton beams in definitive fractionated radiation therapy. Int. J. Radiat. Oncol. Biol. Phys. **8**, 2199–2205 (1982)
37. J.E. Munzenrider, M. Austin-Seymour, P.J. Blitzer, et al., Proton therapy at Harvard. Strahlentherapie **161**, 756–763 (1985)
38. Particles, newsletter of the Particle Therapy Co-operative Group, vol. 36, July 2005. This issue is the most recent available online, at http://ptcog.web.psi.ch/archive_particles.html. Accessed 5 Mar 2010
39. J.M. Slater, I.R. Neilsen, W.T. Chu, et al., Radiotherapy treatment planning using ultrasound-sonic graph pen-computer system. Cancer **34**, 96–99 (1974)
40. I.R. Neilsen, J.M. Slater, D.W. Shreyer, CT Scanner Assumes Key role in Computer-Based Radiotherapy Planning System, in *Medinfo 80: Proc3rd World Conf Med Informatics* ed. by D.A.B. Lindberg, S. Kaihara. (North Holland, Amsterdam, 1980), pp. 25–28
41. M. Goitein, M. Abrams, Multi-dimensional treatment planning: I. Delineation of anatomy. Int. J. Radiat. Oncol. Biol. Phys. **9**, 777–787 (1983)
42. M. Goitein, M. Abrams, D. Rowell, et al., Multi-dimensional treatment planning: II. Beam's eye-view, back projection, and projection through CT sections. Int. J. Radiat. Oncol. Biol. Phys. **9**, 789–797 (1983)
43. J.O. Archambeau, G.W. Bennett, G.S. Levine, et al., Proton radiation therapy. Radiology **110**, 445–457 (1974)
44. J.M. Slater, D.W. Miller, J.O. Archambeau, Development of a hospital-based proton beam treatment center. Int. J. Radiat. Oncol. Biol. Phys. **14**, 761–775 (1988)
45. J.M. Slater, J.O. Archambeau, D.W. Miller, et al., The proton treatment center at Loma Linda University Medical Center: rationale for and description of its development. Int. J. Radiat. Oncol. Biol. Phys. **22**, 383–389 (1992)
46. P.H. Fowler, D.H. Perkins, The possibility of therapeutic application of beams of negative pi-mesons. Nature **189**, 524–528 (1961)
47. M.M. Kligerman, W.C. Black, J.M. Yuhas, et al., Current status of clinical pion radiotherapy. Radiology **125**, 489–492 (1977)
48. C.F. von Essen, M.A. Bagshaw, S.E. Bush, et al., Long-term results of pion therapy at Los Alamos. Int. J. Radiat. Oncol. Biol. Phys. **13**, 1389–1398 (1987)
49. R. Greiner, C.F. von Essen, H. Blattmann, et al., Results of curative pion therapy at SIN. Strahlentherapie **161**, 797–800 (1985)
50. T. Pickles, G.B. Goodman, C.J. Fryer, et al., Pion conformal radiation of prostate cancer: results of a randomized study. Int. J. Radiat. Oncol. Biol. Phys. **43**, 47–55 (1999)
51. C.A. Tobias, J.H. Lawrence, J. Lyman, et al., Response of the Nervous System to Ionizing Irradiation, in *Progress Report on Pituitary Irradiation*, ed. by T.J. Haley, R.S. Snider. (Little, Brown, New York, 1964), pp. 19–35

52. D. Lindstadt, J. Castro, D. Char, et al., Long-term results of helium ion irradiation of uveal melanoma. Int. J. Radiat. Oncol. Biol. Phys. **19**, 613–618 (1990)
53. I.D. Kaplan, J.R. Castro, T.L. Phillips, Helium charged particle radiotherapy for meningioma: experience at UCLBL. Int. J. Radiat. Oncol. Biol. Phys. **28**, 257–261 (1993)
54. J.R. Castro, D.E. Linstadt, J.P. Bahary, et al., Experience in charged particle irradiation of tumors of the skull base: 1977–1992. Int. J. Radiat. Oncol. Biol. Phys. **29**, 647–655 (1994)
55. J.R. Castro, J.M. Quivey, Clinical experience and expectations with helium and heavy ion irradiation. Int. J. Radiat. Oncol. Biol. Phys. **3**, 127–131 (1977)
56. J.R. Castro, W.T. Saunders, C.A. Tobias, et al., Treatment of cancer with heavy charged particles. Int. J. Radiat. Oncol. Biol. Phys. **8**, 2191–2108 (1982)
57. C.A. Tobias, E.A. Blakely, E.L. Alpen, et al., Molecular and cellular radiobiology of heavy ions. Int. J. Radiat. Oncol. Biol. Phys. **8**, 2109–2120 (1982)
58. V. Uhl, J.R. Castro, K. Knopf, et al., Preliminary results in heavy charged particle irradiation of bone sarcoma. Int. J. Radiat. Oncol. Biol. Phys. **24**, 755–759 (1992)
59. R. Schoenthaler, J.R. Castro, F.E. Halberg, T.L. Phillips, Definitive postoperative irradiation of bile duct carcinoma with charged particles and/or photons. Int. J. Radiat. Oncol. Biol. Phys. **27**, 75–82 (1993)
60. R. Schoenthaler, J.R. Castro, P.L. Petti, et al., Charged particle irradiation of sacral chordomas. Int. J. Radiat. Oncol. Biol. Phys. **26**, 291–298 (1993)
61. According to a document available on the PTCOG Web site, at http://ptcog.web.psi.ch/Archive/Patientenzahlen-updateMar2010.pdf (accessed 6 March 2010), 433 patients were treated with heavy ions at Berkeley from 1975 to 1992. Pion trials at Los Alamos yielded 230 patients treated from 1974 to 1982
62. PTCOG Web site, summary of current ion beam therapy facilities. Available at http://ptcog.web.psi.ch/ptcentres.html. Accessed 6 Mar 2010
63. D. Schulz-Ertner, H. Tsujii, Particle radiation therapy using proton and heavier ion beams. J. Clin. Oncol. **25**, 953–964 (2007)
64. D. Schulz-Ertner, The clinical experience with particle therapy in adults. Cancer J. **15**, 306–311 (2009)
65. H. Eickhoff, U. Linz, Medical Applications of Accelerators, in *Reviews of Accelerator Science and Technology*, ed. by A.W. Chao, W. Chou, vol. 1 (World Scientific, Singapore, 2008), pp. 143–161
66. P. Rubin, G.W. Casarett, *Clinical Radiation Pathology*, vols. 1 and 2 (W.B. Saunders, Philadelphia, 1968)
67. P. Rubin, C.J. Johnston, J.P. Williams, et al., A perpetual cascade of cytokines postirradiation leads to pulmonary fibrosis. Int. J. Radiat. Oncol. Biol. Phys. **33**, 99–109 (1995)

Chapter 2
The Place of Ion Beams in Clinical Applications

Paul J. Kim and Helen A. Shih

Abstract The place of ion beam therapy (IBT) in the clinic has evolved amid a dynamic environment of advancements on several fronts: tumor biology, diagnostic imaging, surgical and medical oncology, and radiotherapy treatment planning and delivery. This chapter will present generalized themes of the current place of IBT and current areas of investigation.

2.1 The Role of Proton Therapy

Proton therapy (PT) has played numerous roles in the clinic depending on the site and tumor target. These roles can be grouped as follows: ablative therapy, organ preservation therapy, dose escalation around critical structures, and reduction in acute and long-term morbidity. Clinical areas of investigation will also be discussed. Table 2.1 outlines these clinical applications.

2.1.1 Ablative Intent with Single and Hypofractionated Therapy

2.1.1.1 Pituitary Tumors

The first clinical use of PT in Berkeley inspired similar work in Uppsala, Sweden and the Harvard Cyclotron Laboratory (HCL), which commenced PT in 1956 and 1961, respectively. The HCL's initial clinical experience describes 22 patients with

P.J. Kim (✉)
Massachusetts General Hospital, Department of Radiation Oncology, 100 Blossom St., Cox 3, Boston, MA 02114, USA
e-mail: kimpx1@gmail.com

U. Linz (ed.), *Ion Beam Therapy*, Biological and Medical Physics, Biomedical Engineering, DOI 10.1007/978-3-642-21414-1_2,

Table 2.1 Clinical applications of proton radiotherapy

Ablative intent with single and hypofractionated therapy
Pituitary tumors
Arteriovenous malformations
Vestibular schwannomas
Organ Preservation
Choroidal melanoma
Dose escalation around critical structures with highly fractionated treatment
Base of skull
Prostate cancer
Soft tissue and bone sarcomas
Head and neck cancer
Reduction in morbidity and secondary malignancies
Pediatric tumors
Investigational
Low grade glioma
Lung cancer
Pancreatic adenocarcinoma
Hepatocellular carcinoma
Esophageal cancer
Breast cancer
Lymphoma

acromegaly treated in 1963–1967, delivering a range of 60–140 GyE in a single fraction [1]. Other clinical indications treated with this technique in the early days of the HCL included Cushing's disease, Nelson's syndrome, and diabetic retinopathy [2]. In the following decades, amid advancements in trans-sphenoidal surgical techniques, cobalt- and linac-based radiosurgery, and medical management, modern use of the proton radiosurgical technique continues to have a clinical role in selected cases, including persistent acromegaly or adrenocorticotropin-producing adenomas after surgery and/or medical management [3–5]. Salvage treatment for persistent disease after previous radiotherapy illustrates a distinct role for proton radiotherapy in being able to deliver further treatment while limiting the integral dose to previously irradiated normal structures such as the temporal lobes, cranial nerves, and optic apparatus [5].

2.1.1.2 Arteriovenous Malformations

Treatment of arteriovenous malformations (AVMs) with protons represents another example of ablative use of proton beam therapy. Patients selected for this therapy included those with inaccessible or inoperable malformations, i.e., in Kjellberg's

words “large, centrally located, or lying in the speech areas of the dominant cerebral hemisphere or in the brain stem” [6].

More recent experiences reported by the iThemba LABS in South Africa describe 83 patients treated with hypofractionated PT, ranging from single-fraction equivalents of 10.4–14.52 GyE administered in 1–3 fractions. This resulted in obliteration rates of 43–67% depending on the treated volume [7]. The Svedberg Lab (TSL) in Uppsala achieved similar results for 26 patients treated with 20–25 GyE protons in 2–4 fractions, resulting in obliteration rates dependent on treated volume [8]. These three series describe a clear role of proton radiation with ablative intent for inoperable AVMs. Moreover, with increasing treatment volumes, the benefit of minimizing radiation to uninvolved normal tissues would favor proton radiation as compared to photon-based techniques.

2.1.1.3 Vestibular Schwannomas

Proton radiosurgery has been used to treat vestibular schwannomas to prevent neurological symptoms from progressive growth. The experience of the HCL from 1992 to 2000 found that the role of proton radiosurgery evolved over time to limit patient selection to those with no useful hearing, while reserving fractionated schemes to maximize hearing preservation in inoperable patients with useful hearing [9]. Functional preservation of the facial nerve was found to be dependent on the treatment plan’s inhomogeneity coefficient. This may provide some clinical correlation to the dosimetric improvements seen in tumor coverage, dose homogeneity, and normal tissue sparing when comparing proton versus photon stereotactic radiosurgery techniques, particularly with tumors of medium to large size and of irregular shape [10–12].

2.1.2 Organ Preservation

The role of proton radiation in the treatment of choroidal melanomas was explored as an alternative to enucleation for organ and vision preservation. Episcleral brachytherapy was already in use when Constable and Koehler started developing the proton technique for intraocular tumors at the HCL in 1972 [13]. The rationale came from using the sharp beam profile of protons to deliver a more homogenous high-dose radiotherapy treatment with less exposure of nearby critical structures and decreased morbidity. Since then, PT has been shown to provide excellent local control rates of approximately 95% at 15 years, proving to be an effective eye preservation modality [14, 15]. The experience of the Swiss Paul Scherrer Institute (PSI) supports the role of PT in patients with large tumors unsuitable for brachytherapy or tumors close to the optic disc or macula, achieving 5-year local control and eye retention rates of 99% and 88.9%, respectively, in more than 2,400 patients [16].

2.1.3 Dose Escalation Around Critical Structures with Highly Fractionated Treatment

Fractionated proton radiotherapy was initially developed according to the technology available at the time to account for various complexities of heterogeneity. Three categories of complexities were initially described [17]:

I. No heterodense tissue in the beam path (e.g., perineal fields for prostate cancer)
II. One or two relatively large heterodense structures of simple configuration (e.g., cervical chordoma)
III. Multiple or complex heterodense structures (e.g., nasopharyngeal carcinoma)

Early clinical experience proceeded with patients of Category I, largely those with rectal, anal, and prostate cancers treated with the perineal portal technique.

By 1977, 16 large-field conventional fractionation patients were treated, two of them Category II, and one Category III [17]. Advancements in treatment planning using CT data, immobilization, and verification of treatment position allowed more patients across all three categories to be treated. The second HCL clinical update in 1982 described 187 patients, including those with nonuveal melanomas of the head and neck, tumors of the base of skull, meningiomas, craniopharyngiomas, soft tissue and bone sarcomas, squamous cell carcinomas of the oral cavity and oropharynx, paraaortic metastases from cervical carcinoma, prostate cancer, rectal cancer, and anal cancers [18]. Subsequently, dose-escalation trials targeting tumors of the base of skull and prostate cancer commenced. The following illustrates the current role of PT in dose escalation around critical structures.

2.1.3.1 Base of Skull

Chordomas and chondrosarcomas of the skull base are among the most challenging tumors to treat, as they are often unresectable, closely surrounded by critical structures, and insensitive to systemic therapy. Aggressive surgical resection in a location that is intimately bound to delicate structures including brain stem, cranial nerves, optic apparatus, spinal cord, and brain hemispheres is often incomplete and performed in piecemeal fashion. The extent of resection is also weighed against postoperative morbidity. In their review of the Memorial Hospital experience, Higinbotham reported that radiotherapy served mostly a palliative role and that 70 Gy would be needed to provide a substantial benefit [19]. Because such doses exceed normal tissue tolerances, PT was incorporated into radiotherapy treatments due to its favorable beam profile to allow dose escalation while sparing surrounding critical structures.

By 1999, 290 chordomas and 229 chondrosarcomas of the base of skull were treated at the HCL with 66–83 GyE via combined photon–proton therapy [20]. Local control rates were 64% and 95%. Late severe toxicity affecting 8% was found to be acceptable, considering the relatively high radiotherapy doses delivered and the morbidity and mortality of uncontrolled tumor growth.

Long-term results of a randomized trial comparing 70 GyE versus 76 GyE for chordomas and chondrosarcomas of the skull base and cervical spine were recently reported in abstract form and described no clear differences between the high-dose and low-dose group, except for an improved failure-free survival favoring chondrosarcomas of the base of skull in the low-dose arm [21]. Chondrosarcomas were found to have a distinct favorable behavior with higher rates of local control compared with chordomas despite residual gross disease. Time to adjuvant radiotherapy, volume of residual disease, and in chordomas female gender turned out to be poor prognostic factors. They present challenging issues that may further refine the role of PT in the multidisciplinary management of these tumors.

2.1.3.2 Prostate Cancer

Prostate cancer was identified early as a target for dose escalation with PT. In an initial report from the HCL in 1977, four prostate patients were treated with the perineal field technique as a boost with the intent of dose escalation while limiting irradiation to normal tissues.

The limited range of the 160 MeV HCL beam constrained the approach to low pelvic tumors like the prostate to the perineal field technique rather than the modern opposed lateral field approach through the pelvis. This led to a relatively rapid accrual of clinical experience with a phase I/II study of 17 patients and a comparison study of 64 patients demonstrating the feasibility of the perineal proton boost and lack of significant complications or toxicity despite a 10% increase in dose [22, 23]. By 1990, opposed lateral-field techniques to treat prostate cancer were developed with a 250 MeV proton beam at the first hospital-based proton facility at the Loma Linda University Medical Center. Dose escalation was specifically tested in the Proton Radiation Oncology Group (PROG) trial 95–09, which showed that a higher proton boost of 28.8 GyE had lower biochemical failure rates than a proton boost of 19.8 GyE without increase in sexual dysfunction or RTOG grade 3 long-term urinary or rectal toxicity [24]. Meanwhile, technological advances in transrectal ultrasound-guided brachytherapy and intensity-modulated photon radiotherapy have provided other effective alternatives of dose escalation for prostate cancer. The current role of PT in prostate cancer is to provide an alternative treatment option that is at least equivalent in both cancer control and treatment-related morbidity compared with photon radiotherapy. It clearly does have a reduced integral dose to surrounding pelvic tissues, though the clinical significance has yet to be elucidated. Whether quality of life is superior to photon therapy is an important question that could be answered in a randomized phase III trial.

2.1.3.3 Soft Tissue and Bone Sarcomas

Treatment of sarcomas in close proximity to the spinal cord, pelvis, and abdomen requires a multimodality approach. Gross total resection with minimal morbidity

is often the primary treatment. To this end, radiotherapy techniques, delivered pre-, post-, and intraoperatively are strategies used to increase the likelihood to control any remaining microscopic disease.

A phase II study of 50 patients with sarcomas of the spine and paraspinal tissues managed with surgery and mixed photon–proton therapy delivered up to 77.4, 70.2, and 50.4 GyE for gross, microscopic, and subclinical microscopic disease, respectively, via shrinking field technique. Five-year local control was 78% overall with three sacral neuropathies and no spinal cord injuries [25]. Local control was improved in primary (34 of 36 patients) as compared to recurrent (7 of 14 patients) presentation of disease. This experience shows how the proton component delivered with 3D conformal techniques enables dose escalation while decreasing dose to limiting structures such as the spinal cord, esophagus, and bowel. Incorporating photons into the treatment plan helps with shaping the dose around critical structures with intensity-modulated techniques and to decrease skin dose from the proton component.

2.1.3.4 Head and Neck Cancer

Proton radiotherapy has been used to treat numerous malignancies of the head and neck, including sinonasal tumors, nasopharyngeal, and oropharyngeal carcinomas. At a median dose of approximately 73 GyE, the MGH experience of 99 sinonasal cases (65% T4b), including squamous cell carcinoma, esthesioneuroblastoma, adenoid cystic carcinomas, sarcomas, and adenocarcinomas provided 5- and 8-year local control rates of 87 and 83%, respectively [26].

Toxicity rates remained low among patients treated with an accelerated hyperfractionated schedule. In particular, grade 3 late ocular/visual toxicity (NCI–CTC) was seen in only 2 of 36 patients at a median follow-up of 52.4 months [27, 28]. High local control rates were seen, as well, in 17 patients with T4 nasopharyngeal carcinomas treated at the MGH with a median dose of 73.6 GyE, resulting in 3-year locoregional control and overall survival rates of 92% and 74%, respectively, with a median follow-up of 43 months [29]. This initial experience has prompted an ongoing phase II single institutional trial at MGH to evaluate acute toxicity and compliance of chemotherapy concurrent with PT. Evaluation of quality of life measures is also a primary objective. Oropharyngeal carcinomas were treated with an accelerated hyperfractionation technique at Loma Linda University Medical Center, delivering 50.4 Gy with photons to the larger clinical target volume, and a concomitant boost of 25.5 GyE with protons, resulting in a 2-year locoregional control rate of 92% without an increase in late grade 3 toxicity [30]. In the meantime, intensity modulated photon radiotherapy (IMRT) has now become an accepted standard in the treatment of locally advanced head and neck cancer as it is able to escalate radiotherapy doses to tumor targets while sparing normal tissues such as the parotid gland [31]. Several dosimetry studies have compared 3D conformal proton, IMRT, and intensity modulated proton therapy (IMPT) treatment plans, and have found that the IMPT plans further reduced the integral dose while maintaining dose

conformality to delineated targets [32, 33]. Whether such dosimetric improvements translate into meaningful clinical benefit will require further investigation.

2.1.4 Reduction in Morbidity and Secondary Malignancies

2.1.4.1 Pediatric Tumors

It has been well established that 5-year survival rates of children with cancer have been increasing over the last several decades [34]. The role of PT in this population is to minimize both acute and long-term toxicities associated with radiotherapy treatments by reducing the integral dose to surrounding normal tissues. Treatment planning comparisons have illustrated the substantial sparing of normal tissue during craniospinal irradiation with PT versus photon-based techniques due to the absence of exit dose [35]. Specifically, there was less radiation dose to the cochlea, pituitary, parotid, pharynx, heart, lungs, bowels, and kidneys. This is associated with less acute side effects, including nausea, vomiting, and diarrhea. Quantifying and assessing long-term toxicity reduction continues to be an active area of investigation. A preliminary analysis of patients treated with protons at the HCL from 1974 to 2001 matched to patients treated with photons in the SEER (Surveillance Epidemiology and End Results) database showed that photon treatment had an increased risk of secondary malignancy with an adjusted hazard ratio of 2.73 (95% CI 1.87–3.98) [36]. Neurocognitive toxicities, such as lower IQ and reading scores, have been shown to be reduced with smaller irradiated volumes and dose, providing a clear rationale for the treatment with protons [37,38]. Clinical experience in using PT for specific tumors such as medulloblastomas, rhabdomyosarcomas, retinoblastoma, craniopharyngiomas, low-grade gliomas, and ependymomas continue to grow and will be reviewed in a later chapter.

2.1.5 Investigational

Current protocols seek to expand the clinical indications of PT in different tumor sites. Several of these are briefly described below.

2.1.5.1 Low-Grade Glioma

Low-grade gliomas have a relatively long disease history of slow progression and median overall survivals of approximately 7 years after multimodality treatment. Because radiotherapy has been shown to improve progression-free survival but not overall survival, its use in the adjuvant versus salvage setting is influenced by the concern for long-term neurocognitive impairment. The MGH is currently

conducting a trial (DFCI 06–195) to characterize late radiation effects in patients treated with PT hoping that this will minimize treatment-related adverse effects, e.g., to the pituitary gland or memory.

2.1.5.2 Lung Cancer

Treatment-related pneumonitis and esophagitis are dose-limiting effects of chemoradiotherapy in the treatment of lung cancer. There is preliminary clinical evidence by the MD Anderson Cancer Center (MDACC) in Houston that PT can deliver a dose of 74 GyE for stage III non-small cell lung cancer (NSCLC) with less esophagitis than with photon therapy [39]. To examine the role of PT in lung cancer, MDACC and MGH are conducting a randomized phase III trial (DFCI 09–247) comparing the incidence of treatment-related pneumonitis and locoregional recurrence among locally advanced lung cancer patients treated with image-guided adaptive photon or PT.

2.1.5.3 Pancreatic Adenocarcinoma

Preliminary experience from the MDACC has explored the use of preoperative chemoradiotherapy in the management of resectable pancreatic adenocarcinoma to avoid prolonged postoperative recovery. A short course of chemoradiotherapy over 10 days was found favorable with fewer grade 3 toxicities as compared to a conventionally-fractionated schedule of 25 days [40]. Based on this experience, the MGH is conducting a phase I/II trial (DFCI 06–248) exploring the role of preoperative short course chemoradiotherapy with PT investigating feasibility and grade 3 toxicity rates. Secondary aims include the pathological response rate, surgical morbidity, postoperative mortality, and progression-free survival.

2.1.5.4 Hepatocellular Carcinoma

PT has been utilized in the management of unresectable hepatocellular carcinoma (HCC). Other forms of local treatment such as transarterial chemoembolization and radiofrequency ablation are commonly used in unresectable disease, but have limitations such as tumor size, near proximity to major vessels, and the presence of portal vein thrombosis. Many patients with HCC have cirrhosis with compromised liver function, making it challenging to irradiate these tumors while minimizing the integral dose to uninvolved liver tissue. For this reason, PT has been investigated in these unresectable patients, including those who need aggressive local control while waiting for liver transplantation. The Tsukuba group treated 30 patients with HCCs (cf. also Chap. 13) as part of a phase II trial, demonstrating a 2-year local control rate of 96% with 76 GyE delivered over 5 weeks regardless of vascular invasion in tumors up to 10 cm in size [41]. The Loma Linda University Medical Center (LLUMC) also

reported phase II results in 34 patients with HCC, delivering 63 GyE in 3 weeks with 2-year local control rates of 75%, during which six patients underwent liver transplantation [42]. The MGH is currently conducting a phase II trial (DFCI 09–131) investigating the local control rates with PT in unresectable HCCs and intrahepatic cholangiocarcinomas up to 12 cm in size with a 15-fraction scheme that delivers 67.5 GyE to peripheral tumors and 58 GyE to central tumors. Further research efforts will seek to identify effective treatment schemes and appropriate patient selection factors in HCC to benefit from PT.

2.1.5.5 Esophageal Cancer

Dosimetry-planning studies from MDACC, MGH, and TSL have consistently shown improved sparing of normal tissues, namely lung and heart, when treating esophageal cancers with PT compared with photons [43–45].

Mature results from the Tsukuba group described 46 patients with esophageal cancer (all but one with squamous cell carcinoma) treated between 1985 and 1998 with PT with or without photons [46]. The 5-year actuarial survival rate was 34% and local control rates for T1 and T2–T4 lesions were 83% and 29%, respectively. No chemotherapy or surgery was used. Preliminary results from MDACC showed no difference in esophagitis, pneumonitis, dermatitis, overall survival, or disease-free survival between 53 patients treated with intensity modulated photon irradiation or 18 patients treated with proton radiotherapy [47]. Each group received a median dose of 50.4 GyE. Further analysis of metabolic and pathologic responses may help guide refinements in the approach to esophageal cancers with proton radiotherapy.

2.1.5.6 Breast Cancer

PT has been found to improve sparing of lung, heart, and uninvolved breast tissue in treatment planning comparison studies [48, 49]. The MGH reported their initial clinical results of utilizing PT to deliver partial breast irradiation of 32 GyE in 8 fractions over 4 days in 20 stage I breast cancer patients. They found increased skin toxicity when treating with a one-field technique, resulting in a modification to multiple field techniques [50]. LLUMC developed a prone technique to eliminate or minimize respiratory motion-induced breast movement for partial breast irradiation with PT [49]. A treatment-planning approach of employing 2–4 axial beams of different weightings was used to treat 20 stage I breast cancer patients with 40 GyE in 10 daily fractions. Meanwhile, a randomized phase III trial initiated by the National Surgical Adjuvant Breast and Bowel Project and the Radiation Therapy Oncology Group (NSABP B-39/RTOG 0413), continues to accrue patients in the United States to compare treatment outcomes of hypofractionated partial breast irradiation to conventionally-fractionated whole breast radiotherapy. While the clinical utility of partial breast irradiation remains to be determined, the potential role of PT in the postmastectomy setting to reduce cardiac and pulmonary toxicity

has been demonstrated in planning studies and may represent another therapeutic area [48, 51].

2.1.5.7 Lymphoma

Long-term toxicity of radiation in the management of Hodgkin's lymphoma is well documented, including premature cardiac disease and secondary malignancies. PT has been shown in planning studies to be a potential strategy to further reduce the integral dose to uninvolved normal tissues, such as the heart, lung, thyroid, and breast [52]. Case reports from the MGH and LLUMC have demonstrated the benefit of PT in both Hodgkin's and non-Hodgkin's lymphoma and efforts to determine the clinical utility of PT in Hodgkin's lymphoma are underway at the University of Florida Proton Therapy Institute [53, 54].

2.2 Carbon Ion Radiotherapy

The current place of carbon ions in the clinic comes from their relatively high LET and narrow penumbra compared with PT (cf. Chap. 4 for details). Clinical experience includes the treatment of skull-base chordomas and chondrosarcomas, uveal melanomas, head and neck cancers, NSCLC, HCC, prostate carcinomas, and renal-cell carcinomas (cf. Part IV "*Clinical Results and Indications*" of this book for details).

Suit and colleagues concluded that determining the clinical efficacy of PT versus carbon ion radiotherapy (CIRT) is not yet feasible [55]. The lack of head-to-head trials comparing the two and the typical use of hypofractionation schemes in CIRT complicates direct comparisons with conventionally fractionated PT. It is clear that defining the magnitude of any advantage of CIRT versus PT will take considerable time, resources, and collaboration.

2.3 Conclusion

Proton beam therapy has evolved since its first use in 1954 at the Lawrence Berkeley Laboratory. From its earliest use in ablation of the pituitary gland to its investigational use in the lung or breast, PT continues to be an invaluable addition to the armamentarium in the treatment of both benign and malignant diseases.

Advancements in treatment delivery such as intensity-modulated radiotherapy with scanning beams and image-guided radiotherapy will continue to improve the delivered dose distribution with wider applicability to more clinical sites. Ion beam therapy (IBT) is likely to further evolve in the clinic, not the least due to its inherent physical advantages. Integration with novel surgical approaches and individually

tailored systemic therapies will provide further opportunities for increasing the therapeutic ratio as part of a multimodality approach to cancer management. It will be important to define the magnitude of any advantage of IBT versus other treatment techniques and also of therapeutic protons versus other ions. This, however, will take considerable time, resources, and international collaboration.

References

1. R.N. Kjellberg, A. Shintani, A.G. Frantz, B. Kliman, Proton-beam therapy in acromegaly. New Engl. J. Med. **278**, 689–695 (1968)
2. R.N. Kjellberg, T. Hanamura, K.R. Davis, et al., Bragg-peak proton-beam therapy for arteriovenous malformations of the brain. New Engl. J. Med. **309**, 269–274 (1983)
3. M.K. Aghi, J. Petit, P. Chapman, et al., Management of recurrent and refractory Cushing's disease with reoperation and/or proton beam radiosurgery. Clin. Neurosurg. **55**, 141–144 (2008)
4. J.H. Petit, B.M. Biller, J.J. Coen, et al., Proton stereotactic radiosurgery in management of persistent acromegaly. Endocr. Pract. **13**, 726–734 (2007)
5. J.H. Petit, B.M. Biller, T.I. Yock, et al., Proton stereotactic radiotherapy for persistent adrenocorticotropin-producing adenomas. J. Clin. Endocrinol. Metab. **93**, 393–399 (2008)
6. R.N. Kjellberg, T. Hanamura, K.R. Davis, et al., Bragg-peak proton-beam therapy for arteriovenous malformations of the brain. New Engl. J. Med. **309**, 269–274 (1983)
7. F.J. Vernimmen, J.P. Slabbert, J.A. Wilson, et al., Stereotactic proton beam therapy for intracranial arteriovenous malformations. Int. J. Radiat. Oncol. Biol. Phys. **62**, 44–52 (2005)
8. H. Silander, L. Pellettieri, P. Enblad, et al., Fractionated, stereotactic proton beam treatment of cerebral arteriovenous malformations. Acta Neurol. Scand. **109**, 85–90 (2004)
9. D.C. Weber, A.W. Chan, M.R. Bussiere, et al., Proton beam radiosurgery for vestibular schwannoma, tumor control and cranial nerve toxicity. Neurosurgery **53**, 577–586 (2003)
10. B.G. Baumert, A.J. Lomax, V. Miltchev, J.B. Davis, A comparison of dose distributions of proton and photon beams in stereotactic conformal radiotherapy of brain lesions. Int. J. Radiat. Oncol. Biol. Phys. **49**, 1439–1449 (2001)
11. A. Bolsi, A. Fogliata, L. Cozzi, Radiotherapy of small intracranial tumours with different advanced techniques using photon and proton beams, a treatment planning study. Radiother. Oncol. **68**, 1–14 (2003)
12. L.J. Verhey, V. Smith, C.F. Serago, Comparison of radiosurgery treatment modalities based on physical dose distributions. Int. J. Radiat. Oncol. Biol. Phys. **40**, 497–505 (1998)
13. M.R. Raju, Particle radiotherapy, historical developments and current status. Radiat. Res. **145**, 391–407 (1996)
14. E.S. Gragoudas, M. Goitein, L. Verhey, et al., Proton beam irradiation. An alternative to enucleation for intraocular melanomas. Ophthalmology **87**, 571–581 (1980)
15. E. Gragoudas, W. Li, M. Goitein, et al., Evidence-based estimates of outcome in patients irradiated for intraocular melanoma. Arch. Ophthalmol. **120**, 1665–1671 (2002)
16. E. Egger, L. Zografos, A. Schalenbourg, et al., Eye retention after proton beam radiotherapy for uveal melanoma. Int. J. Radiat. Oncol. Biol. Phys. **15**, 867–880 (2003)
17. H.D. Suit, M. Goitein, J.E. Tepper, et al., Clinical experience and expectation with protons and heavy ions. Int. J. Radiat. Oncol. Biol. Phys. **3**, 115–125 (1977)
18. H. Suit, M. Goitein, J. Munzenrider, et al., Evaluation of the clinical applicability of proton beams in definitive fractionated radiation therapy. Int. J. Radiat. Oncol. Biol. Phys. **8**, 2199–2205 (1982)
19. N.L. Higinbotham, R.F. Phillips, H.W. Farr, H.O. Hustu, Chordoma. Thirty-five-year study at Memorial Hospital. Cancer **20**, 1841–1850 (1967)

20. J.E. Munzenrider, N.J. Liebsch, Proton therapy for tumors of the skull base. Strahlenther Onkol. **175**, S57–S63 (1999)
21. J.E. Munzenrider, B.Y. Yeap, T.F. DeLaney, et al., Long-term results of a dose searching trial in chordomas and chondrosarcomas of the skull base and cervical spine. Int. J. Radiat. Oncol. Biol. Phys. **72**, S104–S105 (2008)
22. J.R. Duttenhaver, W.U. Shipley, T. Perrone, et al., Protons or megavoltage X-rays as boost therapy for patients irradiated for localized prostatic carcinoma. An early phase I/II comparison. Cancer **51**, 1599–1604 (1983)
23. W.U. Shipley, J.E. Tepper, G.R. Prout Jr., et al., Proton radiation as boost therapy for localized prostatic carcinoma. J. Am. Med. Assoc. **241**, 1912–1915 (1979)
24. J.A. Talcott, C. Rossi, W.U. Shipley, et al., Patient-reported long-term outcomes after conventional and high-dose combined proton and photon radiation for early prostate cancer. J. Am. Med. Assoc. **303**, 1046–1053 (2010)
25. T.F. DeLaney, N.J. Liebsch, F.X. Pedlow, et al., Phase II study of high-dose photon/proton radiotherapy in the management of spine sarcomas. Int. J. Radiat. Oncol. Biol. Phys. **74**, 732–739 (2009)
26. M. Cianchetti, J.A. Adams, P. Pommier, et al., Long-term outcome of proton beam therapy for advanced sinonasal malignancies. Presented at PTCOG 48, Heidelberg, Germany, Sep 28–Oct 3, 2009
27. A.W. Chan, N.J. Liebsch, Proton radiation therapy for head and neck cancer. J. Surg. Oncol. **97**, 697–700, (2008).
28. D.C. Weber, A.W. Chan, S. Lessell, et al., Visual outcome of accelerated fractionated radiation for advanced sinonasal malignancies employing photons/protons. Radiother. Oncol. **81**, 243–249 (2006)
29. A.W. Chan, N.J. Liebsch, D.G. Deschler, et al., Proton radiotherapy for T4 nasopharyngeal carcinoma. ASCO Annual Meeting Proceedings J. Clin. Oncol. **22**(Suppl 14), abs 5574 (2004)
30. J.D. Slater, L.T. Yonemoto, D.W. Mantik, et al., Proton radiation for treatment of cancer of the oropharynx, early experience at Loma Linda University Medical Center using a concomitant boost technique. Int. J. Radiat. Oncol. Biol. Phys. **62**, 494–500 (2005)
31. W.T. Ng, M.C. Lee, W.M. Hung, et al., Clinical outcomes and patterns of failure after intensity-modulated radiotherapy for nasopharyngeal carcinoma. Int. J. Radiat. Oncol. Biol. Phys. **79**, 420–428 (2010)
32. U. Mock, D. Georg, J. Bogner, et al., Treatment planning comparison of conventional, 3D conformal, and intensity-modulated photon (IMRT) and proton therapy for paranasal sinus carcinoma. Int. J. Radiat. Oncol. Biol. Phys. **58**, 147–154 (2004)
33. M. Steneker, A. Lomax, U. Schneider, Intensity modulated photon and proton therapy for the treatment of head and neck tumors. Radiother. Oncol. **80**, 263–267 (2006)
34. A.M. Linabery, J.A. Ross, Childhood and adolescent cancer survival in the US by race and ethnicity for the diagnostic period 1975–1999. Cancer **113**, 2575–2596 (2008)
35. W.H. St Clair, J.A. Adams, M. Bues, et al., Advantage of protons compared to conventional X-ray or IMRT in the treatment of a pediatric patient with medulloblastoma. Int. J. Radiat. Oncol. Biol. Phys. **58**, 727–734 (2004)
36. C.S. Chung, N. Keating, T. Yock, T. Tarbell, Comparative analysis of second malignancy risk in patients treated with proton therapy versus conventional photon therapy. Proc. Am. Soc. Ther. Radiol. Oncol. Int. J. Radiat. Oncol. Biol. Phys. **72**, S8 (2008)
37. E. Hoppe-Hirsch, L. Brunet, F. Laroussinie, et al., Intellectual outcome in children with malignant tumors of the posterior fossa, influence of the field of irradiation and quality of surgery. Childs Nerv. Syst. **11**, 340–345 (1995)
38. T.E. Merchant, C.H. Hua, H. Shukla, et al., Proton versus photon radiotherapy for common pediatric brain tumors, comparison of models of dose characteristics and their relationship to cognitive function. Pediatr. Blood Cancer **51**, 110–117 (2008)
39. J.Y. Chang, R. Komaki, M.K. Bucci, et al., Failure patterns and toxicity of concurrent proton therapy and chemotherapy for stage III non–small cell lung cancer. Int. J. Radiat. Oncol. Biol. Phys. **75**, S446–S447 (2009)

40. F.R. Spitz, J.L. Abbruzzese, J.E. Lee, et al., Preoperative and postoperative chemoradiation strategies in patients treated with pancreaticoduodenectomy for adenocarcinoma of the pancreas. J. Clin. Oncol. **15**, 928–937 (1997)
41. M. Kawashima, J. Furuse, T. Nishio, et al., Phase II study of radiotherapy employing proton beam for hepatocellular carcinoma. J. Clin. Oncol. **23**, 1839–1846 (2005)
42. D.A. Bush, D.J. Hillebrand, J.M. Slater, J.D. Slater, High-dose proton beam radiotherapy of hepatocellular carcinoma: preliminary results of a phase II trial. Gastroenterology **127**, S189–S193 (2004)
43. E.M. Crowley, L.A. Kachnic, H.J. Mamon, et al., Optimizing the cardiac and pulmonary dose: a comparison of IMRT photon and 3-D proton treatment planning for distal esophageal cancer. Int. J. Radiat. Oncol. Biol. Phys. **72**, S539–S540 (2008)
44. U. Isacsson, B. Lennernäs, E. Grusell, et al., Comparative treatment planning between proton and x-ray therapy in esophageal cancer. Int. J. Radiat. Oncol. Biol. Phys. **41**, 441–450 (1998)
45. X. Zhang, K.L. Zhao, T.M. Guerrero, et al., Four-dimensional computed tomography-based treatment planning for intensity-modulated radiation therapy and proton therapy for distal esophageal cancer. Int. J. Radiat. Oncol. Biol. Phys. **72**, 278–287 (2008)
46. S. Sugahara, K. Tokuuye, T. Okumura, et al., Clinical results of proton beam therapy for cancer of the esophagus. Int. J. Radiat. Oncol. Biol. Phys. **61**, 76–84 (2005)
47. G. Xiaomao, Z.X. Liao, R. Komaki, et al., Concurrent chemotherapy and proton beam therapy for esophageal cancer. Int. J. Radiat. Oncol. Biol. Phys. **75**, S289–S290 (2009)
48. C. Ares, S. Khan, A.M. Macartain, et al., Postoperative proton radiotherapy for localized and locoregional breast cancer: potential for clinically relevant improvements? Int. J. Radiat. Oncol. Biol. Phys. **76**, 685–697 (2010)
49. D.A. Bush, J.D. Slater, C. Garberoglio, et al., A technique of partial breast irradiation utilizing proton beam radiotherapy: comparison with conformal x-ray therapy. Cancer J. **13**, 114–118 (2007)
50. K.R. Kozak, B.L. Smith, J. Adams, et al., Accelerated partial-breast irradiation using proton beams: initial clinical experience. Int. J. Radiat. Oncol. Biol. Phys. **66**, 691–698 (2006)
51. H. Lu, S.M. MacDonald, P. Paetzold, et al., The potential for proton beam radiation for post mastectomy radiation in patients with unfavorable cardiac anatomy. Int. J. Radiat. Oncol. Biol. Phys. **69**, S219–S220 (2007)
52. B.S. Chera, C. Rodriguez, C.G. Morris, et al., Dosimetric comparison of three different involved nodal irradiation techniques for stage II Hodgkin's lymphoma patients: conventional radiotherapy, intensity-modulated radiotherapy, and three-dimensional proton radiotherapy. Int. J. Radiat. Oncol. Biol. Phys. **75**, 1173–1180 (2009)
53. D.G. Kirsch, D.H. Ebb, A.H. Hernandez, N.J. Tarbell, Proton radiotherapy for Hodgkin's disease in the sacrum. Lancet Oncol. **6**, 532–533 (2005)
54. B. Ronson, C. Rossi, S. Johnson, et al., Locoregional proton radiotherapy of a primary cavernous sinus non-Hodgkin's lymphoma, case report. Technol. Cancer Res. Treat. **5**, 281–284 (2006)
55. H. Suit, T. DeLaney, S. Goldberg, et al., Proton vs carbon ion beams in the definitive radiation treatment of cancer patients. Radiother. Oncol. **95**, 3–22 (2010)

Chapter 3
Socio-Economic Aspects of Ion Beam Therapy

Andre Konski

Abstract Ion beam therapy (IBT) has the promise to improve outcome in cancer patients. IBT facilities are more expensive to build and maintain as compared to conventional radiotherapy facilities. There have been relatively few economic analyses comparing IBT to conventional radiotherapy. Some have argued for randomized clinical trial data prior to adopting IBT as standard of care because of the greater incremental cost without similar improvement in outcome.

3.1 Introduction

Interest in IBT has increased recently because of the beam characteristics and increased radiobiology effectiveness (at least of carbon ion radiotherapy). Currently at least 33 institutions worldwide provide IBT; the majority being proton therapy (PT) centers, with carbon ion radiotherapy (CIRT) centers the next most common type of IBT facilities. Table 3.1 lists the number of operational and proposed facilities by country. Interestingly, the high number of proposed facilities in the United States may be related to the higher reimbursement for PT as compared to photon radiotherapy. Prior to 2004, there were only three PT facilities in the US, but since then five new PT facilities have started to treat patients with more on the drawing board bringing the total to eight IBT facilities in the US. Germany has the most carbon ion radiotherapy facilities.

Unfortunately, socioeconomic issues have brought considerable attention to IBT in the US because of the higher incremental cost associated with IBT as compared to photon beam therapy. Health care expenditures continue to grow; accounting

A. Konski (✉)
Department of Radiation Oncology, Wayne State University School of Medicine, Barbara Ann Karmanos Cancer Center, Detroit, MI 48201, USA
e-mail: akonski@med.wayne.edu

U. Linz (ed.), *Ion Beam Therapy*, Biological and Medical Physics, Biomedical Engineering, DOI 10.1007/978-3-642-21414-1_3,

Table 3.1 Particle therapy facilities

Europe	12
Asia	9
United States	8
Africa	1
Canada	1
Proposed sites	
United States	21
Europe	14
Asia	3
Middle East	1

Modified from the Particle Therapy Cooperative Group (PTCOG) website http://ptcog.web.psi.ch/ptcenters.html

for an ever greater amount of the gross domestic product (GDP) and diverting resources companies and countries could be using for research and development of new products or providing basic healthcare needs to the underserved.

In the US, radiotherapy has come under greater scrutiny, recently, because of the rapid rise in amount of expenditures associated with it. The US dollar (USD) amount for the technical aspect of intensity modulated radiotherapy (IMRT) paid by Medicare, the US federal government payment system for people over the age of 65, is 17th on the list of top 50 claims by dollar amount paid, even though radiation oncologists account for only 0.3% of all practitioners submitting claims for services to Medicare. The total USD expenditures by Medicare Part B for radiotherapy services in 2008, the last year for which data are available, was approximately $1.9 billion USD from 9.8 million allowed services in comparison to approximately $2.4 billion USD from 75 million allowed services for medical oncology (http://www.cms.gov/MedicareFeeforSvcPartsAB/Downloads/BETOS08.pdf).

The current economic climate in the US has highlighted the need to change how health care is reimbursed and forced purchasers of health care to demand value. Value is best defined as outcome divided by cost; e.g., something is of better value if it gives you greater or improved outcome at the same cost, or the same outcome at lower cost. Value can be thought of as the inverse of a cost-effectiveness ratio, where one evaluates cost divided by outcome. In such analyses of the American healthcare system, the US scores very low compared with other countries in the quality of healthcare provided divided by our costs of delivering that healthcare. Other industrialized countries achieve much greater value for their healthcare dollar.

Table 3.2 shows the amount of healthcare spending per person per US dollar with the average life expectancy being the proxy for healthcare quality. Value is measured in average life expectancy/health care spending per person. Sweden and Japan do considerably better than the United States. However, the US policy-making Federal agencies are now beginning to evaluate the efficiency of American healthcare expenses, and the value of the healthcare provided. In value-based purchasing, buyers hold providers of healthcare accountable for both cost and quality of care. Decision-making combines information on quality of healthcare, including patient

Table 3.2 Value for health care spending by selected OECD countries

Country	Annual healthcare spending per person (US$)	Average life expectancy (Years)	Value (Measured in life expectancy/dollar spent)
United States	7290	77.9	0.011
Switzerland	4417	81.9	0.019
Austria	3763	80.2	0.021
Canada (2006)	3696	80.7	0.022
Germany	3588	80.0	0.022
France	3601	80.9	0.022
Sweden	3323	81.0	0.024
Japan (2006)	2581	82.4	0.032
Hungary	1388	73.3	0.053

Adapted from Organization for Economic Co-operation and Development (OECD)
Data from 2009 except for Canada and Japan

outcomes and health status, with data on the expenditures going towards health. "It focuses on managing the use of the healthcare system to reduce inappropriate care, and to identify and reward the best-performing providers." This strategy can be contrasted with more limited efforts to simply negotiate price discounts, which reduce costs but do little to ensure that quality of care is improved [1]. Unfortunately, the moral hazard in the American society is that the end-consumers of healthcare are not the actual buyers of the healthcare. Most of the buyers are government, Medicaid and Medicare, or employers for work-based healthcare. In some cases, buyers may be influenced by total costs to the plan, regardless of outcome, simply to lower costs to the plan. The purchasers of healthcare should combine information on the quality of healthcare and patient outcomes, and these outcomes are the critical factors in the cost analyses that must be objectively measured. Differences in the moral hazard may be experienced by patients in countries where the allocation of healthcare resources are more tightly controlled by a central government agency.

This chapter will try to highlight some of the issues surrounding the controversy within the United States and how this may impact the future development of IBT centers.

3.2 Facility Development Cost

The development of a PT facility is estimated to be between $20 and $100 million USD as compared to the cost of standard linear accelerators usually costing approximately $3–4 million USD. The risks and higher costs, as compared to photon therapy, taken by the Loma Linda University Medical Center (LLUMC), to build their facility were documented in a number of publications [2, 3]. The cost and benefits of the early centers, Loma Linda and the Harvard facility in the US, were also discussed as early as 1989 [4]. Factors influencing the cost of hospital based PT centers include equipment costs and operating costs as well as the importance of

patient throughput [5]. Patient throughput is an important part of the development process of an IBT facility. The data concerning the number of patients and the types of cancers to be treated are an important input into a decision to construct an IBT facility [6–8].

The current facilities consist of one cyclotron and a beam line leading to multiple treatment rooms. The exact cost for each facility will depend upon the number and configuration of the treatment rooms with higher cost for facilities with gantry-mounted treatment nozzles and lower cost for facilities with fixed beam lines.

Still River Systems (Littleton, MA) is in the process of developing a gantry mounted cyclotron in a single room and will be installing the first machine at the Mallinckrodt Institute of Radiology at Washington University School of Medicine in St. Louis in the near future (cf. Chap. 39 for details). The cost of this facility is considerably less as compared to other facilities, since it is a single room treatment facility.

Higher operating costs are also incurred by IBT facilities as compared to standard cancer treatment facilities because of the complexity of the accelerator. Additional personnel, up to 120 full-time employees depending upon the facility, are required for maintenance and patient handling depending upon the system. In addition, the cost for electricity for the facility to power the accelerators can range from US $50,000 to $200,000 per year with yearly facility maintenance cost ranging between US $1.7 and $5 million depending upon the different types of units.

The costs of the facilities mentioned previously are for PT facilities which make up the majority of IBT facilities worldwide. Currently, there are only four carbon-ion facilities operational worldwide, three in Japan (Chiba, Hyogo, and Gunma) and one in Germany. The current construction cost in the United States of a carbon-ion facility has been estimated between US $300 and $350 million with operating costs estimated at US $13–15 million. For the "ETOILE" (Espace de Traitement Oncologique par Ions Légers dans le cadre Européen) project, a light ion therapy center with a gantry, the capital cost is estimated at approx. €88 million. Another €15 million are projected for the operational costs [6]. A variety of ions will be used to treat patients at this facility. There are no carbon-ion facilities under construction within the US with only a few companies with the technical expertise capable of designing and building these facilities. IBA Particle Therapy, Inc (Belgium) is in the process of developing a prototype carbon-ion facility in Caen, France (cf. Chap. 22). An estimation and comparison of the cost of a combined carbon-proton, proton-only and photon facility was recently published by Peeters et al [9]. Capital cost were highest for the combined facility €138.6 million, followed by the proton-only facility, €94.9 million, and the photon-only facility, €23.4 million. Similarly, yearly operational costs for the combined, proton-only and photon-only centers were €36.7 million, €24.9 million, and €9.6 million, respectively. Per fraction cost differences were noted depending upon the anatomic site of treatment. Clinical trials will be needed to determine if the incremental benefit of IBT, either carbon ions or protons, will be worth the investment (cf. Parts IV and IX of this book).

Recently, an interesting analysis was performed by Johnstone and colleagues from the Midwestern Proton Radiotherapy Institute (MPRI) in the United States attempting to quantify the number of patients necessary to cover the fixed costs of a proton radiotherapy center (Johnstone et al., Proton facility economics: the central role of prostrate cancer, personal communication). Public documents were obtained to provide the financial information. To inform their model they assumed 15-year financing at 5% interest, the analysis unit was per room with 14 h of operation a day, the capacity assumptions were based upon the MPRI experience with pediatric cases requiring 1 h per case, simple head and neck and pelvic treatment requiring 30 min room time per treatment, and prostate cancer patients requiring 24 min room time per treatment. Since treatment is 78% of MPRI revenue, they assumed only treatment charges. Pediatric cases were a mix of Medicaid and private payer and Medicare reimbursement was assumed at Indiana rates as MPRI is located in Indiana. They assumed a one room facility costing US $25 million and a four room facility at US $150 million.

A single gantry treating only complex or pediatric patients would have to apply 85% of its treatment slots simply to service debt but the same room could cover debt treating 4 h of prostate cancer patients. On the other hand, a 3-gantry facility treating only complex and pediatric cases would not have enough treatment slots to recoup construction and debt service. A 3-gantry facility could fill one entire room with treating only prostate cancer patients and still fall short of covering debt. A 4-gantry center treating only complex and pediatric cases alone would not have sufficient treatment slots to cover even 60% of its debt service. This analysis underlies the dependence on the treatment of patients with prostate cancer to service the debt of the facility potentially limiting treatment slots for more complex patients such as pediatric patients that would potentially benefit the most from PT.

3.3 Cost-Effectiveness of IBT

A brief review of cost-effectiveness analyses would be in order prior to presenting the data concerning cost-effectiveness of IBT. All cost-effectiveness analyses are an incremental analysis in which the new intervention is compared to a standard or base-case intervention. Costs are located in the numerator and effects are located in the denominator. The cost of the old or standard intervention is then subtracted from the cost of the new intervention giving an incremental cost. The effect of the standard or comparator intervention would likewise be subtracted from the new intervention resulting in an incremental effect. The incremental cost is divided by the incremental effect giving cost/effect or the cost-effectiveness ratio. Figure 3.1 depicts the incremental cost-effectiveness ratio equation.

There are several cost-effectiveness methodologies currently used in health economics. A *cost-minimization analysis* assumes no difference in outcome between

$$\text{ICER} = \frac{\text{Cost of Exp Tx - Cost of Standard Tx}}{\text{Outcome of Exp Tx - Outcome of Standard Tx}}$$

Fig. 3.1 Definition of incremental cost-effectiveness ratio (ICER). *Exp* Experimental; *Tx* Treatment

interventions and the lowest cost item is selected. The *cost–benefit analysis* applies a dollar value to a specific outcome, such as a life-year or number of new cancers detected. This methodology has some associated problems as it is very difficult to assign a dollar value to a year of life or new cancer case detected or prevented. The *cost-effectiveness* analysis is the most widely used methodology. The incremental cost is divided by a unit of outcome of the intervention. The unit of outcome could be a year of life saved or number of cancers prevented. The resultant ratio is cost/life-year or cost/new cancer cases diagnosed. The *cost–utility* analysis results in a dollar value per adjusted life-year gained or lost based on utility or patient preference for a health state, varying from 1.0 for perfect health down to 0 for death. For example, if a person lives a year in a health state which they value as 0.5, the resultant quality-adjustment would be calculated as 1 year $\times$ 0.5 $=$ 0.5 quality-adjusted life year or QALY.

One of the issues confronting researchers performing economic analyses of new technologies is which costs to measure. Costs can be measured from a societal viewpoint including such items as direct medical care, and indirect costs such as lost wages and time away from work, or from the viewpoint of a payer, such as an insurance company or government agency where only costs paid to facilities and physicians are included. The European Society for Therapeutic Radiology and Oncology (ESTRO) established the European Network for Research in Light Ion Therapy (ENLIGHT) to coordinate the European projects focused on carbon ion therapy. A work group was formed to evaluate the health economics aspects (WP6) and to provide reliable estimates of the cost per treated patient when the IBT facility is utilized in the most effective way to cure as many patients as possible [10]. The work group decided to adopt the hospital point of view for the cost assessment and excluded indirect costs and patient transportation, and lodging costs were also excluded. The group decided not to collect follow-up costs including cost of treating recurrences and complications which could be a potential problem for using this method. The true cost of treatment could be underestimated using this method if patients are treated and experience a high rate of failures or toxicity requiring additional treatment.

There have been few economic analyses of IBT as compared to economic analyses of other health care technologies. In a recent review of the literature, Pijls-Johannesma and colleagues identified only five economic analyses of IBT [11]. Four of the analyses used a Markov model while the lone economic analysis of carbon ion therapy used a retrospective analysis of ten patients.

A Markov model is a mathematical modeling technique derived from matrix algebra. It is constructed to enumerate a finite set of mutually exclusive possible

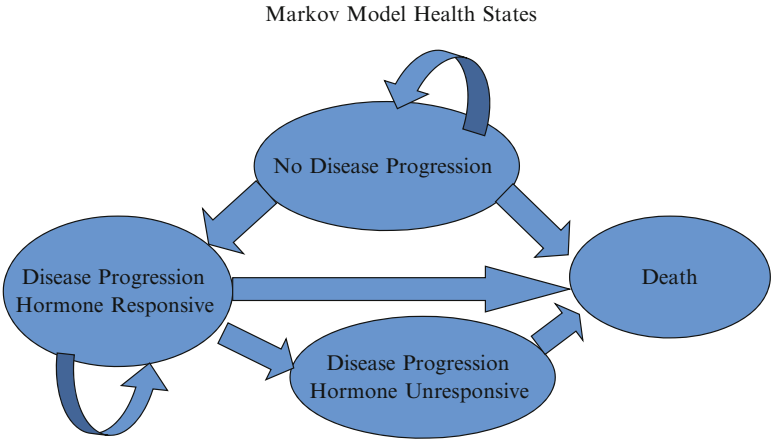

Fig. 3.2 Allowed health states commonly used for a Markov model of prostate cancer treatment

health states. Figure 3.2 illustrates health states and allowed health state transitions commonly used for the evaluation of prostate cancer. The transitions between these health states are allowed and efficiently represent recursive events that occur over time; the time at which these events occur is uncertain. Figure 3.3 depicts a typical Markov model comparing two treatment options for prostate cancer. In addition, many economic analyses utilizing a Markov model will also use a Monte Carlo simulation of the model. In the Monte Carlo simulation, patients traverse the Markov model process one by one with the patient beginning in an initial state and change states as directed by transition probabilities. Another simulation begins upon completion of the simulation with another patient traversing the model. Time spent in each health state combined with each state's utility produces a quality adjusted survival time for each patient. Lundkvist et al. compared PT to conventional photon RT in the treatment of a 55-year-old woman with left-sided breast cancer using a lifetime timeframe [12]. Markov health states included normal death, tumor-related death within the first 10 years, fatal cardiac disease, nonfatal cardiac disease, and pulmonary disease within the first year. The outcome was measured in QALY's and a societal viewpoint was used to estimate costs. The incremental cost-utility ratio (ICUR) was calculated to be €67,000/QALY. A similar analysis, published by the same group in 2005, reported an ICUR of €66,608/QALY with the minor differences being a result of slightly different health states used to inform the models [13].

PT was found to dominate conventional radiotherapy in the treatment of childhood medulloblastoma [13, 14]. Markov health states included hearing loss, IQ loss, hypothyroidism, growth hormone deficiency, osteoporosis, cardiac disease, secondary malignancies, and death (normal death, death due to recurrence, death due to cardiac reasons, death due to subsequent tumor and other death). PT dominated conventional radiotherapy because cost-savings of €23,647 were realized in patients treated with PT. The differences in costs were mostly savings realized in

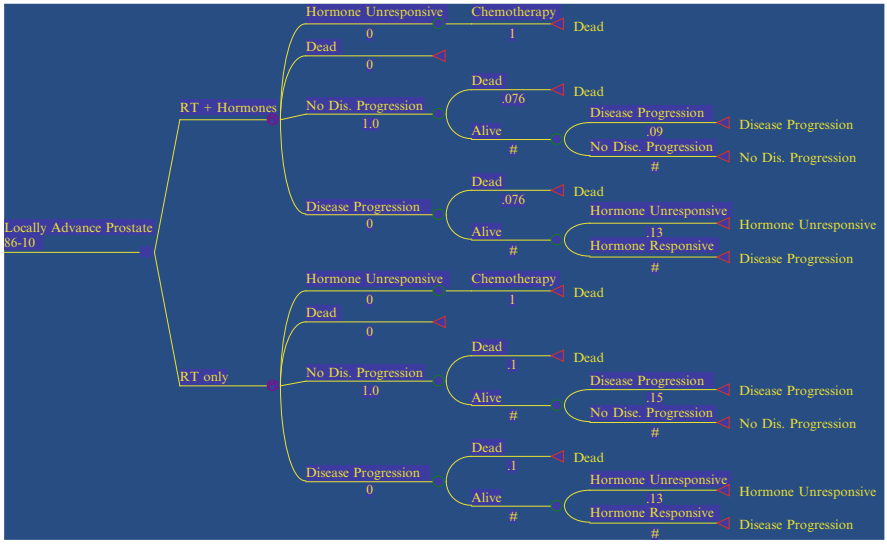

Fig. 3.3 Markov model of prostate cancer therapy

patients treated with PT not having the increased cost of treating the late effects experienced by patients treated with conventional radiotherapy in addition to having a better outcome and not having the increased cost of needing salvage therapy.

PT was also found to be superior to conventional radiotherapy in the treatment of a 65 year old with an unspecified head and neck cancer [13]. The authors assumed a 24% risk reduction in mortality and a reduction in the adverse side effects of radiation with the use of PT. The authors reported an increased total cost of approx. €3,900 per patient with a 1.02 QALY improvement in patients undergoing PT, resulting in an ICUR of €3,811/QALY.

The cost-effectiveness of PT as compared to conventional radiotherapy in the treatment of patients with prostate cancer was evaluated in two studies [13, 15]. Lundkvist and colleagues evaluated PT as compared to conventional RT in a 65-year-old patient with prostate cancer. The authors assumed a 20% reduction in prostate cancer recurrence and a relative risk of adverse events of 0.6 with the use of PT [9]. The increased total cost from the use of PT instead of conventional radiotherapy was approx. €8,000 with an increase of 0.3 QALY's, which results in an ICUR ratio of €26,800/QALY. Konski et al. used a Markov model with a 15-year Markov termination condition. Figure 3.2 shows the allowable transition states for their model.

A Markov termination condition is how long the computer model runs. It is analogous to performing an analysis of a clinical trial at a certain time point. In this case, a 15-year Markov termination condition means the authors examined the outcome and costs after the patients went through the model a maximum of 15 times, since the model was constructed with a 1-year time period for patients to

go through the model. This study was the only study to use a probabilistic analysis to estimate the parameters used to inform the model. In addition, the authors assumed only a 10% improvement in freedom from biochemical recurrence with the use of PT, which was the result of giving a higher radiation dose with PT. The incremental cost–utility ratio for a 70-year-old patient with a Markov termination condition at 15 years was approx. $63,600/QALY. The incremental cost–utility ratio improved the longer the time horizon and the younger the patient. The incremental cost–utility ratio was approx. $55,700/QALY for a 60-year-old patient at 15 years. The differences between the two studies may be a result of the former study doubling the estimate of benefit from PT.

The lone cost-effectiveness analysis for carbon ion radiotherapy (CIRT) was published from the group in Heidelberg, Germany. Costs of conventional radiotherapy treatment were estimated according to the common scale of charges and fees defined within the German health care system [16]. The maximum fee for a full course of conventional radiotherapy was €3,500. CIRT in Germany is currently reimbursed for a few indications after patients obtain consent from their health insurance company. The reimbursement for a full course of CIRT for base of skull tumors, 20 fractions, is €20,000. The reimbursement for carbon ion radiotherapy at the new treatment facility in Heidelberg was agreed to be €19,500. The cost-effectiveness of CIRT was calculated using various scenarios for local control and reimbursements. The authors report the overall treatment costs for CIRT as lower than conventional radiotherapy if the local control rates for CIRT exceeded 70.3%. The cost-effectiveness ratio was €2,539 per 1% increase in survival or €7,692 per additional life year [16].

3.4 Clinical Trials Prior to Adopting IBT

PT is undergoing greater scrutiny as the price differential between PT and IMRT widens without data documenting a similar improvement in efficacy [17]. The increased capital and operating costs to hospitals and universities and the higher reimbursement paid by health insurance companies for IBT has increased the debate on whether clinical trials should be necessary prior to adopting IBT as standard of care [18–21]. Some have argued the higher cost of PT is the only reason why comparison of the two modalities in a clinical trial is even being considered [21]. Others have postulated from a global health care perspective, the cost of PT is not "outrageous at all and should be no justification for denying potentially curative and less toxic treatments to our patients" [22]. It may be unethical to subject certain clinical conditions, such as the treatment of pediatric cancers, to clinical trial assessment. Justification for the high cost of PT as compared to conventional radiotherapy, the 2010 US Medicare Final Ambulatory Payment Classification (APC) is $1,233/treatment for PT compared to $421/treatment for IMRT, may be required given the current worldwide economic conditions. Pharmaceutical companies are required to show efficacy prior to marketing a new drug but

radiotherapy equipment manufacturers only need to demonstrate safety prior to marketing new radiotherapy machines.

IBT has the promise to improve the outcomes of patients treated with radiotherapy both in terms of improved tumor control and survival but also a reduction in late effects in pediatric patients. The current economic conditions, especially in the US, have led to the increased scrutiny of IBT centers with their higher capital and operational costs. Unfortunately, there have been few economic analyses evaluating the cost-effectiveness of IBT compared to conventional radiotherapy.

References

1. J. Meyer, L. Rybowski, R. Eichler, Theory and Reality of Value-Based Purchasing: Lessons form the Pioneers, in *AHCPR Report*, ed. by I. Fraser. (AHCPR pub. No. 98-0004, Rockville, MD, 1997)
2. L. Souhrada, Proton beam accelerator: investing in unconventional medicine. Hospitals **64**, 28–29 (1990)
3. G. Stix, Beam of Hope. A proton accelerator is the most costly medicine yet. Sci. Am. **263**, 24–25 (1990)
4. F. Antoine, Proton beam therapy – cost vs. benefit. J. Natl. Cancer Inst. **81**, 559–562 (1989)
5. P. Cohilis, Y. Jongen, Some factors influencing the cost of a hospital based proton therapy centre. Strahlenther Onkol. **175**(suppl 2), 102–104 (1999)
6. M. Bajard, J.M. DeConto, J. Remillieux, Status of the "ETOILE" project for a French hadrontherapy centre. Radiother. Oncol. **73**, S211–S215 (2004)
7. R. Orecchia, P. Fossati, S. Rossi, The national center for oncological hadron therapy: status of the project and future clinical use of the facility. Tumori **95**, 169–176 (2009)
8. E. Griesmayer, T. Auberger, The status of MedAustron. Radiother. Oncol. **73**, S202–S206 (2004)
9. A. Peeters, J.P. Grutters, M. Pijls-Johannesma, et al., How costly is particle therapy? Cost analysis of external beam radiotherapy with carbon-ions, protons and photons. Radiother. Oncol. **95**, 45–53 (2010)
10. P. Pommier, I. Zucca, I. Naslund, et al., Light ion facility projects in Europe: methodological aspects for the calculation of the treatment cost per protocol. Radiother. Oncol. **73**, S183–S185 (2004)
11. M. Pijls-Johannesma, P. Pommier, Y. Lievens, Cost-effectiveness of particle therapy: Current evidence and future needs. Radiother. Oncol. **89**, 127–134 (2008)
12. J. Lundkvist, M. Ekman, S.R. Ericsson, et al., Economic evaluation of proton radiation therapy in the treatment of breast cancer. Radiother. Oncol. **75**, 179–185 (2005)
13. J. Lundkvist, M. Ekman, S.R. Ericsson, et al., Proton therapy of cancer: potential clinical advantages and cost-effectiveness. Acta Oncol. **44**, 850–861 (2005)
14. J. Lundkvist, M. Ekman, S.R. Ericsson, et al., Cost-effectiveness of proton radiation in the treatment of childhood medulloblastoma. Cancer **103**, 793–801 (2005)
15. A. Konski, W. Speier, A. Hanlon, et al., Is proton beam therapy cost effective in the treatment of adenocarcinoma of the prostate? J. Clin. Oncol. **25**, 3603–3608 (2007)
16. O. Jäkel, B. Land, S.E. Combs, et al., On the cost-effectiveness of carbon ion radiation therapy for skull base chordoma. Radiother. Oncol. **83**, 133–138 (2007)
17. M. Goozner, The proton beam debate: are facilities outstripping the evidence? J. Natl. Cancer Inst. **102**, 450–453 (2010)
18. S.M. Bentzen, Randomized controlled trials in health technology assessment: overkill or overdue? Radiother. Oncol. **86**, 142–147 (2008)
19. B. Glimelius, A. Montelius, Proton beam therapy – do we need the randomised trials and can we do them? Radiother. Oncol. **83**, 105–109 (2007)

20. M. Goitein, J.D. Cox, Should randomized clinical trials be required for proton radiotherapy? J. Clin. Oncol. **26**, 175–176 (2008)
21. H. Suit, H. Kooy, A. Trofimov, et al., Should positive phase III clinical trial data be required before proton beam therapy is more widely adopted? No. Radiother. Oncol. **86**, 148–153 (2008)
22. Y. Lievens, W. Van den Bogaert, Proton beam therapy: too expensive to become true? Radiother. Oncol. **75**, 131–133 (2005)

Part II
Physical and Biological Aspects

Chapter 4
Physical and Biological Rationale for Using Ions in Therapy

Ute Linz

Abstract This chapter reviews the physical and radiobiological properties of accelerated ions which have motivated their clinical application. The effects that lead to the characteristic depth–dose distribution of ions with the Bragg peak are explained. Quantities such as the linear energy transfer (LET) and the relative biological effectiveness (RBE) are defined and their relationships for different types of radiation described.

4.1 Introduction

Since the beginning of clinical radiation therapy (RT), it has been the goal of radiation oncologists to restrict the irradiated volume to the site and shape of the target volume. Of all the different forms of external RT, ion beams are the tool to get closest to this objective.

The strongest argument to consider protons and other accelerated ions for RT is the fact that they are suited to irradiate a tumor at any depth of the body with a minimum dose to the surrounding healthy tissues (Fig. 4.1).

The penetration depth of ions can be tailored precisely to coincide with the location of the tumor to be treated. A finite path with maximum dose deposition close to the end (Bragg peak) is an advantage shared by all ions as compared to photon irradiation. The shallow entrance dose warrants that the radiation burden on the healthy tissue in front of a deep-seated tumor can be kept low. The finite path limits the range of the radiation field to the distal part of the tumor and spares structures beyond from radiation exposure.

U. Linz (✉)
Forschungszentrum Jülich, Leo-Brandt-Str. 1, 52425 Jülich, Germany
e-mail: u.linz@fz-juelich.de

U. Linz (ed.), *Ion Beam Therapy*, Biological and Medical Physics, Biomedical Engineering, DOI 10.1007/978-3-642-21414-1_4,

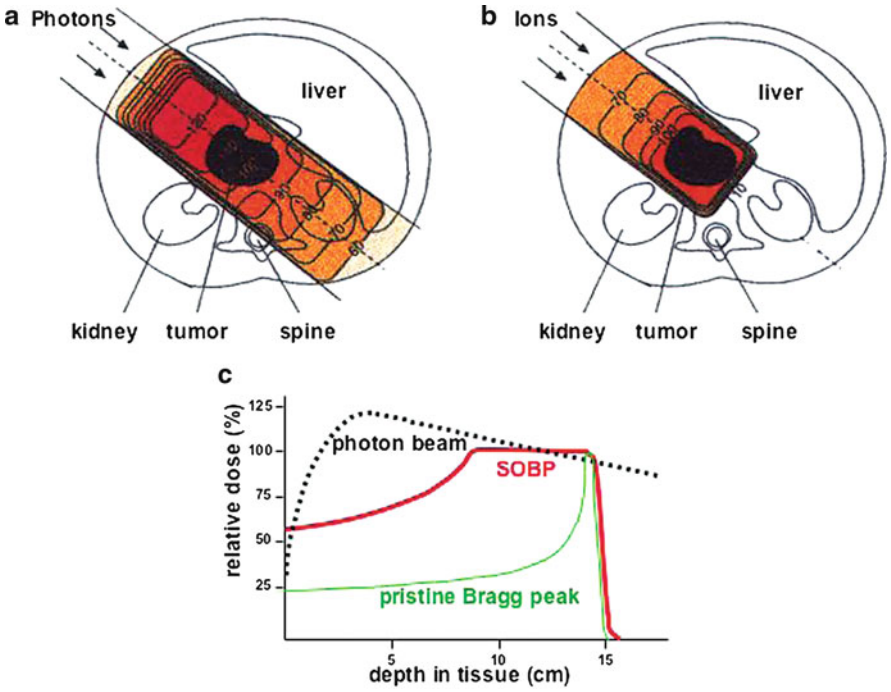

Fig. 4.1 Schematic view of depth-dose distributions of photons and ions. **(a)** megavoltage photon field, **(b)** spread-out ion beam, **(c)** depth–dose profiles of **a** and **b** along the central beam axis. The spread-out Bragg peak (SOBP) is the result of several stacked pristine Bragg curves

The physical rationale to use protons and heavier ions in RT was conceived already decades ago. In 1946, the Harvard physicist, Robert R. Wilson published his pioneering paper on the radiological use of fast protons to "acquaint medical and biological workers" with some of the physical properties and possibilities of ions [1]. Since then, many others have reviewed the properties of ions that give reason for their clinical application (e.g., [2–6], cf. also Chap. 1).

4.2 Physical Properties

4.2.1 Interaction of Photons and Ions with Matter

When photons of short wavelengths (X- or gamma rays) strike condensed matter, they release electrons from the atoms they interact with. The processes by which their energy is transferred to the medium are stochastic events, such as inelastic or Compton scattering, photoelectric processes and – at higher energies – pair production. Due to the statistical nature of the absorption process and the fact that

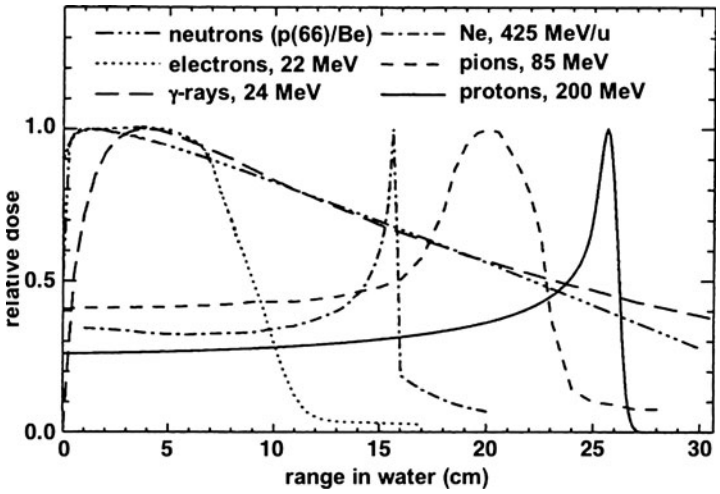

Fig. 4.2 Depth–dose distributions of various kinds of radiation in water

photons are strongly deflected (scattered) during their interactions with atoms, a photon beam entering condensed matter spreads rapidly and has no defined range. The respective absorption curve of a photon beam reveals an initial build-up domain, followed by a region of exponentially decreasing dose (Fig. 4.1c).

In contrast to the indirectly ionizing electromagnetic radiation, radiation consisting of charged particles (electrons, alpha particles, accelerated ions) is directly ionizing.

In classical mechanics, the transfer of kinetic energy is inversely proportional to the square of the velocity v ($\mathrm{d}E/\mathrm{d}x \sim 1/v^2$). Due to their low mass, accelerated electrons reach rapidly high velocities close to the speed of light (at energies > 1 MeV). As the electron velocity approaches the speed of light c, the energy loss per unit length becomes independent of the energy ($\mathrm{d}E/\mathrm{d}x \sim 1/c^2$). As a consequence, relativistic electrons deposit a constant energy dose per unit length. In water with its density similar to tissue, this dose corresponds to approx. 2 MeV/cm. The low mass renders electrons subject to strong lateral scattering. Bremsstrahlung photons which are produced as a by-product of the stopping process of the electrons in the field of the nuclei cause the low-intensity tail at the end of the depth–dose curve (Fig. 4.2).

For protons and all heavier ions, the absorption curve in matter shows a slow initial increase with penetration depth and a steep rise and fall towards the end of the particle's range (Figs. 4.1c and 4.2). Because of their much higher mass, ions experience significantly less lateral scattering than electrons (proton-to-electron mass ratio is 1,836:1).

Accelerated atomic nuclei of the therapeutically relevant kinetic energy (approx. 40–400 MeV/u) interact predominantly via Coulomb forces with the target electrons of the traversed matter. This leads to excitation and ionization of atoms along the track of the traveling particle. Quantitatively, the energy loss per unit path length,

also called stopping power, of these heavy charged particles is described by the Bethe formula

$$\mathrm{d}E/\mathrm{d}x \sim Kn_{\mathrm{o}}(Z_{\mathrm{eff}})^2/\beta^2[\ln((2m_{\mathrm{e}}c^2\beta^2/I(1-\beta^2)) - \beta^2], \tag{4.1}$$

where K is a constant, n_{o} the electron density of the target material, Z_{eff} the effective charge of the projectile ions, β the velocity of the projectile in units of the speed of light ($\beta = v/c$), I the mean ionization energy of the target atoms, and m_{e} the rest mass of the electron.

For low particle velocity ($v << c$, and $\beta << 1$), the Bethe formula can be reduced to

$$\mathrm{d}E/\mathrm{d}x \sim Kn_{\mathrm{o}}(Z_{\mathrm{eff}})^2/v^2[\ln(2m_{\mathrm{e}}v^2/I)]. \tag{4.2}$$

Under these conditions, the stopping power varies mainly with $(Z_{\mathrm{eff}})^2/v^2$. With decreasing speed, $\mathrm{d}E/\mathrm{d}x$ should increase. However, the projectile scavenges electrons, reducing its effective charge Z_{eff}. At $E = 3Mc^2$ (M being the particle mass), the energy loss is minimal. For still lower velocities, $\mathrm{d}E/\mathrm{d}x$ increases logarithmically. Together, these effects produce the sharp rise and fall at the end of the ion track – the Bragg peak – in the graphical representation of energy loss or relative dose as function of penetration depth.

Most ion particles travel the same distance in a monoenergetic beam. But not all experience the same number of collisions. Their range is, therefore, somewhat different. This phenomenon is called straggling. In tissue, the difference is of the order of 1% of the mean range for protons (1, 7). For heavier ions, range straggling varies approximately inversely to the square-root of the particle mass. This means, helium ions show only 50% and neon approx. 22% of the straggle of protons (Fig. 4.3).

As the mass of the lightest ion, the proton ($^1H^+$), is already 1,836 times the mass of the electron, a collision with an electron barely deflects the projectile ion from its initial path. Still, multiple deflections result in lateral spreading or scattering and divergence of the beam. In large parallel beams only the outer edges are affected. In the center, the number of particles scattering out is compensated for by others scattering in. The central dose of narrow beams, however, decreases with depth, as particles scattering out are no longer replaced (Fig. 4.4).

The transverse spread of an infinitely narrow proton beam amounts to approximately 5% of its initial range [1, 7]. Just as for range straggling, the angular deflection from the incident beam direction by multiple scattering decreases with increasing charge and mass. Figure 4.5 illustrates this correlation graphically for several ions. For helium ions, the effect is approximately a factor of two, for carbon a factor of 3.5, and for silicium a factor of five lower than for protons.

4.2.2 Magnetic Deflection for Active Beam Shaping

The narrow Bragg peak of a monoenergetic beam which is only a few millimeters wide, is exploited in specific radiosurgery procedures (cf. Chap. 34). For most

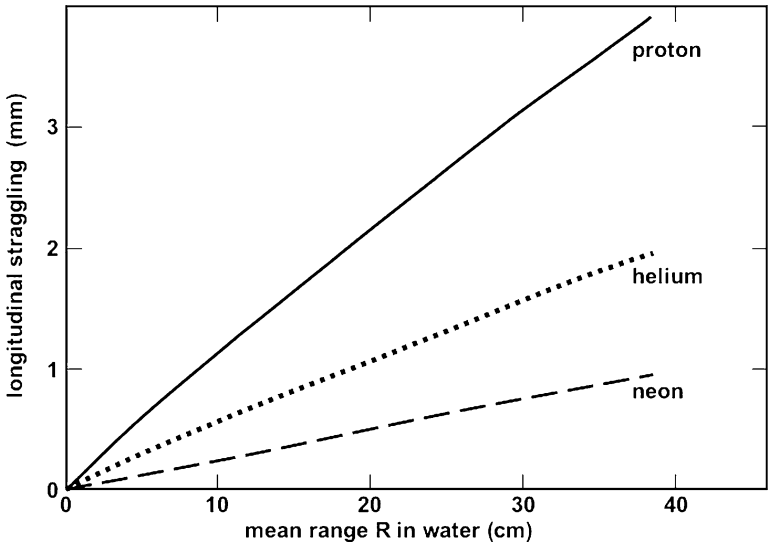

Fig. 4.3 Straggling as function of path length. Comparison of a proton, helium and neon beam in water. Range straggling corresponds to the standard deviation σ_z of the range distribution of a particle beam with mean range R. At first approximation, it varies inversely to the square root of the mass of the particle

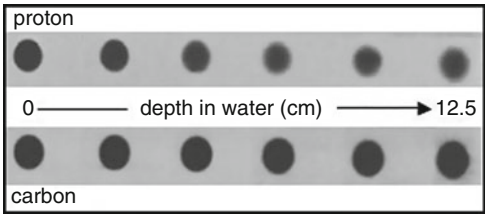

Fig. 4.4 Multiple scattering in a narrow ion beam (Ø 9 mm). Comparison of protons and carbon ions. The higher angular deflection of the particles in the proton beam leads to a visible loss of particle density in the proton spots. Spotsize and particle density of the carbon beam change only slightly. Data from GSI, Darmstadt

practical irradiations, however, it is necessary to spread the radiation field laterally and in depth to cover a larger target area (Fig. 4.1). The classical way has been by passive beam shaping devices, such as scattering foils and energy modulating absorber media, which broaden the beam profile transversely and extend the Bragg-peak dose from the distal to the proximal end of the target volume, respectively (cf. Chap. 25 for details). However, the charge of the ions offers still another way to tailor the irradiated volume very precisely to the shape of the tumor.

A pencil-thin ion beam can be deflected magnetically in horizontal and vertical directions to irradiate a tumor slice of the approximate width of the Bragg peak point by point (Fig. 4.6). By reducing the energy stepwise and repeating the irradiation

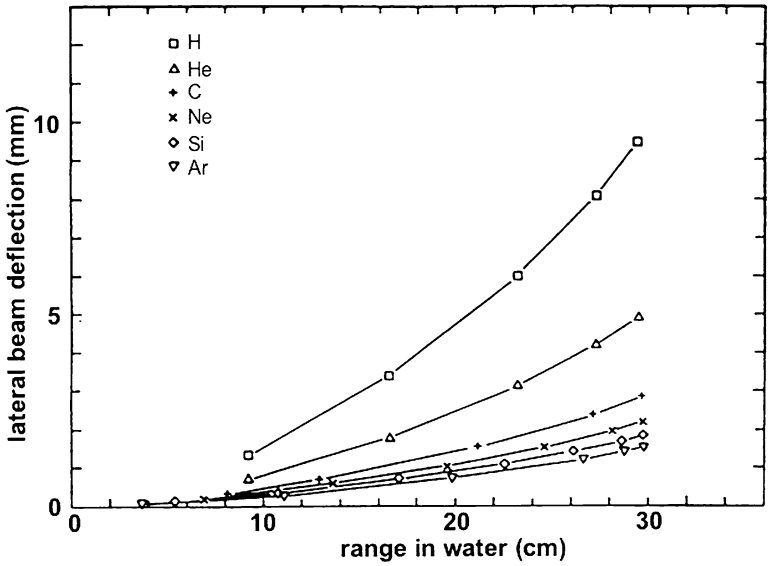

Fig. 4.5 Lateral beam deflection as a function of path length. Data from LBL, Berkeley, USA

for each slice, a tumor of arbitrary shape can be successively irradiated from its most distal to the most proximal part [8–11]. This unique irradiation technique, which is only possible with protons and heavier ions, permits the ultimate in tumor-conform RT, minimizing the radiation burden on healthy tissue. In addition, it facilitates the application of individualized treatments with local boosts or other desired nonhomogeneous dose distributions. It can be applied to increase the dose in the tumor as compared to photon irradiation without increasing the dose in the entrance channel, or to reduce unwanted radiation in the beam entrance without changing the overall tumor dose.

4.3 Biophysical Properties

4.3.1 Stopping Power and LET

The linear energy transfer or LET is a measure for the energy deposited by an ionizing particle traveling through matter. It is closely related to the stopping power described in (4.1). While stopping power can be seen as a material property (depending on electron density), which describes the energy absorbed by matter, LET describes the loss of energy or the "fate" of the particle. If all the secondary electron energies are considered, LET, numerically, equals stopping power.

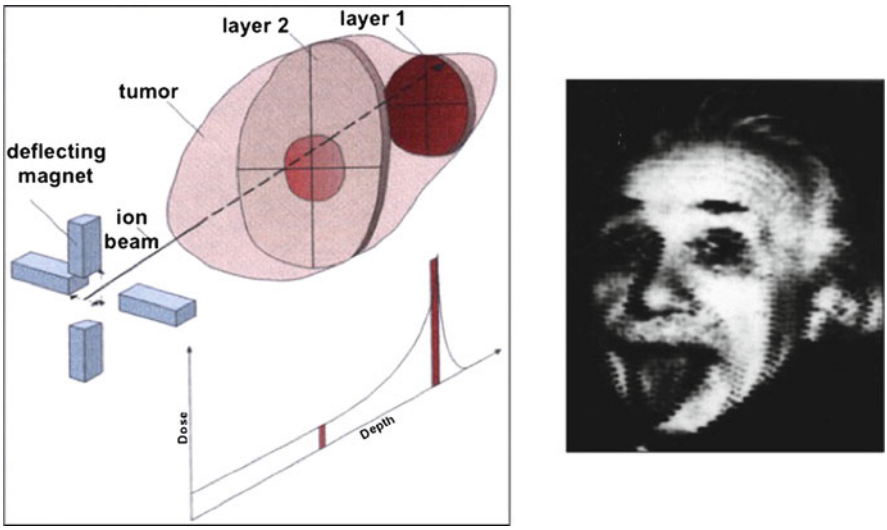

Fig. 4.6 Ion beam scanning. *Left:* Schematic view of the scanning technique. Individual slices of approx. 5 mm (≈Bragg peak width) are irradiated starting from the most distal part of the tumor and gradually moving forward. Within a slice the magnetically controlled ion beam is moved line-wise or from spot to spot to cover the desired target shape. The fact that proximal layers receive some dose (indicated by the dark central spot of layer 2) when more distal layers (1) are treated has to be taken into consideration by appropriately designing the irradiation protocol, e.g., give higher dose to the margin of layer 2 than to the preirradiated core. *Right:* Example of the raster scan capabilities: a pencil beam of carbon ions was used to reproduce a photo of Albert Einstein. Conditions were: 1.5×10^{10} ions delivered in 80 fractions of 5 s each, beam diameter 1.7 mm FWHM, ion energy 480 MeV/u, photo plate 15 cm × 18 cm. Data from GSI, Darmstadt, Germany

LET – generally expressed in units of keV/μm – has long been viewed as a major parameter to discern qualitatively the biological effects of different kinds of radiation [12, 13]. But it is not a constant value. As charge and energy of a projectile ion change along the particle's path, LET changes, as well. Its depth dependence yields the characteristic Bragg maximum. The maximum LET-value of cobalt gamma rays amounts to approx. 10 keV/μm. For protons, the corresponding value is roughly 100 keV/μm and for heavier ions it might be 1,000 keV/μm and more (Fig. 4.7).

Even though LET is not a good parameter to describe the full spectrum of biological radiation effects, it is still a widely used quantity to categorize ion-induced damage.

The limitations of LET become particularly prominent when ions of different atomic number are compared [14–16]. In particular for LET values greater than 100 keV/μm, different biological responses can be observed for particles of the same LET (Fig. 4.7). This is explained by the fact that the energy of accelerated ions is deposited in individual dose "packets" of varying density along individual particle trajectories rather than evenly throughout the overall irradiated volume (for recent review cf. [17, 18]).

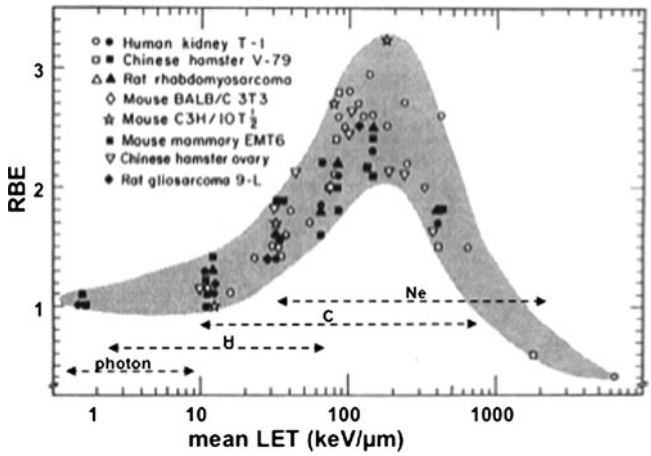

Fig. 4.7 Relative biological effectiveness (RBE) of ion beams as a function of linear energy transfer (LET). The compilation of data for a number of cell types shows that there is a trend but no simple relationship between the two. The *dashed arrows* indicate the approximate LET range for photons and various ions. Adapted from [8]

Ions of the same velocity produce tracks of secondary electrons with the same kinetic energy. But the dose density within the track, i.e., the number of secondary electrons produced, does not need to be identical [17]. According to (4.1), the deposited dose increases with decreasing velocity and the square of the effective charge of the incident ions. As heavier ions can have higher charge states than the singly charged protons, they can also have higher ionization densities.

4.4 Biological Properties

4.4.1 Relative Biological Effectiveness

Prior to the clinical use of accelerated ions, their biological effects were studied with a number of experimental systems. In the late 1950s, the Uppsala cyclotron was intensively used for such studies. Larsson and his colleagues provided a wealth of radiobiological data of protons [19–22]. Similar investigations were performed, thereafter, in Russia [23] and the United States [24–27].

Cultured cells, plant seedlings, healthy and tumor-bearing animals were irradiated and cell survival, chromosomal aberrations, histological changes, LD_{50} etc. examined (for a recent review cf. [28]). The central question of these experiments was the biological effectiveness of the accelerated ions in comparison to the effect by the same physical dose of a reference radiation, mostly 250 kV X-rays or ^{60}Co gamma rays, i.e., the relative biological effectiveness (RBE) (cf. Fig. 4.7).

Early studies revealed an RBE close to one for protons meaning that the proton dose required to produce a given effect was comparable to the reference photon dose causing the same effect. More refined studies indicated, however, that low-energy (<1 MeV) and very high-energy (>1 GeV) protons can have RBE-values of 2 and more, depending on the biological endpoint studied [29–32].

An elevated biological effectiveness in the Bragg peak region has clearly been demonstrated for ions heavier than helium [16]. It is the increase in stopping power of accelerated ions towards the end of their tracks, which leads to more biological damage or an increase in RBE at the site of the Bragg peak. As Fig. 4.7 illustrates, the RBE rises with increasing LET up to approx. 100–200 keV/μm and decreases at higher LET values. This has been interpreted as "overkill" effect, i.e., more dose is deposited in a cell than is necessary to kill it [33].

Precise RBE predictions of heavier ions cannot simply be made on the basis of LET information. As will be discussed in Chap. 6, detailed knowledge of the beam composition, of fluency, charge, and velocity of the particles is required.

4.4.2 Oxygen Enhancement Ratio

Oxygen acts as sensitizer, rendering cells more susceptible to radiation damage [34–36]. When irradiating cells with photons or low-LET ions, they demonstrate different survival behavior, depending on the presence or absence of oxygen (Fig. 4.8).

The oxygen enhancement ratio (OER) of radiation is the dose D required to produce a certain biological effect E in the absence of oxygen (anoxic conditions) to the dose required to produce the same effect in the presence of oxygen (oxic conditions),

$$\mathrm{OER} = \frac{D_{\mathrm{anoxic}}(E)}{D_{\mathrm{oxic}}(E)}. \tag{4.3}$$

For X-rays, the OER ranges from 2.5 to 3 which means, a 2.5–3 times higher X-ray dose is required to kill oxygen-deprived cells rather than the same cells under aerobic conditions. Many independent studies have shown that the OER-value begins to decrease at LET values of ≥100 keV/μm approaching unity between 150 and 300 keV/μm depending on the biological system used [37–39].

For many biological systems the oxygen dependency of radiation response increases up to an oxygen pressure of approx. 20 mmHg (2,700 Pa). Well-vascularized normal tissues exhibit oxygen pressures of ≥40 mmHg. They should, therefore, be fully radiosensitive as far as the oxygen effect is concerned.

In experimentally-induced animal tumors hypoxic cells have routinely been found (cf., e.g., [40]). For human tumors, the existence of hypoxic cells is recognized but their clinical significance is debated. The fact that severe anemia during RT is associated with worse local control in a variety of cancers underlines

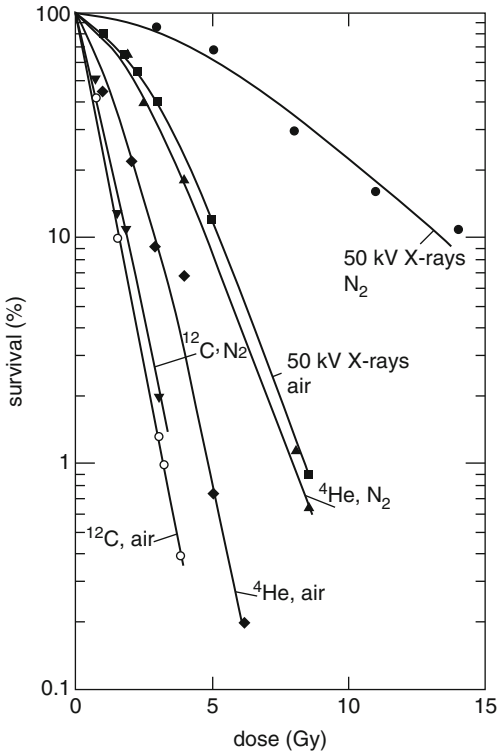

Fig. 4.8 Cell survival curves of human kidney T1 cells after irradiation with ions or X-rays in air or nitrogen atmosphere, respectively. Adapted from [14]

the importance of sufficient oxygen supply [36, 41]. But considerable intra- and inter-individual variations in oxygenation among tumors of the same clinical stage and grade make general statements difficult [42–45]. Still, a reduction in OER has become one of the rationales to use high-LET radiation in cancer therapy.

4.4.3 Variation in Radiosensitivity with the Cell Cycle

The cell cycle of eukaryotic cells is divided into several phases of growth and maturation. The postmitotic rest or gap phase G_1 is followed by the DNA synthesis or S phase and a second gap phase (G_2), which precedes the actual mitosis (M). If the cellular environment is unfavorable, a cell might leave the regular cell cycle and enter a kind of resting state (G_0).

The duration of S, G_2 and M phase is relatively constant for cells from a given species. But G_1 and G_0 can vary widely.

Single-cell survival data with cells in different stages of the cell cycle showed that most cells are sensitive during mitosis and more resistant in G_1 and S phase [46–48]. The effect can be significant with survival rates differing by more than a factor of ten at large single doses (Fig. 4.9).

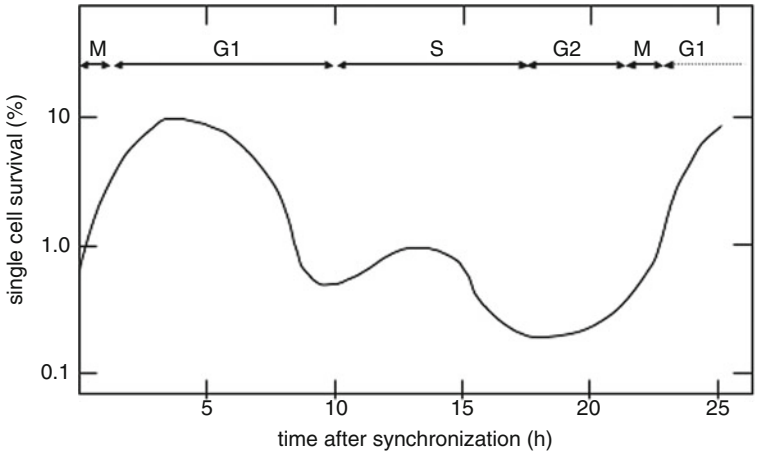

Fig. 4.9 Single cell survival as function of the cell cycle. Synchronized mouse fibroblasts (L929) were exposed to a single dose of 6.2 Gy X-rays at various times after synchronization. The phases of the cell cycle indicated at the *top* are *M* mitosis, G_1 postmitotic gap, *S* DNA synthesis phase, G_2 premitotic gap. Data from [46]

A reduced but not completely eliminated cell-phase dependent radiation sensitivity was also observed for heavy ions. At LET-values of approx. 200 keV/μm and beyond, this dependence seems to vanish. However, results are not fully consistent, not the least because of experimental differences in cell culture synchronization.

4.4.4 Sublethal Cell Damage

Survival curves of exponentially growing cells irradiated by X-rays are characterized by a shoulder (see Fig. 4.8) due to the capacity to accumulate sublethal damage. If the irradiation scheme is divided into multiple fractions, the survival is higher or a shoulder appears with each new fraction, indicating that repair occurs after each treatment.

With increasing LET of the radiation, the shoulder recedes. Heavy ions with an LET of 100–200 keV/μm prompt an exponential survival curve [33, 49]. After fractionated irradiation with heavy ions, the survival curves remain exponential, i.e., no significant repair occurs.

4.5 Comparison of Protons and Heavier Ions

Protons as well as the heavier ions are characterized by a superior depth–dose distribution as compared to photons. While this improved physical dose distribution

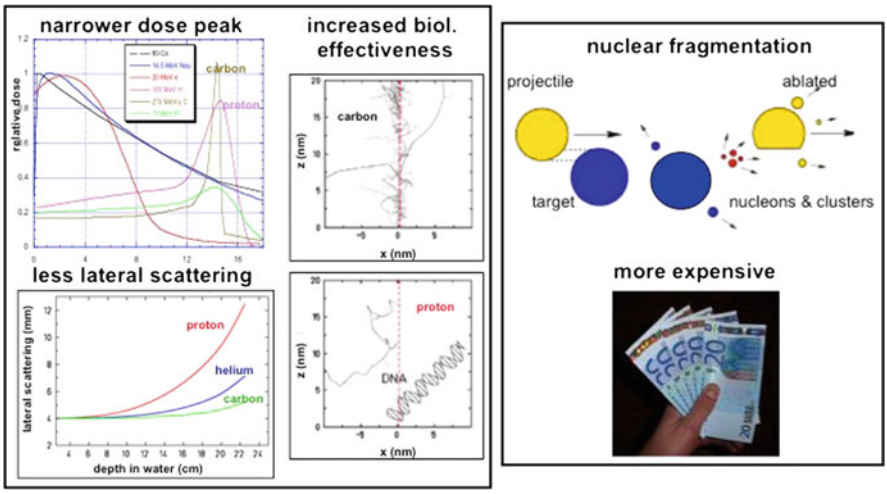

Fig. 4.10 Comparison of protons and heavier ions ($A > 1$). The properties in the *left box* are advantageous. They increase with mass and favor ions with $A > 1$. But the unwanted effects on the *right* increase as well with the ion mass and need to be balanced

is common to all ions, there are several other factors where protons and ions with higher atomic number differ (Fig. 4.10).

As mentioned above, multiple scattering and range straggling effects dwindle with increasing mass, improving the lateral and distal dose fall-off. Clinically exploited, this translates into higher precision of the treatment and, e.g., improved sparing of critical structures immediately adjacent to the tumor.

These physical advantages of helium and the heavier ions are offset, however, by their tendency to fragment after nuclear collisions [50, 51], causing a tailing of the Bragg peak due to the presence of lighter fragment particles, which have longer ranges than the primary beam components and hence, impair the excellent physical dose distribution. Fragmentation, on the other hand, can also produce positron emitting isotopes (^{11}C or ^{15}O), which have successfully been used for real-time monitoring of the spatial dose distribution (cf. Chap. 31 for details).

During the 1980s, when interest in medical applications of heavy ion beams experienced a revival mainly in Europe and Japan, carbon ions were considered the ions of choice, because they demonstrate high-LET qualities within the Bragg peak and low-LET behavior in the entrance channel of their trajectory. Their advantageous biological effects have in the meantime been realized in several thousand successfully treated patients (see Part IV *Clinical Results and Indications* of this book). However, systematic experimental studies to find the optimum ion for clinical use have not yet been pursued.

Kempe and colleagues [52] studied the dose distributional effects of ions of the first ten elements of the periodic table. Their theoretical analysis confirmed that penumbra 80/20, range straggling, Bragg peak width at 60% dose maximum and a

Table 4.1 First order cost estimate for a basic ion beam therapy unit depending on the ion provided (Alonso, Personal communication)

Ion	A	B	C	Total relative cost
Proton	1	1	1	1
Helium	1	1.5	1.4	1.3
Carbon	1	1.9	4.1	2.3
Oxygen	1	2.1	5.8	3.0
Neon	1	2.2	7.6	3.6

Assumptions: normal-conducting synchrotron, fourfold symmetric lattice, vault: 4 m high, 2 m clearance around the edges; 1 transport line: 10 m; 1 treatment room with conventional 45°–45°–90° gantry, 3 m distance to isocenter, ion range: 30 cm; shielding: 1.5 m concrete for protons. Cost components: (A) Fixed costs, (B) Technical components $\sim f$ (magnetic rigidity), (C) Shielding $\sim f$ (beam energy)

number of other parameters show a similar dependency on the number of nucleons $N(1/\sqrt{N})$. The therapeutic value of these properties improves with the square root of the mass number. Hence, the effects are most pronounced from the first to the second element (^{1}H vs. ^{4}He). Due to the exponential dependence, they level off for ions of the heavier elements. The high-LET effects extending into the plateau region and the fragmentation tail beyond the Bragg peak show an opposite trend. It is, therefore, unlikely that ions of $Z > 6$ find a clinical revival. They display too high an LET in the entrance channel, their fragmentation tails vitiate the gain of the Bragg peak, and their production is expensive. But ions with an atomic number between 1 and 6, in particular He, Li, and Be, could be interesting alternatives to carbon ions. They display high-LET effects only in the final Bragg peak region; in the plateau, it is negligible [52]. The tail dose is not yet significant, and not to ignore, their production is less costly (Table 4.1). Clinical studies in this direction are highly recommended. New clinical ion beam centers such as HIT in Heidelberg (Germany) and CNAO in Pavia (Italy) will provide various types of ions. They will offer the technical conditions to perform the necessary trials. It might then be possible to see if a last prediction in Robert Wilson's visionary publication will also be right, namely, that helium ions would be "the most desirable therapeutically" [1].

References

1. R.R. Wilson, Radiological use of fast protons. Radiology **47**, 487–491 (1946)
2. A.M. Koehler, W.M. Preston, Protons in radiation therapy. Radiology **104**, 191–195 (1972)
3. M.R. Raju, *Heavy Particle Therapy* (Academic, New York, 1980)
4. H. Suit, The Gray Lecture 2001: coming technical advances in radiation oncology. Int. J. Radiat. Oncol. Biol. Phys. **53**, 798–809 (2002)
5. J.F. Fowler, What can we expect from dose escalation using proton beams? Clin. Oncol. **16**, S10–S15 (2003)
6. E. Fokas, G. Kraft, H. An, R. Engenhardt-Cabillic, Ion beam radiobiology and cancer: time to update ourselves. Biochim. Biophys. Acta **1796**, 216–229 (2009)

7. M. Hollmark, J. Uhrdin, D. Belkic, et al., Influence of multiple scattering and energy loss straggling on the absorbed dose distributions of therapeutic light ion beams: I. Analytical pencil beam model. Phys. Med. Biol. **49**, 3247–3265 (2004)
8. W.T. Chu, B.A. Ludewigt, T.R. Renner, Instrumentation for treatment of cancer using proton and light-ion beams. Rev. Sci. Instrum. **64**, 2055–2122 (1993)
9. T. Haberer, W. Becher, D. Schardt, G. Kraft, Magnetic scanning system for proton therapy. Nucl. Instrum. Methods Phys. Res. A **330**, 296–314 (1993)
10. E. Pedroni, R. Bacher, H. Blattmann, et al., The 200-MeV proton therapy project at the Paul Scherrer Institute: conceptual design and practical realisation. Med. Phys. **22**, 37–53 (1995)
11. U. Weber, W. Becher, G. Kraft, Depth scanning for a conformal ion beam treatment of deep seated tumours. Phys. Med. Biol. **45**, 3627–3641 (2000)
12. R.E. Zirkle, The Radiobiological Importance of Linear Energy Transfer, in *Radiation Biology* vol. 1, ed. by A. Hollaender. (McGraw Hill, New York, 1954), pp. 315–350
13. G. Kraft, M. Krämer, M. Scholz, LET, track structure and models. Radiat. Environ. Biophys. **31**, 161–180 (1992)
14. P.W. Todd, Fractionated heavy ion irradiation of cultured human cells. Radiat. Res. **34**, 378–389 (1968)
15. A. Perris, P. Pialoglou, A.A. Katsanos, E.G. Sideris, Biological effectiveness of low-energy protons. I. Survival of Chinese hamster cells. Int. J. Radiat. Biol. **50**, 1093–1101 (1986)
16. G. Kraft, W. Kraft-Weyrather, S. Ritter, et al., Cellular and subcellular effect of heavy ions: a comparison of the induction of strand breaks and chromosomal aberration with the incidence of inactivation and mutation. Adv. Space Res. **9**, 59–72 (1989)
17. J. Kiefer, The physical basis for the biological action of heavy ions. New J. Phys. **10**, 075004 (2008) http://iopscience.iop.org/1367--2630/10/7/075004 (accessed 20 Oct 2010)
18. K. Ando, Y. Kase, Biological characteristics of carbon-ion therapy. Int. J. Radiat. Biol. **85**, 715–728 (2009)
19. B. Larsson, L. Leksell, B. Rexed, P. Sourander, Effect of high energy protons on the spinal cord. Acta Radiol. **51**, 52–64 (1959)
20. S. Falkmer, B. Larsson, S. Sténson, Effects of single dose proton irradiation of normal skin and Vx2 carcinoma in rabbit ears. Acta Radiol. **52**, 217–234 (1959)
21. B. Larsson, B.A. Kihlman, Chromosome aberrations following irradiation with high-energy protons and their secondary radiation: a study of dose distribution and biological efficiency using root-tips of Vicia faba and Allium cepa. Int. J. Radiat. Biol. **2**, 8–19 (1960)
22. B. Andersson, C.C. Gale, B. Hökfelt, B. Larsson, Acute and chronic effects of preoptic lesions. Acta Physiol. Scand. **65**, 45–60 (1965)
23. A.A. Wainson, M.F. Lomanov, N.L. Shmakova, et al., The RBE of accelerated protons in different parts of the Bragg curve. Br. J. Radiol. **45**, 525–529 (1972)
24. J.B. Robertson, J.R. Williams, R.A. Schmidt, et al., Radiobiological studies of a high-energy modulated proton beam utilizing cultured mammalian cells. Cancer **35**, 1664–1677 (1975)
25. J. Tepper, L. Verhey, M. Goitein, et al., In vivo determinations of RBE in a high energy modulated proton beam using normal tissue reactions and fractionated dose schedules. Int. J. Radiat. Oncol. Biol. Phys. **2**, 1115–1122 (1977)
26. M. Urano, L.J. Verhey, M. Goitein, et al., Relative biological effectiveness of modulated proton beams in various murine tissues. Int. J. Radiat. Oncol. Biol. Phys. **10**, 509–514 (1984)
27. E.A. Blakely, Cell inactivation by heavy charged particles. Radiat. Environ. Biophys. **31**, 181–196 (1992)
28. E.A. Blakely, P.Y. Chang, Biology of charged particles. Cancer J. **15**, 271–284 (2009)
29. M. Belli, R. Cherubini, S. Finoto, et al., RBE-LET relationship for the survival of V79 cells irradiated with low-energy protons. Int. J. Radiat. Biol. **55**, 93–104 (1989)
30. M. Belli, F. Cera, R. Cherubini, et al., RBE-LET relationships for cell inactivation and mutation induced by low energy protons in V79 cells: further results at the LNL facility. Int. J. Radiat. Biol. **74**, 501–509 (1998)
31. A.N. Kabachenko, B.S. Fedorenko, O.A. Smirnova, Evaluation of the cataractogenic effect of 9 GeV protons (Russ.). Radiobiologiia **26**, 318–322 (1986)

32. T.C. Yang, Proton radiobiology and uncertainties. Radiat. Meas. **30**, 383–392 (1999)
33. H. Wulf, W. Kraft-Weyrather, H.G. Miltenburger, et al., Heavy-ion effects on mammalian cells: inactivation measurements with different cell lines. Radiat. Res. **104**, S122–S134 (1985)
34. L.H. Gray, Radiobiologic basis of oxygen as a modifying factor in radiation therapy. Am. J. Roentgenol. **85**, 803–815 (1961)
35. I. Churchill-Davidson, The oxygen effect in radiotherapy. Proc. R. Soc. Med. **57**, 635–638 (1964)
36. M. Molls, P. Stadler, A. Becker, et al., Relevance of oxygen in radiation oncology. Mechanisms of action, correlation to low hemoglobin levels. Strahlenther Onkol. **174**(Suppl 4), 13–16 (1998)
37. G.W. Barendsen, C.J. Koot, G.R. Van Kersen, et al., The effect of oxygen on impairment of the proliferative capacity of human cells in culture by ionizing radiations of different LET. Int. J. Radiat. Biol. **10**, 317–327 (1966)
38. C.A. Tobias, E.A. Blakely, E.L. Alpen, et al., Molecular and cellular radiobiology of heavy ions. Int. J. Radiat. Biol. Phys. **8**, 2109–2120 (1982)
39. Y. Furusawa, K. Fukutsu, M. Aoki, et al., Inactivation of aerobic and hypoxic cells from three different cell lines by accelerated 3He-, 12C- and 20Ne-ion beams. Radiat. Res. **154**, 485–496 (2000)
40. J.E. Moulder, S. Rockwell, Hypoxic fractions of solid tumors: experimental techniques, methods of analysis, and a survey of existing data. Int. J. Radiat. Oncol. Biol. Phys. **10**, 695–712 (1984)
41. R.S. Bush, R.D. Jenkin, W.E. Allt, et al., Definitive evidence for hypoxic cells influencing cure in cancer therapy. Br. J. Cancer **3**, S302–S306 (1978)
42. W. Müller-Klieser, P. Vaupel, R. Manz, R. Schmidseder, Intracapillary oxyhemoglobin saturation of malignant tumors in humans. Int. J. Radiat. Oncol. Biol. Phys. **7**, 1397–1404 (1981)
43. P. Wendling, R. Manz, G. Thews, P. Vaupel, Inhomogeneous oxygenation of rectal carcinomas in humans: A critical parameter for preoperative irradiation? Adv. Exp. Med. Biol. **180**, 293–300 (1984)
44. P. Vaupel, A. Mayer, Hypoxia in cancer: significance and impact on clinical outcome. Cancer Metastasis Rev. **26**, 225–239, (2007)
45. K.I. Wijffels, I.J. Hoogsteen, J. Lok, et al., No detectable hypoxia in malignant salivary gland tumors: preliminary results. Int. J. Radiat. Oncol. Biol. Phys. **73**, 1319–1325 (2009)
46. J. Fidorra, W.A. Linden, Radiosensitivity and recovery of mouse L cells during the cell cycle. Radiat. Environ. Biophys. **14**, 285–294 (1977)
47. E.A. Blakely, P.Y. Chang, L. Lommel, Cell-cycle-dependent recovery from heavy-ion damage in G1-phase cells. Radiat. Res. Suppl. **8**, S145–S157 (1985)
48. C. Fournier, G. Taucher-Scholz, Radiation induced cell cycle arrest: an overview of specific effects following high-LET exposure. Radiother. Oncol. **73**, S119–S122 (2004)
49. T.K. Hei, K. Komatsu, E.J. Hall, M. Zaider, Oncogenic transformation by charged particles of defined LET. Carcinogenesis **9**, 747–750 (1988)
50. A.S. Goldhaber, H.H. Heckman, High energy interactions of nuclei, Annu. Rev. Nucl. Part Sci. **28**, 161–205 (1978)
51. D. Schardt, I. Schall, H. Geissel, et al., Nuclear fragmentation of high-energy heavy-ion beams in water. Adv. Space Res. **17**, 87–94 (1996)
52. J. Kempe, I. Gudowska, A. Brahme, Depth absorbed dose and LET distributions of therapeutic 1H, 4He, 7Li, and 12C. Med. Phys. **34**, 183–192 (2007)

Chapter 5
Early and Late Responses to Ion Irradiation

Reinhard Schulte and Ted Ling

Abstract Early and late responses to ion beam therapy (IBT) are the result of complex interactions between host, dose volume, and radiobiological factors. Our understanding of these early and late tissue responses has improved greatly with the accumulation of laboratory and clinical experience with proton and heavy ion irradiation. With photon therapy becoming increasingly conformal, many concepts developed for 3D conformal radiotherapy and intensity modulated radiation therapy with photons are also applicable to IBT. This chapter reviews basic concepts and experimental data of early and late tissue responses to protons and ions.

5.1 Basic Concepts

5.1.1 Definition of Early and Late Tissue Responses

Tissue response to ionizing radiation is operationally divided into early (or acute) and late effects reflecting the time after irradiation at which the biological or clinical endpoint is typically observed (Fig. 5.1). The same concept is also applied to normal tissues that are classified as early or late responding depending on the time during or after irradiation at which the clinically relevant effects occur. The latter definition, however, is not always appropriate as early and late reactions may occur in the same tissue. In general, early responses to irradiation are self-limited and heal eventually without consequences. In some patients, however, acute reactions develop into chronic lesions that do not heal. These "consequential" late effects are seen more often with concurrent chemoradiation treatments [1].

R. Schulte (✉)
Department of Radiation Medicine, Loma Linda University Medical Center, 11234 Anderson Street, B 121, Loma Linda, CA 92354, USA
e-mail: rschulte@dominion.llumc.edu

U. Linz (ed.), *Ion Beam Therapy*, Biological and Medical Physics, Biomedical Engineering, DOI 10.1007/978-3-642-21414-1_5,

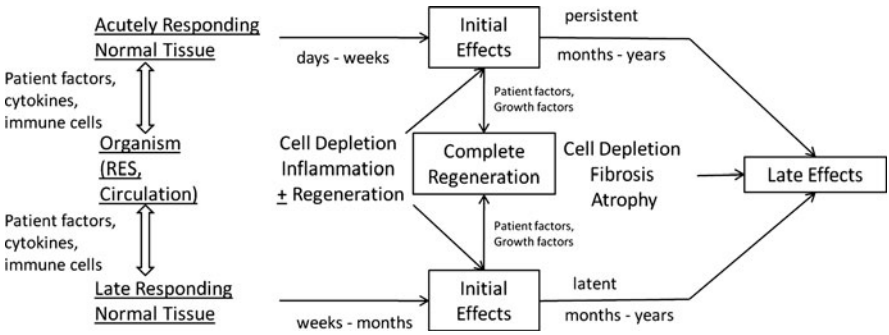

Fig. 5.1 Schematic illustration of the time line of early and late effects and important factors influencing regeneration or progression. *RES:* reticulo-endothelial system

Late effects develop months to years after the radiation treatment. These symptoms are more variable and site and tissue specific. They may range from asymptomatic and self-limited to destructive and progressive. They may develop gradually over years or very suddenly, e.g., as the consequence of vascular occlusion of an irradiated large artery. Severe and progressive late effects are associated with the loss of function and quality of life. Therefore, greater emphasis is usually placed on preventing late responses while early responses, even if they are brisk, are usually accepted.

Most late effects are deterministic, i.e., they occur after a threshold dose is reached and then increase in severity as the cumulative dose increases. Secondary malignant neoplasms (SMN) are stochastic events, i.e., they occur without a known dose threshold and only the event frequency, not severity, increases with dose. A discussion of stochastic late effects of protons and ions is beyond the scope of this chapter, and the clinical perspective on complication rates due to IBT is discussed in Chap. 18.

5.1.2 Cellular and Molecular Origin of Radiation Response

The past decade has seen a number of advances in the tools of molecular biology. This has led to a greater understanding of the molecular mechanisms of radiation-induced tissue damage and response. The original concept of late radiation response stated that primary (not consequential) late effects arise from parenchymal cell depletion secondary to damage to the nonparenchymal stroma. This idea was challenged in the mid-1990s when it was discovered that a multitude of molecular events are triggered in response to primary radiation damage [2]. More recent studies have shown a persistent elevation of cytokine production following tissue irradiation. Late responses are now seen as a continuous and dynamic process involving a number of inflammatory cytokines, chemokines, growth factors as well

as cells of the reticular endothelial system (RES). Late effects can be seen as a systemic response to injury modulated by genetic factors.

Rubin et al. [2] irradiated C57BW6 mice to doses known to induce pneumonitis and pulmonary fibrosis. They demonstrated a marked elevation of proinflammatory cytokines at 2 weeks following thoracic irradiation. These cytokines returned to baseline shortly thereafter, but became persistently elevated again at 8 weeks and remained elevated for many months. This resulted in endothelial damage, edema, and increased permeability, all hallmarks of pneumonitis. An inflammatory response ensued and macrophages were activated, thus perpetuating a continuous nonhealing response leading to chronic radiation injury. Additional studies have shown that inflammation may also lead to vascular damage and subsequent tissue hypoxia. A state of chronic hypoxia generates reactive oxygen species (ROS), which perpetuate tissue injury [3].

One of the prominent cytokines in the late-responding tissue injury pathways is transforming growth factor-beta (TGF-β). It is also a key factor in the development of fibrosis by promoting the influx of fibroblasts and the epithelial to mesenchymal differentiation of cells [4]. Studies have shown that the ability to restore epithelium may protect against further radiation-induced tissue damage [5]. Therefore, the ability to modulate TGF-β may lead to improved tissue healing and decreased fibrosis. Roberts et al. [6] demonstrated that disruption of the TGF-β pathway resulted in resistance to the development of radiation-induced lung fibrosis. Although not fully tested in humans, anti-TGF-β therapy shows promise as an approach to prevent radiation-induced injury.

5.1.3 Dose–Volume Effects

The planning of conformal IBT, like conformal photon therapy, is a balancing act between competing goals: protecting critical organs at risk (OARs) (e.g., spinal cord, optic nerves) from high-dose irradiation and avoiding underdosing the macroscopic tumor when the OARs are in close proximity. Based on an extensive literature review, Emami et al. [7] published the tolerance doses for partial (one third or two thirds) and whole organ irradiation for most of the organs encountered in typical radiation-treated tumor sites. Data from this study have been used extensively in both the clinical setting and in dose-volume–response modeling. Additional mathematical tools were developed to deal with the inhomogeneous dose distribution seen across OARs, which are typical for 3D conformal radiation techniques, including IBT.

Ideally, the treatment planner would use mathematical tools and models that support the planning process, such as cumulative dose–volume histograms (DVHs), and model estimates of tumor control probability (TCP), and normal tissue complication probability (NTCP). These models allow for the preference ranking of different treatment plans. Dose–volume–response models have a long tradition in radiation oncology, but none of the existing models has achieved sufficient maturity to be widely applied.

The underlying concept of early NTCP and TCP models [8–10] was that tissues can be divided into independent subunits (i.e., clonogens in the case of malignant tumors and functional subunits (FSUs) in the case of normal tissues). This concept states that each subunit responds to radiation as if it were isolated from all surrounding units. Another related concept postulates serial and parallel types of tissue architecture. Serial and parallel refers to the arrangement of these independent units and implies an underlying importance of the arrangement of subunits for tissue response. For example, if each functional subunit is critical for the proper function of the organ as a whole then it has serial architecture. Serial organs (e.g., spinal cord) show a volume effect only if the radiation volume is of the order of the subunit volume, otherwise their volume dependence is small. Parallel organs (e.g., lung), on the other hand, have a strong volume dependence as the functional reserve of the organ diminishes with larger fractional volumes irradiated. The relative seriality model [10], postulating a mixture of serial and parallel subunits, has found application in the analysis of late cardiac mortality and in radiation pneumonitis risk studies pertaining to radiation treatment for breast cancer [11] and Hodgkin lymphoma [12].

Lyman [13], who participated in an NCI-sponsored project to evaluate IBT plans, modeled the late-effect threshold doses for partial-volume dependence with a power-law relationship:

$$\mathrm{TD}(V) = \mathrm{TD}(1)/V^n \tag{5.1}$$

where $TD(V)$ is the tolerance dose for a given partial volume (V), $TD(1)$ is the tolerance dose for the full volume, and n is a fitted parameter. A probit model (integral over a normal distribution) was then used to describe the sigmoid dose dependence of the NTCP for a partial volume irradiation:

$$\mathrm{NTCP}(D, V) = \frac{1}{\sqrt{2\pi}} \int_{-\infty}^{t(D)} \exp\left(-t'^2/2\right) \mathrm{d}t' \tag{5.2}$$

where the dose-dependent upper integration limit is given by $t(D) = (D - TD_{50}(\mathrm{V}))/(mTD_{50}(\mathrm{V}))$ with $TD_{50}(V)$ corresponding to the tolerance dose leading to complications in 50% of the population and with m another fitted parameter. In an accompanying paper to the Emami et al. publication [7], Burman et al. [14] fitted Lyman's model to the Emami dose–volume consensus data to derive the model parameters that best predicted the tolerance doses of partial organ volumes. Kutcher et al. [15] further refined Lyman's and Burman's approach by reducing the DVH information, which described the inhomogeneous dose distribution across an OAR, to an equivalent partial volume receiving the maximum dose resulting in the same NTCP as a given inhomogeneous dose distribution. This set the stage for predicting NTCP for arbitrary 3D dose distributions. The Lyman–Kutcher–Burman (LKB) model has since become the most widely used NTCP modeling tool.

The equivalent uniform dose (EUD) concept is another useful DVH-reduction scheme developed by Niemierko [16]. The EUD for inhomogeneously irradiated tumors was defined as the dose that, if given uniformly over the entire tumor,

would lead to the same cell killing as the actual nonuniform dose distribution within that same tumor volume. Furthermore, different dose distributions resulting in the same EUD were postulated to be biologically equivalent. The EUD concept was also extended to normal tissues based on the assumption that the EUD uniformly delivered to an OAR would result in the same reduction in FSUs as the actual inhomogeneous dose [17]. The EUD concept has proven to be useful when performing treatment-dose-plan ranking. The plan with the larger tumor EUD is ranked higher in terms of TCP and the plan with the smaller OAR EUD is ranked higher in terms of NTCP [18]. The EUD concept has also found application in the dosimetric comparison of proton therapy (PT) with other conformal treatment techniques [19, 20].

The progress made in DVH-based TCP and NTCP modeling since the early 1990s, in addition to the increasing number of clinical studies using 3D-conformal radiation techniques, led to the Quantitative Analyses of Normal Tissue Effects in the Clinic (QUANTEC) initiative. A supplemental issue of the International Journal of Radiation Oncology Biology and Physics detailed a group of investigators participating in this effort. They published 16 clinical articles reviewing the dose–volume dependence of late normal tissue toxicities seen in external beam radiotherapy [22]. The compilation of the QUANTEC guidelines will serve as a useful resource for normal tissue effects from radiation therapy, including IBT.

5.1.4 Biological Dose Weighting

While dose-volume effects apply equally to treatment with photons and IBT, a unique characteristic of IBT is the need to apply dose-weighting factors due to differences in relative biological effectiveness (RBE). Additional dose weighting is necessary if dose delivery deviates from conventional practice, as is often the case for IBT, in particular for carbon ion radiotherapy (CIRT). In general, dose-weighting factors are required to accommodate changes in radiation quality as well as the unconventional time-dose-fractionation schedules. The majority of patients receiving conventional radiation therapy are treated with 2 Gray (Gy) per fraction, 5 times a week, so these conditions are generally accepted as the reference conditions for weighting factors related to deviations from this schedule.

The RBE increases with increasing atomic number and increasing linear energy transfer (LET) (below 100 keV/μm) of the particle (cf. previous chapter for details).

The question of dose-weighting factors for reporting and prescribing IBT has recently been addressed in two technical reports. For PT, the International Commission on Radiation Units and Measurements (ICRU) published report 78 [22], and for ions heavier than protons the International Atomic Energy Agency (IAEA) and the ICRU jointly published technical report 461 [23]. Both agencies stressed the importance of reporting and prescribing *absorbed dose* as the underlying physical quantity in radiation therapy. Taking into account the difference between photons and protons, report 78 of the ICRU recommends using a tissue- and depth-independent generic RBE value of 1.10 for all therapeutic applications of protons.

The reason for this recommendation is that the available data on in vitro and in vivo systems, including acute- and late-responding tissues, are consistent with a tissue-independent mean RBE value of 1.10. In the ICRU recommendation, the product of dose and proton RBE is called the *RBE-weighted absorbed dose* (D_{RBE}) and is expressed in units of Gy.

For heavier ions, the ICRU and IAEA recommend multiplying the absorbed dose by a weighting factor, W_{ion}, (e.g., $W_{\mathrm{C+}}$ for carbon beams). This weighting factor takes into account differences in radiation quality, altered fractionation scheme, or other factors specific to IBT. The product of absorbed dose (D) and W_{ion} is called the *weighted absorbed dose* D_{ion} (e.g., $D_{\mathrm{C+}}$ for carbon ions) and is expressed in units of Gy. Report 461 acknowledges that IBT with heavier ions differs from protons in that one needs to consider the variation of RBE with depth within the individual ion beams.

For dose fractions that differ from the conventional 2 Gy per fraction schedule, report 461 recommends using the linear quadratic (LQ) model of cell survival to calculate the isoeffective isodose. The weighting factor W_{ion} is then given by:

$$W_{\mathrm{ion}} = \frac{D_{\mathrm{ref}}}{D_{\mathrm{ion}}} = \frac{n_{\mathrm{ref}} d_{\mathrm{ref}}}{n_{\mathrm{ion}} d_{\mathrm{ion}}} = \frac{\alpha_{\mathrm{ref}} + \beta_{\mathrm{ref}} d_{\mathrm{ref}}}{\alpha_{\mathrm{ion}} + \beta_{\mathrm{ion}} d_{\mathrm{ion}}} \tag{5.3}$$

where D_{ref} and D_{ion}, n_{ref} and n_{ion}, and d_{ref} and d_{ion} are total dose, number of fractions, and dose per fraction for the reference (photon) radiation and the ion or test schedule, respectively, and α_{ref}, β_{ref} and α_{ion}, β_{ion} are the tissue- or effect-specific LQ model parameters for the reference and ion irradiation, respectively. In Appendix II of report 461 [23], Joiner and Marples show that solving this equation for d_{ion} results in an equation that depends only on the tissue- or effect-specific α/β ratios for the reference and ion radiation and the ratio of alpha parameters $\alpha_{\mathrm{ion}}/\alpha_{\mathrm{ref}}$. For photons, it is usually assumed that the α/β ratio is 10 Gy for early-responding tissues and 3 Gy for late-responding tissues.

The formulation recommended by report 461 is generally applied in the setting of "isoeffective" dose and fractionation. Assuming a photon reference scheme of 2 Gy fractions, given 5 times a week, the weighting factor is called W_{IsoE}. When an equal number of fractions is used for the IBT and the photon reference schedule, the weighting factor equals the RBE for the photon reference dose per fraction. Note that the report 461 formalism avoids the use of RBE, and instead employs LQ model parameter ratios. These parameters depend on radiation quality (and, therefore, on depth) as well as on tissue or endpoint, but not on dose per fraction. Assuming validity of the LQ model, the formalism allows conversion of RBE values into LQ model parameters and vice versa, however (cf. also Chap. 8).

Currently, there is no universally accepted approach to estimating weighting factors for a given therapeutic scenario in IBT. Several methods for determining RBE of IBT beams have been described in the literature. The early experimental and clinical human IBT programs performed extensive radiobiological investigations to determine RBE values and RBE–dose relationships (cf. also subsequent chapter). The studies involved cell survival experiments and dose–effect relationships for

various tissues and endpoints. They utilized animal models at various positions within energy-modulated treatment beams. The group performing CIRT at the National Institute of Radiological Sciences (NIRS) in Chiba, Japan, combined their radiobiological data with a previous clinical experience involving neutrons in order to predict values of RBE for carbon beams used for therapy. This approach is described in detail in Annex IV of report 461 [23].

Additional information regarding the weighting of IBT dose has resulted from evaluation with experimental or calculational microdosimetry techniques [24, 25]. Although these data cannot replace biological measurements, they provide a basis for understanding the dependence of ion beam RBE on the position within a spread-out Bragg peak (SOBP). These data can also provide input for biophysical models for deriving RBE and weighting factors.

Various attempts have been made to predict RBE values using biophysical models. These models attempt to connect LET, lineal energy (a microdosimetric quantity), or microscopic subvolume doses to survival data obtained from in vitro or in vivo experiments [26–29]. For example, the local effect model (LEM), developed by the Helmholtzzentrum für Schwerionenforschung (GSI) in Darmstadt, Germany, [26,29], has been utilized in their CIRT program. It can be expected that such models will eventually find application in various commercial treatment planning programs for IBT (cf. Chap. 8 for details).

Aside from dose per fraction and RBE, overall treatment time is another factor affecting the biological effectiveness of radiation therapy, IBT included. This is primarily related to an accelerated proliferation of tumor clonogens and stem cells seen in early-responding normal tissue that often occurs during a course of radiation therapy [30]. When overall treatment time of an IBT course differs from that of the reference treatment technique, the total isoeffective dose needs to be adjusted to take into account this difference in overall time [23]. However, the effect of overall treatment time on tumor control and early and late tissue response is difficult to predict. Solid data on this topic are limited and the interpretation of retrospective clinical data depends on the assumed mechanism [31, 32]. For head and neck squamous cell carcinoma, for example, the suggested compensation for unintentionally missed treatment days is adding 0.6 Gy to the photon dose for each day missed beyond 3–4 weeks when using 2 Gy fractions [33]. For other fraction sizes, tumor types, or normal tissues under consideration, a different correction will likely be required. Additional data are needed before more specific recommendations regarding the time factor can be given.

5.2 Early and Late Tissue Responsess to Proton and Ion Irradiation

In this section, the results of experimental studies of tissue irradiation effects with protons and ions will be reviewed. Recent developments in IBT have favored the use of protons and carbon ions over other ions (e.g., helium and neon), therefore,

the data for protons and carbon will be emphasized. Additional information on specific preclinical studies can be found in later chapters. Some historical results with helium and heavier ions (neon, argon) are still included for comparison.

Radiobiological studies have been an important part of the commissioning programs leading up to the clinical use of IBT and have helped to develop current concepts of dose-volume effects and dose weighting and to define clinical RBE values of ion beams for treatment planning. One must remember, however, that experimentally determined RBE values depend on the particular experimental set-up and that clinical RBE values derived from these studies must be used prudently.

The review of RBE data focuses on major dose-limiting organs and tissues such as skin and the gastrointestinal (GI) tract as indicators for early radiation effects, and lung and spinal cord as important late-responding organs.

5.2.1 Early Normal Tissue Responses

5.2.1.1 Skin

Skin, although not a critical organ in the stricter sense of the term, is a dose-limiting tissue in IBT as its radiation side effects can contribute significantly to both early and late patient morbidity, and has traditionally been used to study RBE effects of new radiation modalities including ion beams. In superficial tumors, proton and ion beams often have to be modulated up to the surface, resulting in intense skin reactions.

Most investigators of skin effects have irradiated the skin of one of the hind legs or feet of mice with the other foot or leg serving as control. The severity of the skin response, which evolves over several weeks and eventually recovers after a period of peak severity, is usually scored on a point scale, ranging from no visible reaction to breakdown of the entire skin [34]. Different scoring systems have sometimes been used for developing and subsiding skin effects, respectively, depending on the extent of redness, hair loss, and skin break down and healing of these side effects. Despite the subjectivity of skin scoring, Douglas and Fowler [35] found that the differences among different observers were less than the biological variation within a group of animals treated to the same dose level.

Investigators who performed comparative studies of different heavy ions [36] found that the time course of the development of skin reactions and subsequent healing was similar for all radiation modalities indicating that epithelial cell depletion and repopulation are not different when high- and low-LET radiations are compared.

Published data on RBE values for skin reactions to protons and carbon ions, supplemented by historic data for helium, argon, and neon ions [36–41] are listed in Table 5.1. They were mostly derived from mice, with the exception of the GSI carbon data, which originated from pig skin.

Table 5.1 Literature review of RBE values for acute skin reactions after irradiation of the epidermis with different ions in different locations relative to the SOBP: entrance region/plateau (pl), middle of SOBP (pk)

Ion	Energy (MeV/amu)	SOBP Wdth (cm)	Beam location	Species (Body Part)	No. of Fx	RBE (95% confidence interval)	First Author Reference No.
Proton	160	10	pk	Mouse (foot)	20	1.14 (±0.08)	Tepper [37]
	160	10	pl	Mouse (foot)	1	1.2 (±0.02)	Raju [36]
			pk			1.1 (±0.02)	
	80	1.8	pk	Mouse (leg)	1	1.15 (1.04–1.40)	Nemoto [38]
					2	1.24 (1.07–1.75)	
					4	1.15 (1.04–1.50)	
					8	1.20 (1.06–1.62)	
Carbon	400	10	pl	Mouse (foot)	1	1.2 (±0.2)	Raju [36]
			Pk			1.5 (±0.2)	
	290	6	pl[a]	Mouse (leg)	1–8	1.25–2.0	Ando [39]
			pk[b]			1.4–3.3	
	185	6	pl	Pig (back)	5	1.32	Zacharias [40]
	320	6	Pl	Mouse (leg)	4	1.30	Kagawa [41]
			Pk			2.16	
Helium	900	10	pl	Mouse (foot)	1	1.2 (±0.02)	Raju [36]
			pk				
						1.2 (±0.02)	
Neon	400	10	pl		1	2.0 (±0.02)	
			pk				
						1.7 (±0.02)	
Argon	400	10	pl		1	2.1 (±0.02)	
			pk				
						1.9 (±0.02)	

The RBE values are for the endpoint with the highest score or after the highest dose (most severe reaction)

[a]Two locations (LET 14 and 20 keV/μm)

[b]Five locations (LET 40, 50, 60, 80, and 100 keV/μm)

For protons, the mean RBE values are in the range of 1.10–1.24 with no apparent effect of fractionation on the RBE nor location in the entrance region or at the center of a SOBP. The slightly higher RBE values of the study at TRIUMPF with 80 MeV protons [38] compared to the study at the Harvard Cyclotron Laboratory (HCL) with 160 MeV protons [37] may be explained by the narrower width of the SOBP at TRIUMF (2 cm vs. 10 cm) leading to a greater concentration of low-energy protons within the SOBP.

Different from protons, the carbon RBE data for skin response show much more dependence on beam location and dose-fractionation parameters. For all ions investigated, including helium, neon, and argon, carbon has the highest RBE ratio between plateau and peak locations, which makes it the preferred high-LET ion for therapy. The most extensive preclinical studies with carbon ions have been performed at the NIRS in Japan [39]. Table 5.1 contains the RBE data from their original study on mouse skin response published in 1998. In that study, more than 1,300 mice were irradiated with either 1, 2, 4, 6, or 8 fractions for two entrance locations and five SOBP locations varying in LET from 14 to 100 keV/μm. The average of the five highest skin response scores was compared for RBE determination. It was found that the RBE increased linearly with LET for all fraction sizes. The slope of the regression lines fitted to the RBE vs. LET data was steepest for 4 fractions, while it was shallowest for the single-dose data. From their studies, the investigators concluded that a four-fraction schedule achieves the highest therapeutic gain in terms of the differential biological effectiveness of SOBP relative to the entrance region.

5.2.1.2 Gastrointestinal Tract

The microcolony assay for jejunal crypt cell survival developed by Withers and Elkind [42], has found wide application as an in vivo clonogenic assay for acutely responding tissues and has been used for intercomparison of protons, heavy ions, and neutron beams for different particle therapy programs. Briefly, in this assay the mice are killed 3–4 days after irradiation and hematoxylin-eosin histologic sections of the jejunum are prepared. The number of regenerating crypt cells per circumference is then determined according to criteria established by Withers and Elkind [42]. The average number of crypt cells per jejunal circumference is of the order of 200 cells. Assuming a Poisson distribution of the number of surviving cells per crypt, the number of surviving cells per circumference is calculated. The RBE is defined as the ratio of doses causing the same level of surviving cells per jejunal circumference, typically 10 or 20 cells.

Table 5.2 gives an overview of published RBE results [37, 43–48] for 10 or 20 surviving crypt cells per circumference obtained with protons, carbon, and other ions. Both single dose and fractionated dose data are included. An increasing effectiveness of ions is seen with heavier ions. As the ion charge and mass increases, the increase of RBE is first observed in the peak region of the SOBP and, for ions heavier than carbon, extends to the plateau region. For ions up to the charge and

mass of carbon, the quality of the plateau region radiation is almost independent of the ion species and is characterized by RBE values in the range of 1.06 and 1.25. An exception is the RBE of 1.72 for single dose and 1.57 for 10 fractions observed in the plateau region of a 135 MeV/u carbon beam with a 3 cm SOBP [48], which can be explained by the lower initial energy (the other carbon studies were done with 400 MeV/u carbon ions).

In the peak region of the SOBP, the RBE of protons and helium is around 1.20, and about 10% higher than in the plateau region. Much higher RBE values are observed for the carbon SOBP with values of the order of 1.5 for a 10 cm SOBP single dose and up to 2.5 for the 135 MeV/u carbon beam with 3 cm SOBP single dose. Distal SOBP RBEs are higher than those in the middle and proximal SOBP, an effect that is more pronounced for carbon than for protons and helium. A comparison of RBE values for single dose and fractionated dose under otherwise equivalent conditions shows a clear increase in RBE with fractionated dose delivery except for protons, where no fractionation effect is seen. The RBE increase is more pronounced for higher ion charge and mass values and in the peak compared to the plateau region. Lastly one should note that, as for skin effects, carbon has the highest plateau to peak RBE ratio (1.5–2), while for ions heavier than carbon this ratio is less than 1.

5.2.2 Late Normal Tissue Responses

Compared to the number of ion beam studies using early endpoints, there is a relative paucity of studies evaluating the late response of OARs to protons and ion beams. Late response studies are more difficult to perform because they are time consuming and expensive and often confounded by the limited life span of rodents. In the following, experimental data on late responses of lung and spinal cord to proton and ion irradiation will be presented.

5.2.2.1 Lung

Lung is an organ where complex cell kinetic changes determine the course of radiation injury [2]. The first late-effect studies on hamster lung after ion beam irradiation were performed during the 1970s by Woodruff and colleagues at the Lawrence Berkeley National Laboratory (LBL) with 375-MeV/u neon irradiation in the plateau region and 230 kV (peak power) X-rays [49]. Single-dose levels for neon irradiation ranged from 1.5 to 10 Gy and for X-rays from 2.25 to 15 Gy. One year after irradiation, the volume density of pulmonary septum, septal cells, connective tissue, and alveolar type II cells was increased, while the volume densities of alveoli, empty alveolar space and capillary lumens were decreased. The RBE of plateau neon compared to X-irradiation was 1.6–1.8 for both excess mortality (>50%) and the volume density of septal cells.

Table 5.2 Literature review of RBE values for jejunal crypt regeneration in mice after proton and ion irradiation in different locations relative to the SOBP: entrance region/plateau (pl), proximal SOBP [pk(p)], middle SOPB [pk(m)], distal SOBP [pk(d)]

Ion	Energy (MeV/amu)	SOBP width (cm)	Beam location	No. of Fx	No. of crypt cells[a]	RBE (95% confidence interval)	First Author Reference No.
Proton	160	10	pl	1	10	1.13 (±0.18)	Tepper [37]
				20		1.17 (±0.06)	
			pk(m)	1		1.19 (±0.06)	
				20		1.23 (±0.02)	
	85	3	pk(m)	1	20	1.08 (±0.03)	Kagawa [43]
	200	7	pl	1	10	1.10 (±0.03)	Gueulette [44]
			pk (p)			1.18 (±0.04)	
			pk (m)			1.12 (±0.03)	
			pk (d)			1.23 (±0.03)	
	200	7	pk (m)	1	20	1.15 (±0.04)	Gueulette [45]
				10		1.14 (±0.07)	
Carbon	400	10	pl	1	10[b]	1.10	Alpen [46]
			pk (p)			1.33	
			pk (d)			1.48	
	400	10	pl	1, 10	10	1.22, 1.25	Goldstein [47]
			pk (p)	1, 10		1.37, 1.46	
			pk (m)	1, 10		1.39, 1.63	
			pk (d)	1, 10		1.45, 1.99	
	135	3	pl	1, 3	10	1.72, 1.57	Fukutsu [48]
			pk (p)	1, 3		2.08, 2.21	
			pk (m)	1, 3		2.22, 2.43	
			pk (d)	1, 3		2.59, 2.97	
Helium	225	8	pl	1,10	10	1.06, 1.19	Goldstein [47]
			pk (d)			1.20, 1.37	

Neon	557	10	pl	1, 10	10	1.42, 1.89
			pk (p)			1.48, 2.37
			pk (m)			1.51, 2.44
			pk (d)			1.61, 2.79
Argon	570	10	pl	1, 2	10	2.07, 2.92
			pk (p)			1.91, 2.52
			pk (m)			1.96, 2.63
			pk (d)			1.79, 2.46

[a]Surviving crypt cells per circumference

[b]RBE for 10 surviving crypt cells per circumference was calculated based on the mean lethal dose (D_0) and the quasi-threshold dose (D_q) for 200 surviving crypt cells per circumference stated by the investigators

Gueulette et al. [50] performed a study providing RBE data of lung tolerance in mice at the dose causing 50% lethality (LD_{50}) with 200 MeV protons at the National Accelerator Centre in South Africa. Protons and cobalt gamma reference irradiation was given in 1, 3, or 10 fractions separated by 12 h. Proton irradiations were performed at the middle of a 7-cm SOBP and additional experiments in the distal third of the SOBP. In this large experiment, a total of 1,008 mice were irradiated, out of which 96 animals underwent autopsy for histopathological evaluation. The analysis revealed the classic signs of radiation-induced pneumonitis and interstitial fibrosis, attributed to a late chronic phase of radiation-induced lung damage. RBEs at the LD_{50} level were found to be insensitive to dose fractionation. The RBE increased with time from 1.0 at 180 days to 1.20 at 270 days (mean values of all fractionation schemes, confidence intervals approximately 20%). Irradiations in 10 fractions in the distal part of the SOBP were about 6% more effective than those at the middle part.

Doerr and coinvestigators [51] studied the response of pig lungs to fractionated irradiation with carbon ions in two experiments at the GSI, to validate the procedures for IBT planning during the late 1990s. Doses in the SOBP of a therapeutic carbon beam were prescribed to be equivalent to 5 fractions of 4 Gy, 5 Gy, and 7 Gy of X-rays in the first experiment and to 5 fractions of 7 Gy and 9 Gy in the second experiment using the LEM. In the first experiment, the lung response in the high-dose region was less than expected, which prompted the investigators to modify the equivalent doses for the second experiment. In addition, pneumonitis reaction and chronic fibrotic changes were observed outside the prescribed high-dose region in both experiments. After 9 months, changes were most intense in the high-dose region. The investigators concluded that the complex irradiation geometry of the pig lung, the changes of body weight between the two experiments, and insufficient accounting for a change in the RBE computation led to substantial deviations of the observed reactions from expectations based on the LEM. The extension of the late fibrotic reaction beyond the planned high-dose region was believed to have resulted from the smear out of the high-dose region due to density variations in tissue structures, respiratory movement, and limited positioning accuracy.

5.2.2.2 Spinal Cord

Similar to the lung, the spinal cord is an important dose-limiting tissue, which sometimes compels the radiation oncologist to underdose nearby tumor tissue. Overdosing of the cord may lead to serious and irreversible injury. Protons and ion beams have emerged as an attractive radiation modality for the treatment of such tumors, as isodoses can literally be “wrapped” around the spinal cord without exceeding tolerance.

First spinal cord studies in rats with heavy ions at LBL were reported by Leith et al. during the period of 1975–1982 [52–54]. These studies showed that, similar to high-LET neutrons, there was a fairly dramatic increase of RBE for 50% radiation myelopathy with decreasing fraction size. For carbon and neon ions, the RBE

increased from values, which were close to those reported in early-responding tissues, to values in the 4–6 range at 2 Gy per fraction and between 6 and 10 in the limit of low doses.

A series of irradiation experiments investigating the tolerance of rat spinal cord (2–20 mm in length) to proton irradiation was performed at the AGOR (Accélérateur Groningen-Orsay) cyclotron of the Kernfysisch Versneller Instituut in Groningen, Netherlands in the early 2000s. These studies were not meant to estimate the RBE of protons but rather to investigate dose-volume effects and the effect of inhomogeneous dose distributions exploiting the sharp lateral penumbra of high-energy proton beams.

In the first experiment [55], the cervical spinal cord of Wistar rats was irradiated at different lengths (2, 4, 8, and 20 mm) with a single fraction of the plateau region of an unmodulated proton beam (150–190 MeV). The goal of this study was to estimate the effective dose causing overt paralysis in the limbs in 50% of the population (ED_{50}). As expected from a serial organ, only a weak increase of ED_{50} was found when decreasing the irradiated cord length from 20 mm ($ED_{50} = 20.4$ Gy) to 8 mm ($ED_{50} = 24.9$ Gy), but a steep increase in ED_{50} was seen when decreasing the length to 4 mm ($ED_{50} = 53.7$ Gy) and 2 mm ($ED_{50} = 87.8$ Gy).

In the subsequent experiment [56], Wistar rats were irradiated with two types of inhomogeneous dose distributions (a) two 4-mm fields with 8- or 12-mm spacing between the center of the fields (referred to as split field) and (b) various combinations of relatively low doses to a large volume of 20 mm combined with high doses to a small volume of 4 mm (referred to as bath and shower). The split-field experiments showed a shift in ED_{50} from 24.9 Gy for a single 8-mm field to 45.4 Gy and 41.6 Gy for 8- and 12-mm spacing, respectively, which was closer to the ED_{50} for a single 4-mm field of 53.7 Gy. The bath and shower experiments showed a large decrease of the ED_{50} values to 15–22 Gy when compared with the 4-mm single field without low-dose bath, even with a bath dose as low as 4 Gy. This effect was not accompanied by histological changes in the low-dose bath regions of the spinal cord.

In the last experiment of this series [57], Wistar rats were irradiated with both symmetric (short and long high-dose segments at the center of a low-dose bath segment) and asymmetric (high-dose segment at the caudal end of a low-dose bath segment) dose distributions. The high-dose bath and shower experiments with a low bath dose of 4 Gy again showed a large shift in tolerance dose compared with a single-field irradiation of the same segment length (2 mm). The ED_{50} value decreased further by increasing the bath dose. Compared to the 2-mm segment, the effect of a 4-Gy bath on ED_{50} was less for the 4-mm and absent for the 8-mm high-dose segments. The asymmetry of the dose arrangement had no influence on the results. The investigators concluded that migration of glial progenitor cells could not explain these results.

Philippens et al. [58] evaluated the time dependence of the sensitizing effect a low-dose bath dose of 4 Gy by separating the low-dose irradiation by intervals of 8 min and 3, 12, and 24 h from the high-dose irradiation of the short segment. The investigators found that the low-dose bath effect diminished with increasing

time but was still noticeable at 12 h and only disappeared after 24 h. This time scale is clearly different from the repair kinetics in spinal cord derived from split dose and fractionation experiments.

Debus et al. [59] from the German Cancer Research Center investigated the radiosensitivity of the spinal cord of Sprague–Dawley rats to single and split doses of carbon ion radiation and estimated the RBE using the ED_{50} for symptomatic neurological complications (paresis grade II) relative to 15 MeV photons. The spinal cord of the rats was placed either in the plateau of a 270 MeV/u carbon beam or in the center of a 10-mm SOBP of a 140 MeV/u carbon beam at the GSI facility. The RBEs, determined from the ratio of ED_{50} values, were 1.43 ± 0.08 and 1.37 ± 0.12 for one and two fractions, respectively, of carbon plateau irradiation and 1.76 ± 0.05, and $2.16 + 0.11$ for one and two fractions, respectively, for carbon SOBP irradiation. The uncertainties were defined as RBE variation when the ED_{50} varied within 1 standard error. Histopathology revealed white matter necrosis in all symptomatic animals.

In a follow-up investigation [60], the RBE and α/β ratios of the LQ model for spinal cord complications were determined for 6 and 18 fractions, while other conditions were unchanged. The RBE values were 1.33 ± 0.02 and 1.42 ± 0.02 for 6 and 18 fractions, respectively, in the carbon plateau, and 2.97 ± 0.05 and 5.04 ± 0.08 for 6 and 18 fractions, respectively, in the SOBP. Combining data from both experiments, the α/β parameter was 2.8 ± 0.4 Gy for photons, 2.1 ± 0.4 Gy for the carbon plateau, and 37.0 ± 5.3 Gy for the carbon SOBP, demonstrating that the repair capacity in the carbon plateau was similar to that of low-LET radiation.

In summary, these experiments demonstrated that therapeutic carbon ions are significantly more effective in the SOBP than in the plateau region for spinal cord complications and that there is a relatively large increase of RBE with decreasing dose per fraction in the SOBP region.

References

1. H.B. Stone, C.N. Coleman, M.S. Anscher, W.H. McBride, Effects of radiation on normal tissue: consequences and mechanisms. Lancet Oncol. **4**, 529–536 (2003)
2. P. Rubin, C.J. Johnston, J.P. Williams, et al., A perpetual cascade of cytokines postirradiation leads to pulmonary fibrosis. Int. J. Radiat. Oncol. Biol. Phys. **33**, 99–109 (1995)
3. Z.A. Haroon, J.A. Raleigh, C.S. Greenberg, et al., Early wound healing exhibits cytokine surge without evidence of hypoxia. Ann. Surg. **231**, 137–147 (2000)
4. K.C. Flanders, Smad3 as a mediator of fibrotic response. Int. J. Exp. Pathol. **85**, 47–64 (2004)
5. W. Dörr, K. Spekl, C.L. Farrell, Amelioration of acute oral mucositis by keratinocyte growth factor: Fractionated irradiation. Int. J. Radiat. Oncol. Biol. Phys. **54**, 245–251 (2002)
6. A.B. Roberts, E. Piek, E.P. Böttinger, et al., Is Smad3 a major player in signal transduction pathways leading to fibrogenesis? Chest **120**, S43–S47 (2001)
7. B. Emami, J. Lyman, A. Brown, et al., Tolerance of normal tissue to therapeutic irradiation. Int. J. Radiat. Oncol. Biol. Phys. **21**, 109–122 (1991)

8. T.E. Schultheiss, C.G. Orton, R.A. Peck, Models in radiotherapy: volume effects. Med. Phys. **10**, 410–415 (1983)
9. H.R. Withers, J.M. Taylor, B. Maciejewski, Treatment volume and tissue tolerance. Int. J. Radiat. Oncol. Biol. Phys. **14**, 751–759 (1988)
10. P. Källman, A. Agren, A. Brahme, Tumour and normal tissue responses to fractionated non-uniform dose delivery. Int. J. Radiat. Biol. **62**, 249–262 (1992)
11. G. Gagliardi, I. Lax, A. Ottolenghi, et al., Long-term cardiac mortality after radiotherapy of breast cancer – application of the relative seriality model. Br. J. Radiol. **69**, 839–846 (1996)
12. F. Eriksson, G. Gagliardi, A. Liedberg, et al., Long-term cardiac mortality following radiation therapy for Hodgkin's disease: analysis with the relative seriality model. Radiother. Oncol. **55**, 153–162 (2000)
13. J.T. Lyman, Complication probability as assessed from dose-volume histograms. Radiat. Res. **8**, S13–S19 (1985)
14. C. Burman, G.J. Kutcher, B. Emami, et al, Fitting of normal tissue tolerance data to an analytic function. Int. J. Radiat. Oncol. Biol. Phys. **21**, 123–135 (1991)
15. G.J. Kutcher, C. Burman, L. Brewster, et al., Histogram reduction method for calculating complication probabilities for three-dimensional treatment planning evaluations. Int. J. Radiat. Oncol. Biol. Phys. **21**, 137–146 (1991)
16. A. Niemierko, Reporting and analyzing dose distributions: a concept of equivalent uniform dose. Med. Phys. **24**, 103–110 (1997)
17. L. Marucci, A. Niemierko, N.J. Liebsch, et al., Spinal cord tolerance to high-dose fractionated 3D conformal proton-photon irradiation as evaluated by equivalent uniform dose and dose volume histogram analysis. Int. J. Radiat. Oncol. Biol. Phys. **59**, 551–555 (2004)
18. J.O. Deasy, A. Niemierko, D. Herbert, et al., Methodological issues in radiation dose-volume outcome analyses: summary of a joint AAPM/NIH workshop. Med. Phys. **29**, 2109–2127 (2002)
19. L. Cozzi, A. Fogliata, A. Lomax, et al., A treatment planning comparison of 3D conformal therapy, intensity modulated photon therapy and proton therapy for treatment of advanced head and neck tumours. Radiother. Oncol. **61**, 287–297 (2001)
20. A. Fogliata, A. Bolsi, and L. Cozzi, Critical appraisal of treatment techniques based on conventional photon beams, intensity modulated photon beams and proton beams for therapy of intact breast. Radiother. Oncol. **62**, 137–145 (2002)
21. A. Jackson, L.B. Marks, S.M. Bentzen, et al., The lessons of QUANTEC: recommendations for reporting and gathering data on dose-volume dependencies of treatment outcome. Int. J. Radiat. Oncol. Biol. Phys. **76**, S155–S160 (2010)
22. International Commission on Radiation Units and Measurements, Prescribing, recording, and reporting proton-beam therapy. J. ICRU. 7, Report 78 (2007)
23. International Atomic Energy Agency and International Commission on Radiation Units and Measurements. *Relative Biological Effectiveness in Ion Beam Therapy*. Technical Report Series no 461 (International Atomic Energy Agency, Vienna, 2008)
24. International Atomic Energy Agency, *International Commission on Radiation Units and Measurements. Microdosimetry*, ICRU Report 36 (ICRU, Bethesda, MD, 1983)
25. T. Loncol, V. Cosgrove, J.M. Denis, et al., Radiobiological effectiveness of radiation beams with broad LET spectra: Microdosimetric analysis using biological weighting factors. Radiat. Prot. Dosim. **52**, 347–352 (1994)
26. M. Scholz, A.M. Kellerer, W. Kraft-Weyrather, G. Kraft, Computation of cell survival in heavy ion beams for therapy. The model and its approximation. Radiat. Environ. Biophys. **36**, 59–66 (1997)
27. R.B. Hawkins, A microdosimetric-kinetic model for the effect of non-Poisson distribution of lethal lesions on the variation of RBE with LET. Radiat. Res. **160**, 61–69 (2003)
28. J.J. Wilkens, U. Oelfke, A phenomenological model for the relative biological effectiveness in therapeutic proton beams. Phys. Med. Biol. **49**, 2811–2825 (2004)
29. T. Elsässer, M. Krämer, M. Scholz, Accuracy of the local effect model for the prediction of biologic effects of carbon ion beams *in vitro* and *in vivo*. Int. J. Radiat. Oncol. Biol. Phys. **71**, 866–872 (2008)

30. J.W. Hopewell, J. Nyman, I. Turesson, Time factor for acute tissue reactions following fractionated irradiation: a balance between repopulation and enhanced radiosensitivity. Int. J. Radiat. Biol. **79**, 513–524 (2003)
31. S.L. Tucker, Pitfalls in estimating the influence of overall treatment time on local tumor control. Acta Oncol. **38**, 171–178 (1999)
32. H.D. Thames, W. D'Souza, D.A. Kuban, Dual radiobiological interpretations of retrospective clinical data: the time factor. Int. J. Radiat. Biol. **79**, 503–509 (2003)
33. R.G. Dale, J.H. Hendry, B. Jones, et al., Practical methods for compensating for missed treatment days in radiotherapy, with particular reference to head and neck schedules. Clin. Oncol. (R. Coll. Radiol.) **14**, 382–393 (2002)
34. R.J. Berry, G. Schwarz, R.E. Ellis, et al., The effect of hypoxia on the skin response of mice to divided doses of 15 MeV electrons. Int. J. Radiat. Biol. Relat. Stud. Phys. Chem. Med. **12**, 293–296 (1967)
35. B.G. Douglas, J.F. Fowler, The effect of multiple small doses of x rays on skin reactions in the mouse and a basic interpretation. Radiat. Res. **66**, 401–426 (1976)
36. S.G. Raju, M.R. Carpenter, A heavy particle comparative study. Part IV: acute and late reactions. Br. J. Radiol. **51**, 720–727 (1978)
37. J. Tepper, L. Verhey, M. Goitein, H.D. Suit, In vivo determinations of RBE in a high energy modulated proton beam using normal tissue reactions and fractionated dose schedules. Int. J. Radiat. Oncol. Biol. Phys. **2**, 1115–1122 (1977)
38. K. Nemoto, T. Pickles, A.I. Minchinton, G.K. Lam, The relative biological effectiveness of the modulated proton beam at TRIUMF. Radiat. Med. **16**, 43–46 (1998)
39. K. Ando, S. Koike, K. Nojima, et al., Mouse skin reactions following fractionated irradiation with carbon ions. Int. J. Radiat. Biol. **74**, 129–138 (1998)
40. T. Zacharias, W. Dörr, W. Enghardt, et al., Acute response of pig skin to irradiation with 12C-ions or 200 kV X-rays. Acta Oncol. **36**, 637–642 (1997)
41. K. Kagawa, M. Murakami, Y. Hishikawa, et al., Preclinical biological assessment of proton and carbon ion beams at Hyogo Ion Beam Medical Center. Int. J. Radiat. Oncol. Biol. Phys. **54**, 928–938 (2002)
42. H.R. Withers, M.M. Elkind, Microcolony survival assay for cells of mouse intestinal mucosa exposed to radiation. Int. J. Radiat. Biol. Relat. Stud. Phys. Chem. Med. **17**, 261–267 (1970)
43. K. Kagawa, M. Murakami, Y. Hishikawa, et al., Preclinical biological assessment of proton and carbon ion beams at Hyogo Ion Beam Medical Center. Int. J. Radiat. Oncol. Biol. Phys. **54**, 928–938 (2002)
44. J. Gueulette, L. Böhm, B.M. De Coster, et al., RBE variation as a function of depth in the 200-MeV proton beam produced at the National Accelerator Centre in Faure (South Africa). Radiother. Oncol. **42**, 303–309 (1997)
45. J. Gueulette, J.P. Slabbert, L. Böhm, et al., Proton RBE for early intestinal tolerance in mice after fractionated irradiation. Radiother. Oncol. **61**,177–184 (2001)
46. E.L. Alpen, P. Powers-Risius, M. McDonald, Survival of intestinal crypt cells after exposure to high Z, high-energy charged particles. Radiat. Res. **83**, 677–687 (1980)
47. L.S. Goldstein, T.L. Phillips, G.Y. Ross, Biological effects of accelerated heavy ions. II. Fractionated irradiation of intestinal crypt cells. Radiat. Res. **86**, 542–558 (1981)
48. K. Fukutsu, T. Kanai, Y. Furusawa, K. Ando, Response of mouse intestine after single and fractionated irradiation with accelerated carbon ions with a spread-out Bragg peak. Radiat. Res. **148**, 168–174 (1997)
49. K.H. Woodruff, J.T. Leith, P. Powers-Risius, et al., Comparison of heavy particle with X-irradiation on the hamster lung. Am. J. Pathol. **95**, 765–774 (1979)
50. J. Gueulette, L. Böhm, J.P. Slabbert, et al., Proton relative biological effectiveness (RBE) for survival in mice after thoracic irradiation with fractionated doses. Int. J. Radiat. Oncol. Biol. Phys. **47**, 1051–1058 (2000)
51. W. Dörr, H. Alheit, S. Appold, et al., Response of pig lung to irradiation with accelerated 12C-ions. Radiat. Environ. Biophys. **38**, 185–194 (1999)

52. J.T. Leith, K.H. Woodruff, B.S. Lewinsky, et al., Letter: Tolerance of the spinal cord of rats to irradiation with neon ions. Int. J. Radiat. Biol. Relat. Stud. Phys. Chem. Med. **28**, 393–398 (1975)
53. J.T. Leith, K.H. Woodruff, J. Howard, et al., Early and late effects of accelerated charged particles on normal tissues. Int. J. Radiat. Oncol. Biol. Phys. **3**, 103–108 (1977)
54. J.T. Leith, M. McDonald, P. Powers-Risius, et al., Response of rat spinal cord to single and fractionated doses of accelerated heavy ions. Radiat. Res. **89**, 176–193 (1982)
55. H.P. Bijl, P. van Luijk, R.P. Coppes, et al., Dose-volume effects in the rat cervical spinal cord after proton irradiation. Int. J. Radiat. Oncol. Biol. Phys. **52**, 205–211 (2002)
56. H.P. Bijl, P. van Luijk, R.P. Coppes, et al., Unexpected changes of rat cervical spinal cord tolerance caused by inhomogeneous dose distributions. Int. J. Radiat. Oncol. Biol. Phys. **57**, 274–281 (2003)
57. H.P. Bijl, P. van Luijk, R.P. Coppes, et al., Influence of adjacent low-dose fields on tolerance to high doses of protons in rat cervical spinal cord. Int. J. Radiat. Oncol. Biol. Phys. **64**, 1204–1210 (2006)
58. M.E. Philippens, L.A. Pop, A.G. Visser, et al., Bath and shower effect in spinal cord: the effect of time interval. Int. J. Radiat. Oncol. Biol. Phys. **73**, 514–522 (2009)
59. J. Debus, M. Scholz, T. Haberer, et al., Radiation tolerance of the rat spinal cord after single and split doses of photons and carbon ions. Radiat. Res. **160**, 536–542 (2003)
60. C.P. Karger, P. Peschke, R. Sanchez-Brandelik, et al., Radiation tolerance of the rat spinal cord after 6 and 18 fractions of photons and carbon ions: experimental results and clinical implications. Int. J. Radiat. Oncol. Biol. Phys. **66**, 1488–1497 (2006)

Chapter 6
The Impact of Radiation Quality on Cure Rate

John Gueulette, Reinhard Gahbauer, Dan T.L. Jones, Jacobus Slabbert, and André Wambersie

Abstract Radiobiological data indicate that high-LET radiations are more effective than low-LET radiations in treating hypoxic, well differentiated, and slowly growing tumors. The clinical outcomes of fast neutron therapy still serve as the basis for the selection of ion beam therapy (IBT). Patient selection is a complex issue and robust predictive tests are needed and in development but not presently validated. Randomized clinical trials comparing modern high- and low-LET radiotherapy machines and treatment planning systems should be organized. For this, protocols and outcomes should be described, reported, and analyzed applying internationally accepted terminology, concepts, and approaches.

6.1 Physical Selectivity and Radiation Quality

The cure rates achieved in radiation therapy can be enhanced by increasing the physical selectivity of the irradiation and/or by improving the differential biological effect. Radiation therapy can be applied alone or in combination with surgery and medical treatment.

Physical selectivity, which enables the delivery of a high dose to the target volume(s) while reducing the dose to the surrounding normal tissues, depends on the beam characteristics, specifically the depth–dose curve and the lateral beam delineation as well as collimation, i.e., the penumbra (Fig. 6.1). Beam properties depend on the nature and energy of the beam and components in the beam delivery system (for details cf. Chap. 4).

Table 6.1 compares the complication rates after neutron therapy for different types of beam collimation: fixed inserts, rectangular moving jaws, and multileaf

J. Gueulette (✉)
Université Catholique de Louvain, UCL – IMRE 5469, Av Hippocrate 55, 1200 Brussels, Belgium
e-mail: john.gueulette@uclouvain.be

U. Linz (ed.), *Ion Beam Therapy*, Biological and Medical Physics, Biomedical Engineering, DOI 10.1007/978-3-642-21414-1_6,

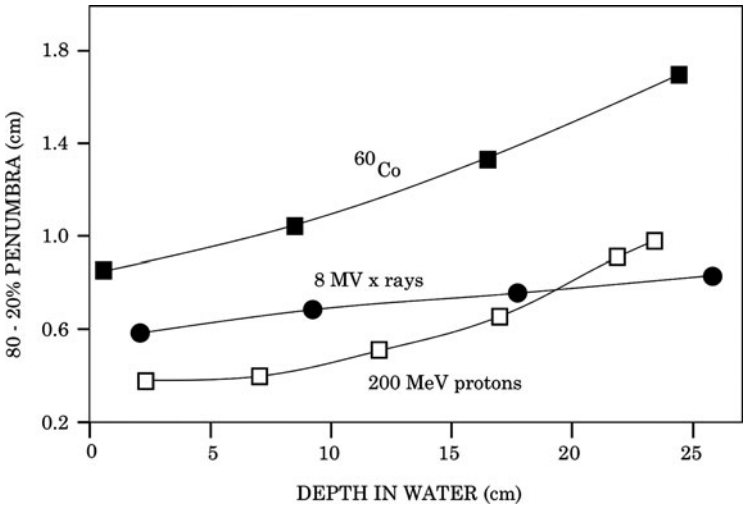

Fig. 6.1 Variation of the 80%–20% penumbrae as a function of depth for various radiation types

Table 6.1 Neutron bowel morbidity by treatment center (Data from 1993)

Institution	Colostomies
University of Washington (50 MeV p-Be, Multileaf collimator)	0/49 (0%)
UCLA (45 MeV p-Be, Movable Jaw collimator)	2/25 (8%)
M. D. Anderson (42 MeV, Fixed cone collimator)	4/10 (40%)

collimators. The table clearly illustrates the importance of collimation systems and the ability of those devices to conform the radiation fields to the target volumes. It should be emphasized that even though fast neutron therapy is limited to a few facilities today, it has provided much of today's knowledge on high-LET radiation. Radiobiological data obtained as long as 50 years ago with fast neutrons have not been contradicted by more recent findings.

Compared to photons, ion beams have the advantage of the Bragg peak which needs to be spread out (spread-out Bragg Peak, SOBP) to closely match the dimensions of the target volume. The dimensions and the depth of the SOBP can be adjusted for a given type of particle and beam delivery system, by adjusting the beam energy. The conformity of the distal edge of the SOBP to the tumor is easily achieved, but it is more difficult to achieve similar conformity to the proximal edge of the SOBP. Scanned beams and special multileaf collimators (MLCs) are needed to optimize the dose distribution proximal to the tumor. In addition to the lower dose in the entrance plateau region, the protection of the normal structures beyond the SOBP is one of the main advantages of charged-particle beams.

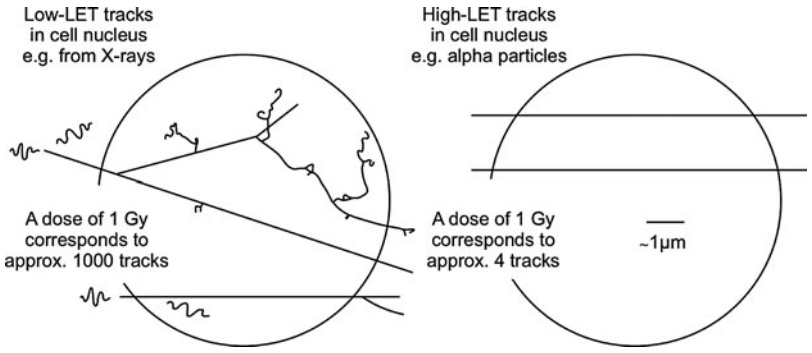

Fig. 6.2 Schematic representation of particle tracks for low-LET (*left*) and high-LET (*right*) radiation. X-rays and alpha particles (^{4}He nuclei) are chosen as examples of low- and high-LET radiations, respectively. The *circles* indicate the typical size of a nucleus for a mammalian cell (adapted from Goodhead [1] as cited in [2])

In a clinical setting, some irradiation of normal tissue is unavoidable and this limits the dose that can be delivered to the target volume. For equal doses, tumor control will improve if the biological effects on the cancer cell population can be increased, while the effects on the surrounding normal tissues are decreased. This leads to the concept of the differential radiobiological effect. Increasing the differential effect can be achieved by adjusting the time–dose distribution (e.g., dose per fraction, overall treatment time, dose rate). Further enhancement can result from combining radiation with drugs that sensitize cancer cells more than normal tissues. Finally, a differential effect can also be obtained by modifying the radiation quality. In this chapter, only the benefits related to the energy deposition at the cellular and subcellular level, as it depends on the nature and energy spectrum of the particles, are discussed.

One measure of the radiation quality is the LET (linear energy transfer) spectrum as described in Chap. 4 and illustrated in Fig. 6.2.

Besides allowing computation of the LET distribution, microdosimetry provides an experimental approach to describe the microscopic pattern of ionizations produced in a volume comparable in size to the nucleus of a mammalian cell. The lineal energy (y) for protons is moderately shifted towards high y values, which is consistent with the generic RBE value of 1.1 recommended in Report 78 of the International Commission on Radiation Units and Measurements (ICRU) [3]. In addition, the modest shift of the microdosimetric spectra as a function of depth within the SOBP explains the additional increase in RBE with depth (see Fig. 6.3). To date, no microdosimetric data are available for carbon ion beams.

6.2 From Absorbed Dose to Radiobiological Effects

Absorbed dose is a fundamental and rigorously defined quantity [7, 8]. Regardless of the type of radiation and biological system, the radiobiological and clinical effects are always a function of absorbed dose. Laboratories for national and

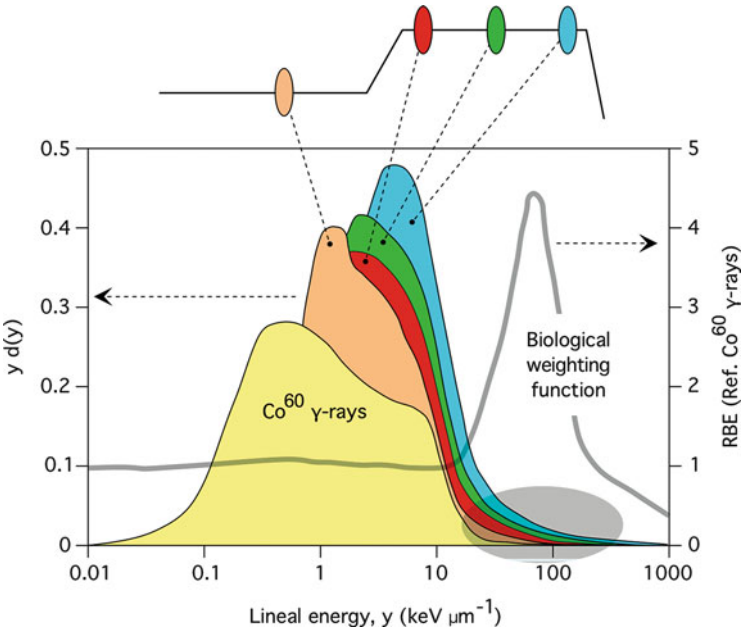

Fig. 6.3 Microdosimetry spectra (lineal energy *y*; *left hand side* ordinate) measured at different depths in a 90 MeV energy-modulated proton beam at the Université catholique de Louvain. Measurements were performed in the initial plateau (*beige*), the proximal (*red*), the middle (*green*), and the distal part (*blue*) of the SOBP (*see the sketch on top*). The biological weighting function for intestinal crypt regeneration has been superimposed (*right hand side* ordinate). This function is flat (RBE = 1) up to LET values of approximately 20 keV/μm. Then it rises rapidly, exhibiting increased RBEs up to LET values of about 100 keV/μm. As the number of single-energy deposition events between 20 and 200 keV/μm increases with depth (i.e., those events having increased RBEs, see the *shaded area*), the RBE of the proton beam increases [4–6]

international standards (e.g., Bureau International des Poids et Mesures, Sèvres, France) guarantee the accuracy and reproducibility of reference absorbed dose measurements. Dosimetry protocols for therapeutic radiations are regularly recommended and improved by medical physics associations or commissions (including ICRU). For all radiation oncology applications, the ICRU has recommended concepts and processes for reporting absorbed dose at reference points and/or in relevant volumes. This goes together with a complete description of the treatment conditions in order to allow full understanding, interpretation, and reconstruction of the treatment [9, 10].

As absorbed dose is a pure physical quantity, there is no need for any biological hypothesis or model. However, the relation between absorbed dose and biological effects is not unique but depends on several factors such as dose rate (including instantaneous dose rate), dose range, dose per fraction, overall treatment time, and other time/dose factors as well as radiation quality (LET) and dose homogeneity. Furthermore, the influence of these factors on the extent of the biological effects

depends on the biological systems and the effects considered (e.g., early or late effects, cf. the previous chapter). Thus, absorbed dose alone is not sufficient to predict the severity of the biological effects. When comparing, adding, or combining doses delivered by treatments performed under different conditions, when altering treatment protocols or designing new protocols, weighting of the absorbed doses is thus necessary. All factors that could influence the clinical outcomes have to be taken into account. The numerical values of these weighting factors may vary significantly with the biological systems or effects considered, physiological conditions of the irradiated system (e.g., degree of oxygenation, temperature), and technical irradiation conditions. They may also be influenced by the pathological conditions of the patient that are known to affect the clinical outcome, such as anemia, previous and/or concomitant chemotherapy. Lastly, comparison of total treatment doses delivered using different therapy modalities implies that they be specified in the same way. The recommendations of ICRU are an attempt to standardize these specifications and have evolved with the development of new techniques and new modalities. There has recently been a move from specifying doses at a point [9, 11] to specifying doses to volumes. Two recent ICRU reports recommend that the dose to the planning target volume (PTV) be specified at a dose level selected on the dose–volume histogram (DVH) (median dose, D_{50} or near-minimum dose, D_{98}) [3, 10].

To facilitate comparisons and combinations of treatments delivered with different therapy modalities or protocols, the concept of *isoeffective absorbed dose* was introduced jointly by the IAEA (International Atomic Energy Agency) and the ICRU for radiation therapy applications [12]. For treatments delivered with high-LET radiations, the influence of radiation quality (and the resulting RBE differences) raises complex issues that are still a matter of clinical and radiobiological debate.

6.3 RBE for the Different Radiation Qualities Used in Therapy

An RBE value can be determined for any two radiation qualities, one of them being taken as the reference. However, in order to facilitate exchange of information and reduce possible confusions, selection of a specific reference radiation quality is needed. Because of their wide availability, 180–220 kV X-rays were initially selected as the reference radiation to define the RBE values [13]. Later, higher photon energies progressively became the preferred reference [14]. No significant variation in RBE could be detected for high-energy photons in the range of that for Cobalt-60 to ~35 MeV. Differences, however, have been observed between 200 kV X-rays and gamma rays from cobalt-60.

An RBE value of 1.1 for proton beams fits best the pooled RBE values observed from in vivo studies. This value is used for all tissue types that are in the direct beam path. Therefore, the use of a generic RBE in proton therapy is judged to be clinically appropriate and has been recommended in ICRU Report 78 [3].

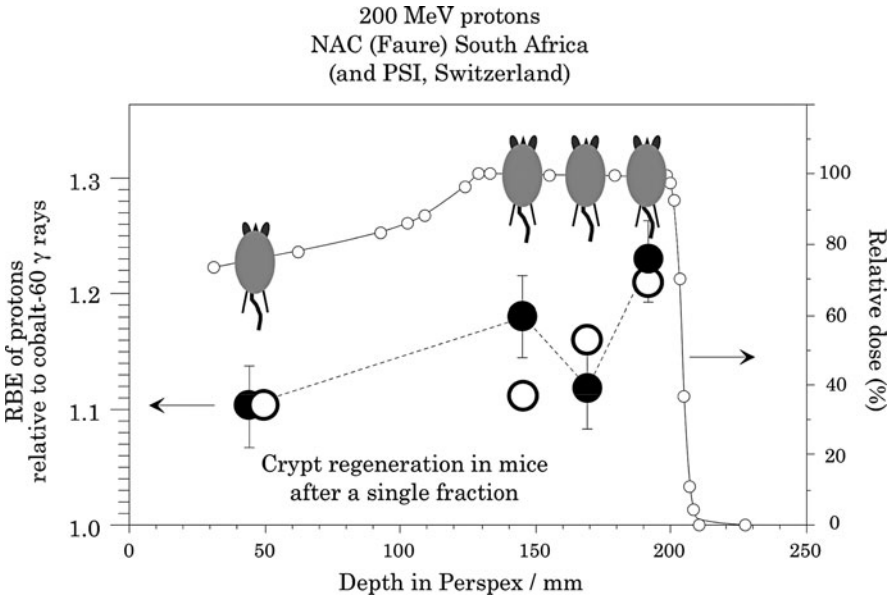

Fig. 6.4 Variation of the RBE with depth in a modulated 200 MeV proton beam produced at iThemba LABS (*closed circles*, *left* ordinate). The width of the SOBP is 7 cm. The *open circles* correspond to the RBE in the unmodulated beam. The *error bars* indicate the 95% confidence intervals. The depth–dose distribution in the modulated beam has been superimposed (*small open points*, *right* ordinate); the *shaded areas* (width = 1.5 cm) indicate the different positions of the mice

While a generic value of 1.1 is recommended by the ICRU to convert the absorbed doses to an RBE-weighted absorbed dose in a proton beam, several experimental observations suggest that an additional RBE increase of 5–10% occurs in the most distal part of the SOBP relative to the middle (Fig. 6.4). There is also evidence that the RBE increases significantly in the declining distal edge of the SOBP. This results in an effective increase in the range of the RBE-weighted dose by 1–2 mm. These effects need to be taken into account in treatment planning, especially for single-field treatments and when organs at risk are located immediately distal to the Bragg peak. However, the clinical relevance of these RBE variations is still a matter of debate. These modest radiobiological RBE variations in clinical proton beams were also expected from the microdosimetric data presented in Fig. 6.5.

The radiobiological data obtained with ions heavier than helium are similar to those from fast neutron data. The RBE increases with LET up to about 150 keV/μm – depending on the type and the energy of the ions. Beyond that LET level the RBE decreases because of the overkill effect (cf. Chap. 4 for details). Differences in the fine structure of the energy deposition of different particle types result in RBE differences for the same LET_∞ values. It indicates that LET_∞, while

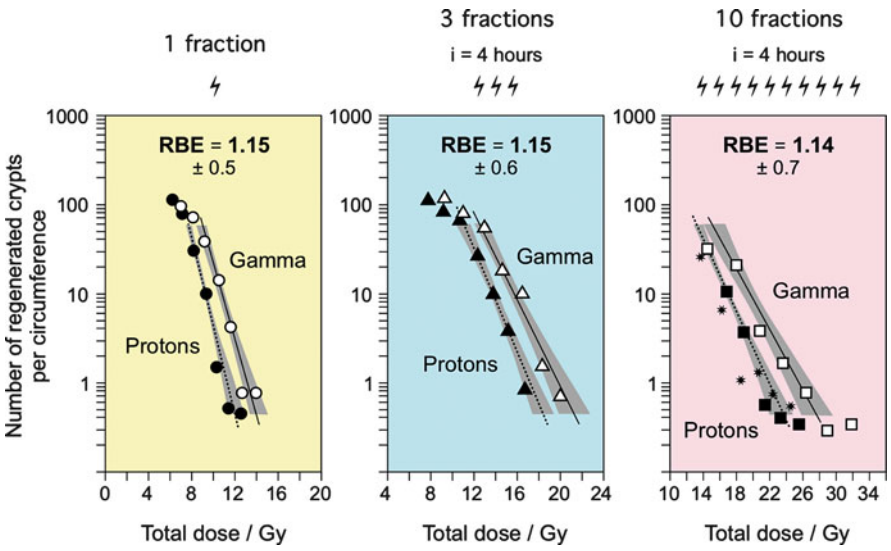

Fig. 6.5 Dose–effect relationships for intestinal crypt regeneration in mice after proton or gamma irradiation in one, three, or ten equal fractions separated by a time interval of 4 h (i). The *shaded areas* correspond to the 95% confidence interval of the slope of the curves. The proton irradiations were performed at the middle of a 7-cm SOBP. The *stars* in the 10-fraction panel correspond to proton irradiations at the end of the SOBP

Table 6.2 RBE values of modulated carbon ion beams of 290 MeV/u from the Heavy Ion Medical Accelerator (HIMAC), Chiba

Position	LET (keV/μm)	RBE values		
		Single fraction		Four fractions
		Cell culture	Skin reaction	Skin reaction
Entrance	22	1.8	2.0	
Proximal SOBP	42	2.1	2.1	2.3
	45	2.2	2.2	
Middle SOBP	48	2.2	2.3	
	55	2.4	2.3	
Distal SOBP	65	2.6	2.3	2.9
	80*	2.8	2.4	3.1
Distal fall-off	100			3.5

*Biological effects of carbon ions at LET of 80 keV/μm are similar to those of fast neutrons previously used at NIRS, Chiba.

often adequate and useful, is not a perfect predictor of RBE. Therefore, a "generic" RBE value (or even a small range of RBE values) cannot be recommended for carbon ions because of the large variations of the RBE with the irradiation conditions. This conclusion is also illustrated from the data in Table 6.2. The influence of LET on RBE with depth is shown in Fig. 6.6.

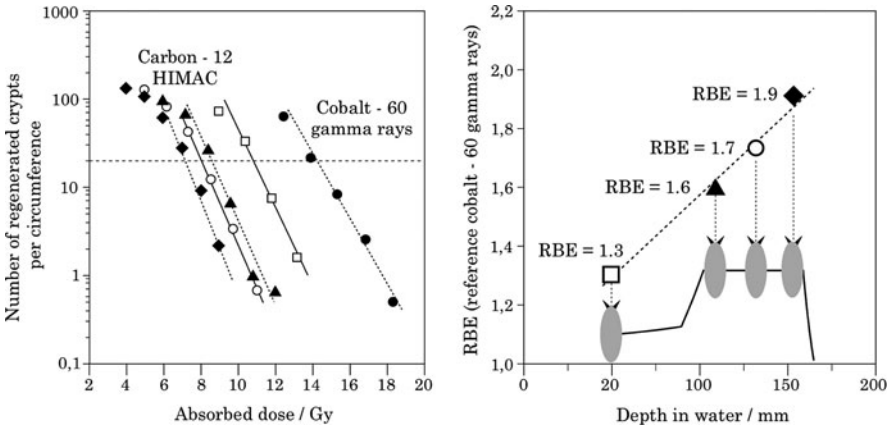

Fig. 6.6 *Left panel*: dose–effect relationships for intestinal crypt regeneration in mice after irradiation with ^{60}Co gamma rays or ^{12}C ions at the entrance plateau and at different positions in a 6-cm SOBP (the positions are shown in the sketch on the panel to the *right*). The corresponding RBEs (reference: ^{60}Co gamma rays), plotted against the depth, indicate a substantial increase of the RBE. As the irradiations were performed with single high doses, these RBEs are much lower than those for fractionated irradiations that reach a value of approximately 3 at the end of the SOBP

6.4 Criteria for Patient Selection for High-LET Radiation Therapy

Hypoxic clonogenic cells are present in most malignant tumors, generally at the level of a few percent. This is the result of fast and anarchic proliferation of the cancer cells. There is chronic hypoxia in cells at the periphery of tumor cords around the microvasculature, as well as transient hypoxia in whole cords caused by the transitory closure of these blood vessels [15]. These hypoxic cells are 2–3 times less radiosensitive to low-LET radiations than normally oxygenated cells. It can be shown that a proportion of hypoxic cells as low as 0.1% can make the tumor radioresistant to large single doses. If the reoxygenation phenomenon during fractionated treatment is inefficient, the continuing presence of hypoxic cells may make the tumor resistant to cure with low-LET radiations.

The radiosensitivity variation according to the oxygenation status is quantitatively expressed by the oxygen enhancement ratio (OER), which is defined as the ratio of the doses necessary to obtain a given biological effect according to whether the cells are irradiated in anoxic or normally oxygenated conditions. The OER for low-LET radiations (e.g., cobalt-60 gamma rays) is about 3. It continuously decreases when the LET increases, down to a value of $\sim$1.9 for carbon ions and close to unity for very high-LET radiations such as alpha particles [16].

A reduction in OER should, in principle, be an advantage when treating poorly reoxygenating tumors because most normal tissues are either well oxygenated or

are homogeneously only slightly hypoxic [15, 17]. However, there is variability in hypoxia between individual tumors, even between tumors of the same type in the same site. Highly hypoxic tumors will benefit most from treatment with high-LET radiations.

Among various techniques capable of detecting hypoxic cells (for review cf. [18]), polarography (e.g., Eppendorf probe) is the only method for which a correlation with treatment outcome has been convincingly demonstrated in different human tumor types, e.g., cervix cancer, head and neck lymph nodes, or sarcomas. Nevertheless, until now, this technique has not been routinely used due to its relatively low sensitivity at low oxygen concentrations and some logistic constraints. The use of the so-called hypoxic-cell markers (e.g., nitroimidazole, EF3, EF5) represents an attractive alternative to polarographic measurements (for review cf. [19]). However, few attempts have been made so far to use these markers for patient selection for high-LET radiation therapy. In principle, the use of cellular markers requires a representative tumor biopsy. Hence, it is only feasible to assess the initial level of hypoxia, but it is more difficult to assess reoxygenation where additional samples are needed during treatment. The requirement for repeated invasive procedures for reoxygenation measurements also applies to the Eppendorf probe. Noninvasive methods have been actively investigated. MRI signals have shown a correlation with Eppendorf probe measurements. PET imaging (e.g., with ^{18}F-misonidazole) represents another promising approach [20, 21].

Because of the large amount of energy deposited in the critical cellular target by a single high-LET particle track, the chance of successful repair of the radiation damage is less. High-LET radiation is thus particularly efficient against cancer cells that have a high capability of repair. There is also less long-term repair and more residual injury in normal tissues after high-LET irradiation [15]. The sparing of late normal tissue reactions by delivering low doses per fraction, the feature that underpins the success of hyperfractionated photon therapy, is reduced with high-LET radiations (cf. the previous chapters).

One feature of high-LET therapy is that the reduced influence of dose per fraction leaves more flexibility for selecting, changing, or shortening a fractionation scheme. Even though radiobiological data indicate a potential benefit of high-LET radiation for the treatment of inherently photon-resistant tumors, the variability in biological characteristics between patients explains why it cannot be expected to bring a benefit in all cases. This stresses the importance of patient selection [14, 17].

6.5 Quality Assurance

Two types of radiobiological experiments have to be performed before applying high-LET radiations in cancer therapy (1) pretherapeutic experiments aimed at confirming the rationale of the new radiation modality, and (2) preclinical experiments dealing essentially with RBE determinations, the results of which are aimed at the

clinical applications and the safe and optimum treatment conditions. Due to the possible RBE variations considered earlier, the clinical RBE (i.e., the ratio of the dose that would have been applied with conventional gamma radiation to the dose actually prescribed for the new type of radiation) is specific to the beam in which it was determined and to the clinical situation for which it was intended. Clinical RBE is an operational concept. Its value depends on the clinical situation and is mainly based on radiobiological experiments determining the RBE with reference to photons, for conditions that are as relevant as possible to the clinical case. These radiobiological calibration experiments are intended to provide RBE values that are representative of the average late tolerance of the normal tissues at risk (e.g., CNS, lung, skin), and for a dose level of 2 Gy gamma-ray equivalent per fraction [16].

Due to the physical and technical factors that could influence the radiation quality and the RBE values, the radiobiological and clinical information gained in a given facility cannot be transferred directly to another facility, even if the type of particle and the nominal energy of the beams are the same. Indeed, RBE differences as high as 15% are observed depending on the type of machine (cyclotron, synchrotron), beam delivery system (passive or active beam modulation for ion), type of collimator, etc. For these reasons, a third type of experiment is justified, needed, and organized in the framework of radiobiological intercomparison programs. In these experiments, the RBE of the beams of participating institutions is determined as accurately as possible for the same biological system and the same irradiation conditions. Such RBE values can further be intercompared between each other, their ratio expressing the RBE of one calibrated clinical beam with reference to another calibrated clinical beam, which would make it possible to transfer radiobiological and clinical information between institutions.

In principle, the biological system and the irradiation conditions to be used for intercomparisons should be similar to those used for the radiobiological calibration of the beam, i.e., as relevant as possible to the clinical situations. However, as pointed out by E.J. Hall more than 30 years ago, the RBE ratio between two "closely related radiation qualities" depends only to a small degree on the biological system, so that the choice of the system for intercomparison should be more dictated by its convenience, portability, and reproducibility [22]. Crypt cell regeneration in mice meets these requirements since this cell lethality-based system is essentially independent of the environmental conditions. It requires relatively simple procedures and yields reproducible results due to its steep dose–effect relationship. The suitability of the system for intercomparison purposes is recognized by the worldwide community of IBT users and neutron users alike. As a consequence, the system has been used for intercomparison of the majority of clinical proton beams worldwide and has recently been employed for intercomparison of the German and Japanese carbon therapy facilities [23, 24]. A particularly relevant example illustrating accuracy and reproducibility of the system is given in Fig. 6.7.

Radiobiological calibrations and radiobiological intercomparisons of beams are an important part of the commissioning procedure of IBT machines. Beyond

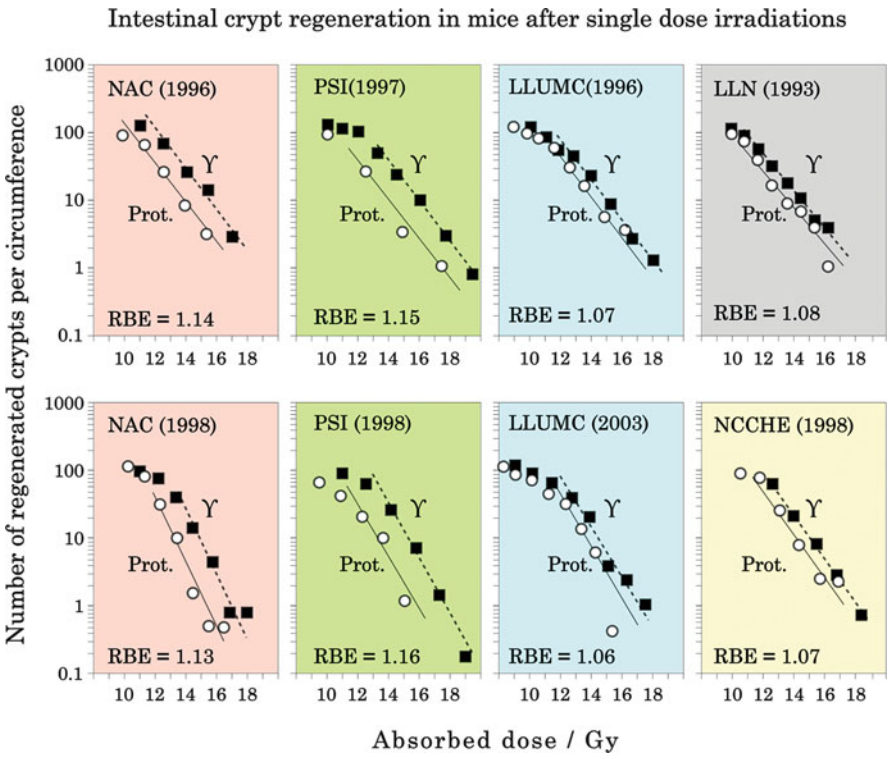

Fig. 6.7 Dose–effect relationships for crypt regeneration in mice after irradiation with protons or ^{60}Co gamma rays. The incident proton beam energy was more than 190 MeV at all facilities (except at LLN, where it was 70 MeV). The proton irradiations were performed at the middle of a 7-cm SOBP and in the middle of a 3-cm SOBP at LLN. The biological system provides RBE values with confidence intervals as small as ±4%, which is compatible with the dose accuracy required in radiation therapy. The system is also particularly reproducible as shown by the similarity of the RBE values obtained at the same institutions for experiments separated by several years. *LLN* Louvain-la-Neuve (Belgium); *LLUMC* Loma Linda University Medical Center, Loma Linda (USA); *NAC* National Accelerator Center, iThemba (South Africa); National Cancer Center Hospital East, Kashiwa (Japan); *PSI* Paul Scherrer Institute, Villigen (Switzerland)

establishing the safety of the irradiations, they are an essential step towards the optimization of the treatments. In this regard, the necessary implementation of intramural or multicenter clinical trials and the pooling of clinical data require harmonization of the concepts and of the terminology used in prescribing, conducting, recording, and reporting the treatments. Agreements are particularly important in expressing the biologically effective dose and the specific location of interest. In this respect, guidelines can be found in different ICRU reports, namely Report 50 [14], 62 [9], and 71 [11].

6.6 Conclusions

Radiobiological data indicate that high-LET radiation is more effective than low-LET radiation for treating hypoxic, well differentiated, and slowly growing tumors. Hypoxic tumors or hypoxic zones in the target volume can now be identified with modern imaging techniques. Areas of rapidly proliferating cells can also be identified using radiopharmaceuticals. Based on the experience with fast neutrons and carbon ions, approximately 20% of the patients referred to therapy departments could benefit from high-LET radiation treatment.

Patient selection between low- and high-LET radiations is a radiobiological issue and it is not related to the technique or the type of machine. It is still complex and difficult because of the lack of accurate and robust predictive tests. A large number of studies carefully undertaken to establish the clinical outcomes of fast neutron therapy still serves as the basis for the initial selection of patients for modern high-LET IBT. This approach was adopted by the two centers with the largest experience in carbon ion therapy: NIRS Chiba, Japan, and DKFZ Heidelberg together with GSI Darmstadt, Germany. Both clinical teams had previous experience with fast neutron therapy.

The recent and important progress in surgery, chemotherapy, and photon irradiation techniques may eventually moderate the gains expected from the use of high-LET radiation. However, the improved physical selectivity of modern ion beam equipment provides new opportunities for high-LET irradiation of selected tumors (e.g., high doses in complex-shaped targets close to critical normal tissues). Modern treatment planning techniques also allow high- and low-LET radiations to selectively target different parts of the tumor volumes (e.g., salivary gland protocols recently applied at the new IBT facility in Heidelberg, Germany). Finally, for all new therapy modalities, it is important that protocols and results be described, reported, and analyzed applying the terminology, concepts, and approaches that are internationally accepted. This would enable investigators to compare, evaluate, interpret, and understand clinical observations in an unambiguous manner [3, 14].

References

1. D.T. Goodhead, Radiation effects in living cells. Can. J. Phys. **68**, 872–886 (1990)
2. M. Tubiana, *Radiobiologie, Radiothérapie et Radioprotection* (Hermann Médecine, Paris, 2008)
3. International Commission on Radiation Units and Measurements (ICRU) and International Atomic Energy Agency (IAEA). Prescribing, recording and reporting proton-beam therapy. ICRU Report 78, jointly with the IAEA. J ICRU 7 (2007)
4. J. Gueulette, M. Octave-Prignot, B.M. De Coster, et al., Intestinal crypt cell regeneration in mice: a biological system for quality assurance in non-conventional radiation therapy. Radiother. Oncol. **73**(Suppl 2), S148–S154 (2004)
5. T. Loncol, V. Cosgrove, J.M. Denis, et al., Radiobiological effectiveness of radiation beams with broad LET spectra: Microdosimetric analysis using biological weighting factors. Radiat. Protect. Dosim. **52**, 347–352 (1994)

6. H.G. Menzel, P. Pihet, A. Wambersie, Microdosimetric specification of radiation quality in neutron radiation therapy. Int. J. Radiat. Biol. **57**, 865–883 (1990)
7. Bureau International des Poids et Mesures (BIPM), *The International System of Units (SI)*, 8th edn. (BIPM, 92312 Sèvres Cedex, 2006)
8. International Commission on Radiation Units and Measurements (ICRU), *Clinical Proton Dosimetry – Part 1: Beam Production, Beam Delivery and Measurement of Absorbed Dose.* ICRU Report 59 (ICRU, Bethesda, MD, USA, 1998)
9. International Commission on Radiation Units and Measurements (ICRU), *Prescribing, Recording and Reporting Photon Beam Therapy*: Supplement to ICRU Report 50. ICRU Report 62 (ICRU, Bethesda, MD, USA, 1999)
10. International Commission on Radiation Units and Measurements (ICRU), *Prescribing, Recording and Reporting Intensity-Modulated Photon-Beam Therapy (IMRT).* ICRU Report 83, J ICRU (in press)
11. International Commission on Radiation Units and Measurements (ICRU), *Prescribing, Recording and Reporting Electron Beam Therapy*. ICRU Report 71, Journal of the ICRU (Oxford University press, Oxford, 2004)
12. International Atomic Energy Agency (IAEA) and International Commission on Radiation Units and Measurements (ICRU), *Relative biological effectiveness in ion-beam therapy*. IAEA-Technical Report Series 461 (IAEA, Vienna, Austria, 2008)
13. International Commission on Radiological Protection (ICRP), Report of the RBE Subcommittee to the International Commission on Radiological Protection (ICRP) and the International Commission on Radiation Units and Measurements (ICRU). Health Phys. **9**, 357–386 (1963)
14. International Commission on Radiation Units and Measurements (ICRU). *Prescribing, Recording and Reporting Photon Beam Therapy*. ICRU Report 50 (ICRU, Bethesda, MD, USA, 1993)
15. J.H. Hendry, Quantitation of the radiotherapeutic importance of naturally-hypoxic normal tissues from collated experiments with rodents using single doses. Int. J. Radiat. Oncol. Biol. Phys. **5**, 971–976 (1979)
16. G.W. Barendsen, The relationship between RBE and LET for different types of lethal damage in mammalian cells: biophysical and molecular mechanisms. Radiat. Res. **139**, 257–270 (1994)
17. A. Wambersie, J.H. Hendry, J. Gueulette, et al., Radiobiological rationale and patient selection for high-LET radiation in cancer therapy. Radiother. Oncol. **73**(Suppl 2), S1–S14 (2004)
18. H.B. Stone, J.M. Brown, T.L. Phillips, R.M. Sutherland, Oxygen in human tumors: correlations between methods of measurements and response to therapy. Radiat. Res. **136**, 422–434 (1993)
19. J.A. Raleigh, M.W. Dewhirst, D.E. Thrall, Measuring tumor hypoxia. Sem. Radiat. Oncol. **6**, 37–45 (1996)
20. S.M. Evans, A.V. Kachur, C.Y. Shiue, et al., Noninvasive detection of tumor hypoxia using the 2-nitroimidazole [18F]EF1. J. Nucl. Med. **41**, 327–336 (2000)
21. P. Mahy, M. De Bast, P.h. Levêque, et al., Preclinical validation of the hypoxic tracer 2-(2 nitroimidazol-1- yl)-N-(3,3,3-[18F]trifluoropropyl)-acetamide, [18F]-EF3. Eur. J. Nucl. Med. Mol. Imaging **3**, 1263–1272 (2004)
22. E.J. Hall, A. Kellerer, Review of RBE Data for Cells in Culture, in *High LET Radiations in Clinical Radiotherapy*. ed. by G.W. Barendsens, J. Broerse, K. Breur. (Pergamon, Oxford, 1979), pp. 171–174
23. A. Uzawa, K. Ando, S. Koike, et al., Comparison of biological effectiveness of carbon-ion beams in Japan and Germany. Int. J. Radiat. Oncol. Biol. Phys. **73**, 1545–1551 (2009)
24. A. Uzawa, K. Ando, Y. Furusawa, et al., Biological intercomparison using gut crypt survivals for proton and carbon-ion beams. J. Radiat. Res. **48**(Suppl A), A75–A80 (2007)

Part III
Models and Preclinical Studies

Chapter 7
Monte Carlo Methods for Dose Calculations

Katia Parodi

Abstract Monte Carlo (MC) methods are increasingly being used at ion beam therapy (IBT) centers to support various dosimetric aspects of treatment planning, from characterization of the beam delivery to forward recalculation of treatment plans. This chapter will review the basic principles of Monte Carlo methods for dose calculations in therapy with protons and heavier ions, discussing the roadmap for clinical application and ongoing investigations at different IBT centers.

7.1 Introduction

Clinical dose calculations of IBT typically rely on pencil beam algorithms, which are considered to offer a reasonable compromise between accuracy and computational speed for inverse treatment planning in current daily clinical practice. The basic idea of pencil beam algorithms is to model the dose delivery to the complex and heterogeneous patient tissue as dose deposition to a patient-specific water-equivalent system in beam's eye view. According to a typical ray tracing from the beam origin to the target volume for each pencil beam or elementary beamlet in which the pencil beam can be decomposed, scaling in depth of the beam range is performed on the basis of the planning X-ray Computed Tomography (CT) image of the patient [1–3]. This is accomplished using facility- and CT-scanner-dependent semiempirical calibration curves between the CT numbers and the ion water-equivalent path length [4, 5] for correction of tissue inhomogeneities along the beam path. The dose deposition in the transformed water-equivalent system

K. Parodi (✉)
Heidelberger Ionenstrahl-Therapiezentrum, Im Neuenheimer Feld 450, 69120 Heidelberg, Germany
e-mail: katia.parodi@med.uni-heidelberg.de

U. Linz (ed.), *Ion Beam Therapy*, Biological and Medical Physics, Biomedical Engineering, DOI 10.1007/978-3-642-21414-1_7,

is then obtained as a properly weighted superimposition of several Bragg peaks. For each considered contribution, the three-dimensional Bragg peak is typically modeled on the basis of prestored or interpolated one-dimensional (central beam axis [1] or laterally integrated [2]) depth–dose profiles in water, complemented by a fixed or depth-dependent two-dimensional lateral spread. The latter off-axis dose contribution is typically assumed to be symmetrically distributed in both the lateral directions according to a single or double Gaussian function, depending on whether only multiple Coulomb scattering of the primary ion beam or also the additional broadening, e.g., due to nuclear products is taken into account [6]. For ions heavier than protons, detailed characterization – in terms of ion energy and charge – of the mixed radiation field resulting from the fragmentation of the primary beam may be additionally required at different penetration depths in water in order to enable biologically based dose calculations [2,7]. More information on pencil beam algorithms as implemented in most of the available ion treatment planning systems (TPS) can be found in [1,2].

Although several efforts have been made over the last years in order to improve the performances of pencil beam algorithms and analytical dose calculations [3,8], typical limitations remain in terms of achievable accuracy in the presence of large tissue heterogeneities or metallic implants. Especially in the case of highly conformal scanned beam delivery, the reliability of the dose calculation engine is of crucial importance for full clinical exploitation of the benefits promised by IBT. Therefore, increasing attention has lately been devoted to MC statistical methods as promising and powerful computational tools for more realistic description of the ion transport and interaction in matter. Indeed, the intrinsic three-dimensional transport capabilities and the faithful representation of the physical interactions undergone by the primary ion beam and the resulting secondary products can help overcome the traditional limitations of analytical pencil beam algorithms, which essentially rely on calculations in water with corrections for tissue inhomogeneity. Although the extensive computational times required still prevent the usage of full MC in clinical routine for dose optimization, MC methods are being increasingly used at state-of-the-art IBT facilities to support several aspects of dose calculation and treatment planning.

7.2 MC Codes for IBT

The suitability of an MC code for application to IBT demands a reliable description of the electromagnetic and nuclear processes which are responsible, on the one hand, for the favorable energy deposition pattern, and, on the other hand, for the alteration/degradation of the primary radiation field while penetrating the tissue. Especially in the case of ions heavier than protons, accurate simulation of the mixed radiation field is required for correctly performing not only physical but also biologically based dose calculations. Reliable prediction of emitted secondary

radiation is also of utmost importance in other emerging areas of research not covered here, such as in vivo treatment verification [9, 10] and risk estimation of secondary cancer induction [11].

Simplified MC solutions tailored to ion (proton) beam therapy treatment planning have already been developed in the last years to combine the advantages of MC statistical methods with a certain number of approximations for the sake of computational efficiency [12–14]. The latter is an extremely important criterion for the applicability of MC methods to inverse dose optimization for eventual clinical treatment planning. However, the main focus is given in the following to full MC implementations which do not introduce approximations for guaranteeing the highest flexibility and accuracy in arbitrarily complex situations, at the expense of still too long computational times for MC-based inverse planning.

At present, full MC applications to IBT have been based on established general purpose codes such as Geant4 [15], FLUKA [16, 17], MCNPX [18], PHITS [19], and Shield-HIT [20]. All these codes were originally developed for high energy physics and are capable to transport a large variety of particles in a wide energy interval, typically from few kiloelectron volt up to several teraelectron volt. Among these codes only Shield-HIT is not supporting the transport of electromagnetic radiation, which is in general not a stopper for performing dose calculations in continuous-slowing-down approximation. However, this might be a limitation for specific applications requiring explicit transport of secondary electrons and positrons as well as propagation of gamma radiation, e.g., for in vivo treatment verification techniques.

The intrinsic suitability of MC methods for a straightforward simulation of particle transport and interaction without resorting to the often complex approximations and models of analytical algorithms was nicely formulated by Rogers and Biekajew for electromagnetic radiation: “The Monte Carlo technique for the simulation of the transport of electrons and photons through bulk media consists of using knowledge of the probability distributions governing the individual interactions of electrons and photons in materials to simulate the random trajectories of individual particles. One keeps track of physical quantities of interest for a large number of histories to provide the required information about the average quantities” [21]. Similar to the problem posed by electron transport, the large number of Coulomb interactions experienced by ion beams in matter (more than 10^6/cm [12]) prevents the simulation of single collision events, as it would be required for a so-called analog simulation approach. Instead, all the above-mentioned codes exploit a “condensed history” technique where the cumulative effect of several “small-effect” interactions can be grouped into relatively few condensed history “steps” by sampling the necessary physics information (e.g., changes of the particle energy, direction, and position) from appropriate distributions of grouped single interactions, like multiple Coulomb scattering or stopping power [22]. In the typically adopted “class II scheme” [23], a distinction is done between “soft” and “hard” collisions, where the former are subject to the condensed history grouping approach while the latter are explicitly simulated in an analog matter. In certain cases, the user can control the boundary between the two categories by inserting appropriate thresholds, such as the definition of

the energy above which explicit delta-electron production is simulated. Particle transport is then performed according to the following four major steps [22]:

- Random selection of the distance to the next "hard" interaction
- Transport of the particle to the interaction site taking into account geometry constraints as well as the cumulative effect of soft collisions
- Random selection of the interaction type
- Simulation of the selected interaction

These steps are iterated until the primary ions and all the descendent secondaries are either locally absorbed (in an inelastic interaction or when falling below the transport threshold) or escape from the simulation geometry.

The main differences between the several codes lie in the models implemented for taking into account the relevant electromagnetic and nuclear physical processes. In general, different strategies are followed by the code developers, giving preference either to theory- or data-driven implementations. Of course, even in the case of theory-driven approaches, the models have to be accurately benchmarked against available data. On the other hand, the scarcity of experimental nuclear cross sections in the energy range of therapeutic interest, in combination with the complexity of the physical correlations to be preserved, makes the usage of purely data-driven implementations for IBT difficult. Without going into detail on the available models and options of the different codes, it should be mentioned that extensive benchmarking activities between the major codes are currently being performed or proposed in the framework of several projects. Similarly, experimental campaigns aiming to extend the nuclear cross section databases are under way. Nevertheless, careful definition of the controllable input physics settings and detailed benchmarking of the MC results against data measured at the individual facilities will likely remain mandatory for reliable application of general purpose MC codes to accurate dose calculations. Fortunately, many codes already support the users by means of predefined physics settings tailored to IBT applications. Still, computational times could largely benefit from deeper investigations on the fine tuning of the optimal transport and production cuts, to avoid spending unnecessary computational time in simulating processes which have only a marginal impact on the dose calculation at the typical millimeter grid used for treatment planning. Moreover, efficiency-enhancing methods like variance reduction are largely established in MC applications for photon and electron radiotherapy [22], whereas in IBT they have so far only marginally been explored [24, 25]. Therefore, improved exploitation of these strategies in the future together with the constantly increasing computing power and the possibilities of parallel computing open perspectives for an eventual application of full MC methods in daily clinical routine and, maybe, even inverse planning for IBT.

Besides the major criterion based on the reliability of the physical models for correct reproduction of the relevant processes in the energy range of therapeutic interest, further factors may influence the preference for a given MC code. Desirable features are, e.g., the capability to import complex geometries including clinical CT scans or to have user-friendly built-in scoring options available. Graphical user interfaces for easy preparation of input files and postprocessing/visualization of

the results, as well as the flexibility for customization of the code to the desired applications at the own facility would be further assets. Although efforts of the several code developers are ongoing in order to ease the burden at the user level, MC implementations reported so far have typically required dedicated and time-consuming user interactions in order to tailor the general purpose codes to the specific needs of IBT at the different treatment sites.

7.3 The Roadmap for MC Dose Calculations in IBT

7.3.1 Modeling of the Beam Delivery System

After the choice of a suitable MC code, the first step to apply an MC method to dose calculation in IBT is the modeling of the beam delivery. This does not refer to the entire simulation of the accelerator complex and of the high-energy beam transport lines in vacuum, but involves only the modeling of the beam line in the last few meters prior to the isocenter of the treatment unit, where the patient is located.

Regardless of the selected ion species, a major distinction between scattered and scanned beam delivery systems is necessary. The former requires detailed modeling of a large amount of components of the beam nozzle which are used in order to broaden (laterally: scatterers and/or wobbling magnets; longitudinally: range modulators) and shape (laterally: collimators; longitudinally: compensators) the patient-specific irradiation field, in addition to the standard beam monitors like transmission ionization chambers. Differently, scanning of pencil beams intrinsically involves only a reduced number of nonpatient-specific materials in the beam line, namely the transmission detectors of the beam monitor system and the few additional optional passive elements which may be used to broaden too narrow Bragg peaks (ridge or ripple filters) or degrade the beam energy (bolus or range shifter). Main considerations with relevant examples of MC implementations for both beam delivery strategies are addressed in the following.

Scattered Beam Delivery. Similar to the challenges in MC modeling of linear accelerator treatment heads in conventional photon and electron therapy [22], the description of the nozzles used to deliver scattered ion beams requires the disclosure of technical drawings and detailed information on the geometry and elemental composition of the various components by the vendors. Moreover, it may require special solutions to import complex geometrical shapes into the MC program, which cannot simply be modeled from the supported regular predefined shapes. Part of the nozzle setup is fixed and patient independent, like in the case of the permanently installed beam monitor system. Therefore, its implementation in the MC geometry needs to be done only once. Other components used for lateral and longitudinal shaping of the beam delivery are specific to the individual patient and treatment field, and thus require the coupling to the treatment planning and/or control system for complete generation of the treatment head geometry. Moreover, elements like

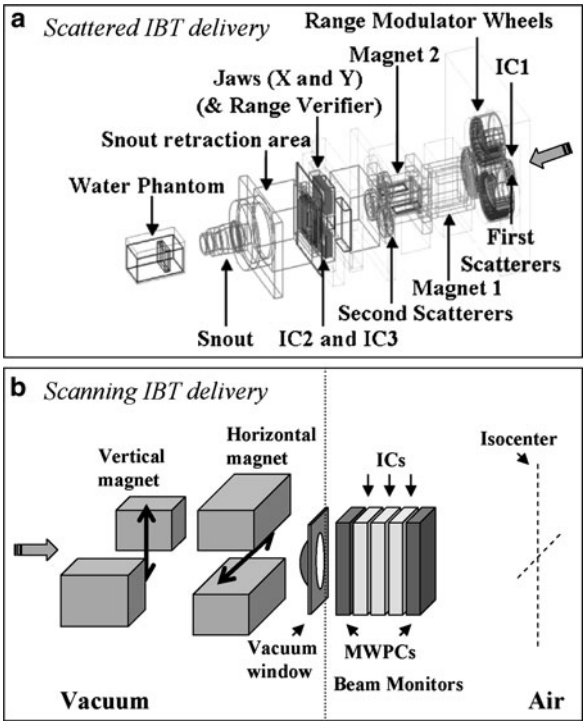

Fig. 7.1 *Top*: Geant4 MC implementation of the universal treatment nozzle for proton therapy at the FHBPTC, adapted from [26]. The beam monitors (ionization chambers, ICs, and range verifier), beam shaping devices (scatterers, range modulationwheel, variable collimator jaws and snout), and wobbling magnets are marked. The beam enters from the right (*arrow*) and is directed to a water phantom. Patient-specific devices to be mounted on the snout are not included in this configuration. *Bottom*: Schematic representation (not to scale) of the scanning beam line at the Heidelberg Ion-Beam Therapy Center (HIT), taken into account in the FLUKA MC implementation of Parodi et al. [30]. The beam enters from the left. Only the permanently installed dipole magnets, the vacuum window, and the beam monitors (ICs and multiwire-proportional chambers, MWPCs) prior to the isocenter are depicted

the beam modulation wheel or the wobbling magnets introduce time-dependent modifications of the irradiation field, to be accounted for by summation of separate simulations or, in a more elegant way, by dynamic update of the geometry or magnetic field settings in the same MC run.

Over the last years an increasing number of groups have reported application of general purpose MC codes to the modeling of beam nozzles at their own IBT facility [26–29]. The example shown in Fig. 7.1 (top) is taken from the pioneering work at the Francis H. Burr Proton Therapy Center (FHBPTC) [26]. A dedicated implementation based on the Geant4 MC code was developed for accurate modeling of the universal gantry treatment nozzle, designed to support the entire spectrum of proton beam delivery strategies from passive broad-beam

modulation to wobbling and, ultimately, scanning, which was, at that time, still under implementation. Various novel solutions needed to be implemented in the MC package for geometrical description of irregularly shaped objects in the beam path, such as contoured scatterers and patient- and field-specific apertures or compensators. Automation was achieved by generating the treatment head setup on the basis of software from the treatment control system and by creating the patient- and field-specific devices via import and interpretation of the TPS files which specify machining of these elements. Dynamic upgrades of the MC settings within the same run were also handled for four-dimensional (i.e., in time and space) simulation of passive range modulation via the rotating wheel or lateral beam broadening via the wobbling magnets. This was achieved by establishing a correlation between the known time dependence and the number of transported primary protons with related secondaries for each considered setting. Introduction of time-dependent geometries for modeling the modulation wheel in passive proton beam delivery was first reported, however, in the work of Biaggi and colleagues [31] using the FLUKA MC code to characterize the ocular beam line of the Paul Scherrer Institute (PSI).

Similar to MC applications for photon therapy, particle transport in the treatment head is a time-consuming process and the loss of primaries in the field-shaping process must be properly accounted for to achieve the desired counting statistics of events reaching the target volume. Final phase-space information on the particle type, position, energy, and direction at the exit of the treatment head can be stored in a file for repeated successive use, e.g., for dose calculations in water and patient CT.

Scanning Beam Delivery. Delivery of scanned ion beams requires less permanently installed items in the beam line (vacuum window and beam monitors, Fig. 7.1 bottom), and only a few fixed-shape elements (ripple/ridge filter, range shifters) which can be introduced into the beam path on demand, depending on the patient treatment field and the passive or active energy selection system. Detailed modeling of the transmission beam monitor system is, in general, not strictly required, especially for ions heavier than protons which are less sensitive to scattering. If information from the manufacturer is unavailable, the approximation as thin layers of measured water-equivalent thicknesses may be adequate, except for precise characterization of the beam perturbations introduced by high Z materials, such as the metallic wires of position-sensitive multiwire proportional chambers [30, 32]. Instead, accurate description of the optional beam shaping devices like the ripple filter is mandatory to correctly reproduce the longitudinal modulation and position of the pristine Bragg peaks, together with the influence on lateral beam scattering.

In addition to modeling of the beam line elements in MC geometry, beam scanning also requires the dynamic delivery of a specified fluence of pencil-like ion beams of selected energy and lateral dimension to each prescribed position in the target volume. Lateral magnetic deflection of the individual pencil beams can be simulated by using either the explicit modeling of the magnetic field of the scanning magnets or the information on beam spot position and focus at isocenter as specified by the TPS. Both approaches have been implemented [26, 33, 34].

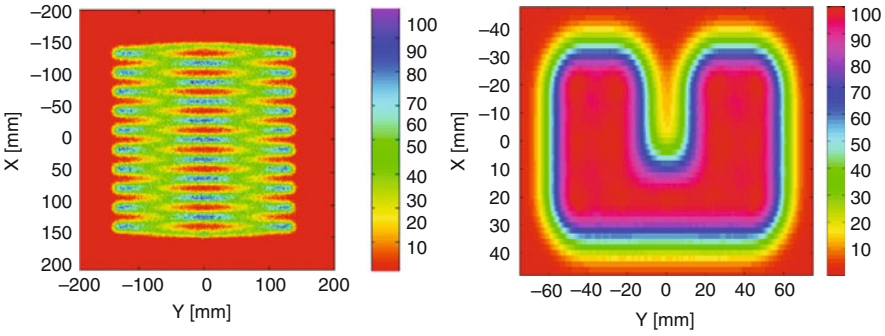

Fig. 7.2 Example of MC-simulated scanning patterns for proton beam delivery implemented in the Geant4 code using the explicit definition of the dipole magnetic fields (*left*, [35]) and in the FLUKA code using the geometrical deflection as defined by the TPS (*right*, adapted from [34])

Examples of scanned patterns are shown in Fig. 7.2. Both methods should actually be equivalent if the correspondence between magnetic field settings and geometrical beam deflection is known.

Regardless of the preferred approach, the MC simulation must be able to handle the input information from the TPS and/or the beam control system for sampling the field-specific properties of the manifold pencil beams building up the entire dose delivery. If for the sake of execution time only a fraction of the total number of ions from the treatment plan is transported, preservation of the relative weight of the different pencil beams must be guaranteed by proper sampling. Since transport in the relatively simple beam line geometry is not as time-consuming and beam modifying as in the case of passive treatment heads, saving the intermediate phase-space beam information prior to entering the phantom or patient target geometry is, typically, not needed.

7.3.2 Dose Calculations in Phantoms

Dose calculations in phantoms are the necessary step to validate the dedicated MC calculation frameworks coupled to the specific beam delivery system at each individual facility. Comparisons with dosimetric measurements have, first of all, to include depth- and lateral-dose profiles in water for pristine and extended Bragg peaks without patient-specific beam modifiers (Fig. 7.3, left). These data enable verification of the activated physical models and fine tuning of the transport parameters for an optimal tradeoff between computational accuracy and speed. In particular, adjustment of sensitive parameters of the average energy loss calculation, such as the ionization potential of water I_w, is mandatory in order to bring the MC ion range calculation in water in agreement with that measured for the same nominal beam energy at each specific facility. This is not only necessary for performing

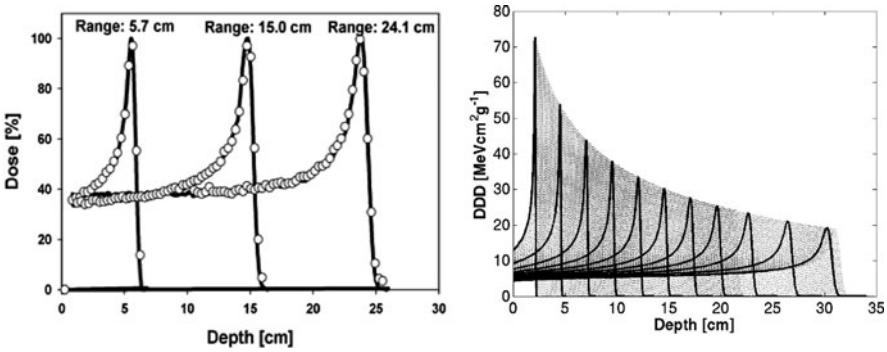

Fig. 7.3 *Left*: Measured (*solid lines*) and Geant4-simulated (*open circles*) pristine depth–dose curves of proton beams in water for different settings of modulator wheel and double scattering system at the FHBPTC [35, 36] (cf. Fig. 7.1, *top*). *Right*: Database of 255 laterally integrated depth–dose distributions (DDD) in water calculated with the MC code FLUKA for pencil-like proton beams at HIT [30] (cf. Fig. 7.1, *bottom*). These data have been stored in the TPS and are used clinically

accurate dose calculations in water, but also to guarantee the correspondence between the range predicted by the TPS and the MC computational engines when using the same CT-range calibration curve, as addressed in the next section. Indeed, several groups have reported different I_w values needed to match the ion ranges or Bragg peaks calculated by MC simulation to the experimental ones. However, rather than uncertainties in the physical quantity itself, the spread of values in the literature reflects mainly the different implementations of energy loss calculations in the miscellaneous codes in combination with likewise small variations of the actual beam energies for the same nominal value at different facilities. In combination with the refinement of the MC physics and transport settings, certain initial beam parameters may also need adjustment if not accurately known or for better reproduction of the measured data. In particular, the beam momentum spread influences the width, height, and distal slope of pristine Bragg peaks. Thus, it can be adjusted on the basis of experimental Bragg curves. Initial beam spot size and angular distributions, on the other hand, mainly affect lateral profiles, especially in beam scanning. Therefore, cross-field fluences in air can be acquired and compared with the MC calculations to validate the characterization of the initial beam profile and the modeling of its transport in the beam line. The additional scattering contribution of the target medium to the overall beam broadening can be assessed in comparison with lateral dose distributions sampled at different depths in water. Further verifications of the MC calculation platforms typically include phantoms with heterogeneities and/or the coupling with patient-specific beam modifiers or beam scanning patterns. As with any other computational engine, all the experimental validations require correct understanding of the influence of the chosen detector systems on the measured data for meaningful comparisons.

Once confidence in the MC engine is gained through dedicated benchmarking against dosimetric measurements of different complexity, the validated MC code can even be used to generate the physical basic data required by the TPS, with a considerable reduction of beam time and related costs. This has been the strategy followed, for example, at the Heidelberg Ion Beam Therapy Center (HIT). Laterally integrated depth–dose distributions in water have been calculated for protons (Fig. 7.3, right) and carbon ion beams with and without the optional ripple filter element on the basis of the FLUKA code, after detailed benchmarking against a representative set of measured Bragg curves [30]. The resulting MC depth–dose data have been given in input to the commercial TPS and are in clinical use for both ion species since the start of patient treatment in November 2009.

In addition to basic data generation, MC tools can be applied to validate dose calculations in pure water or with additional tissue heterogeneities, to support TPS commissioning or further improvement of analytical pencil beam algorithms [34, 37]. Eventually, reliable MC forward recalculations of planned treatment fields in water could replace the time-consuming dosimetric plan verification, which is at the moment routinely performed for each individual clinical treatment field prior to the first day of treatment. MC calculation engines can also be useful tools for sensitivity studies on the influence of different nozzle or beam line components on the dose delivery, e.g., to optimize nozzle or beam line design [26, 27], or for risk assessment on the consequences of erroneous beam applications due to misaligned beam line elements [26] or incorrect pencil beam parameters [38, 39].

7.3.3 Dose Calculations in the Patient CT

After validation and fine tuning of MC dose calculations in phantoms, the computational framework can be further extended to perform forward recalculation of treatment plans in the patient geometry. This requires, first of all, the capability to handle the imaging data from the X-ray CT and time-efficient tracking algorithms for particle transport in voxel geometries [9, 35, 40]. Depending on the chosen code, the translation of the CT image into the MC target geometry can be performed either via direct import of the CT dataset (typically in DICOM or binary format), or mediated by a preprocessor capable to convert the native format of the diagnostic image into a suitable format for input in the MC. An intermediate conversion step is necessary regardless of the data format if the CT image consists of slices of different thicknesses and the respective MC code does only support voxel geometries of fixed slice thickness. Handling CTs of variable slice thickness has already been reported [35, 40], however, it is not the standard. In fact, most institutions and TPS still use CTs of fixed slice thickness. Moreover, CTs with nonequidistant slice spacing tend to exhibit coarser regions outside the tumor area, while a finer and constant thickness is usually employed in the tumor region itself. Thus, the original data in the region of therapeutic interest need not be altered, usually, even if rebinning of the original CT into a grid of equidistant slice separation is needed [9].

Once the CT image is interpreted and imported into the MC voxel geometry taking into account its orientation relative to the beam delivery, additional information must be extracted from the CT Hounsfield Unit (HU) values for particle interaction and transport. In contrast to the ion TPS approach, which relies on the conversion of HU numbers into stopping power ratios relative to water, MC calculations need exact information on the material of the simulated geometry. Conversion of the CT values into material properties can be done on the basis of published data suggesting semiempirical relationships between HU numbers and tissue density and elemental composition, referred to as CT-stoichiometric calibrations [41, 42].

In order to reduce the number of material definitions in the MC procedure and for the sake of faster initialization and reduced memory requirements, the many thousands of gray values in the CT image can be segmented into a smaller amount of HU intervals sharing the same material properties. In the application of MC to conventional photon and electron radiation, emphasis is given to the HU conversion into mass or electron density, and in general only a coarse differentiation of about five tissue types from air to bone is introduced. For IBT, a higher granularity is required because ion interactions are more sensitive to the specific tissue properties. Typically, more than 20 HU intervals of different elemental composition are defined for MC segmentation to represent patient tissue in IBT, mainly following the stoichiometric calibration of Schneider et al. [42]. But even a finer CT-to-tissue segmentation is still insufficient for accurate MC calculations in IBT, since both electromagnetic and nuclear interactions do vary within the grouped HU intervals sharing the same elemental composition and "nominal" mass density. Therefore, special features were introduced, e.g., in the Geant4 [35,40] and FLUKA [9, 17, 43] codes, to correct the "nominal" into the "real" mass density in each voxel during particle transport, using the HU-mass density calibration curve proposed by Schneider et al. [42]. HU-dependent tuning of the MC stopping power calculation was also introduced during runtime to force the MC to reproduce the same CT-range calibration curve (i.e., stopping power ratio to water) as used by the TPS. This adjustment requires (1) calibration of the MC engine to reproduce the same range in water as the TPS (see above) and (2) determination of the (approximately energy-independent) MC stopping power ratio to water for the different HU values on the basis of the defined material segmentation and the "real" density. The resulting correction factors of the MC energy loss calculation are defined from the ratio between the HU-dependent CT-range calibration curve of the TPS and the determined MC stopping power ratios to water. This approach enables a straightforward comparison between the performances of pencil beam algorithms and MC dose calculations in the heterogeneous patient tissue, without introducing uncertainties from different ion beam ranges in the two computational systems (Fig. 7.4). Indeed, the intrinsic accuracy of untuned MC range calculations in the patient CT would be critical due to the unavoidable limitations of stoichiometric calibration curves (especially, if based on single-energy CT scanners) for correct representation of real tissue composition at the voxel level, together with the uncertainties in the knowledge of real tissue physical parameters (e.g., ionization potential) which may strongly influence the energy loss calculation [45].

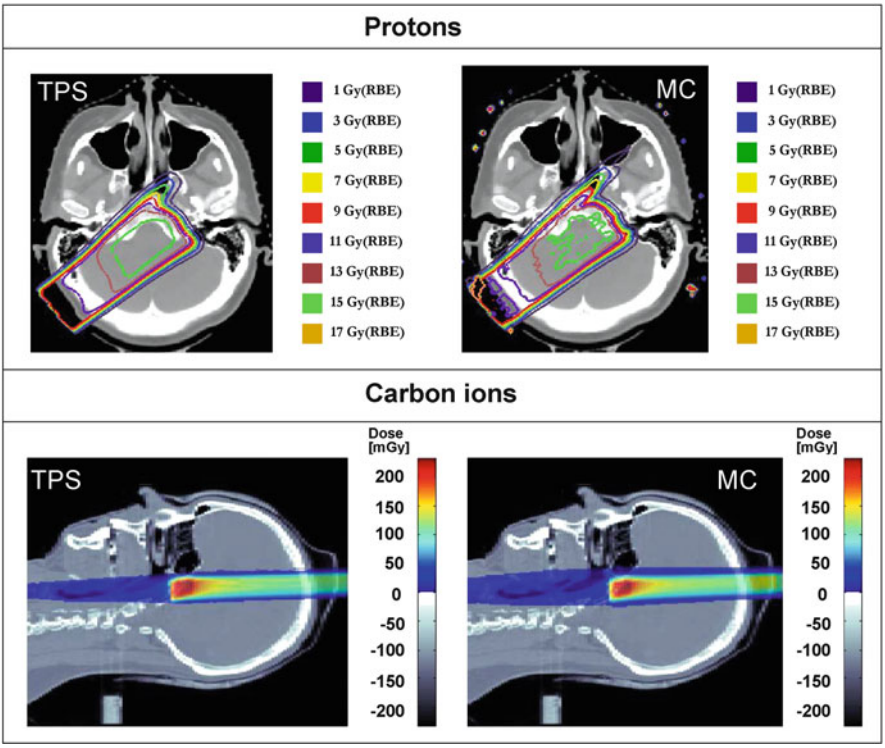

Fig. 7.4 Comparison between clinical doses calculated by TPS (*left*) or by forward recalculations based on MC engines (*right*) using the same CT-range calibration curve. The *top right panel* refers to the Geant4 MC implementation of Paganetti et al. [35] in comparison to the XiO TPS (Computerized Medical Systems Inc., *left*) for a para-spinal tumor treated with scattered proton beams at FHBPTC. The "Gy(RBE)" notation refers to the multiplication of the MC physical dose with a constant factor of 1.1. The *lower right panel* depicts FLUKA MC calculations (*right*, [44]) in comparison to the TRiP TPS (*left*, [2]) for a clivus chordoma patient treated with scanned carbon ions at the GSI

While particle transport should be performed on the CT grid for more detailed characterization of the physical beam interactions, dose deposition can be stored on the typically coarser TPS grid for a straightforward comparison with the planned dose. Using a larger dose grid than the original CT grid offers improved computational efficiency because a reduced amount of primary particles is required to achieve the same tolerable level of statistical uncertainty in the target volume (typically 2–2.5%) [22, 35]. However, the more time-consuming calculation of dose deposition on the original CT grid may still be desirable to analyze MC dose distributions at their maximum resolution [35].

Whereas TPS pencil beam algorithms represent the human tissue as water equivalent and thus report absorbed dose to water D_{w}, MC simulations calculate dose to tissue D_{m}. Due to the different dependency of energy loss on elemental

composition, the differences between dose to water and dose to tissue can exceed 10% in dense, high-Z bone materials. It can be argued that the more realistic consideration of tissue composition in MC calculations should enable a more realistic description of the treatment field interaction in the patient and thus a more reliable CT-based dose calculation. However, clinical dosimetry protocols and clinical experience have been so far based on dose to water, which is also the most important medium for assessment of the radiation action on the cell. Therefore, it is still debated whether dose to tissue should be preferred in the future, e.g., for dose prescription and other dose-related metrics, over the traditional dose to water [22, 46]. As long as the issue is not solved, it is recommended to provide the MC results also as dose to water D_{w} to make them comparable to the traditional TPSs [22]. The converted MC D_{w} should represent the dose to a small volume of water embedded in the actual medium. In conditions of charged particle equilibrium and if neglecting the influence of nuclear interactions, the conversion can simply rely on the Bragg–Gray cavity theory, $D_{\mathrm{w}} = D_{\mathrm{m}}(S/\rho)_{\mathrm{w/m}}$, where $(S/\rho)_{\mathrm{w/m}}$ represents the spectrum-averaged unrestricted water-to-medium mass collision stopping power ratio at the point of interest. If the energy dependence of the relative stopping power is further neglected and only the primary ion beam species are accounted for, the conversion method can be applied retroactively after the MC dose calculation has been completed.

A more detailed calculation has to be performed during runtime to account for the energy- and particle-dependent relative stopping power, as well as for the additional contribution of nuclear reactions to the energy deposition and, ideally, also to the more complex perturbation of the particle fluences in the different media. A comprehensive methodology for implementation and comparison of three different approaches of increasing accuracy has recently been proposed by Paganetti for MC simulations in scattered proton beam therapy [47]. The analysis of 33 treatment fields for five patients confirmed deviations of up to 10% between D_{w} and D_{m} in bony anatomy while only negligible changes were observed in soft tissue, similar to the findings reported for photon therapy [48]. The approximate retroactive conversion method neglecting energy dependence and nuclear reaction effects was found to be sufficiently accurate for mean dose computations, but insufficient for analysis of beam range where the energy dependence of the stopping ratio matters.

For heavier ions, the situation is far more challenging, due to the more relevant role of nuclear interactions causing a complex mixed radiation field. Moreover, the focus for clinical treatments with heavier ion beams is mostly on biological rather than physical dose calculations, as will be addressed in the next section. Therefore, when absorbed dose is considered and no conversion method applied, special care and cautious judgment is required for comparing TPS and MC clinical dose calculations. Shortcomings of the TPS beam modeling have to be recognized and distinguished from intrinsic physical differences between dose to water and dose to tissue.

7.4 Biological Dose Calculations

Dose calculations with MC methods in phantoms are implicitly intended to simulate physical absorbed dose, unless dedicated studies on cell survival or other biological quantities are performed. For clinical dose calculations in the patient, the absorbed dose needs to be corrected for the difference in relative biological effectiveness (RBE, cf. Chap. 4 for details) in order to allow comparison with clinical trials and protocols using conventional photon and electron radiation. In clinical practice of proton therapy a constant RBE of 1.1 is adopted, so that the conversion from physical to RBE-weighted biological dose is only a multiplication factor. For heavier ions, the situation is far more complicated due to the complex dependence of RBE on the components of the mixed radiation field, the irradiated tissue types, and the biological endpoints. Similar to the challenging task for TPS to take this complexity into account for optimized treatment plans, MC computational engines need to be capable to perform at least forward biological dose recalculations in order to support clinical routine in IBT centers using ions heavier than protons.

MC-based biological calculations of complex DNA lesions in water using the FLUKA code were already published for the PSI ocular proton beam back in 1999 [31]. More recent investigations aiming to implement MC calculations of RBE-weighted biological dose for heavier ion beams on the basis of different biological models have been reported using Geant4, FLUKA, and PHITS, respectively [44, 49–52]. Kase et al. [49] adapted the Geant4 code to follow the same approach used in the dedicated TPS for scattered carbon ion therapy at the National Institute of Radiological Sciences (NIRS) in Chiba, Japan. They define biological dose as the product of the physical dose and the RBE at 10% surviving fraction for human salivary gland tumor cells. Despite the simplification of using the LET-dependent alpha and beta parameters of the linear quadratic model for carbon ions only, and regardless of ignoring the mixed field composition, satisfactory results were obtained for the examined case in pure water [49]. The main differences were attributed to the simplified one-dimensional beam model currently used in the NIRS TPS, in comparison to the intrinsic three-dimensional spread of the radiation field in the MC calculation. The approach of Sato et al. [52] extended the capabilities of the PHITS code to accommodate RBE-weighted dose calculations based on the newly proposed microdosimetric kinetic model (MKM) of Hawkins [53]. The authors validated their simulation technique against measurements in different slab phantoms, recognizing its potential to help optimize treatment planning of charged-particle therapy. Indeed, the clinical relevance might increase in the near future if MK models will be incorporated in the next generation of TPS for IBT. Finally, the implementation of RBE-weighted biological calculations in the FLUKA code based on the framework of the Local-Effect-Model (LEM) by Scholz and coworkers [54] deserves to be mentioned [44, 50, 51]. LEM has been used for more than 10 years to plan the clinical treatments in the pilot carbon ion therapy project at the Helmholtzzentrum für Schwerionenforschung (GSI), and is now included in the first commercial TPS for scanned ion beams (syngo^{TM} PT planning, Siemens). Run-time

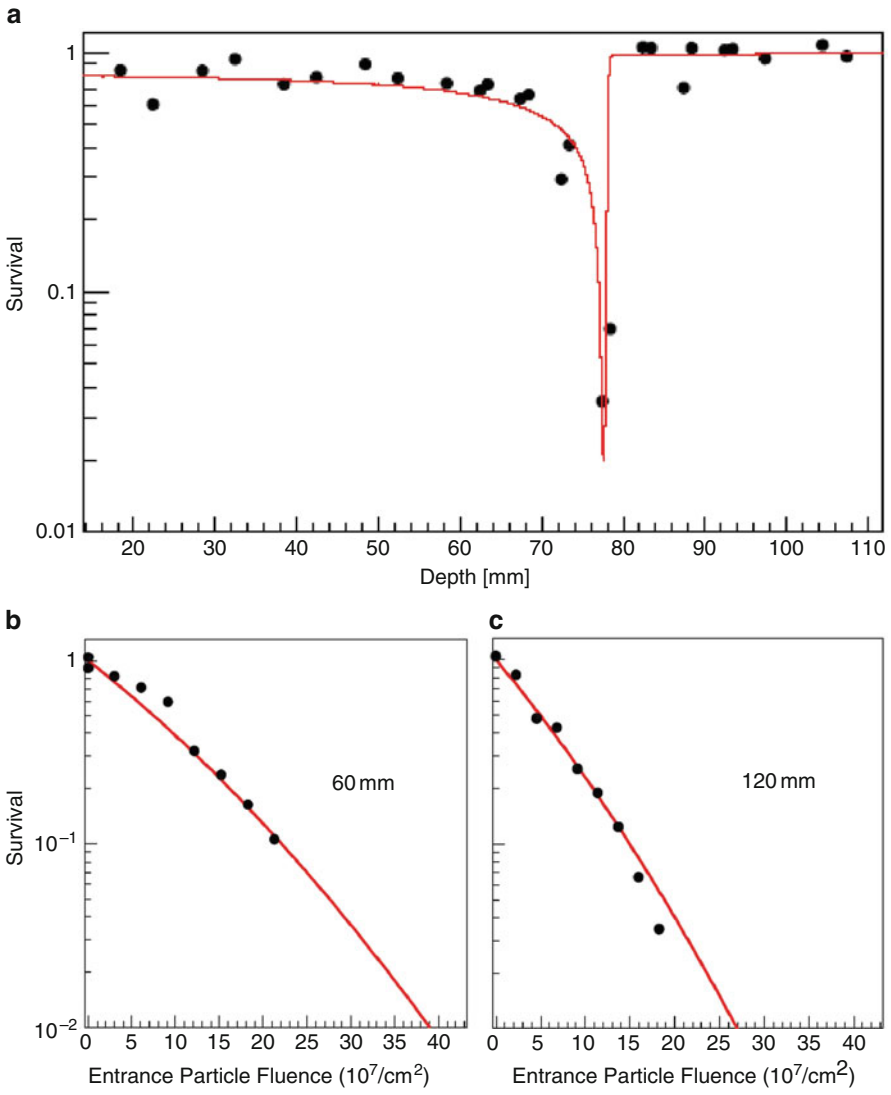

Fig. 7.5 Clonogenic survival of Chinese hamster ovary cells after monoenergetic carbon ion irradiation. The calculations based on the coupling of the FLUKA MC code with the LEM framework are depicted in *red* and benchmarked against measured data (*black full circles*), after [44]. The comparisons are shown as a function of depth in water for (**a**) an initial beam energy of 187 MeV/u and a fluence of $2 \times 10^7/\text{cm}^2$ (*top*), and at water penetration depth of (**b**) 60 mm (*bottom left*) and (**c**) 120 mm (*bottom right*) as a function of the entrance particle fluences for an initial energy of 270 MeV/u

coupling of the MC transport to the LEM framework was validated against cell survival measurements for monoenergetic beams and SOBP fields [44,50] (Fig. 7.5). Successful application to CT-based physical and biological dose calculations has also been demonstrated in comparison to TPS predictions for clinical data [44, 51].

This MC approach will also be used at HIT. Here, the same FLUKA code has been applied to generate the physical input data for the TPS not only of laterally integrated depth dose distributions (see above and [30]) but also of the mixed radiation field in water, the so-called fragment spectra of the primary carbon ion beams [2,44]. Thus, the MC implementation does not only share the same LEM framework and input RBE tables as the TPS for consistent biological dose calculations, but the TPS itself relies on a physical beam model based on physical data from the same MC engine. This is a comfortable situation for a fair comparison between MC and TPS calculations of physical and biological dose. In fact, differences can only be attributed to the approximations introduced by the analytical pencil beam algorithms in comparison to the intrinsic three-dimensional spread of the radiation field in the more sophisticated and time-consuming MC calculations.

7.5 Conclusion

MC calculation tools are commonly recognized as the computational gold standard for accurate dose calculations in IBT. Indeed, the quest for improved tumor–dose conformality and safe dose-escalation studies in IBT has been accompanied by an increasing use of MC methods to support validation and improvement of TPS pencil beam algorithms, and, lately, to generate accurate physical input data for direct use in clinical TPS. Nowadays, most active IBT centers have dedicated MC computational frameworks based on general purpose codes and customized to their specific needs. All the investigations reported so far support the superiority of MC dose calculations as compared to fast-performing analytical TPS algorithms, especially in the case of large tissue heterogeneities or metallic implants (Fig. 7.6).

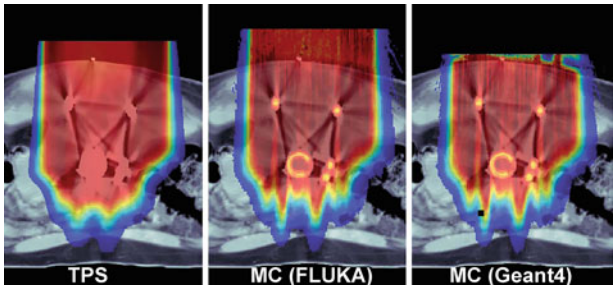

Fig. 7.6 Comparison between a TPS-planned dose (XiO, CMS) for scattered proton beam delivery at FHBPTC and its forward recalculation using two different MC codes (*center*: FLUKA, *right*: Geant4) but the same initial phase space and the same CT-range calibration curve as the TPS. Consistent discrepancies are found between the TPS dose based on a pencil beam algorithm and its recalculation by the two different MC engines, due to the presence of large tissue heterogeneities and metallic implants in this para-spinal case. The differences between the MC doses in the air outside the patient are due to a different scoring implementation and thresholding beyond the patient skin and are of no clinical relevance

MC forward recalculations of treatment plans are important not only for retrospective analysis of the dose delivery in treated patients, but also for prospective revisitation and improvement of the planning process in specific critical cases prior to therapy and, possibly, also for general improvement of pencil beam methods and planning strategies for better future clinical treatments of different tumor indications with different ion species and beam delivery systems.

Ultimately, validated MC methods might eventually replace analytical pencil beam algorithms in the more complex task of inverse dose optimization for real treatment planning, as is the current trend in radiotherapy with conventional photon and electron radiation. Although this latter step will probably be associated with the development of certified commercial solutions, it can be assumed that the described implementations based on general purpose codes will remain important computational tools at the different facilities. Besides offering the advantage of full MC gold standards for benchmarking the time-optimized dedicated solutions, the described programs may serve as powerful and flexible research platform for many other MC applications. These include a large variety of topics from the estimation of shielding to the assessment of secondary cancer induction from secondary neutrons, or the determination of irradiation-associated "surrogate" signals for in vivo treatment verification techniques like positron emission tomography or prompt gamma imaging. In conclusion, it can be predicted that the emerging MC techniques will play an increasing role in the upcoming years supporting and promoting high-precision IBT.

References

1. L. Hong, M. Goitein, M. Bucciolini, et al., A pencil beam algorithm for proton dose calculations. Phys. Med. Biol. **41**, 1305–1330 (1996)
2. M. Krämer, O. Jäkel, T. Haberer, et al., Treatment planning for heavy-ion radiotherapy: physical beam model and dose optimization. Phys. Med. Biol. **45**, 3299–3217 (2000)
3. N. Kanematsu, M. Komori, S. Yonai, A. Ishizaki, Dynamic splitting of Gaussian pencil beams in heterogeneity-correction algorithms for radiotherapy with heavy charged particles. Phys. Med. Biol. **54**, 2015–2027 (2009)
4. B. Schaffner, E. Pedroni, The precision of proton range calculations in proton radiotherapy treatment planning: experimental verification of the relation between CT-HU and proton stopping power, Phys. Med. Biol. **43**, 1579–1592 (1998)
5. E. Rietzel, D. Schardt, T. Haberer, Range accuracy in carbon ion treatment planning based on CT-calibration with real tissue samples. Radiother. Oncol. **23**, 2–14 (2007)
6. E. Pedroni, S. Scheib, T. Böhringer, et al., Experimental characterization and physical modelling of the dose distribution of scanned proton pencil beams. Phys. Med. Biol. **50,** 541–561 (2005)
7. M. Krämer, M. Scholz, Rapid calculation of biological effects in ion radiotherapy. Phys. Med. Biol. **51**, 1959–1970 (2006)
8. H. Szymanowski, U. Oelfke, Two-dimensional pencil beam scaling: an improved proton dose algorithm for heterogeneous media. Phys. Med. Biol. **47**, 3313–3330 (2002)
9. K. Parodi, A. Ferrari, F. Sommerer, H. Paganetti, Clinical CT-based calculations of dose and positron emitter distributions in proton therapy using the FLUKA Monte Carlo code. Phys. Med. Biol. **52**, 3369–3387 (2007)

10. F. Sommerer, F. Cerutti, K. Parodi, et al., In-beam PET monitoring of mono-energetic ^{16}O and ^{12}C beams: experiments and FLUKA simulations for homogeneous targets. Phys. Med. Biol. **54,** 3979–3996 (2009)
11. C.Z. Jarlskog, H. Paganetti, Risk of developing second cancer from neutron dose in proton therapy as function of field characteristics, organ, and patient age. Int. J. Radiat. Oncol. Biol. Phys. **72**, 228–235 (2008)
12. M. Fippel, M. Soukup, A Monte Carlo dose calculation algorithm for proton therapy. Med. Phys. **31**, 2263–2273 (2004)
13. A. Tourovsky, A.J. Lomax, U. Schneider, E. Pedroni, Monte Carlo dose calculations for spot scanned proton therapy. Phys. Med. Biol. **50**, 971–981 (2005)
14. R. Kohno, Y. Takada, T. Sakae, et al., Experimental evaluation of validity of simplified Monte Carlo method in proton dose calculations. Phys. Med. Biol. **48**, 1277–1288 (2003)
15. S. Agostinelli, J. Allison, K. Amako, et al., Geant4 – a simulation toolkit. Nucl. Instrum. Methods Phys. Res. A **506**, 250–303 (2003)
16. G. Battistoni, S. Muraro, P.R. Sala, et al, The FLUKA Code: Description and Benchmarking, in *Proceedings of the Hadronic Shower Simulation Workshop Fermilab*, Batavia, IL, Sept 6–8, 2006, ed. by M. Albrow, R. Raja; AIP Conf Proc 896, 31–49
17. A. Ferrari, P.R. Sala, A. Fassò, J. Ranft, *FLUKA: A Multi-particle Transport Code*. CERN Yellow Report CERN 2005–10 (CERN, Geneva, 2005)
18. J.F. Briesmeister, *MCNP – A General Monte Carlo N-Particle Transport Code*. Los Alamos National Laboratory. Report No. LA-12625-M, 1997
19. K. Niita, T. Sato, H. Iwase, et al., PHITS-a particle and heavy ion transport code. Radiat. Meas. **41**, 1080–1090 (2006)
20. A.V. Dementyev, N.M. Sobolevsky, Shield – universal Monte Carlo hadron transport code: scope and applications. Radiat. Meas. **30**, 553–557 (1999)
21. D.W. Rogers, A.F. Bielajew, Monte Carlo Techniques of Electron and Photon Transport for Radiation Dosimetry, in *Dosimetry of Ionizing Radiation*, vol. 2, ed. by B. Bjarngard, K. Kase, F. Attix. (Academic, New York, 1990), pp. 427–539
22. I. Chetty, B. Curran, J.E. Cygler, et al., Report of the AAPM task group No. 105: issues associated with clinical implementation of Monte Carlo-based photon and electron external beam treatment planning. Med. Phys. **34**, 4818–4853 (2007)
23. M.J. Berger, Monte Carlo Calculation of the Penetration and Diffusion of Fast Charged Particles, in *Methods in Computational Physics*, ed. by S. Fernbach, B. Alder, M. Rotenberg. vol. 1 (Academic, New York, 1963), pp. 135–215
24. J.S. Li, B. Shahine, E. Fourkal, C.M. Ma, A particle track-repeating algorithm for proton beam dose calculation. Phys. Med. Biol. **50**, 1001–1010 (2005)
25. P. Yepes, S. Randeniya, P.J. Taddei, W.D. Newhauser, A track-repeating algorithm for fast Monte Carlo dose calculations of proton radiotherapy. Nucl. Technol. **168**, 736–740 (2009)
26. H. Paganetti, H. Jiang, S.Y. Lee, H.M. Kooy, Accurate Monte Carlo simulations for nozzle design, commissioning, and quality assurance for a proton radiation therapy facility. Med. Phys. **31**, 2107–2118 (2004)
27. M.W. Swanepoel, D.T.L. Jones, Use of Monte Carlo software to aid design of a proton therapy nozzle. Nucl. Instrum. Methods Phys. Res. A **580**, 145–148 (2007)
28. A. Stankovskiy, S. Kerhoas-Cavata, R. Ferrand, et al., Monte Carlo modelling of the treatment line of the Proton Therapy Center in Orsay. Phys. Med. Biol. **54**, 2377–2394 (2009)
29. Y. Zheng, W.D. Newhauser, J.D. Fontenot, et al., Monte Carlo simulation model of the M. D. Anderson Cancer Center's passively scattered proton therapy machine. J. Nucl. Mater. **361**, 289–297 (2007)
30. K. Parodi, A. Mairani, S. Brons, et al., The application of the FLUKA Monte Carlo code to basic data generation for clinical treatment planning of scanned proton and carbon ion therapy, in *Proceedings of the European Workshop on Monte Carlo Treatment Planning*, Cardiff, United Kingdom, Oct 19–21, 2009. http://www.mctp2009.org
31. M. Biaggi, F. Ballarini, W. Burkard, et al., Physical and biophysical characteristics of a fully modulated 72 MeV therapeutic proton beam: model predictions and experimental data. Nucl. Instrum. Methods Phys. Res. B **159**, 89–100 (1999)

32. G. Sawakuchi, U. Titt, D. Mirkovic, et al., Monte Carlo investigation of the low-dose envelope from scanned proton pencil beams. Phys. Med. Biol. **55**, 711–721 (2010)
33. S.W. Peterson, J. Polf, M. Bues, et al., Experimental validation of a Monte Carlo proton therapy nozzle model incorporating magnetically steered protons. Phys. Med. Biol. **54**, 3217–3229 (2009)
34. K. Parodi, S. Brons, F. Cerutti, et al, The FLUKA code for application of Monte Carlo methods to promote high precision ion beam therapy, in *Proceedings of 12th International Conference on Nuclear Reaction Mechanisms*, 15–19 June 2009, Varenna, Italy. CERN-Proceedings-2010–001: 509–516; http://cdsweb.cern.ch/record/1238366/files/p509.pdf.
35. H. Paganetti, H. Jiang, K. Parodi, et al., Clinical implementation of full Monte Carlo dose calculation in proton beam therapy. Phys. Med. Biol. **53**, 4825–4853 (2008)
36. J. Seco, H. Jiang, D. Herrup, et al., A Monte Carlo tool for combined photon and proton treatment planning verification. J. Phys. Conf. Ser. **74**, 021014 (2007)
37. W. Newhauser, J. Fontenot, Y. Zheng, et al, Monte Carlo simulations for configuring and testing an analytical proton dose-calculation algorithm. Phys. Med. Biol. **52,** 4569–4584 (2007)
38. S.W. Peterson, J. Polf, G. Ciangaru, et al., Variations in proton scanned beam dose delivery due to uncertainties in magnetic beam steering. Med. Phys. **36**, 3693–3702 (2009)
39. K. Parodi, A. Mairani, S. Brons, et al., Influence of lateral beam profile modifications in scanned proton and carbon ion therapy: a Monte Carlo study. Phys. Med. Biol. **55**, 5169–5187 (2010)
40. H. Jiang, H. Paganetti, Adaptation of GEANT4 to Monte Carlo dose calculations based on CT data. Med. Phys. **31**, 2811–2818 (2004)
41. F.C.P. du Plessis, C.A. Willemse, M.G. Loetter, L. Goedhals, The indirect use of CT numbers to establish material properties needed for Monte Carlo calculation of dose distributions in patients. Med. Phys. **25**, 195–201 (1998)
42. W. Schneider, T. Bortfeld, W. Schlegel, Correlation between CT numbers and tissue parameters needed for Monte Carlo simulations of clinical dose distributions. Phys. Med. Biol. **45**, 459–478 (2000)
43. K. Parodi, H. Paganetti, E. Cascio, et al., PET/CT imaging for treatment verification after proton therapy: a study with plastic phantoms and metallic implants. Med. Phys. **34**, 419–435 (2007)
44. A. Mairani, *Nucleus-Nucleus Interaction Modelling and Applications in Ion Therapy Treatment Planning*. Ph.D. Thesis, University of Pavia, 2007. http://siba.unipv.it/fisica/ScientificaActa/dottorato_ottobre2007.htm
45. P. Andreo, On the clinical spatial resolution achievable with protons and heavier charged particle radiotherapy beams. Phys. Med. Biol. **54**, N205–N215 (2009)
46. H.H. Liu, P. Keall, Dm rather than Dw should be used in Monte Carlo treatment planning. Med. Phys. **29**, 922–924 (2002)
47. H. Paganetti, Dose to water versus dose to medium in proton beam therapy. Phys. Med. Biol. **54**, 4399–4321 (2009)
48. N. Dogan, J.V. Siebers, P.J. Keall, Clinical comparison of head and neck and prostate IMRT plans using absorbed dose to medium and absorbed dose to water. Phys. Med. Biol. **51**, 4967–4980 (2006)
49. Y. Kase, N. Kanematsu, T. Kanai, N. Matsufuji, Biological dose calculation with Monte Carlo physics simulation for heavy-ion radiotherapy. Phys. Med. Biol. **51**, N467–N475 (2006)
50. A. Mairani, S. Brons, F. Cerutti, et al., The FLUKA Monte Carlo code coupled with the local effect model for biological calculations in carbon ion therapy. Phys. Med. Biol. **55**, 4273–4289 (2010)
51. A. Mairani, K. Parodi, S. Brons, et al., Clinical calculations of physical and biological effective dose distributions in proton and carbon ion therapy using the FLUKA Monte Carlo code. Nuclear Science Symposium Conference Record, NSS '08 IEEE 5612–5615, (2008)
52. T. Sato, Y. Kase, R. Watanabe, et al., Biological dose estimation for charged-particle therapy using an improved PHITS code coupled with a microdosimetric kinetic model. Radiat. Res. **171**, 107–117 (2009)

53. R.B. Hawkins, A microdosimetric-kinetic model for the effect of non-Poisson distribution of lethal lesions on the variation of RBE with LET. Radiat. Res. **160**, 61–69 (2003)
54. M. Scholz, A.M. Kellerer, W. Kraft-Weyrather, G. Kraft, Computation of cell survival in heavy ion beams for therapy – the model and its approximation. Radiat. Environ. Biophys. **36**, 59–66 (1997)

Chapter 8
Modeling Heavy Ion Radiation Effects

Thilo Elsässer

Abstract IBT requires a consideration of the complex dependencies of the relative biological effectiveness (RBE). In this chapter, several approaches based on biophysical modeling are reviewed with an emphasis on the Local Effect Model, since this is the only biophysical model that has been used for treatment planning. Basic considerations, the comparison to experimental data, and the integration into a treatment planning system are summarized.

8.1 Introduction

Biophysical modeling of radiation effects of ions represents a fascinating, challenging, and diverse discipline in the field of radiation research. Besides the complexity of biological processes that follow initial events of radiation damage, also the physics of the interaction of heavy ions with biological materials is more complex than the interaction of photons with biological systems. Therefore, the key for an application of biophysical models in ion beam therapy (IBT) is the simplification and reduction of processes in order to identify and quantitatively describe the most important ones.

Recently, the success of IBT facilities all over the world has intensified research in theoretical radiation biophysics, which was additionally fostered by the identification of heavy ion-induced radiation damage as the major uncertainty of long-term manned missions aiming to explore the deep space [1]. In both cases, the radiation field is strongly inhomogeneous covering a wide range of particles and energies.

T. Elsässer (✉)
Siemens Healthcare AG, Imaging & Therapy, Particle Therapy, Hofmannstr. 26, 91052 Erlangen, Germany

GSI Helmholtzzentrum für Schwerionenforschung, Planckstraße 1, 64291 Darmstadt, Germany
e-mail: thilo.elsaesser@siemens.com; t.elsaesser@gsi.de

U. Linz (ed.), *Ion Beam Therapy*, Biological and Medical Physics, Biomedical Engineering, DOI 10.1007/978-3-642-21414-1_8,

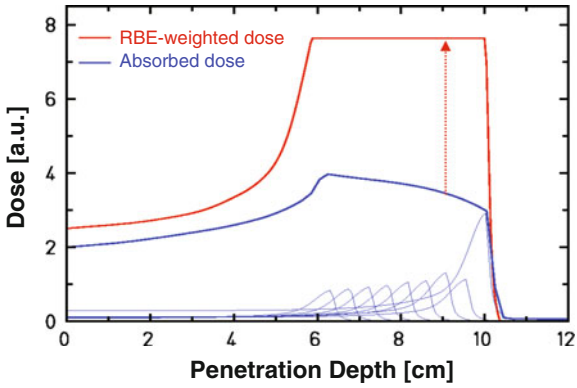

Fig. 8.1 The spread-out Bragg peak (SOBP) consists of several pristine Bragg peaks that are overlaid to produce an extended volume that is covered with the maximum dose. The challenge for biological dose optimization is the generation of a homogenous RBE-weighted dose in the target volume. Courtesy of GSI, Darmstadt

In heavy ion therapy, not only the stopping primary particles (e.g., carbon ions) need to be considered, but also all fragments produced during the stopping process need to be taken into account, because the biological effect depends on the particle type [2]. Moreover, extensive experimental research during the last decades has shown that the biological response to ion irradiation also depends on the particle energy, the dose level, the oxygen status, and the irradiated tissue or cell system [3]. All these dependencies have to be taken into account if one wants to predict the biological response of tissue to a complex radiation field as present in the spread-out Bragg peak (SOBP) of tumor treatments with particles (Fig. 8.1).

The major goal of heavy ion treatment planning is the generation of a particle field that produces a flat distribution of the biological response (e.g., cell survival, tumor control probability), regardless of whether active or passive beam delivery techniques are used. In the early days of particle therapy at Berkeley as well as at the Heavy Ion Medical Accelerator (HIMAC), Chiba, experimental track segment studies were performed to deduce the biological effect of a particular ion/energy combination on representative cell systems. The resulting response to complex fields in an extended Bragg peak was calculated on the basis of a simple formalism that takes into account the biological response of monoenergetic particles [4, 5].

Since in this book, topics relevant to IBT are discussed, only those biological models are considered that were developed with a focus on applications in particle therapy. Their assumptions and main concepts for monoenergetic particles and track-segment conditions are presented in the first section, before the complex particle distribution of mixed fields is considered. Finally, the applicability of the models for treatment planning in IBT is summarized and discussed.

8.2 Amorphous Track Models

Only a selected class of biophysical models qualifies for applications in treatment planning for IBT, since their computational speed and accuracy must meet the needs required in radiation therapy. For that reason, mechanistic models that aim

to calculate the biological effect ab initio starting with the simulation of primary physical interactions of particles with biological systems are too time-consuming. Additionally, they require many parameters to describe the numerous biological processes that are generally not known in great detail. In contrast, models that simplify the physical, chemical, and biological processes have been more successful in IBT. Most of them relate the response of a biological system after ion irradiation to the response after photon irradiation. This approach allows to exploit the large clinical database available for conventional radiation therapy and facilitates a reasonable application of particles.

In the following, the model by Katz and coworkers, the microdosimetric kinetic model (MKM) recently adapted at HIMAC for the potential use in heavy ion therapy, and the Local Effect Model (LEM) successfully applied in the carbon ion pilot project at GSI are introduced. These three models are all based on the assumption that the crucial difference between photon and ion irradiation is the spatial dose distribution and that, in general, the biological mechanisms are not fundamentally different, especially if one considers similar dose levels. Therefore, they commonly use the same three main constituents:

- The photon dose–response as a black box that incorporates the biological characteristics of the irradiated tissue or cell line.
- The cell nucleus as the main target, which is subdivided in smaller domains that are differently motivated and structured in the MKM, the Katz model, and the LEM, respectively.
- An amorphous track structure model that simplifies the complex interaction between swift particles and cells (assumed to consist of water) and considers the radial dose deposition as an average quantity accumulated for many tracks.

However, they differ quite significantly in their respective implementations as we will see in the following sections.

8.3 Early Approaches by Katz and Coworkers

The model by Katz and coworkers was developed in the early 1970s and can be regarded as the origin of the biophysical models that use simplified descriptions of the physical dose distribution in combination with a reference to the photon dose–response. The Katz approach [6, 7] assumes that the relevant target is the cell nucleus which is divided into radiosensitive domains with a radius of approximately a micrometer (“beans in a bag”). The main idea of the Katz approach is the division of radiation action into two different inactivation modes, the ion-kill and γ-kill, respectively, postulating two different mechanisms for the central part of the track (ion-kill) and the outer part (γ-kill). The latter mechanism describes the accumulation of sublethal damages produced by secondary electrons which is considered to be photon like, whereas a single ion traversal is sufficient to directly inactivate the cell in the ion-kill mode. Both mechanisms act independently and the

distribution of the dose to these modes essentially depends on the charge and energy of the particle. The representation of cell inactivation for the γ-mode is based on the multitarget-single hit (MTSH) theory, an alternative way to parametrize cell survival curves, if the most common linear-quadratic model is not used. The MTSH accounts for an exponential slope at high doses and postulates a vanishing slope for low doses. Theoretically, the cross section of the ion-kill mode is determined by considering the absorbed dose in the nuclear domains with an amorphous track structure model. In practical applications for cellular systems, the direct calculation of the cross section is omitted in favor of a fitting procedure to experimental data. As one of the most recent examples, this approach was used to calculate cell inactivation along a SOBP of carbon ions based on experimental in vitro data [8]. Despite good model agreement, the requirement of four free parameters and a vanishing slope for low doses of X-rays – equivalent with an RBE approaching infinity – has hindered the clinical application of the Katz model.

8.4 Microdosimetric Kinetic Model

A promising concept was recently developed at NIRS based on the MKM [9, 10]. Similar to the Katz model, the cell nucleus is divided into microdomains with a radius R_D, which fill up the cell nucleus. The number of lesions in the cell nucleus is related to cell survival by $L_{nucl} = -\ln(S)$ and comprises the sum of all lesions in the individual domains. It was shown that L_{nucl} can be determined by means of the microdosimetric quantity z_{1D} describing the single-event dose mean specific energy:

$$\langle L_{nucl} \rangle = (\alpha_0 + \beta\, z_{1D})\, D + \beta\, D^2, \tag{8.1}$$

where α_0[1] and β are the linear–quadratic parameters following X irradiation and D is the absorbed dose. As a result of the derivation of the MKM, (8.1) shows that the quadratic term β is constant for all radiation qualities and only z_{1D} must be determined in order to describe cell survival, in general. Conveniently, z_{1D} can be either measured with a tissue-equivalent proportional counter [13] or calculated by means of the probability density $f_1(z)$ of the specific energy z deposited by single energy deposition events in the microscopic domain [11]:

$$z_{1D} = \frac{\int_0^\infty z^2 f_1(z)\mathrm{d}z}{\int_0^\infty z f_1(z)\mathrm{d}z}. \tag{8.2}$$

[1] Actually α_0 denotes the linear component of the radiation response for the limit of LET $= 0$. In practical applications, it might be assumed that this limit is also true for X-rays [13], however, this assumption requires extra care [11].

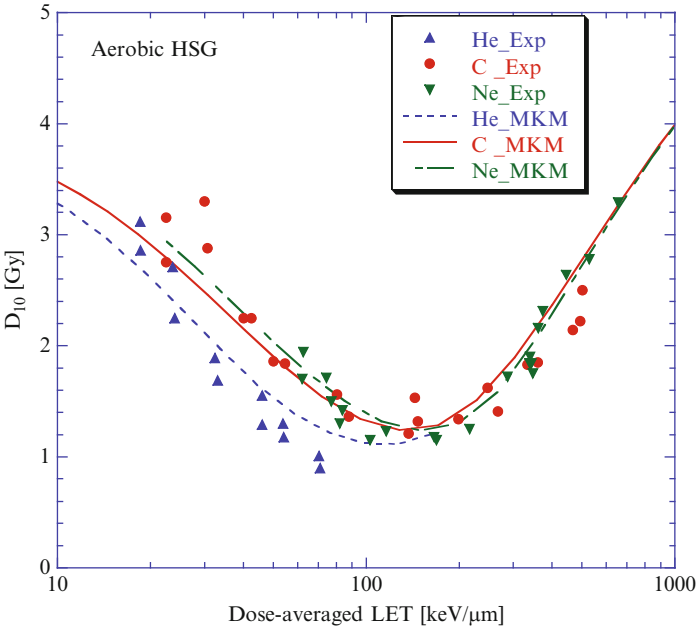

Fig. 8.2 Predictions of the MKM for the dose D_{10} that results in 10% cell survival after irradiation of human salivary gland (HSG) cells with helium, carbon, and neon ions of different energies. Adapted from [11]

For the calculations, the specific energy z can be readily determined by assuming an amorphous track structure model. For the MKM implemented at NIRS, the so-called Kiefer–Chatterjee approximation was used that assumes that the dose falls off with $1/r^2$ for increasing distances from the track center. The inner part of the track (called core) is assumed as a plateau whose outer range depends on the particle's energy. For the radial extension of the track $r_{\max}$ (called penumbra), Kiefer [14] found that $r_{\max}$ depends on the energy E (in MeV/u) only and can be parametrized by

$$r_{\max} = \gamma\, E^{\delta}; \gamma = 0.062, \delta = 1.7, \tag{8.3}$$

with $r_{\max}$ in μm and E in MeV/u.

The MKM achieves good results for monoenergetic in vitro cell measurements as was shown for the standard human salivary gland (HSG) cell line after irradiation with helium, carbon, and neon ions (Fig. 8.2).

Hence, the MKM shows good agreement for in vitro cell inactivation for a large range of LET/particle combinations. However, it has not been used clinically and the applicability remains to be shown, especially if one considers that the domain size R_{D} is a free model parameter.

8.5 Local Effect Model

The LEM was originally developed within the framework of the GSI carbon ion therapy pilot project. In recent years, some deviations between model predictions and experimental data were detected that primarily concerned low-LET particles and light ions. In the following, we introduce the original model LEM I and explain the improvements introduced by the following LEM versions. The latest approach allows to predict RBE values for all particles with similar accuracy.

8.5.1 Original Local Effect Model

The LEM also relates the response of biological systems following ion irradiation to the corresponding response after X irradiation. It assumes that the biological effect of irradiation is determined by the spatial local dose distribution inside the cell nucleus. The accumulated local dose in the cell nucleus from different tracks can be calculated for small subvolumes individually by using a track structure model. With the knowledge of the deposited dose, the biological damage can be extrapolated from data of X-ray experiments for each subvolume and integrated over the cell nucleus. Besides cell inactivation, the LEM can also be applied to determine normal tissue complication probabilities [15,16] and DNA fragmentation [17]. Here, however, the model formulation will be derived for cell inactivation as the most intuitive way to understand the basic ideas.

The LEM assumes that the number of lethal events N follows Poisson statistics. Therefore, the survival after ion irradiation $S = \exp(-N_{\text{ion}})$ is related to the three-dimensional local dose $d(x, y, z)$ to calculate the average number of lethal events N:

$$N_{\text{ion}} = \int_{V_{\text{nucleus}}} \mathrm{d}V_{\nu_{\text{ion}}}[d(x, y, z)], \tag{8.4}$$

where ν_{ion} denotes the lethal event density after ion radiation and V the volume of the sensitive target (see below). The main idea of the LEM states that the local dose effect is independent of the radiation quality ($\nu_{\text{ion}}(d) = \nu_x(d) = -\ln \mathrm{S}_x(d)/V$):

$$N_{\text{ion}} = -\int_V \mathrm{d}V \frac{\ln S_x\,[\mathrm{d}(x, y, z)]}{V}. \tag{8.5}$$

Equation (8.5) represents the most general formulation of the LEM and illustrates the relation of the survival after particle irradiation to the effect of photon irradiation. Similar to the Katz model and the MKM, the LEM is concerned with three input quantities, namely, the volume V of the sensitive target, the local dose distribution d, and the experimental survival curve S_x after X irradiation. Figure 8.3 shows a sketch of the LEM approach.

In the following, the three constituents of the LEM are characterized:

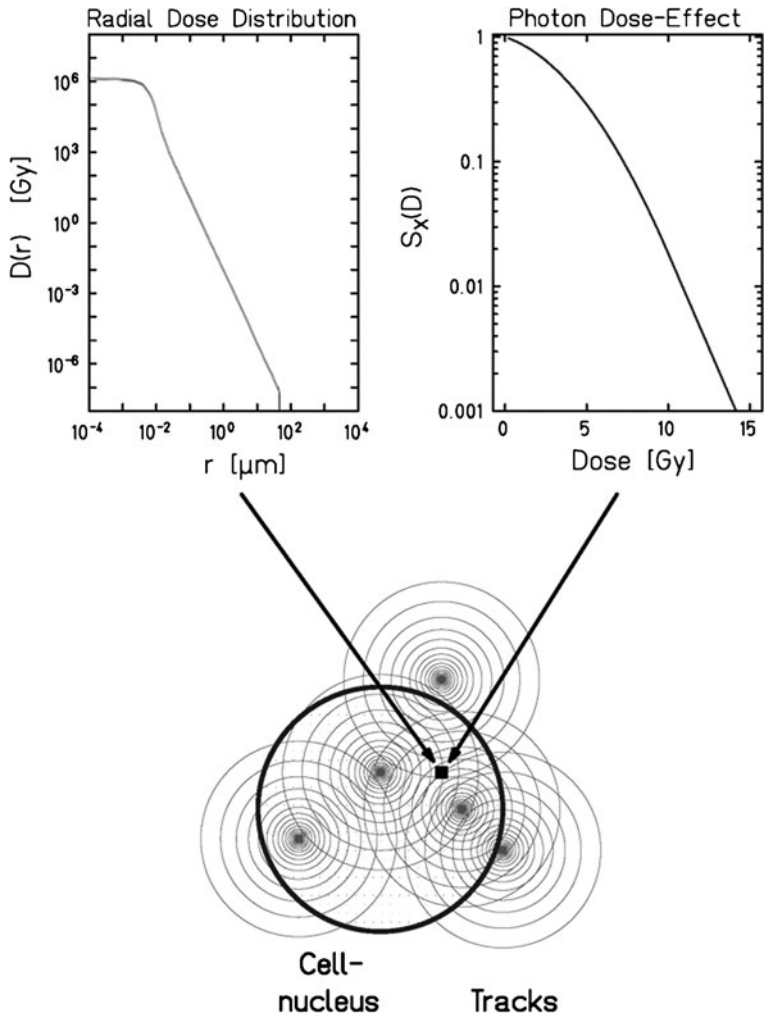

Fig. 8.3 Scheme of the Local Effect Model. Three basic constituents determine the biological response of cells to particle irradiation: the cell nucleus as sensitive target, the microscopic dose distribution around ion tracks, and the photon dose–response. Figure taken from [18]

8.5.1.1 Target

The LEM assumes that the sensitive sites are distributed homogeneously over the cell nucleus and that they exhibit the same radiosensitivity. Therefore, the effective geometrical area A of the cell nucleus and its height h can be used to calculate the sensitive volume V. In general, only the effective size $A = \pi r_n^2$ is considered, which is smaller than the arithmetic mean of the size distribution of cell nuclei [19] accounting for inhomogeneities in DNA density.

8.5.1.2 Photon Response Curve

The LEM incorporates the linear–quadratic approach to parametrize the photon dose–response curve, since it is well accepted and most widely used in the literature. However, experiments and clinical data suggest that a purely linear–quadratic model overestimates the radiation effect for high doses [20–22], and a modification must be introduced to account for this behavior. Above a threshold dose D_t the LEM assumes that the survival curve turns from the shouldered form into a purely exponential part. Therefore, the survival curve takes the following form:

$$S(D) = \begin{cases} \mathrm{e}^{-\alpha D - \beta D^2} & : D \leq D_\mathrm{t} \\ S_\mathrm{t}\,\mathrm{e}^{-s[\eta(D)D - D_\mathrm{t}]} & : D > D_\mathrm{t} \end{cases} \tag{8.6}$$

where α, β denote the linear–quadratic components, $s = \alpha + 2\beta D_\mathrm{t}$ is the slope of the exponential tail for doses above D_t, S_t is the survival at threshold dose D_t, and η quantifies the cluster effect (see next section), which is unity for the original version of the LEM [19].

8.5.1.3 Radial Dose Distribution

The LEM uses an amorphous track structure description which assumes that the track consists of an inner part with a constant inner dose attached to an outer part following a $1/r^2$-dependence. The dose D_track can be expressed by

$$D_\mathrm{track}(r) = \begin{cases} \lambda\,\mathrm{LET}/r_\mathrm{min}^2 & : r < r_\mathrm{min} \\ \lambda\,\mathrm{LET}/r^2 & : r_\mathrm{min} \leq r \leq r_\mathrm{max} \\ 0 & : r > r_\mathrm{max} \end{cases} \tag{8.7}$$

where λ is a normalization constant to assure that the radial integral reproduces the LET for a medium with density ρ. The maximum radius r_max is the same as in the MKM given by (8.3). Originally, the minimum or core radius r_min was chosen to be constant for earlier versions of the LEM (I,II) [18, 23].

8.5.2 LEM II

The first improvement of LEM considers an additional mechanism that increases the radiation damage at large local doses. For the X-ray response curve, for higher doses than the threshold dose D_t above a few hundred Gy, an additional cluster effect due to the enormous ionization densities in the track center must be considered, that results in additional double strand breaks (DSBs) due to nearby single strand breaks (SSBs) [18]. Therefore, the clustering of SSBs on opposite strands within a distance of 25 bp is taken into account. These clusters produce additional DSBs that are responsible for an increased radiation effect for high local doses (quantified by η in (8.6)) in the track center [18].

Additionally, LEM II and the following versions consider the diffusion of radicals explicitly by convoluting $D_{\text{track}}(r)$ with a 2D Gaussian distribution. Radicals can travel a certain distance to generate additional DNA damage at some distance from the primary ionization event. LEM considers an experimentally determined typical radical diffusion length for mammalian cells of 4 nm [24].

8.5.3 LEM III

LEM III applies an energy-dependent track core as a new feature to describe the track center more realistically, following Mozumder [25], who argued that the core radius r_{min} of the inner part of the track can be determined as follows: $r_{\text{min}} = \beta_{\text{ion}} r_{\text{c}}$, with $\beta_{\text{ion}} = v/c$, where v is the velocity of the particle, c the speed of light, and r_{c} describes the largest extension of the inner part of the track for the limit $v = c$. This effect reduces the biological response for fast ions with a wide core as compared to the previous LEM.

8.5.4 Generalization of LEM (LEM IV)

In the previous considerations of the LEM, the radiation damage was directly linked to the local dose deposition, where the considered subvolume was on the order of one or a few nanometers. However, also primary radiation damages induced with a larger distance on the order of a few hundred nanometers have been shown to interact in order to increase the overall radiation damage. In particular, DSBs are important initial radiation events that, in combination, can cause severe biological effects. As a mechanistic explanation one can consider the giant loop model, where an isolated DSB does not suffice to disrupt the giant loop. Only a second or more DSBs may lead to a fragmentation of the loop and cause severe damage to the cell. In the most recent development of the LEM, this situation was taken into account by considering higher order subunits represented by cubes with a side length of about 500 nm. DSBs are located randomly in these subunits according to the local dose deposition in each nanometer-sized subvolume. For ion irradiation, the DSBs are strongly correlated and occupy only a small number of such subunits, whereas for photon irradiation the DSBs are uniformly distributed with the same probability of DSB induction in each subunit. Hence, the spatial arrangement of DSBs is crucial and can be quantified by means of a complexity parameter C that relates the number of subunits with more than one DSB (clustered or cDSB) to the number of subunits with only a single DSB (isolated or iDSB):

$$C = \frac{N_{\text{cDSB}}}{N_{\text{cDSB}} + N_{\text{iDSB}}}. \tag{8.8}$$

In order to transfer the knowledge of photon irradiation to ion irradiation, the photon dose is required, for which the complexity C is the same. Due to the different spatial

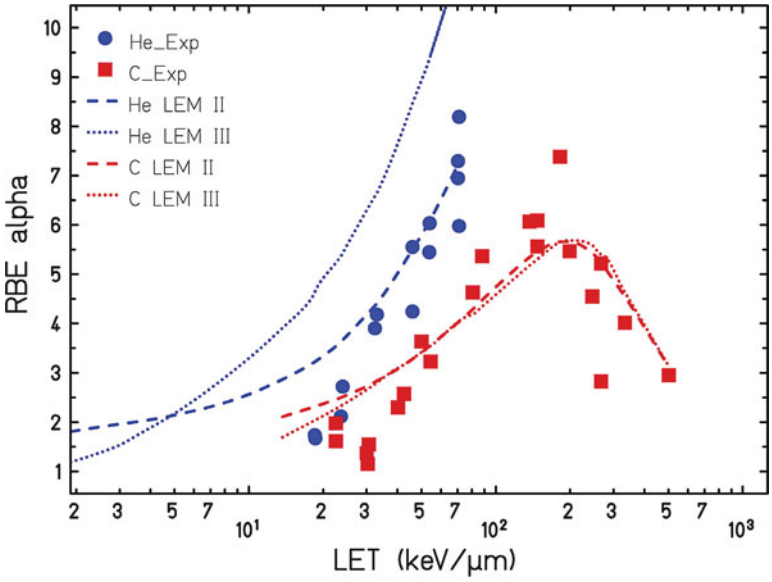

Fig. 8.4 Predictions of LEM II and LEM III for the initial RBE for cell survival for HSG cells after irradiation with carbon and helium ions. Good agreement for carbon ions is found, whereas for light particles such as helium larger deviations occur. Figure taken from [26]

distribution of DSBs, this dose will be higher for photons than for particles, since only at a much larger photon dose level, the number of clustered DSBs relative to isolated DSBs is equivalent. In that case one can imagine that several individual particle tracks with the damage complexity C fill up the nucleus.

Once this photon equivalent dose is determined, the general concept of the LEM can be applied, namely, exploiting the photon dose–response curve as given in (8.6) for the biological system of interest to yield the biological effect E_{eq}. The effect of a single ion $E_{\mathrm{ion}} = \alpha_{\mathrm{ion}}\, d_{\mathrm{ion}}$ can be readily determined by appropriate scaling according to $E_{\mathrm{Ion}} = (N^{\mathrm{Ion}}_{\mathrm{iDSB}}/N^{\mathrm{Photon}}_{\mathrm{iDSB}})E_{\mathrm{eq}}$, where d_{ion} denotes the dose delivered by a single ion. Finally, the same approximation for β_{ion} is applied as for the previous LEM versions.

8.5.5 Comparison to Experimental In Vitro Cell Survival Data

According to (8.5)–(8.7), the dose–response curve can be determined. It can be parametrized by the linear–quadratic parameters α_{ion} and β_{ion}. Typically, the linear component is determined by considering a single ion traversal and utilizing an approximation for β_{ion} [23]. The original LEM has frequently been compared to experimental in vitro data and shows reasonable agreement with various different experimental setups [27, 28]. Here, the comparison is restricted to the reference cell line HSG of HIMAC and the modifications LEM II and LEM III (Fig. 8.4). A

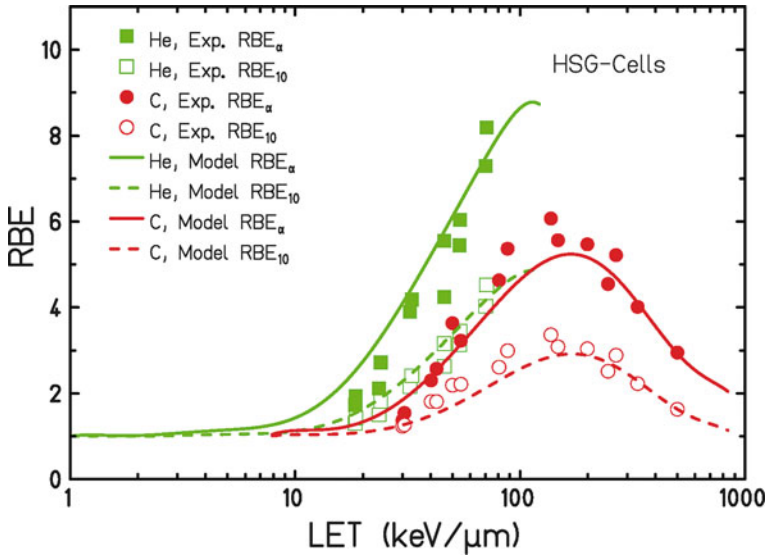

Fig. 8.5 Predictions of the most comprehensive version of LEM (LEM IV) for the initial RBE and the RBE at 10% cell survival for HSG cells after irradiation with carbon and helium ions. Figure taken from [26]

reasonable agreement for carbon ions and a fair agreement for helium ions with larger LET values are demonstrated, whereas for low-LET particles the deviations are more pronounced. This kind of comparisons guided the development of LEM IV in order to achieve a good accuracy for all particles.

As an example for the predictions of LEM IV, Fig. 8.5 presents the initial RBE as well as the RBE at the 10% survival level for the HSG cell line for helium and carbon ions. It shows good agreement for a large range of LET values at two different dose levels for two different particles. Particularly, the higher RBE for lighter particles at the same LET as well as the dose dependence of RBE is well reproduced.

8.6 Applying the Models to Complex Radiation Fields

In the previous sections, we have concentrated on the modeling of biological effects for monoenergetic ions, which are typically compared to experiments with track segment conditions. However, if one is interested in the application for particle therapy, the consideration of the mixed radiation field is of utmost importance. For that purpose, the LEM and the MKM use the same approach, which was initially introduced by Rossi in the 1970s and implemented by Kanai et al. for HIMAC. It is a simple equation that averages the linear–quadratic parameters based on the relative dose contribution f_i of each component i of the mixed radiation field:

$$\alpha_{\text{mix}} = \sum_i f_i \alpha_i \,;\, \sqrt{\beta_{\text{mix}}} = \sum_i f_i \sqrt{\beta_i}\,. \tag{8.9}$$

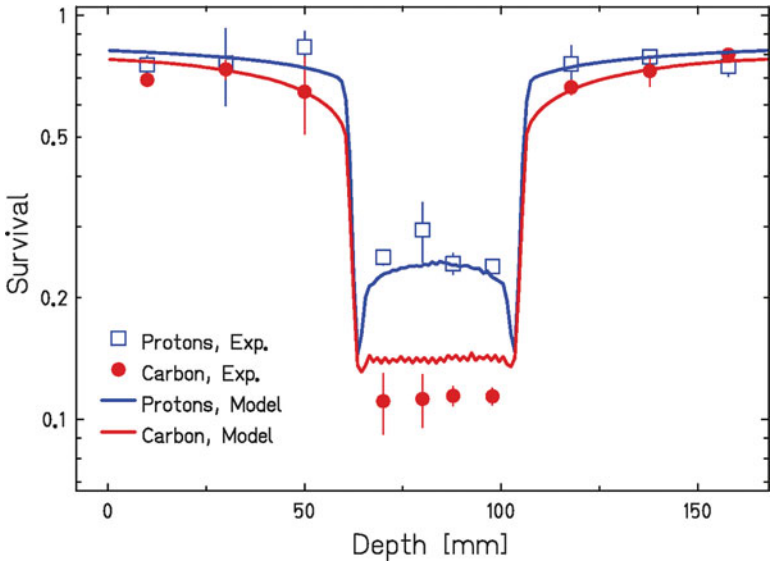

Fig. 8.6 Direct comparison of cell survival of Chinese hamster ovary (CHO) cells after irradiation with carbon ions and protons. A typical treatment scenario of two opposing fields with a 4 cm extended target volume in a depth of 6 cm was chosen. For similar cell survival in the entrance channel, a clear benefit in terms of cell killing is observed for carbon ions in the target volume

Equation (8.9) was used to design the ridge filter at HIMAC considering experimental linear–quadratic parameters. The LEM takes into account all particles present in the treatment field including fragments generated during the ion stopping process. Also the MKM exploits (8.9) and shows good results for mixed radiation fields, though it has not been used for clinical cases yet [13]. Recently, the MKM was used in combination with the Monte Carlo code PHITS to calculate the RBE-weighted dose in complex geometries such as a human voxel phantom [29].

An example for predictions based on the LEM IV is shown in Fig. 8.6. It is a complex irradiation scenario for primary protons and carbon ions including mixed radiation fields. Two opposing fields with a SOBP of 4 cm at a depth of 6 cm were chosen as irradiation geometry in order to simulate typical patient treatments. In this setup, cell survival was measured and calculated by the LEM for the common CHO (Chinese hamster ovary) cell line and compared to each other. The two key findings comprise the larger cell inactivation for carbon ions and the good agreement between model predictions and experimental data. The first result shows the expected superiority of carbon ions over protons in terms of cell killing in the target volume relative to the entrance channel. The second finding offers the opportunity to use a single model with the same model parameters to compare different radiation modalities.

8.7 Comparison of LEM, MKM, and Katz Approach

Although the models introduced in this chapter are similar due to their relation to the photon dose–response and the use of an amorphous track structure model, their implementation of these concepts as well as the target description is quite different. The two main conceptual differences concern the representation of the photon dose–response curve and the target model. In the Katz approach, the MTSH model goes along with a vanishing linear term for small doses, which is different from most experimental observations.

The different representation of photon dose–response between MKM and LEM reflects a current discussion among radiation biologists and oncologists, whether at high doses, one can still assume a quadratic dependence of the biological effect on dose or whether a linear term needs to be considered above a certain threshold dose on the order of $2\alpha/\beta$ [22].

Concerning the target, the Katz model considers domains with a radius of a few micrometers, in which the dose is averaged, thus leveling out the quite large differences in microscopic energy deposition. In contrast, the latest approach of LEM considers target structures of a few hundred nanometers, where isolated DSBs can be tolerated, but clustered defects result in more severe damage. Therefore, especially the interaction of damages within a small distance is crucial. It requires nanometer resolution of the absorbed dose. In contrast, the MKM relies on a statistical distribution of energy resulting in the single-event dose mean specific energy that does not take into account the position of sublethal damages explicitly.

8.8 Application in Treatment Planning for Heavy Ions

In contrast to proton therapy, where it is currently well accepted to use a generic RBE of 1.1, the varying RBE must be taken into account for treatment planning with heavier ions. At the treatment facilities in Chiba and Hyogo, clinical neutron and experimental cell survival data are used in combination with the linear–quadratic model for the design of specifically tailored ridge filters. Since this approach utilizes these passive scattering devices to shape the form of the physical dose distribution, no dedicated radiobiological model is required for the determination of the RBE-weighted dose. However, also for passive scattering systems dedicated radiobiological models could be used, which might enhance the accuracy of the RBE-weighted dose.

In the new treatment facility at Gunma, the layer-stacking irradiation technique offers more flexibility and a better tumor coverage, however, also here the same biological approach as is implemented at HIMAC, which does not take into account an RBE dependence on dose, tissue, and particle type.

Fig. 8.7 View of the treatment planning system syngo^{TM} PT planning by Siemens, Erlangen that uses the LEM to biologically optimize carbon ion treatment plans. Courtesy of HIT, Heidelberg

The only radiobiological model that has been used for IBT planning considering the complex relations of RBE is the LEM. It is an important part of the treatment planning software (TPS) TRiP98 that was developed at GSI and is the computational core of the Siemens TPS syngo^{TM} PT planning. So far, it has been used for patients with chordoma, chondrosarcoma, adenocystic carcinoma, and prostate cancer. However, the LEM can be used for all tumor sites, if the correct input parameters are known. The crucial point for the application of LEM for carbon therapy is the knowledge about the photon parameters α and β required as input for the model calculations in combination with the radius of the cell nucleus and the parameter D_t. For the cases mentioned earlier, an α/β ratio of 2, a nuclear radius of 5 μm, and $D_t = 30$ Gy were used and no clinically detectable deviations between the RBE-weighted doses given by LEM and the clinical results for tumor control probability of chordoma patients and late adverse effect to the brain of patients with skull base tumors were found. A typical treatment plan is depicted in Fig. 8.7, in which the RBE was calculated by LEM in each voxel of the irradiation field in order to optimize the RBE-weighted dose in the target volume.

8.9 Conclusions and Future Directions

Theoretical modeling of biological effects of heavy ions represents a challenging task due to the complexity and limited knowledge of the physical, chemical, and biological processes involved. Therefore, ab initio modeling of radiation effects starting with the very early interactions of ions with biological material covering the entire range of possible processes until the occurrence of late effects is not a reasonable approach for application in IBT. Only those models that rely on the knowledge of the dose–response to photons have been shown to generate results that can be computed fast enough with a desirable accuracy. Currently, only the LEM was used in routine treatments and no significant deviations between predicted outcome and clinical results were observed. However, the application of different biophysical approaches in Japan and Europe poses a serious challenge for dose reporting, since they result in different predictions of the RBE-weighted dose, even if the same cancer or tissue type is considered at the same physical dose level for the same biological endpoint. Therefore, a unification of the approaches or a validated procedure to convert one into the other is highly desirable. The experiment-based approach at HIMAC provides reasonable RBE estimates to shape the SOBP and was shown to back up excellent clinical results [30]. However, the concentration on a single cell line and survival level causes inaccuracies for uncommon treatment protocols as well as tissues with radiobiological characteristics greatly different from the reference cell system. Therefore, the MKM was adapted for the use in treatment planning and is presently investigated as an alternative approach for biological treatment planning. Both the LEM and the MKM as well as future treatment planning approaches should be validated with the steadily growing database of clinical experience with particles. Especially, the new combined proton–carbon machines in Europe and China (Shanghai) as well as the existing center in Hyogo, Japan will produce valuable data for such comparisons.

Furthermore, the use of hypofractionation schemes represents one of the major potential benefits of IBT. It was advanced at the treatment facilities in Japan, where protocols with only four fractions are routinely used for hepatocellular carcinoma and non-small cell lung cancer. Even single-fraction schemes were exploited at HIMAC (for details cf. Chap. 14). Although the application of different fractionation strategies should follow the same principles as applied in conventional radiotherapy [31], the determination of the dose per fraction needs to be calculated properly [32]. Since the RBE models presented in this chapter include an RBE dependence on dose, they should generally be applicable to larger fraction doses as well.

Generally, the LEM and MKM have shown to give reasonable agreement with in vitro measurements for a large range of ions. For that reason, they could guide the quest for the optimum ion species, although the final judgment will be provided by clinical data. State-of-the art accelerators are capable of providing swift ions starting from protons up to neon, possibly allowing for further optimization [33, 34]. The fundamental reason for a benefit of certain ion species is the slope of the RBE-LET dependence, being the steepest for carbon ions. However, for lighter particles like

boron, lithium, or helium a significant increase in RBE is also expected for a SOBP, however, starting at a more distal position.

In conclusion, the application of biophysical RBE models provides a powerful way to improve treatment planning and to guide further development in order to increase the application spectrum of IBT.

Acknowledgment The author expresses his gratitude to Dr. Michael Scholz (GSI) for his valuable input that significantly improved this chapter.

References

1. M. Durante, F.A. Cucinotta, Heavy ion carcinogenesis and human space exploration. Nat. Rev. Cancer **8**, 465–472 (2008)
2. D. Schardt, T. Elsässer, D. Schulz-Ertner, Heavy-ion tumor therapy: Physical and radiobiological benefits. Rev. Mod. Phys. **82**, 383–425 (2010)
3. M. Scholz, Effects of ion radiation on cells and tissues. Adv. Polym. Sci. **62**, 96–155 (2003).
4. T. Kanai, Y. Furusawa, K. Fukutsu et al., Irradiation of mixed beam and design of spread-out Bragg peak for heavy-ion radiotherapy. Radiat. Res. **147**, 78–85 (1997)
5. M. Zaider, H.H. Rossi, The synergistic effects of different radiations. Radiat. Res. **83**, 732–739 (1980)
6. R. Katz, B. Ackerson, M. Homayoonfar et al., Inactivation of cells by heavy ion bombardment. Radiat. Res. **47**, 402–425 (1971)
7. R. Katz, S.C. Sharma, Heavy particles in therapy: an application of track theory. Phys. Med. Biol. **19**, 413–435 (1974)
8. M.P. Waligorski, M. Hollmark, J. Lesiak, A simple track structure model of ion beam radiotherapy. Radiat. Prot. Dosim. **122**, 471–474 (2006)
9. R.B. Hawkins, A statistical theory of cell killing by radiation of varying linear energy transfer. Radiat. Res. **140**, 366–374 (1994)
10. R.B. Hawkins, A microdosimetric-kinetic model for the effect of non-Poisson distribution of lethal lesions on the variation of RBE with LET. Radiat. Res. **160**, 61–69 (2003)
11. Y. Kase, T. Kanai, N. Matsufuji et al., Biophysical calculation of cell survival probabilities using amorphous track structure models for heavy-ion irradiation. Phys. Med. Biol. **53**, 37–59 (2008)
12. R.B. Hawkins, The relationship between the sensitivity of cells to high-energy photons and the RBE of particle radiation used in radiotherapy. Radiat. Res. **172**, 761–776 (2009)
13. Y. Kase, T. Kanai, Y. Matsumoto et al., Microdosimetric measurements and estimation of human cell survival for heavy-ion beams. Radiat. Res. **166**, 629–638 (2006)
14. J. Kiefer, H. Straaten, A model of ion track structure based on classical collision dynamics. Phys. Med. Biol. **31**, 1201–1209 (1986)
15. T. Zacharias, W. Dörr, W. Enghardt et al., Acute response of pig skin to irradiation with 12C-ions or 200 kV X-rays. Acta Oncol. **36**, 637–642 (1997)
16. C.P. Karger, P. Peschke, R. Sanchez-Brandelik et al., Radiation tolerance of the rat spinal cord after 6 and 18 fractions of photons and carbon ions: experimental results and clinical implications. Int. J. Radiat. Oncol. Biol. Phys. **66**, 1488–1497 (2006)
17. T. Elsässer, S. Brons, K. Psonka et al., Biophysical modeling of fragment length distributions of DNA plasmids after X and heavy-ion irradiation analyzed by atomic force microscopy. Radiat. Res. **169**, 649–659 (2008)
18. T. Elsässer, M. Scholz, Cluster effects within the Local Effect Model. Radiat. Res. **167**, 319–329 (2007)

19. M. Scholz, G. Kraft, Track structure and the calculation of biological effects of heavy charged particles. Adv. Space Res. **18**, 5–14 (1996)
20. B. Fertil, I. Reydellet, P.J. Deschavanne, A benchmark of cell survival models using survival curves for human cells after completion of repair of potentially lethal damage. Radiat. Res. **138**, 61–69 (1994)
21. C. Park, L. Papiez, S. Zhang et al., Universal survival curve and single fraction equivalent dose: useful tools in understanding potency of ablative radiotherapy. Int. J. Radiat. Oncol. Biol. Phys. **70**, 847–852 (2008)
22. M. Astrahan, Some implications of linear-quadratic-linear radiation dose-response with regard to hypofractionation. Med. Phys. **35**, 4161–4172 (2008)
23. M. Scholz, A.M. Kellerer, W. Kraft-Weyrather et al., Computation of cell survival in heavy ion beams for therapy. The model and its approximation. Radiat. Environ. Biophys. **36**, 59–66 (1997)
24. V.V. Moiseenko, R.N. Hamm, A.J. Waker et al., Calculation of radiation-induced DNA damage from photons and tritium beta-particles. Part I: Model formulation and basic results. Radiat. Environ. Biophys. **40**, 23–31 (2001)
25. A. Mozumder, J.L. Magee, Track-core radius of charged particles at relativistic speed in condensed media. J. Chem. Phys. **60**, 1145–1148 (1974)
26. T. Elsässer, W. Weyrather, T. Friedrich et al., Quantification of the relative biological effectiveness for ion beam radiotherapy: Direct experimental comparison of proton and carbon ion beams and a novel approach for treatment planning. Int. J. Radiat. Oncol. Biol. Phys. **78**, 1177–1183 (2010)
27. A. Mitaroff, W. Kraft-Weyrather, O.B. Geiss et al., Biological verification of heavy ion treatment planning. Radiat. Environ. Biophys. **37**, 47–51 (1998)
28. M. Krämer, M. Scholz, Treatment planning for heavy-ion radiotherapy: calculation and optimization of biologically effective dose. Phys. Med. Biol. **45**, 3319–3330 (2000)
29. T. Sato, Y. Kase, R. Watanabe et al., Biological dose estimation for charged-particle therapy using an improved PHITS code coupled with a microdosimetric kinetic model. Radiat. Res. **171**, 107–117 (2009)
30. H. Tsujii, J.E. Mizoe, T. Kamada et al., Overview of clinical experiences on carbon ion radiotherapy at NIRS. Radiother. Oncol. **73**(Suppl 2), S41–S49 (2004)
31. J.F. Fowler, The linear-quadratic formula and progress in fractionated radiotherapy. Br. J. Radiol. **62**, 679–694 (1989)
32. C.P. Karger, O. Jäkel, M. Scholz et al., What is the clinically relevant relative biologic effectiveness? A warning for fractionated treatments with high linear energy transfer radiation: in regard to Dasu and Toma-Dasu. (Int J Radiat Oncol Biol Phys 2008;70:867–874). Int. J. Radiat. Oncol. Biol. Phys. **70**, 1614–1615 (2008)
33. A. Brahme, Recent advances in light ion radiation therapy. Int. J. Radiat. Oncol. Biol. Phys. **58**, 603–616 (2004)
34. U. Amaldi, G. Kraft, European developments in radiotherapy with beams of large radiobiological effectiveness. J. Radiat. Res. (Tokyo) **48**(Suppl A), A27–A41 (2007)

Chapter 9
Preclinical Radiobiology and Predictive Assays

Eleanor A. Blakely and Polly Y. Chang

Abstract Physical measurements of absorbed particle radiation doses are currently inadequate to estimate biological outcome at the stopping ranges of particle beams from protons to heavier ions. Estimates of biological significance and clinical impact are essential additional elements to implement ion beam therapy (IBT). This chapter provides a brief review of the current status of preclinical molecular and cellular radiobiology and predictive assays with a focus on the current use of radiobiology to characterize radiation fields of ions, to implement treatment planning with scanned ion beams, and to predict successful clinical outcome.

9.1 Introduction

Radiobiology of ion beams is an essential aspect of treatment planning for ion beam therapy (IBT). There is an ever-increasing literature summarizing radiobiological measurements that have supported the clinical use of particle beams at numerous facilities worldwide [1–3]. Early published work from Europe, the United States, Asia, and Africa characterized both in vitro and in vivo biological endpoints to evaluate cell killing effectiveness in the particle radiation fields, and to screen for any adverse tissue effects under different ambient conditions and different accelerator and beam-shaping parameters. A large variety of human and rodent cell lines, and several rodent and porcine animal strains have been involved in these studies. This variety contributed to a significant range of measured values, adding information about the lower and upper boundaries of the relative biological effectiveness (RBE), but resulting is a dilemma as to which RBE value is the "best" or "most appropriate" to use.

E.A. Blakely (✉)
Life Sciences Division, Mail Stop 977R180, Lawrence Berkeley National Laboratory,
1 Cyclotron Road, Berkeley, CA 94720, USA
e-mail: eablakely@lbl.gov

U. Linz (ed.), *Ion Beam Therapy*, Biological and Medical Physics, Biomedical Engineering, DOI 10.1007/978-3-642-21414-1_9,

With technical advances in particle physics, molecular and cellular laboratory techniques, and increasing clinical experience, relevant measurements are becoming clearer within and among institutions using ion beams. The focus of this chapter is to summarize the basic preclinical radiobiology upon which IBT is based. It will also discuss current issues for physicists, clinicians, and biologists in the field dealing with the commissioning of new facilities and optimizing IBT for safe and effective treatment of cancer at specific target sites in the body.

9.2 Measurements of the Relative Biological Effectiveness

The early literature on RBE was primarily based on measuring dose-dependent cellular survival by colony-forming assays after exposure to photons or radiation with low linear energy transfer (LET) and then comparing the data to equivalent survival after exposure to various ion beams. Established cell lines that are usually immortal and transformed, and therefore not "normal," were used because they provided a reproducible data base that could be compared over the course of several years, rather than primary cells that would be more normal, but are more difficult to use to obtain reproducible outcome because they undergo biological changes in early passage through replicate cultures.

The process of immortalization makes the cultures easy to grow in culture, but can change several physiological and biochemical pathways in the cells [4]. Immortalized cell lines have survival curves with a broad shoulder at low doses, which is absent in survival curves from primary cells. The broad shoulder characterizes the immortalized cells as more radioresistant.

Several studies have revealed an increase of RBE with the LET, reaching a maximum at an LET of approx. 200 keV/μm for carbon and heavier ions (cf. Chap. 4 for details). Even though a rather general phenomenon, clear splits of the LET–RBE spectra were found among ion species and/or cell lines. At a given LET, the RBE value for ^{3}He ions was higher than that for the other ions but at a higher LET value, for example. The position of the maximum RBE shifts to higher LET values for heavier ions. Error estimates for RBE values are difficult to estimate but considerable biological, technical, and theoretical uncertainties exist in determining its accuracy with various models [5].

Two different theoretical approaches have been developed for implementing treatment planning for carbon ion radiotherapy (CIRT): the local effect model (LEM) at GSI, Darmstadt, Germany, and the microdosimetric kinetic model (MKM) at NIRS in Chiba, Japan. Details of these models are summarized in Chap. 8.

In a recent comparison, it was attempted to determine the differences in physical and biological dose resulting from the different treatment planning systems used at NIRS and GSI for certain model tumors. By applying the same cell type [human salivary gland (HSG) cells], the technical differences were reduced as much as possible. Still, the deviations in biological dose calculated across a 6 cm spread-out Bragg peak (SOBP) of carbon ions were approx. 7% and for the physical dose

even 15% [6]. Because the two institutions use RBE values that are independently calculated from historical clinical data of patients receiving fast neutron therapy, the reason for their differences in clinical RBE of carbon ions still requires clarification [6]. Microdosimetric instruments are being developed in two promising studies to measure dose and radiation quality for applications in CIRT [7].

Clinical proton therapy (PT) has been based on the use of a generic RBE of 1.0 or 1.1, worldwide, indicating little dose-dependent biological difference from conventional low-LET radiations.

Paganetti et al. [8] completed a recent comprehensive evaluation of the available literature on proton RBE values for beams with initial energies of 65–255 MeV, following on the earlier summary of Skarsgard [9]. Overall, both in vitro and in vivo data indicate a statistically significant increase in RBE for lower doses per fraction, which is smaller for in vivo systems. However, there is too much uncertainty in the RBE value for any individual human tissue to propose RBE values specific for tissue, dose per fraction, or proton energy [8]. According to the available data summarized, the average RBE value at mid Bragg peak in vivo is approx. 1.1, ranging from 0.7 to 1.6. There is agreement that there is a measurable increase in RBE over the terminal few millimeters of the extended Bragg peak, which results in an extension of the bioeffective range of the beam of approx. 1.2 mm. The variations indicate a need for prospective assessment of normal tissue reactions in the terminal millimeters of therapeutic proton beams.

9.3 Spatial Mapping of RBE

Spatial mapping of the uniformity of RBE values in radiation fields of ions is a method used to check the LET uniformity of the field with direct experimental comparisons of cell inactivation. Novel methods have been devised to irradiate biological samples grown in two and three dimensions and process them to reveal cell-killing effects that allow detection of “hot” or “cold” spots depending on the physical methods used to broaden the ion beam (e.g., passive scattering, wobbling, or scanning, cf. Chap. 25 for details). Early approaches used cells in stirred suspension, sequentially sampled into prepared tubes that were adjusted for expected survival after sequential dose increments [10]. Data from these experiments can produce numerous survival curves within a short time span and with minimal use of beam time.

A second approach grew cells in monolayers within tissue culture flasks that could be stacked and later processed [11] or seeded on plastic discs held in place along the axis of the beam [12]. Finally, a third approach imbedded cells in a stiff gel matrix and irradiated them in a plastic tube that could be extruded, sliced, and melted into warm medium for the biological assay desired [13]. Skarsgard et al. [14] further refined the gel system to use a cell sorter to deliver a known number of cells into the test tubes for the survival assay. A recent 3D tissue-equivalent collagen matrix system similar to the gel matrix has been developed to evaluate

DNA damage intensity of primary human lung fibroblasts imbedded within the matrix [15]. Each of these methods has advantages and limitations that require consideration for the best selection to achieve accuracy, reproducibility, ease of preparation, and completion.

An excellent recent report by Elsässer et al. [16] presented the first direct experimental in vitro comparison of the biological effectiveness of range-equivalent protons and carbon ion beams for Chinese hamster ovary (CHO) cells using a pencil beam scanning technique. They exposed the cells in a three-dimensional phantom to scanned pencil beams of the respective ions and compared the experimental data to the prediction of outcome from the latest version of LEM (see Fig. 8.6). The data clearly demonstrated that higher cell killing is achieved in the target region with carbon ions as compared with protons when the effects in the entrance channel are comparable, and that the model predictions agree reasonably well with the experimental data.

9.4 RBE–LET Relation for Normal and Malignant Tissues

Biological measurements in vivo are essential to careful implementation of IBT. Data from animal experiments to predict the response of specific critical tissues to photons exist for a range of tissues. Among them are skin, intestinal crypt, lung, brain, spinal cord, testes, and lens of the eye. Fewer normal tissues have been investigated with beams of protons or carbon ions.

The time course of the response after exposure is important to investigate. Both acute responses and late appearing effects after single-dose applications and fractionated irradiation regimes at different portions of the Bragg curve have been completed at IBT facilities to mimic established and new clinical irradiation regimes. Each tissue has a different repair capacity and repair kinetics after exposure to photons and ions of different LET. Induction of cancer as a late effect after exposure to ion beams must also be understood. Some animal studies have been completed but little data exist to predict human cancer risk to ion beams [17].

Ando and Kase [18] reviewed RBE values for a number of ion beams from helium to uranium as function of LET for normal tissues (intestinal crypt, skin, spinal cord, and testes) of four rodent species. Regression lines were similar between skin and gut, and steeper than those of testes and spinal cord. They also compared the response of mouse and human tumors to carbon ion exposure. For mouse fibrosarcoma and human esophagus, breast, or tongue cancer grown in nude mice they observed very similar LET-dependent RBE values. In the same study, they compared the RBE–LET regression slopes for numerous endpoints in normal and tumor tissues (including apoptosis, colony formation, chromosome aberrations, normal tissue damage, tumor response, and genetic alterations) and noticed the smallest value for apoptosis and the largest for chromosome damage [18].

RBE values of carbon ions after fractionated irradiation revealed a dependence of the RBE–LET slopes on the number of dose fractions for cultured human tumor

cells of malignant melanoma, glioblastoma, glioma, and lung adenocarcinoma. A steep slope increase along with the number of fractions was observed for all cultured cells except glioma. Similar investigations using normal and malignant tissues demonstrated that the dependence of the RBE–LET slope on fractionation was more prominent for tumor growth delay and spinal cord damage than for skin reaction.

Given that the beam delivery methods are different at NIRS and GSI, Uzawa et al. compared the biological effectiveness of 290 MeV/u carbon ions from both facilities measuring crypt survival in murine small intestine and colony formation in vitro with HSG cells [6]. The overall RBE difference between the two facilities was 0–5% for gut crypt survival and 3–7% for HSG cell kill suggesting that the carbon ion beams had only minor biological differences after single and daily fractionated carbon irradiation. The effectiveness of CIRT for severely radioresistant tumors was demonstrated in a study examining the local control in a syngeneic rat model with the prostate tumor subline R3327-AT1, which represents a hormone-independent anaplastic carcinoma as model of the human prostate tumor [19].

Preclinical effectiveness studies of a new type of radiation should also address the metastatic potential of tumors. For carbon ions Ogata et al. [20] established a mouse osteosarcoma model in syngeneic mice, which showed a significantly reduced number of pulmonary metastases as compared to photon irradiation even at lower doses.

Interestingly, comparative cluster analysis of gene expression profiles of metastatic and primary lung tumors revealed only small differences between the two tissues, suggesting that the expression profiles of the metastatic tumor cells were not affected by the local application of CIRT or photon RT [21].

9.5 Additional Variables in Measuring RBE

The radiation response of cells in vitro or tissues in vivo depends on several important physical and biological variables, including dose, fractionation, size of the irradiation field, time of observation after exposure, condition of the stroma, and vascular supply. This has to be taken into account when studying and measuring biological radiation effects.

9.5.1 Different Doses and Dose Fractionation Regimes

Dose is a general term. In radiation science, it describes the radiation energy deposited in an absorbing medium. Radiation fields of ions are characterized by a nonhomogeneous nature in contrast to the more homogeneous energy distribution of a photon field. Depending on the atomic number and energy, an ion can deposit

extremely high energy in a very small, discrete path along its track. This may lead to clustered biological damage [22]. Particle doses are, therefore, frequently expressed in terms of fluence (particle number per unit area and time).

Dose fractionation reduces effects of low-LET radiation. For high-LET radiation, the situation seems to be more complicated. Fractionation effects are often less pronounced; however, in some cases, even an increased dose effect was observed with fractionation [23].

RBE values of ions tend to increase with the particle dose. However, a significant hypersensitivity at very low doses (<0.1 Gy) of 100 MeV/u carbon ions has been reported with certain Chinese hamster cells [24]. The implications of this hypersensitivity at the edge of carbon ion treatment fields, where the dose decreases significantly, are currently unknown.

9.5.2 Differences in Biological Geometry Relative to the Beam Exposure

The orientation and geometry of a cell in vitro during ion beam exposure can determine the volume of targeted cell material. For example, cells growing in a monolayer irradiated perpendicular to the beam will have less irradiated cell volume at risk than cells irradiated in suspension, where they are in a spherical geometry. In the latter case, concomitant increased effects might occur. They might only be discerned if the sensitivity of the endpoint studied has sufficient resolution.

Using immunofluorescence techniques, it was possible to demonstrate a geometry effect in monolayer cells irradiated from various angles. The radiation-induced expression of the gene CDKN1A provided a "streak" of fluorescence rather than a single "spot" when the cell monolayer was irradiated from an oblique angle [25].

Using a substrate that allowed the parallel alignment of cellular nuclei, Durante et al. [26] illustrated for human cells investigated by mFISH analysis at the same radiation dose that the yield of chromosomal damage and its complexity were indeed modified by the irradiation geometry [27].

9.5.3 Differences in Cell Cycle Status

The growth status of a cell culture is a significant variable when studying radiation effects. Dividing cells are, in general, more sensitive to radiation than cells in stationary phase. Each phase of the cell cycle is known to have variable radiosensitivity to low-LET radiations. In general, there are two "peaks" of low-LET resistance, one in G1-phase, and the other in late S-phase (cf. Fig. 4.9). High-LET radiation quantitatively reduces the amplitude of the wave of cell-cycle-dependent radioresistance, and qualitatively alters the response in the mitotic phase [28, 29].

9.5.4 Differences in Individual Radiosensitivity

There are several human radiosensitivity syndromes that each have their origin in a different genetic defect [30]. Many individuals with these diseases such as Ataxia telangiectasia or Nijmegen breakage syndrome are cancer prone [31]. They are extreme cases of a great genomic variability in normal tissue responses to radiation that can contribute to radiation toxicities in susceptible individuals who carry certain genomic traits [32]. It is important to screen for individuals with clinical family histories if possible, and by examination of their early radiation reactions. It is important to realize that conventional as well as ion dose prescriptions that are usually tolerated may be highly toxic to individuals with the described genomic radiosensitivities.

9.5.5 Differences Between Species

Developing embryos and young organisms are well known to be more radiosensitive than adult organisms. But maturation and longevity can be quite different between species. This can lead to different time courses of effects from radiation, because, for example, signs of aging can appear in a rodent within a couple of years, whereas in man they take several decades to appear. It is not surprising, therefore, that radiation differences exist between species not only in terms of overall radiosensitivity but also in the time course of the appearance of the radiation effects or in the specific kinds of radiation-induced tumors or cancer to which certain strains of laboratory animals are susceptible [33].

9.5.6 Differences in the Gender of the Organism

A few gender-based differences affecting radiation response have been described. Perhaps most important is the radiation sensitivity of the human female breast, especially in early puberty [34], which can result in breast cancer later in life. This effect is not well understood, but is likely due to hormonal influences during early development. Female gender is also associated with increased incidence of radiation-induced chromosomal aberrations in peripheral lymphocytes of hospital workers occupationally exposed to low doses of radiation [35].

On the other hand, estrogen appears to have a protective effect on the appearance of radiation-induced hepatic injury following PT [36] and the induction of early transient performance decrement immediately after a sufficiently large dose of ionizing radiation [37].

Another still unexplained gender difference regards the survival of patients with skull chordomas [38–40]. Females have a shortened overall survival after PT or CIRT for nonchondroidal skull base chordomas (cf. Chap. 12 for details).

9.6 Conclusions

For clinical purposes, it is essential that a radiotherapeutic dose to a patient be legally recorded. To this end, it is essential that the physicist provide the pivotal physical dose parameters for the tumor and treatment volumes to document the therapy administered, as well as the anticipated biological and/or clinical equivalent dose prescribed by the radiation therapist. International standards are still under development (cf. Chap. 6). They are a prerequisite for clinical comparisons between institutions.

Proton clinical facilities have been using a proton RBE of 1.0 or 1.1 for a range of beam energies and treatment plans, but increasing laboratory and clinical evidence argue for an enhanced effectiveness at low proton energies. This concerns potential increased effects at the boundary to critical normal tissues.

Differences exist in beam delivery implementation at the current CIRT facilities. In Japan, wobbled ion beams with fixed ridge filters broaden the field of the beam whereas in Germany, ion beams are delivered with active raster scanning in three dimensions (see Chap. 25). Each carbon ion facility must meet the rigid reporting standards and regulations of their own country in order to begin operation. With more countries planning such facilities, there is a concern for the need to reach an international standard mutually agreed upon by experts in the pertinent fields of medicine, physics, and biology.

The most controversial issue in the reporting of dose is the definition of the biologically or clinically equivalent dose. Different methods to define isoeffective dose profiles exist in Japan and Germany. The Japanese approach is based on experimental measurements with model systems in the laboratory and an RBE that is refined with a clinical component considering the extensive fast neutron experience in patients to temper the evaluation of the anticipated outcome of late effects.

The German strategy is to use a theoretical model of energy absorption in a small local volume, based solely on input parameters from low-LET radiation to predict the response to ions.

Despite the significant differences in these two approaches, new evidence indicates that the clinical outcome of CIRT of non-small cell lung cancer (NSCLC) in Japan is remarkably similar to the outcome predicted by the German theoretical approach [41]. This first encouraging observation comparing the clinical outcome of IBT planned with the Japanese strategy, and then predicted with the theoretical German approach is very important. A more recent paper by Schulz-Ertner [42] shows remarkable agreement in outcome for some additional tumor sites treated with carbon ions in Japan or Germany. Since the German 3D raster beam delivery method is not compatible with the Japanese passive dose optimization approach, one possible next step would be to determine if any differences exist if the NIRS were to test scanning methods. This is being investigated by Inaniwa et al. [43] with a modified microscopic kinetic model. However, we need to reach resolution on how the ion dose reporting should be accomplished.

The strictest definition of RBE requires one to compare a test radiation to ^{60}Co gamma rays. Since cobalt sources are no longer as commonly available as when the RBE definition was made, the high-voltage X-ray machine has gained acceptance in the field as a substitution low-LET reference. But when comparing results obtained by different investigators, it is critical to correct for possible differences due to the choice of the low-LET reference radiation. In the need to establish a common dose-reporting standard, a low-LET reference that is available to the largest number of groups is desirable. It may even be important to propose a low-LET particle as a reference to assure that dosimetric methods used in the comparison are identical [11].

The choice of model systems should not be based on trying to be all-inclusive in determining RBE. Instead, the selection should favor a responding system that is representative either for radiosensitivity or for radioresistance. This would provide the clinician with an appreciation of the range of responsiveness that may be anticipated. Depending on the treatment site, particular normal tissue toxicities should be investigated for individual organs.

The typical photon daily dose fraction is 2 Gy, and equivalent high-LET dose fractions are usually smaller. Biological endpoints must be able to examine the biological responses to a typical clinical dose fraction and to distinguish what may be similar responses at lower doses. Some may argue that measurements of high-dose responses are adequate, since theoretical modeling would allow extrapolation to the low-dose region. However, this statement assumes certainty in selection of an appropriate theoretical model to use for the extrapolation. The "stretch" to low-dose response is well known to be variable with supralinear, linear, and quadratic fits all represented among the various low-LET radiation responses measured [44, 45]. Until recently, very few low-dose responses have been available for high-LET radiations [46].

Since the number of patients treated with ion beams has escalated to many thousands, effort is underway to compare some of the predictive assays of particle response from cells and animals with the actual clinical outcome [47]. However, it would be exceedingly helpful to the international effort if radiobiologists could agree with the clinicians about which representative measurements should be made.

References

1. E. Fokas, G. Kraft, H. An, R. Engenhart-Cabillic, Ion beam radiobiology and cancer: time to update ourselves. Biochim. Biophys. Acta **1796**, 216–229 (2009)
2. N. Hamada, T. Imaoka, S. Masunaga, et al., Recent advances in the biology of heavy-ion cancer therapy. J. Radiat. Res. (Tokyo) **51**, 365–383 (2010)
3. E. Blakely, P.Y. Chang, Biology of charged particles. Cancer J. **15**, 271–284 (2009)
4. M. Kohli, T.J. Jorgensen, The influence of SV40 immortalization of human fibroblasts on p53-dependent radiation responses. Biochem. Biophys. Res. Commun. **257**, 168–176 (1999)
5. T. Friedrich, W. Weyrather, T. Elsässer, et al., Accuracy of RBE: experimental and theoretical considerations. Radiat. Environ. Biophys. **49**, 345–349 (2010)

6. A. Uzawa, K. Ando, S. Koike, et al., Comparison of biological effectiveness of carbon-ion beams in Japan and Germany. Int. J. Radiat. Oncol. Biol. Phys. **73**, 1545–1551 (2009)
7. Y. Kase, T. Kanai, M. Sakama, et al., Microdosimetric approach to NIRS-defined biological dose measurement for carbon-ion treatment beam. J. Radiat. Res. (Tokyo) **52**, 59–68 (2011)
8. H. Paganetti, A. Niemierko, M. Ancukiewicz, et al., Relative biological effectiveness (RBE) values for proton beam therapy. Int. J. Radiat. Oncol. Biol. Phys. **53**, 407–421 (2002)
9. L.D. Skarsgard, Radiobiology with heavy charged particles: a historical review. Phys. Med. **14**, S1–S19 (1998)
10. J.D. Chapman, E.A. Blakely, K.C. Smith, R.C. Urtasun, Radiobiological characterization of the inactivating events produced in mammalian cells by helium and heavy ions. Int. J. Radiat. Oncol. Biol. Phys. **3**, 97–102 (1977)
11. E.A. Blakely, Biological Beam Characterization, in *Ion Beams in Tumor Therapy*, ed. by U. Linz. (Chapman & Hall, New York, 1995), pp. 63–72
12. K. Kagawa, M. Murakami, Y. Hishikawa, et al., Preclinical biological assessment of proton and carbon ion beams at Hyogo Ion Beam Medical Center. Int. J. Radiat. Oncol. Biol. Phys. **54**, 928–938 (2002)
13. L. Skarsgard, B. Palcic, G.K.Y. Lam, RBE Mapping in Pion Beams Using the Gel Technique, in *Proceedings of International Workshop on Pion and Heavy Ion Radiotherapy: Preclinical and Clinical Studies*, ed. by L.D. Skarsgard. (Elsevier North Holland, New York, 1983), pp. 197–210
14. L.D. Skarsgard, B.G. Wouters, G.K.Y. Lam, et al., General considerations in the biological dosimetry of heavy charged particle beams and use of the gelatin/cell sorter in vitro system at TRIUMF. Paper presented in Proceedings of the NIRS international seminar on the application of heavy ion accelerators to radiation therapy of cancer, Chiba, Japan, 14–16 Nov 1994, NIRS-M-103, pp. 172–180, 1994
15. A.I. Roig, S.K. Hight, J.D. Minna, et al., DNA damage intensity in fibroblasts in a 3-dimensional collagen matrix correlates with the Bragg curve energy distribution of a high LET particle. Int. J. Radiat. Biol. **86**, 194–204 (2010)
16. T. Elsässer, W.K. Weyrather, T. Friedrich, et al., Quantification of the relative biological effectiveness for ion beam radiotherapy: direct experimental comparison of proton and carbon ion beams and a novel approach for treatment planning. Int. J. Radiat. Oncol. Biol. Phys. **78**, 1177–1183 (2010)
17. E.L. Alpen, P. Powers-Risius, S.B. Curtis, R. DeGuzman, Tumorigenic potential of high-Z, high-LET charged-particle radiations. Radiat. Res. **136**, 382–391 (1993)
18. K. Ando, Y. Kase, Biological characteristics of carbon-ion therapy. Int. J. Radiat. Biol. **85**, 715–728 (2009)
19. P. Peschke, C.P. Karger, M. Scholz, et al., Relative biological effectiveness of carbon ions for local tumor control of a radioresistant prostate carcinoma in the rat. Int. J. Radiat. Oncol. Biol. Phys. **79**, 239–246 (2010)
20. T. Ogata, T. Teshima, K. Kagawa, et al., Particle irradiation suppresses metastatic potential of cancer cells. Cancer Res. **65**, 113–120 (2005)
21. T. Tamaki, M. Iwakawa, T. Ohno, et al., Application of carbon-ion beams or gamma-rays on primary tumors does not change the expression profiles of metastatic tumors in an in vivo murine model. Int. J. Radiat. Oncol. Biol. Phys. **74**, 210–218 (2009)
22. A. Chatterjee, W.R. Holley, Biochemical mechanisms and clusters of damage for high-LET radiation. Adv. Space Res. **12**, 33–43 (1992)
23. F.Q.H. Ngo, in Effects of Fractionated-Dose Treatments on Mammalian Cells with Heavy-Ion Doses, in *Proceedings of International Workshop on Pion and Heavy-Ion Radiotherapy: Preclinical and Clinical Studies*, ed. by L.D. Skarsgard. (Elsevier North Holland, New York, 1983)
24. G. Bohrnsen, K.J. Weber, M. Scholz, Measurement of biological effects of high-energy carbon ions at low doses using a semi-automated cell detection system. Int. J. Radiat. Biol. **78**, 259–266 (2002)

25. B. Jakob, M. Scholz, G. Taucher-Scholz, Biological imaging of heavy charged-particle tracks. Radiat. Res. **159**, 676–684 (2003)
26. D. Pignalosa and M. Durante, Cellular effects of energetic heavy ions: from DNA breaks to chromosome rearrangements. Radiat. Prot. Dosim. **143**, 391–393 (2011)
27. M. Durante, D. Pignalosa, J.A. Jansen, et al., Influence of nuclear geometry on the formation of genetic rearrangements in human cells. Radiat. Res. **174**, 20–26 (2010)
28. E.A. Blakely, P.Y. Chang, L. Lommel, Cell-cycle-dependent recovery from heavy-ion damage in G1-phase cells. Radiat. Res. Suppl. **8**, S145–S157 (1985)
29. D. Chapman, Biophysical Models of Mammalian Cell Inactivation by Radiation, in *Radiation Biology in Cancer Research*, ed. by R.E. Meyn, H.R. Withers. (Raven, New York, 1980), pp. 21–32
30. C. Alapetite, J.M. Cosset, M.H. Bourguignon, R. Masse, Genetic susceptibility to radiations. Which impact on medical practice? Q. J. Nucl. Med. **44**, 347–354 (2000)
31. J. Hall, S. Angèle, Radiation, DNA damage and cancer. Mol. Med. Today **5**, 157–164 (1999)
32. J.A. Cesaretti, R.G. Stock, S. Lehrer, et al., ATM sequence variants are predictive of adverse radiotherapy response among patients treated for prostate cancer. Int. J. Radiat. Oncol. Biol. Phys. **61**, 196–202 (2005)
33. R.L. Ullrich, N.D. Bowles, L.C. Satterfield, C.M. Davis, Strain-dependent susceptibility to radiation-induced mammary cancer is a result of differences in epithelial cell sensitivity to transformation. Radiat. Res. **146**, 353–355 (1996)
34. C.E. Land, M. Tokunaga, K. Koyama, et al., Incidence of female breast cancer among atomic bomb survivors, Hiroshima and Nagasaki, 1950–1990. Radiat. Res. **160**, 707–717 (2003)
35. F. Maffei, S. Angelini, G.C. Forti, et al., Spectrum of chromosomal aberrations in peripheral lymphocytes of hospital workers occupationally exposed to low doses of ionizing radiation. Mutat. Res. **547**, 91–99 (2004)
36. T. Ahmadi, Y. Itai, H. Onaya, et al., CT evaluation of hepatic injury following proton beam irradiation: appearance, enhancement, and 3D size reduction pattern. J. Comput. Assist. Tomogr. **23**, 655–663 (1999)
37. G.A. Mickley, Antihistamine provides sex-specific radiation protection. Aviat. Space Environ. Med. **52**, 247–250 (1981)
38. E.C. Halperin, Why is female sex an independent predictor of shortened overall survival after proton/photon radiation therapy for skull base chordomas? Int. J. Radiat. Oncol. Biol. Phys. **38**, 225–230 (1997)
39. J.E. Munzenrider, E. Hug, P. McManus, et al., Skull base chordomas: Treatment outcome and prognostic factors in adult patients following conformal treatment with 3D planning and high dose fractionated combined proton and photon radiation treatment. Int. J. Radiat. Oncol. Biol. Phys. **32**(Suppl 1), 209 (1995)
40. J.X. O'Connell, L.G. Renard, N.J. Liebsch, et al., Base of skull chordoma. A correlative study of histologic and clinical features of 62 cases. Cancer **74**, 2261–2267 (1994)
41. M. Scholz, G. Kraft, The physical and radiobiological basis of the local effect model: a response to the commentary by R. Katz. Radiat. Res. **161**, 612–620 (2004)
42. D. Schulz-Ertner, The clinical experience with particle therapy in adults. Cancer J. **15**, 306–311 (2009)
43. T. Inaniwa, T. Furukawa, Y. Kase, et al., Treatment planning for a scanned carbon beam with a modified microdosimetric kinetic model. Phys. Med. Biol. **55**, 6721–6737 (2010)
44. J.W. Denham, C.S. Hamilton, M. O'Brien, et al., Erythema: goodbye LQ! Radiother. Oncol. **44**, 191–193 (1997)
45. C.S. Hamilton, J.W. Denham, M. O'Brien, et al., Underprediction of human skin erythema at low doses per fraction by the linear quadratic model. Radiother. Oncol. **40**, 23–30 (1996)
46. K.M. Prise, G. Schettino, Microbeams in radiation biology: review and critical comparison. Radiat. Prot. Dosim. **143**, 335–339 (2011)
47. T. Yanagi, T. Kamada, H. Tsuji, et al., Dose-volume histogram and dose-surface histogram analysis for skin reactions to carbon ion radiotherapy for bone and soft tissue sarcoma. Radiother. Oncol. **95**, 60–65 (2010)

Part IV
Clinical Results and Indications

Chapter 10
Ocular Proton Therapy Centers

Andrzej Kacperek

Abstract This chapter describes a review of proton therapy (PT) centers and the techniques used for the treatment of ocular lesions. The role of ion beam therapy (IBT) for eye treatments, principally choroidal melanomas, has become well established among the competing treatment modalities. More national centers now offer PT for these lesions, but not necessarily in a hospital environment. Significant improvements in eye treatment planning, patient positioning, and QA dosimetry have been realized, to the benefit of treatment efficiency and accuracy of dose delivery.

10.1 Introduction

The present chapter should be seen as an addition to a previous review [1]. The changes since then have been manifold, from the increased number of centers offering ocular ion beam therapy (IBT) to the improvements in the technique. Today, 16 centers worldwide offer ocular IBT, however, more than 80% of the patients are treated at just six centers.

Uveal melanomas are rare tumors with an incidence of approx. 6–7 per million in western countries; thus, it is advantageous that treatment and expertise is concentrated at a few national centers. There have been over 23,200 ocular IBT patient treatments at the end of 2010, compared with a total of 5,000 in 1994 [2]. All but 400 have been treated with proton beams. Helium ions have been used previously [3], whereas trial treatments are taking place with carbon ion beams [4].

A. Kacperek (✉)
Douglas Cyclotron, Clatterbridge Centre for Oncology, Wirral, CH63 4JY, UK
e-mail: andrzej.kacperek@ccotrust.nhs.uk

U. Linz (ed.), *Ion Beam Therapy*, Biological and Medical Physics, Biomedical Engineering, DOI 10.1007/978-3-642-21414-1_10,

The first proton beam irradiation of uveal melanoma in a patient was initiated in 1975 by a collaboration of the Harvard Cyclotron Laboratory (HCL), the Massachusetts Eye and Ear Infirmary (MEEI), and the Massachusetts General Hospital (MGH) in Boston [5]. Previously, large and medium melanomas were treated by enucleation; smaller sized tumors in the posterior pole were difficult to treat with radioplaques or without detriment to vision; thus charged particle therapy offered the patient conservation of the treated eye as well as the maintenance of some level of visual acuity. The HCL-Boston group pioneered the use of eye-therapy planning software (EyePlan) [6], the use of surgical insertion of tantalum (Ta) fiducial clips on the eye sclera to outline the tumor base and determine eye orientation. Also, the HCL beam line demonstrated the basic elements of an eye therapy treatment, including mouth and head restraints, "propeller" modulators and range shifters, gaze angle device, patient-specific collimators, narrow treatment nozzle, and a precision movement chair. Comparison must be made with other modalities for choroidal tumors; they have also improved in precision and effectiveness, from "trap door" surgical resection of larger tumors, endoresection surgery, radioactive plaques particularly ruthenium-106 (^{106}Ru), and transpupillary thermal therapy [7]. Several decades of experience with proton beams has shown that their main clinical advantage lies in tumors positioned posteriorly adjacent to the optic disk or macula, large anterior tumors unsuitable for radioactive plaques, and ciliary body tumors. Figure 10.1 shows the comparative depth–dose characteristics for shallow penetrating radiations. The very short range characteristics of protons, often less than 5 mm, are employed at some centers for the treatment of iris melanomas,

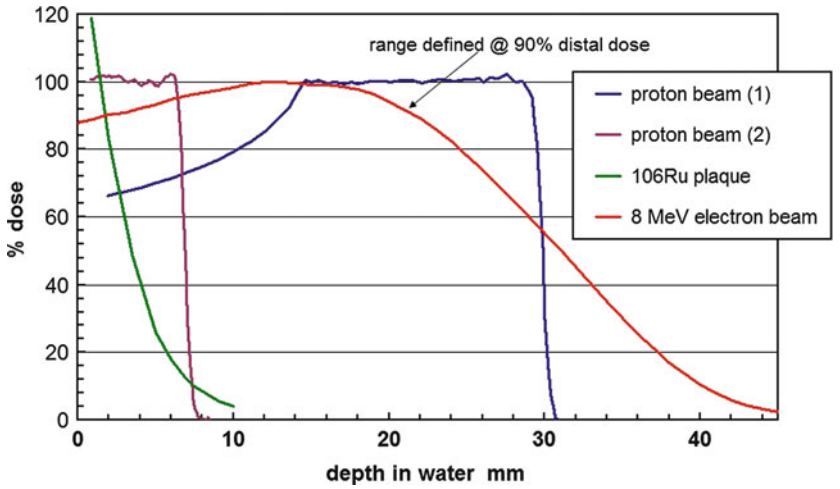

Fig. 10.1 Comparison of central axis depth doses for superficial depths. (1) refers to a clinical modulated beam for a posterior lesion and (2) shows a very shallow range and modulation for iris or ciliary body lesions. The ^{106}Ru plaque data is normalized to 2 mm depth

with or without ciliary body involvement [8] and conjunctival melanomas [9]. The choice of treatment reflects the availability of a particular ocular modality, and also local and national clinical preferences. Often PT is preferred by patients not wishing enucleation, and particularly in cases of recurrences with other techniques. Following advances in mainstream conformal radiotherapy (RT) techniques, their application in uveal melanoma treatment has been described [10, 11]. They offer a combination of 3D imaging techniques and precision head frames, and do not require the surgery for Ta clips. Comparison of treatment plans from PT, gamma knife, Cyberknife™, and IMRT, showed dose to critical eye components was negligible for the proton beam at the expense of slightly higher anterior dose [10, 11].

Excellent local tumor control of better than 98% has been obtained with ocular PT for small choroidal tumors [12]. Follow-up studies of treatments for medium and large tumors show slightly decreased control and eye retention rates [13–16], but PT offers the important eye-conserving alternative to enucleation, especially for patients with a unique eye.

The majority of ocular PT facilities are still located at existing research sites including newer facilities at UC Davies, Catania (INFN) and Krakow (IFJ). The former synchrocyclotron facility for ocular and high-energy beams at the CPO (Orsay) is being recommissioned with a new cyclotron and a reconstruction of the ocular beam line. The cyclotrons at the CCO and CAL (Nice) were initially intended for fast neutron therapy, the former being the first hospital-based facility. Other ocular therapy beam lines or treatment rooms have been commissioned as part of new hospital-based, high-energy PT centers such as at LLUMC (*James M. Slater M.D. Proton Treatment and Research Center*), MGH (*Francis H. Burr Proton Therapy Center*, Boston), MDACC (*PTC-H*, Houston), and WPE (Essen). Since the previous review [1], the ocular beam lines at university facilities at Uppsala and Louvain have ceased treatments, in part due to low patient throughput and beam availability.

In summary, PT has become an important element in the choice of ocular treatment in many countries. This is reflected by the increase in the number of centers, underpinned by substantial patient experience and follow-up studies, as well as technical improvements in treatment planning, patient positioning, beam delivery, and dosimetry. Ocular PT is now a mature modality which provides an important addition to existing techniques. Figure 10.2 shows the new ocular treatment room at PSI that has a configuration typical of other centers.

Although it is a relatively expensive treatment compared to other ocular modalities (e.g., ^{106}Ru plaque, surgery), studies have demonstrated generally better outcomes for PT [12, 14], and the ability of successfully treating large, or critically located posterior tumors. Long-term side effects, [17] such as neovascular glaucoma, “dry or wet eye,” or lid keratinization, have been mitigated by accumulated experience at each center.

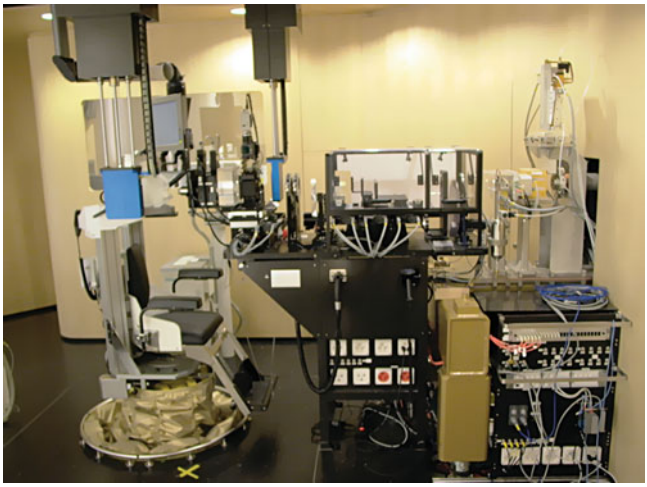

Fig. 10.2 New PT eye treatment room (OPTIS 2) at Paul Scherrer Institute in 2010. Courtesy of PSI, Villigen, Switzerland

10.2 Principal Constituents of a PT Facility

10.2.1 Proton Accelerators

Historically, clinical facilities have been situated in nuclear physics laboratories. Now accelerators are constructed specifically for therapeutic purposes. Recently, Flanz and Smith [18] have reviewed concisely the present and future technologies of clinical beam production, and have described the differences and limitations of the different accelerator types. Table 10.1 lists the accelerators that provide beams for the ocular therapy centers described. Approximately half of the centers have isochronous cyclotrons with energies in the range 60–75 MeV. They require little energy degradation, which is reflected in their sharp distal fall-off characteristics. They also have ample currents for the high-dose fractions. These machines operate in continuous-wave mode at high megahertz frequencies corresponding to the RF (radiofrequency) system driving the dees, thus the beams are considered practically continuous for dosimetry purposes. Synchrocyclotrons have fixed higher energies (>200 MeV) that require significant energy degradation to attain the ocular treatment energy range that affects beam penumbrae and fall-off. Both synchrocyclotrons and synchrotrons have pulsed beam structures, in the kilohertz and hertz range, respectively, which have dosimetric implications [19, 20]. Synchrotrons, constructed as a ring of magnets with RF acceleration gaps, offer energy variation by beam parameter selection of the RF and magnetic fields. Currently, synchrocyclotrons and cyclotrons, and to a lesser extent synchrotrons, are used at multiroom therapy centers, which also have fixed lower energy beams for shallower and ocular treatments.

Table 10.1 Accelerator and beam characteristics

PT eye center	Max. accelerator energy (MeV), type of accelerator	Max. clinical energy (MeV)	Max range in water or eye tissue (mm)	Range shifter type; spacing resolution (mm)	Method of modulation; modulator spacing (mm)	Dose rate range (Gy/min)	Duration of fraction (s)
PSI-OPTIS2, Villigen	250, Synchrocyclotron	75.0	35.0	Wheel 0.05	Four-bladed PMMA propeller 2.0	5–20	30–70
CCO, Wirral	62.5, Isochronous cyclotron	60.0	30.8	Separate PMMA 0.2	Four-bladed PMMA propeller 0.84	0.2–40	30
CPO, Orsay	200, Synchrocyclotron	75.0,	40.5(SOBP 90%)	Separate polycarbonate 0.285	Four-bladed PMMA propeller	4–30	10–30
CAL, Nice	65.0 Isochronous cyclotron	62.5	32.0	Separate PMMA 0.1	Four-bladed PMMA propeller 0.9	0.1–100	10
UCSF	67.5 Cyclotron	59.2	30.1	Water column 0.1	Four-bladed PMMA propeller;	0.2–7	60–120
TRIUMF, Vancouver	500 Isochronous H^{t}-cyclotron	74.0	36.0	Separate 0.01	Four-bladed PMMA propeller 1.0	≤15	50–100
HZB-Charité, Berlin[a]	72.0 Isochronous sector cyclotron	64.7	35.5	Wheel 0.04	Four-bladed PMMA propeller ~1.0	0.2–60	30–65
INFN-LNS, Catania	62 Superconducting cyclotron	60.0	30.5	Separate PMMA0.2	Four-bladed PMMA wheel, 0.7	1–30	40
NIRS-HIMAC Chiba[b] (He–Ar beam)	800/u Synchrotron (2 rings)	140 MeV/u (h and 170 MeV/u (v)	38.3(h) /55.1 (v) mm water	PMMA 0.5	Al ridge filter 5	25–9	33–91
MGH, Boston	230 (162) Isochronous cyclotron	230 (162)	320 (39)	Wheel PMMA 0.1	Multiple PMMA wheels	6–15	36–130
IFJ, Kraków	60.0, Isochronous cyclotron	58.0	28 Water	Wheel PMMA 0.1	Four-bladed PMMA propellers	0.6–36	n.a.

v vertical, *h* horizontal

[a]Formerly HMI

[b]Given data are for carbon ions

10.2.2 Proton Beam Characteristics

The beam must be of sufficient energy to provide range for largest eyes, including any compensators and lid thicknesses. Goitein et al. [21] have suggested that a range of 27 mm would treat 90% of tumors preferably with a minimum energy of 60 MeV. This does not include energy losses due to thickness of the scattering foils, ion chambers, and air distance (approx. 1 MeV loss per air meter). Table 10.1 shows that IFJ, UCSF, CCO, and INFN-LNS have the lowest clinical energies, with a maximum range of approx. 30 mm in water. In these cases, the thickness of scattering foil and monitor ion chamber foils has been kept to a minimum. The required range may be reduced by an appropriate selection of "gaze angle" and lid retraction during treatment planning. Conversely, a higher energy would offer treatment flexibility but would require larger energy degraders, with concomitant increased proton scattering and neutron production. The minimum beam current has to be sufficient to provide (1) dose rates for the high-dose fractions and (2) short fraction times for patient comfort. The minimum beam current is affected by losses, out of the beam area, principally by scattering foil thickness and foil-to-isocenter distance. Gottschalk has produced much work [22] concerning the optimization of passive scattering foils with respect to initial energy, degradation, beam current, and area. The required current for a fraction will also increase significantly (up to a factor of three) with thicker modulators and larger range shifters.

In the case of the CCO beam, a normal treatment time of 30 s requires from 4 to 10 nA. Current loss is also minimized by designing the scattering system to produce a beam area sufficient to cover the collimator area with a uniform field. In practice, this is approximately twice the collimator diameter. While the lack of beam current may cause longer treatment times and changes in beamline design, the availability of much larger currents at former neutron therapy, isotope, or research centers requires the adoption of safety measures such as reduced power ion sources (CCO, CAL) and upstream "pepper pot" collimators (TRIUMF, PSI) for beam current reduction. Generally, several methods of beam opening and shutting are available; an upstream pneumatic or electromagnetic beam shutter may take from 30 to 100 ms, whereas a thick beam ram of steel and plastic, for room isolation, takes 1–2 s. RF and ion source power switching is also used depending on the configuration.

10.2.3 Beam-modifying Devices

These are described for most centers in Table 10.1. Revolving plastic modulators or static ridge filters are positioned upstream to intercept the proton beam in air, thus creating a series of Bragg peaks of different intensity and depth that when integrated over time provide a uniform dose with depth. The requirements for modulator construction have been described elsewhere by HCL/MGH group [23]. The modulator wheel or propeller, shown in Fig. 10.3, should be driven

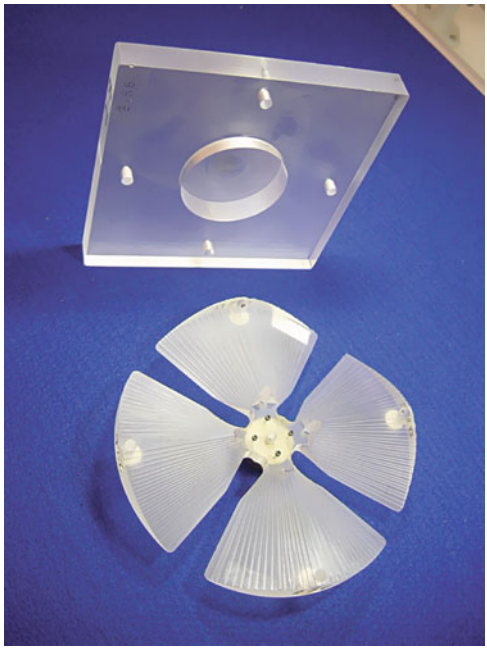

Fig. 10.3 Individual range shifter (*top*) and four-bladed (eight-cycles) modulator at the CCO, typical of many centers. Both are part of a library, and are selected according to prescribed range and modulation

asynchronously at high speeds (say 500–1,200 rpm) to provide a smooth depth–dose and to avoid possible "beating" with the beam frequency or pulse structure. The position of the range shifter and the modulator/filter acts as a virtual beam source; hence, the greater the distance upstream, the smaller the inverse-square law effect and improved lateral penumbrae [24]. The step depths for modulators are shown in Table 10.1, but the range of available modulation depths for treatment is a reflection of local practice e.g., CCO, CPO, CAL have approx. 1 mm steps, whereas others such as UCSF, PSI, and TRIUMF employ larger intervals. This is partially informed by penumbrae and proximal characteristics; typical clinical depth–doses are shown in Fig. 10.4. The effect of scatter off the collimator edge has been studied for small fields, albeit for high proton energies by van Luijk et al. [25], who show a proximal distortion of the SOBP with smaller fields; this has also been demonstrated for ocular SOBPs [26]. However, very small fields (<10 mm diameter) are rarely required for ocular tumors thus avoiding dosimetric and SOBP depth–dose corrections. Range shifters, or "fixed energy absorbers," are required to limit the maximum proton range to that prescribed for a particular treatment; these consist of either a series of fixed-thickness absorbers or adjustable systems that can be "tuned" to the required range, such as sliding wedge pair or a large range shifter wheel (approx. 50–60 cm diameter), similar to the smaller Bragg wheel used for depth–dose checks. As shown in Table 10.1, several centers (PSI, HZB, MGH, and IFJ) have adopted the "range shifting" wheel, normal to the beam, of variable thickness and made of PMMA (Lexan^{TM} at PSI). Technically,

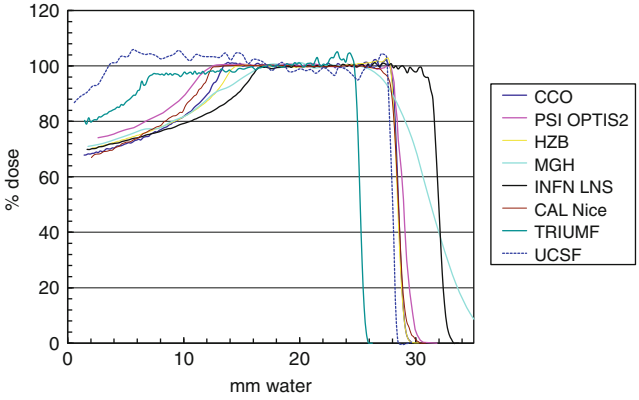

Fig. 10.4 Proton beam depth–dose curves contributed by ocular PT centers. Depth axis normalized to depth in water. These represent a range and modulation required for a medium-sized tumor in the posterior choroid. Measurements performed using either thin diodes or flat ion chambers

this method offers very fine depth resolution but is best used with quite narrow incident beams; also the range wheels have a significant space requirement. At UCSF, a variable water column is used for this purpose. These methods of variable range shifter would require either encoding or additional checks of the prescribed range. Both PMMA range shifters and modulators suffer radiation damage leading to discoloration, brittleness, and eventually fissures. A tubular nozzle construction is required to hold the patient collimators; it should be of sufficient diameter to hold collimators suitable for the largest ocular tumor fields required at a particular center. In Table 10.2 it is shown that several centers have the availability of larger nozzles and collimators, for occasional large fields or research work, at the cost of poorer field uniformity. The isocenter is usually defined, in ocular therapy, as the distance between the patient collimator and the eye/tumor center, along the beam axis; these are shown in Table 10.2. The isocenter is inferred from the bilateral imaging of axial and lateral cross wires, usually positioned just in front of each film holder, or as now, flat panel digital image panels (Fig. 10.5). The cross wires consist typically of thin tungsten (W) wire of 0.15 mm diameter. The axial cross wires are either permanently situated in the beam or removable during irradiation. In the former case, the wire should be sufficiently thick to register on the X-ray images but not to effect beam uniformity. This may be observed in some of the lateral beam profiles in Fig. 10.6. The length, diameter of the nozzle, and the position of the isocenter are arguably a compromise between the proximity of the patient eye to the collimator for the sharpest penumbra [26], and avoiding the patient nose. A longer or a cone-shaped nozzle permits more flexibility in positioning of the close-up eye camera and infrared LED illumination (e.g., LNS, MGH). Clearly the nozzle wall thickness, usually of brass or stainless steel, should be of sufficient thickness to absorb scattered protons. Although the smaller nozzle diameters should be considered as advantageous in most cases, the ability of offering larger fields

Table 10.2 Isocenter details and beam monitoring

PT eye center	Scattering system (material)	Type of in-beam dose monitor	Quad IC for steering	Isocenter-collimator distance (mm)	Isocenter-scattering foil distance (cm)	Isocenter-floor distance (cm)	Max. field diameter (mm)
PSI-OPTIS2, Villigen	Double foil (Ta and PC)	PPIC	Yes	70	~170 (virtual source distance)	142 to floor (152 to concrete floor)	40
CCO, Wirral	Double foil (W + brass)	2 PPICs	No	70	155.0	150.5	34/50[a]
CPO, Orsay	Single foil (Pb)	2 PPICs	No(pixel PPIC)	78	167	140	30
CAL, Nice	Single foil (Ta)	2 PPICs	No	70	1,000.0	150.0	34/60
UCSF	No scattering foil	3 ICs	No	50	n/a	150.0	35
TRIUMF, Vancouver	Single foil (Pb)	2 PPICs + SEM	Yes	100	156.0	137.1	25/50[a]
HZB-Charité, Berlin	Single foil (Ta)	2 PPICs	Yes[b]	68	~908	148	38
NIRS-HIMAC, Chiba (He–Ar beam)	No scattering foil	PPIC +SEM	Yes	80/100	1,070/890[c]	no data	30
INFN-LNS, Catania	Double foil (Ta and Cu)	2 PPICs	No (*X*–*Y* microstrip IC)	84	300	150	35
MGH, Boston	n.a.	PPIC	Yes	70	121.5	136.0	24/50
IFJ, Kraków	Single foil(Ta)	2 PPICs	Yes	92	1,086.5	152	40

Abbreviations: *h* horizontal, *IC* ion chamber, *PP* parallel plate, *SEM* secondary electron monitor, *v* vertical

[a]Larger nozzle used mainly for research

[b]Only beam position measurement. Generates interlock if beam out of position. No active steering

[c]Wobbler magnet is virtual source

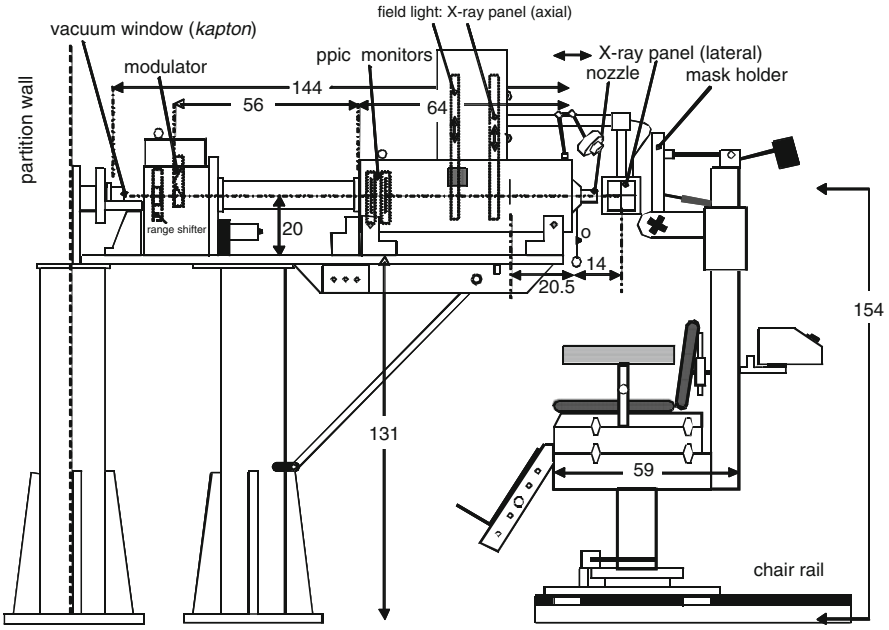

Fig. 10.5 Sketch of the beam line at CCO (in 2009). Measurements are in centimeters. Axial and lateral digital X-ray panels as well as field lights are positioned by pneumatic mechanism

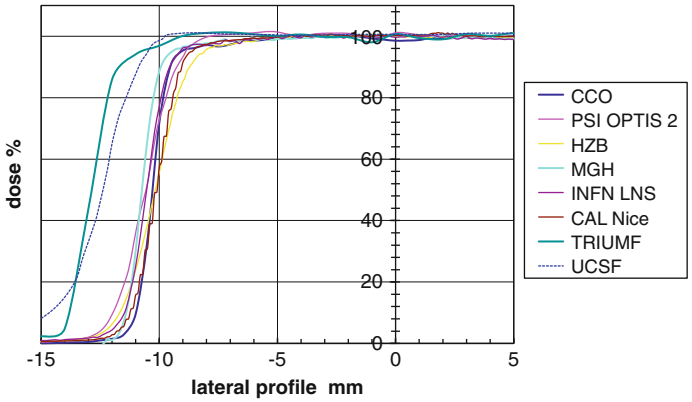

Fig. 10.6 Lateral proton dose profiles, traversing the modulation. Measurements performed with 20 mm collimators, at the isocenter, apart from TRIUMF and UCSF which used a 25 mm collimator. Measurement by thin diodes except MGH and HZB, which used film and scintillator screen, respectively

remains important, e.g., in conjunctival melanomas, as the employment of "patched" proton fields remains problematic due to the matching of sharp dose penumbrae. Several centers have a rotational adjustment of the collimator on the nozzle. This is useful for small changes in eye torsion and avoids the need to remanufacture

a collimator. The nozzle usually holds the fixation light stalk, which provides the angle of "gaze" for the patient, obtained from the planning software. This device consists of a small light, usually a light-emitting diode (LED), which is positioned on a graduated rod (PSI use an LED strip), which can be rotated around the nozzle, to achieve the required polar and azimuthal angle. A red LED is usually used as this is most visible for patients with poor acuity. The intensity of the LED light can be varied and slowly pulsed. This is required as the retina may cease to register too bright a light. The angular extent of the polar axis should be large enough to permit the use of the healthy eye for fixation. Collimators are usually made of brass as it is inexpensive and easy to machine. Most centers have employed CNC (computer numerical control) millers to reproduce the aperture shape obtained as numerical data from the eye therapy planning software. However, as the collimators are at least 8 mm thick, care needs to be exercised during cutting so as not to introduce a "tapering" effect and subsequent dose diffusion at the field edges. Milling one collimator may now take up to an hour. Other centers employ modern compact laser cutting millers. The use of wedges at centers is shown in Table 10.3. They are mounted on the collimator by one or two stalks, the length of which is determined by closest proximity to patient skin surface, as shown in Fig. 10.7. The CNC millers are also used to machine the modulators, which may take up to a day or longer depending on the thickness.

10.2.4 Patient Treatment Chair and Mask

Several decades ago, there were no commercial vendors providing precision treatment chairs for ocular beam lines. Thus, most centers initially developed their own solutions for patient positioning. If the chair is only to be used for ocular tumors, this simplifies movement requirements. In all cases, the patient is in a sitting position, facing the beam; NIRS is a special case where the patient is in a supine position due to the arrangements of the beams [4]. For anesthesia and pediatrics cases, HZB and UCSF have proposed adaptations for horizontal couches; however, the height above the floor may pose safety issues. Generally, the chair has three main movement directions relative to the isocenter: lateral (X), vertical (Y), and forward–backward (Z), with a movement precision of approx. ± 0.2 mm. Further movements on the chair accommodate different patient heights: the height above the seat (H) and an adjustable foot rest. The vertical-axis rotational movement of the chair relative to the beam line allows ease-of-gaze at the fixation light for patients with poor visual field. The patient mask is mounted onto a rigid frame at the top of the chair, which may be rotated by $\pm 20°$ vertically; useful when avoiding a thick brow bone. It should be noted that the former HCL system, now at the FHBPTC (cf. Chap. 35), has the mask frame mounted to the beam line. The chair arms are normally adjustable and can be demounted. Early chair movements were driven by worm screw mechanisms, but CPO and PSI (cf. Fig. 10.2) have chair mechanisms based on six axis hydraulic robotic systems. Mask material has always consisted of perforated thermosetting

Table 10.3 Dosimetry, treatment planning, and positioning

PT eye center	Dosimetry protocol	Treatment planning system	Wedge material; lid modeling	Lid modeling	X-ray imaging recording	X-ray settings: (a) axial (b) lateral
PSI-OPTIS2	IAEA TRS-398	EYEPLAN 3.05	Polycarbonate	No data	Digital panels (Hamamatsu)	(a) 81 kV 8 mAs (b) 66 kV 5 mAs
CCO, Wirral	ECHED 91	EYEPLAN 3.05	Aluminum	Yes	Digital panels (Hamamatsu)	(a) 100 kV 32 mAs (b) 80 kV 4 mAs
CPO, Orsay	IAEA TRS-398	EYEPLAN 3.05	PMMA	Yes	Digital panels (Hamamatsu)	(a) 90 kV 8 mAs (b) 90 kV 2 mAs
CAL, Nice	IAEA TRS-398	EYEPLAN 3.05	PMMA		Digital panels (Hamamatsu)	(a) 96 kV 25 mAs (b) 96 kV 6 mAs
UCSF	ICRU Report 59	EYEPLAN 3.05	No data	No	Digital panels (Hamamatsu)	(a) 100 kV 36 mAs (b) 100 kV 20 mAs
TRIUMF, Vancouver	ECHED 91 (1994 suppl.)	EYEPLAN 3.05	Aluminum	Yes	CMOS camera (Rad-icon)	(a) 100 kV 5 mAs (b) 100 kV 5 mAs
HZB-Charité, Berlin	IAEA TRS-398	OCTOPUS 4.4.9: CT-planning, MRI-planning	PMMA	Occasionally	Image intensifiers (Ziehm)	(a) 110 kV 0.8 mAs (b) 94 kV 0.8 mAs

(continued)

Table 10.3 (continued)

PT eye center	Dosimetry protocol	Treatment planning system	Wedge material; lid modeling	Lid modeling	X-ray imaging recording	X-ray settings: (a) axial (b) lateral
NIRS-HIMAC, Chiba (He-Ar beams)	ECHED 91 (1994 suppl)	CMS XiO-carbon with FocalPro:CT-planning	No	No	Digital panel:axial only (DRTECH)	No data
INFN-LNS, Catania	IAEA TRS-398	EYEPLAN 3.05	No	No	Digital panels (Hama-matsu)	(a) 80 kV, 50 mAs (b) 59 kV, 25 mAs
MGH, Boston	IAEA TRS-398	EYEPLAN 3.05	No	No	CCD camera	(a) 70 kV, 15 mAs, (b) 50 kV, 8 mAs
IFJ, Kraków	IAEA TRS-398	EOPP 8.9 –Varian Eclipse	n.a.	n.a	CR-260 plates (Kodak)	(a) 85 kV 40 mAs (b) 75 kV 8 mAs

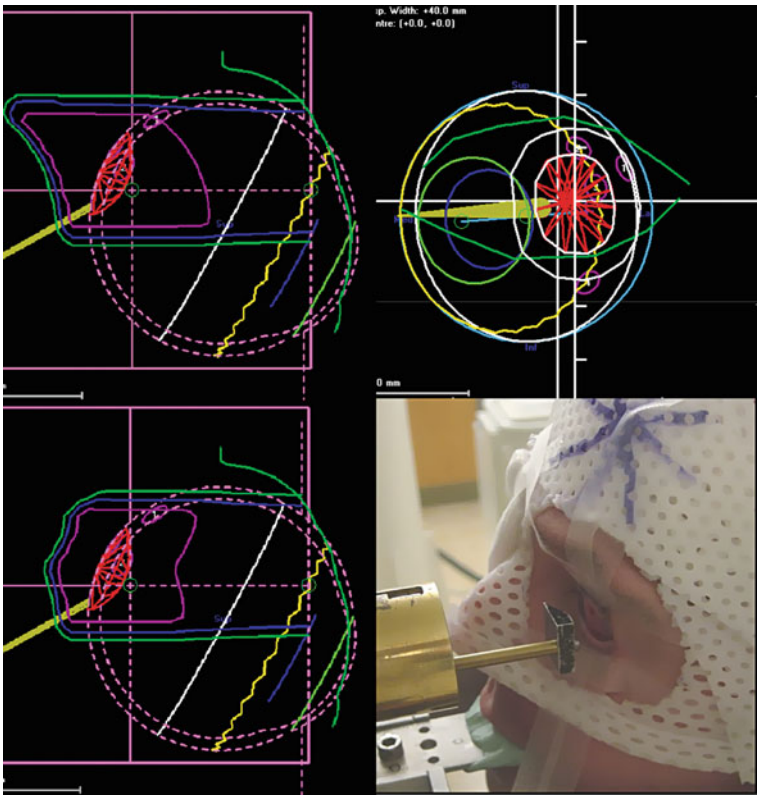

Fig. 10.7 An example using EyePlan (3.05a) views, of an Al wedge (50° tissue-equivalent, vertical, temporal) to reduce modulation from 11.8 to 9.6 mm with the range unchanged at 25.9 mm. The wedge is as near as possible to the eye, consistent with safety

plastic (e.g., ORFIT^{TM} of 2 or 3.2 mm thickness), common in conventional RT. The mask frame also holds a mouth piece of soft dental material. This is well tolerated by patients as only contact with front teeth is required. Earlier mask frames were made of aluminum or steel, more recent designs use carbon fiber, which minimizes interference with X-ray imaging.

10.2.5 Patient Positioning, X-Ray Verification Systems and Markers

Patient positioning for simulation and treatment is dependent on the use of metallic fiducial markers or clips sutured around the tumor. They are chemically inert, radio-opaque and are made of high purity Ta with 2.5 mm diameter and 0.25 mm

thickness, with two holes for suturing [27] (NIRS uses titanium markers [4]). Concern has been expressed over the possible effects of the high-Z Ta with the planned isodose. A Monte Carlo (MC) simulated study revealed some effect principally for anterior markers with edge-on orientation [28]. Usually, however, the markers appear on the periphery of the field or posterior to the tumor. The ophthalmic surgeon determines the edge of the tumor by transillumination or scleral indentation, marks the sclera, and then sutures the Ta marker. This is rendered difficult in the case of posterior tumors by the need to measure (from the back of the eye to the limbus) in two steps, eye muscles, or in determining the edges of diffuse tumors. The majority of the safety margin represents the uncertainty of microscopic tumor spread. The markers are imaged by bilateral X-ray exposures. This process has been discussed in detail elsewhere [12, 16, 29], but the importance of the quality of measurements at surgery cannot be overemphasized for successful outcomes. Table 10.3 shows X-ray exposure parameters, which vary considerably mainly due to distances of the X-ray sets from the imaging panels. Previously, Polaroid^{TM} film (Type 57) with a Lanex^{TM} screen, was used by most centers for bilateral X-ray imaging of patient position for simulation and treatment [1]. Although initially convenient, the time required for film development and the manual matching of the Ta clips with plan-generated views, made this process relatively laborious with limited resolution. HZB had developed a digital imaging system using image intensifiers. A cooperative group of ocular therapy centers (DISPOT) studied possible replacement by digital imaging systems. The requirement of small size ($52 \times 52\,mm^2$) and low cost, led to the selection of a flat digital CMOS-based panel (Hamamatsu 12-bit, $1{,}056 \times 1{,}056$ pixel, with a CsI converter screen). The image data from the panels have been adapted to the EyePlan 3.5 planning system, as illustrated in Fig. 10.8 although most centers have developed their own interface software. There has now been almost a decade of accumulated experience in the use of flat digital panels [29]. Anecdotally, it is considered that the exposure per X-ray pair may be slightly higher than for the Polaroid system, but clip matching by PC software is more rapid and accurate; thus fewer X-ray exposures are required. Initial concern over rapid degradation in image quality, particularly from scattered neutrons, does not appear to be justified. Some degradation in image quality can be sustained as the images are destined for positioning information (clips, cross wires) and not anatomical detail. Several centers (CPO, PSI) retract their X-ray panels laterally or vertically by several meters into shielded housing to minimize neutron exposure during irradiation. Where this is not practical, other beam lines rely on static neutron shielding (e.g., borated plastic, graphite). During the positional X-ray imaging prior to the treatment fraction, the patient's eye position is monitored and convenient features "marked" on a TV monitor. Thus the "marked" image will correspond to the required final patient position, as determined by the X-ray positional images. During treatment, any deviation from the "marked" feature prompts a manual beam interruption until the correct position is regained. If not, further positional X-ray images will be needed. Blinking of the patient eye is minimized by local anesthetic drops. Screen marking was improved quite rapidly upon employing electronic "light pens" to create "markings" (e.g., CPO) that overlaid the eye image on several monitor screens

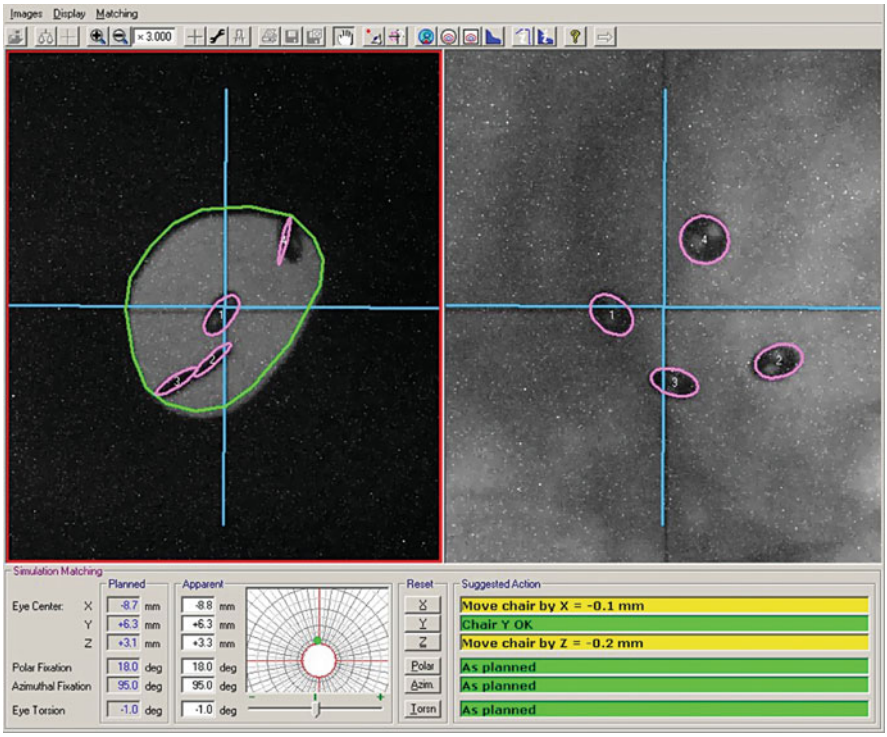

Fig. 10.8 Ta clip matching with patient plan view of clip positions. The *boxes* in *yellow* indicate to the operator the amount of chair movement required. It is also possible to determine changes in gaze angle and eye torsion, with EyePlan 3.05a. The blue cross-wires match those on the X-ray image

simultaneously. Ocular tumor treatments in stereotactic X-ray RT have employed automatic detection of eye movement with beam gating [30] although this technique has not been applied in ocular IBT.

10.3 Radiation Protection

Patients and staff may receive doses from several sources:

(a) *Patient neutron exposure*: Neutrons originate from proton reactions on the passive scattering foils, beam-modifying devices, and principally from the patient collimator. It can be shown to be dependent on the prescribed range, hence, energy. Agosteo et al. [31] has shown that passive scattering systems may produce patient neutron absorbed dose, at 200 MeV, of 10^{-2} Gy per therapy Gy. This ratio is reduced by two orders of magnitude at ocular beam energies.

Several centers have produced measurements and modeling results of neutron dose equivalent in the range 10–40 μSv per therapy Gy [26, 32]. The results are influenced by beam line configuration, measurement position, beam energy, and the scattered neutron spectrum. However, this level of neutron dose equivalent is low compared to the therapy dose range (<0.004%); but it is in the range just measurable with personnel film dosimeters, which are used for female and pediatric ocular patients.

(b) *Patient gamma and X-ray exposure*: The brass collimator is the component closest to the patient and is handled by therapy staff. Nozzle activation products have been described by Cesana [33], albeit for higher proton energies. Immediately following treatment, the patient collimator yields a dose rate of several microsieverts per hour, which originates from the short-lived ^{62}Zn, ^{55}Co, and ^{56}Co isotopes. However, the patient-specific collimator only receives proton fluence during the treatment fractions, whereas the brass nozzle accumulates activity from direct beam continuously. It should be noted that brass contains up to 3% Pb, which produces longer-lived isotopes. The PMMA range shifters and modulators become quite radioactive, principally from induced ^{11}C activity, with dose rates of up to several hundred μSv/h. Photon dose rates up to 300 μSv/h are encountered in the proximity of the W scattering foils at the end of a treatment week, which reduce to 10–20 μSv/h a week later. Their distance from the patient is depicted in Fig. 10.5 for the CCO beam line. Other centers have scattering foils positioned further upstream (Table 10.2). The high-dose fractions induce significant activity from short-lived isotopes of ^{14}O and ^{15}O in the eye; activity levels of up to 0.5 MBq may be produced, with initial dose rates up to 2 μSv/h; however, this is not measurable by the time the patient leaves the treatment room [34].

10.4 Treatment Doses, Fractionation, and RBE

The total dose and fractionation schedules for ocular PT follow those of the pioneering HCL/MGH and PSI groups and are shown in Table 10.4. The total dose was partially based on previous experience of radioactive plaque dose to the tumor apex [35]; the four or five high-dose fraction regimes were based on low levels of normal tissue dose and on the availability of beam time. The efficacy of the 70 GyE MGH dose has been compared with 50 GyE in a randomized control follow-up study. It showed similar tumor control for both dose regimes but slightly fewer side effects with the 50 GyE regime [36]. The optimal fractionation schedule has been examined by Wollensak et al. [37] from isoeffect considerations of tumor and normal tissue response that suggest a three-fraction schedule. Conversely, in order to offer sparing to normal tissue, which receive particularly high doses for large anterior tumor treatments (e.g., lid and cornea), a higher number of fractions has been suggested, although this may pose operational difficulties [12]. A relative biological effectiveness (RBE) of 1.1 (relative to ^{60}Co) has been adopted at the PT

Table 10.4 Dose schedules and patient throughput

PT eye center	No. of fractions/no. of days	Total dose (Gy)[a] (for choroidal melanomas)	Year of first ocular treatment	Total number of treatments up to 2009	No. of patients per annum (approx.)
PSI-OPTIS2	4/4	54.55	1984 (OPTIS), 2010 (OPTIS 2)	5,300 (OPTIS)	200–240
CCO, Wirral	4/4	53.1	1989	1,939	100–120
CPO, Orsay	4/4	54.55	1991	3,936	150–260
CAL, Nice	4/4	52.0	1991	3,935	230–250
UCSF	4/4	56.0	1994	1,200	100–110
TRIUMF, Vancouver	4/4	50.0	1995	145	10
HZB-Charité, Berlin	4/4	60	1998	1,437	200–220
NIRS-HIMAC, Chiba (carbon beams)	5/8	60–70[b,c]	2001	102 (Feb 2010)	∼10
INFN-LNS, Catania	4/4	54	2002	200	185
MGH, Boston	5/5	70 (50[d]) GyE	2002 at MGH (1975 HCL)[e]	1,131 (MGH)	146 (MGH)
IFJ, Krakow	4/4	54.5	2011	NA	40–50 (projected)

[a]RBE = 1.1 (proton)
[b]RBE = 3.0 (modulated carbon)
[c]Depending on tumor size
[d]The lower dose used for smaller tumors adjacent to optic disk.
[e]Beamline was transferred to MGH in 2002

centers listed in Table 10.4. For the modulated carbon beam at NIRS, an RBE of 3.0 is used. The RBE is known to be an approximation as it depends on various factors such as cell type, dose, end point etc. (cf. Chap. 4 for details). The generic RBE value of 1.1 in PT has been examined by Paganetti and Goitein [38]. The mixture of beam energies, due to modulation, may affect the RBE. This is not deemed to be critical, especially, for the large dose fractions in ocular therapy. Radiobiology data have indicated an increase in RBE toward the distal end of SOBP. Modeling by Paganetti [39] demonstrated a significant effect for beams having steeper dose distal fall-offs

Table 10.5 Isodose and collimator characteristics

PT eye center	Mean penumbrae fall-off: 80–20% through modulation. (mm)	Distal fall-off: 90–10% in water (mm)	Normal aperture margin (mm)	Normal range margin (mm)
PSI-OPTIS2	1.8	1.5	2.5	2.5
CCO, Wirral	1.1	0.9	2.5	2.5 (2.0[a])
CPO, Orsay	1.9	2.3	2.5	2.5
CAL, Nice	1.4	1.0	2.5	2.5 (1.0[a])
UCSF	1.0	1.5	2.5	3.0
TRIUMF, Vancouver	1.85	1.25	2.5	2.5
HZB-Charité, Berlin	1.9	0.95	2.5	2.5
NIRS-HIMAC, Chiba (carbon beams)	1.0 (h)/1.0 (v)	<1.5 (90–50%)	1.5	1.0
INFN-LNS, Catania	1.2	0.9	2.5	2.5
MGH, Boston	0.9	6.6	3.0(4.0[b])	2.5–4.0
IFJ, Kraków	1.0[c]	0.7	2.5	2.5

[a]If bare eye

[b]Larger value represents margin for patients that do not have alignment clips

[c]Measured in air (2.15 mm - the mean penumbra falloff measured in water phantom with collimator 25 mm diameter)

(cf. Table 10.5), and a minimal effect with shallower fall-offs. It is noted that the RBE increase at the distal edge occurs in the range margin, which may be adjacent to critical tissue. This effect may be beam line dependent; thus, radiobiological characterization for both RBE and distal edge effects is recommended prior to clinical commissioning. However, no compensation is presently applied to ocular SOBPs for modifying dose uniformity or altering the range margin.

10.5 Ocular PT-planning Systems

The use of the ocular treatment software EyePlan is prevalent. Initially named EYE [6], it was developed at MGH for the eye-therapy beam line at the HCL and included radioactive plaque data. It was further improved by Peret at PSI with an improved graphical user interface (GUI) on color workstation terminals [40] and the addition of wedges. It is a model-based program that simulates a spherical eye model and the position and shape of the tumor. The basic parameters are:

- Eye axis length, sclera thickness, anterior chamber, and lens thickness obtained from ultrasound A- and B-scan, at diagnosis
- Tumor height and base dimensions, tumor shape (from B scans)
- Clinical measurements of tumor base-to-disk or macula

- Clinical measurement of tumor-to-fiducial markers
- Clinical measurements of fiducial markers-to-limbus

The steps of simulating, planning, and treating choroidal tumors have been well described by Egger et al. [41], who also consider in detail the improvements in maximizing tumor control and survival.

Eyeplan uses several simplifying assumptions concerning the constant eye density and the spherical shape of the eye ball. A uniform eye density of 1.05 [1] has been generally adopted. Other user-supplied parameters include:

- Measured beam lateral penumbrae and
- Measured distal and anterior fall-offs
- Magnification factors for X-ray exposures
- Virtual source distance of the beam and position of isocenter

The dose algorithm calculates the maximum and minimum depths required to treat a tumor with a uniform dose for a particular "gaze" angle; calculated doses to critical elements such as the optic disk, macula, lens, iris, ciliary body, and retina are shown in the DVH calculations and may be minimized iteratively with change in the gaze angle. This is assisted by the visualization of isodoses on a user-selected plane through the eye model. The completed plan provides an image of the cross wires and the expected position of the Ta markers; this is compared with the X-ray positional image by overlaying and thus determining the required patient chair movement or adjustment to the "gaze" angle. Safety margins, both for the aperture (in Fig. 10.8) and the proximal and distal depths are shown in Table 10.5 and are determined by local clinical preferences and beam characteristics. The aperture margin, by default 2.5 mm, corresponds approximately to the 50% isodose. It includes patient positioning uncertainties (e.g., overlay of X-ray images and plan) and detectable eye movement during treatment [42–44]. For patients with an unsteady gaze, the margin may be increased by 0.5 or 1 mm. In the case of small juxtapapillary tumors, a small notch (e.g., 0.5–1.0 mm "half-diameter") is edited into the aperture shape to shield fully or partially the optic disk or nerve. The validity of small notches has been demonstrated with film exposures in Fig. 10.9. The CCO version of EyePlan 1.6 included the addition of eyelid modeling in 1992, primarily in order to compensate for range loss. Several centers, such as MGH and HZB, employ robust retraction of lids by use of speculums and thus do not use the eyelid modeling. However, the CCO pioneered the use of treatment fields through the lids, where retraction of lids from the field was not possible. This is used with the proviso that the lid rim and lashes are avoided to prevent keratinization and associated side effects [17]. PSI commissioned a version of EyePlan with ellipsoid eye modeling and two overlapping field treatments in 2000. The software was rewritten in Visual Basic (V6) for transfer onto a PC platform (EyePlan 3.0) by Martin Sheen in 2001. Later,

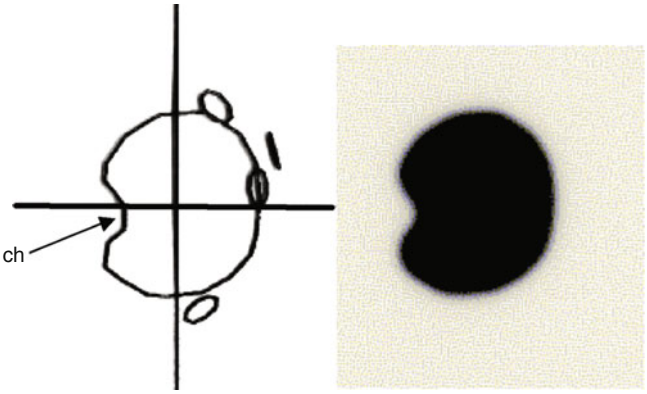

Fig. 10.9 The use of a small notch in the proton field, which appears as a protrusion on the brass collimator. The image on the *left* is an aperture outline from Eyeplan, compared with proton exposure (Kodak V-Omat) to the same collimator (at 5 mm phantom depth)

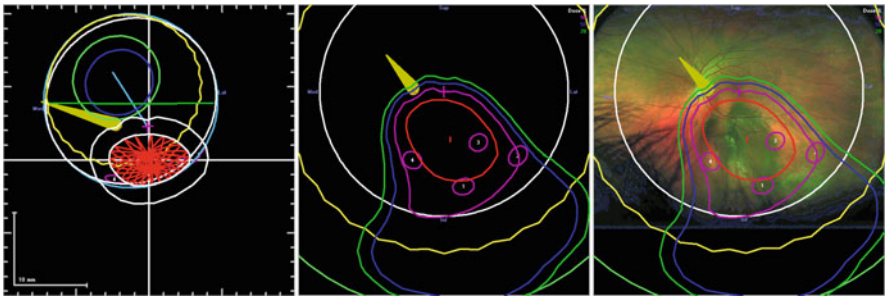

Fig. 10.10 Showing EyePlan PC v 3.05a, where a small, inferior melanoma is modeled without (*center*) and with (*right*) the use of a fundus photo. The optic disk and macula are quite visible for matching the fundus image to the fundus view from EyePlan. The beam's eye view (BEV) is on the *left* and shows the lower lid margin and avoidance of cornea dose

it included the use of transpupillary fundus photographs when drawing the tumor base by matching the fundus image with the fundus view (optic disk and macula as reference points), as presented in Fig. 10.10. Where either is obscured by tumor, an approximation of the position is required. It is considered that this has improved substantially the accuracy and robustness of tumor-base outlining. The experience in correcting tumor base shapes by this method has been described by Daftari et al. [43]. The advent of wide angle fundus cameras (e.g., RetCam, Panoret, Optos) has greatly simplified this procedure. Dobler [44] and Rethfeldt [45] have analyzed the functioning of the EyePlan program and identified improvements in eye and tumor modeling, isodose calculation (including variations in lateral penumbrae), and the inclusion of CT and MRI scans as well as fundus photos. This led to the image-based eye planning system OCTOPUS, used clinically at HMZ-Charité since 2006. In another development, Varian has made available the ocular treatment

planning software ECLIPSE Ocular Proton Planning (EOPP 8.9, 2007), which is being commissioned at IFJ (Kraków) and MDACC (Houston).

10.6 Quality-assurance Methodology

The extent and methods used for quality-assurance measurements and recording respond to local requirements and beam operation.

10.6.1 In-Beam Dose Monitoring

As in conventional RT machines, at least two in-beam parallel-plate ion chambers (PPIC) are used for dose and dose-rate monitoring as shown in Table 10.2. Their outputs, in terms of monitor units (MU), are calibrated at the isocenter, by reference dosimetry, to yield the Gy/MU for each combination of range shifter and modulation. As the PPIC measures incident dose, the Gy/MU factor may vary by up to a factor of five due to differing proximal doses, and beam losses by thicker modulators and range shifters. Several centers (Table 10.2) use SEM (secondary emission monitors) in addition to PPIC; these devices are dose-rate independent and are particularly useful for pulsed beams; however, like thick-walled PPICs, these devices incur significant beam-energy loss and may not be appropriate for beams of minimal clinical energy. A beam reference signal used for beam-scanning purposes may be obtained either from the PPICs or, as in the case of the CCO, from the electrically isolated scattering foil. Table 10.2 indicates the increasing use of quadrant and annular ion chambers for rapid beam steering and indication of field homogeneity.

10.6.2 Daily Beam and Dosimetry Checks for Treatment

Previously, patient beams were scanned in X–Y directions to measure flatness and make steering adjustments iteratively, until clinical uniformity was achieved. This was performed either per patient or each day depending on beam-steering stability. The scanners, using, e.g., 1N4001 reversed-biased diodes (sensitive volume approx. 1 mm^3), are now quite rapid (<1 min). At HZB, linear scanning has been replaced by CCD/scintillator imaging that provides rapid, high-resolution 2D beam information. Patient MU calibration is performed either before each treatment fraction, or alternatively, a standard measurement is performed daily and the patient MUs are obtained by applying a factor that has previously been determined by measurement or calculation. Automatic determination of treatment MUs has been developed with MC modeling or calculation, for combinations of range and modulation [46, 47] to within 1–3% of measurements.

10.6.3 Pretreatment Checks

In practice, the prescribed range and modulation are checked by measurement prior to the treatment week to within locally defined uncertainties, e.g., ±0.2 mm in the distal range but from −0.9 to >5 mm for the proximal edge of the modulation. For convenience, most centers employ a PMMA wheel with a stepped or continuous thickness on its periphery, which intercepts the beam. Depth–dose measurement is usually made with a flat photodiode, e.g., BPW34, which is positioned against the wheel rim. The energy response is similar but slightly greater than that of flat ion chambers by 2–3%. Also, PMMA plastic is susceptible to variations in density, thus dosimetry protocols [19, 20] recommend the use of a flat ion chamber in a water phantom for depth–dose measurements. A particular PMMA wheel requires a depth-scaling factor to be determined periodically by comparison with depth–dose measurements in water.

10.6.4 Reference and Absolute Dosimetry Procedures

Table 10.3 shows that a majority of proton centers have adopted the IAEA 398 dosimetry protocol [20]. This recommends ion chamber calibration in terms of dose-to-water, with traceability to a ^{60}Co reference beam. It also provides chamber-dependent factors for a wide variety of thimble and flat chambers. In practice, ion chambers are either sent to accredited standards laboratories, or reference dosimetry is performed in a local ^{60}Co beam against a secondary standard dosimeter, traceable to the national standards laboratory. Absolute dosimetry with calorimetry has been considered challenging due to the narrow field and limited range of ocular beams; however, with corrections for thermal diffusion and the benefit of high dose rates, the work performed by the National Physical Laboratory of the UK with a graphite calorimeter [48] confirmed the viability of this technique.

The Faraday cup technique obtains dose from a monoenergetic proton fluence conversion. Although being recommended in previous protocols [19, 49], its use remains problematic due to uncertainties in beam area and proton energy spectrum.

10.6.5 Characterization of the Treatment Beam

As with other RT devices, the basic beam parameters must be entered into the treatment planning systems (TPS) with the difference that the fall-off characteristics may change with the prescribed range and modulation. The EyePlan TPS uses lateral penumbra characteristics obtained from a single lateral profile through a typical modulation, by diode or film measurement in water. Similarly, the proximal and distal fall-off curves were obtained from typical depth–dose measurements,

either in water or PMMA. Although the distal fall-off changes very little with range and modulation, the proximal build-up has been shown to be less accurately represented [50]. These approximations were considered sufficient to treat the tumor volume effectively although with slightly less accuracy for nontumor structures. The lateral diffusion of a modulation volume does increase slightly toward maximum range. Recent work by Retheldt [45] and Koch [50] using measurements and MC modeling have shown improvements to isodose accuracy that would be incorporated into the ocular TPS. Improvements in EyePlan (3.05a) include the insertion of several lateral penumbrae with interpolation. Radiochromic films (e.g., EBT2, MD-55) has much improved lateral penumbra measurements in water at therapy dose levels. However, the high LET quenching at the Bragg peak yields a peak-to-entrance ratio of approx. 2.5–1, a slight improvement on the silver halide film ratio of 2–1. Determinations of the proximal dose build-up and distal fall-off are arguably still best obtained in water phantom with flat water–proof ion chambers (e.g., Markus). With improved MC codes and computing speeds, several centers have modeled their ocular beam lines including beam-modifying devices [50,51], in order to determine beam characteristics, neutron production, and shielding information, as well as prediction of dose monitor units.

10.6.6 In Vivo Dosimetry

Much work has been performed to confirm the planned isodose distributions in eye-like phantoms using film, polymer gels, and TLDs [52, 53]. Figure 10.11 illustrates 3D ocular isodose distributions obtained from laser-interrogated PRESAGE™ polymer dosimeters [54]. Measurement of in vivo dose or range would provide invaluable information on treatment accuracy. However, this problem remains intractable, due to LET quenching at the distal fall-off and physical size of existing detectors. Ideally, such a detector would be inserted on the rear of the eyeball at time of Ta marker surgery and withdrawn after treatment. Miniature silicon diodes or wireless MOSFET detectors intended for brachytherapy may offer a development route if dose, dose linearity, and physical constraints can be reconciled, particularly at high-dose fractions [55]. Alternatively, the induced activity from short-lived isotopes following an ocular fraction has been shown to correspond to the prescribed dose [34].

10.7 Discussion

Within two decades, many centers initiated ocular PT in spite of the rare incidence of uveal melanomas and development of alternative treatment modalities. No center has specifically been built to provide ocular PT. Some developed from cyclotrons planned for fast neutron therapy (Clatterbridge, Nice, and Krakow), the majority

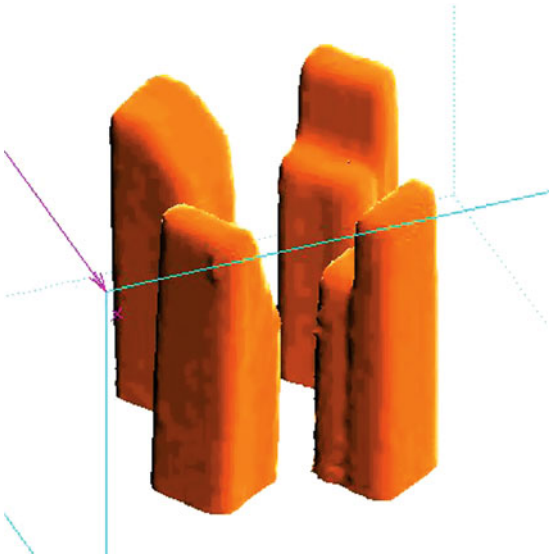

Fig. 10.11 Optical CT of four irradiations of the CCO beam (8 Gy at full modulation) in a PRESAGE™ polymer. The beam direction is from below, and demonstrates the effect of two wedges (*left*) and two "Al-blocked fields" (*right*). With kind permission of S. Doran, ICR UK

are still situated at research institutes rather than hospital sites. Purpose-built high-energy proton centers degrade energy for ocular therapy and the sharp isodose characteristics will not match those of lower-energy cyclotrons.

The world patient throughput for ocular IBT has grown slowly to approx. 1,200 per year. The use of proton beams does, however, reflect local or national clinical preferences. In the United Kingdom, this preference represents approx. 30% of cases but is considerably greater at European centers. The follow-up studies of a large number of patients have indicated the preference for proton beams in cases of small tumors adjacent to critical tissue, large anterior tumors, and where eye retention is paramount. Macular degeneration treatments have decreased mainly due to equivocal results and particularly with the advent of photodynamic therapies, antiangiogenic drug therapies, and epimacular (^{90}Sr) brachytherapy techniques. The development of adjuvant therapies to PT is being pursued to improve clinical outcomes [13]. Both the use of transpupillary thermotherapy (TTT) or laser coagulation therapy for small areas of possible recurrence and anti-VEGF compounds (e.g., bevacizumab, ranibizumab) are novel approaches to reduce macular and papillary edema and possibly improved visual acuity after PT [56].

The reduction of treatment margins, whether in aperture field or in depth, is attractive in order to reduce critical tissue dose. Normal margins of 2–2.5 mm are used at most centers as shown in Table 10.5. As mentioned by Goitein et al. [6], the margins compensate for invisible tumor diffusion, patient-positioning imprecision, and eye movement during irradiation. However, it is emphasized that the optimal application of the proton dose is dependent on the quality of eye and tumor measurements, whether ultrasound biometry, fundus photographs, or measurements at clip-insertion surgery. The latter is affected by tumor type (diffuse or well

differentiated) and proximity of the optic nerve. Decreasing margins may be attractive in reducing visual complications but to the detriment of local tumor control. Egger et al. [41] have provided evidence that reduced local tumor control leads to reduced survival. A localized reduced aperture margin (by 0.5–1 mm) or "notch" on the treatment field for sparing of the optic nerve or macula, with minimal risk of recurrence, is shown in Fig. 10.9.

The treatment of iris melanomas was started tentatively in 1994 by Damato et al. [8], who reported on the largest patient series. This treatment, now performed at several centers, is planned and administered without the use of sutured markers by using a field-light beam positioning technique. The lesion is generally located in the anterior chamber and requires a beam range and modulation of the order of 4–6 mm. EyePlan (v.3.0 and later) offers modeling of iris tumor shapes and the use of iris images.

Many ocular PT centers offered treatments of the "wet" type of age-related macular degeneration (ARMD) with simplified planning techniques (e.g., standard collimators and margins) and benign tumor doses [57]. Proton isodoses were shown to offer smaller integral dose than X-ray beams. Several controlled trials have shown net benefit in longer retention of visual acuity with minimal retinal detriment. However, at present, the preferred treatments for the "wet" type of ARMD are photodynamic therapy (PDT) and intravitreal anti-VEGF compounds. Ocular PT may still fulfill a role where these treatments are not indicated.

10.8 Conclusion

Ocular PT has confirmed its importance among the treatments available for ocular lesions, particularly choroidal melanomas adjacent to critical tissue or large tumors unsuitable for treatment by other techniques. Indeed, in some countries PT is the treatment of choice.

The costs of treatment are relatively high compared to other ocular treatments but are comparable or less than for other conformal RT methods. There are now many years of accumulated experience in the use of this small-field, short-range RT technique including treatment delivery, eye planning software, and both relative and reference dosimetry. These factors have contributed to the high rate of tumor local control and eye retention rates. Total prescribed dose and fractionation have become standardized between centers enabling improved comparison of follow-up results. However, there are different preferences concerning the use of wedges and the positioning of eyelids. Planning experience, coupled with patient follow-up studies has greatly assisted in minimizing side effects such as "dry" eye or lid keratinization. Planning precision has been significantly improved with the inclusion of digital fundus images, as well as CT or MRI data slices into the TPS, and not simply relying on measurements at clip-insertion surgery and ultrasound scans. Follow-up studies at the busier centers should demonstrate whether planning precision improvements translate into improved patient outcomes.

Despite offering advantageous isodose characteristics and high dose rates, low-energy therapy cyclotrons are very unlikely to be built specifically for ocular PT due to high capital costs. Still, many centers have shown that patient treatment income is sufficient to match overall running costs. Thus, it is appropriate that existing facilities, whether former neutron therapy or research institutes, should continue to provide ocular treatments. At present, new ocular therapy facilities are most likely to appear as an additional beamline in high-energy proton centers albeit with less favorable dose conformality. Much progress has been made in the design of compact, low-cost proton accelerators capable of energies up to 200 MeV (see other chapters of this book). If realized, they may be said to represent a third generation of clinical particle accelerators. Although primarily intended for deep-seated tumor treatments, they may be adapted for ocular treatments and should be sufficiently cost-effective to be installed in conventional RT centers.

Acknowledgements I am indebted to my colleagues from the following proton eye therapy centers: Jorn Verwey (PSI, Villigen), Sabine Delacroix (CPO, Paris), Ewan Blackmore (TRIUMF, Vancouver), Jens Heufelder (HZB-Charité, Berlin), Jan Swakon (IFJ, Kraków), Joel Hérault (CAL, Nice), Pablo Cirrone (INFN-LNS, Catania), Inder Daftari (UCSF, San Francisco), and Hanne Kooy (MGH, Boston).

References

1. A. Kacperek, Ophthalmological Proton Facilities, in *Ion Beams in Tumor Therapy*, ed. by U. Linz. (Chapman & Hall, London, 1995), pp. 360–370
2. M. Jermann, Particles Newsletter of the Particle Therapy Co-Operative Group (PTCOG). Available at http://ptcog.web.psi.ch/. Accessed 5 Sep 2011
3. J. Castro, D. Char, P. Petti, et al, 15 years experience with helium ion radiotherapy for uveal melanoma. Int. J. Radiat. Oncol. Biol. Phys. **39**, 989–996 (1997)
4. H. Koyama-Ito, T. Kanai, S. Minohara, et al., Carbon ion therapy for ocular melanoma: planning orthogonal two-port treatment. Phys. Med. Biol. **52**, 5341–5352 (2007)
5. E.S. Gragoudas, M. Goitein, A.M. Koehler, et al., Proton irradiation of small choroidal malignant melanomas. Am. J. Ophthalmol. **83**, 655–673 (1977)
6. M. Goitein, T. Miller, Planning proton therapy of the eye. Med. Phys. **10**, 275–283 (1983)
7. K.K. Mishra, J.M. Quivey, I.K. Daftari, D.H. Char, Uveal Melanoma, in *Leibel and Phillips Textbook of Radiation Oncology*, ed. by R. Hoppe, T. Phillips, M. Roach. 3rd edn. (Saunders, Philadelphia, 2010), pp. 1400–1421
8. B. Damato, A. Kacperek, M. Chopra, et al., Proton beam radiotherapy of iris melanoma. Int. J. Radiat. Oncol. Biol. Phys. **63**, 109–115 (2005)
9. H. Wuestemeyer, W. Sauerwein, D. Meller, et al., Proton radiotherapy as an alternative to exenteration in the management of extended conjunctival melanoma. Graefe's Arch. Clin. Exp. Ophthalmol. **244**, 438–446 (2006)
10. A. Zytkovicz, I. Daftari, T.L. Philips, et al., Peripheral dose in ocular treatments with CyberKnife and gamma knife radiosurgery compared to proton radiotherapy. Phys. Med. Biol. **52**, 5957–5971 (2007)
11. D. Weber, J. Bogner, J. Verwey, et al., Proton beam radiotherapy versus fractionated stereotactic radiotherapy for uveal melanomas: a comparative study. Int. J. Radiat. Oncol. Biol. Phys. **63**, 373–384 (2005)

12. E.S. Gragoudas, Proton beam irradiation of uveal melanomas: the first 30 years. The Weisenfeld Lecture. Invest. Ophthalmol. Vis. Sci. **47**, 4666–4673 (2006)
13. R. Dendale, L. Lumbroso-Le Rouic, G. Noel, et al., Proton beam radiotherapy for uveal melanoma: results of Curie Institut-Orsay proton therapy center (ICPO). Int. J. Radiat. Oncol. Biol. Phys. **65**, 780–787 (2006)
14. J.E. Munzenrider, Proton therapy for uveal melanomas and other eye lesions. Strahlenther Onkol. **175**, S68–S73 (1999)
15. E. Egger, L. Zografos, A. Schalenbourg, et al., Eye retention after proton beam radiotherapy for uveal melanoma. Int. J. Radiat. Oncol. Biol. Phys. **55**, 867–880 (2003)
16. B. Damato, A. Kacperek, M. Chopra, et al., Proton beam radiotherapy of choroidal melanoma: the Liverpool-Clatterbridge experience. Int. J. Radiat. Oncol. Biol. Phys. **62**, 1405–1411 (2005)
17. A.J.E. Foss, I. Whelehan, J.L. Hungerford, et al., Predictive factors for the development of rubeosis following proton beam radiotherapy for uveal melanoma. Br. J. Ophthalmol. **81**, 748–754 (1997)
18. J. Flanz, A. Smith, Technology for proton therapy. Cancer J. **15**, 292–297 (2009)
19. International Commission on Radiation Units and Measurements. Clinical Proton Dosimetry Part I: Beam Production, Beam Delivery and Measurement of Absorbed Dose. ICRU Report 59 (Bethesda, MD USA, 1998)
20. B. Andreo, D.T. Burns, K. Hohlfeld, et al., IAEA TRS-398 Absorbed Dose Determination in External Beam Radiotherapy: An International Code of Practice for Dosimetry Based on Standards of Absorbed Dose to Water (IAEA, Vienna, 2000), pp. 35–50
21. M. Goitein, R. Gentry, A.M. Koehler, Energy of proton accelerator necessary for treatment of choroidal melanomas. Int. J. Radiat. Oncol. Biol. Phys. **9**, 259–260 (1983)
22. B. Gottschalk, Proton Nozzle Design Program NEU. Harvard Cyclotron Laboratory, Internal Report, HCL 3/32/90 (1990)
23. A.M. Koehler, R.J. Schneider, J.M. Sisterson, Range modulators for protons and heavy ions. Nucl. Instrum. Methods Phys. Res. **131**, 437–440 (1975)
24. D.E. Bonnett, A. Kacperek, M.A. Sheen, et al., The 62 MeV proton beam for the treatment of ocular melanoma at Clatterbridge. Br. J. Radiol. **66**, 907–914 (1993)
25. P. van Luijk, A.A. van t' Veld, H.D. Zelle, et al., Collimator scatter and 2D dosimetry in small proton beams. Phys. Med. Biol. **46**, 653–670 (2001)
26. A. Kacperek, Protontherapy of eye tumours in the UK: A review of treatment at Clatterbridge. Appl. Radiat. Isot. **67**, 378–386 (2009)
27. Altomed Limited, Boldon, UK, Ta fiduciary markers (CE marked), http://www.altomed.com/contacts/index.html
28. J. Heufelder, R. Stark, A. Weber, Influence of tantalum marker clips used in eye tumour therapy on the dose distribution of a 68 MeV proton beam. Biomed. Technik. **50**(Suppl 1), 344–345 (2005)
29. I.K. Daftari, T. Essert, T.L. Phillips, Application of flat panel digital imaging for improvement of ocular melanoma patient set-up in proton beam therapy. Nucl. Instrum. Methods Phys. Res. A **598**, 628–634 (2009)
30. J. Bogner, B. Petersch, D. Georg, et al., A non-invasive eye fixation and computer-aided eye monitoring system for linear accelerator–based stereotactic radiotherapy of uveal melanoma. Int. J. Radiat. Oncol. Biol. Phys. **56**, 1128–1136 (2003)
31. S. Agosteo, C. Birattari, M. Caravaggio, et al., Secondary neutron and photon dose in proton therapy. Radiother. Oncol. **48**, 293–305 (1998)
32. F. Trompier, S. Delacroix, I. Vabre, et al., Secondary exposure for 73 and 200 MeV proton therapy. Radiat. Prot. Dosim. **125**, 349–354 (2007)
33. A. Cesana, E. Mauro, M. Silari, Induced radioactivity in a patient-specific collimator used in proton therapy. Nucl. Instrum. Methods Phys. Res. B, **268**, 2272–2280 (2010)
34. A. Kacperek, Dose verification by activation in vivo following proton beam eye radiotherapy. J. Radioanal. Nucl. Chem. **271**, 731–740 (2007)
35. E.S. Gragoudas, M. Goitein, A.M. Koehler, et al., Proton irradiation of small choroidal malignant melanomas. Am. J. Ophthalmol. **83**, 655–673 (1977)

36. E.S. Gragoudas, A.M. Lane, S. Regan, et al., A randomized controlled trial of varying radiation doses in the treatment of choroidal melanoma. Arch. Ophthalmol. **118**, 773–778 (2000)
37. G. Wollensak, L. Zografos, C. Perret, et al., Experimental study on the fractionation schedule for proton irradiation of uveal melanoma. Graef. Arch. Clin. Exp. **228**, 562–568 (1990)
38. H. Paganetti, M. Goitein, Radiobiological significance of beamline dependent proton energy distributions in a spread-out Bragg peak. Med. Phys. **27**, 1119–1126 (2000)
39. H. Paganetti, Calculation of the spatial variation of relative biological effectiveness in a therapeutic proton field for eye treatment. Phys. Med. Biol. **43**, 2147–2157 (1998)
40. C. Perret, R. Greiner, L. Zografos, C. Gailloud, Die Behandlung intraokularer Melanome mit Protonen am Paul Scherrer Institut (PSI). Juli 1988. ID PSI/2000
41. E. Egger, A. Schalenbourg, L. Zografos, et al., Maximising local tumour control and survival after proton beam radiotherapy of uveal melanoma. Int. J. Radiat. Oncol. Biol. Phys. **51**, 138–147 (2001)
42. J. Heufelder, D. Cordini, H. Fuchs, et al., Five years of proton therapy of eye neoplasms at the Hahn-Meitner Institute, Berlin. Z. Med. Phys. **14**, 64–71 (2004)
43. I.K. Daftari, K.K. Mishra, J.M. O'Brien, et al., Fundus image fusion in EYEPLAN software: an evaluation of a novel technique for ocular melanoma radiation treatment planning. Med. Phys. **37**, 5199–5207 (2010)
44. B. Dobler, R. Bendl, Precise modelling of the eye for proton therapy of intra-ocular tumours Phys. Med. Biol. **47**, 593–613 (2002)
45. C. Rethfeldt, H. Fuchs, K.U. Gardey, Dose distributions of a proton beam for eye tumor therapy: hybrid pencil-beam ray-tracing calculations. Med. Phys. **33**, 782–791 (2006)
46. J. Herault, N. Iborra, B. Serrano, et al., Spread-out Bragg peak and monitor units calculation with the Monte Carlo Code MCNPX. Med. Phys. **34**, 680–688 (2007)
47. H.M. Kooy, M. Schaefer, S. Rosenthal, et al., Monitor unit calculations for range-modulated spread-out Bragg peak fields. Phys. Med. Biol. **48**, 2797–2808 (2003)
48. H. Palmans, R. Thomas, M. Simon, et al., A small-body portable graphite calorimeter for dosimetry in low-energy clinical proton beams. Phys. Med. Biol. **49**, 3737–3749 (2004)
49. S. Vynckier, D.E. Bonnett, D.T.L. Jones, Code of practice for clinical proton dosimetry (ECHED). Radiother. Oncol. **20**, 53–63 (1991); Suppl. Radiother. Oncol. **32**, 174–179 (1994)
50. N. Koch, W. Newhauser, Virtual commissioning of a treatment planning system for proton therapy of ocular cancers. Radiat. Prot. Dosim. **115**, 159–163 (2004)
51. C. Baker, D. Shipley, H. Palmans, et al., Monte carlo modelling of a clinical proton beam-line for the treatment of ocular tumours. Nucl. Instrum. Methods Phys. Res. A **562**, 1005–1008 (2006)
52. J. Heufelder, S. Stiefel, M. Pfaender, et al., Use of BANG polymer gel for dose measurements in a 68 MeV proton beam. Med. Phys. **30**, 1235–1240 (2003)
53. L. Czopyk, G.A.P. Cirrone, G. Cuttone, et al., 2D dosimetry of a proton radiotherapy beam using large-area LiF: Mg, Cu, P TL detectors. Radiat. Meas. **43**, 977–980 (2008)
54. S. Al-Nowais, S. Doran, A. Kacperek, et al., A preliminary analysis of LET effects in the dosimetry of proton beams using PRESAGE^{TM} and optical CT. Appl. Radiat. Isot. **67**, 415–418 (2009)
55. A.B. Rosenfeld, D. Cutajar, M.L. Lerch, et al., Miniature semiconductor detectors for in vivo dosimetry. Radiat. Prot. Dosim. **120**, 48–55 (2006)
56. D.H. Char, R. Bove, T.L. Phillips, Laser and proton radiation to reduce uveal melanoma-associated exudative retinal detachments. Am. J. Ophthalmol. **136**, 180–182 (2003)
57. H.J. Zambarakji, A.M. Lane, E. Ezra, et al., Proton beam irradiation for neovascular age-related macular degeneration. Ophthalmology **113**, 2012–2019 (2006)

Chapter 11
Clinical Indications for Carbon Ion Radiotherapy and Radiation Therapy with Other Heavier Ions

Stephanie E. Combs

Abstract A number of studies have shown excellent and convincing clinical results for various indications after treatment with ions heavier than protons. These include skull base chordomas and chondrosarcomas, hepatocellular carcinomas, recurrent rectal cancer, high-risk meningiomas, or soft-tissue and bone sarcomas. This chapter outlines these trials and provides a medical rationale for their choice before they are discussed in depth in subsequent chapters.

11.1 Introduction

The inverted dose profile of ion beams permits to move from *dose redistribution* possible with modern and highly conformed photon techniques to genuine *dose reduction* in the patient. Carbon ion beams offer, additionally, an enhanced biological effectiveness (cf. Chaps. 4 and 6). It is this combination of properties that has favored the use of ion beams in general and of carbon ions in particular. In the beginning of ion beam therapy (IBT), the treatment was restricted to rare tumors that were difficult to treat. This has changed over time and more and more indications have been included for which other treatment modalities do not provide adequate results.

S.E. Combs (✉)
Abt. für Radioonkologie und Strahlentherapie, Universitätsklinikum Heidelberg, Im Neuenheimer Feld 400, 69120 Heidelberg, Germany
e-mail: stephanie.combs@med.uni-heidelberg.de

U. Linz (ed.), *Ion Beam Therapy*, Biological and Medical Physics, Biomedical Engineering, DOI 10.1007/978-3-642-21414-1_11,

11.2 Skull Base Tumors

For tumors of the skull base, especially chordomas and chondrosarcomas, proton therapy (PT) can be considered the treatment standard that should be applied when possible. Clinical data from several proton centers have shown superior results compared to photon radiotherapy (RT), and are described in detail in Chap. 12.

Postoperative RT is recommended, and high local doses are required for long-term local tumor control. Early data on IBT, such as the work published by Colli and Al Mefty [1], demonstrated that proton treatment led to higher local control rates compared to photon data of that time. However, since then, improvements in photon RT have also been achieved with techniques such as step-and-shoot intensity-modulated radiation therapy (IMRT) or helical tomotherapy, enabling higher dose deposition also in regions close to vulnerable organs at risk.

At GSI, local control rates of 70% at 5 years were obtained for chordomas and 89.8% at 4 years for chondrosarcomas [2, 3]. At the National Institute for Radiological Sciences (NIRS) in Chiba, Japan, data on CIRT for skull base chordomas in a comparable patient population have even shown local control rates of 85.1% at 5 years and 63.8% at 10 years [4]. The next likely step is a comparison of PT and CIRT with each other.

Facilities such as the Heidelberg Ion-Beam Therapy Center (HIT) enable the conduction of such clinical trials, since protons and carbon ions are available within the center. Therefore, randomized trials have been initiated to obtain these important clinical data [5, 6].

11.3 Brain Tumors

Subgroups of highly malignant brain tumors, such as high-grade gliomas or high-risk meningiomas, are most likely to benefit from the biological properties of carbon ion beams. To date, only limited clinical data are available for these indications. At NIRS, WHO Grade III and IV gliomas have been treated within a clinical trial with photon RT to the low- and high-grade regions of the tumor, adding a carbon ion boost to the macroscopic, contrast-enhancing lesion seen in magnetic resonance imaging (MRI) or identified by amino acid positron emission tomography (PET) [7].

The median overall survival for glioblastoma patients was 17 months. Considering that within this trial the current treatment standard of temozolomide for radiochemotherapy was not applied [8], these data are highly beneficial as compared to survival data from various photon trials. Therefore, this concept seems worth investigating, and is currently being evaluated in the CLEOPATRA trial at the University Hospital of Heidelberg, Germany. In this trial, standard radiochemotherapy with temozolomide is performed in the standard arm, and patients included into the experimental arm are treated additionally with a carbon

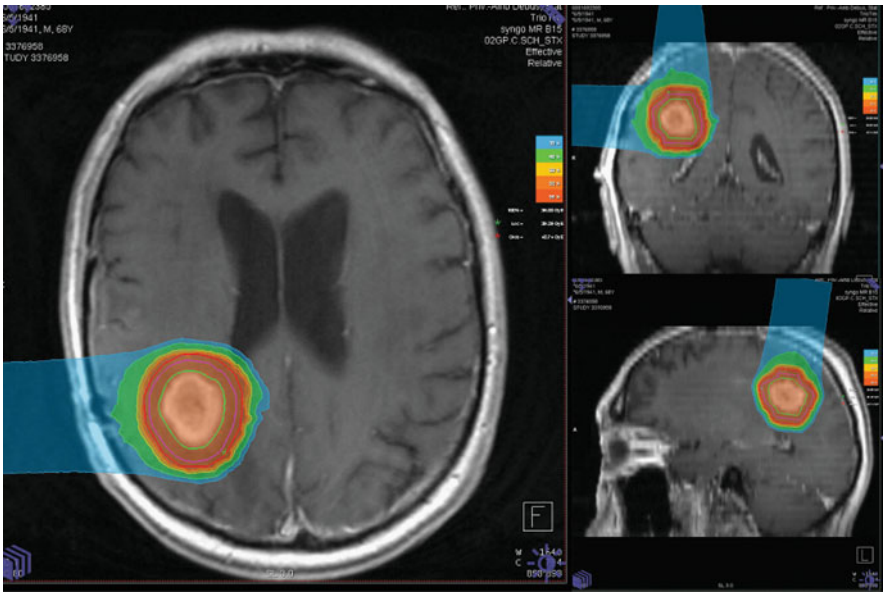

Fig. 11.1 Carbon ion radiation therapy for a patient with a recurrent glioblastoma treated with 10 × 3 GyE as reirradiation

ion boost to the macroscopic high-grade tumor identified by contrast-enhanced MRI as well as amino acid PET [9].

The high precision of carbon ions as well as their high-LET radiation effects (cf. Chap. 4) support the hypothesis that CIRT might also be of benefit for recurrent gliomas. Until now, precision photon RT has been established as a standard for recurrent gliomas, and within the randomized CINDERELLA trial, this technique is considered the standard arm, whereas carbon ions will be explored in a phase I dose escalation scheme, and thereafter as experimental arm in a similar randomized setting [10]. A typical treatment plan for a patient with a recurrent glioblastoma is shown in Fig. 11.1.

High-risk meningiomas, i.e., atypical and anaplastic meningiomas, require high local doses for long-term tumor control. Photon doses exceeding 60 Gy have shown to increase progression-free survival [11]. However, even with advanced photon techniques, such doses can be associated with side effects to normal tissue.

The physical benefits of ion beams should enable local dose escalation without exceeding the tolerance of normal tissues. Unfortunately, treatment of high-risk meningiomas with protons have revealed unsatisfactory local control rates [11–16]. It is assumed that the biological benefit of high-LET ion beams could improve the outcome. Until now, few patients with high-risk meningiomas have been treated with heavier ions.

A group of patients treated with carbon ions at GSI in Germany could show actuarial local control rates of 86% and 72% at 5 and 7 years [17]. The carbon

ions were applied as a boost to macroscopic lesions in combination with photon RT, since the infiltrative nature of the disease requires larger safety margins around the macroscopic tumor. These data are promising, and this concept is currently being investigated within a larger clinical trial (MARCIE [18]).

11.4 Hepatocellular Carcinoma

In the past, RT has played a minor role for the treatment of hepatocellular carcinoma (HCC) since most tumors represent large lesions requiring high local doses and the radiation tolerance of normal liver tissue is limited.

Primary liver cancer is the fifth most common neoplasm in the world, and the third most common cause of cancer-related death; of those, HCC accounts for approx. 75–90% [19]. More than 600,000 new cases are diagnosed per year, corresponding to an incidence rate of 5.5–14.9 per 100,000 [20, 21].

In Western countries, about 30–40% of all patients with HCC are diagnosed in early stages of the disease and potentially curative treatments (surgical resection, liver transplantation) or locoregional procedures such as radiofrequency ablation or chemoembolization can be performed. In such well-selected patient groups, overall survival (OS) rates of 60–70% at 5 years have been observed [22].

Treatment options for patients with advanced HCC are limited and their prognosis is poor [22] without systemic chemotherapeutic treatment [23–25].

The multikinase inhibitor sorafenib has been shown to be effective in patients with HCC: In the multicenter trial SHARP, an increase in OS in patients with advanced HCC from a median of 7.9 months in the placebo group to 10.7 months in the sorafenib group could be demonstrated [26]. Another randomized phase III trial evaluating efficacy and safety of sorafenib in patients with advanced HCC was performed in the Asia-Pacific region, and demonstrated, as well, good tolerability of sorafenib and an increase in OS from 4.2 to 6.5 months [27]. Even though significant, this improvement is still modest and treatment optimization for advanced HCC is needed.

External-beam RT has been applied to HCC also with unsatisfactory results. The low-dose tolerance of the surrounding normal liver tissue limits application of high local doses to larger liver tumors. Radiation-induced liver disease (RILD), defined as a veno-occlusive disease leading to development of ascites, icterus, increase in liver enzymes, and hepatic encephalopathy, is known to develop with total doses of 30–35 Gy delivered to the whole liver [28]. More conformal radiation techniques have shown to be safe, however, only moderately effective in patients with HCC [28–30]. In the past, it could be shown that total doses of >50 Gy lead to significantly better outcome and increased rates of partial tumor responses after RT [31]. Several studies revealed that dose was the only reproducible predictive factor for tumor control [32, 33]. However, as total doses were increased even though using 3D-conformal photon techniques, the rates of radiation-induced side effects increased, as well. Therefore application of higher, locally effective photon

doses is limited to smaller tumors. Stereotactic photon treatments in single-dose or hypofractionated settings could spare functional normal liver tissue more effectively. But with increasing tumor sizes, dose application is again limited [34–37].

New radiation modalities such as IBT may bridge the gap between the required high local radiation dose and the low radiation tolerance of the liver tissue. With ion beams, the precise dose delivery can overcome this obstacle. Moreover, HCC is likely to benefit from the high-LET effects of carbon ions as shown in preclinical experiments [38, 39].

Japanese groups in Chiba and Tsukuba have applied PT to patients with HCC with promising results (cf. Chap. 13 for details). Kato and colleagues achieved 2-year actuarial local progression-free rate of 96% and an actuarial OS rate of 66% [40]. The Tsukuba group demonstrated local control of 93% after 5 years in patients with HCC with limited treatment options other than RT [41]. OS rates were 62% and 33% at 2 and 5 years. No toxicities ≥ grade III were observed, and the treatment was well tolerated. The same group could also demonstrate that high-dose PT may be applied safely to patients with HCC associated with a portal vein tumor thrombus, severe liver cirrhosis, or even to aged patients [42–44].

Carbon ions have been applied in patients with HCC with Child-Pugh A or B in successive dose-escalating protocols. Three-year local control was increased from 81% to 96% as single-fraction doses were increased up to 13.2 GyE. Currently, doses between 32 and 38.8 GyE are applied in two fractions in Japan and local control has been shown to be around 97% at 1 year. Prognostic factors identifying subgroups of patients with an increased benefit from carbon ions were performed without convincing differences. Imada and colleagues published clinical data from 64 patients treated with CIRT with a total dose of 52.8 GyE in four fractions between April 2000 and March 2003 [45]. Patients were grouped with respect to tumor location, which was within 2 cm of the main portal vein in 18 patients (porta hepatis group) and further away from the porta hepatis in 46 patients (non-porta hepatis group). The 5-year overall survival and local control rates were, respectively, 22.2% and 87.8% in the porta hepatis group and 34.8% and 95.7% in the non-porta hepatis group. No difference in the rate of toxicities was noted between both groups.

At the NIRS in Chiba, 24 HCC patients were treated with CIRT in a dose-escalation study increasing total doses from 49.5 to 79.5 GyE in dose increments of 10% in a fixed 15-fraction setting [40, 46]. It could be shown that dose increase was safe without severe treatment-associated side effects, even in the highest dose groups. The authors determined 72 GyE as optimal dose or as lowest dose to yield the highest local tumor control without grade III toxicity. The overall tumor response rate was 71%, with a complete response in 10 out of 24 patients, and a partial response in 7 out of 24 patients.

Although patient cohorts in these IBT studies and the treatment of patients with sorafenib are heterogeneous, the data show that IBT may be a successful treatment alternative for patients with HCC. This could even apply to patients with advanced HCC. To date, patients treated with protons or heavier ions were treated using scattering techniques. Scanned ion beams promise better tumor conformity but they

are much more sensitive to organ motion. This technical challenge is attempted at the HIT with a prospective clinical dose-escalation trial called PROMETHUS-01 [47].

11.5 Prostate Cancer

Prostate cancer cell lines exhibit a low α/β ratio of about 1.5 Gy, which signifies radioresistance. On the other hand, tissue surrounding the prostate, in particular the rectal wall, is highly sensitive to radiation damage and, hence, dose-limiting. This combination of properties is the rationale for the use of carbon ion beams in prostate cancer patients [48].

In Japan, an optimal dose of 66 GyE was established for a regimen of 20 fractions over a time period of 5 weeks [49, 50]. A further phase II study confirmed high effectivity at this dose level with local control in all patients but one. The 4-year biological progression-free survival rate was 87% in the low-risk group and 88% for high-risk patients. In very advanced disease (Stage $\geq$T3a or PSA $\geq$ 20 ng/ml or Gleason score $\geq$ 8), the biological progression-free survival rate was significantly different depending on the period of androgen deprivation therapy (93% for ADT $\geq$ 24 months vs. 73% for ADT $<$ 24 months, $p < 0.01$). Grade 2 late toxicities developed in four patients (2%) for the rectum and nine patients (5%) for the genitourinary system but no grade 3 or higher toxicity was observed [51].

To date, no randomized studies have been conducted that compare CIRT and PT or photon IMRT. This will be a task for the future, especially in centers where all these modalities are available.

11.6 Recurrent Rectal Cancer

Treatment of rectal cancer after primary diagnosis depends on initial staging. Surgical resection is the mainstay for this indication and should be part of the treatment regimen whenever possible. For T1–2 tumors without positive lymph nodes it is considered sufficient if accompanied by close oncological follow-up. For node-negative T3 tumors or node-positive T1–3 tumors, surgery should be followed by radiochemotherapy and adjuvant chemotherapy [52].

There is substantial evidence that RT prior to surgical resection is beneficial for the outcome. Preoperative radiochemotherapy seems to be superior to postoperative RT in stage II–III tumors, for example. Also, significant downstaging could be achieved with radiochemotherapy prior to surgery and local failure rates were reduced from 13% to 6% [53]. Last but not least, toxicity was substantially lower with pre- rather than postoperative radiochemotherapy. Even if advanced surgical techniques such as total mesorectal excision (TME) in combination with radiation and chemotherapy have reduced local failure rates to a few percent [54–56],

recurrences do occur, and treatment options at this stage might be limited because of the size and location of the lesion, as well as due to the prior treatment. It is for these reasons that recurrent rectal cancer remains an entity which is very difficult to tackle by any discipline. Surgery deserves high priority also in the case of recurrence of rectal cancer. It should be evaluated in all instances. If resection remains incomplete or is not possible at all, for example, due to accompanying illnesses adjuvant treatment is required.

RT has been applied for recurrent rectal cancer using several different methods over time. With advanced photon techniques delivering doses precisely through three-dimensional CT- and MRT-based treatment planning, reirradiation can be performed. Doses are commonly limited to 36–45 Gy with small safety margins to account for the normal tissue exposure during prior RT.

IBT using carbon ions has been applied successfully in Japan (see also Chap. 16). Local control rates of up to 81.3% at 3 years were reported. The concept was evaluated within a dose-escalation scheme, starting at 67.2 GyE and increasing the dose up to 73.6 GyE [57]. In the high-dose group, the local control was an excellent 93.7% after 3 years and the 5-year survival rate amounted to 40%. Treatment-related side effects were observed in only about 3% of the patients, remaining significantly lower than side effects associated with surgical resection of recurrent rectal cancer.

To verify if these first results can be corroborated, a dose-escalation study using scanned carbon ion beams is currently in the final preparation phase at the HIT (PANDORA-01 [58]).

11.7 Lung Cancer

For localized non-small-cell-lung cancer (NSCLC), surgery remains the treatment of choice after diagnosis. In inoperable patients, hypofractionated or radiosurgical treatment can be equieffective alternatives.

Some studies have revealed a role for PT in early-stage NSCLC. Four-year local control rates of 89% for stage IA and 39% for stage IB tumors were achieved and the overall survival rates were 70% and 16%, respectively [59]. CIRT was evaluated in two published series: Miyamoto and colleagues analyzed 81 patients with stage I NSCLC. They were treated with carbon ion doses from 59.4 to 96.5 GyE in 18 fractions within the first part of a trial; thereafter, doses of 68.4–79.2 GyE were applied in only nine fractions [60]. In this patient population, the 5-year overall survival was 42%, and the local progression rate 23.2%. With 84% vs. 64%, the local control rate was significantly higher in the 9-fraction group than in the 18-fraction group.

Hypofractionated CIRT up to 72 GyE in nine fractions was evaluated in a phase II study including 50 patients. A 5-year local control rate of 94.7% and a 5-year overall survival of 50% were reported [61]. The authors applied respiratory gating to spare normal lung tissue. Safety was shown in all studies, even in elderly patients with reduced lung function and reduced overall performance.

Sugane et al. published the results of 28 patients aged 80 years and older who underwent CIRT, and analyzed its effectiveness and the impact on the activity of daily life (ADL). The 5-year local control rate for these patients was 95.8%, and the 5-year overall survival rate was 30.7%. No patient had to initiate home oxygen therapy or had decreased ADL [62].

When scanned ion beams are used, more intricate compensation techniques are necessary to avoid massive misalignments due to organ motion. Appropriate techniques are currently under development [63–68]. Together with these modern techniques of organ motion compensation, CIRT promises to be a highly effective treatment for patients with lung cancer. Randomized trials comparing carbon ions with photon or proton treatment or even with surgical resection will be the task of the future.

11.8 Head and Neck Tumors

For tumors in the head and neck region, several proton studies have demonstrated safety and efficacy [69–71]. For carbon ions, especially in radioresistant tumors including malignant melanoma, adenoid cystic carcinoma (ACC), or other non-squamous cell carcinomas, efficacy has also been shown [72]. The largest group of patients with ACC was treated with actively scanned carbon beams in Germany (cf. Chap. 12 for details). Carbon ions were applied as boost to the macroscopic lesion remaining after surgery or biopsy, whereas photon RT was administered to the larger clinical target volume (CTV) accounting for the typical anatomical spread of these tumors. Under these conditions, the locoregional control was considerably higher in the carbon ion boost group, as compared to patients treated with photons alone (72.2% vs. 24.6% at 4 years). However, the overall survival was identical in both groups (75.8% vs. 77.9%) since ACC tends to produce distant metastases ultimately leading to life-limiting tumor progression [73]. Japanese results yielded 50% local control rate for ACC at 5 years [72].

Among head and neck tumors, ACC represent the largest clinical data collection for CIRT, however, direct comparison with protons is warranted, since clinical results from proton treatment at MGH in Boston yielded similar local control rates (93% at 5 years), with distant metastasis-free survival of 62% at 5 years [69]. Therefore, further clinical studies are needed to possibly identify the subgroups of patients which would really benefit from CIRT.

11.9 Soft-Tissue and Bone Sarcomas

Bone tumors or soft-tissue sarcomas have shown convincing clinical responses to CIRT with an improved overall outcome. At NIRS, e.g., the cumulative local control and overall survival rates were 73% and 46% at 3 years for different histological

subtypes [74]. The overall patient numbers for the different entities were too low, however, to permit definite conclusions.

Imai et al. reviewed the data for sacral chordomas only and reported a local control rate of excellent 96% [75]. Unfortunately, location or recurrence were somewhat differently reported. Hence, comparison with other data on sacral chordoma is limited [76, 77].

Doses of carbon ions between 70.4 and 74 GyE seem to be highly effective in controlling chordomas. But further analysis, especially for soft-tissue sarcomas and osteosarcomas, is required. A clinical trial focusing on inoperable osteosarcomas is currently being conducted with scanned carbon ion beams [78].

11.10 Gynecological Malignancies

Tumors of the female pelvis are another indication for which high-LET RT is being considered. Cervical cancer, for example, has yielded excellent clinical results after combined treatment with percutaneous RT and interstitial brachytherapy [79, 80]. With brachytherapy, high local doses can be applied to the macroscopic tumor with steep dose gradients to surrounding normal tissue. Ion beams show comparable conformal dose distributions. Moreover, the biological assets of heavier ion beams are likely to be similar to the biological effect of interstitial high-dose brachytherapy. To date, however, no clinical studies comparing these approaches have been undertaken.

NIRS has the longest experience with CIRT for gynecological cancer (cf. Chap. 15 for details). Initial studies showed substantial late toxicity. The dose to the surrounding normal tissue, to intestine in particular, was obviously too high. Matsushita and colleagues reported that 9 of 94 patients treated in Chiba with carbon ions for cervical cancer developed major long-term side effects [81]. When the doses to the intestines were reduced to under 60 GyE, serious side effects were no longer observed.

To date, no clinical studies have compared treatment with high-LET radiation and combined photon-brachytherapy in these patient groups. This will be a task for the near future, since precise treatment planning for IBT enables selective dose escalation on macroscopic tumor residues.

11.11 Conclusion

A number of studies have shown convincing results for CIRT. Most of these clinical data were generated in Japan using scattered beam techniques, and only few European studies report results from modern scanned carbon ion beams (see Table 11.1).

Table 11.1 Clinical results from carbon ion radiotherapy (CIRT) using active beam delivery

References	Year of Publication	Indication
Combs [23]	2010	High-risk meningiomas
Combs et al. [82]	2010	Recurrent tumors
Combs et al. [83]	2009	Pediatric patients and young adults
Schulz-Ertner et al. [84]	2007	Skull base chordoma
Schulz-Ertner et al. [85]	2007	Skull base chondrosarcoma
Schulz-Ertner et al. [73]	2005	Adenoid cystic carcinoma

Another difference between European and Japanese IBT centers concerns the way biological treatment planning is performed [86–88]. These different approaches require harmonization and standardization to optimally compare the clinical trials and results from the various facilities.

Until now, no randomized clinical trials have been performed to corroborate the benefit of CIRT as compared to PT or advanced photon radiation techniques. This was mainly due to the limited availability of IBT centers and their limited capacity. The first centers to offer various ions opened only recently. They will permit a direct comparison of CIRT to the treatment with other ions or photons. In the years to come, several clinical trials will have to be performed to further define the role of high-LET ions in radiation oncology.

References

1. B. Colli, O. Al Mefty, Chordomas of the craniocervical junction: follow-up review and prognostic factors. J. Neurosurg. **95**, 933–943 (2001)
2. D. Schulz-Ertner, C.P. Karger, A. Feuerhake, et al., Effectiveness of carbon ion radiotherapy in the treatment of skull-base chordomas. Int. J. Radiat. Oncol. Biol. Phys. **68**, 449–457 (2007)
3. D. Schulz-Ertner, A. Nikoghosyan, H. Hof, et al., Carbon ion radiotherapy of skull base chondrosarcomas. Int. J. Radiat. Oncol. Biol. Phys. **67**, 171–177 (2007)
4. J.E. Mizoe, A. Hasegawa, R. Takagi, et al., Carbon ion radiotherapy for skull base chordoma. Skull Base **19**, 219–224 (2009)
5. A.V. Nikoghosyan, I. Karapanagiotou-Schenkel, M.W. Munter, et al., Randomised trial of proton vs. carbon ion radiation therapy in patients with chordoma of the skull base, clinical phase III study (HIT-1-Study). BMC Cancer **10**, 607 (2010)
6. A.V. Nikoghosyan, G. Rauch, M.W. Munter, et al., Randomised trial of proton vs. carbon ion radiation therapy in patients with low and intermediate grade chondrosarcoma of the skull base, clinical phase III study. BMC Cancer **10**, 606 (2010)
7. J.E. Mizoe, H. Tsujii, A. Hasegawa, et al., Phase I/II clinical trial of carbon ion radiotherapy for malignant gliomas: combined X-ray radiotherapy, chemotherapy, and carbon ion radiotherapy. Int. J. Radiat. Oncol. Biol. Phys. **69**, 390–396 (2007)
8. R. Stupp, M.E. Hegi, W.P. Mason, et al., Effects of radiotherapy with concomitant and adjuvant temozolomide versus radiotherapy alone on survival in glioblastoma in a randomised phase III study: 5-year analysis of the EORTC-NCIC trial. Lancet Oncol. **10**, 459–466 (2009)
9. S.E. Combs, M. Kieser, S. Rieken, et al., Randomized phase II study evaluating a carbon ion boost applied after combined radiochemotherapy with temozolomide versus a proton boost after radiochemotherapy with temozolomide in patients with primary glioblastoma: the CLEOPATRA trial. BMC Cancer **10**, 478 (2010)

10. S.E. Combs, I. Burkholder, L. Edler, et al., Randomised phase I/II study to evaluate carbon ion radiotherapy versus fractionated stereotactic radiotherapy in patients with recurrent or progressive gliomas: the CINDERELLA trial. BMC Cancer **10**, 533 (2010)
11. E.B. Hug, A. Devries, A.F. Thornton, et al., Management of atypical and malignant meningiomas: role of high-dose, 3D-conformal radiation therapy. J. Neurooncol. **48**, 151–160 (2000)
12. C. Boskos, L. Feuvret, G. Noël, et al., Combined proton and photon conformal radiotherapy for intracranial atypical and malignant meningioma. Int. J. Radiat. Oncol. Biol. Phys. **75**, 399–406 (2009)
13. G. Noël, M.A. Bollet, V. Calugaru, et al., Functional outcome of patients with benign meningioma treated by 3D conformal irradiation with a combination of photons and protons. Int. J. Radiat. Oncol. Biol. Phys. **62**, 1412–1422 (2005)
14. F.J. Vernimmen, J.K. Harris, J.A. Wilson, et al., Stereotactic proton beam therapy of skull base meningiomas. Int. J. Radiat. Oncol. Biol. Phys. **49**, 99–105 (2001)
15. D.C. Weber, A.J. Lomax, H.P. Rutz, et al., Spot-scanning proton radiation therapy for recurrent, residual or untreated intracranial meningiomas. Radiother. Oncol. **71**, 251–258 (2004)
16. E. Wenkel, A.F. Thornton, D. Finkelstein, et al., Benign meningioma: partially resected, biopsied, and recurrent intracranial tumors treated with combined proton and photon radiotherapy. Int. J. Radiat. Oncol. Biol. Phys. **48**, 1363–1370 (2000)
17. S.E. Combs, C. Hartmann, A. Nikoghosyan, et al., Carbon ion radiation therapy for high-risk meningiomas. Radiother. Oncol. **95**, 54–59 (2010)
18. S.E. Combs, L. Edler, I. Burkholder, et al., Treatment of patients with atypical meningiomas Simpson grade 4 and 5 with a carbon ion boost in combination with postoperative photon radiotherapy: The MARCIE Trial. BMC Cancer **10**, 615 (2010)
19. K. Okuda, Y. Nakanuma, M. Miyazaki, Cholangiocarcinoma: recent progress. Part 1: epidemiology and etiology. J. Gastroenterol. Hepatol. **17**, 1049–1055 (2002)
20. D.M. Parkin, F. Bray, J. Ferlay, P. Pisani, Estimating the world cancer burden: Globocan 2000. Int. J. Cancer **94**, 153–156 (2001)
21. D.M. Parkin, F. Bray, J. Ferlay, P. Pisani, Global cancer statistics, 2002. CA Cancer J. Clin. **55**, 74–108 (2005)
22. J.M. Llovet, A. Burroughs, J. Bruix, Hepatocellular carcinoma. Lancet **362**, 1907–1917 (2003)
23. J.M. Llovet, J. Bruix, Systematic review of randomized trials for unresectable hepatocellular carcinoma: Chemoembolization improves survival. Hepatology **37**, 429–442 (2003)
24. P.M. Lopez, A. Villanueva, J.M. Llovet, Systematic review: evidence-based management of hepatocellular carcinoma – an updated analysis of randomized controlled trials. Aliment Pharmacol. Ther. **23**, 1535–1547 (2006)
25. A. Asnacios, L. Fartoux, O. Romano, et al., Gemcitabine plus oxaliplatin (GEMOX) combined with cetuximab in patients with progressive advanced stage hepatocellular carcinoma: results of a multicenter phase 2 study. Cancer **112**, 2733–2739 (2008)
26. J.M. Llovet, S. Ricci, V. Mazzaferro, et al., Sorafenib in advanced hepatocellular carcinoma. N. Engl. J. Med. **359**, 378–390 (2008)
27. A.L. Cheng, Y.K. Kang, Z. Chen, et al., Efficacy and safety of sorafenib in patients in the Asia-Pacific region with advanced hepatocellular carcinoma: a phase III randomised, double-blind, placebo-controlled trial. Lancet Oncol. **10**, 25–34 (2009)
28. T.S. Lawrence, R.K. Ten Haken, M.L. Kessler, et al., The use of 3-D dose volume analysis to predict radiation hepatitis. Int. J. Radiat. Oncol. Biol. Phys. **23**, 781–788 (1992)
29. J.M. Robertson, T.S. Lawrence, L.M. Dworzanin, et al., Treatment of primary hepatobiliary cancers with conformal radiation therapy and regional chemotherapy. J. Clin. Oncol. **11**, 1286–1293 (1993)
30. J.M. Robertson, T.S. Lawrence, J.C. Andrews, et al., Long-term results of hepatic artery fluorodeoxyuridine and conformal radiation therapy for primary hepatobiliary cancers. Int. J. Radiat. Oncol. Biol. Phys. **37**, 325–330 (1997)
31. H.C. Park, J. Seong, K.H. Han, et al., Dose-response relationship in local radiotherapy for hepatocellular carcinoma. Int. J. Radiat. Oncol. Biol. Phys. **54**, 150–155 (2002)

32. L.A. Dawson, C.J. McGinn, D. Normolle, et al., Escalated focal liver radiation and concurrent hepatic artery fluorodeoxyuridine for unresectable intrahepatic malignancies. J. Clin. Oncol. **18**, 2210–2218 (2000)
33. H.C. Park, J. Seong, K.H. Han, et al., Dose-response relationship in local radiotherapy for hepatocellular carcinoma. Int. J. Radiat. Oncol. Biol. Phys. **54**, 150–155 (2002)
34. H. Blomgren, I. Lax, I. Naslund, R. Svanstrom, Stereotactic high dose fraction radiation therapy of extracranial tumors using an accelerator. Clinical experience of the first thirty-one patients. Acta Oncol. **34**, 861–870 (1995)
35. K.K. Herfarth, J. Debus, F. Lohr et al., Extracranial stereotactic radiation therapy: set-up accuracy of patients treated for liver metastases. Int. J. Radiat. Oncol. Biol. Phys. **46**, 329–335 (2000)
36. J. Wulf, U. Hadinger, U. Oppitz, et al., Stereotactic radiotherapy of extracranial targets: CT-simulation and accuracy of treatment in the stereotactic body frame. Radiother. Oncol. **57**, 225–236 (2000)
37. R. Timmerman, L. Papiez, M. Suntharalingam, Extracranial stereotactic radiation delivery: expansion of technology beyond the brain. Technol. Cancer Res. Treat. **2**, 153–160 (2003)
38. L. Gong, X. Jin, Q. Li, J. Liu, L. An, Heavy ion beams induce survivin expression in human hepatoma SMMC-7721 cells more effectively than X-rays. Acta Biochim. Biophys. Sin. (Shanghai) **39**, 575–582 (2007)
39. X.D. Jin, L. Gong, C.L. Guo, et al., Survivin expressions in human hepatoma HepG2 cells exposed to ionizing radiation of different LET. Radiat. Environ. Biophys. **47**, 399–404 (2008)
40. H. Kato, H. Tsujii, T. Miyamoto, et al., Results of the first prospective study of carbon ion radiotherapy for hepatocellular carcinoma with liver cirrhosis. Int. J. Radiat. Oncol. Biol. Phys. **59**, 1468–1476 (2004)
41. M. Hata, K. Tokuuye, S. Sugahara, et al., Proton beam therapy for hepatocellular carcinoma with limited treatment options. Cancer **107**, 591–598 (2006)
42. M. Hata, K. Tokuuye, S. Sugahara, et al., Proton beam therapy for hepatocellular carcinoma with portal vein tumor thrombus. Cancer **104**, 794–801 (2005)
43. M. Hata, K. Tokuuye, S. Sugahara, et al., Proton beam therapy for hepatocellular carcinoma patients with severe cirrhosis. Strahlenther Onkol. **182**, 713–720 (2006)
44. M. Hata, K. Tokuuye, S. Sugahara, et al., Proton beam therapy for aged patients with hepatocellular carcinoma. Int. J. Radiat. Oncol. Biol. Phys. **69**, 805–812 (2007)
45. H. Imada, H. Kato, S. Yasuda, et al., Comparison of efficacy and toxicity of short-course carbon ion radiotherapy for hepatocellular carcinoma depending on their proximity to the porta hepatis. Radiother. Oncol. **96**, 231–235 (2010)
46. H. Tsujii, J.E. Mizoe, T. Kamada, et al., Overview of clinical experiences on carbon ion radiotherapy at NIRS. Radiother. Oncol. **73**(Suppl 2), S41–S49 (2004)
47. S.E. Combs, et al., Phase II study evaluating the treatment of patients with advanced hepatocellular carcinoma (HCC) with carbon ion radiotherapy: PROMETHEUS-01 Trial. BMC Cancer **11**, 67 (2010)
48. J.F. Fowler, The radiobiology of prostate cancer including new aspects of fractionated radiotherapy. Acta Oncol. **44**, 265–276 (2005)
49. K. Akakura, H. Tsujii, S. Morita, et al., Phase I/II clinical trials of carbon ion therapy for prostate cancer. Prostate **58**, 252–258 (2004)
50. H. Tsuji, T. Yanagi, H. Ishikawa, et al., Hypofractionated radiotherapy with carbon ion beams for prostate cancer. Int. J. Radiat. Oncol. Biol. Phys. **63**, 1153–1160 (2005)
51. H. Ishikawa, H. Tsuji, T. Kamada, et al., Carbon ion radiation therapy for prostate cancer: results of a prospective phase II study. Radiother. Oncol. **81**, 57–64 (2006)
52. R.K. Wong, S. Berry, K. Spithoff, et al., Preoperative or postoperative therapy for stage II or III rectal cancer: an updated practice guideline. Clin. Oncol. (R. Coll. Radiol.) **22**, 265–271 (2010)
53. R. Sauer, H. Becker, W. Hohenberger, et al., Preoperative versus postoperative chemoradiotherapy for rectal cancer. N. Engl. J. Med. **351**, 1731–1740 (2004)
54. R.J. Heald, Total mesorectal excision (TME). Acta Chir. Iugosl. **47**, 17–18 (2000)

55. E. Kapiteijn, E.K. Kranenbarg, W.H. Steup, et al., Total mesorectal excision (TME) with or without preoperative radiotherapy in the treatment of primary rectal cancer. Prospective randomised trial with standard operative and histopathological techniques. Dutch ColoRectal Cancer Group. Eur. J. Surg. **165**, 410–420 (1999)
56. K.C. Peeters, C.A. Marijnen, I.D. Nagtegaal, et al., The TME trial after a median follow-up of 6 years: increased local control but no survival benefit in irradiated patients with resectable rectal carcinoma. Ann. Surg. **246**, 693–701 (2007)
57. S. Yamada, M. Shinoto, Y. Shigeo, et al, [Current status and perspective of heavy ion beam therapy for patients with pelvic recurrence after primarily resected rectal cancer]. Gan To Kagaku Ryoho **36**, 1263–1266 (2009)
58. S.E. Combs, et al., Phase I/II trial evaluating carbon ion radiotherapy for the treatment of recurrent rectal cancer. PANDORA-01-Trial. BMC Cancer (2010)
59. Y. Shioyama, K. Tokuuye, T. Okumura, et al., Clinical evaluation of proton radiotherapy for non-small-cell lung cancer. Int. J. Radiat. Oncol. Biol. Phys. **56**, 7–13 (2003)
60. T. Miyamoto, N. Yamamoto, H. Nishimura, et al., Carbon ion radiotherapy for stage I non-small cell lung cancer. Radiother. Oncol. **66**, 127–140 (2003)
61. T. Miyamoto, M. Baba, N. Yamamoto, et al., Curative treatment of Stage I non-small-cell lung cancer with carbon ion beams using a hypofractionated regimen. Int. J. Radiat. Oncol. Biol. Phys. **67**, 750–758 (2007)
62. T. Sugane, M. Baba, R. Imai, et al., Carbon ion radiotherapy for elderly patients 80 years and older with stage I non-small cell lung cancer. Lung Cancer **64**, 45–50 (2009)
63. C. Bert, A. Gemmel, N. Saito, et al., Dosimetric precision of an ion beam tracking system. Radiat. Oncol. **5**, 61 (2010)
64. C. Bert, A. Gemmel, N. Saito, E. Rietzel, Gated irradiation with scanned particle beams. Int. J. Radiat. Oncol. Biol. Phys. **73**, 1270–1275 (2009)
65. C. Bert, S.O. Grözinger, E. Rietzel, Quantification of interplay effects of scanned particle beams and moving targets. Phys. Med. Biol. **53**, 2253–2265 (2008)
66. C. Bert, N. Saito, A. Schmidt, et al., Target motion tracking with a scanned particle beam. Med. Phys. **34**, 4768–4771 (2007)
67. C. Bert, E. Rietzel, 4D treatment planning for scanned ion beams. Radiat. Oncol. **2**, 24 (2007)
68. E. Rietzel, C. Bert, Respiratory motion management in particle therapy. Med. Phys. **37**, 449–460 (2010)
69. P. Pommier, N.J. Liebsch, D.G. Deschler, et al., Proton beam radiation therapy for skull base adenoid cystic carcinoma. Arch. Otolaryngol. Head Neck Surg. **132**, 1242–1249 (2006)
70. B.L. Ramaekers, M. Pijls-Johannesma, M.A. Joore, et al., Systematic review and meta-analysis of radiotherapy in various head and neck cancers: Comparing photons, carbon-ions and protons. Cancer Treat. Rev. **37**, 185–201 (2011)
71. M.T. Truong, U.R. Kamat, N.J. Liebsch, et al., Proton radiation therapy for primary sphenoid sinus malignancies: treatment outcome and prognostic factors. Head Neck **31**, 1297–1308 (2009)
72. J.E. Mizoe, H. Tsujii, T. Kamada, et al., Dose escalation study of carbon ion radiotherapy for locally advanced head-and-neck cancer. Int. J. Radiat. Oncol. Biol. Phys. **60**, 358–364 (2004)
73. D. Schulz-Ertner, A. Nikoghosyan, B. Didinger, et al., Therapy strategies for locally advanced adenoid cystic carcinomas using modern radiation therapy techniques. Cancer **104**, 338–344 (2005)
74. T. Kamada, H. Tsujii, H. Tsuji, et al., Efficacy and safety of carbon ion radiotherapy in bone and soft tissue sarcomas. J. Clin. Oncol. **20**, 4466–4471 (2002)
75. R. Imai, T. Kamada, H. Tsuji, et al., Carbon ion radiotherapy for unresectable sacral chordomas. Clin. Cancer Res. **10**, 5741–5746 (2004)
76. L. Park, T.F. Delaney, N.J. Liebsch, et al., Sacral chordomas: Impact of high-dose proton/photon-beam radiation therapy combined with or without surgery for primary versus recurrent tumor. Int. J. Radiat. Oncol. Biol. Phys. **65**, 1514–1521 (2006)
77. R. Schoenthaler, J.R. Castro, P.L. Petti, K. Baken-Brown, T.L. Phillips, Charged particle irradiation of sacral chordomas. Int. J. Radiat. Oncol. Biol. Phys. **26**, 291–298 (1993)

78. C. Blattmann, S. Oertel, D. Schulz-Ertner, et al., Non-randomized therapy trial to determine the safety and efficacy of heavy ion radiotherapy in patients with non-resectable osteosarcoma. BMC Cancer **10**, 96 (2010)
79. P.J. Eifel, K. Winter, M. Morris, et al., Pelvic irradiation with concurrent chemotherapy versus pelvic and para-aortic irradiation for high-risk cervical cancer: an update of radiation therapy oncology group trial (RTOG) 90–01. J. Clin. Oncol. **22**, 872–880 (2004)
80. M. Morris, P.J. Eifel, J. Lu, et al., Pelvic radiation with concurrent chemotherapy compared with pelvic and para-aortic radiation for high-risk cervical cancer. N. Engl. J. Med. **340**, 1137–1143 (1999)
81. K. Matsushita, T. Ochiai, H. Shimada, et al., The effects of carbon ion irradiation revealed by excised perforated intestines as a late morbidity for uterine cancer treatment. Surg. Today **36**, 692–700 (2006)
82. S.E. Combs, A. Kalbe, A. Nikoghosyan, et al., Carbon ion radiotherapy performed as re-irradiation using active beam delivery in patients with tumors of the brain, skull base and sacral region. Radiother. Oncol. **98**, 63–67 (2011)
83. S.E. Combs, A. Nikoghosyan, O. Jaekel, et al., Carbon ion radiotherapy for pediatric patients and young adults treated for tumors of the skull base. Cancer **115**, 1348–1355 (2009)
84. D. Schulz-Ertner, C.P. Karger, A. Feuerhake, et al., Effectiveness of carbon ion radiotherapy in the treatment of skull-base chordomas. Int. J. Radiat. Oncol. Biol. Phys. **68**, 449–457 (2007)
85. D. Schulz-Ertner, A. Nikoghosyan, H. Hof, et al., Carbon ion radiotherapy of skull base chondrosarcomas. Int. J. Radiat. Oncol. Biol. Phys. **67**, 171–177 (2007)
86. T. Elsässer, M. Krämer, M. Scholz, Accuracy of the local effect model for the prediction of biologic effects of carbon ion beams in vitro and in vivo. Int. J. Radiat. Oncol. Biol. Phys. **71**, 866–872 (2008)
87. T. Elsässer, M. Scholz, Improvement of the local effect model (LEM) – implications of clustered DNA damage. Radiat. Prot. Dosim. **122**, 475–477 (2006)
88. M. Scholz, N. Matsufuji, T. Kanai, Test of the local effect model using clinical data: tumour control probability for lung tumours after treatment with carbon ion beams. Radiat. Prot. Dosim. **122**, 478–479 (2006)

Chapter 12
Skull Base Tumors

Daniela Schulz-Ertner

Abstract In skull base tumors associated with a low radiosensitivity for conventional radiotherapy (RT), irradiation with proton or carbon ion beams facilitates a safe and accurate application of high tumor doses due to the favorable beam localization properties of these particle beams. Cranial nerves, the brain stem and normal brain tissue can at the same time be optimally spared.

12.1 Introduction

Treatment of skull base tumors is a challenging task. Critical normal tissue structures such as cranial nerves, major brain vessels, eyes and adnexes, the cochlea, brain stem and normal brain tissue limit the application of high radiation doses. Although precision photon RT, such as stereotactic radiotherapy (SRT) and intensity modulated radiotherapy (IMRT), has been shown to yield high control rates in a number of skull base tumors, ion beam therapy (IBT) is assumed to be beneficial especially in chordomas, chondrosarcomas and in some extracranial tumors secondarily invading the skull base such as malignant salivary gland tumors, paranasal sinus tumors and atypical and malignant meningiomas. Based on the hypothesis that protons might lead to a reduction of secondary malignancies, proton therapy (PT) has been considered for benign tumors of the skull base region such as benign meningiomas, neurinomas and pituitary adenomas at some IBT centers, as well. In the following, the expertise with IBT in skull base tumors is summarized.

D. Schulz-Ertner (✉)
Radiologisches Institut am Markus-Krankenhaus, Wilhelm-Epstein-Straße 4, 60431 Frankfurt, Germany
e-mail: daniela.ertner@fdk.info

U. Linz (ed.), *Ion Beam Therapy*, Biological and Medical Physics, Biomedical Engineering, DOI 10.1007/978-3-642-21414-1_12,

12.2 Chordomas and Chondrosarcomas

Chordomas and chondrosarcomas are rare tumors. While the majority of skull base chordomas are located in the region of the clivus, chondrosarcomas show a propensity for the spheno-petrosal and the spheno-occcipital synchondroses. Chondrosarcomas of the nasal cavity and paranasal sinuses might invade the skull base, as well.

Chordomas can be divided into conventional, chondroid and dedifferentiated tumors. Chondrosarcomas are categorized into WHO grade 1–3 tumors based on their degree of cellularity and cytological atypia. Immunohistochemical staining is used to distinguish between chondrosarcomas, chordomas and other skull base tumors.

Since both tumor entities do not tend to metastasize, the treatment strategy consists of local treatments. Surgical removal of chordomas and chondrosarcomas of the skull base is, however, associated with extreme difficulty due to their location in close vicinity to cranial nerves and major vessels. As a consequence, tumor resection with oncologically complete margins is rarely accomplished and high-dose irradiation is recommended after incomplete resection. There is some discussion about the necessity for postoperative high-dose irradiation after complete resections in chondrosarcomas, because local recurrence rates after complete resection have been reported to be lower than 10% [1]. In chordomas, local recurrences are frequently found after incomplete resections. Recently, Takahashi et al. reported a 3-year recurrence-free survival rate of 7.1% for chordoma patients who did not receive adjuvant irradiation after surgery [2]. Upfront postoperative high-dose irradiation is, therefore, recommended in chordomas of the skull base. Ion beams have been found to be ideal for the treatment of chordomas and chondrosarcomas of the skull base, because they permit to deliver higher tumor doses to target volumes located in the skull base as compared to photon RT while adhering to the tolerance doses of normal tissue structures surrounding the tumor. While carbon ions and protons share their physical selectivity, carbon ions furthermore offer enhanced biological efficacy within the Bragg peak which is assumed to be most valuable in slow-growing tumors and tumors with low radiosensitivity for conventional RT, such as chordomas and low-grade chondrosarcomas.

Active beam delivery techniques such as spot-scanning and raster scan techniques, precision head and body immobilization systems, target localization with high accuracy and image-guidance with pretreatment correction of interfractional set-up deviations are used to fully exploit the high spatial accuracy of proton and carbon ion beams at most of the IBT facilities.

Target doses between 70 and 78 GyE are typically chosen for PT in chordomas of the skull base. Chondrosarcomas are treated with somewhat lower target doses between 68 and 75 GyE [3–6]. PT is delivered in a fractionation of 4–5 × 1.8–2.0 GyE per week. Using carbon ion RT (CIRT), total target doses between 60 and 70 GyE are prescribed in chordomas using a fractionation of 7 × 3.0–3.5 GyE per week at GSI. This dose fractionation corresponds to isoeffective doses of 75 to

96 Gy based on a conventional fractionation scheme of 2 Gy per day and assuming an α/β of 2 Gy (α and β being experimentally accessible tissue constants) for late toxicity to the brain tissue and chordoma cells. In chondrosarcomas a lower target dose of 60 GyE (corresponding to an isoeffective dose of 75 Gy) is considered appropriate.

12.2.1 Chordomas

Local control rates after photon RT are unsatisfactory, ranging from 17% to 50% [7–9], most likely due to insufficient radiation doses. A dose–response relationship was found after irradiation of chordoma patients [10, 11]. Based on the published clinical data, doses in the range of 75 Gy are required to achieve satisfactory local control rates in skull base chordomas. Most patients with chordomas of the skull base were treated with ion beams during the last two decades. After delivery of PT, local control rates between 54% and 85% at 5 years were obtained ([3, 4, 6, 12, 13] and Table 12.1).

At NIRS, 33 patients with skull base chordomas were treated with carbon ion beams using passive beam delivery methods between 1995 and 2007. After completion of a dose-escalation trial with target doses between 48.0 and 60.8 GyE given in 16 fractions within 4 weeks, a subsequent clinical phase II trial was performed at a dose level of 60.8 GyE, which was found to be the optimal dose. Preliminary results show a 5-year local control rate of 85% for all patients [13].

At GSI, 44 patients with skull base chordomas were treated with CIRT within a clinical phase I/II trial using the raster scan method for active beam delivery. Initial results were promising with a 3-year local control rate of 87% [16]. An update of the GSI data including 96 patients with skull base chordomas treated between November 1998 and July 2005 showed cumulative 3- and 5-year overall survival rates of 91.8% and 88.5%, respectively. Local control probability was 70% at 5 years and was found to be comparable to the results obtained in large proton series [11].

Prospective randomized phase III trials comparing protons or carbon ions with precision photon RT are not available. Data from retrospective single-center series, however, indicate higher local control rates after RT with protons and carbon ions

Table 12.1 Treatment results in chordomas of the skull base after IBT

References	*n*	RT modality	Dose (GyE)	5y-LCR (%)
Munzenrider [12]	169	Protons (+photons)	66–83	64
Hug [4]	33	Protons	70.7	59
Noel [6]	100	Protons+photons	67	54/4y
Ares [3]	42	Protons	73.5	81
Schulz-Ertner [11]	96	Carbon ions	60[a]	70
Mizoe [13]	33	Carbon ions	60.8	85

LCR local control rate

[a]Corresponding to an isoeffective dose of 75 Gy

as compared to the best photon series. From the available data for chordomas of the skull base it appears likely that doses in excess of 75 Gy will further improve local control [11].

Primary or recurrent tumor status, extent of resection, operability and size of the remaining tumor influence the outcome [3, 4, 6, 11]. Whether gender is a prognostic factor in skull base chordomas is still a matter of controversy. A significantly higher local control rate in male patients reported from some series [17, 18] was not confirmed by others [4, 6, 11].

Hug et al. reported a trend towards better outcome for patients with nonchondroid chordomas treated at the Loma Linda University Medical Center [4], but the presence of chondroid foci in chordomas had no clinical significance in other large series [17]. Furthermore, delivered dose and quality of dose distributions have been identified as prognostic factors. Delivery of CIRT with target doses exceeding 60 GyE (or isoeffective doses of >75 Gy) significantly improved local control probability from 63% to 100% [11]. On the other hand, dose inhomogeneities and cold spots within the target volume might reduce local control probability [4, 6, 19]. Metal implants within the target volume are associated with a reduction of local control rates after protons and CIRT, as well [20, 21].

Based on the available data, PT and CIRT seem to be equally effective at the used dose levels. Randomized phase III trials comparing toxicity of proton and CIRT in chordomas of the skull base at isoeffective dose levels would be needed in order to define the optimal RT modality.

12.2.2 Chondrosarcoma

Postoperative high-dose RT has been performed at most of the IBT centers in low-grade chondrosarcomas after incomplete resections, only. Local control rates between 78% and 94% have been reported in low-grade chondrosarcomas of the skull base after therapy with protons and other ions ([3, 15, 22–24] and Table 12.2).

Rosenberg et al. reported a 5- and 10-year local control rate of 99% and 94%, respectively, for 200 patients with skull base chondrosarcomas treated with proton doses between 64.2 and 79.6 GyE at the MGH in Boston, USA. The majority of

Table 12.2 Treatment results in chondrosarcomas of the skull base after IBT

References	*n*	RT modality	Dose (GyE)	5y-LCR (%)
Rosenberg [22]	200	Protons (+photons)	72.1	99
Hug [4]	25	Protons	70.7	75
Ares [3]	22	Protons	68.4	94
Castro [23]	27	Helium ions	65	78
Noel [24]	26	Protons + photons	67	92/3y
Schulz-Ertner [15]	54	Carbon ions	60[a]	90/4y

LCR local control rate

[a]Corresponding to an isoeffective dose of 75 Gy

patients treated in this series had subtotal (74%) or gross total (5%) resections [22]. Initial results after PT using the spot-scanning technique for 22 patients with skull base chondrosarcomas at the Paul Scherrer Institute in Villigen are promising. Ares et al. reported actuarial 5-year local control and overall survival rates of 94% and 91%, respectively [3]. Helium and neon ions were used for RT of 27 patients with skull base chondrosarcomas at the Lawrence Berkeley Laboratory (LBL) in Berkeley, USA, between 1977 and 1992. Castro et al. achieved a 5-year local control rate of 78% [23].

CIRT was applied at GSI in 54 patients with low- and intermediate-grade chondrosarcomas of the skull base. After target doses between 60 and 70 GyE 4-year local control and overall survival rates of 90% and 98% were reported, respectively [15].

In most of the proton and CIRT series patients with G2 tumors or mixed histology of G1 tumors with focal G2 areas were included, as well. There is only very limited information available on the impact of the histological subclassification and the immunohistochemical characteristics on prognosis. A possible influence of histopathological factors on outcome is discussed. Pritchard et al. found that size and grade significantly influenced prognosis, while age, sex and location were not correlated with outcome [25]. Furthermore, extraskeletal myxoid chondrosarcoma (EMC) are associated with a higher risk for local recurrence and distant metastases as compared to classical low-grade chondrosarcomas [26]. EMC showing histological high-grade features are, therefore, addressed as intermediate-grade tumors by some authors [27].

12.3 Malignant Salivary Gland Tumors

Salivary gland tumors constitute 5–7% of all head and neck tumors. Histology, grading, stage and lymph node metastasis are important prognostic factors. Complete surgical removal and adjuvant radiation therapy is the treatment strategy of choice in high-grade malignant salivary gland tumors, while low-grade malignant salivary gland tumors are treated with surgery alone.

Perineural extension of adenoid cystic carcinomas (ACCs) is associated with poor prognosis. Distant metastases are frequently found, while lymph node metastases might occur in less than 15% of all ACCs [28, 29].

Inoperable tumors with infiltration of the skull base require high target doses. In a randomized clinical phase III trial a significantly higher locoregional control rate was achieved with fast neutron RT as compared to photon RT (56% vs. 17% at 10 years) [30].

Carbon ions offer similar biological properties as neutrons. Between 1998 and 2003, 29 patients with locally advanced ACC were treated with a combination of photon RT and a carbon ion boost to the macroscopic tumor within a clinical phase I/II study at GSI. The total dose was 72 GyE, consisting of conventionally fractionated photon irradiation with 54 Gy to the clinical target volume (CTV) and

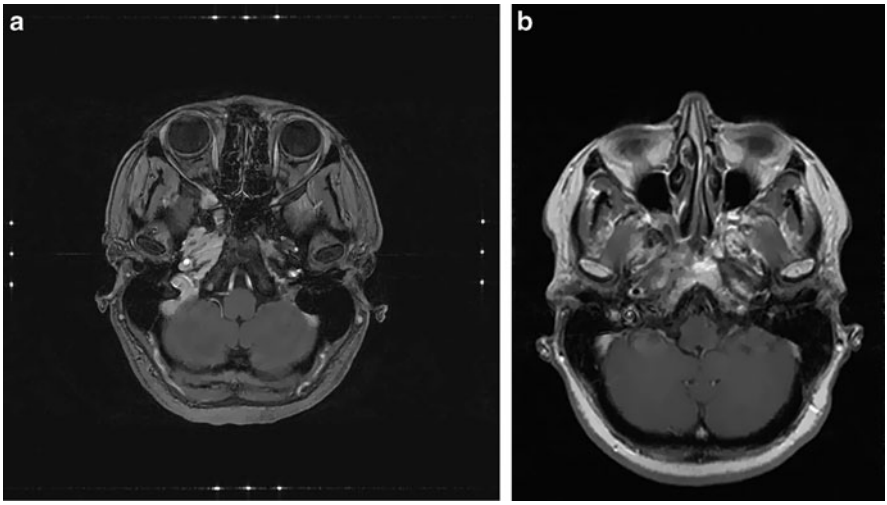

Fig. 12.1 Axial MRI scan of a patient with adenoid cystic carcinoma (ACC) of the skull base (**a**) prior to IBT, (**b**) 6 months after treatment

a carbon ion boost of 18 (6 × 3) GyE to the gross tumor volume (GTV). The 4-year locoregional control and overall survival rates were 77% and 75.8%, respectively (Fig. 12.1). Severe late toxicity grade 4 was observed in one patient, only [31]. For combined photon and CIRT, the CTV for the photon part encompassed the course of the involved cranial nerves up to their entry into the base-of-skull. Elective lymph node irradiation was not performed since occult lymph node metastases are very rare. The GTV to be treated with carbon ions included the macroscopic tumor with a safety margin of 1–2 mm.

Promising results have also been reported for high-dose combined photon and PT in ACCs of the skull base. Pommier et al. reported the results from 23 patients treated at the MGH in Boston. Median dose was approx. 76 GyE. In this retrospective series 13% of the patients were treated after gross tumor resection, the remaining patients were treated after biopsy or partial resection. The 5-year local control rate was 94%, and the overall survival 77% [32].

12.4 Meningioma

Meningiomas represent approx. 15% of all primary CNS tumors. Atypical and malignant meningiomas are rare, amounting to only about 10% of all meningiomas. Neurosurgical resection is considered the treatment of choice. Meningiomas in the skull base region are, however, often difficult to access and incomplete resections are typically followed by recurrences. Salvage therapy consists of repeated surgical

procedures or radiation therapy. High-precision photon RT, such as stereotactic radiosurgery (SRS), fractionated SRT or IMRT with moderate doses between 50 and 60 Gy has been investigated as an alternative to surgery in meningiomas of the skull base. These techniques yield 10-year local control rates between 90% and 96% with low toxicity rates in benign meningiomas [33, 34]. Primary precision photon RT can, therefore, be considered for this tumor entity when complete surgery is unlikely to be accomplished or when surgery is assumed to be associated with a higher risk of morbidity.

Comparable results with respect to control rates and toxicity have been obtained with protons in WHO grade 1 meningiomas. Noel et al. treated 51 patients with WHO Grade 1 meningiomas of the skull base with a combination of photon RT and PT. After combined treatment with a median total dose of approx. 61 GyE the 4-year local control rate was 98%. Severe toxicity occurred in 2 of 51 patients [14].

Gudjonsson et al. treated 19 patients with skull base meningioma with PT in Uppsala, Sweden. They applied 24 GyE in four fractions of 6 GyE. Local control was 100% at 3 years and no patient developed severe toxicity within this time period [35].

Wenkel et al. treated 46 patients with benign skull base meningioma with a median total target dose of 59 GyE using a combination of photons and protons at the MGH in Boston. The 5- and 10-year recurrence-free survival was 100% and 88%, respectively. Survival without severe toxicity was 80% at 5 and 10 years [36].

So far, there are no clinical trials comparing modern fractionated stereotactic photon RT with PT for benign meningioma. Retrospective data do not support the hypothesis that there is a measurable advantage for PT with respect to control rates or toxicity and given the excellent long-term results of SRS and IMRT there might be none.

Patients with atypical and malignant meningiomas show a higher rate of local recurrences after surgery or conventional RT. In a retrospective analysis of the Rare Cancer Network data of 119 patients with atypical and malignant meningiomas from ten academic centers were analyzed. The 5- and 10-year disease-free survival rates were 58% and 48%, respectively. They were significantly influenced by KPS ($p = 0.04$) and high mitotic rate ($p = 0.003$) on univariate analysis [37].

RT doses of 60 Gy are considered insufficient. Dose escalation with IBT has, therefore, been investigated. At the MGH in Boston, dose escalation was realized by combined photon RT and PT in 16 patients, 15 patients received photon RT only. When prognostic factors were analyzed, the use of PT and target doses beyond 60 GyE were associated with significantly higher local control rates [38]. However, this study was not comparing PT with modern photon RT techniques such as IMRT, which allow for dose escalation in atypical and malignant meningiomas, as well [39, 40].

Boskos et al. reported the results of combined photon and PT for 24 patients with atypical and malignant meningiomas (Table 12.3). After irradiation with a median target dose of 65 GyE they observed a local control rate of approx. 47% at 5 years [41].

Table 12.3 Results of IBT for atypical and malignant meningiomas

References	*n*	RT modality	Dose (GyE)	5y-LCR (%)
Hug [38]	31	Photons + protons or photons alone	50–68	AM 19/8y MM 17/8y
Boskos [41]	24	Photons + protons	65.0	47
Combs [43]	10	Photons + carbon ions	68.4	86

LCR local control rate, *AM* atypical meningioma, *MM* malignant meningioma

Treatment results of RT in atypical and malignant meningiomas have to be evaluated with caution, though, because the WHO classification has changed in the meantime [42], and patient recruitment in most of the trials was based on the former WHO classification. The most recent classification is likely to result in a downgrading of many meningiomas. A neuropathological restaging and reanalysis of the data would be necessary in order to prove that the results are valid for the current WHO classification system.

Most recently, Combs et al. reported the results of combined photon and CIRT in ten patients with atypical and malignant meningiomas treated at GSI. All patients had macroscopic tumors at the time of RT. Of ten patients, six received combined treatment as primary treatment. Actuarial local control and overall survival was 86% and 75% at 5 years, respectively. The authors did not observe any severe late effects. At the time of patient inclusion in this phase I/II trial, all tumors were graded as atypical and malignant meningiomas. The pathologic reclassification according to the WHO 2000/2007 classification revealed that only one tumor was anaplastic, five tumors were graded as atypical and three as benign meningiomas. In one patient with previous atypical meningioma, the tumor specimen was not available for reclassification. Histological reclassification did not have an impact on progression-free survival or overall survival in this small patient group [43]. Further prospective trials investigating proton and CIRT in benign and atypical and malignant meningiomas are needed to clearly define their role in the treatment of these tumors.

12.5 Neurinoma and Pituitary Adenoma

The indication for PT in patients with neurinoma and pituitary adenomas is mainly based on the assumption that PT confers a lower risk of secondary cancer induction relative to photons due to a decrease of integral dose delivered to the normal brain tissue. However, many of the current PT facilities still use passive beam delivery techniques, which might lead to significant neutron scatter during RT and thus to a significantly higher effective dose to the patient as compared to photon IMRT [44]. The use of spot-scanning for PT is currently considered one way to overcome this problem [45].

12.5.1 Neurinoma

Five-year local control rates over 90% have been reported for small acoustic neurinomas after surgery, radiosurgery and fractionated SRT [46, 47]. After gamma knife radiosurgery, hearing preservation is achieved in approximately every second patient; after microsurgery, rates between 0% and 84% have been reported [48–50]. For larger neurinomas and neurinomas compressing the brain stem, fractionated stereotactic photon irradiation is the preferred RT modality. Combs et al. reported a 5-year local control probability of 93% for 106 patients treated with fractionated SRT for vestibular schwannomas. The rate of radiation-induced toxicity to the trigeminal and facial nerve was 3.4% and 2.3%, respectively. Noteworthy is the high useful hearing preservation rate of 94% at 5 years [46].

At some of the proton facilities, patients with large acoustic or trigeminal neurinomas and very young patients with neurinomas are accepted for treatment, as well. Weber et al. treated 88 patients with vestibular schwannomas at the Harvard Cyclotron Laboratory (HCL) with proton beam SRS. The median tumor volume was 1.4 cm^3. A median dose of 12 GyE was prescribed to the 70–108% isodose lines (median, 70%). The actuarial 5-year tumor control rate was 94%. Three patients underwent shunting for hydrocephalus, and a subsequent partial resection was performed in one of these patients. Of 21 patients (24%) with functional hearing, 7 (33%) retained serviceable hearing ability (Gardner-Robertson Scale Grade II). Actuarial 5-year normal facial and trigeminal nerve function preservation rates were 91% and 89%, respectively. Univariate analysis revealed that prescribed dose ($p = 0.005$), maximum dose ($p = 0.006$), and dose inhomogeneity ($p = 0.03$) were associated with a significant risk of long-term facial neuropathy [51].

Bush et al. treated 31 acoustic neurinomas in 30 patients with PT at the LLUMC. The mean tumor volume was 4.3 cm^3. Patients were treated with standard fractionated proton RT using daily doses of 1.8–2.0 GyE. Patients with useful hearing before treatment (Gardner-Robertson Grade I or II) received 54 GyE in 30 fractions, patients without useful hearing received 60 GyE in 30–33 fractions. No patients demonstrated disease progression on magnetic resonance imaging scans during follow-up. Of the 13 patients with pretreatment Gardner-Robertson Grade I or II hearing, four (31%) maintained useful hearing. No transient or permanent treatment-related trigeminal or facial nerve dysfunction was observed [52]. With 34 months, the follow-up time in the reported proton series is still short and does not allow a definite conclusion concerning effectiveness and safety of this modality in neurinomas. The reason for the relatively low rate of hearing preservation (< 40%) remains unclear, since target doses were in the same range as compared to recently published fractionated stereotactic photon RT series. A controlled clinical trial comparing fractionated stereotactic photon RT and PT in neurinoma patients seems, therefore, strongly recommended. In addition to local control rate, such a trial should definitely include hearing preservation and toxicity to the facial and trigeminal nerve as clinical endpoints.

12.5.2 Pituitary Adenoma

For pituitary adenomas, transsphenoidal surgery is the treatment of choice. RT is only considered for inoperable tumors because the endocrinological response to irradiation is slow. However, RT has been shown to be effective in recurrences after surgery, in incompletely resected tumors and for postoperatively elevated hormone levels.

In Heidelberg, 68 patients with secreting and nonsecreting pituitary adenomas were treated with SRT or SRS. Overall local tumor control was 93%. After fractionated SRT, 26% with a functional adenoma had a complete remission and 19% had a reduction of hormonal overproduction. Reduction of visual acuity was seen in four patients and partial hypopituitarism in three patients. None of the patients developed brain radionecrosis or secondary malignancies [53].

Minniti et al. treated 102 patients with stereotactic RT and observed a 5-year progression-free survival rate of 98%. In secreting adenomas, hormone levels declined progressively, becoming normal in more than one-third of patients with growth hormone (GH) and prolactin (PRL) secreting pituitary tumors; 50% of baseline GH level was achieved in just under 2 years. The treatment was well tolerated with minimal acute toxicity. Hypopituitarism was the most common long-term effect, 22% of the patients experienced decline in pituitary function [54].

There is only very limited data available on IBT in pituitary gland adenomas. One of the largest patient series was published by Levy et al. in 1991. Since 1956, 475 patients with pituitary adenoma were treated with protons or helium ions at the LBL. Variable degrees of hypopituitarism developed in about one-third of the patients treated solely with radiosurgery [55].

Ronson et al. treated 47 patients with pituitary adenomas with protons. Follow-up was at least 6 months. Approximately half the tumors were functional. The median dose was 54 GyE. Tumor stabilization was obtained in all 41 patients available for follow-up imaging; ten patients had no residual tumor, and three had greater than 50% reduction in tumor size. Seventeen patients with functional adenomas had normalized or decreased hormone levels, progression occurred in three patients. Six patients died, two deaths were attributed to functional progression. Complications included temporal lobe necrosis in one patient, new significant visual deficits in three patients, and incident hypopituitarism in 11 patients [56].

At the MGH, stereotactic proton radiosurgery was used to treat 38 patients with persistent adrenocorticotropin-producing adenomas. After treatment with single doses between 15 and 20 GyE, complete remission was achieved in five patients (100%) with Nelson's syndrome and in 17 (52%) patients with Cushing disease. Fifty-two percent of the patients developed new pituitary deficits, but no other severe side effects or secondary malignancies were observed [57]. Petit et al. treated also 22 patients with persistent acromegaly and 59% attained normal insulin-like growth factor I levels without the use of any medication after a median of 6.3 years [58].

The results after PT in pituitary adenoma patients are in the range of the results reported after modern photon treatments. Follow-up periods are too short

to determine any advantage of protons with respect to late toxicity and secondary malignancies.

References

1. H.L. Evans, A.G. Ayala, M.M. Romsdahl, Prognostic factors in chondrosarcoma of bone. Cancer **40**, 818–831 (1977)
2. S. Takahashi, T. Kawase, K. Yoshida, et al., Skull base chordomas: efficacy of surgery followed by carbon ion radiotherapy. Acta Neurochir. (Wien) **151**, 759–769 (2009)
3. C. Ares, E.B. Hug, A.J. Lomax, et al., Effectiveness and safety of spot scanning proton radiation therapy for chordomas and chondrosarcomas of the skull base: first long-term report. Int. J. Radiat. Oncol. Biol. Phys. **75**, 1111–1118 (2009)
4. E.B. Hug, L.N. Loredo, J.D. Slater, et al., Proton radiation therapy for chordomas and chondrosarcomas of the skull base. J. Neurosurg. **91**, 432–439 (1999)
5. H. Igaki, K. Tokuuye, T. Okumura, et al., Clinical results of proton beam therapy for skull base chordomas. Int. J. Radiat. Oncol. Biol. Phys. **60**, 1120–1126 (2004)
6. G. Noel, J.L. Habrand, E. Jauffret, et al., Chordomas of the base of the skull and upper cervical spine. One hundred patients irradiated by a 3D conformal technique combining photon and protons beams. Acta Oncol. **44**, 700–708 (2005)
7. J. Romero, A. Cardenes, A. la Torre, et al., Chordoma: results of radiation therapy in eighteen patients. Radiother. Oncol. **29**, 27–32 (1993)
8. D.B. Fuller, J.G. Bloom, Radiotherapy for chordoma. Int. J. Radiat. Oncol. Biol. Phys. **15**, 331–339 (1988)
9. J. Debus, D. Schulz-Ertner, L. Schad, et al., Stereotactic fractionated radiotherapy for chordomas and chondrosarcomas of the skull base. Int. J. Radiat. Oncol. Biol. Phys. **47**, 591–596 (2000)
10. P.T.H. Tai, P. Craighead, F. Bagdon, Optimization of radiotherapy for patients with cranial chordoma. Cancer **75**, 749–756 (1995)
11. D. Schulz-Ertner, C.P. Karger, A. Feuerhake, et al., Effectiveness of carbon ion radiotherapy in the treatment of skull-base chordoms. Int J Radiat Oncol Biol Phys **68**, 449–457 (2007)
12. J.E. Munzenrider, N.J. Liebsch, Proton therapy for tumors of the skull base. Strahlenther Onkol. **175**(Suppl 2), 57–63 (1999)
13. J.E. Mizoe, A. Hasegawa, R. Takagi, et al., Carbon ion radiotherapy for skull base chordoma. Skull Base **19**, 219–224 (2009)
14. G. Noel, M.A. Bollet, V. Calugaru, et al., Functional outcome of patients with benign meningioma treated by 3D conformal irradiation with a combination of photons and protons. Int. J. Radiat. Oncol. Biol. Phys. **62**, 1412–1422 (2005)
15. D. Schulz-Ertner, A. Nikoghosyan, H. Hof, et al., Carbon ion radiotherapy in chondrosarcomas. Int. J. Radiat. Oncol. Biol. Phys. **67**,171–177 (2007)
16. D. Schulz-Ertner, A. Nikoghosyan, C. Thilmann, et al., Carbon ion radiotherapy for chordomas and low-grade chondrosarcomas of the skull base. Strahlenther Onkol. **179**, 598–605 (2003)
17. J.X. O'Connell, L.G. Renard, N.J. Liebsch, et al., Base of skull chordoma. Cancer **74**, 2261–2267 (1994)
18. C. Thieblemont, P. Biron, F. Rocher, et al., Prognostic factors in chordoma: role of postoperative radiotherapy. Eur. J. Cancer **31A**, 2255–2259 (1995)
19. A. Terahara, A. Niemierko, M. Goitein, et al., Analysis of the relationship between tumor dose inhomogeneity and local control in patients with skull base chordoma. Int. J. Radiat. Oncol. Biol. Phys. **45**, 351–358 (1999)
20. H.P. Rutz, D.C. Weber, S. Sugahara, et al, Extracranial chordoma: outcome in patients treated with function-preserving surgery followed by spot-scanning proton beam irradiation. Int. J. Radiat. Oncol. Biol. Phys. **67**, 512–520 (2007)

21. O. Jäkel, M. Krämer, C.P. Karger, J. Debus, Treatment planning for heavy ion radiotherapy: clinical implementation and application. Phys. Med. Biol. **46**, 1101–1116 (2001)
22. A.E. Rosenberg, G.P. Nielsen, S.B. Keel, et al., Chondrosarcoma of the base of the skull: a clinicopathologic study of 200 cases with emphasis on its distinction from chordoma. Am. J. Surg. Pathol. **23**, 1370–1378 (1999)
23. J.R. Castro, D.E. Linstadt, J.P. Bahary, et al., Experience in charged particle irradiation of tumors of the skull base: 1977–1992. Int. J. Radiat. Oncol. Biol. Phys. **29**, 647–655 (1994)
24. G. Noel, L. Feuvret, R. Ferraud, et al., Radiotherapeutic factors in the management of cervical-basal chordomas and chondrosarcomas. Neurosurgery **55**, 1252–1260 (2004)
25. D.J. Pritchard, R.J. Lunke, W.F. Taylor, et al, Chondrosarcoma: A clinicopathologic and statistical analysis. Cancer **45**, 149–157 (1980)
26. M. Hisaoka, H. Hashimoto, Extraskeletal myxoid chondrosarcoma: updated clinicopathological and molecular genetic characteristics. Pathol. Int. **55**, 453–463 (2005)
27. J.E. McGrory, M.G. Rock, A.G. Nascimento, A.M. Oliveira, Extraskeletal myxoid chondrosarcoma. Clin. Orthop. Relat. Res. **382**, 185–190 (2001)
28. A.S. Garden, R.S. Weber, W.H. Morrison, et al., The influence of positive margins and nerve invasion in adenoid cystic carcinoma of the head and neck treated with surgery and radiation. Int. J. Radiat. Oncol. Biol. Phys. **32**, 619–626 (1995)
29. R.H. Spiro, Distant metastasis in adenoid cystic carcinoma of salivary origin. Am. J. Surg. **174**, 495–498 (1997)
30. G.E. Laramore, J.M. Krall, T.W. Griffin, et al., Neutron versus photon irradiation for unresectable salivary gland tumors: final report of an RTOG-MRC randomized clinical trial. Int. J. Radiat. Oncol. Biol. Phys. **27**, 235–240 (1993)
31. D. Schulz-Ertner, A. Nikoghosyan, B. Didinger, et al., Therapy strategies for locally advanced adenoid cystic carcinomas using modern radiation therapy techniques. Cancer **104**, 338–344 (2005)
32. P. Pommier, N.J. Liebsch, D.G. Deschler, et al., Proton beam radiation therapy for skull base adenoid cystic carcinoma. Arch. Otolaryngol. Head Neck Surg. **132**, 1242–1249 (2006)
33. J. Debus, M. Wuendrich, A. Pirzkall, et al., High efficacy of fractionated stereotactic radiotherapy of large base-of-skull meningiomas: long-term results. J. Clin. Oncol. **19**, 3547–3553 (2001)
34. M. Brell, S. Villa, P. Teixidor, et al., Fractionated stereotactic radiotherapy in the treatment of exclusive cavernous sinus meningioma: functional outcome, local control, and tolerance. Surg. Neurol. **65**, 28–33 (2006)
35. O. Gudjonsson, E. Blomquist, G. Nyberg, et al., Stereotactic irradiation of skull base meningiomas with high energy protons. Acta Neurochir. (Wien) **141**, 933–940 (1999)
36. E. Wenkel, A.F. Thornton, D. Finkelstein, et al., Benign meningioma: partially resected, biopsied, and recurrent intracranial tumors treated with combined proton and photon radiotherapy. Int. J. Radiat. Oncol. Biol. Phys. **48**, 1363–1370 (2000)
37. D. Pasquier, S. Bijmolt, T. Veninga, et al., Atypical and malignant meningioma: outcome and prognostic factors in 119 irradiated patients. A multicenter, retrospective study of the Rare Cancer Network. Int. J. Radiat. Oncol. Biol. Phys. **71**, 1388–1393 (2008)
38. E.B. Hug, A. DeVries, A.F. Thornton, et al., Management of atypical and malignant meningiomas: role of high-dose, 3D-conformal radiation therapy. J. Neurooncol. **48**, 151–160 (2000)
39. A. Pirzkall, J. Debus, P. Haering, et al., Intensity modulated radiotherapy (IMRT) for recurrent, residual, or untreated skull-base meningiomas: preliminary clinical experience. Int. J. Radiat. Oncol. Biol. Phys. **55**, 362–372 (2003)
40. S. Milker-Zabel, A. Zabel-du Bois, P. Huber, et al., Intensity-modulated radiotherapy for complex-shaped meningioma of the skull base: long-term experience of a single institution. Int. J. Radiat. Oncol. Biol. Phys. **68**, 858–863 (2007)
41. C. Boskos, L. Feuvret, G. Noel, et al., Combined proton and photon conformal radiotherapy for intracranial atypical and malignant meningioma. Int. J. Radiat. Oncol. Biol. Phys. **75**, 399–406 (2009)

42. Louis DN, *WHO Classification of Tumors of the Central Nervous System* (International Agency for Research on Cancer, Lyon, 2007)
43. S.E. Combs, C. Hartmann, A. Nikoghosyan, et al., Carbon ion radiation therapy for high-risk meningiomas. Radiother. Oncol. **95**, 54–59 (2010)
44. E.J. Hall, Intensity-modulated radiation therapy, protons, and the risk of second cancers. Int. J. Radiat. Oncol. Biol. Phys. **65**, 1–7 (2006)
45. U. Schneider, S. Agosteo, E. Pedroni, et al., Secondary neutron dose during proton therapy using spot scanning. Int. J. Radiat. Oncol. Biol. Phys. **53**, 244–251 (2002)
46. S.E. Combs, S. Volk, D. Schulz-Ertner, et al., Management of acoustic neuromas with fractionated stereotactic radiotherapy (FSRT): long-term results in 106 patients treated in a single institution. Int. J. Radiat. Oncol. Biol. Phys. **63**, 75–81 (2005)
47. B.E. Pollock, Vestibular schwannoma management: an evidence-based comparison of stereotactic radiosurgery and microsurgical resection. Prog. Neurol. Surg. **21**, 222–227 (2008)
48. E. Myrseth, P. Moller, P.H. Pedersen, M. Lund-Johansen, Vestibular schwannoma: surgery or gamma knife radiosurgery? A prospective, nonrandomized study. Neurosurgery **64**, 654–661 (2009)
49. I. Yang, M.E. Sughrue, S.J. Han, et al., A comprehensive analysis of hearing preservation after radiosurgery for vestibular schwannoma. J. Neurosurg. **112**, 851–859 (2010)
50. M. Samii, V. Gerganov, A. Samii, Hearing preservation after complete microsurgical removal in vestibular schwannomas. Prog. Neurol. Surg. **21**, 136–141 (2008)
51. D.C. Weber, A.W. Chan, M.R. Bussiere, et al., Proton beam radiosurgery for vestibular schwannoma: tumor control and cranial nerve toxicity. Neurosugery **53**, 577–586 (2003)
52. D.A. Bush, C.J. McAllister, L.N. Loredo, et al., Fractionated proton beam radiotherapy for acoustic neuroma. Neurosurgery **50**, 270–273 (2002)
53. S. Milker-Zabel, J. Debus, C. Thilmann, et al., Fractionated stereotactically guided radiotherapy and radiosurgery in the treatment of functional and nonfunctional adenomas of the pituitary gland. Int. J. Radiat. Oncol. Biol. Phys. **50**, 1279–1286 (2001)
54. G. Minniti, D. Traish, S. Ashley, et al., Fractionated stereotactic conformal radiotherapy for secreting and nonsecreting pituitary adenomas. Clin. Endocrinol. (Oxf) **64**, 542–548 (2006)
55. R.P. Levy, J.I. Fabrikant, K.A. Frankel, et al., Heavy-charged-particle radiosurgery of the pituitary gland: clinical results of 840 patients. Stereotact. Funct. Neurosurg. **57**, 22–35 (1991)
56. B.B. Ronson, R.W. Schulte, K.P. Han, et al., Fractionated proton beam irradiation of pituitary adnomas. Int. J. Radiat. Oncol. Biol. Phys. **64**, 425–434 (2006)
57. J.H. Petit, B.M. Biller, T.I. Yock, et al., Proton stereotactic radiotherapy for persistent adrenocorticotropin-producing adenomas. J. Clin. Endocrinol. Metab. **93**, 393–399 (2008)
58. J.H. Petit, B.M. Biller, J.J. Coen, et al., Proton stereotactic radiosurgery in management of persistent acromegaly. Endocr. Pract. **13**, 726–734 (2007)

Chapter 13
Proton Therapy for Thoracoabdominal Tumors

Hideyuki Sakurai, Toshiyuki Okumura, Shinji Sugahara, Hidetsugu Nakayama, and Koichi Tokuuye

Abstract In advanced-stage disease of certain thoracoabdominal tumors, proton therapy (PT) with concurrent chemotherapy may be an option to reduce side effects. Several technological developments, including a respiratory gating system and implantation of fiducial markers for image guided radiation therapy (IGRT), are necessary for the treatment in thoracoabdominal tumors. In this chapter, the role of PT for tumors of the lung, the esophagus, and liver are discussed.

13.1 Introduction

Thoracoabdominal tumors are common worldwide and mostly include cancers arising from respiratory and gastrointestinal organs such as lung, esophagus, and liver. In comparison with head and neck tumors or urological and gynecological malignancies, most thoracoabdominal tumors are considered to be treatment resistant; i.e., the outcome is insufficient even after several multimodal therapies. The reasons for the poor prognosis include a high rate of distant metastases and a high rate of local recurrences after local therapy, indicating that more intensive local treatment is required for tumors in this category.

A new technique such as stereotactic body radiation therapy (SBRT) has improved local control in early-stage lung and liver cancer through intensive dose delivery. Proton therapy (PT) has a further advantage of excellent dose localization that gives a reduced treatment volume in normal tissues, and dose-escalation protocols with no increase in the dose to normal tissue have been conducted. However, thoracoabdominal tumors in a more advanced stage are more difficult to treat. Concurrent chemoradiotherapy as a multimodal approach is now the standard

H. Sakurai (✉)
Proton Medical Research Center, Department of Radiation Oncology, University of Tsukuba, Tennodai 1-1-1, Tsukuba, Ibaraki 305-8575, Japan
e-mail: hsakurai@pmrc.tsukuba.ac.jp

U. Linz (ed.), *Ion Beam Therapy*, Biological and Medical Physics, Biomedical Engineering, DOI 10.1007/978-3-642-21414-1_13,

treatment for advanced lung and esophageal cancer. In chemoradiotherapy, the high rate of treatment-related morbidity of the lung, heart, and gastrointestinal tract is a concern, because radiosensitization occurs not only in tumor tissue but also in the irradiated normal tissue. PT with concurrent chemotherapy has not been studied widely, but may be a suitable combination because of the reduced volume of irradiated normal tissue.

Thoracoabdominal tumors can also be characterized as tumors that move with respiration. Treatment of lung and liver tumors requires exact patient positioning and precise control of respiratory movement. Intensity-modulated radiation therapy (IMRT) is now used for head and neck and intrapelvic tumors, but because of the complexity of the beam arrangement and the long time required for beam delivery, IMRT is not practical for tumors that are subject to respiratory movement. Conversely, PT with its simple beam arrangement seems predestined for that kind of treatments.

Several technological developments including a respiratory gating system and the implantation of fiducial markers for IGRT have enabled the Proton Medical Research Center (PMRC) at the University of Tsukuba to administer proton beams at high energy levels to deep-seated tumors of the lung, esophagus, and liver.

13.2 Lung

Lung cancer is the leading cause of cancer death worldwide [1]. Surgery plays a major role as curative treatment for non-small cell lung cancer (NSCLC). Patients with inoperable or unresectable NSCLC treated with conventional radiation therapy (RT) show inferior outcomes in terms of local control and survival rates [2, 3]. However, more sophisticated treatment techniques, such as SBRT, have recently produced improvements in local control for early-stage lung cancer. Dosimetric analyses have suggested that PT can achieve a greater reduction of doses to normal tissue, including lung, spinal cord, heart, and esophagus, compared with the dose of 3D conformal RT (3D-CRT) for patients with NSCLC [4–6].

13.2.1 Stage I NSCLC

Five-year survival rates of surgical resection for stage I NSCLC have been reported as 60–70% [2,3]. For patients with inoperable cancer and those who refused surgery 5-year local control and survival rates of only 30–50% and 10–30%, respectively, have been found after conventional, fractionated RT [7, 8]. Since Blomgren et al. showed the potential efficacy of high-dose SBRT for NSCLC [9], high local control rates of stage I NSCLC have been reported in many countries [10–12].

In this context, Bush et al. first reported the results of a prospective study of PT for patients with NSCLC at Loma Linda University Medical Center (LLUMC) [13].

In that study, patients received X-rays of 45 Gy in 25 fractions for a gross tumor including the mediastinum with a concurrent proton boost to the gross tumor of an additional 28.8 GyE in 16 fractions. Thus, a total dose of 73.8 Gy in 41 fractions was given to the tumor. In patients with intercurrent diseases, 51 GyE in ten fractions was given to the tumor using PT alone. The 2-year disease-free and overall survival rates for 27 patients with stage I NSCLC were 87% and 39%, respectively. The majority of patients had poor pulmonary function (average forced expiratory volume in 1 second, FEV1: 1.1 l); none, however, developed clinical radiation pneumonitis. The conclusion from this study was that high-dose PT could be administered safely to patients with poor underlying pulmonary function.

Five years after their first report, Bush et al. reported a second series of results for PT in 68 patients with stage I NSCLC, including 63 with inoperable cancer [14]. Twenty-two patients received 51 GyE in ten fractions and 46 patients received 60 GyE in ten fractions targeted to the primary site using PT alone. The 3-year local control rates in patients with stage IA and IB cancer were 87% and 49%, respectively, and the difference between these rates was significant. The 3-year local control and cause-specific survival rates were 74% and 72%, respectively, which are similar to those reported for surgical series. None of the patients suffered from radiation pneumonitis.

Shioyama et al. reported retrospective results for 28 patients with stage I NSCLC at the University of Tsukuba [15]. Doses of 66–89.1 GyE for stage IA and 66–102.3 GyE for stage IB cases were targeted only to the primary tumor when this was located in a peripheral site or to the primary tumor and the ipsilateral hilum when the tumor was adjacent to the hilum. The 5-year local control and overall survival rates were 89% and 70% respectively, for stage IA cases, and 39% and 16%, respectively, for stage IB. The 5-year local control rate was significantly higher for stage IA cases and similar to the results of Bush et al. [14]. Only one patient suffered from grade 3 toxicity. Nihei et al. reported results for 37 patients who underwent PT of 70–94 GyE targeted to the primary tumor at the National Cancer Center Hospital East (NCCHE) in Kashiwa, Japan [16]. The 2-year local control and overall survival rates were 80% and 84%, respectively, and three patients experienced grade 3 pulmonary toxicity or greater. Based on this study, PT was concluded to be a promising treatment modality for stage I NSCLC.

Nakayama et al. treated 58 tumors (T1: 30, T2: 28) in patients with stage I NSCLC, including 55 inoperable cases, with PT at the new facility of the University of Tsukuba [17]. A total dose of 66 GyE in ten fractions was given to peripherally located tumors, whereas 72.6 GyE in 22 fractions was given for centrally located tumors. The 2-year overall survival and local control rates were 97.8% and 97.0%, respectively, and the 2- and 3-year progression-free survival rates for all patients were 88.7% and 78.9%, respectively. The average FEV1 was limited to 1.1 l in this study; however, only two patients showed deterioration of pulmonary function.

These encouraging results from three institutions indicate that PT may be favorable for treatment of inoperable stage I NSCLC. Representative images of the dose distribution are shown in Fig. 13.1a, and the reports of stage I NSCLC treatment are summarized in Table 13.1.

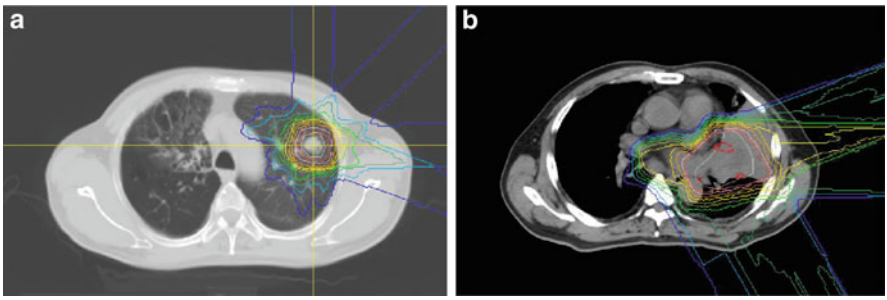

Fig. 13.1 (**a**) A case of proton therapy (PT) for a patient with stage I NSCLC and bronchial ectasia. (**b**) a case of PT for a patient with stage III NSCLC and atelectasis

Table 13.1 PT for stage I NSCLC patients. Reports from the literature

References	Year	Institution	No. of patients	Proton dose (GyE/#Fx)	Local control rate % (at *n* years)	Overall survival % (at *n* years)
Bush et al. [13]	1999	LLUMC	27	51/10	87[a] (2)	39 (2)
				45/25 (Photon)+28.8/16 (Proton)		
Bush et al. [14]	2004	LLUMC	68	51/10	74 (3)	44 (3)
				60/10	IA: 87 IB: 49	
Shioyama et al. [15]	2003	U Tsukuba	28	83.6 (53.9–102.3)	IA: 89 (5)	23[b] (5)
					IB: 39	
Nihei et al. [16]	2006	NCCHE	37	70–94/10	80 (2)	84 (2)
Hata et al. [18]	2007	U Tsukuba	21	55/10	95 (2)	74 (2)
				66/10		
Nakayama et al. [17]	2010	U Tsukuba	55	66/10	97 (2)	97.8 (2)
				72.6/22		

[a]Includes eight stage III patients
[b]Includes nine stage II patients
#Fx number of fractions, *LLUMC* Loma Linda University Medical Center, *NCCHE* National Cancer Center Hospital East, Kashiwa

13.2.2 Stage II–III NSCLC

Five-year survival rates after curative resection in stage II and stage IIIA NSCLC have been reported to be 30–40% and 15–30% [2, 3]. Radiotherapy is mainly performed for the more advanced stage of IIIB, but the outcomes are insufficient. In a study of PT in a small series, Bush et al. found 2-year local control and overall survival rates in eight patients with stage III NSCLC of 87% and 13%, respectively [13]. Shioyama et al. reported 2-year cause-specific and overall survival rates of 70% and 62%, respectively, in nine patients (eight with stage III and one with stage IV NSCLC) [15]. From November 2001 to July 2008, PT alone was performed at the new facility of the University of Tsukuba for 35 patients with stage II–III NSCLC who refused standard therapy or were unsuitable for standard therapy because of intercurrent diseases. The patients included 5, 12, and 18 cases of stage II, IIIA, and IIIB NSCLC, respectively. The total doses were 77.0 GyE in 35 fractions in 13 patients, 83.6 GyE in 38 fractions in seven patients, 72.6 GyE in 22 fractions in six patients, 74.0 GyE in 37 fractions in three patients, and various dose fractionations in six patients. The 1- and 2-year local progression-free survival rates for stage II–III patients were 93.3% and 65.9%, respectively, and the respective 1- and 2-year overall survival rates were 81.8% and 58.9%. No treatment-related toxicity of grade 3 or higher was observed.

Radiation therapy using 3D planning with concurrent chemotherapy is currently increasing the survival rates for advanced-stage NSCLC [19, 20]. Additionally, several phase I/II trials with escalation of radiation doses up to 74 Gy in 37 fractions with combined chemotherapy have resulted in improved survival [21–23]. In principle, PT is advantageous since it allows an increased dose to the target and a decrease to the surrounding organ using Bragg peak properties (Fig. 13.1b). Therefore, further investigations of dose-escalation PT combined with chemotherapy for the treatment of advanced-stage NSCLC is recommended.

13.3 Esophagus

Surgical resection is the current treatment of choice for esophageal carcinoma. Recently, chemoradiotherapy, and combined therapies such as chemoradiotherapy followed by surgery have been established for patients with advanced-stage esophageal cancer [24–26]. From 1983, the Tsukuba group has used PT to treat more than 100 patients with esophageal carcinoma [27–29]. Other than these studies, little information is available on results of PT for esophageal cancer. Therefore, in the following section we introduce our experience in comparison to X-ray treatment.

13.3.1 Survival, Local Control, and Sequelae for Esophageal Cancer

At the former PT facility at Tsukuba [27–29], 46 patients with esophageal cancer who had an intercurrent disease or refused surgery underwent PT or PT combined with X-ray therapy between 1985 and 1998. All patients had locoregionally confined disease and all but one had squamous cell carcinoma. Twenty-three patients had a T1 stage tumor and another 23 had T2, T3, or T4 tumors. Of the 46 cases, 22 were judged inoperable because of intercurrent disease, including cardiovascular ($n = 6$) and chronic pulmonary diseases ($n = 6$), liver cirrhosis ($n = 4$), renal failure ($n = 2$), rheumatoid arthritis ($n = 1$), Crohn's disease ($n = 1$), chronic pancreatitis ($n = 1$), and cerebral infarction ($n = 1$). Four patients had other malignancies: hypopharyngeal cancer ($n = 2$), gastric cancer ($n = 1$), and uterine cervical cancer ($n = 1$), all of which were under control when the esophageal cancer was treated. The characteristics of the 46 patients are shown in Table 13.2. Forty patients received combined therapy of X-rays (median 48 Gy) and protons (median 34 GyE) as a boost. The median total dose of this therapy for the 40 patients was 78 GyE (range 73–90 GyE). The other six patients received PT alone (median 86 GyE, range 82–98 GyE). The 5-year actuarial survival rates for all the patients, for T1, and T2–4 were 34%, 55%, and 13%, respectively, and the respective 5-year disease-specific survival rates were 67%, 95%, and 33%. The 5-year local control rates for T1 and T2–4 lesions were 83% and 29%, respectively. The sites of the first relapse were locoregional for 16 patients and distant for two patients. Acute and late treatment-related toxicities of greater than grade 2 were observed in five patients, each. These data suggest that PT is useful for giving high doses to a limited volume of the esophagus with a low rate of toxicity.

13.3.2 Treatment Procedures for Esophageal Cancer Practiced at the PMRC

Hyperfractionated regimens are currently being used for esophageal carcinoma [29]. To reduce the severe side effects of esophageal ulcer by decreasing the dose fraction, it has been tried to use a schedule of combined X-rays with protons to a total dose of 75 GyE in 44 fractions over approx. 7 weeks. During the first 5 weeks, a larger CTV encompassing the primary tumor and the regional lymph nodes were irradiated with X-rays to a dose of 45 Gy in 25 fractions at 1.8 Gy per day. During the same period, protons were used to deliver a concomitant boost to a smaller target volume encompassing the clinically evident tumor, with 12 GyE given in ten fractions over 5 weeks (twice a week). During weeks 6 and 7, a smaller target volume is irradiated encompassing the clinically evident tumor with protons alone, with 18 GyE in nine fractions over 1.8 weeks. Nineteen patients have been treated with this regimen as of September 2008. The tumors were locally controlled in 13 of 18 patients in whom

Table 13.2 Characteristics of 46 patients treated with PT for esophageal cancer at the PMRC

Age	
Median	72
Range	45–95
Gender [No. of patients and (%)]	
Male	40 (87)
Female	6 (13)
Histology [No. of patients and (%)]	
Squamous cell carcinoma	45 (98)
Adenocarcinoma	1 (2)
Primary length (cm)	
Median	4.0
Range	1.5–15
Primary tumor site [No. of patients and (%)]	
Upper thoracic	4 (8.7)
Middle thoracic	29 (63)
Lower thoracic	12 (26.1)
Abdominal	1 (2.2)
TNM classification [No. of patients and (%)]	
T1	23 (50)
T2	5 (11)
T3	13 (28)
T4	5 (11)
N0	39 (85)
N1	7 (15)

sufficient follow-up data were available. The 5-year survival rate was 41%. Clinical images of a representative case are shown in Fig. 13.2.

We cannot draw any conclusions from our results for PT in patients with esophageal cancer because of the limited number of patients. However, the results appear comparable to the best surgical [30, 31] and chemoradiotherapy [25] series. Definitive chemoradiotherapy followed by surgery has been established as an important therapy for advanced-stage esophageal cancer [24–26]. Data from the RTOG 94–05 trial showed that a total dose of 64.8 Gy in 36 fractions did not improve survival in comparison to 50.4 Gy in 28 fractions in combination with cisplatin chemotherapy, due to increased treatment-related toxicity in the high-dose group [32]. PT has a better dose distribution than conventional RT [33], so simply switching from conventional RT to PT has the potential to reduce toxicity and improve outcomes. A phase II study is ongoing at Tsukuba to examine whether PT increases the local control rate with acceptable toxicity levels in combination with chemotherapy.

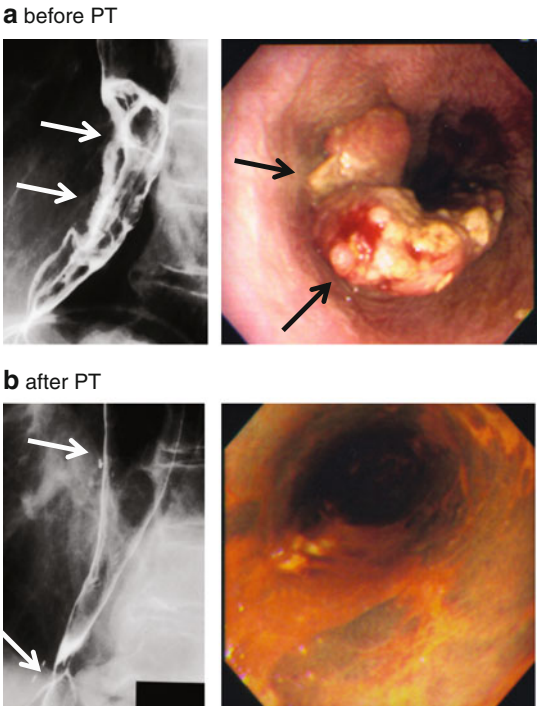

Fig. 13.2 Images of a 77-year-old man who developed esophageal carcinoma staged as cT3N1M0. (**a**) An esophagogram and endoscopic image before PT showed a primary tumor (indicated by the *arrows*). A total dose of 82 GyE was administered in 46 fractions using a concomitant boost regimen. (**b**) An esophagogram and endoscopic image taken 6 months after PT showed complete response of the primary tumor and persistence of a slight esophageal constriction. The *white arrows* indicate fiducial markers implanted at the cranial and caudal boundary of the primary tumor. Normal esophageal function was maintained 27 months after therapy

13.4 Liver

Hepatocellular carcinoma (HCC) is the third leading cause of cancer mortality worldwide [34]. Most HCC cases occur in either sub-Saharan Africa or in Eastern Asia [35]. The geographic variability in the incidence of primary liver cancer is largely explained by the distribution and natural history of the hepatitis B (HBV) and C (HCV) viruses. HBV is the most frequent underlying cause of HCC, whereas chronic HCV infection is a major risk factor in Spain and Japan [35]. The incidence of liver cancer is also increasing in several developed countries, including the United States, where proportional increases occurred in HCV-related HCC as compared to HBV-related HCC, which seems to be stable [35]. Overall age-adjusted incidences of HCC tripled between 1975 and 2005, rising from 1.6 to 4.9 per 100,000 persons [36]. In selected areas of some developing countries, the incidence of liver cancer

has decreased, possibly as a result of the introduction of HBV vaccine [37]. Risk factors for liver cancer other than hepatitis viruses include alcohol, tobacco, oral contraceptives, and aflatoxins [35].

HCC accounts for approx. 85–90% of primary liver cancers [38]. Other histologies of primary liver cancer include intrahepatic cholangiocellular carcinoma (CCC), mixed HCC/CCC, and other rare neoplasms such as hepatoblastoma or sarcoma.

In patients with chronic hepatitis or cirrhosis on the basis of HBV or HCV infection, a variety of hepatocellular lesions, such as dysplastic nodule (DN), adenomatous hyperplasia (AH) and, finally, HCC can be found [39] and a multistep hepatocarcinogenesis process from high-grade DN to HCC has been documented [40, 41].

13.4.1 General Management of HCC

Surgical resection is the mainstay of therapy for HCC, although the majority of patients are not eligible for surgery because of underlying liver cirrhosis or the extent of the tumor. Resection of the gross tumor with a margin of 1–2 cm of normal liver is aimed at. Liver transplantation is another surgical option for patients with a solitary tumor of 5 cm or up to three nodules with a tumor size <3 cm [42]. Radiofrequency ablation (RFA) [43] or percutaneous ethanol injection (PEI) [44] are alternatives for patients with early-stage HCC who are unsuitable for surgical treatment. Since HCC is a highly vascular tumor supplied mainly by the hepatic or adjoining arteries, treatment combining intraarterial embolization with iodized oil and chemotherapy (TACE: transarterial chemoembolization) is also an effective option for unresectable tumors [45].

Radiation therapy has played a limited role in the treatment of hepatic malignancies because of the low tolerance of the whole liver for ionizing radiation. There is a 5% risk for radiation-induced liver disease (RILD) if the whole liver is irradiated with 30–35 Gy of photons in 2-Gy fractions [46, 47]. However, high-dose radiation can be delivered safely provided that a substantial portion of the normal liver is spared. In this context, HCC has recently been recognized as a radiosensitive tumor.

13.4.2 PT Procedure for HCC

Liver tumors are among the most difficult tumors to treat with ion beam therapy because they are difficult to visualize and have a large internal target volume due to respiratory movement. For precise target localization on diagnostic images, in-situ fiducial marker placement or preceding transarterial embolization with iodized oil is recommended [48]. Surgical spacer placement can also be helpful if the tumor lies adjacent to the gastrointestinal tract and is included in a high-dose area [49].

Table 13.3 Clinical results of PT for HCC. Reports from the literature

References	Patient number	Proton dose (GyE/#Fx)	ED (Gy)	Prior therapy %	Local control % (at *n* years)	Overall survival % (at *n* years)
Kawashima et al. [55]	30	76/20	87.4		96 (2)	66 (2)
Bush et al. [56]	34	63/15	74.6		75 (2)	55 (2)
Fukumitsu et al. [57]	51	66/10	91.3	65	94.5 (3)	49.2 (3)
Mizumoto et al. [58]	53	72.6/22	80.5	72	86 (3)	45.1 (3)
Nakayama et al. [54]	318	55/10–79.2/22	78.3–91.3	57(3)	64.7 (3)	

Proton dose (GyE) was calculated with an RBE of 1.1
ED equivalent dose (Gy), *#Fx* number of fractions

Control of respiration-related tumor motion using respiratory gating [50], tumor tracking [51], or restoration of respiratory movement [52] is essential to reduce the internal target volume. IGRT can also help to minimize treatment volumes [53]. Treatment planning CT scans are obtained during the expiratory phase. The clinical target volume (CTV) encompasses the gross tumor volume (GTV) with a 5- to 10-mm margin. The planning target volume (PTV) is designed to cover the CTV with a 5- to 10-mm margin and an additional 5-mm margin in the caudal direction to account for respiratory target movement [54].

13.4.3 Clinical Outcome of PT for HCC

Several institutions have reported the feasibility and effectiveness of PT for HCC (Table 13.3). Clinically significant acute liver toxicity has not been observed during and immediately after focal proton treatment [55, 56, 59–62]. Late toxicity such as RILD, biliary tract stenosis, dermatitis, gastrointestinal bleeding, and rib fracture have been reported, although the incidences were low [54–56, 62]. Slow regression of tumor volumes associated with gradual atrophy of surrounding noncancerous liver tissue is generally observed [63, 64].

Clinical trials for HCC have been performed at the University of Tsukuba. The eligibility criteria for PT for HCC in recent years have included Child-Pugh classification A or B, 3 nodules or less, and tumor sizes up to 15 cm. Most of the cases were considered to be inappropriate for local tumor control using other treatment modalities. All tumors are irradiated using the respiratory gating method. The dose is determined according to the characteristics of the disease in individual patients, as follows:

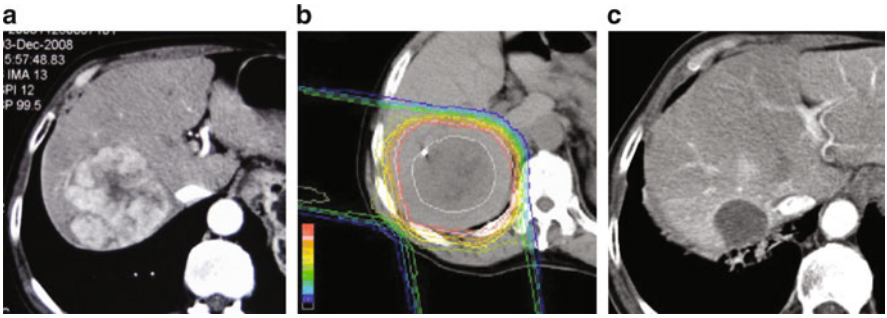

Fig. 13.3 Single nodular type HCC with a maximum dimension of 7.5 cm. The tumor was markedly enhanced with intravenous contrast agent (**a**). Two portals were arranged to encompass the gross tumor volume with a PTV margin of 1 cm. A fiducial marker was implanted on the tumor boundary. The *innermost red line* represents the 95% dose, and the outermost blue line represents the 10% dose (**b**). Lesion shrank and contrast enhancement disappeared 7 months after PT: 66 GyE/10 fractions/15 days (**c**)

Protocol I: 66 GyE/10 fractions for peripheral HCC.
Protocol II: 72.6 GyE/22 fractions for a tumor close to the main portal vein.
Protocol III: 74 GyE/37 fractions for a tumor very close to the stomach or intestine.

The 5-year overall actuarial survival rate in 318 patients treated at PMRC was 44.6%. Child-Pugh liver function, T-stage, performance status, and planning target volume were significant factors affecting survival. The 5-year survival rates were 55.9% for patients with Child-Pugh A disease and 44.5% for those with Child-Pugh B disease [54]

For peripheral tumors, a dose of 66 GyE in ten fractions (2 weeks) was applied to the tumor (Fig. 13.3). This protocol yielded local control rates of 94.5% after 3 and 87.8% after 5 years [57]. Only a minor acute reaction was seen, and 5.9% of the patients developed rib fracture as a chronic complication, which was successfully treated with conservative treatment.

Tumors located within 2 cm of the main portal vein were treated with 72.6 GyE in 22 fractions [58]. Sugahara et al. reported clinical results for tumors larger than 10 cm that were treated using the same dose fractionation. Approximately, half of the patients developed portal vein tumor thrombosis of several grades. The tumor control rate at 2 years was 87% and the overall survival at 2 years was 36% [65]. The predominant tumor progression pattern was new hepatic tumor development outside the irradiated field. These results demonstrate that a large tumor volume can be treated using a high dose without significantly increasing the dose exposure of the functional liver.

Development of a portal vein tumor thrombus (PVTT) is a serious problem in many clinical courses of HCC. RFA and TACE are not effective in such cases and only a few cases can be treated by curative surgery. In a series of 35 cases with tumor thrombi in the main trunk or major branches of the portal vein, PT at a

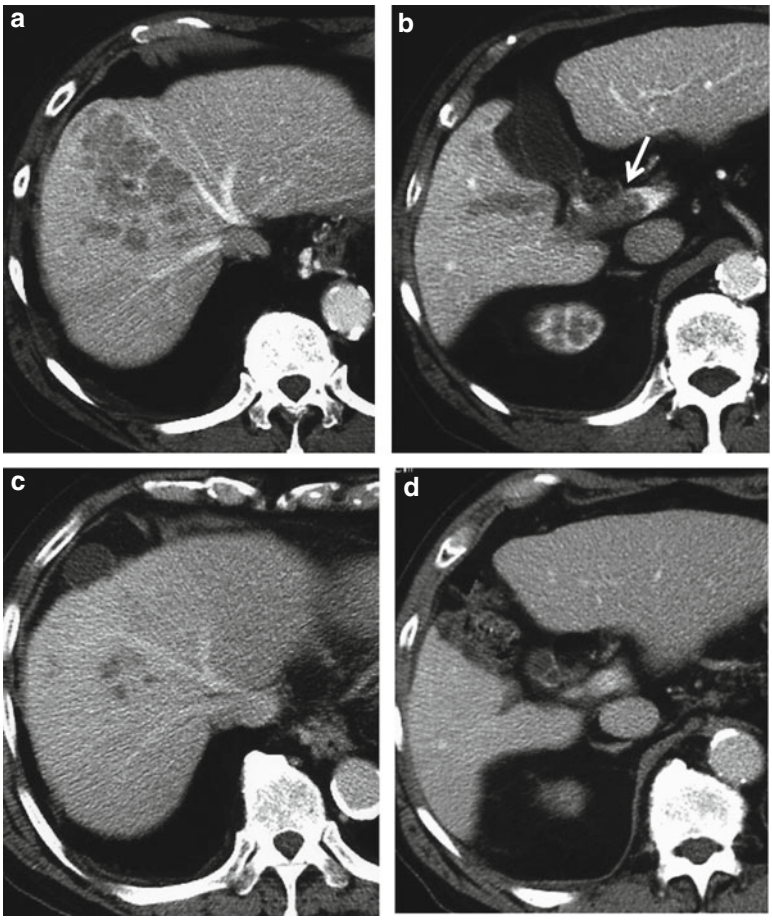

Fig. 13.4 Massive-type HCC with tumor thrombus invading the main portal trunk. The tumor was present in the anterior segment of the right liver (**a**) and a tumor thrombus (*white arrow*) was observed in the main trunk of the portal vein (**b**). Three months after PT (72.6 GyE/22 fractions/37 days), the main tumor showed apparent shrinkage (**c**) and the tumor thrombus had disappeared from the main portal trunk (**d**)

median total dose of 72.6 GyE in 22 fractions was delivered to the PVTT including the primary lesion. The median survival time was 22 months. Local control was achieved in 91% of the patients and about half showed recanalization of the portal vein (Fig. 13.4). These results indicate that PT can improve local control and prolong survival significantly in patients with PVTT [66].

In conclusion, PT gives excellent local control for patients with relatively large and inoperable HCC because a high dose can be delivered to the tumor along with a lower dose to normal liver tissue. The overall local control rate is about 90% and approx. 50% of the patients survive for at least 5 years even if they have a worse condition than those treated with surgery. Especially elderly HCC patients, patients with insufficient liver function, and patients with PVTT seem to profit from PT.

Further studies are required, however, to establish appropriate criteria for patient selection and dose fractionation.

References

1. A. Jemal, R. Siegel, E. Ward, et al., Cancer statistics, CA Cancer J. Clin. **56**, 106–130 (2006)
2. H. Asamura, T. Goya, Y. Koshiishi, et al., A Japanese Lung Cancer Registry study: prognosis of 13,010 resected lung cancers. J. Thorac. Oncol. **3**, 46–52 (2008)
3. M.T. van Rens, A.B. de la Riviere, H.R. Elbers, et al., Prognostic assessment of 2,361 patients who underwent pulmonary resection for non-small cell lung cancer, stage I, II, and IIIA. Chest **117**, 374–379 (2000)
4. C.H. Lee, D. Tait, A.E. Nahum, et al., Comparison of proton therapy and conformal X-ray therapy in non-small cell lung cancer (NSCLC). Br. J. Radiol. **72**, 1078–1084 (1999)
5. C. Wang, H. Nakayama, S. Sugahara, et al., Comparisons of dose-volume histograms for proton-beam versus 3-D conformal x-ray therapy in patients with stage I non-small cell lung cancer. Strahlenther Onkol. **185**, 231–234 (2009)
6. J.Y. Chang, X. Zhang, X. Wang, et al., Significant reduction of normal tissue dose by proton radiotherapy compared with three-dimensional conformal or intensity-modulated radiation therapy in Stage I or Stage III non-small-cell lung cancer. Int. J. Radiat. Oncol. Biol. Phys. **65**, 1087–1096 (2006)
7. D.E. Dosoretz, M.J. Katin, P.H. Blitzer, et al., Radiation therapy in the management of medically inoperable carcinoma of the lung: results and implications for future treatment strategies. Int. J. Radiat. Oncol. Biol. Phys. **24**, 3–9 (1992)
8. G.S. Sibley, T.A. Jamieson, L.B. Marks, et al., Radiotherapy alone for medically inoperable stage I non-small-cell lung cancer: the Duke experience. Int. J. Radiat. Oncol. Biol. Phys. **40**, 149–154 (1998)
9. H. Blomgren, I. Lax, I. Naslund, et al., Stereotactic high dose fraction radiation therapy of extracranial tumors using an accelerator. Clinical experience of the first thirty-one patients. Acta Oncol. **34**, 861–870 (1995)
10. R.C. McGarry, L. Papiez, M. Williams, et al., Stereotactic body radiation therapy of early-stage non-small-cell lung carcinoma: phase I study. Int. J. Radiat. Oncol. Biol. Phys. **63**, 1010–1015 (2005)
11. Y. Nagata, K. Takayama, Y. Matsuo, et al., Clinical outcomes of a phase I/II study of 48 Gy of stereotactic body radiotherapy in 4 fractions for primary lung cancer using a stereotactic body frame. Int. J. Radiat. Oncol. Biol. Phys. **63**, 1427–1431 (2005)
12. J. Wulf, U. Haedinger, U. Oppitz, et al., Stereotactic radiotherapy for primary lung cancer and pulmonary metastases: a noninvasive treatment approach in medically inoperable patients. Int. J. Radiat. Oncol. Biol. Phys. **60**, 186–196 (2004)
13. D.A. Bush, J.D. Slater, R. Bonnet, et al., Proton-beam radiotherapy for early-stage lung cancer. Chest **116**, 1313–1319 (1999)
14. D.A. Bush, J.D. Slater, B.B. Shin, et al., Hypofractionated proton beam radiotherapy for stage I lung cancer. Chest **126**, 1198–1203 (2004)
15. Y. Shioyama, K. Tokuuye, T. Okumura, et al., Clinical evaluation of proton radiotherapy for non-small-cell lung cancer. Int. J. Radiat. Oncol. Biol. Phys. **56**, 7–13 (2003)
16. K. Nihei, T. Ogino, S. Ishikura, et al., High-dose proton beam therapy for Stage I non-small-cell lung cancer. Int. J. Radiat. Oncol. Biol. Phys. **65**, 107–111 (2006)
17. H. Nakayama, S. Sugahara, M. Tokita, et al., Proton beam therapy for patients with medically inoperable Stage I non-small-cell lung cancer at the University of Tsukuba. Int. J. Radiat. Oncol. Biol. Phys. **78**, 467–471 (2010)

18. M. Hata, K. Tokuuye, K. Kagei, et al., Hypofractionated high-dose proton beam therapy for stage I non-small-cell lung cancer: preliminary results of a phase I/II clinical study. Int. J. Radiat. Oncol. Biol. Phys. **68**, 786–793 (2007)
19. K. Furuse, M. Fukuoka, M. Kawahara, et al., Phase III study of concurrent versus sequential thoracic radiotherapy in combination with mitomycin, vindesine, and cisplatin in unresectable stage III non-small-cell lung cancer. J. Clin. Oncol. **17**, 2692–2699 (1999)
20. P. Fournel, G. Robinet, P. Thomas, et al., Randomized phase III trial of sequential chemoradiotherapy compared with concurrent chemoradiotherapy in locally advanced non-small-cell lung cancer: Groupe Lyon-Saint-Etienne d'Oncologie Thoracique-Groupe Français de Pneumo-Cancérologie NPC 95–01 Study. J. Clin. Oncol. **23**, 5910–5917 (2005)
21. J.G. Rosenman, J.S. Halle, M.A. Socinski, et al., High-dose conformal radiotherapy for treatment of stage IIIA/IIIB non-small-cell lung cancer: technical issues and results of a phase I/II trial. Int. J. Radiat. Oncol. Biol. Phys. **54**, 348–356 (2002)
22. S.E. Schild, W.L. McGinnis, D. Graham, et al., Results of a phase I trial of concurrent chemotherapy and escalating doses of radiation for unresectable non-small-cell lung cancer. Int. J. Radiat. Oncol. Biol. Phys. **65**, 1106–1111 (2006)
23. M.A. Socinski, A.W. Blackstock, J.A. Bogart, et al., Randomized phase II trial of induction chemotherapy followed by concurrent chemotherapy and dose-escalated thoracic conformal radiotherapy (74 Gy) in stage III non-small-cell lung cancer: CALGB 30105. J. Clin. Oncol. **26**, 2457–2463 (2008)
24. B.H. Burmeister, B.M. Smithers, V. Gebski, et al., Surgery alone versus chemoradiotherapy followed by surgery for resectable cancer of the oesophagus: a randomised controlled phase III trial. Lancet **6**, 659–668 (2005)
25. J.S. Cooper, M.D. Guo, A. Herskovic, et al., Chemoradiotherapy of locally advanced esophageal cancer: long-term follow-up of a prospective randomized trial (RTOG 85–01). Radiation Therapy Oncology Group. J. Am. Med. Assoc. **281**, 1623–1627 (1999)
26. V. Gebski, B. Burmeister, B.M. Smithers, et al., Survival benefits from neoadjuvant chemoradiotherapy or chemotherapy in oesophageal carcinoma: a meta-analysis. Lancet **8**, 226–234 (2007)
27. S. Sugahara, K. Tokuuye, T. Okumura, et al., Clinical results of proton beam therapy for cancer of the esophagus. Int. J. Radiat. Oncol. Biol. Phys. **61**, 76–84 (2005)
28. N. Fukumitsu, K. Tokuuye, S. Sugahara, et al., A patient surviving for eight years after proton and X-ray irradiation for advanced esophageal cancer. Acta Oncol. **45**, 1132–1134 (2006)
29. M. Mizumoto, S. Sugahara, H. Nakayama, et al., Clinical results of proton-beam therapy for locoregionally advanced esophageal cancer. Strahlenther Onkol. **186**, 482–488 (2010)
30. T. Iizuka, K. Isono, T. Kakegawa, H. Watanabe, Parameters linked to ten-year survival in Japan of resected esophageal carcinoma. Japanese committee for registration of esophageal carcinoma cases. Chest **96**, 1005–1011 (1989)
31. H. Akiyama, M. Tsurumaru, H. Udagawa, et al., Radical lymph node dissection for cancer of the thoracic esophagus. Ann. Surg. **220**, 364–373 (1994)
32. B.D. Minsky, T.F. Pajak, R.J. Ginsberg, et al., INT 0123 (Radiation Therapy Oncology Group 94–05) phase III trial of combined-modality therapy for esophageal cancer: high-dose versus standard-dose radiation therapy. J. Clin. Oncol. **20**, 1167–1174 (2002)
33. X. Zhang, K.L. Zhao, T.M. Guerrero, et al., Four-dimensional computed tomography-based treatment planning for intensity-modulated radiation therapy and proton therapy for distal esophageal cancer. Int. J. Radiat. Oncol. Biol. Phys. **72**, 278–287 (2008)
34. D.M. Parkin, F. Bray, J. Felay, et al., Estimating the world cancer burden: GLOBOCAN 2000. Int. J. Cancer **94**, 153–156 (2001)
35. H.B. El-Serag, K.L. Rudolph, Hepatocellular carcinoma: epidemiology and molecular carcinogenesis. Gastroenterology **132**, 2557–2576 (2007)
36. S.F. Altekruse, K.A. McGlynn, M.E. Reichman, Hepatocellular carcinoma incidence, mortality and survival trends in the United States from 1975 to 2005. J. Clin. Oncol. **27**, 1485–1491 (2009)

37. F.X. Bosch, J. Ribes, M. Diaz, R. Cleries, Primary liver cancer: worldwide incidence and trends. Gastroenterology **124**, S5–S16 (2004)
38. H.B. El-Serag, K.L. Rudolph, Hepatocellular carcinoma: epidemiology and molecular carcinogenesis. Gastroenterology **132**, 2557–2576 (2007)
39. R. Ian, M.D. Wanless, Terminology of nodular hepatocellular lesions. International Working Party. Hepatology **22**, 983–993 (1995)
40. M. Sakamoto, S. Hirohashi, H. Tsuda, et al., Multicentric independent development of hepatocellular carcinoma revealed by analysis of hepatitis B virus integration pattern. Am. J. Surg. Pathol. **13**, 1064–1067 (1989)
41. O. Matsui, M. Kadoya, T. Kameyama, et al., Adenomatous hyperplastic nodules in the cirrhotic liver: differentiation from hepatocellular carcinoma with MR imaging. Radiology **173**, 123–126 (1989)
42. J. Yamamoto, S. Iwatsuki, T. Kosuge, et al., Should hepatomas be treated with hepatic resection or transplantation? Cancer **86**, 1151–1158 (1999)
43. S.A. Curley, F. Izzo, L.M. Ellis, et al., Radiofrequency ablation of hepatocellular cancer in 110 patients with cirrhosis. Ann. Surg. **232**, 381–391 (2000)
44. S.M. Lin, C.J. Lin, C.C. Lin, et al., Randomized controlled trial comparing percutaneous radiofrequency thermal ablation, percutaneous ethanol injection, and percutaneous acetic acid injection to treat hepatocellular carcinoma of 3 cm or less. Gut **54**, 1151–1156 (2005)
45. J.M. Llovet, J. Bruix, Systematic review of randomized trials for unresectable hepatocellular carcinoma: chemoembolization improves survival. Hepatology **37**, 429–442 (2003)
46. J. Ingold, G. Reed, H. Kaplan, Radiation hepatitis. Am. J. Roentgenol. Radium Ther. Nucl. Med. **93**, 200–208 (1965)
47. B. Emami, J. Lyman, A. Brown, et al., Tolerance of normal tissue to therapeutic irradiation. Int. J. Radiat. Oncol. Biol. Phys. **21**, 109–122 (1991)
48. Y. Matsuzaki, T. Osuga, Y. Saito, et al., A new, effective and safe therapeutic option using proton irradiation for hepatocellular carcinoma. Gastroenterology **106**, 1032–1041 (1994)
49. S. Komatsu, Y. Hori, T. Fukumoto, et al., Surgical spacer placement and proton radiotherapy for unresectable hepatocellular carcinoma. World J. Gastroenterol. **16**, 1800–1803 (2010)
50. K. Ohara, T. Okumura, M. Akisada, et al., Irradiation synchronized with respiration gate. Int. J. Radiat. Oncol. Biol. Phys. **17**, 853–857 (1989)
51. H. Shirato, S. Shimizu, K. Kitamura, et al., Four-dimensional treatment planning and fluoroscopic real-time tumor tracking radiotherapy for moving tumor. Int. J. Radiat. Oncol. Biol. Phys. **48**, 435–442 (2000)
52. H. Onishi, K. Kuriyama, T. Komiyama, et al., Clinical outcomes of stereotactic radiotherapy for stage I non-small cell lung cancer using a novel irradiation technique: patient self-controlled breath-hold and beam switching using a combination of linear accelerator and CT scanner. Lung Cancer **45**, 45–55 (2004)
53. D. Verellen, M. De Ridder, G. Storme, A (short) history of image-guided radiotherapy. Radiother. Oncol. **86**, 4–13 (2008)
54. H. Nakayama, S. Sugahara, M. Tokita, et al., Proton beam therapy for hepatocellular carcinoma: the University of Tsukuba experience. Cancer **115**, 5499–5506 (2009)
55. M. Kawashima, J. Furuse, T. Nishio, et al., Phase II study of radiotherapy employing proton beam for hepatocellular carcinoma. J. Clin. Oncol. **23**, 1839–1846 (2005)
56. D.A. Bush, D.J. Hillebrand, J.M. Slater, et al., High-dose proton radiotherapy of hepatocellular carcinoma: preliminary results of a phase II trial. Gastroenterology **127**, S189–S193 (2004)
57. N. Fukumitsu, S. Sugahara, H. Nakayama, et al., A prospective study of hypofractionated proton beam therapy for patients with hepatocellular carcinoma. Int. J. Radiat. Oncol. Biol. Phys. **74**, 831–836 (2009)
58. M. Mizumoto, K. Tokuuye, S. Sugahara, et al., Proton beam therapy for hepatocellular carcinoma adjacent to the porta hepatis. Int. J. Radiat. Oncol. Biol. Phys. **71**, 462–467 (2008)
59. H. Tsuji, T. Okumura, A. Maruhashi, et al., Dose-volume histogram analysis of patients with hepatocellular carcinoma regarding changes in liver function after proton therapy. Nippon Igaku Hoshasen Gakkai Zasshi. **55**, 322–328 (1995)

60. K. Ohara, T. Okumura, H. Tsuji, et al., Radiation tolerance of cirrhotic livers in relation to the preserved functional capacity: analysis of patients with hepatocellular carcinoma treated by focused proton beam radiotherapy. Int. J. Radiat. Oncol. Biol. Phys. **38**, 367–372 (1997)
61. H. Tsujii, H. Tsuji, T. Inada, et al., Clinical results of fractionated proton therapy. Int. J. Radiat. Oncol. Biol. Phys. **25**, 49–60 (1992)
62. T. Chiba, K. Tokuuye, Y. Matsuzaki, et al., Proton beam therapy for hepatocellular carcinoma: a retrospective review of 162 patients. Clin. Cancer Res. **11**, 3799–3805 (2005)
63. K. Ohara, T. Okumura, H. Tsuji, et al., Clearance of parenchymal tumors following radiotherapy: analysis of hepatocellular carcinomas treated by proton beams. Radiother. Oncol. **41**, 233–236 (1996)
64. T. Ahmadi, Y. Itai, H. Onaya, et al., CT evaluation of hepatic injury following proton beam irradiation: Appearance, enhancement, and 3D size reduction pattern. J. Comp. Assist. Tomogr. **23**, 655–663 (1999)
65. S. Sugahara, Y. Oshiro, H. Nakayama, et al., Proton beam therapy for large hepatocellular carcinoma. Int. J. Radiat. Oncol. Biol. Phys. **76**, 460–466 (2009)
66. S. Sugahara, H. Nakayama, K. Fukuda, et al., Proton-beam therapy for hepatocellular carcinoma associated with portal vein tumor thrombosis. Strahlenther Onkol. **85**, 782–788 (2009)

Chapter 14
Carbon Ion Radiotherapy for Peripheral Stage I Non-Small Cell Lung Cancer

Tadashi Kamada, Naoyoshi Yamamoto, and Masayuki Baba

Abstract The National Institute of Radiological Sciences in Chiba, Japan (NIRS) has the highest number of patients with lung cancer treated with carbon ion beams in the world. This report describes the techniques and clinical trials that have been undertaken at NIRS and preliminary results of a current study on single-fraction irradiation. The data are compared to recent results for the treatment of peripheral stage I lung cancer from the literature.

14.1 Introduction

Non-small cell lung cancer (NSCLC) is divided into two groups for radiotherapy (RT). One group is advanced lung cancer, including invasion of the chest wall, mediastinum, and/or mediastinal lymph nodes. The other group is early-stage disease, i.e., peripherally localized T1 or T2 tumors without evidence of lymph node metastases. In general, only early-stage lung cancer is expected to have a long survival.

Surgical resection has played a pivotal role in the treatment of peripherally localized lung cancer and can achieve 5-year survival rates of 60% and 5-year local control rates of more than 80% [1, 2]. The first recommendation for the treatment of early-stage peripheral lung cancer has been surgical resection. However, this is not always feasible or can increase morbidity due to patients' medical conditions, such as pulmonary or cardiovascular disease. RT has played an important role as an alternative treatment. However, conventional RT achieves only poor control of the primary tumor resulting in 5-year survival rates of 30% at best [3]. Dose escalation is essential to improve the effectiveness of RT, but this involves an increasing risk of

T. Kamada (✉)
National Institute of Radiological Sciences, Research Center of Charged Particle Therapy, Anagawa 4-9-1, Inage-ku, Chiba, 263-8555, Japan
e-mail: t_kamada@nirs.go.jp

U. Linz (ed.), *Ion Beam Therapy*, Biological and Medical Physics, Biomedical Engineering, DOI 10.1007/978-3-642-21414-1_14,

normal tissue toxicity, especially pulmonary toxicity [4]. As it can even cause fatal reactions, it limits the applicable dose to the tumor. The goal of RT for lung cancer must, therefore, be a higher dose to the target and lower doses to normal tissues, such as lung parenchyma, esophagus, and spinal cord.

As a substitute for conventional RT, which could only be a palliative treatment for medically inoperable localized NSCLC, various modalities of RT have recently been developed, such as stereotactic body radiotherapy using photon beams (SBRT) and ion beam therapy (IBT). SBRT is spreading worldwide and a variety of new machines and techniques are being developed [5–9]. The radiation doses are usually divided into multiple fractions given in multiple sessions. Hypofractionated SBRT, where few fractions of higher doses are administered, is usually applied for the treatment of peripheral stage I lung cancer [6–10]. Onishi et al. reported SBRT results for 257 patients with stage I NSCLC, which showed lower toxicity and good local control rates (5.4% for the pulmonary complications above grade 2, and 14% for the local progression) [9]. Japan is one of the leading countries in the use of hypofractionated SBRT for early stage lung cancer [5].

Ion beams with their improved dose distribution are a novel promising method to apply a higher dose to the tumor while minimizing the dose to surrounding normal tissues. In particular, carbon ion radiotherapy (CIRT) seems to be an attractive modality due to its excellent dose distribution and increased biological effects in the Bragg peak region (cf. Chap. 4 for details). Our clinical trials led us to conclude that irradiation with ion beams, notably carbon ions, offers a significant potential for improving tumor control without increasing the risk of toxicity [11–15].

14.2 CIRT for Lung Cancer at NIRS

NIRS has conducted clinical trials on CIRT for lung cancer since 1994. For peripheral early-stage NSCLC, a dose-escalation study using 18 fractions in 6 weeks was started in 1994. Between 1994 and 1999, a phase I/II dose-escalation study of the treatment of stage-I peripheral NSCLC was conducted to determine the optimal dose and to evaluate if progression to hypofractionated CIRT was feasible [11]. Another purpose of these trials was to develop precise and safe irradiation techniques with maximum sparing of normal tissue.

The phase I/II study provided the following results:

1. The local control rate was dose dependent. Local control reached more than 90% at 90.0 GyE with a regimen of 18 fractions over 6 weeks and 72.0 GyE with a regimen of 9 fractions over 3 weeks. Both doses were determined to be optimal in each fractionation.
2. Damage to the lung was minimal; grade 3 radiation pneumonitis occurred in 2.7% of the cases. Respiratory-gated and 4-portal oblique irradiations, which excluded opposed ports, proved successful for reducing the incidence of radiation pneumonitis.

3. Survival was significantly related to the local control and tumor size of the primary lesion. Local failure, distant metastasis, and malignant pleurisy accounted for decreases in survival.

After the phase I/II study using this optimized schedule, a phase II clinical trial that enrolled a total of 127 patients was initiated in April 1999 and was closed in December 2003 [12, 13]. In the phase II clinical trial, the total dose was fixed at 72.0 GyE in 9 fractions within 3 weeks, and at 52.8 GyE for stage IA NSCLC and 60.0 GyE for stage IB NSCLC in 4 fractions within 1 week. After confirming the feasibility to irradiate in 4 fractions, a phase I/II dose-escalation clinical trial for single-fraction irradiation for peripheral stage I NSCLC was initiated in April 2003. The initial total dose was 28.0 GyE administered in a single fraction using respiratory-gated and 4-portal oblique irradiation. The total dose was escalated in increments of 2.0 GyE up to 48.0 GyE. This clinical trial is still in progress at this moment (February 2011). This article describes the preliminary results of the phase I/II clinical trial and the recent results of the phase II clinical trial in terms of local control and survival rate after CIRT.

14.3 Treatment Methodology

14.3.1 Staging

Computed tomography (CT) scans of the chest and the whole abdomen, enhanced magnetic resonance imaging (MRI) of the brain, bone scans, and bronchoscopy are routinely performed to permit staging. Enrollment in clinical trials is subject to clear pathological diagnosis of NSCLC based on transbronchial tumor biopsy (TBB), transbronchial aspiration cytology (TBAC), or CT-guided percutaneous needle biopsy (PCNB). If regional lymph nodes are greater than 1 cm in the short axis on contrast-enhanced CT images, as well as positive on a ^{11}C-methionine positron emission tomography (PET) scan, the regional lymph nodes are considered positive for metastasis [16]. Recently, it has been introduced that in such a case endobronchial ultrasound-guided transbronchial needle aspiration (EBUS-TBNA) for the hilar and mediastinal lymph nodes is performed to determine the metastasis status, more clearly. Clinical staging is performed according to the UICC TNM classification [17].

14.3.2 Marker Insertion

Small iridium markers (length: 3 mm, diameter: 0.5 mm) are inserted into the lung to verify position and direction of a patient's body during the irradiation. The markers do not interfere with planning and implementation of the treatment. Routinely, two iridium rods are bronchoscopically placed into the patient's lung (Fig. 14.1). The

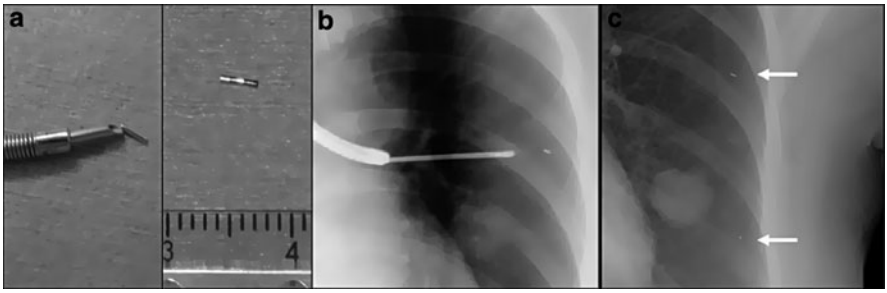

Fig. 14.1 (**a**) *Left*: Size comparison of an iridium marker and the tip of a large-diameter biopsy needle. *Right*: iridium marker with ruler of millimeter gradations. (**b**) X-ray image of bronchoscopic placement of an iridium marker in the lung. (**c**) X-ray image after placement of two iridium markers. The *white arrows* mark their positions

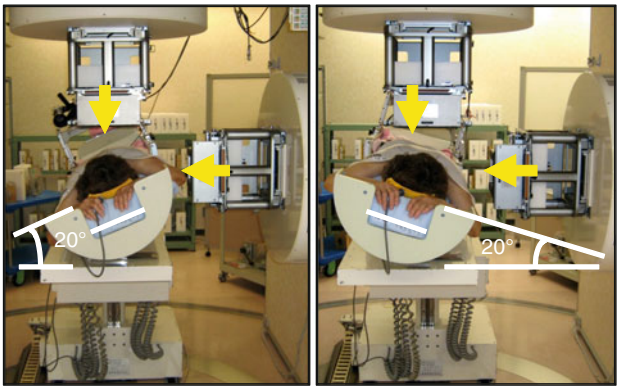

Fig. 14.2 Treatment room with patient fixed in cradle. Irradiation is from four directions. The *yellow arrows* indicate the vertical and horizontal position of the beams. They are directed onto the patient, who is tilted to the left or right by 20°, each

markers serve as fiducial centers to verify the position of the tumor in the lung. In each treatment session, they are visualized by X-ray radiography [18].

14.3.3 Immobilization

The immobilization devices consist of polyurethane fixtures and thermoplastic plates. The fixtures and plates are personalized for each patient before CT scanning for treatment planning. Usually, the patient is in supine position. If the tumor is in the posterior lung, the patient assumes a prone position (Fig. 14.2).

Irradiation is typically from four directions. As the beam lines are fixed in vertical and horizontal directions, respectively, the other two directions are achieved by tilting the patient to the left or right [18].

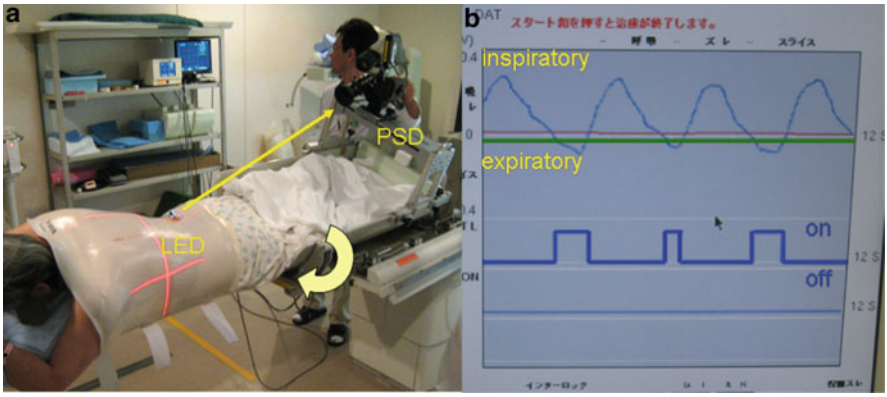

Fig. 14.3 (**a**) Positioning for planning CT-scan. The patient is fixed onto the couch in prone position. The couch is rotated by 20°. A light emitting diode (LED) is attached to the patient's back and the light spot of the LED is focused onto a position-sensitive detector (PSD). (**b**) Respiratory waveform. The *green line* is the threshold of the lung excursion. The *blue line* is the on–off signal of the beam

14.3.4 Respiratory Gating

CT images for treatment planning are taken in synchronization with respiratory motion. Because the displacement of a tumor is generally lowest at the end of the expiratory phase, this is applied for the actual irradiation. Respiration is monitored by measuring the excursions of the chest wall.

The respiratory sensing system uses a position-sensitive detector (PSD) as camera and an infrared light-emitting diode (LED). The LED (5×5 or $3 \times 10\,mm^2$) is attached to the patient's body around the chest wall, and the light spot from the LED is focused on the PSD through a lens system [19]. A change in position is amplified by the zoom lens of the camera. The analog signals of the PSD are directly proportional to the spot position without any software. The camera is typically mounted on the treatment couch at the feet of the patient, where it does not disturb the irradiation and does not interfere with the patient's fixation device. Set-up of the respiratory sensor takes less than 30 s (Fig. 14.3).

Prompt start and stop of beam extraction according to the gate signal are warranted by a special extraction method that provides an efficiency of more than 85% of that of the standard extraction at HIMAC [19, 20].

14.3.5 Treatment Planning

The targets are typically irradiated from four oblique directions without prophylactic elective nodal irradiation. A margin greater than 10 mm is set outside the gross target volume (GTV) to determine the clinical target volume (CTV). Spicula formations

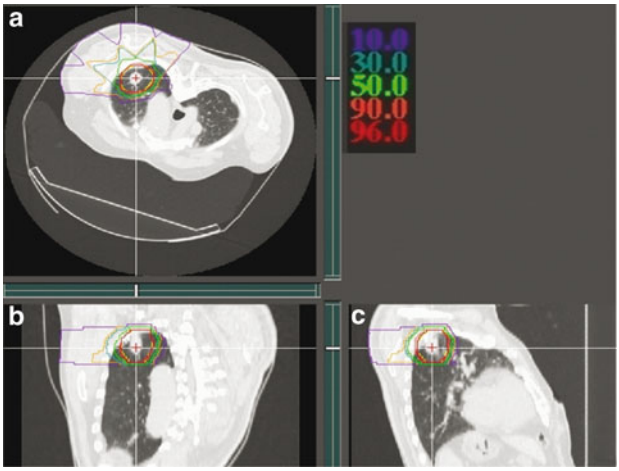

Fig. 14.4 Dose distribution of a single-fraction carbon ion treatment for an 80-year-old male patient with T1 NSCLC. CIRT Dose–Volume histograms showing percentage of prescribed dose of 44.0 GyE. *Red line*: 96%; *orange line*: 90%; *green line*: 50%; *blue line*: 30%; *violet line*: 10%. (**a**) Axial plane. (**b**) Coronal plane. (**c**) Sagittal plane

and pleural indentations are included in the CTV where possible. An internal margin (IM) is set outside the CTV, in order to allow for target motion during gating. The planning target volume (PTV) is defined as CTV plus IM. Three-dimensional treatment planning is performed using the HIPLAN software, developed at NIRS [21]. The IM is determined by extending the target margin in the head and tail direction by a width of 5 mm, which has resulted in the successful prevention of marginal recurrences caused by respiration movement. The dose is prescribed at 90% of the dose distribution. A representative case is illustrated in Fig. 14.4.

14.3.6 Irradiation

For patient positioning, fluoroscopic images are used along with the superposition of the respiration waveform. Each treatment room of the HIMAC has a pair of orthogonal fluoroscopic devices. Fluoroscopic images of the patient in the setting position are digitized and transferred to the positioning computer. They are displayed on the computer monitor screen together with reference images, such as simulation images or digital reconstruction radiography, which is calculated based on the planning CT images. Fluoroscopy is taken from the beam's eye view. The patient's respiration waveform and the gate signal are also superimposed on the TV screen. The treatment couch is then moved to the matching position until the largest deviation from the field edge and the isocenter position is less than 2 mm. The whole procedure including irradiation takes about 20–30 min.

14.4 Clinical Results

14.4.1 Phase II Clinical Trial with 9 or 4 Fractions

After a preliminary report by Miyamoto et al. on phase II clinical trials using a fixed total dose of 72 GyE in 9 fractions over 3 weeks or 52.8/60.0 GyE in 4 fractions over 1 week, a total of 129 patients having 131 tumors were enrolled into a phase II clinical trial on 9- or 4-fraction irradiation [12, 22]. Fifty-one primary tumors of 50 patients were treated using a fixed total dose of 72 GyE in 9 fractions within 3 weeks. The remaining 79 patients with 80 tumors received an applied total dose of 52.8 or 60.0 GyE in 4 fractions within 1 week. A total of 92 males and 37 females were enrolled; their mean age was 74.5 years. Seventy-two tumors were T1 and 59 were T2. The mean tumor size was 31.5 mm in diameter. Of these patients, 75% were inoperable for medical reasons. The median follow-up time was 50.8 months and ranged from 2.5 months to 70.0 months (Table 14.1). The 5-year local control rate for the 131 primary lesions was 91.5%. The 5-year cause-specific survival rate and the overall 5-year survival rate were 67% and 45.3%, respectively (Fig. 14.5).

The 5-year local control rates for the T1 ($n = 72$) and T2 ($n = 59$) tumors were 96.3% and 84.7%, respectively. This difference was statistically significant ($p = 0.0156$). Even more dramatic were the 5-year overall survival rates for the two subgroups with 53.9% for stage IA and 34.2% for stage IB and the cause-specific survival rates with 84.8% and 43.7%, respectively. No significant differences in the local control and survival were observed according to the dose and fractionation pattern. Of 62 (48.8%), who died, half died due to disease progression, the others due to intercurrent diseases.

Toxicities to the skin and lung caused by CIRT were assessed according to the criteria of the RTOG for early, and RTOG/EORTC for late effects [23]. No acute

Table 14.1 Patient characteristics in the studies with 4 and 9 fractions (fx)

Total number of patients (lesions)		129(131)
Gender	Male	92[a]
	Female	37
Mean age (years)		74.5
Tumor stage (no.)	T1	72
	T2	59
Mean tumor diameter (mm)		31.5
Medically inoperable (%)		75
Follow-up (months)	Median	50.8
	Range	2.5–70
Carbon ion dose (GyE)	72/9 fx	51
	52.8 or 60 in 4 fx	80

[a]92 patients with 94 lesions

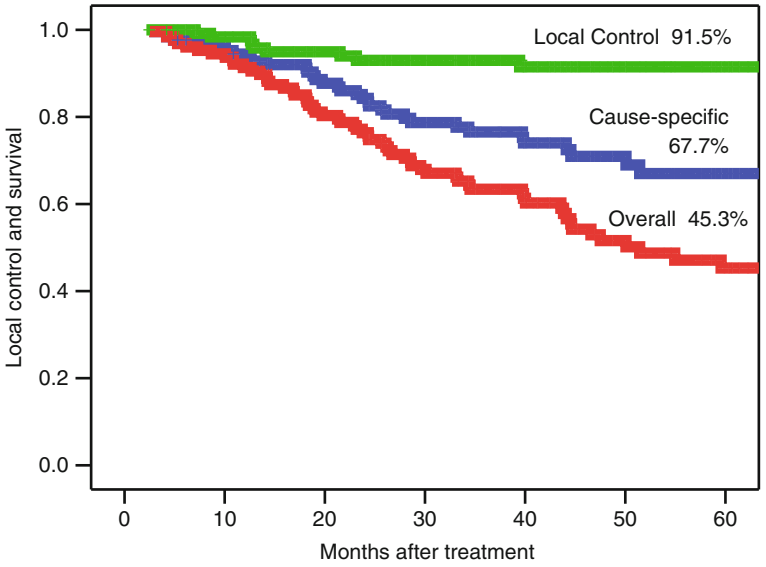

Fig. 14.5 Phase II trial of 9- and 4-fraction CIRT for early-stage NSCLC. The local control rate for 131 primary lesions was 91.5%. The 5-year cause-specific survival rate and the 5-year overall survival rate of 127 patients was 67% and 45.3%, respectively

and only one late grade 3 skin reaction was observed. Of 129 patients assessed, there was no grade 3 early or late reaction. Just two acute and three late grade 2 lung reactions were observed [22].

14.4.2 Phase I/II Clinical Trial: Single Fractionation

More than 200 patients have been enrolled in the dose-escalating clinical trial using a single fraction until February 2011. The trial is still ongoing and the preliminary results are so far quite promising.

The outcome of a first cohort of 72 patients treated between April 2003 and August 2007 was analyzed. The group consisted of 47 patients with T1 and 25 patients with T2 tumors (see Table 14.2). The average tumor size was 28 mm (mean) in diameter and 65% of the patients were medically inoperable. All patients were followed up until death.

The treatment dose was gradually increased from 36.0 GyE per single fraction ($n = 18$) to 38.0 GyE ($n = 14$), 40.0 GyE ($n = 15$), 42.0 GyE ($n = 15$), and 44.0 GyE ($n = 10$), respectively.

The 2-year local control rate for the whole cohort was 89.3%; for patients with T1 tumors, it was 94.6%, and for T2 tumors 78.7%. The overall 2-year survival rate was 85.4% and the cause-specific survival rate an excellent 98.0%.

Table 14.2 Patient characteristics of phase I/II trial with single fractions

Total number of patients		72
Gender (no.)	Male	49
	Female	23
Mean age (years)		75
Tumor stage (no.)	T1	47
	T2	25
Mean tumor diameter (mm)		28
Medically inoperable (%)		65
Follow-up (months)	Median	16.1
	Range	1.6–21.6
Carbon ion dose (GyE)	36	18
	38	14
	40	15
	42	15
	44	10

Skin reactions were, in general, minor with only one acute lesion and one late reaction being of grade 2. None of the 72 patients assessed clinically developed grade 2 or higher acute reactions and no late lung reactions including pneumonitis or fibrosis were observed [24].

The low incidence of complications in patients treated with single-fraction CIRT demonstrated its feasibility not only for patients who refuse surgery but also for medically inoperable candidates.

14.5 Comparisons of CIRT and Other Modalities

Table 14.3 summarizes the clinical results of four institutions treating NSCLC patients with proton therapy (PT).

The first report on PT for NSCLC was published in 1999 by Bush et al. from the Loma Linda University Medical Center (LLUMC) [25]. This report had a heterogeneous patient population with stages I to IIIA, and described a number of irradiation regimens ranging from 10 to 41 fractions. A subsequent report by Bush et al. in 2004 showed good local control rates with hypofractionated PT using 51 or 60 GyE in 10 fractions [26]. In Japan, the same 10-fraction regimen was successfully repeated at the Proton Medical Research Center (PMRC), Tsukuba, and the Hyogo Ion Beam Medical Center (HIBMC) with local control rates ranging from 74 to 95% [27, 28, 30]. A significant improvement in survival was noted for patients who received 60 rather than 51 GyE; their 3-year overall survival rate increased from 27% to 55% [26].

Table 14.3 Overview of clinical IBT studies for early-stage NSCLC

References	Year of publication	Ion/ Institution	Patient No All (IA/IB)	Total dose (GyE)	Fraction No	Total treatment time (w)	Local control (%) All (1A/1B)	Overall survival (%) All (1A/1B)	Lung toxicity ≥ Grade3 (%)	Median follow-up period (months)
Bush et al. [24]	1999	Proton/ LLMC	37[a]	51–73.8	10–41	2–5	2y: 87	2y: 39	No data	14 (3–45)
Bush et al. [25]	2004	Proton/ LLMC	68 (29/39)	51 or 60	10	2	3y: 74 (87/49)	3y: 44	0	30
Shioyama et al. [26]	2003	Proton/ PMRC	51 (9/19)	1A 60–81 1B 60–93	Median 3 Gy/Fr	Median 6	5y: (89/39)	5y: (70/16)	2.0	30 (18–153)
Hata et al. [27]	2007	Proton/ PMRC	21 (11/10)	50 or 60	10	2	2y: 95 (100/90)	2y: 74 (100/47)	0	25 (10–54)
Nakayama et al. [28]	2009	Proton/ PMRC	58[b] (30/28)	66 (peripheral) 72.6 (central)	10 (peripheral) 22 (central)	2 (peripheral) 5 (central)	2y: 97.0	2y: 97.8	3.6	17.7 (1.4–53.3)
Nihei et al. [29]	2006	Proton/ NCCHE	37 (17/20)	70–94	20	4–5	2y: 80 (94/62)[c]	2y: 84 (83/82)	8.1	24 (3–62)

Iwata et al. [30]	2010	Proton/ HIBMC	57 (27/30)	80 or 60	20 or 10	4 or 2	3y: 81	3y: 73	1.8	40
Iwata et al. [30]	2010	Carbon/ HIBMC	21 (14/7)	52.8	4	1	2y: 86	2y: 87	0	24
Miyamoto et al. [11]	2003	Carbon/ NIRS	81 (40/41)	68.4–79.2,59.4–95.4	9 or 18	3 or 6	5y: 74	5y: 42 (64.4/22)	3.7	52.6
Miyamoto et al. [12]	2007	Carbon/ NIRS	50 (29/21)	72	9	3	5y: 94.7	5y: 50 (55.2/42.9)	0	59 (6–83)
Miyamoto et al. [13]	2007	Carbon/ NIRS	79 (42/37)	52.8 or 60	4	1	5y: 90 (98/80)	5y: 45 (62/25)	0	38.6 (3–72)

[a]Stage I: 27, stage II: 2, stage IIIA: 8
[b]58 tumors of 55 patients
[c]Loco-regional free

Nihei et al. at the National Cancer Center Hospital East (NCCHE) in Kashiwa reported results of PT using 20 fractions and total doses of 70–94 GyE. The local control rate of this more classical fractionation scheme was almost the same as that of hypofractionated PT [29].

Iwata et al. compared PT and CIRT for stage I NSCLC. Both are available at HIBMC. The data are preliminary because CIRT began only in April 2005, whereas treatment with protons started already 2 years earlier. Local control and overall survival rates were above 85% after 2 years and compared excellently to X-ray SBRT [30]. The incidence of severe pneumonitis was low with both CIRT and PT. There was a direct correlation between the percentage of the total lung volume receiving a dose $\geq$ 20 Gy (V20) and the incidence of radiation pneumonitis [31]. V20 was lowest for four fractions of CIRT as compared to 10 or 20 fractions of PT due to the reduced penumbra of carbon ion beams (cf. Chap. 4 for details). However, beam directions were constrained in CIRT, because HIBMC has only three fixed beamlines for carbon. Part of the advantageous dose gradient of carbon could be compensated for by having more degrees of freedom for the beam directions using the proton gantry.

In some reports on PT, T1 disease had better local control and survival than T2 disease [26, 31]. A hypothesis for the inferior outcome of more advanced disease was that the total doses used with PT might be insufficient to control larger primary tumors [31], which contain higher numbers of tumor clonogens and areas of relatively radioresistant hypoxic tumor cells [26]. An estimation of the biologically effective dose (BED) administered to these different regimens support this idea. In contrast to a BED value of 123 for 52.8 GyE carbon ions in four fractions, it was only 96 for 10 fractions of 6 GyE protons [29]. In the case of hypofractionated irradiation, a comparison of BED between carbon and proton beams is difficult. A study for RBE of CIRT is currently underway at NIRS.

14.6 Conclusion

IBT is clearly beneficial for stage I NSCLC. Not only physical but also biological properties of carbon ions can bring an extra therapeutic gain for tumor control. It is theoretically possible in CIRT to safely perform hypofractionated irradiation with a significantly smaller number of fractions as compared to PT. However, there are still unclear issues between PT and CIRT, such as RBE for hypofractionated irradiation. To clarify the effectiveness of each modality for early stage NSCLC, well-planned randomized trials will be required.

References

1. H. Asamura, T. Goya, Y. Koshiishi, et al., A Japanese Lung Cancer Registry study: prognosis of 13,010 resected lung cancers. J. Thorac. Oncol. **3**, 46–52 (2008)
2. W.R. Smythe, American College of Chest Physicians. Treatment of stage I non-small cell lung carcinoma. Chest **123**, 181S–187S (2003)

3. B. Jeremic, J. Classen, M. Bamberg, Radiotherapy alone in technically operable, medically inoperable, early-stage (I/II) non-small-cell lung cancer. Int. J. Radiat. Oncol. Biol. Phys. **54**, 119–130 (2002)
4. F.B. Zimmermann, M. Bamberg, M. Molls, et al., Radiation therapy alone in early stage non-small cell lung cancer. Semin. Surg. Oncol. **21**, 91–97 (2003)
5. Y. Nagata, M. Hiraoka, T. Mizowaki, et al., Survey of stereotactic body radiation therapy in Japan by the Japan 3-D Conformal External Beam Radiotherapy Group. Int. J. Radiat. Oncol. Biol. Phys. **75**, 343–347 (2009)
6. F.B. Zimmermann H. Geinitz, S. Schill, et al., Stereotactic hypofractionated radiation therapy for stage I non-small cell lung cancer. Lung Cancer **48**, 107–114 (2005)
7. H. Onishi, T. Araki, H. Shirato, et al., Stereotactic hypofractionated high-dose irradiation for stage I nonsmall cell lung carcinoma: clinical outcomes in 245 subjects in a Japanese multiinstitutional study. Cancer **101**, 1623–1631 (2004)
8. S. Senan, F. Lagerwaard, Stereotactic radiotherapy for stage I lung cancer: current results and new developments. Cancer Radiother. **14**, 115–118 (2010)
9. H. Onishi, H. Shirato, Y. Nagata, et al., Hypofractionated stereotactic radiotherapy (HypoFXSRT) for stage I non-small cell lung cancer: updated results of 257 patients in a Japanese multi-institutional study. J. Thorac. Oncol. **2**(Suppl 3), S94–S100 (2007)
10. Y. Nagata, K. Takayama, Y. Matsuo, et al., Clinical outcomes of a phase I/II study of 48 Gy of stereotactic body radiotherapy in 4 fractions for primary lung cancer using a stereotactic body frame. Int. J. Radiat. Oncol. Biol. Phys. **63**, 1427–1431 (2005)
11. T. Miyamoto, N. Yamamoto, H. Nishimura, et al., Carbon ion radiotherapy for stage I non-small cell lung cancer. Radiother. Oncol. **66**, 127–140 (2003)
12. T. Miyamoto, M. Baba, N. Yamamoto, et al., Curative treatment of Stage I non-small-cell lung cancer with carbon ion beams using a hypo-fractionated regimen. Int. J. Radiat. Oncol. Biol. Phys. **67**, 750–758 (2007)
13. T. Miyamoto, M. Baba, T. Sugane, et al., Carbon ion radiotherapy for stage I non-small cell lung cancer using a regimen of four fractions during 1 week. J. Thorac. Oncol. **2**, 916–926 (2007)
14. T. Sugane, M. Baba, R. Imai, et al., Carbon ion radiotherapy for elderly patients 80 years and older with stage I non-small cell lung cancer. Lung Cancer **64**, 45–50 (2009)
15. T. Kanai, M. Endo, S. Minohara, et al., Biophysical characteristics of HIMAC clinical irradiation system for heavy-ion radiation therapy. Int. J. Radiat. Oncol. Biol. Phys. **44**, 201–210 (1999)
16. T. Yasukawa, Y. Yamaguchi, H. Aoyagi et al., Diagnosis of hilar and mediastinal lymph node metastasis of lung cancer by positron emission tomography using ^{11}C-methionine. Jpn. J. Lung Cancer **36**, 919–926 (1996)
17. International Union Against Cancer (UICC), *TNM Classification of Malignant Tumors*, 6th edn., ed. by L.H. Sobin, Ch. Wittekint (Wiley-Liss, NewYork, 2002)
18. T. Sugane, M. Baba, N. Yamamoto, et al., Treatment planning in carbon ion radiotherapy for lung cancer. Paper presented at Proceedings of NIRS-MD Anderson Symposium on Clinical Issues for Particle Therapy, NIRS-M-210, Houston, TX, 20–21 Mar 2008, pp. 30–35
19. S. Minohara, T. Kanai, M. Endo, et al., Respiratory gated irradiation system for heavy-ion radiotherapy. Int. J. Radiat. Oncol. Biol. Phys. **47**, 1097–1103 (2000)
20. T. Kanai, Y. Furusawa, K. Fukutsu, et al., Irradiation of mixed beam and design of spread-out Bragg peak for heavy-ion radiotherapy. Radiat. Res. **147**, 78–85 (1997)
21. M. Endo, H. Koyama-Ito, S. Minohara, et al., HIPLAN-a heavy ion treatment planning system at HIMAC. J. Jpn. Soc. Ther. Radiol. Oncol. **8**, 231–238 (1996)
22. T. Miyamoto, M. Baba, K. Kagei, et al., Carbon ion radiotherapy in hypofraction regimen for stage I non-small cell lung cancer. Paper presented at Proceedings of NIRS-MedAustron Joint Symposium on Carbon ion Therapy in Cancer, NIRS-M-188, Chiba, 25–26 Feb 2006, pp. 25–28

23. J.D. Cox, J. Stetz, T.F. Pajak, Toxicity criteria of the Radiation Therapy Oncology Group (RTOG) and the European Organization for Research and Treatment of Cancer (EORTC). Int. J. Radiat. Oncol. Biol. Phys. **31**, 1341–1346 (1995)
24. D.A. Bush, J.D. Slater, R. Bonnet, et al., Proton-beam radiotherapy for early-stage lung cancer. Chest **116**, 1313–1319 (1999)
25. D.A. Bush, J.D. Slater, B.B. Shin, et al., Hypofractionated proton beam radiotherapy for stage I lung cancer. Chest **126**, 1198–1203 (2004)
26. Y. Shioyama, K. Tokuuye, T. Okumura, et al., Clinical evaluation of proton radiotherapy for non-small-cell lung cancer. Int. J. Radiat. Oncol. Biol. Phys. **56**, 7–13 (2003)
27. M. Hata, K. Tokuuye, K. Kagei, et al., Hypofractionated high-dose proton beam therapy for stage I non-small-cell lung cancer: preliminary results of a phase I/II clinical study. Int. J. Radiat. Oncol. Biol. Phys. **68**, 786–93 (2007)
28. H. Nakayama, S. Sugahara, M. Tokita, et al., Proton beam therapy for patients with medically inoperable Stage I non-small-cell lung cancer at the University of Tsukuba. Int. J. Radiat. Oncol. Biol. Phys. **78**, 467–471 (2010)
29. K. Nihei, T. Ogino, S. Ishikura et al., High-dose proton therapy and carbon-ion therapy for stage I nonsmall cell lung cancer. Int. J. Radiat. Oncol. Biol. Phys. **65**, 107–111 (2006)
30. H. Iwata, M. Murakami, Y. Demizu, et al., High-dose proton therapy and carbon-ion therapy for stage I non-small cell lung cancer. Cancer **116**, 2476–2485 (2010)
31. K. Tsujino, S. Hirota, M. Endo, et al., Predictive value of dose-volume histogram parameters for predicting radiation pneumonitis after concurrent chemoradiation for lung cancer. Int. J. Radiat. Oncol. Biol. Phys. **55**, 110–115 (2003)

Chapter 15
Ion Beam Therapy for Gynecological Tumors

Tatsuya Ohno and Shingo Kato

Abstract Most of the clinical results for gynecological tumors treated with ion beam therapy (IBT) have been reported from Tsukuba (protons) and NIRS (carbon ions). Several phase I/II dose-escalation studies performed at NIRS indicate that high doses of carbon ion radiotherapy (CIRT) can achieve promising local control without severe complications in patients with locally advanced cervical cancer.

15.1 Introduction

Radiotherapy (RT) is widely used for invasive uterine cervical cancer. Benedet and colleagues estimated that more than 65% of the patients with this type of cancer are treated accordingly [1].

RT with curative intent consists of a combination of external beam irradiation for the pelvis and intracavitary brachytherapy using high-dose rate or low-dose rate sources. The use of concurrent chemotherapy with RT has demonstrated a significant survival benefit for locally advanced cases [2, 3]. However, a 5-year locoregional failure rate of 30% or more has been observed, especially in patients with stage III or IVA disease, with the pelvis being the major site of failure, indicating the need for a more intensive strategy for locally advanced cases [3]. In addition, incidences of grade 3–4 leukopenia and GI toxicities by concurrent chemoradiotherapy were reported to be twice as high as those with RT alone [4]. External beam RT has been performed by conventional anterior–posterior or four-field pelvic irradiation technique.

Recently, investigators have begun to explore ways of reducing the side effects of RT by using highly conformal external beam radiation techniques. Increasing

T. Ohno (✉)
Gunma University Heavy Ion Medical Center, Showa-machi 3-39-22, Maebashi, Gunma, 371-8511, Japan
e-mail: tohno@gunma-u.ac.jp

U. Linz (ed.), *Ion Beam Therapy*, Biological and Medical Physics, Biomedical Engineering, DOI 10.1007/978-3-642-21414-1_15,

interest has focused on intensity-modulated radiation therapy (IMRT) or IBT using protons or carbon ions in gynecological tumors. The potential clinical applications are as (1) alternative to whole pelvis external beam RT (then followed by brachytherapy), (2) alternative to brachytherapy after whole pelvis external beam RT, or (3) integrated boost given during locoregional treatment. At present, most of the clinical results from IBT have been reported from Japanese institutions.

15.2 Proton Therapy for Gynecological Tumors

15.2.1 The Tsukuba University Experience

The initial experience of PT combined with photon external beam therapy for uterine cervical cancer was gained at the Proton Medical Research Center (PMRC) of Tsukuba University. Arimoto et al. reported on the clinical results of 15 patients with uterine cancers, 12 of whom had cervical cancer, and were treated with PT as an alternative to brachytherapy [5]. Among the 12 patients, one recurred locally, one had para-aortic lymph node metastasis, and the remaining ten were alive with no evidence of disease after a median follow-up time of 31 months.

Kagei et al. updated the long-term results of PT for cervical cancer at Tsukuba University [6]. Between 1983 and 1991, a total of 25 patients with histologically confirmed squamous cell carcinoma were treated with combined external photon and proton therapy. They consisted of 9 stage IIB, 15 stage IIIB, and 1 stage IVA. Two patients had pelvic lymph node metastases documented by computed tomography (CT).

Photon irradiation was with a tele-cobalt machine in the case of eight patients; 17 were treated with a linear accelerator (linac) through anterior–posterior opposing fields to the pelvis. Most patients received 50.4 Gy in 28 fractions over 6 weeks with central shielding, depending on the size of the primary tumor, the tumor response to photon irradiation, and the availability of proton beams. The median dose at which the shielding was placed was 25 Gy. Proton irradiation, which was, in most cases, initiated when the central shielding was placed, was given to the primary tumor and adjacent tissue, delivering a median proton tumor dose of 61 Gy (range 37–101 Gy), in 3–4 fractions weekly, with doses per fraction varying from 2.5 to 4 Gy because of the limited availability of beam time and the preference of the attending physicians. A relative biological effectiveness (RBE) value of 1.0 was used. To minimize treatment set-up errors, metal markers were implanted around the tumor at the time of treatment planning, and their relative positions in the treatment field were adjusted by fluoroscopy in every treatment session. Thus, the median combined tumor dose, a sum of both proton and photon tumor doses, was 86 Gy. In order to convert these doses to conventionally fractionated radiation, 2 Gy per fraction-equivalent doses were calculated using a linear quadratic model with α/β ratios of 10 and 3 Gy for early and late responding tissues, respectively. The equivalent

Table 15.1 Late complications in the small/large intestine and urinary bladder in patients with cervical cancer treated with photon and proton radiotherapy (experience of PMRC, Tsukuba, Japan)

Site	RTOG/EORTC late morbidity score					
	Patient no	Grade 1	Grade 2	Grade 3	Grade 4	Grade 5
Small/large intestine	25	7	5	0	1	0
Urinary bladder	25	3	1	0	1	0

median total doses in conventional fractions were 92 Gy for $\alpha/\beta = 10$ and 99 Gy for $\alpha/\beta = 3$, respectively. For the proton tumor doses, median equivalent doses were 68 Gy for $\alpha/\beta = 10$ and 78 Gy for $\alpha/\beta = 3$, respectively.

With a median follow-up time of 139 months, overall and cause-specific survival rates at 10 years for all patients were 59% and 65%, respectively. Overall survival rates at 10 years for stages IIB and IIIB/IVA patients were 89% and 40%, respectively. The 5-year local control rates for all patients, stages IIB and IIIB/IVA, were 75%, 100%, and 61%, respectively. The 5-year distant metastasis-free survival rates for all patients, stages IIB and IIIB/IVA, were 79%, 100%, and 66%, respectively. A combined equivalent dose (2 Gy per fraction, $\alpha/\beta = 10$) >92 Gy was associated with a trend towards better local control rate at 5 years (85% vs. 59%, $p = 0.08$) and improved survival (84% vs. 42%, $p = 0.013\%$). Acute reactions were not significant. One patient had diarrhea requiring a 3-day break in treatment, but no other patients needed a treatment interruption. The incidences of late complications in the small/large intestine and the urinary bladder are shown in Table 15.1. The majority of late complications in the intestine and bladder were grade 1 or 2, but one patient developed a grade 4 complication in the intestine and bladder after receiving equivalent doses of 93 and 102 Gy, respectively. A combined equivalent dose >102 Gy showed a trend for a higher incidence of grade 2 or more late bowel or bladder complications (49% vs. 11%, $p = 0.06$). For proton equivalent doses >78 Gy, that kind of late complications were significantly increased (51% vs. 10%, $p = 0.04$).

15.3 Carbon Ion Radiotherapy for Gynecological Tumors

15.3.1 The NIRS Experience

The National Institute of Radiological Sciences (NIRS) has conducted several prospective phase I/II dose-escalation studies (Protocol 9403 during 1995–1997, Protocol 9702 during 1997–2000, Protocol 9902 during 2000–2006, and Protocol 9704 during 1997–2010) in order to evaluate the toxicity and efficacy of CIRT for locally advanced cervical cancer [7, 8]. In these studies, patients were treated with external carbon ion beams alone with whole pelvis irradiation and local

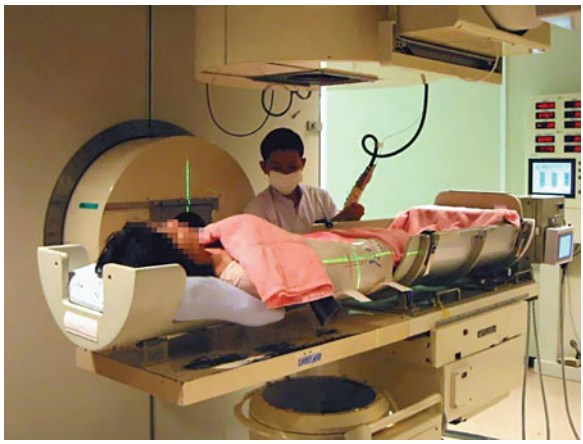

Fig. 15.1 Treatment room for CIRT at NIRS. Patient is placed in customized cradles and immobilized with a low-temperature thermoplastic sheet

boost without brachytherapy. In addition, vaginal malignant melanoma and pelvic recurrence of uterine or ovarian cancer after surgery were treated in a pilot study [9].

For treatment planning, patients were placed in customized cradles, immobilized with a low-temperature thermoplastic sheet, and a set of 5-mm-thick CT images was taken (Fig. 15.1). Three-dimensional treatment planning was performed with HIPLAN software [10] for the planning of carbon ion radiotherapy (CIRT). The treatment consisted of whole pelvic irradiation and local boost. The clinical target volume (CTV) of whole pelvic irradiation included all areas of gross and potentially microscopic disease, consisting of the cervical tumor, uterus, parametrium, at least the upper half of the vagina, and pelvic lymph nodes with common, internal, and external iliac and presacral lymph nodes (CTV-1). Because nonenlarged lymph nodes are poorly visible on CT, these nodal regions were defined by encompassing the pelvic vessels with a 5–10-mm margin. The planning target volume (PTV-1) included CTV-1 plus a 5-mm safety margin for positioning uncertainty. After completing whole pelvic irradiation, local boost irradiation was performed. Because the tumor usually shrank during whole pelvic irradiation, sequential planning CT scans were performed to revise the CTV for the local boost. This revised CTV (CTV-2) included the volume encompassing the gross disease at the primary site, parametrial involvement, the remainder of the uterus, upper vagina, and gross lymph node involvement. Accordingly, the PTV-2 was adjusted to include CTV-2 plus a 5-mm margin. Local boost irradiation was performed via mainly lateral ports. Normal tissue structures, such as the rectum, sigmoid colon, bladder, and the small bowel in the pelvis, were excluded from PTV as much as possible.

CIRT was given once daily on 4 days per week (Tuesday to Friday), for 24 fractions. PTV-1 and PTV-2 were irradiated with 16 and 8 fractions, respectively. At every treatment session, the patient was positioned on the treatment couch with the immobilization devices, and the patient's position was verified with a computer-aided, online positioning system. To minimize internal target positional uncertainty, 100 ml of normal saline was infused into the bladder. Patients were also encouraged

to use laxatives, if necessary, to prevent constipation throughout the treatment period. The radiation dose was calculated for the target volume and surrounding normal structures and was expressed in GyE, defined as the carbon physical dose (Gy) multiplied by an RBE value of 3.0. Acute toxicity was graded according to the system of the Radiation Therapy Oncology Group (RTOG), which considers the highest toxicity within 3 months from the initiation of irradiation. Late toxicity was graded according to the RTOG/EORTC late radiation morbidity scoring scheme.

15.3.2 Locally Advanced Cervical Carcinoma

Protocol 9403 was the first clinical study, and the primary endpoint was acute toxicities of CIRT [7]. Treatment was initiated with a dose of 2.2 GyE per fraction and then gradually increased up to 3.0 GyE by 0.2-GyE increments. At least five patients were treated at each dose level, and dose escalation was performed after careful assessment of the acute normal tissue responses.

Based on the results of Protocol 9403, Protocol 9702 limited the whole pelvic dose to 44.8 GyE in 16 fractions. An additional boost of 28.0 GyE in eight fractions was given to the primary gross tumor. Seven patients were treated according to this regimen, but major (≥grade 3) late gastrointestinal (GI) toxicities in some patients required an adjustment. The dose to the injured bowel was estimated to be over 60 GyE. Therefore, the local boost dose was decreased to 24.0 GyE in eight fractions (total dose, 68.8 GyE) and the treatment technique was revised to keep the dose to the GI tract below 60 GyE. An additional seven patients were treated with this modified scheme.

Kato and colleagues [8] analyzed the results of 44 patients treated according to Protocol 9403 or 9702. No patient developed grade 3 or higher acute toxicity in the skin, GI tract, or genitourinary (GU) tract. In Protocol 9403, grade 2 GI toxicities occurred in four of the nine patients when the whole pelvic dose was increased to 48.0 GyE. After reducing the whole pelvic dose to 44.8 GyE in Protocol 9702, only one patient developed grade 2 GI toxicity. Regarding late toxicities, there were no GU complications of grade 3 or more. Among 25 patients who developed late GI toxicities, 17 patients had mild or intermediate bleeding of the rectum or sigmoid colon, but eight patients had grade 3 or grade 4 GI toxicities. The eight severe complications consisted of three rectovaginal fistulas at 62.4–67.2 GyE, a rectal ulcer at 72.8 GyE, a sigmoid–vesical fistula at 72.8 GyE, a sigmoid perforation at 72.0 GyE, and two ileum perforations at 67.2 and 72.0 GyE. They occurred 11–54 months (median, 20 months) after CIRT. The cervical tumors in these cases were located in very close proximity to the adjacent GI tract. All patients were surgically salvaged and remained free of intestinal problems (follow-up, 35–82 months after surgery). Of these eight patients, five were alive, one died of recurrent cervical cancer and two died of other unrelated disease. In all cases, the doses to the injured GI tract were estimated to be over 60 GyE. After reducing the boost in Protocol 9702 to 24 GyE, no more patients developed late major GI complications. The 5-year local control

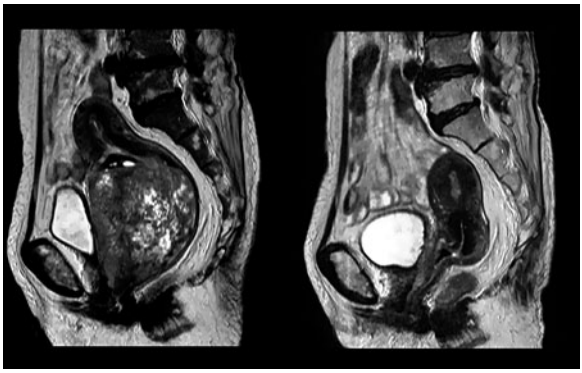

Fig. 15.2 A 74-year-old female with stage IIIB squamous cell carcinoma of the cervix. MRI taken before treatment reveals bulky cervical tumor in the pelvis (*left*). She received CIRT consisting of 72.0 GyE in 20 fractions over 5 weeks. Neither brachytherapy nor concurrent chemotherapy was given. At the end of CIRT, the cervical tumor had disappeared completely (*right*). The patient has remained free of disease and any radiation-related treatment complications over 4 years after treatment. Dose distribution of the treatment plan is shown in Fig. 15.3

rates for patients in Protocols 9403 and 9702 were 45% and 79%, respectively. Local failure was observed in 7 of 11 patients (64%) receiving 52.8–57.6 GyE, and in 11 of 33 patients (33%) receiving ≥62.4 GyE. In Protocol 9702, local failure was observed in only 3 of 14 patients. When treatment was with ≥62.4 GyE, local tumor control was favorable, especially in the patients with stage IVA disease (9 of 13, 69%) and in those with tumors ≥6.0 cm in diameter (14 of 22, 64%).

15.3.3 Locally Advanced Cervical Squamous Cell Carcinoma

In order to shorten the overall treatment time from 6 to 5 weeks, the dose to the whole pelvis was fixed at 39.0 GyE in 13 fractions in Protocol 9902. An additional boost of 15.0 GyE in five fractions was delivered to the cervical tumor and surrounding tissues including the parametrium, uterine body, upper vagina, and adjacent lymph nodes, where tumor infiltration was suspected.

For a further boost, the PTV was restricted to the GTV only, and the GI tracts were completely excluded. The optimum dose was determined in an escalation study beginning with an initial dose of 10.0 GyE in two fractions and moving up to 18.0 GyE in two fractions, also. Thus, the GTV received a total dose of 64.0–72.0 GyE, whereas the dose to the GI tract was limited to <60 GyE. A CT scan was taken before each treatment planning. An example of the dose distribution of CIRT and the clinical outcome is shown in Figs. 15.2 and 15.3.

Twenty-two patients with histologically confirmed squamous cell carcinoma were enrolled into this study. The majority had stage IIIB (82%), bulky tumor ≥6 cm (73%).

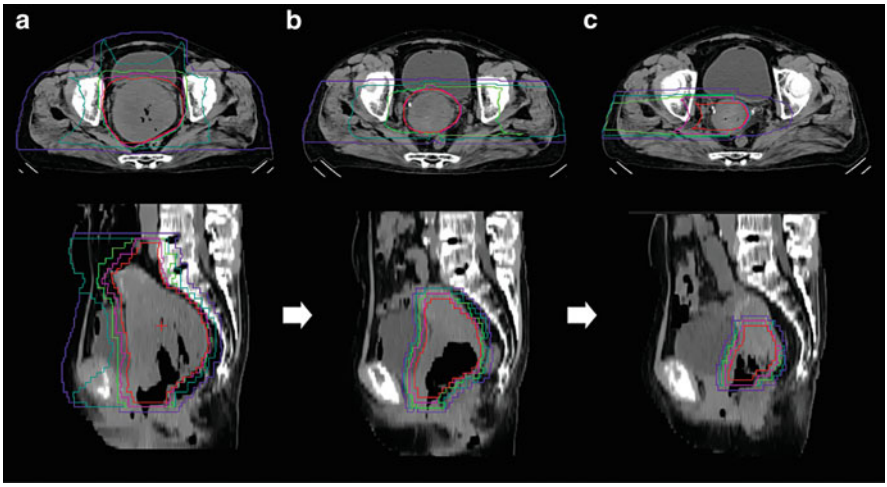

Fig. 15.3 Isodose curves of CIRT for locally advanced cervical cancer (case shown in Fig. 15.2) superimposed on axial and saggital computed tomography images. (**a**) Whole pelvic irradiation to PTV-1: 39.0 GyE in 13 fractions. (**b**) Extended local boost to PTV-2: 15.0 GyE in 5 fractions. (**c**) Local boost irradiation to PTV-3: 18.0 GyE in 2 fractions. Total dose of 72.0 GyE in 20 fractions over 5 weeks was given to the cervical tumor. Highlighted are 95% (*red*), 70% (*pink*), 50% (*green*), 30% (*blue*), and 10% (*purple*) isodose curves

No patient showed grade 3 or higher acute and late toxicities in the GI or GU tract, or the skin. Compared to the incidence of acute GI toxicities of historical cases treated with RT alone or concurrent chemoradiotherapy, toxicity seemed lower with CIRT (Fig. 15.4). After a median follow-up time of 37 months, local control was observed in 7 of 11 patients (64%) receiving 64.0 GyE, in two of five (40%) receiving 68.0 GyE, and in all six patients receiving 72.0 GyE. In 13 patients clinically diagnosed as N0, none developed pelvic lymph node metastases. This result suggested that the prophylactic dose of 39 GyE to the pelvis was effective to control clinically diagnosed N0. The 5-year local control and overall survival rates were 68% and 50%, respectively.

A combined analysis of the treatment according to Protocols 9702 and 9902 revealed local control in 14 of 23 patients (61%) receiving 64.0–68.8 GyE and 12 of 13 patients (92%) receiving 72.0–72.8 GyE. This result may indicate that there is a dose–response relationship in CIRT for cervical squamous cell carcinoma and that a high local tumor control may be obtained with a dose of 72.0 GyE. Distant failure was seen in 16 of the 36 patients (44%) treated, with the most common site of first failure being the para-aortic lymph nodes (10 patients or 28%).

The outcomes of RT for patients with extensive and bulky stage IIIB or IVA disease have been poor. Perez et al. reported significantly worse rates of 10-year pelvic control and disease-free survival of 50% and 32% by RT alone in patients with stage III disease and bilateral parametrial involvement, compared with the corresponding rates of 68% and 48% in those with unilateral parametrial involvement [11].

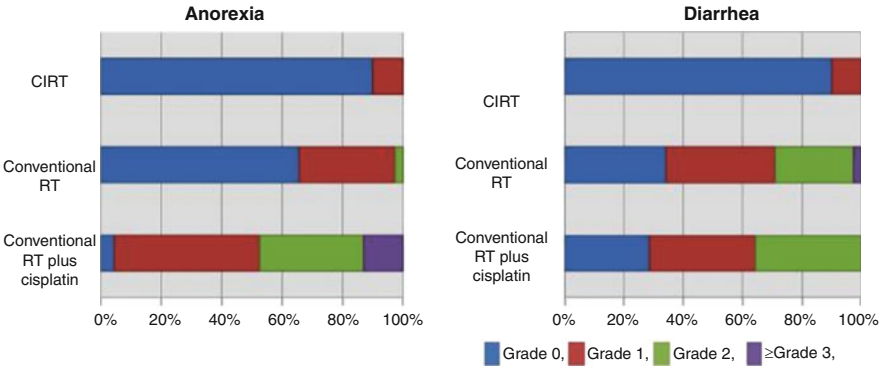

Fig. 15.4 Comparison of the incidence of acute gastrointestinal toxicity by CIRT, conventional RT, and concurrent conventional RT plus 40 mg/m^2 of weekly cisplatin (unpublished data). *Left*: Anorexia. *Right*: Diarrhea. Toxicities were evaluated by the National Cancer Institute Common Toxicity Criteria (NCI-CTC version 2.0). Note that less toxicities of anorexia and diarrhea were seen with CIRT

Regarding concurrent chemoradiotherapy, there have been no reports that compared the treatment results by tumor size or degree of parametrial involvement for stage III–IVA cervical cancer. Kochanski et al. treated 44 stage IB–IIIB cervical cancer patients with IMRT in place of conventional pelvic irradiation [12]. At a median follow-up time of 23 months, the 3-year actuarial pelvic control rates in stage I–IIA and stage IIB–IIIB were 93% and 53%, respectively. Eifel et al. reported that the 5-year local control rates for concurrent chemoradiotherapy and extended-field RT were 71% and 56% in patients with stage III–IVA disease without para-aortic lymph node metastasis in the RTOG 9001 trial [3]. In contrast, the local control rate of CIRT was 61% for patients receiving 64.0–68.8 GyE and 92% for patients receiving 72.0–72.8 GyE. Considering that a larger percentage of stage IVA was included in the carbon ion group (24% vs. 10% in the concurrent chemoradiotherapy arm), CIRT using a high dose (72.0 GyE) seems to be a promising treatment strategy for locally advanced cervical cancer.

15.3.4 Locally Advanced Uterine Adenocarcinoma

The incidence of adenocarcinoma of the uterine cervix has been increasing over the past few decades [13]. Currently, adenocarcinoma accounts for 10–24% of all cervical carcinomas [13, 14]. However, only a few reports described the treatment outcomes of these patients [15–19]. Locally advanced adenocarcinomas allegedly have a poorer prognosis than squamous cell carcinomas because of a poorer local control rate and higher rate of distant metastasis.

Protocol 9704 was initiated to evaluate the toxicity and efficacy of CIRT for locally advanced uterine adenocarcinoma. CIRT was given once daily, 4 days per

Table 15.2 Improvement of incidence of late severe complications in the small/large intestine in patients with cervical cancer treated with CIRT (experience of NIRS, Chiba, Japan)

Protocol	RTOG/EORTC late morbidity score					
	Patient no	Grade 1	Grade 2	Grade 3	Grade 4	Grade 5
9403	30	9	1	0	6	0
9702	14	5	2	1	1	0
9704 and 9902 (I)	24	8	1	0	1	0
9704 and 9902 (II)	30	5	0	0	0	0

During the period of protocol 9702, dose constraints for GI tract were standardized below 60 GyE. Beginning with protocol 9902, the target volume was reduced in three steps so that the highly concentrated dose could be delivered to the tumor without increasing the dose to normal structures. Since 2002, a spacer has been inserted into the vaginal canal before each irradiation to provide a safe distance between the tumor and rectum (9704 and 9902 (II)). Note that complications ≥grade 3 in GI tract were not observed after the latest modification

week, for 20 fractions. The dose to the whole pelvis was restricted to 36 GyE in 12 fractions. Dose escalation was planned for the local boost. It started at 26.4 GyE administered in eight fractions. Increase was in 10% increments up to a total boost dose of 38.4 GyE. Both, whole pelvic plus boost irradiation, yielded a total dose of 62.4–74.4 GyE. The dose to the GI tracts was limited to less than 60 GyE in all cases.

Between 1998 and 2008, 45 patients with cervical adenocarcinoma were treated with CIRT. Histologically, 36 had adenocarcinoma and nine had adenosquamous carcinoma. Fifteen patients had stage IIB, 28 IIIB, and 2 stage IVA disease. Eighteen patients had enlarged lymph nodes in the pelvis. All patients had bulky tumors measuring 3.0–11.0 cm in maximum diameter and a median diameter of 5.5 cm. In the dose-escalation study, three patients received a total dose of 62.4 GyE, four received 64.8 GyE, ten received 68.0 GyE, 21 received 71.2 GyE, and seven received 74.4 GyE. No patient developed severe acute toxicities in the skin, GI, or GU tract. After a median follow-up time of 23 months (range, 6–93 months), no patient except one experienced grade 3 or higher complications in GI, GU, or skin. That patient developed a rectovaginal fistula 14 months after CIRT (grade 4). She has been alive without disease and intestinal problems for 73 months after receiving a colostomy. She had uncontrolled diabetes mellitus, which may have promoted this complication. In addition, tumor shrinkage during the treatment might have resulted in an unexpected dose exposure of the rectum. Since then, a spacer made of cotton was inserted into the vaginal canal before each irradiation to provide a safe distance between the tumor and rectum. Since this modification, no more patient has developed severe late GI toxicities, despite tumor doses beyond 60 GyE (Table 15.2).

Local control rate increased from 57% (4 of 7 pts.) in the lowest dose group receiving 62.4–64.8 GyE to approximately two thirds in the intermediate groups to 100% among the seven patients receiving the highest dose of 74.4 GyE. Before it can be concluded that there is a dose–response relationship and that high local tumor control may be obtained with a dose ≥71.2 GyE longer follow-up periods will be

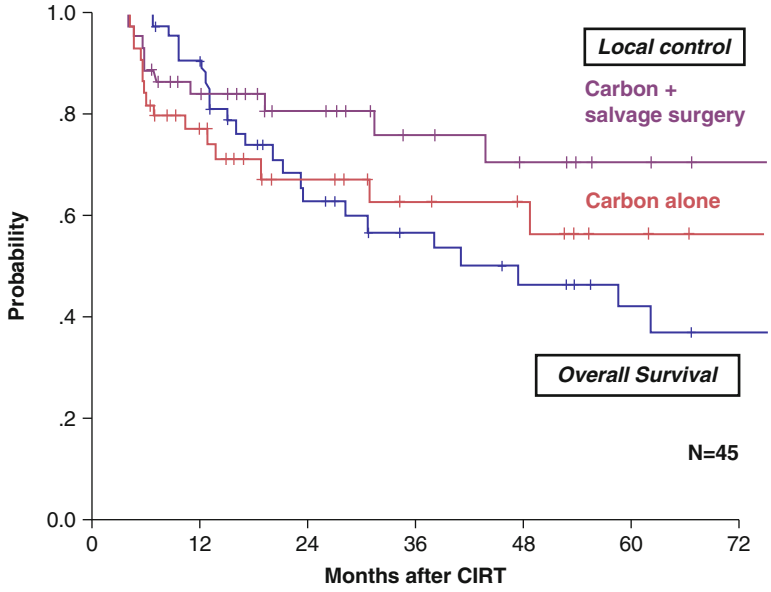

Fig. 15.5 Local control and survival probability for 45 patients with locally advanced adenocarcinoma. The 5-year local control and overall survival rates were 57% and 42%, respectively. Three patients with local recurrences were surgically salvaged, bringing the 5-year local control rate, including the salvage surgery, to 70%

necessary. The 3- and 5-year local control rates were 63% and 57%, respectively. Three patients with local recurrences were surgically salvaged, bringing the 5-year local control rate, including the salvage surgery, to 70% (Fig. 15.5). Twenty-four of the 45 patients (53%) developed distant metastases, 11 of them in the para-aortic lymph nodes. They received subsequent photon RT and/or chemotherapy.

Figure 15.5 illustrates the overall survival rate for the whole cohort with 42% after 5 years.

Several reports have described poorer treatment outcomes for patients with locally advanced cervical adenocarcinoma as compared to patients with squamous carcinoma. Lea et al. treated 83 patients with stage IIB–IVB cervical adenocarcinoma by RT or chemoradiotherapy and reported 5-year survival rates of 30% for stage IIB and 0% for stage III–IV [18]. Eifel et al. in their large series of RT reported 5-year survival rates of 28% for stage IIB and 26% for stage III [16]. In contrast, Grigsby et al. analyzed prognostic factors by multivariate analysis and found that adenocarcinoma was not a significant prognostic factor [20]. However, when comparing treatment outcomes among patients with stage III disease, the 5-year survival rate of adenocarcinoma tended to be lower than that of squamous cell carcinoma (25% vs. 36.7%). However, the effect was not statistically significant [20].

Table 15.3 lists the results of various studies for stage III–IVA cervical adenocarcinoma from the literature [15–20] and compares them to the corresponding

Table 15.3 Outcomes of conventional RT/chemoradiotherapy (CCRT) and CIRT for patients with stage III–IVA cervical adenocarcinoma

References	Year	Patient No.	Stage	Treatment	5y-OS (%)	Follow-up[a] (Months)
Eifel et al. [16]	1990	46	III	RT	26	87
Hopkins and Morley [17]	1991	25	III	RT	8	80
Lea et al. [18]	2002	24	III	RT/CCRT	0	33
Baalbergen et al. [15]	2004	22	III	RT(+HT)	–	61
Quinn et al. [19]	2006	135	IIIB	RT/CCRT	24	NA
NIRS	2008	29	IIIB–IVA	RT/CCRT	19	38
NIRS	2009	24	IIIB–IVA	CIRT (≥68 GyE)	46	26

HT Hyperthermia, *CCRT* Concurrent chemoradiotherapy, *NA* Not available
[a]Median

subgroup from Protocol 9704. With the restriction of a short median follow-up of only 26 months, the 5-year overall survival rate of 46% for the CIRT group seems most favorable (Table 15.3). Where available, local control rate data ranged from 33 to 61%. The corresponding 5-year local control rate for the CIRT patients was 64%. It might, therefore, be concluded that the favorable survival rate achieved for the CIRT group may be attributable to the high local tumor control. However, despite the high local tumor control, distant metastases frequently occurred, and the survival rate of CIRT was still modest. A combination of CIRT with systemic chemotherapy might be necessary to improve it.

15.4 Inter- and Intrafractional Tumor and Organ Motion

When treating with a conventional four-field "box" technique, internal motion is not very critical because the dose distribution is usually so generous that the central structures are kept in the high-dose region even if they move. On the other hand, the conformal dose distributions and steep dose gradients created by IBT planning require an accurate treatment set-up and repeated monitoring to prevent geographic miss during the treatment. Variations in bladder and rectal filling may cause displacement of the uterus and upper vagina, leading to systematic errors throughout the course of treatment [21, 22]. Table 15.4 illustrates the significant interfractional variations that have to be considered for the position of uterus and cervix on two consecutive days [23]. A correlation for uterine up–down movement in relation to bladder filling could be observed, and an antero-posterior motion of cervix and vagina depending on rectal filling. Clinical experience at NIRS using repeated MRI or CT scans during treatment also suggested that the target position changed according to bladder volume (data not shown). To decrease such positional uncertainties, the patients were infused with a fixed volume (usually 100 ml) of

Table 15.4 Mean day-to-day displacement of pelvic organs in millimeters as measured by MRI. Data modified from [23]

	Spatial axis		
	Anterior–Posterior	Superior–Inferior	Lateral
Anterior uterus	7	7.1	0.8
Posterior cervix	2.7	4.1	0.3
Upper vagina	2.6	–	0.3

normal saline into the bladder throughout the CIRT sessions. Patients were also encouraged to use laxatives, if considered necessary, to prevent constipation during treatment.

Tumor volume shrinkage might also result in systematic errors throughout the treatment course, if a treatment plan is generated according to single time-point assessment of the target position. Repeated treatment planning and optimal margins are required to minimize internal target positional uncertainty and prevent underdosing to the target or overdosing to adjacent critical structures. An average regression of the primary GTVs of 46% was shown by repeated MRI after having delivered about 30 Gy to 14 cervical cancer patients [24]. Beadle et al. performed CT scanning before, weekly during, and after conventional chemoradiotherapy for 16 cervical cancer patients [25]. They measured mean cervical volumes before and after 45 Gy of external beam irradiation of 97.0 and 31.9 cm^3, respectively, a reduction of 67%. The results showed that mean maximum changes in the perimeter of the cervix were 2.3 and 1.3 cm in the superior and inferior, 1.7 and 1.8 cm in the anterior and posterior, and 0.76 and 0.94 cm in the right and left lateral directions, respectively [25].

In contrast, Lim et al. studied baseline and weekly pelvic MRI during treatment of 20 patients with cervical cancer [26]. They modeled interfractional organ motion and delivered dose for three treatment scenarios: four-field box, large-margin whole pelvic IMRT (20 mm PTV and 10 mm inferior margin) and small-margin IMRT (5 mm PTV). Surprisingly, the small-margin IMRT plans yielded adequate target coverage in most patients except one who displayed excessive, unpredictable internal target motion [26]. Their results suggested that smaller PTV margins of about 5 mm could be used in most, although not all patients. Daily soft-tissue imaging with correction for intra- and interfractional motion and adaptive replanning are important for future studies on IBT for gynecological tumors.

15.5 Outlook

High linear energy transfer (LET) particle therapy has various advantages in terms of radiobiological effects as well as dose distribution, and it has been expected to offer a therapeutic advantage over conventional photon therapy (cf. Chap. 4 for details). However, little clinical evidence has been provided to show the

minimization of radiation resistance of tumors using high LET particles. Cervical cancer obviously has an advantage for translational research because tumor biopsy samples can easily be obtained and direct measuring of tumor oxygen partial pressure is available. The existence of hypoxic cells is well recognized as one of the major factors affecting resistance against radiation therapy and poor prognosis [27]. The experimental report of carbon beams for usage in clinical trials showed that the *oxygen enhancement ratio* (OER) of carbon beams (70 keV/u) was 2.0 for cultured cell lines and 1.6 for inoculated murine tumors, indicating a distinct advantage in OER over low-LET radiation [28, 29]. Nakano et al reported that oxygen partial pressure (pO_2) was measured by using a needle-type polarographic oxygen electrode for 49 patients treated with CIRT at NIRS [30]. As a control group, pO_2 was also measured in 30 patients treated with conventional RT. In this group, significantly worse local control was noted for patients with hypoxic tumors ($pO_2 \leq$ 20 mmHg) before and during the treatment. On the other hand, similar disease-free survival and local control rates between hypoxic and oxygenated tumors before and during treatment were recognized in the CIRT group. These results indicated that the role of tumor oxygenation was not so important for the local control achieved with CIRT. Hence, high-LET carbon ion irradiation might reduce the influence of the radiation-resistant nature stemming from tumor hypoxia.

Nakano et al. demonstrated that a high mitotic index (MI) of a proliferating cell population (pMI) was a worse prognostic factor in cervical cancer patients treated with photon RT [31]. Suzuki et al. investigated the pMI of 27 consecutive patients with stage IIIB bulky (19 patients) and stage IVA (8 patients) squamous cell carcinoma of the cervix treated with CIRT at NIRS [32]. MI and Ki-67 labeling index (Ki-67-LI) were determined by hematoxylin-eosin and immunohistochemical stainings. The pMI was calculated using the following formula: pMI=MI/Ki-67-LI.

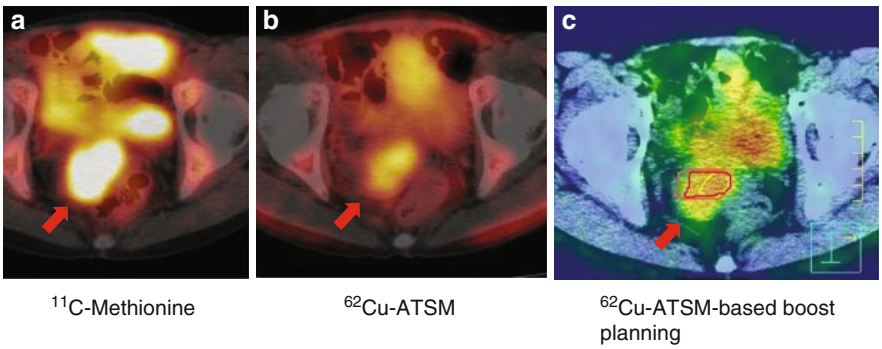

Fig. 15.6 PET-CT with two different imaging agents in a patient with cervical cancer. (**a**) Amino acid ^{11}C-methionine. (**b**) Hypoxia marker ^{62}Cu-ATSM (copper diacetyl-bis(N4-methylthiosemicarbazone)). Note differences in accumulation for (**a**) and (**b**). (**c**) Simulation of the ^{62}Cu-ATSM-PET-CT-based CIRT boost planning for the high-retention area of the compound. *Red arrows* show uterine cervix. *Highlighted* are CTVhypoxia (*yellow*), 96% (*red*), and 90% (*orange*) isodose curves

The local control rate in tumors with a pMI >3.5 was 17%, significantly lower than the 73% in tumors with pMI <3.5 ($p = .005$). These results suggested that a high pMI might be a negative prognostic factor, indicating a poorer prognosis for patients with squamous cell carcinoma of the cervix independent of treatment mode.

The imaging of hypoxia, cell proliferation, angiogenesis, apoptosis, and gene expression can lead to the identification of different areas of a biologically heterogeneous tumor mass that can individually be targeted by IBT. A recently developed PET-based hypoxia measurement technique using the tracer Cu(II)-diacetyl-bis(N4-methylthiosemicarbazone) (Cu-ATSM) is of great interest. Dehdashti et al. studied correlations between 60Cu-ATSM PET uptake and treatment outcome in two small clinical series of patients with lung and cervical cancer treated with radiotherapy, and they suggested that retention of this compound was associated with poor prognosis [33, 34]. Cu-ATSM PET/CT is also of value for integrating functional imaging with PET/CT into the IBT planning process. In the near future, hypoxia-guided CIRT will become one of the challenges for overcoming photon-resistant anoxic tumor cells (Fig. 15.6).

References

1. J.L. Benedet, F. Odicino, P. Maisonneuve, et al., Carcinoma of the cervix uteri. Int. J. Gynaecol. Obstet. **83**, 41–78 (2003)
2. J.A. Green, J.M. Kirwan, J.F. Tierney, et al., Survival and recurrence after concomitant chemotherapy and radiotherapy for cancer of the uterine cervix: a systematic review and meta-analysis. Lancet **358**, 781–786 (2001)
3. P.J. Eifel, K. Winter, M. Morris, et al., Pelvic irradiation with concurrent chemotherapy versus pelvic and para-aortic irradiation for high-risk cervical cancer: an update of Radiation Therapy Oncology Group Trial (RTOG) 90-01. J. Clin. Oncol. **22**, 872–880 (2004)
4. J.M. Kirwan, P. Symonds, J.A. Green, et al., A systematic review of acute and late toxicity of concomitant chemoradiation for cervical cancer. Radiother. Oncol. **68**, 217–226 (2003)
5. T. Arimoto, T.G. Kitagawa, H. Tsujii, et al., High-energy proton beam radiation therapy for gynecologic malignancies. Potential of proton beam as an alternative to brachytherapy. Cancer **68**, 79–83 (1991)
6. K. Kagei, K. Tokuuye, T. Okumura, et al., Long-term treatment results of proton beam therapy for carcinoma of the uterine cervix. Int. J. Radiat. Oncol. **55**, 1265–1271 (2003)
7. T. Nakano, M. Suzuki, H. Tsujii, et al., The phase I/II clinical study of carbon ion therapy for cancer of the uterine cervix. Cancer J. Sci. Am. 362–369 (1999)
8. S. Kato, T. Ohno, H. Tsujii, et al., Dose escalation study of carbon ion radiotherapy for locally advanced carcinoma of the uterine cervix. Int. J. Radiat. Oncol. **31**, 1341–1346 (2006)
9. T. Ohno, S. Kato, E. Sasaki, et al., Carbon ion radiotherapy for vaginal malignant melanoma: a case report. Int. J. Gynecol. Cancer **17**, 1163–1166 (2007)
10. M. Endo, H. Koyama-Ito, S. Minohara, et al., HIPLAN: a heavy ion treatment planning system at HIMAC. J. Jpn. Soc. Ther. Radiol. Oncol. **8**, 231–238 (1996)
11. C.A. Perez, P.W. Grigsby, K.S. Chao, et al., Tumor size, irradiation dose, and long-term outcome of carcinoma of uterine cervix. Int. J. Radiat. Oncol. **41**, 307–317 (1998)
12. J.D. Kochanski, N. Mehta, L.K. Mell, et al., Outcome of cervical cancer patients treated with intensity-modulated radiation therapy. Int. J. Radiat. Oncol. **63**, 214–215 (2005)

13. H.O. Smith, M.F. Tiffany, C.R. Qualls, C.R. Keys, The rising incidence of adenocarcinomas relative to squamous cell carcinomas of the uterine cervix – a 24-year population based study. Gynecol. Oncol. **78**, 97–105 (2000)
14. J.L. Benedet, F. Odicino, P. Maisonneuve, et al., Carcinoma of the cervix uteri. J. Epidemiol. Biostat. **6**, 7–43 (2001)
15. A. Baalbergen, P.C. Ewing-Graham, W.C. Hop, et al., Prognostic factors in adenocarcinoma of the uterine cervix. Gynecol. Oncol. **92**, 262–267 (2004)
16. P.J. Eifel, M. Morris, M.J. Oswald, et al., Adenocarcinoma of the uterine cervix. Prognosis and patterns of failure in 367 cases. Cancer **65**, 2507–2514 (1990)
17. M.P. Hopkins, G.W. Morley, A comparison of adenocarcinoma and squamous cell carcinoma of the cervix. Obstet. Gynecol. **77**, 912–918 (1991)
18. J.S. Lea, E.E. Sheets, R.M. Wenham, et al., Stage IIB-IVB cervical adenocarcinoma: prognostic factors and survival. Gynecol. Oncol. **84**, 115–119 (2002)
19. M.A. Quinn, J.L. Benedet, F. Odicino, et al., Carcinoma of the cervix uteri. FIGO 6th annual report on the results of treatment in gynecological cancer. Int. J. Gynaecol. Obstet. **95**(Suppl 1), S43–S103 (2006)
20. P.W. Grigsby, C.A. Perez, R.R. Kuske, et al., Adenocarcinoma of the uterine cervix: lack of evidence for a poor prognosis. Radiother. Oncol. **12**, 289–296 (1988)
21. A. Ahmad, W. D'Souza, M. Salehpour, et al., Intensity-modulated radiation therapy after hysterectomy: comparison with conventional treatment and sensitivity of the normal-tissue-sparing effect to margin size. Int. J. Radiat. Oncol. **62**, 1117–1124 (2005)
22. A. Buchali, S. Koswig, S. Dinges, et al., Impact of the filling status of the bladder and rectum on their integral dose distribution and the movement of the uterus in the treatment planning of gynaecological cancer. Radiother. Oncol. **52**, 29–34 (1999)
23. A. Taylor, M.E. Powell, An assessment of interfractional uterine and cervical motion: implications for radiotherapy target volume definition in gynaecological cancer. Radiother. Oncol. **88**, 250–257 (2008)
24. L. van de Bunt, U.A. van der Heide, M. Ketelaars, et al., Conventional, conformal, and intensity-modulated radiation therapy treatment planning of external beam radiotherapy for cervical cancer: The impact of tumor regression. Int. J. Radiat. Oncol. **64**, 189–196 (2006)
25. B.M. Beadle, A. Jhingran, M. Salehpour, et al., Cervix regression and motion during the course of external beam chemoradiation for cervical cancer. Int. J. Radiat. Oncol. **73**, 235–241 (2009)
26. K. Lim, V. Kelly, J. Stewart, et al., Pelvic radiotherapy for cancer of the cervix: is what you plan actually what you deliver? Int. J. Radiat. Oncol. **74**, 304–312 (2009)
27. M. Hockel, C. Knoop, K. Schlenger, et al., Intratumoral pO2 predicts survival in advanced cancer of the uterine cervix. Radiother Oncol **26**, 45–50 (1993)
28. K. Ando, S. Koike, C. Ohira, et al., Accelerated reoxygenation of a murine fibrosarcoma after carbon-ion. Int. J. Radiat. Biol. **75**, 505–512 (1999)
29. M.R. Raju, H.I. Amols, E. Bain, et al., A heavy particle comparative study. Part III. OER and RBE. Br. J. Radiol. **51**, 712–719 (1978)
30. T. Nakano, Y. Suzuki, T. Ohno, et al., Carbon beam therapy overcomes the radiation resistance of uterine cervical cancer originating from hypoxia. Clin. Cancer Res. **12**, 2185–2190 (2006)
31. T. Nakano, K. Oka, A. Ishikawa, et al., Correlation of cervical carcinoma c-erb B-2 oncogene with cell proliferation parameters in patients treated with radiation therapy for cervical carcinoma. Cancer **79**, 513–520 (1997)
32. Y. Suzuki, K. Oka, T. Ohno, et al., Prognostic impact of mitotic index of proliferating cell populations in cervical cancer patients treated with carbon ion beam. Cancer **115**, 1875–1882 (2009)
33. F. Dehdashti, M.A. Mintun, J.S. Lewis, et al., In vivo assessment of tumor hypoxia in lung cancer with 60Cu-ATSM. Eur. J. Nucl. Med. Mol. Imaging **30**, 844–850 (2003)
34. F. Dehdashti, P.W. Grigsby, M.A. Mintun, et al., Assessing tumor hypoxia in cervical cancer by positron emission tomography with 60Cu-ATSM: relationship to therapeutic response – a preliminary report. Int. J. Radiat. Oncol. **55**, 1233–1238 (2003)

Chapter 16
Is Prostate Cancer a Good Candidate for Ion Beam Therapy?

Carl J. Rossi Jr.

Abstract Organ-confined prostate cancer now constitutes one of the most commonly treated malignancies with ion beam therapy (IBT). Because of this, questions have been raised regarding the efficacy and cost-effectiveness of such treatment. This chapter details the clinical results obtained with both proton and carbon ion therapy, discusses ongoing clinical trials, and seeks to place IBT in the context of other technological evolutions in radiation oncology.

16.1 Introduction

Prostate cancer presents a major oncologic dilemma for the developed world. In the United States, approx. 218,000 new cases and approx. 32,000 deaths were estimated for the year 2010 [1]. Prostate cancer is the second leading cause of cancer deaths among American men and accounts for approximately 10% of all cancer-related deaths in men. A similar incidence and death rate is seen in Western Europe. The lowest reported incidence is in Eastern/Southern Asia. Over the past 20 years, the discovery and use of prostate specific antigen (PSA) as a screening tool has led to both an increase in the number of cases being diagnosed and a decrease in the proportion of men being diagnosed with advanced disease. This trend toward diagnosis with organ-confined disease has prompted the development and refinement of treatment methods directed at the prostate in the entirely reasonable hope of providing long-term disease-free survival and cure.

From the standpoint of radiation therapy (RT), virtually all technical advances in prostate cancer treatment have been implemented to reduce normal tissue toxicity

C.J. Rossi Jr. (✉)
Department of Radiation Medicine, Loma Linda University Medical Center, 11234 Anderson Street, CSP A-1010, Loma Linda, CA 92354, USA
e-mail: crossi@llurm.org

U. Linz (ed.), *Ion Beam Therapy*, Biological and Medical Physics, Biomedical Engineering, DOI 10.1007/978-3-642-21414-1_16,

by limiting the volume of adjacent bladder and rectum that receives high doses of radiation. A direct consequence of this improvement in dose conformality has been dose escalation [2–7], a concept that has been tested and confirmed in one proton beam-based prospective randomized trial.

The unique physical properties inherent in ion beams – which, for purposes of this chapter, will comprise protons and carbon ions – makes them particularly attractive to the radiation oncologist, for they permit a reduction in "integral dose" (defined as the total radiation dose given to the patient) over and above anything that can be achieved with photon-based external beam-treatment systems [8–11]. Additionally, in the case of carbon ions, radiobiological theory predicts that their high relative biological effectiveness (RBE) may be particularly effective in the treatment of a slowly proliferating tumor such as prostate cancer [12]. The recent commissioning of clinically based carbon ion facilities will permit further testing of this hypothesis.

However, IBT of prostate cancer is not without its detractors. Critics often point out that a multitude of effective treatment methods exist and that modern photon therapy using intensity-modulated techniques (IMRT) and image-guided treatment delivery (IGRT) yield similar outcomes at less monetary cost to society, whereas still others question the wisdom of aggressively treating prostate cancer at all [13, 14]. These criticisms force one to ask the question: Is prostate cancer a good candidate for IBT? Answering this question will first depend on a review of the available data demonstrating the clinical utility of IBT in the treatment of prostate cancer and the future potentials inherent in this modality.

16.1.1 Proton Therapy Results

16.1.1.1 Early Trials

The ability to use IBT to treat deep organs was, and is, greatly dependent on the concurrent development of cross-sectional imaging technology (CT, MRI) and modern computers; hence, it is not surprising that IBT of prostate cancer did not commence until the late 1970s. Beginning in 1977, Shipley and associates at the Massachusetts General Hospital (MGH) initiated a phase I trial in which proton beam RT was used to give a boost dose to patients with locally advanced disease who were also receiving photon RT. At that time, this boost dose was felt to be over and above what could be safely given with existing photon technology. Seventeen patients with stage T2–T4 disease received a perineally directed proton beam boost of 20–26 Gy (given at a rate of 1.8–2 Gy/day) following treatment to the prostate and pelvis to a dose of 50.4 Gy with 10 MV photons. A perineal approach was chosen because this was the only anatomical pathway that allowed the 160 MeV proton beam generated at the Harvard Cyclotron Laboratory (HCL) to reliably encompass the entire prostate gland. Acutely, the treatment was well tolerated and after a

follow-up period ranging from 12 to 27 months no severe late-rectal reactions were noted [15].

These favorable toxicity results led directly to the initiation of a prospective randomized trial designed to test the benefits of proton beam dose escalation in patients with locally advanced disease. Patients with stage T3–T4 tumors were chosen as it was felt that this group stood to gain the most benefit from high doses. All patients received 50.4 Gy to the prostate and pelvis with megavoltage photons. They were then randomized to receive either an additional 16.8 Gy of photons (for a total prostate dose of 67.2 Gy) or 25.2 GyE of protons for a total prostate dose of 75.6 Gy. Adjuvant hormonal therapy was not permitted. The limited availability of the proton beam at the HCL affected patient accrual. Nonetheless, 202 patients were eventually enrolled, with 103 being treated in the high-dose arm and 99 in the standard dose arm.

With a median follow-up of 61 months, there were no differences seen in overall survival, disease-specific survival, total relapse-free survival, or local control between the arms. Patients with high-grade tumors who were treated on the high-dose arm did experience an improvement in local control at 5 and 8 years (92 and 77% vs. 80 and 60%, $p = 0.89$). Patients whose digital rectal exams normalized following treatment and who underwent subsequent prostate biopsy revealed a lower positive biopsy rate in the high-dose arm (28 vs. 45%) and, perhaps most surprisingly, the local control rates for patients with Gleason grade 4–5 tumors (57 patients total) were significantly better at 5 and 8 years in the high-dose patients (94 and 84% vs. 68 and 19%, $p = 0.001$). High-dose treatment was associated with an increase in late-grade 1–2 rectal bleeding (32 vs. 12%, $p = 0.02$) [16].

These results have been erroneously cited by some as evidence that proton beam dose escalation is of doubtful utility [17]. It should be noted that the patients treated in this trial were at a high risk of not only local failure but also of distant failure and, therefore, one should not be surprised that overall survival was unaffected. In addition, patients with these adverse characteristics would not, if diagnosed today, receive RT as monotherapy and instead would be treated with a multimodality approach [18–22]. I believe that the two most important things learned from this study are (1) high-dose RT did decrease local failure, and this decrease was most profound in those patients with the most aggressive tumors, and (2) dose escalation by means of a perineal proton beam (an approach that has largely been abandoned today as higher energy machines have become available) can be performed safely with acceptable toxicity [23].

The improvement in local control seen with dose escalation prompted a very logical question: If patients with earlier stage disease who are less likely to have already experienced metastatic failure are treated with dose escalation, will we see a positive effect on survival? This intriguing hypothesis has been tested in a prospective randomized multiinstitutional trial and its conclusions will be covered presently.

The completion in 1990 of the world's first hospital-based proton treatment center at Loma Linda University Medical Center (LLUMC) marked the beginning of a transition in IBT from the research laboratory setting to that of clinical radiation

Table 16.1 Patient characteristics of 643 prostate cancer patients treated between 1991 and 1995 at LLUMC

		# Patients
Stage	1A/1B	28
	1C	91
	2A	157
	2B	173
	2C	157
	3	37
Gleason	2–5	232
	6–7	324
	8–10	54
Initial PSA	≤4.0	53
	4.1–10.0	280
	10.0–20.0	175
	>20.0	85

oncology [24]. Beginning in late 1991, prostate patients at LLUMC were treated on a clinical trial that set out to confirm the efficacy and toxicity data generated at MGH. Between December 1991 and December 1995, 643 patients were treated to total prostate radiation doses of 74–75 GyE. Patients who were deemed to be at a low risk for occult nodal metastasis were treated with lateral proton beams alone, whereas those who were felt to benefit from elective nodal radiation received 45 Gy to the pelvis with 18–23 MV photons delivered via a multifield 3D conformal technique. Patient characteristics are shown in Table 16.1.

With a median follow-up of 43 months, the overall biochemical disease-free survival (bNED: biochemically no evidence of disease) rate was 79% as per the American Society for Therapeutic Radiology and Oncology (ASTRO) definition of three successively rising PSA values above a nadir equating to biochemical failure (Fig. 16.1). The risk of biochemical failure was strongly dependent on the pretreatment PSA with 5-year bNED survival rates varying from 43% in patients with pretreatment PSA of 20–50 to 100% with PSA < 4.1. BNED survival was also significantly influenced by posttreatment PSA nadir. A multivariant analysis of failure predictors demonstrated that initial stage, PSA, and Gleason score were all strong predictors of biochemical failure at 5 years (Table 16.2). As was also reported in the MGH trial, treatment was by and large well tolerated. Acute toxicity was minimal and all patients completed the prescribed course of RT. Proctitis remained the most common late toxicity with grade 2 toxicity occurring in 21% of patients at 3 years; for the majority of patients, this represented a single episode of rectal bleeding. No toxicity ≥ grade 3 gastrointestinal (GI) was seen. Grade 2 genitourinary (GU) toxicity – primarily gross hematuria – was seen in 5.4% of patients at 3 years, with two patients developing grade 3 bladder toxicity. Interestingly, no significant difference in late toxicity was seen between those patients treated with protons alone and those receiving pelvic X-ray therapy. The excellent biochemical control rates and acceptable toxicity seen in this trial

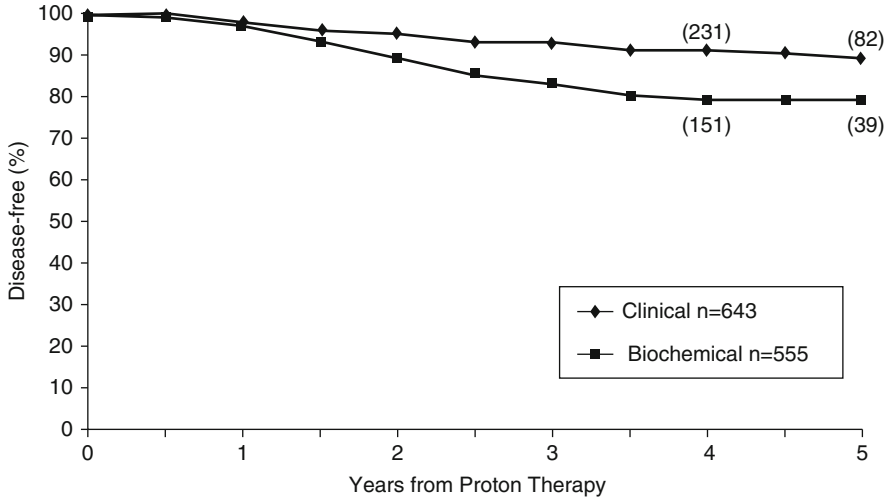

Fig. 16.1 Biochemical disease-free survival in relation to posttreatment PSA nadir for 643 prostate cancer patients treated between 1991 and 1995 at LLUMC. Numbers in *parenthesis* represent patients in analysis at time interval

Table 16.2 Factor analysis of failure predictors

		% Disease-free survival 5 year	Univariate *p*	Multivariate *p*
Initial PSA	≤4.0	100	<0.001	0.001
	4.1–10.0	88		
	10.0–20.0	68		
	>20.0	48		
Gleason	2–5	82	<0.001	0.007
	6–7	76		
	8–10	48		
T stage	1A/1B	79	<0.001	0.003
	1C	94		
	2A	87		
	2B	73		
	2C	59		
	3	59		

confirmed the earlier MGH data and led to the implementation of a prospective randomized dose-escalation study in organ confined prostate cancer [25].

A further update of the initial LLUMC experience was published in 2004. This study encompassed 1,255 patients with stage T1–T3 disease who were treated with proton therapy (PT) alone (i.e., no prior or concurrent hormonal therapy) to a dose of 74–75 GyE. As was seen in the earlier trial initial PSA, Gleason score, and PSA nadir were all strong predictors of bNED survival (Figs. 16.2–16.4). Treatment

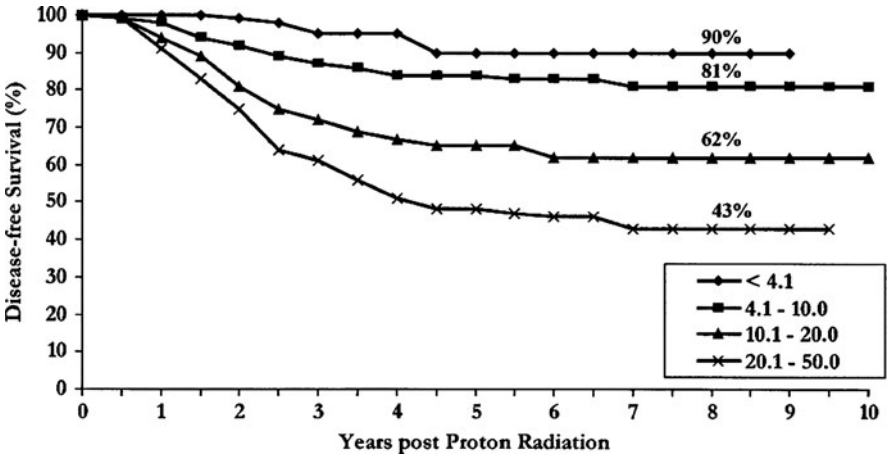

Fig. 16.2 Effect of initial PSA on biochemical disease-free survival (LLUMC)

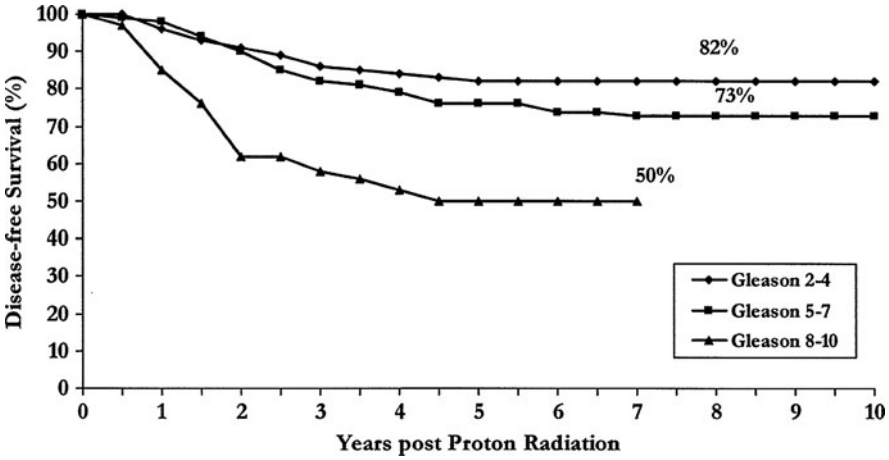

Fig. 16.3 Gleason score in relation to biochemical disease-free survival (LLUMC)

continued to be well tolerated with rates of RTOG grade ≥3 GI/GU late morbidity of <1% [26].

Beginning in 1996, LLUMC and MGH embarked on the Proton Radiation Oncology Group/American College of Radiology (PROG/ACR) 95–09 trial, a prospective, randomized dose-escalation study for patients with organ-confined prostate cancer. This study was designed to test the hypothesis that a dose escalation from 70.2 to 79.2 GyE would result in a statistically significant decrease in local failure, biochemical failure, and overall survival. Eligibility criteria included stage T1b–T2b disease (as per the 1992 American Joint Committee on Cancer-staging system), a PSA of ≤15 ng/ml, and no evidence of metastatic disease on imaging

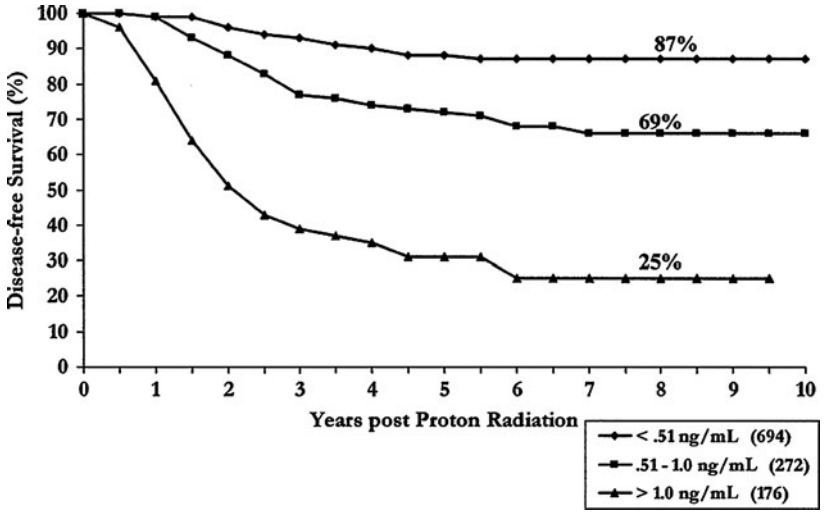

Fig. 16.4 Effect of PSA nadir on biochemical disease-free survival (LLUMC)

studies (bone scan, abdomino-pelvic CT scan). Gleason score was not an exclusion criterion and no prior or concurrent androgen deprivation therapy (ADT) was permitted. Pretreatment patient characteristics are shown in Table 16.3.

Patients were randomly assigned to receive a total prostate dose of 70.2 or 79.2 GyE. RT was administered sequentially in two phases. In phase I, conformal proton beams were used to treat the prostate alone. Depending on randomization, either 19.8 or 28.8 GyE in 11 or 16 fractions was delivered. The clinical target volume (CTV) was the prostate with a 5 mm margin. Beam arrangement was facility dependent with patients at LLUMC being treated with lateral proton beams of 225–250 MeV energy, whereas at MGH a perineal 160 MeV proton beam was employed. Before each proton beam treatment, a water balloon was inserted into the rectum and inflated with 100 ml of saline; this served the dual purpose of distending the rectum lumen to decrease the volume of rectum receiving any radiation and minimizing prostate motion.

In the second phase of treatment, all patients received 50.4 Gy of photons given in 1.8 Gy fractions. The CTV was the prostate and seminal vesicles. No effort was made to include the pelvic lymphatics. Three-dimensional planning was used on all patients and photon energies of 10–23 MV were employed. The use of photons for a portion of the treatment was solely to allow both institutions to participate in this trial, for at the time the trial commenced, MGH patients were still restricted to treatment at the HCL and the limited throughput of that facility meant that the most efficient use of protons was as a boost and not as monotherapy. The randomization scheme is shown in Fig. 16.5. A total of 393 patients were randomized between January 1996 and December 1999.

The results of the trial were initially published in 2005 [27] with an update in 2010. At a median follow-up of 8.9 years, there is a persistent and statistically

Table 16.3 Pretreatment characteristics, PROG/ACR 9509 trial

Characteristic	Assigned dose			
	70.2 GyE ($n = 196$)		79.2 GyE ($n = 195$)	
	No.	%	No.	%
Age (years)				
45–59	43	22	34	17
60–69	92	47	106	54
70–79	61	31	55	28
≥80	1	0.5	0	
Median	67		66	
Range	45–91		47–78	
Race				
White	175	89	178	91
Hispanic	4	2	7	3
Black	12	6	5	3
Other	5	3	5	3
PSA, ng/ml				
<5	54	28	47	24
5 to <10	114	58	119	61
10–15	28	14	29	15
Median	6.3		6.2	
Range	1.24–14.68		0.67–14.30	
Kamofsky performance status				
80	8	4	9	5
90	52	27	47	24
100	136	69	139	71
Combined Gleason				
2–6	148	75	147	75
7	29	15	30	15
8–10	18	9	15	8
Unknown	1	1	3	2
T stage				
T1b	1	1	0	
T1c	120	61	120	61
T2a	43	22	50	26
T2b	32	16	25	13
N stage				
NO	0		2	1
NX	196	100	193	99
Risk groups[a]				
Low	111	57	116	59
Intermediate	75	38	69	35
High	10	5	7	4
Not classified	0		3	2

Abbreviation: GyE Gray equivalent; *PSA* prostate-specific antigen

[a]Risk groups according to D'Amico et al. [23]

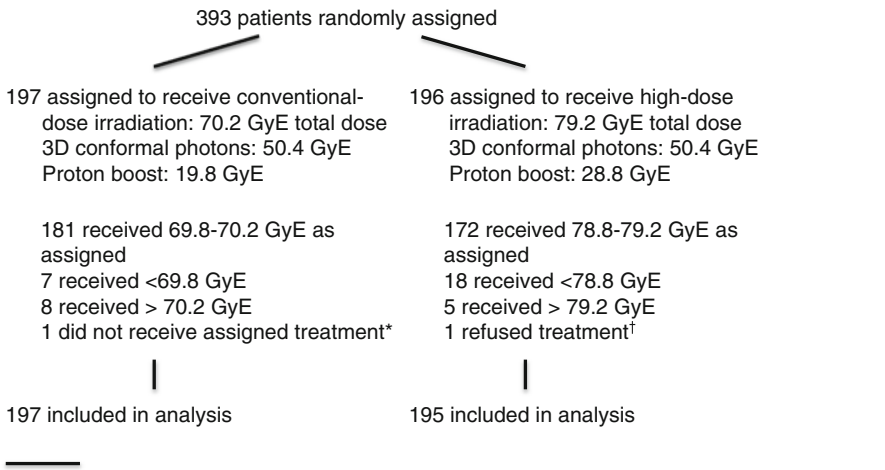

GyE=Gray Equivalent.

*Patient underwent radical prostatectomy rather than radiation therapy because the bowel was too close to the prostate for safe administration of radiation.

†No follow-up data available for analysis.

Fig. 16.5 PROG/ACR 9509 trial randomization scheme

significant increase in biochemical freedom from relapse among patients randomized to the high-dose arm (Fig. 16.6). This difference was seen when using both the ASTRO and the more recent Phoenix definition [28] (in which biochemical failure corresponds to a PSA elevation of $>2\,\mathrm{ng/ml}$ above a nadir). Subgroup analysis showed a particularly strong benefit in 10-year bNED survival among the "low-risk" patients (defined as PSA $<10\,\mathrm{ng/ml}$, and Gleason score <7 and stage $<$T2b), with 92.2% of high-dose patients being disease free vs. 78.8% for standard dose ($p = 0.0001$). A strong trend toward a similar finding was seen in the intermediate risk patients but this has not reached statistical significance (Fig. 16.7). In addition, patients in the standard dose arm are twice as likely to have been started on androgen deprivation therapy as high-dose patients (22 vs. 11, $p = 0.47$) with such treatment usually being initiated due to a rising PSA. To date, there is no difference in overall survival between the arms [29].

As was seen in the previously reported proton trials, treatment was well tolerated. Only 2% of patients in both arms experienced late GU toxicities of grade ≥ 3, and 1% experienced late GI toxicity of grade ≥ 3. Interestingly, as opposed to what has been reported in some photon-based randomized dose-escalation trials, high-dose RT delivered via a conformal proton beam boost did not result in an increase in late-grade ≥ 3 GI morbidity among the high-dose patients (Table 16.4). This encouraging finding has been confirmed in a patient-reported sensitive Quality-of-Life (QoL) questionnaire that did not report any greater morbidity than the physician-reported scores, and which revealed equal and high satisfaction with QoL between both arms [30].

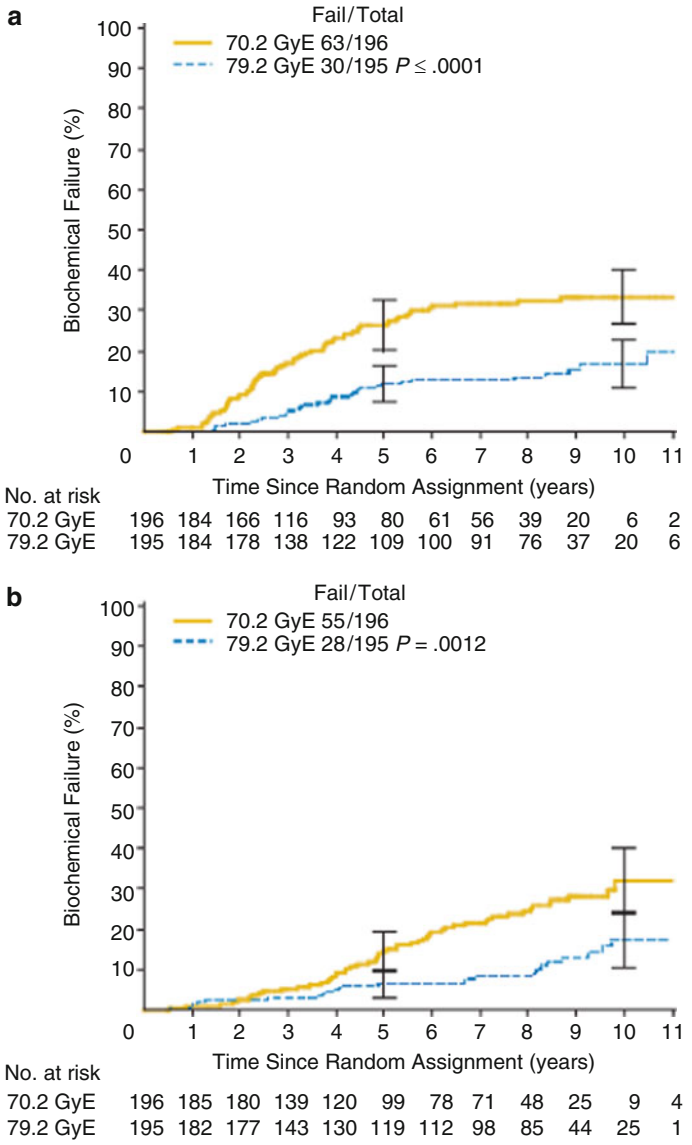

Fig. 16.6 Biochemical failure after either conventional or high-dose conformal RT. (**a**) Biochemical failure by ASTRO Consensus. (**b**) Biochemical failure by the Phoenix Criteria. *GyE* Gray Equivalent

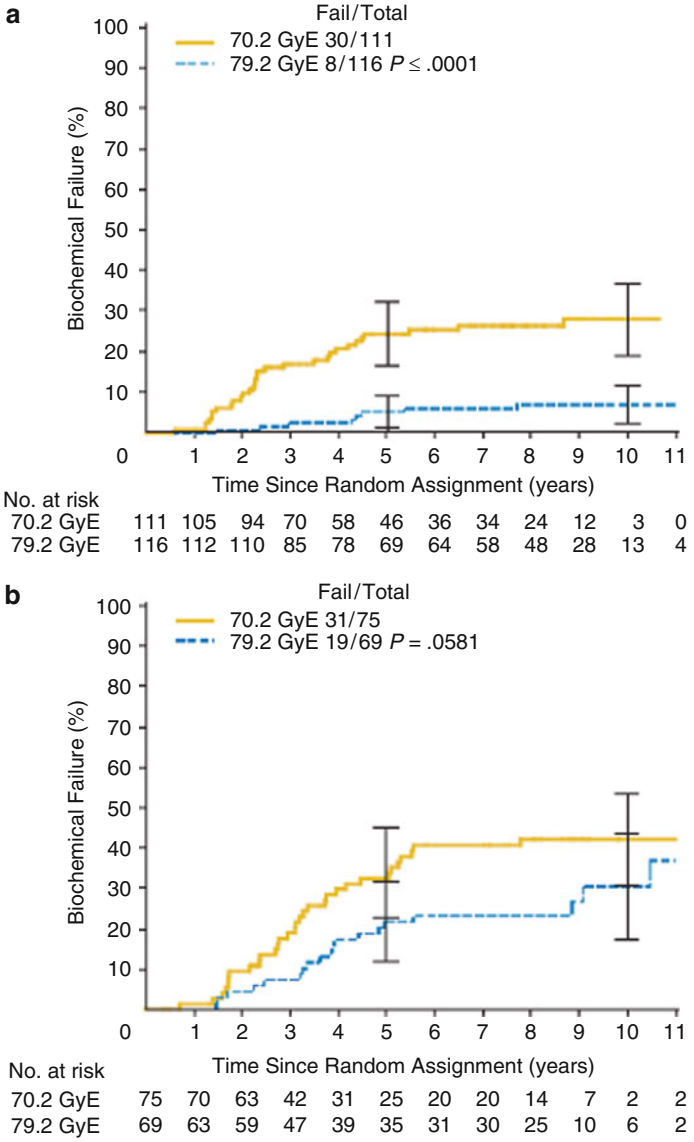

Fig. 16.7 Biochemical failure by ASTRO Consensus after conventional and high-dose conformal RT. (**a**) Biochemical failure for the low-risk group. (**b**) Biochemical failure for the intermediate risk group. *GyE* Gray Equivalent

Table 16.4 Acute and late gastrointestinal (GI) and genitourinary (GU) morbidity for patients treated on the PROG/ACR 9509 protocol

Toxicity	Assigned dose																*P*
	70.2 GyE(n = 196)								79.2 GyE(n = 195)								
	Grade 1		Grade 2		Grade 3		Grade 4		Grade 1		Grade 2		Grade 3		Grade 4		
	No.	%	No.	%	No.	%	No.	%	No.	%	No.	%	No.	%	No.	%	
Acute																	
Gu	72	37	100	51	5	3	0	0	56	29	117	60	4	2	1	1	0.0745
GI	76	39	87[a]	44	2	1	0	0	50	26	123[a]	63	2	1	0	0	0.0006[a]
Late																	
GU	82	42	44	22	4	2	0	0	88	45	52	27	3	2	0	0	0.7934
GI	68	35	25	13	0	0	0	0	79	41	46	24	2	1	0	0	0.0895

[a]Testing grade 1 versus others using X^2 test

Thus, the PROG/ACR 9509 trial provides "Level One" evidence verifying the importance of radiation dose-escalation in organ-confined prostate cancer, and although this study was not designed to directly compare the efficacy of conformal PT against other conformal techniques or modalities it does demonstrate that conformal PT is an effective treatment for this disease, with minimal risk of experiencing severe treatment-induced toxicity.

16.1.1.2 Experience of the Florida Proton Therapy Institute

The Florida Proton Therapy Institute (FPTI) opened in the summer of 2006 with prostate cancer treatment commencing at that time. From August 2006 to October 2007, patients were treated on one of three prospective trials: 78 GyE/39 fractions for low-risk disease, dose-escalation from 78 to 82 GyE for intermediate-risk disease, and 78 GyE with concomitant docetaxel, followed by ADT, for high-risk disease. Preliminary GI and GU toxicity data were reported in 2009 with a minimum of 1 year follow-up. There were 47 grade 2 and 1 grade 3 GU toxicities at 6 months and 48 grade 2 and 1 grade 3 toxicities at 12 months. The overwhelming majority of grade 2 symptoms (98%) were retentive symptoms requiring treatment with alpha blockers. Multivariate analysis suggested that GU toxicities $\geq$ grade 2 were correlated with pretreatment prostatitis, pretreatment International Prostate Symptom Score (IPSS) and, as time progressed, with patient age and pretreatment GU symptom management. This strongly suggests that the predominant predictors of early GU toxicity were pretreatment clinical factors.

GI toxicities were considerably less common, with 1 grade 2 and no grade 3 or greater toxicities at 6 months, increasing to 8 grade 2 and 1 grade 3 at 12 months. Two grade 2 toxicities occurred on both the low-risk and high-risk protocol, whereas the remainder occurred on the dose-escalation intermediate-risk study. Univariate analysis of the low- and intermediate-risk patients revealed a significant correlation between grade 2 or higher GI toxicity and the percentage of rectal wall receiving radiation doses from 25 to 80 GyE. Interestingly, of the ten patients who developed grade 2 or higher symptoms at 12 months, five originally had grade 1 toxicities that progressed to grade 2–3 after colonoscopy intervention, confirming an observation that has also been made at LLUMC. The authors concluded that treatment was well tolerated with minimal and acceptable GI/GU toxicity, again mirroring the results from other proton centers [31].

16.1.1.3 The ACR 0312 Trial

Following the completion of patient accrual to the PROG/ACR9509 randomized trial, LLUMC and MGH opened a phase II dose-escalation study designed to determine the toxicity and efficacy of proton beam-based dose escalation in patients with organ-confined disease. The ACR 0312 trial delivered a total dose of 82 GyE/41 fractions to the prostate, with the initial 50 GyE also including the caudal 2 cm of

the seminal vesicles. Planning target volumes (PTV) were identical to those used in the PROG 9509 patients. The trial enrolled 85 patients who were treated between May 2003 and March 2006. The rate of acute GI/GU ≥ grade 3 complications was 1%. With a median follow-up of 31.6 months, six patients had developed a late-grade 3 GI/GU toxicity with one additional patient developing grade 4 toxicity. The median time to toxicity ≥ grade 3 was 9.5 months with an estimated rate of 6% at 18 months. Dose–volume histogram (DVH) analysis of the radiation dose to the anterior rectal wall failed to reveal a demonstrable association between dose to various volumes of the anterior wall and the risk of subsequently developing toxicity ≥ grade 2 late rectal. The authors noted that the observed late morbidities compare favorably with that reported in IMRT dose-escalation studies, but that the dose of 82 GyE/41 fractions probably represents the safe limit of what can be delivered with passively scattered proton beams. They speculated that further dose escalation should be possible with the forthcoming implementation of intensity-modulated proton therapy (IMPT) and real-time image-guided proton treatment (IGPT).

16.1.1.4 The Japanese Experience

The Hyogo Ion Beam Medical Center (HIBMC) began treating prostate patients with proton radiation in April, 2001. Between 2001 and 2002, a series of phase I–II protocols were performed to verify treatment techniques and assess toxicity. Once these revealed minimal toxicity, proton beam therapy passed into general clinical use [32]. In 2003–2004, 287 patients with stage T1–T4 N0 M0 prostate cancer were treated with lateral proton beams to a dose of 74 GyE in 37 fractions. Planning margins were similar to those used at the US proton centers, although a rectal balloon was not used. Patient characteristics are shown in Table 16.5 [33]. Seventy-one percent of the patients also received ADT.

The observed morbidities are shown in Table 16.6. Mirroring the US experience, grade 3 GU toxicities were extremely rare, and no grade 4 events occurred. On univariate analysis, CTV size and patient age were significantly associated with a greater incidence of grade ≥ 2 GU morbidity. Multivariate analysis confirmed that large CTVs ($p = 0.001$) and the use of androgen suppression therapy ($p = 0.017$) independently predicted acute GU grade 2–3 morbidity. These acute toxicities were comparable to those seen in published IMRT, 3D conformal, and brachytherapy series.

16.1.1.5 Hypofractionation

Modern radiobiological theory predicts that prostate cancer has a low "α/β ratio," a numeric description of the sensitivity of a particular tissue to radiation fraction size. Values typically reported for prostate are in the range of 1.5–2.0 Gy [34]. Tissues with a low α/β are more sensitive to changes in fraction size than those

Table 16.5 Prostate cancer patient characteristics at Hyogo Ion Beam Medical Center (HIBMC). Data from [33]

Characteristic	Patient numbers*
Age (years)	
<70	146 (51)
≥70	141 (49)
T stage	
T1c	107 (37)
T2a	81 (28)
T2b	39 (14)
T3	59 (21)
T4	1 (0.3)
Gleason score	
2–6	91 (32)
7	161 (56)
8–10	26 (9)
Unknown	9 (3)
Initial PSA level (ng/ml)	
<10	135 (47)
10.0–19.9	79 (28)
20.0–49.9	53 (18)
≥50	20 (7)
MSKCC risk group (13)	
Favorable	62 (22)
Intermediate	100 (35)
Unfavorable	125 (43)
Use of AST	
No	83 (29)
Yes	204 (71)
Diabetes mellitus	
No	251 (87)
Yes	36 (13)

Abbreviations: PSA prostate-specific antigen, *MSKCC* Memorial Sloan-Kettering Cancer Center; *AST* androgen suppression therapy

*Data in parentheses are percentages

with a high α/β as, for example, late bladder or rectal toxicity with an assumed α/β ratio of 3–4 Gy. This difference in α/β ratios implies that prostate cancer cells are more sensitive to changes in radiation fraction size than the bladder or rectum, meaning that by increasing the daily fraction size and reducing the total radiation dose, one can potentially shorten the overall treatment time without compromising tumor control and without increasing the risk of incurring a late GI/GU injury.

Hypofractionation has a long-established history in PT, and is now routinely used in the treatment of ocular melanomas [35–37], intracranial metastasis, arteriovenous

Table 16.6 Incidence of acute GI and GU morbidities at HIBMC

Toxicity	Grade 0	Grade 1	Grade 2	Grade 3	Grade 4
Dysuria	52 (18)	134 (47)	101 (35)	0	0
Urinary frequency	69 (24)	179 (62)	36 (13)	3 (1)	0
Urinary retention	204 (71)	73 (25	9 (3)	1 (0.3)	0
Hematuria	231 (81)	50 (17)	5 (2)	1 (0.3)	0
GU, overall	18 (6)	154 (54)	111 (39)	4 (1)	0
Proctitis	282 (98)	5 (2)	0	0	0
Rectal bleeding	0	0	0	0	0
GI, overall	282 (98)	5 (2)	0	0	0

Abbreviations: *GU* genitourinary, *GI* gastrointestinal, *NCI-CTC* National Cancer Institute Common Toxicity Criteria. Data presented as numbers of patients, with percentages in parentheses

malformations [38, 39], lung cancer [40], and breast cancer [41]. It also is being actively investigated in prostate cancer, although to date this investigation has employed primarily IMRT-based approaches [42–46]. There is an emerging body of data supporting its safety and efficacy in this setting to the point that at least one prominent radiation biologist has declared that hypofractionation should be considered the treatment of choice for prostate cancer [47].

At the time of this writing, there are two hypofractionated conformal proton beam treatment protocols actively accruing patients in the United States. At LLUMC, a phase I–II trial of 60 GyE/20 fractions (which is designed to be isoeffective with 81 GyE/45 fractions, if one assumes an α/β ratio of 1.5 for prostate cancer) began accruing patients in 2009. Eligibility is limited to "low-risk" patients (PSA <10 ng/ml, Gleason <7, and Stage <T2b). Preliminary analysis indicates that treatment is well tolerated with no patient ($n = 62$) experiencing grade ≥3 acute GI/GU complication. Posttreatment PSA decreases are consistent with expectations. At the FPTI, hypofractionation is being investigated in a similar protocol in which patients with low- to intermediate-risk prostate cancer are treated on a 5-week hypofractionated regimen to a total dose of 70 GyE/28 fractions for low-risk patients, and 72.5 GyE/29 fractions for intermediate-risk patients.

Hypofractionation has been routinely employed in carbon ion radiotherapy (CIRT) of prostate cancer with all published results based on various hypofractionated treatment regimens. This is largely due to the extremely limited clinical access to carbon ion treatment. Results of these trials will be discussed in the carbon ion section of this chapter.

The published peer-reviewed data conclusively demonstrate that conformal PT is extremely well tolerated and can produce bNED survival rates equivalent to other modern RT modalities and to radical prostatectomy. Conformal proton beam dose escalation has been tested in a prospective randomized trial and has been shown to improve bNED survival without (as opposed to what has been seen in some IMRT trials [48]) concurrently increasing the risk of late GI/GU morbidity ≥ grade 3. However, attempts to escalate dose to 82 GyE have been met with a substantial increase in late GI morbidity; this may reflect the "limit" beyond which treatment with passively scattered beams and their attendant substantial penumbra may not

be safely possible, although it is likely that the pending introduction of IMPT via active beam scanning and the implementation of novel image-guided techniques will permit further increases in dose. Hypofractionation is currently being tested in protocols at several proton centers and preliminary data on the safety and efficacy of this technique will be available within the next 12–18 months.

16.1.2 CIRT Results

The potential benefit of heavy ions in clinical radiation oncology has been discussed for over half a century. Their particular appeal lies in their possession of physical qualities similar to those of protons (the Bragg peak) with an RBE far greater than that of either protons or X-rays (cf. Chap. 4).

Radiation with a high RBE may be particularly effective in killing tumors like prostate cancer that usually have a low proliferative index (the percentage of cells undergoing mitosis at any given time) and are thus relatively resistant to the effects of indirectly ionizing radiation like photons or protons with their low ionization density, but are more likely to be fatally injured by the dense ionization effects produced by heavy ions. Although a good deal of controversy over the precise RBE of heavy ions exists (cf. Chap. 6), the value for carbon ions is felt to be approximately 3 while, in contrast, that of protons is 1.1 [49–54]. Carbon RBE values are the subject of intense investigation as carbon treatment centers seek to be able to more precisely define the RBE for various normal tissues where differences between the assumed and actual RBE could have profound effects on the risk of normal tissue injury.

16.1.2.1 The Japanese Experience

Investigators in Japan have performed a number of phase I/II studies of CIRT in prostate cancer (see also Chap. 36). One of the first published trials was performed by Ishikawa and associates [55]. This was a classic phase I–II dose-escalation study that involved 35 patients with stage T2b–T3b disease. Dose was escalated from 54 GyE/20 fractions/5 weeks (treatment being given on four days per week) to 72 GyE/20 fractions, with the escalation occurring in 10% increments. The investigators found that the 72 GyE dose level produced an unacceptable 36% grade 3 late GI/GU toxicity rate; so a subsequent phase I–II trial was begun in 1998 that utilized a shrinking field technique to deliver a total dose of 60–66 GyE in 20 fractions. At this dose level, there were no late grade 3 GI/GU complications [55].

With this data in hand, a phase II hypofractionation study was initiated. One hundred and seventy-two patients with stage T1–T3 disease were treated to 66 GyE in 20 fractions over 5 weeks at a rate of 3.3 GyE/fraction. Patients were stratified into one of three risk groups based upon initial stage, PSA, and Gleason score. Low-risk patients (T1–T2A and Gleason score <7 and PSA <20) were treated with CIRT

Table 16.7 Characteristics of prostate cancer patients treated with carbon ions at NIRS, Chiba, Japan. Data from [55]

	Low risk ($n = 33$)	High risk ($n = 139$)	All ($n = 172$)
Age (years)			
Median (range)	71 (60 − 80)	70 (53 − 83)	70 (53 − 83)
≤70	16 (48%)	74 (53%)	90 (52%)
≥71	17 (52%)	65 (47%)	82 (48%)
T stage			
T1	22 (67%)	34 (25%)	56 (33%)
T2a	11 (33%)	13 (9%)	24 (14%)
T2b	0 (0%)	29 (21%)	29 (17%)
T3	0 (0%)	63 (45%)	63 (36%)
Gleason score			
4–5	14 (42%)	5 (4%)	19 (11%)
6	19 (58%)	16 (11%)	35 (20%)
7	0 (0%)	77 (56%)	77 (45%)
8–9	0 (0%)	41 (29%)	41 (24%)
Prostate-specific antigen (ng/ml)			
≤19.9	33 (100%)	65 (47%)	98 (57%)
20.0–49.9	0 (0%)	46 (33%)	46 (27%)
≥50.0	0 (0%)	28 (20%)	28 (16%)

alone, whereas intermediate and high-risk patients were treated with neoadjuvant ADT (high-risk patients only) for 2–6 months followed by adjuvant ADT for both intermediate- and high-risk individuals. Adjuvant ADT was administered for a minimum of 12 months post-RT.

Prior to a treatment planning CT scan, all patients were immobilized in the supine position in a custom cradle. The bladder was filled with 100 ml of sterilized water before the CT scan and before each treatment, and patients were asked to empty their rectum. Two PTVs were created. The initial PTV included the prostate and seminal vesicles expanded 10 mm in the anterior and lateral directions and 5 mm posteriorly. This volume received 33 GyE. At this point, the PTV was reduced so that the posterior edge rested on the anterior rectal wall with all other margins being unchanged. A typical treatment plan employed five fields with one field being treated daily. Patient characteristics are shown in Table 16.7.

CIRT was extremely well tolerated with no acute or late grade ≥3 GI toxicities being observed. Late grade 1 rectal bleeding occurred in 13% of patients, whereas only 2% experienced a late grade 2 GI toxicity. The majority of grade 1–2 rectal bleeding events occurred within the first 2 years after CIRT, a time course similar to that seen in patients treated with protons or IMRT (Fig. 16.8). Univariate analysis of rectal DVH data showed that only the V50 predicted for a higher risk of grade 1–2 bleeding, whereas treatment with anticoagulant therapy was also statistically

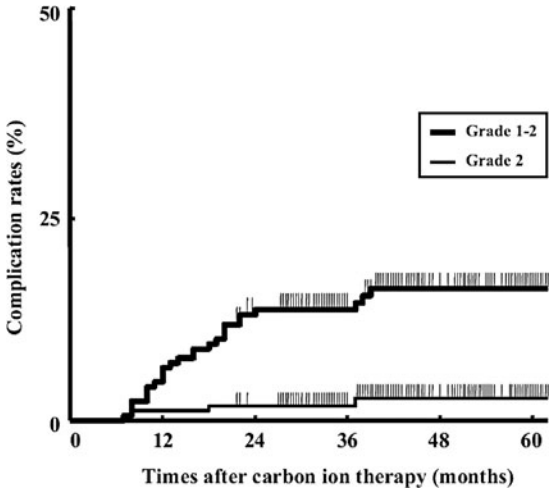

Fig. 16.8 Cumulative incidence curves of late grade 1–2 and grade 2 GI complications after carbon ion therapy

significant. With a median follow-up of 46 months local failure had developed in only one patient, whereas 18 (10.5%) experienced a biochemical failure.

The most recent report from these investigators involves 740 patients who were treated on one of three hypofractionated regimens; 66 GyE/20 fractions, 63 GyE/20 fractions, or 57.6 GyE/16 fractions. No grade $\geq$3 GI/GU toxicities were observed, whereas the incidence of grade 2 GI/GU toxicity among 664 patients followed for a minimum of 12 months were 1.9 and 4.8%, respectively. The lowest rate of GU toxicity was seen in patients treated on the 57.6 GyE arm. The overall biochemical relapse-free survival rate at 5 years was 90.2% with no difference seen between patients receiving 57.6 GyE vs. the other dose schedules. The authors concluded that treatment to 57.6 GyE/16 fractions offered comparable bNED survival to the other tested regimens with lower GU toxicity and that further advances in hypofractionated therapy are possible.

16.2 Conclusion

Now that we have reviewed the available data on IBT at length, it is time to return to the question asked in the introduction: Is prostate cancer a good candidate for IBT? I believe that the evidence-based answer has to be "yes." The rationale supporting this conclusion is found in the data. Treatment-related morbidity is low, whereas biochemical freedom from relapse is equivalent to other RT techniques.

The PROG/ACR 9509 trial provides "Level 1" evidence strongly supporting the benefits of dose escalation in organ-confined prostate cancer. Furthermore, it

demonstrated that when conformal proton beams are employed to escalate the dose, this dose escalation can be achieved without increasing the risk of incurring moderate-severe treatment-related morbidity, something that has not always been the case with IMRT-derived dose escalation. Finally, these results are repeatable, as evidenced by the minimal morbidity reported in the several thousand prostate patients treated at multiple facilities worldwide.

Prostate cancer is an excellent site in which to test and perfect the implementation of new treatment techniques and dose-fractionation schedules. Ongoing technical advances in IBT will lead to further dose specificity within the target organ and a further reduction in normal tissue radiation dose. Development of these techniques, including IMPT and real-time IGPT, will require their testing in a large number of patients having similar disease characteristics and anatomic constraints. Prostate cancer represents an excellent "test bed" for these important developments. It is an extremely common disease and large numbers of potential patients exist. As opposed to some other common tumors (most notably lung cancer), it is typically diagnosed while confined to its organ of origin so that treated patients are likely to live for the many years post treatment required to perform a complete analysis of late effects. Organ motion is minimal, which aids in the development of beam scanning techniques that are inherently more sensitive to target motion than passively scattered arrangements. Perfecting the spot scanning technique in a system with minimal organ motion before moving on to highly mobile tumors makes a great deal more sense than the converse.

The fact that tumor response can be assessed biochemically as opposed to clinically or radiologically, means that the effects of alterations in treatment techniques on tumor can be assessed (and potentially adjusted or even abandoned) far more rapidly than when less exacting measures are available. Lastly, in contrast to other sites like the base of the skull, the prostate is adjacent to only two critical organs about which a good deal is already known concerning dose–volume effects and their impact on acute and late morbidity, thereby providing for a more accurate extrapolation of the effects of any potential treatment alterations than would be true of other, less frequently treated sites.

One of the often-voiced complaints about IBT is the cost of providing this therapy. This concern is commonly raised whenever any new treatment technology or, for that matter, any new technology, is introduced into society. In the health care arena, new technology is increasingly being met with the demand that the new method be subjected to randomized trials vs. existing treatment methods before the new method is accepted by the medical community and health care payers. Although at first examination, this argument seems to have a certain intellectual appeal, it is believed that in the case of IBT such trials are not necessary and may even turn out to be unethical.

The call for randomized data is not new, nor is it confined to the introduction of IBT. Dr. Herman Suit reminds us that similar arguments were made in the early 1960s questioning the introduction of cobalt-60 teletherapy units into radiation oncology, arguments which at this juncture seem to verge upon the ridiculous (would

any of us care to willingly return to the days of orthovoltage treatment?), but at the time were quite popular [56].

In his 2001 Gray Lecture, Dr. Suit goes on to state the following "Four Truisms" of radiation oncology [57]:

- *No* advantage to *any* patient of *any* irradiation of *any* normal tissue exists.
- Direct radiation complications *never* occur in unirradiated tissues.
- That a smaller treatment volume is superior is *not* a medical research question.
- One may only investigate the magnitude of the gain or the cost of achieving that gain.

It must also be noted that virtually all other advancements in RT technology, including the widespread embracement of IMRT, have not occurred only after this technology was first tested in prospective trials but solely because the new technology did a better job of complying to these truisms than its predecessors. When considered from this perspective, IBT is best viewed as a further large step along the same road of technological advancement that has been followed diligently by radiation oncologists for the last century. Considering the relative biological equivalence of protons and X-rays, and that at this juncture roughly the same total radiation dose can be given to the prostate with either technology, it would be difficult if not impossible to compel patients to participate in a trial in which the only difference is not the expected outcome in terms of disease control but the volume of normal tissue which will be irradiated. Mirroring the cost of any new technology (computers being a prime example), it is also very likely that the cost of PT will decline as demand for this technology fosters the continuing development of newer, less expensive treatment units. Again, to echo Dr. Suit, once the cost of PT approximates that of IMRT, arguments over relative efficacy will in all likelihood come to an abrupt end. In order for IBT to achieve this goal, it has to be used for treatment of common cancers like prostate cancer. Again, this pathway is not new, and it simply mirrors the path already trod by other technologies including IMRT.

One area of ion-beam-based prostate cancer treatment where a randomized trial would make sense could be a comparison of modern PT and CIRT. The emergence of dual proton-carbon ion beam centers will allow to test in a clinical setting whether there is a clinical advantage to the use of high-RBE radiation. Unlike the proton-IMRT situation, the possession of a Bragg peak by both particles means that there is not a substantial difference in normal tissue radiation exposure between the two modalities and, thus, the ethical concerns over irradiating large volumes of normal tissue do no longer apply.

The prostate represents perhaps the ideal proving ground for IBT. Rather than discouraging its use on prostate cancer, the author believes that it should be encouraged. The techniques perfected and lessons learned will serve to benefit all patients, including those treated with other RT modalities, and will add invaluable data to the widespread clinical implementation of IBT.

References

1. American Cancer Society, Surveillance and Health Policy Research, Cancer Facts and Figures 2010, http://www.cancer.org/Research/CancerFactsFigures/CancerFactsFigures/cancer-facts-and-figures-2010
2. P. Bergstrom, P.O. Lofroth, A. Widmark, High-precision conformal radiotherapy (HPCRT) of prostate cancer-a new technique for exact positioning of the prostate at the time of treatment. Int. J. Radiat. Oncol. Biol. Phys. **42**, 305–311 (1998)
3. P. Bey, C. Carrie, V. Beckendorf, et al., Dose escalation with 3D-CRT in prostate cancer: French study of dose escalation with conformal 3D radiotherapy in prostate cancer-preliminary results. Int. J. Radiat. Oncol. Biol. Phys. **48**, 513–517 (2000)
4. M. Bolla, What is the role of radiation dose escalation in the treatment of localized prostate cancer? Nat. Clin. Pract. Urol. **5**, 418–419 (2008)
5. R. Cheung, S.L. Tucker, L. Dong, et al., Dose-response for biochemical control among high-risk prostate cancer patients after external beam radiotherapy. Int. J. Radiat. Oncol. Biol. Phys. **56**, 1234–1240 (2003)
6. G. Goldner, J. Dimopoulos, C. Kirisits, et al., Moderate dose escalation in three-dimensional conformal localized prostate cancer radiotherapy: single-institutional experience in 398 patients comparing 66 Gy versus 70 Gy versus 74 Gy. Strahlenther. Onkol. **185**, 438–445 (2009)
7. M.J. Zelefsky, Y. Yamada, Z. Fuks, et al., Long-term results of conformal radiotherapy for prostate cancer: impact of dose escalation on biochemical tumor control and distant metastases-free survival outcomes. Int. J. Radiat. Oncol. Biol. Phys. **71**, 1028–1033 (2008)
8. J.O. Archambeau, G.W. Bennett, S.T. Chen, Potential of proton beams for total nodal irradiation. Acta Radiol. Ther. Phys. Biol. **13**, 393–401 (1974)
9. B. Arjomandy, N. Sahoo, J. Cox, et al., Comparison of surface doses from spot scanning and passively scattered proton therapy beams. Phys. Med. Biol. **54**, N295–N302 (2009)
10. J.S. Loeffler, A.R. Smith, H.D. Suit, The potential role of proton beams in radiation oncology. Semin. Oncol. **24**, 686–695 (1997)
11. H.D. Suit, M. Urie, Proton beams in radiation therapy. J. Natl. Cancer Inst. **84**, 155–164 (1992)
12. U. Amaldi, Conformal radiation therapy with hadron beams and the programs of the TERA Foundation. Rays **23**, 486–507 (1998)
13. A. Konski, W. Speier, A. Hanlon, et al., Is proton beam therapy cost effective in the treatment of adenocarcinoma of the prostate? J. Clin. Oncol. **25**, 3603–3608 (2007)
14. M.L. Steinberg, A. Konski, Proton beam therapy and the convoluted pathway to incorporating emerging technology into routine medical care in the United States. Cancer J. **15**, 333–338 (2009)
15. W.U. Shipley, J.E. Tepper, G.R. Prout, et al., Proton radiation as boost therapy for localized prostatic carcinoma. J. Am. Med. Assoc. **241**, 1912–1915 (1979)
16. W.U. Shipley, L.J. Verhey, J.E. Munzenrider, et al., Advanced prostate cancer: the results of a randomized comparative trial of high dose irradiation boosting with conformal protons compared with conventional dose irradiation using photons alone. Int. J. Radiat. Oncol. Biol. Phys. **32**, 3–12 (1995)
17. G.E. Hanks, A question-filled future for dose escalation in prostate cancer. Int. J. Radiat. Oncol. Biol. Phys. **32**, 267–269 (1995)
18. T. Wiegel, W. Hinkelbein, Lokal fortgeschrittenes Prostatakarzinom (T2b-T4 N0) ohne und lokoregionär fortgeschrittenes Prostatakarzinom (Tx N+) mit Lymphknotenmetastasen. Ist eine Strahlentherapie der pelvinen Lymphabflußwege indiziert oder nicht indiziert? Strahlenther. Onkol. **174**, 231–236 (1998)
19. M. Roach 3rd, Neoadjuvant total androgen suppression and radiotherapy in the management of locally advanced prostate cancer. Semin. Urol. Oncol. **14**, S32–S37, discussion S38, (1996)
20. M. Roach 3rd, Neoadjuvant therapy prior to radiotherapy for clinically localized prostate cancer. Eur. Urol. **32**, S48–S54 (1997)

21. M. Roach 3rd, Current status of androgen suppression and radiotherapy for patients with prostate cancer. J. Steroid Biochem. Mol. Biol. **69**, 239–245 (1999)
22. M. Roach 3rd, Neoadjuvant hormonal therapy in men being treated with radiotherapy for localized prostate cancer. Rev. Urol. **6**, S24–S31 (2004)
23. C.J. Rossi, J.D. Slater, N. Reyes-Molyneux, et al., Particle beam radiation therapy in prostate cancer: is there an advantage? Semin. Radiat. Oncol. **8**, 115–123 (1998)
24. J.M. Slater, The proton treatment center at Loma Linda University Medical Center: rationale for and description of its development. Int. J. Radiat. Oncol. Biol. Phys. **22**, 383–389 (1992)
25. J.D. Slater, L.T. Yonemoto, C.J. Rossi, et al., Conformal proton therapy for prostate carcinoma. Int. J. Radiat. Oncol. Biol. Phys. **42**, 299–304 (1998)
26. J.D. Slater, C.J. Rossi, L.T. Yonemoto, et al., Proton therapy for prostate cancer: the initial Loma Linda University experience. Int. J. Radiat. Oncol. Biol. Phys. **59**, 348–352 (2004)
27. A.L. Zietman, M.L. DeSilvo, J.D. Slater, et al., Comparison of conventional-dose vs high-dose conformal radiation therapy in clinically localized adenocarcinoma of the prostate: a randomized controlled trial. J. Am. Med. Assoc. **294**, 1233–1239 (2005)
28. M.C. Abramowitz, T. Li, M.K. Buyyounouski, et al., The Phoenix definition of biochemical failure predicts for overall survival in patients with prostate cancer. Cancer **112**, 55–60 (2008)
29. A.L. Zietman, K. Bae, J.D. Slater, et al., Randomized trial comparing conventional-dose with high-dose conformal radiation therapy in early-stage adenocarcinoma of the prostate: long-term results from proton radiation oncology group/American College of Radiology 95–09. J. Clin. Oncol. **28**, 1106–1111 (2010)
30. J.A. Talcott, C.J. Rossi, W.U. Shipley, et al., Patient-reported long-term outcomes after conventional and high-dose combined proton and photon radiation for early prostate cancer. J. Am. Med. Assoc. **303**, 1046–1053 (2010)
31. N.P. Mendenhall, Z. Lin, C.G. Morris, et al., Early GI and GU toxicity in three prospective trials of proton therapy for prostate cancer. Int. J. Radiat. Oncol. Biol. Phys. **75**, S11–S12 (2009)
32. I. Hara, M. Murakami, K. Kagawa, et al., Experience with conformal proton therapy for early prostate cancer. Am. J. Clin. Oncol. **27**, 323–327 (2004)
33. H. Mayahara, M. Murakami, K. Kagawa, et al., Acute morbidity of proton therapy for prostate cancer: the Hyogo Ion Beam Medical Center experience. Int. J. Radiat. Oncol. Biol. Phys. **69**, 434–443 (2007)
34. J.F. Fowler, The radiobiology of prostate cancer including new aspects of fractionated radiotherapy. Acta Oncol. **44**, 265–276 (2005)
35. I.J. Constable, Proton irradiation therapy for ocular melanoma. Trans. Ophthalmol. Soc. UK **97**, 430 (1977)
36. E.S. Gragoudas, M. Goitein, L. Verhey, et al., Proton beam irradiation of uveal melanomas. Results of 5 1/2-year study. Arch. Ophthalmol. **100**, 928–934 (1982)
37. J.E. Munzenrider, M. Austin-Seymour, P.J. Bitzer, et al., Proton therapy at Harvard. Strahlentherapie **161**, 756–763 (1985)
38. R.P. Levy, J.I. Fabrikant, K.A. Frankel, et al., Charged-particle radiosurgery of the brain. Neurosurg. Clin. N. Am. **1**, 955–990 (1990)
39. G.K. Steinberg, J.I. Fabrikant, M.P. Marks, et al., Stereotactic heavy-charged-particle Bragg-peak radiation for intracranial arteriovenous malformations. N. Engl. J. Med. **323**, 96–101 (1990)
40. D.A. Bush, J.D. Slater, R. Bonnet, et al., Proton-beam radiotherapy for early-stage lung cancer. Chest **116**, 1313–1319 (1999)
41. D.A. Bush, J.D. Slater, C. Gerberoglio, et al., A technique of partial breast irradiation utilizing proton beam radiotherapy: comparison with conformal x-ray therapy. Cancer J. **13**, 114–118 (2007)
42. D.J. Brenner, Hypofractionation for prostate cancer radiotherapy – what are the issues? Int. J. Radiat. Oncol. Biol. Phys. **57**, 912–914 (2003)

43. P.A. Kupelian, V.V. Thakkar, D. Khunita, et al., Hypofractionated intensity-modulated radiotherapy (70 Gy at 2.5 Gy per fraction) for localized prostate cancer: long-term outcomes. Int. J. Radiat. Oncol. Biol. Phys. **63**, 1463–1468 (2005)
44. P.A. Kupelian, T.R. Willoughby, C.A. Reddy, et al., Hypofractionated intensity-modulated radiotherapy (70 Gy at 2.5 Gy per fraction) for localized prostate cancer: Cleveland Clinic experience. Int. J. Radiat. Oncol. Biol. Phys. **68**, 1424–1430 (2007)
45. V. Macias, A. Biete, Hypofractionated radiotherapy for localised prostate cancer – Review of clinical trials. Clin. Transl. Oncol. **11**, 437–445 (2009)
46. G. Soete, S. Arcangeli, G. De Meerleer, et al., Phase II study of a four-week hypofractionated external beam radiotherapy regimen for prostate cancer: report on acute toxicity. Radiother. Oncol. **80**, 78–81 (2006)
47. J.F. Fowler, A.E. Nahum, C.G. Orton, Point/Counterpoint. The best radiotherapy for the treatment of prostate cancer involves hypofractionation. Med. Phys. **33**, 3081–3084 (2006)
48. D.A. Kuban, S.L. Tucker, L. Dong, et al., Long-term results of the M. D. Anderson randomized dose-escalation trial for prostate cancer. Int. J. Radiat. Oncol. Biol. Phys. **70**, 67–74 (2008)
49. G.T. Chen, J.R. Castro, J.M. Quivey, Heavy charged particle radiotherapy. Annu. Rev. Biophys. Bioeng. **10**, 499–529 (1981)
50. J. Debus, O. Jäckel, G. Kraft, et al., Is there a role for heavy ion beam therapy? Recent Results Cancer Res. **150**, 170–182 (1998)
51. H. Engels, A. Wambersie, Relative biological effectiveness of neutrons for cancer induction and other late effects: a review of radiobiological data. Recent Results Cancer Res. **150**, 54–87 (1998)
52. E. Fokas, G. Kraft, H. An, et al., Ion beam radiobiology and cancer: time to update ourselves. Biochim. Biophys. Acta **1796**, 216–229 (2009)
53. E.J. Hall, The particles compared. Int. J. Radiat. Oncol. Biol. Phys. **8**, 2137–2140 (1982)
54. C.A. Tobias, E.A. Blakely, E.L. Alpen, et al., Molecular and cellular radiobiology of heavy ions. Int. J. Radiat. Oncol. Biol. Phys. **8**, 2109–2120 (1982)
55. H. Ishikawa, H. Tsuji, H. Tsujii, Clinical experience of carbon ion radiotherapy for malignant tumors (Article in Japanese). Gan To Kagaku Ryoho **33**, 444–449 (2006)
56. H. Suit, H. Kooy, A. Trofimov, et al., Should positive phase III clinical trial data be required before proton beam therapy is more widely adopted? No. Radiother. Oncol. **86**, 148–153 (2008)
57. H. Suit, The Gray Lecture 2001: coming technical advances in radiation oncology. Int. J. Radiat. Oncol. Biol. Phys. **53**, 798–809 (2002)

Chapter 17
Rationale for Proton Therapy in Pediatric Malignancies

Shiao Y. Woo

Abstract Proton therapy (PT) is being applied with increasing frequency in the treatment of pediatric malignancies. The principal rationale, selected published clinical results, and remaining challenges will be presented.

17.1 Introduction

During the past four decades, the cure rates for pediatric malignancies have steadily increased [1]. The main reasons are believed to be:

1. Embryonal tumors in children being generally more chemo- and radiosensitive than epithelial tumors in adults
2. Early adoption of multidisciplinary approaches by pediatric cancer physicians
3. Strong participation of patients and pediatric cancer physicians in clinical trials that have answered important therapeutic questions

With improved cure rates came an increasing realization, in long-term follow-up studies, that there are significant late toxicities and decreased quality of life in survivors of childhood cancers [2, 3]. Presently, the overriding philosophy of treatment of pediatric malignancies is to maximize cure while minimizing toxicity.

S.Y. Woo (✉)
Department of Radiation Oncology, University of Louisville, James Graham Brown Cancer Center, 529 S. Jackson Street, Louisville, KY 40202, USA
e-mail: sywoo001@louisville.edu

U. Linz (ed.), *Ion Beam Therapy*, Biological and Medical Physics, Biomedical Engineering, DOI 10.1007/978-3-642-21414-1_17,

17.2 Pediatric Solid Tumors

There are generally two major components of pediatric malignant solid tumors:

1. Loco-regional tumor and
2. Microscopic or macroscopic systemic metastatic disease

Cure is accomplished only if one can eradicate both components. Loco-regional tumor is usually controlled by surgery, radiation therapy (RT), or a combination of both. Chemotherapy, when added, can often further improve the local control rate. It is mandatory in the case of systemic metastases. The importance of the local control of the primary tumor has been particularly understood in primary brain tumors, rhabdomyosarcoma, other soft tissue sarcomas, osteosarcoma, and Ewing's sarcoma [4]. However, both surgery and RT have potential long-term adverse side effects.

17.3 Late Toxicities of RT

The principal late side effects of RT can be categorized into

1. Growth inhibition of bone and soft tissue
2. Organ dysfunction such as hypopituitarism, neurocognitive impairment, ototoxicity, or sterility
3. Second malignant neoplasm

In order to achieve the goal of modern RT, namely, to maintain or improve local control, and to decrease late effects, one needs to expose as little normal tissue as possible to radiation and to use the minimal effective tumoricidal radiation dose for the tumor.

17.4 Methods to Potentially Reduce Late Effects of RT

For photon therapy, the most commonly available modality of RT, a variety of techniques exist to plan and deliver conformal therapy such as fractionated stereotactic RT and intensity-modulated radiation therapy (IMRT). It has been shown that these modalities can conform the high doses of radiation to the size and the shape of the tumor while limiting radiation doses to the adjacent organs at risk. However, because photon beams go through a child's body, a by-product of all these methods is a higher integral dose or a radiation dose "bath," i.e., a relatively large volume of normal tissue outside the tumor zone receiving small doses of radiation. As being argued by some investigators, this higher integral dose could potentially increase the risk of second malignancies [5].

An alternative approach is to use a radiation modality that has physical properties different from photons. PT is such an alternative.

17.5 Rationale for PT in the Treatment of Pediatric Malignancies

A primary rationale is to reduce treatment-related morbidity. An example is the use of protons for cranio-spinal irradiation. Absence of a significant exit dose anterior to the spine with PT as opposed to photon therapy would predict a lower risk for dysfunction of organs such as thyroid gland, heart, and lungs (Fig. 17.1) [6]. A modeling study predicted a lower rate of second malignancies as compared to conventional photon therapy or IMRT [7]. In another study, photon versus proton treatment plans were compared in 40 patients, 10 each with optic pathway glioma, craniopharyngioma, infratentorial ependymoma and medulloblastoma. The supratentorial brain or temporal lobes were found to receive less of the low to intermediate doses with PT than with photon therapy.

When longitudinal models of radiation dose-cognitive effects were applied, it was estimated that PT would result in clinically significantly higher IQ scores than photon therapy in patients with optic pathway glioma, craniopharyngioma, and medulloblastoma [8]. In addition, dosimetric comparisons between protons and photons in the treatment of posterior fossa tumors and orbital rhabdomyosarcoma have all demonstrated lower radiation doses to several organs at risk (e.g., cochlea) and a potential to lower side effects [9, 10].

Proton planning studies for retinoblastoma have shown less volume of orbital bone irradiated than by photon plans [6, 11]. The anterolateral proton beam arrangement with nasally rotated eye could, theoretically, irradiate the least volume of bone and only one growth center. The proton plans would deliver no appreciable dose to the contralateral eye, brain tissue, or pituitary gland. Thus, proton radiotherapy as compared to photon radiotherapy might result in less growth disturbance to the irradiated orbit, possibly less risk of radiation-induced bone tumor, and practically no risk of pituitary dysfunction.

A treatment planning study in patients with neuroblastomas or Wilms' tumors compared two photon techniques [opposing fields and intensity modulated radiotherapy (IMXT)] with two proton beam techniques (passive scattering and scanned beam radiotherapy). In comparison to the opposed photon fields, the proton techniques could reduce the mean dose to liver and kidneys by 40–60% [12]. The volumes of kidneys and liver irradiated at the level of tolerance dose were reduced by 65% and 75%, respectively, for patients with neuroblastoma, and by 10% for patients with Wilms' tumor. The dosimetric improvement was less impressive when compared with IMXT but the volume of normal tissues receiving low doses of radiation was larger with IMXT.

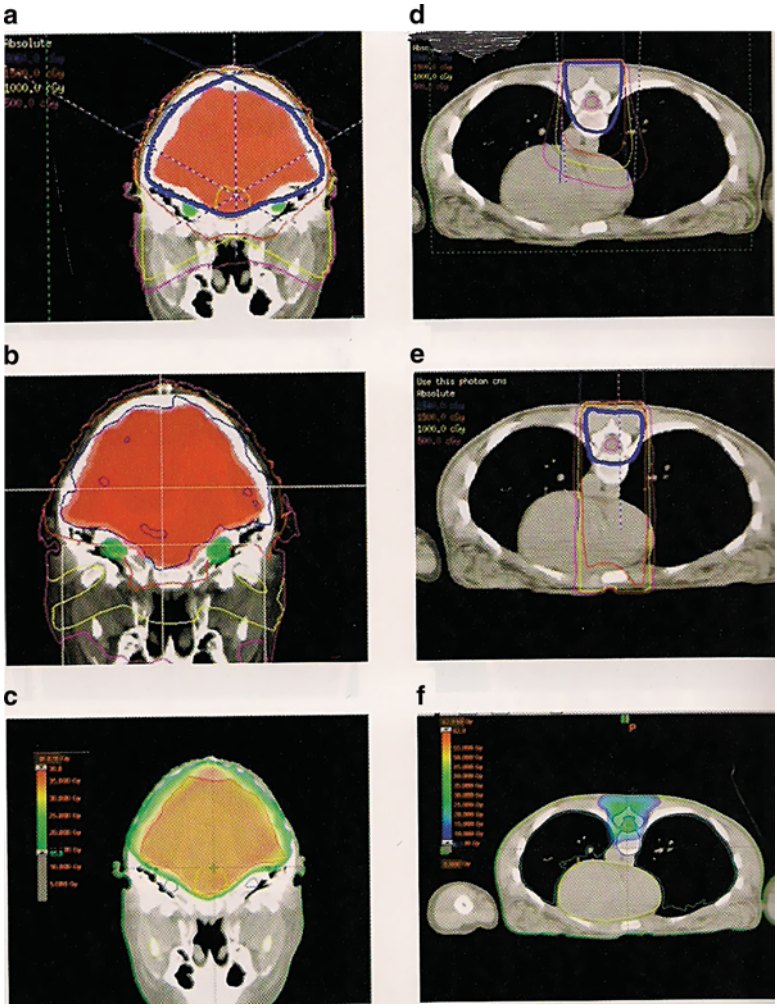

Fig. 17.1 Medulloblastoma plans. *Left*: Posterior fossa, axial slices: (**a**) three-dimensional conformal radiation therapy (3D-CRT); (**b**) IMXT; (**c**) protons. *Right*: Spinal irradiation, axial slices: (**d**) 3D-CRT electrons; (**e**) 3D-CRT photons; (**f**) protons. Reprinted with modification from [6], with permission from Elsevier

For pelvic tumors such as Ewing's sarcoma where chemotherapy and RT are frequently used concurrently, PT could reduce the volume of bone marrow being irradiated, thus not jeopardizing the intensity of the chemotherapy. This may potentially improve both local control and the overall cure rate. Finally, the potential decrease in late morbidity of treatment may improve the quality of life in long-term survivors of childhood cancers.

Carbon ions have a dosimetric advantage over protons because of lesser side scatter. The relative biological effectiveness (RBE), especially at the end of the range is higher with carbon ions (cf. Chap. 4). There is, thus, a theoretical advantage of carbon ion therapy for hypoxic tumors. A major concern about its use in children is the potentially increased toxicity to organs close to the tail of high LET particles at the end of the range of the carbon ions. However, careful investigations of the use of carbon ion therapy in selected tumors in children are ongoing and worthwhile.

17.6 Clinical Results

The use of conformal PT has been reported in 27 children with progressive or recurrent low-grade astrocytomas [13]. The radiation doses were from 50.4 to 63 GyE. After a mean follow-up period of 3.3 years, the local control and survival rates were 87% and 93% for central tumors, 71% and 86% for hemispheric tumors, and 60% each for brainstem tumors, respectively. All children whose tumors were controlled maintained their performance status. All children with optic pathway tumors experienced stable or improved vision. Moyamoya syndrome (stenosis of small cerebral arteries) was diagnosed in one child with Type 1 neurofibromatosis.

PT for children with craniopharyngioma has resulted in 5- and 10-year local control rates of 93% and 85%, respectively [14, 15]. About 20% of the children were found to have learning difficulties and some developed new-onset panhypopituitarism.

A reported series of 17 children with ependymoma treated with PT showed a local control rate and overall survival of 86% and 89%, respectively, at a median follow-up of 26 months [16].

A recent study comparing the hearing outcome of 19 children with medulloblastoma treated with PT against that of a historical cohort of 15 children treated with IMXT showed that high-grade (grade 3 or 4) ototoxicity rates at 1 year were significantly lower following PT versus IMXT (5 vs. 18%, $p < 0.01$) [17].

Both passively scattered and spot-scanning PT have been used to treat chordoma and chondrosarcoma in pediatric patients. A report from the Massachusetts General Hospital, Boston (USA), included children who were treated either with fractionated passively scattered PT or fractionated combined proton and photon irradiation [18]. The local control rates were 60% and 100%, respectively. Late neurological side effects occurred in 7% of the patients.

A report from the Centre de Protonthérapie, Orsay (France), also using fractionated, mostly combined passively scattered proton and photon irradiation, showed a 5-year progression-free survival of 100% and 77% for chondrosarcomas and chordomas, respectively [19].

At the Paul-Scherrer Institute, spot-scanning PT and intensity-modulated PT were used to treat six children with chordomas and four with chondrosarcomas [20]. Median total dose was 75 GyE for chordoma and 66 GyE for chondrosarcoma. At a median follow-up time of 36 months, all patients remained failure-free. One

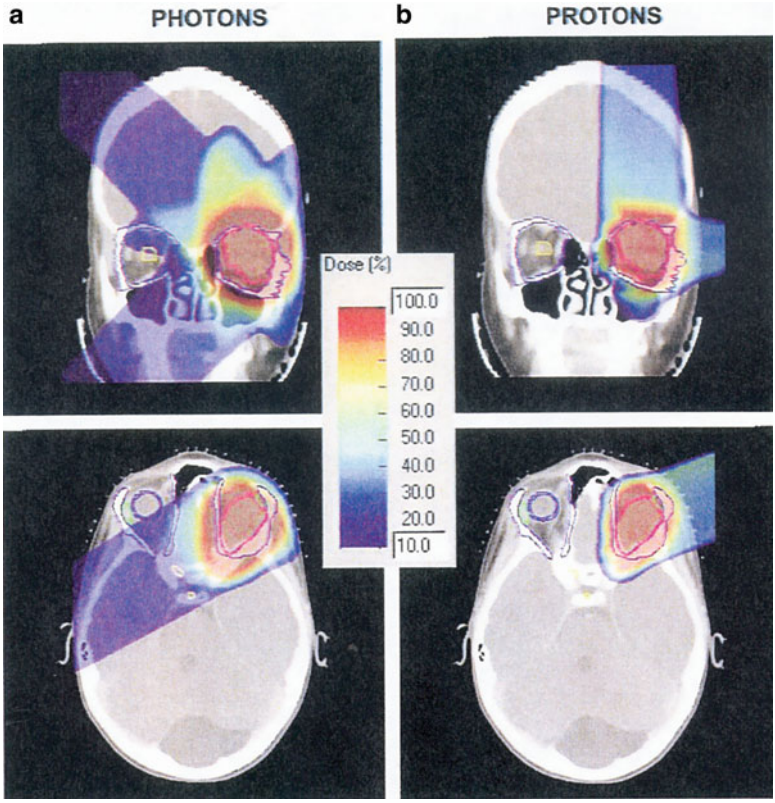

Fig. 17.2 Orbital rhabdomyosarcoma plans: (**a**) coronal and axial photon plan; (**b**) coronal and axial proton plan. Reprinted from [10], with permission from Elsevier

patient developed neurosensory deficit, another developed permanent alopecia and hypoacusis, and a third patient had pituitary insufficiency.

A small series of pediatric patients with orbital rhabdomyosarcoma treated with scattered PT has been reported [10]. At a median follow-up of 6.3 years, six out of seven patients achieved local control. A dosimetric comparison against 3D conformal photon plans showed that protons produced lower doses to the brain, pituitary, hypothalamus, temporal lobes, and contralateral orbital structures (Fig. 17.2). Another small series of children with rhabdomyosarcomas or other soft tissue sarcomas treated with spot-scanning PT showed that after a median follow-up of 18.6 months, 83.3% of the children with rhabdomyosarcomas achieved local control as compared to 50% of those with other subtypes of soft tissue sarcomas [21]. Table 17.1 summarizes all the above results.

Recently, a report from Germany using carbon ion therapy in 17 young patients with chordomas or chondrosarcomas has been published [22]. The dose was 60 GyE (median) in a fractionation scheme of 7 × 3 GyE per week. One patient with

Table 17.1 PT for pediatric malignancies. Summary of clinical results.

Tumor type	Follow-up (months)	Local control (%)	Survival (%)	Ref
Low-grade astrocytoma	39	87 (central)	93	[13]
		71 (hemispheric)	86	
		60 (brainstem)	60	
Craniopharyngioma		93 (5-year)	80 (5-year)	[14]
	157	85 (10-year)	72 (10-year)	[15]
Ependymoma	26	86	89	[16]
Chordoma/chondrosarcoma		60/100		[18]
		77/100		[19]
	36	100/100		[20]
Rhabdomyosarcoma	75	86		[10]
	19	83		[21]

chordoma developed a recurrence at 60 months after therapy. The rest of the patients remained free of tumor progression or severe side effects at a median follow-up time of 49 months.

In summary, the published reports of PT in pediatric patients consist of small series of patients from single institutions most of which had relatively short durations of follow-up. The tumor control rates did not appear to be inferior to the known tumor control rates with photon therapy. Nonetheless, studies on larger cohorts of patients – perhaps with case–control comparisons – especially, on late toxicities and quality of life or more ideally, randomized trials on selected tumor sites will be needed to ultimately prove the value of PT in children.

17.7 Challenges of PT

There are still many challenges of PT, including uncertainties in the in vivo stopping power of protons, in the RBE in different normal tissues and tumors, the production of secondary neutrons both from the PT equipment and in the patient's body, the generally cumbersome referral process to most proton centers, the availability of PT, the lack of mature clinical outcome data especially in children, and the high cost of PT.

Currently, there are only a handful of proton centers that routinely treat infants and children. A proton center needs clinical information such as pathology, images, text results, and treatment records in order to determine if a child is suitable for PT. In addition, authorization for payment, by the insurance company, government or the child's family is usually required before a patient is accepted. This process can be arduous and protracted, and may delay the start time of radiotherapy as specified in some treatment protocols. Whether the delays affect outcome is presently unclear but they are of concern. In addition, most patients have to travel with their parents to cities outside their home towns or even outside their countries for PT. This

might cause a financial burden on the family, interruption of the parents' jobs and disruption of family life. Such social, financial, and emotional impacts have not been fully studied but need to be.

The proton treatment of children especially those who need sedation or anesthesia for the daily treatment is time-consuming and labor-intensive. The safety of repeated prolonged deep sedation over several weeks in even very young children has been demonstrated [23]. However, the sedation process adds time and requires manpower. The in-room time for treating a child could be two to five times more than that for an adult receiving PT for prostate cancer. Administrators at proton centers who have to balance the high capital and operating cost against revenue understandably prefer treating more adult than pediatric patients with complicated needs (cf. also Chap. 3). Whether these considerations affect access of children to proton centers is currently unclear.

There are several factors that affect the stopping power of protons in vivo giving rise to uncertainties regarding the exact location where the proton beam stops in the patient. The existing planning systems use an arbitrary formula to add proximal and distal margins in the direction of a proton beam in order to be sure of coverage of the tumor. These margins decrease the conformity of radiation dose to the target and increase the dose to adjacent normal tissues. Thus, in order to further minimize treatment-related morbidity one needs to reduce these uncertainties and margins. Work in this area is in progress (cf. Chap. 24).

The RBE of 1.1 for protons at the middle of the spread-out Bragg peak, adopted by most proton centers, is not necessarily true in every normal tissue and every tumor. The presence of a small tail of high-LET particles increases the RBE of a proton beam toward the end of its range. Although there have been attempts to incorporate different RBEs at different parts of a proton beam and in different tissues into the planning model, there is not yet a universally accepted system that is clinically useful.

The production of neutrons is higher in passively scattered proton systems than in systems with a scanned proton beam. However, there are potential methods to reduce the exposure to neutrons in passively scattered proton beam lines, e.g., by minimizing the amount of material, modifying the material of the apertures [24], and using external shields for the patient. The quantity of neutrons is generally small (cf. Chap. 21). A modeling study incorporating neutrons has shown that for cranio-spinal irradiation, passively scattered PT still would lead to a smaller second malignancy rate than conventional photon therapy or IMXT [25]. An early report from the Massachusetts General Hospital on a cohort of 1,450 mostly adult patients treated between 1974 and 2001 showed the second malignancy rate to be 6.4% versus 12% in a matched patient cohort from an SEER database [26]. None of the 15 pediatric patients treated by PT in this cohort developed second malignancies.

Despite the high cost of PT, a cost–benefit study from Sweden found it cost-effective for children diagnosed with medulloblastoma when the potential reduction of late effects and the cost associated with managing them were considered [27]. Hopefully, with an increased number of proton centers in the world treating children,

more clinical outcome results will be available and the benefit of PT in children can be convincingly demonstrated.

References

1. L.A. Ries, M.A. Smith, J.G. Burney, et al., *Cancer Incidence and Survival Among Children and Adolescents: United States SEER Program 1975–1995,* SEER Program (National Cancer Institute, Bethesda, MD, 1999)
2. M.M. Geenen, M.C. Cardous-Ubbink, L.C. Kremer, et al., Medical assessment of adverse health outcomes in long-term survivors of childhood cancer. J. Am. Med. Assoc. **297**, 2705–2715 (2007)
3. S.R. Bhat, T.L. Goodwin, T.M. Burwinkle, et al., Profile of daily life in children with brain tumors: an assessment of health-related quality of life. J. Clin. Oncol. **23**, 5493–5500 (2005)
4. S.S. Donaldson, J.R. Anderson, Rhabdomyosarcoma: many similarities, a few philosophical differences. J. Clin. Oncol. **23**, 2586–2587 (2005)
5. E.J. Hall, Intensity-modulated radiation therapy, protons, and the risk of second cancers. Int. J. Radiat. Oncol. Biol. Phys. **65**, 1–7 (2006)
6. C.T. Lee, S.D. Bilton, R.M. Famiglietti, et al., Treatment planning with protons for pediatric retinoblastoma, medulloblastoma, and pelvic sarcoma: how do protons compare with other conformal techniques? Int. J. Radiat. Oncol. Biol. Phys. **63**, 362–372 (2005)
7. R. Miralbell, A. Lomax, L. Cella, et al., Potential reduction of the incidence of radiation-induced second cancers by using proton beams in the treatment of pediatric tumors. Int. J. Radiat. Oncol. Biol. Phys. **54**, 824–829 (2002)
8. T.E. Merchant, C.H. Hua, H. Shukla, et al., Proton versus photon radiotherapy for common pediatric brain tumors: comparison of models of dose characteristics and their relationship to cognitive function. Pedatr. Blood Cancer **51**, 110–117 (2008)
9. W.H. St Clair, J.A. Adams, M. Bues, et al., Advantage of protons compared to conventional X-ray or IMRT in the treatment of a pediatric patient with medulloblastoma. Int. J. Radiat. Oncol. Biol. Phys. **58**, 727–734 (2004)
10. T. Yock, R. Schneider, A. Friedmann, et al., Proton radiotherapy for orbital rhabdomyosarcoma: clinical outcome and a dosimetric comparison with photons. Int. J. Radiat. Oncol. Biol. Phys. **63**, 1161–1168 (2005)
11. M. Krengli, E. Hug, J. Adams, et al., Proton radiation therapy for retinoblastoma: comparison of various intraocular tumor locations and beam arrangements. Int. J. Radiat. Oncol. Biol. Phys. **61**, 583–593 (2005)
12. M. Hillbrand, D. Georg, H. Gadner, et al., Abdominal cancer during early childhood: a dosimetric comparison of proton beams to standard and advanced photon radiotherapy. Radiother. Oncol. **89**, 141–149 (2008)
13. E.B. Hug, M.W. Muenter, J.O. Archambeau, et al., Conformal proton radiation therapy for pediatric low-grade astrocytomas. Strahlenther Onkol. **178**, 10–17 (2002)
14. Q.T. Luu, L.N. Loredo, J.O. Archambeau, et al., Fractionated proton radiation treatment for pediatric craniopharyngioma: preliminary report. Cancer J. **12**, 155–159 (2006)
15. M.M. Fitzek, R.M. Linggood, J. Adams, et al., Combined proton and photon irradiation for craniopharyngioma: long-term results of the early cohort of patients treated at Harvard Cyclotron Laboratory and Massachusetts General Hospital. Int. J. Radiat. Oncol. Biol. Phys. **64**, 1348–1354 (2006)
16. S.M. MacDonald, S. Safai, A. Trofimov, et al., proton radiotherapy for childhood ependymoma: initial clinical outcomes and dose comparisons. Int. J. Radiat. Oncol. Biol. Phys. **71**, 979–986 (2008)

17. B.J. Moeller, M. Chintagumpala, J.J. Philip, et al., Proton radiotherapy for pediatric medulloblastoma: improved early ototoxicity. Int. J. Radiat. Oncol. Biol. Phys. **78**, S18 (2010)
18. E.B. Hug, R.A. Sweeney, P.M. Nurre, et al., Proton radiotherapy in management of pediatric base of skull tumors. Int. J. Radiat. Oncol. Biol. Phys. **52**, 1017–1024 (2002)
19. J. Habrand, R. Schneider, C. Alapetite, et al., Proton therapy in pediatric skull base and cervical canal low-grade bone malignancies. Int. J. Radiat. Oncol. Biol. Phys. **71**, 672–675 (2008)
20. H.P. Rutz, D.C. Weber, G. Goitein, et al., Postoperative spot-scanning proton radiation therapy for chordoma and chondrosarcoma in children and adolescents: initial experience at Paul Scherrer Institute. Int. J. Radiat. Oncol. Biol. Phys. **71**, 220–225 (2008)
21. B. Timmermann, A. Schuck, F. Niggli, et al., Spot-scanning proton therapy for malignant soft tissue tumors in childhood: first experiences at the Paul Scherrer Institute. Int. J. Radiat. Oncol. Biol. Phys. **67**, 497–504 (2007)
22. S.E. Combs, A. Nikoghosyan, O. Jaekel, et al., Carbon ion radiotherapy for pediatric patients and young adults treated for tumors of the skull base. Cancer **115**, 1348–1355 (2009)
23. S. Buehrer, S. Immoos, M. Frei, et al., Evaluation of propofol for repeated prolonged deep sedation in children undergoing proton radiation therapy. Br. J. Anaesth. **99**, 556–560 (2007)
24. D.J. Brenner, C.D. Elliston, E.J. Hall, et al., Reduction of the secondary neutron dose in passively scattered proton radiotherapy, using an optimized pre-collimator/collimator. Phys. Med. Biol. **54**, 6065–6078 (2009)
25. W.D. Newhauser, J.D. Fontenot, A. Mahajan, et al., The risk of developing a second cancer after receiving craniospinal proton irradiation. Phys. Med. Biol. **54**, 2277–2291 (2009)
26. C.S. Chung, N. Keating, T. Yock, N. Tarbell, Comparative analysis of second malignancy risk in patients treated with proton therapy versus conventional photon therapy. Int. J. Radiat. Oncol. Biol. Phys. **72**, S8 (2008)
27. J. Lundkvist, M. Ekman, S.R. Ericsson, et al., Cost-effectiveness of proton radiation in the treatment of childhood medulloblastoma. Cancer **103**, 793–801 (2005)

Chapter 18
Tolerance of Normal Tissues to Ion Beam Therapy

Jean-Louis Habrand, Jean Datchary, Pascal Pommier, Stéphanie Bolle, Loïc Feuvret, Ismael Ghorbel, and Remi Dendale

Abstract This review from the radiation oncology literature provides tolerance doses of normal tissues, mainly late responding. It reports toxicity data for main organs based on the experience with photons, and similar data for various modes of ion beam therapy (protons, light ions, single or multifractionated). Although these data can help compare toxicity of both types of radiations, it should be remembered that clinical historical series are generally not strictly comparable.

18.1 Introduction

Any irradiation modality that selectively spares normal structures in radiotherapy (RT) warrants reduced early and late toxicity. Ion beams with their sharp lateral penumbra and no "exit" dose beyond the target may, therefore, represent a substantial advantage as compared to photon techniques. One can capitalize on these advantages for different purposes: to reduce long-term side effects in very sensitive organs such as those in children, to improve acute tolerance in combined chemo-radiation strategies, or to escalate doses in radioresistant tumor processes while keeping the dose to critical structures at an acceptable level.

In this chapter, the main complications and sequelae along with associated tolerance doses at different dose-fractionation schedules will be summarized for different organs. Dose constraints are, in theory, similar for charged particles and for photons, if dosimetry standards are observed [1], and if biological differences are taken into account. In order to appraise tolerance of normal organs to ion

J.-L. Habrand (✉)
Department Radiation Oncology, Institut Gustave Roussy, 114 rue Edouard Vaillant, 94805 Villejuif, France

ARCHADE - Centre François Baclesse, 3 av. Général Harris, BP 5026, 14076 Caen cedex 5, France
e-mail: habrand@igf.fr; jl.habrand@baclesse.fr

U. Linz (ed.), *Ion Beam Therapy*, Biological and Medical Physics, Biomedical Engineering, DOI 10.1007/978-3-642-21414-1_18,

Table 18.1 Severe radiation-induced toxicity. Data from the photon literature. See text for details

Organ [Reference] Year of Publication	Endpoints	x% Risk: Dose (Gy)	Dose constraints (Gy)	Predisposing factors
Brain [2] 2010	Necrosis	5%: 72 10%:90	60 partial vol	Fraction size, irradiated brain volume, younger age, NF1 mutation, ccmt ChT (MTX)
Spinal cord [3] 2010	Myelitis	≤5% : 54 ≤10% : 60	Max: 45–48	Ccmt intrathecal ChT, fraction size, ccmt ChT (CDDP)
Optic pathway [4] 2010	Blindness	1%: 50 10%: 65	55	Older age, pituitary disorders
Brain stem [5] 2010	Necrosis	1%: 54	59 < 10 cm^3	Hydrocephalus, fraction size, diabetes, hypertension
Cochlea [6] 2010	Deafness	5%: 45 50%: 70	Mean ≤45	Ccmt ChT (CDDP)
Lungs [7] 2010	Pneumopathy	50%: 31	5: 60% vol 20: 4–10% vol Mean < 8 Max < 80	Older age, fraction size, ccmt ChT (gemcitabine, docetaxel)
Liver [8] 2010	Liver failure	Whole gland: 5%: 30 10%: 33 Partial gland: 50%: 66 to >30% 36 to >66% vol	700 cm^3 <15 Mean < 28	Previous or present dysfunction, hepatitis B carrier, ChT (ACTD, ADM), chemoembolization, male gender, portal vein thrombosis
Rectum [9] 2010	Necrosis	6%: 70 50%: 77	50: 50% vol 75: 15% vol	Older age, diabetes, hemorrhoids, inflammatory bowel disease, ccmt hormones
Small bowel [10] 2010	Obstruction, perforation	Whole organ: 5%: 40 50%: 55 Partial organ: 5%: 50 to 30% vol	195 cm^3 <45	Ccmt ChT (CDDP, 5FU), fractionation, irradiated bowel volume, abdominal surgery

(continued)

Table 18.1 (continued)

Organ [Reference] Year of Publication	Endpoints	x% Risk: Dose (Gy)	Dose constraints (Gy)	Predisposing factors
Bladder [11] 2010	Dysuria, hematuria	25%: 62	65: 50% vol 80: 65% vol	Older age, ccmt hormones or ChT (CPM), anticoagulants, smoking, BMI, pelvic surgery
Skin [12] 1991	Necrosis	5%: 60 to 30 cm^2 70 to 10 cm^2	45–50	Ccmt ChT (ACTD, ADM)

Abbreviations: *ACTD* actinomycin D, *ADM* adriamycin, *BMI* body mass index, *CDDP cis*-platinum, *ChT* chemotherapy, *ccmt* concomitant, *CPM* cyclophosphamide, *MTX* methotrexate, *Vol* organ volume

beam therapy (IBT), data from conventional photon series are summarized first in Table 18.1 [2–12]. Most come from the QUANTEC Initiative, a common effort of the American Society for Radiation Oncology (ASTRO) and the American Association of Physicists in Medicine to publish data on normal tissue effects in response to RT. These data are valid in adult patients treated with conventional fractionations (CF) – 1.8 to 2 Gy per fraction, five times a week. Data from IBT programs will be presented according to types of ions and fractionations. Dose is expressed in GyE, which is defined as the physical dose times the estimated RBE value (cf. Chap. 4). Detailed intercomparisons between photons and ions are beyond the scope of this chapter but will be briefly presented.

18.2 Ocular Tumors

The treatment of ocular lesions by IBT is described in detail in Chap. 10. Here, we concentrate on potential side effects.

Acute toxicity includes loss of eye lashes, eyelid desquamation, epiphora, dry eye, and epithelial keratopathy (Table 18.2). Delayed toxicity includes retinopathy, maculopathy, papillopathy, rubeosis iridis, and neovascular glaucoma that can threaten vision or lead to enucleation [13–17].

18.2.1 Protons

Despite the overall selection of larger tumors treated with protons, major toxicity remains in the same range as that of conventional techniques (Table 18.3 and [18]). Posterior subcapsular cataract is the most common long-term side effect. It ranges from 28 to 35% and peaks at 3 years following PT. It seems to occur more frequently

Table 18.2 Toxicity of ion beam therapy (IBT) in ocular melanomas

First Author [Reference] Year of Publication	Tumor stage	Patient No/ FU (months)	Ion type Dose (GyE)/#Fx	Function/ Toxicity (%)
Castro [13] 1997	(54% PP) T1–T2 (37%), T3–T4 (63%)	347/no data	He 48–80/4–5	Useful vision: 36 Glaucoma: 35 Enucleation: 16 Other: 3.5
Courdi [14] 1999	(2/3PP) T1–T2 (38%), T3–T4 (64%)	538/33.8	P 57.2/4	Useful vision: 50.4 Glaucoma: 10.2 Enucleation: 3 Other: 4
Egger [15] 2001	1/2 PP S: 5.1%, M: 42.6%, L: 52.3%	2,645/44	P 60–70/4	Enucleation: 6 Other: 2
Munzenrider [16] 2001		2,815/≅60	P 70/5 (for 95% pt)	Useful vision: 39–67 Cataract: 42
Dendale [17] 2006		1,406/73	P 60/4	Useful vision: 46 Glaucoma: 28.6 Maculopathy: 66.5 Cataract: 62 Papillopathy: 23.5 Enucleation: 7

Tumor Stage: T: according to TNM or SML as follows: S, small: diameter D $\leq$ 10 mm, height H $\leq$ 3 mm; M, medium: D 10–16 mm, H 3–8 mm; L, large: D > 16 mm, H > 8 mm
Abbreviations: *#Fx* number of fractions, *FU* follow-up, *He* helium, *P* proton, *PP* posterior pole, *pt* patient(s)

Table 18.3 Toxicity after treatment of ocular malignancies with various types of treatment

Event	Gamma Knife	Linac	Brachytherapy	Proton therapy	Helium therapy
Retinopathy	23–70	26	22–63	NA	NA
Glaucoma	18–23	9–20	3–11	15–29	35
Enucleation	6–18	12.5	4–21	2–18	19

Numbers are events in percent (after [18])
NA not assessed

at iridal sites [19,20], whereas the risk of dry-eye syndrome is higher at conjunctival sites [21]. Neovascular glaucomas peak at 3 years and range from 15 to 29%. Some patient subgroups are at higher risks (e.g., tumor height >6 mm, >25% of the lens receiving >35 Gy). They make up the majority of enucleations (2–18% cases). Prevention is currently being tested by transpupillary thermotherapy as well as secondary resection of scarred tissue [22]. Toxicity does not appear to be

significantly influenced by different fractionation schedules, e.g., 70 GyE delivered in five fractions, 60 GyE delivered in four fractions, or even a reduction to 50 GyE in five fractions [23].

Vision is preserved or improved in approximately half the cases. Severe loss, seems to be correlated with maculopathy (40%), papillopathy (20%), and more rarely cataract (15%) [24]. A dose–effect relationship has been suggested for tolerance of the optic disc (range: 30–70 GyE), but not the macula (stable at 40 GyE). Diabetes mellitus doubles this risk.

18.2.2 Light Ions

Helium ions seem also attractive for treatment, since they offer a sharper penumbra compared with protons. However, they have never been used on a large scale [13, 25]. A randomized intercomparison with 125I implants (185 cases) showed a significantly reduced rate of enucleation (9 vs. 17%) [26].

18.3 Tumors of the Head and Neck

Table 18.4 summarizes the toxicity reported for skull base and head and neck malignancies treated with IBT [27–35].

18.3.1 Brain

Brain radionecrosis is usually observed within 2 years following RT. It can be purely radiologic or clinically symptomatic [2]. Myelopathy is one of the most dreadful complications that has led to strict dose constraints in conventional therapy ([3] and Table 18.1).

18.3.1.1 Fractionated Protons

Most experiences concerning CNS tolerance refer to skull base malignancies [27–31, 35] and gliomas [36–38]. They represent a paradigm of remarkable tolerance to escalated doses delivered to the target – 65 GyE and more – compared with conventional techniques [39, 40]. Five and 10-year complication-free survival rates are at the order of 90% for the experienced group at the Massachusetts General Hospital (MGH) at Boston [28]. For temporal lobe (a structure generally abutting the target), 8–13% 2- and 5-year risk of necrosis (mainly radiological), has been reported following doses of 66–72 GyE, with a probable adverse influence of male gender [41]. Brain stem tolerance is of the same magnitude and correlated with an organ volume receiving $\geq$60 GyE (V60) of at least 1 ml. Diabetes mellitus and the number of previous surgical procedures can also affect tolerance [42]. Dose

Table 18.4 Toxicity of IBT in skull base and head and neck malignancies

First Author [Reference] Year of Publication	Tumor Type Location	Patient No FU (months)	Radiation Type Dose Range (GyE) Total Dose (GyE)/ Dose per Fx (GyE)	Toxicity
Hug [27] 1999	CD+CS	33 CD + 25 CS Mean : 33	X + P (6pt), P (52pt) 65–79 Mean: 71/1.8–2	G2: 4 pt (7%) hypopituitarism G3: 8 pt (14%) late: 4 pt pituitary, 1 pt optic, 2 pt auditory, 1 pt seizure
Munzenrider [28] 1999	CD+CS skull base/cervical	375 CD+246 CS Median: 36 (spine)–41 (skull)	X + P 66–83 Median: 67/1.8–2	Temporal lobe: 13 pt (5Y) Pituitary/ hypothalamic: 40 pt Optic: 45 Auditory: ≈ 45 Other nerves: 1–5
Igaki [29] 2004	CD	13 Median: 69	X + P (5pt), P (8pt) 63–95 Median 72/2–3.5	≥ G3: 2pt (2 brain necroses ±1 mucosal)
Noël [30] 2005	CD	100 Median: 31	X + P 60–71 Median: 67/1.8–2	Vision < 5/10: 3pt, Uni/ bilateral hypacusis: 16+5pt (1 pt G3), Total+partial hypopituitarism: 9 + 8 pt Cognitive: 11pt (5 pt ≥G3) Temporal lobe (radiological):1 pt
Weber [31] 2005	CD+CS	18 CD+11 CS/ Median: 29	P (spot scanning) CD: 67–74 Median: 74/1.8–2 CS: 64–74 Median: 68/1.8–2	G2: 4 hypopituitarism (1 pt panhypo)
Pommier [35] 2006	ACC skull base+HN	23 Median: 64	P NA 75/1.8–2	≤ G2: 2 pt brain (radiological), 12 pt late ocular, 6 pt thyroid G3: 8 pt brain, 1 pt cataract, 1 pt eyelid, 1 pt lacrymal canal G4: 1 pt retinopathy G5: 2 pt brain (at 9 and 61 months)

(continued)

Table 18.4 (continued)

First Author [Reference] Year of Publication	Tumor Type Location	Patient No FU (months)	Radiation Type Dose Range (GyE) Total Dose (GyE)/ Dose per Fx (GyE)	Toxicity
Mizoe [34] 2004	HN carcinomas/ melanomas	36 Median: 90	C A: 49–70/2.7–3.9 B: 53–64/3.3–4	G1: late cutaneous A:5 pt, B: 10pt ≤ G2: late mucous A: 3 pt, B: 2pt
Schultz-Ertner [32] 2007	CD	96 Mean: 31	C NA Median: 60/3	≤G2: 7.2% temporal lobe G3: 4.1% optic neuropathy
Schultz-Ertner [33] 2007	CS	54 Median: 33	C NA Median: 60/3	≤ G2: 5 pt (9.5%): 1 pt hearing, 1 pt cataract, 1 pt hormoned-eficiency, 2 pt temporal lobe G3: 1 pt (2%): VI nerve

Abbreviations: *ACC* adenoid cystic carcinoma, *C* carbon, *CD* chordoma, *CS* chondrosarcoma, *Fx* fractions, *FU* Follow-up, *G* grade, *HN* head and neck, *P* proton, *pt* patient(s), *tox* toxicity, *X* photons, *Y* year

Table 18.5 Dose–volume constraints in IBT for CNS structures

Organ	Anatomical Structure	PT	CIRT
Brain stem	surface	64–67	NA
	center	53–54	50
	volume $<1 cm^3$	>60	60
Spinal cord	surface	70	
	center	55–58	45
Temporal lobe	surface	<64−67	NA
	volume $<2 cm^3$	<70	
Optic pathway		55–60	54

The maximum tolerated doses in GyE are listed for various anatomical structures and proton therapy (PT) and carbon ion radiotherapy (CIRT), respectively. The data are from [30, 42] for PT, and from [32] for CIRT
Abbreviation: see Table 18.4

constraints specific to charged particles are being tested [30,32,43] and displayed in Table 18.5. Neurocognitive impairment has rarely been explored in adults. It looks very mild following proton therapy (PT) [44]. The potential benefit of technical refinements such as spot scanning is still unknown [45].

18.3.1.2 Radiosurgery with Ions

Proton and helium radiosurgery programs conducted by the MGH group and at the Lawrence Berkeley Laboratory (LBL) provided the basics for brain tolerance to single fractions. The main findings were a relationship between complication rate, dose (approx. $\geq$25 Gy single fraction) and target size (approx. $\geq$6 cm) [46, 47]. Nowadays, fractionation in two to four sessions is favored by several authors [48, 49].

18.3.1.3 Light Ions

Following the pioneering work conducted at the LBL [50], the German group at the GSI (Gesellschaft für Schwerionenforschung) in Darmstadt presented their carbon experience on 150 skull base sarcomas (Table 18.4 and [32, 33]). They reported 7–9% of minor temporal lobe toxicity following a dose of 60 GyE. Using the "Local Effect Model" for treatment planning (cf. Chap. 8 for details), the 5% risk could be set to a biologically equivalent dose of 68 $\pm$ 3 GyE, which is close to 60 GyE for CF and an $\alpha/\beta = 10$ [51].

18.3.2 Cranial Nerves and Cochlea

Cranial nerves have a low sensitivity to radiation with two exceptions: the optic pathway with the optic nerves and chiasm and the auditory nerve extremity including cochlea.

Both structures are organized "serially" (see Chap. 5), and "hot spots" should be avoided. Neurosensory hearing loss (NSHL) becomes clinically relevant at about 20 dB, especially, if it affects speech frequencies (0.5–4 kHz). Radiosurgical data refer to different dose ranges. In the case of NSHL, the effects seem to be influenced by the target size: V15: 40 mm, and V24: 20 mm [6]. The estimated risk for optic neuropathy (ONP) is 5% at 5 years following a dose of 8–10 Gy. For other cranial nerves, a maximum dose of approx. 17.5 Gy seems tolerable [4].

18.3.2.1 Fractionated Protons

Toxicity concerning cranial nerves and internal ear is mostly derived from treating skull base malignancies. The risk of ONP appears to be quite low when dose constraints are strictly observed (Table 18.4), e.g., 4.5% in the Boston series after 41 months median follow-up (FU), 3% in the Orsay series (median FU: 31 months), and one in 16 patients in a series of the Paul Scherrer Institute (PSI). Tolerance can be altered by confounding factors such as beam patching in the optic area

[52], diabetes mellitus, or high blood pressure [53]. The dose to the optic pathway should be estimated on diagnostic imaging, before treatment planning. If the dose is considered excessive, further surgical resection may be warranted. Our rule of thumb for the dose estimate is that each additional mm gap between the organ and the field edge corresponds to 10–15% dose fall-off. NSHL is reported to occur more frequently than OPN following IBT since there is, generally, no attempt to spare auditory structures close to the target if hearing is preserved on the other side. Indeed, the patient can maintain an acceptable quality of life with a single functioning ear, which is not the case when the optic nerve sustains damage. Table 18.4 shows that the risk can be as high as 45% for doses of 65–80 GyE [28]. As mentioned above, other cranial nerves are less sensitive to radiation [54, 55]. An analysis of 27 patients revealed a risk of 1% at 60 GyE and 5% at 70 GyE using logistic regression [56].

18.3.2.2 Proton Radiosurgery

Weber et al. reported on radiation tolerance of cranial nerves in 88 patients with vestibular schwannomas treated at the Harvard Cyclotron Laboratory (HCL). A median dose of 12 GyE was prescribed to the 70–108% isodose lines. Of the patients with functional hearing, 7 out of 21 retained it. Actuarial 5-year preservation of the cranial nerves VII and VIII was approx. 90%. The prescribed maximum dose and the inhomogeneity index were significant predictors of neuropathy of the facial nerve [57, 58].

18.3.2.3 Light Ions

Schulz-Ertner et al. reported a 4% risk of ONP and recommended doses $\leq$54 GyE at 3 GyE/fraction [32]. Demizu et al. from the Hyogo Ion Beam Medical Center (HIBMC) reported 11% (8/75) visual loss in a mixed series of protons (62) and carbon ions (13) with a median FU of 25 months. The 10% risk corresponded to a BED of 80 GyE, which in turn corresponded to 50 Gy photons at CF. The risk was similar for both particles, assuming RBE values of 1.01–1.05, and 1.23–2.56, respectively [59].

18.3.3 Pituitary–Hypothalamic Axis

Anterior pituitary and hypothalamus are sensitive to radiation. This is reflected by low serum hormone or hormone-releasing factor levels. Following irradiation, thyroid, adrenal, and gonadal functions should be checked regularly. Normal values do not exclude deficits. These can only be evidenced by dynamic tests and should be interpreted according to age: for example, normal FSH–LH (follicle-stimulating

hormone and luteinizing hormone) values in postmenopausal women with central hypogonadism – FSH–LH is physiologically elevated in this age range – or low FSH–LH values concomitant with hyperprolactinemia [60].

18.3.3.1 Fractionated Protons

Hypothalamic pituitary injury can develop up to 10 years after irradiation as evidenced in a recent update [60]. Following 68.4 GyE in skull-base sarcomas, 63% of the patients developed hypothyroidism, 36% hypogonadism, and 28% hypoadrenalism. Unlike other hormones, prolactinemia was elevated in 84% of the cases, a symptom related to reduced inhibitory control by the hypothalamus. The risk of endocrinopathies was correlated with a minimum dose of approx. 50 GyE and a maximum dose of 70 GyE to the pituitary.

18.4 Tumors of the Trunk

Prostate, liver, esophagus, lung, and, most recently, also certain cases of breast cancer constitute numerically the major indications for IBT of organs of the trunk (Table 18.6 and [61–70]).

18.4.1 Genitourinary and Lower Digestive Tract

The most common symptoms of bladder toxicity are dysuria and hematuria in part of the bladder. Symptoms usually develop within 3 years. Generally, only toxicity higher than grade II is considered clinically relevant. Dose–volume data should be taken with caution since they can be influenced by bladder repletion at the time of imaging for treatment planning [11]. Rectal toxicity manifests through rectal bleeding and/or diarrhea. Biologically, the rectum corresponds to a serial organ ($n < 0.15$, $\alpha/\beta = 3$) and the maximum dose to the organ seems an important endpoint (cf. [9] and Chap. 5).

18.4.1.1 Fractionated Protons

Prostate carcinoma has been the main pelvic lesion treated in adults since the early 1980s (cf. [61–63] and Chap. 16). Knowledge on toxicity has considerably improved through successive studies (Table 18.6). Clinical investigations evolved from advanced disease (T3–T4) requiring extensive pelvic nodal coverage to less advanced (T1–T3) and early lesions (T1b–T2) treated with more focal RT. Technical approaches, which were initially suboptimal with the administration of a large

Table 18.6 Toxicity of PT with or without photon (X) therapy in adult trunk malignancies

First Author [Reference] Year of Publication	Tumor type stage	Patient No Median FU (months)	Treatment conditions	Toxicity
Shipley [61] 1995	Prostate T3–4, M0	202 61	X and X + P 99 pt: X (67.2) 103 pt: X (50.4) +P (25.2) CF	Rectal X vs X+P (8Y): 12 vs 32 (p: 0.002), 1 pt G4 Urethral X vs X + P (8Y):19 vs 8 (p: NS) Hematuria (8Y):14 vs 8 (p: NS)
Slater [62] 2004	Prostate Ia–III	1255 62	X+P and P 731 pt: X (45)+P (30) 524 pt: P (74) CF	1% ≥ G3 GU or GI (10Y)
Zietman [63] 2005	Prostate T1b–T2 PSA<15	393 66	X + P 197 pt: X (50.4) 4 +P (19.8) 196 pt: X (50.4) +P(28.8) CF	≥ G3: 70.2 vs 79.2 GyE: 1 vs 2 GU or GI G2: 70.2 vs 79.2 GyE: 18vs 20 GU 70.2 vs 79.2 GyE: 8 vs 17 GI (p: 0.005)
Bush [64] 2004	Lung NSCLC I	68 30	P 22 pt: 51/10 fx 46 pt: 60/10 fx	None
Hata [65] 2007	Lung NSCLC I	21 25	P 3 pt: 50/10 fx/15 d 18 pt: 60/10 fx/15 d	2 (Sub)cutaneous G2
Ogino [66] 2007	Lung NSCLC I	61 26	P 70–94/20 fx/4–5 wk	Pulmonary G3: 3
Sugahara [67] 2005	Esophagus T1–T4, M0	46 (23 T1) 35	X+P and P 40 pt: X (48)+P (31.7) Median: 76 (69–87) 6pt: P(82) Median: 82 (75–90)	Late tox: ≤G2: 28% ≥G3: 1% (4 deaths)
Chiba [68] 2005	HCC I–III	162 (192 tumors) 31.7	P 50–88 Median: 72 16 fx/29 d	Late tox ≥G2: 5 pt (ulcers: 2 pt; biliary infection: 2 pt; bile duct fibrosis: 1) PS:4 pt decrease, all others stable
Kawashima [69] 2005	HCC limited disease	30 31	P 76/20 fx/5 wk	Hepatic failure: 8 pt (4 deaths) Increase in hepatic toxicity with severe cirrhosis

(continued)

Table 18.6 (continued)

First Author [Reference] Year of Publication	Tumor type stage	Patient No Median FU (months)	Treatment conditions	Toxicity
Kozak [70] 2006	Breast I	20 12	P 32/8 fx/4 d	Acute cutaneous tox G≥2: 79% cosmesis: 100% good or excellent at 1 Y 3 pt rib pains, 1 pt rib fracture, 3 pt telangiectasia

Dose in Gy for photons, and in GyE for protons
Abbreviations: *CF* conventional fractionation, *d* day(s), *GI* gastrointestinal, *GU* genitourinary, *HCC* hepatocellular carcinoma, *NS* not significant, *NSCLC* non-small cell lung cancer, *p* statistical *p*-value, *PS* performance status, *wk* week(s). Others, see above

photon dose, followed by a perineal proton boost have improved considerably. In the former setting, Shipley et al. compared two dose levels (75.6 vs. 67.2 GyE) and showed a significant increase in rectal toxicity, albeit mild or moderate (G1–2), of 32% in the higher dose arm as compared to 12% [61]. Urinary toxicity was not affected. By comparison, 70–80 Gy photons induced approx. 40% toxicity of level G2 or greater at 7 years, and G3 or greater of 13% [71]. Intensity-modulated photons lower this risk [72]. A recent proton-based randomized study on early cases using similar doses evidenced a very low rate of ≤2% late G3 toxicity in both arms [63].

18.4.1.2 Light Ions

Sixty five patients with postsurgical recurrent rectal adenocarcinoma received carbon ions in a study at the National Institute of Radiological Sciences (NIRS) in Chiba, Japan. The total dose was 67.2–73.6 GyE given in 4–5 GyE per fraction. At a median FU of 38 months, no patient experienced severe toxicity of ≥G3 [73].

18.4.2 Upper Digestive Tract

Late esophageal toxicity consists of dysphagia related to stricture and ulceration [74]. Liver dysfunction [8] is widely reported according to the Child-Pugh scoring system (the sum of five clinical and physiological parameters). The total score is divided into three groups with increasing severity: $A = 5–6$, $B = 7–9$, and $C = 10–15$. Dose constraints are also strongly correlated with the organ volume

(Table 18.1). In hepatocellular carcinomas (HCC), end points are exclusively short- or mid-term due to the limited life expectancy of the patients.

18.4.2.1 Protons

Fractionated PT is well tolerated not only for small volumes. Tolerance appears to be excellent in large and multiple lesions even in the presence of morbidity factors such as cirrhosis [68, 69], and remains good in case of reirradiation [75]. Similarly, esophageal tolerance appeared acceptable in one study following cumulative doses of 76 GyE and 82 GyE in T1–T4, with slightly hypofractionated RT (3 GyE per fraction) [65]. Nonetheless, 48% of the patients (22/46) developed post-RT esophageal ulcers within approx. 7 months, and 4 of the patients died of their unhealed ulcers due to "intercurrent" conditions. There was a significant dose–effect relationship between the BED (80 GyE, at $\alpha/\beta = 3$ Gy) and the risk of ulceration: 75 vs. 37%. Ongoing studies are testing tolerance to different dose fractionation schedules and to combined chemo-RT [76].

18.4.2.2 Light Ions

Advanced HCCs were tested by the Chiba group using carbon ions with dose escalation from 49.5 to 79.5 GyE in 15 fractions/5 weeks. Only Child-Pugh A and B patients were included. No severe early or late toxicity was observed among 24 patients followed, on the average, for almost 6 years [77]. Recently, the same group delivered 52 GyE/4 fractions/1week, with only 3% early and no late severe hepatic toxicity [78].

18.4.3 Lungs

Clinical toxicity of the lung begins with changes in pulmonary function and can lead to dyspnea and, at higher dose levels, to bronchial strictures. More severe dose constraints are applied after a pneumonectomy: Percentage volume and mean dose to the ipsilateral lung are the best prognosticators.

18.4.3.1 Protons

According to dosimetric investigations, only protons seem to be able to treat stage I–III lung malignancies up to 87.5 GyE while keeping the dose to the lung within acceptable limits [79]. Hypofractionation of the dose also appears to be well tolerated when fractionated into 10–20 fractions of 4–5 GyE [64–66, 80, 81]. In contrast, two similar photon studies reported on 13 and 17% high-grade pulmonary

toxicity [82, 83]. Concomitant chemo-RT including protons seems better tolerated than a similar protocol based on photon IMRT [84].

18.4.3.2 Light Ions

Various dose fractionation schedules have been reported for inoperable stage I non-small cell lung cancer with the goal of reducing the number of fractions. It turned out that central lesions needed more fractions to tolerate treatment. At NIRS, it was possible to irradiate peripheral sites with only one fraction of carbon ions (cf. Chap. 14 for details) but central lesions required at least nine fractions [73]. Most of the patients developed minor or mild radiological abnormalities [85]. Pleural reactions that could have been related to RBE changes at the rib–pleura interface affected half of the patients [86]. No G3 toxicity occurred in 79 elderly patients who received 52.8–60 GyE in four fractions [87].

18.4.4 Skin

Skin reactions are divided into acute epidermitis and late dermatitis. The intensity of the reactions is primarily correlated with total dose and exposed skin surface. Therefore, the use of dose–surface histograms seems more appropriate than dose–volume histograms. It is permitted to correlate the severity of acute and late reactions.

Ions lack the sparing effect on skin observed with high-energy photons. This can translate into increased acute [70] and late toxicities [88]. The latter was reported by the Chiba group using carbon ions in sacral malignancies, when the planning target volume (PTV) was close to the skin and treated with a single posterior port. Consequently, they recommended drawing the PTV away from the surface, using multiple portals, and keeping the dose below 64 GyE.

18.5 Pediatric Tumors

In children and adolescents, tissues develop at a more rapid pace than in adults, which makes them more sensitive to radiation [89–98]. Many organs display sensitivity even for doses below 20 Gy administered at CF [99–101]. To mention a few: whole brain in younger children; mammary buds, kidneys, cartilage growth plates, anterior pituitary etc. Since most strategies designed to treat pediatric tumors include large amounts of chemotherapy, sensitivity to radiation can also be enhanced, such as brain necrosis after high-dose busulfan and moderate RT doses [102], or hearing impairment following combined platinum derivatives and low-dose RT [103].

Table 18.7 lists late-toxicity phenomena observed for various indications in children after treatment with protons partly combined with photons and/or chemotherapy.

Table 18.7 Toxicity of PT with or without photon (X) therapy in children

First Author [Reference] Year of Publication	Tumor site	Patient No FU (months)	Treatment conditions	Late toxicity
McAllister [89] 1997	Brain, HN	28 Median: 25	20 pt P and 8 pt X+P P: 40–70/1.8–2.0 X+P: 41–69/1.8–2.0	2 seizures,1 hormonal deficit, 1 cataract
Hug [90] 2002	Low grade glioma	27 Mean: 39	26 pt P and 1 pt X+P 50–63 55.2/1.8	4 hypopituitarism, 1 asymptomatic brain necrosis
Hug [91] 2002	CD+CS	5833CD+ 25CS Mean : 33.2	52 pt P and 6 pt X+P X+P 65–79 70.7/1.8	≥G3: 4 pt (3 symptomatic)
Noel [92] 2003	Brain, HN	17 Mean: 27	20 pt P and 40 pt X+P 50–69 60.0/1.8	1 cerebellar syndrome, 1 hypopituitarism, 1 memory loss
Yuh [93] 2004	Medulloblastoma	3 Max : 36	P Craniospinal axis: 36/1.8 Posterior fossa: 54/1.8	none reported
Yock [94] 2005	Orbital rhabdomyosarcoma	7 Median: 76	P 40–55 46.6/1.8	No endocrine, visual, or cosmetic tox
Luu [95] 2006	Craniopharyngioma	16 Mean: 60	P 50–59/1.8	1 hypopituitarism, 1 cerebrovascular event, 1 meningioma
Timmermann [96] 2007	Soft tissue sarcoma (trunk, HN)	16 (12 RMS) Median: 18.6	P (spot scanning) IMPT in 3 pt 46–61 Median: 50.0/1.8–2.0	Minor
Habrand [97] 2008	CD+CS	3026CD+ 4CS Mean : 26.5	1 pt P and 29 pt X+P 55–71 Mean: 68.3/1.8–2.0	G2: 7 hypopituitarisms G3: 1 hypacusis
MacDonald [98] 2008	Intracranial ependymoma	17 Median: 26	P 52–59 Median: 55.8/1.8	None

Dose in Gy for photons, and in GyE for protons.
Abbreviations: see above

A large body of dosimetric evidence shows improved sparing of anatomical structures in children using protons as compared to photons. For example, temporal lobes in optic pathway gliomas [104], cochleas in cerebellar medulloblastomas [105], orbital bones and contralateral eye in retinoblastomas and orbital rhabdomyosarcomas [94, 106], spine and kidneys in lumbar neuroblastomas [107]. These findings might translate into less long-term toxicity and better quality of life. Clinical evidence is still scarce, though, and comprises limited series with a rather short FU.

18.6 Second Cancers

Approximately, one in ten cancer patients develops a second malignancy [108]. Although considerable uncertainties exist, the increased risk related to radiation exposure has been estimated to be 1.5% per Sv, and seems to be paradoxically enhanced by modern RT technologies such as IMRT to approx. 3–5% per Sv and still higher for children [108].

18.6.1 Protons

Compared to photon RT, PT decreases the dose to adjacent normal tissues and the integral dose – mainly related to medium- and low-dose levels – to the entire body. This might translate into a reduction of second cancers, especially in youngsters. At PSI, mathematical algorithms were developed based on radioprotection estimates, suggesting that the risk could be lowered by a factor of two in parameningeal rhabdomyosarcomas and even 8–15 in medulloblastomas compared with sophisticated photon techniques. On the other hand, some authors pointed out a potential adverse effect due to neutron emission by the proton beam lines, but the extent of such emission remains highly controversial [109]. Preliminary clinical results of two matched cohorts – mainly adults – treated with protons at the MGH, or with photons from the SEER (surveillance, epidemiology, and end results) registry substantiate a clear reduction of risk in the proton group [110].

18.6.2 Light Ions

The risk to induce second cancers is largely unknown for high-LET particles. Concerning fast neutrons, which were widely applied in the clinical setting until the mid 1990s, their RBE for cancer induction was estimated to be higher than for tumoricidal effects – 10 vs. 3 [111]. In the case of fission neutrons, produced as secondary emission by most RT equipment and also by the patients themselves, it

was estimated to be ≥20 relative to photons. A similar estimate was made for carbon ions [112].

If one assumes the integral dose delivered by carbon ions to be only about one third that of photons, the risk for cancer induction would still be 6–7 (20:3) times higher for the ions. This value, could be overestimated since most normal tissues are located in the plateau region of the Bragg curve with lower LET and RBE. Nonetheless, it seems reasonable to cautiously envisage light ion therapy programs in young patients, especially children.

18.7 Conclusion

The dose distribution of ion beams offers, in principle, a substantial benefit concerning toxicity due to improved sparing of normal organs. Clinical data accumulated since the early 1990s have confirmed the low toxicity associated with PT, initially for rare malignancies such as ocular melanomas or skull-base sarcomas and, subsequently, for more common cancers of the lung or prostate. Promising data are also emerging on tolerance to protons in combined radio-chemotherapies and in pediatric malignancies, and to heavier ions in highly hypofractionated regimens. Future directions should also include clinical and economic appraisals comparing advanced photon and particle approaches directed at more common sites. Finally, it should be born in mind that the advantageous dose distribution of ion beams will only translate into a clinical benefit when dose and fractionation schedules, simulation guidelines, physical and biological models, and patient alignment are appropriate. It is, therefore, mandatory to address all these aspects in order to deliver the best possible radiation treatment with a minimum of adverse effects.

Acknowledgement We extend special thanks to Mrs Lorna Sainte-Ange at IGR, for editing.

References

1. International Commission on Radiation Units and Measurements. Report 78: Prescribing, recording and reporting proton-beam therapy. J. ICRU **7**, 49–81 (2007)
2. Y.R. Lawrence, X.A. Li, I. El Naqa, et al., Radiation dose-volume effects in the brain. Int. J. Radiat. Oncol. Biol. Phys. **76**, S20–S27 (2010)
3. J. Kirkpatrick, A.J. van der Kogel, T.E. Schultheiss, Radiation dose-volume effects in the spinal cord. Int. J. Radiat. Oncol. Biol. Phys. **76**, S42–S49 (2010)
4. C. Mayo, M.K. Martel, L.B. Marks, et al., Radiation dose-volume effects of optic nerves and chiasm. Int. J. Radiat. Oncol. Biol. Phys. **76**, S28–S35 (2010)
5. C. Mayo, E. Yorke, T. Merchant, Radiation associated brainstem injury. Int. J. Radiat. Oncol. Biol. Phys. **76**, S36–S41 (2010)
6. N. Bhandare, A. Jackson, A. Eisbruch, et al., Radiation therapy and hearing loss. Int. J. Radiat. Oncol. Biol. Phys. **76**, S50–S57 (2010)

7. L.B. Marks, S.M. Bentzen, J.O. Deasy, et al., Radiation dose-volume effects in the lung. Int. J. Radiat. Oncol. Biol. Phys. **76**, S70–S76 (2010)
8. C.C. Pan, B.D. Kavanagh, L.A. Dawson, et al., Radiation associated liver injury. Int. J. Radiat. Oncol. Biol. Phys. **76**, S94–S100 (2010)
9. J.M. Michalski, H. Gay, A. Jackson, et al., Radiation dose-volume effects in radiation-induced rectal injury. Int. J. Radiat. Oncol. Biol. Phys. **76**, S123–129 (2010)
10. B.D. Kavanagh, C.C. Pan, L.A. Dawson, et al., Radiation dose-volume effects in the stomach and small bowel. Int. J. Radiat. Oncol. Biol. Phys. **76**, S101–S107 (2010)
11. A.N. Viswanathan, E.D. Yorke, L.B. Marks, et al., Radiation dose-volume effects of the urinary bladder. Int. J. Radiat. Oncol. Biol. Phys. **76**, S116–S122 (2010)
12. B. Emami, J. Lyman, A. Brown, et al, Tolerance of normal tissue to therapeutic irradiation. Int. J. Radiat. Oncol. Biol. Phys. **21**, 109–122 (1991)
13. J.R. Castro, D.H. Char, P.L. Petti, et al, 15 years experience with helium ion for uveal melanomas. Int. J. Radiat. Oncol. Biol. Phys. **39**, 989–996 (1997)
14. A. Courdi, J.P. Caujolle, J.D. Grange, et al., Results of proton therapy of uveal melanomas treated in Nice. Int. J. Radiat. Oncol. Biol. Phys. **45**, 5–11 (1999)
15. E. Egger, L. Zografos, A. Schalenbourg, et al., Eye retention after proton beam radiotherapy for uveal melanoma. Int. J. Radiat. Oncol. Biol. Phys. **55**, 867–880 (2003)
16. J.E. Munzenrider, Uveal melanomas. Conservation treatment. Hematol. Oncol. Clin. North Am. **15**, 389–402 (2001)
17. R. Dendale, L. Lumbroso-Le Rouic, G. Noël, et al., Proton beam radiotherapy for uveal melanoma: results of Curie-Institute-Orsay Proton Therapy Center (ICPO). Int. J. Radiat. Oncol. Biol. Phys. **65**, 780–787 (2006)
18. G. Simonova, R. Liscak, J. Novotny, Ocular and Orbital Lesions, in *Principles and Practice of Stereotactic Radiosurgery*, ed. by L.S. Chin, W.R. Regine. (Springer, New York, 2008), pp. 593–610
19. B. Damato, A. Kacperek, M. Chopra, et al., Proton beam radiotherapy of iris melanoma. Int. J. Radiat. Oncol. Biol. Phys. **63**, 109–115 (2005)
20. L. Lumbroso-Le Rouic, S. Delacroix, R. Dendale, et al., Proton beam therapy for iris melanomas. Eye **20**, 1300–1305 (2006)
21. H. Wuestemeyer, W. Sauerwein, D. Meller, et al., Proton radiotherapy as an alternative to exenteration in the management of extended conjunctival melanoma. Graefes Arch. Clin. Exp. Ophtalmol. **244**, 438–446 (2006)
22. L. Desjardins, L. Lumbroso-Le Rouic, C. Levy-Gabriel, et al., Combined proton beam radiotherapy and transpupillary thermotherapy for large uveal melanomas: a randomized study of 151 patients. Ophthalmic Res. **38**, 255–260 (2006)
23. E.S. Gragoudas, A.M. Lane, S. Regan, et al., A randomized controlled trial of varying radiation doses in the treatment of choroidal melanoma. Arch. Ophthalmol. **118**, 773–778 (2000)
24. E.S. Gragoudas, W. Li, A.M. Lane, et al., Risk factors for radiation maculopathy and papillopathy after intraocular irradiation. Ophthalmology **106**, 1571–1578 (1999)
25. D.H. Char, S. Kroll, J. Castro, Ten-year follow up of helium ion therapy for uveal melanoma. Am. J. Ophthalmol. **125**, 81–89 (1998)
26. D.H. Char, J.M. Quivey, J.R. Castro, et al., Helium ions versus 125-I brachytherapy in the management of uveal melanoma: a prospective randomized dynamically balanced trial. J. Ophthalmol. **100**, 1547–1554 (1993)
27. E.B. Hug, L.N. Loredo, J.D. Slater, et al., Proton radiation therapy for chordomas and chondrosarcomas of the skull base. J. Neurosurg. **91**, 432–439 (1999)
28. J.E. Munzenrider, N.J. Liebsch, Proton therapy for tumors of the skull base. Strahlenther Onkol. **175**, 57–63 (1999)
29. H. Igaki, K. Tokuuye, T. Okumura, et al., Clinical results of proton beam therapy for skull base chordoma. Int. J. Radiat. Oncol. Biol. Phys. **60**, 1120–1126 (2004)

30. G. Noël, L. Feuvret, V. Calugaru, et al., Chordomas of the base of the skull and cervical spine. One hundred patients irradiated by a 3D conformal technique combining photon and proton beams. Acta Oncol. **44**, 700–708 (2005)
31. D.C. Weber, H.P. Rutz, E.S. Pedroni, et al., Results of spot-scanning proton radiation therapy for chordoma and chondrosarcoma of the skull base: the Paul Scherrer Institute experience. Int. J. Radiat. Oncol. Biol. Phys. **63**, 401–409 (2005)
32. D. Schulz-Ertner, C.P. Karger, A. Feuerhake, et al., Effectiveness of carbon ion radiotherapy in the treatment of skull-base chordomas. Int. J. Radiat. Oncol. Biol. Phys. **68**, 449–457 (2007)
33. D. Schulz-Ertner, A. Nikoghosyan, H. Hof, et al., Carbon ion radiotherapy of skull base chondrosarcomas. Int. J. Radiat. Oncol. Biol. Phys. **67**, 171–177 (2007)
34. J.E. Mizoe, H. Tsujii, T. Kamada, et al., Dose escalation study of carbon ion radiotherapy for locally advanced head-and-neck cancer. Int. J. Radiat. Oncol. Biol. Phys. **60**, 358–364 (2004)
35. P. Pommier, N. Liebsch, D.G. Deschler, et al., Proton beam radiation therapy for skull base adenoid cystic carcinoma. Arch. Otolaryngol. Head Neck Surg. **132**, 1242–1249 (2006)
36. M.M. Fitzek, A.F. Thornton, J.D. Rabinov, et al., Accelerated fractionated proton/photon irradiation to 90-cobalt gray equivalent for glioblastoma multiforme: results of a phase II prospective trial. J. Neurosurg. **91**, 251–260 (1999)
37. M.M. Fitzek, A.F. Thornton, G. Harsh IV, et al., Dose-escalation with proton/photon irradiation for Daumas-Duport lower grade glioma: results of an institutional phase I/II trial. Int. J. Radiat. Oncol. Biol. Phys. **51**, 131–137 (2001)
38. H. Tatsuzaki, M.M. Urie, R. Linggood, Comparative treatment planning: proton vs. x-ray beams against glioblastoma multiforme. Int. J. Radiat. Oncol. Biol. Phys. **22**, 265–273 (1992)
39. J. Debus, D. Schultz-Ertner, L. Schad, et al., Stereotactic fractionated radiotherapy for chordomas and chondrosarcomas of the skull base. Int. J. Radiat. Oncol. Biol. Phys. **47**, 591–596 (2000)
40. B.G. Baumert, A.J. Lomax, V. Miltchev, J.B. Davis, A comparison of dose distributions of proton and photon beams in stereotactic conformal radiotherapy of brain lesions. Int. J. Radiat. Oncol. Biol. Phys. **49**, 1439–1449 (2001)
41. R. Santoni, N. Liebsch, D.M. Finkelstein, et al., Temporal lobe (TL) damage following surgery and high-dose photon and proton irradiation in 96 patients affected by chordomas and chondrosarcomas of the base of the skull. Int. J. Radiat. Oncol. Biol. Phys. **41**, 59–68 (1998)
42. J. Debus, E.B. Hug, N. Liebsch, et al., Dose-volume tolerance of the brainstem after high dose radiotherapy. Front. Radiat. Ther. Oncol. **33**, 305–314 (1999)
43. L. Marucci, A. Niemierko, N. Liebsch, et al., Spinal cord tolerance to high dose fractionated 3D conformal proton-photon irradiation as evaluated by equivalent uniform dose and dose-volume histogram analysis. Int. J. Radiat. Oncol. Biol. Phys. **59**, 551–555 (2004)
44. G. Glosser, P. McManus, J. Munzenrider, et al., Neuropsychological function in adults after high dose fractionated radiation therapy of skull base tumors. Int. J. Radiat. Oncol. Biol. Phys. **38**, 231–239 (1997)
45. D.C. Weber, A.W. Chan, S. Lessell, et al., Visual outcome of accelerated fractionated radiation for advanced sinonasal malignancies employing photons/protons. Radiother. Oncol. **81**, 243–249 (2006)
46. R.N. Kjellberg, T. Hanamura, K.R. Davis, et al., Bragg-peak proton-beam therapy for arteriovenous malformations of the brain. N. Engl. J. Med. **309**, 269–274 (1983)
47. S. Amin-Hanjani, C.S. Ogilvy, G.J. Candia, Stereotactic radiosurgery for cavernous malformations: Kjellberg's experience with proton beam therapy in 98 cases at the Harvard Cyclotron. Neurosurgery **42**, 1229–1236 (1998)
48. J.C. Flickinger, Radiobiology of Stereotactic Radiosurgery, in *Intracranial Stereotactic Radiosurgery*, ed. by L.D. Lunsford, J.P. Sheehan, 2nd edn. (Thieme Medical, New York, 2009), pp. 5–12
49. H.A. Shih, P.H. Chapman, M.R. Bussière, et al., Central Nervous System, in *Proton and Charged Particle Radiotherapy*, ed. by T.F. DeLaney, H.M. Kooy (Lippincott, Williams & Wilkins, Philadelphia, 2008), pp. 140–150

50. J.R. Castro, D.E. Linstadt, J.P. Bahary, et al., Experience in charged particle irradiation of tumors of the skull base: 1977–1992. Int. J. Radiat. Oncol. Biol. Phys. **29**, 647–655 (1994)
51. I. Schlampp, C.P. Karger, O. Jäkel, et al., Temporal lobe reactions after radiotherapy with carbon ions: incidence and estimation of the relative biological effectiveness by the local effect model. Int. J. Radiat. Oncol. Biol. Phys. **80**, 815–823 (2011)
52. J. Kim, J.E. Munzenrider, A. Maas, et al., Optic neuropathy following combined proton and photon radiotherapy for base of skull tumors. Int. J. Radiat. Oncol. Biol. Phys. **39**, 272, Abstr 2064 (1997)
53. J.L. Habrand, M. Austin-Seymour, S. Birnbaum, et al., Neurovisual outcome following proton radiation therapy. Int. J. Radiat. Oncol. Biol. Phys. **16**, 1601–1606 (1989)
54. E.B. Hug, J.D. Slater, Proton radiation therapy for chordomas and chondrosarcomas of the skull base. Neurosurg. Clin. N. Am. **11**, 627–638 (2000)
55. R. Schoenthaler, B. Fullerton, A. Maas, et al., Relationship between dose to auditory pathways and audiological outcomes in skull-base tumor patients receiving high-dose proton-photon radiotherapy. Int. J. Radiat. Oncol. Biol. Phys. **36**, 291, Abstr 2026 (1996)
56. M.M. Urie, B. Fullerton, H. Tatsuzaki, et al., A dose response analysis of injury to cranial nerves and/or nuclei following proton beam radiation therapy. Int. J. Radiat. Oncol. Biol. Phys. **23**, 27–39 (1992)
57. G.R. Harsh, A.F. Thornton, P.H. Chapman, et al., Proton beam stereotactic radiosurgery of vestibular schwannomas. Int. J. Radiat. Oncol. Biol. Phys. **54**, 35–44 (2002)
58. D.C. Weber, A.W. Chan, M.R. Bussière, et al., Proton beam radiosurgery for vestibular schwannoma: tumor control and cranial nerve toxicity. Neurosurgery **53**, 577–586 (2003)
59. Y. Demizu, M. Murakami, D. Miyawaki, et al., Analysis of vision loss caused by radiation-induced optic neuropathy after particle therapy for head-and-neck and skull-base tumors adjacent to optic nerves. Int. J. Radiat. Oncol. Biol. Phys. **75**, 1487–1492 (2009)
60. H.H. Pai, A. Thornton, L. Katznelson, et al., Hypothalamic/pituitary function following high-dose conformal radiotherapy to the base of the skull: demonstration of a dose-effect relationship using dose-volume histogram analysis. Int. J. Radiat. Oncol. Biol. Phys. **49**, 1079–1092 (2001)
61. W.U. Shipley, L.J. Verhey, J.E. Munzenrider, et al., Advanced prostate cancer: the results of a randomized comparative trial of high dose irradiation boosting with conformal protons compared with conventional dose irradiation using photons alone. Int. J. Radiat. Oncol. Biol. Phys. **32**, 3–12 (1995)
62. J.D. Slater, C.J. Rossi, L.T. Yonemoto, et al., Proton therapy for prostate cancer: the initial Loma Linda University experience. Int. J. Radiat. Oncol. Biol. Phys. **59**, 348–352 (2004)
63. A.I. Zietman, M.L. DeSilvio, J.D. Slater, et al., Comparison of conventional-dose vs high-dose conformal radiation therapy in clinically localized adenocarcinoma of the prostate. A randomized control trial. J. Am. Med. Assoc. **294**, 1233–1239 (2005)
64. D.A. Bush, J.D. Slater, B.B. Shin, et al., Hypofractionated proton beam radiotherapy for stage I lung cancer. Chest **126**, 1198–1203 (2004)
65. M. Hata, K. Tokuuye, K. Kagei, et al., Hypofractionated high-dose proton beam therapy for stage I non small cell lung cancer: preliminary results of a phase I/II clinical study. Int. J. Radiat. Oncol. Biol. Phys. **68**, 786–793 (2007)
66. T. Ogino, K. Nihei, M. Onozawa, et al., Updated results of high dose proton beam therapy (PBT) for stage I non-small-cell lung cancer (NSCLC), in *Proceedings of Particle Therapy Cooperative Group*, Abstract 12, PTCOG 46, Zibo, China, 18–23 May 2007
67. S. Sugahara, K. Tokuuye, T. Okumura, et al., Clinical results of proton beam therapy for cancer of the esophagus. Int. J. Radiat. Oncol. Biol. Phys. **61**, 76–84 (2005)
68. T. Chiba, K. Tokuuye, Y. Matsuzaki, et al., Proton beam therapy for hepatocellular carcinoma: a retrospective review of 162 patients. Clin. Cancer Res. **11**, 3799–3805 (2005)
69. M. Kawashima, J. Furuse, T. Nishio, et al., Phase II study of radiotherapy employing proton beam for hepatocellular carcinoma. J. Clin. Oncol. **23**, 1839–1846 (2005)
70. K.R. Kozak, B.L. Smith, J. Adams, et al., Accelerated partial breast irradiation using proton beams: initial clinical experience. Int. J. Radiat. Oncol. Biol. Phys. **66**, 691–698 (2006)

71. A. Al-Mamgani, W.L. van Putten, W.D. Heemsberger, et al., Update of Dutch multicenter dose-escalation trial of radiotherapy for localized prostate cancer. Int. J. Radiat. Oncol. Biol. Phys. **71**, 1028–1033 (2008)
72. M.J. Zelefsky, E.J. Levin, M. Hunt et al., Incidence of late rectal and urinary toxicities after three-dimensional conformal radiotherapy and intensity-modulated radiotherapy for localized prostate cancer. Int. J. Radiat. Oncol. Biol. Phys. **70**, 1124–1129 (2008)
73. H. Tsujii, J. Mizoe, T. Kamada, et al., Clinical results of carbon ion radiotherapy at NIRS. J. Radiat. Res. **48**(Suppl A), A1–A13 (2007)
74. M. Werner-Wasik, E. Yorke, J. Deasy, et al., Radiation dose-volume effects in the esophagus. Int. J. Radiat. Oncol. Biol. Phys. **76**, S86–S93 (2010)
75. T. Hashimoto, K. Tokuuye, N. Fukumitsu, et al., Repeated proton beam therapy for hepatocellular carcinoma. Int. J. Radiat. Oncol. Biol. Phys. **65**, 196–202 (2006)
76. S. Liu, J. Li, Q. Sun, et al., Preliminary results of proton radiotherapy for esophageal carcinoma, in *Proceedings of Particle Therapy Cooperative Group*, Abstract 13, PTCOG 46, Zibo, China, 18–23 May 2007
77. H. Kato, H. Tsujii, T. Miyamoto, et al., Results of the first prospective study of carbon ion radiotherapy for hepatocellular carcinoma with liver cirrhosis. Int. J. Radiat. Oncol. Biol. Phys. **59**, 1458–1476 (2004)
78. H. Kato, S. Yamada, S. Yasuda, et al., Four-fraction carbon ion radiotherapy for hepatocellular carcinoma. J. Clin. Oncol. **22**(Suppl), S335 (2004)
79. J.Y. Chang, X. Zhang, X. Wang, et al., Significant reduction of normal tissue dose by proton radiotherapy compared with three-dimensional conformal or intensity-modulated radiation therapy in stage I or stage III non small cell lung cancer. Int. J. Radiat. Oncol. Biol. Phys. **65**, 1087–1096 (2006)
80. K. Nihei, T. Ogino, S. Ishikura, H. Nishimura, High-dose proton beam therapy for Stage I non-small-cell lung cancer. Int. J. Radiat. Oncol. Biol. Phys. **65**, 107–111 (2006)
81. Y. Shioyama, K. Tokuuye, T. Okumura, et al., Clinical evaluation of proton radiotherapy for non-small-cell lung cancer. Int. J. Radiat. Oncol. Biol. Phys. **56**, 7–13 (2003)
82. J.S.A. Belderbos, K. De Jaeger, W.D. Heemsbergen, et al., First results of phase I/II dose-escalation trial in non-small cell lung cancer using three dimensional conformal radiotherapy. Radiother. Oncol. **66**, 119–126 (2003)
83. B. Jeremic, Y. Shibamoto, B. Milicic, et al., Impact of treatment interruptions due to toxicity on outcome of patients with early stage (I/II) non-small cell lung cancer (NSCLC) treated with hyperfractionated radiation therapy alone. Lung Cancer **40**, 317–323 (2003)
84. R. Komaki, S.V. Sejpal, X. Wei, et al., Reduction of bone marrow suppression for patients with stage III NSCLC treated with proton and chemotherapy compared with IMRT and chemotherapy, in *Proceedings of Particle Therapy Cooperative Group*, Abstract 010, PTCOG 47, Jacksonville, 19–24 May 2008
85. H. Nishimura, T. Miyamoto, N. Yamamoto, et al., Radiographic pulmonary and pleural changes after carbon ion irradiation. Int. J. Radiat. Oncol. Biol. Phys. **55**, 861–866 (2003)
86. T. Miyamoto, M. Baba, N. Yamamoto, et al., Curative treatment of stage I non-small-cell lung cancer with carbon ion beams using a hypofractionated regimen. Int. J. Radiat. Oncol. Biol. Phys. **67**, 750–758 (2007)
87. T. Miyamoto, M. Baba, T. Sugane, et al., Carbon ion radiotherapy in stage I non-small-cell lung cancer using a regimen of four fractions during one week. J. Thorac. Oncol. **2**, 907–926 (2007)
88. T. Yanagi, T. Kamada, H. Tsuji et al., Dose-volume histogram and dose- surface histogram analysis for skin reactions to carbon ion radiotherapy for bone and soft tissue sarcoma. Radiother. Oncol. **95**, 60–65 (2010)
89. B. McAllister, J.O. Archambeau, M.C. Nguyen, et al., Proton therapy for pediatric cranial tumors: preliminary report on treatment and disease-related morbidities. Int. J. Radiat. Oncol. Biol. Phys. **39**, 455–460 (1997)

90. E.B. Hug, M.W. Muenter, J.O. Archambeau et al., Conformal proton radiation therapy for pediatric low grade astrocytomas. Strahlenther Onkol. **178**, 10–17 (2002)
91. E.B. Hug, R.A. Sweeney, P.M. Nurre, et al., Proton radiotherapy in management of pediatric base of skull tumors. Int. J. Radiat. Oncol. Biol. Phys. **52**, 1017–1024 (2002)
92. G. Noël, J.L. Habrand, S. Helfre, et al., Proton beam therapy in the management of central nervous system tumors in childhood: the preliminary experience of the Centre de Protonthérapie d'Orsay. Med. Pediatr. Oncol. **40**, 309–315 (2003)
93. G.E. Yuh, L.N. Loredo, L.T. Yonemoto, et al., Reducing toxicity from craniospinal irradiation: using proton beams to treat medulloblastoma in young children. Cancer J. **10**, 386–390 (2004)
94. T. Yock, R. Schneider, A. Friedmann, et al., Proton radiotherapy for orbital rhabdomyosarcoma: clinical outcome and dosimetric comparison with photons. Int. J. Radiat. Oncol. Biol. Phys. **63**, 1161–1168 (2005)
95. Q.T. Luu, L.N. Loredo, J.O. Archambeau, et al, Fractionated proton radiation treatment for pediatric craniopharyngioma: preliminary report. Cancer J. **12**, 155–159 (2006)
96. B. Timmermann, A. Schuck, F. Niggli, et al., Spot-scanning proton therapy for malignant soft tissue tumors in childhood: first experiences at the Paul Scherrer Institute. Int. J. Radiat. Oncol. Biol. Phys. **67**, 497–504 (2007)
97. J.L. Habrand, R. Schneider, C. Alapetite, et al., Proton therapy in pediatric skull base and cervical canal low-grade bone malignancies. Int. J. Radiat. Oncol. Biol. Phys. **71**, 672–678 (2008)
98. S.M. MacDonald, S. Safai, A. Trofimov, et al., Proton radiotherapy for childhood ependymoma: initial clinical outcomes and dose comparisons. Int. J. Radiat. Oncol. Biol. Phys. **71**, 979–986 (2008)
99. D.L. Friedman, L.S. Constine, Late Effects of Cancer Treatment, in *Pediatric Radiation Oncology*, ed. by E.C. Halperin, L.S. Constine, N.J. Tarbell, L.E. Kun. 4th edn. (Lippincott, Williams & Wilkins, Philadelphia, 2005), pp. 523–611
100. A.C. Paulino, L.S. Constine, P. Rubin, J.P. Williams, Normal tissue development, homeostasis, senescence and the sensitivity to radiation injury across the age spectrum. Semin. Radiat. Oncol. **20**, 12–20 (2010)
101. R.G. Steen, B.S.M. Coury, C.I. Granja, et al., Effect of ionizing radiation on the human brain: white matter and grey matter T1 in pediatric brain tumor patients treated with conformal radiotherapy. Int. J. Radiat. Oncol. Biol. Phys. **49**, 79–91 (2001)
102. B.M. Seddon, A.M. Cassoni, M.J. Galloway, et al., Fatal radiation myelopathy after busulfan and melphalan chemotherapy and radiotherapy for Ewing's sarcoma: a review of the literature and implications for practice. Clin. Oncol. **17**, 385–390 (2005)
103. T.E. Merchant, C.J. Gould, X. Xiong, et al., Early neuro-otologic effects of three-dimensional irradiation in children with primary brain tumors. Int. J. Radiat. Oncol. Biol. Phys. **58**, 1194–1207 (2004)
104. M. Fuss, E.B. Hug, R.A. Schaefer, et al., Proton radiation therapy (PRT) for optic pathway gliomas: comparison with 3D planned photons and a standard photon technique. Int. J. Radiat. Oncol. Biol. Phys. **45**, 1117–1126 (1999)
105. W.H. St Clair, J.A. Adams, M. Bues, et al., Advantage of protons compared to conventional X-Ray or IMRT in the treatment of a pediatric patient with medulloblastoma. Int. J. Radiat. Oncol. Biol. Phys. **58**, 727–734 (2004)
106. M. Krengli, E.B. Hug, J.A. Adams, et al., Proton radiation therapy for retinoblastoma: comparison with various intraocular tumor locations and beam arrangements. Int. J. Radiat. Oncol. Biol. Phys. **61**, 583–593 (2005)
107. E.N. Hug, M. Nevinny-Stickel, M. Fuss, et al., Conformal proton radiation treatment for retroperitoneal neuroblastoma: introduction of a novel technique. Med. Pediatr. Oncol. **37**, 36–41 (2001)
108. E.J. Hall, Intensity-modulated radiotherapy, protons, and the risk of second cancers. Int. J. Radiat. Oncol. Biol. Phys. **65**, 1–7 (2006)
109. H. Paganetti, T. Bortfeld, T.F. Delaney, Neutron dose in proton radiation therapy: in regard to Eric J Hall. Int. J. Radiat. Oncol. Biol. Phys. **66**, 1594–1595 (2006)

110. C.S. Chung, N. Keating, T. Yock, N. Tarbell, Comparative analysis of second malignancy risk in patients treated with proton therapy versus conventional photon therapy. Int. J. Radiat. Oncol. Biol. Phys. **72**, S8 (2008)
111. A. Wambersie, RBE, reference RBE and clinical RBE: applications of these concepts in hadron therapy. Strahlenther Onkol. **175** S39–S43 (1999)
112. H. Engels, H.G. Menzel, P. Pihet, A. Wambersie, Risk assessment for cancer induction after low- and high-LET therapeutic irradiation. Strahlenther Onkol. **175**, S47–S51 (1999)

Chapter 19
Design and Implementation of Clinical Trials of Ion Beam Therapy

James D. Cox

Abstract Design and implementation of clinical trials are complex even when those trials involve established technologies. Ion beam therapy (IBT) imposes additional requirements including sufficient institutional experience using ions for treatment, credentialing of institutions, formulating hypotheses of interest to investigators and to patients, and securing funding from national and private agencies. The effort, though, is very important to the future of radiation oncology.

19.1 Introduction

Clinical trials of cancer treatments have been the single most important means of advancing the care of patients and improving outcome. Clinical cooperative groups in the United States and their equivalents in the European Organisation for Research and Treatment of Cancer (EORTC) as well as cooperative groups within individual countries, especially France and Germany, have been pivotal. However, as reflected in a review of clinical trials conducted by the Institute of Medicine of the National Academy of Sciences [1], clinical trials suffer from greatly inadequate reimbursement of both participant institutions and individual community-based physicians; a general lack of acknowledgment of the time and effort required; and, for academic physicians, disincentives in terms of tenure and promotion for team-based clinical research.

Clinical trials involving radiation therapy (RT) have special requirements, especially those that deal with new or advanced technology. Trials of ion beam therapy (IBT), in particular, have complexities that are several orders of magnitude greater

J.D. Cox (✉)
Department of Radiation Oncology, University of Texas, M.D. Anderson Cancer Center, Houston, TX, USA
e-mail: jcox@mdanderson.org

U. Linz (ed.), *Ion Beam Therapy*, Biological and Medical Physics, Biomedical Engineering, DOI 10.1007/978-3-642-21414-1_19,

than RT trials, in general. For example, utilization of the advanced technology, including credentialing of individual institutions if cooperative clinical investigations are envisioned, must be addressed. These considerations are all the more problematic if the trials to be undertaken involve institutions in different countries. Cooperative clinical investigations must include repositories where the technical data from the trials can be recorded and archived. This was the original charge in the development of the Radiological Physics Center in Houston, Texas, which was founded in 1968 under the leadership of Dr. Robert Shalek. Since that time, centers for advanced technology have been established at Washington University in St. Louis, the University of Wisconsin, and the University of Florida. Similar reference centers have been established in Europe. Credentialing for IBT can follow the example of advanced X-ray treatments. Credentialing includes measurement of output factors, irradiation of specific phantoms, comparisons of doses estimated in treatment plans with measurements of doses actually delivered, and transmission of data electronically from the site of treatment to a central repository. The data in this repository must be able to be correlated with clinical measures, especially outcomes. Often the repository for the technical data and the headquarters for the cooperative clinical effort are not in the same location.

19.2 Different Types of Clinical Trials

For clinical trials of any type, certain conditions must be met. Adequate numbers of patients must be available to address a question in a timely manner, especially if the study is a randomized comparison. The participating investigators must find the questions being asked sufficiently compelling to enroll their patients in the study. Similarly, the studies proposed must be of sufficient interest to the patients that they are willing to be enrolled. Data management policies and implementation must be strong.

The questions to be addressed in the design of the trials can come from many directions. Many would argue that the advanced technology itself, given the relative lack of clinical experience with it throughout the world, is its own justification for study; such is the case for IBT [2, 3]. Complexities arise when there is a need or desire to compare IBT with another type of treatment such as X-ray therapy. In such cases, statistical considerations become paramount, and it is essential to have active involvement of experienced biostatisticians in the design and conduct of clinical trials, even phase I and phase II studies. The critical difference is the observation period required to achieve the desired endpoints for phase I and phase II trials. Contemporary statistical designs such as Bayesian methodology can permit answers to important questions to be obtained in comparative trials with smaller numbers of patients than would have been required for traditional statistical designs [4, 5].

Another consideration is the length of time needed to observe an effect. Results from phase I trials may be evident within weeks or months, as in the case for esophagitis or pneumonitis arising from radiation treatment of tumors in the

Table 19.1 Clinical trials in oncology: phase/endpoint designations for trials of drugs vs. radiation

Phase	Goal	Endpoints	
		Drug trials	Radiation trials
I	Establish maximum tolerated dose	Toxicity (usually acute effects)	Toxicity (usually late effects)
II	Establish activity	Tumor shrinkage (complete or partial response)	Local tumor control
III	Establish quantitative effect in specific tumor types	Disease-free and overall survival	Disease-free and overall survival

thorax. However, a fundamental difficulty in clinical trials of RT is the duration of observation that is necessary for generating conclusions about the relative safety of one treatment as compared with another (Table 19.1). In most cases, the dose-limiting toxicities of irradiation are late effects that may require years or even decades of observation. Some late effects may begin to become evident within a year, but they continue to progress for many years thereafter [6]. If second malignant tumors are a late-effect endpoint, as would be the case in comparisons of proton therapy (PT) vs. intensity-modulated radiation therapy (IMRT) for cancer of the prostate, 20 or 30 years of observation could be required [7].

Phase II studies are designed to test the efficacy of treatment for specific diseases. The usual endpoint for trials of drug therapy is "response," which could represent as little as 1 or 2 logs of cellular depletion (kill) in a tumor containing 10^9 cells. For RT, control of the tumor within the irradiated volume is the usual endpoint; this also takes at least a year or more of observation.

Randomized trials represent the most sought-after form of evidence. If a standard treatment arm is included in a trial, that trial can be considered phase III. If the comparison is between two arms where neither is considered the standard of care, then the trial is most appropriately designated phase II, even if patient assignment is randomized. Such is the case with the randomized trials described below comparing IMRT and chemotherapy vs. PT and concurrent chemotherapy for locally advanced non-small cell lung cancer (NSCLC).

19.3 Levels of Evidence

Why should clinical trials with ion beams be of interest? Why should their results be considered the "best" or most sought-after form of evidence for decision making in patient care?

The goal of best practice in medicine is to use the evidence that is most applicable to the patient to be treated. "Evidence-based medicine" has become an easily articulated goal but a rarely realized element in the care of patients. The fact is that treatment decisions are always made on more fragmentary evidence than

the physician might wish. Even if a particular patient has a disease in a stage of development that has been addressed by a clinical trial, the evidence from that trial only applies in part to that patient because of differences in age, history of other diseases, comorbid conditions, and other factors.

Numerous hierarchies of evidence have been proposed [8–14]. Most of them require randomized comparative trials to reach the highest level of evidence. In some hierarchies, a meta-analysis of prospective trials is considered the most compelling form of evidence. Nowhere in these rankings is consideration given to the types of evidence that often drive decision making in the treatment of patients with RT. Such evidence may be found on computer screens that display the individual patient's anatomy, usually a computed tomography (CT) scan and radiation beams that have been measured and entered into a computerized treatment planning system. Tepper [15] has contended that radiation treatment plans are models of clinical reality, but are not actual reality. However, hundreds of thousands of patients receive RT based on such plans every year. Where does such evidence rank in the hierarchy?

It is rare for treatment planning to be backed by clinical trials. In part, this is because clinical trials take years to be conceived and completed, whereas treatment-planning systems appear abruptly from vendors and can be adopted within months. Three-dimensional conformal radiation therapy (3D-CRT) was in wide use before the results of the first clinical trial were published [16, 17]. That trial addressed the question of whether higher total doses were of value for treatment of adenocarcinoma of the prostate. However, that trial was based on an initial treatment of all patients with a 2D-planned, 4-field box irradiation of the pelvis, with the dose then escalated to "tolerance" with either a reduced 2D box vs. an 11% higher total dose with 3D-CRT. Three additional trials were conducted comparing 3D-CRT to the then-conventional 2D treatment [18–20]. As the radiation oncology community moved to using IMRT in the late 1990s and early 2000s, the treatment plans themselves formed fairly compelling evidence of the superiority of IMRT. To date, no randomized comparison has been made between 3D-CRT and IMRT, although data have been published regarding the ability of IMRT to spare normal tissues [21, 22] and to escalate the total dose without increasing adverse effects in surrounding normal tissues [23, 24].

19.4 Clinical PT Trials

Thus far, no randomized prospective comparisons of proton beam therapy with X-rays – either 3D-CRT or IMRT – have been undertaken. The closest approximation of such a comparison has come from two studies conducted by investigators from the Massachusetts General Hospital (MGH) using the proton beams at the Harvard Cyclotron Laboratory (HCL) and at Loma Linda University Medical Center (LLUMC). Both trials asked a dose-escalation question, and neither compared protons alone with photons. The first trial compared a photon boost after large-field photon irradiation to the pelvis with a higher dose delivered with protons [25].

The second trial compared two levels of proton boost after large-field photon irradiation (total doses 70.2 GyE vs. 79.2 GyE) [24]. These studies confirmed better tumor control with the higher total doses. Talcott reported the quality of life (as reported by the patients) 8.3 years after treatment [26]. No differences in urinary, bowel, or sexual dysfunction were found between the two treatment arms in spite of the dose escalation.

IMRT is considered the current "state of the art" in external irradiation with photons for carcinoma of the prostate. Calls for a randomized comparison of IMRT with PT for this purpose [27] fail to recognize the requirements of such trials; there is no compelling hypothesis that can be addressed with meaningful endpoints. The major difference between the treatment arms could be second malignant tumors associated with IMRT, especially in the large regions exposed to low doses, that would perhaps occur many years after treatment [28]. Investigators and funding agencies are naturally reluctant to use such a long-term endpoint.

By contrast, NSCLC represents a disease for which comparisons of photons and protons would be favorable. Clinical stage III NSCLC that is locally advanced and unresectable is quite common and is difficult to control with the total radiation doses used in most clinical trials to date [29, 30]. The standard of care at present, based on findings from multiple trials from the United States, Japan, and Europe, is concurrent chemotherapy and RT [30–33]. Preliminary studies of protons delivered with concurrent chemotherapy [34, 35] showed that total doses considerably higher than traditional could be achieved; doses considered to be the maximum tolerated with 3D-CRT using X-rays (74 Gy in 37 fractions) [36].

19.5 Clinical Trials with Protons and Carbon Ions

The design and implementation of clinical trials involving carbon ions and protons have been considerably different from trials involving photons. Phase I trials of dose escalation are appropriate for both particles. Such studies have been carried out with carbon ions at the National Institute of Radiological Sciences (NIRS), which opened in Chiba, Japan, in 1994. Investigators there pursued studies for carcinoma of the prostate [37] and cervix [38]. As might be expected from the nature of RT toxicities, acute effects were minimal. However, severe gastrointestinal late effects were observed that led to detailed evaluations and alterations of the techniques (cf. Chaps. 15 and 36 for details). Notably, these trials were conducted before the use of concurrent chemotherapy plus RT became the treatment standard for carcinoma of the cervix. Moreover, intracavitary applications of radioactive sources were apparently not used.

By February 2010, approx. 5,200 patients had been treated with carbon ion radiotherapy (CIRT) at NIRS (cf. Chap. 36 for details), nearly half of whom for carcinoma of the prostate, lung, or head and neck. Increasing emphasis has been placed on reducing the numbers of fractions, and few if any of these patients received concurrent chemotherapy.

CIRT has also been explored at the Gesellschaft für Schwerionenforschung (GSI) in Darmstadt, Germany, which began treatments in 1997. Findings from a clinical trial of postoperative CIRT for chordomas of the base of the skull conducted there have been considered encouraging ([39, 40] and Chap. 12). Other trials of CIRT or PT for skull base tumors conducted elsewhere have also produced encouraging results [41–44]. The Hyogo Ion Beam Medical Center (HIBMC) in Japan, which offers both PT and CIRT, has reported using carbon ions to treat a variety of radioresistant tumors, including those of the head and neck, melanoma, lung, and liver [45]. A randomized comparison of PT vs. CIRT is being discussed for the Heidelberg Ion Therapy Center (HIT), the clinically integrated successor of the work at GSI. Comparisons between proton and carbon ions are expected to be a main part of the research agenda as carbon ion facilities are developed in Europe [46].

Grutters and colleagues in Maastricht, The Netherlands, published a "meta-analysis" of observational studies comparing the use of ion beams and X-rays for NSCLC [47]. This analysis compared results with photons, given as either 3D-CRT or stereotactic body radiation therapy (SBRT), with those from protons and carbon ions; none of the studies analyzed was a randomized comparison with particles. The endpoints were survival at 2 and 5 years rather than local tumor control, and the vast majority of the patients had stage I tumors. Ions seemed to be equal or superior to photons, with SBRT having the most unfavorable toxicity profile.

The greatest concern with the use of carbon ions comes from their putatively greatest advantage, namely their relative biological effectiveness (RBE), which at approximately 3 is similar to that of fast neutrons. A major research effort with neutron therapy in the United States was mounted between the mid-1970s and the late 1980s. Emphasis was placed on treatment of carcinoma of the prostate, cervix, head and neck as well as salivary gland tumors. The disturbing conclusions reached by most of the participating investigators were that the effects on normal tissues, especially late effects, were more severe than had been predicted by the radiobiological models that had been developed. Moreover, the adverse normal tissue effects seemed to suggest different RBEs for different types of normal tissue, especially those tissues with higher fat content. These experiences have led to a great deal of caution regarding CIRT in the United States as compared to Japan and Europe.

19.6 Design Strategies for Clinical Trials

Conceptually, the strategies for investigations on IBT are almost limitless. Some obvious ones include the following:

1. *Dose escalation*. Because control rates for most epithelial tumors and sarcomas are far lower than desired, strategies to escalate or intensify the doses are warranted. The hypothesis in such a strategy is that a higher dose will control more tumors.

2. *Altered fractionation*. Strategies to manipulate fractionation are mostly directed at reducing the overall number of treatments by giving fewer fractions of larger size (hypofractionation) without having an increase in adverse effects. This has been the prevailing strategy for treating a wide variety of cancer sites at the NIRS (cf. Chaps. 14 and 36). However, the hypothesis could be advanced that using particles with smaller fractions, perhaps to much higher total doses, could achieve even more sparing of normal tissues.
3. *Reducing acute and especially late effects on normal tissues*. This strategy is mostly directed at avoiding irradiation of organs at risk such as bowel, normal lung, esophagus, heart (especially valves and coronary arteries), critical portions of the brain, and even bones and soft tissues in children. Reducing the risk of second malignant tumors is most relevant to the treatment of children, but it also has relevance for men with cancer of the prostate.
4. *Integrating IBT with chemotherapy*. The hypotheses to be tested in this strategy include the following: (a) PT in combination with concurrent chemotherapy will reduce acute toxicity with the same or even increased tumor control; (b) increased radiation doses, either with standard or large fractions, can be used with concurrent chemotherapy to achieve increased tumor control and survival; and (c) increased doses of chemotherapy can be given with PT since organs at risk can be avoided and even effects on the bone marrow can be lessened.
5. *Integrating IBT with surgical resection*. Pre- and postoperative RTs are often used or at least considered in the treatment of many types of tumors. Avoidance of normal tissues can mitigate the adverse effects of this combination of modalities.
6. *IBT as a supplement or "boost" after wider field irradiation with photons*. This was the strategy pursued in both of the dose-escalation studies for carcinoma of the prostate between MGH and LLUMC [24, 25].

Variations on these themes are legion. For example, the different ions can be compared with each other or with photons for any number of disease sites. Dose escalation and altered fractionation can take many forms.

19.7 Equipoise and the Ethics of Clinical Investigations of Ion Beams

Equipoise is a term that has become popular in discussing clinical trials in recent years. It simply means balance. In the context of prospective comparative investigations, it has come to mean the equivalence of two or more proposed treatment arms [48, 49]. However, investigators in oncology are rarely interested in equivalence. Rather, they are interested in improving outcome with a new regimen relative to standard treatment. The equipoise assumption claims that the new regimen will give results that are at least as good as the standard treatment and, according to the hypothesis being tested, better results.

The only investigations actively being discussed in the United States where equivalence is being considered important are those pertaining to carcinoma of the prostate. There are widely diverging views about the effectiveness of various treatments, or even no treatment at all. Some contend that no radiation treatment has ever been proven superior to "watchful waiting" (i.e., no treatment) when survival is used as the endpoint. Those who hold this position discount a study of radical prostatectomy vs. watchful waiting conducted by the Scandinavian Prostate Cancer Group [50]. Coupled with conclusions from consensus conferences that RT and radical prostatectomy produce similar outcomes, the findings from the Scandinavian study are relevant to the discussion of watchful waiting vs. RT. Additional support comes from a study of surrogate endpoints for prostate cancer survival from the Radiation Therapy Oncology Group (RTOG) protocol 92-02 [51], in which men with locally advanced prostate cancer were treated with 4 months of neoadjuvant and concurrent androgen deprivation therapy with external-beam RT, followed by either no additional treatment or 24 additional months of androgen deprivation. Most investigators and most patients wish to pursue treatment that has the possibility of eliminating clinical evidence of prostatic cancer, which is usually measured in the short run by "freedom from biochemical failure" (i.e., a prostate-specific antigen level that does not rise over time). The driving force behind the "no treatment" approach is cost. The fact that IBT or even IMRT costs more than not treating has motivated some to advocate clinical investigations that address the hypothesis that treatment of prostate cancer will result in better survival than no treatment. Of course, the problem is that the usually indolent nature of cancer of the prostate requires years or even decades of observation to get the answer. Most men who present for treatment have little inclination toward observation alone.

At the other extreme of the concept of equivalence is cancer in children. Few would doubt the value of avoiding normal structures if RT is indicated for a child. Indeed, the long-term effects of RT on children have been a driving force behind eliminating RT for many types of childhood cancer. PT is uniquely able to avoid normal structures, including growing bone and muscle. Medulloblastoma is an important childhood tumor that in most cases appears in children less than 10 years old. The long-term consequences of craniospinal irradiation with X-rays are well known and at least two-thirds of children so treated are expected to live 10 years or more. PT can spare normal tissues to a greater degree than can X-rays or electrons [52]. In spite of high initial costs, PT has been estimated to be cost-saving when considered over the life of the patient [53–55]. In this case, there is no equipoise and a clinical trial of protons vs. X-rays would seem unethical [56].

19.8 Mechanisms for Clinical Investigations of IBT

Clinical investigations of IBT have generally been carried out by single institutions or at most two centers (e.g., MGH and LLUMC, or M.D. Anderson Cancer Center). Eventually, multi-institutional cooperative groups studying IBT could be

envisioned. Existing cooperative groups such as the RTOG are funded in part by national agencies. It is not clear when these agencies, which are largely committed to studies of drugs and biological agents, will have any enthusiasm for studies of advanced radiation technology, including therapy with ions.

A new cooperative group could be formed, but the source of funding for such a group is not clear. Ideally, it would be international, given the added complexities that apply. Credentialing of participating centers would be essential, but the mechanisms to do this are available.

19.9 Summary

Clinical investigations of IBT represent a new challenge. Although IBT is used as a form of local–regional treatment for cancer, the potential for it to be integrated with other forms of systemic cancer treatment is great. Defining the credentials needed, hypotheses to be addressed, and the mechanisms by which clinical trials with IBT can be undertaken are all important steps for the future of radiation oncology.

References

1. S.J. Nass, H.L. Moses, J. Mendelsohn (eds.), *A National Cancer Clinical Trials System for the 21st Century: Reinvigorating the NCI Cooperative Group Program* (National Academies, Washington, DC, April 2010). http://books.nap.edu/catalog/12879.html
2. J.P. Grutters, M. Pijls-Johannesma, D.D. Ruysscher, et al., The cost-effectiveness of particle therapy in non-small cell lung cancer: exploring decision uncertainty and areas for future research. Cancer Treat. Rev. **36**, 468–476 (2010)
3. M. Brada, M. Pijls-Johannesma, D. De Ruysscher, Proton therapy in clinical practice: current clinical evidence. Cancer J. **15**, 319–324 (2009)
4. M.D. Wang, Sample size reestimation by Bayesian prediction. Biomet. J. **49**, 365–377 (2007)
5. P.F. Thall, J.D. Cook, E.H. Estey, Adaptive dose selection using efficacy-toxicity trade-offs: illustrations and practical considerations. J. Biopharm. Stat. **16**, 623–638 (2006)
6. I. Turesson, The progression rate of late radiation effects in normal tissue and its impact on dose-response relationships. Radiother. Oncol. **15**, 217–226 (1989)
7. J.D. Fontenot, A.K. Lee, W.D. Newhauser, Risk of secondary malignant neoplasms from proton therapy and intensity-modulated X-ray therapy for early-stage prostate cancer. Int. J. Radiat. Oncol. Biol. Phys. **74**, 616–622 (2009)
8. R.E. Upshur, The ethics of alpha: reflections on statistics, evidence and values in medicine. Theor. Med. Bioeth. **22**, 565–576 (2001)
9. G. Guyatt, R. Drummond, Part 1. The Basics: Using the Medical Literature. 1A. Introduction: The Philosophy of Evidence-Based Medicine, in *Users' Guides to the Medical Literature: A Manual for Evidence-Based Clinical Practice*, ed. by G. Guyatt, R. Drummond. (American Medical Association, Chicago, 2002), pp. 3–12
10. S. West, V. King, T.S. Carey, et al., *Systems to Rate the Strength of Scientific Evidence* (Agency for Healthcare Research and Quality, AHRQ publication 02-E016, Rockville, MD, 2002), pp. 64–88

11. R. Harbour, J. Miller, A new system for grading recommendations in evidence based guidelines. Br. Med. J. **323**, 334–336 (2001)
12. B. Phillips, C. Ball, D. Sackett, et al, *Levels of Evidence and Grades of Recommendations* (Oxford Centre for Evidence-Based Medicine, Oxford, England). Available at: http://www.cebm.net/index.aspx?o=1025. Accessed 4 Jun 2010
13. D. Atkins, D. Best, P.A. Briss, et al, Grading quality of evidence and strength of recommendations. Br. Med. J. **328**, 1490 (2004)
14. V.M. Montori, G.H. Guyatt, Progress in evidence-based medicine. J. Am. Med. Assoc. **300**, 1814–1816 (2008)
15. J.E. Tepper, Protons and parachutes. J. Clin. Oncol. **26**, 2436–2437 (2008)
16. A. Pollack, G.K. Zagars, G. Starkschall, et al., Prostate cancer radiation dose response: results of the M.D. Anderson phase III randomized trial. Int. J. Radiat. Oncol. Biol. Phys. **53**, 1097–1105 (2002)
17. D.A. Kuban, S.L. Tucker, L. Dong, et al., Long-term results of the M. D. Anderson randomized dose-escalation trial for prostate cancer. Int. J. Radiat. Oncol. Biol. Phys. **70**, 67–74 (2008)
18. D.P. Dearnaley, V.S. Khoo, A.R. Norman, et al., Comparison of radiation side-effects of conformal and conventional radiotherapy in prostate cancer: a randomised trial. Lancet **353**, 267–272 (1999)
19. J. Michalski, J.A. Purdy, K. Winter, et al., Preliminary report of toxicity following 3D radiation therapy for prostate cancer on 3DOG/RTOG 9406. Int. J. Radiat. Oncol. Biol. Phys. **46**, 391–402 (2000)
20. E.K. Yeoh, R.H. Holloway, R.J. Fraser, et al., Anorectal function after three- versus two-dimensional radiation therapy for carcinoma of the prostate. Int. J. Radiat. Oncol. Biol. Phys. **73**, 46–52 (2009)
21. K.S. Chao, J.O. Deasy, J. Markman, et al., A prospective study of salivary function sparing in patients with head-and-neck cancers receiving intensity-modulated or three-dimensional radiation therapy: initial results. Int. J. Radiat. Oncol. Biol. Phys. **49**, 907–916 (2001)
22. C.M. Nutting, D.J. Convery, V.P. Cosgrove, et al., Reduction of small and large bowel irradiation using an optimized intensity-modulated pelvic radiotherapy technique in patients with prostate cancer. Int. J. Radiat. Oncol. Biol. Phys. **48**, 649–656 (2000)
23. M.J. Zelefsky, Z.V. Fuks, M. Hunt, et al., High dose intensity modulated radiation therapy for prostate cancer: early toxicity and biochemical outcome in 772 patients. Int. J. Radiat. Oncol. Biol. Phys. **53**, 1111–1116 (2002)
24. A.L. Zietman, M.L. DeSilvio, J.D. Slater, et al., Comparison of conventional-dose vs high-dose conformal radiation therapy in clinically localized adenocarcinoma of the prostate. J. Am. Med. Assoc. **294,** 1233–1239 (2005)
25. W.U. Shipley, L.J. Verhey, J.E. Munzenrider, et al., Advanced prostate cancer: the results of a randomized comparative trial of high dose irradiation boosting with conformal protons compared with conventional dose irradiation using photons alone. Int. J. Radiat. Oncol. Biol. Phys. **32**, 3–12 (1995)
26. J.A. Talcott, C. Rossi, W.U. Shipley, et al., Patient-reported long-term outcomes after conventional and high-dose combined proton and photon radiation for early prostate cancer. J. Am. Med. Assoc. **303**, 1046–1053 (2010)
27. P.L. Nguyen, A. Trofimov, A.L. Zietman, Proton-beam vs intensity-modulated radiation therapy: which is best for treating prostate cancer? Oncology **22**, 748–754, discussion 754, 757 (2008)
28. D.J. Brenner, R.E. Curtis, E.J. Hall, et al., Second malignancies in prostate carcinoma patients after radiotherapy compared with surgery. Cancer **88**, 398–406 (2000)
29. W.J. Curran Jr., Evolving chemoradiation treatment strategies for locally advanced non-small-cell lung cancer. Oncology **17**(Suppl 13), S7–S14 (2003)
30. W.J. Curran Jr, R. Paulus, C.J. Langer, et al., Sequential vs concurrent chemoradiation for stage III non-small cell lung cancer: randomized phase III trial RTOG 9410. J. Natl. Cancer Inst. 8 September 2011 (epub ahead of print)

31. K. Furuse, M. Fukuoka, M. Kawahara, et al., Phase III study of concurrent versus sequential thoracic radiotherapy in combination with mitomycin, vindesine, and cisplatin in unresectable stage III non-small cell lung cancer. J. Clin. Oncol. **17**, 2692–2699 (1999)
32. P. Zatloukal, L. Petruzelka, M. Zemanova, et al., Concurrent versus sequential chemoradiotherapy with cisplatin and vinorelbine in locally advanced non-small cell lung cancer: a randomized study. Lung Cancer **46**, 87–98 (2004)
33. R.M. Huber, M. Flentje, M. Schmidt, et al., Simultaneous chemotherapy compared with radiotherapy alone after induction chemotherapy in inoperable stage IIIA or IIIB non-small cell lung cancer: study CTRT99/97 by the Bronchial Carcinoma Therapy Group. J. Clin. Oncol. **24**, 4397–4404 (2006)
34. Z. Liao, R. Komaki, H.D. Thames, et al., Influence of technological advances on outcomes in patients with unresectable, locally advanced non-small cell lung cancer receiving concomitant chemoradiotherapy. Int. J. Radiat. Oncol. Biol. Phys. **76**, 775–781 (2010)
35. S. Sjpal, R. Komaki, A. Tsao, et al., Early findings on toxicity of proton beam therapy with concurrent chemotherapy for nonsmall cell lung cancer. Cancer **117**, 3004–3013 (2011)
36. J.D. Bradley, J. Moughan, M.V. Graham, et al., A phase I/II radiation dose escalation study with concurrent chemotherapy for patients with inoperable stages I to III non-small-cell lung cancer: phase I results of RTOG 0117. Int. J. Radiat. Oncol. Biol. Phys. **77**, 367–372 (2010)
37. K. Akakura, H. Tsujii, S. Morita, et al, For the Working Group for Genitourinary Tumors, National Institute of Radiological Sciences. Phase I/II clinical trials of carbon ion therapy for prostate cancer. Prostate **58**, 252–258 (2004)
38. S. Kato, T. Ohno, H. Tsujii, et al, for the Working Group of the Gynecological Tumor. Dose escalation study of carbon ion radiotherapy for locally advanced carcinoma of the uterine cervix. Int. J. Radiat. Oncol. Biol. Phys. **65**, 388–397 (2006)
39. D. Schulz-Ertner, A. Nikoghosyan, B. Didinger, J. Debus, Carbon ion radiation therapy for chordomas and low grade chondrosarcomas -current status of the clinical trials at GSI. Radiother. Oncol. **73**(Suppl 2), S53–S56 (2004)
40. S.E. Combs, C. Hartmann, A. Nikoghosyan, et al., Carbon ion radiation therapy for high-risk meningiomas. Radiother. Oncol. **95**, 54–59 (2010)
41. S. Takahashi, T. Kawase, K. Yoshida, et al., Skull base chordomas: efficacy of surgery followed by carbon ion radiotherapy. Acta Neurochir. (Wien) **151**, 759–769 (2009)
42. J.E. Mizoe, A. Hasegawa, R. Takagi, et al., Carbon ion radiotherapy for skull base chordoma. Skull Base **19**, 219–224 (2009)
43. O. Gudjonsson, E. Blomquist, G. Nyberg, et al., Stereotactic irradiation of skull base meningiomas with high energy protons. Acta Neurochir. (Wien) **141**, 933–940 (1999)
44. F.J. Vernimmen, J.K. Harris, J.A. Wilson, et al., Stereotactic proton beam therapy of skull base meningiomas, Int. J. Radiat. Oncol. Biol. Phys. **49**, 99–105 (2001)
45. Y. Hishikawa, Y. Oda, H. Mayahara, et al., Status of the clinical work at Hyogo. Radiother. Oncol. **73**(Suppl 2), S38–S40 (2004)
46. B. Jones, Joint symposium 2009 on carbon ion radiotherapy. Br. J. Radiol. **82**, 884–889 (2009)
47. J.P.C. Grutters, A.G.H. Kessels, M. Pijls-Johannesma, et al., Comparison of the effectiveness of radiotherapy with photons, protons, and carbon ions for non-small cell lung cancer: a meta-analysis. Radiother. Oncol. **95**, 32–40 (2010)
48. B. Freedman, Equipoise and the ethics of clinical research. N. Engl. J. Med. **317**, 141–145 (1987)
49. R.J. Lilford, J. Jackson, Equipoise and the ethics of randomization. J. Roy. Soc. Med. **88**, 552–559 (1995)
50. A. Bill-Axelson, L. Holmberg, M. Ruutu, et al., Radical prostatectomy versus watchful waiting in early prostate cancer. N. Engl. J. Med. **352**,1977–1984 (2005)
51. M.E. Ray, K. Bae, M.H.A. Hussain, et al., Potential surrogate endpoints for prostate cancer survival: analysis of a phase III randomized trial. J. Natl. Cancer Inst. **101**, 228–236 (2009)
52. C.T. Lee, S.D. Bilton, R.M. Famiglietti, et al., Treatment planning with protons for pediatric retinoblastoma, medulloblastoma, and pelvic sarcoma: how do protons compare with other conformal techniques? Int. J. Radiat. Oncol. Biol. Phys. **63**, 362–372 (2005)

53. J. Lundkvist, M. Ekman, S.R. Ericsson, et al., Proton therapy of cancer: potential clinical advantages and cost-effectiveness. Acta Oncol. **44**, 850–861 (2005)
54. J. Lundkvist, M. Ekman, S.R. Ericsson, et al., Cost-effectiveness of proton radiation in the treatment of childhood medulloblastoma. Cancer **103**, 793–801 (2005)
55. J. Lundkvist, M. Ekman, S.R. Ericsson, et al., Economic evaluation of proton radiation therapy in the treatment of breast cancer. Radiother. Oncol. **75**,179–185 (2005)
56. M. Goitein, J.D. Cox, Should randomized clinical trials be required for proton radiotherapy? J. Clin. Oncol. **26**, 175–176 (2008)

Part V
Medical Accelerators and Beam Line Design

Chapter 20
Design Criteria for Medical Accelerators

Hartmut Eickhoff, Udo Weinrich, and Jose Alonso

Abstract Beam and facility requirements for effectively treating patients with ion beams are presented, and their implications on accelerator specifications discussed. Suitability and constraints of different accelerator types are addressed. The chapter concludes with a design example of a synchrotron-based therapy facility, and presents some new concepts being studied for possible applications in medical therapy.

20.1 Introduction

Radiation therapy with beams of protons and heavier ions has reached the stage where intensive clinical research must be performed to develop protocols for the best application of this modality for the treatment of cancer and other lesions. Results from many years of research, both clinical and radiobiological, and many thousands of patients treated have demonstrated the effectiveness of the dose localization abilities of these beams, and have taken advantage of benefits from high-LET radiation.

Within the last years several clinical facilities, both for proton and ion treatment, have been constructed and operated mainly in Asia, Europe, and the United States [1]; other facilities are close to the operation phase [2]. Two primary goals have to be fulfilled at such facilities: they should permit the treatment of large numbers of patients easily and efficiently to accrue statistics and develop the necessary protocols; and they should assist in the development of the best possible beam delivery technology to take maximum advantage of the properties of ion beams in clinical practice.

H. Eickhoff (✉)
GSI Helmholtzzentrum für Schwerionenforschung, Planckstraße 1, 64291 Darmstadt, Germany
e-mail: h.eickhoff@gsi.de

U. Linz (ed.), *Ion Beam Therapy*, Biological and Medical Physics, Biomedical Engineering, DOI 10.1007/978-3-642-21414-1_20,

To accomplish these goals efficiently, careful attention must be paid to the specifications for the performance of the technical components of the treatment facility, including the accelerator, beam delivery, and patient handling system.

Very important is the order in which these specifications are determined: first, there must be the requirements for clinical performance; second, the beam delivery system that will meet these requirements; and, finally, the accelerator that will provide beams tailored to the specified beam delivery system.

20.2 Clinical Specifications

The basic aim of ion beam therapy (IBT) is to be able to place stopping particles in any point of the body, and so to define a treatment volume that conforms as closely as possible to the generally irregular, three-dimensional shape of the diseased tissue to be treated, while keeping the dose to adjacent normal tissue to its lowest possible value. A maximum range of roughly 30 cm in tissue is expected to be able to handle over 95% of the desired treatment plans. While shallow-penetration beams can be obtained by simply degrading the energy of the beam, such degrading if not done properly can spoil the good properties of the beam, losing the precision that is most likely required for these shallow-field treatments, such as for ocular melanomas. Achieving shallow ranges, then, must be accomplished without loss of beam quality (Table 20.1).

Precision in setting the distal extent of the field relates to the accuracy of setting the beam energy. From an accelerator standpoint achieving this accuracy is not a problem, typical accelerator energy resolution and energy control is of the order of 0.1% or better. However, it is more critical to know accurately the density of the material to be traversed to reach this stopping point. This accuracy must emerge from the treatment planning process which must include the translation of CT numbers from patient scans to electron density and the careful accounting for thickness of material traversed. The energy (range) changes or depth steps called for should be related to the natural thickness of the Bragg peak and expected depth dimension of the voxels that would be used in the planning and delivery of treatment.

Table 20.1 Basic clinical specifications (based on Chu et al. [3])

Parameter	Desired specification
Average dose rate	1 Gy/min for a $25 \times 25\,cm^2$ field
Time structure of the beam	Suitable for beam scanning
Dose accuracy	$\pm 2\%$
Range of penetration	2–30 cm
Precision in range setting	0.1 cm
Maximum field size in a fixed-beam room	25×25 cm
Sharpness of distal dose fall-off	0.1 cm above limit (set by range straggling)
Sharpness of lateral penumbra	0.2 cm

As these range changes will occur many times during the treatment, beam-energy changes – either by degrading and cleanup or changing accelerator energy – must be performed efficiently to not add significantly to the treatment time.

The desire of the clinicians is to complete a treatment in the shortest possible time, commensurate with accuracy and safety. Typical times for treatment should be less than 2 min for most fields, which will probably be treated to a dose of around 2 Gy. This of course directly translates to the required beam current from the accelerator. The shape of the treatment volume – and particularly the maximum depth – affects the treatment time and must also be folded into the beam current specifications to minimize treatment times.

The beam time structure is a critical issue which places great constraints on the accelerator parameters and performance. The basic requirement is that the ability to scan the beam across the treatment field should be minimally restricted or constrained by beam time structure. For instance, if the accelerator produces very short pulses with a very low duty factor (e.g., few milliseconds of beam at a 10 Hz rate) one will not be able to move the beam continuously across the field unless the sweep rate is very slow, less than a few beam widths per second. On the other hand, for accelerators that deliver long-duty-factor beams the critical element is not the macroscopic duty factor, but the need to control the intensity of the beam on both long and very short time scales during the period the beam is coming to the treatment room. For instance, if there are sharp irregular spikes in the beam, it will be difficult to control and prevent dose inhomogeneities in the field.

Clinical dose–response data indicate that 5% changes in dose represent about the smallest increment for which a clinical effect can be detected. This sets the allowed tolerance on both differential and integral dose accuracy across the treatment field for compliance with the treatment plan. This regards accuracy of the dose-measuring instrumentation, and control over placement of particles at all coordinates of the treatment field. For the simplest passive beam delivery systems, the requirements are verification of dose uniformity across the field and cut-off when the prescribed dose is reached. For scanning systems, in which the actual dose delivered to each voxel of the treatment field is monitored and controlled, greater accuracy is required to ensure each element receives the proper dose.

The dose accuracy specifications relate to the required precision of the calibration procedures and measurements themselves, as well as to the linearity and stability of the dosimetry instruments employed. The dose detected by an ionization chamber in the nozzle upstream of the patient will be different from what actually is delivered to the relevant voxel in the patient, owing to different energy and particle density profiles at the two locations. Consequently, measurements in the upstream chamber are normally referred to as “monitoring units” rather than “doses.” The relationship between ion chamber reading and actual dose delivered is first determined by a calibration run using a thimble chamber or other standard dosimeter placed at the appropriate depth for each voxel in a water phantom. A measurement of the response of the ion chamber versus the dose delivered to the standard chamber establishes the ratio between “dose” to the voxel and “monitoring unit” read in the upstream ion chamber. This procedure, with the standard chamber moved to the position of

every voxel in the treatment volume, establishes the proper calibration matrix for the entire treatment. With enough measurements, a model can be developed for this calibration matrix, so that a full calibration run for every treatment field becomes unnecessary.

20.3 Technical Design Criteria for Medical Accelerators

An accelerator complex for IBT in a clinical environment must meet several criteria that affect the quality of patient treatment, patient safety, cost, and operational efficiency among others.

20.3.1 Accelerator and Beam Delivery System

The first design decision for such a facility is the accelerator technology to be used which is, of course, influenced by the ion species to be accelerated and the maximum energy required. For protons with a range up to 30 cm in tissue energy of about 220 MeV is required; for carbon ions with the same range an energy of 425 MeV/u is needed. The three major types of accelerators are:

- Linear accelerators (linacs)
- Cyclotrons
- Synchrotrons combined with a low energy linac as an injector

It could be noted that 220 MeV for protons can be conveniently reached with linacs, cyclotrons, or synchrotrons. However, the high rigidity of ion beams, 6.6 Tm in our 425 MeV/u example (with charge/mass ratio $Q/A = 0.5$), presents a challenge for cyclotron designers. Synchrotrons, on the other hand, lend themselves to an easy match for required light-ion performance parameters.

The accelerator performance must be matched to the delivery system selected for the facility, which will optimally place stopping particles in an arbitrarily shaped three-dimensional volume. Best candidates today are the raster scanner employing a small beam spot and tight control over the scanner sweep velocity and beam current and the voxel scanning system which places a planned dose at each coordinate in the field (see Chap. 25 for details). An alternative approach is the range-stacking technique, with a passive scattering or wobbling system for beam spreading and a multileaf collimator to shape the field at each depth slice [4].

The performance specifications discussed below are matched to the needs of these three delivery systems. The discussion will be kept general, to include accelerators suitable for both protons and heavier ions, and, although problems with particular accelerator technologies will be mentioned, particular judgments as to the suitability of accelerator types will be kept to a minimum.

Early work with ion beams was all done with static, mostly horizontal beam lines, whereas nowadays most treatment rooms for facilities using proton beams are equipped with a rotating beam line or gantry, providing considerable additional flexibility to the irradiation. By being able to keep the patient in a supine position for treatment, which corresponds to the orientation of the patient in CT and MRI scanners, one enables treatment planning utilizing the all-important diagnostic images. Much of the cost and technological challenge in bringing ion beam treatments into the realm of practicality have revolved around the development of effective, inexpensive, and practical gantry systems.

20.3.2 Beam Energy

To achieve the required range of approx. 30 cm in tissue with a passive treatment modality, the maximum energy of the beam from the accelerator must be increased (about 25 MeV/u) to compensate for energy loss in material placed in front of the patient such as scattering systems, dosimetry devices, range modulators, and compensators. Active scanning systems are less burdensome in this regard, as there is substantially less material in the beam. The amount of material required for scattering depends on the scattering angle, determined by the maximum field size and the source-to-axis distance (SAD) related to the space between the end of the gantry and the patient, and so to the gantry dimensions.

If possible, the top energy of the accelerator should be designed to be at least 10% higher than the planned longest range. This is easier for some accelerator types (synchrotrons, linacs) than for others (cyclotrons). The maximum energy for a light ion machine is closely related to the heaviest ion that will be used for treatments, and whether this particle must penetrate to the maximum depth. So while 425 MeV/u will yield a 30-cm range carbon beam, a neon beam would need to have 590 MeV/u to achieve the same range.

20.3.3 Beam Energy Variation

In the early days of IBT, when beam energy changes were difficult or impossible to accomplish with the accelerator, a fixed-energy beam was transported to the treatment area, this energy establishing the longest range achievable. This allowed for a standard tune for the accelerator and beam transport lines, a great convenience considering that it took an hour or more to tune and characterize the beam for the day's treatments. Energy (range) was adjusted inside the treatment room via degraders or "water columns" for each treatment. While accomplishing the desired range adjustment, this came at the expense of beam quality due to multiple scattering and range straggling, and the nuclear reactions accompanying the amounts of material in the beam produced a neutron background, which while not overly large

still contributed to the whole-body dose of the patient under treatment. Technology has advanced to where today this method of delivering beam and modulating energy is viewed as the least desirable of available options.

With fixed-energy machines (cyclotrons), a degrading system incorporating an energy spectrometer located in the beam line between the accelerator and the treatment areas can provide rapid and very precise energy changes, with collimators performing the energy selection and masking out the effects of beam spreading from multiple scattering. This technique is accompanied by a substantial loss of beam, ultimately activating material in the beam transport hall. But by increasing the output current from the cyclotron one can maintain the required dose rate.

Synchrotrons are capable of pulse-to-pulse energy variation, and by programming the transport line magnets to track the extraction field one can preserve excellent beam quality over the full required range of beam energies. Modern day control systems make this mode of operation quite routine.

With regard to the energy spread of the primary beam, all accelerators used in therapy extract beams of very high quality, $\Delta E/E < 0.1\%$ typically. The width of the Bragg peak, however, is determined by the range straggling of the beam as it slows in tissue, not by the inherent energy spread from the accelerator or the energy-selection system used.

20.3.4 Lateral Beam Quality

As is the case with the energy spread, the typical emittance of beams coming directly from the accelerator or energy-selection spectrometer is very small, and contributes only little to the lateral penumbra (dose falloff at the edge of the field) experienced in the treatment field. The observed penumbra is mainly driven by the type and geometrical arrangement of material upstream of the patient. Hence, the clinical lateral-penumbra specification relates principally to the design and layout of the beam line "nozzle," which contains dosimetry instrumentation and final field-determining hardware, rather than to the accelerator itself.

However, the beam from the accelerator can contribute to lateral penumbra if positional stability of the beam reaching the isocenter is not adequate. In the case of spot scanning, the precision required for the treatment to define the field boundary, and more particularly, to ensure conformity of the dose to the prescription inside the field, will suffer when the beam spot moves at isocenter due to improper extraction tuning, system noise, or ripple.

Acceptable motion of the beam spot at isocenter is ± 1 mm or about 10% of the best beam size. This places great stress on the stability of the magnet elements, and on excellent control over the extraction process from the accelerator. Synchrotron extraction, in particular, can lead to beam sweeping, and pulse-to-pulse variations. Great care must be taken in the design process to control these effects. The stability requirement at the isocenter can be aided by the design of the beam transport systems and beam optics to be as insensitive as possible to beam motion or fluctuations generated by the extraction process.

20.3.5 Beam Intensity and Time Structure

The beam current must be adequate to meet the specification for maximum dose rate of 1 Gy/min for a 25×25 cm field within the Bragg peak region at a depth of 30 cm.

This translates into a proton current reaching the treatment room of approx. 10^{11} protons per second ($\approx$15 nA); or in the case of carbon, about 3×10^9 ions per second. This number is then carried back to specify the performance of the accelerator and ultimately the ion source, folding in duty factor, as well as energy selection, transport and acceleration efficiencies.

These beam currents can be met by any of the accelerator technologies: linacs and cyclotrons typically produce beam currents in the microampere rather than the nanoampere range, while slow-cycling synchrotrons, which are preferred for their long spills, can reach the 15-nA figure of the requisite characteristics provided care is taken in the design and optimization of accelerator parameters.

Duty factor refers to the fraction of time the beam is on. This can be divided into two basic regimes: macroscopic and microscopic. The dividing line between "micro" and "macro" occurs somewhere between the millisecond and microsecond time scale, so megahertz and higher frequencies are typically considered "microstructure," while lower frequencies will be "macrostructure." The macroscopic nature of the beam can be either CW ("continuous wave" or 100% duty factor) or pulsed. Cyclotron – at least isochronous cyclotron – beams are typically CW, synchrotrons with slow extraction systems produce beams with typically 25–50% duty factor and spills of a few hundred milliseconds to a second or two. Conventional (room temperature) linacs are typically very short-duty-factor machines, beam pulse widths in the microsecond (to millisecond) range, with repetition rates from a few Hertz to a few hundred Hertz. While linacs are normally used for injection into synchrotrons, studies have been done of linacs as energy boosters for cyclotrons. Superconducting linacs offer the possibility of CW beams of protons or ions, but this technology has not yet been considered for medical applications.

The importance of macroscopic duty factor is in the matching of the accelerator with the beam delivery system to be used, particularly, in active (scanning) delivery systems. Passive systems do not sweep the beam across the treatment field, so time structure in the beam is relatively unimportant, except to assure accuracy in cut-off when the desired dose is reached. If the sweep rate of the scanning system is matched to the length of the beam pulse, then a straightforward relationship will exist allowing a painting of the field once per beam spill. A good match exists with the synchrotron spill length of a few hundred milliseconds to a few seconds and scanning rates for magnet systems of conservative design. CW beams place no constraint on the delivery system; beam is simply switched off and on according to the needs of the scanner. Very low-duty-factor machines interface very poorly with a raster-scanning system, sweep rates cannot match a millisecond or shorter pulse, so a short-pulse machine would have to work with a voxel scanner with one or several pulses to be delivered for each voxel. The issue will then be one of control of the

number of particles in each pulse to achieve the required level of dose accuracy per voxel. This is not easy for this type of machine, but a practical system could be designed if the pulse repetition rate were at least 100 Hz to 1 kHz.

Another concern with very short-pulse machines is the high instantaneous dose rate that can lead to saturation of the dose monitoring ion chambers.

Microscopic beam structure is completely unavoidable for any accelerator extracting beam without turning off the RF. The only machine for which this would be possible is the synchrotron, but often even here the RF is left on to provide greater control over the beam during the resonant extraction process. The RF structure ranges from nanoseconds for linacs to tens of nanoseconds for cyclotrons to microseconds for synchrotrons, with pulse trains typically filling only 10% of the time.

The question one must ask is whether this time structure is important for the treatment. From the biological standpoint, effects attributable to accelerator RF structure have not been reported, but it is not clear whether this specific question has really been addressed with adequate experiments. On the physical side, the question is whether this structure will affect the uniformity of a scanned field. One only needs to look at the time between pulses, the distance the beam is swept by the scanning system in this time, and the size of the spot being swept to see that this will or will not be a problem. Fastest sweep rates may approach 1,000 cm/s or 1 cm in a millisecond. If the beam structure is 1 MHz, about 1,000 pulses will strike the target while the beam moves one beam width.

Dose-rate effects could affect ion chamber linearity, hence accuracy of dose measurement, if the current in a very short pulse produces ionization in the chamber gas above a critical density. This might be a concern for very low-repetition-rate systems in which the instantaneous dose in a pulse shorter than 1 ms would be very high. It should be borne in mind and careful calibrations performed to establish that linearity in chamber response is preserved.

20.3.6 Beam Control and Safety Aspects

Very fast beam on–off control is best performed with kickers in the transport line, and does not rely on accelerator response, although most accelerators can easily turn beam off in less than a millisecond. Linear control of the instantaneous beam current is quite difficult with short-pulse linacs, but can be done in a relatively easy fashion with feedback systems for both cyclotrons and synchrotrons.

In the cyclotron, beam current modulation is obtained either by direct control of the ion source, although this is more difficult than the other option: manipulations of the optics in an axial injection line, such as variable transmission through an iris via a rapidly varying focusing or deflecting element. This scheme requires an axial injection line instead of an internal ion source, but such an arrangement has many advantages, in any case.

Linear control for the synchrotron is best obtained by modulating the resonant extraction system parameters, although this is a very sensitive and difficult exercise to perform properly and maintain the desired control over the beam.

Achieving the level of conformation of the dose to the prescribed values at each coordinate in the treatment field requires extremely good control over the dose deposition rate at all times.

Particularly in a scanning system, where the exercise of treating to a prescribed dose is repeated for each coordinate, the presence of uncontrolled beam spikes can be extremely bothersome. Difficult to control, however, is the structure that accompanies resonant extraction in synchrotrons.

Relatively small amount of noise, for example ripple on the magnet power supply, will cause beam to emerge in an uncontrolled fashion bearing the frequency of this noise. Achieving damped feedback response is difficult and proper care is taken in designing the synchrotron and its extraction system. Quiet and controlled spills have been obtained from modern synchrotrons.

System safety requires the ability to rapidly cut-off the beam, either to effect normal termination of the treatment, or to respond to an emergency or detected system abnormality. Following the analysis developed above, cut-off for a scattering system that occurs in a few milliseconds will ensure adequate patient safety, with little chance of patient overdose. For scanning systems, the desired cut-off time is less than 100 μs, to account for a sudden spike at a rate approximately 100 times the normal rate at a voxel. This type of cut-off can be effected by fast magnets (e.g., kicker magnets) in the transport line to divert the beam away from the transport channel, to be followed by clamping of the beam through shut-off of the extraction system, cutting magnet power to a transport magnet, or shutting off the ion source. For the scattering system, the kicker would not be required to ensure proper safety.

20.3.7 Control System

The control system is an essential part of the treatment facility. It must ensure that the beam line instrumentation, beam shaping devices, and positions are all those specified in the patient prescription. While beam is being delivered to the patient, it must monitor and control all the accelerator settings, scanning magnet currents, range adjustments, and a host of other parameters for each increment of time (usually a few milliseconds), and make sure that all these parameters are in compliance with the prescribed treatment plan. It must collect all the data generated by the dosimeters during the treatment and verify that ratios of all measurements are within acceptable limits. It must control the termination of irradiation, either normal termination when desired dose values have been reached, or rapid termination when out-of-range parameters are detected. It must be able to resume the treatment from the point it was prematurely terminated once the problem has been corrected, and deliver the remaining dose to the prescribed accuracy. It must provide archiving services, to keep a record of all parameters associated with each treatment.

Active (scanning) delivery systems present particular challenges for the control systems, because of the very large number of parameters that must be monitored, specified and controlled, including all the dosimetry and beam coordinate parameters, and accelerator settings for beam size, energy, intensity; typically involving major configuration changes on a millisecond time scale.

20.4 Cost Considerations and Availability

Concerning the costs of a medical accelerator system, the following design criteria have to be considered:

- A cost-effective accelerator technology has to be applied that covers the clinical requirements (e.g., ion species, treatment modality, beam delivery systems, number of patients to be treated)
- The facility should be compact to save building costs
- Since high availability is essential, mature and reliable technology is a must

For light ion (e.g., carbon) treatments, the most conservative and proven technology is the normal conducting synchrotron (diameter about 20 m) with a compact injection linac as a preaccelerator. Because of the lower magnetic rigidity for proton beams (about 2.3 Tm for 225 MeV p in comparison to 6.6 Tm for 430 MeV/u C-ions), proton synchrotrons are much smaller and can be realized with diameters of about 7 m. Considering the required space of the building, a cyclotron is even more compact, especially, when superconducting cyclotrons are used. However, it should be noted that in a conventionally laid out facility this would only have a minor effect on saving area, as the beam line, the treatment rooms with gantries and technical infrastructure will occupy most of the area.

Development activities are ongoing for single-room sources of particles, in which the accelerator is located inside the treatment room. Some of these will be addressed later (cf. as well, Chaps. 22 and 39).

The next section will focus on the details of the Heidelberg HIT facility as an example of a modern synchrotron-based facility for treatment with ions and protons [5].

20.5 Design Criteria and Layout of Synchrotron-Based Systems

At present, several hospital-based light ion therapy accelerator facilities are in operation or under construction [2], offering treatments with ions ranging from protons to oxygen. These facilities are all synchrotron-based, and offer advanced beam delivery systems employing raster-scanning or range-stacking techniques.

As an example, Fig. 20.1 shows the accelerator system of the Heidelberg HIT facility. This facility is designed to treat patients with H, He, C, and O

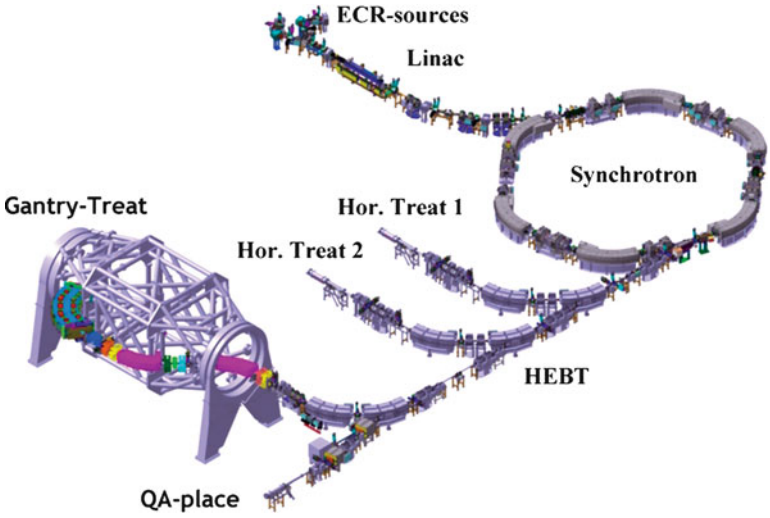

Fig. 20.1 Layout of the HIT facility Abbreviations: *ECR-sources* electron cyclotron resonance ion sources, *HEBT* high-energy beam transport line, *Hor. Treat* treatment room with horizontal beam line, *QA* quality assurance

using intensity-controlled raster scanning in all treatment rooms. For the planned throughput of more than 1,000 patients per year, the facility provides three treatment areas. There are three horizontal beam lines, two for patient treatments and one line for development and quality assurance. In addition, a third treatment room is equipped with an isocentric gantry capable of transporting full-rigidity carbon beams.

Each element of the HIT facility is described in the following sections.

20.5.1 Basic Synchrotron Parameters

The HIT synchrotron has a conventional sixfold symmetric FODO lattice using six large zero-index dipole magnets with maximum fields of 1.5 T. Ring circumference is 65 m, with a single accelerating RF section. Injection energy is 7 MeV/u, corresponding to an injection dipole field of about 0.09 T (for protons), compared to 1.5 T, requested for maximum extracted carbon energy. Multiturn injection provides for stacking of approximately ten turns of beam, reducing the intensity requirements from the injection system and easily providing the 10^9 carbon ions and 4×10^{10} protons per synchrotron cycle needed to achieve the requested dose rates. Frequency swing is 1–7 MHz provided by ferrite-loaded cavities operating in the second harmonic of the beam revolution frequency. Acceleration time to the maximum rigidity of 6.6 Tm (430 MeV/u carbon) is 1 s, and typical flattop times are about 2 s, providing for a typical cycle time of 3–4 s. Flattop fields can be adjusted from

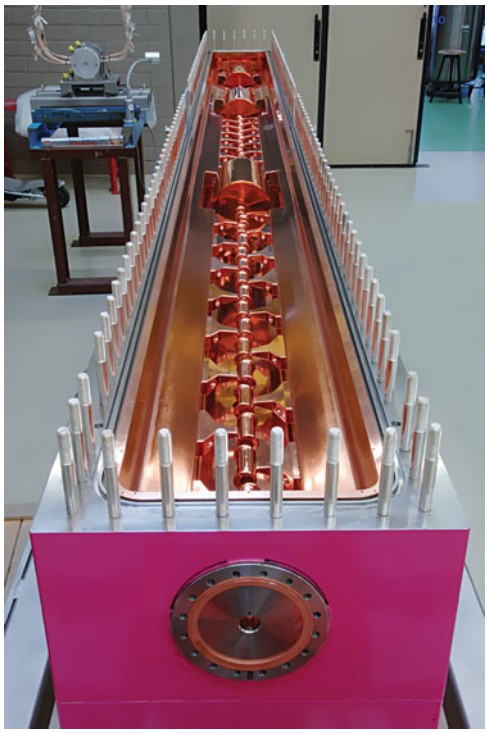

Fig. 20.2 The Interdigital H-mode (IH) LINAC with lid removed, a highly efficient structure for low-beta ion acceleration

about 20% to 100% of maximum on a pulse-to-pulse basis, providing the greatest flexibility in ion energy control.

20.5.2 The Synchrotron Injector System

Based on the HIT model, the injector systems for the synchrotron would consist of the following main components:

1. Two to three ECR ion sources
2. A low-energy beam transport line (LEBT)
3. A radio frequency quadrupole (RFQ)
4. A compact main linac most likely of the Interdigital H-type (IH) type (see Fig. 20.2)
5. A medium-energy beam transport line (MEBT)

ECR ion sources are reliable, cost-effective, and now commercially available solutions for producing the beams needed for medical treatments. All the desired ions can be obtained from standard gas bottles (helium, hydrogen, oxygen, carbon dioxide), and the ECR source easily provides the specified ion currents in the

required charge states. The number of required ECR sources strongly depends on the number of ion types that should either be used in parallel or with very small switching times. The first projects started with a two-source scenario but three ion sources are preferred for the future. Each ion source is coupled to the RFQ through its own LEBT. A switching magnet at the entrance to the RFQ selects the ion source to be used.

Each LEBT isolates the correct charge state of the ions and tailors the beam to fit into the acceptance of the RFQ. It is equipped with a macropulse chopper to cut out beam falling outside the time window for synchrotron injection.

The RFQ transforms the DC ion beam from the macropulse structure to the RF time structure of the linac– 216 MHz in most of the cases. The output energy of the RFQ beam is in the range of 500 keV/u.

The development of very compact IH-structure linacs with top energies of approx. 7 MeV/u was a major step in reducing size and cost of injector systems. The combination of ECR sources, an RFQ, and an IH linac has become the preferred and most economical injection chain for synchrotron-based medical systems.

The MEBT contains a stripper foil and analysis system to strip the ions to the charge state selected for synchrotron injection, and aids in the prevention of ion contamination in the injected beam. The MEBT also serves to match the beam into the synchrotron transverse and longitudinal acceptances.

20.5.3 Beam Extraction from the Synchrotron

The extraction of the ions from the synchrotron should take place in the range of seconds in as homogenous a manner as possible. The conventional slow extraction scheme drives the beam in a controlled fashion into a third-order resonance, using one of several different techniques. The traditional way is to slowly change the machine tune by adjusting quadrupole settings. Achieving a constant, uniform spill is quite difficult, and requires extreme stability of power supplies and very careful ion-optical settings. The recently developed “RF knockout method” [6] has been applied very successfully to achieve controllable and flat intensity beam spills. The amplitude of an RF exciter is increased during the extraction process in a flexible manner in order to achieve a flat spill structure of the extracted beam.

With this method, several spill interruptions are feasible. Recently, the intensity control has been improved to permit active feedback on the exciter.

It has to be emphasized that for full 3D raster scanning, the parameters have to be optimized for about 255 different energy steps. Treatment of moving organs requires either gating and/or repainting and/or an active energy variation during the spill. Though a challenge, extraction systems are now capable of meeting these requirements.

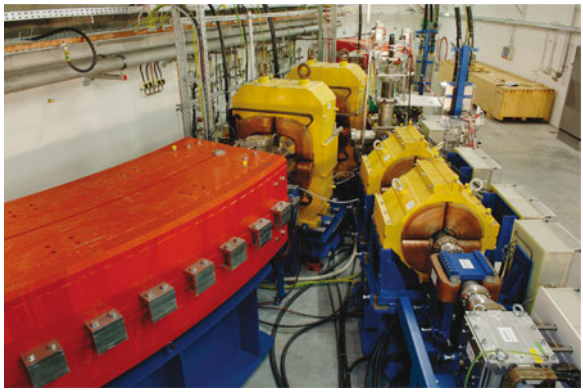

Fig. 20.3 Extraction region of the Heidelberg synchrotron and first part of the high-energy beam transport (HEBT) line

20.5.4 The High-Energy Beam Transport Line with Gantries

The transport lines from the synchrotron to the treatment rooms constitute another challenge. Beam transport has to take place without transmission losses for all ion species and beam energies. In addition, the high-energy beam transport line (HEBT) must focus the beam transversely to the different required beam sizes in the isocenter. This sets constraints on the magnet lattices and required magnet apertures (Fig. 20.3).

Several treatment rooms have to be served, requiring rapid and reliable beam switching to not restrict the patient flow. The beam position must be very stable at the isocenter of each room at all energy steps. All these specifications indicate the need for extremely high-quality components, high-precision instrumentation and controls, and a very sophisticated control system.

The HEBT contains a spill abort system to safely and rapidly interrupt the beam delivery to the patient within about 0.1 ms if required. This is done with a fast switching magnet between two steering magnets operated in a closed beam bump fashion with sufficiently large bending angles. Switching off the fast switching magnet automatically prevents the beam from passing further downstream. An even safer manner is to use a magnet lattice where the beam cannot pass if the switching magnet is off – even if other power supplies fail, as well.

To provide full geometrical flexibility for the tumor treatment, the beam should be able to enter the patient from different directions. For IBT machines this is done via rotating beam lines (gantry systems), which at present are standard installations for proton machines. For carbon accelerators, however, only the gantry at HIT has been built so far and is in the commissioning phase.

For isocentric gantries up to 150°–270° of total bending power is required to bend the beam from the plane of the accelerator to the plane perpendicular to the patient. Basic gantry requirements, taken from [3], are listed in Table 20.2.

Table 20.2 Physical and beam requirements for a gantry delivery system

Description	Specification
Size (diameter)	<13 m
Rotation range	±185° (overlap at the bottom)
Rotation accuracy	±0.3°
Rotation step size	±0.3°
Rotation speed	1 min for full rotation
Braking	1° to complete stop
Spot size	σ_x,σ_y < 3 mm
Spot deviation from circle	$\lvert\Delta\sigma_x - \Delta\sigma_y\rvert < 0.3\sigma_x$
Divergence	σ'_x, σ'_y < 1/200 radian
Spot position accuracy	Δx, Δy < 1 mm

Minimizing the gantry size for high-rigidity ion beams is achieved by positioning the scanning system before the last, i.e., the 90° dipole magnet. Therefore, this magnet has to have a large aperture – at least at the end – which increases its weight.

The Heidelberg gantry contains two 45° dipoles and one 90° dipole with a total weight of about 150 tons due to the large magnetic rigidity of carbon ions. The diameter of this gantry is within the desired 13 m; its length is 25 m.

For the HIT accelerator with its active 3D-scanning system, some ion-optical challenges had to be mastered. Due to the different horizontal and vertical emittances of the extracted beam, the demand for equal beam widths in both planes at the patient at all gantry angles is a nontrivial task.

All gantries need a very stiff support structure to meet the mechanical deformation requirement of beam at isocenter to be ≤1 mm, leading to rather heavy structures and weights; in the case of the HIT gantry, it is 600 tons, total (Fig. 20.4).

20.6 New Accelerator Concepts

20.6.1 FFAG

Organ motion during treatment presents a great challenge to beam delivery technology. Not only is the motion transverse, but in some cases the depth of tissue over the tumor or the shape of the tumor itself will be changing. Assuming that instrumentation can be developed to track these changes, scanning systems can provide rapid corrections for the transverse motion. However, longitudinal corrections require rapid energy changes, on the same order of time as provided by the scanning systems. Millisecond energy changes are not possible with the accelerator systems described above. However, the "rediscovered" concept of a fixed-field alternating-gradient (FFAG) accelerator might provide this energy flexibility [6–10]. In the "nonscaling" FFAG design fixed-field combined-function bending magnets allow fast beam acceleration with compact machines without ramping the magnets. Early

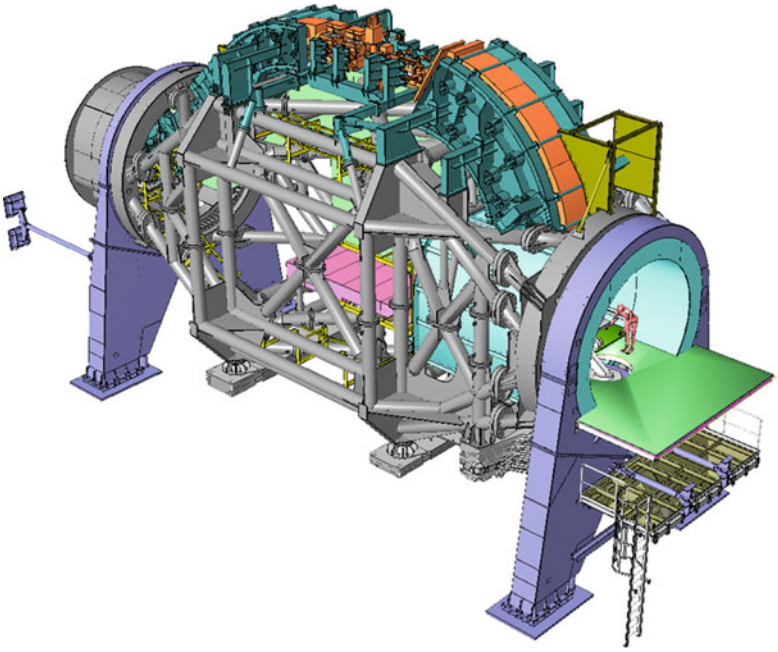

Fig. 20.4 Overview of the Heidelberg gantry

design studies envision the possibility to accelerate carbon beams up to 400 MeV/u, with a repetition rate of 200 Hz, using compact and cost-effective normal- or superconducting structures. Such a system would allow for the fast energy variation required for the treatment of moving organs.

It should be noted that a multistage acceleration concept would be needed, as linear-field FFAGs limit the momentum range that can be accepted to a factor of approx. 3. Hybrid FFAG designs are under investigation which might extend the momentum range to a factor of 6 [11] (Fig. 20.5).

20.6.2 Linac Boosters

One of the initiatives of the TERA foundation in Italy was the design of a linac-booster (LIBO) for proton therapy. LIBO is planned to operate at the very high frequency of 3 GHz, and be able to accelerate protons up to 250 MeV. Fast energy variations would also be featured by turning off accelerating fields from the high-energy end of the linac [13]. The facility reportedly offers the possibility for dual use, i.e., to produce isotopes during the times when no treatments take place. CABOTO (Carbon Booster for Therapy in Oncology) is an evolution of this concept for carbon ions [14].

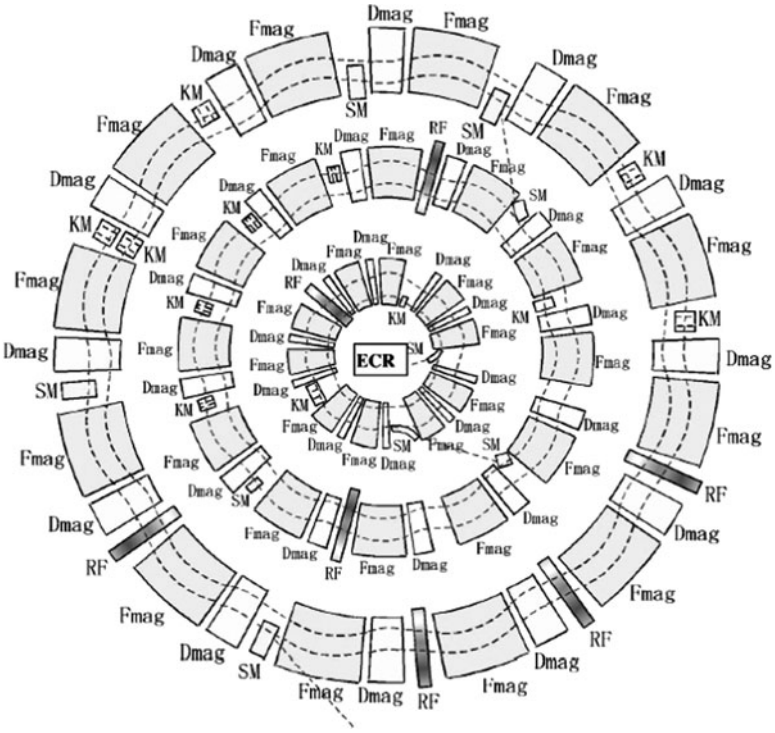

Fig. 20.5 Triple-cascade radial-sector FFAG accelerator [12]

20.6.3 Induction Linacs

A dielectric wall induction-linac accelerator (DWA) is under development at the Lawrence Livermore National Laboratory (LLNL) and the University of California, Davis [15]. It is an approach to enhance the accelerating electric field gradients from about 10 to 100 MV/m, using new dielectrics capable of supporting very high voltages. 250 MeV protons could be produced in a straight structure no more than 3 m long. If accomplished, such a device could be small enough to be mounted on a gantry directly aimed at the patient.

20.6.4 Lasers

As a long-term vision toward compact treatment facilities, developments of ion acceleration by means of high power lasers is under investigation at different laboratories [16]. However, at present the beam properties of laser-accelerated ions are not at all what is required for therapy (high-intensity, well-defined energy) and many technical challenges must be addressed [17].

20.6.5 Antiprotons

In addition to new accelerator concepts, the application of accelerated antiprotons for radiation therapy has been proposed, citing the high RBE-factor associated with annihilation of the antiproton at the stopping point [18]. For one, the enormous investment costs argue against such a facility. In addition, recent simulations [19] point out that the very high energy of the annihilation products distribute the "star" dose over a large volume, leading to overall poor dose localization.

20.7 Summary

Due to the larger investment costs for the accelerator part, IBT is more expensive than conventional radiotherapy. Therefore, a broad use of IBT will only be achieved if the added value of better therapeutic results in clinical practice together with cost-effective accelerator design justify the cost increase.

Nowadays, protons and carbon ions are the only two light ion types finding their way into hospital applications.

Proton accelerators with up to 250 MeV protons are commercially delivered as compact systems, with full gantry functionalities and in multiuser facilities. Active developments are proceeding for further exploration of the full beam potential for dose conformity via improved scanning and gating techniques.

Carbon accelerators with up to 430 MeV/u have the benefit of providing improved RBE and reduced lateral spreading of carbon ions. In addition, combination therapy of protons and carbons and the application of other ions such as helium are possible with such systems. Only a few carbon therapy units have been built or are in the construction phase.

With respect to the treatment modality, all of these facilities are equipped with or are moving toward active beam delivery systems which provide the best control over the treatment field, shape, and quality.

New accelerator concepts and extended scanning functionalities are being investigated worldwide to optimize the treatment modality and to minimize the investment costs for such facilities.

References

1. Particle Therapy Cooperative Group (PTCOG), Table of existing facilities. http://ptcog.web.psi.ch/ptcentres.html. Accessed 12 July 2010
2. PTCOG Planned Facilities. http://ptcog.web.psi.ch/newptcentres.html. Accessed 12 July 2010
3. W.T. Chu, J.W. Staples, B.A. Ludewigt, et al., Performance specifications for proton medical facility. LBL-33749, March 1993. http://www.osti.gov/bridge/product.biblio.jsp?query_id=0&page=0&osti_id=10163935. Accessed 12 July 2010

4. J. Alonso, Medical applications of nuclear physics and heavy-ion beams. LBNL-46036, August 2000. http://www.osti.gov/bridge/product.biblio.jsp?query_id=0&page=1&osti_id=775138. Accessed 9 Sept 2010
5. D. Ondreka, The Heidelberg Ion Therapy (HIT) accelerator coming into operation. Proc EPAC08 Genoa 23–27 (Jun 2008) 979
6. T. Furukawa, K. Noda, Fast beam cut-off method in RF-knockout extraction for spot-scanning. Nucl. Instrum. Methods A **489**, 59–67 (2002)
7. A.G. Ruggerio, Non-scaling FFAG cyclotrons. Presented at the Workshop on Hadron Beam Therapy, Erice, Italy, 24 Apr–1 May 2009. http://erice2009.na.infn.it/TalkContributions/Ruggiero.pdf. Accessed 9 Sept 2010
8. T. Yokoi, Overview of PAMELA: the UK non-scaling FFAC medical facility. Presented at the Workshop on Hadron Beam Therapy, Erice, Italy, 24 Apr–1 May 2009. http://erice2009.na.infn.it/TalkContributions/Yokoi.pdf. Accessed 9 Sept 2010
9. F. Méot, The RACCAM project. Presented at the Workshop on Hadron Beam Therapy, Erice, Italy, 24 Apr–1 May 2009. http://erice2009.na.infn.it/TalkContributions/Meot.pdf. Accessed 9 Sept 2010
10. M.K. Craddock, FFAG accelerators. Presented at the Workshop on Hadron Beam Therapy, Erice, Italy, 24 Apr–1 May 2009. http://erice2009.na.infn.it/TalkContributions/Craddock.pdf. Accessed 9 Sept 2010
11. C. Johnstone, S. Koscielniak, New nonscaling FFAG for medical applications. Presented at PAC07, Albuquerque, NM, 25–29 Jun 2007, Abstract THPMN103. http://ieeexplore.ieee.org/stamp/stamp.jsp?tp=&arnumber=4440631. Accessed 9 Sept 2010
12. T. Misu, Y. Iwata, A. Sugiura, et al., Design study of compact medical fixed-field alternating-gradient accelerators. Phys. Rev. Spl. Top. Accel. Beams **7**, 094701 (2004)
13. U. Amaldi, S. Braccini, A. Citterio, et al., Cyclinacs: Fast-cycling accelerators for hadrontherapy. Nucl. Instrum. Methods A **521**, 512 (2004)
14. U. Amaldi, G. Kraft, European developments in radiotherapy with beams of large radiobiological effectiveness. J. Radiat. Res. **48**(Suppl A), 27–41 (2007)
15. G.J. Caporaso, High gradient induction linacs for hadron therapy. Presented at the Workshop on Hadron Beam Therapy, Erice, Italy, 24 Apr–1 May 2009. http://erice2009.na.infn.it/TalkContributions/Caporaso.pdf. Accessed 9 Sept 2010
16. P.R. Bolton, T. Hori, H. Kiriyama, et al, Toward laser-driven proton therapy of cancer at PMRC in Japan. Presented at the Workshop on Hadron Beam Therapy, Erice, Italy, 24 Apr–1 May 2009. http://erice2009.na.infn.it/TalkContributions/Bolton.pdf. Accessed 9 Sept 2010
17. U. Linz, J. Alonso, What will it take for laser driven proton accelerators to be applied to tumor therapy? Phys. Rev. Spl. Top.– Accel. Beams **10**, 094801 (2007)
18. E.J. Hall, Antiprotons for radiotherapy? Radiother. Oncol. **81**, 231–232 (2006)
19. H. Paganetti, M. Goitein, K. Parodi, Spread-out antiproton beams deliver poor physical dose distributions for radiation therapy. Radiother. Oncol. **95**, 79–86 (2010)

Chapter 21
Shielding and Radiation Protection in Ion Beam Therapy Facilities

Andrew J. Wroe and Steven Rightnar

Abstract Radiation protection is a key aspect of any radiotherapy (RT) department and is made even more complex in ion beam therapy (IBT) by the large facility size, secondary particle spectra and intricate installation of these centers. In IBT, large and complex radiation producing devices are used and made available to the public for treatment. It is thus the responsibility of the facility to put in place measures to protect not only the patient but also the general public, occupationally and nonoccupationally exposed personnel working within the facility, and electronics installed within the department to ensure maximum safety while delivering maximum uptime.

21.1 Introduction

IBT is a useful tool for cancer treatment, but it is imperative that this technology be used in the safest possible manner. In the area of radiation protection, IBT poses some interesting challenges in that it combines the issues associated with conventional RT with those typically associated with nuclear physics or nuclear reactor facilities. Issues that need to be considered include adequate radiation shielding of the accelerator and beam delivery apparatus to maintain dose limits for both the general public and occupationally exposed personnel, activation of both static and removable beam line components, secondary particle spectra including high-energy neutrons, shielding material, maze design and finally, the unwanted radiation dose delivered to the patient outside the treatment field.

An IBT facility covers a large area, all of which must be shielded to protect both workers and the general public. Unlike conventional X-ray therapy facilities which

A.J. Wroe (✉)
Department of Radiation Medicine, Loma Linda University Medical Center, 11234 Anderson Street, CSP A-1010, Loma Linda, CA 92354, USA
e-mail: awroe@dominion.llumc.edu

U. Linz (ed.), *Ion Beam Therapy*, Biological and Medical Physics, Biomedical Engineering, DOI 10.1007/978-3-642-21414-1_21,

are typically self-contained single-room bunkers, an IBT facility encompasses, usually, an accelerator, beam transport, and multiple treatment rooms, increasing the areas which require shielding to protect both occupationally and nonoccupationally exposed persons to federally mandated dose limits.

In conventional X-ray therapy, there is a threshold for neutron production of 10 MV, which removes the need to shield neutrons in low energy applications. However, in IBT all energies of ions have the potential to produce neutrons. The fluence of neutrons produced and the spectra of neutron energies are dependent on the ion energy, delivery technique and materials in the beam line. The presence of these particles creates additional complications for shielding design, including materials used, order of shielding materials, maze dimensions, and the radiation metrology systems used in the overall evaluation of the facilities' shielding. The presence of neutrons also enhances the out-of-field dose equivalent delivered to the patient, which can impact the treatment and may need to be considered by the treatment team.

When shielding and radiation protection issues are correctly considered and accounted for, IBT can be a safe and effective treatment mechanism. As new compact proton centers (cf. Chap. 39), are developed and built, the lessons learned in the larger multiroom facilities will need to be put into practice, producing safe working and treatment environments and allowing this technology to benefit a larger number of patients.

21.2 Dose Limits

Radiation dose limits used in IBT do not vary from those used in X-ray RT or other areas where radiation is employed. As such, only a brief overview is given here and the reader is directed to the references for a more in-depth discussion of this issue. Radiation exposure limits vary based on the individual's declared status. Public and occupational regulatory dose limits are set by federal agencies such as the Nuclear Regulatory Commission (NRC), Department of Energy (DoE) and the Environmental Protection Agency (EPA). In the US, some states are declared as agreement states where state government bodies set and enforce regulations which are based on federal agency guidelines.

The NRC has set the dose limit for radiation workers at 50 mSv per year. Additional annual limits to the lens of the eye and skin is 150 mSv for occupationally exposed workers (NRC 10 CFR 20.1201). In the European Union and many other countries the limit is 20 mSv per year as determined by the International Atomic Energy Agency (IAEA) [1]. For the general public the NRC and IAEA set forth a dose limit of 1 mSv per year. This is the dose limit which needs to be adhered to when shielding uncontrolled areas of the hospital (i.e., waiting rooms, corridors, bathrooms etc.). Occupational exposure for a declared pregnant woman must not exceed 5 mSv (2 mSv in EU) to fetus over the entire course of pregnancy (NRC 10 CFR 20.1208), while it is also recommended that efforts be made to avoid

substantial variation above a uniform monthly exposure rate to a declared pregnant woman.

Fetal dose limits pose a special challenge to the radiation medicine team when attempting to treat a pregnant woman, as while the fetus may not reside within the treatment volume and not be traversed by treatment beams, secondary radiation may interact with the fetus and deliver dose. Such cases have been investigated previously [2] and recommend the use of shielding for the fetus, however, this should be dealt with on a case by case basis as the out-of-field dose equivalent received by the fetus depends strongly on the treatment parameters (i.e., field size, beam energy, etc.).

21.3 Radiation Shielding Basics

Shielding for an IBT facility must address both the primary particles (protons, carbon ions, etc.) and the secondary particles produced from the ions interacting with beam line components and the patient. The secondary particles of primary concern when constructing shielding for the facility are neutrons and photons. Both often have a large range and in the case of neutrons high quality factors for biological damage ($Q = 5$–20) [3] (cf. Chap. 4 for details). The choice of shielding materials is complex as the shielding material itself has a direct impact on secondary particle production. Case in point, as the mass number of the target/shield increases, the total neutron yield increases, yet the ability to absorb photons also increases. For IBT facilities the target is the patient which has a low mass number and a low neutron yield. Other components of the beam line such as the passive scattering system and beam collimation system have a higher mass number and, subsequently, yield a higher number of neutrons that may be shielded to minimize the dose received by humans.

Proton interactions comes in two forms, nuclear evaporation and intranuclear cascade. Nuclear evaporation occurs when the incident particle is absorbed into the nucleus of the target and a new nucleus is formed. The resulting nucleus is left in an excited and unstable state which subsequently decays to a stable state by the emission of radiation. The emitted neutron in this type of interaction has energy up to approx. 8 MeV and the emission is isotropically distributed from the target. The intranuclear cascade is caused by the proton interacting with an individual nucleus. This interaction dominates in incident proton energies above 50 MeV. These neutrons are of higher energy and are more concentrated in the same direction of the incident beam. Heavier ions such as carbon can additionally produce secondary particles including neutrons through fragmentation.

The energy of secondary photons and neutrons is generally the determining factor when designing shields [4, 5]. For simple calculations with a known fluence of secondary photons, the shielding thickness (x) necessary to attenuate the beam $I(x)$ can be estimated using the following formula:

$$I(x) = BI_0 e^{-\mu x} \tag{21.1}$$

where:

B = buildup factor
I_0 = initial intensity
μ = attenuation coefficient

Similarly for neutron attenuation and absorption the following calculation can be used

$$I(x) = BI_0 e^{-\sum_{nr} x} \tag{21.2}$$

where:

$\sum_{nr}$ = neutron removal cross section.

For an approximation of the radiation levels outside the shield, the Moyer model (below) can be used. Assuming neutrons are the only secondary particles produced, the general formula for radiation outside the shield is:

$$H = \frac{1}{r^2} \int g(E) B(E, \theta) e^{-d(\theta)/\lambda(E)} \frac{d^2 n(E, \theta)}{dE d\Omega} dE \tag{21.3}$$

r = distance from source
E = neutron energy
g = fluence to dose-equivalent conversion coefficient
d = shield thickness in the direction Θ
λ = effective removal mean free path
B = buildup factor
$\frac{d^2 n(E,\theta)}{dE d\Omega}$ = yield of neutrons per unit solid angle, at angle Θ, per unit energy interval at E

For a detailed discussion on shielding calculations the reader is referred to [4]. Most shielding is designed using various Monte Carlo (MC) modeling programs and then verified using a range of radiation metrology techniques. The generalized Moyer model, or variants of it, are used to verify computer simulated models and not as the primary shielding calculation method.

21.4 Shielding Materials

Traditionally the three main materials used in IBT facility shielding are earth, concrete and steel. These materials offer good shielding characteristics, while also being cost effective for large facilities with multiple treatment rooms. Other materials such as lead, Lipowitz's metal (low melting point alloys), brass, polymethyl methacrylate (PMMA) and boronated polyethylene are also used for shielding of patients and beam line components, but are typically not employed on a large scale due to the inherent costs involved.

Earth is a cheap and readily available shielding material, and as such most IBT facilities are constructed underground to take advantage of this abundant resource. The attenuation of both primary and secondary radiation is a function of the soil density. Soil density is based on the degree of compaction and soil type, and can range from 1.1 to 1.6 g/cm^3; however, with heavy compaction it can reach to 2.25 g/cm^3. The SiO_2 content of soil also makes it effective in shielding neutrons and photons.

Concrete is another shielding material that is used in facility shielding based on cost and the ease in which it can be poured into the desired shapes and thicknesses. In addition, concrete offers the added benefit of its structural strength. Most modern vaults or treatment rooms utilize concrete extensively as a shielding material. The shielding properties of concrete can vary as material can be added to the concrete to increase its density or thermal neutron capture cross section (see Table 21.1). One disadvantage of concrete is that naturally occurring sodium within the concrete can become activated from interactions with the primary beam, potentially increasing the background radiation levels in the accelerator and treatment areas from the shielding itself. To limit increases in background radiation from primary beam interactions, low-sodium concrete or the addition of boron compounds have been used [4]. Steel can also be used as a shielding material, however, steel alone can

Table 21.1 Typical compositions of representative concretes after curing (Data from [6])

Concrete type	Ordinary	Magnetite[a]	Barytes[b]	Magnetite and steel	Limonite and steel[c]	Serpentine[d]
Element density ($g\,cm^{-3}$)	2.35	3.53	3.35	4.64	4.54	2.1
Hydrogen	0.013	0.011	0.012	0.011	0.031	0.035
Oxygen	1.165	1.168	1.043	0.638	0.708	1.126
Silicon	0.737	0.091	0.035	0.073	0.067	0.46
Calcium	0.194	0.251	0.168	0.258	0.261	0.15
Carbon						0.002
Sodium	0.04					0.009
Magnesium	0.006	0.033	0.004	0.017	0.007	0.297
Aluminum	0.107	0.083	0.014	0.048	0.029	0.042
Sulfur	0.003	0.005	0.361			
Potassium	0.045		0.159		0.004	0.009
Iron	0.029	1.676		3.512	3.421	0.068
Titanium		0.192				
Chromium		0.006				0.002
Manganese		0.007				
Vanadium		0.011		0.003	0.004	
Barium			1.551			

[a]Magnetite ($FeOFe_2O_3$) as aggregate
[b]Barytes, a $BaSO_4$ ore, as aggregate
[c]Limonite, a hydrated Fe_2O_3ore, plus steel punchings, as aggregate
[d]Serpentine ($3MgO\,2SiO_2\,2H_2O$) as aggregate; a concrete usable at high temperatures with minimal water loss

cause a buildup of low-energy neutrons and is usually used in conjunction with concrete. In this arrangement the concrete captures the low-energy neutrons, while the steel attenuates the produced photons.

Polystyrene and other materials with high hydrogen content (plastics, waxes) offer great shielding of neutrons. As neutrons interact with hydrogen nuclei, the energy of the neutron is reduced by approximately half, removing the fast neutrons by reducing them to lower energies. As the lower-energy thermal neutrons are subsequently captured in the material, 2.225 MeV gamma rays are emitted from the (n, γ) reaction with hydrogen, which requires further shielding that is typically achieved using lead or steel downstream of the primary neutron barrier.

Boron can also be incorporated into shielding materials to enhance the capture of thermal neutrons. Natural boron contains approximately 20% of ^{10}B which has an effective absorption cross section for thermal neutrons. In this reaction boron is converted to an alpha particle (with finite energy and range) and a ^{7}Li nucleus. Approximately 94% of the ^{7}Li decays through the emission of a 0.48 MeV gamma ray which is relatively easy to shield using steel or lead [7].

$$^{10}\mathrm{B} + n \rightarrow {}^{4}\mathrm{He}^{2+} + {}^{7}\mathrm{Li}^{3+} + 2.79\,\mathrm{MeV}(6\%),$$

$$^{10}\mathrm{B} + n \rightarrow {}^{4}\mathrm{He}^{2+} + {}^{7}\mathrm{Li}^{3+} + 2.31\,\mathrm{MeV} + \gamma(0.48\,\mathrm{MeV})(94\%).$$

Lipowitz's metal and brass is not routinely used as a facility shielding material. As a collimator material it is used to confirm the passively scattered proton beam to desired field size. Brass alloys are also utilized for beam collimation, even though plastics and waxes might often be preferred due to their lower activation.

21.5 Maze and Door Construction

Any penetration of the room shielding, including ducts for cable routing, tunnels and mazes requires special consideration to minimize the transmission of radiation into potentially uncontrolled areas. The primary goal in designing these openings is to match the shielding characteristics of the walls that make up the room. Two general guidelines should be used when designing penetrations in shielded walls:

1. Never place any penetration so that the primary beam can point directly towards it or so any unshielded particles primary or secondary can be transported unabated.
2. For the maze, the sum of the shield-wall thicknesses between the source and exit point should at least be equivalent to the shield-wall thickness without the maze.

Neutrons have the ability to be reflected off shielding walls, allowing them to penetrate openings in the shielding. To minimize the penetration, mazes are often built into personnel entryways and cable routings. A maze is a series of one or more right angle turns that reduce the neutron dose at either the entry to the treatment room or exit of cables through the shielding (see Fig. 21.1). Data suggest that the

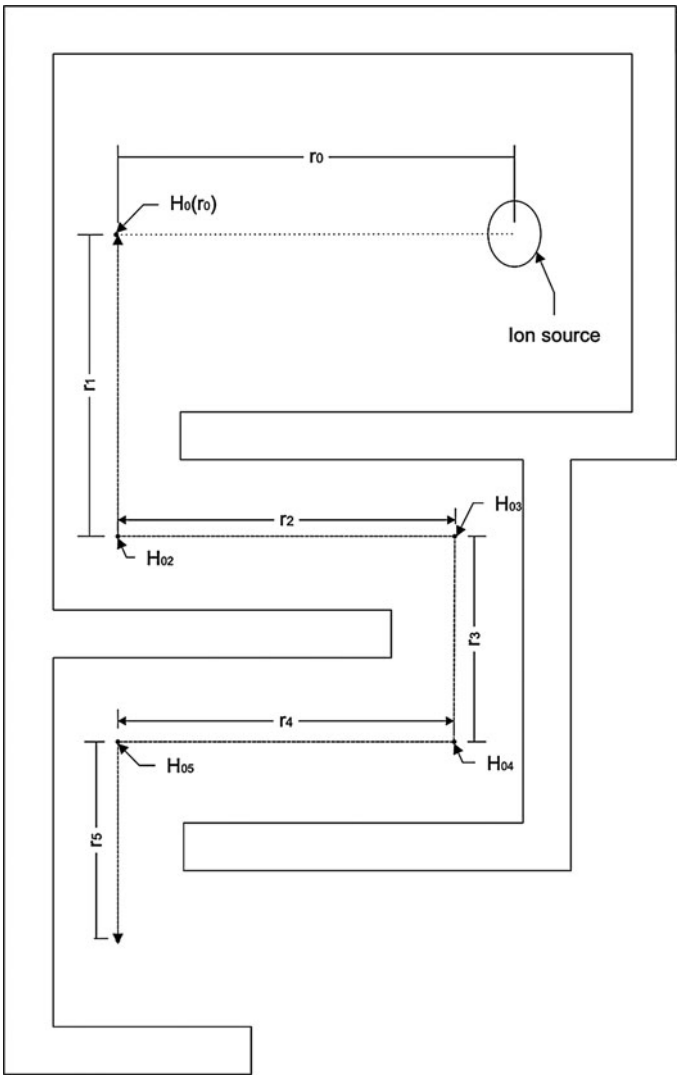

Fig. 21.1 Maze schematic for use with maze equations (21.4) and (21.5)

primary particle energy has little effect on the attenuation of a maze other than an increased neutron yield as a function of primary particle energy and ion type [4]. A simple calculation to determine the dose-equivalent rate attenuation for a single and multilegged maze is below:

$$H(r_1) = 2H_0(r_0)\left(\frac{r_0}{r_1}\right)^2 \text{ for the first leg,} \tag{21.4}$$

$$H(r_i) = \left(\frac{e^{-r_i}/0.45 + 0.022A_i^{1.3}e^{-r_i}/2.35}{1 + 0.022A_i^{1.3}} \right) H_{oi}, \text{ for the } i\text{th leg} (i > 1) \quad (21.5)$$

r_0 = distance from the source to mouth of the maze in meters
r_1 = distance from the source into the first leg in meters
$H_0(r_0)$ = dose equivalent at the mouth from a point source
A_i = cross-sectional area of the maze (m^2)
H_{oi} = dose equivalent at the entrance to the ith leg
r_i = distance into the ith leg in meters

If enough room is available for the construction of a long maze with a number of legs, an entry door is not required from a shielding standpoint, providing that dose limits have been met. In this case, it is common practice to have an interlocked barrier that prevents personnel from entering the room during beam delivery. While this barrier provides no radiation shielding it does provide a useful radiation protection service in preventing unintentional access during beam delivery. In the case where the maze/shielding combination is insufficient to reduce the dose to the entrance of the maze to acceptable limits, a shielded door will be required. This door will serve two purposes: reducing the dose outside the shielded treatment room to acceptable limits and preventing access during beam delivery. Typically, such doors are constructed from a 0.5 cm steel case which contains approximately 10 cm of borated polyethylene and 1.5 cm lead [8]. Traditionally, the borated polyethylene is on the inside of the door and is used to moderate and capture neutrons, while the lead attenuates photons that are produced when the neutrons are captured.

21.6 Activation

Activation of beam line components is an important issue for IBT departments. Activation relates to the induction of radioactivity in a material by an external radiation field. In IBT, this is caused through nuclear reactions with the atoms of the irradiated material, and thus activation is more prevalent in heavier atomic materials which have a higher cross section for nuclear reactions. As the energy of the incident radiation increases, the number of possible reaction channels also increases, resulting in a larger number of produced radionuclides (Fig. 21.2). The composition of the target material and the energy of the ion beam need consideration when assessing possible activation of components.

Activated components can be divided into two main sections for consideration: beam line components and irradiated products. Irradiated products relates to items that have purposely been placed in the beam line for research or testing purposes. This typically includes, but is not limited to cells, animals, phantoms, electronics and all material used within the area of exposure (i.e., cages, stands, tanks, etc). Items of most concern are those which have been irradiated to very high doses such as electronic components. All irradiated items should undergo a radiation survey

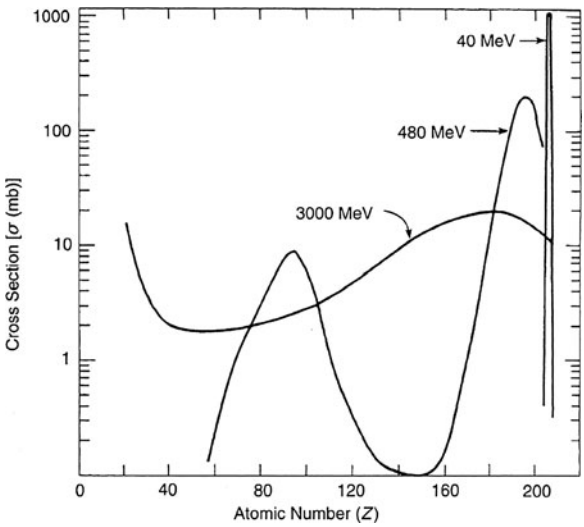

Fig. 21.2 Mass-yield curves (cross section vs. atomic number) for the bombardment of bismuth with protons of varying energy [4]

(details below) before being removed from the premises. If they exceed the radiation limit for release by the department, then they need to be stored in a secure area with posted signage indicating a radiation hazard until a time when they will have decayed sufficiently.

Beam line components regard any component installed in or near the actual beam path. This is typically limited to devices that are located within half a meter of the primary beam path as these items will be irradiated with high fluences of ions under normal beam delivery. Examples of these devices include scattering foils, ion chambers, collimators and bolus materials. Due to the high beam currents passing through these devices and the high atomic numbers of these materials, activation can be quite high, especially for scattering foils and collimators. Typically, these materials are not removed from the beam line, but in the event of service and maintenance care must be taken to conduct a radiation survey before work commences or materials are released for transport.

When completing a radiation survey of potentially activated items a two-step process is typically employed. First, a survey meter with a pancake Geiger–Müller (GM) probe is used to assess either the item or area of work. If the radiation levels are indistinguishable from background, work may proceed or the item can be released for transport. If the surface survey detects radiation levels that are distinguishable from background, an ion chamber survey should be completed. The dose limits for this survey are often set at $5\,\mu Sv/h$ at 30 cm from the surface or $10\,\mu Sv/h$ at the surface, but these should be checked with your radiation safety department or governing organization. If measured values exceed these then maintenance or repair may be delayed and a later survey completed to reassess exposure levels.

21.7 Dose Considerations for Electronics

When considering the longevity and stability of operation of an IBT facility, it is important to consider the dose delivered to electronics that are installed in the radiation environment. Electronics installed in the gantry, accelerator complex, treatment room and beam transport areas of the facility can be subject to radiation from scattered primary ions and also secondary particles such as neutrons and gamma photons. With increasing levels of technology installed in these areas such as multileaf collimators, robot patient positioners, digital imagers and their associated control systems, it is essential that the lessons from electronic system deployment in space be learned and applied. Failure to take this into account can lead to premature equipment failure and extended downtime for a facility. Further, once installed it is often difficult to move electronic systems as this means extensive engineering in areas where space is often at a premium and as a consequence forward planning for this is essential.

In order to complete radiation surveys of potential areas of risk for electronics, it is important to consider the radiation species and energies present. Detection systems need to be able to measure a known portion of the radiation spectra, and it is recommended that multiple detection systems be used to evaluate as much of the spectra as possible. Electronic detectors such as Bonner spheres, REM (Roentgen equivalent man) meters and microdosimeters can be used in this evaluation, however, TLD (thermoluminescent dosimeter), OSL (optically-stimulated luminescence) and CR-39 (a thermoset polymer) detectors used for personnel monitoring are also extremely useful for this work. Such detector systems, typically, provide a number of detectors in a single packaged unit to measure proton, photon, beta, fast neutron and thermal neutron radiation with $\pm 15\%$ dose accuracy at the 95% confidence level. Such detectors have the added advantage in that they do not require extensive power, readout and gas pressurization systems that can be bulky and limit where the detectors can be placed. The main disadvantage with using personnel monitors for this work is that their sensitive volume is quite small making acquisition times long.

Studies on this issue have been completed at Loma Linda University Medical Center (LLUMC) using optically stimulated luminescence technology in conjunction with CR-39 to measure X, gamma, proton, beta, fast and thermal neutron radiation. Detectors were stationed at various positions around the gantry pit and on racks on the gantry itself to evaluate dose to electronics. When a polystyrene phantom at isocenter was irradiated with 250 MeV protons to a dose of approximately 1.4 kGy, the equivalent doses measured ranged from 100 to 6,000 mrem (1–60 mSv). The position of the detector/electronics relative to both isocenter and neutron-producing devices such as the collimators, first and second scatterers had a bearing on the dose received. Interestingly, the addition of 1 in thick wax shielding decreased the fast neutron component by almost 50%, yet this had a corresponding increase in thermal neutron dose of 100% and a 50% increase in photon/proton dose as there was no ^{10}B component to capture thermal neutrons. It is important

to note, however, that despite the increases in photon/proton and thermal neutron dose, the overall dose equivalent decreased by around 30–40% in the presence of wax shielding. This shielding can be further enhanced through the addition of borated polyethylene to reduce the thermal neutron component. This leads to the conclusion that electronics should be installed outside the gantry enclosure. If this is not possible, care should be taken to either mount them outside of the primary beam path, and away from sources of secondary radiation (i.e., collimators and scattering foils) taking advantage of the inverse square law, or to use shielding to limit exposure.

21.8 Out-of-Field Dose Equivalents

Dose delivered to the patient outside of the treatment field is not typically associated with radiation protection, however, as the goal of IBT is to deliver a more conformal radiation dose to the tumor, the dose delivered outside of this volume is an important issue. Protons and other ions provide a significant advantage over other external beam radiation modalities by their depth–dose distribution, which allows for maximum dose to be delivered to the tumor volume with no primary particle dose beyond the distal edge. This allows for significantly fewer beams to be utilized, resulting in a much lower integral dose to surrounding critical structures [9].

Recently, the whole-body dose delivered by protons and other ions was called into question by Dr. Eric Hall [10]. This dose, which is of particular importance in pediatric patients with long life expectancy and greater susceptibility to radiation-induced cancers, is delivered by secondary neutrons that are produced through primary beam interactions with both the patient and beam-modifying devices. The dose-equivalent values per unit of prescribed proton dose presented in the report of Hall [10] have been questioned [11–13], but the concern remains because of the large uncertainties involved in neutron dose measurements and the RBE of neutrons [14].

The main difficulties faced when trying to complete assessments of out-of-field doses in IBT is the range of detection, available quality factors and spatial resolution. The detector system employed needs to be able to detect a wide range of particles over a wide energy range, including scattered high-energy ions, neutrons from a wide range of energies and also nuclear secondaries such as alpha particles. As such, the response of the detector as well as the dead time of collection needs to be considered. Additionally, when evaluating dose equivalents near the edge of treatment fields, spatial resolution becomes an important issue. Large detectors such as Bonner spheres and REM counters become difficult to use in these situations and devices with smaller sensitive volumes such as CR-39 and microdosimeters (whether tissue-equivalent proportional counters or silicon microdosimeters) become more useful in this high-gradient region.

A further complication is the need to measure a mixed radiation field and then assign meaningful quality factors to the measured spectra of radiation. CR-39,

REM counters and microdosimeters are all devices that are suitable for these types of measurements. Microdosimeters and track detectors such as CR-39 have an advantage in that they can assign a quality factor, Q, to the measured radiation that is dependent upon the linear energy transfer (LET). This quality factor is specified by ICRP [1] and ICRU [15], and provides a means for determining the dose equivalent more accurately by varying the value of Q with LET. New detector types such as nanodosimetry [16–18] and $\Delta E - E$ telescope systems [19] are also being applied to these areas of metrology. Their advantage is the ability to use quality factors based on nanodosimetric ionization cluster-size distributions or from actual radiobiological data, which has the potential to provide a more accurate assessment of the radiation field in these applications.

Measurements have been completed by a number of groups concerning the out-of-field doses delivered by proton [2, 20–22] and carbon ion therapy [23]. These are typically of the order of several mSv/Gy close to the edge of the treatment field, where the measured result is influenced by scattered high-energy protons, to sub-mSv/Gy at lateral displacements typically larger than 20 cm.

Figure 21.3 demonstrates the potential of active beam delivery systems such as those used at PSI in reducing the out-of-field dose component to the patient over passive delivery techniques employed, e.g., at HCL, LLUMC and MPRI. The characteristics of the proton beam (field size, proton energy, modulation, etc.) also have a bearing on the dose equivalent delivered out of the field. Figure 21.4

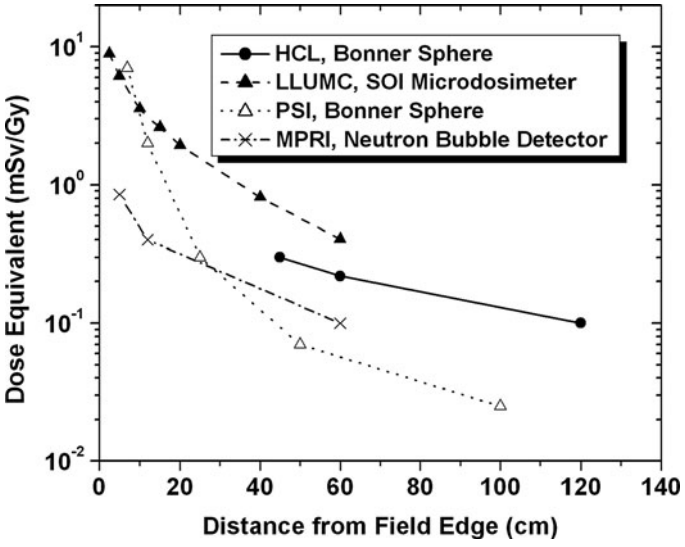

Fig. 21.3 Measured data on out-of-field dose equivalent in proton therapy from a number of centers using a range of measurement techniques and devices. Results are presented from Harvard Cyclotron Laboratory (HCL [24]), Paul Scherrer Institute (PSI [25]), Loma Linda University Medical Center (LLUMC [21]), and Midwest Proton Radiotherapy Institute (MPRI [2]). *SOI* silicon on insulator

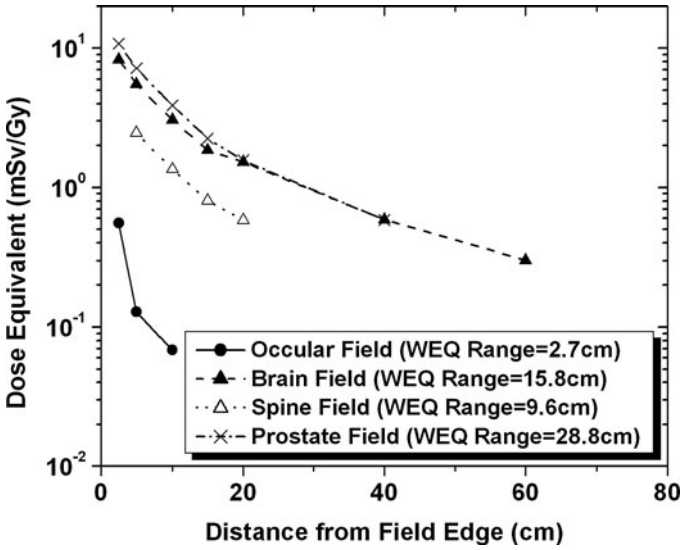

Fig. 21.4 Measured data on out-of-field dose equivalent in proton therapy [20] for a number of different treatment sites and beam configurations. *WEQ* water equivalent

demonstrates how the external field dose equivalent can vary by more than an order of magnitude based on field characteristics.

MC simulation is a very useful tool when evaluating the out-of-field components from proton therapy [26–30]. Once validated they can be used to investigate different beam configurations such as materials for collimator and scatterer design to minimize the component of out-of-field dose equivalent from these structures [31]. Simulations also provide information on particle and energy spectra present in these environments allowing researchers to better tailor their detector choices to the expected radiation field. They are also useful at providing effective doses and secondary cancer risk to various organs in simulated anthropomorphic phantoms which can be used in evaluating the efficacy of a given treatment technique. For a comprehensive summary of the data on this issue, the reader is referred to [32].

A comparison of the studies has shown that the out-of-field doses experienced by passively delivered IBT are comparable or less than those delivered in 3D-CRT and IMRT [33–35], especially close to the field edge. Additionally, the use of fewer treatment beams by passively delivered IBT allows for reduced integral doses to surrounding organs which may be of clinical benefit. Active beam scanning of protons can further reduce the out-of-field dose delivered by external beam RT. However, the method for tumor coverage is more complex and needs careful consideration to ensure that uniform dose to the tumor volume is not compromised. Choice of therapy is an important clinical decision that the physician must make in consultation with the patient weighing in many factors including the inherent

radiation protection issue of out-of-field doses, as these may present an important factor especially for younger patients.

References

1. International Commission on Radiological Protection. (1990) Recommendations of the ICRP. ICRP Report 60. Ann. ICRP **21**, **1–3** (1991)
2. G. Mesoloras, G.A. Sandison, R.D. Stewart, et al., Neutron scattered dose equivalent to a fetus from proton radiotherapy of the mother. Med. Phys. **33**, 2479–2490 (2006)
3. National Council on Radiation Protection and Measurement. *Protection Against Neutron Radiation* (NCRP Report 38, Bethesda, MD, USA, 1971)
4. National Council on Radiation Protection and Measurement. *Radiation Protection for Particle Accelerator Facilities*. (NCRP Report 144, Bethesda, MD, USA, 2003)
5. A.H. Sullivan, The intensity distribution of secondary particles produced in high energy proton interactions. Radiat. Prot. Dosim. **27**, 189–192 (1989)
6. A.B. Chilton, J.K. Shultis, R.E. Faw, *Principles of Radiation Shielding* (Prentice Hall, Englewood Cliffs, 1984)
7. J.E. Martin, *Physics for Radiation Protection: A Handbook*, 2nd edn. (Wiley, Oxford, 2006)
8. P. McGinley, *Shielding Techniques for Radiation Oncology Facilities*, 2nd edn. (Medical Physics, Madison, Wisconsin, 2002)
9. J.M. Slater, Selecting the optimum particle for radiation therapy. Technol. Cancer Res. Treat. **6**, 35–39 (2007)
10. E.J. Hall, Intensity-modulated radiation therapy, protons, and the risk of second cancers. Int. J. Radiat. Oncol. Biol. Phys. **65**, 1–7 (2006)
11. R. Macklis, In regards to Hall: Intensity-modulated radiation therapy, protons, and the risk of second cancers (Int J Radiat Oncol Biol Phys 2006; 65: 1–7). Int. J. Radiat. Oncol. Biol. Phys. **66**, 1593–1594 (2006)
12. B. Gottschalk, Neutron dose in scattered and scanned proton beams: In regard to Eric J Hall (Int J Radiat Oncol Biol Phys 2006; 65: 1–7). Int. J. Radiat. Oncol. Biol. Phys. **66**, 1594–1594 (2006)
13. H. Paganetti, T. Bortfeld, T.F. Delaney, Neutron dose in proton radiation therapy: In regard to Eric J. Hall (Int J Radiat Oncol Biol Phys 2006; 65: 1–7). Int. J. Radiat. Oncol. Biol. Phys. **66**, 1594–1595 (2006)
14. D.J. Brenner, E.J. Hall, Secondary neutrons in clinical proton radiotherapy: a charged issue. Radiother. Oncol. **86**, 165–170 (2008)
15. International Commission on Radiation Units and Measurement. *The Quality Factor in Radiation Protection* (ICRU Report 40, Bethesda, MD, USA, 1986)
16. R.W. Schulte, A.J. Wroe, V.A. Bashkirov, et al., Nanodosimetry-based quality factors for radiation protection in space. Z. Med. Phys. **18**, 286–296 (2008)
17. V. Bashkirov, R. Schulte, A. Breskin, et al., Ion-counting nanodosemeter with particle tracking capabilities. Radiat. Prot. Dosim. **122**, 415–419 (2006)
18. A. Wroe, Developments in Microdosimetry and Nanodosimetry for Space and Therapeutic Applications. PhD Thesis, University of Wollongong, 2007
19. A. Wroe, R. Schulte, A. Fazzi, et al., RBE estimation of proton radiation fields using a Delta E-E telescope. Med. Phys. **36**, 4486–4494 (2009)
20. A. Wroe, B. Clasie, H. Kooy, et al., Out-of-field dose equivalents delivered by passively scattered therapeutic proton beams for clinically relevant field configurations. Int. J. Radiat. Oncol. Biol. Phys. **73**, 306–313 (2009)
21. A. Wroe, A. Rosenfeld, R. Schulte, Out-of-field dose equivalents delivered by proton therapy of prostate cancer. Med. Phys. **34**, 3449–3456 (2007)

22. R. Tayama, Y. Fujita, M. Tadokoro, et al., Measurement of neutron dose distribution for a passive scattering nozzle at the Proton Medical Research Center (PMRC). Nucl. Instrum. Methods Phys. Res. **A 564**, 532–536 (2006)
23. S. Yonai, Y. Kase, N. Matsufuji, et al., Measurement of absorbed dose, quality factor, and dose equivalent in water phantom outside of the irradiation field in passive carbon-ion and proton radiotherapies. Med. Phys. **37**, 4046–4055 (2010)
24. X. Yan, U. Titt, A.M. Koehler, W.D. Newhauser, Measurement of neutron dose equivalent to proton therapy patients outside of the proton radiation field. Nucl. Instrum. Methods Phys. Res. **A 476**, 429–434 (2002)
25. U. Schneider, S. Agosteo, E. Pedroni, J. Besserer, Secondary neutron dose during proton therapy using spot scanning. Int. J. Radiat. Oncol. Biol. Phys. **53**, 244–251 (2002)
26. Y.S. Zheng, W. Newhauser, J. Fontenot, et al., Monte Carlo simulations of stray neutron radiation exposures in proton therapy. J. Nucl. Mater. **361**, 289–297 (2007)
27. Y. Zheng, W. Newhauser, J. Fontenot, et al., Monte Carlo study of neutron dose equivalent during passive scattering proton therapy. Phys. Med. Biol. **52**, 4481–4496 (2007)
28. Y. Zheng, W. Newhauser, J. Fontenot, et al., Study of neutron exposure during passively scattered proton therapy. Med. Phys. **34**, 2549–2550 (2007)
29. C.Z. Jarlskog, C. Lee, W.E. Bolch, X.G. Xu, et al., Assessment of organ-specific neutron equivalent doses in proton therapy using computational whole-body age-dependent voxel phantoms. Phys. Med. Biol. **53**, 693–717 (2008)
30. J.D. Fontenot, Y. Zheng, P. Taddei, W. Newhauser, Stray radiation exposure during proton radiotherapy of the prostate: The influence of the patient on scatter and production. Med. Phys. **34**, 2507–2507 (2007)
31. P. Taddei, J. Fontenot, Y. Zheng, D. Mirkovic, et al., Monte Carlo investigation of local shielding to reduce stray radiation doses to patients receiving proton therapy. Med. Phys. **34**, 2471–2472 (2007)
32. X.G. Xu, B. Bednarz, H. Paganetti, A review of dosimetry studies on external-beam radiation treatment with respect to second cancer induction. Phys. Med. Biol. **53**, R193–R241 (2008)
33. S. Kry, U. Titt, F. Poenisch, D. Followill, et al., A Monte Carlo simulation of out-of-field radiation from an 18-MV beam. Med. Phys. **32**, 1889–1889 (2005)
34. S.F. Kry, M. Salehpour, D.S. Followill, et al., The calculated risk of fatal secondary malignancies from intensity-modulated radiation therapy. Int. J. Radiat. Oncol. Biol. Phys. **62**, 1195–1203 (2005)
35. S.F. Kry, M. Salehpour, D.S. Followill, et al., Out-of-field photon and neutron dose equivalents from step-and-shoot intensity-modulated radiation therapy. Int. J. Radiat. Oncol. Biol. Phys. **62**, 1204–1216 (2005)

Chapter 22
Commercial Ion Beam Therapy Systems

Yves Jongen

Abstract When the first companies took on the challenge of designing and building commercial ion beam systems dedicated to treating patients in the 1990s, the technologies for particle acceleration, transport, and guidance had long been established. Their challenge was to develop the technologies needed to harness ion beams in a medical setting to routinely provide essentially the same capabilities of photon-based radiotherapy (RT). Having met those challenges, a variety of commercial particle beam systems are now being marketed.

22.1 The History of Commercial Ion Beam Therapy Systems

Visionaries at Loma Linda University Medical Center (LLUMC) in California paved the way for commercial manufacturing by opening the first hospital-based proton therapy (PT) facility in 1990. Other manufacturers would emerge over the next two decades with different approaches to facility design, resulting in several reliable and technically sophisticated commercial systems available on the market today.

Even the accelerator of the first hospital-based PT system at LLUMC was designed and built by a group of experienced accelerator physicists from Fermi National Laboratory, while its gantries were developed by Science Applications International Corporation(SAIC, McLean, VA, USA). Optivus, a private company initially named Elekta, was established in Loma Linda, CA, to provide maintenance and continuous development of the PT system at LLUMC. The company is led by Jon Slater, the son of James Slater, the founder of LLUMC's PT center. Optivus is proposing a PT system for sale that is essentially based on the design of the LLUMC system. Although Optivus is probably the oldest company in the PT field,

Y. Jongen (✉)
Ion Beam Applications SA, Chemin du Cyclotron 3, 1348 Louvain-la-Neuve, Belgium,
e-mail: yves.jongen@iba-group.com

U. Linz (ed.), *Ion Beam Therapy*, Biological and Medical Physics, Biomedical Engineering, DOI 10.1007/978-3-642-21414-1_22,

it is the only one that has not designed nor built a PT system. Some members of the company, however, were associated with the development and testing of the LLUMC PT system, first at Fermilab and then at the Loma Linda site.

In the mid-1970s at the Catholic University of Louvain (UCL) in Louvain-la-Neuve, Belgium, Professor André Wambersie and Yves Jongen developed a close collaboration to build a fast neutron therapy facility, which was used to treat a large number of patients. In 1986, Jongen left UCL to start the Belgium-based company Ion Beam Applications (IBA). Wambersie met Jongen in 1989 and suggested that IBA start the design of a cyclotron-based PT facility. The following year, IBA presented the initial design of its PT system based on an isochronous cyclotron and compact, scanning-only gantries at the Particle Therapy Co-Operative Group (PTCOG) XII meeting in Loma Linda.

In 1991, IBA and Sumitomo Heavy Industries (SHI) in Japan signed a 10-year collaboration agreement to jointly develop a PT system based on the IBA concept. Though this collaboration ended in 2001, it explains why the PT systems developed by IBA and SHI share many common features.

The first official tender to acquire a commercially built PT facility was launched by the Massachusetts General Hospital (MGH) in 1992. Several companies responded, but the competition finally narrowed to three groups: Maxwell-Brobeck, in association with Varian, offered a synchrotron-based system; Siemens offered two – one based on a synchrotron and another based on a superconducting isochronous cyclotron. IBA, in association with General Atomics, offered a system based on a resistive isochronous cyclotron. The tender process took a long time, but finally the contract was awarded to the IBA–GA team in April 1994.

The development of the MGH PT facility was very challenging. The specifications were new and demanding and the budget available to MGH was only $20 million for a two-gantry facility. At the time of the contract, an experienced observer dryly commented: “Unfortunately, this contract could mean the death of three good accelerator companies. Perhaps the two companies who did not win the contract, but certainly the company who got it.”

He was partly right. Shortly after the MGH contract was signed, the Brobeck division of Maxwell was disbanded and the special project group of Siemens was sold to its management. The group restarted business under the name of ACCEL Instruments and later returned to PT.

IBA also met serious problems in the development of the MGH PT systems. Although the hardware essentially came on time and on budget, IBA had badly underestimated the effort and the methodology needed to develop the software for a PT facility. The project was seriously delayed and the first patient finally was treated at the Northeast Proton Therapy Center in Boston in November 2001. IBA’s financial loss on the MGH project was huge and might have killed the company if it did not have other, more profitable activities.

In 1995, the National Cancer Center Hospital East (NCCHE) in Kashiwa, Japan, launched a tender for the construction of a PT center. The contract was signed the following year with SHI, who built the system in close collaboration with IBA. Knowing the difficulties IBA had with developing software for MGH’s PT system,

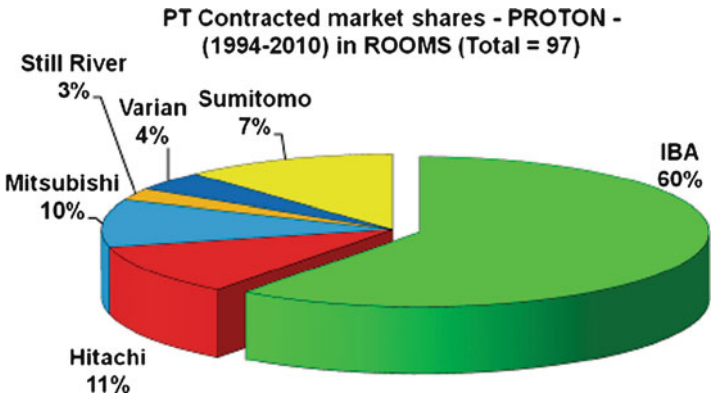

Fig. 22.1 Commercial IBT sales – market shares (1994–2010) in rooms

SHI took a more pragmatic approach in developing control software, which proved very effective. As a result, the PT center at the NCCHE treated its first patient in November 1998, 3 years ahead of MGH.

In the second half of the 1990s, the commercial activity and the number of competitors in the field of PT began to increase dramatically (Fig. 22.1). In Japan, the government funded the construction of several PT facilities. Hitachi and Mitsubishi Electric introduced synchrotron-based PT facilities. In Germany, ACCEL Instruments teamed up with Professor Henri Blosser from the National Superconducting Cyclotron Laboratory at Michigan State University to propose a PT system based on a 250 MeV superconducting isochronous cyclotron (see also Chap. 23).

In contrast to the commercialization of PT, the construction of treatment facilities using heavier particles, such as carbon ions, remained the territory of research institutions and, until a few years ago, it was unclear if any commercial solutions would ever be offered in this field. The reference ion beam therapy (IBT) facility at the National Institute of Radiological Sciences (NIRS) in Chiba, Japan, was designed and built by NIRS, largely using the expertise of Japanese industrial firms such as Mitsubishi and SHI.

But in the mid-1990s, Mitsubishi Electric signed a contract to build a combined proton and carbon ion therapy facility in Hyogo Prefecture, Japan, which opened in 2001.

In Germany, carbon ion radiotherapy (CIRT) was developed at a national research facility, the Gesellschaft für Schwerionenforschung (GSI) in Darmstadt. GSI decided to develop a dedicated, hospital-based proton-ion therapy facility and installed the prototype at the German National Cancer Center (DKFZ) in Heidelberg (cf. Chap. 20). This new facility, named the Heidelberg Ion-Beam Therapy Center (HIT), began treating patients in 2009. Siemens acquired the intellectual rights of the GSI design and is commercially offering this proton-ion therapy facility. Contracts were signed and construction work began for two facilities in Germany (Kiel and

Marburg) and one in Shanghai, China. In 2011, Siemens decided to discontinue the IBT work at the German centers.

IBA has also proposed a proton-carbon therapy facility design based on a superconducting isochronous cyclotron. In September 2010, the prototype of this system was sold to the Archade collaboration in Caen, France. The start-up of the project is still conditioned by the closing of the banks' financing which is expected during 2011.

In Japan, as GSI did at Heidelberg, NIRS designed and built a compact, hospital-based CIRT facility. The prototype is installed at Gunma University in Maebashi. The design of the Gunma facility is accessible to Japanese manufacturers and is offered commercially by Mitsubishi Electric and by SHI.

22.2 Systems and Components of IBT Facilities

As already mentioned, several new companies are offering commercial IBT systems. Some are based on reliable, time-tested designs, some are based on sound design concepts under development, while others are based on radically new ideas. At the time of this writing, eight commercial manufacturers have a total of ten IBT systems on the market. Most of their accelerator systems are either synchrotrons or cyclotrons. Synchrotrons require a linear accelerator to preaccelerate ions before being injected into the synchrotron ring. Cyclotrons do not need a linear accelerator and are self-contained. A typical synchrotron installation, therefore, requires a larger area than a typical cyclotron installation. Some IBT system components are largely standard across all designs and are of minimal interest to readers wishing to compare the commercial offerings. It is beyond the scope of this chapter to describe the operations of the ion source, particle acceleration, energy selection, and beam transport sections.

Commercial companies face many challenges in developing IBT software and hardware for dedicated clinical use. They must design and build a reliable accelerator and beam line, they must couple the beam to a gantry, and they must condition and prepare the beam in a nozzle. They also need to provide patient support systems that accurately and reproducibly position the patient's tumor with respect to the ion beam orientation, including the use of compound angles or "non-coplanar beams." In doing so, manufacturers must strive to keep the size of the facility as small as possible (for the desired number of treatment rooms to meet expected patient load), to automate functions that streamline operations, and to provide monitoring and control systems that make the system as safe and reliable as possible under all circumstances while keeping the cost of the facility as low as possible.

Most manufacturers build a multiroom facility utilizing a single accelerator, in which a central operator oversees the delivery of beams, switching between rooms during the treatment day. Gantries vary in size, shape, and number of degrees of rotation. The relative positioning and distance between the accelerator and treatment rooms affects the size of a facility. To minimize facility footprint, one manufacturer is mounting the accelerator on the gantry inside the treatment room – with the

disadvantage of requiring additional accelerators when adding treatment rooms. IBA has a design that reduces space requirements by placing the cyclotron below the treatment room.

Manufacturers take different approaches to conditioning and preparing the final beam characteristics in the nozzle. In recent years, both scattering and scanning methods of beam delivery have been adapted to clinical use. Energy fine-tuning and range modulationare accomplished with various techniques described elsewhere in this book (Chap. 25). Variable-width snouts are mounted on the end of some nozzles to accommodate various field sizes and to mechanically support field-specific collimating apertures and range compensators. Motorized beam accessories for range shifting during scanning delivery further simplify and optimize operations.

Depending on the manufacturer, cancer site, and type of treatment room, various support systems are used to precisely position the patient's tumor and anatomy with respect to beam orientation. Early commercial systems utilized traditional radiotherapy, employing either a right-hand screw mechanism or a scissors-lift hydraulic mechanism for height adjustment. It is now common to see an industrial robot adapted for medical use in the radiotherapy treatment room, offering precise computer control, multiple degrees of freedom, and high reliability and stability (cf. Chap. 33 for details). Chairs for treating a patient seated upright are also common and are typically interchangeable with the tabletop using the same motion mechanisms.

22.3 Commercial PT Systems

22.3.1 IBA

IBA's Proteus^{TM} 235 is an expandable PT system for hospitals or freestanding settings that is built around an isochronous cyclotron. It can be expanded from one to six treatment rooms as patient demand requires and budget permits. The system's 230 MeV resistive magnet cyclotron (Fig. 22.2) is 4.34 m in diameter, 2.1 m high, weighs 220 tons, and requires 9 m × 17 m floor space.

IBA's Vbeam technology is a design that reduces space requirements by placing the cyclotron below the treatment room. Available treatment rooms include gantry (Fig. 22.3), fixed-beam, dual incline, dedicated eye-line, and research rooms. The isocentric gantry has 370° of rotation with 0.4 mm radius precision, and a gantry rolling floor. Each gantry room includes a patient positioning system featuring a robot-controlled patient couch. The robot permits three orthogonal linear motions, rotation about the vertical axis, and ±3° of pitch and roll of the patient couch. Another robot is available that allows ±10° of pitch and roll plus additional features for a variety of applications.

The energy selection system (ESS) permits precise tuning of the continuous proton beam, from 70 to 230 MeV/u, in under 1 s. The beam range delivered to

Fig. 22.2 IBA's 235 MeV cyclotron for PT, Proteus™

Fig. 22.3 Gantry treatment room of the IBA PT System

treatment rooms is 0–32 cm. Beam delivery modalities include three nozzles: a universal nozzle with four automated delivery modes (single scattering, double scattering, uniform scanning, and pencil beam spot scanning); a dedicated, pencil beam spot scanning nozzle; and a single scattering eye treatment nozzle. Patient alignment and imaging systems include laser, orthogonal X-ray, fluoroscopy, cone beam (CBCT) and respiratory gating accessories. Unique PatLog™ technology automates many aspects of patient set up, positioning, and transport for imaging and treatment – enabling 4D image guidance and enhancing throughput.

Fourteen of the 35 commercial PT systems sold to date were designed and built by IBA:

- The Francis H. Burr Proton Therapy Center (FHBPTC) at MGH, Boston, MA, USA
- Midwest Proton Radiotherapy Institute (MPRI), Bloomington, IN, USA (phase 2: gantries)
- Wanjie Proton Therapy Center (WPTC), Zibo, China

- University of Florida Proton Therapy Institute (FPTI), Jacksonville, FL, USA
- National Cancer Center, Ilsan, Korea
- Roberts Proton Therapy Center, University of Pennsylvania Health System, Philadelphia, PA, USA
- Procure Proton Therapy Center, Oklahoma City, OK, USA
- Centre de Protonthérapie de I'Institut Curie, Orsay (CPO), France
- Hampton University Proton Therapy Institute, Hampton, VA, USA (treating patients since 2 Sept 2010)
- Central DuPage Hospital (a Procure Center), Warrenville, IL, USA (treating patients since 27 Oct 2010)
- Westdeutsches Protonentherapiezentrum, Essen (WPE), Germany
- ATreP Proton Therapy Center, Trento, Italy
- PTC Prague, University Hospital Bulovka, Czech Republic (scheduled to open in 2012)
- Somerset Procure Proton Therapy Center, Somerset, NJ, USA.

22.3.2 Sumitomo

SHI is marketing a PT system that provides proton beams from a 230 MeV cyclotron with a resistive magnet for up to five treatment rooms (Fig. 22.4). The system features both a conventional isocentric and a compact gantry to save space and building cost. A gantry rolling floor and a fixed-beam treatment room are available.

The system uses a multipurpose nozzle for a variety of beam delivery modes, including double scattering, single scattering (wobbling nozzle), uniform scanning,

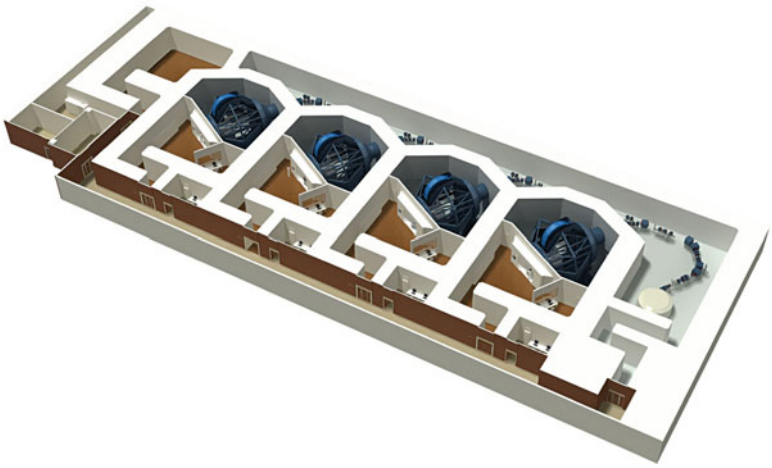

Fig. 22.4 Facility concept of the SHI PT system for Chang Gung Memorial Hospital, Taipei, Taiwan. Courtesy of SHI Ltd

IMPT spot scanning, and an eye treatment nozzle, as well as stereotactic radiosurgery. The system can deliver 2 Gy to a 1 l volume (10 cm × 10 cm with a range from 25 to 15 cm) in under 1 min with pencil beam scanning and under 20 s with double scattering.

For more flexible and faster operation without patient collimators, SHI's system features a multileaf collimator with 3 mm-wide leaves and an isocenter field size of 200 mm × 200 mm.

Patient positioning is facilitated by a robotic couch with the help of lasers and a Digital Radiography (DR) System with CBCT function. In addition to on-line PET for verification of beam accuracy, the system includes orthogonal X-rays, X-ray in beam axis, and fluoroscopy. To compensate for tumor motion, the system uses respiratory gating.

SHI has only one system currently treating patients, built in collaboration with IBA, but it was the first commercial system to do so. Their PT facility at the NCCHE, in Kashiwa, Japan, has been treating patients since 1998. The company reports that firm contracts have been signed for two systems, one in Taiwan and one in the United States. Although construction of the systems is underway, installation has not yet begun.

22.3.3 Hitachi

Hitachi proposes the PROBEAT^{TM} PT system based on a synchrotron, which has been sold to four institutions. The first, at the Proton Medical Research Center (PMRC) at the University of Tsukuba in Japan, began treating patients in 2001. The second, at the University of Texas M.D. Anderson Cancer Center (MDACC) in Houston, went into operation in 2006. These systems are based on a slow-cycle synchrotron that provides 70–250 MeV protons. Hitachi PT systems have also been sold to the Wakasa Wan Energy Research Center (WERC) in the Fukui Prefecture in Japan, and more recently to the Nagoya City Proton Center, in Aichi Prefecture, Japan.

The system at MDACC is equipped with three rotating gantry treatment rooms – two with passive scattering and one with a pencil beam scanning nozzle; one room with a large-field passive scattering beam plus a small-field passive scattering beam for eye therapy; and a research room with a passive scattering beam. The maximum beam range for passive scattering is approx. 33 cm in tissue, for the pencil beam scanner, it is approx. 36 cm, adjustable in 1-mm steps over a maximum field size of 30 cm × 30 cm. Time needed to deliver 2 Gy into 1 l volume is 1 min. Maximum range for the eye beam corresponds to 38 mm in tissue.

The four treatment rooms are equipped with rotating patient couches, plus a patient positioning chair for the eye beam. With the help of orthogonal X-rays and X-ray in-beam imaging, a patient information alignment system compares treatment planning position with actual tumor position to guide movement of the couch or

chair. The patient positioning system can accommodate patients weighing up to 136 kg.

22.3.4 Mitsubishi

Mitsubishi Electric markets a PT system powered by a synchrotron that delivers 70–250 MeV protons to up to six treatment rooms at a maximum dose rate of 2 Gy/min. Available treatment rooms include rotating gantries and fixed-angle rooms with horizontal, 45°, or vertical beam lines. Available beam modification includes wobbler, ridge filter, range shifter, and a multileaf collimator. Patient positioning is achieved by laser pointer and orthogonal X-ray systems. A typical PT system, including treatment rooms, requires an area of approx. 28 m × 55 m.

Two of the PT systems are now in clinical use, one at the Shizuoka Cancer Center and the other at the Southern Tohoku Proton Therapy Cancer Center in Koriyama, Japan. Two additional systems are under construction at the Fukui Prefecture Proton Therapy Center and at the Medipolis Medical Research Institute, in Kagoshima Prefecture, Japan.

22.3.5 Varian

The PT system of Varian Medical Systems features an isochronous superconducting cyclotron, which provides 70–250 MeV/u protons for up to six treatment rooms (Fig. 22.5). The 3-m diameter, 1.6 m-high cyclotron weighs 90 tons and requires a floor space of approximately 5 m × 5 m. The system's fixed-beam treatment rooms

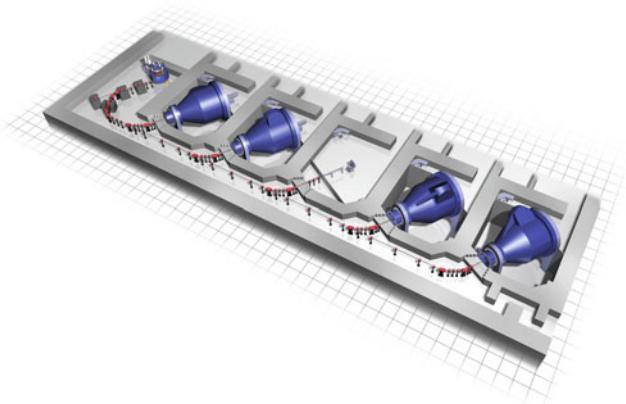

Fig. 22.5 Example of a Varian PT Facility (RPTC Munich). Courtesy of Varian Medical Systems

offer a horizontal beam that can be optimized for head, neck, or eye treatments, while its rotating gantry rooms provide 380° of beam coverage around the patient. A rolling floor is available.

To eliminate the need for custom-milled compensators and heavy brass apertures, and to reduce the generation of neutrons, the system uses intensity-modulated spot scanning (pencil beam scanning), which can be expanded to uniform scanning to cover a field of up to 30 × 40 cm. A separate eye line with single scattering nozzle is available. The maximum beam range delivered to the treatment rooms is 37.6 cm and the minimum treatment time to deliver a dose of 2 Gy to a 1-l volume (10×10 cm range from 25 cm to 15 cm) is ≤1 min. Treatment rooms are equipped with a robotic patient couch and patient positioning is guided by orthogonal X-rays (and CBCT in the near future). Organ motion is compensated by respiratory gating (Real-Time Position Management System).

In 2007, Varian bought ACCEL, who designed and was in the process of building the PT system at the Rinecker Proton Therapy Center in Munich, Germany. Varian took over the project, which began treating patients in March 2009.

22.3.6 Still River Systems

Still River Systems is offering a single-room PT system that requires much less space and capital investment than typical multitreatment room systems. Its miniaturized 250 MeV superconducting synchrocyclotron accelerator is mounted directly on the rotating gantry within the treatment room (Fig. 22.6). The diameter of the accelerator's magnetic iron yoke is just 1.8 m and the external magnetic shield is 2.2 m in diameter. While required space and building costs are lower with this approach, increasing patient–treatment capacity requires purchasing additional rooms with integrated accelerators.

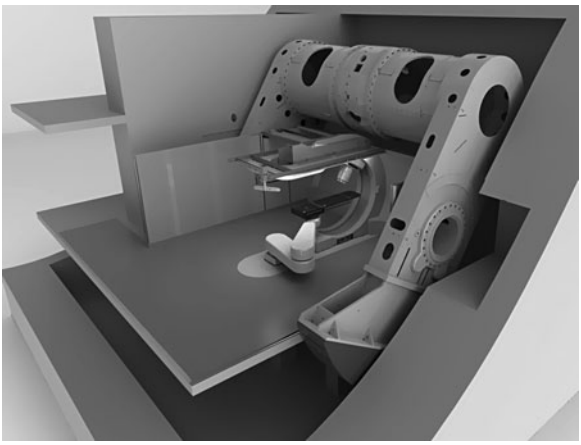

Fig. 22.6 Monarch250™ PT system of Still River Systems

The Monarch250™ system includes a gantry that rotates 190° and a treatment couch that turns 270° so that all clinically required beam orientations can be achieved. Single scattering, double scattering, and an eye line are provided and an intensity-modulated spot scanning nozzle and multileaf collimator are being developed. Tumor motion is compensated by respiratory gating. Clinical workflows are supported by a 6D robotic couch and an image-guided positioning system using lasers, orthogonal X-ray, CBCT, and fluoroscopy. Integration with third-party motion tracking is supported.

The system's beam delivery range is 5–32 g/cm^2 and the time needed to deliver 2 Gy in a 1-l volume (10 × 10 cm from 25 to 15 cm) is less than 1 min for double scattering beam modality. Total power consumption is 43 kVA on standby and 85 kVA with the beam on.

Installation of the company's first system is underway at Barnes Jewish Hospital at Washington University in St. Louis, MO, USA, with the gantry elements in place and delivery of the accelerator to follow later in 2011 (cf. Chap. 39 for details). First patient treatment is expected in 2012. The company is in sales negotiations with 16 centers in the United States and abroad.

22.3.7 Optivus

Optivus Proton Therapy is marketing a PT system similar to the first hospital-based system at LLUMC. Since their founding in 1993, Optivus has helped to maintain and design improvements for the LLUMC system. Its commercial system, the Conforma 3000, based on a synchrotron designed and built by accelerator physicists from Fermi National Laboratory, includes one fixed-beam and three gantry treatment rooms, which can be expanded to five gantry rooms to meet the therapy needs of the market area. Optivus also markets Odyssey, an FDA-cleared radiation treatment planning software application for PT.

22.4 Commercial Systems for Ions Heavier than Protons

22.4.1 Sumitomo

SHI offers a CIRT system with a resistive magnet synchrotron to deliver C^{4+} and C^{6+} ions to three treatment rooms, its standard facility configuration. Its 20-m diameter synchrotron and 10-m length ion injector require a floor space of approximately 35 × 70 m. Total power consumption for a three-treatment-room configuration is about 2,000 kW.

The system's beam delivery modalities include a wobbling nozzle for single scattering, uniform scanning, and IMPT spot scanning. A multileaf collimator is available with 3-mm wide leaves and a 150 × 150 mm field size at isocenter.

Minimum and maximum range sent to the treatment rooms is 4 and 30 cm. The minimum time to deliver a 2-Gy dose to 1-l volume with its wobbling system is 30 s. Patient positioning is accomplished by a robotic couch guided by lasers, orthogonal X-rays, X-ray in beam axis, CBCT, fluoroscopy, and online PET. Respiration gating is used to compensate for organ movement.

Although SHI has installed its ion sources and injectors at NIRS, the Hyogo Ion Beam Medical Center (HIBMC), and the Gunma University Heavy Ion Medical Center (GHMC) in Japan, it has not yet sold a complete IBT system.

22.4.2 Mitsubishi

Mitsubishi's combined proton/carbon ion system delivers either 70–250 MeV protons or 70–380 MeV/u carbon ions at a maximum dose rate of at least 2 Gy/min. Treatment rooms with fixed-horizontal, fixed-vertical, and fixed-45° angle beam lines are available as well as a room with a fixed-horizontal beam for seated patients. Modifications from these standard beam types and patient-positioning systems similar to those of the company's proton beam system are optional. This system requires an approximate area of 63×78 m, which is more than three times the space needed by the PT system.

Mitsubishi's combined proton/carbon ion system is being used to treat patients at the HIBMC in Tatsuno and NIRS in Chiba. Another Japanese center has been ordered to be installed at the Saga Heavy Ion Medical Accelerator Facility in Tosu, Saga Prefecture.

22.4.3 Siemens

Siemens markets one of the only two commercial CIRT systems currently in clinical use. The IONTRIS^{TM} system at the HIT began treating patients in November 2009 and treated more than 250 patients within the first year.

The system employs a 22-m diameter synchrotron with resistive magnets to accelerate ions from hydrogen up to oxygen from 50 to 250 MeV for hydrogen and 80 to 430 MeV/u for carbon.

IONTRIS^{TM} (Fig. 22.7) generally, provides three or four treatment rooms, all of which are equipped with intensity- and position-controlled raster scanning for precise delivery of ions to target tissues without the need of compensators, collimators, or other passive devices. The combination of dual fixed beams (horizontal, horizontal and oblique, horizontal and vertical) with a robotic patient positioner in all treatment rooms allows the coverage of nearly all clinically required beam angles using identical equipment. A laser system enables stereotactic patient alignment, and a robot imager mounted at the ceiling in each treatment room allows tumor and surrounding tissue position verification with orthogonal X-ray, CBCT, and fluoroscopy.

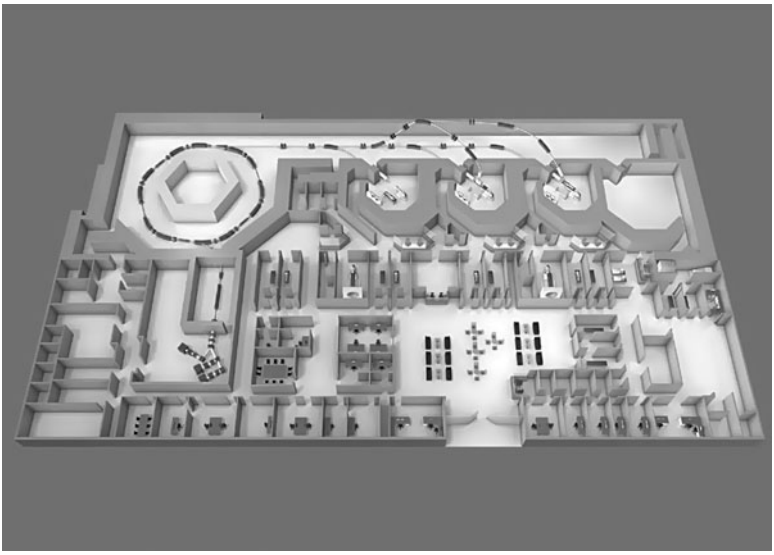

Fig. 22.7 The Siemens IONTRIS^{TM} typical facility layout

Multiturn injection into the synchrotron assures best treatment conditions from a few millimeters up to 30 cm water-equivalent penetration depth through the use of a range shifter. Minimum penetration without the range shifter is 2 cm water-equivalent. The minimum time required to deliver a 10 Gy dose of protons to a 1-l spherical volume (centered at 17 cm depth) is 2 min and 4 min for carbon ions.

In summer 2011, Siemens surprisingly announced that it would discontinue the work on the nearly finished particle therapy units at Rhön-Klinikum Marburg and NRoCK, Kiel. However, work at a third, more research-oriented installation in Shanghai, China, should continue (http://www.siemens.com/press/en/pressrelease/index.php?content=healthcare).

22.4.4 IBA

IBA has designed a compact isochronous cyclotron using a magnet for CIRT in collaboration with scientists from Dubna, Russia. Dubbed the C-400, the cyclotron will accelerate ions with a charge–mass ratio of 1/2, up to and including neon-20. IBA has signed a letter of intent with the Archade group in France to receive and test the prototype which will be ready for construction as soon as the bank financing has been confirmed.

The C-400 supports the use of hydrogen, helium, lithium-6, boron-10, carbon-12, nitrogen-14, oxygen-16, and neon-20 ions. Only hydrogen, helium, and carbon

ion beams will be fully supported for clinical use, however, the other ions will be available for research.

All ion species will be accelerated to 400 MeV/u except for hydrogen, which will be accelerated in the form of H_2^+ to achieve the desired Q/M, then split and extracted at 260 MeV. Live ion sources for hydrogen, helium, and carbon will be incorporated on the bottom of the cyclotron, which will allow for a quick switch without having to physically change ion sources.

IBA designed a compact gantry for CIRT. The reduction in gantry size, weight, and cost was achieved by using a superconducting magnet to reduce the radius at the final bend.

The C-400 features three new types of treatment rooms for the delivery of protons, helium, and carbon beams: a compact gantry; a dual fixed-beam room with ports at 45° and 90°; and a horizontal fixed-beam room with a 90° port. All treatment rooms employ pencil beam scanning nozzles. A fourth room for research features a horizontal 90° port that can deliver all eight ion species. Four types of proton rooms are also available. A facility can typically handle up to six treatment rooms.

IBA is also collaborating with the Istituto Nazionale di Fisica Nucleare (INFN) in Italy to develop a biologically optimized treatment planning engine for ions. The development time line calls for the new engine to be ready for testing in 3 years.

22.5 Outlook

Today, several facilities are operating based on the reliable, technically sophisticated, time-tested designs of the early commercial manufacturers. As most of these designs have been refined and improved over the years, new facilities are able to benefit from the latest advances in the field – such as scanned beams and image guidance.

In the last 5 years, radically new concepts have appeared on the PT market. The company Still River Systems was founded in Boston to develop and commercialize a single-room PT system based on a very high magnetic field superconducting synchrocyclotron mounted on a gantry that rotates around the patient. PROTOM International Inc., based in Flower Mound, TX, was founded to commercialize a very simple and inexpensive synchrotron developed in Russia by Professor V. Balakin. At the Lawrence Livermore National Laboratory, the concept of the Dielectric Wall Accelerator was developed by George Caporaso and his team (see also Chap. 20). It will be commercialized by Compact Particle Acceleration Corporation, a spin-out of Tomotherapy. The focus of PT system manufacturers, both established and new entrants alike, over the next decade will be to maintain the quality of their systems, introduce and refine beam shaping, modulation and delivery technologies while continuing to reduce the size of the facilities along with manufacturing and construction costs.

The first commercial carbon and ion beam systems are now treating patients while others are in development. Although fewer companies are expected to offer

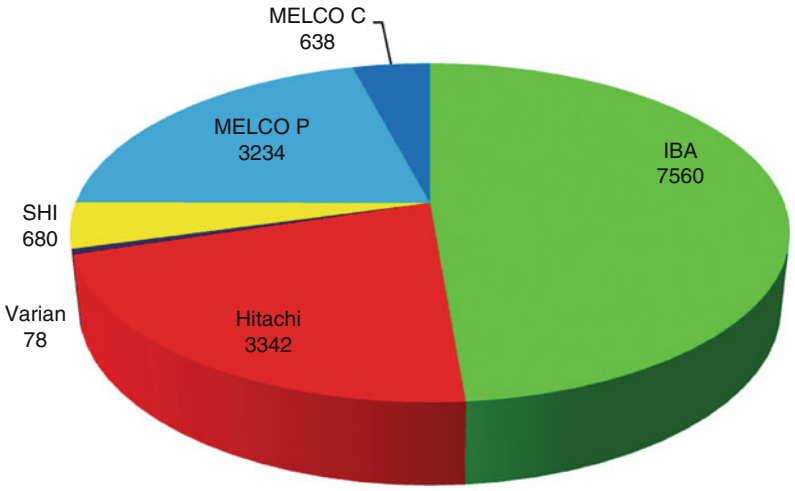

Fig. 22.8 Distribution of 15,532 total patients treated in commercially-built IBT facilities by manufacturer. The total of all patients who received IBT at all facilities in operation as of December 2009 was 62,017. Data from PTCOG's report, *Hadron Therapy Patient Statistics* http://ptcog.web.psi.ch/Archive/Patientenzahlen-updateMar2010.pdf

heavy ion systems than proton systems, leading academic research institutions will continue to pursue higher radiobiological effectiveness, shortened treatment courses, and less damage to normal tissues, which will likely generate some demand for heavier ion systems. Accelerators, gantries, nozzles, and treatment planning systems for heavy ions are certain to be the focus of development over the next several years for those manufacturers participating in this early market.

Perhaps the most important change resulting from the commercialization of IBT has been the increase in the number of patients who are able to receive treatment. According to a PTCOG report, 25% of all 62,017 patients who received treatment at IBT facilities in operation as of December 2009, had been treated with one of the commercial IBT systems (Fig. 22.8). That percentage should rise even more quickly as commercial systems under construction begin operation and new ones are sold.

Chapter 23
Advantages and Challenges of Superconducting Accelerators

Detlef Krischel

Abstract After a short review of the history toward high-energy superconducting (SC) accelerators for ion beam therapy (IBT), an overview is given on material properties and technical developments enabling to use SC components in a medical accelerator for full body cancer treatment. The design concept and the assembly of a commercially available SC cyclotron for proton therapy (PT) are described and the potential advantages for applying superconductivity are assessed. The discussion includes the first years of operation experience with regard to cryogenic and magnetic performance, automated beam control, and maintenance aspects. An outlook is given on alternative machine concepts for protons-only or for heavier ions. Finally, it is discussed whether the application of superconductivity might be expanded in the future to a broader range of subsystems of clinical IBT accelerators such as SC magnets for transfer beam lines or gantries.

23.1 Introduction

Before the 1990s, hardly any accelerator had been built as dedicated machine for IBT. Instead, IBT developed as a parasitic usage of existing accelerators for fundamental physics (cf. Chap. 1 for details), which had been designed and built to collide beams or to provide particle beams at external experimental sites [1]. Those accelerators require several hundred square meters in size which is hard to imagine in a clinical environment. The large machines require large buildings, a vast infrastructure, and a large number of accelerator specialists for machine operation, i.e., high cost in investment and operations. Some of those accelerators, e.g., the old

D. Krischel (✉)
Bruker Advanced Supercon GmbH, Friedrich-Ebert-Str. 1, 51429 Bergisch Gladbach, Germany
e-mail: detlef.krischel@bruker-asc.com

U. Linz (ed.), *Ion Beam Therapy*, Biological and Medical Physics, Biomedical Engineering, DOI 10.1007/978-3-642-21414-1_23,

590 MeV cyclotron at the Paul Scherrer Institute (PSI) were not even available year round because of too high energy cost.

An attempt to overcome this unfortunate situation was to build limited-energy synchrotrons. In 1990, Loma Linda University Medical Center (LLUMC) was the first hospital which started operation of a dedicated proton synchrotron for cancer treatment [2].

Only when a stronger demand for dedicated clinical machines came up, cyclotrons were proposed as well for proton energies from 200 to 250 MeV. In a paper of Pierre Mandrillon at the EPAC in 1990 [3], he pointed especially to the European EULIMA (European Light-Ion Medical Accelerator) project for which alternatively to a conventional synchrotron a light-ion cyclotron with SC coils was proposed. Other machines mentioned for protons were the SC synchrocyclotron proposed by Henry Blosser and the team of the National Superconducting Cyclotron Laboratory (NSCL) in East Lansing, MI [4] and the development of a dedicated 235 MeV cyclotron [5] which made use of normal-conducting magnets. This so-called CYCLONE was later selected by the Massachusetts General Hospital for their NPTC system [6]. In addition to a synchrotron-based layout, Siemens also proposed an SC cyclotron. This proposal set forth the idea to make use of SC magnet coils to squeeze the accelerator to clinical size and to reduce energy cost, as proposed by Mandrillon in [3].

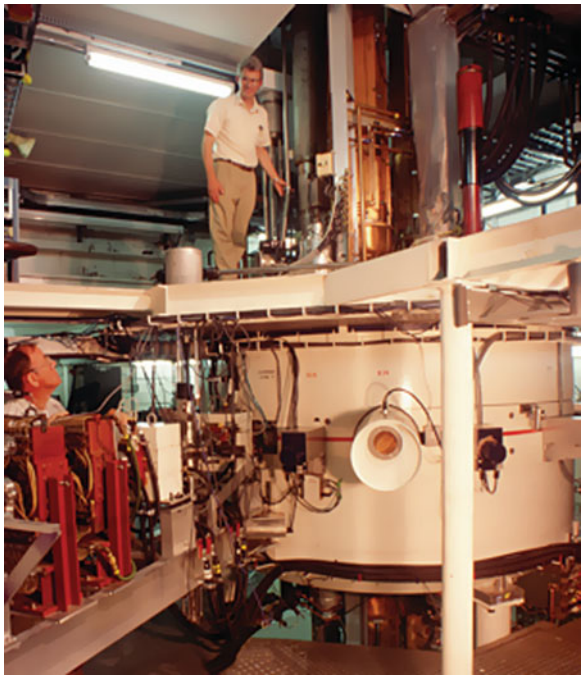

Fig. 23.1 The head of the Cyclotron Operations group standing on the decking around the top of the K500 cyclotron main magnet, the large white cylinder. Courtesy of NSCL Michigan State University

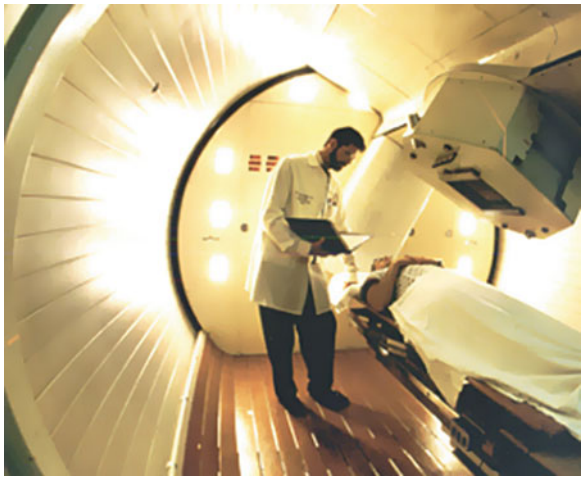

Fig. 23.2 Jeffrey Forman, M.D., present Lead Medical Doctor of the medical cyclotron project, checks the alignment of a patient about to receive treatment. Courtesy of NSCL Michigan State University

The K500 (Fig. 23.1) at the NSCL was the world's first SC cyclotron, which has since been used for physics research, but not for medical purposes [7].

A forerunner of later cyclotrons for medical usage of protons or heavier ions was a low-energy machine also designed and built by Henry Blosser and his team from the NSCL [8]. It was an isochronous SC cyclotron (K100) which was developed for neutron therapy at the Harper Hospital in Detroit (Fig. 23.2). This accelerator was the world's first SC cyclotron for cancer treatment. The machine has been operated since 1993 with short interruptions until today. However, though being a small, low-energy machine it needed a full room equipped with a helium liquefier to enable continuous operation. This infrastructural complexity was unavoidable at that time but not acceptable to other customers in a clinical environment. Also for the EULIMA project, the synchrotron was finally preferred by the expert group because of the then better-known technology [9].

It is, therefore, not surprising that among the existing therapy centers worldwide [1], only one single commercial and another research-oriented facility are making use of SC accelerators for PT [10]. This cyclotron, as described later, is designed based on the NSCL proposal of 1993 [11].

The technical challenge to combine the knowledge in the design of accelerators, of SC magnets and cryogenic systems into an SC cyclotron did appear to be too high a hurdle for a long time – with no economic prosperous market being visible. As long as SC technology did not seem to be the last resort going beyond some technical boundaries, it was not used. However, several advantages have been claimed, which may justify the effort to introduce higher complexity as long as it can be handled without risk. Despite quite some challenges, there must be good reasons nowadays for some industrial suppliers to make use of superconductivity in some IBT accelerators.

23.2 Material Properties of Superconductors in Comparison to Normal-Conducting Materials

The fundamental advantage in the application of superconductivity is to make use of the much higher current-carrying capacity of superconductors as compared to normal-conducting (e.g., copper) wires. Superconductors at low temperatures carry high currents without resistive or "Ohmic" losses, whereas such losses in a resistive magnet coil need to be compensated for by powering the system continuously. This advantage can be quantified by comparing the achievable current densities J_c of superconductors versus normal-conducting materials like copper or aluminum. The J_c of copper is around $3\,A/mm^2$ with no active cooling, and can be brought up to about $10\,A/mm^2$ when being water-cooled. The values for aluminum are very similar.

In contrast to this, an SC NbTi-filament can carry current densities of more than $3{,}000\,A/mm^2$ even in magnetic fields of about 4–10 T, see Fig. 23.3 [12] (Aubele A, Bruker-HTS, Personal communication, 2010), which is the relevant field range for the accelerators to be considered. However, such values are reduced to approx. $200\,A/mm^2$, the so-called engineering or overall current density for an SC wire or "strand" with a copper matrix embedding the SC filaments for thermal stabilization. Despite these technical limitations, it is safe to say that for the low-field regime the relative current densities of superconductors are at least a factor of 10–30 higher than for normal-conducting wires.

High current densities provide high magnetic fields, which transform into higher magnetic forces being exerted on elementary particles for bending or focusing. Altogether, this allows to build much more compact accelerators. As an example, we may look at a nonmedical accelerator like the Large Hadron Collider (LHC) at CERN, Geneva.

The LHC was built into an existing tunnel (27 km circumference including some straight intersections) with a bending radius of 2.8 km for the two 7 TeV proton rings providing a magnetic rigidity of about 23 T m. To achieve that energy, the magnetic field in the magnets must be operated at 8.3 T, which is only possible with the most sophisticated SC NbTi cable at 11.9 kA and an operating temperature of 1.9 K. With normal-conducting, water-cooled magnets providing dipole bending fields of about 2 T maximum, the bending radius of the LHC would be about 11 km or more than a factor of 4 larger, and the tunnel circumference would be in the order of 100 km. In the case of the LHC, superconductivity must be regarded primarily as the enabling technology. Transferred to medical accelerators, the usage of superconductivity facilitates to build compact machines which should be less expensive and easier to integrate into a clinical environment.

Another dream of superconductor experts has been to replace the metallic, low-T_c (T_c is the temperature at which SC materials become resistive again) superconductors by high-T_c superconductors (HTS), which can be operated at liquid nitrogen temperature of 77 K. However, their production costs which are about a factor 10–30 higher than low-T_c materials, a current-carrying performance which is not much

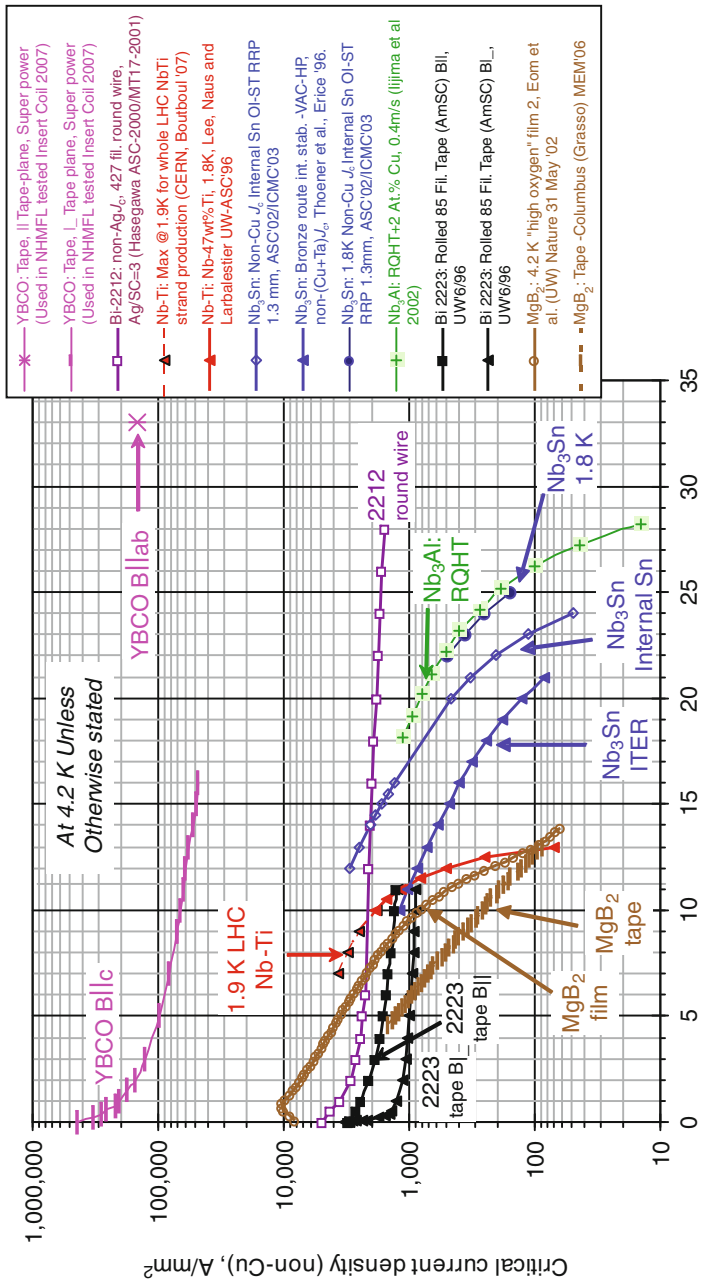

Fig. 23.3 Critical current densities j_c of different types of SC materials. Copper for comparison would be at only 10 A/mm^2, i.e., at the lowest scale figure of the ordinate

better at 77 K than for copper, and a strong nonisotropic dependency from magnetic fields (see Fig. 23.3) prevent the wide usage of HTS for large-scale projects.

23.3 Definition of a "Superconducting" Accelerator for IBT

The main misunderstanding prevailing with the medical users about an SC accelerator concerned the accessibility to the various elements of such a piece of equipment. Thinking of the accelerator vacuum chamber and devices installed therein being at a temperature of 4 K caused some reservations and wrong assumptions about the time needed for operational changes or routine maintenance. "Cold parts" would indeed impose unacceptable operational restrictions like time-consuming warm-up and cool-down procedures for maintenance purposes. However, the accelerator to be considered is using SC coils housed in their cryostat, which provides all the necessary transitions between low temperature and room temperature within a few centimeter distance from the coils such that all the conventional parts of the accelerator are kept at room temperature. Neither the RF cavities nor the ion source or the extraction elements are cold. Instead, they are accessible as in a normal-conducting cyclotron.

23.4 Specifications of a Possible SC Accelerator for IBT

The best medical accelerator must be compliant with the general performance requirements as summarized in Table 23.1. These requirements are equally important for end users as for manufacturers.

At first glance, the general performance parameters can be fulfilled by both cyclotrons or synchrotrons. For the tender of the NPTC at the Massachusetts General Hospital (MGH), several companies had developed proposals based on a cyclotron (normal-conducting or SC) or a synchrotron concept, indicating that none of the current accelerator concepts is a primary candidate in itself. However, compliant synchrotron lattices can be built in standard magnet technology and are

Table 23.1 General requirements of IBT accelerators and claims of advocates for SC cyclotrons for proton therapy (PT)

General requirements	Potential advantages of SC PT cyclotrons
High reliability	Low power consumption
Low activation	Compactness, i.e., smallest possible footprint and weight
Ease of maintenance	Ample room for particle acceleration
Fast morning start-up	Very good conditions for beam production both in quality and extraction efficiency
Ease of operation	Best suitability for advanced scanning techniques
Low-cost operation	Low contamination due to particle losses
	Faster accessibility by personnel for maintenance

Table 23.2 Beam specifications for PT cyclotrons

Parameter	Specified value
Energy	230–250 MeV
Current (at full energy)	>800 nA
Emittance of extracted beam	
Horizontal	$\leq 2\pi$ mm mrad
Vertical	$\leq 5\pi$ mm mrad
Momentum spread $\Delta p/p$	$\pm 0.2\%$
Extraction efficiency	>80%
Fast intensity modulation	$\Delta I/I > 90\%$ in 100 ms (beam switch off) with 1 kHz max. repetition rate

not considered in detail in this paper. Some aspects about SC beam line components and gantry magnets, which will be discussed at the end of the paper, are equally relevant, though, for both cyclotrons and synchrotrons.

Suppliers of SC cyclotrons do not only claim to optimally fulfill the general requirements but, in addition, they claim the advantages listed in Table 23.1 [13]. This will be assessed in detail in the following paragraphs along with the typical specifications for a proton beam as defined by PSI for their PROSCAN project and listed in Table 23.2 [10].

23.5 The ACCEL/Varian Isochronous Cyclotron for PT

23.5.1 Overview

ACCEL Instruments (ACCEL), now Varian Medical Systems Proton Therapy (VMSPT), designed, engineered, and built a 250 MeV SC proton cyclotron [14], specifically for cancer treatment. Figure 23.4 shows the cut-view of the opened cyclotron and details of the SC coils:

Two solenoidal SC magnet coils symmetric to the mid plane are embedded in a cryostat. All accelerator parts other than the SC coils are at room temperature. A distinct part of the cyclotron is the iron yoke consisting of the flux return yoke rings and the motorized upper and lower pole caps. Each pole cap has four spiral poles (or hills) that provide the needed vertical focusing for the proton beam. The RF structure consists of four dees placed between the hills and a copper liner shielding the iron from the RF power. The resonator is surrounded vertically by the pole caps and radially by the coil cryostat.

The cryogenic system is split into a supply cryostat serving as helium reservoir and the toroidal coil cryostat clamped between the yoke rings for the split main coil. A "neck" joins both parts and connects all instrumentation and the current leads to

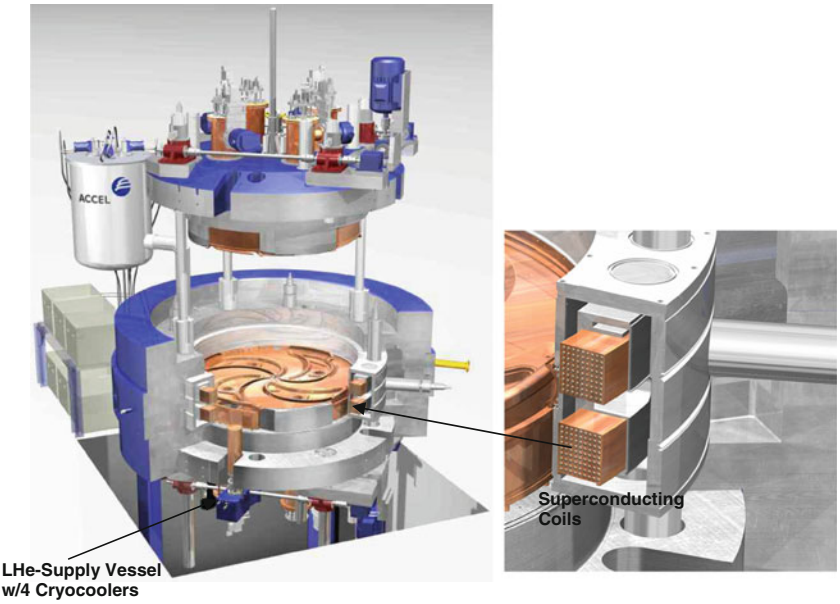

Fig. 23.4 Schematic view of the 250 MeV SC cyclotron of Accel/Varian. Main components are the iron yoke with its motorized pole caps (*the upper one* is in open position), the supply cryostat and the coil cryostat clamped between the flux return yoke rings

the coils. A radiation shield is surrounding the cold mass of the coil cryostat and the helium reservoir in the supply cryostat. Even penetrations through the median plane of the coil cryostat, e.g., for the particle extraction tube, are equipped with radiation shields.

There are four 2-stage cryocoolers assembled to the supply cryostat with 1.5 W cooling power each at 4 K and about 35 W at 50 K providing cooling power for "zero-LHe-boil-off conditions." This concept was possible only because high-T_c current leads between the first and second stage were applied. Such leads bring down the total heat loss at the 4-K level to a range which can be covered by a few cryocoolers. Provisions were made to enable the exchange of each cooler for maintenance without warming up the system. For the radiation shield of the coil cryostat separated cryocoolers are used, in addition. As for the recondensing cryocoolers, each shield cooler can be exchanged in cold condition of the magnet.

Two such identical SC cyclotrons were delivered to the customers by ACCEL in spring and summer 2004. These machines were the first ones of their kind being engineered and built solely by industry (Table 23.3).

The first cyclotron for medical purposes had been delivered, installed, and commissioned at PSI (see Fig. 23.5), for the PROSCAN project [15]. This cyclotron, called COMET, replaced a dual-use, separated-sector cyclotron, which will continue to serve as physical accelerator. The second ACCEL cyclotron was delivered to the Rinecker Proton Therapy Center (RPTC) in Munich, Germany. Whereas COMET

Table 23.3 Main parameters of the Accel/Varian cyclotron

Accelerator type	Isochronous cyclotron
Particles	Protons
End energy	250 MeV (fixed)
Extracted beam current	Up to 800 nA
Expected and measured extraction efficiency	80% in multiturn extraction mode, designed for single-turn extraction
Number of turns	650
Ion source	PIG cold cathode, internal
Total weight	Approx. 90 tons
Outer diameter	3.1 m
Magnetics	
Average magnetic field	2.4 T@center 3.0T@extraction radius
Stored field energy	2.5 MJ
Iron yoke	
Outer diameter	3.2 m
Weight	90 t
Coils	
Operating current	160 A
Ampere-turns	10^6 A-turns
Maximum field at coil	<4 T
Rated power of cryocoolers	40 kW
Wire	Conventional low-T_c, monolithic, wire-in-channel Cu/Sc ratio: approx. 10
Current leads	High T_c superconducting (BSCO bulk)
RF Cavity	
Frequency	72.8 MHz
Operation	2nd harmonic
Voltage source to puller/@ extraction radius	80/130 kV
Number of dees	4
Power	Approx. 120 kW

serves three treatment rooms, the RPTC cyclotron delivers protons to up to five rooms.

23.5.2 Cyclotron Design Parameters and Performance Data

Starting from the 1993 NSCL proposal [11], ACCEL refined and finalized the design in close collaboration with NSCL. In particular, the cryogenics had to be adapted to the special user-friendly needs of a medical environment.

The design features of the cryosystem are given in Table 23.4.

After assembly, both cyclotrons were tested with respect to their magnetic and cryogenic properties. Figure 23.6 shows a photograph of the cyclotron during tests at

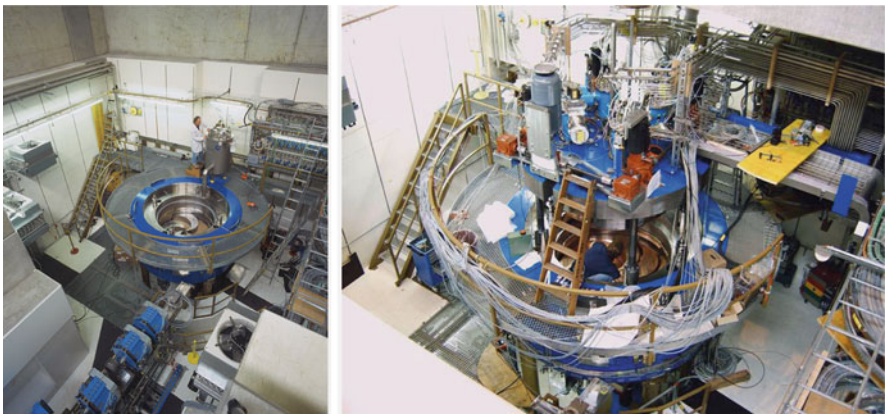

Fig. 23.5 The Accel/Varian cyclotron during assembly and commissioning at PSI. Commissioning of the superconducting cyclotron at PSI; Courtesy of PSI and Varian Medical System

Table 23.4 Design features of the Accel/Varian cryosystem

Type	Bath cooling, zero boil-off system, inherent quench safety no active protection necessary
Heat balance	<3 W at 4.2 K for normal operation
Refrigeration capacity	4 × 1.5 W at 4.2 K and 4 × 35 W at 50 K provided by four 2-stage Sumitomo cryocoolers, one redundant cooler
	2 × 60 W at 70 K provided by two single-stage CTI Cryodyne cryocoolers
Maintenance interval of cryocoolers	>10,000 h, no warming up needed
Helium reservoir	16 h of normal operation w/o cryocoolers possible
Power requirements	6 × 6.5 kW

ACCEL. At this stage, no RF components were in place but a magnetic field mapper was installed. Cryogenic tests included the verification of cryogenic properties such as heat balance, cool-down and warm-up times, and quench tests. In December 2003, the first cyclotron was energized to about 10% above the design current of 160 A without a single quench. This was a very important step as cryogenic superconductor stability is a must for the successful implementation in a PT facility.

With the power supply providing a maximum voltage of 60 V, ramp rates of 20 A/min were run during the tests at high excitation. Even at the limit of ramp rates, it was impossible to initiate a quench in the system. Instead, quench heaters that are attached directly onto the coil windings were used to trigger a safety quench. That way, heat can be applied directly to the coil locally distributed over an area of 10 cm^2. This area is much smaller than the area that would be heated by neutrons produced by a locally stopped proton beam as shown in Fig. 23.7. The calculated neutron-induced heat load in the 4-K mass of about 1.25 W from a proton current of 500 nA and 80% extraction efficiency could later be confirmed by measuring

Fig. 23.6 The SC cyclotron at the ACCEL premises during magnetic and cryogenic system tests. Courtesy of Varian Medical Systems

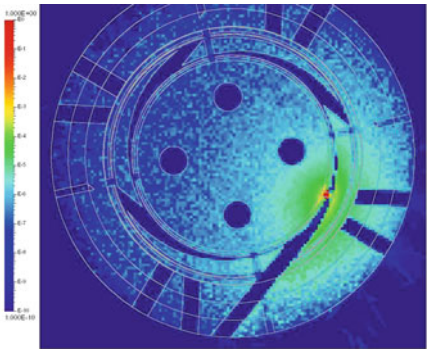

Fig. 23.7 Power density of neutrons produced by a 250 MeV proton beam stopped inside the cyclotron in the radial probe head at extraction radius; color-coded logarithmic scale ranges from 10^{-10} to 10^{0} W/cm^3. Courtesy of Varian Medical Systems

the cryogenic heat balance at the 4-K level. Stepwise increasing the power of the heater, the magnet quenched as the power was set from 4 to 5 W. This result proved the general cryogenic layout to be conservative and reliable.

When the second cyclotron was tested in spring 2004, the excellent results were reproduced indicating that the production procedures were appropriate and satisfied all needs for reliable manufacturing of this kind of machines. Figure 23.8 shows the cyclotron and the first section of the beam line toward the patient treatment rooms.

During the factory tests as well as during the first years of operation at the customers' sites, the conservative layout of the cryogenics was confirmed for both machines. The design current was exceeded without a single quench, and cooling power is more than sufficient. Therefore, it can be concluded that the cryogenic design (zero boil-off) is compliant with an IBT environment.

Fig. 23.8 The ACCEL/Varian cyclotron installed at the RPTC in Munich. The beam line with some quadrupoles is visible *on the right*. Courtesy of Varian Medical Systems

Commissioning / Verification

Isochronism: Smith–Garren measurement

Smith-Garren:
- Variation of main coil current

Goal:
- Verification of magnetic field shimming
- Verification of energy gain per turn

Result:
- excellent agreement between phase curve derived from measured field maps and Smith-Garren measurement

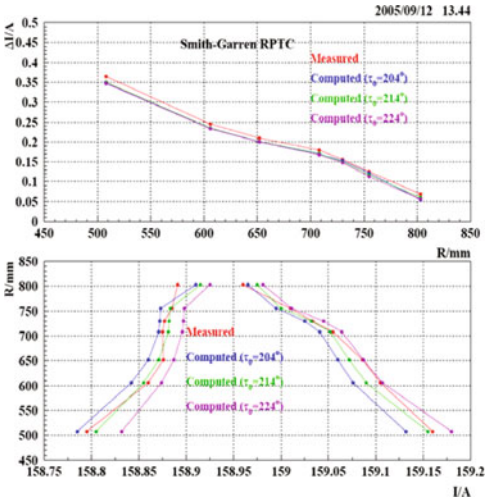

Fig. 23.9 Verification of isochronism conditions. Courtesy of Varian Medical Systems

23.5.3 Operational Routines and Maintenance Aspects

For an automated operation of the cyclotron without a continuous control by a dedicated operator, it was essential to know, anticipate, and verify as best as possible the behavior of the machine under all thinkable conditions. Figure 23.9 illustrates an example for such verification showing the agreement between phase curves derived from measured field maps and from so-called Smith-Garren measurements when the coil current was slightly varied [16].

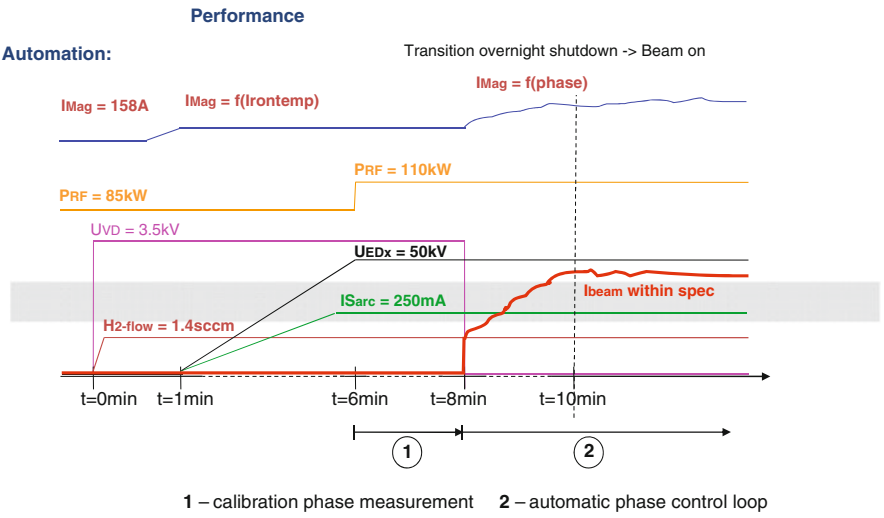

Fig. 23.10 Automated operation. Courtesy of Varian Medical Systems

Another essential criterion for the applicability in a hospital environment is a fast warm-up period in the morning and a high repeatability of the start-up behavior. Figure 23.10 demonstrates that this is met. A typical automated operation to restart after an overnight shut-down of the machine demonstrates beam availability according to specifications within only approx. 10 min. Of course, such performance needs repeated calibrations and daily QA checks.

One step in that procedure is the automated cyclotron tuning using beam phase measurements [17]. During operation of the cyclotron, heat dissipation of the RF system induces a small drift in the iron temperature. This temperature drift slightly detunes the magnetic field and small corrections must be made. Using a fast nondestructive beam detector mounted directly behind the last flange of the extraction channel of the cyclotron, the detuning of the cyclotron can be measured and a feedback loop is used to correct the current in the main coil to achieve stable operational conditions [18]. Activating a continuous feedback on the main coil current allows to run the machine in a kind of two-button operation.

After 2 years of operation, Accel reported about relevant maintenance operations for internal components [13]. The maintenance of cold heads and shield coolers every 12–18 months is the only maintenance activity which is due to superconductivity! The expectations on the consequences of the good extraction efficiency for maintenance of parts within the cyclotron vacuum chamber were confirmed by measurements 24 h after beam off when the effective dose rate at the opened cyclotron was only 250 μSv/h which is considered very low.

23.6 Assessing the Potential Advantages of an SC Cyclotron

The usage of an SC main coil for a cyclotron is not new. There are many examples in the USA (NSCL), Italy (INFN), and the Netherlands (KVI) where this technique was successfully applied. In all these cases, individual designs were established by scientific institutes. However, ACCEL brought the first commercially available SC cyclotrons on the market, featuring a modern and easily maintainable cryosystem as it is used in other medical products such as MRI magnets. This points at an issue associated with the operation of an SC accelerator: the cryogenic system. An SC accelerator still needs a cryogenic "medium," either liquids or a "heat sink," which cools down the coldmass in a cryostat. The cryostat, which typically provides at least three temperature levels, must be operated under vacuum and must contain security devices for a possible failure of the magnet coil if getting resistive under a "quench."

Acceptance in the market, i.e., by medical users, is found only if the system can be run as a "zero-boil-off" bath or a "dry" system, where the magnet is cooled by thermal conduction from the cold finger of a cryocooler. Given this fact, one can reflect the advantages to use SC coils for the operation of a medical cyclotron.

The discussion will go along the claims listed in Table 23.1.

23.6.1 Low Power Consumption

The cryogenic system needs approximately 40 kW of electrical power, whereas the power consumption of the magnet for a comparable normal-conducting cyclotron is in the order of 300 kW. Besides the fact that the running costs for a normal-conducting cyclotron are higher, the higher dissipated power also asks for a more powerful water cooling system.

23.6.2 Fast Morning Start-Up Time

An SC cyclotron magnet stays continuously electrically powered because the power from the 500 W supply is negligible. In contrast, it takes a long time for the large amount of copper and iron in a normal-conducting accelerator to get into thermal equilibrium when being switched on in the morning. This is very critical, since for the operation of a cyclotron relative field accuracies in the order of $\Delta B/B \sim 10^{-4}$ have to be reached. In fact, when facing such small allowable deviations, the iron yoke of a normal-conducting cyclotron will not even reach thermal equilibrium within 1 day of operation.

23.6.3 Compactness

The weight of an SC cyclotron is approximately 90 tons as compared to 200 tons for a normal-conducting unit. The outer diameter of 3 m for a 250 MeV SC cyclotron is approximately 1 m smaller than for a normal-conducting one. All this reduces the requirements for transportation, reinforcements in the building, and the weight of activated material for later waste disposal.

23.6.4 Ample Room for Particle Acceleration

To compensate for relativistic effects (the protons will reach more than 60% of the speed of light), the magnetic field has to be higher at large radii. Since there are limits for the hill width, the only method to increase the average field in a normal-conducting cyclotron is to reduce the magnetic gap at higher radii (elliptical pole shape). This reduces the space at the extraction radius and leads to increased nonlinearities in the magnetic field. Higher-order effects and a more distorted phase space, which may cause beam losses, unpredictable beam behavior, and a reduced extraction efficiency are the consequence.

The SC coils, in contrast, are providing very good conditions for beam "production" both in quality and extraction efficiency, resulting in low contamination losses allowing also for fast accessibility for maintenance.

Table 23.5 summarizes the pros and cons of an isochronous SC proton-only cyclotron.

23.7 Other SC Medical Accelerators for Protons

Synchrocyclotrons have played an important role in IBT. The old Harvard cyclotron providing an energy of up to 165 MeV was used to treat more than 9,000 patients until the year 2002. It was a huge machine with normal-conducting coils.

The concept of the synchrocyclotron was adopted a few years ago by the company Still River Systems in Littleton, MA, for a very compact machine [19]. It comprises a magnet of 10 T maximum field strength wound from Nb_3Sn conductor. The accelerator is directly mounted on a rotating gantry (see Fig. 23.11 and Chap. 39).

In a design study, ACCEL proposed a similar synchrocyclotron [20]. Different from the Still River concept, it should feed protons into a beam line on a gantry which could include degrader functionality, beam transfer, and nozzle.

However, such synchrocyclotrons deliver a pulsed proton beam with a 1 kHz time profile of the beam. Such a beam could still comply with the spot scanning techniques as applied at PSI if the dose to each spot is an integral during the

Table 23.5 Summary of assessments and conclusions on SC cyclotrons

	Impact on system or performance due to superconductivity	Comment
Pros		
1. Compared to synchrotron	Continuous beam with steady intensity	
2. Compared to synchrotron or normal-conducting cyclotron	Smaller footprint	
3. Compared to normal-conducting cyclotron	Less power consumption	
	Larger space for particle acceleration → good extraction efficiency	
	Less particle losses → Less neutron contamination → better maintenance conditions	
Cons	Uncommon to medical users	MRI experience should help
	Need for joint know-how in accelerators, superconducting magnet technology and cryogenics	Probably the most critical issue
	Less operational experience	True, but existing systems will provide good references
	Risk of operational malfunctions Quenches Loss of cryostat vacuum	Can be avoided by design, hardware devices, and strict control of handling instructions

hold time of the beam at the spot location. Experience is necessary to find out if the synchrocyclotron will also comply with the requirements for future continuous raster scanning with fast intensity modulation.

23.8 SC Medical Accelerators for Ions Heavier than Protons

To this writing in 2010, no SC accelerators for IBT other than for protons have been built. But several design studies have been published.

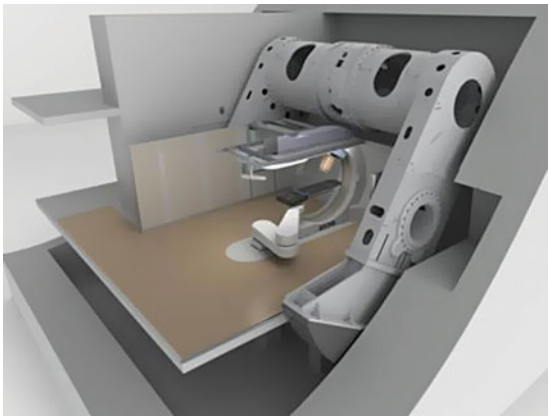

Fig. 23.11 Still River Systems Monarch 250™ synchrocyclotron. Courtesy of Still River Systems

23.8.1 EULIMA

The acronym EULIMA stands for European Light-Ion Medical Accelerator. In the 1980s, the EULIMA project became the flagship of the idea to build a light ion accelerator for a European therapy center [9, 21]. A project group at CERN developed concepts for two 400 MeV/u accelerators, a synchrotron and an SC cyclotron [9] but none of these machines has been built.

23.8.2 SCENT300

Since 2005, the cyclotron group of the INFN in Catania, Italy, is making "parasitic" use of their SC research cyclotron for eye treatments. At about the same time they proposed to develop a 300 MeV/u SC cyclotron for fully stripped carbon ions and ionized hydrogen molecules H_2^+ [22].

Although such a medium energy accelerator would not allow to treat the deepest seated tumors with carbon, INFN claims that about 70% of all tumor locations could be treated at much reduced cost of the accelerator compared to a 400 MeV/u machine. Superconductivity in this case would keep the dimensions of the accelerator within "reasonable size", the cyclotron weight is calculated to be less than 350 tons and the diameter approx. 5 m. Whereas the main coils of the cyclotron should be SC producing a maximum magnetic field of 4.95 T, the small difference in the charge-to-mass ratio of the selected ion species C^{6+} and H_2^+ does require a pair of room-temperature tuning coils to correct for isochronism during acceleration. INFN pursued the concept with two different industrial partners but at this writing (fall 2011), it had not been realized.

23.8.3 C400 IBA

The Belgian company IBA in collaboration with the Joint Institute of Nuclear Research (JINR), Dubna, Russia, designed an SC isochronous cyclotron called C400 for carbon ions of a maximum energy of 400 MeV/u [23]. The ions are extracted by an electrostatic deflector. The C400 is intended to accelerate H_2^+ ions to 265 MeV/u and extract them by stripping. To achieve the high particle energy at low enough stray fields around the cyclotron, the yoke diameter becomes 6.9 m and the total weight is about 660 tons (cf. Chap. 22). Obviously, such a cyclotron although being by itself still relatively compact compared to a synchrotron is not a small machine and does require special means for an eventual installation in a nonresearch environment. The design has made good progress [24] but a start to build the cyclotron has not yet been confirmed.

23.9 SC Beam Line Magnets and SC Gantry Magnets

The use of SC magnets for transfer beam lines or gantry magnets was discussed at several PTCOG or EPAC conferences but no magnet has been built or even introduced in a clinical environment so far. Superconductivity must compete with the well established standard technology of resistive water-cooled copper-wound magnets providing excellent field quality by using magnetic iron poles made from low-carbon steel laminations. Whereas the copper magnets have been built in thousands around the world, SC ones replacing low-field magnets must still be developed and prove compliance with the specified requirements. The clear advantage of much less power consumption must compete with the established procedures in design, standardized assembly processes as well as beam control, alignment, and operation.

A PT facility with four gantry-equipped treatment rooms will need an installed power for the transfer and gantry beam lines, i.e., lattice achromatic dipoles, all quadrupoles, and bending dipoles in the order of 3 MVA. Assuming a duty cycle for ramping the magnets of 50% for settings to the required energies and switching between rooms and typical times for clinical operations of 14 h per day (QA and start up excluded), total cost in the order of several 100 k€/a need to be covered assuming 0.10 €/kWh. Part of the cost may be reduced by an optimal sequence of ramping operations, but the criticality of high cost is still relevant.

SC gantry magnets appear to be even more attractive because they could reduce the steel structure both in size and weight and, hence, in cost. Two crucial aspects prevent a wide implementation of SC magnets: the need for fast ramping and the gantry rotation.

The problem of fast ramping which creates unavoidable AC-losses in the conductor beyond the steady-state Ohmic losses can be avoided when the transfer beam line magnets are designed for fix, maximum energy as far as possible toward

the patient rooms and degraders are installed only at the minimum distance to the beam isocenter, i.e., in front of the gantry or on the gantry itself. Running the transfer beam line magnets in steady-state would allow to cut the power needs by several hundred kW corresponding to approx. 100–200 k€ savings per year in the energy bill. Although the advantages of SC magnets are clearly recognized, there is still some reservation concerning the usage of liquid helium and misunderstandings about cryogenic options as expressed in [25].

The economical impact of an SC accelerator on the necessary investment for the building is relatively minor, when the total facility is considered. However, the much smaller size of the caves for SC gantries could reduce the investment quite dramatically, especially for ion machines. Also the operation cost could be reduced by several hundred thousand Euros per year.

23.10 Conclusions

SC cyclotrons have been operated for more than 20 years in research institutes and for more than 5 years in IBT in a clinical environment. Superconductivity is not necessarily the exclusive enabling technology for IBT accelerators but the expected operational and cost advantages of SC cyclotrons have been verified successfully. However, some lack of knowledge on the user side about the maturity of superconductivity as a state-of-the-art technology and the very limited number of industrial suppliers prevent a widespread use. Combined know-how about accelerators, SC magnet design, and cryogenic operations are considered a great challenge to enter into the development of SC accelerators for IBT. Increasing experience with the successful operation of the existing SC accelerators should help to overcome remaining hurdles.

Gaining experience should also encourage the industry to develop more SC components for future IBT accelerator systems when aiming for more compact and less expensive facilities.

References

1. Particle Therapy Co-Operative Group (PTCOG), Particle therapy facilities in operation. http://ptcog.web.psi.ch/ptcentres.html. Accessed April 2010
2. J. Slater, Applying charged particle physics technology for cancer control at the Loma Linda University Medical Center, Proceedings of EPAC, pp. 286–288, 1990. http://www.protons.com/proton-therapy/proton-videos/proton-therapy-at-loma-linda.html. Accessed 29 Nov 2010
3. P. Mandrillon, High energy medical accelerators. Proceedings of EPAC90,Nice, 12–16 Jun 1990, p. 263
4. H. Blosser, Present and future superconducting cyclotrons. Proceedings of Particle Accelerator Conference (PAC), Washington DC, 16–19 Mar 1987. Bull. Am. Phys. Soc. **32**, 171 (1987)

5. Y. Jongen, Preliminary design of a reduced cost proton therapy facility using a compact, high field isochronous cyclotron. Presented at PTCOG XII, Loma Linda, 7–9 May 1990
6. Northeast Proton Therapy Center. Request for Proposal to design and construct the Proton Therapy Equipment for the NPTC at the MGH, NPTC-10, 12/18/92
7. H. Blosser, National Superconducting Cyclotron Laboratory, NSCL. http://www.nscl.msu.edu/tech/accelerators/k500. Accessed 15 Sept 2010
8. H. Blosser, G. Blosser, J. Dekamp, et al., Compact superconducting cyclotrons for neutron therapy. IEEE T. Nucl. Sci. NS-**32**, 3287 (1985)
9. P. Mandrillon, C. Carli, G. Cesari, et al., Feasibility study of the EULIMA light ion medical accelerator. Proceedings of EPAC92, Berlin, 24–28 Mar 1992, pp. 179–181
10. M. Schillo, A. Geisler, A. Hobl, et al., Compact superconducting 250 MeV proton cyclotron for the PSI PROSCAN therapy project. Proceedings of 16th International Conference Cyclotrons and Their Applications, East Lansing, MI, 13–17 May 2001, p. 37
11. H. Blosser, Proposal for a Manufacturing Prototype Superconducting Cyclotron for Advanced Cancer Therapy -MSUCL-874, 1993. http://www.nscl.msu.edu/tech/accelerators/k250
12. P.J. Lee, D.C. Larbalestier, Microstructural factors important for the development of high critical current density Nb3 Sn strand, Cryogenics **48**, 283–292 (2008)
13. A.E. Geisler, J. Hottenbacher, H.U. Klein, et al., Commissioning of the ACCEL 250 MeV proton cyclotron. Proceedings of 18th International Conference on Cyclotrons and their Applications, Giardini Naxos, Italy, 1–5 Oct 2007, pp. 9–14
14. D. Krischel, C. Baumgarten, A. Geisler, et al., Design aspects and operation experience with a novel superconducting cyclotron for cancer treatment. IEEE T. Appl. Superconduct. **17**, 2307–2310 (2007)
15. J.M. Schippers, J. Duppich, G. Goitein, et al., The use of protons in cancer therapy at PSI and related instrumentation. Proceedings of EPS Euroconference XIX Nuclear Physics Division Conference. J. Phys. Conf. Ser. **41**, 61–71 (2006)
16. C. Baumgarten, A. Geisler, H.U. Klein, et al., Isochronism of the Accel 250 MeV medical cyclotron. Nucl. Instrum. Methods Phys. Res. A **570**, 10–14 (2007)
17. H. Röcken, C. Baumgarten, T. Stephani, et. al., Automatic tuning and operation of the Accel 250 MeV superconducting proton cyclotron. Presented at European Cyclotron Progress Meeting (ECPM) Berlin, 15–18 Oct 2008
18. J.H. Timmer, H. Röcken, T. Stephani, et al., Automated cyclotron tuning using beam phase measurements. Nucl. Instrum. Methods Phys. Res. A **568**, 532–536 (2006)
19. J.B. Flanz, What's new in particle therapy accelerator technology? Nucl. Instrum. Methods Phys. Res. B **261**, 768–772 (2007)
20. J. Timmer, C. Baumgarten, A. Geisler, et al., The ACCEL single-room proton therapy facility. Presented at PTCOG 45, Houston, TX, 7–11 Nov 2006. http://ptcog.web.psi.ch/PTCOG45/PTCOG45%20Abstracts.pdf. Accessed 29 Nov 2010
21. U. Amaldi, G. Kraft, European developments in radiotherapy with beams of large radiobiological effectiveness. J. Radiat. Res. **48**, A27–A41 (2007)
22. M. Maggiore, L. Calabretta, D. Campo, et al., SCENT 300, A superconducting cyclotron for hadron therapy. Proceedings of EPAC08, Genoa, Italy, 23–27 Jun 2008, pp. 1812–1814
23. Y. Jongen, M. Abs, A. Blondin, et al., Current status of the IBA C400 cyclotron project for hadron therapy. Proceedings of EPAC08, Genoa, Italy, 23–27 Jun 2008, pp. 1806–1808
24. F. Forest, D. Albertini, S. Antoine, et al., Superconductive coils and cryostat status for the C400 cancer therapy cyclotron. Presented at Int Conf on Magnet Technology (MT-21), Hefei, China, 18–23 Oct 2009
25. M. Pullia, Improving ion gantries. Presented at PTCOG 48, Heidelberg, 28 Sep–3 Oct 2009. http://ptcog.web.psi.ch/PTCOG48/presentations/M.%20Pullia%20-%20Improving%20ion%20gantries.pdf. Accessed 12 Oct 2010

Part VI
Beam Preparation and Control

Chapter 24
All-in-One: An Attempt to Integrate the Full Potential of Proton Pencil Beam Scanning in a New Gantry System

Eros Pedroni

Abstract This article describes the main ideas underlying the design of the new Gantry 2 (G2) system of PSI. Based on a conceptually simple but very powerful scanning technology, the new second-generation scanning system is derived from the positive experience of using the previous gantry, Gantry 1 (G1). This article will provide a general overview on the various technological options faced when realizing such a new device. The reasoning for the present system will be discussed, and alternative solutions will be described, where appropriate.

24.1 Introduction

The only long-term experience with a proton gantry based on the spot scanning technique has been the one with G1 of PSI. The new system G2 has been designed for maximum flexibility without any compromise in performance. It offers a wide range of scanning modalities, since the main intention of the G2 project is to explore the potential of scanning in its full extent.

Published information of the performance of commercial scanning gantries is still very scarce. For this reason, this article does not attempt to provide a review article on gantries. The main goal is rather to discuss in which direction the proton therapy (PT) technology could or should evolve in the next decade. The author's hope is that the presentations will be useful for extracting specifications and ideas for future systems. The points relevant for this purpose are highlighted in *italic*.

E. Pedroni (✉)
Center for Proton Therapy (CPT), Paul Scherrer Institut, 5232 Villigen, Switzerland
e-mail: eros.pedroni@psi.ch

U. Linz (ed.), *Ion Beam Therapy*, Biological and Medical Physics, Biomedical Engineering, DOI 10.1007/978-3-642-21414-1_24,

24.2 The First Scanning Gantry at PSI

The first PSI gantry G1 was built in 1992 with limited resources as a side project of physics experiments [1]. The major goal in the 1990s was the development of a very basic pencil beam scanning approach. The confidence to treat human patients with pencil beam scanning was achieved only after a long phase of veterinary treatments from 1994 until 1997 (dogs with spontaneous tumors). Until 2008, when the Hitachi scanning gantry came into operation at the M.D. Anderson Cancer Center (MDACC) in Houston [2], G1 was the only proton scanning gantry in the world. Today, G1 is mainly used for complex treatments and it is the only system delivering intensity modulated proton therapy (IMPT) on a regular basis [3]. This is a major feature derived from the pion therapy project in the 1980s [4]. G1 represents a unique major first clinical experience of using proton pencil beam scanning on a gantry [5].

The major characteristic of the original system is the very compact design. With a radius of the rotating structure of only 2 m, it is the most compact proton gantry in the world (Fig. 24.1). The patient table is mounted eccentrically on the rotating support and turns with the gantry (*eccentrical gantry*). A counter-rotation maintains the patient table horizontal at any time. A major disadvantage of the eccentric approach is that the patient is moved away from the ground floor when treated with the beam from below. In fact, patients have never been treated in this situation. This is probably the major drawback of G1. Even though we would know how to improve this point in a new system [6], we decided to use an isocentric layout for G2. At G1, the scanned beam has about 3–4 mm sigma in air at isocenter [7]. Spot scanning is applied as a step-and-shoot method where the beam is switched off in between spots

Fig. 24.1 Photograph of Gantry 1, the first proton scanning gantry of the world, which treats patients since 1996

(*discrete spot scanning*). Dose control is performed by measuring with a parallel plate ionization chamber (beam monitor) the number of protons delivered per spot. Once the desired amount is reached, the beam is switched off with a fast kicker magnet upstream of the gantry. The reaction time of controlling the dose is only a fraction of the delay time of switching off the beam, which is in the order of $<100\,\mu s$.

The scanning procedure is as follows. The beam is moved by *magnetic deflection* first, followed by changing the proton range with a *range shifter*, and by moving the *patient table* in the second lateral direction as the slowest element in the scanning loops. The sweeper magnet is mounted before the last bending magnet (*upstream scanning*). The beam is scanned magnetically only within the dispersion plane of the last 90° dipole, in order to keep the gap of the last bending magnet small (7 cm). An appropriate design of the shape of the poles of the last magnet permits *parallel magnet scanning* along the dispersive direction. The apparent source of scanning on G1 is at infinity, and the scanning system is completely Cartesian.

Due to the slow motion of the patient table, which is used as a scanning axis, it is not possible to apply target repainting with G1. The slow scanning speed is the weak point of this system, which is reflected in an inherently *high sensitivity of the beam delivery to organ motion* [8, 9]. Organ motion can produce significant errors in the dose homogeneity within the target caused by the interference of the motion of the target with the pattern of scanning. For these reasons, G1 is only used for tumors of the base of the skull, the spinal cord and the lower pelvis.

The G1 system was realized step by step with limited resources and many compromises. Today, it is conceptually a 20-year-old system. Despite these limitations, G1 has essentially contributed to spreading the scanning technique. Many new PT facilities with gantries are now realized based solely on this technique (in Munich and Essen, Germany, and Trento, Italy).

The appreciation of scanning has grown substantially since the introduction of IMPT with this system [10, 11].

24.3 The Rationale of Using a Proton Gantry

Despite the fact that PT can deliver a conformal dose just from a single direction, the use of a gantry as compared to fixed beam lines brings substantial advantages.

With a gantry, one can apply several fields or "beam incidences" – typically 1–3. The plateau dose can be distributed within the body and the local dose reduced below the tolerance of organs at risk (OAR). The patient is treated in supine position in order to minimize displacements of internal organs. The supine position is the same as for CT-data-taking for treatment planning and is also the most comfortable for the patient.

A gantry offers maximum flexibility in choosing beam directions. The criteria for selecting the most adequate beam incidence(s) can prevent treatments with the beam going through sensitive organs. Similarly, also complex density heterogeneities in

the patient body can be avoided. Carefully selected beam angles can reduce dose errors due to the interplay of multiple Coulomb scattering (MCS) with range, i.e., avoid shadow effects at interfaces parallel to the beam direction like bones or metallic implants [12, 13].

A gantry permits beam angles with low ranges. This minimizes the amount of dose delivered to the healthy tissues outside the target (dose sparing).

If one wants to apply IMPT in the sense of *simultaneous dose optimization of multiple fields*, the use of a gantry is mandatory. IMPT provides complex dose distributions, for example, for target shapes having concavities. It permits to optimize the overlap of the dose fields while keeping disabled selected pencil beams from pointing at sensitive OARs.

Today, the use of a gantry is the established standard solution for PT.

24.4 The Motivation for a Gantry with Pencil Beam Scanning

Many advantages of using a scanning gantry have already been demonstrated with the G1 system.

With scanning, the dose is delivered conformally in three dimensions with *variable modulation of the range* as opposed to scattering which works with a fixed spread-out Bragg peak (SOBP), which limits its conformal capability. With variable modulation of the range, one avoids unnecessary dose in the proximal region of the target and reduces the skin dose.

Scanning is fully automated by design. Field- and patient-specific equipment, such as collimators and compensators are dispensable. This saves time in the treatment room. One can deliver multiple fields in one go without personnel entering the room in between fields.

Each delivered proton is stopped in the patient. The activation of equipment in the area is minimized. The *neutron dose* applied to the patient is limited to the neutrons generated within the patient body as opposed to passive scattering where the additional neutron background from beam modifiers and apertures in the nozzle is a point of possible concern (cf., as well, Chap. 21). To keep the beam utilization efficiency of a scattered beam similarly high, one needs very sophisticated beam spreading systems for a large variety of field sizes.

With scanning one can deliver from very small up to very large fields using the same equipment. Scanning is well suited for IMPT. The simultaneous optimization of dose fields is used at PSI for about one-third of all patients.

Scanning is also well suited for *biological targeting*, i.e., the planned delivery of nonhomogeneous dose distributions, where dose shaping in the interior of the target is driven by imaged biological tumor activity. There are similar developments in conventional therapy with IMRT. Scanning is today considered a necessary prerequisite in PT to successfully compete with IMRT and tomotherapy.

Scanning is also expected to provide better precision of the dose distribution than scattering, i.e., *better conformity* of the dose field and *sharper lateral fall-off*.

For deep-seated tumors, one can take advantage of the *edge enhancement capability* of scanning. This is of interest, especially, when the unavoidable MCS in the patient body is the major contribution to the spot size. By placing highly weighted largely spaced spots at the target boundary, one can obtain a sharper lateral fall-off than by using a uniform proton flux shaped through collimation. The effect can be understood as the difference between Gaussian and error-function, which is Gaussian folded with a step function (for more details cf. [1] and figure 4 therein).

For superficial tumors, it is rather the width of the beam in air which limits the dose precision. In this special case, the dose precision can be improved by adding *collimation on top of scanning*, i.e., apertures or simple shielding blocks are machined to cover the edge of the projection of the OAR. Since there is no other material in the beam path, the dose penumbra is governed solely by the phase space of the undisturbed pencil beam. For scattering, one usually needs a compensator, in addition. The MCS generated in the compensator and propagating in the air gap to the patient produces additional deterioration of the dose penumbra, which makes scattering possibly less competitive than scanning. Scanning with properly selected options – *with/without additional collimation* – is, therefore, superior to scattering in terms of dose lateral fall-off in most situations.

There have been attempts to realize gantries capable of delivering both – scattering and scanning in the same nozzle – starting from scattering. The practical experience has shown that this approach is not going without complications and compromises. A major issue is the deterioration of the beam spot size affecting the dose shaping precision of scanning due to many devices in the beam path and the long distance that the beam travels in air. In the end, a "universal nozzle" implies the parallel development of two completely different types of beam delivery systems. The control system, equipment and treatment planning are correspondingly complex.

With G2 we could show the technical feasibility of *simulated scattering* on a scanning gantry [14], by implementing very fast and flexible *uniform scanning* with the capability to apply a *high number of volumetric repaintings* to reduce organ motion sensitivity. Simulated scattering on a scanning gantry could improve scattering beyond its known performance. The deepest uniform dose energy layer can be delivered to just cover the shape of the projected target (including a collimation margin), to reduce neutrons. The shape of the proximal isoenergy layers can be eroded in function of the target shape, when moving the Bragg peak to shallower depths. This way, one can provide *simulated scattering with variable modulation of the range*. On G2, scattering is simulated with a two-dimensional parallel scanned beam. The *parallelism of simulated scattering* brings additional advantages. Collimators can be machined with normal edges. Dose homogeneity errors introduced by compensators can be avoided because of the parallel beam. It is much easier to simulate scattering or wobbling on a scanning system than the reverse.

The main goal of G2, however, remains the development of fast, repetitive, volumetric, conformal scanning to deliver uniform and intentionally nonuniform dose distributions without the need for field-specific collimators and compensators.

The new system of G2 at PSI was designed with these goals in mind [15].

24.5 The Open Problem of Scanning: Sensitivity to Organ Motion

There are two types of dose errors in the context of organ motion, *blurring of the edges of the dose distribution*s and disturbances in the *homogeneity of the dose*.

Blurring of the lateral fall-off of the dose distribution due to organ motion is the same for scanning and for scattering. This error can be compensated by safety margins, or can be reduced by using gating or tracking [16].

With scattering, the dose can be delivered quickly and uniformly over the full volume. If the whole dose volume is applied within a fraction of the breathing cycle (e.g., a SOBP cycle <100–200 ms with a rotating wheel) scattering can be applied without dose-homogeneity errors within the target. This is the major advantage of scattering.

With scanning, it is not possible to paint a full volume in a fraction of the breathing cycle. The interference between organ motion and the sequence of scanning can, therefore, produce substantial dose-homogeneity errors. This major drawback of scanning is a known issue for any dynamic therapy including IMRT in conventional therapy.

Possible solutions to the organ motion problem of scanning are investigated today with *respiration gating* and *tumor tracking*. But both modalities have still to be clinically explored with scanning. In any case, one has to investigate whether the residual motion error within the gating window is sufficiently small. If the residual precision is not good enough, one has to apply a certain amount of *repainting* (statistically uncorrelated regating or retracking).

If the time needed for painting a small volume is below 5–10 s one could also consider treating the whole volume within a breath-hold cycle and repeat this as often as required – *breath-hold mode with volumetric repainting*.

If the amount of organ motion is not reproducible or not detectable online, repainting might be the only strategy. This would be the case for tumors in the abdominal region, breast cancer, and tumors in the trunk with motions below 5–10 mm. The preferred approach for these tumors at PSI is isolayered, volumetric, repainted spot scanning as described in [17].

Delivery of a very *fast conformal scanning* with *volumetric repainting* capability is the major goal of the further development of G2.

Volumetric repainting, whether used alone or in combination with gating and tracking, is a key issue to allow treating all body regions with scanning.

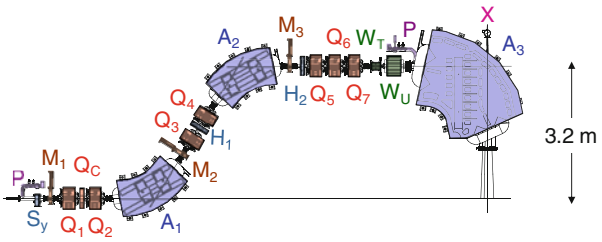

Fig. 24.2 Beam optics design of G2. The beam line consists of three main dipoles (A), seven quadrupoles (Q) three steering magnets (S), realized in combination with hexapoles (H), and pump (P) and beam profile monitors (M). The sweeper magnets WT and WU are controlled directly by the scanning system. The corrector quadrupole QC is wired in series to the U sweeper, in order to keep the beam well focused at the isocenter independently of scanning

24.6 Mechanical Layout of the New Gantry 2

The major difference between G2 and the present commercial gantries is that the PSI system displays *upstream scanning*, i.e., scanning started before the last bending magnet (Fig. 24.2) rather than the more usual approach with *downstream scanning* which starts after the last bending magnet [18].

Upstream scanning was chosen as it can provide *parallel scanning* in both scanning directions rather than divergent scanning in the case of a downstream solution. The PSI solution implements, as well, the beam's eye-view (BEV) X-ray solution for QA control of moving targets, described further below. Since no extra space is needed in the radial direction for mounting the scanning magnets and for the lateral spreading of the beam, the size of G2 could be kept rather compact (diameter: 8 m). In fact, a downstream gantry would never have fit into the available space at the PSI facility.

A major disadvantage of the upstream approach is, however, that the last 90° bending magnet must be designed with large pole faces and with a large gap (15 cm for G2) to accommodate for the lateral motion of the beam within the magnet. The weight of the last magnet is, therefore, quite high (43 tons). The G2 design limits further the range of magnetic scanning to a square of $12 \times 20\,\text{cm}^2$ as compared to the $20 \times 20\,\text{cm}^2$ up to $30 \times 40\,\text{cm}^2$ often stated for commercial systems.

It is planned to expand the range of scanning by combining the magnetic motion of the beam with displacements of the patient table. With a parallel beam, it should be straightforward to interpret a shift of the table position as a displacement of the origin of the magnetic scan coordinates. The idea is to combine and exchange at wish table and sweeper motion without the need to reoptimize the treatment plan. The dose could thus be planned for an infinitely wide parallel beam. Once implemented, it is expected that this solution will be very efficient for treating elongated tumors such as medulloblastoma cases, which require treating the brain

plus the whole spinal cord. For such large fields the "shifted-parallel" scanning of G2 should provide a more elegant approach than the patching techniques with divergent fields used with downstream scanning or scattering.

The main advantages of using a parallel scanned beam are of practical nature. The absolute dose delivery is less sensitive to the nozzle distance. This simplifies treatment planning and dosimetry. Since there are no inverse distance squared corrections, the dose measured directly in the dosimetric phantom is essentially the same as within the patient.

On a downstream gantry the source-to-tumor distance is usually very short to keep the gantry radius reasonably small. This implies a strong divergence of the beam. With parallel scanning, we have a lower plateau dose and reduced skin dose. The limited range of the magnetic scanning of G2 makes it easier to use a smaller vacuum window and to place it close to the exit of the nozzle. The thickness of the foils of the monitors and of the vacuum window is kept thin, in order to have a sharp pencil beam for highest dose precision. Due to the limited scan range, it is also easier to provide a higher scanning speed.

All existing gantries are built similarly with full gantry rotation of 360°. The usual solution is to support on the front side the rotating gantry with a cylindrical treatment cell. The beam exits the nozzle at the isocenter within the cylinder. The patient table is mounted in front of the cylinder. If one wants to treat the patient in supine position from all directions (for example from the top of the head), the radius of the cylinder must be larger than 2 m. This implies a more than 2 m deep *pit below the patient table at the isocenter*. A full gantry rotation makes it difficult to have a permanent fixed floor below the patient table, since the gantry rotation "cuts" the supporting structure of the floor. A very elegant but complex solution to the gantry pit problem has been realized in Japanese gantries, by mounting a flexible rolling floor, which adapts to the rotation of the gantry and the nozzle within the cylindrical cell.

For the PSI Gantry 2, we have chosen a simpler approach, a *left-right-handed solution*. The gantry rotates only on one side by at least 180° (−30° to +180°), to include all beam directions from above to below with respect to gravitation (Fig. 24.3). Rotation in the horizontal plane of the patient table, mounted on the opposite side of the gantry head, is then used to achieve complete coverage of the solid angle for the requested beam incidences (in analogy to the geographic coordinate system with latitude and longitude).

The support of the gantry is on a commercial pivot bearing (Fig. 24.4). There is no need to construct a large precise ring for supporting the treatment cell during rotation.

With this choice, a *fixed floor* could be mounted underneath the patient table providing rapid access to the patient at any time. *Fixed walls* and a *fixed ceiling* are used for mounting commercial positioning equipment (like Vision-RT) around the isocenter. As they do not rotate with the gantry the diagnostic images should be easier to interpret.

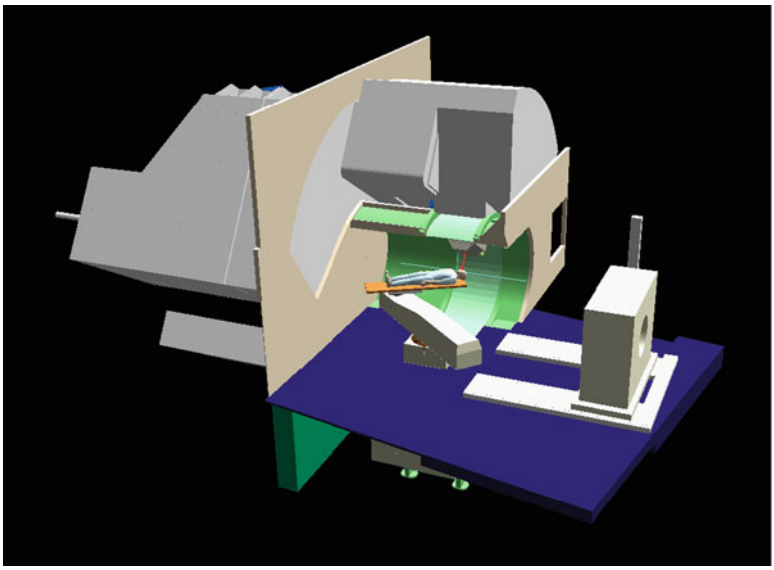

Fig. 24.3 The new layout of Gantry 2 (G2), with limited rotation from −30° to +185°, fixed environment of the patient table and integration of a sliding CT

The layout of G2 is open from the side and from the front. This offers the possibility to use an in-room CT scanner. The *sliding CT* will be used for patient positioning before treatment and for optional checks at the end of a session. The use of such a full-fledged modern commercial diagnostic tool will open new possibilities in the context of treating moving targets (use of the CT for set-up of respiration gating). The flexibility to mount commercial equipment within the reach of the gantry could bring new solutions in the future, like PET-CT or possibly, even MRI.

The upstream scanning feature has permitted to equip G2 with a *BEV X-ray system*. The last 90° magnet of G2 was built with a small hole in the rear yoke along the back projection of the exit beam axis (see Fig. 24.5). This provides room for an X-ray tube above the magnet to image the patient, possibly also during proton beam delivery, through the nozzle in the same direction as the applied proton beam. As proton beam scanning normally does not require the use of collimators or compensators, the nozzle is otherwise free of material apart from the exit window of the vacuum tube and the thin windows in the beam monitors.

The system is completed by a removable flat panel detector, which can be placed immediately behind the patient to acquire the X-ray image. A major advantage is that it acquires images in the proton beam direction, i.e., the most useful direction for assessing motions orthogonal to the beam delivery, which are likely to be the most damaging. Using a single BEV imager also reduces the dose to the patient, saves on equipment costs, and simplifies the analysis of displacement errors. The

Fig. 24.4 Phases of realization of G2 at PSI

only possible disadvantage of this system is potential radiation damage to the imager from neutrons emerging from nuclear interactions of the protons in the patient body. This issue will be explored in more detail with the first prototype of G2. The use of the BEV equipment and of the sliding CT underlines the trend towards

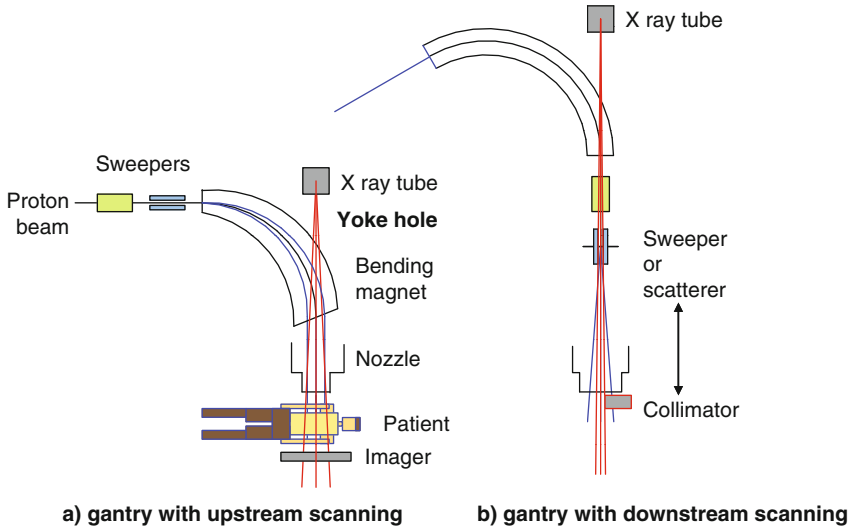

Fig. 24.5 BEV X-ray conceptual design (**a**) Upstream scanning system (short distance; large field of view) (**b**) Downstream scanning or scattering (long distance; reduced field of view)

image-guided proton therapy (IGPT), a development strongly needed in order to follow the developments in conventional radiation therapy.

A further option of G2 is the planned possibility to install *two fixed orthogonal* 45° *X-ray tubes* with corresponding imaging panels to perform QA controls of patient positioning during beam delivery. The G2 system is also compatible with the use of a *patient transporter* to bring the patient ready for treatment from outside the treatment room (the basic solution adopted for G1). This approach will be considered for treating children under anesthesia with G2.

24.7 Gantry Beam Optics

A beam optics solution with a 1:1 imaging – a "focus-to-focus" transport solution – was chosen from the coupling point to the isocenter (Fig. 24.2). At the first intermediate focus, the vacuum of the gantry can be separated from the vacuum of the accelerator. The beam can be injected into the gantry through a collimator hole mounted on its rotational axis. The diagnostic elements, which are permanently in the beam, do not significantly disturb the beam quality. Adding MCS at a focal point is only slightly altering the divergence of the pencil beam but not its size.

The shape of the 90° bending magnet and the position of the two sweeper magnets have been designed so as to obtain a *double parallel scanned beam*.

The beam transport is designed for fully *achromaticity* (in Transport code terms $R16 = R26 = 0$). Transport calculations were performed for a pencil beam of ± 3 mm, ± 10 mrad and $\pm 0.6\%$ $\Delta p/p$.

24.8 Nozzle Design

We have designed the nozzle with the vacuum window placed very close to the patient. The nozzle is very *compact* (Fig. 24.6). There is just enough space to mount two *transmission monitors* and a *strip monitor* for controlling online dose and position of the beam during beam delivery. There is also the option to have a motorized *preabsorber block* moving in and out of the beam in combination with scanning. The preabsorber option should be of interest for treating superficial tumors. The preabsorber is inserted into the beam for stopping the beam with the lowest proton ranges within the patient, i.e., those which would otherwise require energies below 70 MeV, which is the minimal value in the gantry beam line.

The whole nozzle can be moved longitudinally along the beam axis. The *telescopic motion of the nozzle* will be used to reduce the air gap between nozzle and patient while keeping the patient at the isocenter. That way, the tumor can be kept at the optical beam focus and at the place where 45° orthogonal X-ray images could be taken during beam delivery if we would decide later to implement that option.

At the exit of the nozzle, we have a support plate for mounting *optional collimators and compensators*. We plan to explore this possibility to protect OAR with shielding blocks in addition to conformal scanning and also to simulate scattering with the scanning beam.

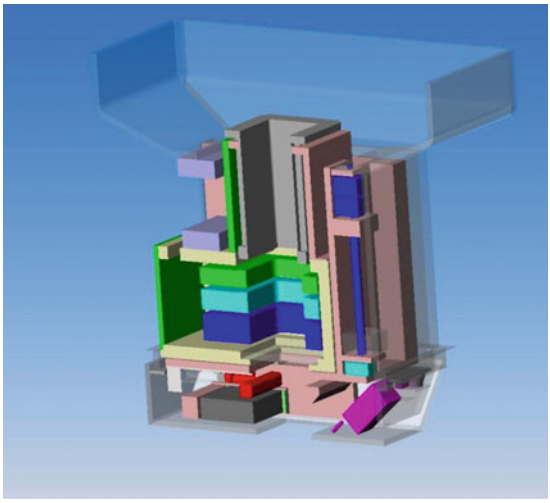

Fig. 24.6 Compact layout of the nozzle of G2. The vacuum chamber of the 90° magnet is extended into the nozzle (*upper gray section*) up to the box containing the monitors (monitor 1, monitor 2 and strip monitor are shown in *green*, *turquoise* and *blue*, respectively). Additional space below the box is needed for the movable preabsorber (*dark gray*), lasers and TV camera (*magenta*). The moving support for mounting collimators and compensator is not visible in the picture. It requires changing the type of nozzle cover. The nozzle (whole section below the vacuum chamber) can be moved along the beam axis

The nozzle is enclosed within *collision-detecting plates* to protect the patient in case of collisions during mechanical motion performed under *remote control*. The freedom to steer the patient table remotely during beam delivery allows treatment of multiple fields in one go without personnel in the treatment area.

For G2 we abandoned the idea to use a range shifter in front of the patient as with G1. The energy of the beam will instead be scanned dynamically with the beam line.

In order to achieve the best possible lateral fall-off of the dose distribution, it is mandatory to design the nozzle with a minimal amount of material in the beam. Since the broadening of the pencil beam size is linear with distance to the source of MCS, the nozzle elements should be placed as close as possible to the patient. Ideally, we want to have only the minimal amount of material necessary for the beam monitoring.

Figure 24.7 shows the measured beam size as a function of the proton energy, a possible benchmark for future gantry systems.

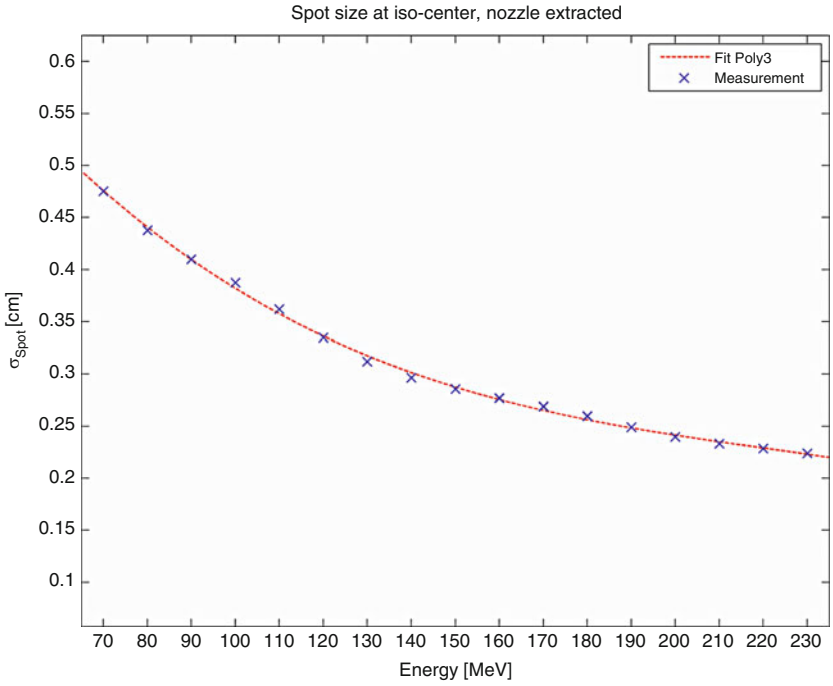

Fig. 24.7 Measured beam size (sigma) at the isocenter at the nozzle exit of G2 as a function of proton energy

24.9 Development of Novel Scanning Techniques

The main goal of G2 is to provide sufficiently *fast scanning* with *volumetric repainting* to deliver the dose with tolerable dose-homogeneity errors due to the interplay of beam delivery and organ motion.

Reliability, reproducibility, safety and precision of the beam delivery are of paramount importance. The beam should be very stable in intensity, energy, position and shape – ideally a round Gaussian. The aimed absolute precision in position and range of the beam should be of the order of <1 mm, the short-term relative precision from spot to spot of the order of a few tenths of a millimeter.

The control system of G2 is configured for the delivery of *discrete spots* (the basic mode), but also *lines* and *contours*, which means continuous dose painting with variable speed and/or variable modulation of the beam intensity.

Dynamic control of the beam intensity for dose painting is performed with a *vertical deflector* (voltage plate followed by collimators) in the first beam orbit after the ion source. The beam intensity can be changed from 0 to 100% in a programmed way at a time scale of 100–200 μs (the electronics resolution is 10 μs), which is of the same order as the time delay of the proton beam from the source to the patient.

At the exit of the cyclotron, a *fast kicker* is used, which allows discrete spot scanning (as with G1). This mode brings better precision in controlling the dose at the expense of a larger dead time. It avoids dose uncertainties during the time when the beam is moved to the next spot. Keeping the beam on during uncontrolled transient dose depositions could be deleterious when applying repainting. From the experience with G1 it is expected that discrete spot scanning yields a more precise relationship between applied and calculated dose.

A *fast degrader* ahead of the gantry is used for changing the beam energy. It consists of a series of opposed carbon wedges, which can be positioned mechanically very quickly into the beam [19]. The energy changes actuated by the degrader are followed dynamically by the whole beam line with analyzing section, switchyard and gantry up to the patient.

The disadvantage of using a degrader is the beam-broadening with large intensity losses due to MCS and energy straggling when reducing the energy. At 100 MeV, for example, the beam intensity at the patient is reduced by about two orders of magnitude as compared to the current extracted from the cyclotron. Most of the beam is stopped in the beam-defining collimators at the exit of the degrader box.

The speed to change the energy of G2 is mainly limited by the speed of changing the magnetic field in the last 90° dipole. Preliminary results have shown that energy changes corresponding to proton range differences of $\sim$5 mm can be achieved within approx. 80 ms.

We work with a *continuous* selection of the *beam energy* (variable energy tunes) and we scan the energy in both SOBP directions with cyclic magnet ramping up-down and down-up, including corrections for hysteresis effects in the magnets.

Since there are several locations in the beam line upstream of the gantry where the beam is focused on round collimators, we decided to provide an *equalization of*

the intensity losses in the energy range from 100 to 200 MeV. The beam transmission was first optimized for 100 MeV. When going to the higher energies the beam is defocused and gets partially lost in collimator holes at two focal locations along the beam line (one focus is in front of the degrader, the other is before the separation wall to the gantry room). The beam is detuned in the energy range from 100 to 200 MeV in order to obtain a constant beam monitor unit (MU) rate at the isocenter while keeping the extracted intensity from the cyclotron unchanged. In this energy range, we can thus fully reserve the dynamic use of the deflector plate for dose painting.

For discrete spot scanning, the full *energy range* from 70 to 230 MeV, is envisaged. In the energy intervals 70–100 and 200–230 MeV, the deflector plate will be used to adjust the MU rate as a function of the beam energy. The possibility to work with variable energies down to 70 MeV – together with the option of using a 3–4 cm bolus on the patient's skin for lower ranges – should permit discrete spot scanning of highest precision at all energies without material in the beam. That way, the need for a very *small air gap between nozzle and patient* could be avoided. The air gap problem is well known to us from the G1 experience, where it is caused by the range shifter in front of the patient.

Lateral scanning is performed by *double magnetic scanning*. A velocity of 2 cm/ms is aimed at to move the beam in the transverse direction (inner loop in the sequence of scanning). The velocity in the second lateral, dispersive direction is 0.5 cm/ms (the second inner loop).

Discrete spot scanning alone and in combination with collimators will be used for treating static and moderately moving tumors. This mode should be easy to achieve, as it is very similar to the scanning mode of G1.

For moving tumors, a *continuous line scanning* technique will be explored, where dose elements are painted with high beam velocities and variable dose rates.

The control system is based on the use of Field Programmable Gated Arrays (FPGA). Whole dose patterns programmed as trajectories of the U and T sweepers and with variable beam intensity can be downloaded, to be delivered as a function of real time. The control of the dose of these time-driven scans is performed with a feedback loop which takes the difference of the output of the dose monitor to the desired dose rate value and corrects it back to the vertical deflector plate. Figure 24.8 shows the result of a first exploratory experiment. Ten-centimeter long dose lines, each painted in 5 ms, were shaped by variable modulation of the beam intensity. The images were obtained with a scintillating screen seen by a CCD camera through a 45° mirror. Currently, work is in progress to substantiate this proof of principle of the advanced scanning modes.

Repainting should be performed as painting of single lines with 5 mm spacing. It is intended to move the beam with nearly maximum speed and shape the dose by modulation of the beam intensity. The goal is to paint with 10 ms per 10 cm line. A $10 \times 10\,\text{cm}^2$ surface should be covered in about 200 ms, i.e., 300 ms if we add 100 ms dead time for the energy change. Accordingly, a tumor volume of 1 l could be treated in about 6 s, if 20 energy layers are considered. This estimate, however, considers only the time of moving the beam; it neglects possible limitations given by the available dose rate. At the end, we hope to achieve volumetric repainting in

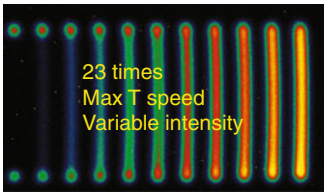

Fig. 24.8 Scanning of dose lines (re)-painted with modulation of the beam intensity (work in progress). The 10-cm lines were painted each in 5 ms. The dose was controlled with a feedback loop from the main G2 beam monitor to the deflector plate. The dose image was taken with a scintillating screen seen by a CCD camera. *From the left to the right* the dose level in the central portion of the *vertical lines* increases in steps of 10%

the order of 10 repaintings per liter in a couple of minutes. The feasibility of these ideas has still to be corroborated experimentally. This holds, as well, for the safety issues of these advanced irradiation modes.

In the further future, the G2 scanning system should also be able to paint the dose with beam intensity modulation along *contours*. This should offer highest repainting capability with the best possible dose fall-off characteristics. However, treatment planning for this mode is expected to be correspondingly challenging.

24.10 Conclusions

G2 is a new system under development at PSI to explore the physical and practical limits of pencil beam scanning. The system has an open design for a stepwise implementation of new scanning methods. They will be realized as software releases using the same basic simple equipment. We aim at reaching the best possible performance in terms of dose precision and dose shaping capability as an attempt to prove a general superiority of scanning versus scattering. Another goal is to demonstrate the capability of scanning for moving tumors, using repainting and gating, in order to establish scanning as a universal beam delivery method. The final goal would then be to replace scattering by scanning for all types of ion beam treatments.

Acknowledgements This article was written on behalf of the R&D technology group of the Proton Therapy Center of PSI. I would like to thank, in particular, David Meer, Christian Bula, Silvan Zenklusen, Sairos Safai, and Roland Kobler as major contributors to the G2 project.

References

1. E. Pedroni, R. Bacher, H. Blattmann, et al., The 200-MeV proton therapy project at the Paul Scherrer Institute. Conceptual design and practical realization. Med. Phys **22**, 37–53 (1995)
2. A. Smith, M. Gillin, M. Bues, et al., The M. D. Anderson proton therapy system. Med. Phys. **36**, 4068–4083 (2009)

3. A.J. Lomax, T. Böhringer, A. Coray, et al., Intensity modulated proton therapy: a clinical example. Med. Phys. **28**, 317–324 (2001)
4. E. Pedroni, Therapy Planning System for the SIN Pion Therapy Facility, in *Treatment Planning for External Beam Therapy with Neutrons*, ed. by G. Burger, J.J. Broerse. (Urban & Schwarzenberg, Munich, 1981), pp. 60–69
5. B. Timmermann, A. Schuck, F. Niggli, et al., Spot-scanning proton therapy for malignant soft tissue tumors in childhood: First experiences at the Paul Scherrer Institute. Int. J. Radiat. Oncol. Biol. Phys. **67**, 497–504 (2007)
6. E. Pedroni, System for performing proton therapy. Wipo patent WO/2004/026401 (2004)
7. E. Pedroni, S. Scheib, T. Böhringer, et al., Experimental characterization and physical modeling of the dose distribution of scanned proton pencil beams. Phys. Med. Biol. **50**, 541–561 (2005)
8. M. Phillips, E. Pedroni, H. Blattmann, at al. Effects of respiratory motion on dose uniformity with a charged particle scanning method. Phys. Med. Biol. **37**, 223–234 (1992)
9. J. Gueulette, H. Blattmann, E. Pedroni, et al., Relative biologic effectiveness determination in mouse intestine for scanning proton beam at Paul Scherrer Institute, Switzerland. Influence of motion. Int. J. Radiat. Oncol. Biol. Phys. **62**, 838–845 (2005)
10. M. Goitein, A.J. Lomax, E. Pedroni, Treating cancer with protons. Phys. Today **55**, 45–50 (2002)
11. A.J. Lomax, T. Böhringer, A. Coray, et al., Intensity modulated proton therapy: a clinical example. Med. Phys. **28**, 317–324 (2001)
12. B. Schaffner, E. Pedroni, A. Lomax, Dose calculation models for proton treatment planning using a dynamic beam delivery system: an attempt to include density heterogeneity effects in the analytical dose calculation. Phys. Med. Biol. **44**, 27–41 (1999)
13. M. Goitein, *Radiation Oncology: A Physicist's-Eye View* (AIP, Springer Science + Business Media, New York, 2008)
14. S. Zenklusen, E. Pedroni, D. Meer, et al, Preliminary investigations for the option to use fast uniform scanning with compensators on a gantry designed for IMPT. Accepted for publ. in Med. Phys. in July 2011
15. E. Pedroni, Pencil Beam Scanning, in *Proton and Charged Particle Radiotherapy*, ed. by T. DeLaney, H. Kooy. (Lippincott Williams & Wilkins, Baltimore, 2008), pp. 40–50
16. A. Knopf, C. Bert, E. Heath, et al., Special report: Workshop on 4D-treatment planning in actively scanned particle therapy – recommendations, technical challenges, and future research directions. Med. Phys. **37**, 4608–4614 (2010)
17. S. Zenklusen, E. Pedroni, D. Meer, A study on repainting strategies for treating moderately moving targets with proton pencil beam scanning at the new Gantry 2 at PSI. Phys. Med. Biol. **55**, 5103–5121 (2010)
18. E. Pedroni, R. Bearpark, T. Böhringer, et al., The PSI Gantry 2: a second generation proton scanning gantry. Z. Med. Phys. **14**, 25–34 (2004)
19. J.M. Schippers, R. Dölling, J. Duppich, et al., The SC cyclotron and beam lines of PSI's new protontherapy facility PROSCAN. Nucl. Instrum. Methods Phys. Res. B **261**, 773–776 (2007)

Chapter 25
Beam Spreading Devices

Jay Flanz

Abstract Effective use of a particle beam for radiotherapy necessitates delivery of that beam in such a way that it covers the target volume with a prescribed dose distribution. The particle beam extracted from an accelerator normally has beam dimensions smaller than that of a typical target. Therefore, that beam has to be spread out to match the target volume. This chapter will discuss aspects of the transverse and longitudinal spreading techniques using scattering and scanning techniques and some of the devices used to implement these techniques.

25.1 Introduction

The goal of radiotherapy implementation is to deliver the prescribed dose to the target with the prescribed dose distribution. Every volumetric element of a target (a voxel) should receive energy from the ions traveling through or up to that voxel as described by the prescription. This requires that the ions are directed to the right place with the correct number of ions at that place. Generally, a beam coming from an accelerator has a spatial intensity (I) distribution of Gaussian form such as given by (25.1).

$$I = \mathrm{e}^{-\frac{x^2}{2\sigma^2}}. \tag{25.1}$$

The beam size is characterized by the value of sigma (σ), which is related to the full width at half maximum amplitude (FWHM) by FWHM $= 2.35\,\sigma$ as shown in Fig. 25.1. The beam is a collection of particles described not only by size but also by its divergence since each ion in the beam has a position and angle that describes its trajectory. The area of the beam phase space (distribution of positions and angles of the particles in the beam) is given by $\pi\varepsilon$, where ε is the emittance of the beam.

J. Flanz (✉)
Francis H. Burr Proton Therapy Center, Massachusetts General Hospital, Harvard Medical School, 30 Fruit Street, Boston, MA 02114, USA
e-mail: flanz@hadron.mgh.harvard.edu

U. Linz (ed.), *Ion Beam Therapy*, Biological and Medical Physics, Biomedical Engineering, DOI 10.1007/978-3-642-21414-1_25,

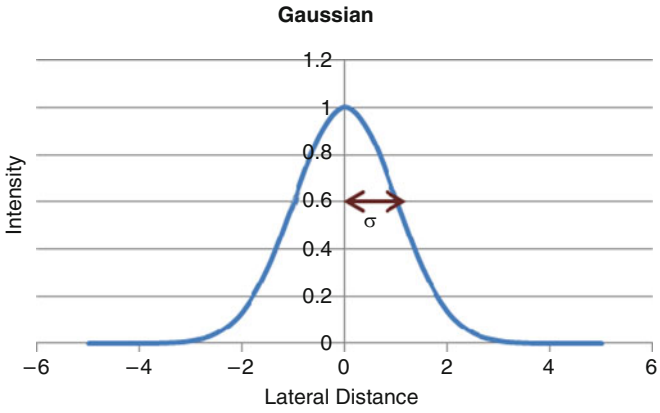

Fig. 25.1 Intensity distribution of a Gaussian beam along the lateral axis with the definition of σ

The beam phase space is represented as an ellipse, owing to the Gaussian form of the canonical components.

A typical emittance for an accelerator that uses a degrader is about 20 mm-mrad, and a typical emittance for a beam directly from the accelerator is about 5 mm-mrad or less. This results in a beam size from mm to cm in a beam line. A smaller beam transported to the patient results in a smaller and less-expensive beam transport system. However, the main point is that the size of the beam in the transverse direction is of this dimension.

In the longitudinal direction, a large fraction of the dose is delivered in the Bragg peak, which has a width dependent upon the beam energy and penetration depth from a couple of millimeters for low energy to several millimeters for higher energy as shown in Fig. 25.2. This width is dependent upon the spread of beam energies intrinsic to the beam and the energy straggling caused by the ion interaction in the medium in which it is traveling.

Given that a treatment target can have an arbitrary shape with characteristic dimensions from millimeters for radiosurgery fields, to tens of centimeters for craniospinal irradiations, the beam transported to the patient must be spread out in both transverse and longitudinal directions. There are a variety of mechanisms to accomplish this. Many of these mechanisms make use of the properties of an ion beam interacting with matter.

25.2 Ion Beams Interacting with Matter

25.2.1 Scattering

Equation (25.2) shows the relation of the growth of the root mean square (rms) angle θ of a beam when it is scattered through a target [1].

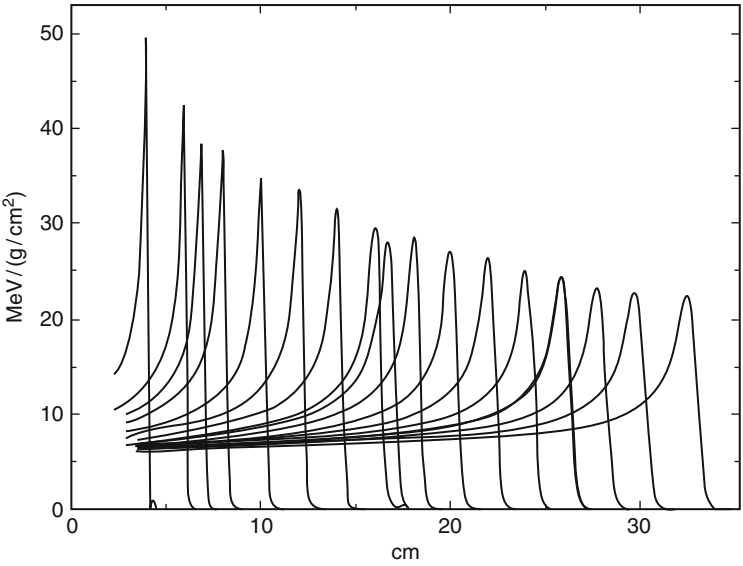

Fig. 25.2 Depth dose distribution of protons in water, or the shape of the Bragg peak as a function of energy (courtesy of Hanne Kooy). Note that the width of the Bragg peak is larger with higher energy and deeper depth

$$\theta_{\text{rms}} \approx \frac{\text{Constant}}{pv} Z \sqrt{\frac{L}{L_{\text{R}}}} \left[1 + \frac{1}{9} \log_{10} \frac{L}{L_{\text{R}}} \right]. \tag{25.2}$$

The quantities are as follows:

L = Length of penetration in the medium.
L_{R} = Radiation length of the material (a constant of the material).
p = Momentum of the incident particle.
v = Velocity of the incident particle.
Z = Charge of the atoms in the medium.

This mechanism is basically the result of the Coulomb interaction between the charged particle and the charged nucleus. Each of the individual interactions with atoms results in a change of direction of the incident ion, and the statistical average of all these particles results in a spread of overall divergence angles, which are summarized by the rms divergence angle of the beam. The result of this approximates a Gaussian distribution. Exploring the dependence of the rms Gaussian divergence, in (25.3), one finds, approximately:

$$\theta_{\text{rms}} \approx Z \sqrt{\frac{L}{L_{\text{R}}}} \quad \text{and} \quad L_{\text{R}} \alpha \frac{A}{Z^2} \Rightarrow \theta \approx Z^{3/2} \sqrt{L}, \tag{25.3}$$

where A is the atomic number of the medium.

25.2.2 Energy Loss

One of the representations of the energy loss per unit distance ($\mathrm{d}E/\mathrm{d}x$) that an ion experiences while traveling in an absorbing medium is given by [2]:

$$\frac{\mathrm{d}E}{\mathrm{d}x} = \frac{4\pi}{m_e v^2} \quad z^2 e^4 \, NZB \tag{25.4}$$

with

$$B = \ln(2m_0 v^2) - \ln(I(1-\beta^2)) - \beta^2 \tag{25.5}$$

and

E = Instantaneous total energy of the particle (at any location along its path)
e = Electron charge
m_e = Electron mass
v = Speed of the ion particle
ze = Charge of the ion particle
Z = Atomic number of the absorbing material
N = Number of atoms/cm^3 of the absorbing material
I = Mean ionization energy of the absorbing material

Looking only at the dependence on the target material one finds that

$$\mathrm{d}E/\mathrm{d}x \sim NZ = N_\mathrm{A}\rho Z/A = (N_\mathrm{A} Z/A)\rho = \text{Constant} \cdot \rho \tag{25.6}$$

where N_A is Avogadro's number.

In other words, the energy loss of the ion is proportional to the density of the penetrated matter and the penetration depth.

25.2.3 Relative Effects

According to the relations identified above, energy loss and scattering have different dependencies on the atomic number of the material. A higher Z material produces more scattering, but does not yield more energy loss than a lower Z material. Therefore, one can use materials of different compositions in order to control the degree to which the energy loss or scattering has to be modified, at least relatively. This is shown in Fig. 25.3 [3].

25.3 Longitudinal Beam Conformance

25.3.1 Longitudinal Beam Spreading

To spread the beam longitudinally implies adding dose over a larger longitudinal extent than the pristine Bragg peak. By adding multiple pristine Bragg peaks of

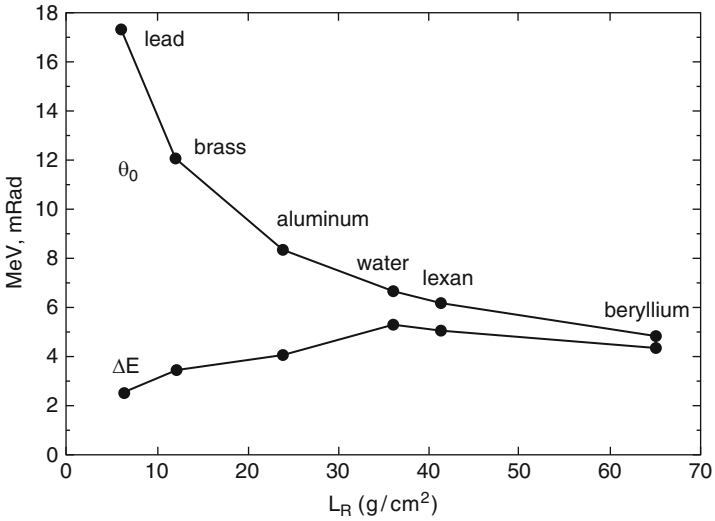

Fig. 25.3 The *upper curve* is a plot of the scattering angle, Θ_0 (mRad), as a function of radiation length, L_R(g/cm^2), of various materials and the lower curve is the energy loss, ΔE (MeV), in the given radiation length of the same materials. Adapted from [3]

different range and intensity one can create a "spread-out Bragg peak" (SOBP) as shown in the blue curve of Fig. 25.4. Thus, it is necessary to utilize methods that will create multiple Bragg peaks of different range. This can be done by changing the beam energy coming from the accelerator, or by introducing additional energy-degrading material between the accelerator and the patient, as needed. The relative number of ions delivered to the target at any given range depends on the desired physical longitudinal dose distribution and will then be controlled by the number of ions delivered for each of the Bragg peaks. Of course, at any given depth in the target, the absorbed physical dose results from the superposition of all the Bragg peaks. The actual effective dose delivered will also depend upon the relative biological effectiveness (RBE) of the ion at its particular energy.

The appropriate relative weights can be determined by a linear weighting scheme. Figure 25.5 shows an example of the procedure [3]. The appropriate matrix equations can be solved to achieve the desired weight of the individual Bragg peaks needed to achieve the desired physical dose distribution and, in turn, the desired biological dose distribution.

Delivering a certain amount of ions of a given energy can be achieved in different ways. Here are two methods:

1. Deliver N_1 ions at a range R_1. Then change the beam energy extracted from the accelerator and deliver N_2 ions at a range R_2, and continue until the desired dose distribution is achieved.

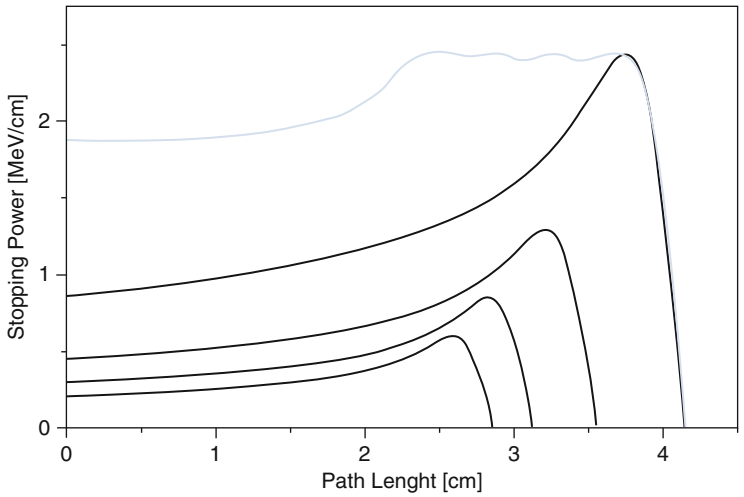

Fig. 25.4 Example how multiple Bragg peaks of different ranges can be added to approximate a flat spread-out depth dose distribution. The wiggles in the *uppermost* (*blue*) *curve*, which is the sum of the other curves, show that there are insufficient Bragg peaks used in this example to create a smoother SOBP for the desired SOBP width

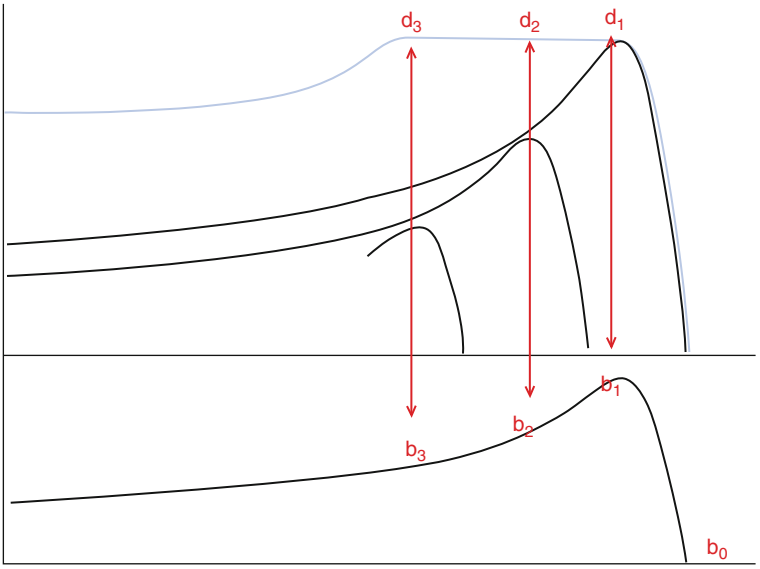

Fig. 25.5 Curves demonstrating how the components of an individual Bragg peak add to the overall SOBP. One must superimpose the contributions of the individual Bragg peaks (e.g., b_1, b_2, and b_3) to achieve the overall desired dose distribution (e.g., d_1, d_2, and d_3)

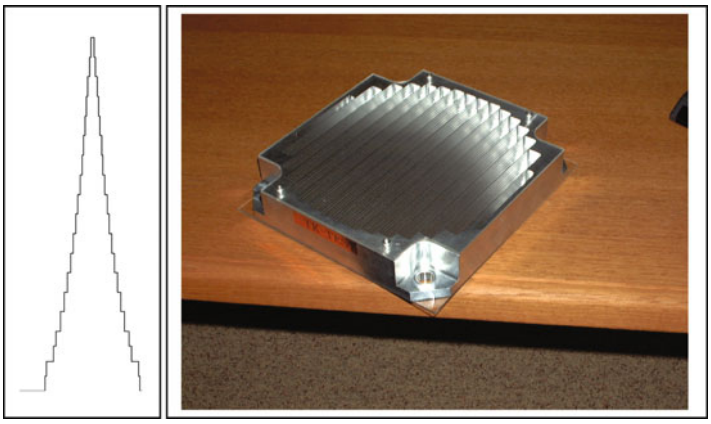

Fig. 25.6 Cross section of an individual ridge (*left*) in the ridge filter shown on the *right* (courtesy of Yoshihisa Takada)

2. Deliver N_1 ions at a range R_1. Then change the material in the beam path keeping a constant accelerator energy and deliver N_2 ions at a range R_2, and continue until the desired dose distribution is achieved.

These methods can be differently implemented, depending on how one varies the beam fluence at a given energy and whether the process is dynamic or not.

25.3.1.1 Constant Beam Fluence and Materials in the Beam Path

Ridge Filter. A ridge filter is the only truly passive device for longitudinal beam spreading. This device depends upon an incident uniform transverse distribution and there are multiple ridges across the beam area as shown in Fig. 25.6. The shape of the ridge filter is determined in such a way as to have the appropriate number of ions lose the correct amount of energy, according to the results of the matrix analysis above. The beam is also scattered in this filter so that all the ion energies that entered the ridge filter and those created by the degrading effects of the ridge filter are mixed over the entire field and, therefore, at any one transverse location there is a statistical mix of these ions. An advantage of this approach is that, since it is truly passive, all energies are delivered simultaneously, i.e., there is no time dependence. This could be an advantage when considering moving targets and a desired averaging. A disadvantage of this system is that the width of the SOBP is fixed according to the height of the ridge and each one is designed for a specific energy range. Thus the selection of ranges and SOBP widths is limited by the number of these devices that are used. One either has to insert a different one for every treatment or have an automated (limited number) library insert the appropriate filter into the beam path [4].

Range Modulator Wheel. The range modulator wheel is a dynamic version of longitudinal beam spreading. Assuming that this wheel rotates at a constant rate and

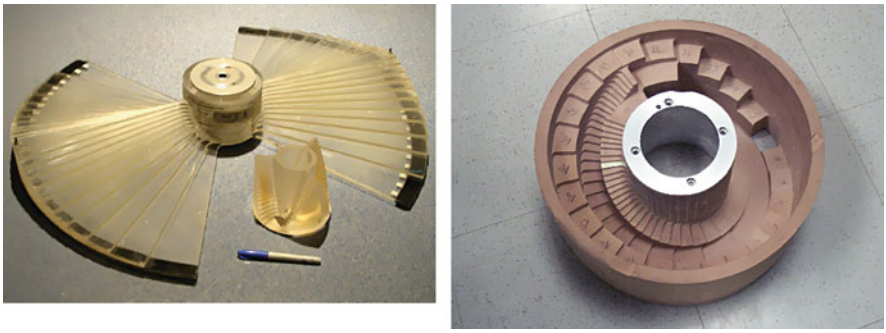

Fig. 25.7 *Left*: a conventional "downstream" range modulator with two cycles of range modulation (courtesy of Bernard Gottschalk). *Right*: a model of a multitrack range modulator wheel (each with one cycle) provided by Ion Beam Applications (IBA)

that the incident beam fluence is constant, then the number of ions that are degraded to a given energy will depend upon the amount of time a given thickness of the degrader wheel is in the path of the beam. Thus, in the wheel geometry, the angular extent of a given thickness of the wheel will correspond to the appropriate relative weights of the ranges calculated in the matrix formalism noted above as shown in Fig. 25.7. An advantage of this technique, although not passive, is that the wheel-revolution frequency can be fairly high. It is typically on the order of ten revolutions per second, and therefore all the energies that make up the SOBP are delivered in about 0.1 s, which is much faster than typical target motion [5].

One implementation of this, by Ion Beam Applications (IBA), conceived by Miles Wagner, shown in Fig. 25.7 (right), is to design multiple tracks on one wheel. By laterally shifting the position of the wheel a different track can be used. This is helpful, in that a wheel is positioned automatically, as needed. However, without any additional changes, much like the ridge filter, a given range modulator wheel is only good for a limited range of incident beam energy and SOBP width.

Lamination. Finally, one can consider a different method of delivering the appropriate energy distribution. This can be accomplished by putting a certain amount of degrader material into the beam and letting that material stay in the beam path until the appropriate number of ions have been delivered at that energy. Then a different amount of material is inserted until the appropriate number of ions are delivered, etc. This is typically done with a binary degrader system, which includes plastic degraders and lead scatterers in a binary sequence of thicknesses as shown in Fig. 25.8. This method is not as fast as the ridge filter and range modulator wheel for depositing dose over the full set of ranges desired, if one waits for each energy to be fully delivered, but one can think of a compromise where the degraders are put in the beam path in sequence repeatedly.

Wedge. A wedge degrader system is a variation of the binary lamination scheme; however, the combination of plastic and lead is more difficult. The usefulness of this

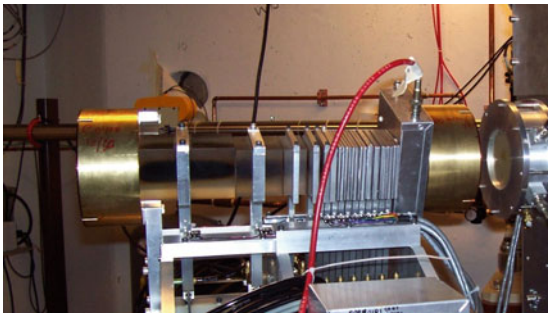

Fig. 25.8 Binary range modulationsystem used in the stereotactic beam line of the Massachusetts General Hospital (MGH). A variant of this system was used briefly at the Harvard Cyclotron Laboratory. Courtesy of Ethan Cascio

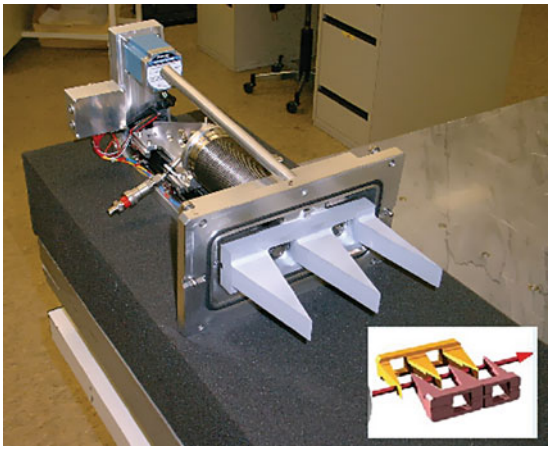

Fig. 25.9 Photo of the wedge degrader system used at the Paul Scherrer Institute. Courtesy of Marco Schippers

will be made clearer later. A system like this is used at the Paul Scherrer Institute to modulate the energy of the cyclotron beam. It is shown in Fig. 25.9 (cf. also [6]).

Other Methods. Other techniques that have been used include variable water columns or other forms of wheels. The author apologizes for accidental omission of methods not described herein.

25.3.1.2 Beam Current Modulation

In the case of a range modulator wheel, one can, in principle, deliver any subset of an SOBP if the beam is turned off during the wheel rotation at some proximal range position. One then requires synchronization of the beam turning on and off and the wheel revolution phase.

Another aspect of a range modulator wheel design is that it works over a limited range of incident energy. If the wrong distal energy is delivered, then the SOBP will not be of the desired shape as shown in the red part of Fig. 25.10. By varying the beam current during the range modulator rotation, one can effectively change the

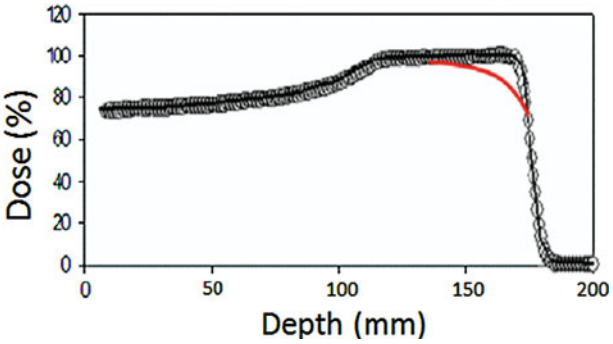

Fig. 25.10 Standard SOBP (*in black*) compared to the perturbation caused by using the wrong energy incident on the range modulator system, without correction. Courtesy of Harald Paganetti

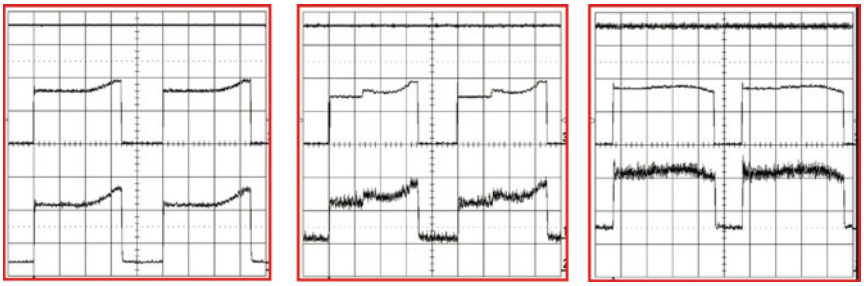

Fig. 25.11 Three examples of beam current modulation files such as those used to correct the issue demonstrated in Fig. 25.10, as implemented in the system provided by IBA for double scattering. The *vertical axis* is the beam intensity, and the *horizontal axis* is the time. Each scope trace shows two range modulator rotation cycles. The *middle curve* on each trace is the desired and the *lower curve* the actual beam current signal

relative weight of the amount of ions delivered at a given range. Some examples of beam current modulations are shown in Fig. 25.11.

25.3.1.3 Range Compensation

Delivering a beam whose range has a fixed longitudinal extent given by the extremes of the target is not always appropriate for optimal conformance to the target. The actual range to the distal end of the target can be affected by tissue and organs of different densities across the target's cross-sectional area. A range compensator made of material like plastic is used to mitigate those irregularities as shown in Fig. 25.12. It is aligned with the aperture and helps to conform quite precisely to the distal edge; however, the width of the range modulationis still fixed and this contributes sometimes to unwanted proximal dose. Balancing between the distal and

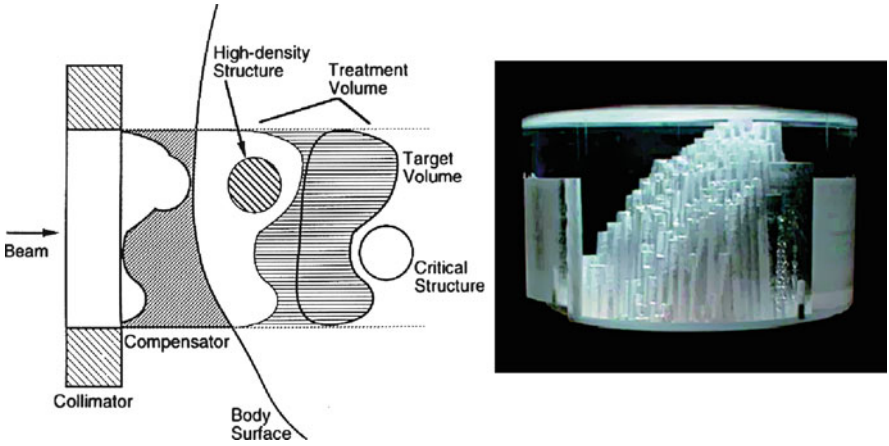

Fig. 25.12 Representation (*left*) of how a compensator (*right*) is used to account for density variations in the target and allow for conformality to the distal edge despite a fixed distal range of the beam

proximal ends is a clinical decision. One can consider whether critical structures are distal or proximal to the target and modify the region of high dose, but this does not appear to be typically done.

25.4 Transverse Beam Spreading

To spread the beam transversely, implies delivering dose over a region larger than the size determined by the unmodified transverse beam diameter from the accelerator beam. One can consider adding multiple spots by moving the beam over the target transverse dimension, or one can consider spreading the beam in what has (erroneously) been called a "passive" method.

All methods that do not involve moving the unmodified beam spot over the target, in fact, modify the beam spot. This modification makes use of the effect of scattering, discussed earlier.

25.4.1 Single Scattering

The simplest way to increase the size of the beam is to scatter it by passing the beam through a scattering material. As noted above, the relative dependencies of scattering and energy loss are different for different materials, so the best material to affect the scattering without losing too much energy is lead. An incident Gaussian beam passing through lead will end up as a Gaussian beam with a larger divergence,

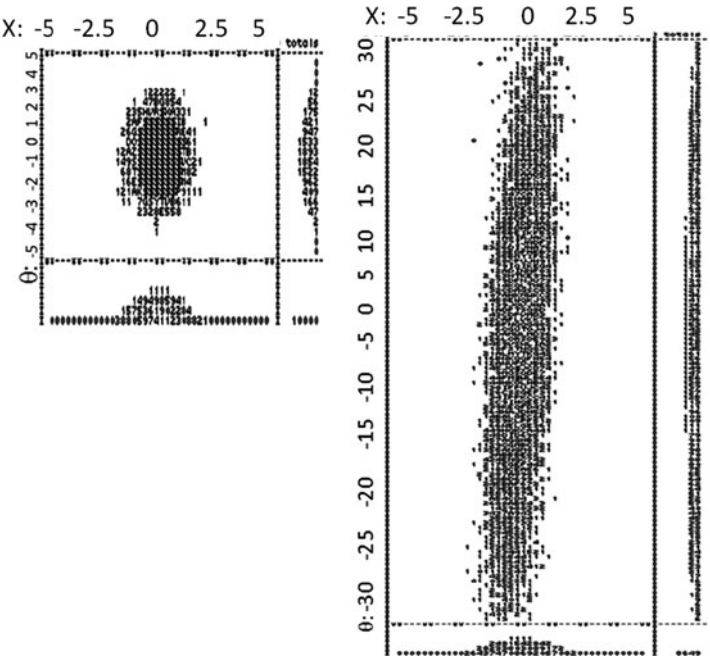

Fig. 25.13 Example of how the beam phase space increases in divergence after scattering and after a finite drift length. The *horizontal axis* is the lateral position (x) in cm and the *vertical axis* is the horizontal angle (θ) in mrad. The *right side* and *bottom* of each figure shows the projection of the particles in the phase space area, in each dimension. Also note how the ellipse starts to rotate to the right after drifting a finite length

as shown in the phase space plot of Fig. 25.13. In this plot, each point represents a particle in the beam plotted with its position (x in cm) and angle (θ in mrad). Thus, the rounder beam spot is turned into an ellipse due to the larger spread of angles (vertical axis). After some drift distance, the larger angles result in a larger beam size (tilting ellipse) since particles with larger angles drift to larger transverse distances.

If one wants to use this for treatment, keeping the overall transverse dose distribution within $\pm 2.5\%$, then one can only use the top 5% of the Gaussian amplitude. Integrating the Gaussian over this range results in using only 5% of the incident beam or a 95% loss of the beam, quite an inefficient system.

25.4.2 Double Scattering

Used for electron beam therapy [7, 8], the idea of combining two scattering devices in order to optimize the percentage of ions in a uniform field area, was developed for ion beam delivery, as well [9, 10]. In this scheme, the first scatterer is similar

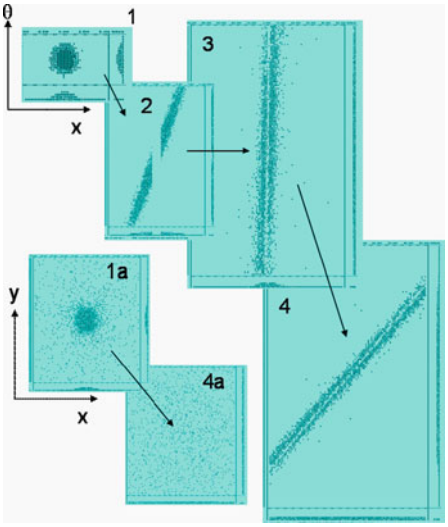

Fig. 25.14 Phase space representation of double scattering with an occluding post. Graphs 1 through 4 have the same units as those used in Fig. 25.13. Graphs 1a and 4a are the x, y position plots (do not include angular dependencies)

to a single scatterer, acting to spread out the beam and create a Gaussian beam profile with a larger divergence, which translates to larger width after a short drift. The second element of this system, provides a differential scattering power along the transverse dimension. The way in which one such example works is shown in Fig. 25.14 where a post in the center of the beam occludes a portion of the beam and produces a hole [11]. A view in the phase space plane (x, θ) shows the initial beam (1), followed by a scattered beam after a short drift (rotated ellipse) wherein the physical post has removed the protons in the middle (2). After a second scatterer, the angular spread on each half grows (3) and then the beam phase space rotates further after the final drift (4). In space, at a given location, only the positions are known and, therefore, the special projections, or the xy plots of (1a) and 4(a) are relevant, and one can see the resulting uniform distribution obtained by this second scattering method. More modern techniques use a contoured scatterer system together with a scattering power-compensated first scatterer, developed by Gottschalk et al. [3], as shown in Fig. 25.15.

25.5 Three Dimensional Dose Conformation

In order to spread the beam in three dimensions over the target volume, it is necessary to spread out the beam both longitudinally and transversely. The longitudinal spreading results from energy modulation. This energy modulation will result in a different scattering divergence when these different energy beams

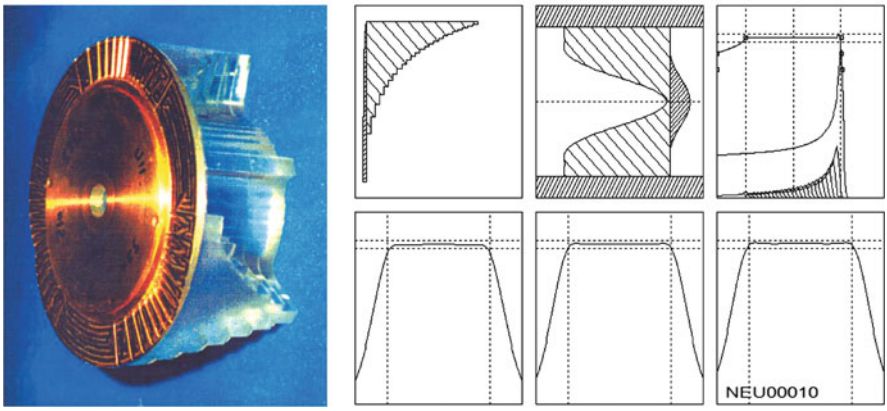

Fig. 25.15 An example of a scattering power-compensated range modulator (*left*), and a calculation including the use of a contoured scatterer (*right*: *upper middle graph*), as part of a calculation to optimize a double scattering system using NEU [3]. The graphs to the *right* (from Bernard Gottschalk) include the thickness of the range modulator wheel (*upper left*), the resulting Bragg peak distribution (*upper right*), and the transverse distributions at three depth locations (*lower three graphs*)

pass through the next (or previous) transverse scatterer(s). Therefore, the effective field size varies, or is different for different ranges. Ideally, the combined system would result in a constant overall scattering power; thus, the effective ion-usage efficiency would be the same over the full SOBP. This is accomplished by making the device that modulates the beam energy, to have a scattering power independent of that energy. Thus, for a range modulator wheel, a combination of materials can result in different energy losses but the same scattering divergence, independent of location on the wheel. This can be done similarly with a binary degrader system.

Much work at the Harvard Cyclotron Laboratory was devoted to an optimized usage of the proton beam, with these scattering systems. Originally, the range modulator used was the most downstream component. In this case, the size of the wheel was large since it was downstream of the beam scattered by the first scatterer. The concept of upstream modulation versus downstream modulation was developed.

Using a compensated upstream combination of scatterer and degrader results in a smaller device and the most efficient use of ions. Optimization of the distance between the first and second scatterers and the target is also important in the most effective and efficient use of ions in this scattering modality.

25.5.1 Additional Hardware and Related Beam Properties

Mechanisms for spreading out a beam using the scattering techniques have been discussed. A uniform transverse dose distribution can be obtained and a desired longitudinal, physical dose distribution can be obtained. These are part of the

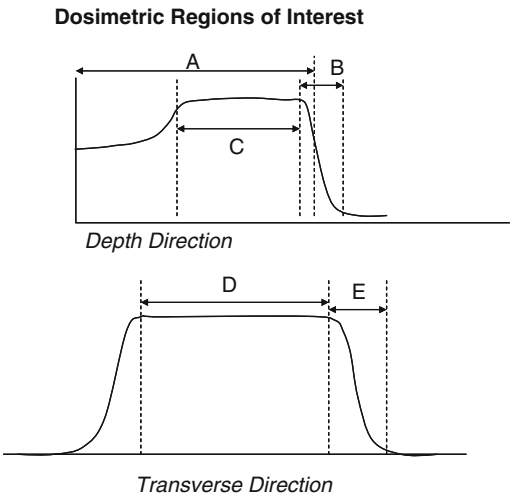

Fig. 25.16 Areas of dosimetric interest in the longitudinal (*top*) and transverse (*bottom*) regions

properties needed for treatment of a patient target. However, these are necessary, but not sufficient. Figure 25.16 identifies some areas of dosimetric interest for treatment with a scattered beam.

- Region A indicates the particle range. In some cases, it is defined as the distance in water that a particle penetrates up to the point at which the Bragg peak reaches 80% of the value of the maximum amplitude of the SOBP. This definition can change, but what is important is that the treatment-planning algorithms use consistent definitions.
- Region B is the distance of the distal fall-off, or the length from 80% to 20% amplitude on the distal side of the Bragg peak.
- Region C is the modulation width or the length of the uniform part of the Bragg peak. There are various definitions including starting from one distal fall-off length proximal to the range to 95% on the proximal side of the SOBP uniform field region.
- Region D, in the transverse dimension, is the region of uniform dose distribution defined by a distance inward on each side relative to the lateral penumbra (e.g., 2 penumbra widths from the 90% point on the penumbra).
- Region E defines the lateral penumbra, starting from the dose amplitude 80% of the uniform dose going down to 20%, on both sides of the transverse dose distribution.

In order to tailor the transverse part of the beam for treating a target, one has to confine the beam to hit only the target, which is generally irregularly shaped. The scattered beam previously discussed is circularly symmetric and has a size dependent upon the scattering power of the scattering system. It is necessary to further conform the beam to the target. This is done by interposing an aperture between the scattered beam and the target. This aperture can be any material thick

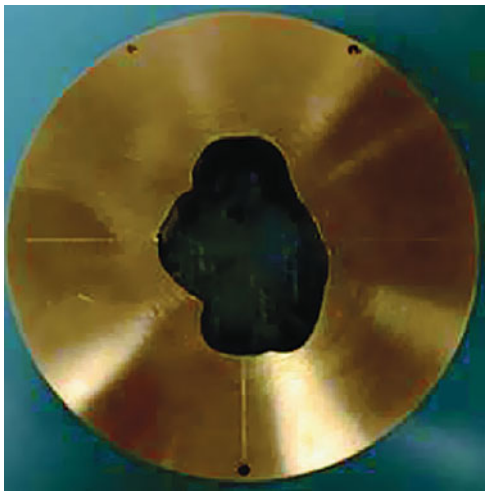

Fig. 25.17 Photo of a brass aperture for patient treatment

enough to stop the transport of ions before entering the patient. Typically, this aperture can be brass. The aperture is machined with an opening that conforms to the transverse projection of the target in the direction of the beam field as shown in Fig. 25.17. Thus, only ions that will enter the target are allowed to continue.

This aperture, also known as a collimator, absorbs the ion beam outside of the treatment field. However, it also results in lateral penumbra (cf. Region E in Fig. 25.16). This is basically the transition from the flat, uniform dose region to the region of zero dose. When a beam of finite effective source size is scattered and then collimated, and there is a finite distance between collimator and target, the final distribution of the beam contains an intensity fall-off at the edges called a penumbra. This is shown geometrically in Fig. 25.18a, as well as more accurately via the phase space representation of the beam in Fig. 25.18b. The latter shows the initial elliptical beam phase space area (distribution in position and angle for one dimension), and the collimator effect, after a finite drift distance. The collimator cuts off the edges of the beam and creates a sharp edge. However, the third graph indicates that after additional drift distance, and owing to the angles in the beam, the vertically cut-off beam grows to a trapezoid shape, shown in orange. If one were to integrate the beam vertically, achieving the profile of the projection along the transverse dimension as shown in the lower graphs, one would achieve a flat central distribution (since the integral of all angles along a given x position results in the same number in the curved portion of the phase space area) with a finite reduction of particle number beyond that at each end, or the penumbra.

In a similar way, the longitudinal distribution obtained through the creation of the SOBP provides a specific SOBP width and a specific distal range in a uniform medium. Patient targets and material in the beam path do not constitute a uniform medium and one would like to tailor the beam to better match the longitudinal properties of the target. The range compensator previously described is used for this.

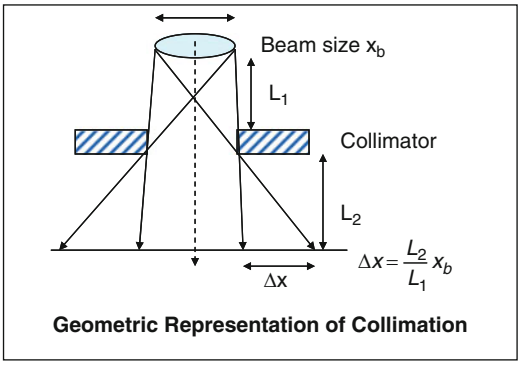

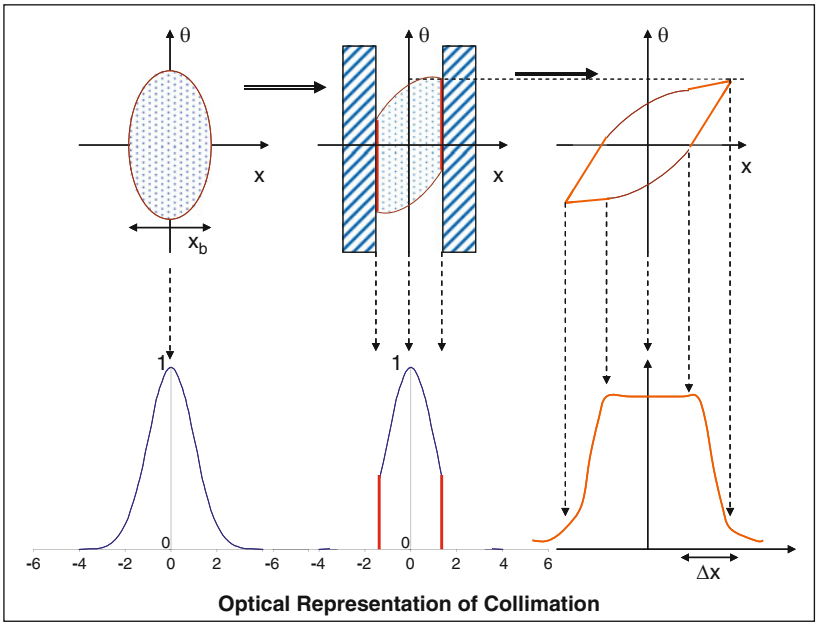

Fig. 25.18 Geometric representation of the evolution of the penumbra (Δx in **a**, *top*), and the same effect shown in a phase space representation (**b**, *bottom*). The *lower graphs* in (**b**) are the projections, or sums along the *vertical lines* in the *upper graphs*, resulting in the intensity distribution with position

The distal dose fall-off is primarily determined by the shape of the Bragg peak. This is determined by the spread of energies in the beam, and the addition of range straggling as the beam passes through the material on its way to, and inside the target. Therefore, the distal fall-off will be sharper, for a beam of the proper energy delivered to reach the distal edge of the target, when compared with a beam of higher energy, but degraded by material in the beam path before the target, owing to the additional range straggling introduced [12].

25.5.2 Scanning

Another way to transversely spread the beam is by moving an unmodified beam across the target. Beam scanning is quite a general technique, and while it has acquired many acronyms such as PBS (pencil beam scanning), IMPT (intensity-modulated proton therapy), and SS (spot scanning), coming from specific implementations of the technology and limitations of accelerator beam properties; these acronyms only serve to minimize the power and generality of this beam spreading approach. Beam scanning is achieved by moving a charged particle beam of particular properties and/or changing one or more of the properties of that beam as it is moved. Physical equipment is used to modify these properties; however, for the most part, this is done without use of extraneous material in the beam path. Thus, the unmodified beam size and properties can be used for the beam delivery.

This is not a new technique, its advantages were recognized early, having first been implemented in Japan in 1980 [13], and used for routine clinical treatments at the Paul Scherrer Institute (PSI) [14], and the Gesellschaft für Schwerionenforschung (GSI) [15].

The regions of dosimetric interest for a scanned beam are different from those of Fig. 25.16. They are represented in Fig. 25.19.

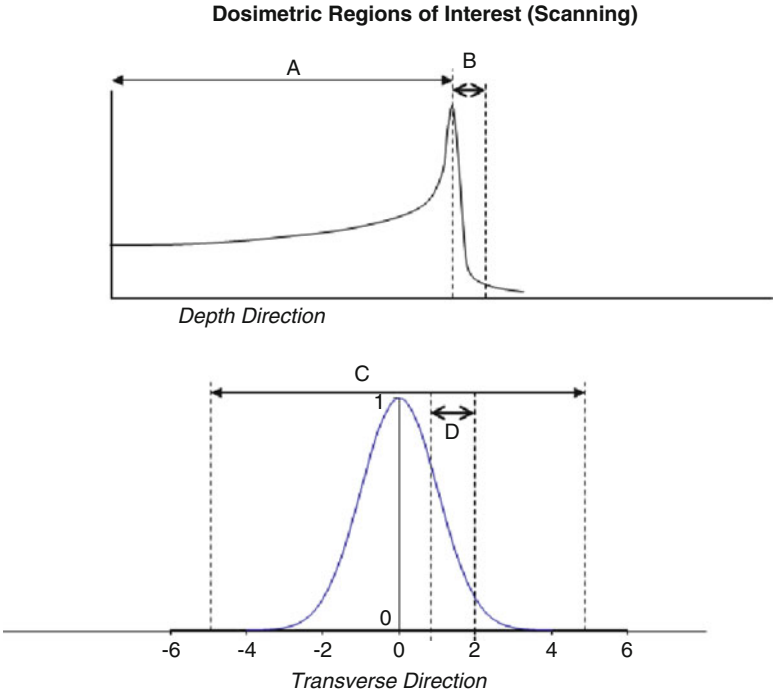

Fig. 25.19 Areas of Dosimetric interest in the longitudinal (*top*) and transverse (*bottom*) regions for a scanned beam

- Region A represents the Bragg peak. Since the beam has not been modified, the only relevant longitudinal parameter is given by the unmodified Bragg peak. Multiple Bragg peaks can be formed to distribute the dose over the depth of the target region, but this is very dependent upon the scanning technique and the treatment plan. There is no SOBP necessary. Other than the range, the only other relevant quantity is the distal fall-off in region B, since this will determine the distal penumbra.
- Region C represents the Gaussian transverse beam distribution. Since the beam has not been modified, the only relevant transverse parameter is given by the raw beam transverse distribution. The transverse penumbra of the Gaussian in region D will determine the overall extent of the penumbra. Multiple beams can be added together to form virtually any transverse distribution. The concept of a uniform field region is not relevant, since the transverse distribution can be uniform or not, depending upon the treatment plan.

There are a variety of methods to scan the beam over the target. These can include mechanical motions, such as moving the target or a bending dipole, or even using an adjustable collimator to localize the beam in a certain region. The faster and potentially more flexible method is by using a magnetic field to bend the beam trajectory as shown in Fig. 25.20. There are two scanning dipoles (one for each direction), a pair of quadrupoles to focus the beam, and ion chamber instrumentation. For the sake of completeness, a place for apertures and compensators (a snout) is identified as an option. Combinations of these methods are possible.

In the case that the beam is magnetically scanned transversely across the target, this process can be discrete or continuous. In either case, the dose deposited in any given region can be controlled either by measuring the dose and controlling the beam accordingly (turning it on or off, or moving it faster or slower), or it

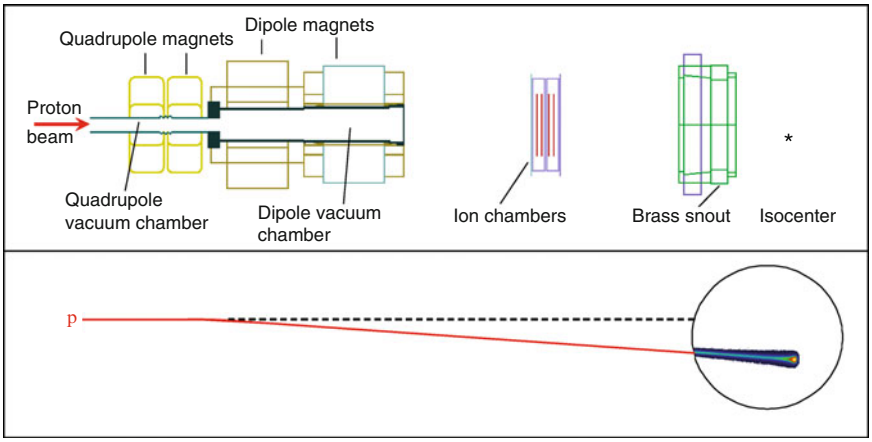

Fig. 25.20 Example of some components used for magnetic beam scanning. The *red line* represents a deflected scanned beam

can be controlled by time, assuming that the beam current and transverse velocity is appropriately controlled. The former can be called "*dose-driven*" and the latter "*time-driven.*" Spot scanning can be implemented in either mode, and it is this mode description that is more critical in the implementation of a scanning system. One important aspect of the choice between these two implementations is that of the ability of the accelerator to deliver a well-controlled beam, and whether the beam is continuous or pulsed.

25.5.2.1 Motion Effects

It is well known that the dose delivered to the target can be affected by the relative motion of the beam and the target (cf. Chap. 32 for details). In the case of spot scanning, the beam-on time is on the order of milliseconds, and this is a very short time compared to organ motion. In principle, given the ability to modify the beam parameters for each spot, it should be possible to track the motion in the transverse direction. However, a difficulty arises if target density and/or organs in the beam path change. This brings up the question whether the beam energy should be changed quickly to compensate for a different effective range, and whether the accelerator and beam line system can be adjusted to change quickly enough.

25.5.2.2 Time Sequence

The events that take place during a scanning sequence will determine the time required to deliver the treatment plan, and depending upon the motion effects, will actually determine the dose distribution delivered. How a treatment map is delivered might have nothing to do with the treatment plan, but rather with the scanning and accelerator implementation.

It is helpful to consider, within safety limits, how to best deliver an efficiently scanned beam. One can identify the contributions to the scanning time per layer.

- Beam control
  - Time to change the beam intensity or to turn it on and off.
- Time to irradiate a location
  - For safety reasons, the maximum dose rate will be inversely proportional to the time to stop the beam.
- Time to move from spot to spot
  - Note that in time-driven scanning mode, the maximum dose rate depends upon maximum scan speed and the instrumentation time constants; the maximum scanning speed depends upon the time for beam current change and the desired effective penumbra.

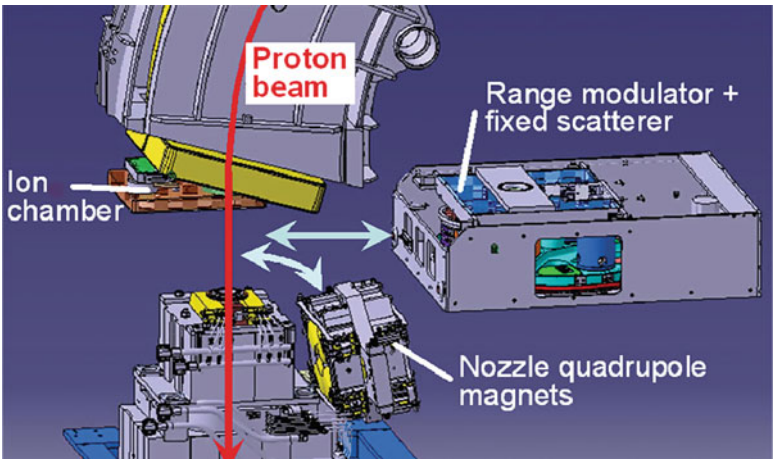

Fig. 25.21 A universal nozzle, including scanning elements developed by IBA and MGH. Some of the scattering elements can be removed and the nozzle quadrupole magnets inserted which results in the configuration shown in Fig. 25.20

- Scanning magnets
  - Time to change the magnetic field is a balance between speed and accuracy. Some practical limitations such as the voltage available also comes into play. Also important is the time to detect that the magnets are settled.
- Instrumentation
  - As in all the above contributions, instrumentation plays a crucial role. For example, the time to read dose is determined by a number of factors including the ion drift time in the ion chambers, to the speed of the electronics readout.

25.5.2.3 Hardware

The hardware required to spread out the beam in the scanning modality includes equipment to control the beam properties and instrumentation to measure the beam properties. The equipment used for this in the system of the Massachusetts General Hospital (MGH) was jointly developed with IBA. It is summarized in Fig. 25.21.

The beam range is given by the accelerated beam energy or the beam energy resulting from a degrader system. The beam size is determined by the intrinsic emittance of the beam and any beam focusing elements in the beam line. The position on the target is controlled by the beam angle bent through the scanning dipoles. The overall system of scanning magnets and power supply will determine

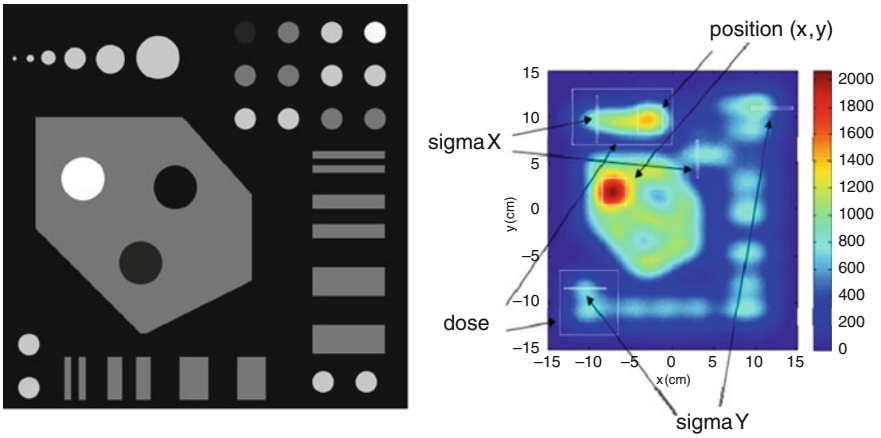

Fig. 25.22 *Left*: Theoretical design scan test pattern. *Right*: Result of a measurement with a larger beam size and some of the analysis that can be achieved using this pattern

the speed of the scan (limited, of course, by the speed of the instrumentation used to measure the beam properties).

Instrumentation to measure the fluence, position, and beam profile is generally included in the beam path just before the patient.

25.5.2.4 Quality Assurance (QA)

Figure 25.19 highlights the regions of dosimetric interest in the case of a scanned beam. These, in fact, represent the raw beam parameters. A challenge is to measure these parameters in a reasonably quick and accurate fashion. One method, jointly devised by MGH and IBA is through the use of a test pattern. Figure 25.22 displays a scanning beam pattern with perfect resolution and a realistic pattern measured with the MGH scanning beam. The illustrated case used an unfocused beam with a sigma of 1 cm. Also indicated are some of the regions of the pattern which can be used to analyze the beam position, dose, and beam size. Finally, parameters such as the gradient - the difference in fluence per unit distance - can be evaluated.

25.6 Summary

The basic principles of methods to modify the raw beam properties that emerge from an accelerator, in order to deliver a uniform dose to a target, have been described. Spreading out the beam by scanning is a method that has the promise to provide the most conformal treatment, but is also most sensitive to organ motion. There are advantages and disadvantages of each of these methods and some of these are impor-

tant to consider when addressing typical and atypical aspects of treatment delivery. The issue of conformality and target motion is one example that must be considered.

Basic physical principles of the interaction of ions with matter is the basis of the optimization of these methods. Practical implementation, particularly automation and efficiency of treatment operations, are important to consider. It is useful to regard the important dosimetric regions of interest and the efficiency of ion usage and to identify how both are affected by the design of the beam spreading system. The practical implementation of patient-specific hardware to optimize the treatment field and to allow reasonable handling by therapists is also worth considering. Of course, the beam scanning method affords the possibility to eliminate patient-specific hardware.

In almost all scattering implementations (with the exception of those using ridge filters), the term "passive" scattering has been misused. Most modern scattering systems require synchronization of the beam with a moving device, either a wheel or paddles, for example. In some cases, the beam current is further modulated. In fact, the implementation of an "active" beam scanning system can, in some ways, be considered less complex than some "passive" scattering systems that are used.

Single scattering provides the smallest penumbra, but is very inefficient in terms of beam usage and can result in secondary radiation produced. Double scattering is more efficient, in some cases up to 40%, if not combined with patient-specific apertures. Beam scanning is essentially 100% efficient and minimizes the secondary radiation delivered to the patient. However, it may not provide the best penumbra depending upon the size of the unmodified beam. Creating a very small beam is very difficult and expensive and can lead to longer treatment times (under some conditions), and it may be worth considering some cases for which lightweight apertures can produce an advantage.

A scanned beam delivery may provide the most efficient treatment scenario. This can afford the possibility to deliver multiple fields without entering the room. On the other hand, there may be some situations in which the use of a range compensator is useful to minimize the beam-on delivery time (by reducing the number of energy layers required), when complex three-dimensional concave shapes are involved. Many thousands of patients have been successfully treated using these techniques. Although beam scanning can produce a more conformal field distribution, quite complex cases can be treated using any of the techniques described herein. However, the application of these techniques, both in the design of patient-specific hardware, implementation of tolerances, and the use of treatment planning optimization is a nontrivial skill that must be developed for the most effective treatments.

References

1. G. Molière, Theorie der Streuung schneller geladener Teilchen: II Mehrfach- und Vielfach-streuung. Z. Naturforsch. **3a**, 78–97 (1948)
2. H.A. Bethe, Zur Theorie des Durchgangs schneller Korpuskularstrahlen durch Materie. Ann. Physik. **5**, 325–400 (1930)

3. B. Gottschalk, Passive Beam Spreading in Proton Radiation Therapy. Draft (Oct. 2004). Available as pdf file under http://physics.harvard.edu/∼gottschalk/. Accessed 15 Nov 2010
4. V. Kostjuchenko, D. Nichiporov, V. Luckjashin, A compact ridge filter for spread out Bragg peak production in pulsed clinical beams. Med. Phys. **28**, 1427–1430 (2001)
5. A.M. Koehler, R.J. Schneider, J.M. Sisterson, Range modulators for protons and heavy ions. Nucl. Instrum. Methods Phys. **131**, 437–440 (1975)
6. M.J. van Goethem, R. van der Meer, H.W. Reist, J.M. Schippers, Geant4 simulations of proton beam transport through a carbon or beryllium degrader and following a beamline. Phys. Med. Biol. **54**, 5831–5846 (2009)
7. A. Brahme, *The Optimal Choice of Scattering Foils for Electron Therapy* (Report of the Royal Institute of Technology, Stockholm, Sweden, TRITA-EPP-72–17, 1972)
8. H. Svensson, L. Johnson, L.G. Larsson, et al., A 22 MeV microtron for radiotherapy. Acta Radiol. Ther. Phys. Biol. **16**, 145–156 (1977)
9. M.A. Koehler, R.J. Schneider, J.M. Sisterson, Flattening of proton dose distributions for large-field radiotherapy. Med. Phys. **4**, 297–301 (1977)
10. P.L. Petti, J.T. Lyman, T.R. Renner, et al., Design of beam-modulating devices for charged particle therapy. Med. Phys. **18**, 513–518 (1991)
11. E. Grusell, A. Montelius, A. Brahme, et al., A general solution to charged particle beam flattening using an optimized dual scattering foil technique, with application to proton therapy beams. Phys. Med. Biol. **39**, 2201–2216 (1994)
12. G. Arduini, R. Cambria, C. Canzi, et al., Physical specifications of clinical proton beams from a synchrotron. Med. Phys. **23**, 939–951 (1996)
13. T. Kanai, K. Kawachi, Y. Kumamoto, et al., Spot scanning system for proton radiotherapy. Med. Phys. **7**, 365–369 (1980)
14. E. Pedroni, R. Bacher, H. Blattmann, et. al., The 200-MeV proton therapy project at the Paul Scherrer Institute: conceptual design and practical realization. Med. Phys. **22**, 27–53 (1995)
15. T. Haberer, W. Becher, D. Schardt, G. Kraft, Magnetic scanning system for heavy ion therapy. Nucl. Instrum. Methods Phys. Res. A **330**, 296–305 (1993)

Chapter 26
Dosimetry Techniques for Ion Beams

Giacomo Cuttone

Abstract Beam dosimetry is a key issue in ion beam therapy (IBT). In order to get a real clinical advantage from the physical and radiobiological features of ions, it is mandatory to develop a novel approach for determining the absolute and relative dose. New detectors and innovative measurement techniques have been implemented following the recommendations of International Standardization Committees.

26.1 Introduction

The decades of research and treatment with ion beams have gradually coalesced to an agreement across the spectrum of radiation oncology that once the gross tumor volume (GTV), the clinical target volume (CTV), and the planning target volume (PTV) have been delineated, there are two key decisions remaining. The first decision is how to optimize the 3D conformality of the delivered dose to the defined target volumes; here, lower-LET ions (protons) have excelled in the tests of time and experience. Even better, 3D conformality is appearing with the development of beam scanning and with the incorporation of access to a greater selection of nonorthogonal beam entry angles. The second decision is to select the desired RBE of the radiation treatment and to choose the appropriate radiation source. If high-LET irradiation is desired, the choice is to use heavier ions (from lithium to oxygen). If the combination of both excellent 3D dose distribution and increased RBE is preferred, carbon ions are presently considered the radiation source of choice. For pediatric tumors the use of lithium beams seems feasible and clinical attractive, though. The primary charged-particle beams, which can then be spread out in three dimensions to accommodate the target volume, are quite narrow

G. Cuttone (✉)
Laboratori Nazionali del Sud –INFN, Via S. Sofia 64, 95123 Catania, Italy
e-mail: cuttone@lns.infn.it

U. Linz (ed.), *Ion Beam Therapy*, Biological and Medical Physics, Biomedical Engineering, DOI 10.1007/978-3-642-21414-1_26,

in cross section and very thin along the z-axis of the Bragg peak, constraining tightly the volume of tissue with the highest dose. This high degree of 3D shaping of the radiation dose to the target volume permits an improvement of the therapeutic ratio of the target-volume dose to the adjacent normal tissue dose. These features have a great impact on dosimetry. In fact, both absolute dosimetry and relative dosimetry are strongly conditioned by the physical properties of ions. In the following the physical features of proton and heavy ion beams will be presented. The main dosimetry techniques will then be reported.

26.2 Properties and Requirements of Ion Beams

The use of ions, particularly protons, in radiotherapy is one of the major innovations in the fight against cancer. However, the level of the specifications of an ion beam is not yet as well defined as in the case of other, more conventional radiation therapies. It is necessary to define a beam of ions in terms of path, modulation of the Bragg peak, adjustment of the depth of penetration (range), dose rate, field size, uniformity and symmetry of the field, penumbra side, and dose distal fall-off (see Fig. 26.1).

The characteristics of the ions used for treatment influence decisively the choice of the accelerator and consequently of the detectors for dosimetry. Considering the dose curve as a function of depth, practical range defines the distance between the surface of the entering ion beam and the distal point where the dose is reduced by

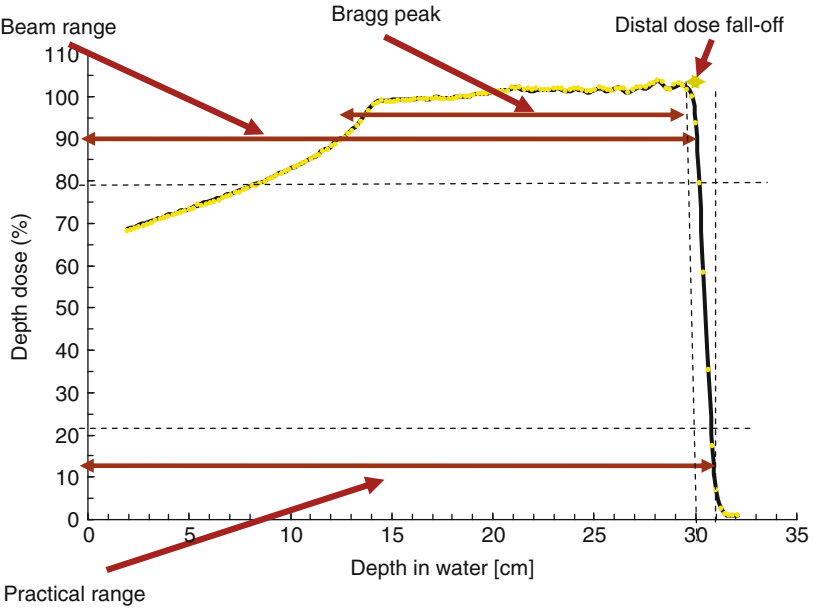

Fig. 26.1 Spread-out Bragg peak features

10%. It depends on the energy and materials along the beam line (e.g., tools for beam monitoring, range adaptation, and beam modulation).

The depth extension of a beam of ions, the so-called spread-out Bragg peak (SOBP), is defined as the distance between two points proximal and distal where the dose is reduced to 95% compared to the standardized nominal value. The SOBP should vary in steps of 0.1–0.2 mm (in water) for beams with energies lower than 70 MeV and in 1–2 mm steps for higher energies.

The field size depends on the kind of beam line used. For fixed, horizontal beams, used in the treatment of ocular tumors, field sizes vary between 5 and 35 mm in diameter. Horizontal beams used to treat diseases of the head and neck, require fields up to $15 \times 15\,\text{cm}^2$. If full flexibility is required treating tumors in any part of the body, field variation between 2×2 and $40 \times 40\,\text{cm}^2$ might be considered. In any case, the field size should be modified by steps of 1 mm with an accuracy of 0.5 mm.

The lateral penumbra (80–20%) has to be measured in water at the entrance and it should be less than 2 mm. Also the lateral penumbra at the maximum depth of treatment has to be measured. In fact, the beam straggling in the tissue strongly affects the lateral penumbra, increasing it. Nevertheless, we have to take into account that this contribution cannot be reduced or eliminated. In beam lines modulating the energy with passive systems, the penumbra is not only determined by the accelerator's characteristics but also by diffusing materials, set along the beam path. It can be reduced by using collimators, minimizing the distance between collimator and skin and increasing the distance between the source and the collimator. With an active system, the lateral penumbra is mainly influenced by the divergence of the "pencil beam" related to the optics of the accelerator extraction system and to the beam-scanning pattern. It should also be noted that an active scanning beam system uses a superposition of many beams of different energies and quality with a FWHM of 0.5–1 cm. Then the following considerations are necessary:

- The dose rate can be extremely high because the dose needed for the treatment could, in principle, be extracted all at once.
- Dose deposited in every elementary volume is obtained as a superposition of many spots; in order to achieve a total accuracy of $\pm 3\%$ in the dose measurement, an accuracy of 1% is needed in each spot.
- The size of the beam spot can also be smaller than 0.5 cm FWHM; this must be considered in the design of the room monitor, for a granularity and a spatial resolution of a few mm. The size of the beam and its position are two spatial parameters to be measured and verified during treatments. Many factors can influence the mean dose rate to the target such as the beam intensity, the beam extraction system, the transport efficiency, and the technique used to change the energy. For a field $40 \times 40\,\text{cm}^2$, the recommended dose rate should be 1–3 Gy min^{-1}. For a field $5 \times 5\,\text{cm}^2$ at 70 MeV, it is recommended to be 5 Gy min^{-1}. Moreover, for the treatment of ocular tumors still higher dose rates (10 Gy min^{-1}) are required.

The accuracy in dose determination should be $\pm 2.5\%$, according to international protocols or a code of practice [1–5]. The dose uniformity should be $\pm 5\%$ in the target volume.

The skin-to-target dose ratio is influenced by the source-to-axis distance (SAD). For a monoenergetic beam, the geometrical contribution to this ratio is the ratio between the area irradiated at the Bragg peak depth and that irradiated at the patient surface:

$$D^2/(D-R)^2 \tag{26.1}$$

- where D is the SAD and R the proton range. The skin-to-target dose ratio can be expressed as function of the source-to-surface distance (SSD) rather than SAD considering that both are correlated. The ratio in any case decreases with SSD. In a gantry, an SAD $>$ 3 m is typically unfeasible. An acceptable value of SAD is 2–3 m.

The time structure of the extracted beams has to be reported in relation to the detectors to be used for dose determination. In general, no drawbacks can be reported implementing a passive scattering system. Designing an active scanning system, particular care has to be devoted to the maximum intensity fluctuations that can be handled by the detectors in a fixed time window. On the other hand, the ion current intensity for pulse mode accelerators (when synchrotron and linac-based facilities are used) has to be carefully assessed from the dosimetric point of view. In fact, collection efficiency has to be carefully evaluated in order not to introduce errors in the dose determination. No major drawbacks are reported in this field for cyclotron-based facilities being characterized by a practically continuous beam and, from this point of view, any detector can be used for dosimetry. The readout speed must be fast enough to react to any malfunctioning to minimize the maximum error in the treatment delivery. A reasonable value of this feedback time is 100 μs.

26.3 Absolute Dosimetry

The absorbed dose to tissue is one of the basic quantities used in dosimetry for radiotherapy. The comparability of tumor treatment with different types of radiation fields, requires high-accuracy measurement devices that allow an absolute and direct dose determination. To date, the dose calibration is standardized for all types of radiation fields and is traced back to a primary standard. It has been internationally agreed upon to use the absorbed dose to water as the calibration quantity for all types of radiation fields. The dose delivered to tissue should be measured with an accuracy of $\leq 3\%$.

First of all, we have to define the residual range R_{res} at a measurement depth z, as

$$R_{\mathrm{res}} = R_{\mathrm{p}} - z \tag{26.2}$$

where z is the depth of measurement and R_p the practical range (both expressed in $g\,cm^{-2}$).

Typically, R_{res} is chosen as the beam quality index. This has the advantage of being easily measurable. Although this choice will slightly underestimate the stopping power ratios in the middle of the SOBP, this effect is unlikely to exceed 0.3%.

Clinical proton dosimetry has been based on different types of dosimeters, such as calorimeters, ionization chambers, Faraday cups, track detectors, activation systems and diodes. Existing proton dosimetry protocols [2–4] provide recommendations for ionization chamber dosimetry, based on in-air calibrations in a ^{60}Co beam or in terms of absorbed dose to water [1, 5].

Air kerma (kinetic energy released per unit mass of air) is easy to measure in an ionization chamber. The measurement device is calibrated in a well-known photon reference field to absorbed dose to water and traced back to a national primary standard reference chamber.

Plane-parallel or cylindrical ionization chambers can be used. The combined standard uncertainty in the absorbed dose to water for plane-parallel ionization chambers (PPICs) will be slightly higher than for cylindrical ones due to their higher uncertainty for p_{wall}, the response correction for nonmedium equivalence of the chamber wall and any waterproofing material, in the ^{60}Co reference beam quality.

Cylindrical ionization chambers are preferred for reference dosimetry. Their use is, however, limited to proton beams with qualities at a reference depth or residual range $R_{res} > 0.5\,g\,cm^{-2}$. The reference point for these chambers is chosen on the central axis at the center of the cavity volume; this point is positioned at the reference depth in the phantom.

PPICs can be used for reference dosimetry in all proton beams and must be used for proton beams at reference depths $R_{res} < 0.5\,g\,cm^{-2}$. For these chambers, the reference point is taken on the inner surface of the entrance window, at the center of the window and positioned at the point of interest in the phantom. The outer diameter for cylindrical ionization chambers should not be larger than half the SOBP width.

The absorbed dose to water at the reference depth z_{ref} in water, in a proton beam of quality Q and in the absence of the chamber is given by

$$D_{wQ} = M_Q N_{D\,w\,Qo} k_{Q\,Qo} \tag{26.3}$$

where M_Q is the reading of the dosimeter at the reference point of the chamber positioned and corrected for pressure, temperature, electrometer calibration, polarity effect, and ion recombination. N_{DwQo} is the calibration factor in terms of absorbed dose to water for the dosimeter at reference quality Q_o, and k_{QQo} is a chamber-specific factor that corrects for differences between the reference beam quality Q_o and the actual quality Q being used. All these factors are reported in [1].

Clinical dosimetry requires the measurement of central-axis percentage depth-dose distributions, transverse beam profiles, output factors, etc. Such measurements should be made for all possible combinations of energy, field size, and SSD used for

radiotherapy. Depth-ionization distributions are measured using PPICs. They can be converted into a depth-dose distribution on the basis of the depth dependence of the stopping-power ratio $s_{w,air}$, particularly, in the low-energy region. Values for $s_{w,air}$ as a function of R_{res} can be calculated [1]. Perturbation factors are assumed to have a value of unity. The influence of ion recombination and polarity effects on the depth-ionization distribution should be investigated and taken into account if there is a variation with depth.

If the field size is smaller than twice the diameter of the cavity of the plane-parallel chamber, then a detector with a better spatial resolution (e.g., minichamber, diode or diamond detector) has to be used. The resulting distribution must also be converted using appropriate stopping-power ratios depending on the detector materials used (e.g., water-to-air, water-to-silicon, or water-to-graphite) as reported in the literature [5, 6].

The suitability of such detectors for depth-dose measurements should be verified by test comparisons with a PPICs at a larger field size. For clinical proton beams produced by dynamic beam delivery systems such as spot scanning, measurement times should be long compared to the scanning cycle of the field in order to yield reproducible readings.

Reference dosimetry (beam calibration) of heavy ion beams is based on a calibration factor in terms of absorbed dose to water of an ionization chamber in a reference beam which, owing to the lack of primary standards for heavy ions, is taken from ^{60}Co gamma rays. An international Code of Practice was developed for ions ranging from 2 to 30 g cm^{-2} in water [1]. For carbon ions, this corresponds to an energy range of 100–450 MeV/u.

For heavy ions, the biological effective dose (BED) has to be determined. It is defined as the physical absorbed dose multiplied by the relative biological effectiveness (RBE) of the beam for the tissue under consideration. In the case of heavy ions, the RBE varies with depth and with dose delivered to the tissue. By using BED, it is possible to compare results from conventional radiotherapy with those from heavy ion radiotherapy. Dosimetry of heavy ions is restricted to the determination of the physical dose with standards of absorbed dose to water disseminated through an ionization chamber calibrated in terms of absorbed dose to water, $N_{D,w,Qo}$ [1].

Ion beams for radiotherapy have a distinct physical characteristic for radiation dosimetry compared to other therapeutic radiation beams [7]. Heavy ions passing through beam-modulating devices or human tissues, produce fragment nuclei mainly due to the fragmentation of the incident projectiles. The fragmented nuclei have a longer range than the incident ions (because A/Z^2 increases). Many nuclei are present, all with different energy distributions. Other nuclear reaction mechanisms involving target fragmentation are possible but their cross section is so low that they need not be taken into account. The projectile fragmentation affects considerably the dose profile of heavy ions and the biological response to this kind of radiation. A more or less significant tail dose at the distal end of the Bragg peak results from this nuclear fragmentation.

To measure the dose deposited by a beam of ions heavier than protons with an ionization chamber requires knowledge of the energy spectra of the incident ions and the projectile fragments. Very few experimental and theoretical data on the spectral distribution of heavy ion beams are available in the literature and new measurements are, finally, in progress.

Cylindrical chambers and PPICs are also the reference dosimetry instruments for clinical heavy ion beams. However, the combined standard uncertainty on D_{wQ} for PPICs will be slightly higher due to their higher uncertainty for p_{wall} in the ^{60}Co reference beam quality. For this reason, cylindrical ionization chambers are preferred for reference dosimetry. However, their use is limited to heavy ion beams with a SOBP width $\geq 2.0\,g\,cm^{-2}$. The reference point for these chambers is set on the central axis of the chamber at the center of the cavity volume. In the case of heavy ion beams, an effective point of measurement of the chamber, P_{eff}, should be used because the depth-dose distribution in the SOBP is not flat and the slope depends on the width of the SOBP [8]. The reference point of the cylindrical chamber should be positioned a distance of $0.75\,r_{cyl}$ deeper than the point of interest in the phantom, with r_{cyl} being the inner radius of the chamber.

PPICs can be used for reference dosimetry in all heavy ion beams; they must be used for heavy ion beams with a SOBP width $<2.0\,g\,cm^{-2}$. For PPICs, the reference point is taken to be on the inner surface of the entrance window, at the center of the window.

The absorbed dose to water at z_{ref} in a heavy ion beam of quality Q is calculated according to (26.3).

When beams are generated by scanning techniques, the dose rate might be very high and general recombination effects must be taken into account. The correction factor for general recombination should be obtained experimentally by the well-known two-voltage method [1]. When general recombination is negligible, initial recombination should be taken into account for heavy ion beams, especially when the dose is measured using PPICs. All the details are reported in [1].

At present, no primary standard of absorbed dose to water for heavy ion beams is available. The stopping-power ratios and W-values for heavy ion beams are taken to be independent of the beam quality, owing to a current lack of experimental data. The contribution of fragmented nuclei to stopping-power ratios and W values are also assumed to be negligible. Constant values for the stopping-power ratio and W-value are, therefore, adopted as 1.130 and 34.50 eV, respectively. Recently, a new determination of the W-value has been reported [9]. The respective value is 3.5% larger than that estimated for heavy ion beams [1]. In the therapeutic energy range, the W-values in air for carbon beams indicated slight energy dependence, but these should be applied as a constant value for practical use because of the large uncertainty and unknown perturbation factors of the ionization chambers. Otherwise, the value of the stopping power ratio has recently been confirmed [6].

For clinical use, depth-dose distributions, transverse beam profiles, penumbra size of the radiation fields, and output factors for the various conditions of treatments with heavy ion beams should be measured. PPICs are recommended for the measurement of depth-dose distributions. For the measurement of transverse profiles or

3D dose distributions, very small chambers with a cavity volume $<0.1\,cm^3$ can be used. For dosimeters other than ionization chambers, the energy dependence of the detector response should be checked versus ionization chambers.

26.4 Detector Requirements for Relative Dosimetry

Relative dosimetry in IBT is strongly affected by the presence of

- Small radiation fields with high-dose gradients
- Dose rate variations in space and time
- Beam energy variations in space and time

Measurements that have to be performed can be classified in three categories:

- *Beam monitoring during irradiation*. In this case, the detector is placed up-stream of the patient and the most important issue is not to perturb the radiation beam, significantly.
- *In phantom measurements*. They are required to verify the dose calculations of the treatment planning system (TPS) prior to treatment. Phantoms can be square cylindrical, or anthropomorphic.
- *In vivo measurements*. They are performed during patient treatment to verify the absorbed dose in a certain point, e.g., to record the threshold dose in the entrance channel or the dose distribution in a plane.

The beam monitoring during irradiation is performed with specialized detectors, the *monitor chambers.* When heavy ions are used, distinction has to be made between passive and active beam delivery. In the former, a full area PPIC can be used as in the case of photons. In the latter, the dose distribution is obtained as a superposition of many elemental beamlets, typically Gaussian shaped with 0.5–1.0 cm FWHM. Thus the verification has to be done both on the fluence and the center of gravity. To reach this goal, position sensitive fluence detectors are needed.

Different devices can be developed for point dosimetry, dose profiles, or planar dose distributions (mono- and bidimensional) and for volumetric measurements. If the phantom has a regular shape and a homogeneous composition, the control of the TPS calculation can be done thanks to a simulation, i.e., by calculating the dose that would be absorbed at the selected depth, in the actual experimental conditions, using the field shape and the monitor units of the patient treatment. In the case of anthropomorphic phantoms, the verification has to take into account inhomogeneity and the treatment geometry. These measurements are less user-friendly and, in practice, only passive or off-line dosimeters can be used.

The assessment of the absolute dose in a point is necessary for each treatment verification. Considering the steep dose gradients of an IBT plan and the potentially very small field sizes, the need for accurate dose determination becomes evident.

A spatial resolution of 1–2 mm is sufficient for almost all applications of point dosimetry. The response should be widely independent of the dose rate in the range of 0.01–100 Gy/min. Full independence is often not achievable. The dependence effects must then be well known and considered. A correction is possible when the dose rate does not change during a single charge acquisition or when the measured response is current versus time and the integration is subsequently performed numerically. Point dosimeters have to respond linearly to absorbed dose in a wide range (approx. 1 mGy to 20 Gy).

The detector response has to be fast compared to the beam delivery modalities. The detector has to be able to follow the output variation of the accelerator. For a monitor unit from an accelerator being delivered in a time of approx. 0.15 s, the acceptable value for the rising time of the detector signal can only be some tenths of a second.

A negligible leakage current, a low LET dependence, and water equivalence are further important issues, as are a low angular dependence, good radiation hardness, and long-term time stability.

Point dosimeters have to be matched between different samples. This is essential when multiple sensors have to be used at different points (for instance, thermoluminescent dosimeters in an anthropomorphic phantom): their application becomes more laborious if each one has to be characterized individually. The detector has to be waterproof to facilitate the dose measurements in water phantoms. It is usually recommended for dose calibration operations in external radiotherapy by the international dosimetry protocols. This requirement is of concern for detectors to be employed for beam calibration in reference conditions. It does not apply to devices planned for in vivo or in anthropomorphic phantom measurements.

Bidimensional dosimetry is mainly used for beam monitoring: Typically, three independent dosimeters are required to provide continuous monitoring of the dose delivered to the patient. One dosimeter has to be located at a distance of less than 1 m from isocenter. At least one dosimeter must not saturate at the highest possible beam current focused into a 3 mm^2 area. A secondary electron emission monitor fulfils this requirement. A dose detector with a two-dimensional position resolution of 5 mm or better must be provided. The detector must be able to generate a beam cut-off signal when any spot has reached the specified dose limit. It can thus serve as one of the three independent dosimeters.

In order to satisfy the specifications for the maximum beam diameter at isocenter and to cause minimal perturbation to the radiation beam (transparency), the detectors have to be as thin as possible [10]. In order to reach a level of accuracy on the measured dose that can be considered acceptable for the treatment, the 2D detectors must satisfy a number of requirements, which include most of the requirements previously quoted for the point detector: a specific requirement is the possibility of working in charge integration. The spatial resolution depends on the sensor dimensions and on the distance between each component of the matrix (granularity). A short distance between matrix elements is necessary to determine a good spatial sampling of the dose distribution. The two parameters (size and

distance) have to be evaluated considering the grid of the TPS dose matrix. Then the pixel dimension has to be typically better then 5 mm.

The current response has to be independent of the dose rate and a short- and long-term stability of the detectors is requested. Ideally, the sensitivities of all the sensors (for a matrix device) should be the same, and stable in time. This cannot exactly be achieved. However, at least the calibration factors need to remain constant for a longer period.

Three-dimensional dosimetry represents the most complete solution for in-phantom simulation of conformal treatments. This kind of measurement has to be performed before the treatment as check of the TPS. Dose calculations and the phantom can have any shape (square, cylindrical, anthropomorphic). Standard commercial detectors are not well established for this type of application. The same requirements as for the 2D dosimetry are valid, but tissue equivalence issues become a major concern.

26.5 Current Detector Types for IBT

A number of small-field detectors exist that were specifically developed for dosimetry measurements in radiosurgery, but are applicable to IBT, as well. In Table 26.1, some basic information for ion chambers and other detectors is presented.

For absolute point dose measurements, ionization chambers are the devices of choice. The one usually considered as reference is the Farmer-type ionization chamber, which is calibrated at a national reference laboratory. Smaller chambers can be calibrated to a ^{60}Co beam by the user.

PPICs are recommended for depth-dose distribution measurements in proton and heavy ion beams in water phantoms [1]. They are available with 1 mm electrode spacing, giving high spatial resolution, as the Advanced Markus^{TM} chamber (Fig. 26.2). Both cylindrical and plane-parallel chambers can be used for proton beam calibration, but PPICs have to be used for the measurement of dose in a narrow SOBP adopted, e.g., in proton beams <70 MeV for the treatment of uveal melanoma [11–13].

Silicon diodes are of interest as small-volume devices with reasonable sensitivity. High-doped p-type silicon diodes have recently been used in proton beams [14, 15]. They confirmed good features in terms of short- and long-term repeatability, linearity, dose rate, and LET independence.

Natural diamond detectors have proven to be suitable for clinical dosimetry. Diamond compares favorably with ion chambers and silicon diode systems in terms of sensitivity, spatial accuracy, and tissue equivalence [16]. PTW diamond showed also excellent characteristics with respect to angular spread and penumbra width [17]. Nevertheless, there are some drawbacks: the signal shows a dose-rate dependence that must be accounted for [17–21], and it needs a preirradiation dose before daily use to stabilize the response [22]. Moreover, the response characterization in low-energy proton beams showed a strong energy dependence

Table 26.1 Basic features of point dosimeters

Detector type	Volume (cm^3)	Cavity length (mm)	Cavity diameter (mm)
IC NE FARMER	0.6	24	6.3
IC PTW PIN POINT	0.015	5	2
IC EXRADIN T1	0.05	5.7	4
IC Exradin T14	0.009	6	1.5
IC SCANDITRONIX RK	0.12	10	4
IC EXRADIN A16	0.007	2.7	1.5
		Collecting diameter (mm)	Electrode spacing (mm)
IC Markus	0.055	5.3	2
IC Advanced Markus	0.02	5.3	1
IC PPC05	0.046	10	0.5
		Sensitive diameter (mm)	Sensitive thickness (μm)
p-Si diode SCANDITRONIX SFD	1.7×10^{-5}	0.6	60
p-Si diode SCANDITRONIX	0.3×10^{-3}	2.5	0.060
Natural Diamond PTW	1.4×10^{-3}	4.5	0.31
TLD-100 Microcubes	1×10^{-3}	1[a]	1[b]
MOSFET	–	2.3	1[b]

[a]Edge length (mm)
[b]Total thickness
Abbreviations: *IC* ion chamber, *MOSFET* metal-oxide semiconductor field-effect transistor, *SFD* stereotactic field diode, *TLD* thermoluminescent dosimeter

of the natural diamond and an unsuitable dimension of the detector [23]. Finally, the detector cost is not necessarily competitive.

Metal-oxide semiconductor field-effect transistors (MOSFETs), revealed a lower sensitivity in low-energy proton beams (<70 MeV) than in photon beams [24]. This was attributed to the LET effect in the interaction between protons and oxide, significantly affecting the trapping. Another peculiarity was a strong dependence of the calibration factor on the proton energy.

Thermoluminescent dosimeters (TLDs) are versatile and easy to use instruments to measure radiation in IBT. Their advantages include small size, versatility in placement, and readily available readout. However, TLDs must be characterized individually [25] and their accuracy is limited to 2–3% [26, 27].

Film dosimetry is a well-established method to verify 2D dose distributions in phantoms or to perform quality control tests of radiation beams. A radiographic film for extended dose range (Kodak EDR-2), however, showed low sensitivity for proton and carbon ion beams of different energies [28]. In the case of small animal and cell culture irradiations and for narrow, high-intensity beams or particle scattering experiments, this drawback can be turned into a feature. Radiographic films can also be helpful in quality assurance programs to check beam parameters such as lateral dose uniformity, penumbra width, and range uniformity for consistency over time.

Limitations regard the large energy- and ion-dependent response. This may require prior knowledge of the energy spectrum of the particles and a weighting scheme to calculate the dose conversion factors.

Bidimensional dosimetry measurements can further be performed with radiochromic films, which change color with irradiation. They are insensitive to visible light and need not be processed. They offer high spatial resolution but their sensitivity to low-energy photons is lower than for radiographic films. Their application is limited because their response is time and temperature dependent and presents effects of spatial nonuniformity. Radiochromic films are also more expensive than radiographic film. Newly marketed products (EBT, HS, and NHS) are said to compensate for these drawbacks. Radiochromic films are routinely used for proton beams for eye treatments because their dose response is largely independent of the ion energy and LET. This offers the possibility to have a unique calibration curve in an energy range from 20–250 MeV.

A new type of radiochromic film (Gafchromic^{TM} EBT) has recently been studied for its applicability in heavy ion therapy [29]. Significant improvements were recognized with respect to previous products. In particular, an excellent spatial resolution was observed, making the new film a promising candidate for dosimetry in scanned medical ion beams.

A bidimensional position-sensitive dosimetry system based on a scintillating gas detector for pretreatment verification of dose distributions in IBT was described [30]. The dosimetry system consists of a chamber filled with an argon/carbon tetrafluoride (Ar/CF_4) scintillating gas mixture, inside which two cascaded gas electron multipliers (GEMs) are mounted. A GEM is a thin polymer film (e.g., Kapton^{TM}) with copper cladding structured with a regular pattern of micrometer holes. The primary electrons, created in the detector's sensitive volume by the incoming beam, drift in an electric field toward the GEMs and undergo gas multiplication in the GEM holes. During this process, photons are emitted by the excited Ar/CF_4 molecules and detected by a mirror-lens-CCD camera. Since the amount of emitted light is proportional to the dose deposited in the sensitive volume of the detector by the incoming beam, the intensity distribution of the measured light spot is proportional to the 2D ion dose distribution. Consequently, the scintillating gas detector is a promising device for verifying dose distributions in high-LET beams, for example, to check treatment plans comprising ion beams of different energies.

Three-dimensional dosimetry is the most complete solution for conformal treatment verification, but standard commercial detectors are not readily available. Gel dosimetry is the only choice in practice. Some detectors are based on Fricke dosimeters, others on polymer gels. A review on polymer gel dosimetry can be found in [31]. Polymer gel dosimeters can be purchased as a ready-to-mix package and their usefulness for 3D dose measurements was demonstrated [32]. The response of polymer gels is dependent on exposure to light and oxygen, the composition, and the temperature of the gel during readout. The readout can either be done by an MRI or CT scanner. In any case, there are technical challenges to overcome. Recently, such a detector has been applied to carbon dosimetry [33].

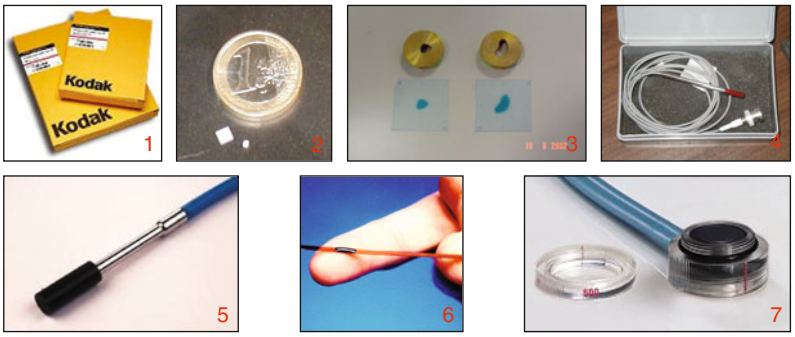

Fig. 26.2 Detectors for dosimetry: (1) Radiographic film for extended dose range (EDR-2), (2) Thermoluminescent dosimeter (TLD), (3) Gafchromic™ EBT (External Beam Therapy) film, (4) Hi-p silicon diode, (5) Tissue equivalent natural diamond, (6) Metal-oxide semiconductor field-effect transistor (MOSFET), (7) Plane parallel ion chamber Advanced Markus™

A novel approach for reconstruction of the 3D dose distribution was reported from HIMAC. A fluorescent screen with a CCD camera was used to measure the fluence distribution for each isoenergy slice (i.e., the unit of the depth scanning). The measured images were then superimposed to rebuild the dose distribution [34]. This system was installed at the HIMAC experimental port and tested with carbon ions. Since the maximum difference between the reconstructed dose and the ionization chamber measurement was around 5% in the target volume, this system could be useful for quick verification of 3D dose distributions.

At GSI, Darmstadt, an in-beam PET camera was installed to determine the 3D dose distribution during carbon ion treatment (cf. Chap. 31 for details). It is capable to perform simultaneously with the therapeutic irradiation a beam-delivery independent, noninvasive control of the ion beam irradiation. It permits an in-vivo measurement of the ion range, validation of the physical model of treatment planning, and evaluation of the whole process of treatment from planning to dose delivery.

For head and neck tumors, it could be demonstrated that the system is able to detect and quantify unpredictable deviations between planned and really applied dose distributions due to mispositioning or anatomical changes [35].

The potential of in-beam PET appears to be of special interest in cases where new ion species, e.g., helium or oxygen ions, are introduced into therapeutic applications. It could be of help when new components or algorithms are introduced into the technological chain from diagnostic imaging to beam delivery, and in any delicate therapeutic situation, where high-precision dose delivery is required, as, for example, during hypofractionation or single-dose irradiation.

26.6 Summary

As shown, beam dosimetry is a key issue in IBT. A dedicated approach for the determination of absolute and relative dose has been developed to get a real clinical advantage from the physical and radiobiological features of ions. New detectors

and innovative measurement techniques have been implemented even considering the experience gained in nuclear physics. Today, ion dosimetry can be assessed as mature field with respect to the clinical requirements in IBT. The dosimetry developments are continuing as the other scientific and technological main topics involved in radiotherapy with external ion beams ensuring a high quality in clinical treatments.

References

1. International Atomic Energy Agency. *Absorbed Dose Determination in External Beam Radiotherapy: An International Code of Practice Based on Standards of Absorbed Dose to Water*. IAEA Techn Report Series 398 (IAEA, Vienna, 2000)
2. J.T. Lyman, M. Awshalom, P. Berardo, et al., *Protocol for Heavy Charged-Particle Therapy Beam Dosimetry*. AAPM Task Group 20, Report 16 (AIP, New York, 1986)
3. S. Vynckier, D.E. Bonnett, D.T.L. Jones, Code of practice for clinical proton dosimetry. Radiother. Oncol. **20**, 53–63 (1991)
4. S. Vynckier, D.E. Bonnett, D.T.L. Jones, Supplement to the code of practice for clinical proton dosimetry. Radiother. Oncol. **32**, 174–179 (1994)
5. International Commission on Radiation Units and Measurements. *Clinical Proton Dosimetry, Part I: Beam Production, Beam Delivery and Measurement of Absorbed Dose*. ICRU Report 59 (ICRU, Bethesda, MD, 1999)
6. H. Paul, A comparison of recent stopping power tables for light and medium-heavy ions with experimental data and applications to radiotherapy dosimetry. Nucl. Instrum. Methods Phys. Res. **B247**, 166–172 (2006)
7. J.J. Broerse, L.T. Lyman, J. Zoetelief, Dosimetry of External Beams of Nuclear Particles, in *The Dosimetry of Ionizing Radiation*, ed. by K.R. Kase, B.E. Bjärngard, F.H. Attix. vol. 1 (Academic, New York, 1987), pp. 229–290
8. G.H. Hartmann, O. Jäkel, P. Heeg, et al., Determination of water absorbed dose in a carbon ion beam using thimble ionization chambers. Phys. Med. Biol. **44**, 1193–1206 (1999)
9. M. Sakama, T. Kanai, A. Fukumura, K. Abe, Evaluation of *w* values for carbon beams in air, using a graphite calorimeter. Phys. Med. Biol. **54**, 1111–1130 (2009)
10. W.T. Chu, J.W. Staples, B.A. Ludewigt, et al., Performance specifications for proton medical facility. Lawrence Berkeley Laboratory, LBL-33749, UC-000, 1993. http://www.osti.gov/energycitations/product.biblio.jsp?osti_id=10163935. Accessed 29 Oct 2010
11. G. Cuttone, L. Raffaele, M.G. Sabini, et al., First dosimetry intercomparison results for the CATANA project. Phys. Med. **15**, 121–130 (1999)
12. H. Palmans, F. Verhaegen, On the effective point of measurement of cylindrical ionization chambers for proton beams and other heavy charged particle beams. Phys. Med. Biol. **45**, L20–L22 (2000)
13. A. Kacperek, E. Egger, G. Cuttone, et al., Intercomparison Using Parallel Plate Ionization Chambers in Proton Eye Therapy Beam, in *IAEA Standards and Codes of Practice in Medical Radiation Dosimetry*, vol. 2 (IAEA, Vienna, 2003), pp. 311–319
14. J. Medin, E. Grussel, General characteristics of the use of silicon diode detectors for clinical dosimetry in proton beams. Phys. Med. Biol. **45**, 2573–2582 (2000)
15. M. Pacilio, C. De Angelis, S. Onori, et al., Characteristics of silicon and diamond detectors in a 60 MeV proton beam. Phys. Med. Biol. **47**, N107–N112 (2002)
16. M. Bucciolini, F. Banci Buonamici, S. Mazzocchi, et al., Characteristics of silicon and diamond detectors in a 60 MeV proton beam. Med. Phys. **30**, 2149–2154 (2003)
17. S.N. Rustgi, Evaluation of the dosimetric characteristics of a diamond detector for photon beam measurements. Med. Phys. **22**, 567–570 (1995)

18. A. Fidanzio, L. Azario, R. Miceli, et al., PTW-diamond detector: Dose rate and particle type dependence. Med. Phys. **27**, 2589–2593 (2000)
19. F. Haryanto, M. Fippel, W. Laub, et al., Investigation of photon beam output factors for conformal radiation therapy Monte Carlo simulations and measurements. Phys. Med. Biol. **47**, N133–143 (2002)
20. W. Laub, M. Alber, M. Birkner, F. Nüsslin, Monte Carlo dose computation for IMRT optimization. Phys. Med. Biol. **45**, 1741–1754 (2000)
21. W. Laub, T.W. Kaulich, F. Nüsslin, A diamond detector in the dosimetry of high-energy electron and photon beams. Phys. Med. Biol. **44**, 2183–2192 (1999)
22. C. De Angelis, S. Onori, M. Pacilio, et al., An investigation of the operative characteristics of two PTW diamond detectors in photon and electron beams. Med. Phys. **29**, 248–254 (2002)
23. S. Onori, C. De Angelis, P. Fattibene, et al., Dosimetric characterization of silicon and diamond detectors in low-energy proton beams. Phys. Med. Biol. **45**, 3045–3058 (2000)
24. G.A.P. Cirrone, G. Cuttone, P.A. Lojacono, et al. Preliminary investigation on the use of the MOSFET dosimeter in proton beams. Phys. Med. **22**, 29–36 (2006)
25. M.G. Sabini, L. Raffaele, M. Bucciolini, et al., The use of thermoluminescent detectors for measurements of proton dose distribution. Radiat. Prot. Dosim. **101**, 453–456 (2002)
26. D.A. Low, S. Mutic, J.F. Dempsey, et al., Quantitative dosimetric verification of an IMRT planning and delivery system. Radiother. Oncol. **49**, 305–316 (1998)
27. M.G. Sabini, M. Bucciolini, G. Cuttone, et al., TLD-100 glow-curve deconvolution for the evaluation of the thermal stress and radiation damage effects. Nucl. Instrum. Methods Phys. Res. **A476**, 779–784 (2002)
28. M.F. Moyers, EDR-2 film response to charged particles. Phys. Med. Biol. **53**, N165–N173 (2008)
29. M. Martisikova, B. Ackermann, S. Klemm, O. Jäkel, Use of Gafchromic EBT film in heavy ion therapy. Nucl. Instrum. Methods Phys. Res. **A591**, 171–173 (2008)
30. E. Seravalli, M. de Boer, F. Geurink, et al., A scintillating gas detector for 2D dose measurements in clinical carbon beams. Phys. Med. Biol. **53**, 4651–4665 (2008)
31. M. McJury, M. Oldham, V.P. Cosgrove, et al., Radiation dosimetry using polymer gels: methods and applications. Br. J. Radiol. **73**, 919–929 (2000)
32. D.A. Low, J.F. Dempsey, R. Venkatesan, et al., Evaluation of polymer gels and MRI as a 3-D dosimeter for intensity-modulated radiation therapy. Med. Phys. **26**, 1542–1551 (1999)
33. I. Kantemiris, L. Petrokokkinos, A. Angelopoulos, et al., Carbon beam dosimetry using VIP polymer gel and MRI. Presented at 5th International Conference on Radiotherapy Gel Dosimetry, Hersonissos, Greece, 29 Sep–3 Oct 2008, IOP Publishing Journal of Physics, Conference Series 164 (2009)
34. T. Furukawa, N. Saotome, T. Inaniwa, et al., Delivery verification using 3D dose reconstruction based on fluorescence measurement in a carbon beam scanning irradiation system. Med. Phys. **35**, 2235–2242 (2008)
35. K. Parodi, T. Bortfeld, W. Enghardt PET imaging for treatment verification of ion therapy: implementation and experience at GSI Darmstadt and MGH Boston Nucl. Instrum. Methods Phys. Res. **A59**, 282–286 (2008)

Chapter 27
Control and Safety Systems for Ion Beam Therapy

Hiroshi Akiyama and Kazuo Tomida

Abstract The control and safety system (CSS) is a crucial component of an ion beam facility. Measuring agreement of planned and actual treatment, controlling the irradiation process, and feedback to treatment planning are among the many tasks. This article describes general considerations for upstream design of a CSS for ion beam therapy.

27.1 Overview

There is a variety of designs for control and safety systems (CSSs) depending on the accelerator type, the irradiation scheme, and the positioning method. Even if accelerator and beam delivery system design are the same, the CSSs may not necessarily be identical owing to differences in experience, level of understanding of the system, and interpretation of the system functionality. Therefore, this article describes only general considerations for upstream design of a CSS rather than a "recipe."

The CSS should be designed with respect to the processes of users and major components of the ion beam therapy (IBT) facility; in other words, the users should be determined, their behavior analyzed, features of various components characterized, and the functionality of the system extracted in order to define the specifications. Based on these conditions, the system configuration including the required software and hardware is defined and projected. A major difference in planning an entire IBT system is that the design should be based on a comprehensive risk analysis. The risk analysis for the system may be performed by a hazard base approach. Based on the identified hazards, the risk level is evaluated and the safety

H. Akiyama (✉)
Particle Therapy Systems Design Department, Hitachi Ltd. Power Systems Company, Saiwai-cho 3-1-1, Hitachi-shi, Ibaraki 317-8511, Japan
e-mail: hiroshi.akiyama.qj@hitachi.com

U. Linz (ed.), *Ion Beam Therapy*, Biological and Medical Physics, Biomedical Engineering, DOI 10.1007/978-3-642-21414-1_27,

measures such as redundant monitoring systems or alert to the users with a warning label are implemented. This article describes the requirements for the safety system and gives an overview on hazard-based safety design.

It also addresses the connection of the oncology information system (OIS), an important component of any modern radiation therapy unit.

27.2 Control System Design

27.2.1 Characteristics of an IBT System

An IBT system is first of all a radiation therapy unit that shares its basic operation procedures with conventional photon therapy facilities. The major difference between the two seems to be the scale. Whereas for photons the typical unit configuration is one treatment room per accelerator, in most IBT facilities one accelerator serves multiple treatment rooms. Hence, one first prerequisite is that the extracted beam is efficiently delivered to all treatment rooms.

A second difference is the test procedure. Because of its large size, it is hardly possible to test all parts and equipment of an IBT unit and the performance of the total system at the vendor's factory. Instead, the system tests are carried out at the client's site.

A third difference concerns the life cycle of the two systems. Most parts of an IBT facility including the building are constructed and optimized for the current layout. It might not be trivial to dispose of existing equipment and replace it with a new one. Therefore, long equipment lifetime and functional upgrade by modification are typical for an IBT facility. These unique characteristics have to be considered when designing a CSS for IBT.

27.2.2 User and Mode Definitions

The users who operate the irradiation unit are mainly radiologists, therapists, medical physicists, and vendor engineers. The therapists position a patient based on a treatment plan and perform the actual irradiation procedure. The radiologists judge the validity of the positioning and irradiation. The medical physicists monitor the system conditions and perform QA procedures to maintain safety and accuracy of the treatment. The vendor engineers, finally, perform system commissioning, machine parameter setting, and maintenance. If errors occur, they recover and repair the system within the specified scope.

Corresponding to these three levels of operations, there are three user modes – for treatment, physics, and service.

In the treatment mode, the interlock is usually fully activated and machine parameters can hardly be changed. For the QA mode, part of the interlocks are disabled and parameters can be changed. It is only in the service mode that basically

all parameters and interlocks can be changed. Access to the various levels is restricted by compulsory user and password control.

Most IBT systems have multiple treatment rooms. When one room is in treatment mode, sometimes the QA procedures have to be conducted in another room. It is, therefore, required to select the operation modes in each room individually.

27.2.3 Requirement Definition

All radiation therapy systems comprise the tasks patient set-up and treatment beam delivery.

Basic functions of any CSS for radiation therapy are, therefore, to select an irradiation direction, position a patient at the isocenter, focus on the target volume, and shape the dose distribution to provide the prescribed dose to the target volume. This could be described in a flow diagram as follows:

- Prescription download
- Preparation of the patient-specific items such as range compensator, aperture, immobilization device
- Patient check
- Initial positioning of the patient (laser, X-ray imaging)
- Gantry angle rotation
- Patient positioning in the treatment position
- Request for beam extraction
- Equipment setting, irradiation field, and shape
- Accelerator and beam line settings
- Start irradiation
- Interrupt irradiation (triggered by respiration or organ motion)
- Finish irradiation
- Save irradiation record
- Patient release

A careful process analysis is central to the design of the treatment control system. The actual implementation is then similar to software development, in general. Unified Modeling Language (UML) is often used for system software design. A description of UML in detail can be found in [1].

Operator and equipment behavior might also be described in an activity diagram. This is a flowchart which comprises the multiple components and devices and their activity profiles in parallel (Fig. 27.1). An activity diagram analysis does not only help in the implementation of the control system but also in hazard identification and the design of the safety system (see below).

27.2.4 Structure of the Control System

Within the three main sectors – treatment, physics, and service – further subdivisions are made to structure the various functions of a control system. Individual functions

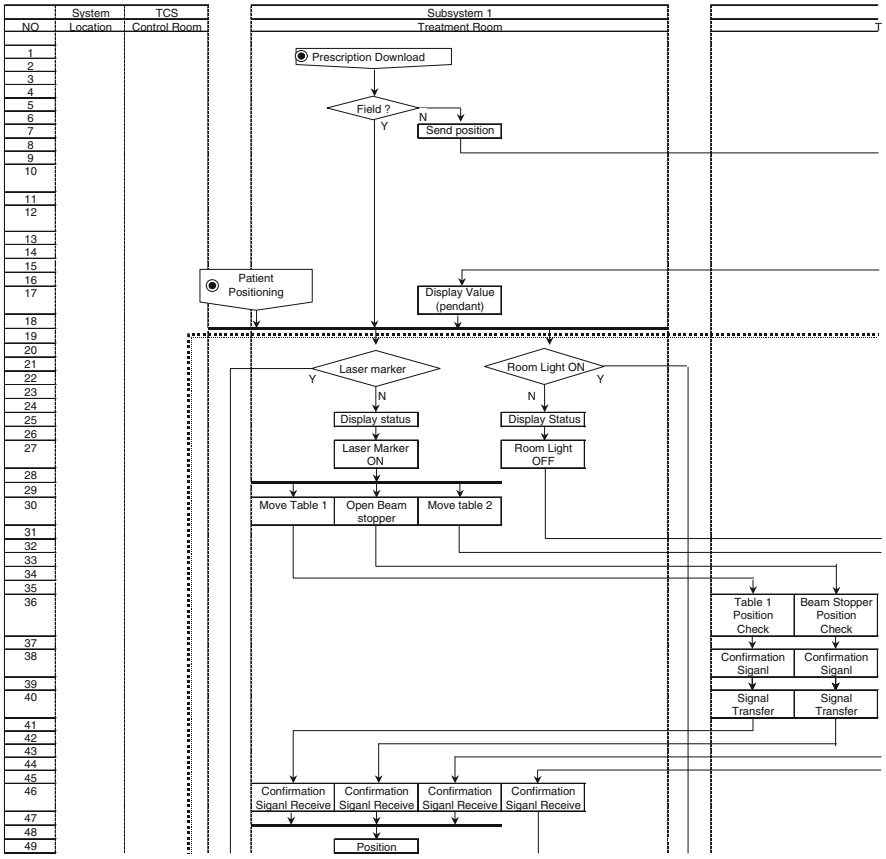

Fig. 27.1 Example of an activity diagram describing the workflow in a treatment room

are interlinked to subsystems. The accelerator components from ion source to beam transport, for example, are such subsystems. Similarly, the components of a treatment room (e.g., gantry, nozzle, couch) are controlled individually but also communicating with each other. A subsystem controller for a treatment room manages these components and communicates with the total control system (TCS). In addition, it controls the human–machine interface (HMI) for the components, accepting input from terminal and pendant controller. All the functions from beam production, beam delivery, and treatment room are merged in the next level of supervision, which is the TCS. It communicates with all the subsystems and with the external information system.

An example for the hierarchical structure of the control systems is shown in Fig. 27.2. It also illustrates that the safety system is linked to the TCS but runs as redundant system separately.

It should be noted that the system configuration presented here is very basic. A variety of individual configurations exists in the operating IBT centers.

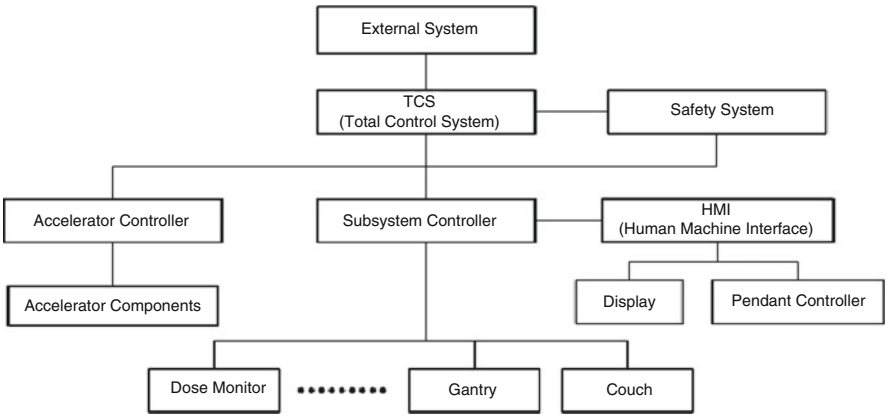

Fig. 27.2 Hierarchical structure of the CSS

The control functions are very diverse and require specific tools that might range from preset interlocks to manual intervention.

The actual process of irradiation of the patient, e.g., is a preprogrammed process that requires very short response time for effective control in the range of microseconds. Therefore, when the start button has been pushed by the operator, the control system usually operates the irradiation process automatically until the specified dose is reached. This requires rapid and repeated measurement of the beam parameters to maintain and satisfy the clinical dose specifications. If the prescribed value is reached, the beam is turned off. Any excess dose should cause an alarm and beam stop. Independent of this automatic control, the operator can follow each monitor value displayed on the HMI, and also keeps an eye on the patient via TV camera to be prepared for eventual beam pause, interruption, or termination.

In the case of couch, gantry, and snout activity, the operator mainly uses the pendant controller for visually checking the conditions. The control cycles of these mechanical items are more typically in the millisecond range and tolerate interactive operation. However, operations that rely on human decisions, require measures against incorrect operation and reaction rates. A simple means to prevent incorrect or inadvertent operation is, for example, to hold down two switches together to initiate an action.

27.3 Design of the Safety System

27.3.1 Safety Philosophy

Safe and accurate delivery of the prescribed dose to the target volume is essential for achieving the desired benefit to the patient and preventing an overdose of irradiation. In addition to that, appropriate safety measures for conceivable failure

conditions should be provided in order to minimize the risk of harm to the patient. Finally, safety is not only a built-in feature but also a task for the whole staff. In their various roles and responsibilities, radiation oncologists, radiation therapists, medical physicists, and service personnel need to contribute to achieve safe and effective treatments.

27.3.2 Role of the Safety System

The built-in safety system provides measures to turn the IBT system into a safe state in case of a hazardous situation or prevent further operation in case of deviation from a prescribed condition.

Hazardous situations are not only those associated with irradiation, e.g., overdosing, underdosing, wrong dose distribution, or misaligned exposures but also mechanical hazards such as contact between moving parts and a patient during patient and/or equipment setting.

27.3.3 Function of the Safety System

In order to achieve the roles described above, the safety system is expected to have the following functions:

- To monitor critical parameters or status signals
- To detect hazardous situations
- To turn off the operation
- To drive the IBT system into safe state
- To display status or alert
- To disable or override interlocks
- To perform an emergency stop

Critical parameters or signals are monitored continuously or in fixed intervals depending on the purpose and method of monitoring (e.g., hardware with analog signal, software with digital signal).

They are compared to a lookup table to decide whether the parameter is within an acceptable limit of tolerance to the prescribed values. If not, the safety system should decide if the treatment procedure has to be interrupted, terminated, or whether the IBT system enters otherwise into a safe state.

The action initiated by the safety system depends on the stage of the treatment process (see Table 27.1).

Upon detecting a hazardous situation associated with a moving part, the movement should be stopped and the accumulated energy could be released by shutting off the power. In certain cases, it might be necessary to lock the brakes. If it is possible that the patient becomes trapped between certain components, means should be provided to permit safe release.

Table 27.1 Typical critical parameters or signals to be monitored and possible actions initiated by the safety system

System component	Type of failure	Possible action
Patient or equipment setting stage	Unintended movement of the moving parts Collision	Stop movement Shut-off power Lock brake Release patient
Irradiation ready stage	Wrong patient or equipment setting	Prevent beam delivery
Treatment delivery stage	Wrong dose (distribution), Malfunctioning of field-shaping devices	Terminate or interrupt beam delivery Save dose data Prevent restart until all faulty conditions are removed

An interlock should be installed to prohibit starting a treatment unless all necessary conditions are met. An active action that permits the IBT system to start irradiation should only be made by a human operator. In case a hazardous situation is discovered after beam delivery has already begun, there must be a function for automatic termination or interruption. In addition, the safety system must provide a way to terminate or interrupt the irradiation manually. In any case, the data of the already administered dose need to be retained for a certain period. Resuming the irradiation should not be possible until all faulty conditions are removed and the system is reset.

A HMI should display the status of the IBT system and alert any anomalous situation. A standardized set of error messages, eventually accompanied by an audible alarm, should communicate the situation to the operator via the operator's console. The level of importance or emergency can be identified by a color code. Ideally, the error messages include a direction as to what type of action should be taken for each message. All failure conditions and messages may be recorded as a log for later analysis.

When the IBT system is in physics or service mode, the interlock functions may be partially or fully disabled. In such cases, appropriate safety measures such as access control by ID and password are mandatory in order to prevent treatment delivery with disabled interlocks.

A means of protection should also be provided for cases of emergency that the safety system cannot discern (unintended movement, fire, explosion, panic etc.). For these situations, emergency stop buttons should be installed in appropriate positions within the facility and on the equipment.

27.3.4 Configuration of the Safety System

To safeguard the patient, the system design must adhere to the following principles [2]:

- For all devices, monitoring and control functions are performed independently.
- The hardware to terminate the irradiation is independent of the control system.
- The beam parameters position, size, intensity, etc., are continuously monitored independently of the accelerator control system.
- Functioning of the field-shaping devices is monitored by measuring online the dose distribution of the radiation field.
- At fixed intervals, detector readings are compared with standard values to verify correct function of the beam modulation and field-shaping devices.
- Absolute dose measurements are continuously monitored and displayed for operator surveillance.
- Any detected inconsistency or "out-of-tolerance" value initiates a termination or interruption of the irradiation.
- The response and action of the safety system is fast enough to avoid excessive dose in case of failure.

In addition to the listed principles, the design philosophy should strive for fail-safe, redundant, and fault-tolerant solutions.

Fail-safe design means that common failures will result in a safe state. Moreover, a safety confirmation system should be installed that allows operation only when safety is assured rather than a hazard detection system that stops operation when an error is detected. This eliminates the risk to operate the system in an uncertain state, which is not clearly determined as safe or hazardous. Critical safety functions such as dose monitoring or termination of the irradiation need to be hardwired or of equivalent reliability.

All critical components of the safety system should be redundant and/or employ different methods to prevent failure of the entire system from a single hardware or software error.

27.3.5 Risk Management and Safety Measures

Used as a medical device, the IBT system has to comply with the national or regional regulatory requirements and obtain approval, certification, or permission from the respective authorities. Safety is one of the most important issues for regulatory agencies. Product safety should be ensured based on recognized international standards such as the IEC60601–1 Series [3]. This standard requires risk management based on ISO14971 [4]. The aim is to ensure risk mitigation of potential hazards to patients, operators, and service personnel associated with the use of the medical device.

To do so, hazards and hazardous situations have to be identified related to defined categories including radiation, electricity, mechanics, electromagnetic compatibility, programming, and environment. Each risk is evaluated on the basis of severity and frequency, and appropriate safety measures are considered to mitigate the risk to an acceptable level. This level can be determined from a risk–benefit analysis.

Inherent safety by design, protective measures, and safety information are major priorities for risk mitigation, in general.

Examples for inherently safe design in an IBT facility would be the limitation of the beam intensity by the accelerator, or that a single failure of the bending magnet would prevent the beam from entering the treatment room.

The second level of measures includes interlocking devices, emergency stop, etc., while the third level includes warning labels, user manuals, or the like. All relevant safety measures described above are applied even for such complex systems as an IBT unit.

27.3.6 Typical Hazardous Situations and Safety Measures

There is a variety of designs and operating procedures for IBT systems requiring individual safety measures even for similar hazardous situations. This section will present some typical hazardous situations and possible safety measures considering the general principles discussed above.

27.3.6.1 Errors in the Transfer of Treatment Information

Wrong computer settings are a frequent source of error. Consistency checks, frequent verification, and validation measures are required not to proceed with wrong settings.

An interruption in the transfer of treatment plan or prescription data, for example, could be resolved by a read-back check (handshake) and/or by using a DICOM-compliant protocol [5].

Errors in the conversion of clinical parameters into machine parameters can be avoided by applying multiple methods for verification and validation.

Errors in conversion from physical dose (pulse counts) to MU (monitor units) can be avoided by double checking by the multiple medical staff.

27.3.6.2 Errors in Patient/Equipment Set-Up

The use of barcodes or IC (identification chip) tags together with appropriate readers can help prevent mix-up of patients, immobilization devices, table tops, compensators or patient collimators.

A much-feared hazard is collision of or trapping by moving parts such as the rotating gantry, the patient couch, or the moving parts of the irradiation nozzle or an imaging device. Although the specific safety measures will depend on the type and design of the equipment, a few general considerations for an effective safety measure can be made.

The speed of travel should be fully controllable at any time either on-site or remote.

The moving parts should only be operated under surveillance of an operator with a double-switched operating console. In case a collision course is noted, an optical or acoustical alarm could be given or the intended movement could be disabled. In addition, contact sensors located on the moving parts can be helpful. Finally, an emergency stop should be provided for unintended movement, etc.

27.3.6.3 Treatment Delivery

Irradiation with incorrect or conflicting parameter settings could cause a serious hazard.

Many parameters are necessary to prepare for the actual treatment. This includes (depending on the specific system) selection of ion type, beam line, irradiation nozzle, beam energy, beam spreading device, beam limiting device, range modulation device, snout, patient collimator and compensator, setting of range shifter, confirmation of staff's exit and closing the door to the treatment room, setting of the target dose (MU value), and the limit on the control timer. An interlock that prohibits treatment delivery until all these necessary conditions are met is an essential safety measure. In addition, verification by a qualified person and positive action such as pushing a confirmation button would be a meaningful redundant safety measure.

If abnormal dose or dose distribution occurs during the treatment, immediate termination, or interruption of the beam delivery upon detection of the abnormal condition are necessary measures.

Redundant and differing beam stop mechanisms should be employed in order to ensure a safe beam stop. Appropriate mechanisms include stop of beam extraction at the accelerator, shutting off the current of the bending magnet or insertion of a mechanical beam stop. All these mechanisms should consist of hardware independent of the control system.

Because they are of utmost importance for success and safety of the treatment, the monitoring systems for dose and dose distribution have to meet high standards.

While deviation in dose distribution will not necessarily cause overdosing since the irradiation can be interrupted or terminated immediately upon detection of the deviation, a failure to stop the irradiation, however, could result in overdosing because it would already have occurred when the failure is detected.

In other words, the dose monitoring system needs to exist in triplicate to prevent overdosing. When the preset value of the main dose monitor is reached, the irradiation needs to be terminated. If the main dose monitor fails to stop the irradiation, a subdose monitor or field timer will be redundant stops. Termination by the main dose monitor only, will be considered as normal operation, whereas termination by the subdose monitor or the control timer will be treated as abnormal condition.

Each critical parameter representing dose distribution should be monitored in real time or ensured by a quality assurance (QA) process before irradiation with direct or indirect methods. Since errors in the dose distribution will not necessarily result in overdosing, duplicate monitoring systems should be sufficient. For example, failure

Table 27.2 Measuring devices and QA methods for various beam parameters

Critical parameter	Measuring device or QA method
Dose	Redundant dose monitors Control timer
Dose rate (beam flux)	Dose monitors
Field size	Dose monitors Field shaping devices (setting and/or functioning)
Range	Operation parameters of the accelerator Range shifter (setting and/or functioning)
SOBP	Range modulator (setting and/or functioning)
Beam spot position	Wire radiation detector Current of the scanning magnet
Beam spot size	Wire radiation detector Beam profile monitor

of a wire radiation detector will result in an unbalance of the dose distribution and should result in abnormal termination or interruption without overdosing.

The methods to monitor dose and dose distribution are largely dictated by the safety considerations for each type of IBT system such as passive beam spreading versus active beam scanning, synchrotron versus cyclotron, or mechanical range shifter versus energy stacking with different extracted beam energies. The typical direct or indirect means for monitoring the critical parameters are listed in Table 27.2.

When treatment delivery is interrupted, the beam extraction should be prohibited until the faulty condition is removed and the system reset.

27.3.7 Other Safety Considerations

In addition to the aforementioned safety measures, the following aspects should be considered as well for the design of an IBT system:

- Mechanical beam stop in case of wrong beam direction.
- Safety measures in case of leakage/stray radiation outside the radiation field.
- Communication tools between patient and medical staff, e.g., via interactive television (ITV).
- A back-up system for electric power failure or disaster such as earthquake by means of an uninterruptable power supply (UPS) or emergency power supply system.

27.4 Interface to Other Systems

In recent years, as in many other areas of business, electronic networking has also become relevant in health care. Likewise, it is normal that radiation therapy is embedded into the entire oncology workflow within a hospital or treatment center.

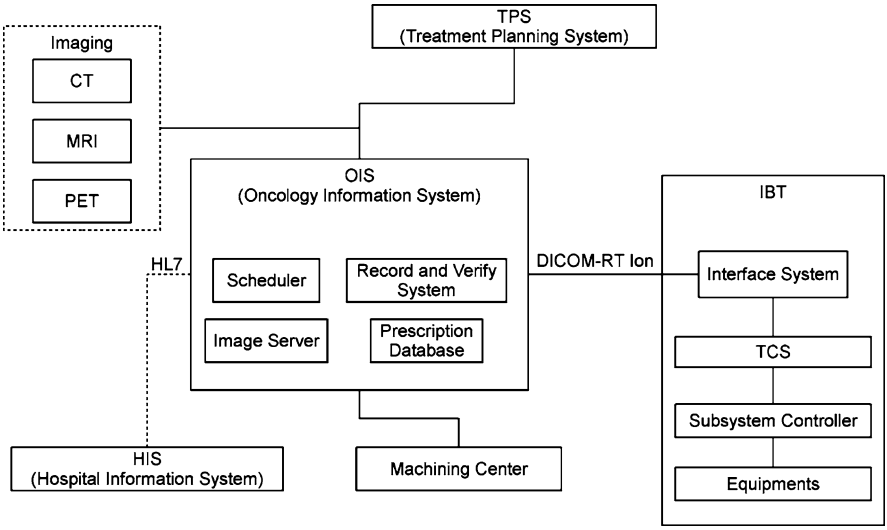

Fig. 27.3 Basic structure of an oncology information system with IBT integration. *DICOM*: Digital Imaging and Communications in Medicine is a standard for handling and exchange of electronic images. *HL7*:Health Level 7 is a standard for electronic healthcare applications. *TCS*: Total control system

Figure 27.3 shows an example of the configuration of such a network as part of the facility management.

At the central core is an OIS, which manages the treatment process in the facility. The OIS is connected to the IBT system, to treatment planning, imaging, the machining center, but also to other departments via the hospital information system.

The OIS includes the function of prescription database for the treatment plans, scheduler, verification system, and image archiving system.

The scheduler manages the treatment flow with date, time, and room selection. Recording and verification concerns primarily the irradiation data such as monitor units, couch position, or gantry angle and checks of the clinical parameters before an irradiation. The OIS transfers the planning and imaging data to the TCS on demand of the operator. The IBT system returns the clinical parameters to the OIS after all machine parameters have been set. They are then verified by the OIS and saved as irradiation record.

27.5 Product Life Cycle

Most IBT facilities consist of large-scale equipment in a dedicated building. This increases the cost as compared to conventional radiation therapy. The higher

construction cost is partly compensated for by a longer lifetime of the hardware. However, this does not apply to the lifetime of the hardware and software of the CSS. Periodic updates are required, e.g., to adapt more sophisticated positioning or irradiation techniques. This requires care and attention and cannot always be performed during operation. A major modification, such as replacing a scattering with a scanning system, for example, will require a system shutdown with significant impact on the operating ability of the facility. Other than for most conventional medical equipment, reliability and approval tests often have to be performed at the user's site.

As commercial IBT systems are still relatively new, there are still many open questions that need further discussions between users and vendors.

27.6 Conclusions

There is no single solution for the design of a CSS for IBT. Different approaches yield different solutions that influence and depend on the operation of the facility, the number of staff, the country-specific regulations, and so on. A CSS should be designed considering these conditions and it should be born in mind that risk analysis is one of the most important processes in the design of any CSS.

Acknowledgements The authors wish to thank Dr. Alfred R. Smith for many discussions about CSSs during the design and construction of the new proton therapy facility at MD Anderson Cancer Center. The authors are also grateful to Dr. Jay Flanz for helpful suggestions concerning the safety system.

References

1. T. Pilone, N. Pitman, UML 2.0 in a Nutshell. O'Reilly Media; 2nd edition, June 1, (2005)
2. W.T. Chu, B.A. Ludewigt, T.R. Renner, Instrumentation for treatment of cancer using proton and light-ion beams. Rev. Sci. Instum. **64**, 2055–2122 (1993)
3. IEC60601–1, Medical electrical equipment – Part1: *General Requirements for Basic Safety and Essential Performance* (International Electrotechnical Commission, Geneva, 2005)
4. ISO14971, *Medical Devices – Application of Risk Management to Medical Devices* (International Organization for Standardization, Geneva, 2007)
5. National Electrical Manufacturers Association. *Digital Imaging and Communications in Medicine* (DICOM), Parts 3.1–3.18 (NEMA, Rosslyn, VA, 2009)

Chapter 28
Considerations for an Effective Quality Assurance Program for Proton Therapy

Michael Gillin, X. Ronald Zhu, and Narayan Sahoo

Abstract Treatment with protons requires a high level of quality control over the entire process from the initial simulation to the final treatment fraction. This chapter provides an overview of recommendations and actual processes for a comprehensive proton therapy (PT) quality assurance program. There are a large number of parameters and a limited amount of time, so programs must be wise in the development and analysis of a PT quality program.

28.1 Introduction

High energy protons stop, whether in a water phantom or a patient. Unless there is careful attention to a large number of details of imaging, planning, information transfer, and treatment delivery, it is easy to deliver poor quality PT. Over the last several decades, the concept of quality in radiation oncology has been maturing. It has evolved from an equipment-focused quality assurance (QA) program, performed by the physicists during the dark of the night, to a comprehensive Quality Management program, which brings all elements of the process of radiation therapy (RT) into the light of the day for review. A comprehensive and recent overview of this topic can be found in the chapter entitled "Quality Management in Radiotherapy" by Guenther Hartmann, in *New Technologies in Radiation Oncology* [1]. The focus of this chapter is on QA for the technical and physics aspects of PT equipment, dosimetry, and treatment planning. In his book entitled *Radiation Oncology: A Physicist's Eye View*, Michael Goitein provides a succinct answer to the question of assuring safety and quality in RT, namely "Quality is assured through meticulous attention to myriads of small details" [2].

M. Gillin (✉)
Department of Radiation Physics, University of Texas, M.D. Anderson Cancer Center, Houston, TX, USA
e-mail: mgillin@mdanderson.org

U. Linz (ed.), *Ion Beam Therapy*, Biological and Medical Physics, Biomedical Engineering, DOI 10.1007/978-3-642-21414-1_28,

Education and quality are linked. To provide the patient with high-quality treatment, it is important that all radiation oncology practitioners (therapists, dosimetrists, physicists, and oncologists) understand not only their job but also how all of the elements in the RT process interrelate. A broad continuing education program covering the entire process and which, in addition, can focus on highly specific details, helps insure quality.

The various individual components in the PT process are subject to preventive and corrective maintenance and system upgrades. Every change in any component has the potential of affecting the range of protons in the patient. There must be a strong interface with the service and maintenance organizations for every component of the delivery system. No changes should be made without prior review and an estimate of the impact of such changes on the existing system.

Time is the ultimate constraint, especially in the world of PT. It is not unusual for a busy PT center to treat for 17–18 h per day beginning in the early morning and finishing around midnight. During nontreatment weekday hours and on the weekends, both new patient and machine-specific QA activities must be performed, as well as program development, corrective maintenance, and preventive maintenance. The QA program must be focused and efficient to accomplish all of the desired tests within the limited time available.

28.2 Quality Assurance on CT Simulators for Protons

CT based simulation has been an integral part of radiation oncology treatment planning for approximately three decades. In 2003, the American Association of Physicists in Medicine (AAPM) Radiation Therapy Task Group No. 66 published their report, Quality assurance for computed-tomography simulators, and the computed-tomography-simulation process [3]. Daily, monthly, and annual test intervals are described for the various tests.

One parameter in this report to be tested is the CT number accuracy with the recommendation of daily testing of water with tolerance limits of ± 5 HU (Hounsfield units), monthly tests of 4–5 different materials, and annual tests of an electron density phantom. For photon dose calculations, HU are converted to electron density, while for proton dose calculations, HU are converted to stopping powers.

Report 78 of the International Commission on Radiation Units and Measurements (ICRU) describes two different methods to determine the relationship between Hounsfield number and the mass stopping power, namely a direct fit method and a stoichiometric method [4]. This report states that typically this conversion results in a 1–2% uncertainty (1 standard deviation) in calculating the effective range of near-monoenergetic protons within the patient.

From a QA perspective, the relationship between Hounsfield number and the mass stopping power must initially be established for each CT scanner used for proton patient simulation with the specific kilovoltage used for imaging and then

tested on a periodic basis [5]. For a modern, well-maintained CT scanner, it is our experience that the scanner produces consistent HUs over time, assuming a constant imaging technique.

28.3 Quality Assurance on PT Planning Systems

The IAEA (International Atomic Energy Agency) Technical Report Series 430, is a large comprehensive report intended to provide guidance for commissioning and QA of treatment planning systems (TPS) [6]. It states that education, verification, documentation, and communication are the four key words that "summarize the goals, objectives, and outcomes of a well structured QA program." Ten general recommendations are presented. Some of these recommendations highlight the significant responsibilities of the medical physicists who commission and manage the TPS. This report may understate the efforts required when new versions of PT software are implemented, as this can be a major project. The final recommendation calls for in-house training and periodic refresher training to ensure no errors or inconsistencies have emerged in the use of the TPS.

The IAEA published a subsequent report, which provides a protocol for specification and acceptance testing of TPS [7]. The quality assurance issues associated with TPS are also described in detail in the report of the AAPM Task Group No. 40 [8]. Section III of this report has two major sections, namely Program Documentation and Test Procedures. The test procedures include initial manufacturer's tests, initial user test procedures, tests after program modification, and ongoing tests. Table V of this report contains QA recommendations for TPS and monitor unit calculations for commissioning and future upgrades, on a daily, monthly, and annual basis.

Proton TPS are substantially less mature than photon planning systems. For example, in 4 years of treating with protons, we have upgraded our commercial TPS twice and have rejected possible new version upgrades four times, due to limitations discovered during our testing of the updated versions. We have a commissioning box configured as both client and server, upon which new software versions are installed for testing purposes. Approximately 9 person-months were used for testing the latest new version before it was released to the clinic. Separate physics teams worked on the scattered and the scanned portion of the system. The calculated beam and treatment field characteristics with the new versions of the TPS were compared with available baseline data. New measurements were made whenever necessary to validate the accuracy of the TPS dose calculation schemes. An end-to-end test of the patient treatment process using a phantom is highly desirable to ensure all aspects of data and image transfer are both functional and accurate. Both a commissioning report and user release notes were generated at the time of clinical release of a new version of treatment planning software.

28.4 Quality Assurance on the Electronic Medical Record for Protons

Digital Imaging and Communications in Medicine (DICOM) is a very important step forward in breaking down the barriers to communication between various individual digital systems, e.g., the proton TPS of vendor A to the proton electronic medical record (EMR) of vendor B to the proton delivery system of vendor C. DICOM Working Group 7 deals with radiotherapy and remains active in addressing specific issues. The Ion Therapy subgroup, WG 07, continues to address specific questions, such as clarification of ion control point sequence. Despite substantial progress, there is not one single standard agreed upon by all ion beam therapy vendors.

The EMR may be used by the entire practice, to include photons, electrons, protons, brachytherapy, and satellites. Frequent updates of EMR versions are needed in order to incorporate new technology, to address issues with the current version, and to meet new expectations of the users. The EMR vendor generally does not have a real or virtual proton delivery interface to test new versions of the EMR. Rather, it is the user who has the proton testing environment. Thus, substantial testing in the proton (and photon) environment is performed before any migration of the EMR. The tester can download actual treatments and deliver and record such treatments onto the test database to confirm that delivery and recording processes work.

There are proton-specific features of the EMR, which need to be tested. For example, one important scanned proton beam feature to be tested is the ability of the EMR to calculate the remaining spots when the delivery system crashes while delivering a scanned beam treatment field. In addition to proton treatment parameters, reference images may also be downloaded into a patient imaging analysis module. The reference images can then be compared with daily images, the patient position can then be adjusted, and final images uploaded back to the EMR.

The practice of radiation oncology at M.D. Anderson Cancer Center (MDACC) is a filmless, paperless practice, which has ten different physical locations. A new version of the EMR is introduced every 6–9 months. It is our practice to test on every beam line the new version of the EMR to insure that it supports routine patient treatments, has addressed specific issues which were identified in previous versions, and has implemented appropriately the promised new features. This testing requires at least 4 h per beam line after IT Services has set up the test environment. Generally, it is the physicist using the test database, who works in Treatment Mode (as opposed to Physics Mode) to download, image, treat, and upload the data. One beneficial, but unintended consequence is to remind the physicist of the challenges and frustrations encountered by the therapists in the daily treatment routine. By tradition on the weekend that the entire practice is migrated to a new version of the EMR, the migration starts with protons. The first step is the conversion of the patient data base, which requires multiple hours and begins after all treatments have been delivered on Friday night. Plans for new patients are uploaded on Saturday morning to the new version of the EMR and then downloaded to the proton delivery system.

A check is made to insure that all interlocks are cleared, up to actual treatment delivery, on all beamlines for new and existing patients. If the proton migration is not successful, then the migration will be aborted and the older version of the EMR will be used.

28.5 Quality Assurance on the PT Delivery System

Treatment delivery QA can be divided into two different categories, namely machine and patient QA. Both test the machine in some fashion. Recommendations for machine QA have been published in ICRU Report 78 [4] and by Maughan and Farr (M&F) [9]. Both sets of recommendations address scattered and scanned beams.

The ICRU recommendations are divided into daily, weekly, and annual checks, whereas M&F include monthly checks as well. In addition, they divide the tests into the following major categories: dosimetry and beam delivery, mechanical, and safety. Moyers in 1999 has also provided a comprehensive list of quality assurance procedures, which reflects actual tests for a hospital-based PT system and contains daily, weekly, monthly, and annual recommendations [10].

Finally, Appendix A of ICRU Report 59 contains a check list from Loma Linda University Medical Center (LLUMC) for new treatment ports, daily, weekly, biannual, and yearly QA checks [11].

28.6 Daily Machine QA Tests

The recommended daily tests are quite ambitious and would require significant time to perform. Both the ICRU and M&F recommendations for dosimetry and beam delivery include:

1. Proton beam output check to confirm that the proton nozzle dosimetry system is functioning, as expected, including the back-up monitor.
2. Measurement of the Bragg peak width and lateral profile, including flatness and symmetry.
3. For a scattered beam, correct operation of the scatters, including range shifters.

The recommendations include at least one two-dimensional (2D) measurement of the profile and another measurement of the Bragg Peak width and range. Neither recommendation is explicit on the number of different energies, widths of the spread-out Bragg peak (SOBP), ranges, and profiles to be measured. Moyer's recommendations are consistent with the above and also include a review of the maintenance and safety logbook.

The mechanical tests include alignments of snouts, apertures, and compensators. Visual inspection is mentioned. The alignment of lasers is recommended, but this assumes that lasers are used in patient alignments. One modern update of laser

Table 28.1 Daily QA program at the Proton Therapy Center of MDACC, Houston (PTC-H) with estimation of time spent per task

Log into proton console, spreadsheets, and EMR	1 min
Phantom, ion chamber, electrometer set-up	2 min
Four different single-point output measurements at four different depths in the phantom	4 min
Safety including door interlock	1 min
Breakdown dosimetry and set-up imaging	2 min
Change from physics mode to irradiation mode and test patient download from EMR	2 min
X-ray phantom, review images in patient alignment software, and upload images to EMR	5 min
Breakdown imaging phantoms	1 min

alignment is alignment of the patient positioning X-ray system with the mechanical isocenter and the proton beam. The recommended safety checks are the same as with photons (door interlocks, AV operational, radiation monitors functioning), except that M&F also recommend testing of functioning of the motion stops on all moving systems. This interesting recommendation may not be practical because it may require a nontrivial time to recover. Tests of communication with the EMR are not mentioned. In a filmless, paperless environment, this communication is an absolute essential if treatments are to be delivered using the EMR. Occasionally, changes in the network will occur overnight. Moyers suggests a 20-min time limit for daily tests and that these tests are performed by therapists. At PTC-H, the Proton Therapy Center of MDACC, Houston, it takes, generally, 30 min from the time the unit is released after overnight maintenance to the time the first two beamlines are treating patients.

Table 28.1 summarizes the various steps in the morning QA program and the approximate time required to complete them at our facility. One energy option per day is being tested for the scattered systems. Thus a total of five different energies per week are reviewed with measurements taken in the proximal, center, and distal portion of the SOBP and beyond the range for the energy being reviewed. (Fig. 28.1). Depending on the week, measurements are made at zero degrees, 90°, or 270°. The point measurements at these locations are performed using an ionization chamber in water and solid phantoms with known water equivalent thickness (Fig. 28.2). The baseline values of the expected readings were established during the commissioning for the specific dosimetry system used for daily QA measurement. Any change in the SOBP characteristics would also lead to a change in the dose output per monitor unit (MU) and SOBP width. Although no explicit measurement of the entire SOBP depth dose curve is performed, the four point measurement is considered to be adequate to ensure the consistency of the beam output or proper functioning of dose monitors, the range of the beam, and the generation of the programmed SOBP by the range modulator wheel (RMW). Field flatness and symmetry are not measured daily at MDACC, although they are monitored by the dosimetry system in the nozzle. Use of 2D ion chamber arrays for measuring flatness

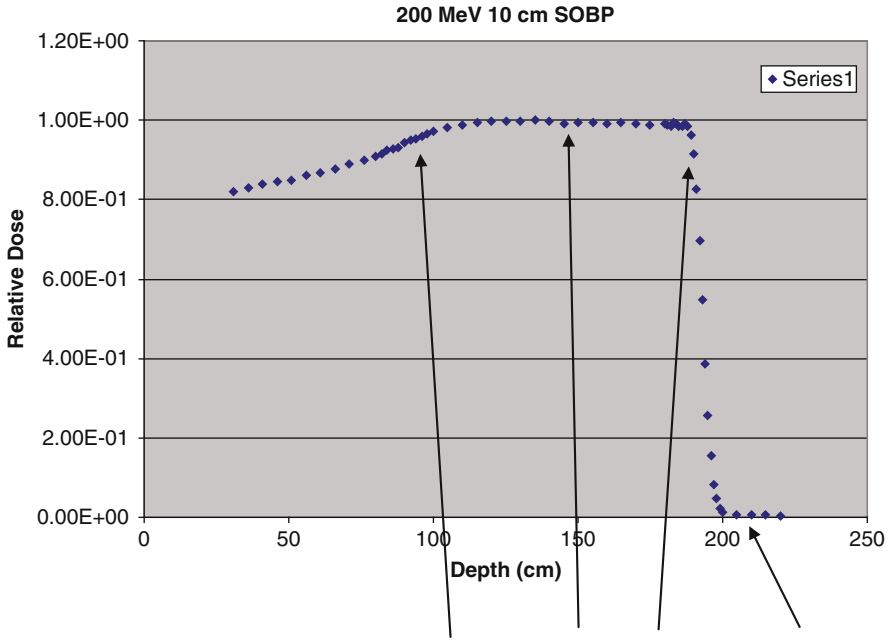

Fig. 28.1 Daily scattered-beam QA point measurements made at proximal, center, distal, and past the spread-out Bragg peak (SOBP)

Fig. 28.2 Morning SOBP measurement set-up. The alignment plate is indexed to the couch and is holding the water phantom (10 cm depth in one direction, 5 cm depth in the other), which contains a Farmer-type chamber. Plates of various thicknesses are placed in front of the phantom to adjust the depth of measurement

and symmetry together with point doses along the central axis at four different locations of the SOBP is currently being explored. Data are recorded on specially designed forms, which contain explicit instructions on the measurement being made. These forms are reviewed weekly by a qualified medical physicist. By the end of the

morning QA tests, all elements in the delivery system (treatment control, in room imaging, safety, and communication with the EMR in both directions) have been exercised and reviewed.

28.7 Weekly Machine QA Tests

M&F recommend a comparison of measured dose to the calculated dose at selected depths in a phantom, for a randomly selected patient. They also recommend to check weekly the respiratory gating equipment, the alignment of the imaging devices, and the gantry and collimator angle indicators.

Moyers recommends verification of the accuracy of the gantry angle readouts at the four cardinal angles, of the integrity and alignment of the scatterers, the monitor detector chain, patient calibration system, in addition to checking the proper functioning of the door interlock and backup dose monitor.

According to ICRU 78, the patient positioning and alignment systems, beam-line apparatus, and respiratory-gating equipment should be checked once a week. For scattered beams, the dose delivered to randomly selected patients (comparison of planned dose distributions to those measured in a water phantom) and for scanning beams, a qualitative three-dimensional check of the outline and range of the dose distribution for one patient's irradiation field in a water phantom should be performed weekly. The components of the beam-line apparatus are not defined, but could include various devices that can change as the range and field size changes, e.g., scattering foils, range shifters, and the RMWs.

One goal of weekly machine QA at PTC-H is to measure the output in standard conditions for every new combination of energy and scattering parameters used for patients who are starting their treatment. For example, the output will be measured for 140 MeV, large field scattering, in a standard configuration, if this combination is not in use by a patient under treatment but will be used for a new patient.

The accuracy of the patient imaging and alignment system is checked on a weekly basis by taking images of a 2 mm steel ball at the center of a cubic phantom placed at the isocenter of the gantry and then retaking the images after the couch is shifted by a known distance in all three directions. The amount of shift is then measured by software tools and compared with the applied shift. For scanned proton beams, a simple film test is performed weekly to confirm coincidence between the central axis of the X-ray field and the proton spot scanning system. Tolerance for any observed deviation is 1 mm.

28.8 Monthly Machine QA Tests

ICRU 78 does not make any recommendations for monthly QA tests. Moyers and M&F provide dosimetry, mechanical, and safety recommendations. The verification of the modulation system is recommended by both parties. One method to verify the

modulation system is to measure at least one SOBP width for each energy/scattering system that is being used that month to treat patients. Assuming 30 patients are under treatment per beamline and 10 min per measurement, the total time that this would require is more than 5 h. If there are four beamlines, then a substantial time would be required each month to verify the integrity of the modulation system. However, if there are tests inherent to the delivery system, then the frequency of the recommended QA can decrease. For example, the PTC-H system has, for the scattered beams, a "Beam Checking" function, in which prior to each field approximately 10 MUs are delivered to a mutlilayer Faraday cup that is moved to intercept the beam. The SOBP is measured by this technique. If there is agreement between the measured and specified SOBP, then treatment can continue. If the criteria for agreement are not met, then the measurement can be repeated by the therapist two additional times. If it continues to fail, then either the physics or service section must be notified. This can be viewed as a daily SOBP check for every scattered field.

PTC-H performs a number of monthly tests, which focus on verifying the parameters which are being used to treat patients during that month. The goal is to insure that some test is performed each month to confirm proper performance of key dosimetric parameters and to measure flatness and symmetry at various gantry angles. The monthly QA includes gantry, couch, and nozzle mechanical alignment tests, and verification of the X-ray and proton field coincidence. Dose per MU consistency checks and distal range checks for all passively scattered RMWs that are being used, are performed, as are beam flatness and symmetry tests at one gantry angle. In addition, output vs. gantry angle is measured. The range uniformity is also checked by comparing the beam profiles at distal 90% depth and 1 mm distal to this depth. Since a change of 1 mm of range can lead to a dose change of as much as 15%, up to 15% difference in the beam flatness and symmetry between these two profiles is a good indicator of the range uniformity. Alternatively, one can use a picket fence with 1 mm difference in thickness at different sections and measure the profile at the distal 90% depth. The dose uniformity of 15% in the flat region of this profile, which can either be measured with a film or ion chamber array, should indicate the range uniformity of a broad field.

28.9 Annual Machine QA Tests

Elaborate recommendations are made for annual tests, as is the case for photons. ICRU 78 states comprehensive tests of the therapy equipment. Separate dosimetric measurements for scanning beams are suggested, including calibration of the whole dosimetry system and performance in terms of dose linearity and dose-rate dependence. In addition to dosimetric tests, there are recommendations for mechanical and safety checks. Especially, the mechanical tests are challenging, given the size of the gantry and the number of moving elements, such as the snout [12].

The M&F report recommends an extensive recalibration of the output under a wide variety of operating conditions, as well as a number of standard annual

measurements. Moyers also provides a detailed list of recommended tests of the therapy equipment and associated systems.

Some of the common features in the various recommendations for the annual QA check of a passive scattering beam delivery system include:

1. The dose/MU calibration in water under the reference condition and relative output factors for all other options.
2. Monitor system linearity, reproducibility, and end effect.
3. Depth-dose curve measurement of selected SOBPs to check the consistency of the beam range, SOBP width, dose uniformity in the flat region of the SOBP and the entrance dose.
4. Beam flatness and symmetry consistency (can be a review of the past monthly measurements already performed for some of the RMWs and measurement for the others).
5. Verification of the validity of inverse square effect.
6. Coincidence of the gantry mechanical, proton, and X-ray field isocenters.
7. Coincidence of the couch mechanical isocenter with proton radiation field isocenter.
8. Imaging system performance QA.
9. Radiation and mechanical safety tests.
10. The stability of the CT Hounsfield number calibration for each CT unit that is used for proton simulation.

At PTC-H, one beam line per quarter receives an annual QA check. These tasks are generally performed on Saturdays, consuming more than 50 h per beam line. Annual measurements are compared to the initial commissioning measurements and to output from the TPS. The official date of the annual check is the day that the calibration of the main and subdose monitor is reaffirmed, using IAEA Technical Report Series 398, which simplifies interactions with regulators and the 365-day rule [13]. The final step at the end of the calibration process is to irradiate thermoluminescence dosimeters (TLDs) from the Radiological Physics Center (RPC) at MDACC, which provide an independent confirmation of the calibration. The RPC provides TLDs for both the scattered and the scanned beam lines. The order in which tests are performed depends, in part, on clinical needs, program development status, and personnel schedules. Formal annual reports are generated and signed and reviewed. An ideal schedule and and the estimated time spent per task is shown in Table 28.2. PTC-H has recently published a description of the initial commissioning of its discrete spot scanning beam [14] and an overview of its machine QA procedures [15].

28.10 Patient-specific QA

Patient-specific QA is an integral part of the overall QA program, but one focused on a limited number of parameters, which pertain to a specific patient. This process begins after the oncologist approves the plan and signs the prescription. The major

Table 28.2 Annual QA program at PTC-H with estimation of time spent per task

Mechanical tests of isocenter for gantry and couch	6 h
X-ray systems (three tubes and three flat panel detectors)	4 h
Alignment of photon field and X-ray beam for X-ray system in the nozzle at several gantry angles	2 h
TRS 398 calibration and establishing daily factors for the field chamber at various gantry angles	8 h
Measurement of SOBPs for scattered beams (depending on the beam line there are 6–24 combinations plus range shifters)	6–24 h
Lateral profiles and symmetry at various gantry angles	8 h
Safety systems	4 h
CT unit Hounsfield calibration	1 h per CT unit
Report generation	8 h
Report review	2 h

elements of this process include a technical review of the plan, calculation of a verification plan in a water phantom based on the parameters from the patient's plan, determination or verification of the MUs to deliver the prescribed dose from each field, aperture and compensator tests after their construction, and review and approval of data in the EMR. The physicist must approve both the calibration and the plan in the EMR prior to the first treatment.

At PTC-H, this patient-specific QA process is performed by the physicists and physics assistants. The approved plan is reviewed with the goal of determining that the plan can be delivered in a safe and accurate manner. Typical questions to be answered include if the dose prescription were defined for a "reasonable" volume, a collision between the snout and the couch could occur, gaps between spinal fields were reasonable, etc. The physicist then performs a verification plan calculation, using essentially the same approach as is used for IMRT. A point in the verification plan must be identified that is a good representative of the prescription dose volume. This process requires, on the average, less than 1 h for a simple two-field prostate plan and at least 6 h for a patient with several fields and junction changes, e.g., cranial and spinal fields.

Following a long-established precedent in the photon world, PTC-H uses two independent methods to determine the MUs. The vast majority of patients being treated with scattered beams have measurements made in a water phantom, as one method to determine MUs. At least one point of measurement in a region of stable dose is identified and a measurement is made, generally, at a gantry angle of 270°. This measurement, which is made before the patient is treated by a physics assistant, confirms that the respective combination of energy and scattering condition can run without difficulty. Generally, this measurement, which requires less than 15 min to perform, is done during the week, after all patient treatments have been delivered. The second method of determining the MUs is based on independent measurements of each of the dosimetric parameters that change the MUs, e.g., relative output factor for energy or SOBP. This system has been described in a paper by Sahoo et al. [16]. The TPS can be configured to provide the MU for patient treatment fields, as done at

LLUMC or as available in commercial programmes (e.g., Eclipse™). Alternatively, an MU calculation formalism like that used at Massachusetts General Hospital (MGH) can be adopted. It may also be possible to develop MU calculation models based on prior patient treatment fields. For example, we are no longer performing measurements for the most common conditions, e.g., prostate, small-field, 9 cm SOBP, 225 MeV. For this condition, previous measurements have been reviewed and the MUs vs. range have been plotted. The result is a straight line, which can be used to determine the MUs for a new patient based on measurements made for previously treated patients. For approximately 90% of the small-field 9 cm SOBP, 225 MeV patients, this approach is used to determine the MUs. The second check, using the individually measured dosimetry parameters is used for the remaining 10% of patients.

The patient-specific QA for scanned beam patients is substantial and more elaborate. It begins with the calculation of a verification plan in a water phantom. Multiple depth dose points are measured for each patient, in order to confirm the SOBP width. In addition, the dose is measured in several planes perpendicular to the central axis, so that the measured dose pattern can be compared with the calculated dose pattern. The TPS has been configured to provide the MUs. The accuracy of the TPS-calculated MUs are confirmed by dose measurements in a "fish bowl" type phantom using an ion chamber. These measurements are performed at the gantry angle for which the fields will be delivered. Some of these measurements are made at night, while others are performed on Saturdays. The time required to perform patient QA for a simple scanned beam plan is approximately 1 h. Complex plans take substantially more time for measurements.

Adequate staffing is essential for the success of QA tasks. For example, machine and patient QA activities at PTC-H are managed by four full-time equivalent (FTE) physics assistants and more than six medical physicists. The pace of the QA machine and patient program is steady until there is a new version of software or a major repair of the delivery system or some other unique event, which requires highly focused efforts. Saturday is a very important day for the QA program, as well as for program development activities.

28.11 Summary

Proton QA programs provide assurance that complicated imaging, planning, and delivery systems are functioning as expected. A recent QA Symposium provided four general recommendations [17]: to update conventional QA programs, using risk-assessment methods; to better balance clinical processes vs. device operations; to improve modern RT quality management and QA needs, and to support research directed toward QA problems in image-guided therapies. These recommendations are pertinent for PT, especially considering the fact that there are currently and soon will be many first-generation proton planning and proton delivery systems.

Risk assessment of discrete spot scanning, concerning both planning and delivery, should be an essential part of the QA program. The balancing of clinical processes and device operations is important in making the proton environment of multiple vendors function in a safe and efficient manner. Modern quality management should involve the oncologists, who need to have a basic understanding of issues associated with information flow and treatment delivery. Especially with PT, the exquisite dose distributions produced by the TPS may not be what is delivered to the patient. Research, which addresses QA challenges, should be supported both by funding and also by acknowledging the importance of such contributions within the academic environment.

Quality assurance of the therapeutic use of protons can become an all-consuming activity with patient QA, machine QA, upgrades to the TPS and the EMR, and preventive and corrective maintenance of the delivery system. In addition to its primary function, a QA program can collect more dosimetric data and can help

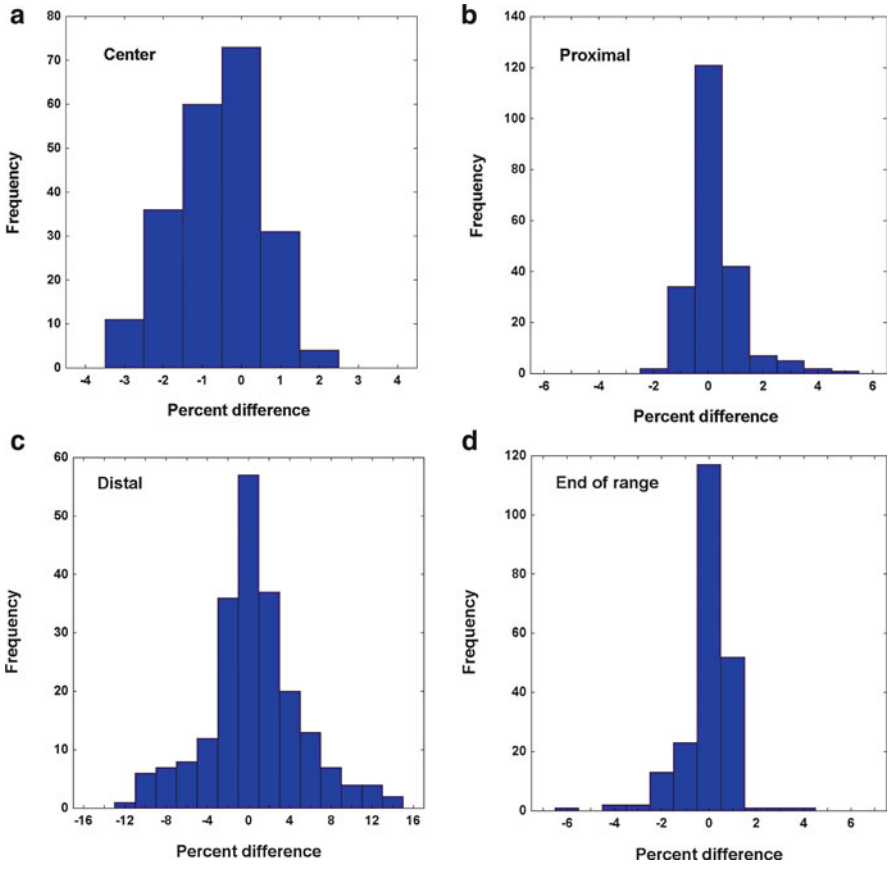

Fig. 28.3 Summary of all 2009 daily output data for Gantry 1. Measurements at the proximal and center points generally fall within $a \pm 2\%$ window. The measurements at the distal point are much broader, showing the challenges of point measurements in a rapidly changing dose gradient

to train less-experienced physicists. One potential pitfall is failing to devote time to a high-level review of the QA activities with the goal of identifying priorities (Fig. 28.3). It is not possible to confirm that every component of the delivery system is functioning as expected. Issues with the planning system are discovered on a regular basis and placed on the list of TPS issues. The exciting focus in PT tends to be on program development and clinical results, especially by the oncologists. However, given the resources consumed by PT quality programs, it is important that there be a formal periodic report devoted to quality, which is reviewed by the practice leadership. In his very short chapter on QA, Michael Goitein notes that "Quality assurance is the *sine qua non* of any practice, but especially one in which people's lives and health are at stake" [18].

References

1. G.H. Hartmann, Quality Management in Radiotherapy, in *New Technologies in Radiation Oncology*, ed. by W. Schlegel, T. Bortfeld, A.-L. Grosu. (Springer, Berlin, 2004), pp. 425–447
2. M. Goitein, *Radiation Oncology: A Physicist's-Eye View* (Springer, Berlin, 2007), p. 288
3. S. Mutic, J.R. Palta, E.K. Butler, et al., Quality assurance for computed-tomography simulators and the computed-tomography-simulation process: Report of the AAPM Radiation Therapy Committee Task Group No. 68. Med. Phys. **30**, 2762–2792 (2003)
4. ICRU Report 78, *Prescribing, Recording, and Reporting Proton-Beam Therapy* (Oxford University Press, Oxford, 2007)
5. U. Schneider, E. Pedroni, A. Lomax, The calibration of CT Hounsfield units for radiotherapy treatment planning. Phys. Med. Biol. **41**, 111–124 (1996)
6. J. Van Dyk, J.C. Rosenwald, B. Fraass, et al., *Commissioning and Quality Assurance of Computerized Planning Systems for Radiation Treatment of Cancer*, IAEA TRS-430 (IAEA, Vienna, 2004)
7. G. Ibbott, R. Schmidt, J. Van Dyk, et al., *Protocol for Specification and Acceptance Testing of Radiation Treatment Planning Systems*, IAEA TECDOC Series No. 1540 (IAEA, Vienna, 2007)
8. G. Kutcher, L. Coia, M. Gillin, et al., Comprehensive QA for Radiation Oncology: Report of AAPM Task Group 40. Med. Phys. **21**, 581–618 (1994)
9. R.L. Maughan, J.B. Farr, Quality Assurance for Proton Therapy, in *Proton and Charged Particle Radiotherapy*, ed. by T.F. DeLaney, H.M. Kooy. (Lippincott Williams and Wilkins, Philadelphia, 2008)
10. M.F. Moyers, Proton Therapy, in *The Modern Technology of Radiation Oncology. A Compendium for Medical Physicists and Radiation Oncologists*, ed. by J. Van Dyk. (Medical Physics, Madison, WI, 1999)
11. ICRU Report 59 Clinical Proton Dosimetry Part I: *Beam Production, Beam Delivery and Measurement of Absorbed Dose* (ICRU, Bethesda, MD, 1998)
12. X. Ding, M. Bues, M. Zhu, et al., Measurement of the mechanical isocenter of a proton gantry. Med. Phys. **34**, 2468 (2007)
13. B. Andreo, D.T. Burns, K. Hohlfeld, et al., IAEA TRS-398 *Absorbed Dose Determination in External Beam Radiotherapy: An International Code of Practice for Dosimetry Based on Standards of Absorbed Dose to Water* (IAEA, Vienna, 2000)
14. M. Gillin, N. Sahoo, M. Bues, et al., Commissioning of discrete spot scanning proton delivery system at the University of Texas M.D. Anderson Cancer Center, Proton Therapy Center, Houston, Med. Phys. **37**, 154–163 (2010)

15. B. Arjomandy, N. Sahoo, X.R. Zhu, et al., An overview of the comprehensive proton machine quality assurance procedures implemented at the University of Texas M.D. Anderson Cancer Center Proton Therapy Center-Houston. Med. Phys. **36**, 2269–2282 (2009)
16. N. Sahoo, X.R. Zhu, B. Arjomandy, et al., A procedure for calculation of monitor units for passively scattered proton radiotherapy beams. Med. Phys. **35**, 5088–5097 (2008)
17. J.F. Williamson, P. Dunscombe, M. Sharpe, et al., Quality assurance needs for modern image-based radiotherapy: Recommendations from 2007 interorganizational symposium on "quality assurance of radiation therapy: challenges of advanced technology". Int. J. Radiat. Oncol. Biol. Phys. **71**(Suppl), S2–S12 (2008)
18. M. Goitein, *Radiation Oncology: A Physicist's-Eye View* (Springer, Berlin, 2007), p. 287

Part VII
Patient Positioning and Treatment Planning

Chapter 29
Imaging and Tumor Localization for Ion Beam Therapy

Oliver Jäkel

Abstract Ion beam therapy (IBT) requires an increased degree of precision in patient positioning, treatment planning, and monitoring in order to exploit the full potential of this treatment modality. This chapter discusses aspects of imaging for treatment planning and treatment set-up that are specific for this form of high precision radiotherapy. Special considerations about functional imaging, which are connected to the radiobiological properties of heavier ions, are also highlighted.

29.1 Introduction

In the following, imaging issues relevant for the treatment planning and set-up process of IBT are discussed, whereas prior diagnostic imaging needed to classify the disease is not regarded here. Also, the various possibilities of patient immobilization are not addressed since they are, in general, not different from any other form of high precision radiotherapy.

Throughout the treatment planning and set-up procedures, imaging information is required for various purposes. They are outlined in more detail. A more extensive description of the various imaging modalities is beyond the scope of this chapter but can be found in the literature [1].

O. Jäkel (✉)
Klinik für Radioonkologie und Strahlentherapie, Universitätsklinikum Heidelberg, Heidelberg, Germany

Heidelberger Ionenstrahl-Therapiezentrum, Im Neuenheimer Feld 450, 69120 Heidelberg, Germany,
e-mail: oliver.jaekel@med.uni-heidelberg.de

U. Linz (ed.), *Ion Beam Therapy*, Biological and Medical Physics, Biomedical Engineering, DOI 10.1007/978-3-642-21414-1_29,

29.2 Segmentation

The definition of target volumes and organs at risk (OARs) is the basis for treatment planning and also the starting point for dose optimization, during which a compromise between target coverage and sparing of organs at risk has to be found. The beam directions are selected on the basis of a three-dimensional (3D) model of the patient anatomy. In IBT, in addition, tissue parameters important for the radiobiological modeling may be assigned to different volumes of interest.

Three-dimensional treatment planning is still mainly based on radiological imaging techniques, namely X-ray computed tomography (CT) and magnetic resonance imaging (MRI). Both imaging techniques allow visualization of anatomical structures with high spatial accuracy. Tumor tissue becomes visible mainly due to its different density or due to contrast enhancement. Due to the low soft-tissue contrast in CT imaging, MR images are routinely used in many cases to support the delineation of normal structures but also to identify tumor tissue by using dedicated imaging sequences (see [2] for details).

The delineation of normal structures and OARs is usually a straightforward procedure as anatomical variations between patients are relatively small (except for situations, where the tumor and OARs are overlapping or when organs are deformed by an expanding tumor). The definition of the target volume is much more complex, due to the large variability and the different growth patterns.

In IBT, the general nomenclature introduced by ICRU is used accordingly (see [3] for the latest version of this nomenclature). The gross target volume (GTV) is the macroscopic extent of the tumor as visualized, e.g., in the planning images. It may include not only the primary tumor but also macroscopically involved lymph nodes, macroscopic residual tumor after partial resection, or regions of tumor recurrence. The GTV, by definition, is independent of the treatment modality and should be defined, accordingly. On the other hand, the extent of the GTV may have an important impact on the choice of treatment. The GTV together with surrounding microscopic spread of tumor cells defines the clinical target volume (CTV), which is much more difficult to define, as these microscopic extensions are not visible in radiographic imaging. Furthermore, the extent of the CTV depends on anatomical and tumor-specific growth patterns. A lot of clinical experience is required for an adequate definition of the CTV and, consequently, a large uncertainty is involved in its definition (variations in volume of up to a factor of 2 have been observed [4]). Like the GTV, the CTV is, as well, a clinical concept independent of the treatment modality.

In many cases, a higher dose is prescribed to the GTV as compared to the CTV, which is justified by the lower number of tumor cells in the part of the CTV outside the GTV. In many cases, it is beneficial to deliver the additional dose to the GTV using IBT, either because of the higher dose-sparing potential of ion beams or because of a higher biological effectiveness of, e.g., carbon ions in the case of a higher radiation resistance of the tumor (see below for combined treatments).

Finally, the planning target volume (PTV) is defined. It includes a margin around the CTV to ensure the coverage of the CTV with respect to uncertainties in the beam

delivery and set-up of the patient. The PTV is, thus, depending on the individual technical installations used for patient set-up but also on the beam modality, i.e., the different physical properties of ion beams and also the details of the beam delivery system (see Chap. 25 for details).

Especially the limitations of radiographic imaging with respect to CTV definition have led to the introduction of functional imaging based on positron emission tomography (PET), single photon emission tomography (SPECT), or functional MRI (fMRI). Functional imaging allows visualization of microscopic disease outside the region of the highest tumor cell density visible in anatomical images. The possibilities to detect differences in molar masses can be picomolar (PET), nanomolar (SPECT), or micromolar (fMRI) as compared to millimolar in the case of CT.

The possibility to image dedicated processes such as oxygen perfusion or metabolic activity, allows also a differentiation between various parts of the tumor in terms of biological behavior. This is sometimes referred to as the concept of biological target volume (BTV).

Involvement of functional images in radiotherapy planning is, however, just at the very beginning and only few systematic attempts have been made to modify target volumes or dose distributions according to that kind of information [5]. The BTV concept will certainly be of great importance for IBT because of the potential to boost subvolumes of the GTV to higher doses using IBT and the potential of high-LET radiation to more efficiently kill radioresistant or hypoxic tumor cells.

Figure 29.1 gives an example of CT and MR images of a patient undergoing carbon ion radiotherapy (CIRT) for a chondrosarcoma of the base of the skull. The steep gradients in the resulting dose distribution underline the need for precise targeting techniques.

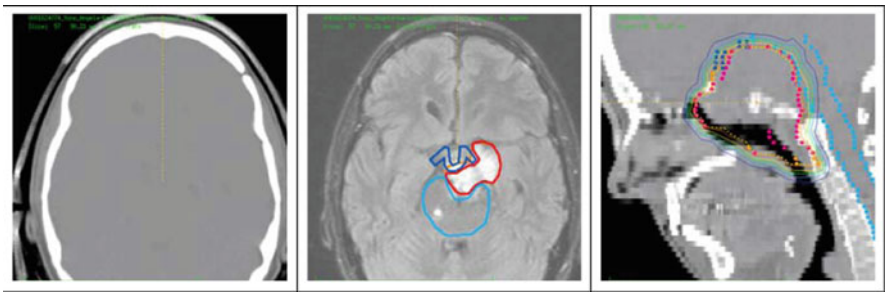

Fig. 29.1 Example of treatment planning images for the treatment of a patient with a skull base chordoma using carbon ion radiotherapy (CIRT). The *left image* shows the CT data used for dose calculation, the *image in the center* shows a T1-weighted MR image of the same anatomical location, which is colocalized with the CT data set and is used for the delineation of the tumor and organs at risk. The *deep* and *light blue contours* represent the optic chiasm and brain stem, respectively, the *red line* the target volume. The *image on the right* depicts the dose distribution on the CT image resulting from two opposing fields of carbon ions. The *red*, *yellow*, *green* and *blue lines* represent the 90%, 70%, 50% and 30% isodose, respectively

29.3 Dose Calculation

All dose calculation algorithms for ions are currently based on the quantitative electron density information provided by X-ray CT data of the patient. Due to the much higher sensitivity of the particle range (and thus also dose) to tissue inhomogeneities as compared to photons, accurate density information is crucial for IBT [6, 7]. MRI data are not suitable to provide quantitative information about the electron density.

The currently used relation between X-ray CT data and ion ranges – also called CT-to-range calibration – is to a large extent empirical and depends critically on the imaging protocol used at the CT scanner [8, 9]. As an example, real tissue phantoms are used for the determination of the CT-to-range relation, together with the resulting calibration curve are shown in Fig. 29.2.

The method has intrinsic uncertainties in the order of 3–5% depending on the region under investigation. Much larger errors are found in the presence of metal artifacts or, to a lesser extent, in tissue with very low or high density such as lung or bones [10]. To overcome these problems, various attempts are currently undertaken to introduce dual energy CT (DECT), which provides information about additional tissue parameters for the dose calculation. An alternative would be megavoltage CT available at tomotherapy treatment machines. It can significantly suppress metal artifacts.

The ultimate goal would be to use ion beams for tomographic imaging. Such images based on a sequence of radiographic projections would allow a reconstruction of the volumetric distribution of the ion stopping power, which is the information needed in the dose calculation. Currently no such system is available, but within several research projects the principle of ion beam radiography is being exploited.

29.3.1 Position Verification

To align the patient in the treatment position prior to treatment, a 3D model of the anatomy is required, which is compared to images acquired in treatment position. This procedure is called image-guided radiotherapy. It has been used in IBT for nearly 50 years [11]. Typically, X-ray images are acquired after the initial positioning procedure prior to each fraction and they are compared to digital radiographs, reconstructed from the planning CT data. By doing so, a correction of the initial position can be obtained and interfractional deviations can be corrected for.

An example of position verification images, together with the digitally reconstructed radiograph as reference is depicted in Fig. 29.3.

Images used for position verification may include external landmarks serving as reference frame like in stereotactic procedures, or they may be used to directly match the patient model to the verification images taken in treatment position, either by fiducial surface markers or anatomical landmarks (e.g., distinct bony structures).

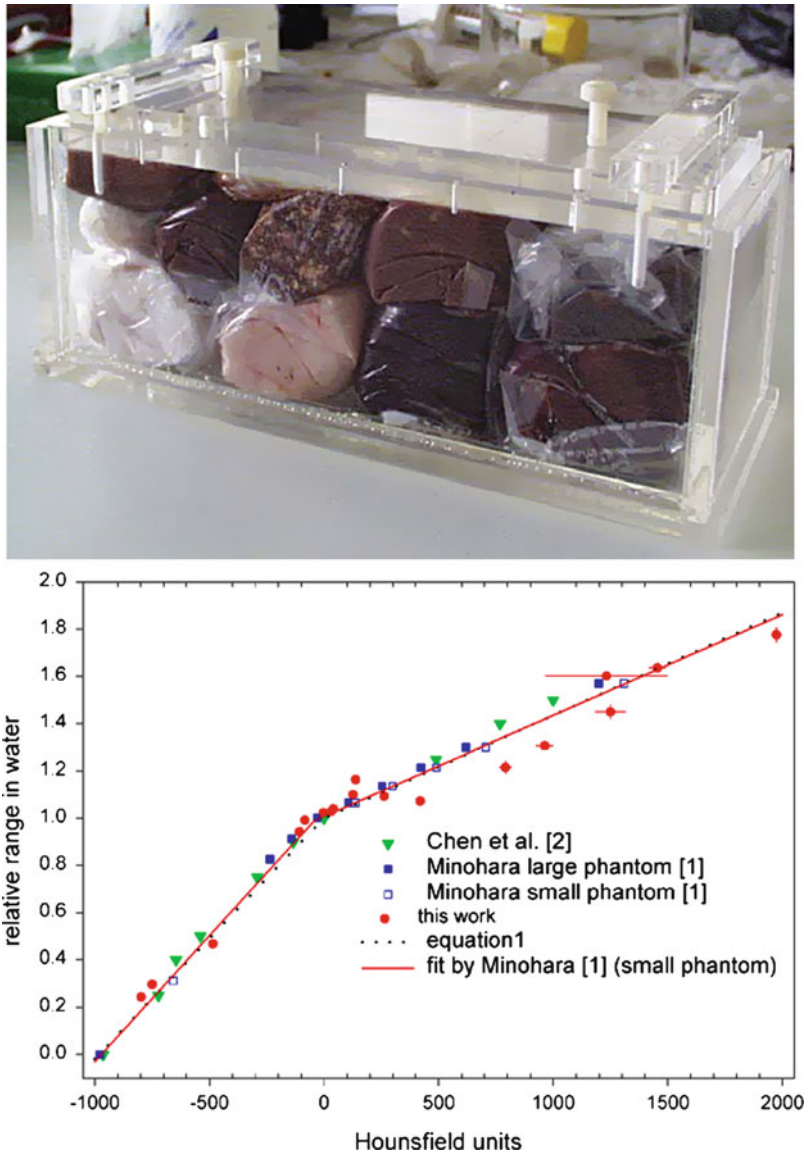

Fig. 29.2 *Top*: Typical phantom to validate the Hounsfield-to-range relation for ion beams as used, e.g., in [9]. It is composed of real animal tissue samples of different organs and put into a box of PMMA (polymethyl methacrylate), in order to have a well defined thickness for the range measurement. *Bottom*: Relation of the X-ray CT numbers to relative ranges of ions in water as derived from [8]. Several measured data sets are plotted together with a step-wise linear interpolation

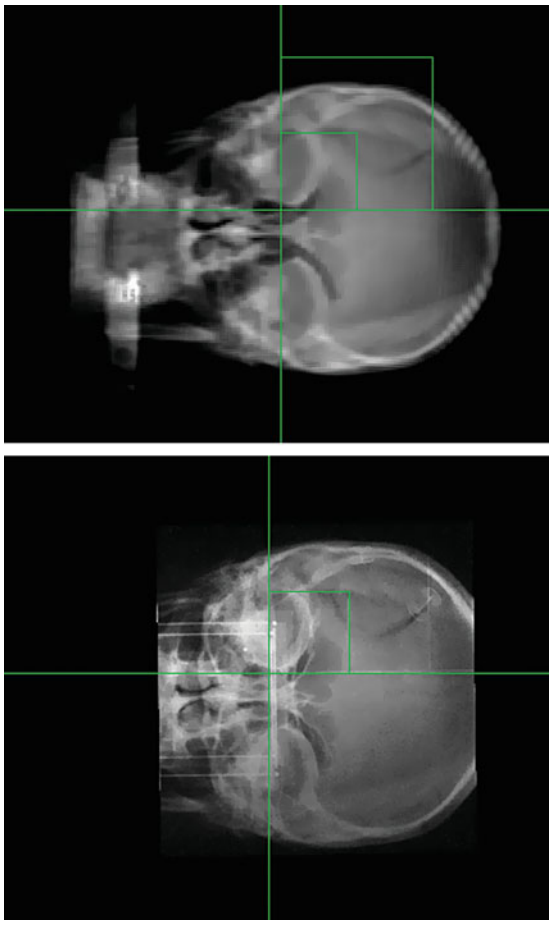

Fig. 29.3 Set-up verification of a patient being prepared for IBT. The *upper image* shows the digitally reconstructed radiograph, which is derived from the planning CT. The *green crosshairs* denote the position of the isocenter. The *lower image* shows the actual X-ray radiograph taken in treatment position. Deviations of the bony anatomy from the reference can be measured and corrected for prior to treatment. Data acquisition from GSI, Darmstadt

29.4 Monitoring of Interfractional Motion

The monitoring of organ motion during treatment plays a special role. Interfractional motion of internal organs may be addressed by set-up corrections as for position verification. Depending on the organ, it requires, however, volumetric imaging in the treatment room like cone beam or CT imaging on rails. Repeated CT imaging may also be required in order to quantify the amount of movement from day to day and to identify the proper internal margin. This information may also be used to precalculate treatment plans for various target positions and select the most appropriate plan in each fraction ("plan of the day").

In Fig. 29.4, an example of repeated imaging using a CT scanner on rails in the treatment room is shown for a patient receiving a carbon ion boost for a prostate

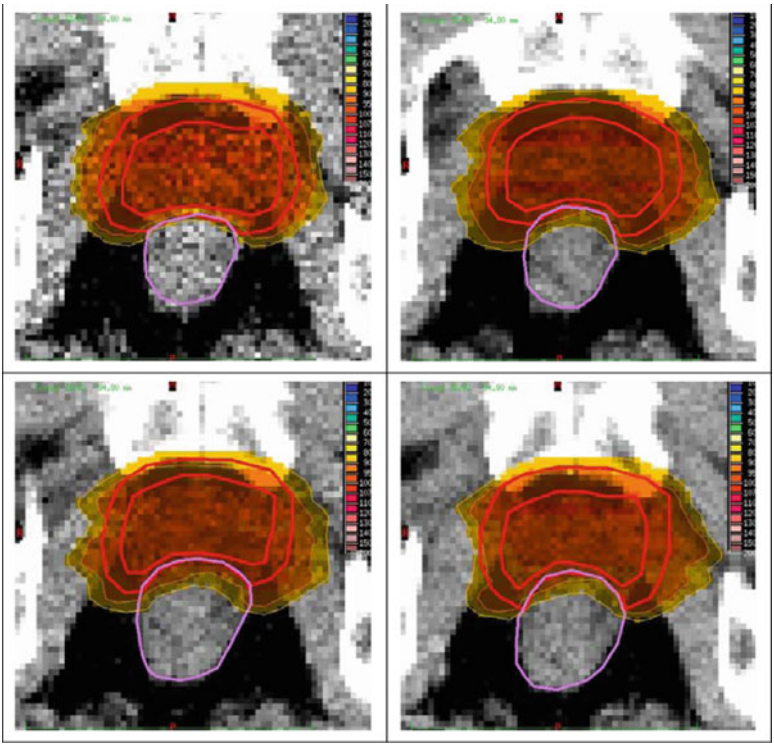

Fig. 29.4 Variation of the anatomy due to interfractional motion and the corresponding dose distributions for a carbon ion boost of a prostate carcinoma patient. The CT data were taken as reference and planning image (*upper left*) and as control scans taken on three different days during the prior irradiation with photons using an in-room CT scanner on rails (*upper right* and *two lower images*). The doses were calculated on these control CTs using the applied treatment plan. The analysis of the distributions shows the mean difference (standard deviation of the 95%- and 90%-coverage for the gross tumor volume (GTV) of 4.9% (SD 3.6) and 2% (SD 1.5), respectively. The corresponding values for the clinical target volume (CTV) were 3.6% (SD 3.7) and 2.8% (SD 2.8), respectively. Data from [12]

cancer. The images were acquired during the prior photon treatments at DKFZ [12]. The resulting dose distribution for the applied treatment plan for three control images is shown together with the reference plan.

29.5 Monitoring of Intrafractional Motion

Intrafractional organ motion poses a more severe problem, especially for a dynamic beam delivery like scanning. Generally, IBT depends significantly more on density variations than conventional RT. Dealing with intrafractional motion requires time-resolved imaging (4D-CT or 4D-MRI) during treatment planning in order to provide the information needed for various motion mitigation techniques.

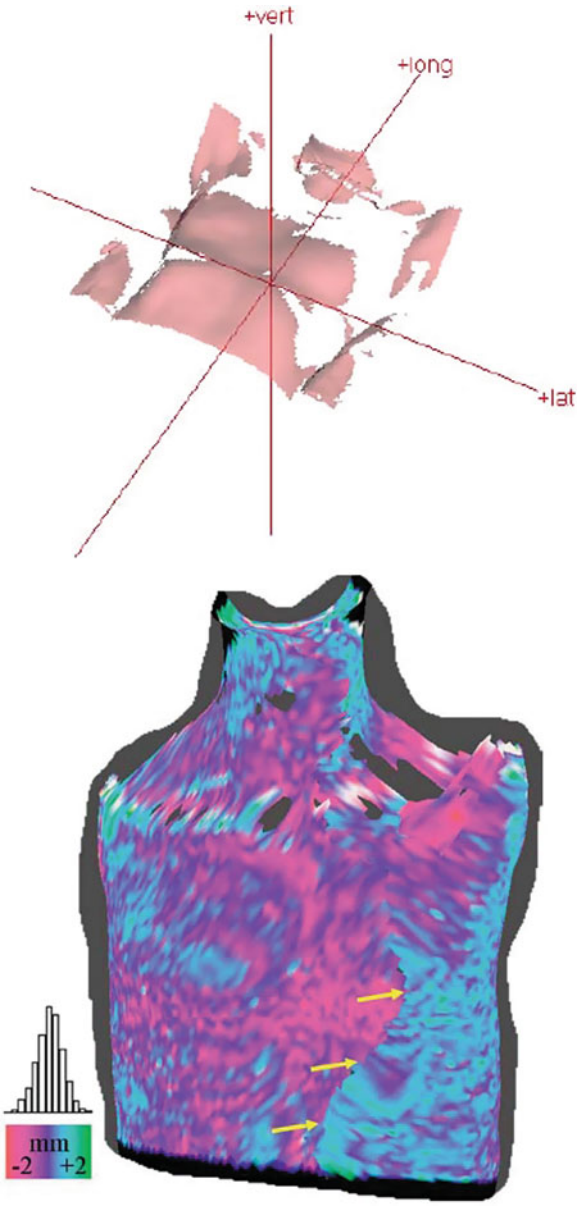

Fig. 29.5 3D-reconstruction of the surface of a patient being treated for breast cancer. From the reconstructed surface data of the patient and the data from a reference position, the deviation of each point on the surface can be calculated. The surface data were obtained with a laser system in the treatment room. Reprinted from [17]. *Bottom*: Example of the measured 3D map of deviations. Color-coded difference of the surface reconstructed from a CT and an optically measured surface. Black regions correspond to areas where the optical system could not acquire data. The *histogram* displays the distribution of the differences between the surfaces. Reprinted from [18]

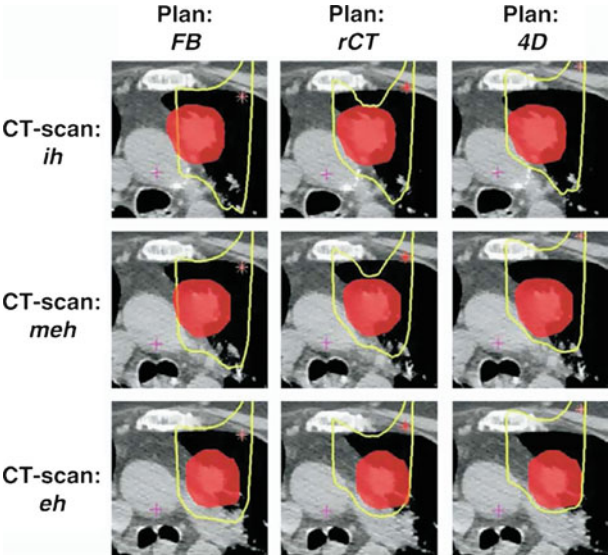

Fig. 29.6 Treatment planning for proton therapy of a lung tumor. 4D-CT images were used to account for intrafractional motion. Dose distributions for 1 of 3 beam directions and for three treatment plans calculated on end-inhalation (ih), mid-exhalation (meh), and end-exhalation (eh) phases are shown. The three plans were created for a CTV constructed from a normal free-breathing CT including margins (FB), from the 4D motion for a CTV derived from a reference image in mid-exhale phase with the same margin as in FB (rCT), and a CTV derived from all three breathing phases encompassing all possible target positions (4D). The *yellow line* indicates the 95% isodose level, the *red* area the CTV. Plan FB does not cover the target volume over all breathing phases. Plan rCT slightly underdoses the target in some slices. Target coverage is best for plan 4D. Reprinted from [19]

This may either be an appropriate internal safety margin that covers the tumor in every state of motion or the correlation of a movement with external markers such as breathing belts related to 4D-MRI [13] or laser tracking systems for gating techniques [14, 15]. From these results, the detailed definition of the trajectory of the tumor and changes in the tissue needed for full 4D treatment planning [16].

Figure 29.5 displays the 3D reconstruction of a patient's surface based on a laser tracking system [17]. The reconstructed surface of the patient can be used to calculate the deviations from reference positions. This is illustrated in a 3D map for another patient in the lower part of Fig. 29.5 [18].

An example of the use of 4D-CT in the treatment of lung tumors with a proton beam is shown in Fig. 29.6. The resulting dose distribution is displayed. It was recalculated from the applied treatment field based on 4D-CT images in different phases of the breathing cycle [19]. Various strategies for designing the CTV are shown, with only the 4D approach leading to a reasonable coverage.

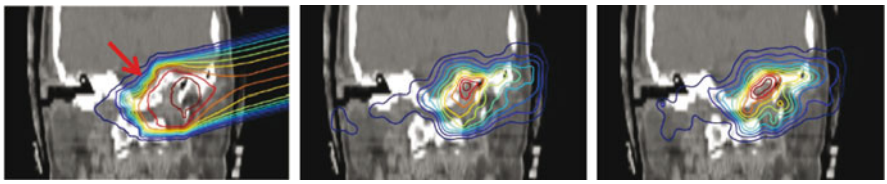

Fig. 29.7 PET imaging acquired during CIRT at GSI using an in-beam PET [20]. The example shows the lateral treatment field for a chondrosarcoma of the skull base with a maximum dose of 0.63 Gy (*left*). The treatment plan aims at sparing the brain stem just behind the target (*red arrow*). A comparison of the predicted (*middle*) and the measured (*right*) β^+-activity distribution shows good agreement and, hence, correct delivery. The isodose and isoactivity lines correspond to 5%, 15% ... 95% of the maxima

29.6 Treatment Verification

A special feature of ion beams is the possibility to monitor the delivered radiation through activation of the tissue. Imaging information is also needed in this case to relate the measured activity to the anatomical site in the patient. The most advanced technique is the measurement of induced positron emitters, by using PET (cf. Chap. 31 for details). The 3D activity information, as measured with either an in-beam or an off-line PET has to be correlated to the morphological images in order to derive meaningful information from it. This is no longer needed if modern PET-CT scanners are used for monitoring, which intrinsically provide correlation of both images.

Biological washout effects, the temporal pattern of the irradiation as well as the activity measurement are important to understand the measured pattern. Based on the X-ray CT planning images, the expected activity can be modeled for a given treatment plan. Figure 29.7 shows the applied dose distribution for a single treatment field of carbon ions and the induced pattern of positron activity for a patient with a skull base tumor [20]. The measured activation pattern is compared against the simulated pattern based on the treatment plan.

29.7 Future Developments

Despite the enormous technological developments in radiotherapy, there are still many cases where it is not possible to control local tumor growth. The explanation may be that the knowledge on what should be included in the target volume is still insufficient. The Canadian physicist Harold Johns aptly summarized this situation in the phrase “If you can’t see it, you can’t hit it, and if you can’t hit it, you can’t cure it” [4].

In the past, the main goal of development in imaging was morphology, which helped to define the GTV. Also the CTV definition is mostly based on morphological structures. In a recent review on the future of imaging in radiation therapy, Schlegel rightly concluded that tumor and normal tissue characterization needs to be based on three “M”s, namely morphology, movement, and molecular profile [21].

29.7.1 Morphology: Increasing Imaging Resolution

Resolution of modern 3D imaging used for radiotherapy planning is in the order of 1 mm. But the CTV concept requires information about microscopic tumor extensions in normal tissue, which are not visible with modern 3D imaging. In the near future, a significant increase of imaging resolution may be achievable with PET and SPECT scanning, leading to comparable resolution as CT [21]. Together with the enormous sensitivity of PET and SPECT this will allow improved accuracy in the CTV definition, especially using hybrid systems, like SPECT- and PET-CT or PET-MRI.

High-field MRI in the range of up to 7 T, which already allows for resolution well below 1 mm, may be introduced into the RT process. Also the resolution of functional MRI is improved by high-field scanners. These methods are, however, not yet established as standard imaging techniques for radiotherapy, in general, nor for IBT, in particular.

29.7.2 Movement: Integration of Imaging and Treatment

The ongoing development of image-guided radiation therapy (IGRT) is mainly addressing the problem of motion. Associated with it is the integration of imaging devices into treatment machines such as in-room CTs, linac-integrated MV- or kV-imaging, tomotherapy, or linac-integrated MRI scanners. This development in conventional therapy will certainly be extended to IBT and attempts will be made to integrate advanced imaging modalities into the treatment rooms. First steps in this direction already available today are robot-controlled cone beam CTs and CT-on-rail systems.

An example of such a robotic imaging device, based on a conventional C-arm for X-ray imaging is installed at the Heidelberg Ion-Beam Therapy Center (Fig. 29.8). The system can perform X-ray imaging from any angle, allows for fluoroscopic

Fig. 29.8 The robotic imaging system installed in the treatment rooms at the Heidelberg Ion-Beam Therapy Center (HIT). The C-arm can be used for X-ray and fluoroscopic imaging in any direction, and is prepared for cone beam CT imaging

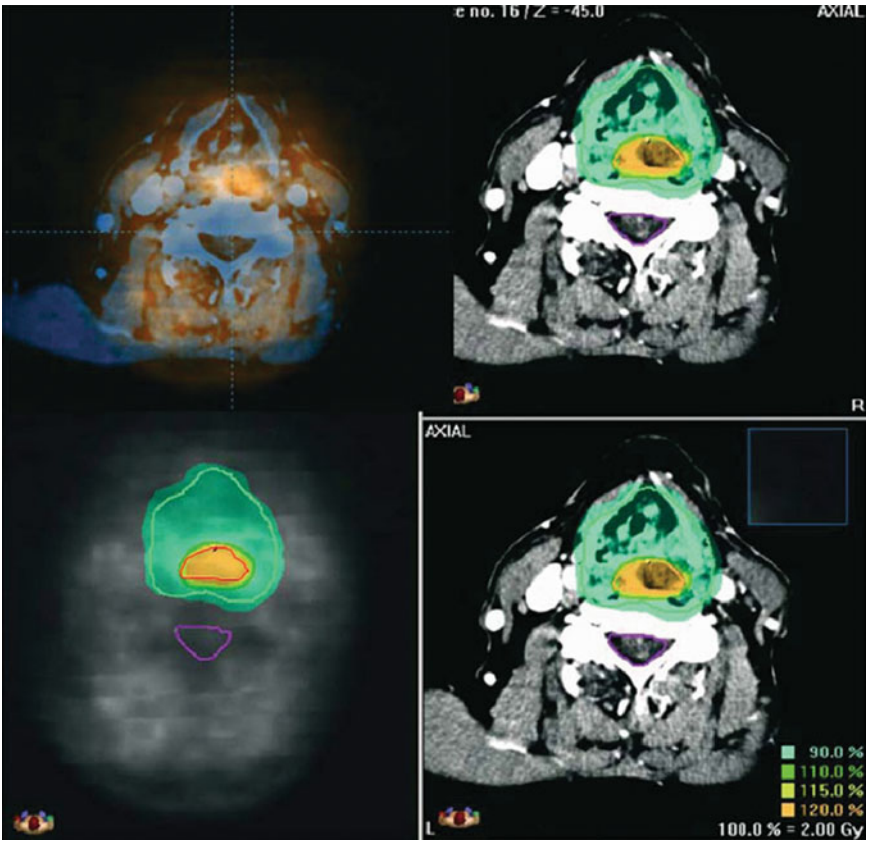

Fig. 29.9 Example of a functional PET image, showing hypoxic regions in a patient with a laryngeal cancer (T4N2M0 G2). The hypoxia tracer [18F]-fluoroazomycin arabinofuranoside (FAZA) was used for the PET image, which was fused with the CT data. During treatment with IMRT, the hypoxic area is encompassed in the high-dose area or biological target volume (BTV, *red contour*). The CTV is encompassed in the lower dose area displayed in *green* (reprinted from [5])

imaging with a frequency of 30 Hz, and is prepared for cone beam imaging in treatment position [22].

29.7.3 Molecular Profiling

Molecular profiling will become especially important for IBT. Today, it is evident that the assumption of a tumor being a homogeneous mass of cancer cells is too simplistic. Therefore, the necessity of delivering a homogeneous dose to the target must be questioned, as well. As has been shown with modern PET-tracers, e.g., a tumor may consist of subvolumes with very different radiobiological properties like

radioresistant hypoxic areas or regions with uncontrolled cellular proliferation. This phenomenon may be addressed by delivering inhomogeneous dose distributions, sometimes called “dose painting.”

An example for this concept using conventional photon IMRT is shown in Fig. 29.9, where a higher dose is delivered as a boost treatment to hypoxic tumor areas [5]. In IBT, the question may be even more important, as it is reasonable to restrict high-LET radiation to regions with a high concentration of radioresistant cells. Given the possibility of using different ions like protons, helium, carbon, etc. or combinations of them, the final goal may be to perform an “LET painting” within the target volume. This line of development is of special importance since it is known that the mean LET delivered with a certain ion type will decrease with increasing target volume. It may, therefore, be much more effective to restrict high-LET radiation to small subvolumes of the target.

Understanding the role of other molecular processes like apoptosis (programmed cell death) or angiogenesis (formation of new blood vessels) is still limited for conventional radiotherapy. For IBT, it is merely nonexistent and much more research will be required in this area.

The advent of 3D molecular imaging modalities (e.g., PET, PET/MRI, MRI spectroscopy, and fMRI) will provide new functional data on the target, and it will be a challenge to include them into radiotherapy planning, especially for ion beams.

References

1. W. Schlegel, T. Bortfeld, A.L. Grosu (eds.), *3D Imaging for Radiotherapy. New Technologies in Radiation Oncology* (Springer, Heidelberg, 2006), p. 176
2. L. Schad, Magnetic Resonance Imaging for Radiotherapy Planning, in *3D Imaging for Radiotherapy. New technologies in Radiation Oncology*, ed. by W. Schlegel, T. Bortfeld, A.L. Grosu. (Springer, Heidelberg, 2006), pp. 99–111
3. International Commission on Radiation Units and Measurements. Report 83. Prescribing, Recording, and Reporting Photon-Beam Intensity-Modulated Radiation Therapy (IMRT) J. ICRU. **10**, 1 (2010)
4. C.F. Njeh, Tumor delineation: the weakest link in the search for accuracy in radiotherapy. J. Med. Phys. **33**, 136–140 (2008)
5. A.L. Grosu, L.D. Sprague, M. Molls, Definition of Target Volume and Organs at Risk. Biological Target Volume, in *3D Imaging for Radiotherapy. New Technologies in Radiation Oncology*, ed. by W. Schlegel, T. Bortfeld, A.L. Grosu. (Springer, Heidelberg, 2006), pp. 167–177
6. M. Krämer, O. Jäkel, T. Haberer, G. Kraft, et al., Treatment planning for heavy ion radiotherapy: physical beam model and dose optimization. Phys. Med. Biol. **45**, 3299–3317 (2000)
7. O. Jäkel, M. Krämer, C.P. Karger, J. Debus, Treatment planning for heavy ion radiotherapy: clinical implementation and application. Phys. Med. Biol. **46**, 1101–1116 (2001)
8. O. Jäkel, C. Jacob, D. Schardt, C.P. Karger, et al., Relation between carbon ion ranges and X-ray CT numbers. Med. Phys. **28**, 701–703 (2001)
9. E. Rietzel, D. Schardt, T. Haberer, Range accuracy in carbon ion treatment planning based on CT-calibration with real tissue samples. Radiat. Oncol. 2 (2007)
10. O. Jäkel, P. Reiss, The influence of metal artifacts on the range of ion beams. Phys. Med. Biol. **52**, 635–644 (2007)

11. H.D. Suit, W. Chu, History of Charged Particle Radiotherapy, in *Proton and Charged Particle Radiotherapy*, ed. by T.F. Delaney, H.M. Kooy. (Lippincott Williams and Wilkins, Philadelphia, 2008)
12. A. Nikoghosyan, D. Schulz-Ertner, B. Didinger, et al., Evaluation of therapeutic potential of heavy ion therapy for patients with locally advanced prostate cancer. Int. J. Radiat. Oncol. Biol. Phys. **58**, 89–97 (2004)
13. M. Feng, J.M. Balter, D. Normolle, et al., Characterization of pancreatic tumor motion using cine MRI: surrogates for tumor position should be used with caution. Int. J. Radiat. Oncol. Biol. Phys. **74**, 884–91 (2009)
14. S. Minohara, T. Kanai, M. Endo, et al., Respiratory gated irradiation system for heavy-ion radiotherapy. Int. J. Radiat. Oncol. Biol. Phys. **47**, 1097–1103 (2000)
15. H. Shirato, S. Shimizu, T. Kunieda, K. Kitamura, et al., Physical aspects of a real-time tumor-tracking system for gated radiotherapy. Int. J. Radiat. Oncol. Biol. Phys. **48**, 1187–1195 (2000)
16. C. Bert, E. Rietzel, 4D treatment planning for scanned ion beams. Radiat. Oncol. **2**, 24 (2007). http://www.ro-journal.com/content/2/1/24. Accessed on 26 Oct 2010
17. T. Moser, S. Fleischhacker, K. Schubert, et al., Verification of the Accuracy in Patient Alignment Using a Laser-Optical 3D-Surface Imaging System, in *WC 2009 IFMBE Proceedings 25/2009*, ed. by O. Dössel, W. Schlegel. pp. 295–298
18. C. Bert, K.G. Metheany, K. Doppke, G.T.Y. Chen, A phantom evaluation of a stereo-vision surface imaging system for radiotherapy patient setup. Med. Phys. **32**, 2753–2763 (2005)
19. M. Engelsman, E. Rietzel, H. Kooy, Four-dimensional proton treatment planning for lung tumors. Int. J. Radiat. Oncol. Biol. Phys. **64**, 1589–1595 (2006)
20. W. Enghardt, P. Crespo, F. Fiedler, et al., Charged hadron tumour therapy monitoring by means of PET. Nucl. Instrum. Methods Phys. Res. A **525**, 284–288 (2004)
21. W. Schlegel, If you can't see it, you can miss it: the role of biomedical imaging in radiation oncology. Radiat. Prot. Dosim. **139**, 321–326 (2010)
22. O. Jäkel, C.P. Karger, J. Debus, The future of heavy ion radiotherapy. Med. Phys. **35**, 5653–5663 (2008)

Chapter 30
Treatment Planning for Ion Beam Therapy

Oliver Jäkel

Abstract The special aspects of treatment planning for ion beams are outlined in this chapter, starting with positioning and immobilization of the patient, describing imaging and segmentation, definition of treatment parameters, dose calculation and optimization, and, finally, plan assessment, verification, and quality assurance.

30.1 Introduction

Treatment planning is a process to design radiation beams that yield the optimum balance between high dose conformation to the target and sparing of normal tissue. It further allows to estimate the clinical effect of the beams to the patient. Treatment planning for radiotherapy (RT) with protons and ions heavier than protons, in general, is very similar with only one major difference arising from the larger variability of the relative biological effectiveness (RBE) for ions other than protons.

For all clinical applications of proton therapy (PT), the RBE is assumed to be constant throughout the planning process. For ions heavier than protons this is no longer a useful concept. As shown below, the RBE will be varying as a function of particle type, energy, penetration depth, fraction dose, clinical end point, etc. In principle, all these dependencies should be considered during the process of treatment planning.

Depending on the flexibility of the beam delivery system, however, not all these parameters will be varying during beam delivery and, hence, some of these

O. Jäkel (✉)
Klinik für Radioonkologie und Strahlentherapie, Universitätsklinikum Heidelberg, Heidelberg, Germany

Heidelberger Ionenstrahl-Therapiezentrum, Im Neuenheimer Feld 450, 69120 Heidelberg, Germany
e-mail: oliver.jaekel@med.uni-heidelberg.de

U. Linz (ed.), *Ion Beam Therapy*, Biological and Medical Physics, Biomedical Engineering, DOI 10.1007/978-3-642-21414-1_30,

dependencies may be disregarded during the planning process. Consequently, the choice of the beam delivery system for the ion beams has important implications for the treatment planning system (TPS) and process.

The systems to be discussed here are the 3D beam scanning system (called *active* system) and the conventional technique using beam shaping elements like modulators, range shifters, compensators, scattering systems (or wobblers), and collimators (called *passive* system).

Many of the aspects of treatment planning for conventional photon therapy also apply to ion beam therapy (IBT). In this contribution, the focus will primarily be on the specific aspects of treatment planning for ions heavier than protons. Differences to photons mainly arise from their different physical properties that are discussed in detail in Chap. 4.

30.2 Aspects of Patient Positioning and Immobilization

The same methods for patient positioning can be used in IBT as in any other precision RT modality. Due to the enormous increase in complexity and costs of IBT as compared to conventional RT, all existing facilities still use fixed beam lines for beam delivery (at least in some of the treatment rooms). This means that there is a severe restriction in flexibility as compared to PT where rotating gantries are considered the standard today. This restriction is often compensated for by using a variety of treatment positions for a patient, typically in supine, prone, and sometimes in sitting positions.

Many positioning units, therefore, exhibit special features to tilt and roll the patient to gain additional flexibility. At HIMAC, e.g., a special whole-body half-shell with a rolling mechanism - called *patient cradle* - has been introduced for that purpose (see Fig. 15.1). The patient can be rolled by approximately 15° in both directions. This feature is especially important when treatments with only few fractions are performed and normal tissue sparing is only achieved by using many fields, as in the case of lung tumors, for example [1]. For this procedure, it is very important that an appropriate imaging modality in the treatment position is available which allows soft tissue imaging, since organ movement and deformation due to the positioning will generally appear as compared to a treatment planning CT in supine position. Consequently at HIMAC, the patient is imaged in the CT under the same angle (and separately for each angle) as during treatment. This has important consequences for the planning procedure: first, the roll angles have to be defined prior to the imaging and second, the resulting CT images for each field (or angle) have to be merged in order to allow for calculation of the resulting dose distribution from all fields. This may introduce additional uncertainties during the process of elastic matching of the images and dose distributions.

Similarly, at HIT, a robotic patient positioning system is used which allows tilt and roll movements of up to 15° in both directions. This feature is currently only used for position corrections and is limited to small angle corrections only. In some

cases, however, a defined roll angle of the patient may be used for the treatment, based on a single fixed-angle CT planning image. To ensure accurate positioning of the internal organs and tumor after rotation, kilovoltage cone beam CT imaging in treatment position is foreseen. This will be performed with a second robot, carrying an X-ray system, which can be rotated around the patient (cf. Chap. 33 for details).

Also at HIMAC, patients can be treated while sitting in a treatment chair. For this special case, a vertical CT scanner is available, that allows imaging of the patient in the treatment room in seated position, in order to detect and correct for internal motion [2].

The immobilization devices used for IBT should fulfill some additional requirements as compared to conventional RT, because they may introduce additional heterogeneities into the beam. Generally, it should be ensured, that any material that may be traversed by a treatment beam, should be as homogeneous as possible and manufactured with a low density. This especially excludes systems, which are reinforced by metal elements in this area.

30.3 Aspects of Imaging and Segmentation

The aspect of imaging and tumor localization for treatment planning is extensively discussed in Chap. 29. Only the calibration of Hounsfield units (HU) to range is discussed here in some more detail, as it is important for the dose calculation.

Since the CT numbers are the only quantitative source of information to obtain the ranges of the particles in tissue, the quality of these data is of high importance. The procedures to obtain the HU-density calibration have to be carefully defined and documented. The conversion curves from CT number or HU (cf. Fig. 29.2) to the effective density in terms of stopping power has a specific structure due to the varying composition of the biological tissues [3]. In particular, bones may exhibit strongly varying HU due to increased attenuation of kilovoltage X-rays for high-atomic number materials such as calcium. The relation depends primarily on X-ray energy spectrum and beam-hardening effects [4]. It is thus necessary to define quality assurance (QA) procedures for CT images to be used in IBT planning. These should include regular checks of the HU of various phantom materials throughout the scale [5] as well as real tissue measurements [6]. For dose calculations, only native CT scans should be used since the presence of contrast agent may disturb the HU of tissue and can lead to range uncertainties [4, 7].

The presence of metals (dental fillings, prostheses, neurosurgical implants) causes special problems. First, the range calculation for metal may be wrong. Most CT scanners do not yield reasonable HU for metals and the HU-density correlation for human tissue may no longer be valid. In treatment planning practice, the region of metal implants should be outlined and a proper density should be assigned to this region [8]. Secondly, metal artifacts also may cause large range uncertainties especially for patients with hip prosthesis made of surgical steel [9]. Several effects can be separated here; streak artifacts in the surrounding normal tissue, incorrect

size of the metal implants in the CT images, and a low-density artifact around the high-density region. The effect of these artifacts on the ion range strongly depends on the beam direction, the density and size of the metal, and the imaging protocol. Imaging protocols that reduce these artifacts have to be properly examined to avoid additional uncertainties in the HU due to the use of artifact reduction algorithms.

The additional use of MR and PET images for an improved definition of anatomical structures is common practice in IBT and is discussed in Chap. 29.

30.4 Definition of Treatment Parameters

The definition of treatment parameters includes the selection of the number of treatment beams, treatment angles, the appropriate margins to ensure target coverage, and, finally, the therapeutic prescription including dose, fractionation scheme, and ion species. This also includes a decision on RBE values for various tissues that are involved in the treatment.

30.4.1 Selection of Beam Directions

Currently, the selection of treatment angles is done manually, although there are some attempts to include beam angle optimization in IBT. This possibility will be discussed below. Due to the excellent dose conformation possibilities of IBT, typically only a few beam directions (2–3) are used [10]. Consequently, selecting appropriate beam angles becomes more important as for techniques where many beams are used. In Fig. 30.1, an example of a treatment plan consisting of two horizontal fields of carbon ions is shown, which were delivered using the beam scanning technique at GSI.

Treatment angles are usually selected such that

- The restrictions of the positioning system and beam delivery are taken into account.
- The aims of the treatment tissue sparing, can be achieved, i.e., good target coverage and normal.
- The uncertainties of the delivered dose to the patient are reduced as much as possible.

The first point is of importance not only in the case of fixed-beam treatments, where the selection of appropriate angles is obviously very restricted and the choice of angles critical. Also in gantry systems, the table angle is often restricted. This restriction can be quite severe, if the space inside the gantry is limited and not all table angles are available, as is the case on many proton gantries but also the only ion beam gantry operating at HIT. These limitations should be visualized in accurate 3D models of the treatment in the planning system in order to avoid planning of unrealistic treatment configurations.

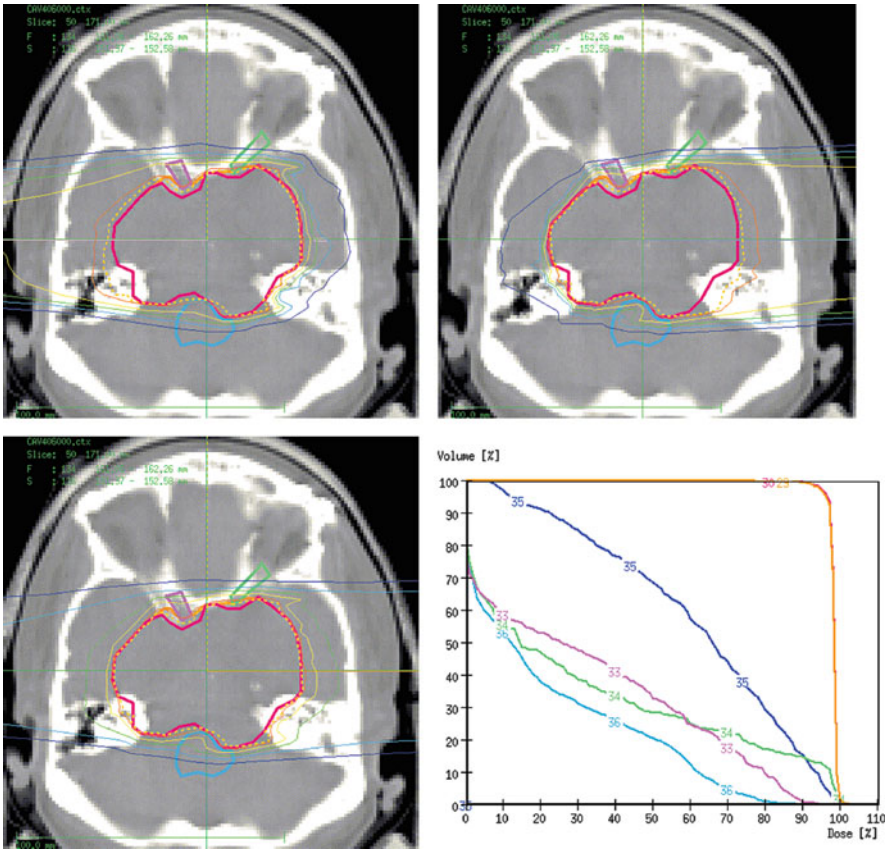

Fig. 30.1 Example of a treatment plan for a skull base chordoma, using two scanned fields of carbon ions. The dose distribution for the two single beams is shown on the *top images*. The isodose lines correspond to 10% (*dark blue*), 30% (*light blue*), 50% (*green*), 70% (*yellow*) and 90% (*red*) of the dose prescribed per field, respectively. The *contours* of the planning target volume (*red line*, dose-volume histogram/DVH line 30), optical nerves (*purple* and *green contours*, DVH line 33 and 34) and brain stem (*light blue*, DVH line 36) are shown. The DVH comprises, in addition, the optical chiasm (DVH line 35) The combined dose distributions are shown in the same color code but relative to the dose prescribed per plan on the CT image (*lower left*) and in the DVH (*lower right*)

Other restrictions on the number of treatment fields may arise in some systems, as the dose delivered per field may become quite low in some areas and the monitoring system may not be able to deliver these fields with the appropriate accuracy. This is an issue for heavier ions only, where the particle number is about two orders of magnitude lower than for proton beams.

A second aspect influences the number of fields chosen for a treatment. If, for example, a relatively low dose is to be delivered to a simple target volume, a single beam treatment may be chosen while in complex cases, e.g., in the case of skull base

chordoma, high doses are needed and critical structures are in close vicinity to the target. In these cases, three or four beams may be needed.

The last point in the above list is probably the most important. It is associated with the *robustness* of a treatment plan [11], which is part of the plan assessment. The major uncertainties in IBT come from the uncertainty in ion range and RBE. In order to limit range uncertainties, treatment angles will be chosen such that

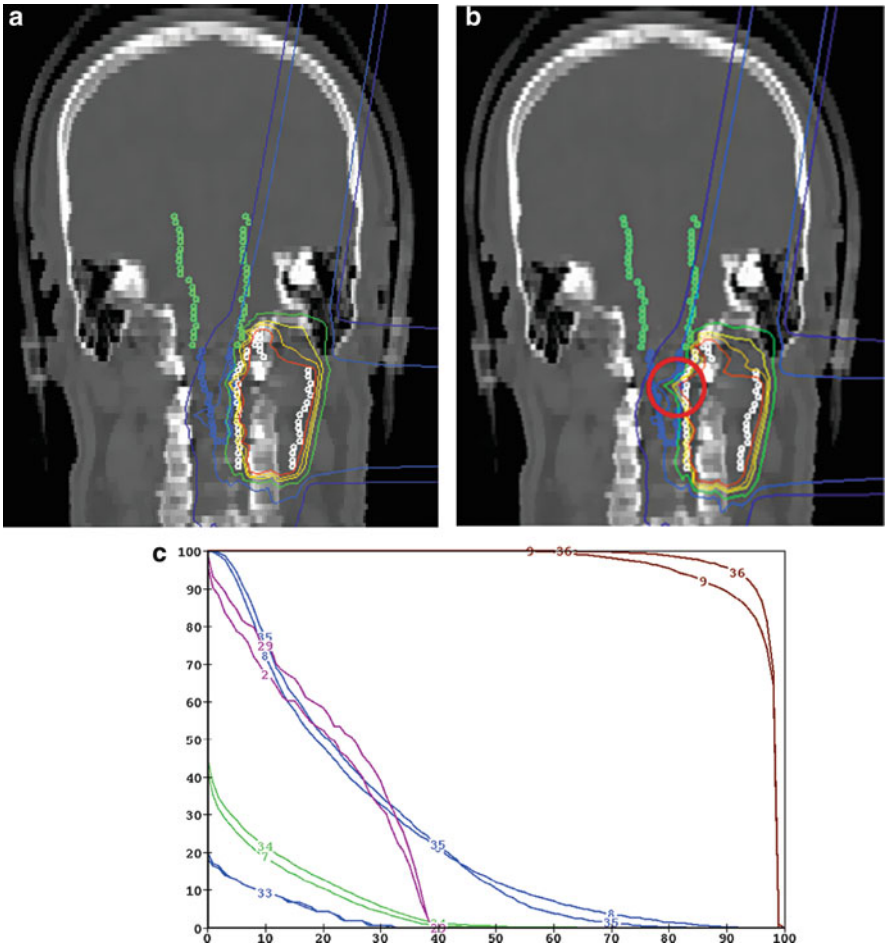

Fig. 30.2 Example of a robustness test of a treatment plan for a cervical chordoma. The same isodose lines as in Fig. 30.1 are shown. The treatment plan is based on a vertical field arrangement, where the left lateral field stops close to the spinal cord (*blue circles*). The dose distribution for the planned patient position is shown on the *upper left*. The dose distribution in the upper right results when the patient moves 5 mm in cranial direction. It exhibits a critical hot spot (shown in the *red circle*) in the spinal cord (*light green contour*). In the dose-volume histogram, both dose distributions are compared for the target (lines 36 and 9), spinal cord (lines 35 and 8), brain stem (34 and 7), and the optical chiasm (lines 2 and 29), respectively

beam paths through very inhomogeneous tissue or areas with larger movement are avoided, since they will suffer from a larger range uncertainty than paths through very homogeneous nonmoving tissue. Also, beam angles perpendicular to the organ motion will give larger dose deviations than beams parallel to it. An example of a calculation of the robustness of a dose distribution against position errors for a cervical chordoma is shown in Fig. 30.2.

A common technique that may be used in difficult treatment situations is to irradiate different parts of a target volume with different beams. This is called field patching and may be achieved either by lateral patching or distal patching, depending on where the fields are joined together [10]. Obviously, this technique critically

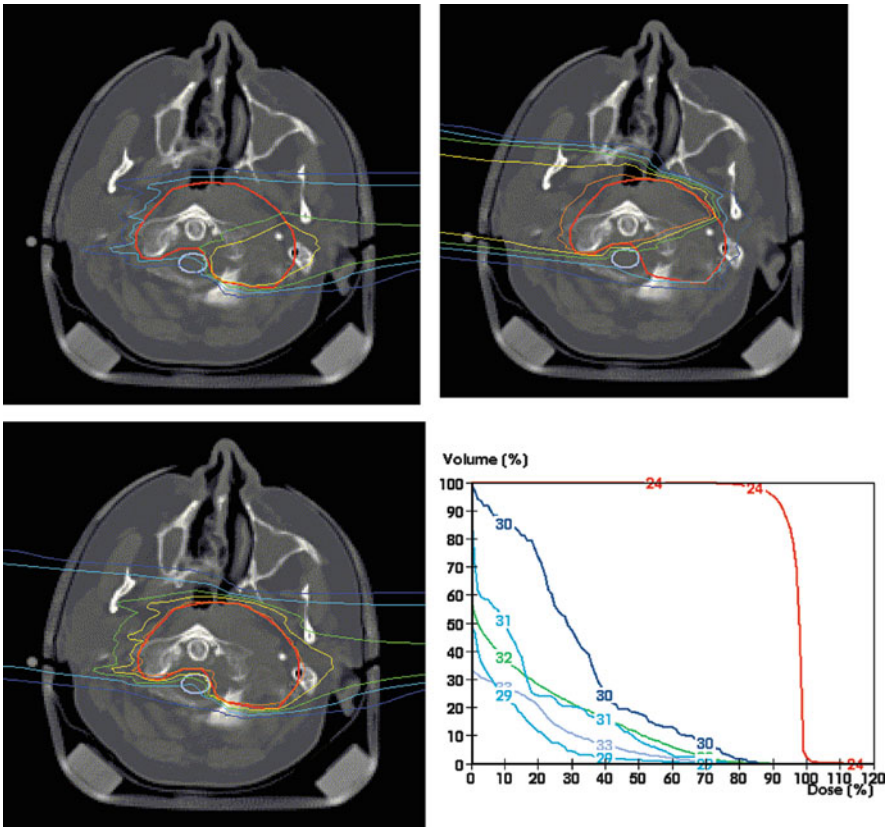

Fig. 30.3 Example of a so-called wedge field technique: the two treatment fields cover only part of the target volume and are optimized so that a decrease of dose around the patch-plane is achieved (*top*). The same isodose lines as in Fig. 30.1 are shown. The combined dose for both fields yields a homogeneous dose distribution (*bottom*). The dose-volume histogram shows the excellent sparing of the brain stem (*gray line*, DVH line 33), but also the increased maximum dose in the target volume (*red line*, DVH line 24), which results in the small volume of the patch plane. Both fields are optimized separately and the resulting biological effective dose is calculated

depends on the correct beam position (lateral patching) or range calculation (distal patching) and will be inherently less robust.

There are two strategies to increase the robustness of these plans:

1. Treatment plans with different patch lines (or without any patching) are combined (moving patch plane).
2. In the case of beam scanning, a smooth patching can be achieved by smearing out the dose gradient at the patch line over a larger volume.

The latter procedure is sometimes called wedge field technique and is shown in Fig. 30.3.

The robustness against set-up errors and patient or organ motion can usually be assessed only by simulating these variations and their influence on the dose distribution. This process is tedious and time consuming, for which reason automatic beam angle selections would be very attractive for IBT.

The aspect of RBE uncertainties may also play a role in beam angle selection. One example would be the RBE in the fragmentation tail of carbon ions. The absolute dose deviations due to these RBE uncertainties would become significant and it may, therefore, be reasonable to avoid the fragment tail in critical structures. Another example of how uncertainties in RBE are limited is the selection of opposing beams. It leads to an averaging of LET and thus also RBE variations in the target volume. An opposing-field arrangement is very robust also with regard to range uncertainties, since over- or undershooting from one side will be partially compensated by the other field.

Currently, only few attempts are made to develop algorithms for automatic beam selection. These algorithms are mainly based on simple and fast dose calculation algorithms to search beam angles that minimize the heterogeneity along the beam path, the uncertainty due to set-up errors [12, 13], or simply to get the best dose distribution [14, 15].

30.4.2 Definition of the Planning Target Volume

Defining the planning target volume (PTV) based on the clinical target volume (CTV) is another important step in the treatment planning process. It is important to determine appropriate margins to ensure target coverage in the presence of uncertainties in the planning and delivery process. This extension of the target volume by the use of margins may be limited by adjacent critical normal tissue structures in the individual case, though [16].

The most critical uncertainties to be regarded during PTV definition, are range uncertainties due to heterogeneities, set-up errors, and organ motion. The aspect of organ motion is dealt with in more detail in Chap. 32, where also the concept of the internal target volume or ITV is mentioned. As discussed already above, these effects are difficult to assess and usually require repeated simulations of various positions and motion phases to quantify the appropriate margin. In the presence of

organ motion with large density heterogeneity such as in lung cancer cases, PTV and ITV are not just geometrical concepts but should be defined with the density variation for adequate range control.

Uncertainties of the beam delivery are easier to determine, as they are independent of the individual treatment plan. They are connected to the accuracy of the beam position, energy, penumbra, the position and tolerances of beam shaping devices (like collimators, ridge filters, compensators), and other basic parameters. These uncertainties should be quantified during the commissioning procedure of the facility.

In general, the optimum treatment margin strongly depends on the treatment site, the patient set-up, immobilization, motion management, beam delivery system, but also the individual treatment plan. Since the latter is mainly due to the range uncertainties, field-specific margins may be needed, in order to reduce the amount of normal tissue in the high-dose region.

In order to facilitate the definition of margins, automated algorithms are being investigated. One currently used approach relies on a probabilistic approach to optimize the PTV in such a way that the robustness of the resulting dose distribution is maximized while the volume of the high-dose region is limited as far as possible [17]. This approach is a novel concept of PTV definition and an alternative to the ICRU concept [16].

30.4.3 Selecting a Particle Type

The experience with different ion types for therapy is very limited. In Berkeley, just 433 patients were treated using beams of carbon, silicon, argon, and neon ions between 1977 and 1992 [18]. Since then, all other ion beam facilities have solely used carbon ions. The Heidelberg facility and several others are already offering protons as well as carbon ions. In the near future, HIT will also provide helium and oxygen ions for therapy [19]. Selecting the optimum ion type will consequently become an important task in treatment planning. Several aspects have to be regarded when considering various ions for RT:

- When using ions heavier than carbon, the number of nuclear fragments beyond the Bragg peak is increasing; for a carbon beam, the tail dose beyond the spread-out Bragg peak (SOBP) approximates to 10–30%, depending on the modulation depth.
- LET for ions heavier than carbon is increasing and also their effectiveness is increased. This is true not only for the Bragg peak region but also for the entrance region. For argon ions, for example, it has been shown, that in contrast to carbon the RBE in the entrance region may even be higher than in the peak region (see Fig. 30.4).

Light ions like helium ions, show a slightly increased RBE, but not a significant increase between entrance and peak region. These ions, however, may be interesting as lateral scattering is strongly reduced compared to protons and they can easily be

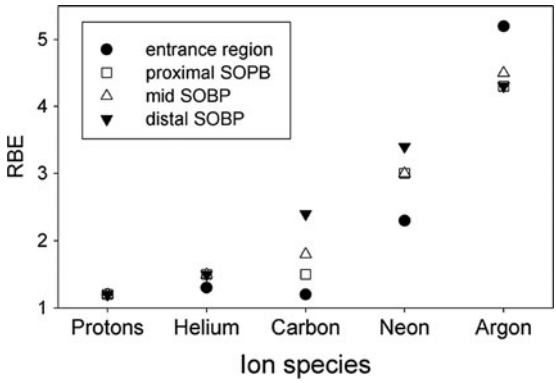

Fig. 30.4 The relative biological effectiveness (RBE) for a fractionated irradiation of jejunal crypt cells of mice for different ions in different positions of a spread-out Bragg peak (SOBP). The modulation depth of the SOBP was 8–10 cm and the initial beam energy was 160, 225, 400, 557 and 570 MeV/u for protons, helium, carbon, neon and argon ions, respectively (image reproduced from [20])

produced in relatively small cyclotrons. More biological and clinical data are needed to decide the question, which ion type is best suited for which tumor type.

30.5 Dose-Calculation Algorithms

Depending on the dose delivery system (passive scattering vs. scanning), different dose calculation algorithms of different complexity are needed: whereas for passive systems, only a single (modulated) beam is applied, the algorithm for scanning has to deal with many different beam energies and focus levels.

30.5.1 Absorbed-Dose Calculation

For therapeutic beams, basically three different dose calculation algorithms have been proposed: ray trace, pencil beam, and Monte-Carlo (MC)-based algorithms. They differ considerably in complexity (and thus computation time) and accuracy.

Typically, the dose calculation is separated into two parts: the depth-dose calculation along the central axis of the beam, and the lateral or "off-axis" distribution. While the depth-dose curve is determined mainly by the energy loss through ionization, the off-axis terms are determined by multiple Coulomb scattering of the incident particles. Nuclear fragmentation affects both parts and can thus only be included empirically into these algorithms.

Ray-tracing methods, which are used for passive systems only, are extremely fast, but provide only limited accuracy, especially, of the lateral scattering processes [21]. The beam is simply traced from the source along straight lines ("rays") through the patient and the energy deposited is calculated using depth-dose curves measured along the central axis of broad beams. Since multiple scattering for heavier ions is very limited (unlike protons), this is already a good approximation. The dose $D(z, r, E_0)$ at any depth z, distance r to the central axis, and for each primary energy E_0, can be parametrized as:

$$D(z, r, E_0) = D_{\mathrm{CAX}}(z, E_0) \cdot L_F(z, r, E_0), \tag{30.1}$$

where $D_{\mathrm{CAX}}(z, E_0)$ denotes the measured central axis depth-dose curve and $L_F(z, r, E_0)$ the relative lateral dose distribution for a given field size F.

More common are pencil beam algorithms [22, 23]. Here, the treatment beam is subdivided into elementary pencil beams. The pencil beam $P(z, r, E_0)$ is defined as the dose deposited in a semi-infinite water phantom by an infinitely narrow beam of incident particles with initial energy E_0 at depth z and radial distance r from the central axis. In particular, this distribution includes the dose due to particles that are scattered away from the central axis.

These beams are transported separately through the tissue and the resulting dose is calculated from the superposition of all partial beams, i.e., by integration over the beam aperture and energy spectrum. In the case of scanning pencil beams, the primary beams may directly be used as discrete pencil beams. In this case, the dose calculation can be simplified to a weighted sum of precalculated finite pencil beam dose distributions $P_{\mathrm{f}}(z, r, E_0)$ for a nominal energy of E_0, which accounts for the machine-dependent particle phase space of the delivery device. It can again be separated into a central axis term and an off-axis term [24].

$P(z, r, E_0)$ can be obtained either from MC simulations [23, 25], or it can be separated again into a central axis and an off-axis term [26], $L(z, r, E_0)$, which usually is assumed to be Gaussian:

$$L(z, r, E_0) = \frac{1}{2\pi\sigma(z, E_0)^2} \exp\left(-\frac{r^2}{2\sigma(z, E_0)^2}\right) \tag{30.2}$$

$L(z, r, E_0)$ is normalized such that an integral over a plane perpendicular to the beam direction equals 1.

The lateral width of the beam is composed of the machine-dependent term $\sigma_0(E_0)$ and a second term $\sigma_{\mathrm{MCS}}(z, E_0)$, which accounts for multiple Coulomb scattering in the tissue in depth z:

$$\sigma(z, E_0)^2 = \sigma_0(E_0)^2 + \sigma_{\mathrm{MCS}}(z, E_0)^2. \tag{30.3}$$

Pencil beam algorithms can handle multiple Coulomb scattering and the energy loss of all individual beams and lead to a more realistic dose calculation. More complex effects, arising, for instance, from nuclear fragmentation or lateral inhomogeneities,

can only be handled empirically by these algorithms [27, 28]. While it is straightforward to include nuclear fragments empirically in the depth dose [24], it is more difficult to model the lateral penumbra arising from the production and scattering of secondary particles in depth [29–31] or the effect of lateral inhomogeneities.

The potentially most accurate algorithms are MC techniques, which are, however, very time-consuming. Their application in clinical routine is still very limited, but they are increasingly used [32–34]. Among the most popular codes, able to model the nuclear fragmentation, are FLUKA, GEANT, SHIELD, and MCNPX, with only FLUKA being used in clinical routine for carbon ions (cf. Chap. 7 for more details).

An important application of the MC simulation for treatment planning is the beam modeling for pencil beam algorithms. In the case of the Heidelberg facility, 252 energies are available at four different focus levels each. Since the measurement of all the depth-dose curves and beam profiles would be very time-consuming, it was decided to use an MC algorithm to model the measured database and interpolate between the measurements [32–34].

30.5.2 Nuclear Fragmentation

In IBT, the biologically effective dose has to be calculated in addition to the absorbed dose. Since the RBE depends strongly on the particle type and energy, it is necessary to model also the particle spectrum arising from nuclear fragmentation in depth. This can be done by dedicated transport algorithms using empirical models [24]. If an MC algorithm is used for generation of the pencil beam kernels, it is, however, much more straightforward to employ them also for the particle spectra needed to determine the radiobiological effects.

It should be noted that most model calculations are restricted to the generation of projectile fragments, i.e., protons, helium, lithium, beryllium, and boron ions in the case of a carbon beam. Target fragments are produced as recoil nuclei at very low energies and are expected to deposit their energy locally at the point of creation. A special issue is the production of neutrons, which are created at very high energies in passive elements of the beam line and in the patient [35, 36]. They are usually also neglected for the dose calculation, since they leave the patient without significant loss of energy. They are, however, important for considerations about radiation protection, shielding, and late radiation risks for the patient (cf. Chap. 21 for details).

There are only very few data available for any other medium than water. All semiempirical transport codes will, therefore, assume that the fragmentation yield in all tissues can be derived from the yield in water, scaled by the relative density.

In the case of passive systems, this problem does not arise since the depth modulation is constant and, thus, also the particle spectrum is just a function of depth. In this case, RBE can be modeled as a fixed function of depth (see below).

30.5.3 Biological Modeling

Due to energy loss and nuclear interactions of ions in matter, the RBE of ion beams varies strongly with depth in tissue. It further varies with the applied dose, and depends on cell type, and biological endpoint. This has to be kept in mind, when calculating treatment plans and comparing different modalities.

30.5.3.1 RBE Modeling for Passive Beam Delivery

When using a passive beam delivery system, the above-mentioned dependencies of the RBE are usually ignored and only a single fixed-range modulator is designed for a certain fractionation scheme, cell type, and endpoint.

Due to the high dose and LET in the proximal parts of the target region, acute reactions of the skin are usually defined as dose-limiting endpoint. Once a certain design of the modulator has been chosen, no further biological modeling is needed in the process of treatment planning. The RBE-weighted depth-dose curves for the SOBP are stored in the beam library for various beam energies and modulation depths [37,38]. The curves are normalized at the reference depth, which is typically the center of the SOBP. During dose calculation these depth-dose curves are scaled by the prescribed dose.

Figure 30.5 shows the depth-dose curves for various depth modulations produced with the range modulator at the HIMAC facility for a fixed energy. The underlying RBE model is based on an RBE for human salivary gland cells measured in vitro as a function of dose mean LET. It is scaled to a clinical RBE for neutrons gained in prior clinical studies at a point in the SOBP, where the dose mean LET is the same as for the neutrons ($65\,\mathrm{keV}\,\mu\mathrm{m}^{-1}$) [37]. This RBE value is based on an endpoint for acute skin reactions.

As explained above, the model is useful only for a well-defined clinical situation for which the modulator was optimized. When, for example, the dose per fraction is changed, a different tumor type, or clinical end point is considered, the validity of this model has to be questioned. It should also be noted that the tabulated isoeffective depth doses are only valid, if a single field of a treatment plan is applied per day. If several fields were superimposed, the dose distribution and, consequently, the RBE changes. Also, the use of complex techniques like intensity modulation is not feasible.

30.5.3.2 RBE Modeling for Active Beam Delivery

When using a 3D scanning beam delivery system, nearly any arbitrary depth modulation can be achieved. Therefore, a more general method is needed to describe the respective depth-dose curves. The most obvious effect is an adaption of the modulation depth at every point in the field to reach the desired dose conformation.

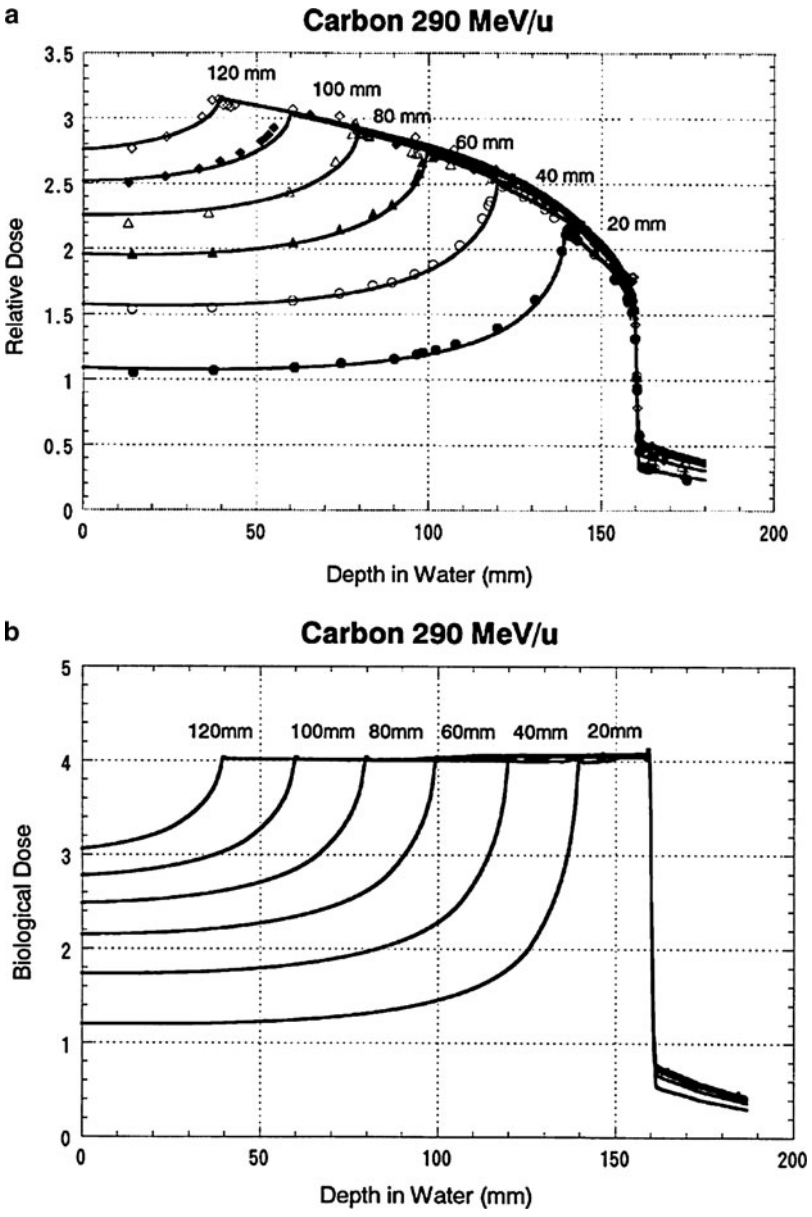

Fig. 30.5 Absorbed depth-dose distribution(**a**) and resulting biological depth dose (**b**) for a single fixed-energy beam of carbon ions, using different depth modulations. The decrease in absorbed dose in the SOBP is designed in a way to compensate the increase of RBE towards the distal end (image reproduced from [37])

Currently, only the so-called local effect model (LEM) developed at GSI has been used for treatment planning of scanned ion beams (cf. Chap. 8 for details). This model takes into account the different effectiveness of the nuclear fragments as well as the dependencies of the resulting RBE on applied dose, cell type, and endpoint. The main input data that are required to calculate RBE values for a certain tumor type and endpoint are merely the α and β values for photons for the same endpoint. This means that the LEM model permits to estimate the biological effects of ions, as long as data for photons for the respective endpoint are available.

The database for α and β values for clinical endpoints is still rather limited. Since also a wide patient-to-patient variability of tumor cells even for the same histology had to be expected, a different strategy was followed when the LEM was applied to the first patient treatments at GSI in 1997: rather than attempting to estimate the RBE for tumor control directly, the RBE of the dose-limiting normal structures were used [39]. This procedure has some advantages, as the variability of normal tissue sensitivity is less pronounced and a better database exists for these tissues. By performing dose-escalation studies, the tumor control rate can then be gradually adjusted while still avoiding unwanted side effects. By using best-available data for the different involved tissues, the resulting dose distributions can be simulated in the treatment planning. A typical example of this procedure is shown in Fig. 30.6 for a prostate cancer patient. This procedure of using a dose-dependent RBE has important implications for treatment planning: it is necessary to calculate all dose distributions in absolute values as simple scaling of the distribution is not possible.

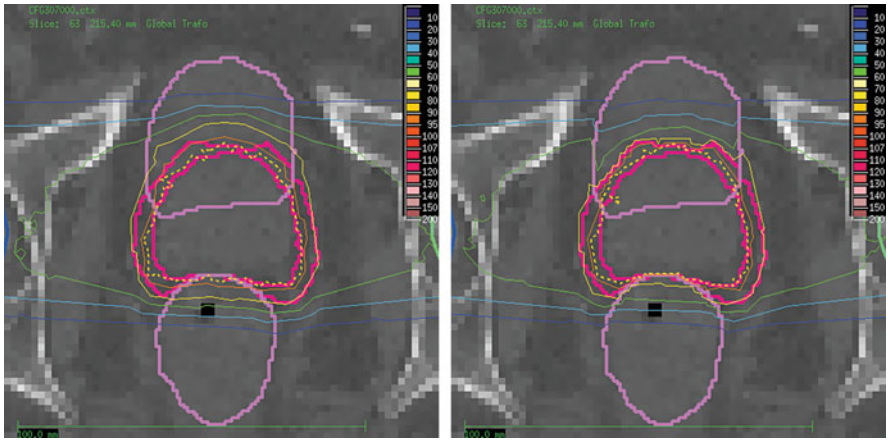

Fig. 30.6 The isoeffective dose distribution for a prostate cancer patient being treated with two horizontal opposing fields of carbon ions. The biological optimization is based on a single fixed α/β-value of 2. In the *left image* a fixed α/β-value was used for all tissues, while in the *right image*, a varying α/β-value of 2, 4, and 5 was used for prostate, rectum, and bladder, respectively. The isodose lines are as in Fig. 30.1. The changes of isoeffective dose at the border of the outlined volumes are visible

The advantage is, however, that simultaneous optimization of many beams can be done. That way, multiple fields can be treated in one day and intensity-modulated IBT becomes feasible, as well.

30.6 Optimization Algorithms

Treatment planning for a passive system is very similar to conventional forward planning, with no further degree of freedom, once a beam direction has been defined. A 3D scanning system, on the other hand, can produce nearly arbitrary shapes and dose levels of the SOBP. A TPS to support this flexibility needs a certain structure. A few relevant components are exemplified here:

- Before calculating the dose, the target volume is divided into slices of equal radiological depth corresponding to available energies of the accelerator. For each energy slice, either a grid of scan points (which need not be equidistant) or a scan path is defined, depending on the type of delivery system.
- The particle number delivered to each point or during a scan line for each energy has to be optimized in such a way as to obtain a predefined level of isoeffective dose. This may include the optimization of the scan path, i.e., the definition of a sequence of the scan points or lines.
- Optimization of isoeffective dose distributions is provided.
- The algorithm respects constraints that are imposed on the dose distribution in the organs at risk in order to tailor the dose to the target volume while limiting the dose to normal tissue.

Furthermore, not any optimized scan pattern may be feasible to deliver with a given scanning system. For example, there is a minimum number of particles at each scan spot, which can be delivered. The feasibility of each plan has also to be warranted with regard to the delivery time, which means that not too many spots of low particle number should be used. These constraints have to be taken into account during the optimization procedure. It is, therefore, useful to directly calculate and optimize the dose distributions on the basis of the machine capability and not to rely on an algorithm that matches desired dose distributions with possible beam parameters.

30.6.1 Single-Field Uniform Dose

Dose optimization in a single scanned treatment field intrinsically includes optimization of particle fluences, since otherwise, no homogeneous dose or isoeffect could be obtained. In doing so, dose constraints for the target volume and the organs at risk can already be included. The separate optimization of single treatment fields

is called single-field uniform dose (SFUD) optimization. It is a very easy, fast, and robust way to define a treatment plan that is not very demanding in terms of computing power.

30.6.2 Intensity-Modulated IBT

Although SFUD already involves fluence modulation, this is not considered to be the equivalent of IMRT. The important aspect of intensity-modulated IBT sometimes also called IMPT (for intensity-modulated particle therapy) is the simultaneous optimization of all treatment fields in a plan including all scan spots. This has so far only been introduced in combination with active beam scanning. It should be stressed that it is the particle number rather than the beam intensity that is modulated here.

IMPT is quite computing time and memory intensive since particle numbers at typically 30,000–50,000 scan spots per field have to be optimized in terms of isoeffective dose. This involves sampling of a large fragmentation database for each scan spot. The procedure is further complicated by a nonlinear dose dependence of the RBE values. But even if a number of approximations are introduced to speed up the optimization times, the method is still limited to only few fields [40].

Biologically optimized IMPT was used clinically for the first time at the GSI facility in 2005 and approximately 15 patients have since been treated with this procedure at GSI [41]. An example of the additional gain that can be achieved with IMPT is shown in Fig. 30.7.

Although IMPT results in better sparing of normal tissues, the resulting plans may not be as robust as SFUD plans, depending on the optimization strategy. Range uncertainties, for example, may become more important, since IMPT will try to

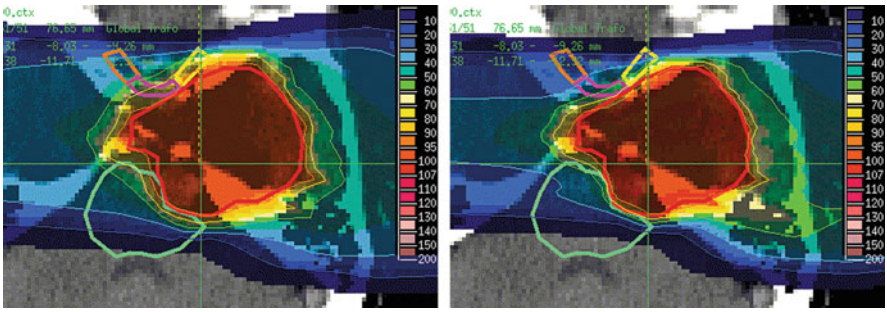

Fig. 30.7 Comparison of two treatment plans for carbon ion therapy of a patient with a skull base chordoma. *Left*: Single-field uniform dose (SFUD) plan. *Right*: Intensity-modulated IBT plan. It can be seen that additional dose sparing can be achieved in the brain stem, optical nerves and optical chiasm. The isodose lines are as in Fig. 30.1

make use of the finite range of the particles. In some cases IMPT can, however, be even more robust than SFUDs [42]. This is especially true, if range uncertainty is already included in the optimization procedure, as mentioned above [43].

30.7 Plan Review and Assessment of Dose Distributions

In general, all common tools for treatment planning are useful for IBT, too. In most cases, the RBE-weighted dose will be of particular importance and of clinical relevance. But the distributions of absorbed dose and (in the case of detailed modeling) also the RBE distributions should be displayed. For active beam delivery, it is also useful to display the distribution of scan spots on the patient CT and the weight of the spots in order to anticipate potential problems arising from limitations of the beam delivery or from uncertainties for the specific plan.

An estimate of the delivery time should be included in the plan assessment, to avoid unrealistic parameters that could lead to an exceedingly large number of scan spots or energy layers to be delivered.

Since IBT is critically dependent on the correct patient position, accuracy of CT data, range calculation, etc., it is important to provide tools in the TPS that assess the arising dose uncertainties. This may include best- or worst-case versions of a single treatment plan [10, 11, 41] or the same plan calculated with different input parameters (e.g., for patient position or α/β values assigned to various organs) [39]. These aspects are still under investigation and commercial solutions are not readily available to tackle these issues.

30.8 Planning of Combined Treatments

IBT may be combined with other RT modalities, like conventional 3D RT or various types of modern intensity-modulated RT (IMRT). The reason for this is certainly the large potential of IBT as a boost after low-LET irradiation as was demonstrated in a clinical trial at GSI [44].

An example for a combination treatment of photon IMRT and a carbon ion boost for a patient with an adenoid cystic carcinoma, is shown in Fig. 30.8.

In the near future, a combination therapy of protons and carbon ions or, more general, of two different ions may be used to selectively deliver a high-LET beam into a dedicated region.

In order to select the best option, the final dose distributions should be reviewed in terms of the isoeffective dose with respect to a standard treatment scheme. The common fractionation scheme 2 Gy/fx delivered in 5 days/week could serve as reference. When calculating combined dose distributions, it is important to select the appropriate weights of each treatment based on the fraction dose and the weekly delivery scheme. In order to account for different fraction doses in different

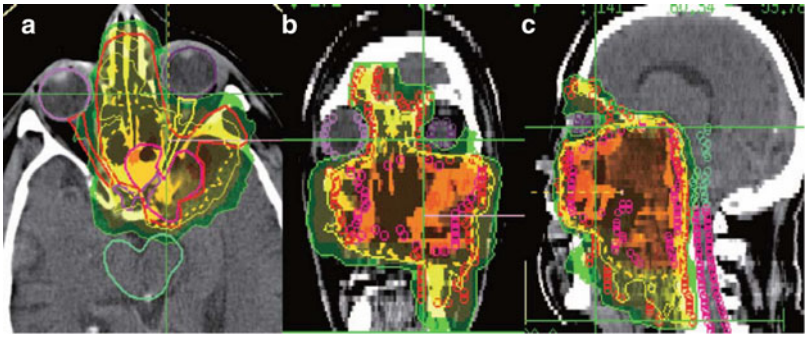

Fig. 30.8 Example of a combination therapy for a patient with adenoid cystic carcinoma. The larger PTV I (including microscopic tumor spread) was treated with photon IMRT in 30 fractions of 1.8 Gy and only the PTV II (defined as GTV plus a margin) was treated with carbon ions with an additional dose of 18 Gy in six equal fractions. The *thin yellow line* corresponds to 60 Gy, the *dotted line* to 54 Gy, and the *thin green line* to 39 Gy, respectively (Image taken from [44])

treatments, it should be noted that the α/β-value for photons is needed to adjust the appropriate dose values. As an example, the combined dose resulting from the photon dose of 54 Gy (in 1.8 Gy/fx) and an RBE-weighted ion dose of 18 Gy (in 3 Gy/fx) as shown in Fig. 30.8 is isoeffective to a dose of 77.7 Gy (54 Gy+23.7 Gy) with a fraction dose of 1.8 Gy, when an α/β-value of 2 is used.

This procedure should ideally be run on a voxel-by-voxel basis using appropriate weighting factors calculated from the α/β-value for the specific organ that incorporates that voxel. This procedure would then include the different behavior of various tissues when changing the fractionation.

30.9 Quality Assurance and Dosimetric Plan Verification

Quality assurance of a TPS includes the commissioning and acceptance testing of the TPS prior to its clinical use as well as regular constancy checks of the system during its clinical application. A number of general recommendations exists for the QA of TPSs in RT, which apply to IBT, accordingly [45–50].

While most aspects of QA are similar for conventional TPSs and those for IBT (e.g., checks of the software version, database, and dose calculation algorithms), there are some aspects that require specific checks in the case of ion beams:

- Imaging parameters and protocols of the treatment planning CT data that are important for the range calculation algorithms.
- Correct calculation of ion ranges based on the CT data and the transfer of ranges to required beam energies or range shifter settings.
- Correct selection of beam parameters (in the case of scanned beams) or correct definition of field-specific devices (collimators and compensators).

- Geometric accuracy of digital reconstructed radiographs, which may be used as a reference for set-up verification in the treatment room using X-ray imaging.
- Performance of the applied dose calculation algorithms in various phantoms, with a focus on range calculation and scattering effects behind inhomogeneities or in anthropomorphic phantoms.
- Database used for the calculation of biological effects and RBE, and correct absolute number of delivered particles (avoid dose errors due to wrong RBE values).

It needs to be stressed that although the clinically relevant quantity is isoeffective dose, the measurement and control of absorbed dose is of utmost importance, as this is the quantity which is controlled and monitored during beam delivery.

Measurements of biological endpoints in in-vitro cell samples in various phantoms may also be useful to validate the algorithms used for the calculation of isoeffective dose [51, 52]. Due to the inherently larger uncertainty of biological experiments as well as the large complexity involved in these measurements, it is currently not recommended to perform regular in-vitro measurements for QA purposes.

Another important question is the dosimetric verification of individual patient plans. In the case of a passive beam delivery technique, the dosimetric verification of a beam of protons or ions is practically identical to conventional (non-IMRT) RT. Here, the treatment field can be verified, e.g., by scanning a single ion chamber through the treatment field in a water phantom. For calibration purposes, the measurement of absorbed dose in the reference point is sufficient.

If active beam delivery is used, scanning of ion chambers is not possible. Hence, multichannel dosimetry systems are needed for an efficient dose verification. For this purpose, dedicated systems were developed that allow, for instance, to position a set of ion chambers in a water phantom and measure doses at various points in the field simultaneously [53]. Another possibility is to use multichannel detectors (e.g., the segmented ion chamber array PTW 729). Film detectors, although inappropriate for quantitative dose measurements for high-LET beams, are important to check geometric parameters of the treatment field [54, 55].

Verification of individual treatment plans is very time-consuming. There are attempts to restrict such measurements to randomly selected cases and rely on a TPS-independent dose check for all other plans instead. Such a check could, for example, be performed by an algorithm which calculates the absorbed dose, based on the optimized machine control data and compares it to the dose calculated by the TPS.

30.10 Conclusion

Treatment planning for IBT has undergone an enormous development over the last two decades. While the first systems were specially developed “homegrown” systems, dedicated to certain facilities, today, several commercially available TPSs

exist, which offer the same functionality as planning systems for conventional RT. The inclusion of biological modeling and intensity modulation techniques can also be considered a standard in a modern TPS for IBT. Currently ongoing developments concentrate on optimization algorithms aiming at improved robustness of treatment plans by taking into account various uncertainties in the delivery as well as optimization of treatment parameters. Another important area of ongoing development is treatment planning for moving organs and the introduction of imaging systems in the treatment room.

Taking these developments into account, there is still a large potential for future improvements in treatment planning for IBT.

References

1. T. Miyamoto, M. Baba, T. Sugane, et al., Carbon ion radiotherapy for stage I non-small cell lung cancer using a regimen of four fractions during 1 week. J. Thorac. Oncol. **2**, 916–926 (2007)
2. T. Kamada, H. Tsujii, J.E. Mizoe, et al., A horizontal CT system dedicated to heavy-ion beam treatment. Radiother. Oncol. **50**, 235–237 (1999)
3. W. Schneider, T. Bortfeld, W. Schlegel, Correlation between CT numbers and tissue parameters needed for Monte Carlo simulations of clinical dose distributions. Phys. Med. Biol. **45**, 459–478 (2000)
4. B. Schaffner, E. Pedroni, The precision of proton range calculations in proton radiotherapy treatment planning: experimental verification of the relation between CT-HU and proton stopping power. Phys. Med. Biol. **43**, 1579–1592 (1998)
5. O. Jäkel, G.H. Hartmann, C.P. Karger, et al., Quality assurance for a treatment planning system in scanned ion beam therapy. Med. Phys. **27**,1588–1600 (2000)
6. E. Rietzel, D. Schardt, T. Haberer, Range accuracy in carbon ion treatment planning based on CT-calibration with real tissue samples. Radiat. Oncol. **2**, 14 (2007)
7. H. Wertz, O. Jäkel, Influence of iodine contrast agent on the range of ion beams for radiotherapy. Med. Phys. **31**, 767–773 (2004)
8. O. Jäkel, Ranges of ions in metals for use in particle treatment planning. Phys. Med. Biol. **51**, N173–N177 (2006)
9. O. Jäkel, P. Reiss, The influence of metal artefacts on the range of ion beams. Phys. Med. Biol. **52**, 635–644 (2007)
10. O. Jäkel, M. Krämer, C.P. Karger, et al., Treatment planning for heavy ion radiotherapy: clinical implementation and application. Phys. Med. Biol. **46**, 1101–1116 (2001)
11. A.J. Lomax, Intensity modulated proton therapy and its sensitivity to treatment uncertainties 1: the potential effects of calculational uncertainties. Phys. Med. Biol. **53**, 1027–1042 (2008)
12. G. Cabal, S. Luan, O. Jäkel, An algorithm for optimizing beam angle configuration in particle therapy, Proceedings of 48th Meeting of the Particle Therapy Co-Operative Group (PTCOG), Heidelberg, Germany, 28 Sep–3 Oct 2009, German Medical Science Publishing House, Düsseldorf, 2009. http://www.egms.de/static/en/meetings/ptcog2009/09ptcog033.shtml. Accessed 21 Oct 2010
13. G. Cabal, S. Luan, O. Jäkel, A beam angle selection algorithm for particle therapy. Presented at 52nd Annual Meeting of American Association of Physicists in Medicine (AAPM), Philadelphia, PA, 18–22 Juy 2010
14. S. Speer, J. Karg, M. Schmidt, R.G. Müller, Beam Angle Optimization in Particle Therapy with OPTiC. Proceedings of IFMBE World Congress Munich, Germany, 7–12 Sept 2009, pp. 562–565

15. M. Bangert, U. Oelfke, A novel framework for beam angle optimization in intensity modulated hadron therapy, Proceedings of 48th Meeting of the Particle Therapy Co-Operative Group (PTCOG), Heidelberg, Germany, 28Sep–3 Oct 2009 (German Medical Science Publishing House, Düsseldorf, 2009). http://www.egms.de/static/en/meetings/ptcog2009/09ptcog015.shtml. Accessed 21 Oct 2010
16. International Commission on Radiation Units and Measurements. Report 83: Prescribing, Recording, and Reporting Photon-Beam Intensity-Modulated Radiation Therapy (IMRT). J. ICRU **10**, 1 (2010)
17. G. Cabal, O. Jäkel, Towards a novel approach for PTV definition in particle therapy. Presented at 49th Annual Meeting of the Particle Therapy Co-operative Group (PTCOG) Gunma, Japan, 20–22 May 2010
18. J.R. Alonso, Review of Ion Beam Therapy: Present and Future. Report of Lawrence Berkeley National Laboratory, LBNL – 45137, 2000. http://www.escholarship.org/uc/item/3nm7286j?display=all#page-1. Accessed 21 Oct 2010
19. O. Jäkel, C.P. Karger, J. Debus, The future of heavy ion radiotherapy. Med. Phys. **35**, 5653–5663 (2008)
20. O. Jäkel, Medical physics aspects of particle therapy. Radiat. Prot. Dosim. **137**, 156–166 (2009)
21. M. Endo, H. Koyama-Ito, S. Minohara, et al., HIPLAN – a heavy ion treatment planning system at HIMAC. J. Jpn. Soc. Ther. Radiol. Oncol. **8**, 231–238 (1996)
22. P.L. Petti, Evaluation of a pencil-beam dose calculation technique for charged particle radiotherapy. Int. J. Radiat. Oncol. Biol. Phys. **35**, 1049–1057 (1996)
23. P.L. Petti, Differential-pencil-beam dose calculations for charged particles. Med. Phys. **19**, 137–149 (1992)
24. M. Krämer, O. Jäkel, T. Haberer, et al., Treatment planning for heavy-ion radiotherapy: physical beam model and dose optimization. Phys. Med. Biol. **45**, 3299–3317 (2000)
25. A.K. Carlsson, P. Andreo, A. Brahme, Monte Carlo and analytical calculation of proton pencil beams for computerized treatment plan optimization. Phys. Med. Biol. **42**, 1033–1053 (1997)
26. L. Hong, M. Goitein, M. Bucciolini, et al., A pencil beam algorithm for proton dose calculations. Phys. Med. Biol. **41**, 1305–1330 (1996)
27. T. Inaniwa, T. Furukawa, A. Nagano, et al., Field-size effect of physical doses in carbon-ion scanning using range shifter plates. Med. Phys. **36**, 2889–2897 (2009)
28. T. Inaniwa, T. Furukawa, T. Tomitani, et al., Optimization for fast-scanning irradiation in particle therapy. Med. Phys. **34**, 3302–3311 (2007)
29. U. Weber, G. Kraft, Comparison of carbon ions versus protons. Cancer J. **15**, 325–332 (2009)
30. N. Kanematsu, M. Komori, S. Yonai, et al., Dynamic splitting of Gaussian pencil beams in heterogeneity-correction algorithms for radiotherapy with heavy charged particles. Phys. Med. Biol. **54**, 2015–2027 (2009)
31. N. Kanematsu, Semi-empirical formulation of multiple scattering for the Gaussian beam model of heavy charged particles stopping in tissue-like matter. Phys. Med. Biol. **54**, N67–N73 (2009)
32. A. Mairani, S. Brons, F. Cerutti, et al., The FLUKA Monte Carlo code coupled with the local effect model for biological calculations in carbon ion therapy. Phys. Med. Biol. **55**, 4273–4289 (2010)
33. K. Parodi, A. Mairani, S. Brons, et al., The influence of lateral beam profile modifications in scanned proton and carbon ion therapy: a Monte Carlo study. Phys. Med. Biol. **55**, 5169–5187 (2010)
34. F. Sommerer, K. Parodi, A. Ferrari, et al., Investigating the accuracy of the FLUKA code for transport of therapeutic ion beams in matter. Phys. Med. Biol. **51**, 4385–4398 (2006)
35. K. Gunzert-Marx, D. Schardt, R.S. Simon, The fast neutron component in treatment irradiations with 12C beam. Radiother. Oncol. **73**(Suppl 2), S92–S95 (2004)
36. K. Gunzert-Marx, D. Schardt, R.S. Simon, Fast neutrons produced by nuclear fragmentation in treatment irradiations with 12C beam. Radiat. Prot. Dosim. **110**, 595–600 (2004)
37. T. Kanai, M. Endo, S. Minohara, et al., Biophysical characteristics of HIMAC clinical irradiation system for heavy-ion radiation therapy. Int. J. Radiat. Oncol. Biol. Phys. **44**, 201–210 (1999)

38. N. Kanematsu, M. Torikoshi, M. Mizota, et al., Secondary range shifting with range compensator for reduction of beam data library in heavy-ion radiotherapy. Med. Phys. **34**, 1907–1910 (2007)
39. O. Jäkel, D. Schulz-Ertner, J. Debus, Specifying carbon ion doses for radiotherapy: the Heidelberg approach. J. Radiat. Res. (Tokyo) **48**, A87–A95 (2007)
40. M. Krämer, M. Scholz, Rapid calculation of biological effects in ion radiotherapy. Phys. Med. Biol. **51**, 1959–1970 (2006)
41. M. Ellerbrock, O. Jäkel, M. Krämer, et al., Clinical implementation of multiple field dose optimization in heavy ion treatment planning. Radiother. Oncol. **81**, S358 (2006)
42. M. Ellerbrock, O. Jäkel, M. Krämer, et al., Clinical implementation of intensity modulated heavy ion therapy. Radiother. Oncol. **84**, 129 (2007)
43. D. Pflugfelder, J.J. Wilkens, U. Oelfke, Worst case optimization: a method to account for uncertainties in the optimization of intensity modulated proton therapy. Phys. Med. Biol. **53**, 1689–1700 (2008)
44. D. Schulz-Ertner, A. Nikoghosyan, B. Didinger, et al., Therapy strategies for locally advanced adenoid cystic carcinomas using modern radiation therapy techniques. Cancer **104**, 338–344 (2005)
45. International Atomic Energy Agency. *Commissioning and Quality Assurance of Computerized Planning Systems for Radiation Treatment of Cancer*, IAEA Tech Rep Ser 430 (IAEA, Vienna, 2004). http://www-pub.iaea.org/MTCD/publications/PDF/TRS430_web.pdf. Accessed 21 Oct 2010
46. International Atomic Energy Agency. *Specification and Acceptance Testing of Radiotherapy Treatment Planning Systems*. IAEA-TECDOC-1540 (IAEA, Vienna, 2007)
47. International Atomic Energy Agency. *Commissioning of Radiotherapy Treatment Planning Systems – Testing for Typical External Beam Treatment Techniques*. IAEA-TECDOC-1583 (IAEA, Vienna, 2008)
48. B.A. Fraass, QA issues for computer-controlled treatment delivery: this is not your old R/V system any more! Int. J. Radiat. Oncol. Biol. Phys. **71**, S98–S102 (2008)
49. D.J. Van, R.B. Barnett, J.E. Cygler, et al., Commissioning and quality assurance of treatment planning computers. Int. J. Radiat. Oncol. Biol. Phys. **26**, 261–273 (1993)
50. J. Jacky, C.P. White, Testing a 3-D radiation therapy planning program. Int. J. Radiat. Oncol. Biol. Phys. **18**, 253–261 (1990)
51. A. Gemmel, B. Hasch, M. Ellerbrock, et al., Biological dose optimization with multiple ion fields. Phys. Med. Biol. **53**, 6991–7012 (2008)
52. A. Mitaroff, W. Kraft-Weyrather, O.B. Geiss, et al., Biological verification of heavy ion treatment planning. Radiat. Environ. Biophys. **37**, 47–51 (1998)
53. C.P. Karger, O. Jäkel, G.H. Hartmann, A system for three-dimensional dosimetric verification of treatment plans in intensity-modulated radiotherapy with heavy ions. Med. Phys. **26**, 2125–2132 (1999)
54. M. Martisikova, O. Jäkel, Dosimetric properties of Gafchromic(R) EBT films in medical carbon ion beams. Phys. Med. Biol. **55**, 5557–5567 (2010)
55. B. Spielberger, M. Krämer, G. Kraft, Three-dimensional dose verification with x-ray films in conformal carbon ion therapy. Phys. Med. Biol. **48**, 497–505 (2003)

Chapter 31
Online Irradiation Control by Means of PET

Fine Fiedler, Daniela Kunath, Marlen Priegnitz, and Wolfgang Enghardt

Abstract Positron emission tomography (PET) is a dedicated tool for quality assurance in IBT. By measuring the spatial distribution of positron emitters generated via nuclear interactions between projectiles and atomic nuclei of the tissue during the therapeutic irradiation, conclusions on the accuracy of the dose localization can be drawn. In the following, the physical background as well as the technical realization of PET is depicted. Furthermore, current PET installations for quality assurance of proton and IBT are presented.

31.1 Introduction

Despite its great potential for tumor-conform irradiation, ion beam therapy (IBT) bears the risk that, under certain conditions, the applied dose can severely deviate from the planned distribution. Since the depth profile of the dose strongly depends on the particle range, and thus, on the types of irradiated tissues, modifications in the tissue density along the ion beam path may change the dose distribution considerably. Minor errors in the particle range can already lead to severe underdosing in the tumor volume or to an excessive dose in neighboring organs at risk. Such unpredictable range deviations may especially occur during fractionated therapy due to slight variations in patient positioning or local anatomical changes since the planning CT was performed. Therefore, a method for real-time verification of the dose delivery is highly desirable. Positron emission tomography (PET) complies with the requirements for such a verification method and can serve as a dedicated tool for beam-delivery-independent dose monitoring and quality assurance in IBT.

F. Fiedler (✉)
Helmholtz-Zentrum Dresden-Rossendorf, Institute of Radiation Physics, PO Box 510119, 01314 Dresden, Germany
e-mail: f.fiedler@hzdr.de

U. Linz (ed.), *Ion Beam Therapy*, Biological and Medical Physics, Biomedical Engineering, DOI 10.1007/978-3-642-21414-1_31,

31.2 Physical Background

PET is based on the radioactive decay of positron emitters followed by the annihilation of the positrons with electrons of the tissue. The two resulting collinear annihilation photons with an energy of 511 keV each can be detected, and by using tomographic techniques the spatial positron emitter distribution can be reconstructed. For a comprehensive description, see, e.g., Valk et al. [1].

For PET-based verification of the deposited dose distribution in IBT, various approaches have been chosen. At the Heavy Ion Medical Accelerator (HIMAC) in Chiba, Japan, beams of positron emitting ^{11}C and ^{10}C ions are used [2, 3]. These nuclides are produced via nuclear fragmentation of ^{12}C projectiles. Their production rates are only about 0.1% of the primary beam current. To produce the beam intensity of approx. 10^8 ions s^{-1} required for carbon ion therapy, a primary ^{12}C-beam current of approx. 10^{11} ions s^{-1} is necessary. This requires expensive measures for shielding and absorption of these high-intensity beams. The mean activity density reached with a therapeutic ^{11}C beam in the irradiated volume is comparable to that of PET tracer imaging ($10^3 - 10^5$ Bq Gy^{-1} cm^{-3}).

An alternative to a treatment beam of positron emitting ions is a low-intensity radioactive probing beam for dose verification prior to the therapeutic irradiation with a stable ion beam. This technique was pioneered at the former heavy ion therapy unit at the Lawrence Berkeley Laboratory (LBL), USA [4], and is applied at the HIMAC as well [5].

A more efficient way, is to measure the positron-emitting nuclides produced as a byproduct of each therapeutic irradiation with stable ion beams via nuclear reactions – predominantly peripheral collisions – between the ions of a stable therapeutic beam and the nuclei of the irradiated tissue (also called autoactivation). For example, the predominant nuclei of the tissue, ^{16}O and ^{12}C, can fragment into the positron emitting target fragments ^{15}O, ^{11}C, and ^{10}C. Additionally, positron emitters can emerge as projectile fragments from the delivered ions if their atomic number is greater than 5.

Figure 31.1 shows schematically a nuclear fragmentation reaction ^{12}C atom of the beam and an ^{16}O resulting from the collision of a atom of the tissue. The positron emitters ^{15}O and ^{11}C are produced as target and projectile fragments, respectively. Fig. 31.2 displays the positron emitter production from the collision of protons (^{1}H) as projectiles with oxygen atoms of the tissue. This latter reaction produces only target fragments, e.g., ^{15}O, since the proton does not disintegrate via nuclear reactions.

Table 31.1 compiles reactions of carbon and proton projectiles with the most abundant atoms of human tissue leading to the most relevant positron emitters for online PET irradiation control (^{11}C with half-life $T_{1/2} = 20.4$ min, ^{10}C with $T_{1/2} = 19.2$ s, ^{15}O with $T_{1/2} = 122$ s, and ^{13}N with $T_{1/2} = 9.96$ min).

The depth distribution of the positron emitter-induced activity (also referred to as β^+-activity) depends strongly on the type of the projectile. For projectiles which can disintegrate into positron emitters, two components in the activity depth distribution

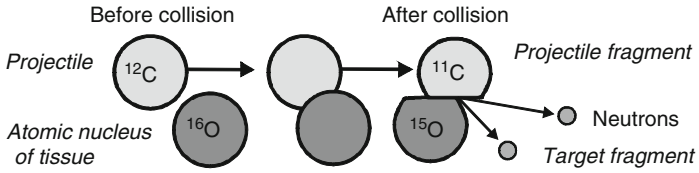

Fig. 31.1 Schematic illustration of the $^{16}O(^{12}C, ^{11}C\ 2n)^{15}O$ reaction. A ^{12}C projectile collides peripherally with an ^{16}O atom of the tissue. Both nuclides may lose a neutron and disintegrate into the projectile fragment ^{11}C and the target fragment ^{15}O, respectively

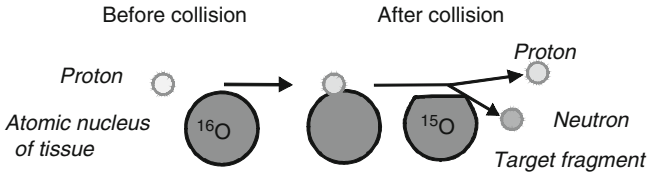

Fig. 31.2 Schematic illustration of the $^{16}O\,(p,\ 2n)^{15}O$ reaction. A proton projectile collides peripherally with an ^{16}O atom of the tissue. The target atom loses a neutron and disintegrates into the positron emitting target fragment ^{15}O

Table 31.1 Partial cross sections σ of the reactions of ^{12}C and proton beams with the most abundant nuclei of human tissue

Target atom	Positron emitting fragment	Projectile ^{12}C			Projectile ^{1}H		
		σ (mb)	$E(A\text{MeV})^a$	Reference	σ (mb)	E(MeV)	Reference
^{12}C	^{11}C	55.97 ± 4.06	250	[6]	45 ± 2	150	[7]
	^{10}C	5.33 ± 0.81	250	[6]	2.6 ± 0.3	155	[8]
^{16}O	^{15}O	28.3 ± 0.2	290	[9]	38 ± 4	155	[8]
	^{11}C	16.3 ± 0.2	290	[9]	11 ± 1	155	[8]
	^{10}C	1.65 ± 0.02	290	[9]	1 ± 0.2	155	[8]
	^{13}N	6.09 ± 0.09	290	[9]	4.5 ± 1	155	[8]
^{14}N	^{13}N	13.3 ± 0.4	600	[10]	8.3 ± 0.5	155	[8]
	^{11}C	27.5 ± 0.4	600	[10]	15 ± 1	155	[8]
	^{10}C	2.1 ± 0.2	600	[10]	1.6 ± 0.3	155	[8]

[a] AMeV = MeV/nucleon

occur. A prominent activity maximum near the end of the range of the primary particles is superimposed onto a pedestal. Since the produced positron emitters are predominantly a result of peripheral collisions with small momentum transfer, the target fragments remain at rest after the collision, forming this flat pedestal in the activity distribution, which extends over the whole path of the projectiles except the last few millimeters, where the kinetic energy of the projectiles is below the reaction threshold. The observed activity maximum originates from projectile fragments, which have the same velocity as the projectiles before the collision.

According to the Bethe–Bloch [11] equation, the range R of these fragments is proportional to

$$R(A, Z) \sim A/Z^2,$$

where A is the mass number and Z the atomic number of the projectile. As a result, the position of the activity maximum depends on the projectile, the projectile fragment species, and the time of the activity measurement. For activity measurements during the irradiation, projectile fragments with short half-lives (e.g., ^{10}C) dominate the activity maximum and define its position, whereas it is shifted to the range of positron emitters with longer half-lives when the measurements start several minutes after the irradiation.

Figure 31.3 shows the measured activity distribution in a polymethyl methacrylate (PMMA, $[CH_2C(CH_3)COOCH_3]_n$) target induced by different types

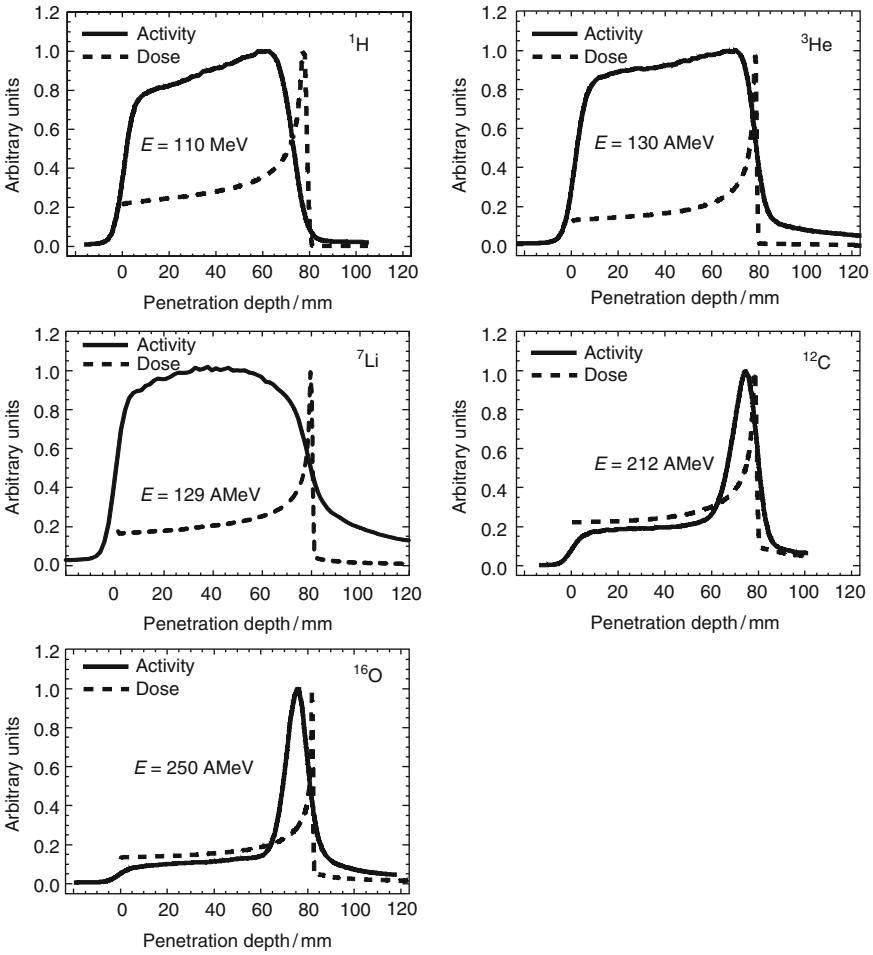

Fig. 31.3 Measured positron emitter activity distribution and irradiation dose distribution in a PMMA target irradiated with protons (^{1}H), ^{3}He, ^{7}Li, ^{12}C, and ^{16}O ions, respectively. The energy of the impinging ions was chosen to result in the same particle range of approx. 80 mm for each projectile. AMeV corresponds to MeV/nucleon

Table 31.2 Mean dose-related activity density α for different therapy-relevant ions impinging onto a PMMA target [12]

Therapy beam	^{1}H	^{3}He	^{7}Li	^{12}C	^{16}O
α (Bq Gy^{-1} cm^{-3})	6,600 ± 2,100	5,300 ± 1,000	2,500 ± 1,500	1,600 ± 510	1,030 ± 130

of monoenergetic ion beams (^{1}H, ^{3}He, ^{7}Li, ^{12}C, ^{16}O) with a range of approx. 80 mm. For carbon and oxygen beams, the pronounced maximum caused by projectile fragments is clearly visible, whereas the other activity distributions only show the flat component of the target fragments. As mentioned above, the lighter projectiles do not disintegrate into positron-emitting projectile fragments. In addition, Fig. 31.3 displays the dose distribution resulting from the irradiation. Both distributions, irradiation dose and radioactivity distribution, cannot be compared directly as they result from different physical processes. The irradiation dose deposition is a product of electron–ion interactions, whereas the radioactivity production is a result of nucleus–ion interactions. Accordingly, the exact correlation between deposited irradiation dose and generated positron emitter activity has to be determined for a correct analysis of the resulting PET images.

Experimental irradiation of PMMA targets with different beams and measurement of the induced positron emitter activity at the in-beam PET scanner at GSI Helmholtzzentrum für Schwerionenforschung (short GSI), Darmstadt, Germany, revealed a rather low mean activity density. Typical experimental values [12] are summarized in Table 31.2.

31.3 Technology and Implementation

The detection principle for PET-based radiation therapy control is similar to diagnostic PET in nuclear medicine [13]. However, the technical implementation differs considerably. For online therapy control, the PET scanner needs to be integrated into the treatment site. Other than in nuclear medicine, a full-ring PET detector is not feasible. Patient positioning and handling as well as protection of the scanner from damage by the therapeutic beam favor a technical solution as installed at the former experimental carbon ion therapy site at the GSI in Darmstadt [14].

It comprises a double-head system based on conventional PET components (cf. Fig. 31.4). The aperture between both detector heads allows beam entrance and exit of the secondary particles as well as free access of the medical staff to the patient. Furthermore, the detectors can be rotated around the central beam to provide monitoring also for patients in sitting position [15].

The two large-area (42 × 21 cm^2) detector heads were built from components of an ECAT EXACT PET scanner (CTI PET Systems Inc., Knoxville, TN). Each head consists of 8 × 4 position-sensitive scintillation block detectors of bismuth germanate (BGO). The two detector heads are operated in coincidence, resulting in 2,048^2 lines of response within the field of view of the camera. Data acquisition is

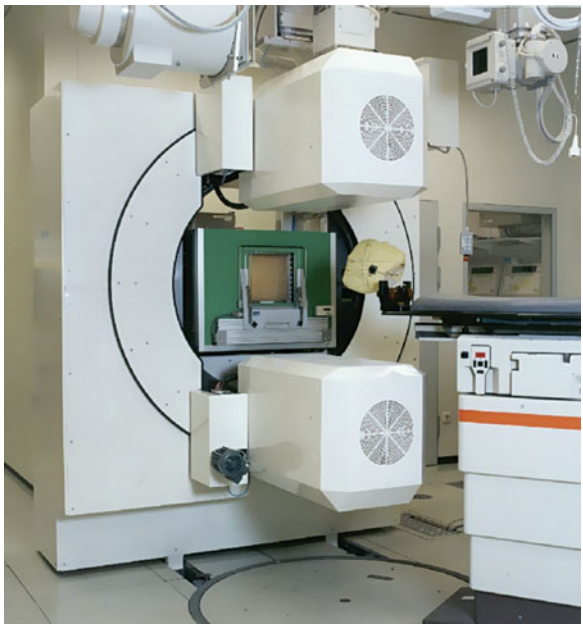

Fig. 31.4 The double-head positron camera at the GSI treatment site. The horizontal carbon ion beam leaves the beam pipe through a $20 \times 20\,\mathrm{cm}^2$ window visible in the center of the picture. To provide sufficient space for patient positioning, the PET scanner can be moved parallel to the beam between the measuring position (displayed) and the parking position [14]

based upon the standard solution of the manufacturer with modifications, required for the in-beam application. For valid events, i.e., prompt and delayed (by 128 ns) coincidences within 12-ns wide time windows, the identification of the fired crystals is transmitted from the coincidence processor to the data acquisition station. During the off-line tomographic reconstruction only those events are taken into account, which are registered in the periods between the beam pulses. Coincidences being acquired during the beam pulses are massively corrupted by random events caused by the γ-ray background from projectile-induced nuclear reactions [16]. Therefore, each data word is completed by the information on the synchrotron beam status (extraction on or off) which is derived from the output of an ionization chamber which the beam passes before it reaches the patient. Usually, the data are stored in list mode, where a time tag is inserted into the data stream every 10 ms. This allows a flexible setting of time frames for reconstruction, since the target activation during dose delivery by raster scanning is a dynamic process that has to be resolved in some critical therapeutic situations. For data evaluation, the beam energy, intensity, and diameter of each beam pulse are needed. Therefore, the accelerator control unit is connected with the PET data acquisition and these parameters are recorded. The PET data acquisition is controlled by a dedicated workstation, or alternatively during the patient irradiation from the treatment control console [14].

Shakirin et al. [17] evaluated three concepts for PET monitoring in IBT according to image quality criteria, integration costs and their influence on irradiation workflow.

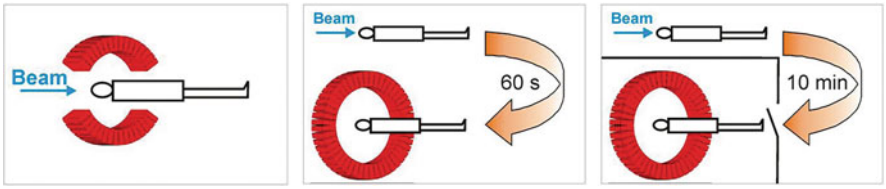

Fig. 31.5 The three different scenarios for PET monitoring in IBT. *Left*: In-beam PET; the data are acquired during the irradiation. *Middle*: In-room PET; the PET scan is taken very shortly after the irradiation by a conventional PET/CT scanner installed in close vicinity to the treatment site. *Right*: Off-beam PET; the measurement is performed by a PET/CT in a separate room at least 10 min after irradiation of the last field

The in-beam PET concept relies on a measurement performed simultaneously with the irradiation. A double-head PET scanner with different detector arrangements is fully integrated into the treatment site.

In-room PET applies a conventional PET/CT scanner placed very close to the irradiation site inside the treatment room.

An off-beam PET scenario means measuring the remaining activity after 10–30 min in a stand-alone PET/CT (cf. Fig. 31.5) in a separate room.

The most valuable data are produced by an in-beam PET scanner, because data are taken simultaneously with the therapeutic irradiation. These data are only marginally corrupted by metabolic washout processes and it is also possible to measure the short-lived isotopes. Therefore, the image quality is highest. However, the image quality suffers from the limited angle acceptance of the double-head geometry of this scanner type. For clinical routine, in-beam PET would require the development of a new scanner, possibly with different detector arrangements [18, 19], including sophisticated mechanical movement, data acquisition and processing. As a consequence, the installation costs of such a scanner are high, even if components of commercially available PET scanners could be used and adapted. In combination with time-of-flight measurements, real-time in-vivo dosimetry would be feasible.

For off-line PET, a conventional PET scanner can be used. Specific software for data evaluation has to be developed, though, and the image quality is compromised due to low measurement statistics. Short-lived positron emitters decay during the transport time from the treatment room to the scanner and are no longer available for the PET analysis. Therefore, long measurement times are required resulting in highly corrupted images due to washout processes. The application of off-line PET is also limited to certain irradiation scenarios. It is, e.g., hardly possible to measure the ion range when two opposing fields are applied, and, finally, the correlation of the PET image to the anatomy requires an additional CT scan [17].

A compromise between the disadvantages of an off-beam scanner and the high costs of an in-beam PET scanner may be an in-room system. In combination with robot-assisted positioning of the patient, a conventional full-ring scanner can be efficiently operated in the treatment cave. Accepting 50% reduction in counting

statistics together with the elimination of limited angle artifacts by a closed-ring PET scanner, in-room PET is superior to in-beam PET in terms of installation costs. Without substantial modifications a commercially available scanner can be integrated into the treatment room. Nevertheless, the measurement time has to be extended, causing increased metabolic washout. Additionally, for some clinical scenarios such as probing irradiation in hypofractionation, where a low-dose probing beam is applied for range verification prior to the actual therapeutic irradiation, in-room PET is hardly feasible.

31.4 Current PET Installations

As mentioned earlier, the technology of in-beam positron emission imaging for quality assurance in IBT was pioneered at the LBL [4]. The first instrument for imaging was a one-dimensional camera constructed in 1979 with 48 NaI(Tl) detectors in a geometric arrangement, called PEBA-I (Positron Emission Beam Analyzer) ([20, 21]) and references therein). This imaging device was used until 1982, followed by a high-accuracy and high-sensitivity two-dimensional camera, PEBA-II [21]. This camera consisted of two opposing heads of detectors with 64 BGO crystals each, resulting in a size of the detector heads of $10 \times 10\,\mathrm{cm}^2$. A substantial number of measurements with human phantoms and animals were performed, predominantly with radioactive ^{19}Ne beams followed by measurements with a few patients treated with the radioactive beam technique [4]. But this imaging method was not translated into clinical routine at the LBL.

Further experiments and investigations on the feasibility of PET to verify IBT were reported by Bennett et al. [22], Vynckier et al. [23], Paans et al. [24], Oelfke et al. [25], and Litzenberg et al. [26], to name but a few. To the best of our knowledge, none of these approaches has been implemented.

31.4.1 GSI Helmholtzzentrum für Schwerionenforschung, Darmstadt, Germany

Within the framework of the German heavy-ion therapy pilot project (1997–2008) at GSI, more than 440 patients were treated with stable beams of ^{12}C and nearly all irradiation fractions were monitored by in-beam PET measuring the autoactivation of the tissue [27]. As shown in Fig. 31.4, the PET scanner at GSI is completely integrated into the treatment unit. It consists of two detector heads ($42 \times 21\,\mathrm{cm}^2$) with position-sensitive detector blocks of BGO [14]. The positron emitter-induced activity was measured during the irradiation of the patient and continued on for approx. 40 s after the treatment [28]. It was compared with a predicted distribution calculated on the basis of the treatment plan. This approach permitted to verify

the field position in 3D and to quantify local dose deviations with respect to the treatment plan [29].

Typical treatment plans consisted of two opposing fields. Since the remaining activity of the first irradiated field corrupts the measurements in the second field only the PET measurements of the first field were evaluated on each day. By changing the order of the fields from day to day, data from both fields were obtained during the 20 days of a treatment period.

31.4.2 HIMAC, Chiba, Japan

At HIMAC, Chiba, a positron camera consisting of a pair of Anger-type scintillation detectors was developed for in-situ range verification in IBT. It is integrated into the irradiation site. Each detector is equipped with an NaI(Tl) crystal with a diameter of 60 cm. The positron activity is measured while the radioactive probing beam of positron emitting ions is implanted. The actual treatment with either a radioactive or stable ion beam follows immediately [5, 30]. In addition, volumetric PET measurements can be performed with a conventional PET scanner installed near the irradiation site after the treatment [3]. Various experiments with different radioactive beams have been performed and it seems that ^{10}C suits best as a probing beam for subsequent irradiation with ^{12}C. Furthermore, successful animal experiments with ^{10}C and ^{11}C were conducted in order to investigate the metabolic washout of implanted activity [31, 32]. Stable beams of ^{12}C and ^{16}O have been investigated in different settings using this camera [33]. Recently, an "Open PET" geometry was proposed consisting of two detector rings with a gap in between to allow for the passing of the ion beam [34,35]. But none of these positron activity imaging systems has been used in clinical routine, so far.

31.4.3 National Cancer Center Hospital East, Kashiwa, Japan

The National Cancer Center Hospital East (NCCHE) in Kashiwa has a beam online PET system (BOLPs) integrated in the irradiation site. It is mounted on a rotating gantry port, consists of two opposing detector heads of a planar positron imaging system with BGO scintillators and a field of view of $16.5 \times 16.7\,\text{cm}^2$ [36, 37]. In order to simulate and estimate the activity image acquired with the BOLPs, an experimental study with 20 patients was performed where the positron activity after treatment with protons was measured using a conventional PET-CT [38]. Recently, activity measurements using the BOLPs were performed for 48 patients irradiated with protons [37]. The measurement started directly after the therapeutic irradiation and took 200 s. The obtained activity images of every fraction were compared with the image from the first day of the therapeutic irradiation. Reduction of the tumor size or changes of the body shape could, thus, be detected.

31.4.4 Hyogo Ion Beam Medical Center, Tatsuno, Japan

Since 2001, the Hyogo Ion Beam Medical Center (HIBMC) has treated patients suffering from different cancers with proton or stable carbon ion beams. Accuracy of the irradiation is verified by measuring the positron activity distribution from autoactivation of the tissue with a commercial PET scanner (BGO detectors) several minutes after the treatment and comparing the result visually with the planned dose distribution [39, 40].

31.4.5 CATANA, Catania, Italia

At the CATANA beamline in Catania ocular pathologies are treated. They developed an in-beam PET prototype for therapy monitoring. This so-called DoPET system (dosimetry with a positron emission tomograph) consists of two small opposing planar heads – active area of about $5 \times 5\,\mathrm{cm}^2$ each – with lutetium yttrium orthosilicate (LYSO) detectors [41]. PET measurements directly after irradiation were performed on several homogeneous and inhomogeneous plastic phantoms [41, 42]. A larger clinical version of this in-beam PET system is now under construction.

31.4.6 University of Florida Proton Therapy Institute, Jacksonville, USA

At the PTI of the University of Florida a total of 50 PET/CT imaging studies were performed on ten patients with prostate cancer. Within 15 min after the daily proton therapy sessions, a PET image was taken using a conventional LYSO-based PET/CT. The acquisition time was 30 min. Patient-specific information on prostate motion and patient position variability was obtained by comparing the measured positron activity distribution with the planned beam path determined by implanted markers visible in the CT [43].

31.4.7 Massachusetts General Hospital, Boston, USA

In order to investigate the feasibility of off-line PET for routine proton treatment, numerous experiments with different phantoms irradiated with proton beams were performed at the Massachusetts General Hospital (MGH) in Boston [44]. These experiments were followed by a patient study including nine patients with different tumors treated with protons. Positron activity measurements were performed within

20 min after treatment for a period of 30 min using a commercial lutetium oxyorthosilicate (LSO)-based PET/CT scanner [45]. The measured PET images were compared with predicted distributions obtained from Monte-Carlo simulations and analytical calculations [46], respectively.

Furthermore, phantom measurements were carried out on a small moveable PET scanner on wheels to test whether it is feasible for in-room proton treatment verification [47].

31.5 Clinical Examples

With 440 patients and 12 years of in-beam PET experience, the GSI accumulated a wealth of information. The PET verifications served several prime purposes: to determine the range of the ions in vivo, to identify the lateral field position and to detect unexpected density modifications within the irradiated tissue. Figure 31.6 is an example for the anatomical agreement of the planned ion dose and the measured positron activity.

A dedicated software tool was developed [29] to quantify local dose deviations if discrepancies between the measured and predicted positron activity occur. It allows to interactively manipulate a CT, i.e., to change Hounsfield units in well-defined regions and to translate or rotate a CT to test the observer's assumption on the origin of the deviation. If fast recalculations of the β^+-activity confirm the assumed type of deviation, a dose recalculation on the basis of the modified CT can be performed to quantify the difference to the prescribed dose (cf. Fig. 31.7).

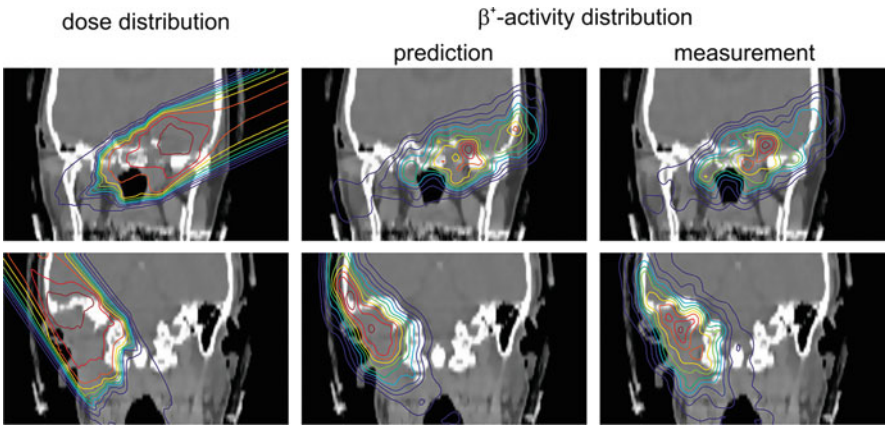

Fig. 31.6 Two examples of the clinical implementation of in-beam PET. *Left column*: Planned dose distributions superimposed onto the patient CT. *Middle column*: Predicted β^+-activity distributions from a Monte Carlo simulation. *Right column*: Measured β^+-activity distributions. The isodose and isoactivity lines are decoded in rainbow colors and denote levels of 5% (*blue*), 15%, ... 95% (*red*) of the maxima

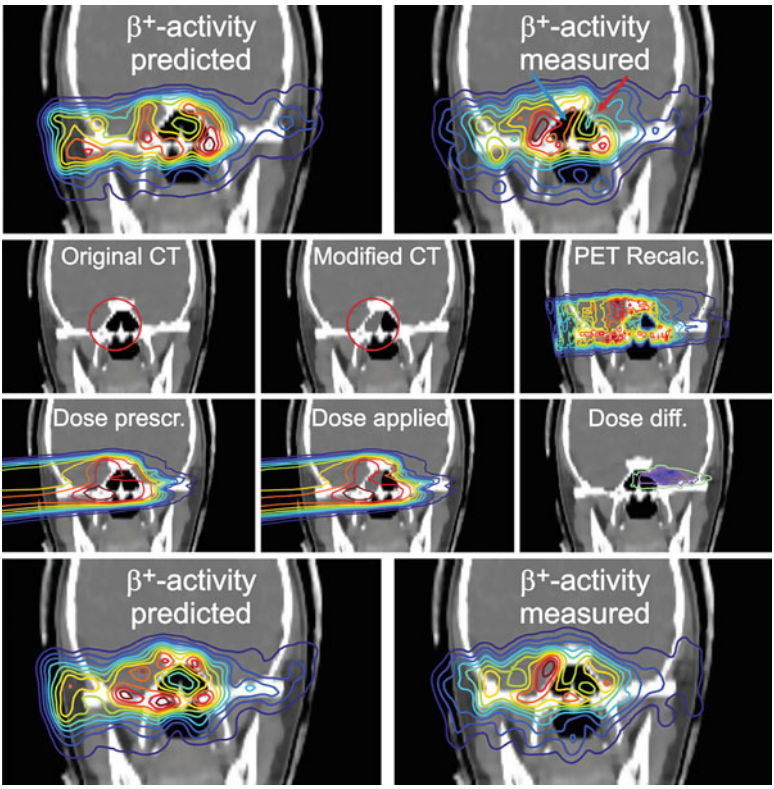

Fig. 31.7 Anatomical changes, their effects on dose and the approximate quantification of dose deviations from the treatment plan. *First row*: Comparison of predicted and measured β^+-activity. The *blue arrow* indicates a dose deposition in the nasal cavity, the *red arrow* shows missing dose at the distal edge of the irradiation field. *Second row*: on the basis of the assumption of a mucus-filled cavity the planning CT was interactively modified. A fast recalculation of the positron activity confirmed this hypothesis. *Third row*: The difference between the prescribed dose and the dose actually deposited in the tissue recalculated on the basis of the modified CT can be quantified. The maximum deviation is −214 mGy, the maximum dose in this field is 525 mGy. *Fourth row*: Comparison between predicted and measured β^+-activity 3 days later, after administration of a mucolytic. The nasal cavity is no longer stuffed, the dose is applied as planned

In-beam PET does not only detect anatomical changes but also inaccuracies in patient positioning. An example is given in Fig. 31.8.

During therapeutic treatment, random modifications as for example anatomical changes and inaccuracies in patient positioning occur in approximately 10–15% of the measurements. Besides this, in-beam PET is also capable of detecting systematic errors in the treatment planning procedure. The basis for charged particle treatment planning is the correlation between ion range and Hounsfield number. Uncertainties in this calibration result in particle range deviations and consequently in incorrect dose applications. This is of utmost relevance since ions have to be reliably stopped

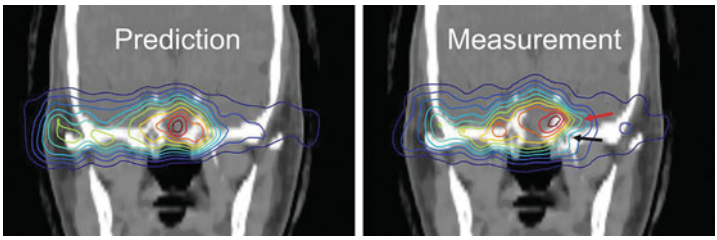

Fig. 31.8 Prediction of β^+-activity vs. in-beam PET measurement. The measurement indicated a slight rotation of the patient counterclockwise. The *red arrow* indicates an area of unwanted high activity in the base of the skull, the *black arrow* marks a lack in activity. Both findings indicate a density change in the beam path

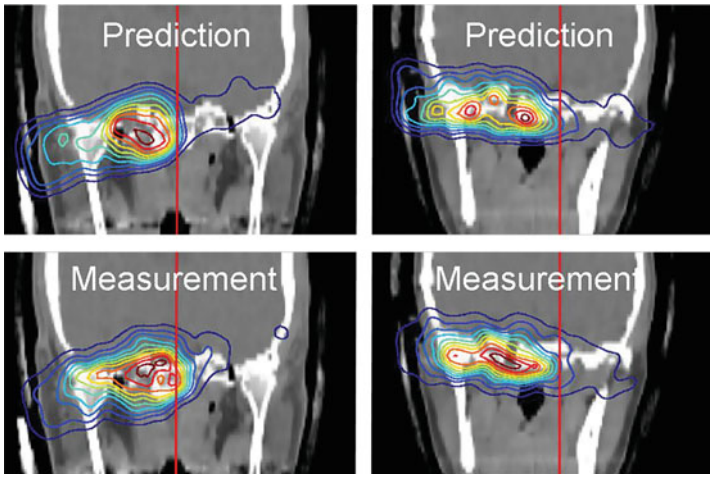

Fig. 31.9 Comparison of measured and predicted positron activity. *Left*: Overrange of several millimeters arising from an inaccurate Hounsfield unit–ion range correlation. *Right*: Improvement of correspondence between the predicted and measured particle ranges after precision measurements of the ion ranges as a function of the Hounsfield unit

before reaching organs at risk. For the very first patients treated at the GSI ion therapy site, deviations between predicted and measured positron activity were detected. After this observation, precision measurements led to a refining of the Hounsfield unit-range calibration and to modifications in the physical beam model and the algorithm of the treatment planning program [48]. Subsequently, the measured ranges were in agreement with the prediction (cf. Fig. 31.9) [49, 50].

The large pool of clinical data obtained at the GSI therapy unit was used to determine the accuracy of the in-beam PET [51]. A sensitivity of 91 ± 3% and a specificity of 96 ± 2% were calculated for overrange detection with a confidence interval of 95%. Curtailed ranges could be identified with similar accuracy (sensitivity 92 ± 3%; specificity 96 ± 2%) [52].

Semiautomatic approaches to support the analysis are under development and are evaluated with real measured data. First results yield a sensitivity of $64 \pm 8\%$ for the detection of a range modification of any sign at the specificity level of the manual analysis. By changing the classification threshold, it is possible to achieve a higher specificity of $94 \pm 8\%$ while keeping the sensitivity at $46 \pm 6\%$ [51].

Despite the fact that in-beam PET has proven to be a valuable tool to improve the quality of IBT, it is up to now not possible to deduce the dose directly from the data measured during patient irradiation, i.e., from the β^+-activity distribution. The reason for this constraint is the inability to acquire quantitative data. One particular effect is the blurring as well as the reduction of the measured activity distribution due to washout. A biological half-life of 170.89 ± 8.6 s was estimated. The effective half-life, however, was found to be highly dose dependent [28]. In the high-dose area it was longer, probably due to reduced perfusion of the tumor. Even an indication for tumor response was observed when the dependence of the effective half-life was correlated to the number of fractions delivered. Generally, the effective half-life seems to decrease during the treatment. This effect was even more pronounced in the high-dose region. The most likely explanation for this observation might be an increase in tumor perfusion with treatment time [28].

Further investigations on metabolic washout of positron emitters deduced from animal experiments with radioactive ^{10}C and ^{11}C beams were reported by Tomitani et al. [31] and Mizuno et al. [32].

The image quality of in-beam PET is further limited by the spatial layout of the therapeutic site. A full-ring PET scanner would impede motion capability of other treatment-related equipment. Therefore, an in-beam PET scanner has to be a limited-angle device. This hampers the image reconstruction, however, because signals from certain angles are missing. An attempt to overcome this issue turned out to cause artifacts and reduced resolution perpendicular to the opening of the ring [14]. In the meantime, simulations have shown that the time-of-flight (TOF) difference between the two opposing γ-rays provides shift-variant (fixed dual-head), artifact-free tomograms from in-beam PET for a time resolution $\tau \leq 200$ ps full width at half maximum (FWHM). This would not only allow a reconstruction in real-time but would also bring the in-beam PET method a step closer to full quantitative data [53].

Even though the half-lives of the positron emitters are only in the range of a couple of minutes, they are prohibitive for quantitative measurement. In case of multiple field irradiations, only the first field can be evaluated by in-beam PET. The following fields are corrupted by remaining activity from the previously irradiated portals.

Given these limitations, a new approach is under development. It makes use of the prompt γ-rays from nuclear reactions between projectiles of the therapeutic beam and atomic nuclei of the tissue. The novel technique, in-beam single-photon emission computed tomography (in-beam SPECT) has the potential to overcome the inherent sensitivity of in-beam PET to metabolic processes. Potentially useful radiation modalities are also light charged particles. Recently published experimental

investigations indicate that the distribution of single γ-rays reflect the range of the therapeutic ions [54]. Either a Compton camera or a collimated camera can be used to monitor the emitted photons [48].

References

1. P.E. Valk, D.L. Bailey, D.W. Townsend, M.N. Maisey (eds.), *Positron Emission Tomography* (Springer, London, 2003)
2. E. Urakabe, T. Kanai, M. Kanazawa, et al., Spot scanning using radioactive C-11 beams for heavy-ion radiotherapy. Jpn. J. Appl. Phys. **40**, 2540–2548 (2001)
3. M. Kanazawa, A. Kitagawa, S. Kouda, et al., Application of an RI-beam for cancer therapy: in-vivo verification of the ion-beam range by means of positron imaging. Nucl. Phys. A **701**, 244–252 (2002)
4. J. Llacer, Positron emission medical measurements with accelerated radioactive ion beams. Nucl. Sci. Appl. **3**, 111–131 (1988)
5. Y. Iseki, H. Mizuno, Y. Futami, et al., Positron camera for range verification of heavy-ion radiotherapy. Nucl. Instrum. Methods A **515**, 840–849 (2003)
6. J.M. Kidd, P.J. Lindstrom, H.J. Crawford, G. Woods, Fragmentation of carbon ions at 250 MeV/nucleon. Phys. Rev. C **37**, 2613–2623 (1988)
7. C. Brun, M. Lefort, X. Tarrago, Determination of proton beam intensities from 40 to 150 MeV. J. Phys. **23**, 371–376 (1962)
8. L. Valentin, G. Albouy, J.P. Cohen, M. Gusakow, Réactions induites par des protons de 155 MeV sur des noyaux légers. Phys. Lett. **7**, 163–164 (1963)
9. S. Momota, M. Notani, S. Ito, et al., Production of projectile-like fragments at intermediate energies. Nucl. Phys. A **701**, 150–155 (2002)
10. W.R. Webber, J.C. Kish, D.A. Schrier, Individual isotopic fragmentation cross sections of relativistic nuclei in hydrogen, helium, and carbon targets. Phys. Rev. C **41**, 547–565 (1990)
11. W.R. Leo, *Techniques for Nuclear and Particle Physics Experiments* (Springer, Berlin, 1987), pp. 21–32
12. M. Priegnitz, D. Möckel, K. Parodi, et al., In-beam PET measurement of $^{7}Li^{3+}$ irradiation induced β^{+}-activity. Phys. Med. Biol. **53**, 4443–4453 (2008)
13. D.L. Bailey, J.S. Karp, S. Surti, Physics and Instrumentation in PET, in *Positron Emission Tomography*, ed. by P.E. Valk, D.L. Bailey, D.W. Townsend, M.N. Maisey. (Springer, London, 2003), pp. 41–67
14. W. Enghardt, P. Crespo, F. Fiedler, et al., Charged hadron tumour therapy monitoring by means of PET. Nucl. Instrum. Methods A **525**, 284–288 (2004)
15. F. Fiedler, M. Sobiella, W. Enghardt, PET-CT Co-Registration for In-Beam PET. Proceedings, 2008 Nuclear Science Symposium, Medical Imaging Conference and 16th Room Temperature Semiconductor Detector Workshop, Dresden, Germany, 19–25 Oct 2008
16. K. Parodi, P. Crespo, H. Eickhoff, et al., Random coincidences during in-beam PET measurements at microbunched therapeutic ion beams. Nucl. Instrum. Methods A **545**, 446–458 (2005)
17. G. Shakirin, H. Braess, F. Fiedler, et al., Implementation and workflow for PET monitoring of therapeutic ion irradiation: a comparison of in-beam, in-room, and off-line techniques. Phys. Med. Biol. **56**, 1281 (2011)
18. G. Shakirin, System solution for in-beam positron emission tomography monitoring of radiation therapy. PhD Thesis (TU Dresden, Germany, TUD Press, 2009), ISBN: 978–3–941298–33–0
19. P. Crespo, G. Shakirin, W. Enghardt, On the detector arrangement for in-beam PET for hadron therapy monitoring. Phys. Med. Biol. **51**, 2143–2163 (2006)

20. J. Llacer, A. Chatterjee, H.C. Jackson, et al., An imaging instrument for positron emitting heavy ion beam injection. IEEE Trans. Nucl. Sci. **26**, 634–647 (1979)
21. J. Llacer, A. Chatterjee, E.L. Alpen, et al., Imaging by injection of accelerated radioactive particle beams. IEEE Trans. Med. Imaging **3**, 80–90 (1984)
22. G.W. Bennett, J.O. Archambeau, B.E. Archambeau, et al., Visualization and transport of positron emission from proton activation in vivo. Science **200**, 1151–1153 (1978)
23. S. Vynckier, S. Derreumaux, F. Richard, et al., Is it possible to verify directly a proton-treatment plan using positron emission tomography? Radiother. Oncol. **26**, 275–277 (1993)
24. A.M.J. Paans, J.M. Schippers, Proton therapy in combination with PET as monitor: A feasibility study. IEEE Trans. Nucl. Sci. **40**, 1041–1044 (1993)
25. U. Oelfke, G.K.Y. Lam, M.S. Atkins, Proton dose monitoring with PET: quantitative studies in Lucite. Phys. Med. Biol. **41**, 177–196 (1996)
26. D.W. Litzenberg, D.A. Roberts, M.Y. Lee, et al., On-line monitoring of radiotherapy beams: Experimental results with proton beams. Med. Phys. **26**, 992–1006 (1999)
27. D. Schardt, T. Elsässer, D. Schulz-Ertner, Heavy-ion tumor therapy: physical and radiobiological benefits. Rev. Mod. Phys. **82**, 383–425 (2010)
28. F. Fiedler, M. Sellesk, P. Crespo, et al., In-beam PET measurements of biological half-lives of ^{12}C irradiation induced β^+-activity. Acta Oncol. **47**, 1077–1086 (2008)
29. W. Enghardt, K. Parodi, P. Crespo, et al., Dose quantification from in-beam positron emission tomography. Radiother. Oncol. **73**(Suppl 2), S96–S98 (2004)
30. Y. Iseki, T. Kanai, M. Kanazawa, et al., Range verification system using positron emitting beams for heavy-ion radiotherapy. Phys. Med. Biol. **49**, 3179–3195 (2004)
31. T. Tomitani, J. Pawelke, M. Kanazawa, et al., Washout studies of ^{11}C in rabbit thigh muscle implanted by secondary beams of HIMAC. Phys. Med. Biol. **48**, 875–889 (2003)
32. H. Mizuno, T. Tomitani, M. Kanazawa, et al., Washout measurement of radioisotope implanted by radioactive beams in the rabbit. Phys. Med. Biol. **48**, 2269–2281 (2003)
33. T. Inaniwa, T. Kohno, T. Tomitani, S. Sato, Monitoring the irradiation field of ^{12}C and ^{16}O SOBP beams using positron emitters produced through projectile fragmentation reactions. Phys. Med. Biol. **53**, 529–542 (2008)
34. T. Yamaya, T. Inaniwa, E. Yoshida, et al., Simulation studies of a new "OpenPET" geometry based on a quad unit of detector rings. Phys. Med. Biol. **54**, 1223–1233 (2009)
35. E. Yoshida, T. Yamaya, K. Shibuya, et al., Simulation study on sensitivity and count rate characteristics of "OpenPET" geometries. IEEE Trans. Nucl. Sci. **57**, 111–116 (2010)
36. T. Nishio, T. Ogino, K. Nomua, H. Uchida, Dose-volume delivery guided proton therapy using beam on-line PET system. Med. Phys. **33**, 4190–4197 (2006)
37. T. Nishio, A. Miyatake, T. Ogino, et al., The development and clinical use of a beam on-line PET system mounted on a rotating gantry port in proton therapy. Int. J. Radiat. Oncol. Biol. Phys. **76**, 277–286 (2010)
38. T. Nishio, A. Miyatake, K. Inoue, et al., Experimental verification of proton beam monitoring in a human body by use of activity image of positron-emitting nuclei generated by nuclear fragmentation reaction. Radiol. Phys. Technol. **1**, 44–54 (2008)
39. Y. Hishikawa, K. Kagawa, M. Murakami, et al., Usefulness of positron-emission tomographic images after proton therapy. Int. J. Radiat. Oncol. Biol. Phys. **53**, 1388–1391 (2002)
40. M. Abe, Charged particle radiotherapy at the Hyogo Ion Beam Medical Center: characteristics, technology and clinical results. Proc. Jpn. Acad. Ser. B **83**, 151–163 (2007)
41. S. Vecchio, F. Attanasi, N. Belcari, et al., A PET prototype for "in-beam" monitoring of proton therapy. IEEE Trans. Nucl. Sci. **56**, 51–56 (2009)
42. F. Attanasi, N. Belcari, S. Moehrs, et al., Characterization of an in-beam PET prototype for proton therapy with different target compositions. IEEE Trans. Nucl. Sci. **57**, 1563–1569 (2010)
43. W.C. Hsi, D.J. Indelicato, C. Vargas, et al., In vivo verification of proton beam path by using post-treatment PET/CT imaging. Med. Phys. **36**, 4136–4146 (2009)
44. K. Parodi, H. Paganetti, E. Cascio, et al., PET/CT imaging for treatment verification after proton therapy: a study with plastic phantoms and metallic implants. Med. Phys. **34**, 419–435 (2007)

45. K. Parodi, H. Paganetti, H.A. Shih, et al., Patient study of in vivo verification of beam delivery and range, using positron emission tomography and computed tomography imaging after proton therapy. Int. J. Radiat. Oncol. Biol. Phys. **68**, 920–934 (2007)
46. K. Parodi, T. Bortfeld, A filtering approach based on Gaussian-powerlaw convolutions for local PET verification of proton radiotherapy. Phys. Med. Biol. **51**, 1991–2009 (2006)
47. A. Knopf, K. Parodi, T. Bortfeld, et al., Systematic analysis of biological and physical limitations of proton beam range verification with offline PET/CT scans. Phys. Med. Biol. **54**, 4477–4495 (2009)
48. F. Pönisch, K. Parodi, B.G. Hasch, W. Enghardt, The modelling of positron emitter production and PET imaging during carbon ion therapy. Phys. Med. Biol. **49**, 5217–5232 (2004)
49. M. Krämer, O. Jäkel, T. Haberer, et al., Treatment planning for scanned ion beams. Radiother. Oncol. **73**, S80–S85 (2004)
50. E. Rietzel, D. Schardt, T. Haberer, Range accuracy in carbon ion treatment planning based on CT-calibration with real tissue samples. Radiat. Oncol. **2**, 14 (2007)
51. F. Fiedler, G. Shakirin, J. Skowron, et al., On the effectiveness of ion range determination from in-beam PET data. Phys. Med. Biol. **55**, 1989–1998 (2010)
52. A. Santiago, F. Fiedler, G. Shakirin, et al., Development of an automatic evaluation routine for in-beam PET in the ion therapy. Presented at the ESTRO 29, Barcelona, Spain, 12–16 Sept 2010
53. P. Crespo, G. Shakirin, F. Fiedler, et al., Direct time-of-flight for quantitative, real-time in-beam PET: concept and feasibility study. Phys. Med. Biol. **52**, 6795–6811 (2007)
54. E. Testa, M. Bajard, M. Chevallier, et al., Monitoring the Bragg peak location of 73 MeV/u carbon ions by means of prompt γ-ray measurements. Appl. Phys. Lett. **93**, 093506 (2008)

Chapter 32
Compensation of Target Motion

Christoph Bert and Eike Rietzel

Abstract In ion beam therapy (IBT), organ motion requires special procedures. Of general concern is the impact on the dose distribution as a result of motion-related changes in the beam's range. In addition, interplay effects can arise for scanned beam application which cannot be addressed by the so-called margins to increase the treated volume. Dedicated motion mitigation techniques and/or 4D treatment planning are required. This chapter introduces the main concepts for management of respiratory motion in IBT.

32.1 Introduction

IBT for tumors, which are subject to motion during application of the beam (intrafractional target motion [1]), requires additional methods and techniques to ensure adequate dose deposition to the clinical target volume (CTV) despite motion. Typically, internal margins (IM) that contribute to the planning target volume (PTV) are used to cover uncertainties and motion-induced variations [2, 3]. However, this concept requires modifications for IBT, especially in the case of IBT with a scanned beam [4]. In this chapter, the current status of quantification and monitoring of organ motion, treatment planning incorporating organ motion, and ion beam-specific mitigation techniques, namely rescanning, gating, and beam tracking, is presented. The chapter focuses on respiration-induced target motion as this is the most dominant cause of intrafractional motion.

C. Bert (✉)
GSI Helmholtzzentrum für Schwerionenforschung, Planckstraße 1, 64291 Darmstadt, Germany
e-mail: c.bert@gsi.de

U. Linz (ed.), *Ion Beam Therapy*, Biological and Medical Physics, Biomedical Engineering, DOI 10.1007/978-3-642-21414-1_32,

32.2 Impact of Organ Motion

In radiotherapy, in general, intrafractional motion results in blurring of the delivered dose distribution that results in smoothed gradients at the lateral field edges of the PTV. In addition to this effect, organ motion further influences the dose deposition in IBT because of the possible changes of the ion beam's range if the density distribution in the beam's entrance channel changes (Fig. 32.1).

In IBT with a passively shaped beam, specific PTVs that incorporate the change in ion beam range, e.g., by compensator smearing [6], are sufficient to guarantee adequate dose deposition in the CTV but are often used in combination with beam gating to reduce dose deposition in normal tissues [7]. For scanned beams, the PTV concept is not appropriate as the interference of scanning beam delivery and moving target volume result in misdosage [8, 9]. This interference is typically referred to as interplay. Overdosage but more importantly underdosage can also occur if the interference of the two motions leads to more (or less) dose deposition in an area of the CTV. Figure 32.2 illustrates the formation of interplay in scanned IBT of intrafractionally moving targets. Because of interplay, dedicated techniques are required when treating moving organs with a scanned ion beam. To date, these techniques have not been established in the existing IBT facilities and thus, intrafractionally moving targets have only been treated with passively shaped beams.

32.3 Motion Monitoring

The goal of motion monitoring, also referred to as motion tracking, is real-time surveillance of the target's motion. Motion-monitoring techniques are required for

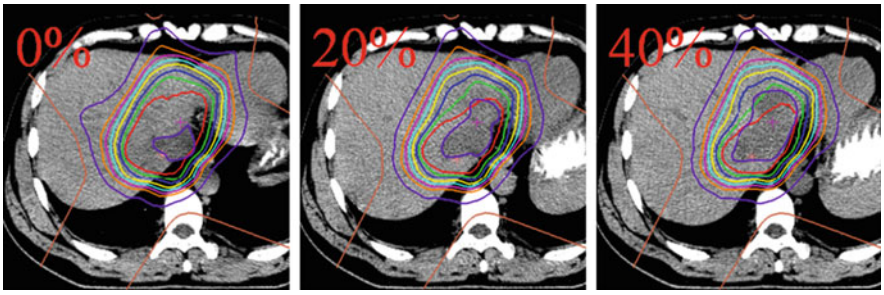

Fig. 32.1 Impact of organ motion (breathing phases 0%, 20%, 40%) on dose distributions for protons (four fields, gantry angles 20°, 115°, 210°, 315°); prescription dose 60 Gy. Relative isodose lines: *red* 99%, *green* 95%, *blue* 90%, *yellow* 80%, *cyan* 70%, *magenta* 60%, *orange* 50%, *purple* 30%, and *brown* 10%. Reprinted from [5] with kind permission from Elsevier Ltd

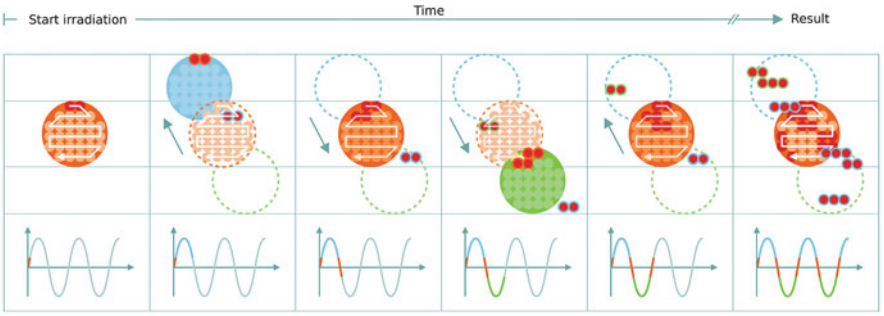

Fig. 32.2 Formation of interplay: in the presence of target motion, rasterscan beam delivery can result in deteriorated dose distribution. During beam scanning along the predefined scan path within a slice, the target moves as indicated by the blue, orange, and green motion phases. The scanning process delivers the pencil beams to stationary room coordinates. Target motion then changes the relative positions between pencil beams in the target volume. The result is a deteriorated dose distribution as shown on the right. Reprinted from [9] with permission of IOP Publishing Ltd

time-resolved quantification of organ motion. During treatment planning, motion monitoring techniques are combined with imaging protocols to reconstruct time-resolved data sets such as 4D computed tomography (4D-CT). At the time of treatment delivery, motion monitoring provides the actual position of moving organs.

Three classes of monitoring techniques can be differentiated: direct measurement of internal target motion, motion surrogates, e.g., the chest wall, and combination techniques that use models to allow precise estimation of internal motion based on a motion surrogate. Measurement of internal target motion is currently achieved using kV fluoroscopy [10, 11]. Implanted radio-transmitting markers [12] and ultrasound are currently in scientific evaluation. Fluoroscopy deposits an additional low dose to the patient and typically requires radio-opaque implants, especially in sites with low-imaging contrast like the liver. Fluoroscopy alone is used clinically in photon beam therapy at NTT hospital in Sapporo, Japan [10]. Several groups evaluate the potential of MV fluoroscopy with the exit beam of photon beam treatments [13].

Monitoring by motion surrogates is a wide field with numerous techniques in use. They measure a surrogate rather than target motion itself. The height of the chest wall and the temperature/flow of the expired air are typical parameters. These surrogates can be measured without additional imaging dose but cannot guarantee a steady correlation to the target's actual motion.

The most promising method is a combination of internal and surrogate monitoring that can be achieved by applying the technique in parallel, correlated by a motion model. After a short training sequence of the correlation model at the beginning of a session, fluoroscopic images are acquired occasionally (e.g., 1 frame per minute) while measurements with the motion surrogate are performed continuously at 10–40 Hz. On the basis of the trained parameters of the correlation model, the internal target position can be determined at high sampling rates with increased precision

in comparison with using motion surrogates only. A commercial version of such a tracking system is Synchrony™ by the company Accuray, a clinically used photon beam therapy system that provides the possibility to track and correct target motion because of respiration [14, 15].

32.4 Time-Resolved Volumetric Imaging

Treatment planning requires volumetric data to determine the extent of the motion of tumor and organs at risk and, in particular, CT data to determine the range of the ion beam within the patient. For intrafractionally moving sites, volumetric imaging has thus to incorporate the changing anatomy, i.e., time-resolved 4D imaging modalities are required [16–18].

The acquisition of time-resolved data can be performed by oversampling the image data in combination with a temporally registered motion monitoring signal such as the height of the chest wall. Following the image reconstruction, the acquired data are then grouped into multiple, typically 10, segments of the respiratory period either by respiratory amplitude or respiratory phase. Each of the segments represents a 3D data set. The ten segments – also referred to as motion phases – form a 4D-CT that includes 3D anatomical changes over the time of a respiratory period. An example of a 4D-CT is shown in Fig. 32.3 in comparison with a regular 3D-CT of the object that results in interference patterns comparable to interplay.

For quantification of motion, nonrigid registration techniques can be used to calculate the transformation parameters from all motion phases to an arbitrary reference phase. These data can be used to propagate delineations of the target volume or organs at risk from the reference to other motion phases, e.g., for formation of an internal target volume. As part of treatment planning, the transformation data can further be used for 4D dose calculations.

32.5 Treatment Techniques for Intrafractionally Moving Organs

Motion monitoring, as well as 4D data acquisition, forms the basis for treatment techniques for tumors moving with respiration. Development of dedicated treatment techniques is especially required for scanned IBT to eliminate detrimental interplay effects during irradiations. In addition, gating and beam tracking allow reduction of internal margins because the effective motion amplitude is reduced or even eliminated. Apart from specific motion mitigation techniques, a change of the respiration process can also be used to reduce the motion amplitude and, therefore, provide the possibility to mitigate intrafractional motion artifacts. Effective ways are, for example, irradiation during breath-hold, abdominal press devices to limit abdominal motion, or even invasive methods such as jet-ventilation or apnea under anesthesia.

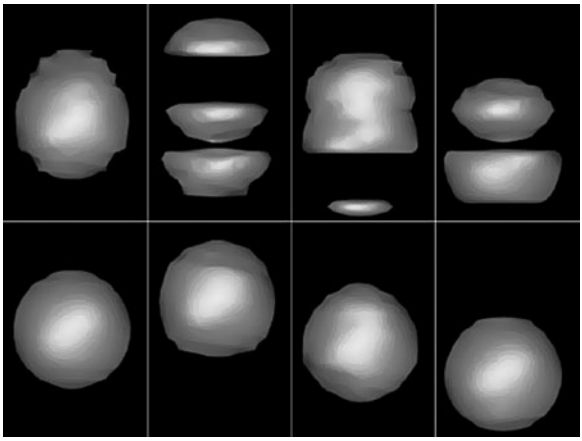

Fig. 32.3 Isosurface renderings of a spherical object (radius 1.2 cm), CT scanned while periodically moving on a sliding table (amplitude 1 cm, period 4.4 s). *Top row*: different artifacts obtained by standard axial CT scanning. Artifacts depend on the interplay (relative motion phase) between CT data acquisition and object motion; to measure different artifacts, CT scans were started at different motion phases. Note that slices of the object can be imaged in mixed order. *Top row*, *right image* shows two disconnected parts of the sphere, the upper part consists of the top and the bottom of the sphere. *Bottom row*, *left*: a CT scan of the static object. Other images show three positions of the sphere while moving as imaged with 4D-CT (29 images per couch position reconstructed). Only small residual artifacts on the surface remain, the object is imaged at different positions of the motion cycle. Reprinted from [17] with kind permission from AAPM

32.6 Rescanning

Rescanning or "repainting" is a technique for scanned beam therapies that aims at reducing the sensitivity of the delivered dose distribution to interplay-caused underdosage by irradiating the PTV multiple times [8]. Because of the strong dependence of not only the under- and overdose pattern in the dose distribution on the motion parameters such as period, initial phase, and amplitude but also the speed of the scan process or the scanning direction, multiple scans with a proportionally reduced dose will lead to an averaging effect of the interference pattern. If sufficient rescans are applied, the averaging effect will lead to homogeneous dose coverage of the CTV and a blurred dose distribution in the region of the internal margins.

Multiple rescan options have been proposed in the last years [19–22]. The underlying options are rescanning energy slice by energy slice (*slice-by-slice rescanning*) or rescanning of the volume (*volumetric rescanning*). Volumetric rescanning will not be applicable in synchrotron-based facilities with the current methods of active energy variation since these need several seconds to change the energy of the beam. In a typical case of 50 energy slices and 10 rescans, the integral time to change the energy would take longer than the total irradiation time that the clinical centers aim at.

Currently, a detailed 4D treatment plan optimization recipe that estimates the necessary number of rescans, e.g., as function of motion amplitude, is not available. But studies indicate that the number of rescans will be below 10 for the typical target motion amplitudes dealt with in IBT. Studies and an estimation of the temporal patterns of the issue further reveal that averaging over the multiple motion phases does not necessarily occur as planned since the irradiation might always take place in the same fraction of the motion phases [21]. An example might illustrate this situation. In slice-by-slice rescanning, irradiating one isoenergy slice requires ∼1 s. Irradiation of adjacent slices starts at 5 s intervals. Since such a rhythm is also typical for a normal respiratory period, irradiation always takes place in the same sections of the motion cycle [21]. One option to avoid such synchronism is random pauses or random modulations of the irradiation process (e.g., a change in scan speed). A more elegant alternative to ensure irradiations averaged over the motion cycle can be achieved by incorporating the respiration pattern in the rescanning process. By using the data from a motion monitoring system in combination with a modulated dose rate, it is possible to spread the rescans throughout the respiration period. This so-called *phase-controlled rescanning* or *breath-sampled rescanning* requires the extraction rate from the synchrotron to be adjusted so that the given parameters (treatment plan, period of the patient's motion, number of rescans) are met and rescans are executed in each motion phase of the respiratory cycle [19, 20].

Apart from the different rescan options mentioned above, for the actual delivery two different options were also proposed [22]: *scaled rescanning* is characterized by proportional reduction of the dose per scan; alternatively, *iso-layered rescanning* has been proposed to deliver a certain number of particles per spot and scan. Because of the inhomogeneous particle deposition map in each layer, this will lead to different spot positions in each rescan since some of the spots will have received sufficient dose from the already completed number of scans. Slice-by-slice rescanning has been implemented for study purposes at GSI Helmholtzzentrum für Schwerionenforschung (GSI), Darmstadt, Germany. Figure 32.4 shows the results of the irradiation of a vertically moving radiographic film (amplitude 3 cm peak-to-peak) with different numbers of rescans. The quadratic CTV is homogeneously covered after 15 rescans if 1.5-cm margins in the direction of the motion are used.

32.7 Gating

Different from rescanning, gating reduces the effective amplitude of the motion. It is thus a mitigation technique that is not limited to scanned beams. In fact, it has been applied for many years in scattered beam IBT [7, 23]. On the basis of the signal from the motion-monitoring device, the beam is interrupted (gated) if the tumor is outside of the gating window defined in 4D treatment planning. Typical gating windows comprise 30% of the respiratory cycle either defined by the motion amplitude or phase. This extends the treatment time for cyclotrons proportionately. For synchrotrons the extension of the treatment duration is, in

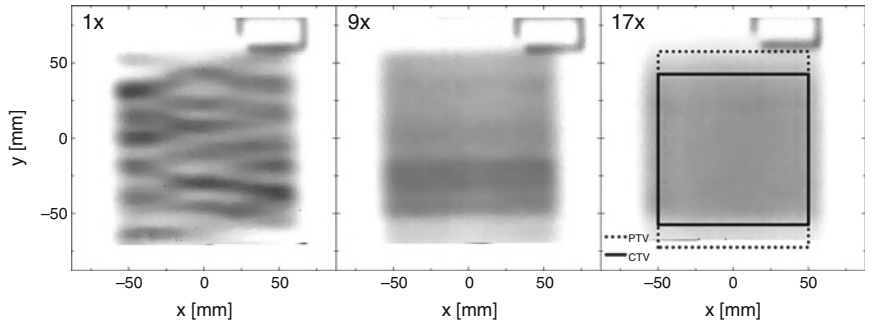

Fig. 32.4 Rescanning example. In case of one rescan (1x), interplay deteriorates the dose homogeneity within the CTV despite using a PTV. With increasing number of rescans (9x, 17x) homogeneity can be restored at least in the CTV, a blurred dose distribution will be present in the CTV–PTV margins as expected

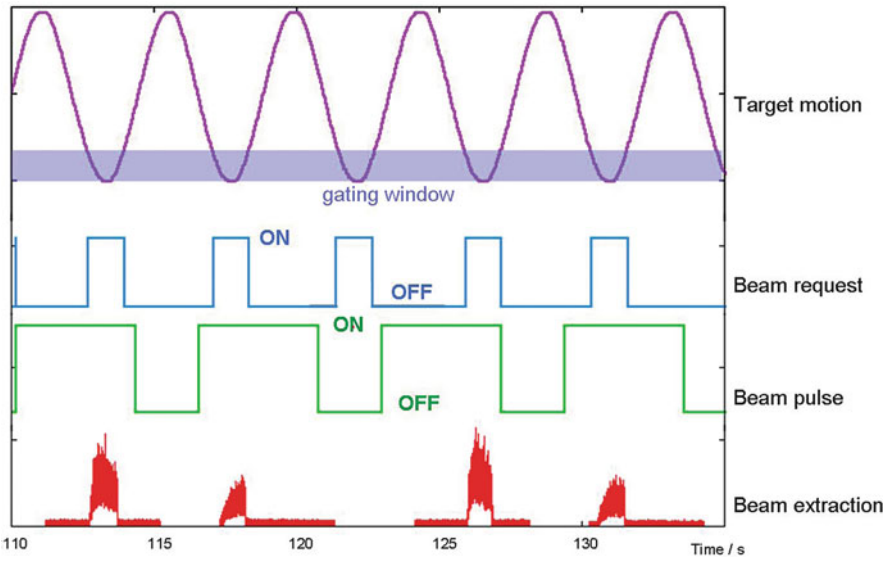

Fig. 32.5 Gating scheme similar to the one introduced in [7]. A motion monitoring system measures target motion. Depending on the size of the gating window, beam is requested. If beam request and beam pulse from the synchrotron overlap, particles are extracted from the accelerator

general, less pronounced since a significant amount of time is lost for refilling and acceleration, anyway [24].

The longest experience with gating exists at the National Institute of Radiological Sciences (NIRS), Chiba, Japan, where this treatment mode has been applied with a passively scattered carbon beam since 1996. Figure 32.5 shows the schematic outline of the gated irradiation system.

Gating with a scanned beam is also feasible but requires methods to reduce the dosimetric impact of interplay between residual motion within the gating window and the scanned beam. Currently, two methods have been proposed to accomplish this task.

NIRS plans a combination of (phase-controlled) rescanning and gating to achieve a homogeneous coverage of the CTV [19]. GSI together with the Heidelberg Ion-Beam Therapy Center (HIT) focus on using an increased overlap of pencil beams that ensures an increased number of beam positions contributing to an anatomical position. This increase in overlap ensures that residual interplay does not cause relevant underdosage [25]. Initial studies reveal a linear relationship between the acceptable gating window size (residual motion amplitude) and the beam's full width at half maximum at a given grid spacing of beam positions. Clinical implementation is currently ongoing with the first patient treatment expected in 2011.

32.8 Beam Tracking

The beam monitoring signal in combination with the data from 4D-CT can be used to adjust the parameters of the treatment plan in real-time such that the motion of the tumor is compensated. This motion compensation technique is called beam tracking. In principle, beam tracking does not require internal margins that cover for motion uncertainties but only margins that cover for the uncertainty of the method. Beam tracking was originally proposed for photon beam therapy for which a compensation of the lateral target motion by the multileaf collimator of a LINAC is sufficient [26]. For IBT, the changes in beam range have also to be compensated. Figure 32.6 shows schematically the experimental beam tracking system that was implemented at GSI [27]. Lateral compensation of target motion is achieved by changing the beam position via the scanning magnets. The compensation of changes in beam range can currently not be achieved with the accelerator because compensation has to occur for each beam position, i.e., each $\sim$10 ms. Therefore, an energy modulation system based on double wedges mounted on fast moving linear motors directly upstream of the isocenter is used for range compensation.

The performance of the system has been tested for accuracy [29] and speed as well as dosimetric aspects [30, 31]. Laterally, system speed and accuracy were determined to $<$1 ms and $<$0.16 mm, respectively. For compensation of ion beam range, a global communication delay of 11 ms was measured. The compensation speed was 16 ms for a 5 mm water-equivalent range shift. Dosimetric precision assessed by an array of 24 ionization chambers deviates by 1% from comparable measurements without target motion (SD 2%, maximal deviation 4%). Parallel radiographic film measurements revealed a lateral tracking accuracy of 0.75 mm at film homogeneities of 96.6% in comparison with 97.3% for a stationary target.

Recent investigations focus on an alternative beam energy modulation system which is based on an ion-optical method in combination with a stationary

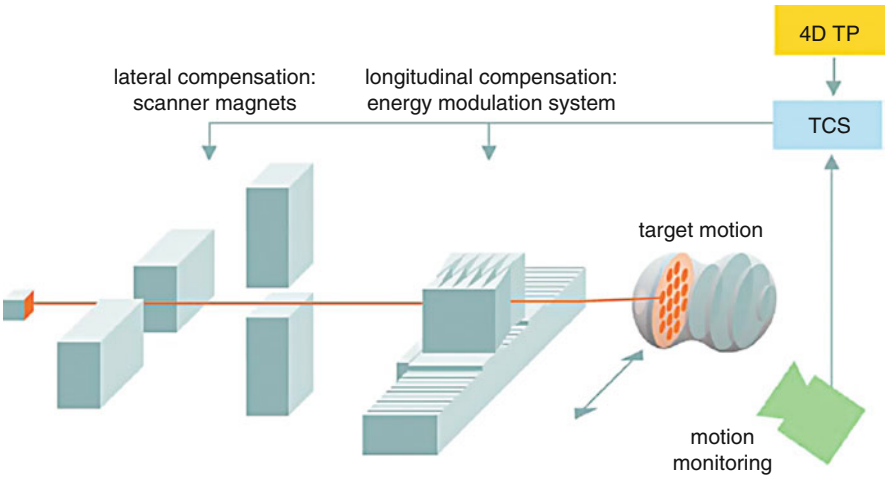

Fig. 32.6 Schematic outline of the beam tracking system currently installed at GSI, Darmstadt, Germany. On the basis of the data from a motion monitoring device and a library of compensation parameters determined in 4D treatment planning (4D TP) [28], lateral as well as range compensation parameters for the currently irradiated beam position are communicated to the scanning magnets and the energy modulation system, respectively (from [21])

wedge-shaped absorber in the beam line. A feasibility study concerning beam parameters gave promising results [32]. For full implementation including compensation speeds comparable to the scanning process, hardware modifications in the beam line are required. In addition, nontranslational target motion components that change the dose in the proximal parts of the target volume need to be compensated. These dose changes can be incorporated in 4D treatment planning and adjusted during irradiation for example by real-time modulation of the nominal dose [33].

32.9 Comparison of Motion Mitigation Techniques

The three motion mitigation techniques, rescanning, gating, and beam tracking, can be compared with respect to target conformation, robustness, and implementation complexity.

Target conformation is dominated by the size of the required PTV and addresses mainly the dosimetric burden for normal tissues and organs at risk in the vicinity of the CTV. All three techniques warrant coverage of the CTV and effective suppression of interplay-related dose inhomogeneities. Minimal CTV–PTV margins are given by the uncertainties that are present in irradiations of stationary targets.

Beam tracking aims to realize target coverage by compensating target motion-related changes. The PTV does not require IM to cover organ motion-related

uncertainties. Most likely, it requires, however, margins slightly larger than for stationary irradiations because of the complex technical system (see below).

Effective gating means irradiating a CTV with small motion amplitudes. This is achieved by pausing the beam during long periods of the respiratory cycle. The residual motion has to be covered by IM in scattered as well as scanned IBT. For scanned beams interplay effects have to be mitigated, in addition. At least for the technique of an enlarged beam overlap, it is likely that the lateral gradients will be slightly increased because of the larger pencil beam width. The margins required because of technical uncertainty are most likely smaller than for beam tracking but the entire motion mitigation-related expansion of the CTV will most likely be larger than for beam tracking. Of the three techniques, rescanning is the only one that does not reduce the effective motion amplitude but focuses on suppression of the interplay influence only. CTV coverage relies on IM only. For a given motion amplitude, margins are consequently larger than for beam tracking or gating. Similarly, the smearing of lateral gradients will be larger than for the other techniques. Since rescanning does not involve any specific hardware, margins related to technical complexity will be low and most likely comparable to stationary irradiations. In summary, normal tissue involvement will increase in the following order: beam tracking, gating, and rescanning. Figure 32.7 compares the corresponding dose distributions.

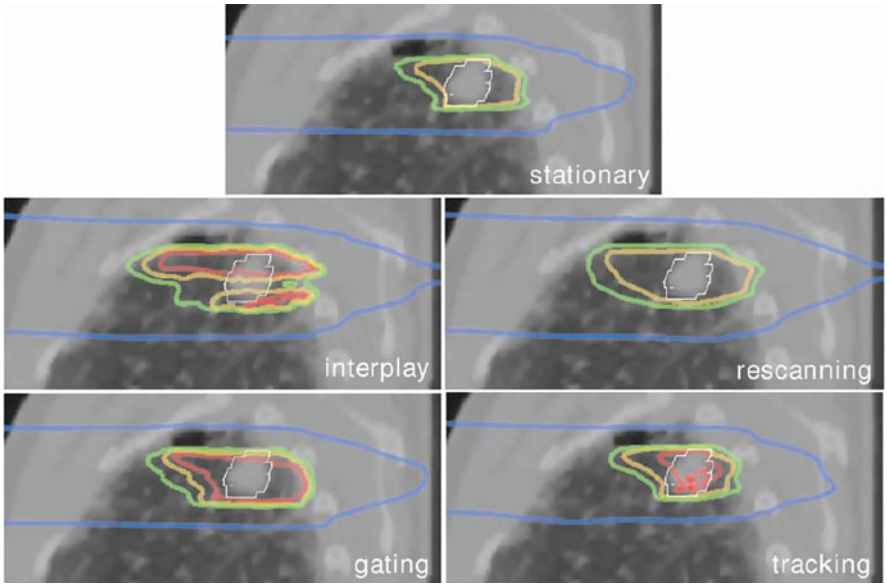

Fig. 32.7 Dose distributions of scanned ion beams for a lung tumor treatment calculated for a stationary reference, moving (period: 4 s) without as well as with different motion mitigation techniques. Isodose lines correspond to 100%, 95%, 90%, and 10%. Reprinted with permission from [21]

A discussion on technique-related margins is incomplete if sensitivity to expected uncertainties is not considered. Patient studies have shown that the respiratory pattern of, e.g., patients with lung cancer is not constant but changes at least interfractionally [34]. In addition, gating and beam tracking (and for certain implementation modes rescanning) rely on motion monitoring data that potentially have a limited precision, especially if surrogates such as the chest height are measured to determine the position of the target.

Rescanning is least sensitive to these uncertainties since margins are used to cover them, and these margins can be increased to meet the degree of uncertainty (lateral and longitudinal margins for range uncertainties). The precision of the method might be reduced further but CTV coverage can be assured. The situation is different with gating since motion monitoring is involved. In case of a respiratory phase mismatch between gating signal and target motion, e.g., because of an unreliable motion surrogate, there is the risk of geometrical miss of the CTV resulting in distinct underdosage. If this uncertainty is controlled, CTV coverage and interplay mitigation can be ensured by a conservative choice of margins and overlap parameters.

For beam tracking the sensitivity to expected uncertainties is highest. Beam tracking relies on precise motion monitoring during all parts of the respiratory cycle. In addition, a valid modeling of the patient's moving geometry by 4D-CT and the corresponding deformation maps, which are used to calculate the compensation parameters, are necessary. In case of changing anatomy or motion pattern between 4D treatment planning and treatment delivery, the adaptation of the beam is not matching which might result in changes of the dosimetric coverage of the CTV. In summary, it can be stated that the robustness against uncertainties decreases in the order rescanning – gating – beam tracking. This will likely determine the choice of the mitigation technique for a specific patient; patients with small motion amplitudes and/or unstable motion patterns are candidates for rescanning. At intermediate or large motion amplitudes, gating or beam tracking will be the preferred options. In case of unstable motion patterns these patients could be treated in a combined treatment rescanning with gating. For stable breathers at large amplitudes beam tracking is the method of choice because CTV coverage can be achieved at minimal dose to normal structures.

Similar to the robustness assessment, the technical challenges are minor for rescanning, more significant for gating, and highest for beam tracking. The speed of the scanner magnets can typically be assumed to be sufficient, and therefore, it is mainly the treatment control system that needs to be adapted for rescanning. Gating requires controlled pausing and resuming of the beam delivery based on a motion surrogate. Pausing and resuming the ion beam can be achieved with radiofrequency knockout (RF-KO) extraction for facilities with a synchrotron. For cyclotrons, the current can be modulated directly at the ion source. Beam tracking requires the functionality of gating (pausing the beam is essential to cope with coughing or other imponderabilities). Additional changes concern the therapy control system to allow for lateral adaptation of the beam based on 4D treatment planning data and motion monitor input. Furthermore, a fast energy modulation system is needed.

Ideally, all three methods should be used in combination with a 4D treatment planning system. But only for beam tracking 4D treatment planning is essential as the motion compensation parameters have to be calculated. Rescanning and gating can most likely rely on published studies or experiences gained from research 4D treatment planning systems that give instructions for certain motion characteristics on how many rescans to apply or which gating window to consider.

In view of the technical complexity and the current situation, the implementation order of the motion mitigation techniques can be foreseen as follows: most facilities rely on rescanning followed by gating, whereas beam tracking is a research topic with a long-term clinical perspective because of best target conformation and least treatment time. In an ideal facility all techniques are available with the option to combine them. Then, a patient-specific compromise between target coverage, target conformation, and treatment time can be achieved by selecting an appropriate motion mitigation technique.

32.10 Conclusions

The use of IBT for tumors moving with respiration is almost exclusively limited to centers that use a scattered beam. Carbon ion treatments of intrafractionally moving tumors are limited to the centers in Japan, mainly NIRS. Treatments at NIRS are performed with gating in combination with appropriate internal margins. In their new facility, which is currently commissioned, a scanned ion beam will be used and it is planned to treat moving tumors with phase-controlled rescanning in combination gating (see also Chap. 37). For motion monitoring, NIRS will continue to use an in-house developed laser distance sensor that monitors the motion of the abdomen as a surrogate.

At the combined proton-ion facility HIT in Heidelberg, Germany, gating with an increased overlap of pencil beams will be the first method to be implemented. Currently, medical physics and commissioning studies are ongoing to develop strategies for optimization and patient-by-patient quality assurance of treatment plans. A major focus are beam overlap data as function of the respiration parameters. Most likely, HIT will use the expansion of the chest or abdomen as a motion surrogate. After successful clinical implementation of gating, beam tracking will be further developed and considered for patients with large and reproducible tumor excursions.

Most of the other ion and proton beam centers that are using a scanned beam for treatment of intrafractionally moving sites will rely on one of the rescanning methods potentially in combination with gating for tumors with a larger motion amplitude.

References

1. K.M. Langen, D.T.L. Jones, Organ motion and its management. Int. J. Radiat. Oncol. **50**, 265–278 (2001)
2. International Commission on Radiation Units and Measurements, *Prescribing, Recording, and Reporting Photon Beam Therapy*. (ICRU Report 50, Bethesda, MD, USA, 1993)
3. International Commission on Radiation Units and Measurements. *Prescribing, Recording and Reporting Photon Beam Therapy*: Supplement to ICRU Report 50 (ICRU Report 62, Bethesda, MD, USA, 1999)
4. T. Haberer, W. Becher, D. Schardt, G. Kraft, Magnetic scanning system for heavy ion therapy. Nucl. Instrum. Methods A **330**, 296–305 (1993)
5. E. Rietzel, G.T.Y. Chen, N.C. Choi, C.G. Willet, Four-dimensional image-based treatment planning: Target volume segmentation and dose calculation in the presence of respiratory motion. Int. J. Radiat. Oncol. **61**, 1535–1550 (2005)
6. M. Urie, M. Goitein, M. Wagner, Compensating for heterogeneities in proton radiation therapy. Phys. Med. Biol. **29**, 553–566 (1984)
7. S. Minohara, T. Kanai, M. Endo, et al., Respiratory gated irradiation system for heavy-ion radiotherapy. Int. J. Radiat. Oncol. **47**, 1097–1103 (2000)
8. M.H. Phillips, E. Pedroni, H. Blattmann, et al., Effects of respiratory motion on dose uniformity with a charged particle scanning method. Phys. Med. Biol. **37**, 223–233 (1992)
9. C. Bert, S.O. Grözinger, E. Rietzel, Quantification of interplay effects of scanned particle beams and moving targets. Phys. Med. Biol. **53**, 2253–2265 (2008)
10. H. Shirato, S. Shimizu, T. Kunieda, et al., Physical aspects of a real-time tumor-tracking system for gated radiotherapy. Int. J. Radiat. Oncol. **48**, 1187–1195 (2000)
11. H. Shirato, M. Oita, K. Fujita, et al., Feasibility of synchronization of real-time tumor-tracking radiotherapy and intensity-modulated radiotherapy from viewpoint of excessive dose from fluoroscopy. Int. J. Radiat. Oncol. **60**, 335–341 (2004)
12. J.M. Balter, J.N. Wright, L.J. Newell, et al., Accuracy of a wireless localization system for radiotherapy. Int. J. Radiat. Oncol. Biol. Phys. **61**, 933–937 (2005)
13. W. Mao, R.D. Wiersma, L. Xing, Fast internal marker tracking algorithm for onboard MV and kV imaging systems. Med. Phys. **35**, 1942–1949 (2008)
14. J.R. Adler, M.J. Murphy, S.D. Chang, S.L. Hancock, Image-guided robotic radiosurgery. Neurosurgery **44**, 1299–1307 (1999)
15. A. Schweikard, G. Glosser, M. Bodduluri, et al., Robotic motion compensation for respiratory movement during radiosurgery. Comput. Aided Surg. **5**, 263–277 (2000)
16. E.C. Ford, G.S. Mageras, E. Yorke, C.C. Ling, C.T. Respiration-correlated spiral, A method of measuring respiratory-induced anatomic motion for radiation treatment planning. Med. Phys. **30**, 88–97 (2003)
17. E. Rietzel, T. Pan, G.T.Y. Chen, Four-dimensional computed tomography: Image formation and clinical protocol. Med. Phys. **32**, 874–889 (2005)
18. S.S. Vedam, P.J. Keall, V.R. Kini, et al., Acquiring a four-dimensional computed tomography dataset using an external respiratory signal. Phys. Med. Biol. **48**, 45–62 (2003)
19. T. Furukawa, T. Inaniwa, S. Sato, et al., Design study of a raster scanning system for moving target irradiation in heavy-ion radiotherapy. Med. Phys. **34**, 1085–1097 (2007)
20. J. Seco, D. Robertson, A. Trofimov, H. Paganetti, Breathing interplay effects during proton beam scanning: simulation and statistical analysis. Phys. Med. Biol. **54**, N283–N294 (2009)
21. E. Rietzel, C. Bert, Respiratory motion management in particle therapy. Med. Phys. **37**, 449–460 (2010)
22. S.M. Zenklusen, E. Pedroni, D. Meer, A study on repainting strategies for treating moderately moving targets with proton pencil beam scanning at the new Gantry 2 at PSI. Phys. Med. Biol. **55**, 5103–5121 (2010)
23. H.D. Kubo, B.C. Hill, Respiration gated radiotherapy treatment: a technical study. Phys. Med. Biol. **41**, 83–91 (1996)

24. Y. Tsunashima, S. Vedam, L. Dong, et al., Efficiency of respiratory-gated delivery of synchrotron-based pulsed proton irradiation. Phys. Med. Biol. **53**, 1947–1959 (2008)
25. C. Bert, A. Gemmel, N. Saito, E. Rietzel, Gated irradiation with scanned particle beams. Int. J. Radiat. Oncol. Biol. Phys. **73**, 1270–1275 (2009)
26. P.J. Keall, V.R. Kini, S.S. Vedam, R. Mohan, Motion adaptive x-ray therapy: a feasibility study. Phys. Med. Biol. **46**, 1–10 (2001)
27. S.O. Grözinger, C. Bert, T. Haberer, et al., Motion compensation with a scanned ion beam: a technical feasibility study. Radiat. Oncol. **3**, 34 (2008)
28. C. Bert, E. Rietzel, 4D treatment planning for scanned ion beams. Radiat. Oncol. **2**, 24 (2007)
29. N. Saito, C. Bert, N. Chaudhri, et al., Speed and accuracy of a beam tracking system for treatment of moving targets with scanned ion beams. Phys. Med. Biol. **54**, 4849–4862 (2009)
30. C. Bert, N. Saito, A. Schmidt, et al., Target motion tracking with a scanned particle beam. Med. Phys. **34**, 4768–4771 (2007)
31. C. Bert, A. Gemmel, N. Saito, et al., Dosimetric precision of an ion beam tracking system. Radiat. Oncol. **5**, 61 (2010)
32. N. Chaudhri, N. Saito, C. Bert, et al., Ion-optical studies for a range adaptation method in ion beam therapy using a static wedge degrader combined with magnetic beam deflection. Phys. Med. Biol. **55**, 3499–3513 (2010)
33. R. Lüchtenborg, N. Saito, N. Chaudhri, et al., On-line compensation of dose changes introduced by tumor motion during scanned particle therapy. Proceedings of World Congress on Med Phys Biomed Engin, Munich, Germany, 7–12 Sept 2009.IFMBE **25**(1), 449–452 (2009)
34. J.J. Sonke, J. Lebesque, M. van Herk, Variability of four-dimensional computed tomography patient models. Int. J. Radiat. Oncol. Biol. Phys. **70**, 590–598 (2008)

Chapter 33
Industrial Robots for Patient Support

Andres Sommer

Abstract Flexibility, precision, and capability to support the clinical workflow make robots the ideal choice for ion beam therapy (IBT) facilities for use in patient positioning. To fulfill the clinical needs in IBT, an industrial robot patient positioner needs to be carefully designed regarding applications and safety issues as well as precision and handling.

33.1 Introduction

IBT is known for the ability to apply a pencil beam of ions with high precision to a target inside a patient's body. A lot of effort is spent to transport the beam with submillimeter accuracy to the isocenter of the treatment room. The target needs to be positioned exactly as planned for precise treatment. The actual position and the beam's pathway are controlled by imaging and corrected with the table if necessary and possible. This needs to be done at least with a similar precision as for the beam itself, in order to maintain treatment accuracy.

Today's patient tables for conventional radiation therapy (RT) do not provide all the features necessary for IBT. There was a need to improve the design, improve precision and allow for more flexibility in positioning. Finally, cost aspects need to be considered with respect to the lifecycle and protection of such an investment.

Today, immobilization and position verification are performed within the treatment room. This takes time and slows down the patient throughput. By changing the table design, it should be possible to immobilize and image a patient outside the treatment room and then move him or her to the treatment position [1].

A. Sommer (✉)
Siemens Healthcare AG, Imaging & Therapy, Particle Therapy, Hofmannstraße 26, 91052 Erlangen, Germany
e-mail: andres.sommer@siemens.com

U. Linz (ed.), *Ion Beam Therapy*, Biological and Medical Physics, Biomedical Engineering, DOI 10.1007/978-3-642-21414-1_33,

Industrial robots are primarily designed to work in production lines well secured behind fences and safety barriers. For robots handling humans, special care has to be taken to ensure safety and comfort for patients and operators.

33.2 Patient Tables for Conventional RT

Cobalt sources and later linear accelerator-based treatment modalities have been used for quite some time. A C-shaped gantry transports the photon source 360° around the patient. The patient is fixed on a tabletop positioned by the mechanics of the table.

The characteristics of photon dose delivery require irradiation from multiple directions. Movements of the patient support system are performed in the following ways (see IEC 61217 and Fig. 33.1):

Isocentric rotation
Vertical up/down
Lateral left/right
Longitudinal forward/backwards
Tabletop rotation around the table base

The precision needed is in the millimeter range or half-degree angle. Special care is taken for the isocentric rotation. The tables use large bearings placed in the floor of the treatment room to provide precise turns. For this purpose, the table needs a special base frame.

Since 1999, when the first commercially available accelerator with CT image guidance was installed in Morristown NJ, image guidance with CT image quality

Fig. 33.1 Present-day treatment table for conventional RT with movement characteristics. The column rotation axis is used to move the table out of the isocenter. This axis is used for extended SSD (source-to-surface distance) treatments. Not all commercial tables share this feature though

has been more and more accepted as a necessary tool to increase accuracy in radiation treatment. With the ability to plan, simulate and verify in 3D, the need of pitch and roll movement to correct for rotational setup variations in patient position came up. The conventional tables were not capable of handling these movements. Tabletop adapters were designed to provide pitch and roll [2]. They were mounted on top of the existing tables thereby reducing the convenience of handling the tables, and they lowered their load capacity. But it helped to apply the correction without redesigning the whole table.

33.3 Patient Tables for IBT

33.3.1 Positioner for a Gantry

The mechanics of the beam generation systems changed dramatically when using ions. While the gantry of a photon linac has a height of about 2.5 m, a proton gantry has a diameter of up to 10 m. The enormous weight of the last bending magnet needs a very stable gantry construction which does not allow to place the patient positioner inside the gantry mechanics. A table customized for this type of gantry needs to be designed with a very long extension to place the patient in the center of the gantry. It also requires a patient to step-on outside the gantry's mechanics to avoid a moving floor with all its disadvantages in design and operation.

The inner diameter of the gantry drives the overall cost and is kept to a minimum. This very much limits the length of the tabletop as well as possible movements within this inner gantry space. Short tabletops (<2 m) may reduce the applicability.

33.3.2 Positioner for a Fixed Beam

The increased radiobiological effectiveness (RBE) of heavier ions in the Bragg peak region relative to the entrance channel of the beam permits to reduce the number of beam angles in comparison to irradiation with photons and protons. A combination of fixed beamlines is used to provide the few beam angles necessary, e.g., at 90° (horizontal), 45°, 30° and 0°. The entrance angles needed are achieved by moving the patient around the beam and not the beam around the patient.

Another option to position a patient at a fixed beam is a chair. A newly designed positioner should move a chair 360° in front of a horizontal beam to allow treatment similar to a rotating gantry (see below).

Today, chairs are used for uveal melanoma treatments with fixed beam angles and passive scattering techniques for lateral spreading with 60–70 MeV proton beams [3, 4]. These small ocular targets call for higher precision than any other indication treated with protons. The treatment chairs designed just for this purpose are not further discussed here.

33.3.3 Precision

The first parameter discussed in specifying the quality of a patient positioner is the submillimeter accuracy. The specifications for patient positioning in IBT by the oncologist are similar to those used in conventional RT today, i.e., 6 degrees of freedom (DoF) with submillimeter precision. This high precision is necessary to safely deposit the high-energy dose of the narrow focal spot (few mm FWHM). This requires X-ray image guidance with submillimeter pixel size. These images are compared to digitally reconstructed radiographs (DRR) based on planning CT data. Depending on the slice width of these data, the resulting position accuracy is at best in the order of 1 mm (Fig. 33.2). This assumes that the target is visible, which is questionable in a lot of applications even with 3D cone beam computed tomography (CBCT) due to the lack of soft tissue contrast. In RT, fiducials are used as a reference. But metal inserts must not be placed in the beam entrance channel/course of the beam as they could cause changes to the dose distribution.

Unfortunately, often patient comfort and precision are contradictive. To be precise, positioning has to be reproducable which may not be possible when being smooth and comfortable. But fixation has its limits where respiration is impaired or, to avoid a respiration induced target movement, an abdominal press causes

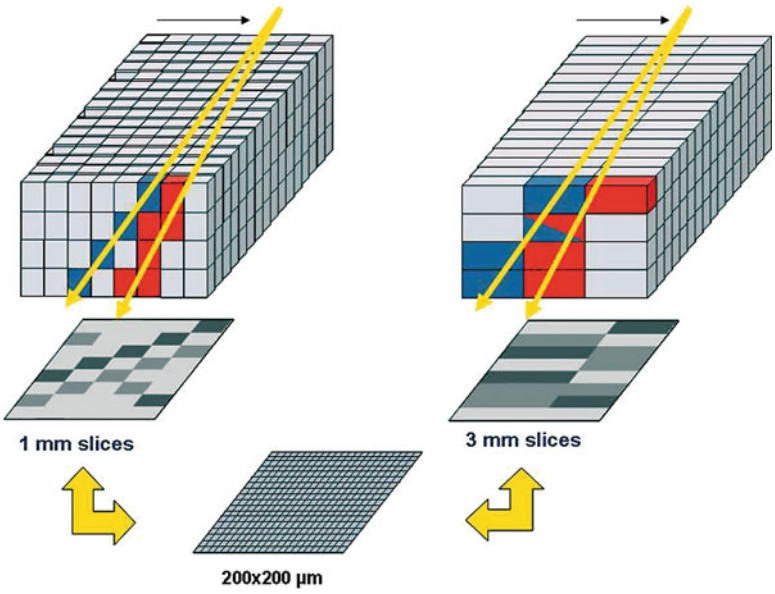

Fig. 33.2 The 3D planning-CT dataset (*top*) is used to calculate the DRRs (*middle*). Depending on the slice width used for the planning CT (*left*: 1 mm, *right*: 3 mm) the resulting 2D DRRs show at best $1 \times 1\,mm^2$ or $1 \times 3\,mm^2$ pixels, respectively. The accuracy of the calculated shift vector for position correction can hardly be better

discomfort and pain. Motion and acceleration patterns of the positioner have to be adapted accordingly. But they should not be limited by the positioner mechanics which should provide flexibility in controlling the pathways and speed. Roll angles up to 25° are applied today in cradle-like tabletops, e.g., at the Loma Linda University Medical Center (LLUMC) in the USA or at the National Institute of Radiological Sciences (NIRS) in Chiba [5], Japan. This flexibility provides, as well, new options for future applications and/or immobilization needs.

Cost and precision is another pair of parameters which is linked very closely: for every tenth of a millimeter the price at least doubles. This requires careful reasoning when defining the minimum specifications.

Absolute repetitive 3D positioning along with high precision, for example, is an expensive feature. The accuracy requirements should not ask for more than 0.5 mm radius. Relative positioning in small steps of 0.1 mm over a travel range of a few centimeters might be an acceptable compromise, which fulfills the clinical needs for high-precision applications such as position correction in stereotactic treatments.

33.4 Imaging Capability

Imaging at every fraction is a standard procedure in IBT. X-ray sources and detectors mounted close to the isocenter are state-of-the-art devices. Other solutions comprise C-arms mounted on robots or special mechanics to allow CBCT scanning. A newly designed patient positioner should allow imaging in every treatment position to ensure correct target position.

CBCT imaging with conventional flat panel detectors still does not offer sufficient low-contrast resolution for target volume contouring. For better results, a real CT scanner on rails should be considered.

33.5 Tabletop

In conventional RT, the tabletop comprises removable frames or open fiber mesh panels (tennis racket inserts). In order to avoid high skin dose, these inlays can be taken out. This, however, compromises the stability of the tabletop and a balance has to be found between the two conditions. The use of carbon fiber tops is growing but is still not a standard.

In IBT, the stability of the tabletop must not be compromised. This results in a very stiff design, which needs to meet the following basic criteria:

- Low material density if the beam has to pass it (e.g., in a gantry or cradle design); a maximum of 1.5 mm Al-equivalent absorption is acceptable when used for X-ray, CT or PET imaging.
- Smooth changes in the material density to avoid changes in the beam entrance path which might be hard to correct for if the beam is applied from underneath

through the tabletop (90° < beam angle < 270°). This is also appropriate to reduce imaging artifacts. If this is not possible, the treatment plan needs to be adapted to avoid the high-density areas.
- No sharp edges, no bore holes, no inserts or metal inclusions to avoid imaging artifacts and unplanned modifications in the particle range within the treated area.
- Very low bending even for loads exceeding 130 kg.

Priorities have to be set when a single tabletop is to be used for all treatments and QA tasks. It might be preferable to have at least two different designs of the tabletop, one for patient treatments and another for QA tasks.

The imaging artifacts do not play a role when a water phantom is placed at isocenter on the tabletop but it facilitates the QA workflow essentially, if, e.g., bore holes are available on the tabletop for phantom fixation. If more than one tabletop is available, they should be exchangeable without the necessity for a tool. For heavier items such as a water tank, it might be helpful to move the QA devices mounted on the dedicated tabletop with a shuttle between the treatment rooms and let the positioner automatically adapt.

The existing add-on tabletops which are transported with a shuttle and slide on top of the treatment tabletop [6] may not be the best choice for treatment beam angles from below the table. The double layer of dense material and the variations will add hard-to-predict density changes and, hence, range fluctuations. It will also reduce imaging quality.

A well-designed exchangeable tabletop can be implemented into the therapy planning system or measured by the CT scanner (if used). A nice "side effect" of such a solution is a better overall precision of the entire treatment process. It can also reduce sagging effects between planning imaging and consecutive treatment sessions. If the positioner is combined with a CT-on-rails system for treatment planning, and the positioner mechanics are similar in their specifications and layout, the overall deviation between the planning and treatment geometry caused by the mechanics comes close to zero.

33.6 Facility Workflow and QA

To build IBT facilities requires a large investment. Availability and patient throughput are relevant for their profitability. By reducing the patient's time in the treatment room, the usage of the beam can be increased. Here, a robotic patient positioner can help to improve the workflow. Proper immobilization needs time. It is, therefore, more favorable to immobilize the patient outside the treatment room and transfer the patient with a shuttle to and from the treatment room as has been shown in various presentations by PSI [1], the Heidelberg group, and others.

Another possibility to speed up the workflow is automation. Robotic patient positioners are ideal for this purpose. Automated movement under visual control

and automated docking procedures are programmable. It also reduces the overall treatment time. The time a therapist needs to walk through the maze can be used for patient setup with remote control by another operator.

33.7 Safety Aspects in Medical Equipment

Robots are the main actors in numerous science fiction stories. Other than in fiction, control of robots still needs to be done by a bundle of sensors, preprogrammed electronics and human interaction.

Robots are powerful, fast, and can be – if not properly controlled – dangerous to humans. When used as medical equipment, however, special care has to be taken to avoid any risk to the patient, the user, the service and maintenance staff, or the machine itself.

The medical industry has implemented processes into their design procedures to avoid such risks. It begins with a risk analysis based on the available functions. Mitigations are described, implemented, tested and documented. To find a balance between acceptable and feasible mitigations without impeding the applicability and the treatment is a challenge which will be discussed with some examples.

33.7.1 Collision Control

To prevent collisions is a primary concern when working with robots. The collision control system needs to be designed so that collisions with all known barriers (walls, beam outlets, imaging devices, etc.) are avoided. At the same time, the robot should perform its clinical tasks and impair the workflow as little as possible. This is always a conflict for the designer which needs to be solved individually.

33.7.2 Speed

The maximum permitted speed must be limited deep down in the control system, in order not to be reprogrammed unintentionally by the user. Stopping a movement needs to fulfill certain standards. This is also necessary for the maximum acceleration a patient accepts or the clinical procedure allows.

33.7.3 Control Standards

Medical standards ask for two independent ways of monitoring in a control system. There are various ways to design it. One is to duplicate as much as possible in the

controls. The control processors have to be fail-safe for the first error (e.g., bit flip in the main memory, sensor defect, or cable break). It needs “brain power” and a lot of experience in medical equipment design to find feasible mitigations. Safety integrity level controllers that reduce risks by 2–3 orders of magnitude (SIL 2) help in some cases.

33.7.4 Power Failure

Positioners used with a gantry are generally mounted outside the gantry structure for stability reasons. Some gantries have moveable floors which allow the patient to step on or off the tabletop if the gantry is in 0° angle. If power fails, there must be a backup solution to rescue the patient.

33.8 Design Principles of Robotic Patient Positioners

In combination with patient positioning, the term “robotic” is used today for any table solution which does not look like a conventional patient table or positioner at a conventional linac. Linear and rotating drives are used for positioners in various combinations.

Linear drives are precise on a submillimeter level, but only if mounted carefully and balanced correctly. The point of gravity of the weight to transport must be close to the drives. Otherwise their lifecycle will be degraded and the specifications cannot be met very long. Linear drives are sensitive to dirt and dust and need, therefore, to be covered well.

Rotational drives are precise down to some 10 μm accuracy. Bearings can handle extreme loads in all directions and can be sealed against dust, water, etc. easily. Special designs are available for every type of load and environmental conditions.

33.8.1 Custom Manufactured Solutions

The first installations in IBT used individually designed patient positioners using standard mechanical parts. These tables were exactly adapted to the specific environment they had to fit in. The designers of these solutions used linear drives for most of the movements.

Figure 33.3 shows the design principle. The base allows the whole structure to move between both ends of the gantry opening. Three linear drives and one vertical rotating axis bring the tabletop into position. Precision might be reduced when the horizontal arm is in its outermost position. Bending of the whole structure is then maximum. However, this table position is not very often used clinically.

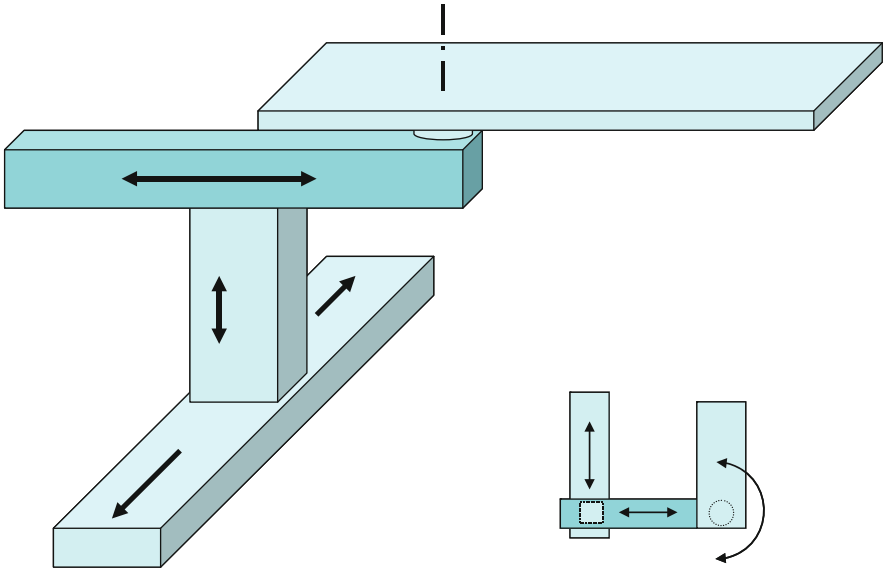

Fig. 33.3 Patient table as it is used at multiple sites in combination with proton gantries [7]. Sketch in lateral and top view

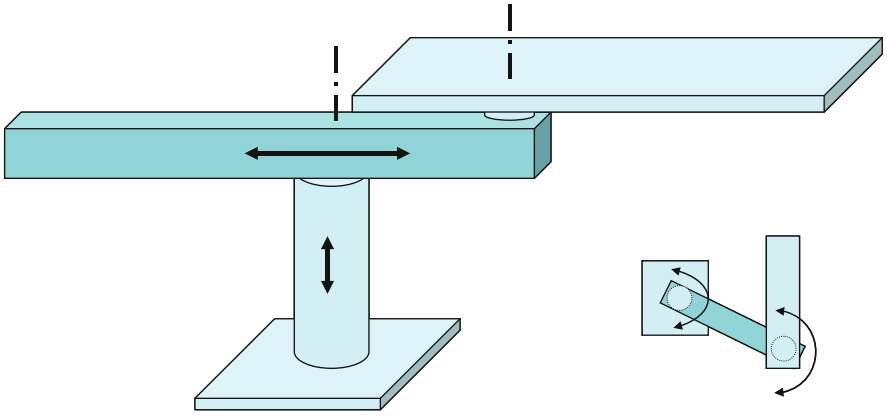

Fig. 33.4 Another concept of a patient positioner. Two linear and two rotational drives allow a flexible movement with improved precision

The construction, made by the Swiss company Schär for the Varian/Accel proton gantry (Fig. 33.4), uses two linear drives for horizontal and vertical movement and two vertical rotating-axis drives for positioning. The vertical moving column and the horizontal drive are built extremely heavy to maintain high precision. Because of the size of the vertical drive, this construction is probably designed only for usage

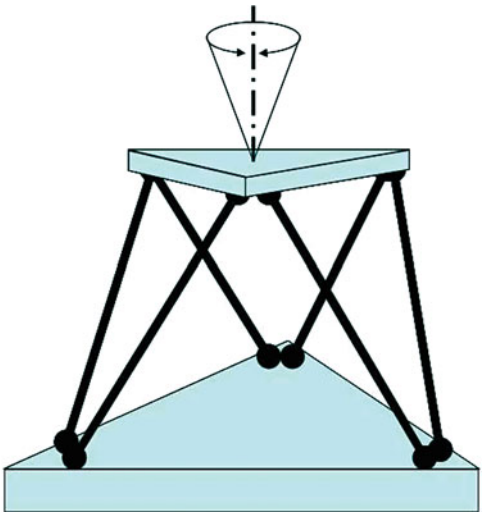

Fig. 33.5 A hexapod design using six hydraulic cylinders or linear drives to swivel the top platform

in combination with a gantry. It is possible to pitch and roll the tabletop within small angles for position correction.

A third, very interesting solution is the so-called "hexapod" (Greek for "six-footed"), originally designed for flight simulators (Fig. 33.5). The design is more than half a century old. It was probably developed in parallel by Steward, Gough and Cappel [8, 9]. The hexapod connects a stationary platform with a moving one using six independent linear drives. These drives are hydraulic cylinders or electrical spindle drives. At least two drives need to be controlled together for a movement. The design offers very complicated movements within a limited range of movements for the top platform. It is available as an off-the-shelf component including the control systems. This construction is used with add-on devices for conventional RT tables to enable pitch and roll capability [2] as well as in IBT in combination with a treatment chair at a fixed beam. Conceptually, the platform is not able to rotate within a wide range or to provide lateral or sagittal movements of several ten centimeters depending on the size of the platform. This limits the use of the hexapod to very specific treatment applications.

33.8.2 Standardized Solutions

The various solutions for patient positioners seem to have met their specifications and requirements reasonably well up to now. However, when designing an industrial product which should last more than 20 years, one needs to look into a more standardized solution which responds to the clinical needs of today and is also flexible enough to meet new demands in the future.

In the early phase of the design, it was logical to look into the industrial robot world to see what these mechanical miracles could do for patient support.

Industrial robots as we use them today are designed to work in large-scale production lines as in the car industry or in high risk areas. The specifications of these heavy-duty engines are impressive. They can transport more than a ton of load with a repetitive precision of ± 0.1 mm. The speed of the robot head is more than $2\,\mathrm{m\,s^{-1}}$ over a distance of 5–6 m, and they execute their tasks on preprogrammed paths for approx. 10 years with high reliability. The technology is in a mature state. But it is a bit more expensive than a conventional patient table.

Robots come in various mechanical variations depending on their specific tasks. Some general rules for the conceptual design can be distinguished:

- Longer arms => larger work space => less precise.
- More axes => more flexible => less precise.
- More load capability => less precise.
- Less linear drives => more precise.

The challenge for all manufacturers is to combine high flexibility with high precision and high load at a reasonable price. Today, mainly two types of industrial robots are used for patient positioning.

The first type is a vertical axis robot (Fig. 33.6). It has two vertical rotating axes to position a third vertical moving linear axis at any place in a circle around its base. This robot is typically used for precise positioning of parts (electronic parts on PC boards) or for precision drilling. For patient positioning in a clinical environment, it is a good choice if pitch and roll are not necessary.

The most common type of robots used today is the six-axes robot (Fig. 33.7).

This robot is highly flexible and is used for a great variety of applications. Some challenges need to be overcome, though, before it can be used to position patients.

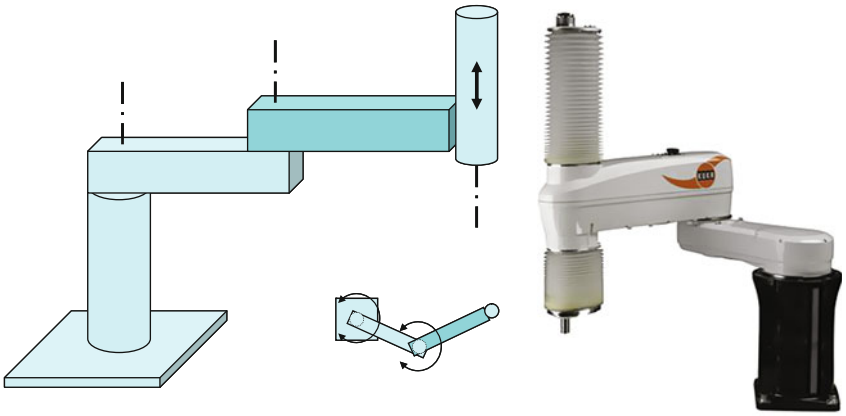

Fig. 33.6 Vertical axis robot. *Left*: Sketch in lateral and top view. The accessible range is a circle around the base. *Right*: Example of a vertical axis robot. Positioning accuracy: 0.02 mm; loading capacity: 10 kg. Courtesy of KUKA Roboter GmbH, Augsburg, Germany

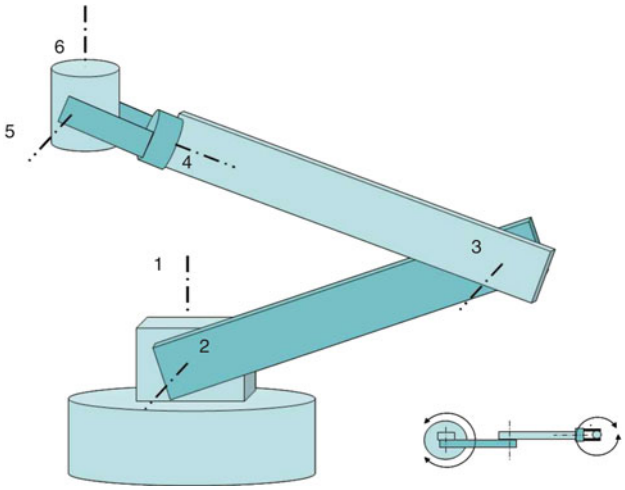

Fig. 33.7 Six-axes robot. The small sketch provides a view from the top

33.9 Design Steps and Challenges

Several features of six-axes industrial robots need to be modified when they are intended for the clinic:

Production robots move fast – a patient positioner should not.
Production robots move on predefined pathways – a patient positioner needs to move on any path.
Production robots are optimized for fast dynamic positioning procedures – a patient positioner should rather operate in "slow motion".
Production robots move their arms to any position – a patient positioner should not interfere with the therapist coming close to the patient.

Only some aspects of the design can be discussed here.

A first step towards modeling a 3D problem is a simulation. The robot manufacturers offer excellent simulation tools which can be adapted to the specific medical environment by adding CAD-edited tabletops, patients, etc. These tools can demonstrate all movements in 3D and allow implementing room limits and other possible obstacles or add-ons.

The first limitation in using an in-stock robot was that the standard 270° position opposite to a fixed beam could not be reached properly. Without major redesign of the robotic arms, it would have been necessary to lower the robot a little into the floor to permit a low table position in this alignment used mainly for head treatments.

To warrant safety, significant additions were required because in industrial applications humans are not allowed to work close to a robot! Accidents reported between humans and robots are mainly caused by bypassing the safety mechanisms or wrong handling in maintenance [10].

The arms of the clinical robot are equipped with collision switches. Room sensors detect if a person enters the treatment room while the positioner is operating. The control of all robotic devices is embedded in the room's safety system.

The final product is safe to use, fits into the overall machine control and fulfills all design and manufacturing standards.

If planning CT and treatment are not performed with the same positioner, weight-dependent corrections should be implemented. This will reduce positioning errors caused by bending mechanics. While weight cells are industrial standard, other sensors are also available.

33.9.1 Service and Maintenance

The patient positioner is a decisive part of the treatment room. If it fails, treatment and room are blocked.

Industrial robots, which are used in high-speed and dynamic modes, are designed for a life span of approx. 10 years. For slow-motion applications, it can be expected that they last longer. Nevertheless, when projecting an IBT facility, the possibility to replace the positioner or parts of it within the lifetime of the facility needs to be considered. The heavy machines have to fit through the maze of the treatment rooms and the floor needs to tolerate the transportation load.

Service and replacement periods should last less than 24 h. But this is only possible when standard parts are used. Additional service and medical QA time might also be necessary when the robot needs to be readjusted to its specifications.

33.9.2 The User Interface

It is nearly impossible for untrained people to perform a linear movement of a tabletop using the single-axis control provided by the robot companies. For a medical user, an interface similar to the single-pushbutton version for a conventional patient table needs to be provided. The only single-axis movement might be an eccentric tabletop turn using axis 6 (Fig. 33.7).

Since a robot patient positioner needs some space to move the arms, the personnel has to keep away from it. The user interface, e.g., a hand control, should, therefore, be remotely operable. A good choice is a wireless hand control with integrated safety button for emergency stop.

For the user, the hand control is the key to the robot positioner day by day. The more "intelligent" or intuitive this interface is designed, the better the acceptance will be. A robotic patient positioner is a challenge for a user who worked with conventional patient tables before. The satisfaction factor of this little piece of electronics should, therefore, not be underestimated!

33.10 History and Today's Solutions

33.10.1 The Pioneers of Robotic Positioners

The idea to use robots for patient positioning was patented in 1987 (Fig. 33.8). Implementation, however, was hardly possible at that time. In particular, 3D multiple axis controls were hard to design with the then existing technology.

In the mid-1990s, Niek Schreuder was one of the pioneers to build a robotic patient positioner for use at a proton therapy site at the iThemba Labs in South Africa and a second one at the MPRI [11]. Both were based on commercial robot arms.

Another pioneer in robotic positioning is Alejandro Mazal. He used a palletizing robot as a medical treatment table at the former Centre de Protonthérapie d'Orsay (today part of the Institut Curie). To this robot, he attached a tabletop as well as a chair. He also designed a treatment chair based on a hexapod robot.

33.10.2 Current Solutions

Positioning robots are still exceptions in IBT centers. One example is the six-axes robot positioner installed at the HIT facility in Heidelberg. Figure 33.9 shows some possible treatment positions and the step-on position at a 90° fixed beam. Any body

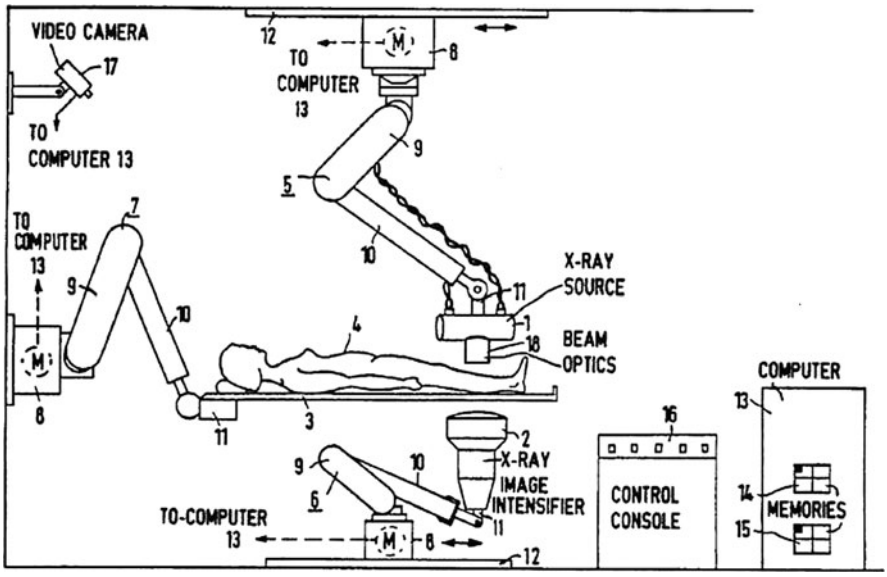

Fig. 33.8 An early patent to use a robot for patient positioning and two additional robots for imaging (H. Kresse, Siemens AG, 1987)

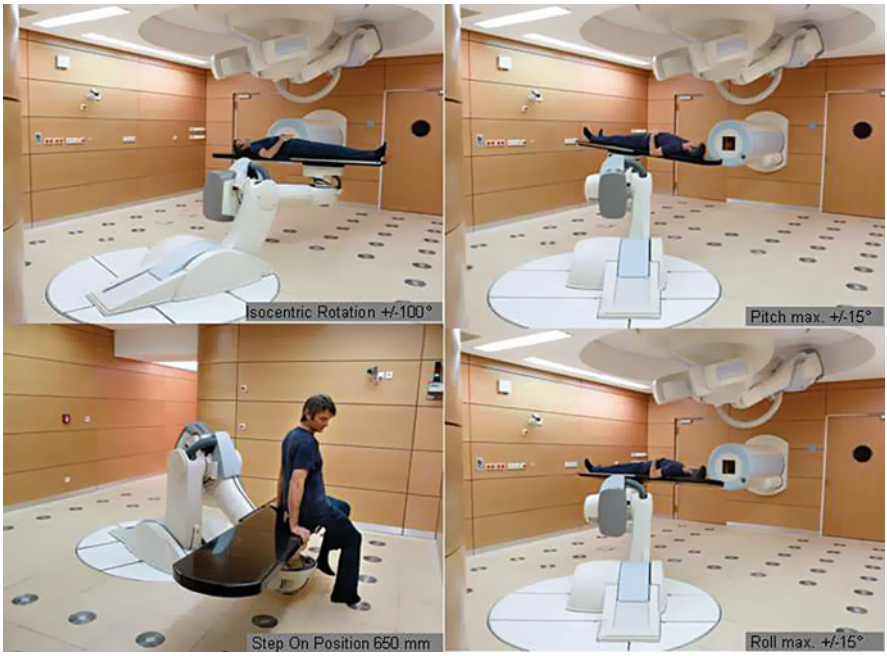

Fig. 33.9 Robotic patient positioner manufactured by Siemens for the Heidelberg Ion-Beam Therapy Center (HIT). Some of the possible positions typically used during patient treatment are shown

part of the patient from the head to the pelvic region can be positioned including pitch and roll. Position correction of a misaligned angle in immobilization set-up is corrected by extending the isocentric rotation or yaw to 200°.

The patient tabletop can be removed by pulling a handle or fully automatically. That way dedicated tabletops (e.g., flat or cradle-like) for specific applications can be connected easily. The QA tabletop illustrated in Fig. 33.10 is one example. The QA devices are permanently fixed on that top. If not in use, it is placed on a transport shuttle. The robot positioner picks up the complete set-up. Power and electrical controls, Ethernet links and sensors are directly connected to the tabletop and the lines are fed through the robotic arms. This allows automated procedures and positioning of the devices without taking care of cables or the necessity to enter the room in between measurements or QA steps.

The robot control system used supports more than six axes. It can, therefore, be used for additional functions, e.g., imaging for position verification (Fig. 33.11). Another six-axes robot mounted to the ceiling carries a C-arm comprising an X-ray tube and a detector. This allows imaging in a wide variety of treatment positions at isocenter and also off-center if compatible with the safety margins. Using this system, imaging can be performed as 2D X-ray in multiple axes and/or as 3D-CBCT. Complex movements for tomosynthesis or extension of the field of view can be programmed. Similar set-ups are in use in modern angiography systems.

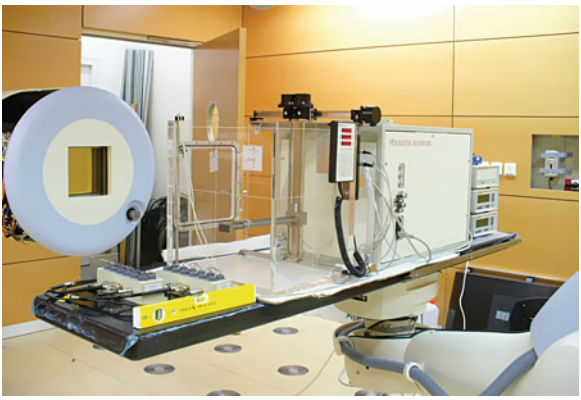

Fig. 33.10 A dedicated QA platform adapted to the robot positioner including a water tank and the necessary measurement equipment

Fig. 33.11 Robots in a treatment room of the HIT facility. The ceiling-mounted robot is used for imaging. In CBCT mode it rotates around the patient. The floor mounted robot positions the patient. The aligned system requires control of 12 degrees of freedom

A robot-based solution is not a low-cost solution for a patient positioner. But it is an excellent investment in the future of an IBT center. It can be upgraded without major downtime of the overall system. When planning a new IBT facility, robotic patient handling should be a must-have item. Adding features on conventional solutions will lead to limited flexibility and, more importantly, to lower-grade implementation and poor user interfaces. Upgrades of the robotic positioner will mostly be restricted to software adaptations which will improve the functionality, the user interface and lead to better integration.

33.11 Outlook

Robot positioners offer an enormous flexibility which will not only speed up the workflow, but might also have the potential to improve the treatment outcome.

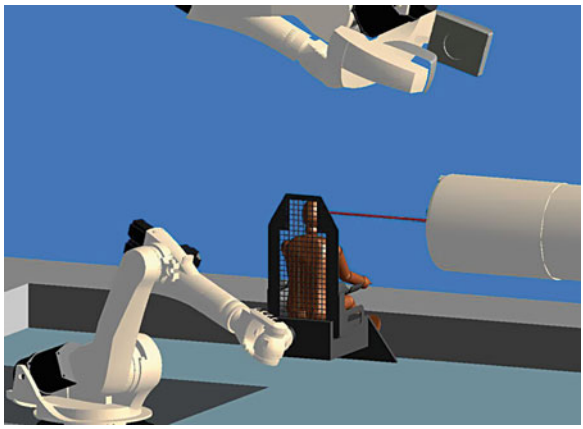

Fig. 33.12 Simulation of a treatment chair adapted to the robot positioner at a fixed beam. A patient can be rotated by 360° allowing all treatment angles similar to a gantry

Treatments in specially designed chairs are already provided at some IBT facilities. It is likely that most active centers will soon equip their treatment rooms with fully robotic tables. Patient- or disease-specific chairs and tables with exchangeable tabletops can easily be used as parts of the same system by reprogramming the common control system and user interface (Fig. 33.12).

In the future, patient chairs might not be restricted to treatments in the head and neck area. This will not only be a challenge for immobilization and imaging, but clinically, it would also mean to turn away from the supine position as general standard.

Treatment planning could be based on CTs from patients in upright or seated position. A robotic imager could be programmed to image a patient in other orientations than just horizontally lying. The upright position might need some habituation, but it might as well be of clinical advantage for targets below the diaphragm because respiration-coupled organ movements should be less pronounced than in the horizontal position.

Other novelties apply to user interfaces. Tactile surfaces and zero-force control systems will allow the user to manually move a patient into treatment position just by pushing the tabletop or a robot arm. New stronger and lighter materials for the mechanics may add even more precision for treatment with heavier ions.

Multimodality imaging will become more important for position control (e.g., MRI for prostate, liver and brain) or online beam control (e.g., in-beam PET). However, placing the imaging modalities close to the beam exit will limit the space for proper patient positioning. Even a redesign of the imaging modalities may be necessary. An MRI scanner in the vicinity of an ion beam will possibly change the beam path in an unpredictable way. If there is enough space in the treatment room, one can add conventional imaging gantries (PET, CT, MRI) on rails and let the robot move the patient between the imaging modalities and the beam outlet. If optimization of treatment planning will be automated and faster than today, a "see–plan–treat" machine could be designed using a single robotic patient positioner combined with the best imaging and treatment in a single room (Fig. 33.13).

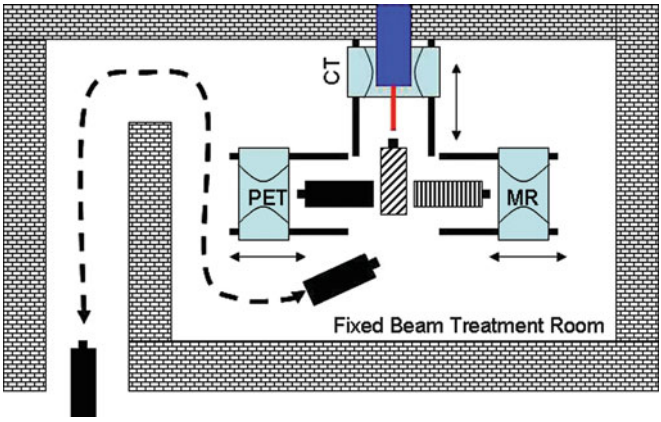

Fig. 33.13 Sketch of a "see-plan-treat" machine combining CT on rails parked over the fixed beam outlet combined with PET and MR imaging. The robot positioner moves the patient between the imaging modalities and the treatment positions

Probably a bit further on the horizon but conceivable is the idea of a "see–plan and treat-in-one-day" cancer treatment. After all, single-fraction treatment with carbon ion beams has already successfully been applied in Japan (cf. Chap. 14).

References

1. A. Bolsi, A. Lomax, O. Stadelmann, G. Goitein, Remote patient positioning in proton therapy. Proceedings of 14th International Conference on Medical Physics, Nuremberg, Germany, 14–17 Sept 2005, in Biomed Technik **50**(Suppl 1, Part 1), 2005
2. R.A. Sweeney, M. Vogele, A. Wegmayr, et al., The patient positioning concept for the planned MedAustron centre. Radiother. Oncol. **73**(Suppl 2), S64–S67 (2004)
3. E.W. Blackmore, B. Evans, M. Mouat, Operation of the TRIUMF proton therapy facility. Proceedings of Particle Accelerator Conference (PAC), Vancouver, Canada, 12–16 May 1997, in IEEE PAC 1997 Proc. 3831–3833, 1998. http://epaper.kek.jp/pac97/papers/pdf/7P109.PDF. Accessed Mar 2011
4. D.E. Bonnet, A. Kacperek, M.A. Sheen, et al., The 62 MeV proton beam for the treatment of ocular melanoma at Clatterbridge. Br. J. Radiol. **66**, 907–914 (1993)
5. K. Noda, Overview of NIRS Accelerator Activity. Presented at the Workshop on Hadron Beam Therapy, Erice, Italy, 24 Apr–1 May 2009. http://erice2009.na.infn.it/TalkContributions/Noda.pdf. Accessed Mar 2011
6. K. Nemoto, K. Seiji, K. Sasaki, et al., A Novel support system for patient immobilization and transportation for daily computed tomographic localization of target prior to radiation therapy. Int. J. Radiat. Oncol. Biol. Phys. **55**, 1102–1108 (2003)
7. G. Silke, L. Nissley, T. Hurn, et al., An advanced six axis patient positioner for use in proton therapy. Presented at Seventh ANS Topical Meeting on Robotics and Remote Systems, Augusta, GA, USA, 27 Apr–1 May 1997
8. V.E. Gough, S.G. Whitehall, Universal tyre test machine. Proceedings of FISITA IX International Technical Congress, 1962, pp. 117–137

9. D. Stewart, A platform with six degrees of freedom. IMechE Proc. Arch. **180**, 371–386 (1965)
10. United States Department of Labor, http://www.osha.gov/oshstats/index.html. Accessed 20 Nov 2010
11. J.E. Katuin, A.N. Schreuder, W.M. Starks, J. Doskow, The use of industrial robot arms for high precision patient positioning. Proceedings of Int Conf on the Application of Accelerators in Research and Industry, 17th CAARI, Denton, TX, 12–16 Nov 2002, ed. by J.L. Duggan, I.L. Morgan. AIP Conference Proceedings 680 (AIP, Melville, NY, 2003), pp. 1138–1141. www.iucf.indiana.edu/proton/docs/denton02a.pdf. Accessed 20 Nov 2010

Part VIII
Individual Facilities and Management Issues

Chapter 34
Twenty Years of Proton Radiation Therapy at Loma Linda University Medical Center

Jerry D. Slater

Abstract The proton treatment center at Loma Linda is the first hospital-based proton facility in the world. Dr. James M. Slater spearheaded its development in response to the need to reduce normal tissue injury and unacceptable side effects. Loma Linda physicians treat a wide range of cancers and other conditions with protons; studies are ongoing to expand applications and realize the still-evolving potential of the modality.

34.1 Introduction

At this writing, the proton treatment facility at Loma Linda University Medical Center (LLUMC) is completing its second decade of clinical operation. When the facility, now named the *James M. Slater, M.D., Proton Treatment and Research Center*, opened in October 1990, it was the world's first hospital-based proton treatment facility. Today, eight proton centers, mostly hospital based, serve or soon will serve patients in the United States; worldwide, 31 facilities deliver protons or carbon ions to patients [1]. The LLUMC center began with the vision and pioneering investigations of Dr. Slater more than two decades before it opened; in the years since, it has remained a state-of-the-art facility (for the history cf. Chap. 1).

J.D. Slater (✉)
Department of Radiation Medicine, Loma Linda University Medical Center, 11234 Anderson Street, CSP A-1010, Loma Linda, CA 92354, USA,
e-mail: jmslater@dominion.llumc.edu

U. Linz (ed.), *Ion Beam Therapy*, Biological and Medical Physics, Biomedical Engineering, DOI 10.1007/978-3-642-21414-1_34,

34.2 The Origin of Proton Therapy at LLUMC

Normal tissue sparing was the fundamental reason for Dr. Slater to study alternatives to X-ray-based radiation therapy. Key concerns were (1) to reduce doses to normal tissues, which required better means of identifying the target volume, and (2) conforming the needed dose to that volume.

Dr. Slater and others at LLUMC addressed the first concern with the pioneering development of digital-image-based, computer-assisted radiotherapy planning in 1971 (Fig. 34.1, see also Fig. 1.1); the first system used ultrasound images, followed in the mid-1970s by a system employing CT scans when the technology became available [2, 3].

Studies addressing the second concern began in 1970 and continued until the mid-1980s, when the decision was made to build the LLUMC facility. From the outset it was clear that some form of heavy charged particle irradiation would be an excellent way of delivering conformal therapy. In 1970, when studies began at LLUMC, heavy charged particles were being investigated for therapy at several physics laboratories around the world. Most offered proton therapy (PT), but other particles, such as negative pi-mesons and heavy ions, were being employed. Researchers of LLUMC studied all available options and participated in investigations, including pion trials at Los Alamos National Laboratory, Los Alamos, NM, USA [4] and studies of heavy ions at Lawrence Berkeley Laboratory (LBL), Berkeley, CA, USA [5]. Eventually, the proton was selected because its combination of capabilities seemed ideal for routine radiation therapy.

In 1986, therefore, LLUMC administration decided to proceed with a proton treatment center. The medical center entered into agreements with Fermi National Accelerator Laboratory (Fermilab) to perform conceptual and engineering design studies, and Fermilab later built the proton synchrotron [6]. Further contributions came from the architectural firm NBBJ; the McCarthy firm of general contractors, which built the structure; Scientific Applications International Corporation (SAIC), which assisted in transferring the technology from Fermilab to LLUMC; Martinez and Turek, a California firm that built the gantries used to rotate the proton beam

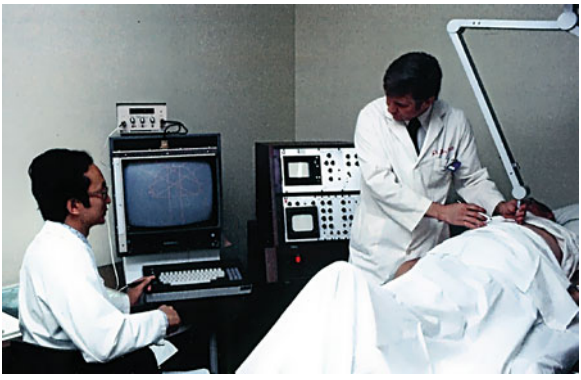

Fig. 34.1 James M. Slater, M.D., (*right*) and William Chu, Ph.D., medical physicist, in 1972, demonstrating the initial, ultrasound-based treatment planning system

around the patient; Loma Linda University Radiation Research Laboratories, forerunner of Optivus Proton Therapy, Inc., which played a leading role in developing the facility's control systems for the accelerator and treatment rooms; and faculty and staff of the LLUMC department of radiation medicine, who helped develop guidelines and specifications necessary for employing the synchrotron and facility to benefit patient care. The facility opened in October 1990 as the Proton Treatment Center [7]. In 2007, in recognition of his leading role in developing the facility and hospital-based PT generally, the LLUMC center was formally renamed in Dr. Slater's honor.

34.3 Developing Clinical Strategies for PT

By 1990, PT was known to be excellent for treating certain kinds of tumors and diseases, usually difficult-to-treat conditions such as ocular melanomas and lesions intimate to vital structures. When planning the LLUMC facility, however, it was intended to use protons for virtually any localized or regional solid tumor, in any anatomic site. After all, patients ordinarily treated with photon irradiation would almost all benefit from the ability to deliver highly conformal treatments to the intended target while avoiding normal tissue and thus minimizing side effects.

In order to evaluate protons in many clinical sites, it was important that the facility had the capabilities to treat not only more sites but also admit a significantly larger volume of patients than was previously possible in nonhospital centers, in order to accumulate significant clinical data. Presently, about 150 patients are treated per day. As of 1 April 2010, the number of patients treated with protons at LLUMC was nearly 14,500. This extensive clinical experience results in part from the efficiency designed into the facility, in terms of the placement of clinics, simulation rooms, dressing rooms, physician offices, control rooms, and so on; from the reliability designed into the treatment system; and because of the capacity designed into the facility, with several beam lines and treatment rooms, permitting accumulation of a sufficient body of patient data to validate outcomes (Fig. 34.2).

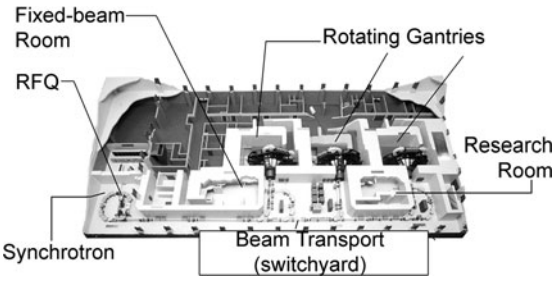

Fig. 34.2 Cutaway model of the proton treatment floor. The fixed-beam room has two beam lines, for eye and for head-and-neck treatments. The research room has three beam lines. The unlabelled rooms at top include dressing rooms for patients, control rooms for the gantries and the fixed-beam room, and rooms for physicians and technologists to evaluate plans and consult on individual cases

The large patient throughput results not only from the initial facility design but also from exploiting technological advances and upgrading regularly. For example, power supplies for the accelerator have been upgraded often; new gantry devices have been installed, notably hardware modifying the manner in which beam exits the gantry; and the beam control and treatment planning systems have been upgraded as needed. One major advance facilitating patient throughput, accuracy, and daily operational efficiency was a computer-assisted digital alignment system. In addition, a new accelerator control system was implemented, enabling further future upgrades such as beam scanning and intensity-modulated proton therapy (IMPT). Efforts to maintain optimal operating efficiency have permitted high patient throughput with safety to patients and personnel [8], while retaining individualized treatment for each patient.

Exploiting the therapeutic potential of protons has been ongoing since the facility opened. Initial goals were to: (1) build on prior experience with photon and proton irradiation by investigating additional anatomic sites; (2) develop therapy protocols and evaluate outcomes; and (3) improve or develop technology to investigate additional anatomic sites.

Using protons to: (1) reduce treatment-related morbidity for patients having conditions for which curative treatments exist but have been associated with significant morbidity, and (2) improve control rates for tumors not well controlled by other means were the main objectives of the clinical investigations. Studies proceeded in small steps. Initial dose-escalation studies for prostate cancer, for example, explored whether total doses only 10% higher than that used in conventional photon treatment could be administered without increasing morbidity. If desired outcomes occurred, further dose-escalation studies were pursued. Other studies investigated whether lower morbidity rates occurred using the same total doses as with photons.

Investigations proceeded on the premise that ionizing radiation from any source will destroy targeted tissue if the total dose is sufficiently high. The chief consideration was whether the needed doses could be delivered to patients without causing unacceptable permanent damage to untargeted tissues. Given that protons permitted one to control the physical dose distribution and avoid much normal tissue, the slightly higher proton radiobiologic effect (RBE of 1.1) was not considered significant but is taken into account in prescribing dose.

34.4 Clinical Applications

The clinical program at LLUMC has undergone significant changes over the past two decades. We typically divide these into different phases, which were defined by technology, operative, and clinical developments. The initial phase began with the opening in 1990 and was primarily focused on quality assurance and integration. Our clinical programs attempted to reproduce outcomes other proton facilities had achieved. During this phase, sites were limited, and prescribed doses were those that had previously been reported at other institutions. The second phase began

Table 34.1 Overview of anatomic sites treated with protons at LLUMC, 1990 to present

1990–1994	Ocular melanomas
	Orbital tumors
	Chordomas
	Chondrosarcomas
	Meningiomas
	Acoustic neuromas
	Pituitary adenomas
	Craniopharyngiomas
	Radiosurgery (AVM)
	Locally advanced prostate cancer
1995–2008	Pediatric CNS
	Oropharyngeal cancer
	Recurrent nasopharyngeal cancer
	Early lung cancer (Medically Inoperable)
	Early prostate cancer
	Radiosurgery (Brain Metastasis)
	Macular degeneration
	Pediatrics (Non-CNS)
	Hepatocellular cancer
	Locally advanced lung cancer
	Early breast cancer
2009–Present	Early prostate cancer (Hypofractionated)
	Pancreatic cancer
	Recurrent para-aortic nodes (in development)
	Locally advanced cervix cancer (in development)

in approximately 1994, with the opening of the second and third gantries and completion of our prototype treatment planning system. The clinical foci were on expanding to other anatomic sites and modifying the fractionation schedules; the latter concentrated primarily in the direction of hypofractionation and accelerated fractionation in different anatomic sites. These studies continue: priority is given to patients on clinical trials, and patients are only accepted outside of clinical trials when beam time permits. The third phase, just begun, emphasizes more difficult therapeutic problems.

An overview of some of the sites treated at Loma Linda is presented in Table 34.1. For many anatomic sites, treatment strategies and sites evolved over time, as experience and technology accumulated. Discussions of some of these evolutions are noted in the sections below.

34.4.1 Stereotactic Radiosurgery of the Central Nervous System and Base of Skull

Proton radiosurgery is used to treat brain metastases and arteriovenous malformations (AVMs). In comparison with photon beams from a linac or gamma knife,

protons produce less normal tissue radiation, especially for larger volumes and peripheral lesions; offer better coverage for irregularly shaped volumes; and yield more uniform doses within target volumes. One application pioneered at LLUMC has been in treatment of large AVMs. Investigators from the departments of radiation medicine, neurosurgery, and neuroradiology are collaborating with investigators from the departments of neurosurgery and neuroradiology at Stanford University to evaluate a program for treating large (>3 cm) AVMs with surgery, embolization, and hypofractionated protons. The program has been pursued since 1994; doses of 20–25 GyE in 1–5 fractions are given, based on the volume of the target.

34.4.2 Fractionated Proton Treatment for Tumors of the Central Nervous System

Loma Linda clinicians employ fractionated protons for most lesions occurring in the central nervous system (CNS) and the base of the skull, including chordomas and chondrosarcomas [9, 10]; acoustic neuromas, including large, recurrent, and unresectable cases [11]; meningiomas, and pituitary adenomas [12]. Proton radiation therapy offers new potentialities for treating glial tumors of the CNS [13], and is used as primary treatment or in combination with other modalities. Further, proton radiation is a primary treatment option for patients with benign CNS tumors, traditionally viewed as candidates for primary surgery. Although stereotactic treatment approaches, featuring one or a few treatments, are often used for these lesions, the precision of the proton beam and modern methods of positioning patients in effect make fractionated PT as precise as stereotactic methods [14].

34.4.3 Diseases of the Eye

Historically, proton irradiation yields control rates exceeding 95% for small ocular melanomas, and rates of eye retention typically reach 90%. Loma Linda clinicians evaluated the efficacy and safety of PT for medium-size and large melanomas, as well [15]. Overall, our results are consistent with other institutions' outcomes and indicate that protons are effective and safe for melanomas of all sizes, and often can preserve the eye and its function.

34.4.4 Tumors of the Head and Neck

At LLUMC, protons are used to treat locally advanced oropharyngeal cancer. It has been shown that protons, used as a concomitant boost, effectively deliver an accelerated time–dose schedule to the cancer with a more tolerable schedule to surrounding

normal tissues. Results thus far have revealed increased locoregional control without increased toxicity, as compared to other radiation techniques delivering lower doses. Studies are ongoing to optimize the time–dose schedule [16]. We also employ PT for nasopharyngeal cancers, including retreatment following photon radiation [17].

34.4.5 Lung Cancer

Of new cases of lung cancer diagnosed annually in the US, about 20% of patients have clinical stage I disease; about 15% are medically inoperable, although many have technically resectable disease. Conventional irradiation can control early-stage inoperable lung cancer but can also result in irreversible injury to functional lung tissue. LLUMC studied not only whether protons could be used to control the disease, but also whether protons could deliver the total dose in fewer fractions than conventional photon radiation, while continuing to spare adjacent lung tissue and minimize side effects. Preliminary studies indicated that it could, owing to reduced integral volume doses when compared with photon plans [18]. A prospective phase II clinical trial to determine the efficacy and toxicity of high-dose hypofractionated proton radiotherapy was conducted. Doses as high as 60 GyE were delivered in ten fractions over 2 weeks. No symptomatic radiation pneumonitis or late esophageal or cardiac toxicities were seen. It could be concluded that high-dose hypofractionated PT can be administered safely and with minimal toxicity, and that local tumor control appears to be improved when compared to results of conventional radiotherapy, with a good expectation of disease-specific survival [18, 19]. More recently, investigations have begun for locally advanced non-small cell lung carcinoma (NSCLC) using altered fractionation and concurrent chemotherapy.

34.4.6 Breast Cancer

At LLUMC, hypofractionated PT is also being used for early-stage breast cancer. However, protons are not used to treat the entire breast, as is commonly the case in photon regimens following lumpectomy or partial breast resection. They are delivered instead to a more circumscribed volume around the postoperative site (Fig. 34.3) [20].

Two clinical trials have been conducted: each delivered a total dose of 40 GyE in 10 fractions of 4 GyE each; treatment, typically, was given with three or four beams, with several fields treated daily. Preliminary analysis showed excellent local control with no treatment-related sequelae seen. Data from the first trial have been accumulated and have been submitted for publication. The second trial has finished accrual. Results have been good in terms of the patients' ability to complete the program with minimal side effects.

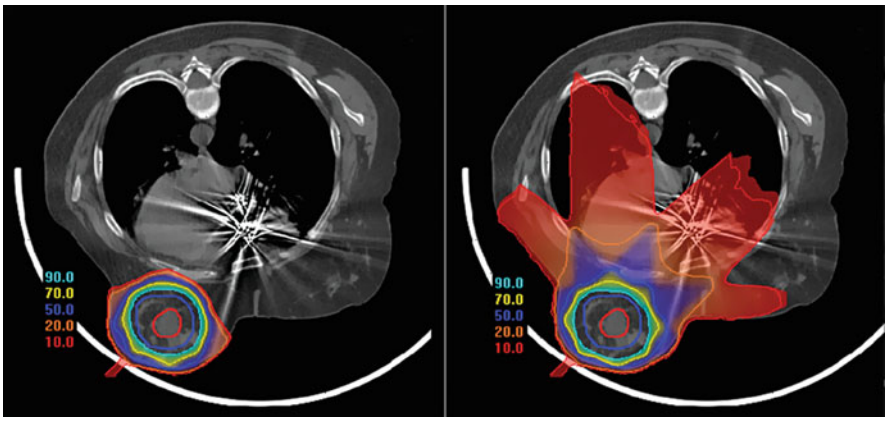

Fig. 34.3 Proton irradiation of the breast (*left*), compared with an intensity-modulated photon plan. The lumpectomy site is indicated by a *red circle* within the breast. *Color washes* indicate that the proton plan allows for complete sparing of both lungs, the heart, and the contralateral breast

34.4.7 Hepatocellular Carcinoma

Primary liver cancers are associated with a high mortality rate, in part because many patients cannot undergo surgery due to concomitant cirrhosis. A first phase II clinical trial using an accelerated fractionation schedule to determine the efficacy and toxicity of PT for patients with locally unresectable hepatocellular carcinoma (HCC) revealed local tumor control rates superior to conventional radiation therapy, and comparable overall survival. Most patients have demonstrated markedly reduced posttreatment alpha-fetoprotein levels, and some, given protons to prepare for liver transplantation, have been found to have no evidence of residual carcinoma in the explanted liver. Posttreatment toxicity has been minimal [21]. An updated report has been completed and is being submitted for publication.

34.4.8 Prostate Cancer

LLUMC has a long experience with protons for prostate cancer (cf. also Chap. 16). Current treatment programs were developed within a conservative approach aimed at optimizing PT. Because the proton treatment facility was designed to treat up to 200 patients per day, a large, intrainstitutional clinical experience could be accumulated. The initial treatment scheme was not very different from standard photon protocols (the total dose was increased by only 10%). Preliminary results showed that conformal PT at that dose level yielded disease-free survival rates

comparable with other forms of local therapy, with only minimal morbidity [22]. Results were even more favorable when patients with early-stage disease were evaluated [23]. Further, in reference to the common perception that younger men (less than 60 years of age) should be treated by surgery rather than radiation, studies demonstrated no significant difference when groups were divided by age [24].

As experience accumulated, it gradually emerged that the precise proton dose distribution would enable higher doses, to increase the probability of disease control while retaining low rates of side effects. A phase III randomized trial in collaboration with investigators from Massachusetts General Hospital (MGH) demonstrated that men with clinically localized, early-stage prostate cancer had a significantly increased likelihood of biochemical control if they received high-dose conformal radiation, without increasing grade 3 acute or late urinary or rectal morbidity [25, 26].

Most of the patients treated for prostate cancer at LLUMC receive total doses of 80 GyE or more. At this writing, patients are being enrolled in a clinical trial of hypofractionated PT, delivering the total dose in 4 weeks rather than eight to nine. Experience with hypofractionated regimens for other disease sites underlies the prostate trial, as well as the repeated demonstration from dose-escalation studies that high total doses can be delivered with protons without increasing the side effects. The same proton dose distribution that enables dose-escalation studies makes hypofractionation studies possible.

34.4.9 Pediatric Tumors

Tumors in children have always presented a special problem for radiation treatment: damage to growing normal tissues can lead to a progressive series of side effects that persist throughout the patient's lifetime.

When treating children with ionizing radiation, avoiding even moderate doses to normal tissues is essential. A reduced dose and a smaller irradiated volume should reduce radiation effects, but full expression of late effects may occur decades after treatment.

At LLUMC, the physical dose distribution of protons is exploited to spare growing tissues as much as possible for a variety of pediatric treatment problems [27–34].

Protons limit treatment-related morbidity in children with tumors in or near the developing brain and spinal cord. A dramatic example can be seen in the case of a very young child treated with PT for medulloblastoma: craniospinal protons reduced the dose to the cochlea and vertebral bodies and essentially eliminated the exit dose through the thorax, abdomen, and pelvis (Fig. 34.4). Radiation-related sequelae were minimal; the technique may be especially advantageous in children having a history of myelosuppression [33].

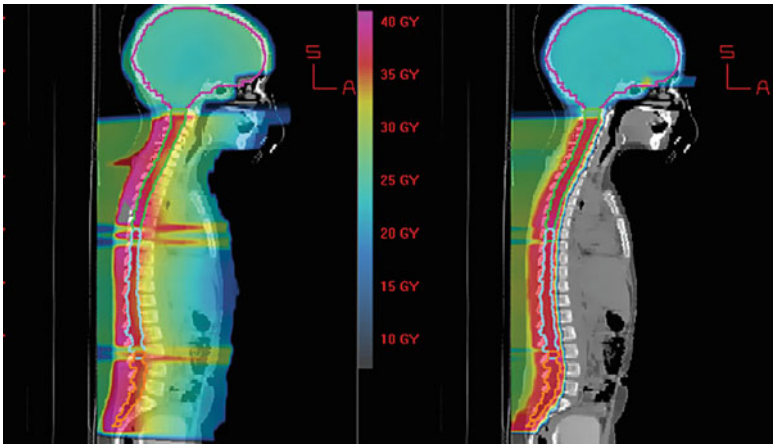

Fig. 34.4 Comparison of dose distribution using X-rays (*left*) and protons (*right*) in the irradiation of the craniospinal axis and posterior fossa for the treatment of medulloblastoma in a 3-year-old child. Note the substantial reduction in the dose to the vertebral bodies, and virtual elimination of the exit dose through the chest, abdomen, and pelvis

34.5 Clinical Perspective

The fundamental objective of using protons is sparing the normal tissue. The greater the extent to which the dose to normal tissues can be reduced, the lesser is the likelihood of compromising radiotherapy because of unacceptable side effects. Reducing or eliminating the radiation dose to normal tissues not only allows one to deliver the total needed dose but also affords opportunities to deliver that dose in fewer fractions without increasing side effects. This has been borne out in several comparative dosimetry studies and clinical trials: sites as disparate as the breast, lung, liver, and prostate illustrate the use of hypofractionation; conformal dose distributions and attendant sparing of normal tissues make this possible. We are examining hypofractionation as a possible way to reduce treatment time and costs, provided that control rates are maintained and side effects do not increase. Results obtained thus far are promising.

Minimizing the integral dose to normal tissues is a salient goal. Much attention centers around eliminating the dose to normal tissues where possible, or otherwise minimizing the volume of normal tissue receiving some dose of radiation. We presume that there is no "safe" radiation dose. Studies dating back more than 40 years support the notion that there is no "safe" radiation exposure of normal tissue. Tissues have varying ranges of radiation tolerance; some express radiation injury soon after relatively low doses; others may not express clinical injury till many years after larger doses. Given enough time, however, any irradiated tissue will demonstrate chronic radiation-related injury [35, 36].

34.6 The Research Foundation

When the proton facility was designed, a dedicated research beam line was included in addition to the four treatment rooms. Further, a program of basic radiobiological studies was established to lay foundations for treatment programs later developed for PT of various anatomic sites. Needs for a separate and comprehensive suite of laboratories and laboratory personnel were foreseen; plans to develop the laboratory complex were made before the hospital-based treatment facility opened.

An important part of the research program is collaboration with the National Aeronautics and Space Administration (NASA). Both NASA and LLUMC have similar needs to understand the outcomes of radiation in animals and humans: NASA, for understanding risks to astronauts undergoing long-duration space missions; LLUMC, to better understand radiation effects in normal tissue. Both are interested in ways to minimize those risks, and the proton beam affords a useful tool for studying them, given the prevalence of protons in intergalactic radiation and the increasing use of different proton dose schedules such as hypofractionation.

Various basic and translational studies have been performed over the last two decades. Some investigators are studying fundamental issues involving radiation and its interaction in cells and subcellular components, and the potential synergistic effects of radiation in association with other factors, such as drugs or the rigors of space travel. Low-dose/low-dose rate gamma and proton irradiation is being studied in terms of background radiation in space and possible synergistic effects when used prior to high-dose therapeutic irradiation. Radiation protection is the focus of another line of investigation; some antioxidants have been studied to determine whether normal cells can be protected without also protecting tumor cells against radiation. The effects of space flight on biological responses are being studied, as are the biological effects of scanned vs. passive proton radiation and radiation effects on CNS-immune interactions. An intriguing area of study is the bystander effect. Technologies are being developed to manipulate interactions between specific cells in a population, and to understand how they influence each other's responses to irradiation. Other studies are ongoing with regard to the effects of protons and heavier ions on CNS functions [37–43].

The preclinical research program includes several translational studies. A major effort is a Precision Patient Alignment System, now installed in one of the gantry rooms. It has been commissioned by physics and physician personnel, and is in clinical use. The system calculates and adjusts patient alignment automatically to place the treatment target within 1 mm of the patient's treatment plan, and will help to decrease daily patient treatment time and improve precision (Fig. 34.5). Work also continues on active beam scanning; a system is operational in the research room. A scanned proton beam will be an important tool to treat a greater variety of patients with larger and more irregular tumors.

Translational studies are also proceeding on studies of proton track structure; investigators have developed and tested the concept of a compact ion detector that allows imaging the individual ionizations of individual particle tracks with

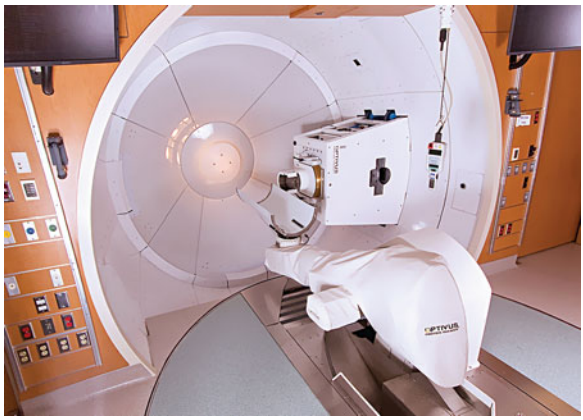

Fig. 34.5 Robotic positioner in place, Gantry Room 1, James M. Slater, M.D., Proton Treatment and Research Center

nanometer resolution. The project studies the spatial distribution of ionizations in the vicinity of charged particles, to better understand the effects of protons and other particle radiation on DNA, chromosomes, cells, tissues, and organisms [44]. In a related investigation, the accuracy of PT depends on accurate knowledge of the penetration depth of the beam and the actual electron density or relative proton stopping power distribution of materials and tissues in the proton path. Proton CT (pCT) offers a means to more accurately determine penetration depth [45].

Finally, PT is being evaluated for neuroscience applications. Long-term goals are to: (1) further improve the safety of PT and radiosurgery for lesions of the brain and spinal cord, and (2) to treat functional disorders of the central nervous system such as intractable epilepsy and central pain syndromes with protons. Technical preparations are being made for this use [46].

34.7 Looking Ahead

Hospital-based centers are increasing worldwide. The existence of more large clinical facilities, and the large numbers of patients they will serve, will permit multi-institutional cooperative clinical trials that lead to valuable clinical data about employing PT. This amplifies a process begun at LLUMC: one reason that the facility has several treatment rooms and is located on the hospital campus is to offer a full spectrum of evaluation and necessary treatment services. This is important to patients and also for developing meaningful clinical data.

Further advances in technology, and radiobiological investigations, will facilitate the ability to exploit capabilities even more in the future. One example, noted above, is the use of robotic patient positioning devices and real-time monitoring of patient and tumor during treatment. An active beam delivery system is another. Such developments will increase precision and repeatability.

Protons hold promise for treatment planning, replacing the photon-based CT systems commonly employed today with a system that uses protons. Because conformal proton radiation therapy requires accurate prediction of the Bragg peak position, proton imaging may be more suitable than conventional X-rays for this task.

Hypofractionation studies will continue; hypofractionated paradigms will deliver the necessary total doses while still reducing or eliminating normal-tissue radiation and resultant side effects. They will also reduce overall costs. Given that costs such as beam time and therapists' salaries are a fixed part of each treatment fraction delivered, hypofractionated regimens will lead to cost reductions.

LLUMC will continue to concentrate on advancing technology for PT. Clinicians and researchers are working toward several outcomes, including

1. Fully computer-assisted treatment rooms, featuring automated patient alignment systems and a scanning beam
2. Continued investigation of alternate fractionation schedules, including accelerated programs and hypofractionation
3. Adjunctive radioprotection of crucial anatomic sites to enhance treatments and protect crucial sensitive tissues intimate to radiation fields
4. Studies to enhance tumor radiosensitivity and
5. Proton treatment of benign diseases and neurological disorders

PT is still a relatively young discipline, and, as the foregoing suggests, its optimal uses are yet to come, even granting the remarkable results in disease control and reduced side effects that have already been achieved at centers around the world. The ability to spare normal tissue opens up opportunities for uses and strategies that are difficult, if not impossible, to undertake with photon regimens. Research and clinical studies to realize this potential – in therapeutic efficacy, new applications, and reduced costs of treatment – must continue.

References

1. PTCOG Web site, summary of current ion beam therapy facilities. http://ptcog.web.psi.ch/ptcentres.html. Accessed 6 Mar 2010
2. J.M. Slater, I.R. Neilsen, W.T. Chu, et al., Radiotherapy treatment planning using ultrasound-sonic graph pen-computer system. Cancer **34**, 96–99 (1974)
3. I.R. Neilsen, J.M. Slater, D.W. Shreyer, CT Scanner Assumes Key Role in Computer-Based Radiotherapy Planning System, in *Medinfo 80: Proceedings of the Third World Conference on Medical Informatics*, ed. by D.A.B. Lindberg, S. Kaihara. (North Holland, Amsterdam, 1980), pp. 25–28
4. C.F. von Essen, M.A. Bagshaw, S.E. Bush, et al., Long-term results of pion therapy at Los Alamos. Int. J. Radiat. Oncol. Biol. Phys. **13**, 1389–1398 (1987)
5. J.R. Castro, W.T. Saunders, C.A. Tobias, et al., Treatment of cancer with heavy charged particles. Int. J. Radiat. Oncol. Biol. Phys. **8**, 2191–2108 (1982)
6. J.M. Slater, D.W. Miller, J.O. Archambeau, Development of a hospital-based proton beam treatment center. Int. J. Radiat. Oncol. Biol. Phys. **14**, 761–775 (1988)

7. J.M. Slater, J.O. Archambeau, D.W. Miller, et al., The proton treatment center at Loma Linda University Medical Center: rationale for and description of its development. Int. J. Radiat. Oncol. Biol. Phys. **22**, 383–389 (1992)
8. M.F. Moyers, D.A. Lesyna, Exposure from residual radiation after synchrotron shutdown. Radiat. Meas. **44**, 176–181 (2009)
9. E.B. Hug, J.D. Slater, Proton radiation therapy for chordomas and chondrosarcomas of the skull base. Neurosurg. Clin. N. Am. **11**, 627–638 (2000)
10. E.B. Hug, L.N. Loredo, J.D. Slater, et al., Proton radiation therapy for chordomas and chondrosarcomas of the skull base. J. Neurosurg. **91**, 432–439 (1999)
11. D.A. Bush, C.J. McAllister, L.N. Loredo, et al., Fractionated proton beam radiotherapy for acoustic neuroma. Neurosurgery **50**, 270–273 (2002)
12. B.B. Ronson, R.W. Schulte, K.P. Han, et al., Fractionated proton beam irradiation of pituitary adenomas. Int. J. Radiat. Oncol. Biol. Phys. **64**, 425–434 (2006)
13. D.S. Gridley, R.S. Grover, L.N. Loredo, et al., Proton-beam therapy for tumors of the CNS. Expert Rev. Neurother. **10**, 319–330 (2010)
14. W.D. Johnson, L.N. Loredo, J.D. Slater, Surgery and radiotherapy: complementary tools in the management of benign intracranial tumors. Neurosurg. Focus **23**, E2 (2008)
15. M. Fuss, L.N. Loredo, P.A. Blacharski, et al., Proton radiation therapy for medium and large choroidal melanoma: preservation of the eye and its functionality. Int. J. Radiat. Oncol. Biol. Phys. **49**, 1053–1959 (2001)
16. J.D. Slater, L.T. Yonemoto, D.W. Mantik, et al., Proton radiation for treatment of cancer of the oropharynx: early experience at Loma Linda University Medical Center using a concomitant boost technique. Int. J. Radiat. Oncol. Biol. Phys. **62**, 494–500 (2005)
17. R. Lin, J.D. Slater, L.T. Yonemoto, et al., Nasopharyngeal carcinoma: repeat treatment with conformal proton therapy: dose-volume histogram analysis. Radiology **213**, 489–494 (1999)
18. D.A. Bush, R.D. Dunbar, R. Bonnet, et al., Pulmonary injury from proton and conventional radiotherapy as revealed by CT. Am. J. Roentgenol. **172**, 735–739 (1999)
19. D.A. Bush, J.D. Slater, B.B. Shin, et al., Hypofractionated proton beam radiotherapy for stage I lung cancer. Chest **126**, 1198–1203 (2004)
20. D.A. Bush, J.D. Slater, C. Garberoglio, et al., A technique of partial breast irradiation utilizing proton beam radiotherapy: comparison with conformal x-ray therapy. Cancer J. **13**, 114–118 (2007)
21. D.A. Bush, D.J. Hillebrand, J.M. Slater, J.D. Slater, High-dose proton beam radiotherapy of hepatocellular carcinoma: preliminary results of a phase II trial. Gastroenterology **127**(5 Suppl 1), S189–S193 (2004)
22. J.D. Slater, C.J. Rossi Jr, L.T. Yonemoto, et al., Proton therapy for prostate cancer: the initial Loma Linda University experience. Int. J. Radiat. Oncol. Biol. Phys. **59**, 348–352 (2004)
23. J.D. Slater, C.J. Rossi Jr, L.T. Yonemoto, Conformal proton therapy for early-stage prostate cancer. Urology **53**, 978–984 (1999)
24. C.J. Rossi Jr, J.D. Slater, L.T. Yonemoto, et al., Influence of patient age on biochemical freedom from disease in patients undergoing conformal proton radiotherapy of organ-confined prostate cancer. Urology **64**, 729–732 (2004)
25. A.L. Zietman, M.L. DeSilvio, J.D. Slater, et al., Comparison of conventional-dose vs high-dose conformal radiation therapy in clinically localized adenocarcinoma of the prostate: a randomized controlled trial. J. Am. Med. Assoc. **294**, 1233–1239 (2005) erratum: J Am Med Assoc 299, 899–900, 2008
26. A.L. Zietman, K. Bae, J.D. Slater, et al., Randomized trial comparing conventional-dose with high-dose conformal radiation therapy in early-stage adenocarcinoma of the prostate: long-term results from Proton Radiation Oncology Group/American College of Radiology 95–09. J. Clin. Oncol. **28**, 1106–1111 (2010)
27. B. McAllister, J.O. Archambeau, M.C. Nguyen, et al., Proton therapy for pediatric cranial tumors: preliminary report on treatment and disease-related morbidities. Int. J. Radiat. Oncol. Biol. Phys. **39**, 455–460 (1997)

28. E.B. Hug, J.D. Slater, Proton radiation therapy for pediatric malignancies: status report. Strahlenther. Onkol. **175**, S89–S91 (1999)
29. M. Fuss, E.B. Hug, R.A. Schaefer, et al., Proton radiation therapy (PRT) for pediatric optic pathway gliomas: comparison with 3D planned conventional photons and a standard photon technique. Int. J. Radiat. Oncol. Biol. Phys. **45**, 1117–1126 (1999)
30. E.B. Hug, M. Nevinny-Stickel, M. Fuss, et al., Conformal proton radiation treatment for retroperitoneal neuroblastoma: introduction of a novel technique. Med. Pediatr. Oncol. **37**, 36–41 (2001)
31. E.B. Hug, R.A. Sweeney, P.M. Nurre, et al., Proton radiotherapy in management of pediatric base of skull tumors. Int. J. Radiat. Oncol. Biol. Phys. **52**, 1017–1024 (2002)
32. E.B. Hug, M.W. Muenter, J.O. Archambeau, et al., Conformal proton radiation therapy for pediatric low-grade astrocytomas. Strahlenther. Onkol. **178**, 10–17 (2002)
33. G.E. Yuh, L.N. Loredo, L.T. Yonemoto, et al., Reducing toxicity from craniospinal irradiation: using proton beams to treat medulloblastoma in young children. Cancer J. **10**, 386–390 (2004)
34. Q.T. Luu, L.N. Loredo, J.O. Archambeau, et al., Fractionated proton radiation treatment for pediatric craniopharyngioma: preliminary report. Cancer J. **12**, 155–159 (2006)
35. P. Rubin, G.W. Casarett, *Clinical Radiation Pathology*, vols. 1 and 2 (W. B. Saunders, Philadelphia, 1968)
36. P. Rubin, R.A. Cooper, T.L. Phillips (eds.) *Radiation Biology and Radiation Pathology Syllabus* (American College of Radiology Publications, Chicago, 1978)
37. R.D. Pearlstein, Y. Higuchi, M. Moldovan, et al., Metalloporphyrin antioxidants ameliorate normal tissue radiation damage in rat brain. Int. J. Radiat. Biol. **86**, 145–163 (2010)
38. J. Tian, M.J. Pecaut, J.M. Slater, D.S. Gridley, Spaceflight modulates expression of extracellular matrix, adhesion, and profibrotic molecules in mouse lung. J. Appl. Physiol. **108**, 162–171 (2010)
39. J. Tian, M.J. Pecaut, G.B. Coutrakon, et al., Response of extracellular matrix regulators in mouse lung after exposure to photons, protons and simulated solar particle event protons. Radiat. Res. **172**, 30–41 (2009)
40. D.S. Gridley, A. Rizvi, X. Luo-Owen, et al., Low dose, low dose rate photon radiation modifies leukocyte distribution and gene expression in CD4(+) T cells. J. Radiat. Res. (Tokyo) **50**, 139–150 (2009)
41. F.P. Baqai, D.S. Gridley, J.M. Slater, et al., Effects of spaceflight on innate immune function and antioxidant gene expression. J. Appl. Physiol. **106**, 1935–1942 (2009)
42. A.Y. Makinde, X. Luo-Owen, A. Rizvi, et al., Effect of a metalloporphyrin antioxidant (MnTE-2-PyP) on the response of a mouse prostate cancer model to radiation. Anticancer Res. **29**, 107–118 (2009)
43. J.R. Williams, Y. Zhang, H. Zhou, et al., Overview of radiosensitivity of human tumor cells to low-dose-rate irradiation. Int. J. Radiat. Oncol. Biol. Phys. **72**, 909–917 (2008)
44. R.W. Schulte, A.J. Wroe, V.A. Bashkirov et al., Nanodosimetry-based quality factors for radiation protection in space. Z. Med. Phys. **18**, 286–296 (2008)
45. S.N. Penfold, A.B. Rosenfeld, R.W. Schulte, K.E. Schubert, A more accurate reconstruction system matrix for quantitative proton computed tomography. Med. Phys. **36**, 4511–4518 (2009)
46. D. Kittle, B. Holshouser, J.M. Slater, et al., Technical note: rapid prototyping of 3D grid arrays for image guided therapy quality assurance. Med. Phys. **35**, 5708–5712 (2008)

Chapter 35
The Francis H. Burr Proton Therapy Center

Jay Flanz, Hanne Kooy, and Thomas F. DeLaney

Abstract The Francis H. Burr Proton Therapy Center (FHBPTC) is one of the first hospital-based proton therapy (PT) facilities. Its development was the natural evolution of several decades of PT experience of the Massachusetts General Hospital treating patients at the Harvard Cyclotron Laboratory. The operations of the FHBPTC reflect the combined missions of patient care, clinical and physics research, technological developments, and education. This chapter will discuss aspects of the history, evolution, and performance of this unique PT center.

35.1 Introduction

The Massachusetts General Hospital (MGH), in collaboration with the Massachusetts Eye and Ear Infirmary, has been treating patients with high-energy proton beams for cancer and other diseases. This work, which started at the Harvard Cyclotron Laboratory (HCL) in the 1960s for stereotactic intracranial radiosurgical procedures and in the 1970s for fractionated large-field radiotherapy, continued through 2002 [1].

The limited range of the HCL protons (16 cm) restricted their clinical utility to the treatment of head and neck tumors and few, relatively superficial tumors at other sites including the prostate and the sacrum. In order to reach deeper seated tumors in all body sites, higher energy was needed. In addition, the HCL treatment beams were oriented horizontally which made it cumbersome to position some patients for their treatments. However, in the more than 30 years of clinical work at HCL more than 9,000 patients were treated.

J. Flanz (✉)
Francis H. Burr Proton Therapy Center, Massachusetts General Hospital, Harvard Medical School, 30 Fruit St., Boston, MA 02114, USA
e-mail: flanz@hadron.mgh.harvard.edu

U. Linz (ed.), *Ion Beam Therapy*, Biological and Medical Physics, Biomedical Engineering, DOI 10.1007/978-3-642-21414-1_35,

Approximately 56% of the large-field patients and 48% of the uveal melanoma patients treated at the HCL lived in Massachusetts and neighboring states in the northeastern USA. The number of referrals dropped off at a radius beyond 250 miles. Within this 250-mile radius, however, lives a population of over 38 million. This created pressure to develop the capability to treat a wider range of clinical sites where protons might be advantageous and which could not be treated at the HCL. This called for a modern facility, accessible to and equipped with the full range of hospital services, capable of satisfying the cancer treatment needs of the geographic region, and with the technical capacity to support more advanced treatment techniques. Such a new facility, the Northeast Proton Therapy Center (NPTC) was funded by the MGH and the National Cancer Institute of the United States [2].

35.2 The Facility

The NPTC began construction in 1995 and was renamed the Francis H. Burr Proton Therapy Center (FHBPTC) in 2005 after the former Chairman of the MGH Board of Trustees.

Previously, PT was primarily delivered in physics laboratories where the capabilities existed to accelerate high-energy proton beams and onto which clinical facilities had been retrofitted. One notable exception was the Loma Linda University Medical Center (LLUMC), which was the first hospital-based PT center. This facility was built by a collaboration of national laboratory personnel (e.g., FermiLab) and private technical firms. The NPTC in contrast was built mostly by a commercial firm, Ion Beam Applications (IBA), under a fixed-price contract with full responsibility for the technical equipment of the accelerator and two gantry rooms. In addition to the cyclotron and the beam lines for the two gantry rooms provided by IBA, the MGH staff constructed three more beam lines to service equipment that was moved from the HCL, including the eye treatment station, the later to be installed stereotactic alignment for radiosurgery (STAR) positioner for high precision intracranial proton treatments, and a large-field beam line that could also be used for nonclinical experiments.

The elements of an ion beam therapy system consist of a beam production unit, a beam delivery system and a positioning device, with interfaces to seamlessly connect them. The choice and integration of various types of available system components may affect the time or efficiency of the particular anatomic site being treated, which may also be differentially affected by the choice of passively or actively scanned beams. Vice versa, the population to be treated and the treatment technique to be used are likely to have significant impact on the choice of therapy system components.

Some of the clinical specifications for the FHBPTC and the actual performance are listed in Table 35.1.

The FHBPTC equipment includes the following major components which are subsequently described:

Table 35.1 FHBPTC initial specifications and actual performance. In brackets, date when first achieved

	Desired specification	Actual performance
1. Beam range and shape		
a. Range in patient	$Max = 32\,g/cm^2$	$32.8\,g/cm^2$ (3/97)
	$Min = 3.5\,g/cm^2$	$3.5\,g/cm^2$ (3/97)
b. Range modulation	Steps of $0.5\,g/cm^2$ ($0.2\,g/cm^2$ for ranges $<5\,g/cm^2$)	$0.5\,g/cm^2$
c. Range adjustment	Steps of $0.1\,g/cm^2$ ($0.05\,g/cm^2$ for ranges $<5\,g/cm^2$)	$0.1\,g/cm^2$
d. Distal dose fall-off	$\leq 0.1\,g/cm^2$ above physical limit	Energy spread fixed (3/97)
e. Field size	$40 \times 30\,cm^2$ in scanning mode	20 cm scattered; $30 \times 40\,cm^2$ wobbled (7/98)
f. Lateral penumbra	≤ 2 mm over penumbra due to physical limits	$\sim 4 - 5$ mm
g. Dose uniformity	$\pm 2.5\%$ over treatment field within physical limits	$<2.5\%$
2. Beam dose		
a. Average dose rate	2 Gy/min for $25 \times 25\,cm^2$ field at $32\,g/cm^2$ full modulation	300 nA extracted cyclotron current (3/97)
b. Dose accuracy	Daily accuracy and reproducibility $\pm 1.5\%$	Achieved according to daily QA
3. Beam trajectory		
a. Beam position	Beam directed to the target better than ± 1.0 mm (Results from several components including gantry mechanical isocenter accuracy, and PPS accuracy)	Gantry measured mechanical isocenter accuracy of ± 0.6 mm (3/98) PPS reproducibility <0.3 mm (12/97)

- Fixed-energy 235-MeV cyclotron
- Beam transport system (BTS) including a degrader and energy analyzer
- Two isocentric gantries (rotating beam lines)
- Beam delivery systems (nozzles)
- Patient positioning system (PPS)
- Two fixed-beam treatment rooms
- Computer control system
- Safety system
- Building

35.2.1 Cyclotron Accelerator

The IBA cyclotron is capable of delivering more than 300 nA of protons continuously. The dynamic range of the delivered current is over a factor of 1,000 with the ability to vary the current within tens of microseconds. The cyclotron has a

maximum field strength of 3.2 T using room temperature coils (cf. Chap. 22 for more details). It was delivered to the FHBPTC site in 1997, and was working in about 2 months, just in time to host the US Particle Accelerator School course on beam measurements.

35.2.2 The BTS Including Degrader and Energy Analyzer

The beam line contains a degrader which is a material of variable thickness that can be placed in the beam path to degrade the energy of the beam. The degrading process increases the dimensions and the energy spread of the beam. A collimator downstream of this degrader is used to limit the emittance transmitted to the remainder of the beam line. The energy of this beam is analyzed in an achromat which also includes slits to limit the momentum spread of the transported proton beam. This part is called the energy selection system (ESS).

The BTS directs the energy-selected beam to the treatment rooms. These beam lines provide the required focusing to deliver a round beam with the appropriate trajectory for transmission through the gantries or the fixed beam lines. The layout for a section of the ESS and BTS is presented in Fig. 35.1.

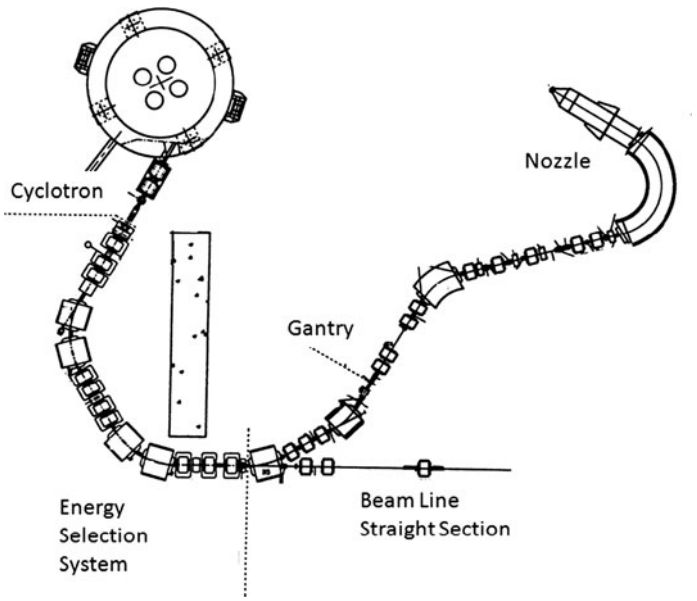

Fig. 35.1 Layout of the beam transport system (BTS) including the energy selection system (ESS), the beam line through the gantry of the first treatment room, and part of the remaining beam line

35.2.3 Gantries

The gantries are conventional in the sense that all the bends are in the same plane. They are capable of rotation about an isocenter over 360°. The distance between the virtual source and the isocenter is approx. 2.3 m.

The beam lines and gantry were initially designed by General Atomics (GA) of San Diego, California, a subcontractor to IBA. The first gantry began patient treatment in 2001 and the second initiated treatments 1 year later.

35.2.4 Beam Delivery Systems

The beam delivery system included, initially, a passive scattering and a wobbling system. Wobbling is accomplished using a slow raster scanning technique with beam spread by a single scatterer. Other modes of beam delivery have since been developed.

35.2.5 PPS

The PPS holds the patient securely in the supine or prone position, and permits proton beam entry from any oblique direction, without danger of collision with the gantry or nozzle. The PPS and gantry are capable of allowing accurate and reproducible alignment of beam to the patient within ± 0.5 mm. The PPS has six degrees of freedom including tilt and roll adjustments. A photo of the gantry treatment area with the PPS in place is shown in Fig. 35.2.

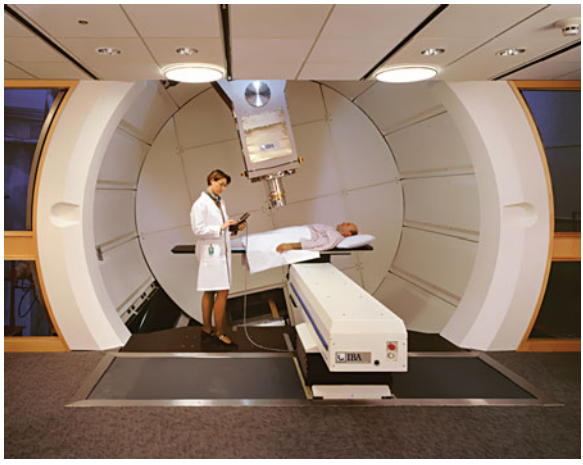

Fig. 35.2 View of a treatment room with gantry, including the beam delivery nozzle (*hanging from above*) and the patient positioning system (PPS)

Fig. 35.3 Treatment equipment in the fixed-field room of the FHBPTC moved from the Harvard Cyclotron Laboratory (HCL). *Left*: Eye treatment station; *Right*: STAR (Stereotactic Radiation) positioner

35.2.6 Fixed-Beam Treatment Rooms

Some treatment equipment from the HCL was moved to the FHBPTC to provide continuity of the successful MGH/Harvard programs for the treatment of ocular tumors using a small-field fixed-beam treatment station with the STAR patient gantry positioner and the treatment of intracranial tumors using the stereotactic radiotherapy patient treatment system as displayed in Fig. 35.3.

35.2.7 Computer Control System

The control system helps to perform rapid beam switching, set-up, and shutdown of the entire system. It provides the required monitoring of the dosimetry and diagnostic information. It also provides the necessary interfaces for the radiation therapists, engineers, and physicists as well as the interface required for treatment verification and validation.

35.2.8 Safety System

The safety system has two main aspects. One, essentially hard-wired system is responsible to ensure that no interlock conditions exist which should prevent treatment. There is also a computer component of the control system which records the safety status and independently monitors conditions required for safe facility operation.

Fig. 35.4 Start of construction of the Proton Therapy Center in 1995 in the narrow space of the MGH parking lot, formerly the exercise yard of the Charles Street Jail

35.2.9 Building

The FHBPTC building houses the PT equipment and related program space such as clinical and administrative rooms. It contains approximately 2,100 m^2 of program space including three clinical treatment rooms, accelerator equipment, and offices. The treatment floor of the building is underground and has pits to accommodate the gantry rotation extending below that floor. The building was constructed in a narrow corner on the hospital site, a former parking lot, as shown in Fig. 35.4.

The layout of the lower level is depicted in Fig. 35.5. It contains the accelerator, treatment rooms, and some equipment support space. It also includes clinical space for patient examination and care. The ground level comprises administrative, staff, and miscellaneous support space as well as aspects of equipment support and clinical space. The FHBPTC space programming underwent a rigorous optimization procedure and the space remaining is probably as lean as possible. This is evident in comparisons with other facilities which often cover twice the area of the FHBPTC [1].

One unique challenge in the early life of the FHBPTC was to maintain and expand the clinical and research operations while a new ten-story outpatient hospital building was constructed above and adjacent to the center. Subsequently, a hotel was built adjacent to the center. The beam delivery system functioned despite the transmitted vibrations associated with pile-driving and other construction activities. In fact, the beam was always on target and the treatment program continued uninterrupted. Photos of the FHBPTC before and after the construction are presented in Fig. 35.6.

35.3 Mission and Capacity

The FHBPTC system was designed to allow a wide variety of beam delivery modalities. At the time of construction, double scattering with a range modulator wheel was the primary mode of beam spreading. The current beam delivery capabilities include:

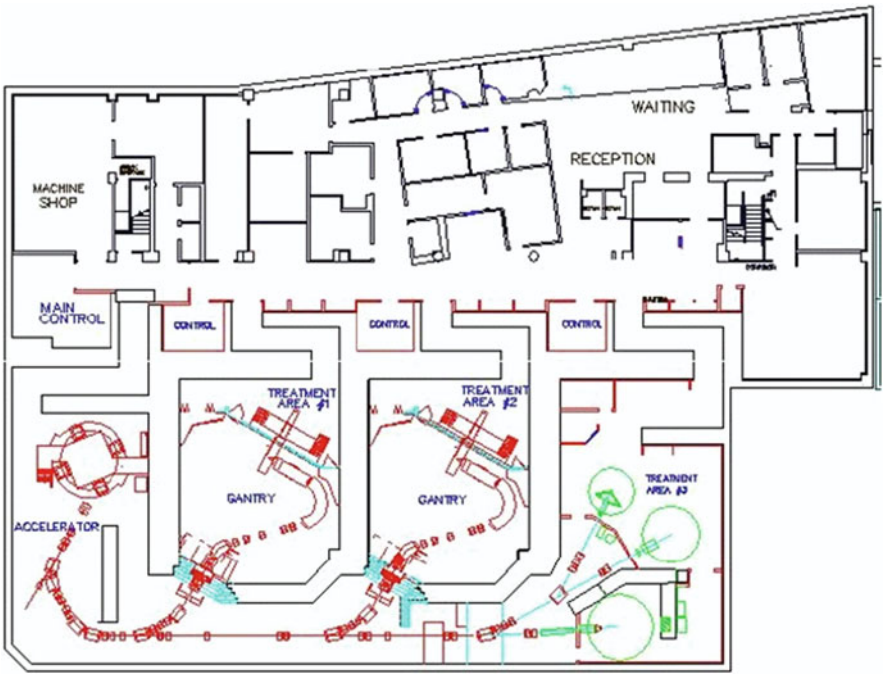

Fig. 35.5 Layout of the lower level of the FHBPTC including clinical rooms and most of the treatment equipment

- Single scattering
- Double scattering
- Wobbling
- Scanning
- Beam gating
- Gantries
- Fixed beam lines

The primary missions of the FHBPTC are to: (1) treat patients, (2) perform clinical research studies designed to improve patient treatment outcome, (3) develop, implement, and refine the treatment techniques, and (4) train physicians, physicists, and other personnel engaged in PT. It was originally envisioned, and proved, that it would take some time to gain treatment efficiencies. It should be said, however, that the facility quickly assumed the full capacity of the HCL. The evolution of patient treatment consistently increased from approx. 200 patients in the first year to roughly 800 at present. Until winter 2010, more than 4,000 patients were treated.

It is useful, perhaps, to explore what determines patient capacity. Capacity is inversely proportional to the time for a treatment, which in turn is proportional to the complexity of the treatment. Patient number is inversely proportional to the number

Fig. 35.6 Views of the FHBPTC before and after hospital construction projects

of fractions per patient. Of course, capacity is also dependent upon the number of rooms, number of hours used for treatment, and the availability of the system. The three rooms of the FHBPTC being used for 10 h/day result in approx. 60 patients/day. In fact, if one scaled these numbers from 3 to 4 rooms and from 10 to 16 h/day one would reach an impressive 144 patients/day.

One of the key factors in enhancing the efficiency of the facility is the ability to fully characterize the system performance. A special effort was applied to characterize beam parameters and use novel, thorough and yet highly efficient quality assurance procedures.

35.4 Clinical Results

In 2009, 755 patients were treated at the FHBPTC (Table 35.2). With 84%, the majority were adults. But the children occupied approximately two-thirds of the gantry time.

Table 35.2 Summary of diseases treated at the FHBPTC in 2009

Type of disease	Number of patients	%
CNS	292	39
Eye	135	18
Bone/soft tissue sarcomas	121	16
Skull base sarcomas	53	7
Prostate	50	7
Head/neck	35	5
Lung	17	2
Pancreas	12	2
Liver	8	1
Other	32	4
Total	755	

Factors that contribute to the given patient population include the selection of patients for whom protons with their 50–60% lower integral dose as compared to photons are felt to reduce acute or late morbidity or allow dose escalation without significant increase in morbidity. A last group are patients who are being treated for new investigational indications such as locally advanced lung cancer [3, 4].

The high preponderance of sarcomas reflects the excellent success of PT for skull base and other sarcomas as well as physician and institutional expertise with these tumors [5, 6].

It must be noted that the treatment of many of these indications is highly complex and requires motion management strategies including respiratory gating of the proton beam. This contributes to the technical demands of the PT system. A better measure of the clinical use of the system might, therefore, be the number of fields treated. This is shown in Fig. 35.7, indicating that over 100,000 fields have been delivered at the FHBPTC.

Proton clinical research is underway for nearly all anatomic sites being treated including pediatric tumors, brain and central nervous system malignancies, nasopharyngeal and paranasal sinus carcinomas, liver and pancreatic cancers, skull base, spine, retroperitoneal, and pelvic sarcomas, eye tumors, lung cancers, prostate cancer, and (left-sided) breast cancer. PT is considered by most clinicians to offer perhaps the greatest clinical advantage for pediatric patients. Currently, treatments within prospective clinical research studies are underway at the FHBPTC for pediatric patients with medulloblastoma (craniospinal irradiation), retinoblastoma, rhabdomyosarcoma and non-rhabdomyosarcoma soft tissue, and bone sarcomas [7].

35.5 System Statistics

A PT system comprises thousands of parts including mechanical and electrical components as well as software. It is designed to be extremely safe, but many things can prevent the system from being able to deliver a beam to the patient.

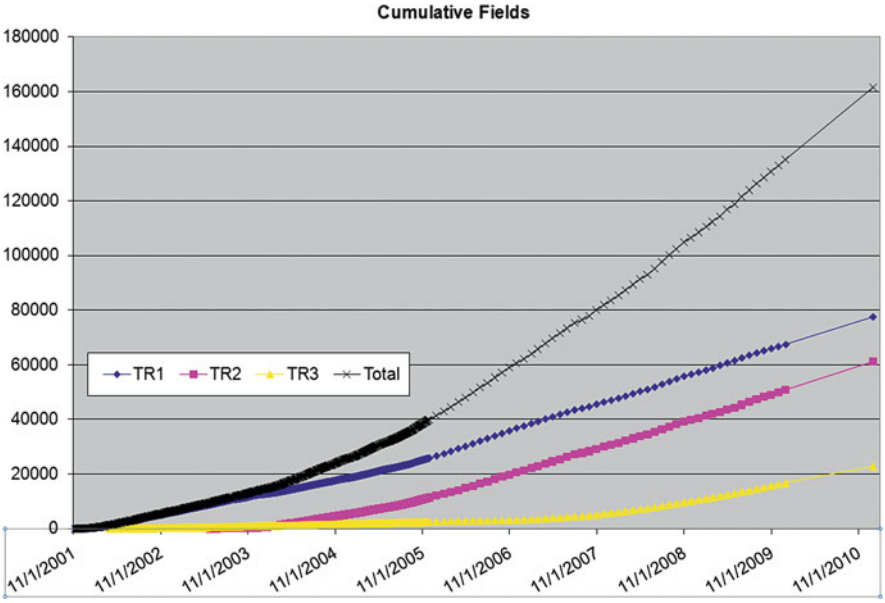

Fig. 35.7 Cumulative number of fields treated in each room (and total) of the FHBPTC since the facility was opened for treatment in November 2001

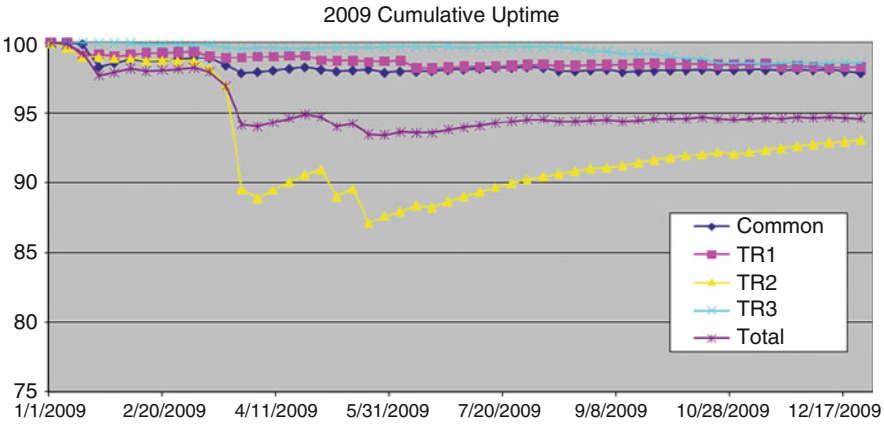

Fig. 35.8 Cumulative percentage of availability during the year 2009. Each of the treatment rooms and the common systems are shown individually. The largest contributing factor comes from the large gantry dipole magnet in treatment room two which partially failed that year

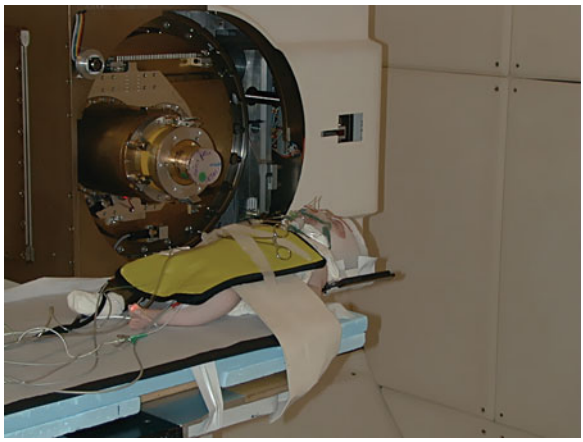

Fig. 35.9 Photo of a pediatric retinoblastoma treatment under anesthesia

As mentioned above, delivering over 100,000 fields implies that the gantries have circled well over 100,000 times; the range modulator wheels have spun up and down more than 100,000 times and the accelerator has produced beam for thousands of hours.

Yet, with all of this, the availability of the system, measured by the number of minutes that beam is available for treatment when requested, is on the order of 95%. Some measures of availability count the number of patient treatments per day compared to the number scheduled, but our measure of availability is more severe and accurate since, even if all the patients scheduled for a day can be treated, but there was some time that the system was not available, then the availability for that day would be below 100%. The cumulative availability for the year 2009 is illustrated in Fig. 35.8. Many of the smaller system components have had to be replaced in order to achieve this level of reliability.

Through all of this, it is most important to keep in mind the treatment mission and to enhance safety, efficiency, and ability of the treatment professionals to do their job, as depicted in the treatment scenario of Fig. 35.9.

35.6 Outlook

Much of the system components have been on site since 1997, and the facility has been used for patient treatment for approx. a decade. In the near future, some of the original patient positioning devices will be replaced by more modern robotic ones. Newer imaging techniques leading to adaptive beam therapy will be developed, and clinical treatments using a scanning proton beam will become more routine.

References

1. J. Flanz, S. Durlacher, M. Goitein, et. al, Overview of the MGH-Northeast Proton Therapy Center plans and progress. Nucl. Instrum. Methods Phys. Res. B **99**, 830–834 (1995)
2. H.D. Suit, W. Chu, History of Charged Particle Radiotherapy, in *Proton and Charged Particle Radiotherapy*, ed. by T.F. DeLaney, H.M. Kooy. (Lippincott Williams & Wilkins, Philadelphia, 2007), pp. 1–7
3. T.F. DeLaney, Clinical Issues in Proton Radiotherapy, in *Proton and Charged Particle Radiotherapy*, ed. by T.F. DeLaney, H.M. Kooy. (Lippincott Williams & Wilkins, Philadelphia, 2007), pp. 108–114
4. D. Schulz-Ertner, The clinical experience with particle therapy in adults. Cancer J. **15**, 306–311 (2009)
5. J.E. Munzenrider, N.J. Liebsch, Proton therapy for tumors of the skull base. Strahlenther. Onkol. **175**, 57–63 (1999)
6. T.F. DeLaney, N.J. Liebsch, F.X. Pedlow, et al., Phase II study of high-dose photon/proton radiotherapy in the management of spine sarcomas. Int. J. Radiat. Oncol. Biol. Phys. **74**, 732–739 (2009)
7. T.F. DeLaney, Clinical proton radiation therapy research at the Francis H. Burr Proton Therapy Center. Technol. Cancer Res. Treat. **6**, 61–66 (2007)

Chapter 36
HIMAC: A New Start for Heavy Ions

Tadashi Kamada and Hirohiko Tsujii

Abstract In 1994, carbon ion radiotherapy (CIRT) was initiated at the National Institute of Radiological Sciences (NIRS) in Japan using the Heavy Ion Medical Accelerator in Chiba (HIMAC), which was the world's first heavy ion accelerator complex dedicated to medical use. Among several types of ion species, carbon ions were chosen for cancer therapy because they were presumed to possess optimal properties in terms of biologically effective dose localization.

This chapter will cover the evolution of CIRT over the last 15 years and highlight the clinical results achieved at NIRS.

36.1 Introduction

In Japan, the decision for a medical accelerator using ions heavier than protons was made in 1984 at NIRS. HIMAC was the world's first heavy ion accelerator complex intended primarily for clinical use (Fig. 36.1). The accelerator complex took almost a decade to build and was completed by the end of 1993. One year later, in 1994, clinical trials using carbon ion beams generated from the HIMAC were initiated [1]. Carbon was chosen because of the favorable properties (cf. Chap. 4 for details). The HIMAC has operated since its opening as a multipurpose facility available for joint cancer treatment and research in biology and physics by both Japanese and foreign investigators.

T. Kamada (✉)
National Institute of Radiological Sciences, Research Center of Charged Particle Therapy, Anagawa 4-9-1, Inage-ku, Chiba, 263-8555, Japan
e-mail: t_kamada@nirs.go.jp

U. Linz (ed.), *Ion Beam Therapy*, Biological and Medical Physics, Biomedical Engineering, DOI 10.1007/978-3-642-21414-1_36,

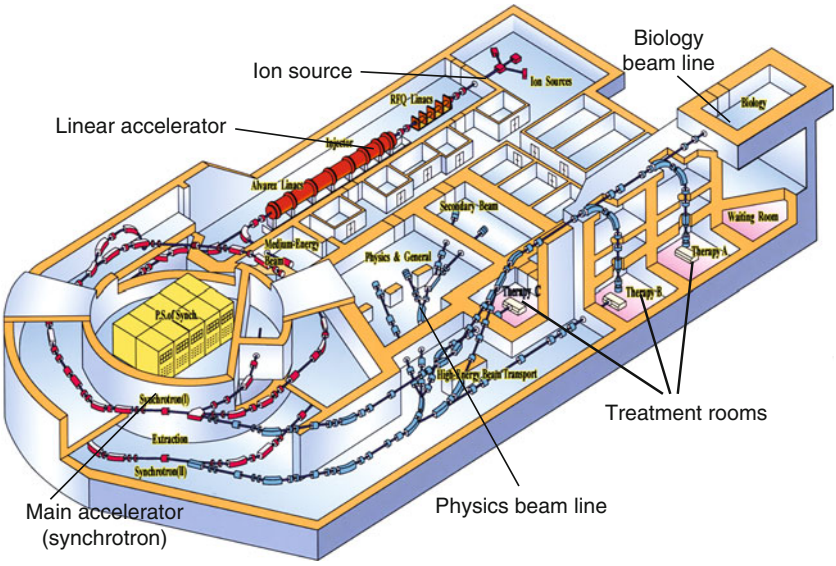

Fig. 36.1 Heavy ion medical accelerator in Chiba (HIMAC)

36.2 CIRT at NIRS

Since June 1994 until spring 2011, almost 50 protocols have been conducted in an attempt to determine the optimal dose fractionation and irradiation method for the treatment of specific diseases. The number of patients has increased year by year, and the facility has meanwhile reached a capacity permitting nearly 700 patients to be treated each year (Fig. 36.2). In February 2011, nearly 5900 patients had been registered. The categories of disease that can be treated in routine clinical practice include lung cancer, prostate cancer, head and neck cancer, skull base tumors, ocular melanoma, bone and soft-tissue sarcoma, liver cancer, and pelvic recurrences of rectal cancer (Fig. 36.3).

The clinical trials began with a small dose per fraction. At first, the average number of fractions was almost 18. All these early trials were carried out as dose-escalation studies. It was found that a very high dose per fraction could be administered and the average number of fractions could be reduced from 18 to 12–13 over the last several years leading to improvements in patient throughput (Fig. 36.4).

HIMAC has three treatment rooms with fixed vertical and/or horizontal beam lines. In order to conform the dose to a target volume, the beam lines in the treatment room are equipped with a pair of wobbler magnets to modulate the beam width, plus beam scatterers, ridge filters, multileaf collimators, and the ability to administer a compensation bolus (see also next chapter). An appropriately sized ridge filter,

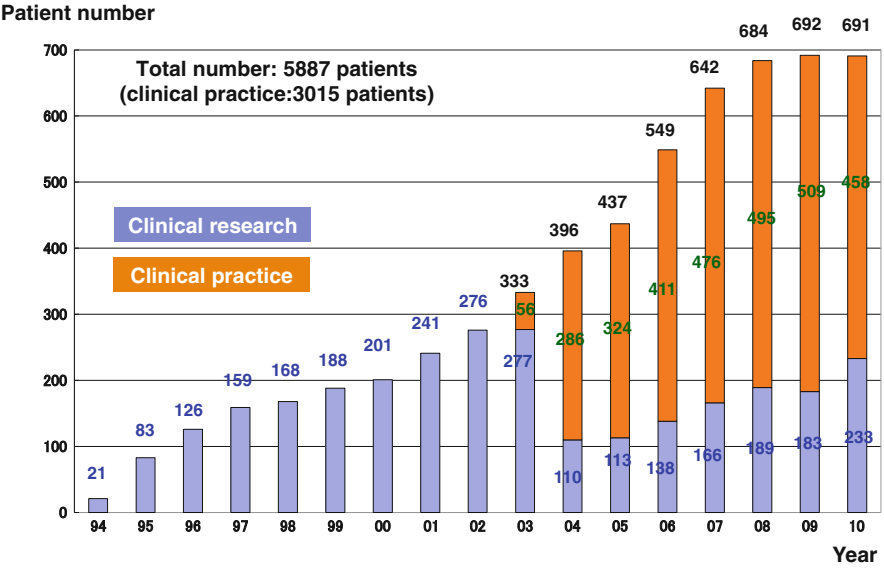

Fig. 36.2 Annual patient accrual in carbon ion radiotherapy (CIRT) at NIRS

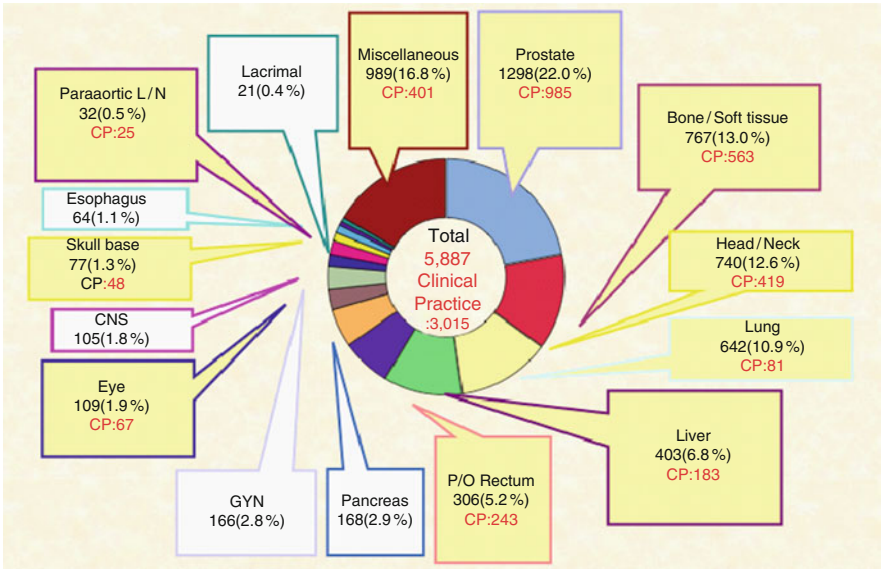

Fig. 36.3 Patient distribution enrolled in CIRT at NIRS (Treatment Period: June 1994 to February 2011)

which corresponds to, and determines the size of the spread-out Bragg peak (SOBP), is selected to avoid unnecessary dose to normal tissues along the beam path in each port.

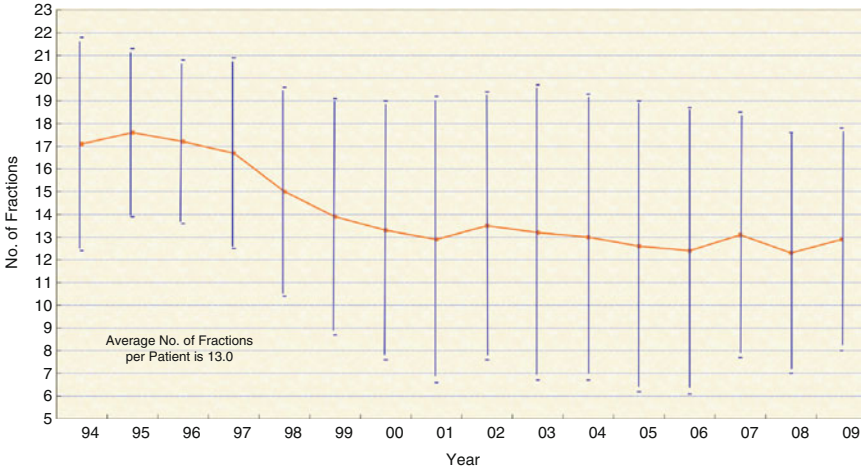

Fig. 36.4 Average number of fractions used in CIRT at NIRS

The patients are positioned in customized cradles and immobilized with a low-temperature thermoplastic. A set of 5-mm thick CT images is taken for treatment planning with the immobilization devices in place. Respiratory gating of both the CT acquisition and the therapy is performed when indicated [2].

Three-dimensional treatment planning is performed using HIPLAN software, which was developed for CIRT [3]. A margin of 5 mm is usually added to the clinical target volume to create the planning target volume. Dose is calculated for the target volume and any nearby critical structures and expressed in Gray-Equivalent (GyE = carbon physical dose in Gray × Relative Biological Effectiveness {RBE}) [4, 5].

CIRT is given once daily, on 4 days per week (Tuesday to Friday). At every treatment session, the patient's position is verified with a computer-aided online positioning system (Fig. 36.5).

36.3 Treatment Results by Tumor Type

Head and neck cancer, lung, liver, and prostate cancer, postoperative rectal cancer recurrences, and bone and soft-tissue sarcomas are the six most commonly treated tumors in NIRS studies.

36.3.1 Head and Neck Cancer

CIRT was first applied to the treatment of patients with head and neck tumors and five clinical trials were conducted at NIRS (Fig. 36.6). Two dose optimization studies with different fractionation (protocols of 18 fractions over 6 weeks and

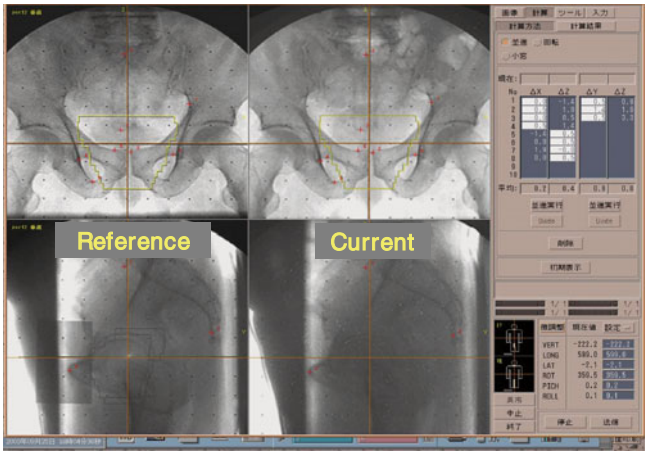

Fig. 36.5 Online positioning using an orthogonal X-ray TV system

16 fractions over 4 weeks) were followed by a phase II fixed dose study [6]. During the phase II study, a high distant metastasis rate in melanoma and a poor local control rate in sarcoma with standard doses (total doses of 57.6 GyE or 64 GyE over 4 weeks) were found by subgroup analysis. New protocols modified for melanoma and sarcoma were created; a concurrent chemocarbon therapy protocol for melanoma and a high-dose protocol (70.4 GyE in 16 fractions over 4 weeks) for sarcoma.

More than 700 locally advanced tumors were treated with carbon ions in these five studies. The treatment results obtained so far can be summed up by stating that a very favorable local control rate of 70–80% has been achieved for locally advanced adenocarcinoma, adenoid cystic carcinoma, malignant melanoma in the nasal cavity and paranasal sinus, squamous cell carcinoma, and sarcomas.

36.3.2 Lung Cancer

Patients with inoperable stage I non-small cell lung cancer (NSCLC) were treated in several protocols. The results have been quite promising and more than 600 patients were enrolled in the lung studies. Clinical trials in lung cancer were started with 18 fractions over a 6-week dose-escalation study. Two subsequent protocols shortened the overall treatment time to 3 weeks. The 3-year local control rates were 65–95%, and the 5-year survival rates were 40–50%. The results of these studies are better than those of conventional radiotherapy, and almost the same as those of surgery [7]. We have conducted a fixed 4-fractions-in-1-week protocol since 2000. That way, a very high dose can be given with acceptable side effects. A single-fraction dose escalation study was started in 2003 (cf. Chap. 14 for details).

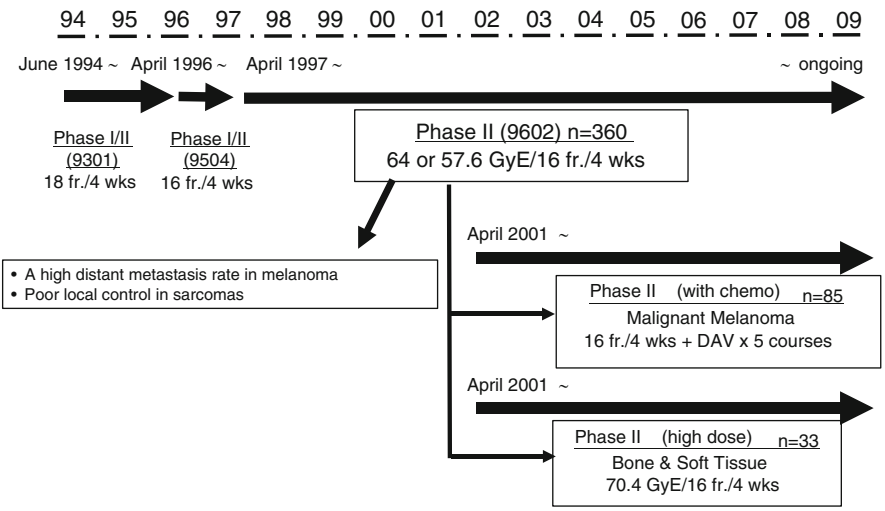

Fig. 36.6 Protocols for head and neck tumors

36.3.3 Liver Cancer

For liver cancer, 15 fractions over 5 weeks were employed as initial dose optimization study [8]. The overall treatment time of 5 weeks was then shortened to 3, 2, and 1 week in subsequent studies [9]. More recently, a fourth clinical trial using an even shorter irradiation schedule of 2 fractions over 2 days has just been completed with encouraging results in terms of a favorable local control rate and the absence of any particular serious adverse reactions. No unwanted skin reactions of grade 2 or higher were observed. For liver function, no toxicities greater than grade 3 occurred. Almost 400 patients with liver cancer have been treated with CIRT using these protocols.

36.3.4 Prostate Cancer

A total of three clinical trials have been carried out for patients with prostate cancer. The first CIRT trial protocol (20 fractions over 5 weeks) with concomitant endocrine therapy was conducted for B2-C stage patients [10]. The eligibility criteria for the second trial were less stringent. CIRT-only was applied to stage A2–B1 prostate cancer and CIRT plus endocrine therapy for stage B2–C disease. In the first clinical trial, the most serious toxicities were recorded in the rectum among patients exposed to the highest dose level of 72 GyE. Dose volume histogram (DVH) analysis was performed to identify the tolerance dose of the rectum, using a rectal DVH curve that permits prediction of the risk of rectal reactions. This curve has made it possible

to prevent severe rectal reactions in new patients at the time of treatment planning. As a result, the safe dose distribution for the digestive tract was established and no serious toxic reactions were encountered in the subsequent clinical trials. A total dose of 63 GyE was found to be an optimal dose for 20 fractions over a 5-week protocol. The overall treatment time was then shortened to 4 weeks and showed better outcomes [11]. The total number of prostate cancers treated with carbon ions is now nearly 1,300. We are now proceeding to a clinical trial with an even shorter regimen of 12 fractions in 3 weeks.

36.3.5 Bone and Soft-Tissue Sarcomas

Bone- and soft-tissue sarcomas are generally considered to be radioresistant. Advanced tumors originating in the trunk, in particular, are in many cases not resectable and have a poor prognosis. The use of carbon ion beams does offer a favorable prospect of improved local control in view of their superior biological dose distribution (Fig. 36.7). The patients enrolled in our initial dose escalation trial were primarily subjects not responding to surgery or they were totally inoperable. This trial produced favorable local control of approx. 85% at 5 years. It has been realized that chordoma and osteosarcoma are the prime candidates for CIRT [12–15]. In some 10% of those patients, the lesions were close to the body surface so that it was not possible to avoid exposure of the skin to high-radiation doses. They developed severe reactions such as skin ulceration. In the meantime, more experience has been gained and significant improvements in irradiation techniques have been achieved that such severe toxicity has no longer been observed (Fig. 36.8).

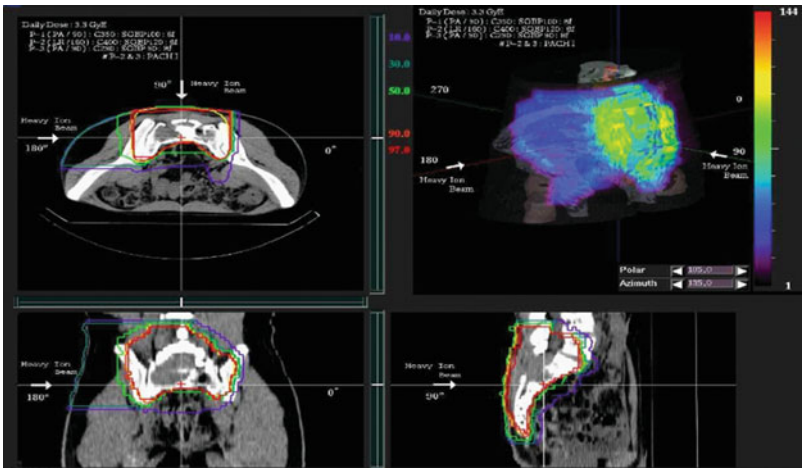

Fig. 36.7 Example of the dose distribution of CIRT in an osteosarcoma

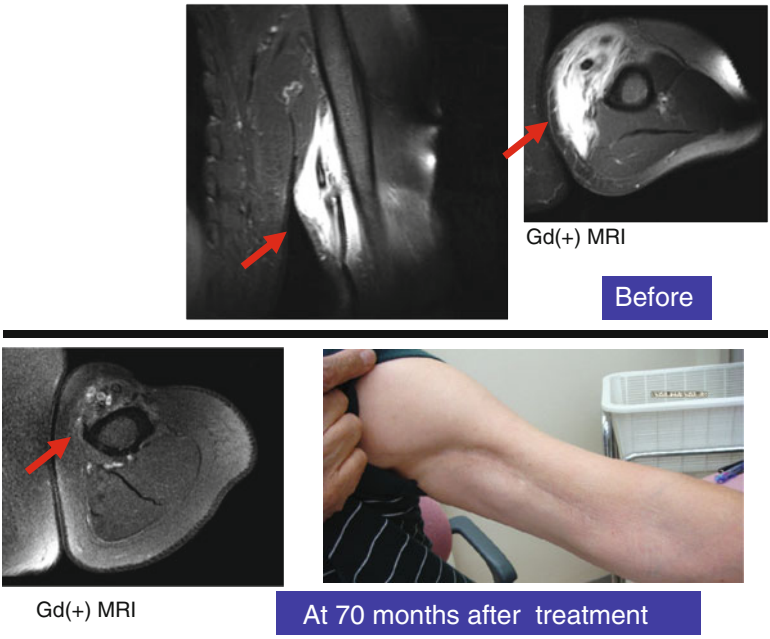

Fig. 36.8 Malignant fibrous histiocytoma of the left arm. The tumor received 70.4 GyE of carbon ions in 16 fractions over 4 weeks. Complete tumor regression and almost no skin reaction were observed at 70 months after treatment

Bone and soft-tissue tumors in the trunk are the most typical lesions qualifying for CIRT and more than 750 patients have been treated.

36.3.6 Rectal Cancer

Although postoperative rectal cancer recurrence in the pelvis has decreased as a result of improvements in surgical procedures, the incidence is still almost 20% [16–18]. Many of the patients with local recurrence are not eligible for surgical resection and are frequently referred to conventional radiation therapy; yet the results are still far from being acceptable. Many of the literature reports give a 50% survival period of 12 months and a 3-year survival rate of approxrimately 10%, and the role of radiotherapy is often described as palliative [19].

Over 300 patients have so far been treated with CIRT and no particularly serious toxic reactions have been discovered. The results in terms of local control and survival rate are extremely favorable in comparison with conventional radiotherapy and are comparable to those achieved with surgery.

Table 36.1 Activity numbers of CIRT facilities in the world

Name	Start	No. of Pts.	Until	Country
NIRS	1994	5,887	2011.2	Japan
GSI	1997	440	2008.7	Germany (closed)
HIBMC	2002	915	2010.9	Japan
IMP	2006	126	2010.11	China
HIT	2009	200	2010.10	Germany
GHMC	2010	90	2010.12	Japan
		7,658		

NIRS National Institute of Radiological Sciences *GSI* GSI Helmholtzzentrum für Schwerionenforschung *HIBMC* Hyogo Ion Beam Medical Center *IMP* Institute of Modern Physics *HIT* Heidelberg Ion-Beam Therapy Center *GHMC* Gunma University Heavy Ion Medical Center

36.4 Future Prospects for CIRT

CIRT is an effective treatment modality for many cancers. Compared with other treatment modalities, however, it has to be admitted that it is rather costly. HIMAC with its 42-m-diameter synchrotron ring was built at costs of roughly 33 billion yen (US $360 million). For the benefits of carbon ions to be available to the public at large, it is of paramount importance to develop a lower cost and more compact system. In view of this, NIRS embarked on the development of a compact system that has the same performance as the HIMAC at about one third of its cost and size (cf. Chap. 37). In March 2010, the new compact facility at Gunma University in Maebashi, Japan, was completed. They have just started their carbon beam treatment as the third CIRT facility in Japan – after NIRS and Hyogo Ion Beam Medical Center.

More than 7500 patients have been treated with carbon ion beams worldwide since 1994, and nearly 80% were treated at NIRS (Table 36.1). Now five carbon ion beam facilities are operating, including the facility at Gunma University. Three more facilities are under construction in Europe and planning is in progress at ten or more institutions worldwide (cf. Chap. 41). There has been a growing interest in using CIRT for cancer treatment in the last decade. NIRS has been pivotal in providing the preclinical and clinical data for this field, and other facilities have successfully reproduced them [20].

The future development and expansion of CIRT requires further progress. The new NIRS system with respiration-gated scanning and a compact rotating gantry should be instrumental in that respect.

36.5 Summary

CIRT at NIRS has made significant progress with a total of 5,887 patients registered by the end of February 2011.

By location, it is effective in the head and neck (including the eye), the base of the skull, lung, liver, prostate, bone and soft tissue, and pelvic recurrence of rectal cancer. By pathological type, CIRT is effective against adenocarcinoma for which photon beams are relatively ineffective, as well as against sarcomas of the bone and soft tissue.

CIRT offers significant advantages over conventional radiotherapy due to its extremely favorable physical and biological dose distribution. These unique features lend themselves to convenient hypofractionated regimens. For lung and liver cancer, in particular, an ultrashort irradiation schedule with only 1 or 2 sessions is available. For prostate, head and neck, base of the skull, pelvic recurrence of rectal cancer, and bone and soft-tissue sarcomas, treatments with 12 fractions over 3 weeks are possible.

Toxicities initially associated with dose escalation are no longer encountered. But clinical trials need to be continued not the least to investigate if the therapeutic outcome of up to now intractable tumors such as malignant glioma or cancer of the pancreas, can also be improved.

References

1. H. Tsujii, S. Morita, T. Miyamoto, et al., Preliminary results of phase I/II carbon-ion therapy at the NIRS. J. Brachyther. Int. **13**, 1–8 (1997)
2. S. Minohara, T. Kanai, M. Endo, et al., Respiratory gated irradiation system for heavy-ion radiotherapy. Int. J. Radiat. Oncol. Biol. Phys. **47**, 1097–1103 (2000)
3. M. Endo, H. Koyama-Ito, S. Minohara, et al., HIPLAN - a heavy ion treatment planning system at HIMAC. J. Jpn. Soc. Ther. Radiol. Oncol. **8**, 231–238 (1996)
4. T. Kanai, Y. Furusawa, K. Fukutsu, et al., Irradiation of mixed beam and design of spread-out Bragg peak for heavy-ion radiotherapy. Radiat. Res. **147**, 78–85 (1997)
5. T. Kanai, M. Endo, S. Minohara, et al., Biophysical characteristics of HIMAC clinical irradiation system for heavy-ion radiation therapy. Int. J. Radiat. Oncol. Biol. Phys. **44**, 201–210 (1999)
6. J. Mizoe, H. Tsujii, T. Kamada, et al., Dose escalation study of carbon ion radiotherapy for locally advanced head and neck cancer. Int. J. Radiat. Oncol. Biol. Phys. **60**, 358–364 (2004)
7. T. Miyamoto, N. Yamamoto, H. Nishimura, et al., The working group for lung cancer: carbon ion radiotherapy for stage I non-small cell lung cancer. Radiother. Oncol. **66**, 27–140 (2003)
8. H. Kato, H. Tsujii, T. Miyamoto, et al., Liver Cancer Working Group. Results of the first prospective study of carbon ion radiotherapy for hepatocellular carcinoma with liver cirrhosis. Int. J. Radiat. Oncol. Biol. Phys. **59**, 1468–1476 (2004)
9. H. Kato, S. Yamada, S. Yasuda, et al., Four-fraction carbon ion radiotherapy for hepatocellular carcinoma. Proc of 40th Ann Meeting Am Soc Clin Oncol, New Orleans, USA, June 5-8, 2004 J. Clin. Oncol. **22**, 4090 (2004)
10. K. Akakura, H. Tsujii, S. Morita, et al., The Working Group for Genitourinary Tumors: Phase I/II clinical trials of carbon ion therapy for prostate cancer. Prostate **55**, 252–258 (2004)
11. H. Tsuji, T. Yanagi, H. Ishikawa, et al., Working Group for Genitourinary Tumors. Hypofractionated radiotherapy with carbon ion beams for prostate cancer. Int. J. Radiat. Oncol. Biol. Phys. **32**, 1153–1160 (2005)
12. T. Kamada, H. Tsujii, T. Yanagi, et al., Working Group for Bone and Soft Tissue Sarcomas: Efficacy and safety of carbon ion radiotherapy in bone and soft tissue sarcomas. J. Clin. Oncol. **20**, 4466–4471 (2002)

13. R. Imai, T. Kamada, H. Tsuji, et al., Working Group for Bone and Soft Tissue Sarcomas. Carbon ion radiotherapy for unresectable sacral chordomas. Clin. Cancer Res. **10**, 5741–5746 (2004)
14. R. Imai, T. Kamada, H. Tsuji, et al., Working Group for Bone and Soft Tissue Sarcomas. Effect of carbon ion radiotherapy for sacral chordoma. Results of phase I-II and phase II clinical trials. Int. J. Radiat. Oncol. Biol. Phys. **77**, 1470–1476 (2009)
15. Y. Nishida, T. Kamada, R. Imai, et al., Clinical outcome of sacral chordoma with carbon ion radiotherapy compared with surgery. Int. J. Radiat. Oncol. Biol. Phys. **79**, 110–116 (2010)
16. S. Galandiuk, H.S. Wieand, C.G. Moertel, et al., Patterns of recurrence after curative resection of carcinoma of the colon and rectum. Surg. Gynecol. Obstet. **174**, 27–32 (1992)
17. F. Bozzetti, L. Mariani, R. Micel, et al., Cancer of the low and middle rectum: local and distant recurrence and survival in 350 radically resected patients. J. Surg. Oncol. **62**, 207–213 (1992)
18. J.L. McCall, M.R. Cox, D.A. Wattchow, Analysis of local recurrence rates after surgery alone for rectal cancer. Int. J. Colorectal. Dis. **10**, 126–132 (1995)
19. H.J. Wanebo, R.J. Koness, M.P. Vezeridis, et al., Pelvic resection of recurrent rectal cancer. Ann. Surg. **220**, 586–595 (1994)
20. D. Schulz-Ertner, C.P. Karger, A. Feuerhake, et al., Effectiveness of carbon ion radiotherapy in the treatment of skull-base chordomas. Int. J. Radiat. Oncol. Biol. Phys. **68**, 449–457 (2007)

Chapter 37
A National Action Plan in Japan: From Experimental Studies to Highly Advanced Medical Technology

Koji Noda

Abstract Since 1994, cancer treatments in Japan have successfully progressed with HIMAC as a heavy ion radiotherapy facility. On the basis of these successful experiences with carbon ion radiotherapy (CIRT) at HIMAC, several new developments and construction projects for Japanese CIRT facilities have been promoted in order to boost the application of this treatment modality.

37.1 Introduction

The Heavy Ion Medical Accelerator in Chiba (HIMAC) project was promoted by the Japanese government as one of the major projects in the "Comprehensive 10-Year Strategy for Cancer Control". In October 1993, the HIMAC facility was completed by the National Institute of Radiological Sciences (NIRS) as the world's first heavy ion accelerator dedicated to medical use. Cancer treatments utilizing HIMAC were initiated on June 21, 1994, and until December 2010 NIRS has treated more than 5,700 patients (cf. the previous chapter).

The clinical efficiency of CIRT has been demonstrated for various diseases. Owing to the accumulated protocols, the Japanese government approved the HIMAC treatment as a highly advanced medical technology in 2003, which means that it is covered by the Japanese health insurance. From 2004 to 2005, NIRS studied and designed a downsized version of the HIMAC facility for more widespread use in Japan. After completing these works, Gunma University Heavy Ion Medical Center (GHMC) began construction of a pilot facility of the downsized version in February 2007, and the construction was completed in July 2009. After a beam commissioning and preclinical phase, cancer treatments in GHMC have been

K. Noda (✉)
Department of Accelerator and Medical Physics, National Institute of Radiological Sciences, Research Center of Charged Particle Therapy, Anagawa 4-9-1, Inage-ku, Chiba, 263-8555, Japan
e-mail: noda_k@nirs.go.jp

U. Linz (ed.), *Ion Beam Therapy*, Biological and Medical Physics, Biomedical Engineering, DOI 10.1007/978-3-642-21414-1_37,

successfully carried out since March 2010. On the other hand, NIRS has carried out the new treatment research facility project since 2006, for further development of the HIMAC treatments. The goal of the project is to realize adaptive cancer therapy for both fixed and moving targets using the 3D pencil beam rescanning method. These technologies have been transferred to various Japanese industrial companies. By 2015, it is expected that five CIRT facilities and eight proton radiotherapy facilities will be providing ion beam therapy for cancer in Japan.

37.2 Progress of HIMAC

The HIMAC design parameters were based on radiological requirements. In the design stage, the required ion species were chosen in the range from He to Ar. The maximum range of ions in tissue was determined to be 30 cm, based on the clinical experience with conventional radiotherapy at NIRS. The maximum beam energy was determined by the range–energy relationship for the silicon ion, which is one of the heaviest ions suited for treatment of deeply seated and radioresistant tumors. It was 800 MeV/u and this energy could provide a range in tissue greater than 30 cm for ions lighter than silicon. The dose rate for any ion beam was required to be 5 Gy/min to permit completion of one fractional treatment within 1 min. The beam intensities for various ion species were determined from the required dose rate. The irradiation field size was determined as 22 cm in diameter based on the clinical experience at NIRS. Using both vertical and horizontal beams is essential to obtain a highly controlled dose distribution in heavy ion treatments. The HIMAC facility, thus, has three treatment rooms, which are equipped with a horizontal beam delivery system, with a vertical one, and with both horizontal and vertical ones, respectively. Further, an appropriate accelerator system, consisting of an injector, linear accelerator cascade, and a synchrotron was chosen in consideration of the medical requirements. Two experimental rooms for physics and one for biology were also prepared in order to carry out basic research related to heavy ion radiotherapy. The specifications of the HIMAC facility are summarized in Table 37.1, and a cut-away view of the HIMAC facility is shown in Fig. 37.1.

At the beginning of the HIMAC project, a carbon ion beam was selected for heavy ion radiotherapy because of the similarity of its LET characteristics to those of the neutron beam which was used for clinical trials at NIRS [1]. After preclinical research with a carbon ion beam, the first clinical trial was carried out on three patients in June 1994 with 290 MeV/u carbon ions.

At an early stage of the clinical trials, the number of fractions was typically 18 and the treatment required 6 weeks excluding the time for diagnostics and treatment planning. The number of fractions, however, could be decreased for some protocols, especially liver and lung, without additional serious side effects. Today, the typical number of fractions is as low as four for liver cancer. For lung cancer treatment, even single-fraction irradiations have been tried since April 2003 (cf. Chap. 14 for details). By reducing the number of fractions, the number of treatments could

Table 37.1 Specifications of the HIMAC facility

Ion species	He, C, Ne, Si, Ar
Range	30 cm in soft tissue
Max. energy	800 MeV/u (Si)
Maximum irradiation field	22 cm diameter
Dose rate	5 Gy/min
Beam direction	Horizontal, vertical
Number of treatment rooms	Three (H, V, H&V)[a]
Number of research rooms	Two for physics, one for biology
Irradiation method	Broad beam (wobbler)

[a] *H* Horizontal beam delivery system, *V* Vertical beam delivery system

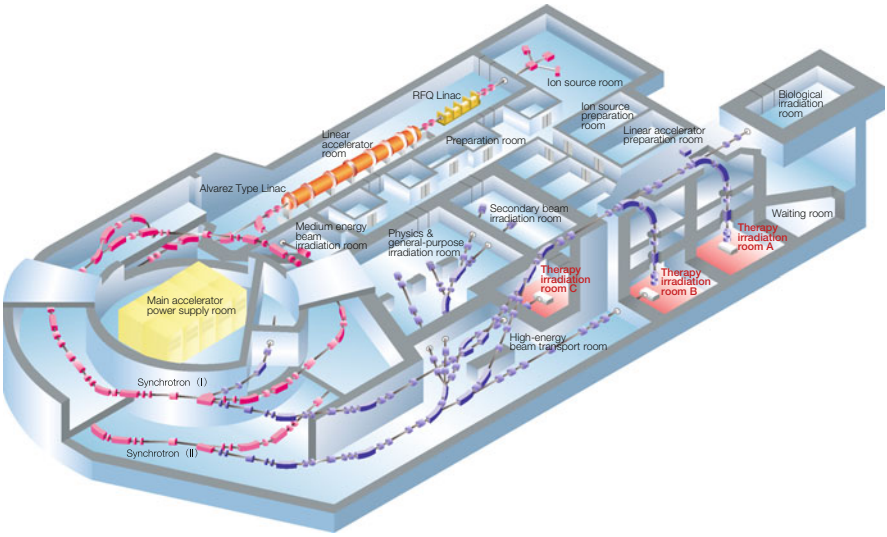

Fig. 37.1 Cut-away view of the HIMAC facility

significantly be increased and in the meantime, CIRT at HIMAC is approved as a highly advanced medical technology.

37.3 Technology Development and Medical Physics at HIMAC

Since HIMAC began operation, various technologies related to heavy ion radiotherapy have been developed and basic research related to medical physics has been performed.

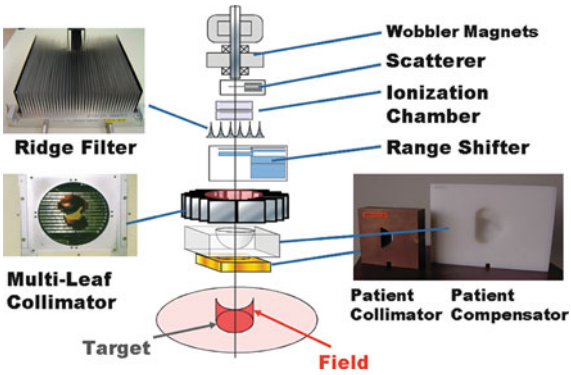

Fig. 37.2 Beam wobbling method with devices

37.3.1 Beam Delivery System

37.3.1.1 Layer-Stacking Irradiation Method

As schematically shown in Fig. 37.2, a beam wobbling method, which is one of the broad-beam irradiation methods, has been utilized at HIMAC. In comparison to 3D pencil beam scanning, dose management is considered easier and it is less sensitive to beam misplacement. A pair of beam wobbling magnets rotates the beam in a circular orbit at high frequency so as to generate a pseudostationary broad beam in conjunction with a heavy metal scatterer. A ridge filter modulates the beam range in the field to spread out the Bragg peak (SOBP) longitudinally. In the HIMAC beam delivery system, a ridge filter consisting of identical aluminum bar ridges spreads the beam range to give a uniform biological dose distribution to the SOBP region. A range shifter system, consisting of variable thickness energy absorbers, can adjust the beam range. The field aperture is defined by a multileaf collimator (MLC) with movable metal elements and a customized patient collimator. A patient compensator, a sculptured plastic device, compensates the beam ranges so that the ions' range conforms to the distal part of the target volume in the field.

In the beam wobbling method, a constant SOBP across the field area results in an undesirable dose to the normal tissue proximal to the target. In order to avoid such undesired doses, layer stacking was proposed [2] and has been routinely used for carbon therapy at HIMAC [3, 4]. In this method, a miniature SOBP is produced with a ridge filter. The full widths at 60% dose level of the SOBP layer are about 11.9, 12.8, and 15.9 mm for 290, 350, and 400 MeV/u carbon ion beams, respectively. During irradiation, the centroid of the SOBP is sequentially shifted in the longitudinal direction and in steps of 2.5 mm by changing the beam energy using a range shifter. The patient compensator and the MLC are also used as in ordinary beam wobbling while the aperture shape of the MLC conforms to each slice of the target. Once the planned dose is delivered to each slice, beam extraction is quickly cut off during the transition time to set the range shifter and the MLC for the next slice. Beam-on/off is controlled by using the radiofrequency knock-out (RF-KO)

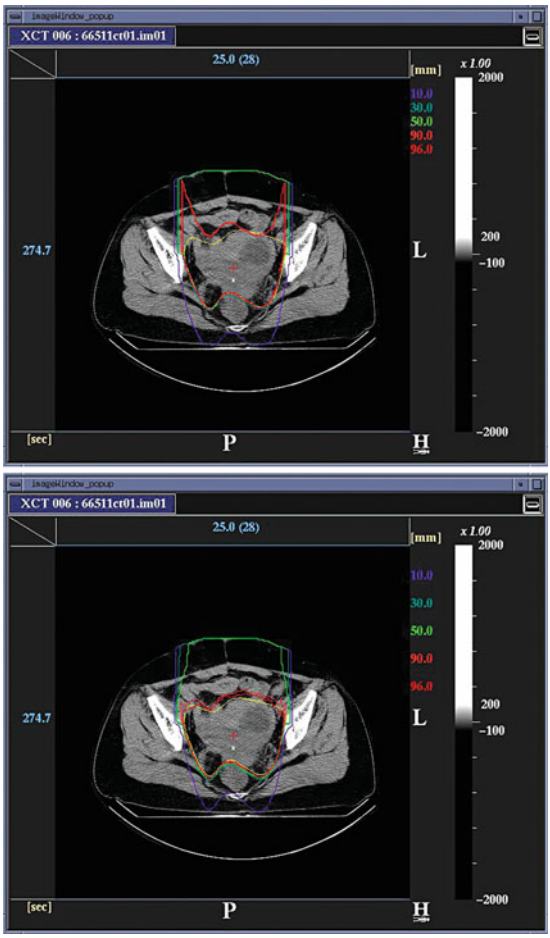

Fig. 37.3 Treatment planning (*Top*) with the conventional broad-beam method and (*Bottom*) with the layer stacking method

slow extraction [5]. Currently, the mechanical movement of the range shifter limits the transition time to within a fraction of a second. As shown in Fig. 37.3, layer stacking clearly suppresses the undesired dose to the surface observed with the conventional method.

37.3.1.2 Respiratory-Gated Irradiation

Organ motion during patient positioning and beam delivery degrades targeting precision. In particular, breathing causes movements up to a few centimeters in the lung and liver. Respiratory movements may even influence the whole body when the patient is in the prone position. Respiratory-gated irradiation effectively mitigates such motion by controlling the timing of the beam extraction synchronously with respiration. At HIMAC, breathing can be detected with an infrared light spot and a

position-sensitive detector, which gives a respiration waveform signal. The organs are normally most stable at the end of expiration. Therefore, beam extraction is gated to this phase of the respiration cycle [6].

The respiration pattern and its reproducibility are patient-dependent. Real-time detection of the respiration waveform, fast and robust gating logic, and responsiveness of the beam extraction system are, therefore, essential for the respiratory gating system. In the case of HIMAC, beam extraction is turned on and off within submilliseconds owing to RF-KO slow extraction. The respiratory-gated irradiation method has been applied to approx. 30% of the HIMAC treatments.

37.3.2 Medical Physics Program

37.3.2.1 Analysis of Tumor Control Probability

On the basis of dose-escalation studies, clinical results from HIMAC have been analyzed in order to reduce the number of fractions per treatment. The clinical dose distributions of the therapeutic carbon ion beam currently used at NIRS are based on the survival of human salivary gland (HSG) cells in vitro and on clinical experience with fast neutron therapy. The moderate radiosensitivity of HSG cells is assumed to be similar to the typical response of a tumor to carbon beams.

For a new protocol, the biological dose distribution is designed so as to cause a flat biological effect on HSG cells in the SOBP region. Then, the entire biological dose distribution is evenly raised in order to reach a relative biological effectiveness (RBE) of 3.0 at a depth where the dose-averaged linear energy transfer (LET) is 80 keV/μm. It could be demonstrated experimentally that at that point carbon ions have a biological effect identical to fast neutrons [7].

The resulting clinical dose distribution in this approximation does not depend on dose level, tumor type or fractionation scheme and, thus, reduces the unknown parameters in the analysis of the clinical results. The width of the SOBP and the ratio of clinical to physical dose at the center of the SOBP specify the dose distribution.

The clinical results of non-small cell lung cancer (NSCLC) treated at HIMAC depicted a very strong dependency of the local control rate (LCR) on the dose. A dose-escalation study was performed with a treatment schedule of 18 fractions in 6 weeks [7]. Dose dependency of tumor control probability (TCP) with the photon beam was fitted by the following formula proposed by Webb:

$$TCP = \sum_i \frac{1}{\sqrt{2\pi}\sigma} \left\{ -\frac{(\alpha_i - \alpha)^2}{2\sigma^2} \right\} \exp\left[-N \exp\left\{ -n\alpha d \left(1 + d/(\alpha + \beta)\right) + \frac{0.693(T - T_k)}{T_p} \right\} \right],$$

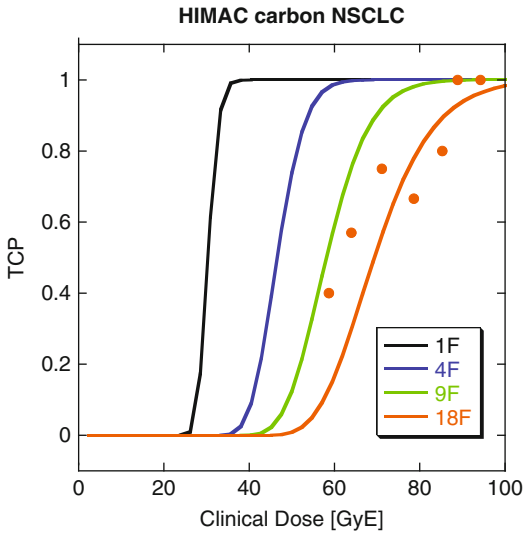

Fig. 37.4 Tumor control probability (TCP) curve of non-small cell lung cancer (NSCLC) by CIRT. The curves for 1, 4, and 9 fractions are calculated from clinical data derived from 18 fractions

where α and β are coefficients of the linear–quadratic (LQ) model of the cell survival curve for HSG cells, σ is the standard deviation of the coefficient α, which reflects patient-to-patient variation of radiosensitivity, N is the number of clonogens in a tumor (a fixed value of 10^9 was used), n and d are the total fraction number and the dose/fraction, respectively. T (42 days), T_k (0 day) and T_p (7 days) are overall time for treatment, kick-off time, and average doubling time of tumor cells, respectively.

The analysis was carried out for 18 fractions in order to determine the tumor-specific radiosensitivity parameter α and its variation σ. Once the parameters were fixed, it was possible to estimate the dose–response curve for various fraction schedules.

Figure 37.4 gives an example of the TCP for NSCLC as function of the dose and fraction number. TCP curves for 1, 4, and 9 fractions were estimated from the parameters derived from the data of the 18 fractions. This approach is applicable to estimate appropriately prescribed doses when initiating hypofractionated radiotherapy.

37.3.2.2 Radiation Quality of Carbon Ions

The mechanism underlying the clinical effect of carbon ions is still not fully understood, and the complicated physical interactions in a patient are hard to predict. In order to obtain a feasible solution, some approximations were introduced into the treatment planning system (TPS) [8].

When heavy ions travel in a patient's body, some of them undergo fragmentation reactions with target nuclei, generating various fragment species which become

widely distributed. The biological effectiveness of heavy ions is affected not only by the deposited energy, but also by the particle species [9]. Thus, precise calculation of the spatial distribution of the radiation quality such as dose, dose-averaged LET, fluence, and energy distributions for each particle species plays a crucial role.

The deflection angle of fragment particles in matter should be described by considering both multiple scattering [10] and Fermi momentum transfer [11]. The angular distribution of fragment particles was measured with a monoenergetic 290 MeV/u ^{12}C beam by a nuclear reaction in a thick water target [12]. A parameter describing the extent of transferred momentum in the Goldhaber model [11] was determined so as to reproduce the observed angular distribution.

On the basis of these studies, a semianalytical beam transportation code was developed for energetic heavy ion beams in which the 3D distribution of the radiation quality can be calculated for each particle type [13]. The production of secondary and tertiary fragments was considered and the effects of the Fermi momentum transfer at their production point were taken into account.

Despite its simplicity, the developed code was able to reproduce the experimental results well. Another approach to derive the spatial distribution of radiation quality in matter is the utilization of Monte Carlo methods [14], although it is time-consuming and currently not practical for implementation into the TPS of heavy ion therapy.

37.4 Downsized Version of HIMAC

In order to reduce construction cost and to widen the applicability of CIRT, NIRS designed a downsized version of the HIMAC facility.

37.4.1 Design and R&D Work

The specifications were determined, as summarized in Table 37.2, considering the statistics from HIMAC treatments as to residual range, irradiation field size, beam intensity, and number of treatment rooms [15].

37.4.1.1 Beam Delivery System

The beam delivery system employs the broad-beam method, for the same reasoning as mentioned above. Spiral beam wobbling, a modification of conventional wobbling, was developed in order to reduce the beam energy; it uses a relatively thin scatterer. As a result, it was experimentally verified that this method could produce an irradiation field with a uniformity of $\pm 2.5\%$ [16]. It could also easily be applied to respiratory-gated irradiation and layer stacking.

Table 37.2 Specifications of the downsized carbon therapy facility

Ion species	Carbon
Energy	140–400 MeV/u
Max. residual range	25 cm
SOBP	4–15 cm
Max. lateral field size	22 cm
Max. dose rate	5 GyE/min/l
Beam intensity	1.2×10^9 pps
Irradiation methods	Gating, layer stacking
Number of treatment rooms	Three rooms, equipped with H&V, H, V[a]
Number of treatments	>800 patients/year

[a] *H* Horizontal beam delivery system, *V* Vertical beam delivery system

Spiral beam wobbling was designed for carbon ions having a residual range of 25 cm under the initial energy of 400 MeV/u and an irradiation field of 22 cm in diameter. The system consists of dose monitors, scanning magnets, a scatterer, a ridge filter, a range shifter, and collimators.

The ridge filter is designed to change the SOBP size from 4 to 15 cm. The range shifter is installed so as to precisely adjust the residual range in a patient. MLC and patient compensators precisely define the lateral and distal irradiation fields, respectively. Since the MLC employs thin leaves (3.7 mm thick), a separate patient collimator is not required. The length of this beam delivery system could be downsized to 8.5 m whereas that of HIMAC is more than 10 m long.

37.4.1.2 Accelerator System

The accelerator system in the downsized treatment unit consists of an injector and a synchrotron ring. The injector comprises a compact 10 GHz ECR ion source [17] and a linac cascade, which consists of an RFQ linac and an alternating phase focused interdigital H-mode (APF-IH) linac [18], both with an operating frequency of 200 MHz. The output energy of the injector linac cascade is designed to be 4.0 MeV/u. The required intensity is 200 μA C^{6+} after a charge stripper. A prototype of this compact injector system was constructed in order to verify its performance. From a beam test result, the intensity of 500 μA for 4.0 MeV/u C^{6+} was obtained as designed.

Design and R&D work on the proposed synchrotron [19] were carried out in order to reduce the synchrotron size while keeping the required performance. The synchrotron was designed to accelerate a C^{6+} beam from 4 to 400 MeV/u. Multiturn injection is used to increase the intensity. Because of the quick response to beam-on/off, the RF-KO slow-extraction method is applicable to both the gated irradiation and layer stacking. The lattice structure employs a FODO missing magnet design while each cell contains three dipole magnets and two kinds of quadrupole magnets

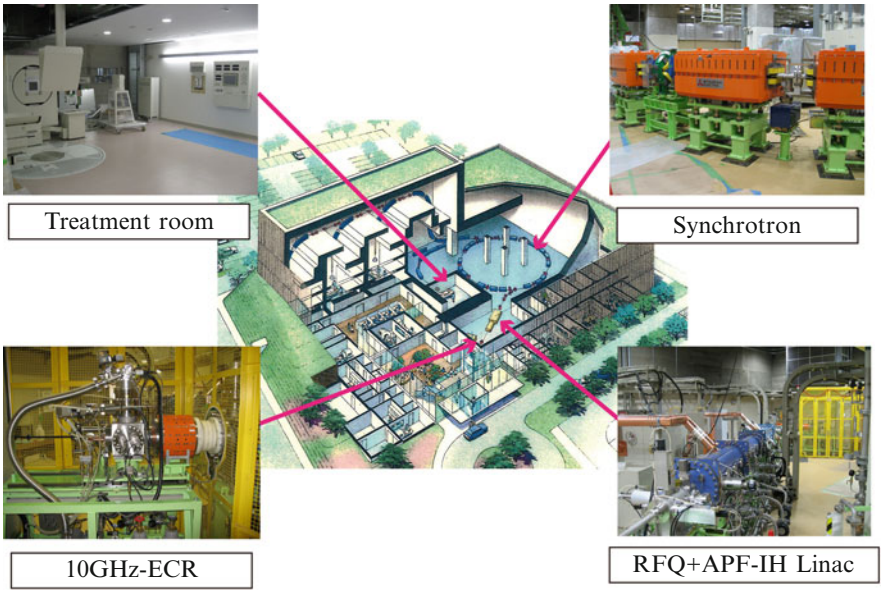

Fig. 37.5 Sketch of the GHMC and installed devices

(QF/QD). As a result, the ring circumference could be considerably reduced to approx. 63 m, half the size of the HIMAC synchrotron.

37.4.2 Construction of a Pilot Facility

On the basis of the design and R&D work at NIRS, construction of a downsized pilot facility began at GHMC in February 2007. It was projected for a compact injector system, a synchrotron ring, three treatment rooms with spiral beam wobbling technique, and one experimental room for basic research. A view of the GHMC facility with some of the equipment is presented in Fig. 37.5. The area is only about one-third the size of the HIMAC facility. The first beam from the synchrotron was obtained in August 2009. After commissioning and a preclinical phase, the first patient was successfully treated in March 2010.

37.5 New Treatment Research Facility Project at NIRS

NIRS proposed a new treatment research facility aiming at adaptive cancer therapy with heavy ions, e.g., by putting the 1-day treatment of lung cancer into effect. Further, the new facility should accurately treat fixed targets, moving targets with breathing and/or targets near critical organs. For these purposes, 3D rescanning with

Table 37.3 Main specifications of the new treatment research facility at HIMAC

Ion species	^{12}C, ^{16}O, ^{11}C, ^{15}O	
	Fixed port	Rotating gantry
Energy	140–430 MeV/u	140–400 MeV/u
Lateral field	22 × 22 cm	15 × 15 cm
SOBP	15 cm	15 cm

a pencil beam [20] is intended plus or minus a rotating gantry [21]. The design study and the related R&D work have been carried out at HIMAC since 2006. Construction of the facility building was completed in March 2010. Treatment of the first patient started successfully in May 2011.

37.5.1 Facility Planning

As in the case of the downsized version of the HIMAC facility, the main specifications of the new treatment research facility at NIRS were deduced from more than 10 years of experience with HIMAC. The main specifications are summarized in Table 37.3.

The maximum ion energy is designed to be 430 MeV/u in the fixed-beam delivery system, corresponding to a range of 30 cm in tissue for ^{12}C and 22 cm for ^{16}O ions. The rotating gantry is configured for a maximum energy of 400 MeV/u and a smaller lateral field size of 15 × 15 cm in order to limit its dimensions. Further, positron emitting beams such as ^{11}C and ^{15}O will be used to verify the irradiation area and their ranges in a patient's body. They should be accelerated directly in the HIMAC [22] rather than being produced by projectile fragmentation.

The ion beams are to be delivered from the upper ring of the HIMAC synchrotron. The treatment hall, placed underground, will comprise three treatment rooms allowing to treat more than 800 patients per year.

Two rooms are equipped with fixed-beam delivery systems in both horizontal and vertical direction, the third room will accommodate the gantry. Two treatment simulation rooms with X-ray CT are prepared for patient test positioning and position monitoring during all treatment sessions. Six rooms are devoted to patient preparation just before irradiation. A schematic view of the new treatment facility is shown in Fig. 37.6.

37.5.2 3D Pencil Beam Rescanning

It is well known that 3D beam scanning is suitable for adaptive cancer radiotherapy because it does not require any patient compensators, which can take a week to manufacture. NIRS applied beam scanning with protons first [23]. In the 1990s, PSI and GSI developed scanning methods for proton and carbon ion radiotherapies,

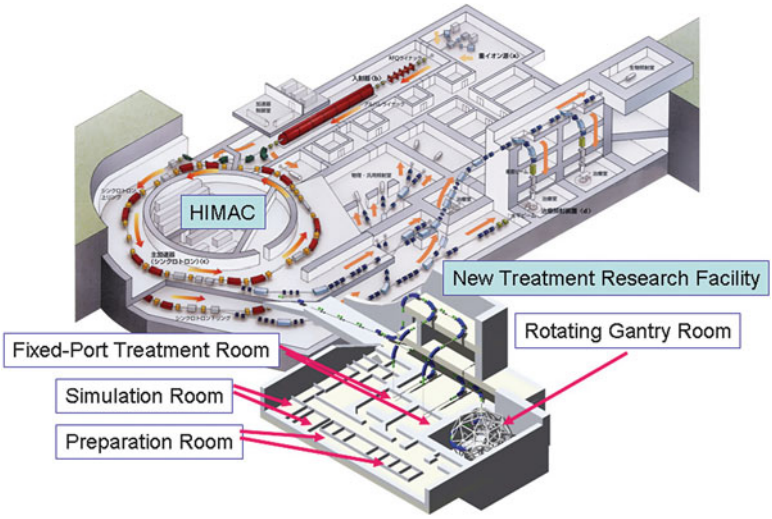

Fig. 37.6 Schematic view of the new treatment research facility at NIRS

respectively [24, 25]. However, scanning has not yet been applied to moving targets such as lung or liver cancer because the dose management is difficult. The new 3D pencil beam scanning method of NIRS will just offer this option.

After a simulation study, the respiration phase-controlled rescanning method was developed [20]. In this method, irradiation of one slice is completed during one gated period. A uniform dose distribution can be obtained even for a moving target, because during irradiation the target motion is close to "zero" on average.

The phase-controlled rescanning method requires mainly two technologies: an intensity modulation which ensures a constant irradiation time for all the slices independent of their cross sections and a fast scanning technique to complete several rescans within one gating period.

37.5.2.1 Intensity Modulation

A beam spill control system was developed [26], based on the improvement of the time structure of an extracted beam from the synchrotron [27, 28]. The core part of this system required the following functions:

- Calculation and output of an amplitude modulation signal according to request signals from a beam delivery system
- Real-time processing with a time resolution less than 1 ms and
- Feed-forward and feedback controls to realize the extracted intensity as requested

As illustrated in Fig. 37.7, this system allows dynamic control of the beam intensity as required.

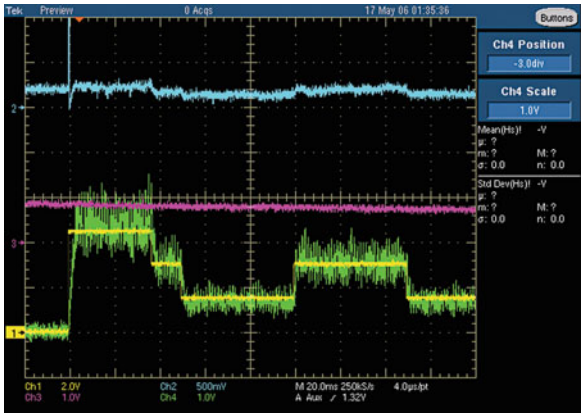

Fig. 37.7 Time structure of extracted beam obtained by the spill control system. The time structure (*green*) can be modulated by the request signal (*yellow*)

37.5.2.2 Fast Scanning Technique

Three techniques are proposed for fast scanning:

(a) A new TPS
(b) Extended flattop operation of the HIMAC synchrotron and
(c) Design and construction of a high-speed scanning magnet system

(a) A new TPS has been developed for fast 3D scanning with a pencil beam. The biological dose distribution of a pencil beam is obtained by combining the measured physical dose distribution and the RBE obtained through measured α and β values in the LQ model. Using the biological dose distribution, the new TPS optimizes the assignment of spot positions and their weights so as to give the prescribed dose to the target and to significantly reduce the dose to surrounding normal tissues. For the fast 3D scanning, raster scanning is employed instead of spot scanning, in order to save the beam-on/off time during beam movement between spot positions. In the raster scanning method, however, it is inevitable that the prescribed dose distribution is disturbed by an extra dose due to beam movement between spot positions. In addition, the extra dose is proportional to the delivered beam intensity. On the other hand, fast scanning requires high beam intensity. Consequently, the high extra dose makes uniform dose distributions difficult for fast raster scanning. Since the HIMAC synchrotron delivers a highly reproducible beam with a uniform time structure [26], the extra dose can be predicted and taken into account in the new TPS. As a result, the new TPS can increase the scanning speed by approx. a factor of 5. By applying a modified "traveling-salesman problem", the path length of raster scanning could be shortened by 20–30%.
(b) Owing to the high beam utilization efficiency of nearly 100% in the scanning method and an intensity upgrade to 2×10^{10} carbon ions at the HIMAC

synchrotron, single-fraction irradiations of almost all treatment procedures can, in principle, be completed in a single operation cycle of the HIMAC synchrotron. This single-cycle operation can significantly reduce dead time for beam injection, acceleration, and deceleration. Beam stability was tested in this operation mode, and position and profile stability were less than ± 0.5 mm at the isocenter during 100 s of extended flattop operation. This extended flattop operation can shorten the irradiation time by a factor of 2 and has been routinely utilized for 3D scanning experiments at HIMAC.

(c) The scanning speeds are designed to be 100 mm/ms and 50 mm/ms in horizontal and vertical directions, respectively. This is nearly one order of magnitude faster than for conventional spot scanning. To achieve this, the scanning magnet was designed with slits at both ends of the magnetic pole, based on a thermal analysis including eddy-current loss and a hysteresis loss.

The power supply of the scanning magnet consists of two-stage circuits: the first stage for voltage forcing by IGBT (insulated gate bipolar transistor) switching elements and the second stage for flattop current control by FET (field-effect transistor) switching elements. The results of a preliminary test showed a maximum temperature increase of approx. 30°, which was consistent with the thermal analysis, for the designed scanning speed.

A test irradiation port was designed and constructed for the fast raster scanning experiment in order to verify the proposed performance (Fig. 37.8). The measured dose response of the pencil beam with various energies was adapted. The beam size at the entrance and the width of the Gaussian-shaped minipeak were 3.5 and 4 mm at 1 standard deviation, respectively. Experimental results verified the validity of the beam model and the optimization calculation [29]. Furthermore, experimentally, the desired physical dose distribution was successfully obtained for both fixed and moving targets, and HSG cell survival was also obtained as expected. In comparison to conventional spot scanning, the irradiation time could be shortened by approx. two orders of magnitude.

37.5.3 Rotating Gantry

In order to reduce the size of the gantry, the final dipole magnet is divided into a 30° and a 60° unit, and the two scanners are placed in between the dipoles to extend the effective length from the scanners to the isocenter.

The total weight of the rotating gantry is estimated to be roughly 350 tons. In order to avoid any change of the beam size depending on the rotation angle, a compensation method for the asymmetric phase space distribution will be adapted [30].

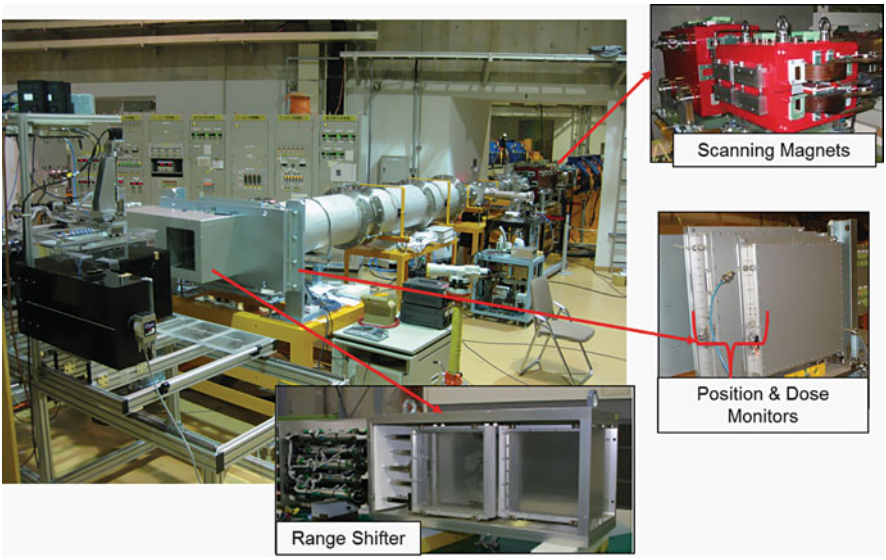

Fig. 37.8 The fast 3D-rescanning test port installed in the HIMAC facility

37.6 Japan's National Action Plan

CIRT at NIRS has proven to be effective against a wide variety of tumors including radioresistant ones. Serious side effects were rare and quality of life (QoL) could be kept high.

The fraction number could be reduced as compared to low-LET radiotherapy, making short-course or even single-fraction treatments possible.

The number of cancer patients continues to grow in Japan since cancer has become the leading cause of death in the 1980s. Therefore, NIRS proposed a new facility in order to boost applications of CIRT, with emphasis on a less costly, downsized version of HIMAC. The design of the new facility was based on the more than 10 years of experience with HIMAC treatments.

Key technologies for more compact accelerator and beam delivery systems were developed and their performances verified by beam tests with HIMAC.

GHMC was the first pilot facility on the basis of the new concept. It was built in about 2 years and began with patient treatments in March 2010.

NIRS itself has been engaged in a new treatment research facility project since April 2006. The goal is adaptive cancer radiotherapy, i.e., treatment which remains accurate and tumor conform even if changes of size and shape occur during the treatment period.

Since NIRS treats both fixed and relatively mobile tumors, it proposed a fast 3D rescanning method with gated irradiation to move toward the goal of treating both classes of tumors.

Following the GHMC pilot facility, two additional CIRT projects have been initiated in Japan: The Saga Heavy Ion Medical Accelerator in Tosu (Saga-HIMAT) project and the Kanagawa Prefectural project.

The Saga-HIMAT project was initiated in February 2010 and is expected to open in April 2014. Although this facility has three treatment rooms, it will open with only two exhibiting the spiral beam wobbling method as first step. Both rooms will have two beam lines each, either horizontal and vertical, or horizontal and 45°. In a second step, the third room will be equipped with horizontal and vertical beam delivery systems. It will offer the new 3D rescanning method developed by NIRS.

Design work for the Kanagawa Prefectural Cancer Center is ongoing since April 2010, and it is expected to be operational by April 2015.

More than 500,000 persons are diagnosed with cancer every year in Japan, and it is expected that this number will continue to rise. After HIMAC and the Hyogo Ion Beam Medical Center (HIBMC), the newly opened GHMC facility is expected to further boost CIRT applications. By April 2015, a total of five carbon ion and eight proton facilities will be operating in Japan, and they will certainly play an important role in cancer therapy.

References

1. H. Tsunemoto, T. Arai, S. Morita, et al., Japanese experience with clinical trials of fast neutrons. Int. J. Radiat. Oncol. Biol. Phys. **8**, 2169–2172 (1982)
2. T. Kanai, K. Kawachi, H. Matsuzawa, T. Inada, Broad beam three-dimensional irradiation for proton radiotherapy. Med. Phys. **10**, 344–346 (1983)
3. Y. Futami, T. Kanai, M. Fujita, et al., Broad-beam three-dimensional irradiation system for heavy-ion radiotherapy at HIMAC. Nucl. Instrum. Methods Phys. Res. A **430**, 143–153 (1999)
4. T. Kanai, N. Kanematsu, S. Minohara, et al., Commissioning of a conformal irradiation system for heavy-ion radiotherapy using a layer-stacking method. Med. Phys. **33**, 2989–2997 (2006)
5. K. Noda, M. Kanazawa, A. Itano, et al., Slow beam extraction by a transverse RF field with AM and FM. Nucl. Instrum. Methods Phys. Res. A **374**, 269–277 (1996)
6. S. Minohara, T. Kanai, M. Endo, et al., Respiratory gated irradiation system for heavy-ion radiotherapy. Int. J. Radiat. Oncol. Biol. Phys. **47**, 1097–1103 (2000)
7. T. Miyamoto, N. Yamamoto, H. Nishimura, et al., Carbon ion radiotherapy for stage I non-small cell lung cancer. Radiother. Oncol.**66**, 127–140 (2003)
8. T. Kanai, M. Endo, S. Minohara, et al., Biophysical characteristics of HIMAC clinical irradiation system for heavy-ion radiation therapy. Int. J. Radiat. Oncol. Biol. Phys. **44**, 201–210 (1999)
9. E.A. Blakely, F.Q. Ngo, S.B. Curtis, C.A. Tobias, Heavy ion radiotherapy: cellular studies. Adv. Radiat. Biol. **11**, 295–390 (1984)
10. G. Molière, Theorie der Streuung schneller geladener Teilchen: II Mehrfach- und Vielfach-streuung. Z. Naturforsch. **3a**, 78–97 (1948)
11. A.S. Goldhaber, Statistical models of fragmentation processes. Phys. Lett. B **53**, 306–308 (1974)
12. N. Matsufuji, M. Komori, H. Sasaki, et al., Spatial fragment distribution from a therapeutic pencil-like carbon beam in water. Phys. Med. Biol. **50**, 3393–3403,(2005)
13. T. Inaniwa, T. Furukawa, N. Matsufuji, et al., Clinical ion beams: semi-analytical calculation of their quality. Phys. Med. Biol. **52**,7261–7279 (2007)

14. H. Nose, Y. Kase, N. Matsufuji, T. Kanai, Field size effect of radiation quality in carbon therapy using passive method. Med. Phys. **36**, 870–875 (2009)
15. K. Noda, T. Furukawa, T. Fujisawa et al., New accelerator facility for carbon-ion cancer therapy. J. Radiat. Res. **48**, A43–A54 (2007)
16. S. Yonai, N. Kanematsu, M. Komori, et al., Evaluation of beam wobbling methods for heavy-ion radiotherapy. Med. Phys. **35**, 927–938 (2008)
17. M. Muramatsu, A. Kitagawa, Y. Sakamoto, et al., Development of a compact electron-cyclotron-resonance ion source for high-energy carbon-ion therapy. Rev. Sci. Instrum. **76**, 1133041–1133046 (2005)
18. Y. Iwata, S. Yamada, T. Murakami, et al., Performance of a compact injector for heavy-ion medical accelerators. Nucl. Instrum. Methods Phys. Res. A **572**, 1007–1021 (2007)
19. T. Furukawa, K. Noda, K. Yoshida, et al., Design of synchrotron and transport line for carbon therapy facility and related machine study at HIMAC. Nucl. Instrum. Methods Phys. Res. A **562**, 1050–1053 (2006)
20. T. Furukawa, T. Inaniwa, S. Sato, et al., Design study of a raster scanning system for moving target irradiation in heavy-ion radiotherapy. Med. Phys. **34**, 1085–1097 (2007)
21. T. Furukawa, T. Inaniwa, S. Sato, et al., Design study of a rotating gantry for the HIMAC new treatment facility. Nucl. Instrum. Methods Phys. Res. B **266**, 2186–2189 (2008)
22. S. Hojo, T. Honma, Y. Sakamoto, S. Yamada, Production of 11C-beam for particle therapy. Nucl. Instrum. Methods Phys. Res. B **240**, 75–78 (2005)
23. T. Kanai, K. Kawachi, Y. Kumamoto, et al., Spot scanning system for proton radiotherapy. Med. Phys. **7**, 365–369 (1980)
24. T. Haberer, W. Becher, D. Schardt, G. Kraft, Magnetic scanning system for heavy ion therapy. Nucl. Instrum. Methods Phys. Res. A **330**, 296–305 (1993)
25. E. Pedroni, R. Bacher, H. Blattmann, et al., The 200-MeV proton therapy project at the Paul Scherrer Institute: Conceptual design and practical realization. Med. Phys. **22**, 37–53 (1995)
26. S. Sato, T. Furukawa, K. Noda, Dynamic intensity control system with RF-knockout slow-extraction at HIMAC synchrotron. Nucl. Instrum. Methods Phys. Res. A **574**, 226–231 (2007)
27. K. Noda, T. Furukawa, S. Shibuya, et al., Advanced RF-KO slow-extraction method for the reduction of spill ripple. Nucl. Instrum. Methods Phys. Res. A **492,** 253–263 (2002)
28. T. Furukawa, K. Noda, M. Muramatsu, et al., Global spill control in RF-knockout slow extraction. Nucl. Instrum. Methods Phys. Res. A **522**, 196–204 (2004)
29. T. Inaniwa, T. Furukawa, S. Sato, et al., Development of treatment planning for scanning irradiation at HIMAC. Nucl. Instrum. Methods Phys. Res. B **266**, 2194–2198 (2008)
30. T. Furukawa, K. Noda, Compensation of the asymmetric phase–space distribution for a slowly extracted beam from a synchrotron. Nucl. Instrum. Methods Phys. Res. A **565**, 430–438 (2006)
31. H. Tsunemoto, S. Morita, T. Ishikawa, et al., Proton therapy in Japan. Radiat. Res. **104**(Suppl), S235–S243 (1985)
32. J.R. Castro, *Treatment of Cancer with Heavy Charged Particles* (Lawrence Berkeley National Laboratory, LBL-Report PUB-5301, Berkeley, 1991)

Chapter 38
Operational and Training Issues Related to Facility Start-Up

Nancy P. Mendenhall and Zuofeng Li

Abstract Proton and other ion beam centers are few in number, but hold great promise that is driving widespread demand for more facilities. Such facilities are expensive and complex. This chapter discusses special considerations in planning, staffing, and operating a full-scale proton therapy (PT) unit.

38.1 Introduction

38.1.1 Governing Principles

The planning of a PT program should include defining principles to guide facility operations that will be reflected in physical-plant design, equipment selection, staff composition, business models, workflow, and training, then continually monitored, reinforced, and refined by administration during start-up.

Eliminating error is a major focus in medicine; therefore, the first and most important guiding principle for a facility based on new medical technology is *accuracy*. With PT there is less margin for error in treatment planning and delivery than with conventional X-ray-based radiation. With any new technology, the supporting infrastructure will be less robust than more mature technology, so a focus on recognizing potential sources of error at the beginning is critical. Facility design, staffing, and operations should facilitate the attainment of accuracy.

PT facilities also demand a focus on *efficiency*. Biologically, PT is more efficient than X-ray therapy since a greater proportion of deposited energy reaches the targeted cancer. Wasted energy injures normal tissues, leading to side effects

N.P. Mendenhall (✉)
University of Florida Proton Therapy Institute, Department of Radiation Oncology, 2015 North Jefferson Street, Jacksonville, FL 32206, USA
e-mail: menden@shands.ufl.edu

U. Linz (ed.), *Ion Beam Therapy*, Biological and Medical Physics, Biomedical Engineering, DOI 10.1007/978-3-642-21414-1_38,

and complications. The dosimetric efficiency in PT is likely to improve clinical outcomes by both reducing toxicity and increasing disease control, which will increase clinical applications and patient demand. In addition, the high cost of these facilities makes fiscal viability difficult without large-volume patient throughput. So the likelihood of a broad spectrum of clinical applications and fiscal viability requires that facilities be designed for large patient volumes, a broad spectrum of applications, and efficient operations.

The third guiding principle of a new PT facility should be the creation and maintenance of a culture that is both *patient centric* and focused on *quality improvement*. Accuracy and efficiency must be achieved in an environment of compassion and individualized care. Because this technology is relatively new, there is significant opportunity for improvement in technology and operations; therefore, the organizational culture should be permeated at all levels with a focus on continual quality improvement in all aspects of the facility's operation.

38.2 Operational and Training Issues

38.2.1 Program Design

38.2.1.1 The Structure

The physical plant should be designed with the patient and workflow in mind.

Patients will ambulate to many critical functions. Patient ambulation paths should be as short as possible, well lit, and attractive. Specifically, the clinic, simulation area, and treatment rooms need to be within an easy walk from the facility entrance and reception area. Patient bathrooms should be close to the reception and the treatment rooms. Young children may require anesthesia; for operational efficiency, anesthesia should be induced and the patient awakened outside the treatment room, which mandates that anesthesia induction and recovery areas are adjacent to the treatment rooms.

The facility design should support staff efficiency. Although some staff will function primarily in one part of the facility the majority of the time, others need to move efficiently from one activity to the next to facilitate efficiency. For example, physicians may need to be in attendance at simulation, treatment planning, the clinic, and the treatment rooms; optimally these functions will be located in close proximity to each other and to physician offices. Similarly, physicists may be required in treatment planning, simulation, device manufacture, and treatment gantries. These functions should, therefore, be placed together and in proximity to physics offices. Ideally, passageways between activities can be created for staff separate from patient pathways.

Access to conventional radiation therapy equipment is important in facilities providing PT. Many clinical situations may benefit from both protons and conventional radiation therapy and, in the event of PT equipment issues, conventional radiation

therapy can serve as a backup preventing treatment delays that could compromise patient outcomes. Ideally, both photon and proton sources will be situated under the same roof, with common simulation equipment, physicians, physicists, and treatment planning personnel. Important equipment that should be located on site includes computed tomography (CT) simulator(s), positron emission tomography (PET)-CT scanner(s), and magnetic resonance imaging (MRI) for the simulation suite as well as milling machines for fabricating apertures and compensators.

38.2.1.2 Context

PT is but one weapon in the radiation therapy armamentarium, and radiation therapy is but one part of the overall cancer management program. While the business model of a proton facility may stand alone, its function occurs in the broader context of managing cancer patients. It is important, therefore, that the PT facility be sited in a location with access to diagnostic radiology and other critical support services, as well as complementary cancer therapies.

Ideally, PT should be provided amid a spectrum of radiation modalities, such as external-beam photon treatment (including orthovoltage X-rays, electrons, three-dimensional conformal photons, intensity-modulated radiotherapy (IMRT), image-guided radiotherapy (IGRT), stereotactic radiosurgery (SRS), and stereotactic radiotherapy (SGRT)), brachytherapy (interstitial and intracavitary, high dose rate and low dose rate, permanent and temporary), and radioactive isotopes (e.g., iodine-131, phosphorus-32, strontium-89, or yttrium-90). Whether hospital based or free standing, there should be diagnostic and clinical services available for all needed diagnostic and therapeutic interventions associated with optimal delivery of ion beam therapy (IBT). A high-priority population for PT are children, so the facility should be close to pediatric oncology, anesthesia, social, and hospital services.

38.2.1.3 Infrastructure

The infrastructure for an ion beam facility consists of both the electronic information system and the administrative personnel responsible for support of the clinical and technical activities. To create an infrastructure that facilitates efficiency and accuracy as well as the cultural goals of the organization, the workflow process must be understood, the operational impact of variations in the process must be analyzed, and technology must be leveraged to support the process.

Workflow

The limiting resource in a PT facility should be beam time, so its use must be maximized by the workflow process. If there is a single proton source serving multiple treatment rooms, the operations of the treatment rooms are interdependent.

Many technical, medical, and operational factors discussed below impact both the maximum number of treatment rooms that a single ion accelerator can serve and the minimum number of treatment rooms necessary to maximize clinical use of available beam time.

Technical factors. The accelerator, beam delivery, and control-system specifications will affect the time available for beam use. For example, the beam-switching time, which includes deenergizing and reenergizing the magnets along the beam line that directs the particle beam into the treatment rooms, may differ with equipment and power supply impacting clinically useful beam time. Beam-tuning time may vary to meet the required dosimetry specifications of a given treatment plan. The availability of multileaf collimation may reduce time required for applying patient-specific apertures and compensators, thereby increasing room time available for beam use. The time required for the delivery of a given dose with passive versus scanning beam techniques will differ and thus affect the number of patients who can be treated with a given amount of beam time. Digital positioning systems can significantly enhance both accuracy and efficiency in treatment set-ups also enhancing room time available for beam use.

Medical factors. Patient mix and complexity of treatment plans and set up will have a significant impact on throughput and thus optimization of beam-time use. Some tumors and anatomic sites require more complicated treatment plans with multiple, noncoplanar fields and intense quality assurance (QA) procedures; consequently, fewer complicated treatment plans can be delivered in a given time than more simple treatment plans. For example, patients with mobile thoracic tumors may require gating of the beam to a respiratory phase. Respiratory gating necessitates an additional piece of equipment in the treatment room that must be set-up, turned on, and monitored. It requires that the patient be compliant and active rather than passive in the set-up process and results in the use of only part of the available beam for treatment. The impact of beam gating is significant. Additional set-up time is required in the reference treatment room, significant additional beam time for delivery of a given dose, and significant additional beam time not available to other treatment rooms. Other examples of more resource-intense treatments that impact the number of patients that can be treated in a given period include pediatric patients requiring anesthesia and patients requiring multiple daily treatment fractions usually separated by a minimum of 6 h, for the purpose of minimizing damage to normal tissues.

Operational factors. Sequential scheduling of patients whose set-ups are similar and require the same treatment nozzle, devices, and/or beam orientations may reduce room turnover time by minimizing the number of times a nozzle, device, or floor position must be changed. Importantly, optimal staffing will permit concurrent task performance, rather than sequential task performance, minimizing the time the room is not available for beam use.

At the facility level, optimizing beam time means that the patient intake operation, clinical evaluation, and treatment simulation must all be coordinated to generate a steady source of patients to fill all treatment slots created by the beam

time without jeopardizing individual patient care. Some cancer patients can be safely queued; others require expeditious treatment and must be referred to another facility if a treatment slot is not available within an acceptable time.

Limitations to beam sharing include the actual beam-on time for each patient, typically not more than 1 min using passive scattering technique, or several minutes using active scanning technique, for each standard treatment fraction; beam-switching time, during which the beamline magnets are de-energized and re-energized to direct the particle beam from one treatment room to another; and beam tuning, when the beam quality is finely tuned to meet patient treatment dosimetry requirements. The expected patient setup and localization time vs. actual beam-on time must be considered and understood for the intended patient disease mix, such that the optimal number of treatment rooms may be specified.

Impacting Workflow Through the Infrastructure

To leverage technology to support the workflow process, all clinical and technical processes should be detailed, ordered, and mapped to maximize efficiency and accuracy. The infrastructure (human and electronic) necessary to support each process must be identified. The process must be staffed for efficiency. And staff must be trained both in specific tasks as well as the overall workflow process and infrastructure. When all operations depend on a single ion source, there must be close coordination between the clinical, technical, and administrative processes, from initial patient inquiry and intake to the last day of treatment, to ensure maximum use of available treatment slots.

38.2.1.4 Integration and Communication

All available technological solutions for integration and communication should be employed to ensure accurate and real-time information transfer between all operations. Information, when possible, should be transferred digitally rather than manually. For example, a bar-coded name tag for a patient can be read on patient arrival at reception, notifying staff that the patient is present. This bar code can then be used to accurately retrieve treatment plans, select patient-specific treatment devices (i.e., mask, mold, aperture, compensator), deliver patient-specific treatment, as well as accurately track patient progress through the system, providing an excellent source of data for time-management studies.

38.2.2 Operational Issues

38.2.2.1 Phases

In planning a new facility, it is useful to consider the development process in terms of phases during which certain tasks must be accomplished. These tasks can be mapped on a timeline, as in Table 38.1, and monitored.

Preopening Phase

The preopening phase begins after facility construction and at least 1 year before treating the first patient. In this phase, concurrent tasks are completed by technical, clinical, and administrative staff. Equipment is accepted, tested, and commissioned – meaning it will be thoroughly tested to assure reliable performance according to clinical specifications. Clinical protocols are developed – meaning particular treatment regimens are devised for certain cancers. Processes are designed for how patients will be accepted into the system, housed, supported, and billed; how the building and equipment will be maintained; and how quality will be assured.

These tasks may require significant understanding and expertise in the clinical, technical, and administrative aspects of IBT for which local expertise should be developed. Designated members of the clinical, physics, and administrative teams may be chosen at the beginning of the preopening phase for in-depth training at existing facilities. Ideally, these members should be leaders of an institution's existing leadership team so that their experiences with the existing clinical flow may be utilized in developing PT-specific protocols and processes. Additional education and training opportunities exist in the symposiums and educational workshops hosted by professional organizations, including the Particle Therapy Cooperative Group (PTCOG), American Society of Radiation Oncologists (ASTRO), and American Association of Physicists in Medicine (AAPM).

Some tasks will be unique and require customized local solutions. For example, as long as ion facilities are uncommon, patients will be travelers in need of housing, transportation, and social support for up to 3 months. Resources within the institution's community must be identified to handle the itinerant population drawn by the proton facility.

The length of time budgeted for system commissioning and integration should be carefully determined, especially for a single-source, multiple-room facility. Vendors typically complete the system installation and calibration in the order of accelerator first, beam line second, and treatment rooms third, one at a time. There are two approaches to user-acceptance testing and commissioning: waiting for the vendor to deliver all treatment rooms before any user commissioning starts, or starting user commissioning as soon as the first treatment room is delivered.

The first approach allows maximum time available for user commissioning and patient treatment delivery after system acceptance testing, but leaves the largest

Table 38.1 Phases of development for new ion beam facilities

	Phase							
	Planning	Facility construction	Equipment installation	Preopening		Opening	Ramp-up	Capacity
Phase owner	Owners/Board of directors	Facility management, architect, building construction team	Vendor with physics participation	Physics	Clinical, technical, and administrative management teams	Clinical, technical, and administrative management teams	Clinical, technical, and administrative management teams	Clinical, technical, and administrative management teams
Phase tasks	Task force	Coordinated monitoring by architect, building crew, facility management, physicists, and clinicians	All equipment installed	Acceptance testing and commissioning of equipment (verification by in-house team that all equipment functions predictably and to specifications)	Protocol development	Initial activity and process optimization	Additional activities and hours of operation	Optimization and prioritization
	Site selection				Process definition			
	Equipment selection				Process practice			
	Legal issues							
	Building design							
	Financing							
	Governance plan							

time interval between vendor equipment delivery and the first patient treatment. In the second scenario, patient treatments may start as soon as the first treatment room is commissioned while vendor installation and user commissioning continue in the remaining treatment rooms. Patient treatment, vendor installation, and user commissioning activities all require beam time, but beam and software-integration requirements vary and are difficult to combine. It is unlikely these three activities could be performed efficiently concurrently, so, typically, they would be allotted sequential beam time, limiting the hours available for patient treatment.

Each facility must determine whether to adapt one of these two extreme approaches, or design a variation, depending on the number of treatment rooms to be commissioned and the daily working hours allocated to each of the three activities requiring beam time; the relative priorities are start patient treatment deliveries at the earliest time possible with the fastest facility ramp-up possible while maintaining the project schedule.

After equipment has been installed and commissioned, staff have been trained, and all aspects of the program appear ready, a minimum of 2 weeks, but optimally 2 months, is set aside for dry runs, which include treatment planning, device fabrication and testing, and treatment delivery with phantom dosimetry verification. If the institution has decided to begin treating only one clinical site, e.g., prostate, then the shorter 2-week preopening interval may suffice. If more complicated sites will be treated at the opening of the facility, the preopening dry-run time should be extended to allow staff to run through as many phantom cases as possible from start to finish. If the facility is entirely new, as opposed to being attached to a fully functional radiation therapy department, the preopening time required may be longer as all standard equipment will also require integration and testing.

Facility Opening

The second phase is the opening, when the first patient is treated. One popular strategy for facilities planning to treat a large volume and broad mix of patients has been to select a single clinical site of focus at the beginning. This strategy permits physicians, physicists, dosimetrists, therapists, and nurses to focus on the technical aspects and process of one treatment type. As experience grows, procedures and policies are refined. If multiple clinical programs are developed simultaneously, there may be varying strategies that lead to confusion among dosimetrists or therapists and potential errors. Once the first site and process has been mastered, the lessons learned and process developed can be applied to the next site.

Prostate cancer has been a popular first site for three reasons. First, the disease is prevalent, resulting in an abundance of knowledge from conventional radiation therapy that can be applied to IBT. Second, prostate cancer is relatively indolent, permitting patient queueing, an important factor in facility opening and ramp-up when capacity is developing and unpredictable. The third and most important reason, however, is the relatively simple treatment technique, which requires only two lateral or slightly angled fields, standard body immobilization methods, and

standard prostate stabilization devices. In prostate cancer, the issue of organ motion has been well studied and several strategies for dealing with it have been described. Field design and arrangement are partially customized class solutions that can be mastered easily. In contrast to prostate cancer, many of the other high-priority indications for IBT, such as base of skull sarcomas, craniospinal irradiation, lung cancer, and pancreatic cancer, require complicated multiple-field plans, consideration of significant organ motion, avoidance of critical normal tissues, field abutment, and anesthesia. These cancers are less common, making it more difficult to develop expertise, find class solutions, and define processes. As these more complicated sites are added to the repertoire of the facility, each new technique (i.e., field abutment, patched fields), each immobilization device (i.e., the active breathing coordinator (ABC) device, anesthesia, the abdominal compression device), and each alignment strategy (i.e., radiographic fiducial markers, ultrasound, CT alignment, or cameras) will require hours of physicist and physician time in equipment testing, process definition, and verification.

Ramp-Up

The third phase, ramp-up, occur between opening and full capacity. As the facility ramps up, it is critical that each additional staff be thoroughly trained in a systematic way, perhaps with a formal check-off system, in each step in the process.

Ramp-up will be faster and smoother if all steps in the process (i.e., intake, financial review, scheduling, patient support, clinical evaluation, treatment simulation, planning, and delivery) are codified in a written procedure. An important part of the ramp-up is the selection and training of additional staff to support additional treatment rooms and additional hours. Training will also be greatly facilitated and standardized by written procedures and policies. All aberrations in the process, including delays, deviations, and errors, are opportunities to refine the process and strengthen the procedures. All team members must be encouraged to participate in process improvement at all times, but particularly in the ramp-up phase when weaknesses in the initial procedures may be discovered and can be addressed before full-scale operation. It is critical that all knowledge be shared among team members and that adequate time is provided in a nonstressed environment for education and information exchange; thus there should be regular educational sessions focusing on reviewing and developing various processes (e.g., operating a positioning system, a new imaging device); any errors or deviations should be thoroughly analyzed for root cause, and the process revised and reviewed with all members of the team. Ideally, there should be a regularly scheduled forum for training and process improvement issues with required attendance by all team members involved.

Capacity

The final phase is capacity during which maximum use of the rate-limiting operation (in this case beam time) has been achieved, optimization continues, and

prioritization takes place. The hours of clinical operation will be limited due to time allotments for required daily equipment maintenance and patient-specific quality-assurance activities. Capacity (within the clinical hours of operation) is a function of both the number and mix of patients, assuming optimal process and staffing. For example, a pediatric craniospinal irradiation case with five separate treatment fields and anesthesia delivery may require an hour of time in the treatment room, whereas a simple prostate, sarcoma, or head-and-neck treatment necessitating only one or two fields may require only 15 min of room time. General principles for maximum operational efficiency and capacity include moving all activities not necessarily conducted in the treatment room to another room (e.g., patient disrobing, bathroom use, partial patient positioning), minimizing equipment changes (e.g., all patients treated with anesthesia, a particular nozzle, or a set gantry position should be scheduled consecutively), and optimizing staffing. For example, treatment room staffing should be more generous during hours when labor-intensive treatments (e.g., anesthesia, ABC devices, multiple fields, etc.) are being given. All activities should be optimally sequenced, with as many concomitant processes as possible; for example, with three staff members in a treatment room, a nontherapist can escort the patient to the treatment room while apertures are being retrieved by a second person, and a third person is retrieving the treatment plan on the computer, thereby reducing the treatment room time committed to a particular patient to one-third of what it might have been with suboptimal staffing.

38.2.3 Tasks

38.2.3.1 Administrative Tasks

Staffing

In planning the composition and number of staff, it is useful to consider the progressive operational phases since required staffing and composition will vary with progression through these phases.

During the concurrent tasks of preopening – equipment commissioning, policy and procedure development, and staff training – *pro formas* for a new facility should allow key technical, clinical, and administrative staff to be on site to establish accuracy, efficiency, and facility culture before the first patient arrives.

Physicists play a key role in equipment commissioning, managing and supervising equipment operations, treatment planning and delivery, and QA. Key physicists should be on staff during the planning phase to participate in facility design and equipment selection. Some physicists, who will be involved in equipment commissioning and day-to-day activities, should be included at least a year in advance of opening to participate in equipment installation before equipment commissioning. An excellent training strategy for these key physicists is to permit them to participate and help in the installation and commissioning of another

cyclotron or synchrotron, gantry system, or control system before being solely responsible for these activities – this is a 2–3-month labor-intensive process and other facilities may be willing to have extra physicists on hand to help. If any equipment installation and/or user commissioning occurs after the first patient is treated, the physics staffing level must adequately support these nonoverlapping activities. Additional physicists beyond the number required for patient treatment activities (simulation, planning, and delivery) will be necessary to support the many additional installation and commissioning of activities. The addition of physics staff should therefore follow a schedule coincident with the increasing activities and manpower requirements during the preopening, opening, ramp-up, and capacity phases.

Physicians will need to be involved at least part time for approximately a year in advance in the development of clinical protocols. Protocol development requires a functioning treatment planning system dosimetry-practice exercises, protocol writing, submission to the institutional review board (IRB), and protocol training for nursing personnel.

Dosimetrists experienced in all high-technology external-beam treatment planning techniques for complicated tumors, including IMRT and stereotactic treatment planning require at least 3 months of training and practice at an ion beam facility since treatment planning for IBT differs substantially from photon treatment planning. An inexperienced but motivated junior dosimetrist may require 6 months to a year of mentoring to master basic planning techniques.

Therapists with substantial experience will require 3–6 weeks of training; inexperienced therapists may require 6 months of mentorship.

Nurse coordinators will be required during protocol development to aid in creating roadmaps. Ideally, these nurses will serve as care coordinators, maintaining contact with the patient from initial consultation, through treatment planning, during weekly on-treatment evaluations, and in posttreatment surveillance. Whereas this process is not specific to PT, it is critical that at least the nursing director be involved during protocol development and on site at least 3 months before opening to become fully familiar with all aspects of the process including intake, treatment planning, daily flow of patients in the facility, and clinic flow during pre-, post-, and on-treatment evaluations.

The *chief administrative officer*, and ideally key staff such as the medical, physics, therapy and nursing directors, should be involved in facility design during the planning phase; their input into patient and work flow can be critical to facility design. Other staff, such as the facility, billing, and patient-services directors should be brought on 6 months to a year before opening to help develop facility management procedures, relationships with providers, and relationships with potential providers of patient housing and transportation.

Staffing expansion during ramp-up significantly impacts budget performance, the accuracy and efficiency of operations, and the culture of the organization. Flexibility is important as expansion is linked to medical priority, patient demand, staff availability for new program development, and equipment capacity. With a new facility, patient demand in particular tumor sites may not correlate with medical priority or

program development goals. Marketing by administration and educational efforts by staff can help build patient interest and a referral base, but excessive demand may overwhelm the infrastructure or place premature pressure on processes like prioritization. Prioritization of program development must factor in medical gains from PT, research potential, program maturity, operational feasibility, and patient demand. Thus, marketing must be closely coordinated with programmatic maturity, needs, and prioritization.

Maximum performance of new equipment may not be achieved at opening; operator proficiency, equipment adjustments, and optimization of preventative maintenance programs will develop during the ramp-up. Close monitoring of these independent processes is needed to staff optimally during ramp-up until maximum capacity stabilizes.

The American College of Radiology (ACR) has made data available in its Radiation Oncology Accreditation Program Requirements that describe staffing trends and equipment levels for currently accredited conventional radiation oncology practices that are either hospital based, free standing, or academic [1]. These data, which are based on patient volume, can be used as a starting point for planning the staffing capacity. Two important differences exist between conventional and proton facilities. Few conventional facilities in the United States actually operate at equipment capacity; work is generally organized around a single shift of personnel. In contrast, the economics of PT facilities demand that the use of beam time be maximized, so workflow is organized around available beam time and most facilities aim to treat at machine capacity, with potentially over 15 h of daily clinical operation including machine- and patient-specific QA activities. The second difference is that the novelty and complexity of PT operations, treatment planning, and treatment delivery require more staff training and staff numbers than conventional therapy. In general, staffing for specific medical and technical roles should be increased over ACR guidelines by 25–100%, depending on the particular position and the nature of the practice. Table 38.2 includes excerpts from ACR data for conventional radiation oncology practices; included is a column describing current staffing for a contemporary PT facility that is operating at capacity.

Whereas the number of physicians needed for an IBT facility is similar to an academic conventional radiotherapy program, the number of physicists, dosimetrists, and therapists is significantly greater. When technical development is required of the physicists, staffing levels will further increase. Examples of activities that might require additional physicists are developing techniques for evaluating and minimizing the site-specific dosimetric effects of organ motion and other uncertainties, both for passive scattering and for active scanning techniques; implementing and improving simulation, planning, and delivery techniques for new disease sites; developing dosimetry measurement techniques for active scanning beams; and developing a PET-activation program. In Table 38.2, the increase in patients treated per machine at a proton facility compared to a conventional radiation therapy facility is somewhat misleading in that conventional facilities generally operate the equipment for a single shift each day and proton facilities may use the equipment for

Table 38.2 Radiation oncology staffing trends[a]

Staff	All ACR-accredited facilities	AC/MS	H1	H2	H3	F1	F2	F3	PF[b]
New patients/ radiation oncologist	209	127	250	217	161	236	225	144	125
New patients/ physicist	325	166	333	298	294	429	418	309	130
New patients/ FTE dosimetrist	302	337	360	314	160	270	337	201	130
New patients/ FTE therapist	76	63	94	75	76	85	62	67	36
FTE therapist/ Rx machine	3	3.8	3.6	3.2	2.3	3.5	2.2	2.4	5.8
New patients/ Rx machine	236	248	308	233	141	300	260	134	207

Abbreviations: *FTE* full-time equivalent, *Rx* treatment, *ACR* American College of Radiology, *AC* academic, *MS* medical school, *H* hospital-based, *F* free-standing, *P* proton facility, 1*X* new patients per year, 2 facilities with *Y* new patients per year; 3 facilities with *Z* new patients per year

[a]Data in columns 2–9 taken from ACR

[b]Data in column 10 is from the University of Florida Proton Therapy Institute with 15 h of treatment time per day and 3 staggered shifts of personnel

up to two shifts per day. Staffing during preopening, opening, and ramp-up phases will require a higher ratio than needed for an efficient practice at full capacity.

Training

It is likely that most staff will not have had previous work experience at a proton facility. Additional training will, therefore, be necessary. For ongoing daily processes, such as treatment planning, for which space and personnel in already operational facilities are fully committed, it may be difficult to incorporate extra physicists, physicians, dosimetrists, or therapists into the established daily schedule. Therefore, short periods of a week to a month for off-site training, including at workshops or facilities with a dedicated training mission, can be very helpful to gaining insight into the treatment planning strategies and delivery operations used in IBT. Although some of the training can be done off-site, much will have to be done on-site. If the facility is free standing and new, then key technical staff (physicists, dosimetrists, and radiation therapists) must be on staff at least 3–6 months before opening to become familiar with the equipment, develop procedures (i.e., intake, patient services, nursing, dosimetry, therapy, physics, physicians, billing, etc.), and train the remainder of the team at opening and during ramp-up. Because of novel equipment and rapidly evolving technology, regular training sessions for all staff, even those with experience, should be part of the routine operation during its subsequent phases. If the facility is part of a fully staffed extant radiation oncology practice, staff associated with the clinical and technical operations should be on hand well in advance of opening to participate in equipment installation

and commissioning, QA procedure development, clinical protocol development, treatment planning practice, radiation therapy, and dosimetry training.

Many operations with PT are similar or identical to those of conventional radiation therapy, so training strategies will be comparable. The main areas of difference are in equipment QA, operation, and maintenance as well as treatment planning and delivery. It is vital, therefore, that personnel involved in equipment, treatment planning, and treatment delivery have ample time to visit at least one operational facility for thorough on-site training before opening to become familiar with the equipment, treatment planning systems, and QA programs.

Process Definition and Monitoring

As the organization and operation grows and new situations arise, opportunities to deviate from the initially defined processes will increase, potentially resulting in errors. These new situations may occur at the busiest, most intense time of operation or in early or late hours when staffing is minimal. At these times, it is critical that a culture exists where all personnel have access to supervision, feel free to ask questions, and feel empowered to help improve the process by reporting deviations. These new situations or deviations should be viewed as opportunities to improve the operation because they expose weaknesses in processes or the need for training. Once such a concern is raised, the issue must be thoroughly analyzed, the process strengthened, and the event and resulting changes in process communicated to all team members. Occasionally, a deviation may require reporting to a regulatory agency, which may also be helpful in suggesting process revisions. All processes, whether clinical, technical, or administrative, should be periodically reviewed and refined as new information, technology, or circumstances develop.

Intake and Patient Services

Patient access should be available through multiple methods (i.e., phone, e-mail, Internet) and facilitated with sufficient numbers of knowledgeable staff. Training of the intake staff is key; their initial interaction with the patient sets the tone for the rest of the patient experience and they, in essence, serve as partial gatekeepers. Intake is the best place to screen patients for basic eligibility for protocols; this activity need not necessarily involve professional staff if intake staff is adequately trained in the basics of the disease processes, and protocols have been developed and prioritized with clear eligibility requirements. It is important at this step that potential patients be given realistic expectations. Ideally, most patients accepted through the intake process will be appropriate candidates for PT, making for the most efficient use of nursing, physician, and clinic time. Along with direct patient access to the intake process, physicians from each area of interest in PT should be available to discuss potential cases with referring physicians. In facilities operating at capacity, prioritization will be necessary, so a weekly conference involving key members

of the team can help assure the best use of treatment slots; at such conferences, various types of information may be considered, such as open protocols, individual imaging studies, and resource utilization. In most cancer cases, it is important to avoid treatment delay, so efforts to identify and address barriers to treatment should begin immediately and alternative treatments be identified if necessary. During the medical suitability assessment, an insurance coverage review can occur so that any potential coverage issues can be determined and addressed proactively before the patient arrives for a consultation.

38.2.3.2 Technical Tasks

Equipment Commissioning

When preparing this manuscript, there were no existing guidelines for the acceptance testing and commissioning of IBT systems. This is in part due to the rapidly progressing status of ion beam technologies. The facility physics team responsible for this task must therefore obtain an in-depth understanding and knowledge of the system to be installed and develop a commissioning plan at the earliest possible time, with clearly defined endpoints and timelines. It is possible that equipment will be prototypes or second generation requiring extensive commissioning to ensure reliable clinical performance. Equipment commissioning will take up to 3 months per machine with appropriate staff (2–4 physicists' FTEs per piece of equipment). The more personnel trained and available for commissioning, the less time it will take, but regardless of skill and number of staff, it is unlikely that commissioning time could be reduced below 3 months given the myriad functions requiring verification. Critical pieces of equipment requiring commissioning include the accelerator, the treatment delivery system (gantry or fixed beam), its associated patient localization and support systems, the simulation equipment (CT, PET-CT, MRI, immobilization devices), the treatment planning system, the treatment control system, the treatment accessory fabrication system, and the facility management system. Less than comprehensive commissioning could lead to a disastrous systematic error, so this phase must be neither rushed nor understaffed. If there is new conventional radiation equipment, such as linear accelerators, they too will require commissioning.

Technical Process Development

There are a number of steps in the process of treatment delivery – identifying the patient, retrieving the patient treatment prescription and plan, requesting the appropriate ion beam (range), positioning the patient with the appropriate patient-specific immobilization devices and set-up parameters, retrieving and positioning appropriate patient-specific dose distribution modifiers such as apertures and compensators, delivering the beam for the appropriate exposure time, etc. Accuracy

and efficiency can best be achieved if the steps are ordered optimally, codified in a process that requires conscious check-offs, accomplished and documented electronically in real time.

Every effort should be made to assure the timely execution and completion of each of the tasks in the entire patient management process without sacrificing accuracy to assure maximum use of available beam time. Completing a task after its designated timeline will either cause a delay in the start of treatment or create a rushed effort to make the timeline, thereby increasing the risk of errors. In addition, many patients may have traveled a long distance to seek the benefit of this technology and delays can have an added impact on costs of relocation, lost work time, etc. Facility management systems or other in-house clinical flow management systems can assure the most accurate and efficient data flow and facilitate a task assignment and completion check-off list for all steps in the process, including the diagnostic workup, simulation, planning, QA testing, and treatment delivery for each patient. A certain degree of accuracy can be assured if all variables (treatment plan, immobilization device, apertures, compensators, etc) are labeled with the patient bar codes. Each step should be checked by two people to improve accuracy. A time-out process should be applied during each treatment session so that every parameter of every treatment field is reviewed by two therapists independently. In the treatment planning process, the use of detailed protocols with specific doses specified in standard ways and specific normal-tissue constraints will maximize efficiency and minimize the chance of an ill-advised treatment planning decision. Therefore, clinical protocols should include specific guidelines for both target coverage and normal-tissue avoidance for use by the dosimetrists in treatment planning.

Technical QA

Technical QA requires daily equipment monitoring and preventative maintenance by engineering staff, and daily machine QA tests by physicists. No standards of practice exist for periodic ion beam QA activities, so the physics team is responsible for developing such a QA program, and for continually improving it based on reviews of QA results and a better understanding of the system. A facility will probably develop an initial periodic QA program that includes many extensive, in-depth daily tests supplemented by additional weekly, monthly, and annual tests (cf. Chap. 28 for details). As the physics team gains more experience and greater confidence with how the system functions, the periodic QA program will need to be reviewed and revised appropriately. For example, the number and comprehensiveness of daily QA tests may be reduced and transferred to less frequent weekly and monthly QA tests to allow more daily treatment delivery hours. On the other hand, tests for detecting system failures that occur more often than expected, or failures that would negatively impact the accuracy of treatment delivery, may need to be performed more frequently. In addition, patient-specific treatment plan verification with phantoms, output measurements, and checks of patient-specific apertures and

compensators may also require daily beam time, and must be appropriately budgeted for in facility capacity estimates. Lastly, implementing new techniques after the facility has reached capacity will require reallocation of beam time for clinical use.

38.2.3.3 Clinical Tasks

Clinical Protocol Development

At least a year in advance of opening, medical staff will consider which sites to treat, in what order the programs will be started, and what criteria will be used for prioritizing treatments when capacity is reached. Specific protocols should be developed that include pretreatment selection criteria, required evaluation, treatment details, and surveillance requirements. Ideally, these protocols should be submitted for IRB approval, a process that may take as little as a few weeks or as much as 6 months depending on the complexity of the protocol and the efficiency of the IRB. In addition to preparing the protocols, development work with physicists and dosimetrists will be needed to determine the best treatment simulation process and treatment planning solutions, and with nursing for clinical assessment needs during and after treatment.

Nursing Coordination

Navigating the entire treatment process from intake, to clinical evaluation, to treatment planning, to treatment and posttreatment surveillance can be difficult. Regardless of the strategy, someone needs to shepherd and coordinate all activities for the patient. One option is a nurse coordinator. This person will be involved in evaluating the patient for protocol eligibility, know the management roadmap, see the patient for on-treatment visits, and be responsible for arranging posttreatment surveillance and care. Under the best-case scenario, this nurse coordinator will be involved at an early stage with protocol development and be responsible for accruing clinical research information during the course of treatment and follow-up care. The nurse coordinator will be the main contact for the patient after consultation as well as throughout and after treatment.

Clinical QA

Although every clinical situation is unique and each treatment plan must be customized, it is important that the team provides oversight for individual treatment decisions and plans. Therefore, every patient's case should be reviewed in a QA conference to verify the appropriate treatment recommendation and optimal treatment plan. One popular strategy is the weekly chart review in which all new cases are discussed using clinical information, pertinent imaging, and treatment

plans. Any deviations from treatment plan protocol guidelines can be explained and discussed among the team. In addition, a periodic conference to review outcomes is important to identify what is and what is not working, where improvements might be made. This can take the form of an adverse events conference and a clinical research forum in which outcomes are reported. These regular meetings communicate to all clinical personnel important information for future protocol development and specific patient surveillance.

38.3 Conclusion

The expense and complexity of PT facilities require planning, creative modeling, efficient operation with flexible staffing, specialized staff training, and enhanced coordination over and above what is necessary in traditional conventional radiation therapy facilities. Although much can be learned from the early experiences in PT, each IBT facility will have unique challenges requiring customized solutions.

Reference

1. American College of Radiology. *Radiation Oncology Accreditation Program Requirements*. http://www.acr.org/accreditation/radiation/requirements.aspx. Accessed 29 Sept 2010

Part IX
Future Developments

Chapter 39
The Single-Room Ion Beam Facility

Kenneth P. Gall

Abstract Proposals to develop compact, less-costly systems have been made for many years. A single-room system that has been developed by the Still River Systems corporation has shown comparable treatment capabilities to currently available multiroom systems. A detailed description of that system is given as an example of a single-room IBT solution.

39.1 Introduction

Since its inception, external beam radiation therapy (RT) has usually been carried out by a single practitioner on a single patient using a single radiation source. With the development of the X-ray tube and extension of X-ray energies into the orthovoltage range, the one-source/one-patient model was continued for the Co-60 therapy systems developed in the post-WWII era. To this day, conventional RT is still practiced in this manner with electron linear accelerator (linac) systems. The standard treatment facility has one radiation source within a single radiation-shielded vault and is typically run by radiation therapists or radiographers who assist and position the patients and initiate the irradiations. The history of the efforts to cure human disease with these radiation sources are well covered in the literature [1].

Ion beam therapy (IBT) evolved somewhat differently from conventional gamma- and X-ray-based RT. In the early years of IBT, patients were brought to high-energy particle accelerator facilities that were initially set up as physics research institutions. These facilities were naturally arranged with multiple beam lines to accommodate a number of experiments or, later, patient treatment rooms.

K.P. Gall (✉)
Still River Systems, 300 Foster Street, Littleton, MA 01460, USA
e-mail: kgall@stillriversystems.com

U. Linz (ed.), *Ion Beam Therapy*, Biological and Medical Physics, Biomedical Engineering, DOI 10.1007/978-3-642-21414-1_39,

The natural reasons for this architecture are obvious from a purely financial perspective. The high-energy accelerators were vastly more expensive than the cost of bend magnets that could switch the beam path into many different branches. Experimental physicists as well as radiation oncologists found that there was often more time taken to set-up at the end of the beam line than it took to take data or treat a patient. As IBT accelerator systems were developed specifically for patient treatments, the relative operational inefficiencies of treating patients sequentially only as the therapy beam was available or concurrent failure of the entire facility due to an accelerator failure were still considered small operational costs compared to the cost of another high-energy particle accelerator.

It remains clear, however, that if the cost of a single-room system could be brought down enough in comparison to comparable multiport systems, the preference would likely be the single-room solution. The question of what cost reduction is sufficient to meet this condition is perhaps not simple to answer. The tabulation of costs really must include not only the initial price of the treatment equipment but also the price of the facility (including the financing costs associated with longer construction times for larger facilities), the ongoing operating costs including utilities and personnel, the maintenance costs, and the less-tangible costs associated with those previously mentioned operational efficiencies of system redundancy and availability. There might also be trade-offs of technical specification versus cost, for which a correlation coefficient could be difficult to find consensus on.

For the purpose of this chapter, we assume the goal of a single-room treatment solution, which maintains a comparable ability to treat patients as the available multiroom systems. The development of a one-room IBT facility can be viewed as a simple problem of making a system with a low-enough cost averaged over the lifetime of the equipment and facility.

39.2 Proton Therapy System Cost

The cost to produce a proton therapy (PT) system is usually dominated by the cost to produce the particle accelerator itself. Housing a large accelerator also requires a large radiation-shielded vault. So in the effort to reduce system cost, it is reasonable to first look at how one can reduce the size, and, therefore, cost of the proton accelerator. In having reduced the size, the complexity must not be increased so much that it offsets the cost advantages of smaller size.

For circular accelerators (cyclotrons and synchrotrons), the only meaningful way of reducing their size is to increase the magnetic field used to define the bend radius of the beam during acceleration. For linacs, one must increase the acceleration gradient. Both of these approaches have been proposed. In most cases, the proposals are extrapolations of existing accelerator architectures [2, 3], whereas others are for more novel approaches to increase the electromagnetic field strength [4].

Viable solutions for low-cost PT accelerators have been slow to emerge, which ultimately has led to the predominance of the multiple-room facilities being built

Table 39.1 Peak magnetic field of various PT facilities

Facility	Beginning of operation	Magnetic field (T)
Harvard Cyclotron Laboratory (HCL)	1961	1.6
Loma Linda University Medical Center (LLUMC)	1990	1.8
Massachusetts General Hospital (MGH)	2000	2.4
Paul-Scherrer Institute (PSI)	2006	4.5

up to this day. However, this trend toward higher magnetic and electric fields is apparent as accelerator technologies advance. For instance, peak magnetic fields of the proton accelerators used for therapy have trended higher as shown in Table 39.1.

Proposals for novel linacs with acceleration gradients of 100 MV/m are currently being explored [4] and single-room treatment systems are proposed for their use.

39.3 An Example of a PT System that Reduces Size and Complexity

Early in 2004, a private company, Still River Systems, was founded with the plan to develop a single-room PT system based on the designs of the author. This is likely to be the first compact IBT device to treat patients that is purpose built as a single-room facility. Installation at the first clinical site is due to be complete in 2011. The remainder of the chapter describes the details of this system.

The primary requirements for the system were

1. To provide proton beams with sufficient energy, intensity, and geometric properties (angle of approach and lateral extent) so that they could be used for the vast majority of patients considered for treatment and
2. To reduce system cost through size and complexity reduction

Requirement 1 led to the more specific requirements for the treatment beam properties:

Maximum depth of penetration: 32 cm in water
Maximum field size: $20 \times 20\,\text{cm}^2$ up to a depth of 25 cm in water; $10 \times 10\,\text{cm}^2$ to full depth of penetration
Dose rate: 2 Gy/min (minimum), 4 Gy/min (preferred)

The essential elements of the initial conceptual design:

- A superconducting (SC) synchrocyclotron would provide the proton source, as this accelerator type is more readily translated to higher magnetic fields than other circular accelerator architectures.

- The synchrocyclotron would be mounted to a gantry so that the beam coming out of the accelerator would be directed straight toward the patient, eliminating the need for a beam transport line.
- The cyclotron gantry would rotate by 180°, from beam straight up to beam straight down.
- A treatment floor would be cantilevered past isocenter to allow for full access to the patient with just a small slot left open in the floor where the beam could penetrate.
- A patient-positioning couch would be capable of rotating over 270° in this space, allowing for all beam-entry points of interest in RT to be delivered.

The proposed design has other attendant advantages:

- Because the forward direction of the beam is limited to a 180° arc, radiation-shielding volume could be drastically reduced when the vault is sited underground and especially when three of the walls are bordered by earth. This reduces facility construction costs.
- The room layout allows for all support equipment (control racks, power supplies, etc.) to be located within the vault itself, reducing facility footprint and further reducing facility cost.
- Conventional control systems can be used with no more complexity than conventional RT linac system controls, increasing reliability and reducing developmental testing time.
- The control system simplicity allows for conventional clinical workflow, with radiation therapists or radiographers entirely running the operation of the system. The reduction in personnel needed to run the system further reduces operating costs.

In order to make the smallest possible cyclotron, a relatively old, yet reliable cyclotron architecture was used. Synchrocyclotrons achieve acceleration of charged particles to relativistic energies by gradually changing the driving RF frequency rather than increasing the magnetic field with radius as is done in isochronous cyclotrons. The magnet for a synchrocyclotron can be much simpler than for other cyclotron designs since axial focusing can be achieved with an azimuthally uniform magnetic field. An additional benefit of the synchrocyclotron architecture is the relative robust nature of operation [5].

The final design of the system resulted in an SC synchrocyclotron operating at a peak magnetic field in excess of 10 T.

Specifications for the cyclotron system include:

Beam energy >250 MeV.
Extracted beam current >10 nA.
Beam spot size at extraction channel exit <0.5 cm FWHM.
External radiation leakage <0.1% of proton dose rate at isocenter.

39.4 System Description

The Still River PT system is shown in Fig. 39.1. The view shows the vault walls cut away and the treatment room enclosure removed at the top.

The cyclotron is housed at the middle of a cylindrical *accelerator module* that is supported by two gantry arms. The gantry arms rotate about bearings mounted into the side walls of the vault and hold the counterweights for the accelerator.

Figure 39.2 shows the view of the treatment space with all the enclosures in place. As can be appreciated from this view, the treatment room takes advantage of the floor surrounding isocenter to provide for a comfortable clinical setting.

The outer cyclotron gantry moves separately from the inner *treatment gantry*. The treatment gantry carries the final collimation and range compensation elements as well as the field light and transmission ionization chambers that monitor dose.

The field-shaping system (not shown) is mounted to the accelerator module. It forms treatment beams from the cyclotron's pencil beam following the design principles developed by Gottschalk [6] and commonly referred to as double scattering. The field-shaping system can readily be swapped out for beam-scanning magnets

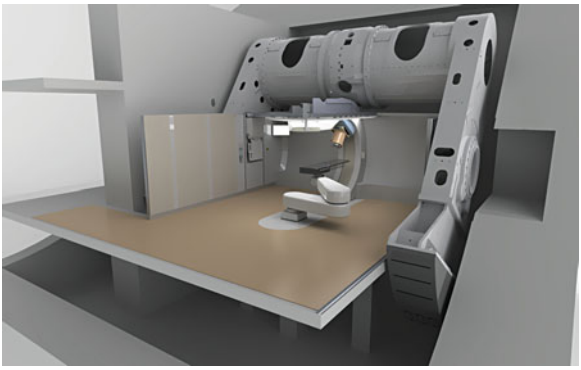

Fig. 39.1 The Still River PT system shown with vault and treatment room enclosure cut away

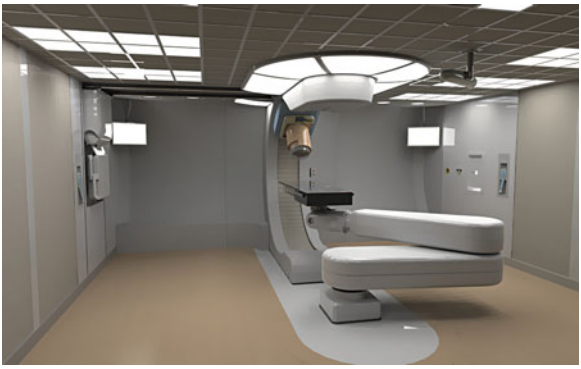

Fig. 39.2 The Still River PT system treatment room

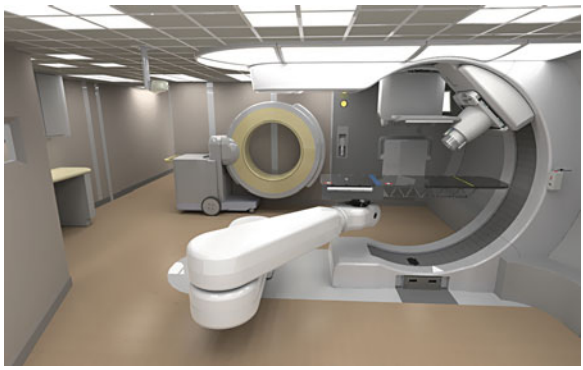

Fig. 39.3 The Still River PT system treatment room showing planar radiographic receptors deployed at isocenter and the cone beam CT (CBCT) scanner in its storage location (*center backdrop of the image*)

to implement intensity-modulated proton therapy (IMPT) with a scanned beam. The final collimation system holds conventional aperture and range-compensating boluses for individual RT field dose tailoring. The applicator can equally well be swapped out for a multileaf collimator for automated field blocking or implementation of IMPT, as discussed below.

Within the treatment room, there is a robotic couch that offers 6 degrees of freedom (DoF). The couch is capable of submillimeter positioning precision throughout the usable work space of ±135° of couch rotation, ±5° of couch pitch and roll and ±25 cm lateral, ±47.5 cm longitudinal, +10/−39 cm vertical translation moves.

Figure 39.3 shows the treatment room with the radiographic imaging systems. Planar X-ray receptors are provided and positioned for lateral and posterior–anterior (PA) radiographic views of a supine patient at isocenter. These retract to the side wall when not in use. Figure 39.3 also illustrates the cone beam CT (CBCT) scanner that can be deployed at or near isocenter for full 3D soft-tissue imaging. The position of the CBCT within the room is determined with a stereoscopic camera and correlated to the treatment coordinate system. A patient positioning algorithm running on a dedicated computer uses the captured planar or CT radiographic images and compares them to the planning CT to compute rotational and translational corrections to the patient position for treatment. These corrections are transmitted to the couch controller.

39.5 Dosimetric Properties

The Still River PT system provides a therapy beam with dosimetric properties comparable to other commercially available systems. Figure 39.4 shows the raw Bragg peak and a spread-out Bragg peak (SOBP) from the system. Figure 39.5 depicts a series of lateral profiles taken through the proximal, middle, and distal portion of a 10 cm SOBP.

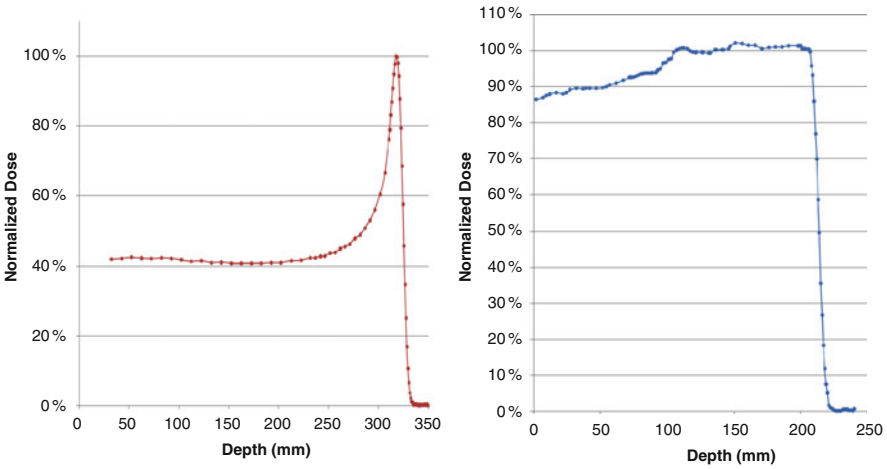

Fig. 39.4 Bragg peak and SOBP

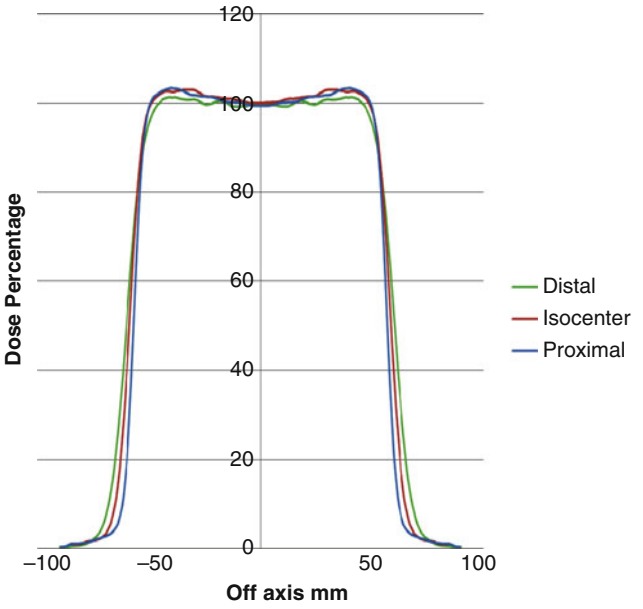

Fig. 39.5 Lateral profiles through distal, middle, and proximal portions of a 10 cm SOBP

39.6 Facility

A great deal of time and cost can be consumed in the planning and building of the "bricks and mortar" facility surrounding IBT equipment. Service utilities for electric power, chilled water, heating, ventilation, and air conditioning (HVAC) can

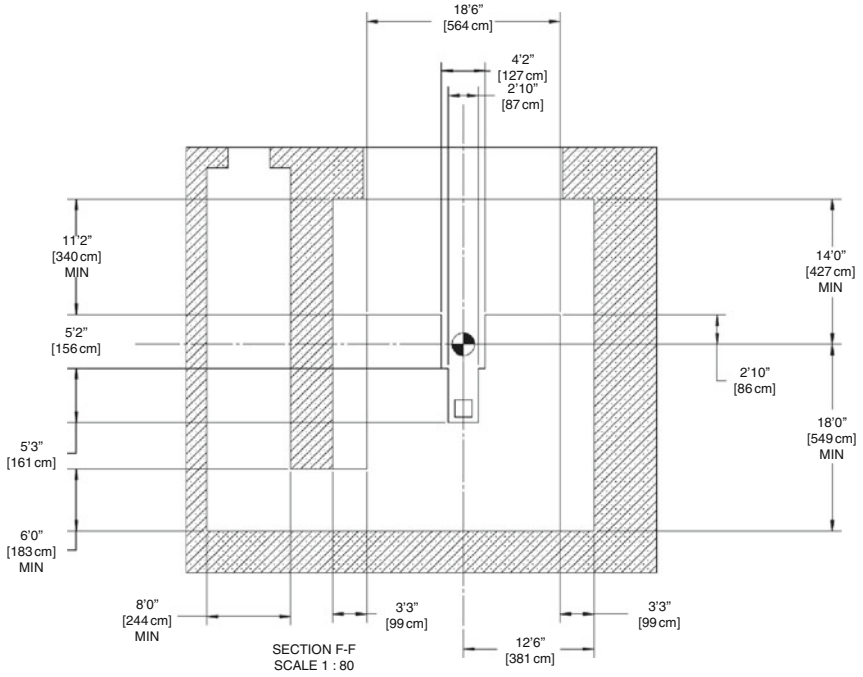

Fig. 39.6 The Still River PT system standard vault plan view. *At the left* is the entrance maze. The wall at the *top of the view* shows an access way which is blocked in following accelerator module installation

become expensive if they are unusually large. The bulk of an RT facility is taken up in radiation shielding, which is most often provided for with thick concrete walls.

The single-room system described here also facilitates the reduced cost of the treatment facility around it. Total electric power requirements are reduced through the use of the SC magnet and comparatively low power is required for the radiofrequency (RF) system in a synchrocyclotron. The chiller plant for cooling is not unusually large given the low energy dissipation of the low-power RF.

As described above, the radiation-shielding volume is reduced in comparison to other systems since the inner dimensions of the vault are smaller and the radiation beam forward direction is limited to an arc of 180°. Neutron dose rate and attenuation lengths are highest in the direction of the incident proton beam.

A horizontal section of the standard vault plan layout is presented in Fig. 39.6, and a vertical section in Fig. 39.7.

The treatment level provides space for the patient positioning couch as well as plane view X-ray panels, a CBCT scanner, and imaging workstations behind an X-ray shielded partition (not shown).

The lower level of the vault provides room for system control electronics, RF power systems, imaging system X-ray generator, couch controller, and magnet cooling. The upper levels of the vault provide access way for system and facility wiring and HVAC.

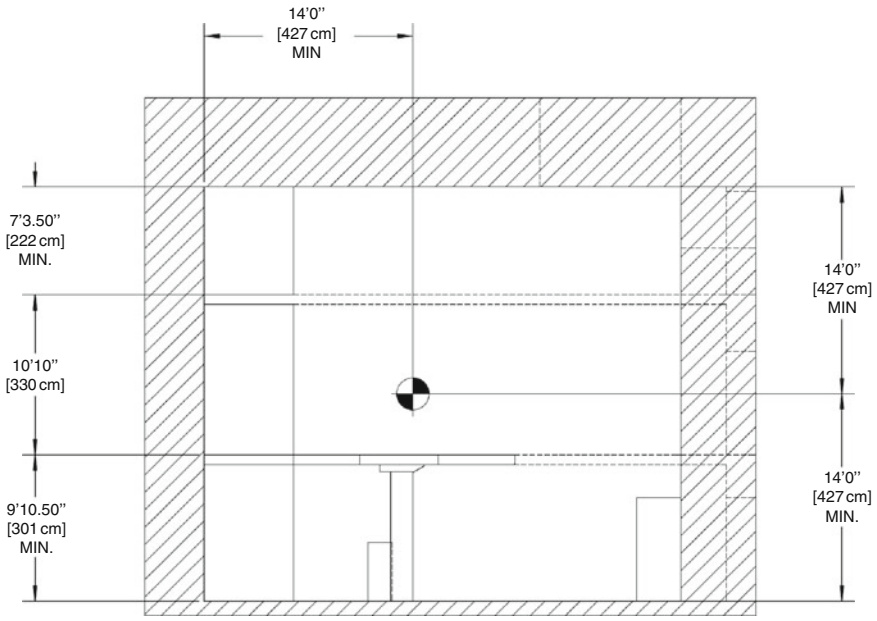

Fig. 39.7 The Still River PT system standard vault vertical section

Since the vertical height of the vault is dictated by the outer radius of the accelerator swing, the upper, and lower levels of the maze are already preset. Taking advantage of this space for equipment location thus reduces the need for additional facility footprint if, for instance, an equipment room were designed next to the vault.

The inner dimensions of the vault are approximately 7.6 m wide, 9.8 m deep, and 8.5 m high. An entrance maze 2.4 m wide provides significant attenuation of neutron flux, thus reducing the door thickness.

With an outer footprint, including nominal shield wall thickness, of approximately $13.5 \times 13.5\,m^2$, the vault can be readily incorporated into a conventional RT department layout as another treatment room alongside the electron linac vaults.

39.7 Challenges

Certain design challenges arose during system design that are specific to the single-room solution. For the system described here, these challenges were:

Reduction of stray magnetic field.
Meet stray radiation (head leakage) constraints.
Provide compatibility with IMPT.

Each of these challenges were met and are described below.

39.7.1 Stray Magnetic Field

In order to be widely accepted as a treatment system available to all RT practitioners, the unit had to accommodate typical clinical work flow. So, stray magnetic fields should not be so large in the treatment area that forces on ferromagnetic objects became problematic. At magnetic field levels less than 0.01 T, there are typically no concerns for forces on ferromagnetic objects, although personnel would still need to be screened for potential pacemaker interference. Careful magnetic design of the cyclotron steel yoke and surrounding magnetic shield confirmed that fields in excess of 10^{-2} T could be kept to within centimeters of the accelerator housing. This, however, did come at the cost of significant weight increase of the accelerator module. Measurements confirm that the stray magnetic field at isocenter is less than 5×10^{-4} T; a value below which personnel need not be screened before being exposed and all areas within the treatment room are below the limit of 10^{-2} T.

39.7.2 Head Leakage

The radiation leakage from the accelerator itself must meet regulatory requirements. These requirements are defined for conventional electron accelerators, for instance by the IEC (International Electrotechnical Commission), as the average dose rate at 2 m from the treatment beam axis in the plane of isocenter being below 0.1% of the treatment dose rate [7]. Here too, a careful analysis of beam efficiency and local shielding of areas of anticipated beam loss show head leakage requirements are easily met. Indeed, as has been reported by a large number of authors, the total secondary radiation burden for patients undergoing PT is dominated by the reduction in the volume irradiated by the primary beam. When the regulatory head-leakage requirements are met for a PT system, the result is a treatment system that vastly reduces doses to healthy tissues in the patient in comparison to conventional high-energy X-ray systems.

Measurements on the first Still River PT system irradiating a water phantom with a $10 \times 10\,\text{cm}^2$ proton field with a SOBP of 10 cm and a maximum penetration depth of 32 cm show less than 0.1% of treatment dose equivalent at a distance of 1 m from the beam axis. This is better than the IEC standard for conventional RT systems.

39.7.3 Compatibility with IMPT

IMPT can be delivered in a fashion analogous to the predominant mode of delivering X-ray IMRT, namely with multileaf collimators (MLC). Various methods for variable collimation were proposed as early as 1989 [8] and have been used for patient treatments with ion beams [9].

A concern cited by a variety of authors is an increased secondary neutron dose imparted to the patient when an MLC is used to stop a portion of the beam. In X-ray IMRT, it is commonplace to deliver many more machine monitor units per unit target dose than would be done with open-beam techniques for 3D treatment. With IMPT, it is possible to keep the machine monitor units exactly the same and only stop the beam corresponding to various depths in an MLC. This should result in an overall reduction in secondary dose to the patient since the source of neutrons is removed from the patient to the MLC.

Providing for compatibility with an MLC for IMPT in a single-room system is straightforward. A portion of the beam-shaping applicator is replaced with the MLC. The design, manufacture, and clinical use of MLCs is now a mature technology, and the widespread adaptation of MLCs to IBT systems is expected.

Many IBT practitioners insist that the ultimate dose distribution is obtained with the use of scanned beams (cf. [10], and Chaps. 24 and 25). Compatibility with scan beam techniques for the single-room system requires that an adequately sized beam spot can be delivered with sufficient efficiency at the penetration depths required for the vast majority of treatments. The nominal distance from the cyclotron exit port to isocenter is over 2 m in the system described here. This is adequate space for incorporation of bend magnets and energy degraders to achieve similar field size specifications as those delivered with scattering techniques.

The pulsed time structure of the beam extracted from a synchrocyclotron can be used in a spot-scanning system quite readily. The pulse rate of the Still River PT system is approximately 500 Hz and is readily increased to 1,000 Hz. With sufficiently fast lateral and depth beam position changes, over 60,000 individual beam spots can be painted in a given treatment volume in a 1-min treatment. This should allow for multiple *repaintings* of the field for the majority of treatments, a key parameter for minimizing the influence of physiological motion perturbations on the dose distribution.

It is worthwhile to note that the final word on what constitutes an optimized IMPT system may not yet have been heard. In reality, what the radiotherapist would like to maximize is the rate of increased quality years of extended patient life. Complex treatment techniques that are prone to higher rates of treatment errors may not win out over more robust techniques. Nor is it clear whether highly sophisticated techniques can be uniformly established as quickly over as widespread a base of facilities. It is likely that these less tangible but nonetheless important factors will play a part in determining which IMPT techniques ultimately proliferate on single-room systems.

39.8 Outlook

As of this writing, over one dozen RT treatment providers have signed contracts for the single-room PT system described in this chapter and interest is growing throughout the RT community for compact single-room PT capabilities. The author

is aware of several other single-room system proposals and commercial developments (cf. also Chap. 23). As accelerator costs are reduced further through system refinement, and perhaps additional size reduction, it is possible that the single-room solution for providing IBT will become the norm.

References

1. L. Gandt, J.L. Dodson, *A Century of Oncology* (Greenwich Press, Greenwich, CT, 1997)
2. H. Blosser, Compact superconducting synchrocyclotron systems for proton therapy. Nucl. Instrum. Methods **B40/41**, 1326–1330 (1989)
3. L. Picardi, C. Ronsivalle, A. Vignati, et al, Preliminary design of a very compact proto-synchrotron for proton therapy, in Proceedings of European Particle Accelerator Conference (EPAC), London, UK, 27 Jun–1 Jul 1994, pp. 2607–9. http://cdsweb.cern.ch/record/922490/?ln=cs. Accessed 10 Jan 2011
4. G.J. Caporaso, T.R. Mackie, S. Sampayan, et al., A compact linac for proton therapy based on a dielectric wall accelerator, Presented at 1st European Conference on Medical Physics, Pisa, Italy 20–22 Sept 2007
5. J.R. Richardson, A short anecdotal history of cyclotrons, in *Proceedings of the 10th International Conference on Cyclotrons and Their Applications*, 1984, ed. by F. Marti, East Lansing, MI, 30 Apr–3 May (IEEE, New York, 1984)
6. B. Gottschalk, *Passive Beam Spreading in Proton Radiation Therapy*. Draft Oct. 2004. http://physics.harvard.edu/$\sim$gottschalk/. Accessed 11 Jan 2011
7. International Electrotechnical Commission, *Medical electrical equipment* – Part 2–1: Particular requirements for the safety of electron accelerators in the range of 1 MeV to 50 MeV. IEC 60601–2–1, Edition: 2.0, (IEC, Geneva, 1998)
8. M.M. Urie, M. Goitein, Variable versus fixed modulation of proton beams for treatments in the cranium. Med. Phys. **16**, 593–601 (1989)
9. Futami Y, Kanai T, Fujita M, et al. Broad-beam three-dimensional irradiation system for heavy-ion radiotherapy at HIMAC. Nucl. Instrum. Methods Phys. Res. A, **430**, 143–153 (1999)
10. Schippers JM. Beam delivery systems for particle radiation therapy. Rev. Accel. Sci. Technol. **2**, 183–198 (2009)

Chapter 40
Smaller – Lighter – Cheaper: New Technological Concepts in Proton Therapy

John Cameron and Niek Schreuder

Abstract The demand for proton beam cancer treatment is on the rise worldwide. The only way to make proton therapy (PT) available to more patients is to develop smaller and less expensive PT systems. The challenge is to accomplish this without compromising their efficacy.

40.1 Introduction

The demand for proton beam cancer treatment is on the rise worldwide. Because most cancer patients are treated in community and private practice settings, the only way to make PT available to more patients is to develop smaller and less expensive PT systems. Our challenge has been to accomplish this without compromising the efficacy of the PT systems. In this chapter, we examine the processes and pitfalls of such cost reduction designs. Herein, we delineate the minimum requirements for less expensive systems and show how these requirements continue to drive our design and implementation efforts.

In our opinion, a lack of support from the radiation therapy (RT) community itself is what has inhibited development of PT most over the past 50 years. Only a handful of companies worldwide were able to obtain contracts to provide systems for PT. In addition, there was a demand that every new system had to be "better" than the previous one that together with a lack of cohesive clinical specifications led users to ask for vastly different features. The resulting global paucity of proton centers and a lack of well-directed clinical research to prove efficacy did not provide the financial motivation to further develop PT technology.

J. Cameron (✉)
ProCure Treatment Centers, 420 N Walnut Street, Bloomington, IN 47404, USA
e-mail: john.cameron@procure.com

U. Linz (ed.), *Ion Beam Therapy*, Biological and Medical Physics, Biomedical Engineering, DOI 10.1007/978-3-642-21414-1_40,

40.2 PT Technology Circa 2010

Proton equipment available today has the following typical specifications (cf. previous chapters for details):

(a) 230–250 MeV accelerators to provide a reliable proton beam.
(b) Particle accelerators of two types: cyclotrons and synchrotrons.
(c) Fast energy variation systems capable of changing the energy of the beam by 10% in less than 2 s.
(d) Evacuated beam transport systems using multiple magnets to switch the beam into each of the treatment rooms. Typical beam switching times using such systems varies between 10 and 120 s.
(e) Fixed beam rooms with beams projected horizontally, and/or inclined at 60° to the horizontal.
(f) Gantry treatment rooms with a large rotating gantry that delivers the beam from 0° to 360°.
(g) Therapy control systems that provide the interface to drive and monitor the PT equipment.
(h) Therapy safety systems to monitor multiple safety concerns for the patient and clinical personnel.

Until recently, all of the centers that were developed according to the above-mentioned specifications were primarily built in conjunction with large academic medical research centers. The costs to construct these facilities became almost prohibitive and the overall complexity and project coordination was daunting for any institution. In addition, few people in the world had any experience using PT.

It has become clear that the field of PT would not progress much faster in this manner. Furthermore, the systems being produced would not keep up with technological advances occurring in standard X-ray RT.

In the past decade, dramatic changes have started to occur in many aspects of the PT treatment rooms. Double foil passive scattering systems, historically used to get large (up to 30 cm diameter) uniform fields, have been replaced by systems that use active beam scanning to achieve the desired treatment field [1]. Elimination of the need for the scattering foils and the resulting interactions of many of the scattered protons with collimators and other material close to the patient significantly reduce the undesirable whole body neutron dose to the patient [2, 3]. Following pioneering work done in Switzerland, the use of spot beam scanning is now included in the specifications for all new facilities [4, 5].

Patient positioning for proton treatment most often has been achieved by placing the patient on a flat bed affixed to a positioning mechanism to move the bed along any of three axes. Position verification is obtained using orthogonal X-ray films. For PT, this has provided an early form of image-guided radiation therapy (IGRT). New positioning systems allow for more accurate control of position around six axes by attaching the bed to a robotic positioning device (cf. [6] and Chap. 33).

An individual room in a typical four-room facility should be able to deliver about 10,000 fractions per year. Detailed modeling, using attributes from queuing theory

to evaluate probable patient waiting times, shows that four rooms is the optimal number that can be serviced with one accelerator when treatment times average from 15 to 30 min (M. Leuschner, ProCure Treatment Centers, INC, Personal Communication).

More efficient methods are being explored in which patients are set up and positioned outside of the treatment room, and then transported into the room ready for treatment. These methods can further reduce the average time per patient in the treatment room below 20 min. With this methodology, the optimal number of rooms per facility may actually decrease to three for each accelerator.

From these calculations, to achieve full system availability of over 96%, the beam delivery system must maintain an uptime approaching 98%, 18 h per day, 250 days per year for many years. This, in turn, implies simplicity and, hopefully, a long record of successful operation. The typical overall clinical specifications for a PT beam delivery system of this type would be:

- Range at nozzle exit of $32 \pm 0.15\,\mathrm{g/cm^2}$
- Range modulationsteps of $0.5\,\mathrm{g/cm^2}$ or less over full depth
- Range that can be adjusted continuously between 4 and $32 \pm 0.15\,\mathrm{g/cm^2}$
- Average dose rate with a beam intensity sufficient to treat a 20 cm diameter field at a depth of $30\,\mathrm{g/cm^2}$, modulated over 10 cm, to a dose of 2 Gy in 30 s or less (this translates to about 10^{10} protons per second at the tumor.)
- Delivery of a sufficient number of voxels of $5 \times 5 \times 10\,\mathrm{mm^3}$ size to treat tumor volumes specified above in 2 min (this translates to at least 6,600 voxels or about 50 per second)
- Maximum treatment field size of 30 cm diameter. Dose uniformity of $\pm 2.5\%$ over the reference volume (see below). Effective source-to-axis distance (SAD) for a gantry beam of at least 2.3 m
- Distal dose falloff (80–20%) with not more than $0.25\,\mathrm{g/cm^2}$ above the physical limit
- Lateral penumbra (80–20%) with not more than 4 mm over the penumbra due to multiple scattering in the patient, as a function of clinical parameters chosen
- An in-room system of position and target verification (e.g. cone beam computed tomography/CBCT)

The reference volume is defined as that portion of the high dose volume in the proton beam where the variation in dose must be $< \pm 2.5\%$. This is typically the portion of the beam that will cover the target area. The reference volume is specified across the beam in the in-plane and cross-plane directions as well as along the spread-out Bragg peak (SOBP).

Interestingly, only the first five items in this list depend on the capability of the actual accelerator. The rest are determined by other parts of the system, in particular, the dose delivery system within the treatment room.

Due to the nature of proton beam delivery, almost every proton beam ever delivered to patients has been with the use of some form of image guidance. One can rightly say that IGRT was invented and first implemented in PT systems. However, with the advent of intensity-modulated radiation therapy (IMRT), the

requirement for accurately positioned X-ray beams provided the needed stimulus for a significant growth period in the development of IGRT systems for X-ray therapy. The most prominent recent developments in image guidance include: CBCT systems, ultrasound, radiofrequency, and optical guidance systems. Sadly, almost none of these is employed with existing PT systems. Hence, the PT community began to significantly lag behind developments in the IGRT arena. It is our opinion that this must be rectified in future systems. One might even argue that IGRT remains significantly more important in the use of proton beams than for lower dose gradient X-ray beams.

40.3 Future Systems

It is evident that a new generation of PT systems is needed to enable wider implementation and adequately serve the population of cancer patients. The question became: "How can we reduce the costs to allow for the needed proliferation of PT?" These are the issues we address in the following sections.

40.4 Define What You Want to Treat

Ideally, the design of PT systems should be tailored to the demands of particular treatment requirements. In the past, the notion was adopted that proton systems needed to do exactly what X-ray systems could do in terms of the types and sizes of targets to be treated. This misperception led to the addition of certain features which are very expensive, and never used in practice.

We have performed an analysis of the most common and desirable PT treatment protocols currently in use, or planned in the USA. Figure 40.1 shows typical ranges and field sizes for the most common treatment sites in PT derived from this analysis. These data indicate that there are three distinctive groups of treatments:

1. The small-volume treatments that can have a lateral extent of the radiation field up to 15 cm and can occur at various depths in the patient. We estimate that these treatments comprise more than 50% of the typical fields delivered in PT. This group is illustrated by the ellipses below the horizontal dashed line in Fig. 40.1.
2. The second major group covers shallower tumors, which can have a large lateral extent of up to 40 cm but ranges less than 16 cm. One example of such a field would be a tumor of the spinal axis. This group is illustrated by the ellipses to the left of the vertical dashed line in Fig. 40.1.
3. The third group is comprised of exotic treatments where the deep-seated tumors may have large lateral dimensions (e.g. large pelvic masses). This group is illustrated by the ellipses above the horizontal dashed line and to the right of the vertical dashed line in Fig. 40.1.

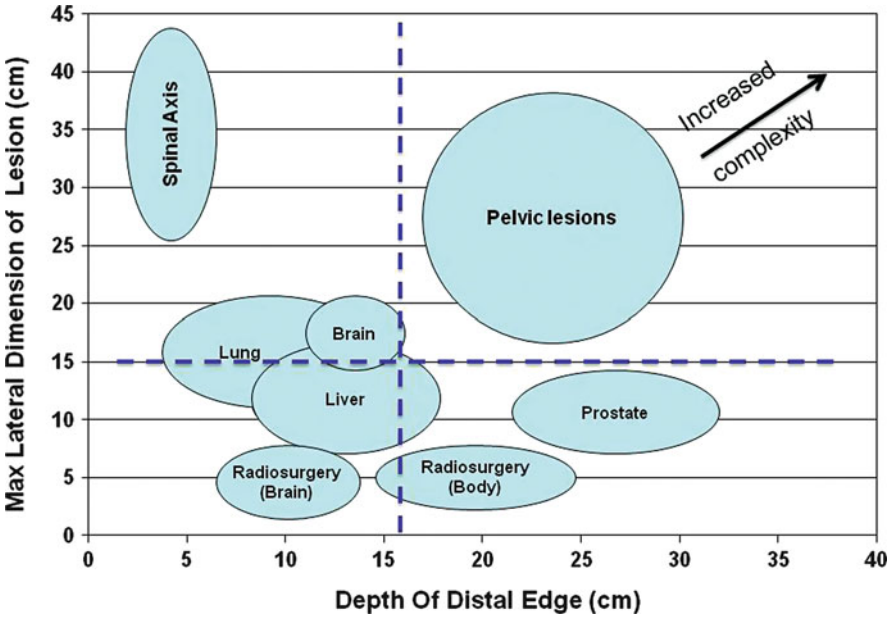

Fig. 40.1 A schematic illustration of typical cases treated with proton beams. The *ellipses* illustrate the parameter space of the typical beams used to treat such cases. The *horizontal axis* dimension of each ellipse indicates the variation in beam ranges (min to max range) and the *vertical axis* dimension indicates the variation in field size (min to max of the lateral extent) for the proton beams required

Fig. 40.2 One of the two dual inclined beam treatment rooms in the ProCure Oklahoma City facility. Shown here is a patient treated for a mediastinum tumor using the 30° off vertical position of the inclined beam system

It is clear that the requirements for these three distinct groups can be significantly different and hence establishing such delivery systems can vary significantly in cost. It can be argued that, on the basis of this analysis, for a multiroom facility, these groups are each represented in a different treatment room rather than all the treatment rooms being able to cover the entire spectrum of treatments. This analysis together with a study done at the iThemba Labs in South Africa [7] was used when

ProCure decided to replace some of the 360° rotating gantries in the Procure centers with a dual inclined beam system shown in Fig. 40.2.

Researchers from the University of Wisconsin School of Medicine and Public Health have carried out similar studies, quantified the maximum proton energy necessary to treat a given percentage of patients, and examined the implications of this energy threshold when building a gantry-mounted proton-accelerator treatment system. The team analyzed 100 randomly selected treatment plans from patients treated with IMRT for cancers of the breast, brain, head and neck, lung and bronchus, abdomen and pelvis and prostate. For each case, they calculated the maximum proton-beam energy required to treat the patient [8].

These calculations reveal that treating all patients would need proton energies of up to 240 MeV. However, 90% of patients could be treated at 200 MeV and 95% at 210 MeV. In the Wisconsin study, a beam with kinetic energy of 200 MeV as it enters into the patient was determined to be sufficient to treat all breast, brain, head and neck cases, as well as a majority of the tumors of the lung, bronchus, abdomen, pelvis, and prostate.

The Wisconsin group also performed Monte Carlo simulations of the neutron production due to interactions of a mono-energetic proton pencil beam in a water phantom representing the patient. They demonstrated that decreasing the proton kinetic energy from 250 to 200 MeV decreased the total neutron fluence produced by a factor of 2.29. This reduction in neutron production reduces not only the unwanted dose to the patient but also reduces the amount of concrete required for shielding. The authors conclude that it is presently feasible to significantly lower the maximum kinetic-energy requirements of a compact proton accelerator in some centers if the ability to treat a small percentage of patients could be sacrificed. We suggest that such a decrease could reduce costs and ease engineering constraints when setting up such a facility. Such simple adjustments could allow more patients access to this promising treatment modality.

40.5 Maintain the Ballistic Advantages of Proton Beams

The next important aspect in cost reduction is the need to maintain the ballistic advantages of protons while reducing the costs. This is illustrated with the horizontal arrow in Fig. 40.3. However, the possibility exists that manufacturers can compromise on certain design aspects to reduce the cost while sacrificing important features of the system. One example is to build PT systems that cannot do pencil beam scanning (PBS). Another way to cut cost and efficacy is to provide only simple patient alignment systems unable to provide precise and rapid corrections. Such systems will track along the declining diagonal arrow in Fig. 40.3.

On the other hand, it is actually possible to sacrifice redundant, underutilized, and nice-but-not-essential features, and use the costs saved to implement the latest features that will enhance the ballistic effect of the proton beam. One example of this tactic is to reduce the number of expensive gantry systems and, at the same time, add state-of-the-art patient alignment and IGRT systems [7]. Targeting systems such as

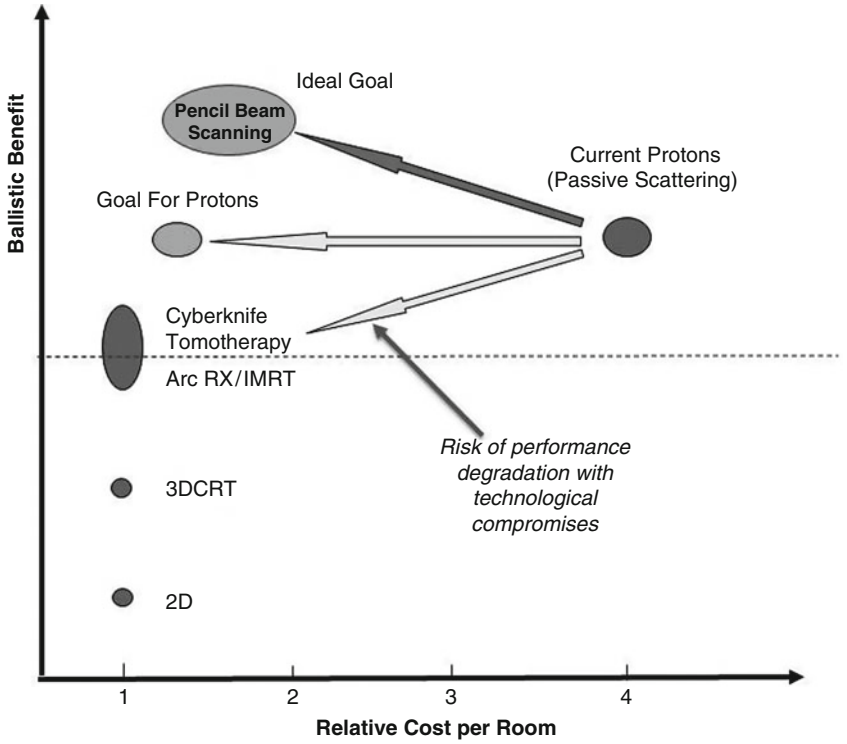

Fig. 40.3 A graphical illustration of the ultimate goal for cost reduction, i.e. reducing costs while increasing the ballistic benefits (*rising arrow*). The immediate goal is to reduce costs while maintaining the current ballistic benefits (*horizontal arrow*). However, reducing costs while sacrificing ballistic benefits (*declining arrow*) is to be avoided. Adapted from P Scalliet, IBA SAPOTE Workshop, Belgium 2009

the Calypso^{TM} radiofrequency system should allow for a reduction in the time and complexity of treatment set-up, as well. Such systems will track along the rising diagonal arrow in Fig. 40.3.

40.6 Smaller and Lighter Accelerators, Gantries, and Beam Lines

The technology in available FDA-approved PT systems dates from developments in research laboratories many decades ago. This technology does not reflect recent advances in subatomic science research, in particular, the use of superconductors. This technology can be used effectively in innovations that will revolutionize the way in which PT can be delivered (cf. Chaps. 23 and 39 for details).

The main challenge is to reduce the size and associated costs of the systems now available commercially without reducing the ballistic advantages of the proton beam [9]. The heaviest and most costly element in extant proton systems is the accelerator. A number of new concepts are under development for smaller accelerators to provide the beam necessary for PT. There are two cyclotron accelerators on the market today based on superconducting magnet technology. In these machines, the coils of the electromagnet are made from superconducting wire and must be operated below 30 K. This results in a magnetic field strength that can be as high as five times that of a conventional magnet coil. The increased field strength results in a smaller radius of the cyclotron. These accelerators are much smaller and lighter and should be cheaper than their room-temperature predecessors. Superconducting units require cryogenerator systems that add to the complexity of the equipment, but the units will require much less power to run.

Research teams are continuing to develop other lower-cost accelerator options based on either a high-gradient dielectric wall accelerator or a laser-driven accelerator. While these emerging technologies have a potential of reducing the size of medical proton accelerators, they are still in very early stages of development (cf. Chap. 20 for details). Having an accelerator in the treatment room, as is the case with photons, may not be the optimal solution in terms of minimizing the whole body dosages to the patient when using proton beams. In addition, this configuration may not be optimal for spot beam scanning. In particular, there are significant medical safety issues associated with neutron dose from beam energy degraders, beam spreading foils and any other neutron producing items, as these are major contributors to secondary tumor incidence rates [10, 11]. Stray electromagnetic fields are also of concern for some patients. With spot scanning, it is desirable to have the scanning magnets at least 2.3 m from the patient to keep skin dose as low as possible.

Interestingly, the accelerator is not the dominant component in the layout of a conventional PT facility. When one takes a bird's eye view of a traditional four-room facility, it is evident that the largest component of the system is, in fact, the isocentric gantry. Figure 40.4 shows a two-dimensional view of a system in which the gantry has a clearly larger size and footprint than the accelerator. The reduced size of the fixed-beam rooms is also evident.

The size of the gantry becomes even more evident if one looks at all three dimensions, and takes into account that the diameter of the typical gantry exceeds 13 m. Conventional gantries now on the market, that are capable of performing spot scanning, weigh over 100 tons and cost in the range of US$ 10–15 million. Much will be gained through the design of smaller and lighter gantries, or by eliminating the need for such gantries entirely. Superconducting technology offers the possibility to reduce the installed cost of the gantry by 50%. A superconducting gantry will be half the size and one-tenth of the weight of existing gantries. Superconducting technology has been proposed in the past for gantries for use in carbon ion therapy. However, it was concluded at that time that the complexity of the cryogenic system and difficulty of ramping the superconducting magnets would make the application of low-temperature high-field magnets technically too challenging [12].

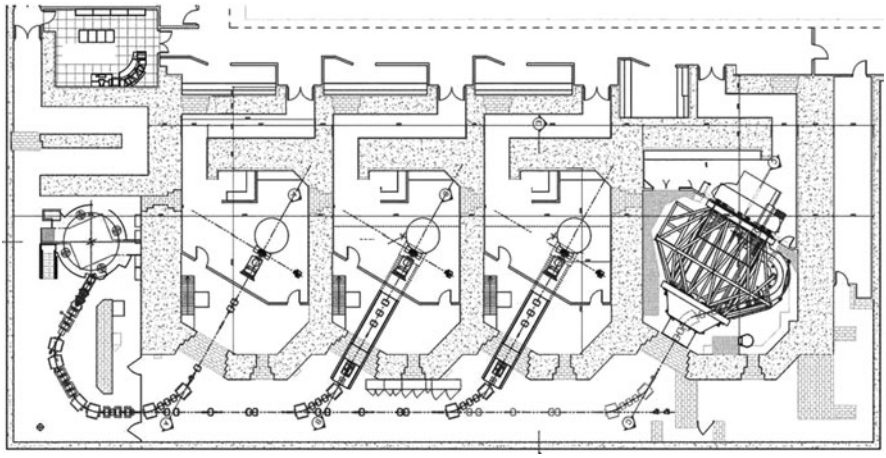

Fig. 40.4 A layout drawing of the concrete section of a typical PT center illustrating the larger size of the 360° rotating gantry in comparison with the accelerator (cyclotron) and a fixed-beam room (Courtesy of IBA and ProCure)

Beyond the accelerator and gantry, significant cost benefit can be realized by having the beam transport system designed with superconducting or permanent magnets. The system design in use at Midwest Proton Radiation Institute, Bloomington, IN, employs separate energy selection systems (ESS) at the entry to each treatment room. This allows the main beam transport line to run at fixed energy and with excellent momentum acceptance [13]. This, in turn, greatly simplifies the design and allows for much greater ease of operation along with automation of that part of the system.

By replacing the majority of the room temperature magnets in the system with superconducting technology, we can greatly reduce the overall power needed for operation. This is the cost most likely to increase significantly as the general cost of energy increases.

We propose that through the use of advanced accelerator technology, together with the use of advanced magnet technology for both beam transport and beam delivery systems, it is possible to reduce the capital cost of proton systems to be competitive with that of advanced X-ray systems on a per-treatment fraction use basis.

40.7 Spread of PT

Indications are that the spread of PT will need to undergo a significant change with a transition from the extant large facilities to smaller facilities that more closely mirror the distribution of conventional radiation centers. Depending on the types of

cancer treated, each four-room center now treats about 1,500–2,000 patients per year. However, if one addresses a more local market, smaller centers (500–750 patients annually) could satisfy much of the local demand.

If small centers are to become a reality, it is clear we need smaller and cheaper systems. Suppliers are beginning to move in that direction now. At present, we see a need for one- or two-room facilities to complement the current standard of four- and five-room freestanding centers being built today.

40.8 Treatment Times and System Availability

Any extended unavailability of the treatment system has many consequences for the patient, and all of these are bad. The consequences range from just wasting of the patient's time, all the way to potentially serious issues that might affect survival. To achieve full system availability of over 96%, the beam delivery system must maintain an uptime approaching 98%, 18 h per day, 250 days per year over many years. This, in turn, implies simplicity and a long record of successful operation of equipment.

A typical four-room treatment facility should be able to deliver more than 40,000 fractions per year. Depending on the type of cancer, this would equate to about 1,500–2,000 patients per year. To achieve this number of patients, the facility would have to operate for 16 h per day and 5 days per week. That means that the typical time in the treatment room per patient has to be about 25 min. Detailed modeling, using attributes from queuing theory to evaluate probable patient waiting times, shows that with a typical mix of patients, four rooms is the optimal number that can be serviced with one accelerator with 25 min per treatment and a total of 2 min of beam-on time per patient spread over two different times for two fields (M. Leuschner, ProCure Treatment Centers, INC, Personal Communication). Indeed, if patient positioning outside of the treatment room can significantly reduce the time per patient in the room [14], that number may go down to three rooms. Adding more rooms only results in the undesirable situation that, for a large fraction of time, both a room and a patient are waiting for beam.

40.9 General Considerations of Cost Reduction

The total cost of technical operations of a PT facility depends on many factors ranging from the capital cost of the equipment to the electrical power bill. Many of these factors are interrelated in a complicated manner. A proton center capital cost has three major components: first is the land and building costs, second are the equipment costs and finally are the financing costs that depend on the time taken to develop the center. From an equipment perspective, factors that enter into this equation obviously start with the capital cost. However, that also includes the

time to construct the various components, the time for integration and installation, and time for commissioning. Once the system is up and running, the operating and maintenance costs continue to be a major expense. Consideration of all these costs should be included as part of the equipment design considerations.

To minimize the building and land costs, one needs to minimize the footprint of the facility, in order to minimize the concrete needed for shielding, and to standardize the design once it is completed. Ease and speed of equipment installation also needs to be a design consideration. Obviously smaller, lighter components are going to be easier and quicker to install. Operating costs are generally dominated by staffing costs. Thus, reduction in staffing requirements is necessary. This reduction might be achieved both through system simplification and, whenever possible, through automation.

There are several factors that drive the preference to have a facility with a much smaller footprint than is the case with extant centers. The smaller land requirements might allow integration with or installation in close proximity to an existing photon treatment facility or comprehensive cancer care center. If the footprint of the building can be reduced to something in the range of 5,000 sq ft or roughly 500 qm, there can be many more sites in cities that can accommodate such a facility as an addition to their existing complex. This size constraint will most likely dictate a vertically oriented facility with the various functions installed on different floor levels and thus dictates much smaller and lighter components.

40.10 Commissioning and Staff Training

Current commercially available PT systems are assembled on site after the building is available. Commissioning of all subsystems is also performed on site, followed yet by full system compliance testing. The commissioning process can take between 1.5 and 2 years to complete. This is in great contrast of the time scale for installation and verification of a photon/electron accelerator, where the whole process may be completed in a few weeks. The huge difference in commissioning times is dictated by the relative size and scale of the equipment. A linear accelerator can be delivered in a few preassembled and tested subsystem sections. Full system testing of these machines can commence after a period of about 3 weeks. The next generation of PT systems must incorporate these more efficient procedures to become competitive. Consider, for example, a room-temperature magnet 230 MeV accelerator that today weighs about 220 tons. By going to high-field superconducting magnets, the weight could be reduced by a factor of 10. Such a device could be commissioned at the factory, transported intact and installed leaving again only the need for full system verification testing on site as with linacs.

Another constraint on the rapid ramp-up of the utilization of facilities is often the need to train staff on the actual system once it is fully commissioned. This is very inefficient and costly. In 2007, ProCure opened the world's first and only training facility dedicated to PT. The ProCure Training and Development Center

(TDC), located in Bloomington, Indiana, provides hands-on simulation and training for radiation oncologists, medical physicists, dosimetrists, radiation therapists, and other staff involved in delivering PT [15, 16]. At the TDC, ProCure offers clinical, technical, interpersonal, and administrative training in an exact replica of a PT center without an accelerator and beam line. The facility includes two treatment rooms for training equipped with the actual equipment found in the ProCure treatment centers except for the 360° rotating gantry which is a lightweight replica of the real gantries. This comprehensive hands-on training enables higher efficiency and standardized processes that can commence even before individual center operations begin.

The TDC also allows ProCure to be a leader in technological research for PT, by providing an innovative environment with experts in all aspects of PT. With standardization across the complete process of creating a proton center, and by training all staff off-line (referred to as "before the job" training) at the TDC, ProCure has reduced many of the barriers to efficient implementation of PT. The resulting capital cost reduction for ProCure is 25–30% on a per-treatment basis compared to other existing proton facilities.

40.11 Summary

To summarize, a next generation PT system should incorporate many of the ideas discussed in this chapter:

- An accelerator that can be transported and installed in one piece. The size and weight (<40 tons) of a 5-T magnetic field device should meet that goal.
- An ability to get beam out of the accelerator within a few weeks after all services are installed.
- A 50% cost reduction compared to the accelerators currently available.
- A fixed-energy main beam transport line that would be a fully automated system using superconducting technology to reduce size and operating cost.
- A separate degrader and ESS for each room that could be automated.
- A gantry of less than 20 tons that comes in a few preassembled major components and with a total cost of about half of current configurations.
- A lightweight nozzle designed only for use with scanned beams.
- A control system with modular software and simple troubleshooting features that would allow for totally automated operation.
- A reduction in overall power requirements by 50%.
- A reduction in on-site operations and maintenance staff by 50%.

If these technical goals can be met, it should be possible to provide PT at a cost very competitive with that of IMRT today. If the cost differential is removed, the ballistic advantages of protons should place this modality in a dominant role for the future of radiation therapy.

References

1. V.A. Anferov, Scan pattern optimization for uniform proton beam scanning. Med. Phys. **36**, 3560–3567 (2009)
2. W.D. Newhauser, J.D. Fontenot, A. Mahajan, et al., The risk of developing a second cancer after receiving craniospinal proton irradiation. Phys. Med. Biol. **54**, 2277–2291 (2009)
3. D. Hecksel, G.A. Sandison, J.B. Farr, A.C. Edwards, Scattered neutron dose equivalent from an active scanning proton beam delivery system. Australas. Phys. Eng. Sci. Med. **30**, 326–330 (2007)
4. S. Lin, T. Boehringer, A. Coray, et al., More than 10 years experience of beam monitoring with the Gantry 1 spot scanning proton therapy facility at PSI. Med. Phys. **36**, 5331–5340 (2009)
5. O. Jäkel, D. Schulz-Ertner, C.P. Karger, et al., Experience with carbon ion radiotherapy at GSI. Nucl. Instrum. Methods Phys. Res. B **241**, 717–720 (2005)
6. C.E. Allgower, A.N. Schreuder, J.B. Farr, et al., Experiences with an application of industrial robotics for accurate patient positioning in proton radiotherapy. Int. J. Med. Robot. Comput. Assist. Surg. **3**, 72–81 (2007)
7. A.N. Schreuder, D.T.L. Jones, J.L. Conradie, et al., *Applications of Accelerators in Research and Industry*, ed. by J.L. Duggan, I.L. Morgan. (American Institute of Physics, Melville, NY, 1999), pp. 963–966
8. E. Sengbusch, A. Pérez-Andújar, P.M. DeLuca Jr, T.R. Mackie, Maximum proton kinetic energy and patient- generated neutron fluence considerations in proton beam arc delivery radiation therapy. Med. Phys. **36**, 364–372 (2009)
9. J. Matthews, Accelerators shrink to meet growing demand for proton therapy. Phys. Today **62**, 22–24 (2009)
10. G. Mesoloras, G.A. Sandison, R.D. Stewart, et al., Med. Phys. **33**, 2479–2490 (2006)
11. X.G. Xu, B. Bednarz, H. Paganetti, A review of dosimetry studies on external-beam radiation treatment with respect to second cancer induction. Phys. Med. Biol. **53**, R193–R241 (2008)
12. U. Weinrich, Gantry design for proton and carbon hadrontherapy facilities. Proceedings of European Particle Accelerator Conference EPAC-2006, Edinburgh, UK, 26–30 June 2006, pp 964–968
13. V. Anferov, J. Collins, D.L. Friesel, et al., The Indiana University proton therapy system. Proceedings of European Particle Accelerator Conference EPAC-2006, Edinburgh, UK, 26–30 June 2006, pp. 2349–2351
14. A. Bolsi, A.J. Lomax, E. Pedroni, G. Goitein, et al., Experiences at the Paul Scherrer Institute with a remote patient positioning procedure for high-throughput proton radiation therapy. Int. J. Radiat. Oncol. Biol. Phys. **71**(5), 1581–1590 (2008)
15. M. Skoufalos, Proof is in the protons. RT-Image **22**, 14–18 (2009)
16. T. Bove, Learning Accelerated, Chief Learning Officer, Published Feb 2010

Chapter 41
New Facilities: Plans and Proposals

Ramona Mayer and Stanislav Vatnitsky

Abstract Ion beam facilities that have either become operational since 2001 or are at present under construction or in development are reviewed. The concepts of four upcoming European dual ion beam facilities will be described in more detail.

41.1 Introduction

In contrast to the early years of ion beam therapy (IBT), where patients were treated at physics research facilities when beam time was available, the last decade has clearly seen a trend towards hospital-based facilities. The overview on new and upcoming facilities shows a distinct market for proton facilities in the United States. In contrast to that, in Asia and Europe an interest in both, proton and carbon ion treatments, or combined treatments as provided in dual ion beam facilities can be noticed. A comprehensive summary of all existing, closed, and planned ion beam facilities can be found on the homepage of the Particle Therapy Cooperative Group (PTCOG), where also the number of patients treated worldwide is regularly updated (http://ptcog.web.psi.ch/).

R. Mayer (✉)
EBG MedAustron GmbH, Viktor Kaplan-Straße 2, 2700 Wiener Neustadt, Austria
e-mail: ramona.mayer@ebgmedaustron.at

U. Linz (ed.), *Ion Beam Therapy*, Biological and Medical Physics, Biomedical Engineering, DOI 10.1007/978-3-642-21414-1_41,

41.2 Situation in Europe

41.2.1 Proton Therapy Facilities

The first ion beam patient in Europe was treated with protons in Uppsala, Sweden, in 1957. The first proton therapy (PT) facility in Western Europe has been in operation at the Paul Scherrer Institute (PSI) in Villigen, Switzerland, since 1984. The spot scanning technique with a proton gantry was established in this institution in 1996 [1].

In 2010, a total of nine proton facilities are operational in Europe, four of them are dedicated to eye treatment, only. Additionally, three centers are running in Russia; however, none of them is hospital-based.

Four new proton centers (Table 41.1) are under construction or in development stage in Europe. The existing facility in Orsay will be enlarged and at the final stage, it will be equipped with one gantry and four fixed-beam rooms. The facility at PSI in Villigen, Switzerland, will soon start to use an additional gantry with modern beam scanning technology (cf. [2] and Chap. 24 for details).

41.2.2 Carbon Ion Beam Facilities

Pioneer work in carbon ion radiotherapy (CIRT) has been done at the Helmholtz Research Centre for Heavy Ions (GSI) in Darmstadt, Germany. For example, much of the important research work on the relative biological effectiveness (RBE) was performed at the GSI [3, 4]. At this research center from 1997 to 2008, beam time was used during several weeks per year to treat more than 440 patients for tumors in the head or neck region [5, 6]. For many years, the GSI was the only facility in Europe providing CIRT. With the opening of the dual ion beam facility at Heidelberg, Germany, in 2009, patient treatment at GSI was abandoned.

A carbon ion facility called ARCHADE is under development in Caen, France. At this center, in contrast to all other carbon ion facilities worldwide, a cyclotron will be used instead of a synchrotron. The facility, which is primarily research orientated, will be equipped with one research room and one fixed-beam treatment room.

41.2.3 Dual Ion Beam Facilities

In 2009, the first European dual ion beam facility HIT (Heidelberg Ion-Beam Therapy Center) started operation in Heidelberg, Germany. Currently, however, the patients are only treated with the fixed-beam lines. The first carbon ion beam gantry worldwide shall start operation within 2011. Additional dual ion beam centers are under construction or in development in Europe. Four of these are introduced, here, in more detail.

Table 41.1 New ion beam facilities in Europe. Top: Opening after 2001. Bottom: Under construction or in development

Center	City	State	Particle	Max. clin. energy (MeV)	Beam delivery system		Start
					Gantry	Fixed-beam	
European facilities which opened after 2001							
Istituto Nazionale di Fisica Nucleare Laboratori Nazionali del Sud (INFN-LNS)	Catania	Italy	p	60	~	1	2002
Rinecker Proton Therapy Center	Munich	Germany	p	250	4	1	2009
Heidelberger Ionenstrahl-Therapiezentrum (HIT)	Heidelberg	Germany	p, C-ion	430/u	1	2	2009
Central Military Hospital Proton Therapy Center	Ruzomberok	Slovak Republic	p	250	~	1	2010
Narodwe Centrum Radioterapii Hadronowej	Krakow	Poland	p	60	~	1	2011
New European facilities under construction or in development							
Centro Nazionale di Adroterapia Oncologica (CNAO)	Pavia	Italy	p, C-ion	430/u	~	4	2011
Westdeutsches Protonentherapiezentrum (WPE)	Essen	Germany	p	230	3	1	2011
Partikel-Therapie Zentrum (PTZ)	Marburg	Germany	p, C-ion	430/u	~	3	2011[a]
Nordeuropäisches Radioonkologisches Centrum Kiel (NRoCK)	Kiel	Germany	p, C-ion	430/u	~	4	2012[a]
Proton Therapy Center Czech	Prague	Czech Rep.	p	230	3	1	2012
Skandion Clinic	Uppsala	Sweden	p	250	2		2013
Agenzia Provinciale Per la Protonterapia (ATreP)	Trento	Italy	p	230	1	1	2013
HollandPTC	Delft	The Netherlands	p	n.a.	n.a.	n.a.	n.a.
MedAustron	Wiener Neustadt	Austria	p, C-ion	400/u	1	3	2015
ARCHADE	Caen	France	p, C-ion	400/u	~	1	2014
ETOILE	Lyon	France	p, C-ion	400/u	2	2	2015

[a] In the summer of 2011, the provider Siemens announced to disontinue any IBT work in this facility

Fig. 41.1 Artist's view of NRoCK. Courtesy of NRoCK GmbH, Kiel, Germany

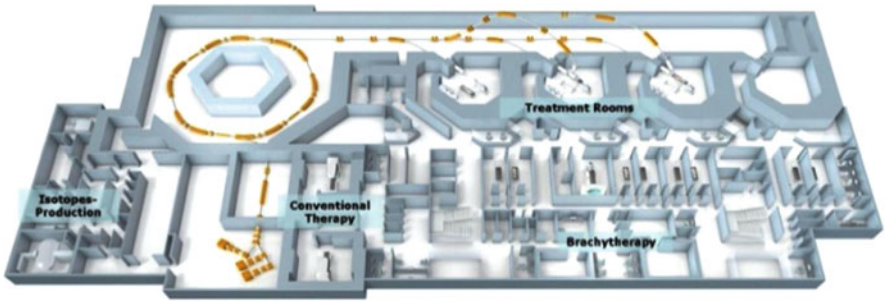

Fig. 41.2 Treatment level at NRoCK. Courtesy of NRoCK GmbH, Kiel, Germany

41.2.3.1 North European Radiooncological Center Kiel (http://www.nrock.de)

The North European Radiooncological Center Kiel, Germany (NRoCK), was intended to be the first center worldwide to offer external beam therapy with photons, electrons, protons and carbon ions, brachytherapy, systemic therapy, and state-of-the-art diagnostic imaging under one roof (Figs. 41.1 and 41.2). Construction of NRoCK began in July 2008. A public-private partnership wanted to share the estimated cost of 250 million Euros. Patients should receive (R. Kampf, Personal communication 2010). Advanced radiation therapy as well as systemic therapy in close cooperation with partner institutions in Northern Germany and the neighboring Baltic states.

Projected Technical details: Protons and carbon ions are generated in an ion source and injected into a two-stage linear accelerator where they are brought to an energy of approx. 7 MeV/u. A medium energy beam transport line guides the particles to a synchrotron where they are accelerated up to 250 MeV/u for protons and 430 MeV/u for carbon ions. Inside the treatment rooms two fast scanning magnets deflect the ion beam in directions perpendicular to the beam axis to fully cover the shape of the tumor (raster scanning). All beam parameters with the exceptions of energy should be switched within tenths of a second.

Three treatment rooms are projected, each with a horizontal beam line, one with an additional vertical beam line and one with an additional 45° beam line.

The use of robots together with kV imaging should provide highest treatment precision and a new level of comfort for the patient.

The equipment for conventional radiotherapy at NRoCK comprises two state-of-the-art linacs to perform photon and electron radiation treatments across a wide energy range. Image-guided radiation therapy (IGRT) and intensity-modulated radiotherapy (IMRT) can be performed. In addition, two bunkers are dedicated to brachytherapy capable of delivering high, low, and pulsed dose rate brachytherapy. The imaging area is equipped with a sliding gantry computed X-ray tomography unit, a whole-body 1.5 T magnetic resonance imaging (MRI) system, and a combined positron emission tomography and computed X-ray tomography (PET-CT) system.

In September 2011, when most of the technical equipment was already installed, Siemens announced that it would only equip the facility with conventional radiotherapy instrumentation and would discontinue the work related to IBT [7].

41.2.3.2 ETOILE: The First French CIRT Center in Lyon (http://www.centre-etoile.org)

The ETOILE project has emerged since the beginning of 2007. It gained governmental support and juridical structure as a Health Cooperation Grouping (Groupement de Coopération Sanitaire, GCS-ETOILE). The call for bids was released in February 2008 in the frame of a public–private partnership. Three industrial consortia initiated the competitive dialog with the GCS-ETOILE in July 2008. This negotiation phase ended in March 2010. Finalization of the contract and launching of the construction are expected in 2011 (J. Balosso, P. Pommier, G. Wasmer, et al., Personal communication). The project is characterized by the parallel course of seven programs, which are all together necessary for the final success of the project. These are

1. Application to the health authorities for the validation of the initial core indications
2. Detailed economical modeling to define the level of reimbursement for the carbon ion treatments in close relation with the governmental health services
3. A new round of epidemiological studies to obtain a real-scale image of the recruitment, and the organization of the national network
4. Discussions with neighboring countries to attract patients from a larger area than France only for the early indications
5. Information and lobbying activities to ascertain the national position of the ETOILE Center
6. Necessary financial conditions to obtain state warranties for the loan and the financial security of the project
7. Research and technological developments other than the clinical activities of CIRT and PT

Fig. 41.3 Projection of the ETOILE facility in the city of Lyon. Courtesy of Centre ETOILE, Lyon, France. *ETOILE – The First French CIRT Center at Lyon* (http://www.centre-etoile.org)

The French Higher Health Authority issued a preliminary favorable evaluation in March 2010 with recognition of most of the so-called "consolidated" indications for CIRT that comprise the former neutron indications and the major indications investigated by NIRS and GSI/HIT. These indications accumulate to an incidence of about 1,200 cases per year in France. A set of more frequent (3,000–6,000 cases per year) but less investigated "prospective" indications will necessitate successful clinical trials to be progressively added to the first set. This second set will be subjected to multicentric prospective clinical trials in the frame of the ULICE (Union of Light Ion Centres in Europe) network, an EU-funded project set up by 19 research organizations and European industrial partners.

The ETOILE Project has generated a strong scientific environment with specific funding since 2000. Many doctoral and postdoctoral positions have thus been financed. Researchers are supported by specific funding from various public regional institutions, such as the City of Lyon, and constitute the so-called Regional Program of Research in Hadron therapy (PRRH: Programme de Recherche Régional en Hadronthérapie), linked to a similar national program (PNRH). Research teams involved in PRRH are part of established research and teaching institutions such as neighboring universities or the French Public Research Institutions INSERM and CNRS. Major PRRH topics are the medical project itself; economic simulations; in-silico modeling; study of the particles generated in the target volume and real-time control imaging; radiobiology of particles; dosimetry and dose deposition simulation; moving targets, organ motion and distortion; and technological developments associated with the former (Fig. 41.3).

41.2.3.3 CNAO: The National Center for Oncological Hadron Therapy in Pavia, Italy (http://www.cnao.it)

The founders of CNAO are five major hospitals, seated in Milan and Pavia, plus the Italian TERA Foundation. Since 2003, the National Institute of Nuclear Physics (INFN), the Universities of Milan and Pavia, the Polytechnic of Milan, and the Town

Fig. 41.4 Outside view of the CNAO ion beam facility in Pavia. With permission of Fondazione CNAO, Milan, Italy

of Pavia are additional institutional participants of CNAO (P. Fossati, M. Pulia, R. Orrecchia, S. Rossi, Personal communication).

The CNAO project has a long history which began in 1996 at CERN, Geneva, Switzerland, with the design of an optimized synchrotron for proton and light ion therapy with the acronym PIMMS (Proton-Ion Medical Machine Study) [8]. PIMMS was a collaboration of CERN, Med-AUSTRON (Austria), Oncology 2000 (Czech Republic), and TERA. GSI contributed and gave expert advice.

The PIMMS group had as mandate the design of a synchrotron and beam lines for center unconstrained by financial and/or space limitations. In fact, PIMMS was never intended to be built in its final layout. It was more an open design study from which different modules could be taken for the design of various centers according to their requirements.

Based on that work, the TERA Foundation, with the collaboration of many institutions, including INFN, CERN, GSI and a few Italian universities, engineered the PIMMS synchrotron and made a more compact design of the extraction and injection lines. The resulting project has recently been completed in Pavia (Fig. 41.4).

The CNAO synchrotron, shown in Fig. 41.5, has a diameter of approximately 25 m and accelerates protons and carbon ions to 250 MeV and 400 MeV/u, respectively.

The injector is almost identical to that of the HIT facility differing only in the geometry of the low-energy beam transport (LEBT) system. Sources and linac are placed inside the main ring, making the accelerator very compact. The two ion sources run continuously and can be individually monitored; the particle species to be accelerated are selected by just changing the LEBT magnet settings.

The CNAO facility has three treatment rooms in which the beam can be delivered with horizontal lines. The design of the extraction lines is particularly compact thanks to the use of a “switching” magnet that directs the beam to the selected treatment room. In one of the rooms, a vertical line is available, additionally, to deliver the beam at the same isocenter as the horizontal one. CNAO will employ an active spot scanning system.

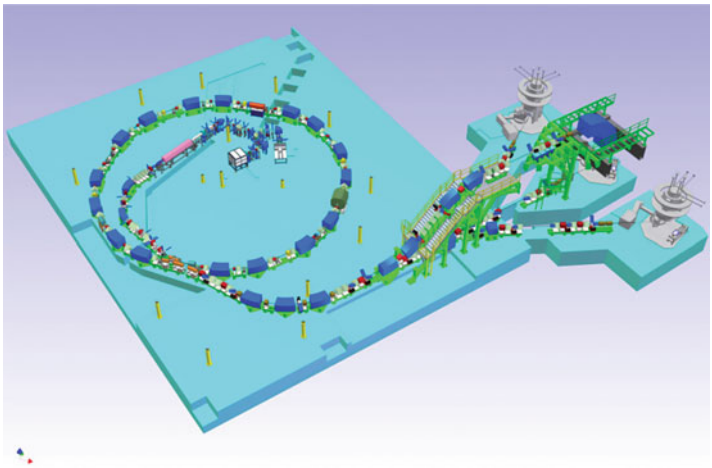

Fig. 41.5 CNAO accelerator complex. With permission of Fondazione CNAO, Milano, Italy

The CNAO building has been constructed to allow expansion by two additional treatment rooms. The reserved space for such a second phase is dimensioned to also provide sufficient room for two carbon ion gantries.

The facility will be equipped with one CT scanner, one PET/CT scanner, and one MRI scanner dedicated to treatment simulation and in-treatment response evaluation. Treatments will be performed with patients immobilized on specially designed couches or chairs that will be docked to a state-of-the-art, 6-degrees-of-freedom positioning device. Set-up verification will be performed with orthogonal kV images of diagnostic quality. Additionally, an optoelectronic system with marker detection and surface detection capability is projected. CNAO aims to have a high patient throughput. Therefore, dedicated positioning rooms exist for computer-aided positioning (CAP) on a couch or on a chair outside the treatment room. The patients will be transported into the treatment room on a trolley which docks to the positioning device. Three-dimensional set-up verification will be available in the CAP room with CT on rails [9].

Seven areas of interest have been identified for treatment: lung cancer, liver cancer, head and neck malignancies, pediatric solid cancers, eye tumors, sarcoma, and central nervous system cancers. In the future, gynecological and digestive (pancreas, biliary tract, and rectum) tumors might be further indications. Disease-specific working groups will define selection criteria and protocols to be used at CNAO. All patients will participate in clinical trials in order to establish optimal indications for IBT.

Commissioning of the first treatment room was completed, recently, and the first patient was treated in September of 2011.

41.2.3.4 MedAustron, Wiener Neustadt, Austria (http://www.medaustron.at)

The ion beam cancer treatment and research center MedAustron in Wiener Neustadt, Austria is designed to be a dual ion beam center, where proton and carbon IBT can be compared under identical technical conditions. The company EBG MedAustron GmbH has the overall responsibility for the construction and operation. Collaborations for the realization of the MedAustron accelerator complex have been established with CERN and CNAO. Recently, a scientific collaboration was also signed with PSI. The planning and construction of the building were contracted to a consortium of architects (Fig. 41.6).

In 2009, the civil engineering preplanning was finished and the documents for the mandatory Environmental Impact Assessment were submitted. Approval was obtained in December 2010 and the construction work started in February 2011. The first patient treatment is scheduled in 2015.

The ground floor of the MedAustron facility will house the medical, the research, and the accelerator wing. The technical infrastructure for the building services and the accelerator will be accommodated in the basement and the administrative area will be situated in the upper floor. The MedAustron accelerator complex is designed to support active beam delivery. The accelerator complex will cycle with a typical repetition rate of 0.5 Hz. Beam energy, size, and intensity can be changed on a cycle-to-cycle basis. A change of the ion type, i.e., protons or carbon ions will also be possible on a subminute level.

The injector will comprise three ion sources with the possibility of adding a fourth source. Protons and carbon ions will be the standard configuration for medical treatment, the third source will serve as spare and the alternative fourth source is intended for research with a further ion type. The LEBT brings the beam from the active source to the RFQ, which serves as preinjector for a drift tube linac. The synchrotron is based on the PIMMS concept [8] and was further developed into a

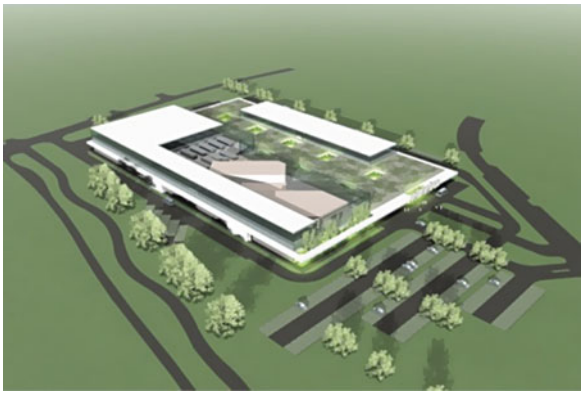

Fig. 41.6 Schematic view of MedAustron. *MedAustron, Wiener Neustadt, Austria* (http://www.medaustron.at)

technical design by the CNAO group. Its energy range is 60–250 MeV for protons and 120–400 MeV per nucleon for carbon ions.

The MedAustron facility will be equipped with one horizontal beam line for protons and carbon ions, one horizontal and vertical beam line for protons and carbon ions and one proton gantry. A fourth treatment room, possibly equipped with a carbon ion beam gantry, is a medium- to long-term idea. Its implementation, however, will depend on the experience of existing facilities and further technological progress.

Beam scanning will be available at all beam lines in order to provide greater flexibility in treatment plan optimization and superior dose distributions with reduced neutron doses to the patient.

The MedAustron facility and the hospital nearby will be equipped with CT, MRI, PET-CT, and ultrasound to meet the requirements for adaptive radiotherapy. Thus, time-variable effects, such as weight loss, changes in organ filling, or tumor shape could be accounted for in the course of the treatment by repeated imaging.

41.2.4 Cooperations Within the Ion Beam Community

The European Commission helped to establish active cooperations between European ion beam facilities and interested institutions. One example is the European Network for Light Ion Hadron Therapy (ENLIGHT), which was established in 2002 [10] and comprises, presently, more than 50 partners from academia and industry. The more recent projects ULICE (http://ulice.web.cern.ch) or the Particle Training Network for European Radiotherapy (PARTNER) (http://partner.web.cern.ch) are equally intended to strengthen collaboration and exchange in IBT. Moreover, cooperations with facilities beyond the European Union are also strongly encouraged.

41.3 Situation in the USA

In 2010, there are seven clinical proton facilities operational in the United States and eight centers are under construction or in development (Table 41.2). All facilities have at least one rotating gantry. The maximum energy varies between 200 and 250 MeV with a tendency to higher maximum energy for the projected units.

The University of Florida Proton Therapy Institute (FPTI) in Jacksonville is the first facility in the USA where the accelerator floor is at ground level. Previously, this was underground to facilitate radiation shielding. But due to the high water table in Florida, the entire building was raised to ground level and the exterior walls had to be thickened in some areas to approx. 5.5 m to obtain the same level of radiation shielding.

Table 41.2 New ion beam facilities in the United States. Top: Opening after 2001. Bottom: Under construction or in development

Center	City	State	Particle	Max. clin. energy (MeV)	Beam delivery system		Start
					Gantry	Fixed-beam	
US facilities which opened after 2001							
Francis H. Burr Proton Center at MGH (FHBPC)	Boston	MA	p	235	2	1	2001
Midwest Proton Therapy Institute (MPTI)	Blomington	IN	p	200	2	1	2004
M.D. Anderson Proton Therapy Center (MDAPTC)	Houston	TX	p	250	3	1	2006
Univ. of Florida Proton Therapy Institute (FPTI)	Jacksonville	FL	p	230	3	1	2006
ProCure Proton Therapy Center	Oklahoma City	OK	p	230	1	1	2009
Roberts Proton Therapy Center	Philadelphia	PA	p	230	4	1	2010
Hampton Univ. Proton Therapy Institute	Hampton	VA	p	230	4	1	2010
New US facilities under construction or in development							
Northern Illinois Proton Therapy Center	W. Chicago	IL	p	250	2	2	2011
ProCure CDH Proton Therapy Center	Warrenville	IL	p	230	1	3	2011
ProCure Proton Therapy Center	Somerset	NJ	p	230	1	3	2012
ProCure Proton Therapy Center	Seattle	WA	p	230	1	3	2012
South Florida Proton Center	Miami	FL	p	250	1	2	2012
Broward General Medical Center	Fort Lauderdale	FL	p	250	1		2012
King Center for Proton Therapy, Barnes-Jewish Hospital	St. Louis	MI	p	250	1		201?

The PT center in Oklahoma City and three of those under development are supplied by the US company Procure in cooperation with local hospitals or institutions. This company is the only worldwide to provide a Training and Development Center dedicated to PT (cf. Chap. 40). In addition to the PT facilities listed in Table 41.2 as being under construction or in development, there are several more hospitals considering the construction of similar facilities. Regularly, updated information can be found on the homepage of the National Association for Proton Therapy (NAPT) (http://www.proton-therapy.org/), an independent, nonprofit, public benefit corporation founded in 1990 to promote the clinical benefits of PT for cancer patients and their affiliates.

In contrast to Europe or Asia, there is no carbon ion beam center running in the United States, and other than in Europe, there is hardly any public funding for it. The National Institutes of Health (NIH), e.g., the most relevant funding agency of medical research in the USA, is not supporting CIRT [11]. Alleged scarcity of data and difficulty to predict long-term effects are common explanations. They ignore, however, the fact that the Lawrence Berkeley Laboratory (LBL) in Berkeley, California, pioneered the therapy with ions heavier than protons already in the 1970s or that more than 7,000 patients have been treated with carbon in the meantime, most of them at NIRS in Chiba, Japan, with up to 15 years of follow-up (cf. Chap. 36 for details). It is more likely that cost and the differences in the reimbursement of medical services between the US and other industrial countries (cf. also Chap. 3) are the major barriers for more commitment.

A few US institutions intend to invest, nevertheless, in CIRT; among them the Mayo Clinic in Rochester, NY, Vanderbilt University in Nashville, TN, and Touro University in Vallejo, CA [11].

41.4 Situation in Asia

41.4.1 PT Facilities

In 2010, a total of eight PT facilities are running in Asia, most of them are located in Japan. In the near future at least five more centers will be added, three of them also in Japan (cf. also Chap. 37).

41.4.2 Carbon Ion Beam Facilities

Japan has the longest experience in the clinical application of CIRT. At the Heavy Ion Medical Accelerator (HIMAC) at the National Institute of Radiological Sciences (NIRS) in Chiba, the first patient in the world was treated with carbon ions in 1994. Until 2010 more than 5,000 patients underwent this treatment option in the framework of clinical studies performed in Chiba ([12, 13], cf. also Chaps. 14 and 36).

Table 41.3 New ion beam facilities in Asia. Top: Opening after 2001. Bottom: Under construction or in development

Center	City	State	Particle	Max. clin. energy (MeV)	Beam delivery system		Start
					Gantry	Fixed-beam	
Asian facilities which opened after 2001							
Proton Medical Research Center (PMRC)	Tsukuba	Japan	p	250	2	~	2001
Hyogo Ion Beam Medical Center (HIBMC)	Hyogo	Japan	p + C-ion	320/u	1	2	2001
Wakasa Wan Energy Research Center (WERC)	Tsuruga	Japan	p	200	~	2	2002
Shizuoka Cancer Center	Shizuoka	Japan	p	235	1	1	2003
Wanjie Proton Therapy Center (WPTC)	Zibo	China	p	230	2	1	2004
National Cancer Center	IIsan	South Korea	p	230	2	1	2007
Southern Tohoku Proton Therapy Cancer Center	Koriyama	Japan	p	n.a.	n.a.	n.a.	2008
Gunma Heavy Ion Medical Center (GHMC)	Gunma	Japan	C-ion	400/u	1	1	2010
New Asian facilities under construction or in development							
Fukui Prefecture Proton Therapy Center	Fukui	Japan	p	250	2	1	2011
Chang Gung Memorial Hospital	Taipei	Taiwan	p	235	4	~	2012?
Sino-Japanese Friendship Hospital	Beijing	China	p	230	1	1	n.a.
Fudan University	Shanghai	China	p + C-Ion	430/u	~	4	n.a.
Heavy Ion Tumor Therapy Facility	Lanzhou	China	C-ions	430/u	n.a.	n.a.	n.a.
Southern Tohoku Proton Therapy Cancer Center	Fukushima	Japan	p	n.a	n.a.	n.a.	n.a.
Medipolis Medical Research Institute	Kagoshima	Japan	p	n.a.	n.a.	n.a.	n.a.

A project to construct a new treatment facility as an extension of the existing HIMAC facility has been initiated for the further development of CIRT. In the new facility, one of the treatment rooms will be equipped with an isocentric gantry employing a 3D pencil beam scanning method. Two other rooms will be equipped with fixed-beam delivery systems providing beams in both horizontal and vertical directions (cf. [14] and Chap. 37 for details).

In 2010, a new facility started CIRT at Gunma University. This project has been strongly supported by NIRS.

In the near future, CIRT should also be available in China, at the Heavy Ion Tumor Therapy Facility in Lanzhou, China.

41.4.3 Dual Ion Beam Facilities

The world's first dual ion beam facility, providing protons and carbon ions at the same center was opened in 2002 in Hyogo, Japan. This facility is equipped with five treatment rooms; three rooms with fixed-beam lines and two rooms with isocentric proton gantries. Fudan University in Shanghai, China, is planning to have the number two dual IBT facility with fixed-beam lines in Asia (Table 41.3).

41.5 Conclusion

Different trends can be observed in Europe, the United States, and Asia. In the US, there is a clear priority for proton facilities, whereas in Asia and Europe there is interest in both PT and CIRT, and hence, also in dual IBT facilities.

References

1. E. Pedroni, R. Bacher, H. Blattmann, et al., The 200-MeV proton therapy project at the Paul Scherrer Institute: conceptual design and practical realization. Med. Phys. **22**, 37–53 (1995)
2. E. Pedroni, R. Bearpark, T. Böhringer, et al., The PSI Gantry 2: a second generation proton scanning gantry. Z. Med. Phys. **14**, 25–34 (2004)
3. M. Scholz, A.M. Kellerer, W. Kraft-Weyrather, G. Kraft, Computation of cell survival in heavy ion beams for therapy: the model and its approximation. Radiat. Environ. Biophys. **36**, 59–66 (1997)
4. T. Elsässer, M. Krämer, M. Scholz, Accuracy of the local effect model for the prediction of biologic effects of carbon ion beams in vitro and in vivo. Int. J. Radiat. Oncol. Biol. Phys. **71**, 866–872 (2008)
5. D. Schulz-Ertner, The clinical experience with particle therapy in adults. Cancer J. **15**, 306–311 (2009)
6. D. Schulz-Ertner, C.P. Karger, A. Feuerhake, et al., Effectiveness of carbon ion radiotherapy in the treatment of skull-base chordomas. Int. J. Radiat. Oncol. Biol. Phys. **68**, 449–457 (2007)

7. Joint press release from the Ministry of Science and Economics of the state of Schleswig-Holstein and Siemens AG, Agreement in Kiel: UKSH to receive top-quality conventional radiotherapy at advantageous rates, 14 Sept 2011, http://www.siemens.com/press/en/pressrelease/?press=/en/pressrelease/2011/corporate_communication/axx20110983.htm. Accessed 5 Oct 2011
8. L. Badano, M. Benedikt, B.J. Bryant, et al, Proton–Ion Medical Machine Study (PIMMS) Part I. CERN-PS-99- 010-DI. http://cdsweb.cern.ch/record/385378/files/ps-99--010.pdf. Accessed 20 Jan 2011
9. R. Orecchia, P. Fossati, S. Rossi, The National Center for oncological hadron therapy: status of the project and future clinical use of the facility. Tumori **95**, 169–176 (2009)
10. M.K. Dosanjh, H.F. Hoffmann, G. Magrin, Status of hadron therapy in Europe and the role of ENLIGHT. Nucl. Instrum. Methods Phys. Res. A **571**, 191–194 (2007)
11. V. Brower, Carbon ion therapy to debut in Europe. J. Natl. Cancer Inst. **101**, 74–76 (2009)
12. H. Tsujii, J.E. Mizoe, T. Kamada, et al., Overview of clinical experiences on carbon ion radiotherapy at NIRS. Radiother. Oncol. **73**, S41–S49 (2004)
13. D. Schultz-Ertner, H. Tsujii, Particle radiation therapy using proton and heavier ion beams. J. Clin. Oncol. **25**, 953–964 (2007)
14. K. Noda, T. Furukawa, T. Inaniwa, et al., New heavy-ion cancer treatment facility at HIMAC. Proceedings of European Particle Accelerator Conference (EPAC), Genoa, Italy, 23–27 June 2008, pp. 818–1820

Chapter 42
Future Directions in Ion Beam Therapy

Daniel Habermehl, Stephanie Combs, and Jürgen Debus

Abstract There is a growing interest in ion beam therapy (IBT) worldwide which has led to an increasing number of new treatment facilities. This development is accompanied by intensive radiobiological, physical and clinical research of both proton therapy (PT) and carbon ion radiotherapy (CIRT). Current developments in IBT with high impact for future challenges will be summarized in this chapter.

42.1 Introduction

Over the last few years, there was a growing interest in IBT with protons and carbon ions due to excellent clinical results. The main goal of modern radiotherapy (RT) is the delivery of a lethal radiation dose to the tumor tissue while sparing surrounding normal tissue. Even with precision techniques, photon-based RT is limited because of its physical dose distribution. IBT offers a breakthrough modality which can be used for patient treatment, and the benefits are based on distinct radiobiological and physical properties (cf. Chap. 4).

These biophysical benefits are currently translated into a clinical benefit for certain oncological patients. To date, the therapeutic effectiveness and safety of IBT has been shown for certain types of tumors, including skull base tumors, lung cancer, liver cancer, head and neck cancer, prostate cancer, bone/soft tissue sarcoma and some others. Furthermore several PT facilities have focused on brain and pediatric tumors, head and neck tumors and prostate cancer.

Clinical use of IBT requires sophisticated therapy facilities with a high level of technical and medical equipment thus limiting its broad application as yet. While

D. Habermehl (✉)
Klinik für Radioonkologie und Strahlentherapie, Universitätsklinikum Heidelberg,
Im Neuenheimer Feld 400, 69121 Heidelberg, Germany
e-mail: daniel.habermehl@med.uni-heidelberg.de

U. Linz (ed.), *Ion Beam Therapy*, Biological and Medical Physics, Biomedical Engineering, DOI 10.1007/978-3-642-21414-1_42,

more than 50,000 patients worldwide have been treated with PT, IBT with ions heavier than protons is still restricted to a few facilities.

This chapter focuses on future trends in IBT and attempts to anticipate short- and long-term developments. The following three issues will be discussed, in particular:

1. *Future contributions of radiobiology to IBT.*
2. *Future challenges of clinical trials in IBT.*
3. *Future advances in medical physics of ion beams.*

42.2 Future Contributions of Radiobiology to IBT

The biophysical gain of IBT in comparison to conventional RT is the impact of the physical dose distribution and the increased relative biological effectiveness (RBE). In general, RBE calculations are derived from in vitro cell survival curves representing the radiobiological gold standard. The RBE of protons is approximately 1.1 [1] and substantially larger for heavy ions [2]. Since the RBE depends on LET, each particle shows an increasing RBE with increasing LET for low doses which cumulates in a defined peak (approximately 100–200 keV/μm) after which the RBE decreases again with higher LET. The biological explanation of this finding is the so-called *overkill effect* which results from an extensively high dose deposition in one cell, leading to higher DNA damage than actually required (cf. Chap. 4 for details).

Different treatment planning strategies are pursued at different heavy ion beam facilities. At the National Institute of Radiological Sciences (NIRS) in Chiba, Japan, the estimation of clinical RBE values is based on the radiobiological properties of human salivary gland cells which are considered to be representative for the treated tumors [3]. The generated RBE values are used for all tumor entities independently of the applied dose level.

At GSI (Gesellschaft für Schwerionenforschung, Darmstadt, Germany) a different treatment planning strategy was developed. The researchers originally came up with the development of the *local effect model* (LEM) in the mid-1990s [4] which implies specific tumor biology information and physical parameters with the ambitious aim of calculating RBE values pixelwise for the planning target volume (PTV) (cf. Chap. 8 for details).

In 2008, Elsässer et al. published an update of the LEM which includes an extensive analysis and improvement of the model [5]. The authors observed slight deviations between model prediction and experimental data in a manner that the old model led to an overestimation of the effective dose in the entrance channel of the beam, whereas the effective dose in the tumor volume was underestimated. This gap was bridged by upgrading the model with the cluster extension (LEM II) and a more detailed track structure description (LEM III) [6, 7]. In general, the improved version of the model seems to be an accurate representation of in vivo effects of heavy ion therapy. To date, more than 600 patients underwent CIRT based

on treatment planning calculations derived from LEM I. Excellent clinical results and low toxicity have proven the effectiveness of the LEM-based treatment planning approach [8, 9].

Even if LEM has already undergone a lot of changes, there are still some weaknesses which have to be resolved in the future.

Radiosensitivity of human tumor cells is usually described by the steepness of a cell survival curve. As mentioned above, tumors with low α/β value are considered rather radioresistant but also more sensitive to changes in fractionation in conventional RT. To date we know that two of the main cancer diseases – breast and prostate cancer – are having comparatively low α/β values (prostate cancer approx. 1.1–3.7 Gy, breast cancer approx. 3–4 Gy) indicating higher sensitivity to changes in fractionation [10–12]. Together with the finding that surrounding normal tissues have an approximately equal or higher α/β ratio, accelerated hypofractionated radiation schedules suggest a benefit. Large clinical trials using photon RT recently confirmed these findings [13–15].

From a radiobiological point of view, tumors with a small α/β ratio such as chordoma, chondrosarcoma, or adenoid cystic carcinoma, are especially suitable for IBT, an assumption which is strongly supported by clinical data [8, 16]. In principle, tumors suitable for high-LET IBT are slowly proliferating and almost radioresistant due to their high DNA repair capacity which overcomes the induced amount of DNA damage.

Conventional fractionation in photon-based RT is necessary to minimize side effects in normal tissue by allowing interfractional repair. Since IBT allows sparing of normal tissue in the entrance channel from high integral doses, fractionation is not as important. This is one of the reasons why ion beam facilities in Japan and Germany use accelerated or hypofractionated therapy regimens with promising results of both normal tissue and antitumor effects.

This knowledge finally leads to the following issues that have to be elucidated in the future:

Until now we have an α/β-based understanding of tumor radiosensitivity. In some cases the underlying data are of limited significance because only few publications deal with experimental or clinical data. In some cases, it might be that α/β values differ significantly in both settings. Furthermore, application of α/β values derived from the linear–quadratic model is somehow controversial for single fractions with doses higher than 5–8 Gy according to some authors [17–20]. This is the reason why mathematical extensions of the model were proposed to better describe the radiobiological effects with underlying mechanistic modeling of the biological response [21–23].

In case of more (dose escalated) hypofractionated therapy regimens, as proposed for example for heavy ion therapy of hepatocellular carcinoma (HCC), the therapeutic gain and validity of the linear quadratic approach has to be evaluated carefully, even when higher α/β ratios are described for these tumor entities [24, 25]. As was demonstrated by Kato et al. for liver tumors [25], a therapeutic benefit can possibly be explained by the better dose distribution and, therefore, higher dose deposition

in the target volume in contrast to photon therapy. This may even compensate a hypothetical α/β "handicap".

Another area of investigation will be the further examination of the tumor microenvironment in IBT effects. Recent publications have interestingly proposed different mechanisms for ions as compared to X-rays. A special focus of these investigations was on the integrin family and matrix-metalloproteinases (MMPs) on the protein level and on migration behavior of irradiated cells on the cellular level. Heavy ion irradiation led to inhibition of cellular adhesiveness and migration in some cases and moreover to a suppression of MMPs and integrins in a model of human umbilical vein endothelial cells [26], whereas X-ray-irradiation promoted endothelial cell migration. Results of further investigations were basically comparable to these findings and also showed a decreased cell migration and inhibition of MMPs in an in vitro human fibrosarcoma model and a human colon cancer model after irradiation with ions and the opposite effects after X-ray application [27]. In summary, there is certain evidence supporting qualitative differences of ion beam and photon irradiation in terms of antiangiogenic and antimigrative effects. It, therefore, remains an open question in which manner these findings will be translated into future radiobiological understanding of IBT. Future models founding on the linear quadratic model such as (partially) the LEM will have to be extended by more precise biological and tumor-specific data to guarantee an individualized and optimal treatment planning.

There is a broad consensus with regard to the outstanding physical and biological advantages of IBT compared to conventional X-ray therapy. In this context, one tends to forget that these identified amenities can also be appalling enemies. A basic therapeutic principle in clinical RT is the addition of a safety margin which extends the contoured gross target volume thus implicitly approving a certain (*high-LET*) dose deposition in the normal tissue. The applied dose can be as high as the tumor dose and lead to severe early and late tissue effects (necrosis, perforations, bleedings, etc.) in nontumoral areas. Furthermore, hypofractionated therapy regimens often used in IBT can possibly contribute to more severe normal tissue damage, as well.

Associated to this subject is the further investigation of early and late normal tissue reactions induced by IBT. Whereas the so-called *radiogenomics* is a field of growing interest in X-ray RT – as can be seen by recent efforts [28–30] – comparable investigations should be initiated in IBT to predict individual radiosensitivity with further impact on treatment by means of fractionation and overall dose concepts. Attempts should be made with regard to analysis on a microscopic and a macroscopic dimension. Normal tissue reactions can be measured by histopathological analysis of original biopsies, by animal studies or by in vitro experiments. Studies of whole-organ and organism responses to various patterns and intensities of radiation would be of high interest. From a clinical point of view, morphological reactions of normal tissues in vivo that can be seen in computed tomography or magnetic resonance scans after IBT would represent the most elegant way of short- and long-term monitoring of normal tissue reactions.

The different radiobiological and biophysical models used for IBT at the facilities in Japan and Germany, lead to different photon-equivalent doses for the treated tumor and the surrounding tissue. The best fractionation schedules for different cancer types are unknown because basic parameters such as the RBE are mainly derived from experimental in vitro data and, therefore, need to be proven in clinical applications.

Finally the following questions will define the future of IBT from a radiobiological point of view:

- How can we improve the predictions of our models of radiobiological effects for ions in tumor and normal tissue and define the width of the therapeutic window?
- Can we generate a more holistic model that includes radiation effects on DNA, protein, cellular, and microenvironmental level in normal and tumor tissue?
- Can we identify patients with the highest potential benefit from IBT by biological markers?

42.3 Future Challenges of Clinical Trials in IBT

IBT has already shown an impressive potential in anticancer treatment because of improved physical and radiobiological characteristics. But despite a growing number of encouraging reports in the last decade, one has to realize that there is in fact limited evidence of the benefit of protons or carbon ions as compared to X-ray therapy [31, 32].

Usually medical progress is defined by evidence-based medicine which is founded on *randomized clinical trials* (RCT) including large patient numbers and comparing at least two different therapies in reference to defined end points. For the achievement of statistical significance to detect a difference between two treatment modalities, a RCT has to be powered adequately by means of patient numbers. In a best-case scenario, there would be clinical studies which compare a standard conventional RT with a proton or heavy ion therapy for a distinct cancer type.

There is a first limitation: The low number of proton and especially heavy ion facilities impedes the conduction of large clinical trials. Even if trials comparing protons to photons in a therapeutic setting could be initiated, trials with other ions will only be conducted in a few centers worldwide with limited capacities for phase-III clinical trials.

The second difficulty results from ethical concerns of conducting clinical trials comparing IBT to photon therapy because of a possible lack of equipoise, which generates questions regarding ethical considerations and acceptance of randomization. One has to be aware of the fact that clinical trials will in some cases hurt this principle because of obvious differences between ion beam and X-ray therapy in dose distribution and the potential to save organs at risk from significant radiation-induced toxicity.

Apart from these theoretical reflections, the promising results obtained with both PT and CIRT need further confirmation in controlled clinical trials with large patient numbers comparing different treatment modalities. To date almost all published clinical trials with protons and heavier ions examine single-modality treatment. Therefore, further efforts have to be made in organizing multicenter clinical trials to achieve sufficient and adequate patient numbers for meaningful trials.

The conceptual designs of future clinical trials have to consider both nonrandomized and randomized settings. Besides practical feasibility of their conduction and ethical reflections, one also has to consider overall treatment costs which differ significantly between carbon ion, proton, and X-ray RT. The following suggestions of trial concepts would appear ethically appropriate and of clinical relevance.

42.3.1 Combined Treatment of Intensity-Modulated X-Ray RT (IMRT) and IBT

In some indications, advantages of both high-precision X-ray RT techniques and IBT can reasonably be combined. One such design, for example, consisting of a two-step treatment has been successfully applied to the treatment of adenoid cystic carcinoma of the head and neck region [16]. In a first step, X-ray-irradiation is used to a larger volume (clinical target volume or CTV) which may include surrounding normal tissue at risk for microscopic tumor spread and/or (cervical) lymph node regions at risk. Usually, an overall dose of 50 Gy is given in 1.8–2 Gy fractions to this enlarged CTV. The second step of the treatment schedule consists of an IBT *boost* (usually with carbon ions) to the macroscopic tumor with or without a small CTV-expansion.

Hereby, large areas of normal tissue can be spared from irradiation by IBT and delivery of a high dose to the macroscopic tumor can be performed by conventional RT and IBT. This is an attractive schedule especially for large tumors and target volumes which tend to spread microscopically or involve lymph node regions.

42.3.2 Comparison of IBT with Nonradiotherapeutic Modalities

In the case of liver metastases or liver cancer (HCC, cholangiocarcinoma), it was suggested that PT or CIRT might be compared with surgical resection or methods of local ablation such as TACE (transarterial chemoembolization) or PEI (percutaneous ethanol injection). Such comparisons offer the potential to define new indications for IBT.

42.3.3 Testing of Different Fractionation Schedules with Curative Intent Using IBT in Both Arms

In this setting, there are both potential risks and potential benefits of hypofractionation which might be considered to counterbalance one another. The assignment of cancer types to a distinct fractionation schedule has ideally to be based on radiobiological estimations of radiosensitivity. As described above, radiosensitivity characterization derived from X-ray RT has to be critically examined when transferred to IBT.

42.3.4 Dose-Searching Trials Comparing IBT at Different Dose Levels

Recently, dose-escalation studies were performed for HCC and stage-I non-small cell lung cancer (NSCLC) with minimal side effects even in case of highly accelerated hypofractionated regimens [33–36]. Nevertheless, the amount of late toxicities induced by (hypofractionated) IBT has still to be examined in detail by means of normal tissue complication probability.

42.3.5 Combination of Concurrent Systemic Therapies with IBT as Compared to Concurrent Chemotherapy with X-Ray RT

Combination of chemo- and radiotherapy is a therapeutic gold standard in many diseases such as glioblastoma, locally advanced head and neck tumors, adenocarcinoma of the rectum, etc. The therapeutic benefit of combined regimens is an additive or a supraadditive effect of the tumoricidal properties resulting in a higher local control rate and reduced distant failure. Nevertheless, a higher antineoplastic effect comes at the cost of a higher amount of side effects and normal tissue toxicity. In case of improved dose conformality and a higher (local) RBE with sparing of normal tissue as in IBT, one can suggest a higher dose of systemic therapies (e.g., cytotoxic or receptor-targeted agents such as fluoropyramidines and EGFR-antibodies with reduction of mucositis or dermatitis) with impact on local and distant control rates (higher impact on control of metastases).

42.3.6 Comparison of Heavy Ion Therapy with PT

This setting is ethically highly appropriate and is the only way to answer the basic question if a higher RBE in the tumor volume results in an improved clinical benefit

by almost comparable physical dose distributions in the normal tissue. All of these issues listed above will have to be considered in the near future to further define the role of IBT.

Moreover, clinical trials must be carefully designed as to the cancer indications and treatment schedules. By now, a certain clinical benefit is reported for the following diseases after PT: head and neck tumors (4 studies), prostate cancer (3 studies), ocular tumors (15 studies), gastrointestinal cancer (5 studies), lung cancer (4 studies), CNS tumors (15 studies), and sarcomas (2 studies) (recently reviewed by [33, 37]).

CIRT was successfully applied to the following indications as shown by several retrospective analyses or phase-I/-II studies: skull base tumors, prostate cancer, HCC, NSCLC, chordoma, chondrosarcoma, osteosarcoma, head and neck tumors, and adenoid cystic carcinoma (recently reviewed by [38,39], (cf., as well, Chaps. 11 and 12)).

Combined therapy regimens including chemotherapy and other systemic therapies with antibodies, small molecules, multikinase inhibitors, and RT are standard procedures in a variety of oncological diseases such as head and neck cancer, cancer of the gastrointestinal tract, gynecological cancers, brain tumors, and lung cancer. There are plenty of possible combinations of these antineoplastic treatment modalities which are currently studied in nearly all types of cancer. While normal tissue toxicitiy is higher in some cases, the principal aim of a combined therapy is a higher antineoplastic efficacy which is in particular due to different modes of tumoricidal action.

To date, there is an almost complete lack of combined regimens in the field of IBT. Further research in this area is, therefore, absolutely required. One can imagine that a combination of protons or carbon ions with a systemic therapy can possibly lead to different effects as compared to X-ray RT. As RBE and LET are increased in the Bragg peak, it can be speculated if the tumoricidal effect of additional substances will be remarkably higher or if it will fail to potentiate the antineoplastic damage in the target volume because the radiation-induced cellular injury has already reached a maximum (saturation). Another aspect is the potential to increase the dose of a systemic therapy as the integral radiation dose to the normal tissues can be reduced with ion beams. This leads to (1) application of a higher local dose implicating an improved local tumor control and (2) potential application of higher doses of a systemic therapy due to a reduced radiation-induced normal tissue toxicity. Both offer the potential to decrease the number of distant metastases.

Finally, it also has to be considered that addition of chemotherapy, unfortunately, can lead to an enhanced effect in surrounding normal tissue (also in IBT) which partially is affected by high-dose regions thus resulting in severe acute or late tissue complications (necrosis, bleedings, fibrosis, etc.).

Some preclinical studies suggest an increased cytotoxicity for combined treatment of CIRT and standard chemotherapeutic drugs. Recently, it could be shown that addition of the chemotherapeutic drug temozolomide to carbon ion treatment

of several glioblastoma cell lines exerted increased cytotoxicity and decreased cell survival as compared to monotherapy [40]. In a human esophageal SCC cell model, combined therapy of carbon ion irradiation and application of various chemotherapeutic drugs such as fluorouracil, *cis*-platinum, doxorubicin and gemcitabine led to additive antitumor effects, whereas simultaneous treatment with docetaxel showed a significant potentiated effect in cell growth suppression [41]. Even newer drugs such as histone deacetylase inhibitors have been tested in the same cancer type in combination with CIRT with promising results in vitro [42].

Future clinical trials will be conducted to evaluate combination therapies including PT or CIRT and systemic treatment with cytostatic drugs, antibodies (e.g., targeting of EGFR, VEGF, or PDGF), small molecules (inhibitors of mTOR, histone deacetylase, bcl-2/-xl, or multikinase pathways) and/or hormone therapy. Therefore, preclinical investigations have to identify potential molecular targets for IBT which can serve as basis for well-designed clinical studies.

Of special interest for IBT will be the treatment of radioresistant tumors. Radioresistance can basically consist of intrinsic resistance (low α/β, slow proliferation or tumor doubling time, elaborated repair mechanisms) or therapy-induced resistance after chemo- or radiotherapy. A central issue will be the investigation of the effectiveness for hypoxic tumors which are considered to be highly radioresistant to low-LET RT. It is expected that this effect is significantly smaller for heavy ion RT than for photon irradiation. This potential advantage has to be proven clinically because up to now, only very few study data on the comparison of the effectiveness of heavy ions for hypoxic and normoxic tumors are available [43].

There is a broad consensus that IBT is an innovative and technically sophisticated method of modern therapeutic ionizing radiation. In the last few years many new ion beam facilities were constructed, especially, for the delivery of protons. Advances in the field of medical physics, beam delivery, and radiobiology have led to high expectations among health professionals and medical laypersons. Retrospective analysis and small phase-I/-II trials suggest promising results for many oncological indications for both proton and heavy ion therapy.

Unfortunately, only limited evidence exists for the superiority of IBT over the best possible X-ray-therapy in all treated cancer types at the moment. Dose distribution characteristics and superior RBE of IBT represent a clear benefit for the patients, theoretically. They have to be translated into measurable endpoints in well-designed clinical trials which might also include testing of additional systemic therapies.

In summary, the future direction of IBT will be defined by the following three questions:

- Does high-LET IBT result in higher local tumor control rates when compared directly to highly conformal proton and photon therapy (applied with biologically equivalent dose)?
- Which cancer types will be the most suitable for carbon or proton beam therapy?
- What can be the impact of additional systemic therapies in combined therapy regimens?

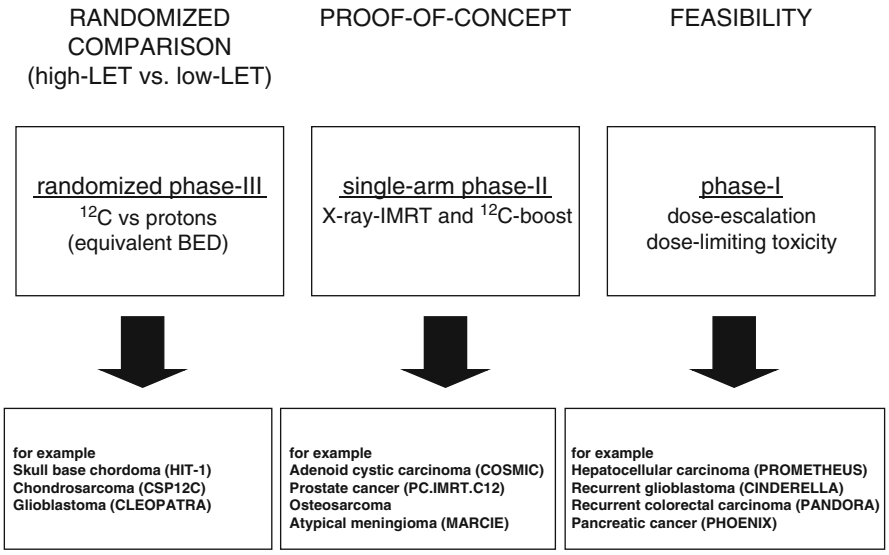

Fig. 42.1 Selected overview of current and future clinical trials at the Heidelberg Ion-Beam Therapy Center (HIT). Classification is according to trial design (phase-I, -II, and –III) with examples of trial names in *parentheses*

One approach to answer these questions will be the ongoing clinical trials in the new Heidelberg Ion-Beam Therapy Center (HIT) which started patient treatment in November 2009. A brief overview and classification of current clinical trials of this institution are given in Fig. 42.1.

42.4 Future Advances in Medical Physics of IBT

There are undoubtedly numerous challenging developments mainly in the field of medical physics and engineering which build the background of modern IBT facilities. One of the developments with highest importance for patient treatment is the irradiation of moving targets.

42.4.1 Moving Organs

Most tumors treated by IBT up to now are located in the head (e.g., chordoma and chondrosarcoma of the skull base, adenoid cystic carcinoma, malignant melanoma of the paranasal sinuses, glioblastoma). Many other cancer types with epidemiological relevance are located in quasimobile organs such as rectum, prostate, lung, or liver. This requires elaborated radiotherapeutic techniques, especially in the case of

IBT. The role of IBT for these indications has still to be defined and will finally decide over the future significance in comparison to X-ray RT.

In the case of skull base tumors, the target volume can be considered fixed when the patient's head is immobilized by external aids such as individual head masks, bite blocks, specially adapted frames, or vacuum fixation.

The basic problem which is also apparent in X-ray therapy is the movement of a target volume in the lateral position and, especially, in the radiological depth, the latter with implications for the range of the ion beams. For heavy ions, the treatment planning system has to assess optimization algorithms for computation of the biologically effective dose when changes in depth modulation appear. *Interfractional* movements can be detected best by direct imaging and can be compensated by set-up corrections and if necessary by adaptation of the treatment plan. In the future, cone beam imaging may be used to detect translational and rotational set-up errors between fractions. In the case of adequate reproduction of the patient's position, translational set-up corrections and – with a robotic couch – rotational corrections around three axes might also be feasible.

Intrafractional organ motion as, for example, in the case of lung or liver tumors results from respiratory movement. Meanwhile, several concepts have been developed to compensate respiratory-associated motions.

One solution considers the extension of the PTV to assure target coverage. Usually, a 4D-CT or MRI is previously performed to record the shifting of the target volume. As known from photon IMRT, motion-related alterations of the ion range lead to an increased inclusion of surrounding normal tissue in the target volume and, therefore, to an increase of RT-induced toxicity. For scanned ion beams expansion of the target volume is not sufficient since it does not prevent the interplay of beam and target motion [44]. Generation of an expanded target volume has to ensure that the beam energy is sufficiently high to cover the distal end of the volume at every moment of the respiratory cycle [45, 46].

If dose is delivered by an active scanning system target coverage can be disturbed by interaction between beam scanning and target motions, thus, eventually, leading to under- or overdosage in the target (*cold* or *hot spots*). These effects can be compensated for by the so-called rescanning techniques which average the effect of irradiations at different breathing phases (cf. Chap. 24 for details). While rescanning studies are under way, there are still some problems to be solved. The particle fluence has to be lowered so that all irradiated fields deliver the correct dose which leads to longer irradiation times and difficulties in dose-monitoring.

There are still more technically advanced attempts to tackle the challenge of the moving target. While *gating* on a stable breathing phase to compensate respiratory motion is in clinical application with passive beam application systems [47], the so-called tumor *tracking* (cf. Chap. 32 for details) promises improved dose deposition to the target while sparing normal tissue, but it is limited to scanning beam systems [48, 49]. Advanced beam delivery systems are able to choose the best adapted treatment plan for a specific breathing phase which ideally requires treatment planning based on a 4D-CT [50].

42.4.2 Role of Positron Emission Tomography

Advances in technology have accounted for implementation of positron emission tomography (PET) as a promising technique for in vivo and noninvasive 3D verification of both carbon ion and proton beam treatment [51, 52]. From a clinician's point of view, it will be favorable to evaluate the applied dose distribution by means of modern imaging techniques, especially when no additional radiation exposure is required.

Treatment with ^{12}C ion beams produces the nuclear fragments ^{11}C and ^{10}C as byproducts. Because of their lower mass, their range is slightly shorter than that of the parent particle of the same energy and they accumulate right in front of the primary beam range. Protons do not disintegrate into positron-emitting fragments. However, proton beams can induce positron activity (mainly ^{15}O) by reacting with the atomic nuclei of the irradiated tissue. The positron activity induced by these two different mechanisms enables quantification of dose activity even shortly after beam delivery (*offline PET*) or immediately during treatment (*in-beam PET*). Finally, activity distributions can be compared to the treatment plan and correction of imprecisely applied doses will be possible (see Chap. 31).

When treating moving targets with scanned ion beams, time-resolved acquisition and motion compensation are required because of a prolonged scan interval. Feasibility of 4D in-beam PET verification of carbon ion tracking of a moving target has recently successfully been performed in a phantom [53]. Volumetric extension of irradiation-induced activity distribution can hence be processed by both in-beam as well as offline PET imaging, even in a more complex setting of target motion.

It will be challenging to implement these new techniques into clinical routine. Hereby, a more precise evaluation and quality assurance of scanned IBT for moving targets (e.g., lung cancer, liver cancer) will be possible in the near future.

42.5 Summary

There have been many important innovations in the area of radiobiology and, especially, in medical physics which represent the preconditions of modern IBT. Nevertheless, improvements of existing standards raise new questions leading to new directions. To date the significance of IBT and, especially, of high-LET CIRT is still undetermined for a wide variety of cancer types. Even if for some rare indications such as skull base tumors and adenoid cystic carcinomas, heavy ion therapy is of clear benefit, it is still an open question whether and how the therapeutic spectrum can be extended, reasonably.

Therefore, it will be a challenge for all radiation oncologists involved to examine the full potential of IBT and to probably pull it out of its therapeutic niche.

Moreover, further attempts have to be made towards the selection of PT indications. Will protons be the "better" but "costly" photons? The above-mentioned biophysical advantages argue for their clinical application but clinical decision making will, finally, also depend on related therapy costs. The aim and challenge

of all hereby related efforts will be improvements of patient treatment which need to be confirmed in adequately conducted clinical trials.

References

1. H. Paganetti, A. Niemierko, M. Ancukiewicz, et al., Relative biological effectiveness (RBE) values for proton beam therapy. Int. J. Radiat. Oncol. Biol. Phys. **53**, 407–421 (2002)
2. W.K. Weyrather, G. Kraft, RBE of carbon ions: experimental data and the strategy of RBE calculation for treatment planning. Radiother. Oncol. **73**(Suppl 2), S161–169 (2004)
3. T. Kanai, M. Endo, S. Minohara, et al., Biophysical characteristics of HIMAC clinical irradiation system for heavy-ion radiation therapy. Int. J. Radiat. Oncol. Biol. Phys. **44**, 201–210 (1999)
4. M. Scholz, A.M. Kellerer, W. Kraft-Weyrather, G. Kraft, Computation of cell survival in heavy ion beams for therapy. The model and its approximation. Radiat. Environ. Biophys. **36**, 59–66 (1997)
5. T. Elsässer, M. Krämer, M. Scholz, Accuracy of the local effect model for the prediction of biologic effects of carbon ion beams in vitro and in vivo. Int. J. Radiat. Oncol. Biol. Phys. **71**, 866–872 (2008)
6. T. Elsässer, M. Scholz, Cluster effects within the local effect model. Radiat. Res. **167**, 319–329 (2007)
7. C.P. Karger, P. Peschke, R. Sanchez-Brandelik, et al., Radiation tolerance of the rat spinal cord after 6 and 18 fractions of photons and carbon ions: experimental results and clinical implications. Int. J. Radiat. Oncol. Biol. Phys. **66**, 1488–1497 (2006)
8. D. Schulz-Ertner, C.P. Karger, A. Feuerhake, et al., Effectiveness of carbon ion radiotherapy in the treatment of skull-base chordomas. Int. J. Radiat. Oncol. Biol. Phys. **68**, 449–457 (2007)
9. D. Schulz-Ertner, A. Nikoghosyan, H. Hof, et al., Carbon ion radiotherapy of skull base chondrosarcomas. Int. J. Radiat. Oncol. Biol. Phys. **67**, 171–177 (2007)
10. V. Macías, A. Biete, Hypofractionated radiotherapy for localised prostate cancer. Review of clinical trials. Clin. Transl. Oncol. **11**, 437–445 (2009)
11. J. Yarnold, A. Ashton, J. Bliss, et al., Fractionation sensitivity and dose response of late adverse effects in the breast after radiotherapy for early breast cancer: Long-term results of a randomised trial. Radiother. Oncol. **75**, 9–17 (2005)
12. J.R. Owen, A. Ashton, J.M. Bliss, et al., Effect of radiotherapy fraction size on tumour control in patients with early-stage breast cancer after local tumour excision: Long-term results of randomised trial. Lancet Oncol. **7**, 467–471 (2006)
13. T.J. Whelan, J.P. Pignol, M.N. Levine, et al., Long-term results of hypofractionated radiation therapy for breast cancer. N. Engl. J. Med. **362**, 513–520 (2010)
14. START Trialists' Group, A. Bentzen, et al., The UK Standardisation of Breast Radiotherapy (START) Trial A of radiotherapy hypofractionation for treatment of early breast cancer: a randomised trial. Lancet Oncol. **9**, 331–341 (2008)
15. The START Trialists' Group, S.M. Bentzen, R.K. Agrawal, et al., The UK Standardisation of Breast Radiotherapy (START) Trial B of radiotherapy hypofractionation for treatment of early breast cancer: a randomised trial. Lancet **371**, 1098–1107 (2008)
16. D. Schulz-Ertner, A. Nikoghosyan, B. Didinger, et al., Therapy strategies for locally advanced adenoid cystic carcinomas using modern radiation therapy techniques. Cancer **104**, 338–344 (2005)
17. S.M. Bentzen, M.C. Joiner, The Linear-Quadratic Approach in Clinical Practice, in *Basic Clinical Radiobiology*, ed. by M. Joiner, A. van der Kogel. (Hodder Arnold, London, 2009), pp. 120–134

18. J.P. Kirkpatrick, J.J. Meyer, L.B. Marks, The linear-quadratic model is inappropriate to model high dose per fraction effects in radiosurgery. Semin. Radiat. Oncol. **18**, 240–243 (2008)
19. D.J. Brenner, The linear-quadratic model is an appropriate methodology for determining isoeffective doses at large doses per fraction. Semin. Radiat. Oncol. **18**, 234–239 (2008)
20. H. Iwata, Y. Shibamoto, R. Murata, et al., Estimation of errors associated with use of linear-quadratic formalism for evaluation of biologic equivalence between single and hypofractionated radiation doses: an in vitro study. Int. J. Radiat. Oncol. Biol. Phys. **75**, 482–488 (2009)
21. M. Carlone, D. Wilkins, P. Raaphorst, The modified linear-quadratic model of Guerrero and Li can be derived from a mechanistic basis and exhibits linear-quadratic-linear behaviour. Phys. Med. Biol. **50**, L9–L13 (2005)
22. M. Guerrero, X.A. Li, Extending the linear-quadratic model for large fraction doses pertinent to stereotactic radiotherapy. Phys. Med. Biol. **49**, 4825–4835 (2004)
23. C.S. Park, L. Papiez, R. Timmerman, The unifying (hybrid) survival curve and single fraction equivalent dose: useful tools in understanding the potency of ablative radiation therapy. Int. J. Radiat. Oncol. Biol. Phys. **69**, 623–624 (2007)
24. A. Tai, B. Erickson, K.A. Khater, X.A. Li, Estimate of radiobiologic parameters from clinical data for biologically based treatment planning for liver irradiation. Int. J. Radiat. Oncol. Biol. Phys. **70**, 900–907 (2008)
25. H. Kato, S. Yamada, S. Yasuda, et al., Four-fraction carbon ion radiotherapy for hepatocellular carcinoma: results of a phase II clinical trial. Proceedings of 40th ASCO Annual Meeting, 5–8 June 2004. J. Clin. Oncol. **22**, 4090 (2004)
26. Y. Takahashi, T. Teshima, N. Kawaguchi, et al., Heavy ion irradiation inhibits in vitro angiogenesis even at sublethal dose. Cancer Res. **63**, 4253–4257 (2003)
27. T. Ogata, T. Teshima, K. Kagawa, Y. Hishikawa, Particle irradiation suppresses metastatic potential of cancer cells. Cancer Res. **65**, 113–120 (2005)
28. C. West, B.S. Rosenstein, Establishment of a radiogenomics consortium. Radiother. Oncol. **94**, 117–118 (2010)
29. A.M. Rutman, M.D. Kuo, Radiogenomics: creating a link between molecular diagnostics and diagnostic imaging. Eur. J. Radiol. **70**, 232–241 (2009)
30. N.G. Burnet, R.M. Elliott, A. Dunning, C.M.L. West, Radiosensitivity, radiogenomics and RAPPER. Clin. Oncol. **18**, 525–528 (2006)
31. M. Goitein, Trials and tribulations in charged particle radiotherapy. Radiother. Oncol. **95**, 23–31 (2010)
32. H. Suit, H. Kooya, A. Trofimova, et al., Should positive phase III clinical trial data be required before proton beam therapy is more widely adopted? No. Radiother. Oncol. **86**, 148–153 (2008)
33. M. Brada, M. Pijls-Johannesma, D. De Ruysscher, Current clinical evidence for proton therapy. Cancer J. **15**, 319–324 (2009)
34. T. Miyamoto, N. Yamamoto, H. Nishimura, et al., Carbon ion radiotherapy for stage I non-small cell lung cancer. Radiother. Oncol. **66**, 127–140 (2003)
35. T. Miyamoto, M. Baba, N. Yamamoto, et al., Curative treatment of Stage I non-small cell lung cancer with carbon ion beams using a hypofractionated regimen. Int. J. Radiat. Oncol. Biol. Phys. **67**, 750–758 (2007)
36. H. Kato, H. Tsujii, T. Miyamoto, et al., Results of the first prospective study of carbon ion radiotherapy for hepatocellular carcinoma with liver cirrhosis. Int. J. Radiat. Oncol. Biol. Phys. **59**, 1468–1476 (2004)
37. M. Brada, M. Pijls-Johannesma, D. De Ruysscher, Proton therapy in clinical practice: current clinical evidence. J. Clin. Oncol. **25**, 965–970 (2007)
38. D. Schardt, T. Elsässer, D. Schulz-Ertner, Heavy-ion tumor therapy: Physical and radiobiological benefits. Rev. Mod. Phys. **82**, 383–425 (2010)
39. E. Fokas, G. Kraft, H. An, R. Engenhart-Cabillic, Ion beam radiobiology and cancer: Time to update ourselves. Biochim. Biophys. Acta **1796**, 216–229 (2010)
40. S.E. Combs, J. Bohl, T. Elsässer, et al., Radiobiological evaluation and correlation with the local effect model (LEM) of carbon ion radiation therapy and temozolomide in glioblastoma cell lines. Int. J. Radiat. Oncol. Biol. Phys. **85**, 126–137 (2009)

41. H. Kitabayashi, H. Shimada, S. Yamada, et al., Synergistic growth suppression induced in esophageal squamous cell carcinoma cells by combined treatment with docetaxel and heavy carbon-ion beam irradiation. Oncol. Rep. **15**, 913–918 (2006)
42. M. Kano, S. Yamada, I. Hoshino, et al., Effects of carbon-ion radiotherapy combined with a novel histone deacetylase inhibitor, cyclic hydroxamic-acid-containing peptide 31 in human esophageal squamous cell carcinoma. Anticancer Res. **29**, 4433–4438 (2009)
43. T. Nakano, Y. Suzuki, T. Ohno, et al., Carbon beam therapy overcomes the radiation resistance of uterine cervical cancer originating from hypoxia. Clin. Cancer Res. **12**, 2185–2190 (2006)
44. C. Bert, S.O. Grözinger, E. Rietzel, Quantification of interplay effects of scanned particle beams and moving targets. Phys. Med. Biol. **53**, 2253–2265 (2008)
45. M. Engelsman, E. Rietzel, H.M. Kooy, Four-dimensional proton treatment planning for lung tumors. Int. J. Radiat. Oncol. Biol. Phys. **64**, 1589–1595 (2006)
46. C. Bert, E. Rietzel, 4D treatment planning for scanned ion beams. Radiat. Oncol. **2**, 24 (2007)
47. S. Minohara, T. Kanai, M. Endo, et al., Respiratory gated irradiation system for heavy-ion radiotherapy. Int. J. Radiat. Oncol. Biol. Phys. **47**, 1097–1103 (2000)
48. C. Bert, N. Saito, A. Schmidt, et al., Target motion tracking with a scanned particle beam. Med. Phys. **34**, 4768–4771 (2007)
49. C. Bert, S.O. Grözinger, E. Rietzel, Quantification of interplay effects of scanned particle beams and moving targets. Phys. Med. Biol. **53**, 2253–2265 (2008)
50. S.O. Grözinger, E. Rietzel, Q. Li, et al., Simulations to design an online motion compensation system for scanned particle beams. Phys. Med. Biol. **51**, 3517–3531 (2006)
51. K. Parodi, H. Paganetti, H.A. Shih, et al., Patient study of in vivo verification of beam delivery and range, using positron emission tomography and computed tomography imaging after proton therapy. Int. J. Radiat. Oncol. Biol. Phys. **68**, 920–934 (2007)
52. K. Parodi, T. Bortfeld, T. Haberer, Comparison between in-beam and offline positron emission tomography imaging of proton and carbon ion therapeutic irradiation at synchrotron- and cyclotron-based facilities. Int. J. Radiat. Oncol. Biol. Phys. **71**, 945–956 (2008)
53. K. Parodi, N. Saito, N. Chaudhri, et al., 4D in-beam positron emission tomography for verification of motion-compensated ion beam therapy. Med. Phys. **36**, 4230 (2009)

Index

U. Linz (ed.), *Ion Beam Therapy*, Biological and Medical Physics, Biomedical Engineering, DOI 10.1007/978-3-642-21414-1,

Name Index

U. Linz (ed.), *Ion Beam Therapy*, Biological and Medical Physics, Biomedical Engineering, DOI 10.1007/978-3-642-21414-1,